Christos Comninellis • Guohua Chen
Editors

Electrochemistry for the Environment

Springer

Electrochemistry for the Environment

Christos Comninellis · Guohua Chen
Editors

Electrochemistry for the Environment

Springer

Editors
Christos Comninellis
Dept. Chemical Engineering
Ecole Polytech. Fed. Lausanne
1015 Lausanne
Switzerland
christos.comninellis@epfl.ch

Guohua Chen
Dept. Chemical Engineering
Hong Kong University of Science
and Technology
Clear Water Bay
Kowloon
Hong Kong SAR
kechengh@ust.hk

ISBN 978-0-387-36922-8 e-ISBN 978-0-387-68318-8
DOI 10.1007/978-0-387-68318-8
Springer New York Dordrecht Heidelberg London

Library of Congress Control Number: 2009927499

Preface

Wastewater treatment technology is undergoing a profound transformation due to the fundamental changes in regulations governing the discharge and disposal of hazardous pollutants. Established design procedures and criteria, which have served the industry well for decades, can no longer meet the ever-increasing demand.

Toxicity reduction requirements dictate in the development of new technologies for the treatment of these toxic pollutants in a safe and cost-effective manner. Foremost among these technologies are electrochemical processes.

While electrochemical technologies have been known and utilized for the treatment of wastewater containing heavy metal cations, the application of these processes is only just a beginning to be developed for the oxidation of recalcitrant organic pollutants.

In fact, only recently the electrochemical oxidation process has been recognized as an advanced oxidation process (AOP). This is due to the development of boron-doped diamond (BDD) anodes on which the oxidation of organic pollutants is mediated via the formation of active hydroxyl radicals.

In this volume, our goals are to first lay down the fundamentals involving the environmental electrochemistry, introducing the basic techniques in selecting the electrode materials and fabricating them, followed by the theoretical analysis of the electrochemical processes, the green electrochemical operation, discuss about the electrochemical technologies in water/wastewater treatment using BDD, and then examine the established wastewater treatment technologies such as electrocoagulation and electroflotation. The electrochemical reduction technologies are discussed in two chapters with main focus on the treatment of halogenated compounds. Electrooxidation using Ti/SnO_2 has received lots attention in the past decades, one chapter is devoted to this topic. One chapter discusses about the treatment of wet sludge, a type of waste to generate along with the water/wastewater treatment development. The emerging technologies based on solar energy are analyzed toward the end of the book with a closing chapter on using both redox half-reactions, reduction and oxidation in wastewater treatment.

We are grateful to the contributors from eight countries in Asia, Europe, and North America. We hope this collective work of internationally renowned experts on electrochemical technologies can help the environmental engineers, academic

researchers, and environmental protection officials/agencies to better protect our precious earth. We are confident that together people can preserve the natural environment for us and many generations to come!

Lausanne, Switzerland — *Christos Comninellis*
Kowloon, Hong Kong — *Guohua Chen*

Contents

Contributors

Detlef W. Bahnemann Institut für Technische Chemie, Leibniz Universität Hannover, Hannover, Germany, bahnemann@iftc.uni-hannover.de

M.E. Henry Bergmann Departments 6/7, Anhalt University of Applied Sciences, Koethen/Anh., Germany, h.bergmann@emw.hs-anhalt.de

Enric Brillas Laboratori d'Electroquímica dels Materials i del Medi Ambient, Departament de Química Física, Facultat de Química, Universitat de Barcelona, Martí i Franquès 1–11, 08028 Barcelona, Spain, brillas@ub.edu

Pere Lluís Cabot Laboratori d'Electroquímica dels Materials i del Medi Ambient, Departament de Química Física, Facultat de Química, Universitat de Barcelona, Martí i Franquès 1–11, Barcelona, Spain, p.cabot@ub.edu

Pablo Cañizares Department of Chemical Engineering, Universidad de Castilla La Mancha, Campus Universitario s/n, Ciudad Real, Spain

Guohua Chen Department of Chemical and Biomolecular Engineering, Hong Kong University of Science and Technology, Clear Water Bay, Kowloon, Hong Kong, kechengh@ust.hk

Xueming Chen Environmental Engineering Department, Zhejiang University, Hangzhou, China, chenxm@zju.edu.cn

Hua Cheng School of Chemical Engineering & Advanced Materials, Newcastle University, Merz Court, Newcastle Upon Tyne, UK, hua.cheng@ncl.ac.uk

Christos Comninellis Institute of Chemical Sciences and Engineering, Ecole Polytechnique Fédérale de Lausanne (EPFL), Lausanne, Switzerland, christos.comninellis@epfl.ch

Yujie Feng State Key Laboratory of Urban Water Resource & Environment, Harbin Institute of Technology, No 73, Huanghe Road, Harbin 150090, Heilongjiang, People's Republic of China, yujief@hit.edu.cn

György Foti Institute of Chemical Sciences and Engineering, Ecole Polytechnique Fédérale de Lausanne (EPFL), Lausanne, Switzerland, gyorgy.foti@epfl.ch

Ulrich Griesbach Care Chemicals, BASF SE, Ludwigshafen, Germany, ulrich.griesbach@basf.com; cpr@adamant_technologies.com

Liang Guo Environmental Engineering Program, The Hong Kong University of Science and Technology, Clear Water Bay, Kowloon, Hong Kong, guol2008@hotmail.com

Nicolas Hermant Adamant Technologies SA, La Chaux-de-Fonds, Switzerland

Agnieszka Kapałka Institute of Chemical Sciences and Engineering, Ecole Polytechnique Fédérale de Lausanne (EPFL), Lausanne, Switzerland, agnieszka.cieciwa@epfl.ch

Xinyong Li Key Laboratory of Industrial Ecology and Environmental Engineering, School of Environmental & Biological Science & Technology, Dalian University of Technology, Dalian, China, xyli@dlut.edu.cn

Huijuan Liu State Key Laboratory of Environmental Aquatic Chemistry, Research Center for Eco-Environmental Sciences, Chinese Academy of Sciences, Beijing, China, hjliu@rcees.ac.cn

Justo Lobato Department of Chemical Engineering, Universidad de Castilla La Mancha, Campus Universitario s/n, Ciudad Real, Spain

Itamar M. Malkowsky Chemicals Research and Engineering, BASF SE, Ludwigshafen, Germany, itamar.malkowsky@basf.com

M. Mascia Dip. Ingegneria Chimica e mat., University of Cagliari, Cagliari, Italy, mmascia@dicm.unica.it

S. Palmas Dip. Ingegneria Chimica e mat., University of Cagliari, Cagliari, Italy, sipalmas@dicm.unica.it

Marco Panizza Department of Chemical and Process Engineering, Genoa University, Genoa, Italy, marco.panizza@unige.it

Anna Maria Polcaro Dip. Ingegneria Chimica e mat., University of Cagliari, Cagliari, Italy, polcaro@dicm.unica.it

Christophe Provent Adamant Technologies SA, La Chaux-de-Fonds, Switzerland

Cesar Pulgarin Division of Chemistry, Ecole Polytechnique Fédérale de Lausanne Suisse, cesar.pulgarin@epfl.ch

Laurent Pupunat Adamant Technologies SA, La Chaux-de-Fonds, Switzerland

Jiuhui Qu State Key Laboratory of Environmental Aquatic Chemistry, Research Center for Eco-Environmental Sciences, Chinese Academy of Sciences, Beijing, China, jhqu@rcees.ac.cn

Angela Guiovana Rincón Division of Engineering and Applied Science, California Institute of Technology, Pasadena, CA, USA, agrincon@caltech.edu

Manuel A. Rodrigo Department of Chemical Engineering, Universidad de Castilla La Mancha, Campus Universitario s/n, Ciudad Real, Spain, manuel.rodrigo@uclm.es

Sandra Rondinini Dipartimento di Chimica Fisica ed Elettrochimica, Università degli Studi di Milano, Via Golgi, 19-20133 Milan, Italy, sandra.rondinini@unimi.it

Philippe Rychen Adamant Technologies SA, La Chaux-de-Fonds, Switzerland

Cristina Sáez Department of Chemical Engineering, Universidad de Castilla La Mancha, Campus Universitario s/n, Ciudad Real, Spain

Keith Scott School of Chemical Engineering & Advanced Materials, Newcastle University, Merz Court, Newcastle Upon Tyne, UK, k.scott@ncl.ac.uk

Roberto M. Serikawa Applied Chemistry Laboratory, Ebara Research Co., LTD., Honfujisawa, Fujisawa-shi, Japan, serikawa.roberto@er.ebara.co.jp

Ignasi Sirés Laboratori d'Electroquímica dels Materials i del Medi Ambient, Departament de Química Física, Facultat de Química, Universitat de Barcelona, Martí i Franquès 1–11, Barcelona, Spain, isires@catalonia.net

A.Vacca Dip. Ingegneria Chimica e mat., University of Cagliari, Cagliari, Italy, vacca@dicm.unica.it

N. Vatistas Chemical Engineering Department, University of Pisa Via Diotisalvi, Pisa, Italy, vatistas@ing.unipi.it

Alberto Vertova Department of Physical Chemistry and Electrochemistry, University of Milan, Italy, alberto.vertova@unimi.it

Siegfried R. Waldvogel Kekulé-Institute for Organic Chemistry and Biochemistry, University of Bonn, Bonn, Germany, waldvogel@uni-bonn.de

Huanjun Zhang Department of Chemical and Biomolecular Engineering, Hong Kong University of Science and Technology, Clear Water Bay, Kowloon, Hong Kong, zhanghj@ust.hk

Xu Zhao State Key Laboratory of Environmental Aquatic Chemistry, Research Center for Eco-Environmental Sciences, Chinese Academy of Sciences, Beijing, China, zhaoxu@rcees.ac.cn

Chapter 1
Basic Principles of the Electrochemical Mineralization of Organic Pollutants for Wastewater Treatment

Agnieszka Kapałka, György Fóti, and Christos Comninellis

1.1 Introduction

Biological treatment of polluted water is the most economical process and it is used for the elimination of "readily degradable" organic pollutants present in wastewater. The situation is completely different when the wastewater contains toxic and refractory (resistant to biological treatment) organic pollutants. One interesting possibility is to use a coupled process: partial oxidation – biological treatment. The goal is to decrease the toxicity and to increase the biodegradability of the wastewater before the biological treatment. However, the optimization of this coupled process is complex and usually complete mineralization of the organic pollutants is preferred. The mineralization of these organic pollutants can be achieved by complete oxidation using oxygen at high temperature or strong oxidants combined with UV radiation. Depending on the operating temperature, the type of used oxidant, and the concentration of the pollutants in the wastewater, the mineralization can be classified into three main categories:

(a) *Incineration*. Incineration takes place in the gas phase at high temperature (820–1,100°C). Its main characteristic is a direct combustion with excess oxygen from air in a flame. The process is nearly instantaneous. Incineration by-products are mainly in the gas (including NO_x, SO_2, HCl, dioxins, furans, etc.) and solid phases (bottom and fly ashes). The technology is applied mainly for concentrated wastewater with chemical oxygen demand, COD $> 100\,g/L$.

(b) *Wet air oxidation process (WAO)*. WAO can be defined as the oxidation of organic pollutants in an aqueous media by means of oxygen from air at elevated temperature (250–300°C) and high pressure (100–150 bar). Usually Cu^{2+} is used as a catalyst in order to increase the reaction rate. The efficiency of the mineralization can be higher than 99% and the main by-products formed in the aqueous phase after the treatment are acetone, methanol, ethanol, pyridine, and

A. Kapałka (✉)
Institute of Chemical Sciences and Engineering, Ecole Polytechnique Fédérale de Lausanne (EPFL), CH-1015 Lausanne, Switzerland
e-mail: agnieszka.cieciwa@epfl.ch

C. Comninellis and G. Chen (eds.), *Electrochemistry for the Environment*,
DOI 10.1007/978-0-387-68318-8_1,

methanesulfonic acid. The technology is attractive for treatment of wastewater with moderate concentration. The optimal COD is in the domain: $50\,g/L > COD > 15\,g/L$.

(c) *Oxidation with strong oxidants*. The oxidation of organic pollutants with strong oxidants (H_2O_2, O_3) takes place generally at room temperature. In order to increase the efficiency of mineralization, the oxidation takes place in the presence of catalyst and UV radiation. This technology is interesting for the treatment of dilute wastewater with $COD < 5\,g/L$.

The electrochemical method for the mineralization of organic pollutants is a new technology and has attracted a great deal of attention recently. This technology is interesting for the treatment of dilute wastewater ($COD < 5\,g/L$) and it is in competition with the process of chemical oxidation using strong oxidants. The main advantage of this technology is that chemicals are not used. In fact, only electrical energy is consumed for the mineralization of organic pollutants. Besides our contribution in this field (Comninellis and Plattner 1988; Comninellis and Pulgarin 1991; Seignez et al. 1992; Comninellis 1992; Comninellis and Pulgarin 1993; Pulgarin et al. 1994; Comninellis 1994; Comninellis and Nerini 1995; Simond et al. 1997; Fóti et al. 1997; Ouattara et al. 2004), many other research groups are very active in this promising technology (Comninellis and De Battisti 1996; Iniesta et al. 2001a; Chen et al. 2003; Ouattara et al. 2003; Zanta et al. 2003; Polcaro et al. 2004; Brillas et al. 2004; Haenni et al. 2004; Martinez-Huitle et al. 2004; Polcaro et al. 2005; Chen et al. 2005; Boye et al. 2006).

The aim of the present work is to elucidate the basic principles of the electrochemical mineralization (EM) using some model organic pollutants. The following points will be treated:

- Thermodynamics of the electrochemical mineralization (EM) of organics
- Mechanism of the electrochemical oxygen transfer reaction (EOTR)
- Influence of anode material on the reactivity of electrolytic hydroxyl radicals
- Determination of the current efficiency in the electrochemical oxidation process
- Kinetic model of organics mineralization on BDD anodes
- Intermediates formed during the EM process using BDD
- Electrical energy consumption in the EM process
- Optimization of the EM process using BDD
- Fouling and corrosion of BDD anodes.

1.2 Thermodynamics of the Electrochemical Mineralization

Thermodynamically, the electrochemical mineralization (EM) of any soluble organic compound in water should be achieved at low potentials, widely before the thermodynamic potential of water oxidation to molecular oxygen (1.23 V/SHE under standard conditions) as it is given by (1.1):

$$2H_2O \rightarrow O_2 + 4H^+ + 4e^- \tag{1.1}$$

A typical example of EM is the anodic oxidation of acetic acid to CO_2 (1.2):

$$CH_3COOH_{(aq)} + 2H_2O\,(l) \rightarrow 2CO_{2(g)} + 8H^+_{(aq)} + 8e^- \tag{1.2}$$

The thermodynamic potential of this reaction E^0 (V) can be calculated using (1.3):

$$E^0 = \frac{-\Delta_r G^0}{nF}, \tag{1.3}$$

where $\Delta_r G^0$ $\left(\text{J mol}^{-1}\right)$ is the standard free energy of the reaction, n is the number of exchanged electrons ($n = 8$), and F is Faraday's constant $\left(\text{C mol}^{-1}\right)$. The standard free energy of the reaction $\Delta_r G^0$ can be calculated from the tabulated values of the standard free energy of formation $\left(\Delta_r G^0\right)$ of both reactants and products (1.4):

$$\begin{aligned} -\Delta_r G^0 &= 2\Delta_f G^0(CO_2) - \Delta_f G^0\,(CH_3COOH) - 2\Delta_f G^0\,(H_2O)\,, \\ -\Delta_r G^0 &= 2 \times \left(-394.4 \times 10^3\right) - \left(-399.6 \times 10^3\right) - 2 \times \left(-237.13 \times 10^3\right) \\ &= 85.1 \times 10^3\ \text{J mol}^{-1}. \end{aligned} \tag{1.4}$$

From the calculated standard free energy, the thermodynamic potential of reaction (1.2) under standard conditions $\left(1\ \text{mol dm}^{-3},\ CH_3COOH,\ P = 1\ \text{atm},\ T = 25°\text{C}\right)$ can be calculated using (1.3):

$$E^0 = \frac{-\Delta_r G^0}{nF} = \frac{85.1 \times 10^3}{8 \cdot 96485} = 0.11\ \text{V/SHE}.$$

Similarly, the thermodynamic potential for EM of some model organic compounds (alcohols, carboxylic acids, ketenes, phenols, and aromatic acids) can be calculated. Typical values are reported in Table 1.1. This table shows that the thermodynamic potential for EM of organics never exceeds 0.2 V/SHE.

Table 1.1 Standard free energy $\Delta_r G^0$, thermodynamic potential for organics mineralization E^0 and thermodynamic cell potential ΔE^0_{cell} calculated for various organic compounds

Organic compound	$\Delta_r G^0$ $\left(\text{kJ mol}^{-1}\right)$	E^0 (V/SHE)	ΔE^0_{cell} (V/SHE)
CH_3OH	−17.2	0.030	1.20
C_2H_5OH	−99.6	0.086	1.14
C_3H_7OH	−173.2	0.100	1.13
CH_3COOH	−85.1	0.110	1.12
CH_3COCH_3	−157.9	0.102	1.13
C_6H_5OH	−292.9	0.108	1.13
C_6H_5COOH	−330.1	0.114	1.11

Taking into consideration this result, it will be theoretically possible to treat an aqueous organic pollutants stream as a fuel cell with co-generation of electrical energy. In this device, the organic pollutant is oxidized at the anode [(1.2) in case of acetic acid] and oxygen is reduced at the cathode (1.5):

$$\frac{1}{2}O_2 + 2H^+ + 2e^- \rightarrow H_2O \tag{1.5}$$

The total reaction of this fuel cell, considering acetic acid as a fuel, is given by (1.6):

$$CH_3COOH + 2O_2 \rightarrow 2CO_2 + 2H_2O \tag{1.6}$$

The standard free energy change of this fuel cell can be calculated from the tabulated standard free energy of formation of reactant and products:

$$\begin{aligned}\Delta_r G^0 &= 2\Delta_f G^0\,(CO_2) + 2\Delta_f G^0\,(H_2O) - \Delta_f G^0\,(CH_3COOH)\,,\\ \Delta_r G^0 &= 2 \times \left(-394.4 \times 10^3\right) + 2 \times \left(-237.13 \times 10^3\right) - \left(-399.6 \times 10^3\right)\\ &= -863.5 \times 10^3\,\mathrm{J\,mol^{-1}}.\end{aligned}$$

Finally, the standard thermodynamic potential of the cell, based on (1.6) (i.e., incineration of the pollutant with co-generation of energy), can be calculated using the relation:

$$E^0_{\mathrm{cell}} = \frac{-\Delta_r G^0}{nF} = \frac{-\left(-863.5 \times 10^3\right)}{8 \cdot 96485} = 1.12\,\mathrm{V}.$$

In Table 1.1, the thermodynamic cell potentials calculated for some other organics are given. Values close to 1 V can be achieved under standard conditions. Figure 1.1 shows a schematic presentation of a hypothetical fuel cell for the incineration of organic pollutants with co-generation of electrical energy.

In contrast to these promising thermodynamic data, the kinetics of the electrochemical mineralization is very slow and in practice it can be achieved close to the thermodynamic potentials only in very limited cases. In fact, only platinum-based electrodes can allow EM of simple C_1 organic compounds. A typical example is the use of Pt–Ru catalyst in the electrochemical mineralization of methanol.

In conclusion, in the actual state of the art, the electrochemical mineralization of organic pollutants with co-generation of electrical energy is not feasible due to the lack of active electrocatalytic anode material. However, recently we have demonstrated that the electrochemical mineralization of organics can be achieved on some electrode material by electrolysis at potentials largely above the thermodynamic potential of oxygen evolution (1.23 V/SHE under standard conditions). Even if in this process electrical energy is consumed, this system opens new possibilities for the treatment at room temperature of very toxic organic pollutants present in

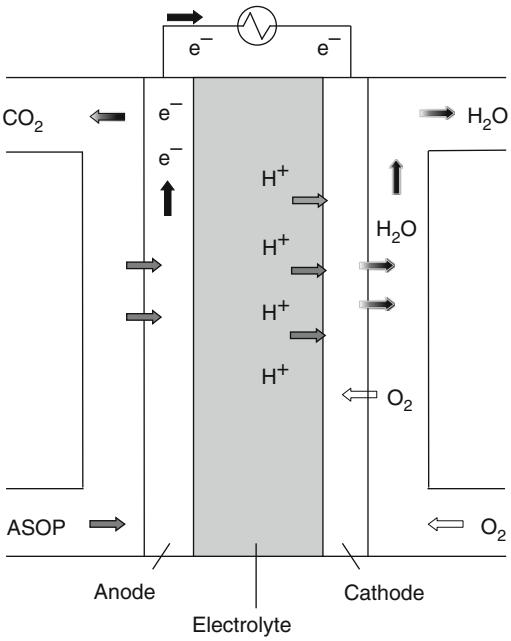

Fig. 1.1 Schematic representation of a hypothetical fuel cell for the mineralization of organic pollutants; *ASOP* aqueous solution of organic pollutants

industrial wastewater (Boye et al. 2004; Gandini et al. 2000; Rodrigo et al. 2001; Panizza et al. 2001a, b; Iniesta et al. 2001b; Fryda et al. 1999; Montilla et al. 2001; Bellagamba et al. 2002; Boye et al. 2002; Montilla et al. 2002).

1.3 Mechanism of the Electrochemical Mineralization

In general, anodic oxidation reactions are accompanied by transfer of oxygen from water to the reaction products. This is the so-called EOTR. A typical example of EOTR is the EM of acetic acid (1.2). In this anodic reaction, water is the source of oxygen atoms for the complete oxidation of acetic acid to CO_2. However, in order to achieve the EOTR, water should be activated. Depending on electrode material, there are two main possibilities for the electrochemical activation of water in acid media (1) by dissociative adsorption of water in the potential region of the thermodynamic stability of water (fuel cell regime) and (2) by electrolytic discharge of water at potentials above its thermodynamic stability (electrolysis regime).

1.3.1 Activation of Water by Dissociative Adsorption

According to this mechanism, in acid media, water is dissociatively adsorbed on the electrode (1.7) followed by hydrogen discharge (1.8) resulting in the formation of chemisorbed (chemically bonded) hydroxyl radicals on the anode surface (1.9):

$$H_2O + M \rightarrow M - OH + M - H \tag{1.7}$$

$$M - H \rightarrow M + H^+ + e^- \tag{1.8}$$

$$H_2O + M \rightarrow M - OH + H^+ + e^- \tag{1.9}$$

The reaction can take place at anode potentials largely lower than the thermodynamic potential of water oxidation to oxygen (1.23 V/SHE under standard conditions). However, in order to achieve the dissociative activation of water (1.7), electrocatalytic electrodes are needed. In fact, the dissociative adsorption of water can be achieved only at electrodes (M) on which the bonding energy of M–OH and M–H exceeds the dissociation energy of water to $H^\bullet + HO^\bullet$. This is the case of Pt–Ru-based electrodes on which water activation can be achieved at 0.2–0.3 V/SHE.

The EOTR between the organic compound (R) and the hydroxyl radicals take place at the electrode surface (both adsorbed) according to a Langmuir–Hinshelwood type mechanism. This process has been extensively studied mainly for fuel cell applications. However, as it has. been reported in Sect. 1.2, it is limited for simple C_1 organic compounds (methanol, formic acid). Furthermore, there are problems with electrode deactivation due to CO chemisorption on the electrode active sites.

We stress again here that in the actual state of the art, the EM of organic pollutants with simultaneous production of electrical energy (fuel cell regime) is not feasible due to the lack of active electrocatalytic anode material. Bio-electrocatalysis is a new active field and can overcome this problem as it has been demonstrated recently in the development of bio-fuel cells.

1.3.2 Activation of Water by Electrolytic Discharge

According to this mechanism, in acid media, water is discharged (1.23 V/SHE under standard conditions) on the electrode producing adsorbed hydroxyl radicals (1.10), which are the main reaction intermediates for O_2 evolution (1.11).

$$H_2O + M \rightarrow M(^{\cdot}OH) + H^+ + e^- \tag{1.10}$$

$$M(^{\cdot}OH) \rightarrow M + \frac{1}{2}O_2 + H^+ + e^- \tag{1.11}$$

The reactivity of these electrolytic hydroxyl radicals is very different from the chemically bonded hydroxyl radicals formed by the dissociative activation of water (1.9).

Even if the exact nature of the interactions between the electrolytically generated hydroxyl radicals (1.10) and the electrode surface (M) is not known, we can consider that these hydroxyl radicals are physisorbed on the anode surface.

The EOTR between an organic compound R (supposed none adsorbed on the anode) and the hydroxyl radicals (loosely adsorbed on the anode) takes place close to the anode's surface:

$$R_{(aq)} + M\,(^{\cdot}OH)_{n/2} \rightarrow M + \text{Oxidation products} + \frac{n}{2}H^{+} + \frac{n}{2}e^{-}, \qquad (1.12)$$

where n is the number of electrons involved in oxidation reaction of R.

1.4 Influence of Anode Material on the Reactivity of Electrolytic Hydroxyl Radicals

The reaction of organics with electrogenerated electrolytic hydroxyl radicals (1.12) is in competition with the side reaction of the anodic discharge of these radicals to oxygen (1.11). The activity [rate of reaction (1.11) and (1.12)] of these electrolytic hydroxyl radicals are strongly linked to their interaction with the electrode surface M. As a general rule, the weaker the interaction, the lower is the electrochemical activity [reaction (1.11) is slow] toward oxygen evolution (high O_2 overvoltage anodes) and the higher is the chemical reactivity toward organics oxidation. Based on this approach, we can classify the different anode materials according to their oxidation power in acid media as it is shown in Table 1.2. This table shows that the oxidation potential of the anode (which corresponds to the onset potential of oxygen evolution) is directly related to the overpotential for oxygen evolution and to the adsorption enthalpy of hydroxyl radicals on the anode surface, i.e., for a given anode material the higher is the O_2 overvoltage the higher is its oxidation power.

A low oxidation power anode is characterized by a strong electrode–hydroxyl radical interaction resulting in a high electrochemical activity for the oxygen evolution reaction (low overvoltage anode) and to a low chemical reactivity for organics oxidation (low current efficiency for organics oxidation). A typical low oxidation power anode is the IrO_2-based electrode (Fóti et al. 1999). Concerning this anode, it has been reported that the interaction between IrO_2 and hydroxyl radical is so strong that a higher oxidation state of oxide IrO_3 can be formed. This higher oxide can act as mediator for both organics oxidation and oxygen evolution.

In contrast to this low oxidation power anode, the high oxidation power anode is characterized by a weak electrode–hydroxyl radical interaction resulting in a low electrochemical activity for the oxygen evolution reaction (high overvoltage anode) and to a high chemical reactivity for organics oxidation (high current efficiency for organics oxidation).

Boron-doped diamond-based anode (BDD) is a typical high oxidation power anode (Fóti and Comninellis 2004). By means of spin trapping, the evidence for the formation of hydroxyl radicals on BDD is found (Marselli et al. 2003). The

Table 1.2 Oxidation power of the anode material in acid media

Electrode	Oxidation potential (V)	Overpotential of O_2 evolution (V)	Adsorption enthalpy of M-OH	Oxidation power of the anode
RuO_2–TiO_2 ($DSA–Cl_2$)	1.4–1.7	0.18	Chemisorption of OH radical	
IrO_2–Ta_2O_5 ($DSA–O_2$)	1.5–1.8	0.25		
Ti/Pt	1.7–1.9	0.3		
Ti/PbO_2	1.8–2.0	0.5		
Ti/SnO_2–Sb_2O_5	1.9–2.2	0.7		
p-Si/BDD	2.2–2.6	1.3	of OH radical	

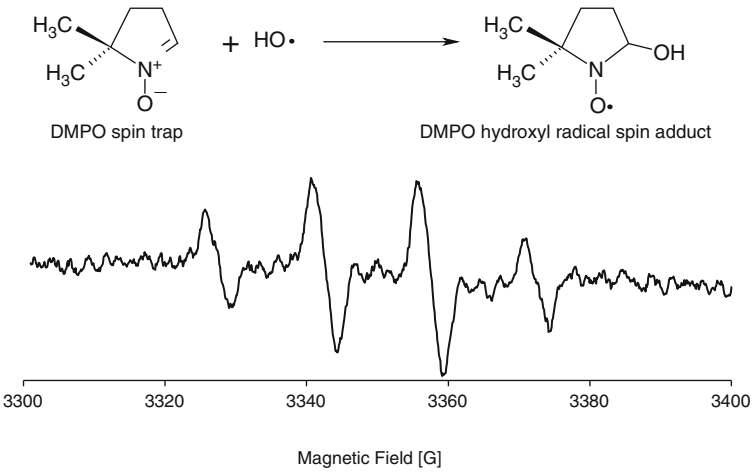

Fig. 1.2 ESR of DMPO adduct obtained after electrolysis of 8.8 mM DMPO solution in 1 M $HClO_4$ for 2 h on BDD electrode at 0.1 mA cm^{-2}

ESR (Electron Spin Resonance) spectrum (Fig. 1.2) recorded during electrolysis of DMPO (5.5 dimethyl-1-pyrroline-N-oxide) solution on BDD confirms the formation of OH during anodic polarization of diamond electrodes. It has been reported that the BDD–hydroxyl radical interaction is so weak (no free p or d orbitals on BDD) that the OH can even be considered as quasi-free. These quasi-free hydroxyl

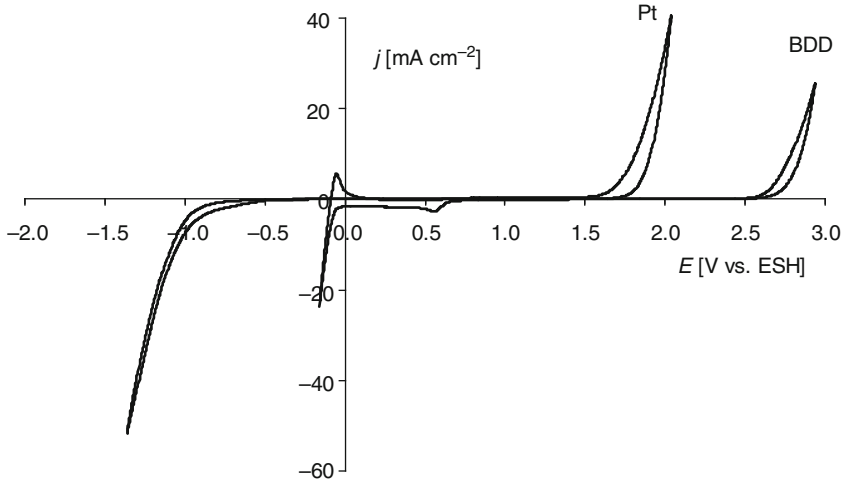

Fig. 1.3 Cyclic voltammograms of BDD and platinum electrodes

radicals are very reactive and can result in the mineralization of the organic compounds (1.13):

$$R_{(aq)} + BDD\,(^{\cdot}OH)_{n/2} \rightarrow BDD + \text{Mineralization products} + \frac{n}{2}H^{+} + \frac{n}{2}e^{-} \quad (1.13)$$

Furthermore, BDD anodes have a high overpotential for the oxygen evolution reaction compared with the platinum anode (Fig. 1.3). This high overpotential for oxygen evolution at BDD electrodes is certainly related to the weak BDD–hydroxyl radical interaction, what results in the formation of H_2O_2 near to the electrode's surface (1.14), which is further oxidized at the BDD anode (1.15):

$$2^{\cdot}OH \rightarrow H_2O_2 \quad (1.14)$$

$$H_2O_2 \rightarrow 2H^{+} + 2e^{-} + O_2 \quad (1.15)$$

In fact H_2O_2 has been detected during electrolysis in $HClO_4$ using BDD anodes as it is shown in Fig. 1.4 (Michaud et al. 2003).

1.5 Determination of the Current Efficiency of the Electrochemical Mineralization

For the determination of the current efficiency of organics mineralization we consider two parallel reactions:

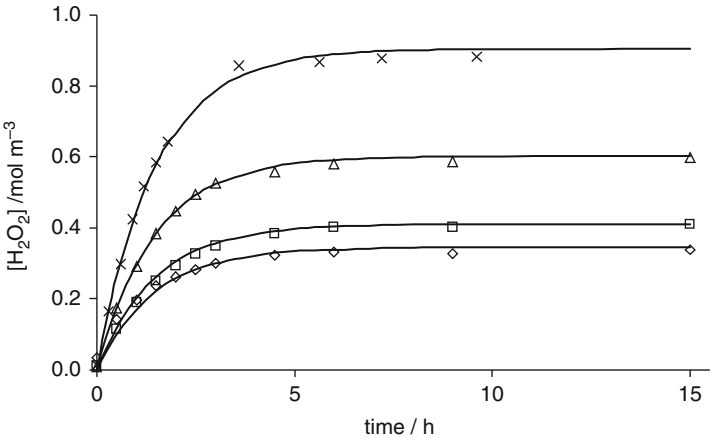

Fig. 1.4 Production of H_2O_2 at different current densities; (*open diamond*) 230 A cm^{-2}, (*open sqaure*) 470 A cm^{-2}, (*open triangle*) 950 A cm^{-2}, (*cross*) 1,600 A cm^{-2} during electrolysis of 1 M $HClO_4$ on BDD electrode

(a) The main reaction of oxygen transfer from water toward the organic compound

$$\mathrm{R} + \frac{n}{2}\mathrm{H_2O} \rightarrow \text{Mineralization products} + n\,\mathrm{H^+} + n\,\mathrm{e^-} \tag{1.16}$$

(b) The side reaction of oxygen evolution

$$2\mathrm{H_2O} \rightarrow \mathrm{O_2} + 4\mathrm{H^+} + 4\mathrm{e^-} \tag{1.17}$$

In the basis of this simplified reaction scheme, two techniques have been proposed for the estimation of the instantaneous current efficiency (ICE) during electrolysis: the chemical oxygen demand (COD) and the oxygen flow rate (OFR) techniques.

1.5.1 Determination of ICE by the Chemical Oxygen Demand Technique

In this technique, the COD of the electrolyte is measured at regular intervals (Δt) during constant current (galvanostatic) electrolysis and the instantaneous current efficiency (ICE_{COD}) is calculated using the relation:

$$\mathrm{ICE_{COD}} = \frac{FV}{8I}\frac{\left[(\mathrm{COD})_t - (\mathrm{COD})_{t+\Delta t}\right]}{\Delta t}, \tag{1.18}$$

where $(COD)_t$ and $(COD)_{t+\Delta t}$ are the chemical oxygen demand $\left(\mathrm{mol\ O_2\ m^{-3}}\right)$ at time t and $t + \Delta t$ (s), respectively; I is the applied current (A); F is Faraday's constant $\left(\mathrm{C\ mol^{-1}}\right)$; and V is the volume of the electrolyte $\left(\mathrm{m^3}\right)$.

1.5.2 Determination of ICE by the Oxygen Flow Rate Technique

In the OFR technique, the OFR is measured continuously in the anodic compartment during constant current (galvanostatic) electrolysis in a two-compartment electrochemical cell. The instantaneous current efficiency (ICE_{OFR}) is then calculated using the relation:

$$ICE_{OFR} = \frac{\dot{V}_0 - \left(\dot{V}_t\right)_{org}}{\dot{V}_0}, \tag{1.19}$$

where $\dot{V}_0\left(m^{-3}s^{-1}\right)$ is the theoretical OFR calculated from Faraday's law (or measured in a blank experiment in the absence of organic compounds) and $\left(\dot{V}_t\right)_{org}\left(m^{-3}s^{-1}\right)$ is the OFR obtained during electrochemical treatment of the wastewater.

Both the COD and OFR techniques have their limitations as given below:

- If volatile organic compounds (VOC) are present in the waste water only the OFR technique will give reliable results.
- If for example Cl_2 (g) is evolved during the treatment (due to the oxidation of Cl^- present in the wastewater) only the COD technique will give reliable results.
- If insoluble organic products are formed during the treatment (for example polymeric material) only the OFR technique will give reliable results.
- Furthermore, simultaneous application of both the COD and OFR techniques during the electrochemical process will allow a better control of the side reactions involved in the electrochemical treatment.

1.6 Kinetic Model of Organics Mineralization on BDD Anode

In this section, a kinetic model of electrochemical mineralization of organics (RH) on BDD anodes under electrolysis regime is presented. In this regime, as reported in Sect. 1.4, electrogenerated hydroxyl radicals (1.20) are the intermediates for both the main reaction of organics oxidation (1.21) and the side reaction of oxygen evolution (1.22).

$$BDD + H_2O \rightarrow BDD\left(^{\cdot}OH\right) + H^+ + e^- \tag{1.20}$$

$$BDD\left(^{\cdot}OH\right) + R \rightarrow BDD + \text{Mineralization products} + H^+ + e^- \tag{1.21}$$

$$BDD\left(^{\cdot}OH\right) \rightarrow BDD + \frac{1}{2}O_2 + H^+ + e^- \tag{1.22}$$

Considering this simplified reaction scheme (1.20)–(1.22), a kinetic model is proposed based on following assumptions: (1) adsorption of the organic compounds at the electrode surface is negligible; (2) all organics have the same diffusion coefficient D; and (3) the global rate of the electrochemical mineralization of organics is a fast reaction and it is controlled by mass transport of organics to the anode surface.

The consequence of this last assumption is that the rate of the mineralization reaction is independent on the chemical nature of the organic compound present in the electrolyte. Under these conditions, the limiting current density for the electrochemical mineralization of an organic compound (or a mixture of organics) under given hydrodynamic conditions can be written as (1.23)

$$i_{\text{lim}} = nFk_{\text{m}}C_{\text{org}}, \tag{1.23}$$

where i_{lim} is the limiting current density for organics mineralization $\left(\text{A m}^{-2}\right)$, n is the number of electrons involved in organics mineralization reaction, F is Faraday's constant $\left(\text{C mol}^{-1}\right)$, k_{m} is the mass transport coefficient $\left(\text{m s}^{-1}\right)$, and C_{org} is the concentration of organics in solution $\left(\text{mol m}^{-3}\right)$. For the electrochemical mineralization of a generic organic compound, it is possible to calculate the number of exchanged electrons, from the following electrochemical reaction

$$\text{C}_x\text{H}_y\text{O}_z + (2x - z)\,\text{H}_2\text{O} \rightarrow x\,\text{CO}_2 + (4x + y - 2z)\,\text{H}^+ + (4x + y - 2z)\,\text{e}^- \tag{1.24}$$

Replacing the value of $n = (4x + y - 2z)$ in (1.23) we obtain

$$i_{\text{lim}} = (4x + y - 2z)\,Fk_{\text{m}}C_{\text{org}}. \tag{1.25}$$

From the equation of the chemical mineralization of the organic compound (1.26)

$$\text{C}_x\text{H}_y\text{O}_z + \left(\frac{4x + y - 2z}{4}\right)\text{O}_2 \rightarrow x\,\text{CO}_2 + \frac{y}{2}\text{H}_2\text{O}, \tag{1.26}$$

it is possible to obtain the relation between the organics concentration (C_{org} in mol $\text{C}_x\text{H}_y\text{O}_z\,\text{m}^{-3}$) and the chemical oxygen demand $\left(\text{COD in mol O}_2\,\text{m}^{-3}\right)$:

$$C_{\text{org}} = \frac{4}{(4x + y - 2z)}\text{COD}. \tag{1.27}$$

From (1.25) and (1.27) and at given time t during electrolysis, we can relate the limiting current density of the electrochemical mineralization of organics with the COD of the electrolyte (1.28):

$$i_{\text{lim}}(t) = 4Fk_{\text{m}}\text{COD}(t). \tag{1.28}$$

At the beginning of electrolysis, at time $t = 0$, the initial limiting current density $\left(i^0_{\text{lim}}\right)$ is given by

$$i^0_{\text{lim}} = 4Fk_{\text{m}}\text{COD}^0, \tag{1.29}$$

where COD^0 is the initial chemical oxygen demand.

Let us define a characteristic parameter α of the electrolysis process (1.30):

$$\alpha = i \,/ i^0_{\text{lim}}. \tag{1.30}$$

Working under galvanostatic conditions α is constant, and it is possible to identify two different operating regimes: at $\alpha < 1$ the electrolysis is controlled by the applied current, while at $\alpha > 1$ it is controlled by the mass transport control.

(a) Electrolysis under current limited control ($\alpha < 1$):

In this operating regime ($i < i_{\text{lim}}$), the current efficiency is 100% and the rate of COD removal $\left(\text{mol O}_2\ \text{m}^{-2}\text{s}^{-1}\right)$ is constant and can be written as (1.31)

$$r = \alpha \frac{i_{\text{lim}}^0}{4F}. \tag{1.31}$$

Using relation (1.29), the rate of COD removal (1.31) can be given by

$$r = \alpha k_{\text{m}} \text{COD}^0. \tag{1.32}$$

It is necessary to consider the mass balances over the electrochemical cell and the reservoir to describe the temporal evolution of COD in the batch recirculation reactor system given in Fig. 1.5. Considering that the volume of the electrochemical reactor V_{E} $\left(\text{m}^3\right)$ is much smaller than the reservoir volume V_{R} $\left(\text{m}^3\right)$, we can obtain from the mass balance on COD for the electrochemical cell the following relation:

$$Q\ \text{COD}_{\text{out}} = Q\ \text{COD}_{\text{in}} - \alpha k_{\text{m}} A\ \text{COD}^0, \tag{1.33}$$

where Q is the flow rate $\left(\text{m}^3\text{s}^{-1}\right)$ through the electrochemical cell; COD_{in} and COD_{out} are the chemical oxygen demands $\left(\text{mol O}_2\ \text{m}^{-3}\right)$ at the inlet and at the outlet of the electrochemical cell, respectively; and A is the anode area $\left(\text{m}^2\right)$. For the well-mixed reservoir (Fig. 1.5), the mass balance on COD can be expressed as

$$Q\ (\text{COD}_{\text{out}} - \text{COD}_{\text{in}}) = V_{\text{R}} \frac{\text{d}\,(\text{COD}_{\text{in}})}{\text{d}t}. \tag{1.34}$$

Combining (1.33)–(1.34) and replacing COD_{in} by the temporal evolution of chemical oxygen demand, COD, we obtain

$$\frac{\text{d}\,(\text{COD})}{\text{d}t} = -\alpha \frac{\text{COD}^0 A k_{\text{m}}}{V_{\text{R}}}. \tag{1.35}$$

Integrating this equation subject to the initial condition $\text{COD} = \text{COD}^0$ at $t = 0$ gives the temporal evolution of $\text{COD}(t)$ in this operating regime ($i < i_{\text{lim}}$):

$$\text{COD}(t) = \text{COD}^0 \left(1 - \alpha \frac{A k_{\text{m}}}{V_{\text{R}}} t\right). \tag{1.36}$$

This behavior persists until a critical time (t_{cr}), at which the applied current density is equal to the limiting current density, what corresponds to:

$$\text{COD}_{\text{cr}} = \alpha\ \text{COD}^0. \tag{1.37}$$

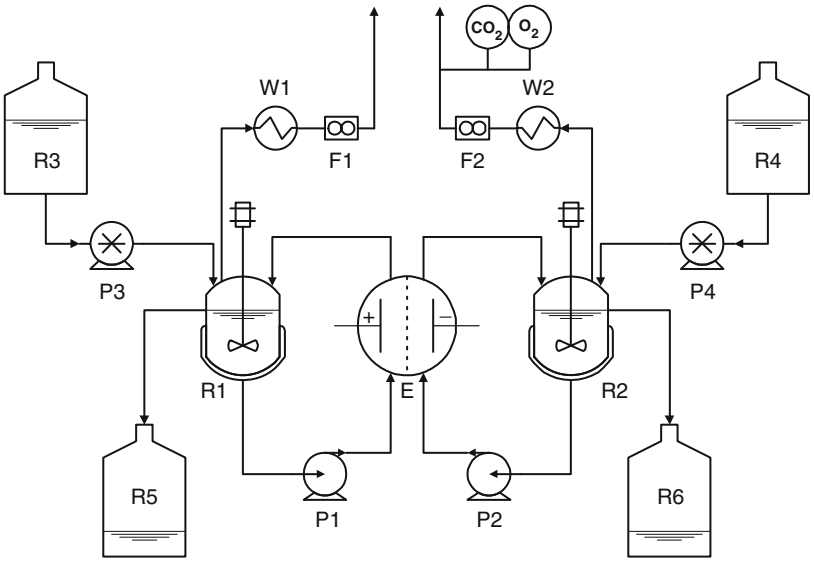

Fig. 1.5 Schematic view of the two-compartment electrochemical flow cell. *R* reservoirs, *P* pumps, *E* electrochemical cell with membrane, *W* heat exchangers, *F* gas flow controllers

Substituting (1.37) in (1.36), it is possible to calculate the critical time:

$$t_{\mathrm{cr}} = \frac{1-\alpha}{\alpha}\frac{V_{\mathrm{R}}}{Ak_{\mathrm{m}}} \tag{1.38}$$

or in term of critical specific charge $\left(\mathrm{A\ h\ m^{-3}}\right)$:

$$Q_{\mathrm{cr}} = i^{0}_{\mathrm{lim}}\frac{(1-\alpha)}{k_{\mathrm{m}} \times 3{,}600} = \frac{4F\left(\mathrm{COD}^{0}\right)(1-\alpha)}{3{,}600}. \tag{1.39}$$

(b) Electrolysis under mass transport control ($\alpha > 1$):

When the applied current exceeds the limiting one ($i > i_{\mathrm{lim}}$), secondary reactions (such as oxygen evolution) commence resulting in a decrease in the ICE. In this case, the COD mass balances on the anodic compartment of the electrochemical cell E and the reservoir R2 (Fig. 1.5) can be expressed as

$$\frac{\mathrm{d}\,(\mathrm{COD})}{\mathrm{d}t} = -\frac{Ak_{\mathrm{m}}\mathrm{COD}}{V_{\mathrm{R}}}. \tag{1.40}$$

Integration of this equation from $t = t_{\mathrm{cr}}$ to t, and $\mathrm{COD} = \alpha\,\mathrm{COD}^{0}$ to $\mathrm{COD}\,(t)$ leads to

$$\mathrm{COD}\,(t) = \alpha\,\mathrm{COD}\exp\left(-\frac{Ak_{\mathrm{m}}}{V_{\mathrm{R}}}t + \frac{1-\alpha}{\alpha}\right). \tag{1.41}$$

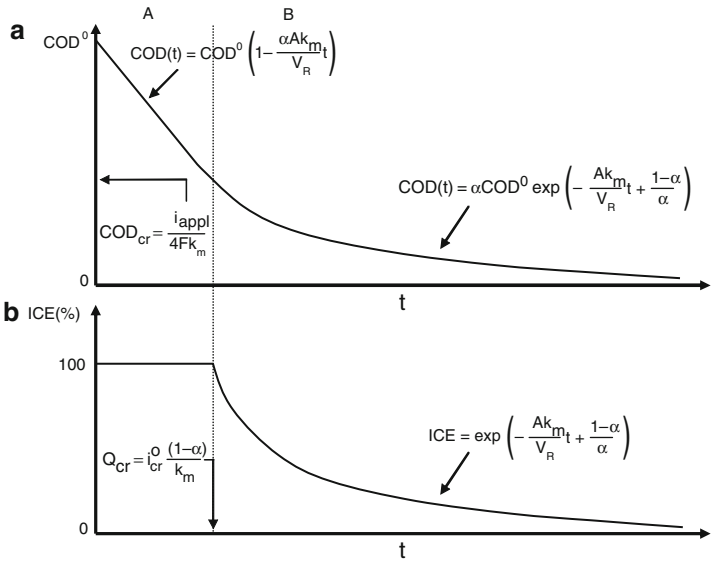

Fig. 1.6 Evolution of (**a**) COD and (**b**) ICE in function of time (or specific charge); A represents the charge transport control; B represents the mass transport control

The ICE can be defined as

$$\mathrm{ICE} = \frac{i_{\mathrm{lim}}}{i} = \frac{\mathrm{COD}\,(t)}{\alpha \mathrm{COD}^0}. \tag{1.42}$$

And from (1.41) and (1.42), ICE it is now given by

$$\mathrm{ICE} = \exp\left(-\frac{Ak_{\mathrm{m}}}{V_{\mathrm{R}}}t + \frac{1-\alpha}{\alpha}\right). \tag{1.43}$$

A graphical representation of the proposed kinetic model is given in Fig. 1.6. In order to verify the validity of this model, the anodic oxidation of various aromatic compounds in acidic solution has been performed varying organics concentration and current density.

1.6.1 Influence of the Nature of Organic Pollutants

Figure 1.7 shows both the experimental and predicted values (continuous line) of both the ICE and COD evolution with the specific electrical charge passed during the anodic oxidation of different classes of organic compounds (acetic acid, isopropanol, phenol, 4-chlorophenol, 2-naphtol). This figure demonstrates that the

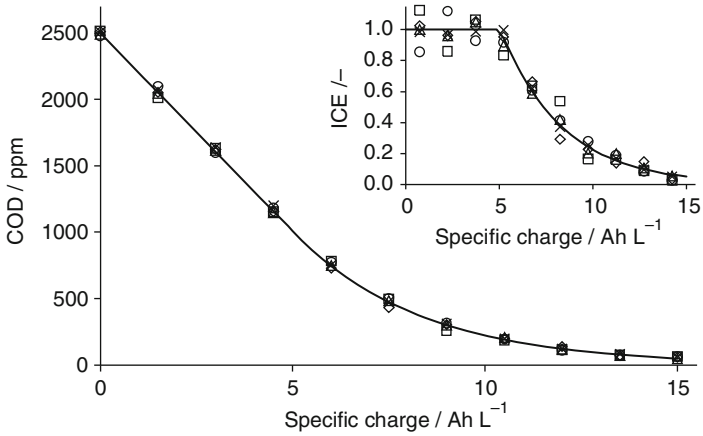

Fig. 1.7 Evolution of COD and ICE (*inset*) in function of specific charge for different organic compounds: (*cross*) acetic acid, (*open square*) isopropanol, (*open circle*) phenol, (*open triangle*) 4-chlorophenol, (*open diamond*) 2-naphtol; $i = 238\,\mathrm{A\,m^{-2}}$; $T = 25°\mathrm{C}$; Electrolyte: $1\,\mathrm{M\,H_2SO_4}$. The *solid line* represents model prediction

electrochemical treatment is independent on the chemical nature of the organic compound. Furthermore, there is an excellent agreement between the experimental data and the predicted values from proposed model.

1.6.2 Influence of Organic Concentration

Figure 1.8 presents both ICE and COD evolution with the specific electrical charge passed during the galvanostatic oxidation $\left(238\mathrm{A\,m^{-2}}\right)$ of 2-naphtol $(2-9\,\mathrm{mM})$ in $1\,\mathrm{M\,H_2SO_4}$. As predicted from the model, the critical specific charge Q_{cr} (1.39) increases with increase in the initial organic concentration (reported as initial COD^0). Again, there is an excellent agreement between the experimental and predicted values.

1.6.3 Influence of Applied Current Density

The influence of current density on both ICE and COD evolution with the specific electrical charge passed during the galvanostatic oxidation of a 5 mM 2-naphtol in $1\,\mathrm{M\,H_2SO_4}$ at different current densities $\left(119-476\,\mathrm{A\,m^{-2}}\right)$ is shown in Fig. 1.9. As previously noted, an excellent agreement between the experimental and predicted values is observed.

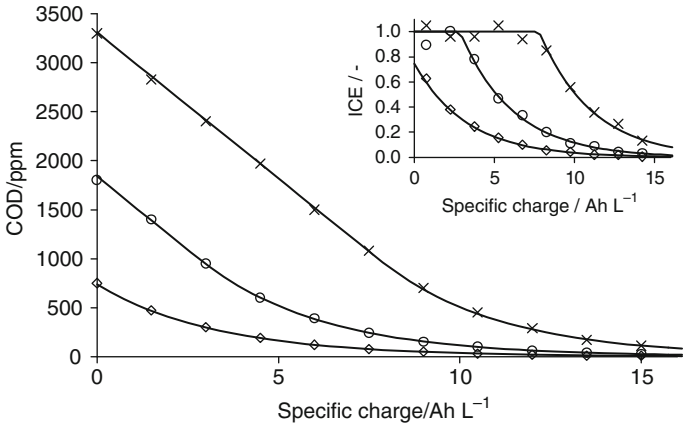

Fig. 1.8 Influence of the initial 2-naphtol concentration: (*cross*) 9 mM, (*open circle*) 5 mM, (*open diamond*) 2 mM on the evolution of COD and ICE (*inset*) during electrolysis on BDD; $i = 238\ \mathrm{A\ m^{-2}}$; $T = 25°\mathrm{C}$; Electrolyte: 1 M H_2SO_4. The *solid line* represents model prediction

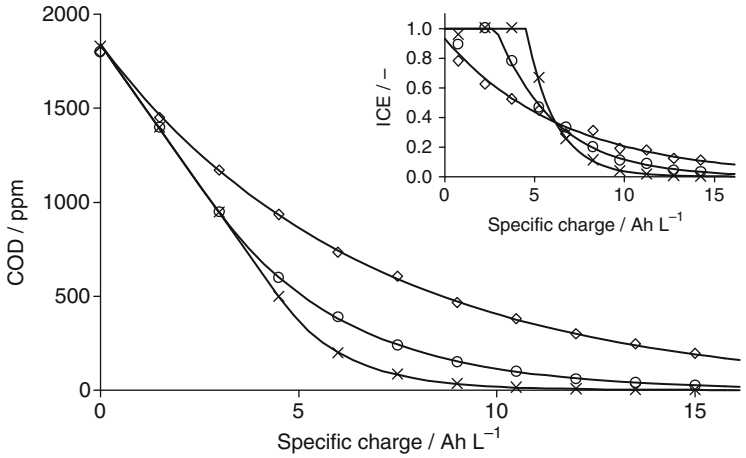

Fig. 1.9 Influence of the applied current density: (*cross*) 119 A m^{-2}, (*open circle*) 238 A m^{-2}, (*open diamond*) 476 A m^{-2} on the evolution of COD and ICE (*inset*) during electrolysis of 5 mM 2-naphtol in 1 M H_2SO_4 on BDD; $T = 25°\mathrm{C}$. The *solid line* represents model prediction

1.7 Intermediates Formed During the Electrochemical Mineralization Process Using BDD

It has been found, that the amount and nature of intermediates formed during the electrochemical mineralization of organics on BDD anodes depends strongly on the working regime. In fact, electrolysis under conditions of current limited control

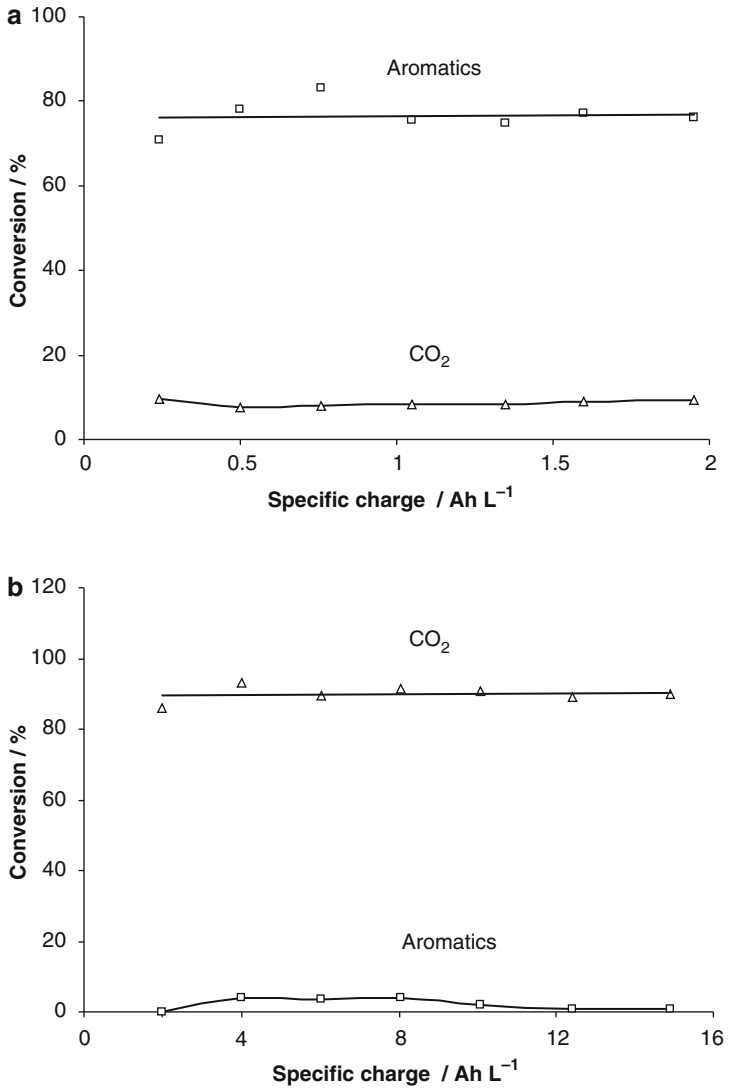

Fig. 1.10 Trend of the percentage of phenol converted to CO_2 (*open triangle*) and to aromatic compounds (*open square*) during phenol electrolysis in 1 M $HClO_4$ on BDD under (**a**) current limited control, initial phenol concentration: 20 mM, current density 5 mA cm^{-2}; (**b**) mass transport control, initial phenol concentration: 5 mM, current density 60 mA cm^{-2}

results usually in the formation of an important number of intermediates in contrast to electrolysis under mass transport regime, where practically no intermediates are formed and CO_2 is the only final product. Figure 1.10 shows a typical example of phenol oxidation under conditions of current limited control (formation of aromatic intermediates) and mass transport regime (no intermediates, only CO_2).

1.8 Electrical Energy Consumption in the Electrochemical Mineralization Process

In contrast to the chemical oxidation process in which strong oxidants (usually in the presence of catalysts) are used in order to achieve efficient treatment, the electrochemical process consumes mainly electrical energy. The specific energy consumption for the electrochemical treatment of a given wastewater can be estimated from the relation (Panizza et al. 2001a, b):

$$E_{sp} = \frac{4FV_c}{3{,}600\text{EOI}} \quad \text{with } 0 \leq \text{EOI} \leq 1, \tag{1.44}$$

where E_{sp} is the specific energy consumption (kW h/kmol COD), F is Faraday's constant $\left(\text{C mol}^{-1}\right)$, V_c is the cell potential (V), and EOI is the electrochemical oxidation index (which represents the average current efficiency for organics oxidation) given by (1.45):

$$\text{EOI} = \frac{\int_o^\tau \text{ICE}\, dt}{\tau} \quad \text{with } 0 \leq \text{EOI} \leq 1, \tag{1.45}$$

where ICE is the instantaneous current efficiency (–) and τ is the duration of the electrochemical treatment (s). Using the numerical values, (1.44) can be written as

$$E_{sp} = 107.2\frac{V_c}{\text{EOI}} \quad \text{with } 0 \leq \text{EOI} \leq 1. \tag{1.46}$$

The cell potential can be related to the current density by the relation (1.47):

$$V_c = V_0 + \rho di, \tag{1.47}$$

where V_0 is a constant depending on the nature of the electrolyte (V), ρ is the resistivity of the electrolyte (Ω m), d is the interelectrode distance (m), and i is the current density $\left(\text{A m}^{-2}\right)$. Combining (1.46) and (1.47) we obtain

$$E_{sp} = 107.2\frac{(V_0 + \rho di)}{\text{EOI}} \quad \text{with } 0 \leq \text{EOI} \leq 1. \tag{1.48}$$

This relation shows that the specific energy consumption decreases with increasing average current efficiency reaching a minimum value at EOI = 1.

1.9 Optimization of the Electrochemical Mineralization Using BDD Anodes

As it has been shown in Sect. 1.8, the specific energy consumption for the electrochemical mineralization of organics decreases strongly with increasing average current efficiency (EOI) and reaches a minimum value at EOI = 1. In order to work

under these favorable conditions (at which EOI = 1), electrolysis has to be carried out under programmed current, in which the current density during electrolysis is adjusted to the limiting value. The following steps are proposed for an optimal treatment of a wastewater using BDD anodes:

(a) Measure the initial chemical oxygen demand $\left(\mathrm{COD}^0\right)$ of the wastewater.
(b) Estimate the mass transfer coefficient (k_m) of the electrolytic cell under fixed hydrodynamic conditions (stirring rate). This can be achieved using a given concentration of $\mathrm{Fe(CN)_6}^{4-}$ (50 mM) in a supporting electrolyte (1M $\mathrm{Na_2SO_4}$) and measuring the limiting current (I_lim) for the anodic oxidation of $\mathrm{Fe(CN)_6}^{4-}$ under fixed stirring rate. The mass transfer coefficient (k_m) can then be calculated using the relation:

$$k_\mathrm{m} = \frac{I_\mathrm{lim}}{FA\left[\mathrm{Fe(CN)_6}^{4-}\right]}, \tag{1.49}$$

where k_m is the mass transfer coefficient $\left(\mathrm{m\,s^{-1}}\right)$, I_lim is the limiting current (A), $\left[\mathrm{Fe(CN)_6}^{4-}\right]$ is the concentration of $\mathrm{Fe(CN)_6}^{4-}$ $\left(\mathrm{mol\,m^{-3}}\right)$, F is Faraday's constant $\left(\mathrm{C\,mol^{-1}}\right)$, and A is the anode surface area $\left(\mathrm{m^2}\right)$.
(c) Estimate the initial limiting current density (i_lim) for the electrochemical mineralization using (1.29).
(d) Calculate the time constant of the electrolytic cell (τ_c) using the relation:

$$\tau_\mathrm{c} = \frac{V_\mathrm{R}}{Ak_\mathrm{m}}, \tag{1.50}$$

where τ_c is the electrolytic cell time constant (s) and V_R is the volume of the reservoir R2 in Fig. 1.5 $\left(\mathrm{m^3}\right)$.
(e) Using (1.29), (1.41), (1.50) and considering $\alpha = 1$ (initial applied current density = calculated initial limiting current density), we obtain the theoretical temporal evolution of the limiting current during electrolysis (1.51).

$$i_\mathrm{lim} = i_\mathrm{lim}^0 \exp\left(-\frac{t}{\tau_\mathrm{c}}\right). \tag{1.51}$$

(f) Start electrolysis by application of a current density corresponding to the limiting value [calculated as in point (c)].
(g) Adjust the current density during electrolysis to the time dependent limiting value according to (1.51).
(h) From (1.29) and (1.51), calculate the electrolysis time (τ) in order to achieve the target final COD value ($\mathrm{COD_{final}}$) using the relation:

$$\tau = -\tau_\mathrm{c} \log \frac{\mathrm{COD_{final}}}{\mathrm{COD}^0}. \tag{1.52}$$

Table 1.3 Corrosion rate and current efficiency of BDD corrosion for various electrolytes

Electrolyte	Corrosion rate (μg/Ah)	Current efficiency (%)
1M $HClO_4$	0.3 ± 0.1	0.0003
1M H_2SO_4	<0.3	<0.0003
1M H_2SO_4 + 9M CH_3OH	3 ± 1	0.003
1M H_2SO_4 + 3M CH_3COOH	12 ± 2	0.011

1.10 Fouling and Corrosion of BDD Anodes

One of the major problems in the application of the electrochemical technology for wastewater treatment is the fouling of the electrode's surface caused by the deposition of oligomeric or polymeric material and the electrode's deactivation. It has been reported, that BDD electrodes are not sensible to fouling due to the electrogeneration of active, electrolytic hydroxyl radicals which can oxidize any polymeric material deposited on the anode's surface. However, BDD anodes are susceptible to deactivation mainly due to the anodic corrosion. The corrosion rate depends strongly on the reaction media as it is shown in Table 1.3. In the same table, the current efficiency of BDD corrosion is also given, considering (1.53).

$$C \rightarrow C^{4+} + 4e^- \tag{1.53}$$

References

Bellagamba, R., Michaud, P.-A., Comninellis, Ch. and Vatistas, N. (2002) Electro-combustion of polyacrylates with boron-doped diamond anodes. Electrochem. Commun. 4, 171–176.

Boye, B., Michaud, P.-A., Marselli, B., Dieng, M.M., Brillas, E. and Comninellis, Ch. (2002) Anodic oxidation of 4-chlorophenoxyacetic acid on synthetic boron-doped diamond electrodes. New Diam. Front. Carbon Technol. 12, 63–72.

Boye, B., Brillas, E., Marselli, B., Michaud, P.-A., Comninellis, Ch. and Dieng, M.M. (2004) Electrochemical decontamination of waters by advanced oxidation processes (AOPS): Case of the mineralization of 2,4,5-T on BDD electrode. Bull. Chem. Soc. Ethiop. 18, 205–214.

Boye, B., Brillas, E., Marselli, B., Michaud, P.-A., Comninellis, Ch., Farnia, G. and Sandonà, G. (2006) Electrochemical incineration of chloromethylphyenoxy herbicides in acid medium by anodic oxidation with boron-doped diamond electrodes. Electrochim. Acta 51, 2872–2880.

Brillas, E., Boye, B., Sires, I., Garrido, J.A., Rodriguez, R.M., Arias, C., Cabot, P.-L. and Comninellis, Ch. (2004) Electrochemical destruction of chlorophenoxy herbicides by anodic oxidation and electro-Fenton using a boron-doped diamond electrode. Electrochim. Acta 49, 4487–4496.

Chen, X., Gao, F., Chen, G. and Yue, P.L. (2003) High-performance Ti/BDD electrodes for pollutants oxidation. Environ. Sci. Technol. 37, 5021–5026.

Chen, X., Gao, F. and Chen, G. (2005) Comparison of Ti/BDD and Ti/SnO_2-Sb_2O_5 electrodes for pollutants oxidation. J. Appl. Electrochem. 35, 185–191.

Comninellis, Ch. (1992) Electrochemical treatment of wastewater. Gas Wasser Abwasser 72, 792–797.

Comninellis, Ch. (1994) Electrocatalysis in the electrochemical conversion/combustion of organic pollutants for waste water treatment. Electrochim. Acta 39, 1857–1862.

Comninellis, Ch. and De Battisti, A. (1996) Electrocatalysis in anodic oxidation of organics with simultaneous oxygen evolution. J. Chim. Phys. 93, 673–679.

Comninellis, Ch. and Nerini, A. (1995) Anodic oxidation of phenol in the presence of NaCl for wastewater treatment. J. Appl. Electrochem. 25, 23–28.

Comninellis, Ch. and Plattner, E. (1988) Electrochemical wastewater treatment. Chimia 42, 250–252.

Comninellis, Ch. and Pulgarin, C. (1991) Anodic oxidation of phenol for wastewater treatment. J. Appl. Electrochem. 21, 703–708.

Comninellis, Ch. and Pulgarin, C. (1993) Electrochemical oxidation of phenol for wastewater treatment using tin dioxide anodes. J. Appl. Electrochem. 23, 108–112.

Fóti, G. and Comninellis, Ch. (2004) Electrochemical oxidation of organics on iridium oxide and synthetic diamond based electrodes. In: R.E. White, B.E. Conway, C.G. Vayenas and M.E. Gamboa-Adelco (Eds.), *Modern Aspects of Electrochemistry*, Vol. 37. Plenum, New York, NY, pp. 87–130.

Fóti, G., Gandini, D. and Comninellis, Ch. (1997) Anodic oxidation of organics on thermally prepared oxide electrodes. In: M. Armand, J.O'M. Bockris, E.J. Cairns, M. Froment, Z. Galus, Y. Ito, R.F. Savinell, Z.W. Tian, S. Trasatti and T.J. VanderNoot (Eds.), *Current Topics in Electrochemistry*, Vol. 5. Research Trends, Trivandrum, pp. 71–91.

Fóti, G., Gandini, D., Comninellis, Ch., Perret, A. and Haenni, W. (1999) Oxidation of organics by intermediates of water discharge on IrO_2 and synthetic diamond anodes. Electrochem. Solid-State Lett. 2, 228–230.

Fryda, M., Herrmann, D., Schäfer, L., Klages, C.-P., Perret, A., Haenni, W., Comninellis, Ch. and Gandini, D. (1999) Properties of diamond electrodes for wastewater treatment. New Diam. Front. Carbon Technol. 9, 229–240.

Gandini, D., Mahé, E., Michaud, P.-A., Haenni, W., Perret, A. and Comninellis, Ch. (2000) Oxidation of carboxylic acids at boron-doped diamond electrodes for wastewater treatment. J. Appl. Electrochem. 30, 1345–1350.

Haenni, W., Rychen, P., Fryda, M. and Comninellis, Ch. (2004) Industrial applications of diamond electrodes. Semiconduct. Semimet. 77, 149–196.

Iniesta, J., Michaud, P.-A., Panizza, M. and Comninellis, Ch. (2001a) Electrochemical oxidation of 3-methylpyridine at a boron-doped diamond electrode: Application to electroorganic synthesis and wastewater treatment. Electrochem. Commun. 3, 346–351.

Iniesta, J., Michaud, P.-A., Panizza, M., Cerisola, G., Aldaz, A. and Comninellis, Ch. (2001b) Electrochemical oxidation of phenol at boron-doped diamond electrode. Electrochim. Acta 46, 3573–3578.

Marselli, B., Garcia-Gomez, J., Michaud, P.-A., Rodrigo, M.A. and Comninellis, Ch. (2003) Electrogeneration of hydroxyl radicals on boron-doped diamond electrodes. J. Electrochem. Soc. 150, D79–D83.

Martinez-Huitle, C.A., Quiroz, M.A., Comninellis, Ch, Ferro, S. and De Battisti, A. (2004) Electrochemical incineration of chloranilic acid using Ti/IrO_2, Pb/PbO_2 and Si/BDD electrodes. Electrochim. Acta 50, 949–956.

Michaud, P.-A., Panizza, M., Ouattara, L., Diaco, T., Foti, G. and Comninellis, Ch. (2003) Electrochemical oxidation of water on synthetic boron-doped diamond thin film anodes. J. Appl. Electrochem. 33, 151–154.

Montilla, F., Michaud, P.-A., Morallon, E., Vazquez, J.L. and Comninellis, Ch. (2001) Electrochemical oxidation of benzoic acid on boron doped diamond electrodes. Portug. Electrochim. Acta 19, 221–226.

Montilla, F., Michaud, P.-A., Morallon, E., Vazquez, J.L. and Comninellis, Ch. (2002) Electrochemical oxidation of benzoic acid at boron-doped diamond electrodes. Electrochim. Acta 47, 3509–3513.

Ouattara, L., Duo, I., Diaco, T., Ivandini, A., Honda, K., Rao, T., Fujishima, A. and Comninellis, Ch. (2003) Electrochemical oxidation of ethylenediaminetetraacetic acid (EDTA) on BDD electrodes: Application to wastewater treatment. New Diam. Front. Carbon Technol. 13, 97–108.

Ouattara, L., Chowdhry, M.M. and Comninellis, Ch. (2004) Electrochemical treatment of industrial wastewater. New Diam. Front. Carbon Technol. 14, 239–247.

Panizza, M., Michaud, P.-A., Cerisola, G. and Comninellis, Ch. (2001a) Anodic oxidation of 2-naphthol at boron-doped diamond electrodes. J. Electroanal. Chem. 507, 206–214.

Panizza, M., Michaud, P.-A., Cerisola, G. and Comninellis, Ch. (2001b) Electrochemical treatment of wastewaters containing organic pollutants on boron-doped diamond electrodes: Prediction of specific energy consumption and required electrode area. Electrochem. Commun. 3, 336–339.

Polcaro, A.M., Mascia, M., Palmas, S. and Vacca, A. (2004) Electrochemical degradation of diuron and dichloroaniline at BDD electrode. Electrochim. Acta 49, 649–656.

Polcaro, A.M., Vacca, A., Mascia, M. and Palmas, S. (2005) Oxidation at boron doped diamond electrodes: Effective method to mineralise triazines. Electrochim. Acta 50, 1841–1847.

Pulgarin, C., Adler, N., Peringer; P. and Comninellis, Ch. (1994) Electrochemical detoxification of a 1,4-benzoquinone solution in wastewater treatment. Water Res. 28, 887–893.

Rodrigo, M.A., Michaud P.-A., Duo, I., Panizza, M., Cerisola, G. and Comninellis, Ch. (2001) Oxidation of 4-chlorophenol at boron-doped diamond electrode for wastewater treatment. J. Electrochem. Soc. 148, D60–D64.

Seignez, C., Pulgarin, C., Peringer, P., Comninellis, Ch. and Plattner, E. (1992) Degradation of industrial organic pollutants. Electrochemical and biological treatment and combined treatment. Swiss Chem. 14, 25–30.

Simond, O., Schaller, V. and Comninellis, Ch. (1997) Theoretical model for the anodic oxidation of organics on metal oxide electrodes. Electrochim. Acta 42, 2009–2012.

Zanta, C.L.P.S., Michaud, P.-A., Comninellis, Ch., De Andrade, A.R. and Boodts, J.F.C. (2003) Electrochemical oxidation of p-chlorophenol on SnO_2-Sb_2O_5 based anodes for wastewater treatment. J. Appl. Electrochem. 33, 1211–1215.

Chapter 2
Importance of Electrode Material in the Electrochemical Treatment of Wastewater Containing Organic Pollutants

Marco Panizza

2.1 Introduction

In recent decades, oxidative electrochemical technologies, providing versatility, energy efficiency, amenability to automation, environmental compatibility, and cost effectiveness have reached a promising stage of development and can now be effectively used for the destruction of toxic or biorefractory organics (Rajeshwar et al. 1994; Rajeshwar and Ibanez 1997; Chen 2004).

The overall performance of the electrochemical processes is determined by the complex interplay of parameters that may be optimized to obtain an effective and economical incineration of pollutants. The principal factors determining the electrolysis performance will be (Pletcher and Walsh 1982) as follows:

1. *Electrode potential and current density*. Control which reaction should occur and its rate and commonly determine the efficiency of the process
2. *Current distribution*. Determines the spatial distribution of the consumption of reactants and hence, it must be as homogeneous as possible
3. *Mass-transport regime*. A high mass-transport coefficient that leads to a greater uniformity of pollutant concentration in the reaction layer near the electrode surface and to generally a higher efficiency
4. *Cell design*. The cell dimension, the presence or the absence of a separator, the design of the electrode, etc. affect the figures of merit of the electrochemical process
5. *Electrolysis medium*. The choice of electrolyte and its concentration, pH, temperature
6. *Electrode materials*. The ideal electrode material for the degradation of organic pollutants should be totally stable in the electrolysis medium; cheap; and exhibit high activity toward organic oxidation and low activity toward secondary reactions (e.g., oxygen evolution).

M. Panizza (✉)
Department of Chemical and Process Engineering, University of Genoa, Italy
e-mail: marco.panizza@unige.it

C. Comninellis and G. Chen (eds.), *Electrochemistry for the Environment*,
DOI 10.1007/978-0-387-68318-8_2,

Even if we still remain far from meeting all these requirements for an electrode, a significant step has been made toward the production of better electrode material. The present chapter reviews and discusses the crucial role of the electrode materials in the electrochemical treatment of wastewater containing organic pollutants.

2.2 Electrochemical Parameters

Before analyzing the influence of the electrode material on the electrooxidation of organic pollutants, it is necessary to review some global parameters commonly used to estimate the progress and the efficiency of electrochemical treatments.

The instantaneous current efficiency (ICE) of the electrooxidation is determined by chemical oxygen demand (COD) measurements, using the relationship (Comninellis and Pulgarin 1991):

$$\mathrm{ICE} = \frac{(\mathrm{COD}_t - \mathrm{COD}_{t+\Delta t})}{8 I\, \Delta t} F V, \tag{2.1}$$

where $(\mathrm{COD})_t$ and $(\mathrm{COD})_{t+\Delta t}$ are the chemical oxygen demands at times t and $t + \Delta t$ $\left(\text{in } g_{O2}\, dm^{-3}\right)$, respectively; I is the current (A); F is Faraday's constant $\left(96{,}500\mathrm{C\ mol}^{-1}\right)$; and V is the volume of the electrolyte $\left(dm^3\right)$.

The Electrochemical Oxidation Index (EOI), which is the average value of the current efficiency during the oxidation, is determined from the ICE using the relationship (Comninellis and Pulgarin 1991):

$$\mathrm{EOI} = \frac{\int \mathrm{ICE}\, dt}{\tau}, \tag{2.2}$$

where τ is the time at which the ICE is almost zero.

The Electrochemical Oxygen Demand is calculated using the relationship (Comninellis and Pulgarin 1991):

$$\mathrm{EOD} = \frac{8\,(\mathrm{EOI} \times I \times \tau)}{F\,[\mathrm{organic}]}, \tag{2.3}$$

where [organic] is the amount of the organic in the electrolyte (g) and EOD is expressed in $g_{O2}\left(g_{\mathrm{organic}}\right)^{-1}$.

The General Current Efficiency for the anodic oxidation is calculated from the COD values, using the following relationship (Martinez-Huitle et al. 2004b):

$$\mathrm{GCE} = F V \left(\frac{(\mathrm{COD}_0 - \mathrm{COD}_t)}{8 I t} \right), \tag{2.4}$$

where $(\mathrm{COD})_0$ and $(\mathrm{COD})_{t+\Delta t}$ are the chemical oxygen demands $\left(g\, dm^{-3}\right)$ at times $t = 0$ (initial) and t, respectively; I is the current (A), F is Faraday's constant

$(96{,}500\text{C mol}^{-1})$; V the volume of the electrolyte (dm^3), and 8 is the oxygen equivalent mass (g eq^{-1}). This equation is similar to that proposed by Comninellis and Pulgarin (1991) for the determination of the ICE, although the expression used for the GCE represents an average value between the initial time t and $t + \Delta t$.

The overall capacity of the electrochemical oxidation is expressed in terms of space–time yield (YST) using the following relationship (Chen 2004):

$$Y_{\text{ST}} = \frac{a \times i \times \text{CE} \times M_{\text{FW}}}{nF} \times 3{,}600, \tag{2.5}$$

where a is the specific electrode area (m^{-1}), defined as the ratio of the electrode area to the reactor volume; i is the current density (A m^{-2}); CE is the current efficiency; n is the number of electrons in the reaction involved; F is Faraday's constant $(96{,}500\text{C mol}^{-1})$; and M_{FW} is the molar mass (g mol^{-1}).

2.3 Oxidation Mechanisms

Electrooxidation of organic pollutants can be performed in several different ways, including direct and indirect oxidation, which are schematized in Fig. 2.1.

It has been generally observed that the nature of the electrode material, the experimental conditions, and the electrolyte composition strongly influence the oxidation mechanism.

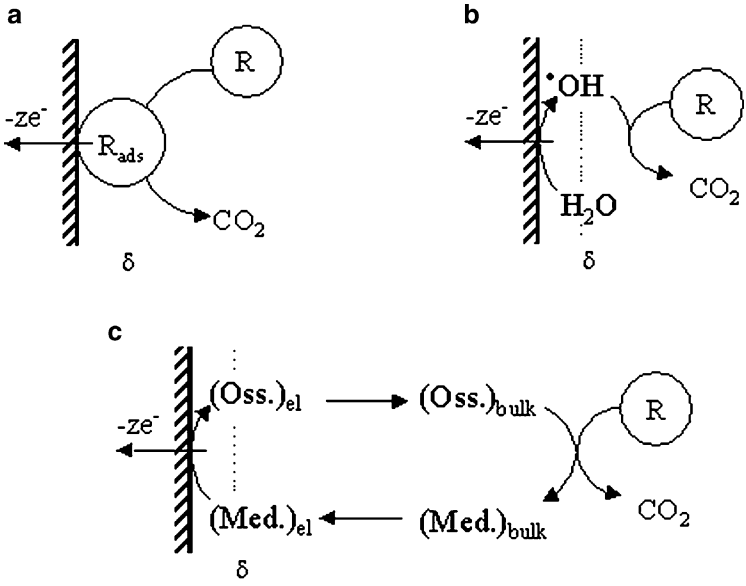

Fig. 2.1 Scheme of the electrochemical processes for the removal of organic compounds (R): (**a**) direct electrolysis; (**b**) via hydroxyl radicals produced by the discharge of the water; and (**c**) via inorganic mediators

In direct electrolysis, the pollutants are oxidized after adsorption on the anode surface without the involvement of any substances other than the electron, which is a "clean reagent":

$$R_{ads} - ze^- \rightarrow P_{ads} \tag{2.6}$$

Direct electrooxidation is theoretically possible at low potentials, before oxygen evolution, but the reaction rate usually has low kinetics that depends on the electrocatalytic activity of the anode. High electrochemical rates have been observed using noble metals such as Pt and Pd, and metal-oxide anodes such as iridium dioxide, ruthenium–titanium dioxide, and iridium–titanium dioxide (Foti et al. 1997).

However, the main problem of electrooxidation at a fixed anodic potential before oxygen evolution is a decrease in the catalytic activity, commonly called the poisoning effect, due to the formation of a polymer layer on the anode surface. This deactivation, which depends on the adsorption properties of the anode surface and the concentration and the nature of the organic compounds, is more accentuated in the presence of aromatic organic substrates such as phenol (Gattrell and Kirk 1993; Foti et al. 1997), chlorophenols (Rodgers et al. 1999; Rodrigo et al. 2001), naphthol (Panizza and Cerisola 2003b), and pyridine (Iniesta et al. 2001b).

In indirect oxidation, organic pollutants do not exchange electrons directly with the anode surface; but they exchange through the mediation of some electroactive species regenerated there, which act/acts as an intermediary for shuttling electrons between the electrode and the organics. Indirect electrolysis can be a reversible or an irreversible process.

In the reversible process, the redox reagents are turned over several times and recycled. The reversible mediators of oxidation can be a metallic redox couple, such as Ag^+/Ag^{2+}(Farmer et al. 1992), Co^{2+}/Co^{3+}(Leffrang et al. 1995), Ce^{3+}/Ce^{4+}(Nelson 2002), Fe^{2+}/Fe^{3+}(Dhooge and Park 1983), or inorganic ions such as Cl^-/ClO^- (Comninellis and Nerini 1995; Szpyrkowicz et al. 1995; (Panizza and Cerisola 2003a) or Br^-/BrO^- (Martinez-Huitle et al. 2005) added to or present in the electrolyte. The main drawback of the use of a solution redox couple is the need to subsequently separate the oxidation products from the mediator.

In the irreversible process, a strong oxidizing chemical (e.g., ozone (Foller and Tobias 1982; Tatapudi and Fenton 1993; Feng et al. 1994), hydrogen peroxide (Do and Chen 1993; Brillas et al. 1995, 2003; Alvarez-Gallegos and Pletcher 1998; Boye et al. 2002), etc.) is generated in situ to mineralize the organic pollutants.

Another mechanism for the indirect electrochemical oxidation of organics at high potential, proposed by Johnson et al. (Chang and Johnson 1990; Johnson et al. 1999), is based on intermediates of the oxygen evolution reaction. This process involves the transfer of anodic oxygen from H_2O to the organics via adsorbed hydroxyl radicals generated by the water discharge:

$$S[\cdot] + H_2O \rightarrow S[OH^{\cdot}] + H^+ + e^- \tag{2.7}$$

$$S[OH^{\cdot}] + R \rightarrow S[\cdot] + RO + H^+ + e^- \tag{2.8}$$

where S represents the surface sites for adsorption of the $OH^{\cdot}$ species.

An inevitable but undesirable concomitant reaction is the evolution of oxygen by the oxidation of the water

$$S\,[OH^{\cdot}] + H_2O \rightarrow S\,[\cdot] + O_2 + 3H^+ + 3e^- \tag{2.9}$$

Comninellis et al. (Comninellis 1994; Comninellis and De Battisti 1996; Simond et al. 1997; Foti et al. 1999) found that the nature of the electrode material strongly influences both the selectivity and the efficiency of the process and, in particular, several anodes favored the partial and selective oxidation of pollutants (i.e., conversion), while others favored complete combustion to CO_2. In order to interpret these observations, they proposed a comprehensive model for the oxidation of organics at metal oxide electrodes with simultaneous oxygen evolution.

In a similar way to the mechanism proposed by Johnson, the first step in the oxygen transfer reaction is the discharge of water molecules to form adsorbed hydroxyl radicals

$$MO_x + H_2O \rightarrow MO_x\,(^{\cdot}OH) + H^+ + e^- \tag{2.10}$$

The following steps depend on the nature of the electrode materials, and make it possible to distinguish between two limiting classes of electrodes, defined as "active" and "nonactive" anodes:

(a) At "active" electrodes, where higher oxidation states are available on the electrode surface, the adsorbed hydroxyl radicals may interact with the anode, forming the so-called higher oxide:

$$MO_x\,(^{\cdot}OH) \rightarrow MO_{x+1} + H^+ + e^- \tag{2.11}$$

The surface redox couple MO_{x+1}/MO_x, which is sometimes called chemisorbed "active oxygen," can act as a mediator in the conversion or selective oxidation of organics on "active" electrodes:

$$MO_{x+1} + R \rightarrow MO_x + RO \tag{2.12}$$

(b) At "nonactive" electrodes, where the formation of a higher oxide is excluded, hydroxyl radicals, called physisorbed "active oxygen," may assist the nonselective oxidation of organics, which may result in complete combustion to CO_2:

$$MO_x\,(^{\cdot}OH) + R \rightarrow MO_x + m\,CO_2 + n\,H_2O + H^+ + e^- \tag{2.13}$$

However, both the chemisorbed and the physisorbed "active oxygen," also undergo a competitive side reaction, i.e., oxygen evolution, resulting in a decrease in the efficiency of the anodic process.

As a general rule, anodes with low oxygen evolution overpotential (i.e., anodes that are good catalysts for the oxygen evolution reaction), such as carbon, graphite, IrO_2, RuO_2, or platinum, have "active" behavior and only permit the partial oxidation of organics, while anodes with high oxygen evolution overpotential (i.e., anodes

that are poor catalysts for the oxygen evolution reaction), such as antimony-doped tin oxide, lead dioxide, or boron-doped diamond (BDD), have "nonactive" behavior and favor the complete oxidation of the organics to CO_2 and so are ideal electrodes for wastewater treatment. Moreover, radical trap experiments using *N*, *N*-dimethyl-*p*-nitrosoaniline (DMPO) as an $OH^{\cdot}$ scavenger have demonstrated that a larger concentration of $OH^{\cdot}$ is present on nonactive anodes than on active ones (Comninellis 1994; Marselli et al. 2003). The larger $OH^{\cdot}$ concentration has been suggested as the cause of the complete combustion of organics to CO_2 on nonactive anodes.

2.4 Electrode Materials

As mentioned above, the nature of the electrode material influences the selectivity and the efficiency of an electrochemical process for the oxidation of organic compounds and for this reason, in literature, many anodic materials have been tested to find the optimum one. According to the model proposed by Comninellis (1994), anode materials are divided for simplicity into two classes as follows:

Class 1 anodes, or active anodes, have low oxygen evolution overpotential and consequently are good electrocatalysts for the oxygen evolution reaction:

- Carbon and graphite
- Platinum-based anodes
- Iridium-based oxides
- Ruthenium-based oxides

Class 2 anodes, or nonactive anodes, have high oxygen evolution overpotential and consequently are poor electrocatalysts for the oxygen evolution reaction:

- Antimony-doped tin oxide
- Lead dioxide
- Boron-doped diamond

The oxygen evolution potentials in H_2SO_4 of the most extensively investigated anode materials are compared in Table 2.1.

2.4.1 Carbon and Graphite

Carbon and graphite electrodes are very cheap and have a large surface area and so they have been widely used for the removal of organics in electrochemical reactors with three-dimensional electrodes (e.g., packed bed, fluidized bed, carbon particles, porous electrode, etc.). However, with these materials the electrooxidation is generally accompanied by surface corrosion, especially at high current densities. Gattrell and Kirk (1990) used reticulated glassy carbon anodes in a flow-by cell for the oxidation of phenol. During the electrolysis there was a rapid decrease in the

Table 2.1 Potential for oxygen evolution of different anodes in H_2SO_4

Anode	Value vs. SHE	Conditions
RuO_2	1.47	0.5 M H_2SO_4
IrO_2	1.52	0.5 M H_2SO_4
Pt	1.6	0.5 M H_2SO_4
Oriented pyrolytic graphite	1.7	0.5 M H_2SO_4
SnO_2	1.9	0.05 M H_2SO_4
PbO_2	1.9	1 M H_2SO_4
BDD	2.3	0.5 M H_2SO_4

Standard potential for oxygen evolution is 1.23 V vs. NHE (Panizza and Cerisola 2006b)

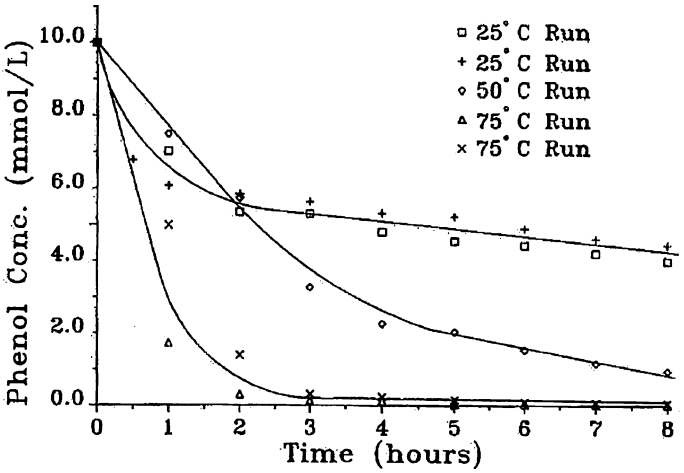

Fig. 2.2 The effect of temperature on the rate of phenol oxidation at a glassy carbon electrode (Gattrell and Kirk 1993)

reaction rate due to the blocking of the electrode surface with insoluble polymeric products that were slow to oxidize or desorb. Moreover, increasing the phenol concentration from 0.005 to 0.02 M increased the current efficiency but also increased the fraction of phenol that reacted to form polymeric products. They observed that high-temperature (Fig. 2.2) and high-applied potentials (i.e., greater than 1.9 V vs. SCE) not only resulted in a more complete oxidation of the phenol, but also resulted in a decrease in the current efficiency and faster electrode corrosion.

The electrochemical 2-chlorophenol and 2,6-dichlorophenol removal from aqueous solutions using porous carbon felt (Polcaro and Palmas 1997) or a fixed bed of carbon pellets (Polcaro et al. 2000) as three-dimensional electrodes was investigated by Polcaro's group. The group's experimental setup consisted of a two-compartment electrochemical cell separated by an anionic membrane where the carbon felt or pellets could be lodged and the solution was recirculated by peristaltic pumps. Both carbon-based anodes effectively removed the chlorophenols as well as their reaction

intermediates. The HPLC chromatographs showed that the main intermediates were aliphatic compounds such as oxalic and maleic acids, while phenol, cathecol, and benzoquinone were not observed; this may indicate that cleavage of chlorine occurs at the same time as the ring opening. They also demonstrated that the electrolyte velocity through the electrode did not affect the reaction behavior, while the most important parameter was the current density per unit electrolyte volume: Using an applied current density of 5 mA cm^{-2} of electrode, average current efficiency values were from 25 to 30%. Moreover, under these conditions, they observed only low corrosion effects on the superficial characteristics of the anodes after they had been working for several hours.

The electrochemical treatment of phenol using graphite electrodes was recently investigated by (Awad and Abuzaid 1997, 1999, 2000) and the effect of residence time at different applied currents was elucidated. Phenol removal efficiency was found to increase with the increase in current and residence time and reached about 50% at a current of 2.0 A and a residence time of 35 min (Fig. 2.3).

Other types of carbon-based electrodes, such as activated carbon (Canizares et al. 1999), graphite particles (Piya-areetham et al. 2006), graphite Rashig rings (Ogutveren et al. 1999), and carbon black slurry (Boudenne et al. 1996; Boudenne and Cerclier 1999) have also been employed sometimes for the treatment of organic compounds.

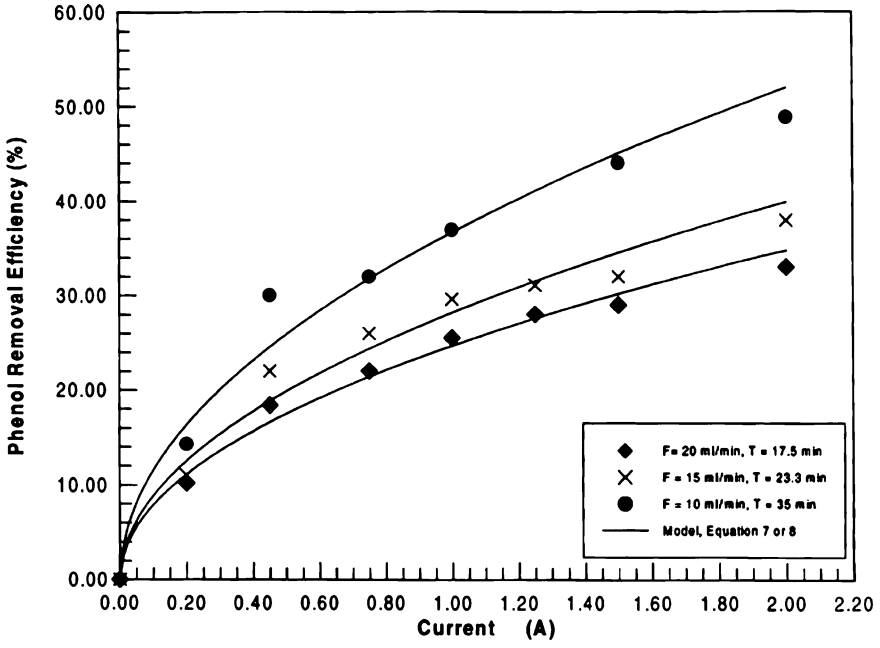

Fig. 2.3 Relationship between phenol removal efficiency and current, under different flow rates and residence time values, during phenol oxidation at porous graphite anodes (Awad and Abuzaid 2000)

Carbon-based materials have also been widely used as cathodes in indirect electrolyses of organics generating in situ hydrogen peroxide, by two-electron reduction of oxygen on the cathode surface:

$$O_2 + 2H^+ + 2e^- \rightarrow H_2O_2 \tag{2.14}$$

In fact, carbon and graphite exhibit good electrochemical activities for oxygen reduction, high overpotential for hydrogen evolution, and low catalytic activity for hydrogen peroxide decomposition (Do and Chen 1994a, b; Ponce-de-Leon and Pletcher 1995).

It is well known that in acidic solutions, the addition of a small concentration of Fe(II) to the electrogenerated H_2O_2 enhances the rate and the efficiency of the oxidation of organics, due to the formation of highly oxidizing $OH^{\cdot}$ radicals, according to Fenton's classical mechanism (Brillas et al. 1996):

$$Fe^{2+} + H_2O_2 \rightarrow Fe^{3+} + OH^- + OH^{\cdot} \tag{2.15}$$

This reaction is propagated by Fe^{2+} regeneration, which takes place through the reduction of Fe^{3+} with H_2O_2, the hydroperoxyl radical $HO_2^{\cdot}$ previously formed, and the organic radical intermediates and by reduction at the cathode:

$$Fe^{3+} + H_2O_2 \rightarrow Fe^{2+} + OH^+ + OH_2^{\cdot} \tag{2.16}$$

$$Fe^{3+} + HO_2^{\cdot} \rightarrow Fe^{2+} + H^+ + O_2 \tag{2.17}$$

$$Fe^{3+} + e^- \rightarrow Fe^{2+} \tag{2.18}$$

In this field, several authors have reported the complete removal of organic pollutants, such as formaldehyde (Do and Chen 1993), aniline (Brillas et al. 1996), phenol (Alvarez-Gallegos and Pletcher 1999), pesticides (Guivarch et al. 2003), herbicides (Boye et al. 2002), and industrial effluent containing naphthalene- and anthraquinone-sulfonic acids (Panizza and Cerisola 2001) by in situ electrogenerated hydrogen peroxide catalyzed by iron ions.

2.4.2 Platinum

The platinum electrode is one of the most commonly used anodes in both preparative electrolysis and synthesis because of its good chemical resistance to corrosion even in strongly aggressive media. The behavior of platinum electrodes in the electrochemical oxidation of organic pollutants has been widely reported in literature, showing a significant electrocatalytic activity (Soriaga and Hubbard 1982; Lamy et al. 1983; Foti et al. 1997; Rodgers et al. 1999).

For example, Lamy (1984) studied the oxidation of organic compounds (e.g., methanol, ethanol, butanol, ethylene-glycol, C_2 oxygenated compounds, etc.) on

noble metal electrodes (e.g., platinum, gold, rhodium, and palladium) in aqueous solutions and verified that platinum appears to be the best electrocatalyst, particularly in an acidic medium.

Gattrell and Kirk (Gattrell and Kirk 1993) investigated the oxidation of phenol at platinum and peroxidized platinum anodes using cyclic voltammetry and chronoamperometry. Their studies demonstrated that the phenol can be irreversibly adsorbed on metallic platinum, quickly passivating the electrode. However, the presence of a platinum oxide layer on the electrode surface slightly inhibited the formation of the passivating film due to the decreased adsorption strength of the reaction products at the oxide surface. In long-term electrolyses, the activity of metallic platinum and platinum oxide had the same behavior.

The electrochemical oxidation of phenol at platinum anodes was also studied in depth by Comninellis and Pulgarin (Comninellis and Pulgarin 1991) under different conditions for wastewater treatment. A yellow-brown polymeric product was formed during the oxidation of phenol, and this film formation strongly depended on the experimental conditions. They showed that the process was not limited by mass transfer at the anode and the oxidation occurred through an electrophilic attack on the aromatic ring by the $OH^{\cdot}$. The EOI and the EOD values were slightly influenced by the current density and temperature, but they increased with the pH (Table 2.2) and phenol concentration (Fig. 2.4). However, even at pH $=$ 12.5 the EOI obtained during the electrochemical oxidation of 0.01 M of phenol at $T = 70°C$ and $i = 57 mA\ cm^{-2}$ was only 0.143. Such a low value was due to the formation of reaction intermediates, mainly aliphatic acids (e.g., maleic, fumaric, and oxalic acid), which resisted further electrooxidation.

The oxidation of a wide range of phenol and other biorefractory organic compounds (e.g., ethanol, aliphatic acids, naphthalene and anthraquinone sulfonic acids, aniline, nitrobenzene, etc.) on platinized titanium was also studied by Kotz et al. (Kotz et al. 1991; Stucki et al. 1991). The elimination of TOC was rather ineffective due to the leakage current for oxygen evolution, and the average EOI was about 0.05.

More recently, Bonfatti et al. (1999) have verified that the reactivity of glucose at Ti/Pt electrodes was acceptable in all current densities, slightly higher at $600 A\ m^{-2}$; however, the electrochemical mineralization was low, particularly over a long electrolysis time, due to the accumulation of intermediates, mainly glucaric acid, which resisted further attack at the platinum electrode. The situation improved by increasing the temperature to 56°C.

Table 2.2 Influence of pH and temperature on the EOI and EOD during the oxidation of phenol at a platinum anode

pH	T (°C)	EOI	EOD
1.3–2.0	70	0.078	0.99
12–13	70	0.143	1.14
1.5–1.7	15	0.048	0.76
12–13	15	0.121	1.20

Initial phenol concentration: $0.01 mol\ dm^{-3}$, $i = 57 mA\ cm^{-2}$ (Comninellis and Pulgarin 1991)

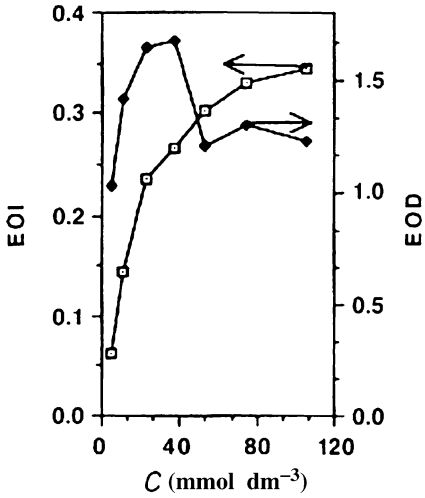

Fig. 2.4 Influence of the initial phenol concentration on the EOI and EOD values obtained during electrochemical oxidation at platinum electrodes. $I = 57$ mA cm^{-2}, $T = 70$°C, pH 12.5 (Comninellis and Pulgarin 1991)

Table 2.3 Dependence of 1-aminonaphthalene-3,6-disulfonic acid (ANDS) conversion on the electrooxidation temperature of the platinum anode, $c = 10^{-3}$ mol dm^{-3}, volume of solution = 60 mL (Socha et al. 2005)

Temperature (°C)	η_{TOC} (%)	η_{COD} (%)	η_{Abs} (%)
30	13.83	35.14	76.76
40	16.45	33.78	76.76
50	15.67	33.58	77.82
60	15.23	35.14	78.21
70	17.63	36.48	78.93
80	18.75	36.48	78.93

Similar results were also obtained by Socha et al. (2005) for the electrochemical treatment of 1-Aminonaphthalene-3,6-disulfonic acid (ANDS), a component of the wastewater produced during the synthesis of many synthetic dyes. An increase in the temperature caused a slight increase in the efficiency of the substrate oxidation (Table 2.3), but even at 80°C the removal of TOC and COD was only 18 and 36%, although the decolorization of the solution, i.e., decrease of absorbance, was achieved.

2.4.3 Dimensionally Stable Anodes

The dimensionally stable anodes (DSA®) consist of a titanium base metal covered by a thin conducting layer of metal oxide or mixed metal-oxide oxides. Since their discovery by Beer (1966) in the late 1960s, a lot of work has been done on DSA® and on finding and preparing new coating layers for many electrochemical

applications. The development of anodes coated with a layer of RuO_2 and TiO_2 brought about significant improvements in the chlor-alkali industry ($DSA-Cl_2$), while the anodes coated with IrO_2 have been commercially used for oxygen evolution reactions ($DSA-O_2$) in acidic media in several electrochemical processes, such as water electrolysis and metal electrowinning. Recently, DSA® anodes with a different coating composition have been also studied for applications in the oxidation of organics (Bock and MacDougall 2000; Lanza and Bertazzoli 2002; Malpass et al. 2006).

Johnson et al. (Houk et al. 1998; Johnson et al. 1999) studied the incineration of 4-chlorophenol and benzoquinone using quaternary metal-oxide anodes (Ti, Ru, Sn, and Sb). They demonstrated that this type of electrode is stable and electrochemically active for the oxidation of organic compounds when it is used in the absence of a soluble supporting electrolyte, with a Nafion® membrane as solid-state electrolyte; however, the electrolysis time for complete COD and TOC removal was excessively long and current efficiency was low.

The electrocatalytic behavior of olefins was studied by Zanta et al. (2000) at thermally prepared ruthenium–titanium- and iridium–titanium-dioxide-coated anodes. The aliphatic olefins were shown to be inactive in the region before oxygen evolution, while aromatic ones showed one or two oxidation peaks, and the catalytic activity seemed to be the same for both substrates. However, as for platinum anodes, voltammetric studies and FTIR analyses have also shown the formation of a polymeric film that blocks the surface of the electrode and decreases its activity.

Many studies of the oxidation of organic compounds with Ti/IrO_2 electrodes have been carried out by Comninellis' group (Pulgarin et al. 1994; Foti et al. 1997, 1999; Simond et al. 1997). In the region before oxygen evolution, Ti/IrO_2 did not show any electrocatalytic activity for the oxidation of alcohols (methanol, propanol, and butanol) and carboxylic acids (maleic, oxalic, and formic acid). Instead, in the presence of phenol, Ti/IrO_2 had high electrocatalytic activity, but this was quickly diminished because of the formation of a polymer film on the surface of the electrode.

Studies of the electrochemical detoxification of 1,4-benzoquinone (Pulgarin et al. 1994) showed that the primary oxidation, i.e., elimination of benzoquinone, was obtained with Ti/IrO_2 anodes, resulting in an accumulation of carboxylic acids: maleic, fumaric, mesoxalic, and oxalic acids that were only poorly degraded at the Ti/IrO_2 anode (Fig. 2.5).

Several authors have reported that DSA-type anodes coated with a layer of RuO_2 or IrO_2 and other oxides can be used efficiently for organic disposal by indirect electrolysis generating in situ active chlorine by the oxidation of chloride ions present in the solution, according to the following reaction:

$$2Cl^- \rightarrow Cl_2 + 2e^- \tag{2.19}$$

As a function of pH, chlorine remains in the solution as aqueous chlorine ($pH < 3$) or disproportionates to hypochloric acid ($pH < 7.5$) or hypochlorite ions ($pH > 7.5$):

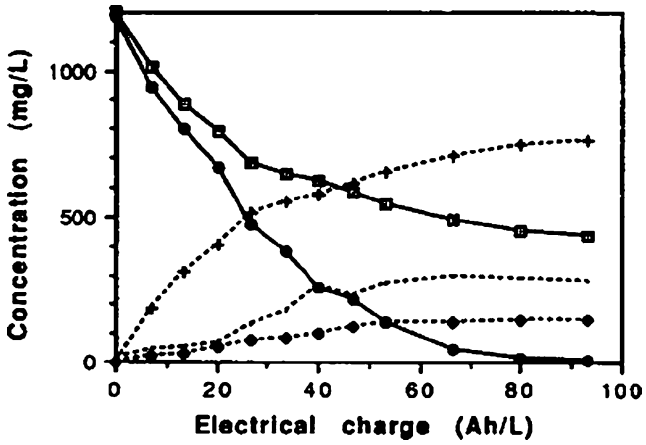

Fig. 2.5 Evolution of benzoquinone, intermediates and COD during the oxidation of benzoquinone at Ti/IrO_2 anodes as a function of charge: *open square with dot* COD; *filled circle* benzoquinone; *open diamond* aliphatic acids, *dashed line* others; *plus* CO_2. Reprinted from Pulgarin et al. (1994), Copyright (1994), with permission from Elsevier

$$Cl_2 + H_2O \rightarrow HOCl + H^+ + Cl^- \tag{2.20}$$

$$HOCl \rightarrow H^+ + OCl^- \tag{2.21}$$

This process can effectively oxidize many pollutants, however, it has the drawback of permitting the formation of chlorinated organic compounds during the electrolysis.

Comninellis and Nerini (1995) studied the oxidation of phenol with Ti/SnO_2 and Ti/IrO_2 anodes in the presence of sodium chloride. They showed that the addition of 85 mM of NaCl to the solution catalyzed the oxidation of phenol at Ti/IrO_2 anodes due to the participation of electrogenerated ClO^-, increasing the EOI from about 0.06 to 0.56. Surprisingly, the COD elimination was independent of the NaCl concentration and the applied current density. Unfortunately, in their experimental conditions, organochlorinated intermediates, which were further oxidized to volatile organics ($CHCl_3$), were formed.

A systematic study of the kinetics and the influence of operating conditions on the anodic mineralization of formaldehyde with electrogenerated hypochlorite ions at a mixed-oxide anode of SnO_2–PdO–RuO_2–TiO_2 (SPR) was undertaken by Do and Yeh (Do and Yeh 1995; Do et al. 1997). During the oxidation of the formaldehyde the current efficiency increased with the stirring of the solution, the concentration of the chloride ions, the pH, and the concentration of the formaldehyde, while it decreases with current density. The maximum degradation fraction during the electrolysis at $i = 75 \text{mA cm}^{-2}$, at pH = 13, and in the presence of 1 M NaCl was about 90%.

The influence of the DSA®-coating composition and experimental condition on the electrochemical treatment of disperse dyes mediated by chloride ions was

Table 2.4 Results of electrooxidation of a dyeing bath obtained after 40 min of electrolysis applying a current of 2 A dm^{-2} using various anodes (Szpyrkowicz et al. 2000)

Anode material	Anode potential (V)	Cell potential (V)	Color removal (%)	COD removal (%)	Faraday efficiency (%)
Ti/Pt	4.36	8.0	40	9	21.4
$Ti/RuO_2–TiO_2$	4.33	7.8	42	26	60.4
$Ti/SnO_2–Sb_2O_5$	4.59	8.6	45	23	61.7
Ti/Pt–Ir	4.56	8.6	50	39	104.8
$Ti/MnO_2–RuO_2$	4.44	8.2	46	10	23.9
$Ti/RhO_x–TiO_2$	4.41	8.6	47	29	77.6
$Ti/PdO–Co_3O_4$	4.32	8.6	48	25	57.9

investigated by Szpyrkowicz et al. (2000). The efficiency of the treatment depended on the nature of the supporting electrolyte and the bulk pH in the reactor and, to a lesser degree, on the type of the anode material. The best results were obtained in a chloride-rich medium under acidic pH using a Ti/Pt–Ir anode (Table 2.4). However, despite the excellent destruction of the synthetic dyes, the indirect electrooxidation resulted in the production of many chloroorganic compounds, which was a major disadvantage of this method (Naumczyk et al. 1996).

More recently, Panizza (Panizza and Cerisola 2003a) investigated the oxidation of 2-naphthol with in situ electrogenerated active chlorine using an undivided flow cell with a Ti–Ru–Sn ternary oxide anode and a stainless steel cathode. The degradation rate increased with the NaCl concentration and pH, but it was almost independent of the current density. A higher EOI value, about 0.302, was achieved with a concentration of NaCl of 7.5 g dm^{-3} at pH 12 (Fig. 2.6). A small quantity of organochlorinated compounds was detected in the solution during oxidation, but these compounds were then mineralized to CO_2 or oxidized to volatile chlorinated compounds (i.e., chloroform).

On the contrary, Bonfatti et al. (2000a, b) demonstrated that by choosing optimal experimental conditions, glucose can be incinerated by chlorine-mediated electrolysis without the formation of any chlorinated organics. In the presence of 2–5 g dm^{-3} of NaCl, the formation of active chlorine makes the mineralization process substantially insensitive to the nature of the electrode surface, its rate being the same at Ti/PbO_2, Ti/SnO_2, and Ti/Pt electrodes. In particular, the removal of glucose was found to be faster at a chloride concentration of 5 g dm^{-3}, a lower temperature, and a higher current density.

Chlorine-mediated electrolysis has also been used efficiently for the treatment of real wastewater such as landfill leachate (Chiang et al. 1995; Vlyssides et al. 2003), textile effluents (Lin and Chen 1997; Vlyssides et al. 2000; Yang et al. 2000; Iniesta et al. 2002), olive oil wastewater (Israilides et al. 1997; Panizza and Cerisola 2006c), industrial effluent containing aromatic sulfonated acids (Panizza et al. 2000), and tannery wastewaters (Vlyssides and Israilides 1997; Szpyrkowicz et al. 2001; Panizza and Cerisola 2004a).

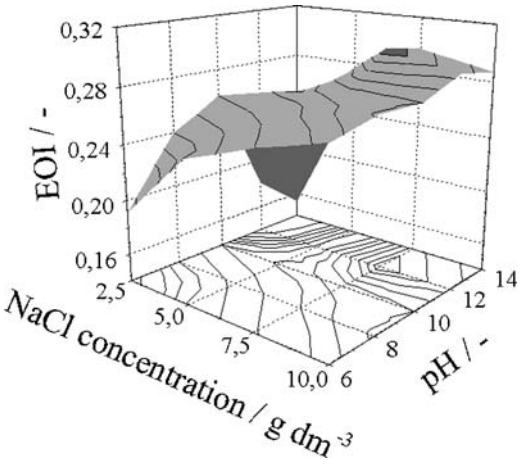

Fig. 2.6 3D representation of the combined effect of NaCl concentration and pH on the EOI values during the electrolyses of 2-naphthol on a Ti–Ru–Sn ternary oxide anode. Initial 2-naphthol concentration = 5mM; $i = 75$ mA cm^{-2}; flow rate = 180 l h^{-1} (Panizza and Cerisola 2004b)

2.4.4 Tin Dioxide

During the last 10 years, many papers have demonstrated that conductive Sb-doped SnO_2 anodes, which have an onset potential for O_2 evolution of about 1.9 V vs. SHE, are highly effective for the electrooxidation of organics in wastewater treatment (Pulgarin et al. 1994; Cossu et al. 1998; Bock and MacDougall 1999; Grimm et al. 2000).

Kotz et al. (Kotz et al. 1991; Stucki et al. 1991) reported that anodic oxidation of a wide range of organic compounds at SnO_2 was very much unselective, which means that the electrode can be applied to a multitude of different wastewater compositions, and proceeded with an average efficiency that was five times higher than with Pt anodes (Table 2.5).

The electrochemical oxidation of phenol on doped SnO_2 and platinum anodes was studied by Comninellis and Pulgarin (1993). The rate of phenol removal was almost the same for both anodes but the rate of TOC elimination and the ICE were much higher for the SnO_2 electrode (Fig. 2.7).

The intermediate products of the oxidation of phenol, mainly aliphatic acids, were oxidized rapidly by the Ti/SnO_2–Sb anode, but on the contrary, they were practically unaffected by the Pt anodes.

Similar results were also obtained by Li et al. (2005) for the oxidation of phenol at Ti/SnO_2−Sb, Ti/RuO_2, and Pt anodes. The best result for phenol oxidation and TOC removal was obtained with the Ti/SnO_2 − Sb anode, followed by the Pt anode and then by the Ti/RuO_2 anode.

Polcaro et al. (1999) compared the performance of Ti/PbO_2 and Ti/SnO_2 anodes for the electrochemical oxidation of 2-chlorophenol, showing that, although both electrodes gave similar Faradic yields, the Ti/SnO_2 anode was preferred because of its greater ability to oxidize toxic compounds. Stopping the electrolysis when only a small amount of easily biodegradable oxalic acid was present in the effluent (i.e., COD = 300 mg dm^{-3}), the current efficiency was 50%.

Table 2.5 Initial electrochemical oxidation index (EOI) determined for the various test substances using Pt and SnO_2 anodes (Stucki et al. 1991)

Initial electrochemical oxidation index (EOI)		
Organic species	Platinum anode	Ti/SnO_2 anode
Ethanol	0.02	0.49
Acetone	0.02	0.21
Acetic acid	0.00	0.09
Tartaric acid	0.27	0.34
Formic acid	0.01	0.05
Oxalic acid	0.01	0.05
Malonic acid	0.01	0.21
Maleic acid	0.00	0.15
Benzoic acid	0.10	0.79
Phenol	0.15	0.60
Aniline	0.1	0.50
EDTA	0.30	0.30
Average	0.05	0.34

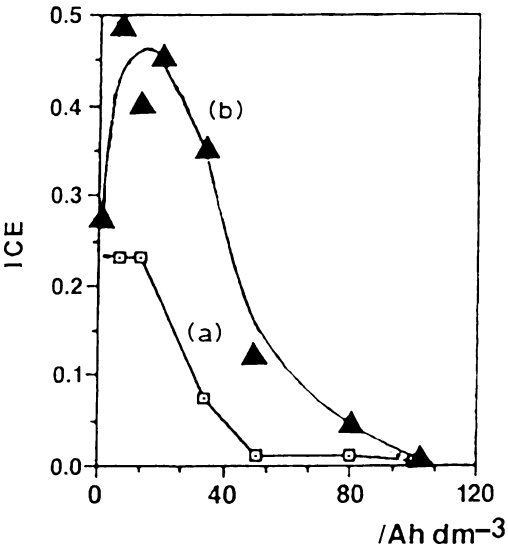

Fig. 2.7 Evolution of the ICE with a specific charge during the oxidation of phenol at (**a**) Pt anode; (**b**) SnO_2 anode. Conditions: $T = 70°C$, pH = 2, Initial phenol concentration: 21 mM, $i = 50$ mA cm^{-2} (Comninellis and Pulgarin 1993)

However, despite the high removal ability of organic pollutants, the SnO_2 anodes have the major drawback of a short service life that limits their practical applications (Lipp and Pletcher 1997). Correa-Lozano et al. (1997) investigated the stability of the Ti/Sb_2O_5 − SnO_2 and found that the service life of those produced by spray pyrolysis can be improved by using a high electrode loading (about 100 g m^{-2}) and a preparation temperature of 550°C, but even under these conditions their life remained less than 12 h at 100 mA cm^{-2} in 1 M H_2SO_4 at $T = 25°C$.

Ways of improving these anodes are now being investigated in many laboratories and it has been demonstrated that the service life of Sb-doped SnO_2 electrodes

can be increased by the incorporation of new dopants such as platinum (Vicent et al. 1998); by the introduction of interlayers between the titanium and the active oxide (Zanta et al. 2003), such as IrO_2; or by improvements to the preparation method (Lipp and Pletcher 1997). However, the EOI values for the incineration of glucose at composite $Pt - SnO_2$ electrodes were even lower than those at pure Pt electrodes (Bonfatti et al. 1999), while the onset potential for oxygen evolution of $Ti/IrO_2/SnO_2$ decreased significantly up to 1.5 V vs. NHE (Chen et al. 2002).

2.4.5 *Lead Dioxide*

Lead dioxide anodes have a long history of use as electrode materials for the oxidation of organics because of their good conductivity and large overpotential for oxygen evolution in acidic media, enabling the production of hydroxyl radicals during water discharge (Cossu et al. 1998; Saracco et al. 2000; Gherardini et al. 2001; Keech and Bunce 2003). The possible release of toxic ions, especially in basic solutions, is the main drawback of these electrodes.

Early papers (Smith-de-Sucre and Watkinson 1981; Kirket et al. 1985; Sharifian and Kirk 1986) studied the oxidation of phenol and aniline using a packed-bed reactor of PbO_2 pellets with a recirculating anolyte. The phenol and aniline in the solution were oxidized readily, but further oxidation of intermediates to carbon dioxide was more difficult. The extent of organic and TOC removal increased with the applied current density. Bonfatti et al. (1999), comparing the oxidation of glucose on different electrode materials such as Ti/PbO_2, Ti/Pt, and $Ti/Pt - SnO_2$, showed that the incineration of glucose and its oxidation intermediates (i.e., gluconic and glucaric acid) took place at a reasonable rate only at Ti/PbO_2 electrodes, and the highest Faradic yield was found at 300 A m^{-2}.

The electrochemical oxidation of phenol was thoroughly investigated under different experimental conditions Belhadj and Savall (Tahar and Savall 1998, 1999a, b) in a two-compartment cell. Phenol and its intermediates (benzoquinone, maleic, and fumaric acids) were completely eliminated at a pure Ta/PbO_2 anode through the intermediation of hydroxyl radicals adsorbed at the active site of the electrode (Fig. 2.8). The consumption rate of the phenol was mass-transport limited, and was favored by a high-temperature and low-current density. The mean Faradic yield reached 70% at the beginning of the electrolysis at $T = 70°C$ for an anodic current density of 100 mA cm^{-2}. These authors also studied the effect of the type of substrate (Pb, $Ti/IrO_2–Ta_2O_5$, and Ta) or electrode formulation on the stability and efficiency of PbO_2 deposits for phenol degradation. The efficiency of the electrodes for complete TOC removal decreased according to the type of substrate used, as follows: Ta > $Ti/(IrO_2–Ta_2O_5)$ > Pb, andTa/PbO_2 was also more stable. Regarding the composition of the electrode, the pure PbO_2 anode was more efficient for phenol degradation than $Bi_2O_5–PbO_2$ or perchlorate-doped PbO_2.

On the contrary, other studies by Johnson's group (Chang and Johnson 1990; Kawagoe and Johnson 1994; Feng et al. 1995) showed that the electrocatalytic

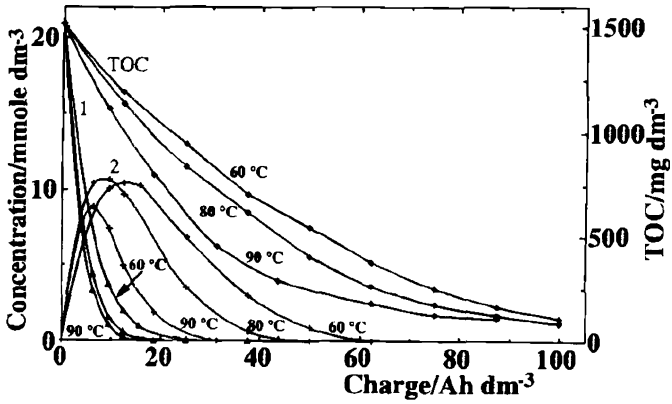

Fig. 2.8 Variation of the concentration of (1) phenol, (2) 1,4-benzoquinone, and TOC during electrochemical oxidation of phenol on a Ta/PbO_2 anode at different temperatures. Initial phenol concentration 0.021 mol dm^{-3}; $i = 100$ mA cm^{-2} (Tahar and Savall 1998)

properties and fouling resistance of PbO_2 film electrodes was enhanced by the incorporation of metallic species, such as Fe(III) or Bi(V), in the films. For example, the current efficiency for the electrochemical incineration of 10 mM of benzoquinone at 10 mA cm^{-2} increased from 7.4 to 23.5% when the PbO_2 anode was replaced with the Fe–PbO_2 one. They also observed that a significant increase in the efficiency of the anodic degradation of benzoquinone was observed as a result of raising the temperature from 20 to 80°C.

The electrochemical degradation of phenol with several metal-oxide electrodes (i.e., PbO_2, $Ti/Sb–Sn–RuO_2$, $Ti/Sb–Sn–RuO_2–Gd$, and Ti/RuO_2) and Pt anodes was carried out by Feng (Feng and Li 2003) and different TOC removal and phenol degradation rates were observed for different anodes (Fig. 2.9). Phenol was completely oxidized with all the electrodes, more rapidly at PbO_2 and Pt anodes, however, complete removal of TOC only took place on PbO_2-coated anodes.

Martinez-Huitle et al. (2004a) studied the electrochemical oxidation of oxalic acid at Ti/PbO_2, highly BDD, Pt, Au, and $Ti/IrO_2–Ta_2O_5$ electrodes showing that oxalic acid was oxidized to CO_2 with different results at several substrates. Higher current efficiencies were obtained at Ti/PbO_2 because the interaction of the oxalic acid with the PbO_2 surface was particularly strong, and its anodic oxidation was only limited by mass transfer at higher current densities and lower substrate concentrations.

2.4.6 Boron-Doped Diamond

High-quality BDD electrodes possess several technologically important characteristics including an inert surface with low adsorption properties, remarkable

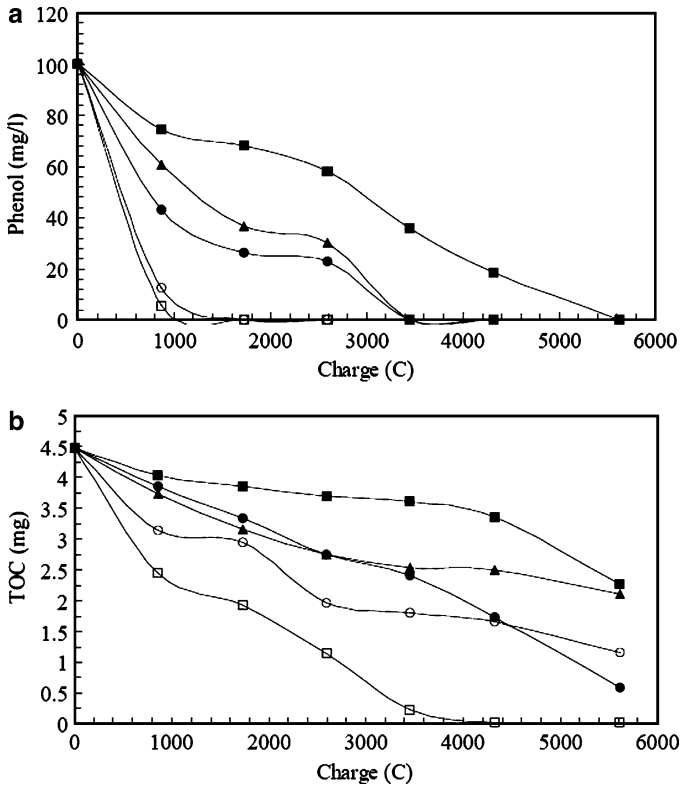

Fig. 2.9 Electrochemical degradation of 100-ppm phenol as a function of charge passed for different electrode materials, $i = 10$ mA cm^{-2}, (**a**) Phenol removal; (**b**) TOC removal; (*filled square*) Ti/RuO_2; (*filled triangle*) Ti/Sb-Sn-RuO_2; (*filled circle*) Ti/Sb–Sn–RuO_2–Gd; (*open square*) Ti/PbO_2; and (*open circle*) Pt. Reprinted from Feng and Li (2003), Copyright (2003), with permission from Elsevier

corrosion stability even in strong acidic media, and extremely high oxygen evolution overpotential. Thanks to these properties. During electrolysis in the region of water discharge, a BDD anode produces a large quantity of the $OH^{\cdot}$ that is weakly adsorbed on its surface, and consequently it has high reactivity for organic oxidation, providing the possibility of efficient application to water treatment (Comninellis et al. 2005; Panizza and Cerisola 2005).

So far, many papers have demonstrated that BDD anodes allow complete mineralization of several types of organic compounds, such as carboxylic acids (Gandini et al. 2000; Canizares et al. 2003a), polyacrilates (Bellagamba et al. 2002), herbicides (Brillas et al. 2004), cyanides (Perret et al. 1999), wastewater from automotive industry (Troster et al. 2002), surfactants (Lissens et al. 2003; Panizza et al. 2005), benzoic acid (Montilla et al. 2002), industrial wastewaters (Kraft et al. 2003; Panizza and Cerisola 2006a), naphthol (Panizza et al. 2001a), phenol (Perret et al. 1999; Iniesta et al. 2001a; Canizares et al. 2002; Morao et al. 2004),

chlorophenols (Gherardini et al. 2001; Rodrigo et al. 2001; Canizares et al. 2004a), nitrophenols (Canizares et al. 2004b), synthetic dyes (Hattori et al. 2003; Fernandes et al. 2004), and other pollutants, with high current efficiency.

It has been shown that the oxidation is controlled by the diffusion of the pollutants toward the electrode surface, where the hydroxyl radicals are produced, and the current efficiency is favored by high mass-transport coefficient, high organic concentration, and low current density. Performing electrolysis under optimum conditions, without diffusion limitation, the current efficiency approaches 100%.

Comninellis and coworkers (Foti et al. 1999; Gandini et al. 1999, 2000; Perret et al. 1999; Gherardini et al. 2001; Rodrigo et al. 2001) thoroughly investigated the behavior of Si/BDD anodes in an acidic solution for the oxidation of a wide range of pollutants, and they observed that complete mineralization was obtained with all the experimental conditions studied, and the current efficiency was influenced by the initial concentration and applied current. In particular, for high organic concentrations and low current densities, the COD decreased linearly and the ICE remained about 100%, indicating a kinetically controlled process, while for low organic concentrations or high current densities, the COD decreased exponentially and the ICE began to fall due to the mass-transport limitation and the side reactions of oxygen evolution. For example, Fig. 2.10 shows the trend of the COD and ICE during the electrochemical oxidation of different concentrations of 4-chlorophenol. In order to describe these results, the authors developed a comprehensive kinetic model that made it possible to predict the trend of the COD and current efficiency for the electrochemical combustion of the organic with BDD electrodes and estimate the energy consumption during the process (Panizza et al. 2001b).

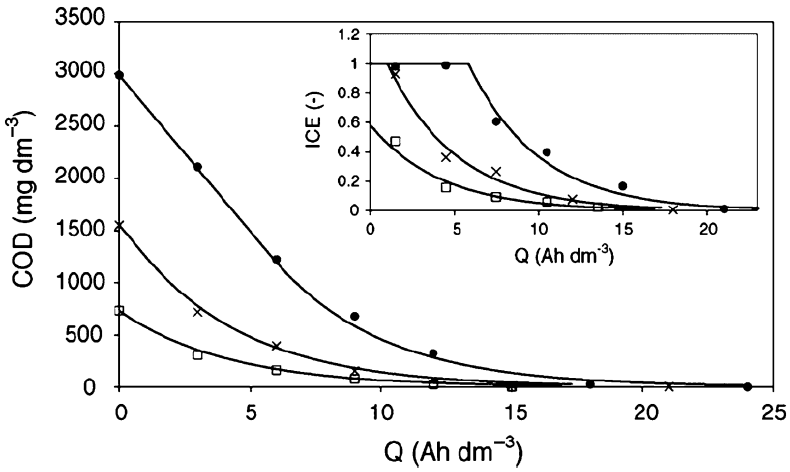

Fig. 2.10 Evolution of COD and ICE (*inset*) with the specific electrical charge passed during the oxidation of 4-chlorophenol (4-CP) on a boron-doped diamond anode. Electrolyte: sulfuric acid 1 M; $T = 30°C$; $i = 30\,mA\,cm^{-2}$; initial 4-CP concentration: (*open square*) 3.9 mM; (*cross*) 7.8 mM; (*filled circle*) 15.6 mM (Rodrigo et al. 2001)

Table 2.6 Initial current efficiency for the electrochemical oxidation of 4-chlorophenol (MCP), 2,4-dichlorophenol (DCP), and 2,4,6-trichlorophenol (TCP) using BDD anode at $T = 25°C$ (Canizares et al. 2004a)

Compound	Concentration ($mg\,dm^{-3}$)	pH	Current density ($mA\,cm^{-2}$)	Electrolyte	Initial ICE
MCP	140	2	30	Na_2SO_4	0.1
MCP	140	12	30	Na_2SO_4	0.14
MCP	140	2	30	Na_3PO_4	0.1
MCP	2,000	2	30	Na_2SO_4	1
MCP	2,000	2	60	Na_2SO_4	0.95
DCP	180	2	30	Na_2SO_4	0.25
DCP	180	12	30	Na_2SO_4	0.16
DCP	180	2	30	Na_3PO_4	0.16
DCP	2,000	2	30	Na_2SO_4	1
DCP	2,000	2	60	Na_2SO_4	0.65
TCP	220	2	30	Na_2SO_4	0.15
TCP	220	12	30	Na_2SO_4	0.2
TCP	220	2	30	Na_3PO_4	0.15

The oxidation of different phenolic compounds (phenol, chlorophenols, and nitrophenols) and carboxylic acids on BDD anodes was also studied by the group of Canizares et al. (2002, 2003b, 2004a, c). They reported that the organic compounds were completely mineralized regardless of the characteristics of the wastewater (initial concentration, pH, and supporting media) and operating conditions (temperature and current density) used. In particular, high concentration and low current density values increased the efficiency of the electrochemical oxidation of different chlorophenols (Table 2.6).

They also found that, depending on the electrolyte composition, the organics were oxidized on both the electrode surface by reaction with hydroxyl radicals and in the bulk of the solution by inorganic oxidants electrogenerated on the BDD anodes, such as peroxodisulfuric acid from sulfuric acid oxidation:

$$2H_2SO_4 \rightarrow H_2S_2O_8 + 2H^+ + 2e^- \tag{2.22}$$

Polcaro et al. (2003, 2005) verified that during the oxidation of organic compounds, such as phenol, diuron, 3,4-dichloroaniline, and triazines, the crucial point to obtain high Faradic yields is the rate of mass transfer of the reactant toward the electrode surface (Fig. 2.11). Thus, they developed an impinging cell that enabled them to obtain high mass-transfer coefficients (e.g., $10^{-4}\,m\,s^{-1}$). With this cell, at a current density of $150\,A\,m^{-2}$, they achieved a Faradic yield of 100%, up to the almost complete disappearance of the organic load.

Some investigations have also tried to compare the behavior of BDD with other electrodes, such as SnO_2, PbO_2, IrO_2, for the oxidation of organic pollutants. Chen et al. (2003) reported that the current efficiency obtained with Ti/BDD in oxidizing acetic acid, maleic acid, phenol, and dyes was 1.6–4.3-fold higher than that obtained with the typical $Ti/Sb_2O_5–SnO_2$ electrode. Other papers have demonstrated that

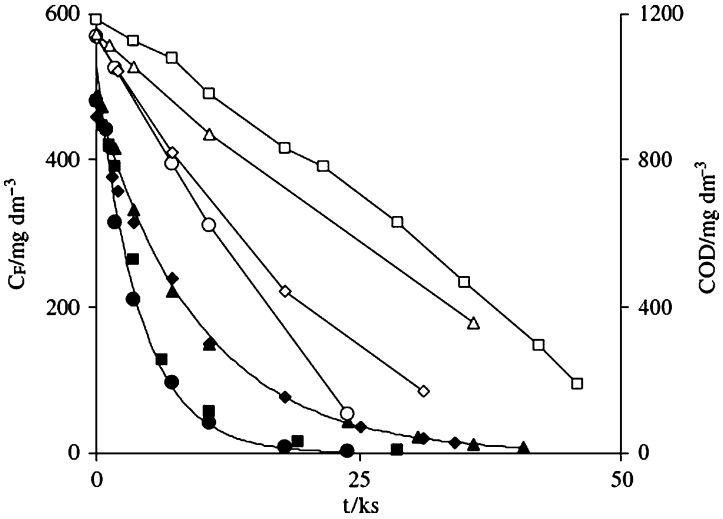

Fig. 2.11 Trend of phenol concentration (*solid symbols*) and COD (*hollow symbols*) as function of electrolysis time during the oxidation of phenol at BDD: (*open circle, filled circle*) $i = 305\,\text{A m}^{-2}$, Re = 13,250; (*open triangle, filled triangle*) $i = 153\,\text{A m}^{-2}$, Re = 3,500; (*open square, filled square*) $i = 153\,\text{A m}^{-2}$, Re = 13,250; and (*open diamond, filled diamond*) $i = 305\,\text{A m}^{-2}$, Re = 3,500 (Polcaro et al. 2003)

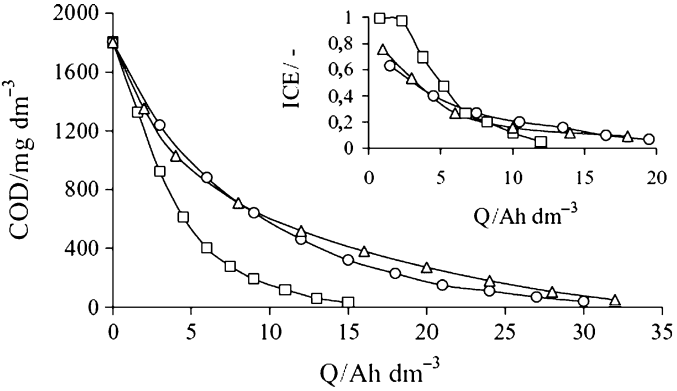

Fig. 2.12 Comparison of the trend of COD and ICE (*inset*) during the oxidation of 2-naphthol at the (*open circle*) Ti/PbO_2 anode, $i = 25\,\text{mA cm}^{-2}$; flow rate $180\,\text{dm}^3\,\text{h}^{-1}$; the (*open square*) BDD anode; $i = 25\,\text{mA cm}^{-2}$; flow rate $180\,\text{dm}^3\,\text{h}^{-1}$; and the (*open triangle*) Ti–Ru–Sn ternary oxide anode, NaCl = $7.5\,\text{g dm}^{-3}$; $i = 50\,\text{mA cm}^{-2}$; flow rate $180\,\text{dm}^3\,\text{h}^{-1}$. (Panizza and Cerisola 2004b)

Si/BDD electrodes are able to achieve faster oxidation and better incineration efficiency than Ti/PbO_2 in the treatment of naphthol (Panizza and Cerisola 2004b) (Fig. 2.12), 4-chlorophenol (Gherardini et al. 2001), and chloranilic acid (Martinez-Huitle et al. 2004b).

Diamond electrodes have also been studied with the aim of developing highly efficient electrochemical processes for water disinfection for domestic water treatment purposes or industrial water cooling systems. The good electrochemical stability and high overpotential for water electrolysis allows the production of a mixture of very strong oxidants under several disinfection mechanisms, without using any chemicals. In fact, besides hydroxyl radicals and hydrogen peroxide, directly produced by the water, the presence of chlorides, sulfates, and carbonates induces a very efficient generation of free chlorine, peroxodisulfate, and percarbonates, respectively (Rychen et al. 2003).

However, despite the numerous advantages of diamond electrodes, their high cost and the difficulties in finding an appropriate substrate on which to deposit the thin diamond layer are their major drawbacks. In fact, stable diamond films can really only be deposited on Silicon, Tantalum, Niobium, and Tungsten, but these materials are not suitable for large-scale use. In fact, a silicon substrate is very brittle and its conductivity is poor and Tantalum, Niobium, and Tungsten are too expensive. Titanium possesses good electrical conductivity, sufficient mechanical strength, electrochemical inertness, and is inexpensive. However, the stability of the diamond layer deposited on the Titanium substrate is still not satisfactory, because cracks may appear and may cause the detachment of the diamond film during long-term electrolysis.

2.5 Conclusions

This paper has presented and briefly discussed the performance of different electrode materials for the electrochemical oxidation of organic pollutants for wastewater treatment. Literature results have demonstrated that anodes with low oxygen evolution overpotential, such as graphite, IrO_2, RuO_2, or Pt only permit the primary oxidation of organics (i.e., conversion), but not the complete mineralization, due to the accumulation of oxidation intermediates, mainly aliphatic acids, which are quite stable against further attack at these electrodes.

The complete mineralization of the organics to CO_2 and good Faradic efficiency can be obtained using high oxygen overpotential anodes, such as SnO_2, PbO_2, and BDD, because these electrodes involve the production of oxygen evolution intermediates, mainly hydroxyl radicals, that nonselectively oxidize the organic pollutants and their intermediates.

Despite their notable ability to remove organics, doped-SnO_2 anodes have the major drawback of a short service life that limits their practical applications and, consequently, ways to improve the service life of these anodes is now under investigation.

Even the application of Ti/PbO_2 anodes to wastewater treatment may be limited by the possible release of toxic lead ions, due to their dissolution under specific anodic polarization and solution composition.

On the contrary, conducting diamonds offer significant advantages over other electrode materials in terms of current efficiency and stability for a variety of

electrochemical processes. However, further improvements, such as finding an appropriate substrate on which to deposit the thin diamond layer and the reduction of production costs, are required before their wide industrial application.

Acknowledgments The author wishes to express his sincere thanks to Prof. Giacomo Cerisola for his helpful discussions during the preparation of this article and to the journals and all the authors who gave permission for the reproduction of figures and tables.

References

Alvarez-Gallegos, A. and Pletcher, D. (1998) Removal of low level organics via hydrogen peroxide formed in a reticulated vitreous carbon cathode cell, Part 1. The electrosynthesis of hydrogen peroxide in aqueous acidic solutions. Electrochim. Acta 44, 853–861.

Alvarez-Gallegos, A. and Pletcher, D. (1999) The removal of low level organics via hydrogen peroxide formed in a reticulated vitreous carbon cathode cell, Part 2. The removal of phenols and related compounds from aqueous solutions. Electrochim. Acta 44, 2483–2492.

Awad, Y. M. and Abuzaid, N. S. (1997) Electrochemical treatment of phenolic wastewater: Efficiency, design considerations and economic evaluation. J. Environ. Sci. Health A 32, 1393–1414.

Awad, Y. M. and Abuzaid, N. S. (1999) Electrochemical oxidation of phenol using graphite anodes. Sep. Sci. Technol. 34, 699–708.

Awad, Y. M. and Abuzaid, N. S. (2000) Influence of residence time on the anodic oxidation of phenol. Sep. Purif. Technol. 18, 227–236.

Beer, H. B. (1966) US Patent Appl. 549 194.

Bellagamba, R., Michaud, P. A., Comninellis, C. and Vatistas, N. (2002) Electro-combustion of polyacrylates with boron-doped diamond anodes. Electrochem. Commun. 4, 171–176.

Bock, C. and MacDougall, B. (1999) Anodic oxidation of p-benzoquinone and maleic acid. J. Electrochem. Soc. 146, 2925–2932.

Bock, C. and MacDougall, B. (2000) Influence of metal oxide properties on the oxidation of organics. J. Electroanal. Chem. 491, 48–54.

Bonfatti, F., Ferro, S., Lavezzo, F., Malacarne, M., Lodi, G. and De Battisti, A. (1999) Electrochemical incineration of glucose as a model organic substrate. I. Role of the electrode material. J. Electrochem. Soc. 146, 2175–2179.

Bonfatti, F., De Battisti, A., Ferro, S., Lodi, G. and Osti, S. (2000a) Anodic mineralization of organic substrates in chloride-containing aqueous media. Electrochim. Acta 46, 305–314.

Bonfatti, F., Ferro, S., Lavezzo, F., Malacarne, M., Lodi, G. and De Battisti, A. (2000b) Electrochemical incineration of glucose as a model organic substrate. II. Role of active chlorine mediation. J. Electrochem. Soc. 147, 592–596.

Boudenne, J. L. and Cerclier, O. (1999) Performance of carbon black-slurry electrodes for 4-chlorophenol oxidation. Water Res. 33, 494–504.

Boudenne, J. L., Cerclier, O., Galea, J. and Vlist, E. V. D. (1996) Electrochemical oxidation of aqueous phenol at a carbon black slurry electrode. Appl. Catal. A: General 143, 185–202.

Boye, B., Dieng, M. M. and Brillas, E. (2002) Degradation of herbicide 4-chlorophenoxyacetic acid by advanced electrochemical oxidation methods. Environ. Sci. Technol. 36, 3030–3035.

Brillas, E., Bastida, R. M., Llosa, E. and Casado, J. (1995) Electrochemical destruction of aniline and chloroaniline for wastewater treatment using a carbon PTFE O_2-fed cathode. J. Electrochem. Soc. 142, 1733–1741.

Brillas, E., Mur, E. and Casado, J. (1996) Iron(II) catalysis of the mineralization of aniline using a carbon-PTFE O_2-fed cathode. J. Electrochem. Soc. 143, L49–L53.

Brillas, E., Boye, B. and Dieng, M. M. (2003) Peroxi-coagulation and photoperoxi-coagulation treatments of the herbicide 4-chlorophenoxyacetic acid in aqueous medium using an oxygen-diffusion cathode. J. Electrochem. Soc. 150, E148–E154.

Brillas, E., Boye, B., Sires, I., Garrido, J. A., Rodriguez, R. M., Arias, C., Cabot, P. L. and Comninellis, C. (2004) Electrochemical destruction of chlorophenoxy herbicides by anodic oxidation and electro-Fenton using a boron-doped diamond electrode. Electrochim. Acta 49, 4487–4496.

Canizares, P., Dominguez, J. A., Rodrigo, M. A., Villasenor, J. and Rodriguez, J. (1999) Effect of the current intensity in the electrochemical oxidation of aqueous phenol wastes at an activated carbon and steel anode. Ind. Eng. Chem. Res. 38, 3779–3785.

Canizares, P., Diaz, M., Dominguez, J. A., Garcia-Gomez, J. and Rodrigo, M. A. (2002) Electrochemical oxidation of aqueous phenol wastes on synthetic diamond thin-film electrodes. Ind. Eng. Chem. Res. 41, 4187–4194.

Canizares, P., Garcia-Gomez, J., Lobato, J. and Rodrigo, M. A. (2003a) Electrochemical oxidation of aqueous carboxylic acid wastes using diamond thin-film electrodes. Ind. Eng. Chem. Res. 42, 956–962.

Canizares, P., Garcia-Gomez, J., Saez, C. and Rodrigo, M. A. (2003b) Electrochemical oxidation of several chlorophenols on diamond electrodes: Part I. Reaction mechanism. J. Appl. Electrochem. 33, 917–927.

Canizares, P., Garcia-Gomez, J., Saez, C. and Rodrigo, M. A. (2004a) Electrochemical oxida-tion of several chlorophenols on diamond electrodes: Part II. Influence of waste character-istics and operating conditions. J. Appl. Electrochem. 34, 87–94.

Canizares, P., Saez, C., Lobato, J. and Rodrigo, M. A. (2004b) Electrochemical treatment of 2,4-dinitrophenol aqueous wastes using boron-doped diamond anodes. Electrochim. Acta 49, 4641–4650.

Canizares, P., Saez, C., Lobato, J. and Rodrigo, M. A. (2004c) Electrochemical treatment of 4-nitrophenol-containing aqueous wastes using boron-doped diamond anodes. Ind. Eng. Chem. Res. 43, 1944–1951.

Chang, H. and Johnson, D. C. (1990) Electrocatalysis of anodic oxygen-transfer reactions. J. Electrochem. Soc. 137, 2452–2457.

Chen, G. (2004) Electrochemical technologies in wastewater treatment. Sep. Purif. Technol. 38, 11–41.

Chen, G., Chen, X. and Yue, P. L. (2002) Electrochemical behavior of novel $Ti/IrO_x - Sb_2O_5 - SnO_2$ anodes. J. Phys. Chem. B 106, 4364–4369.

Chen, X., Chen, G., Gao, F. and Yue, P. L. (2003) High-performance Ti/BDD electrodes for pollutant oxidation. Environ. Sci. Technol. 21, 5021–5026.

Chiang, L. C., Chang, J. E. and Wen, T. C. (1995) Indirect oxidation effect in electrochemical oxidation treatment of landfill leachate. Water Res. 29, 671–678.

Comninellis, C. (1994) Electrocatalysis in the electrochemical conversion/combustion of organic pollutants for waste water treatment. Electrochim. Acta 39, 1857–1862.

Comninellis, C. and De Battisti, A. (1996) Electrocatalysis in anodic oxidation of organics with simultaneous oxygen evolution. J. Chim. Phys. 93, 673–679.

Comninellis, C. and Nerini, A. (1995) Anodic oxidation of phenol in the presence of NaCl for wastewater treatment. J. Appl. Electrochem. 25, 23–28.

Comninellis, C. and Pulgarin, C. (1991) Anodic oxidation of phenol for wastewater treatment. J. Appl. Electrochem. 21, 703–708.

Comninellis, C. and Pulgarin, C. (1993) Electrochemical oxidation of phenol for wastewater treatment using SnO_2 anodes. J. Appl. Electrochem. 23, 108–112.

Comninellis, C., Duo, I., Michaud, P. A., Marselli, B. and Park, S. M. (2005) Application of syhthetic boron-doped diamond electrodes in electrooxidation processes. In: A. Fujishima, Y. Einaga, T. N. Rao and D. A. Tryk (Eds.), *Diamond Electrochemistry. Elsevier*, Amsterdam, pp. 449–476.

Correa-Lozano, B., Comninellis, C. and De Battisti, A. (1997) Service life of $Ti/SnO_2 - Sb_2O_5$ anodes. J. Appl. Electrochem. 27, 970–974.

Cossu, R., Polcaro, A. M., Lavagnolo, M. C., Mascia, M., Palmas, S. and Renoldi, F. (1998) Electrochemical treatment of landfill leachate: Oxidation at Ti/PbO_2 and Ti/SnO_2 anodes. Ind. Eng. Chem. Res. 32, 3570–3573.

Dhooge, P. M. and Park, S. M. (1983) Electrochemistry of coal slurries - 2. Studies on various experimental parameters affecting oxidation of coal slurries. J. Electrochem. Soc. 130, 1029–1036.

Do, J. S. and Chen, C. P. (1993) In situ oxidative degradation of formaldehyde with electrogenerated hydrogen peroxide. J. Electrochem. Soc. 140, 1632–1637.

Do, J. S. and Chen, C. P. (1994a) In situ oxidative degradation of formaldehyde with hydrogen peroxide electrogenerated on the modified graphite. J. Appl. Electrochem. 24, 936–942.

Do, J. S. and Chen, C. P. (1994b) Kinetics of in situ oxidative degradation of formaldehyde with electrogenerated hydrogen peroxide. Ind. Eng. Chem. Res. 33, 387–394.

Do, J. S. and Yeh, W. C. (1995) In situ degradation of formaldehyde with electrogenerated hypochlorite ion. J. Appl. Electrochem. 25, 483–489.

Do, J. S., Yeh, W. C. and Chao, I. Y. (1997) Kinetic of the oxidative degradation of formaldehyde with electrogen hypochlorite. Ind. Eng. Chem. Res. 36, 349–356.

Farmer, J. C., Wang, F. T., Hawley-Fedder, R. A., Lewis, P. R., Summers, L. J. and Foiles, L. (1992) Electrochemical treatment of mixed and hazardous wastes: Oxidation of ethylene glycole and benzene by silver(II). J. Electrochem. Soc. 139, 654–662.

Feng, Y. J. and Li, X. Y. (2003) Electro-catalytic oxidation of phenol on several metal-oxide electrodes in aqueous solution. Water Res. 37, 2399–2407.

Feng, J., Johnson, D. C., Lowery, S. N. and Carey, J. (1994) Electrocatalysis of anodic oxygen-transfer reactions evolution of ozone. J. Electrochem. Soc. 141, 2708–2711.

Feng, J., Houk, L. L., Johnson, D. C., Lowery, S. N. and Carey, J. J. (1995) Electrocatalysis of anodic oxygen-transfer reactions: The electrochemical incineration of benzoquinone. J. Electrochem. Soc. 142, 3626–3632.

Fernandes, A., Morao, A., Magrinho, M., Lopes, A. and Goncalves, I. (2004) Electrochemical degradation of C. I. Acid Orange 7. Dyes Pigm. 61, 287–296.

Foller, P. C. and Tobias, C. W. (1982) The anodic evolution of ozone. J. Electrochem. Soc. 129, 506–515.

Foti, G., Gandini, D. and Comninellis, C. (1997) Anodic oxidation of organics on thermally prepared oxide electrodes. Curr. Top. Electrochem. 5, 71–91.

Foti, G., Gandini, D., Comninellis, C., Perret, A. and Haenni, W. (1999) Oxidation of organics by intermediates of water discharge on IrO_2 and synthetic diamond anodes. Electrochem. Solid State Lett. 2, 228–230.

Gandini, D., Comninellis, C., Perret, A. and Haenni, W. (1999) Anodic oxidation of organics on synthetic diamond thin-film electrodes. ICHEME Symp. Series 145, 181–190.

Gandini, D., Mahe, E., Michaud, P. A., Haenni, W., Perret, A. and Comninellis, C. (2000) Oxidation of carboxylic acids at boron-doped diamond electrodes for wastewater treatment. J. Appl. Electrochem. 30, 1345–1350.

Gattrell, M. and Kirk, D. (1990) The electrochemical oxidation of aqueous phenol at a glassy carbon electrode. Can. J. Chem. Eng. 68, 997–1003.

Gattrell, M. and Kirk, D. (1993) A study of the oxidation of phenol at platinum and preoxidized platinum surfaces. J. Electrochem. Soc. 140, 1534–1540.

Gherardini, L., Michaud, P. A., Panizza, M., Comninellis, C. and Vatistas, N. (2001) Electrochemical oxidation of 4-chlorophenol for wastewater treatment. Definition of normalized current efficiency. J. Electrochem. Soc. 148, D78.

Grimm, J. H., Bessarabov, D. G., Simon, U. and Sanderson, R. D. (2000) Characterization of doped tin dioxide anodes prepared by a sol-gel technique and their application in an SPE-reactor. J. Appl. Electrochem. 30, 293–302.

Guivarch, E., Oturan, N. and Oturan, M. A. (2003) Removal of organophosphorus pesticides from water by electrogenerated Fenton's reagent. Environ. Chem. Lett. 1, 165–168.

Hattori, S., Doi, M., Takahashi, E., Kurosu, T., Nara, M., Nakamatsu, S., Nishiki, Y., Furuta, T. and Iida, M. (2003) Electrolytic decomposition of amaranth dyestuff using diamond electrodes. J. Appl. Electrochem. 33, 85–91.

Houk, L. L., Johnson, S. K., Feng, J., Houk, R. S. and Johnson, D. C. (1998) Electrochemical incineration of benzoquinone in aqueous media using a quaternary metal oxide electrode in the absence of a soluble supporting electrolyte. J. Appl. Electrochem. 28, 1167–1177.

Iniesta, J., Michaud, P. A., Panizza, M., Cerisola, G., Aldaz, A. and Comninellis, C. (2001a) Electrochemical oxidation of phenol at boron-doped diamond electrode. Electrochim. Acta 46, 3573–3578.

Iniesta, J., Michaud, P. A., Panizza, M. and Comninellis, C. (2001b) Electrochemical oxidation of 3-methylpyridine at a boron-doped diamond electrode: Application to electroorganic synthesis and wastewater treatment. Electrochem. Commun. 3, 346–351.

Iniesta, J., Exposito, E., Gonzalez-Garcia, J., Montiel, V. and Aldaz, A. (2002) Electrochemical treatment of industrial wastewater containing phenols. J. Electrochem. Soc. 149, D57-D62.

Israilides, C. J., Vlyssides, A. G., Mourafeti, V. N. and Karvouni, G. (1997) Olive oil waste-water treatment with the use of an electrolysis system. Bioresource Technol. 61, 163–170.

Johnson, S. K., Houk, L. L., Feng, J., Houk, R. S. and Johnson, D. C. (1999) Electrochemical incineration of 4-chlorophenol and the identification of products and intermediates by mass spectrometry. Environ. Sci. Technol. 33, 2638–2644.

Kawagoe, K. T. and Johnson, D. C. (1994) Electrocatalysis of anodic oxygen-transfer reactions. Oxidation of phenol and benzene at bismuth-doped lead dioxide electrodes in acidic solutions. J. Electrochem. Soc. 141, 3404–3409.

Keech, P. G. and Bunce, N. J. (2003) Electrochemical oxidation of simple indoles at a PbO_2 anode. J. Appl. Electrochem. 33, 79–83.

Kirk, D., Sharifian, H. and Foulkes, F. R. (1985) Anodic oxidation of aniline for waste water treatment. J. Appl. Electrochem. 15, 285–292.

Kotz, R., Stucki, S. and Carcer, B. (1991) Electrochemical wastewater treatment using high overvoltage anodes. Part I: physical and electrochemical properties of SnO_2 anodes. J. Appl. Electrochem. 21, 14–20.

Kraft, A., Stadelmann, M. and Blaschke, M. (2003) Anodic oxidation with doped diamond electrodes: A new advanced oxidation process. J. Hazard. Mater. 103, 247–261.

Lamy, C. (1984) Electrocatalytic oxidation of organic compounds on noble metals in aqueous solution. Electrochim. Acta 29, 1581–1588.

Lamy, C., Leger, J. M., Clavilier, J. and Parsons, R. (1983) Structural effects in electrocatalysis: A comparative study of the oxidation of CO, HCOOH and CH_3OH on single crystal Pt electrodes. J. Electroanal. Chem. 150, 71–77.

Lanza, M. R. V. and Bertazzoli, R. (2002) Cyanide oxidation from wastewater in a flow electrochemical reactor. Ind. Eng. Chem. Res. 41, 22–26.

Leffrang, U., Ebert, K., Flory, K., Galla, U. and Schmeider, H. (1995) Organic waste destruction by indirect electrooxidation. Sep. Purif. Technol. 30, 1883–1899.

Li, X.-y., Cui, Y.-h., Feng, Y.-j., Xie, Z.-m. and Gu, J.-D. (2005) Reaction pathways and mechanisms of the electrochemical degradation of phenol on different electrodes. Water Res. 39, 1972–1981.

Lin, S. H. and Chen, M. L. (1997) Treatment of textile wastewater by chemical methods for reuse. Water Res. 31, 868–876.

Lipp, L. and Pletcher, D. (1997) Preparation and characterization of tin dioxide coated titanium electrodes. Electrochim. Acta 42, 1091–1099.

Lissens, G., Pieters, J., Verhaege, M., Pinoy, L. and Verstraete, W. (2003) Electrochemical degradation of surfactants by intermediates of water discharge at carbon-based electrodes. Electrochim. Acta 48, 1655–1663.

Malpass, G. R. P., Neves, R. S. and Motheo, A. J. (2006) A comparative study of commercial and laboratory-made $Ti/Ru_{0.3}Ti_{0.7}O_2$ DSA electrodes: "In situ" and "ex situ" surface characterisation and organic oxidation activity. Electrochim. Acta 52, 936–944.

Marselli, B., Garcia-Gomez, J., Michaud, P. A., Rodrigo, M. A. and Comninellis, C. (2003) Electrogeneration of hydroxyl radicals on boron-doped diamond electrodes. J. Electrochem. Soc. 150, D79–D83.

Martinez-Huitle, C. A., Ferro, S. and De Battisti, A. (2004a) Electrochemical incineration of oxalic acid: Role of electrode material. Electrochim. Acta 49, 4027–4034.

Martinez-Huitle, C. A., Quiroz, M. A., Comninellis, C., Ferro, S. and De Battisti, A. (2004b) Electrochemical incineration of chloranilic acid using Ti/IrO_2, Pb/PbO_2 and Si/BDD electrodes. Electrochim. Acta 50, 949–956.

Martinez-Huitle, C. A., Ferro, S. and De Battisti, A. (2005) Electrochemical incineration in the presence of halides. Electrochem. Solid State Lett. 8, 35–39.

Montilla, F., Michaud, P. A., Morallon, E., Vazquez, J. L. and Comninellis, C. (2002) Electrochemical oxidation of benzoic acid at boron-doped diamond electrodes. Electrochim. Acta 47, 3509–3513.

Morao, A., Lopes, A., Amorim, M. T. P. d. and Goncalves, I. C. (2004) Degradation of mixtures of phenols using boron doped diamond electrodes for wastewater treatment. Electrochim. Acta 49, 1587–1595.

Naumczyk, J., Szpyrkowicz, L. and Zillio-Grandi, F. (1996) Electrochemical treatment of textile wastewater. Water Sci. Technol. 34, 17–24.

Nelson, N. (2002) Electrochemical destruction of organic hazardous wastes. Plainum Met. Rev. 46, 18–23.

Ogutveren, U. B., Toru, E. and Koparal, S. (1999) Removal of cyanide by anodic oxidation for wastewater treatment. Water Res. 33, 1851–1856.

Panizza, M. and Cerisola, G. (2001) Removal of organic pollutants from industrial wastewater by electrogenerated Fenton's reagent. Water Res. 35, 3987–3992.

Panizza, M. and Cerisola, G. (2003a) Electrochemical oxidation of 2-naphthol with in situ electrogenerated active chlorine. Electrochim. Acta 48, 1515–1519.

Panizza, M. and Cerisola, G. (2003b) Influence of anode material on the electrochemical oxidation of 2-naphthol. Part 1. Cyclic voltammetry and potential step experiments. Electrochim. Acta 48, 3491–3497.

Panizza, M. and Cerisola, G. (2004a) Electrochemical oxidation as final treatment of synthetic tannery wastewater. Environ. Sci. Technol. 38, 5470–5475.

Panizza, M. and Cerisola, G. (2004b) Influence of anode material on the electrochemical oxidation of 2-naphthol: Part 2. Bulk electrolysis experiments. Electrochim. Acta 49, 3221–3226.

Panizza, M. and Cerisola, G. (2005) Application of diamond electrodes to electrochemical processes. Electrochim. Acta 51, 191–199.

Panizza, M. and Cerisola, G. (2006a) Electrochemical oxidation of aromatic sulphonated acids on a boron-doped diamond electrode. Int. J. Environ. Pollut. 27, 64–74.

Panizza, M. and Cerisola, G. (2006b) Electrochemical processes for the treatment of organic pollutants. In: D. V. Zinger (Eds.), *Advances in Chemistry Research*, Vol. 2. Nova Science, New York, NY, pp. 1–38.

Panizza, M. and Cerisola, G. (2006c) Olive mill wastewater treatment by anodic oxidation with parallel plate electrodes. Water Res. 40, 1179–1184.

Panizza, M., Bocca, C. and Cerisola, G. (2000) Electrochemical treatment of wastewater containing poliaromatic organic pollutants. Water Res. 34, 2601–2605.

Panizza, M., Michaud, P. A., Cerisola, G. and Comninellis, C. (2001a) Anodic oxidation of 2-naphthol at boron-doped diamond electrodes. J. Electroanal. Chem. 507, 206.

Panizza, M., Michaud, P. A., Cerisola, G. and Comninellis, C. (2001b) Electrochemical treatment of wastewater containing organic pollutants on boron-doped diamond electrodes. Prediction of specific energy consumption and required electrode area. Electrochem. Commun. 3, 336.

Panizza, M., Delucchi, M. and Cerisola, G. (2005) Electrochemical degradation of anionic surfactants. J. Appl. Electrochem. 35, 357–361.

Perret, A., Haenni, W., Skinner, N., Tang, X. M., Gandini, D., Comninellis, C., Correa, B. and Foti, G. (1999) Electrochemical behavior of synthetic diamond thin film electrodes. Diam. Relat. Mater. 8, 820–823.

Piya-areetham, P., Shenchunthichai, K. and Hunsom, M. (2006) Application of electrooxidation process for treating concentrated wastewater from distillery industry with a voluminous electrode. Water Res. 40, 2857–2864.

Pletcher, D. and Walsh, F. C. (1982) *Industrial Electrochemistry*. Chapman and Hall, London.

Polcaro, A. M. and Palmas, S. (1997) Electrochemical oxidation of chlorophenols. Ind. Eng. Chem. Res., 1791–1798.

Polcaro, A. M., Palmas, S., Renoldi, F. and Mascia, M. (1999) On the performance of Ti/SnO_2 and Ti/PbO_2 anodes in electrochemical degradation of 2-chlorophenol for wastewater treatment. J. Appl. Electrochem. 29, 147–151.

Polcaro, A. M., Palmas, S., Renoldi, F. and Mascia, M. (2000) Three-dimensional electrodes for the electrochemical combustion of organic pollutants. Electrochim. Acta 46, 389–394.

Polcaro, A. M., Vacca, A., Palmas, S. and Mascia, M. (2003) Electrochemical treatment of wastewater containing phenolic compounds: Oxidation at boron-doped diamond electrodes. J. Appl. Electrochem. 33, 885–892.

Polcaro, A. M., Vacca, A., Mascia, M. and Palmas, S. (2005) Oxidation at boron doped diamond electrodes: An effective method to mineralise triazines. Electrochim. Acta 50, 1841–1847.

Ponce-de-Leon, C. and Pletcher, D. (1995) Removal of formaldehyde from aqueous solutions via oxygen reduction using a reticulated vitreous carbon cathode cell. J. Appl. Electrochem. 25, 307–314.

Pulgarin, C., Adler, N., Peringer, P. and Comninellis, C. (1994) Electrochemical detoxification of a 1,4-benzoquinone solution in wastewater treatment. Water Res. 28, 887–893.

Rajeshwar, K. and Ibanez, J. G. (1997) *Environmental Electrochemistry. Fundamentals and Applications in Pollution Abatement*. Academic, London.

Rajeshwar, K., Ibanez, J. G. and Swain, G. M. (1994) Electrochemistry and environment. J. Appl. Electrochem. 24, 1077–1091.

Rodgers, J. D., Jedral, W. and Bunce, N. J. (1999) Electrochemical oxidation of chlorinated phenols. Environ. Sci. Technol. 33, 1453–1457.

Rodrigo, M. A., Michaud, P. A., Duo, I., Panizza, M., Cerisola, G. and Comninellis, C. (2001) Oxidation of 4-Chlorophenol at boron-doped diamond electrodes for wastewater treatment. J. Electrochem. Soc. 148, D60–D64.

Rychen, P., Pupunat, L., Haenni, W. and Santoli, E. (2003) Water treatment applications with BDD electrodes and the DiaCell concept. New Diam. Front. Carbon Technol. 13, 109–117.

Saracco, G., Solarino, L., Aigotti, R., Specchia, V. and Maja, M. (2000) Electrochemical oxidation of organic pollutants at low electrolyte concentrations. Electrochim. Acta 46, 373–380.

Sharifian, H. and Kirk, D. (1986) Electrochemical oxidation of phenol. J. Electrochem. Soc. 113, 921–924.

Simond, O., Schaller, V. and Comninellis, C. (1997) Theoretical model for the anodic oxidation of organics on metal oxide electrodes. Electrochim. Acta 42, 2009–2012.

Smith-de-Sucre, V. and Watkinson, A. P. (1981) Anodic oxidation of phenol for wastewater treatment. Can. J. Chem. Eng. 59, 52–59.

Socha, A., Chrzescijanska, E. and Kusmierek, E. (2005) Electrochemical and photoelectrochemical treatment of 1-aminonaphthalene-3,6-disulphonic acid. Dyes Pigm. 67, 71–75.

Soriaga, M. P. and Hubbard, A. T. (1982) Determination of the orientation of adsorbed molecules at solid–liquid interfaces by thin-layer electrochemistry: Aromatic compounds at platinum electrodes. J. Am. Chem. Soc. 104, 2735–2742.

Stucki, S., Kotz, R., Carcer, B. and Suter, W. (1991) Electrochemical wastewater treatment using high overvoltage anodes. Part II: Anode performance and applications. J. Appl. Electrochem. 21, 99–104.

Szpyrkowicz, L., Naumczyk, J. and Zilio-Grandi, F. (1995) Electrochemical treatment of tannery wastewater using Ti/Pt and Ti/Pt/Ir electrodes. Water Res. 29, 517–524.

Szpyrkowicz, L., Juzzolino, C., Kaul, S. N., Daniele, S. and DeFaveri, M. (2000) Electro-chemical oxidation of dyeing baths bearing disperse dyes. Ind. Eng. Chem. Res. 39, 3241–3248.

Szpyrkowicz, L., Kelsall, G. H., Kaul, S. N. and DeFaveri, M. (2001) Performance of electrochemical reactor for treatment of tannery wastewaters. Chem. Eng. Sci. 56, 1579–1586.

Tahar, N. B. and Savall, A. (1998) Mechanistic aspects of phenol electrochemical degradation by oxidation on a Ta/PbO_2 anode. J. Electrochem. Soc. 145, 3427–3434.

Tahar, N. B. and Savall, A. (1999a) A comparison of different lead dioxide coated electrodes for the electrochemical destruction of phenol. J. New Mat. Electr. Sys. 2, 19–26.

Tahar, N. B. and Savall, A. (1999b) Electrochemical degradation of phenol in aqueous solution on bismuth doped lead dioxide: A comparison of the activities of various electrode formulations. J. Appl. Electrochem. 29, 277–283.

Tatapudi, P. and Fenton, J. M. (1993) Synthesis of ozone in a proton exchange membrane electrochemical reactor. J. Electrochem. Soc. 140, 3527–3530.

Troster, I., Fryda, M., Herrmann, D., Schafer, L., Haenni, W., Perret, A., Blaschke, M., Kraft, A. and Stadelmann, M. (2002) Electrochemical advanced oxidation process for water treatment using DiaChem electrodes. Diam. Relat. Mater. 11, 640–645.

Vicent, F., Morallon, E., Quijada, C., Vazquez, J. L., Aldaz, A. and Cases, F. (1998) Characterization and stability of doped SnO_2 anodes. J. Appl. Electrochem. 28, 607–612.

Vlyssides, A. G. and Israilides, C. J. (1997) Detoxification of tannery waste liquors with an electrolysis system. Environ. Pollut. 97, 147–152.

Vlyssides, A. G., Papaioannou, D., Loizidoy, M., Karlis, P. K. and Zorpas, A. A. (2000) Testing an electrochemical method for treatment of textile dye wastewater. Waste Manage. 20, 569–574.

Vlyssides, A. G., Karlis, P. K. and Mahnken, G. (2003) Influence of various parameters on the electrochemical treatment of landfill leachates. J. Appl. Electrochem. 33, 155–159.

Yang, C. H., Lee, C. C. and Wen, T. C. (2000) Hypochlorite generation on Ru–Ti binary oxide for the treatment of dye wastewater. J. Appl. Electrochem. 30, 1043–1051.

Zanta, C. L. P. S., Andrade, A. R. d. and Boodts, J. F. C. (2000) Electrochemical behaviour of olefins: Oxidation at ruthenium-titanium dioxide and iridium-titanium dioxide coated electrodes. J. Appl. Electrochem., 467–474.

Zanta, C. L. P. S., Michaud, P. A., Comninellis, C., Andrade, A. R. D. and Boodts, J. F. C. (2003) Electrochemical oxidation of p-chlorophenol on SnO_2-Sb_2O_5 based anodes for wastewater treatment. J. Appl. Electrochem. 33, 1211–1215.

Chapter 3
Techniques of Electrode Fabrication

Liang Guo, Xinyong Li, and Guohua Chen

3.1 Thermal Decomposition Method

Metal oxides belong to a class of widely used catalysts. Application of the metal oxide electrodes expands into several areas, including environmental decontamination, analytical chemistry, fuel cells, materials science and catalysis, microelectronics, etc. (Fierro 2006). In this part, the fabrication of these electrodes applied in environmental decontamination field, mainly for pollutant mineralization and gas evolution, will be discussed.

Dimensional stable anodes (DSAs) are such kind of catalytic electrodes, which consist of a mixture of metal oxides coated on metal, mainly titanium, substrate. Large-scale use of DSAs in chlor-alkali electrolysis industry came in the 1960s when Henri Beer invented this type of electrodes (Beer 1968, 1969, 1972, 1973). In the Journal of Electrochemical Society in 1980, Henri Beer reviewed his research and development on DSAs and the further industrial applications of the electrodes (Beer 1980). Due to the high stability under high current density loading and high electrical efficiency for chlorine gas production, mixed oxide of ruthenium and titanium on titanium substrate has become the most useful electrode in industrial application (Beer 1980). High stability means long working life time with stable working performance and little contamination to the environment from the dissolving of the metal oxides. High electrical efficiency is closely related with the electrocatalysis performance. Oxygen and chlorine gas evolution reactions are two competitive steps in chlor-alkali process. High-quality electrodes can improve the electrocatalytic activity of the desired reactions, such as chlorine gas evolution, but depress the electrocatalytic activity of the side reactions, such as oxygen gas evolution. Even for very low chloride concentrations, chlorine formation occurs on Ir–Ru oxide electrode and side reactions show significantly lower efficiency in this case (Bergmann and Koparal 2005). Bergmann and coworkers demonstrated that Ir–Ru

G. Chen (✉)
Chemical and Biomolecular Engineering Department, The Hong Kong University of Science and Technology, Clear Water Bay, Kowloon, Hong Kong
e-mail: kechengh@ust.hk

C. Comninellis and G. Chen (eds.), *Electrochemistry for the Environment*,
DOI 10.1007/978-0-387-68318-8_3,

oxide have a higher chlorine production efficiency than IrO_2 anodes (Bergmann et al. 2002). High stability and high electrocatalysis performance are the two most important research topics for studying or developing electrodes.

Modified DSA-type electrodes have been developed recently. For example, iridium oxides have been investigated as electroactive component for the oxygen evolution reaction (Kotz and Stucki 1986; Rolewicz et al. 1988; Duby 1993; Ferrer and Victori 1994). Tantalum is the most suitable anode material owing to its high conductivity and excellent corrosion resistance in aggressive media because of its protective oxide film formation (Rolewicz et al. 1988; Comninellis and Vercesi 1991a; Cardarelli et al. 1998). DSA-type electrodes are becoming more interesting because proper selection of the material allows a good degree of reaction selectivity. In terms of the components, the DSA electrodes can be categorized into single metal-oxide, binary metal-oxide, and ternary or more phase metal-oxide electrodes. Furthermore, the proper combination of different metal oxides is known to show synergistic effects toward electron-transfer reactions and electrode stability. Its application has been broadened into various industrial and academic areas, in addition to the chlor-alkali industry.

More recently, DSA-type electrodes have been used for the mineralization of various organic molecules that constitute water pollutants. As pointed out in many publications, an indirect electrochemical oxidation may take place via mediators produced at metal-oxide electrodes surface during anodic polarization (Lyons et al. 1993; Lodowicks and Beck 1994). Treatment of dye and/or textile wastewater has been reported with DSA-type electrodes employed. Electrochemical discoloration and chemical oxygen demand (COD) degradation of textile dye wastewater containing various reactive, acidic or basic dyes were conducted by using titanium-based DSAs, including IrO_2, PbO_2, RuO_2, SnO_2, Ru–Pb–Sn oxide, Ti–Ta–Pt–Ir oxide, Ti–Ru–Sn–Sb oxide, and Bi-doped PbO_2 (Kim et al. 2003a; Awad and Galwa 2005; Yang et al. 2005b; Chatzisymeon et al. 2006; Da Silva et al. 2006; Mohan and Balasubramanian 2006; Rajkumar and Kim 2006; Rajkumar et al. 2007). Tin oxide is claimed to increase the overpotential for oxygen evolution and improve the anodic stability of precious metal oxides (Iwakura et al. 1981; Spasojevic et al. 1984). The rate of phenol removal was much higher on SnO_2 than on PbO_2 or Pt electrodes (Kotz et al. 1991). The SnO_2–Sb coating provides a catalytic function for rapid organic oxidation, compared with Ti/RuO_2 and Pt (Li et al. 2005). Comninellis proposed a simplified mechanism for the electrochemical oxidation or combustion of organics. Selective oxidation occurs with oxide anodes (MO_x) forming the higher oxide MO_{x+1} and combustion occurs with electrodes at the surface of which ·OH radicals are accumulated (Comninellis 1994).

Electrochemical disinfection systems have been studied by employing Ir–Sb–Sn oxide anode to inactivate bacteriophage MS2 in synthetic solutions with sodium chloride addition. Compared with chlorination, the EC disinfection system exhibited superior inactivation capability especially with a longer contact time or in the presence of ammonium (Fang et al. 2006). Inactivation of blue-green algae was successfully performed by the electrochemical treatment with RuO_2 anode (Liang et al. 2005). Electrochemical disinfection power is similar to that of ozone and much

stronger than that of chlorine. The major killing function of EC disinfection is proposed by short-lived and high-energy intermediate EC products, such as free radicals (Li et al. 2004).

Suspended solid (SS), heavy metals, and organic chemicals, especially oil and grease, can be removed from the wastewater with electroflotation (EF) technique using gas evolution DSA-type electrodes. EF has certain desirable characteristics, compared with dissolved and dispersed air flotation, particularly in regard to the small bubble size distribution of the process. O_2 evolution is a critical reaction when electrodes are working as gas evolution anodes. Only RuO_2 and IrO_2 have been thus far extensively investigated as anodes for O_2 evolution in acid solution. While RuO_2 is more active than IrO_2 (Angelinetta et al. 1989), the latter is much more corrosion resistant than the former (Kotz and Stucki 1986). In particular, $IrO_2 + Ta_2O_5$ mixed oxides are indicated as the most stable anodes for O_2 evolution in strong acid (Morimitsu et al. 2000). Accelerated life test showed that with addition of Sb–Sn the electrochemical stability of IrO_x anode was effectively improved (Chen et al. 2002b). With RuO_2 anode, removal efficiency of heavy metal from metal finishing plants wastewater can reach 98–99% (Khelifa et al. 2005). Dispersed oil was separated from oil-water emulsions by using RuO_2 gas evolution anode and the removal efficiency reached 70% at optimum conditions (Ben Mansour and Chalbi 2006). A combination of electrocoagulation (with sacrificed anode, mainly iron and aluminum) and electroflotation with Ir–Sb–Sn, and Ir–Ta oxide electrodes was designed to remove the total Cr from wastewater (Gao et al. 2005) and to treat restaurant wastewater (Chen et al. 2000).

DSA-type metal oxides can be prepared in various ways, but the most applied procedure in technology is the thermal decomposition of appropriate precursors, mainly metal chloride salts, dissolved in suitable solvents and painted on the metal substrates, mainly titanium (Trasatti 1991). The thermal decomposition method is preferred, due to its specialties of simple conduction and low cost. Figure 3.1 shows the schematic diagram for the metal-oxide electrodes fabrication process with thermal decomposition methods. Pretreatment on the metal substrate should be conducted before thermal deposition, in order to enhance the adhesion of produced metal oxide on the substrate. Normally, pretreatment process includes: first, thoroughly cleaning of the substrate by organic solvent and degreasing agent and

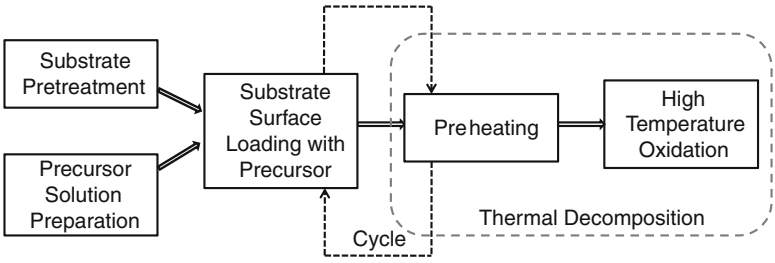

Fig. 3.1 Schematic diagram of thermal decomposition method for making DSA type electrodes

second, etching of the substrate in concentrated HCl at high temperature for 30 min to 1 h, to remove the original surface oxides and increase the surface roughness. The chemical composition, crystallinity and crystal grain size, surface morphology, electrical conductance, electrocatalysis performance, and electrode stability are determined by the precursor composition, solvents and loadings, substrate pretreatment, and thermal decomposition parameters especially the temperature and duration of the preparation and calcinations processes (Trasatti 1991; Santana et al. 2005).

3.1.1 Ruthenium-Oxide-Based Electrode (RuO_x)

The stock solution is prepared with $RuCl_3$ salt dissolved in 1:1 v/v HCl. The oxide electrodes can be prepared by carefully brushing the precursor solution on all sides of the etched Ti substrate, dried at 90°C for 10 min, sintered at 350°C for 10 min, and finally annealed at 350–650°C for 1 h (Kim et al. 2001). Nonstoichiometric oxide, RuO_x (a mixture of Ru^{3+} and Ru^{4+} in the oxide) (Galizzioli et al. 1974, 1975), shows catalytic performance supplying the sites to adsorb hydroxyl radicals from water, which convert to active hydroxyl radicals to destroy the organics (Trasatti 1980; Kinoshita 1992). It is reported that RuO_x exists the most when annealed at around 450°C, and disappears at 600°C (Kim et al. 2001). RuO_2-based electrodes are generally known to be unstable for O_2 evolution. In order to improve the electrode stability, Sb and Sn elements are added to make RuO_2-based $Ti/RuO_2–Sb_2O_5–SnO_2$ ternary oxide electrode (Chen and Chen 2005b). RuO_2 serves as the catalyst, SnO_2 as the dispersing agent, and Sb_2O_5 as the dopant. It is reported that the $Ti/RuO_2–Sb_2O_5–SnO_2$ electrode containing 12.2 mol% of RuO_2 nominally in the coating had a service life of 307 h in 3 M H_2SO_4 solution under a current density of 0.5 A cm^{-2} at 25°C, more than 15 times longer than other types of RuO_2-based electrodes (Chen and Chen 2005b).

3.1.2 Iridium-Oxide-Based Electrode (IrO_2)

The precursor solution (10 μl of 0.2 g $H_2IrCl_6 \cdot 6H_2O$ in 5-ml isopropanol) was spread onto the pretreated Ti-base metal surface. The sample was dried at 80°C for 10 min and then the dried layer was fired at 500°C for 10 min in a preheated oven. These steps were repeated ten times and followed by 1 h of annealing procedure at 500°C (Rolewicz et al. 1988). The performance of IrO_2 electrode for the catalytic oxidative mineralization to organics was evaluated related with the calcinations temperature. A sintering temperature of around 650°C enhanced the organic destruction rather than 400–550°C, and the electrode surface was sufficiently converted to IrO_2 from the precursor under the high temperature (Kim et al. 2002). In terms of electrode stability, IrO_2 presents a service life about 20 times longer than that of the equivalent RuO_2 as oxygen evolution anode (Alves et al. 1998). In

Chen's group, a ternary IrO_2-based electrode is investigated for O_2 evolution, where SnO_2 serves as a dispersing agent, Sb_2O_5 as a dopant, and IrO_2 as a catalyst (Chen et al. 2001, 2002a). Its good conductivity, compact structure, and high homogeneity with metastable solid solution nature make it more stable than IrO_2. The electrochemical stability and activity of the ternary oxide Ti/IrO_2–Sb_2O_5–SnO_2 electrodes prepared under different conditions were investigated (Chen and Chen 2005a). It was found that the calcination temperature and Sb and Ir contents could affect the stability and activity significantly. The optimal calcination temperature and Sb content are 550°C and 15 mol%, respectively. The stability and activity increased with an increase in the Ir content in the investigated range of 0–10 mol%. Physicochemical analysis showed that the ternary oxide coatings obtained were oxide solid solutions even at a Sb content of up to 25 mol% and had compact microstructure when Sb content was less than 15 mol%.

3.1.3 Tin-Dioxide-Based Electrode (SnO_2)

Tin dioxide crystallizes in a rutile-type structure and it is quite inert toward chemical etching with common acid or alkalis. With high-oxygen evolution overpotential, the main application of supported SnO_2-film electrodes is the electrochemical incineration of organic compounds in aqueous solutions. SnO_2 is frequently added to MO_2/TiO_2 (M = Ru or Ir) layers to enhance the electrochemical oxidation of organic compounds. These nonactive anode materials (Ti/SnO_2; Ti/PbO_2) show high efficiency in the complete oxidation of organic compounds to CO_2, due to the formation of hydroxyl radicals (Comninellis 1994). At 0.1 mA cm^{-2}, the oxygen evolution reaction potentials (vs. SCE) were 1.5 V (on Pt), 1.65 V (on PbO_2), and 1.95 V (on SnO_2). Kotz reported that the SnO_2 electrode presented a higher efficiency for the oxidation of phenol, compared with Pt and PbO_2 (Kotz et al. 1991; Stucki et al. 1991). Since $SnCl_4$ volatilization happens at temperatures above 114°C, the greatest difficulty in preparing electrodes containing Sn by this thermal decomposition process is the proper control of the amount of SnO_2 in the coating (Comninellis and Vercesi 1991b). Careful control of the preparation parameters is essential to maintain the desired SnO_2 content and enhance the deposition yield. The conductivity can be enhanced by the addition of an appropriate dopant such as In(III), Sb(V), or F into the SnO_2 film (Chopra et al. 1983). The most common dopant for the electrochemical oxidation application is Sb (Comninellis and Pulgarin 1993; Correa-Lozano et al. 1996; Lipp and Pletcher 1997; Vicent et al. 1998).

Sb-doped SnO_2 film electrode can be fabricated with the following procedure (Kotz et al. 1991; Lipp and Pletcher 1997). The coating solution was prepared with 20% w/v $SnCl_4 \cdot 5H_2O$, 0.2% w/v $SbCl_x$, and reagent grade 2-propanol. A thin layer of a solution was applied to the freshly pretreated Ti substrate at room temperature with a soft hair paintbrush. The excess alcohol was allowed to evaporate by heating it in the air at 90°C for 10 min. This stage was then repeated one more time. After two applications of the solution, the oxide layer was formed thermally

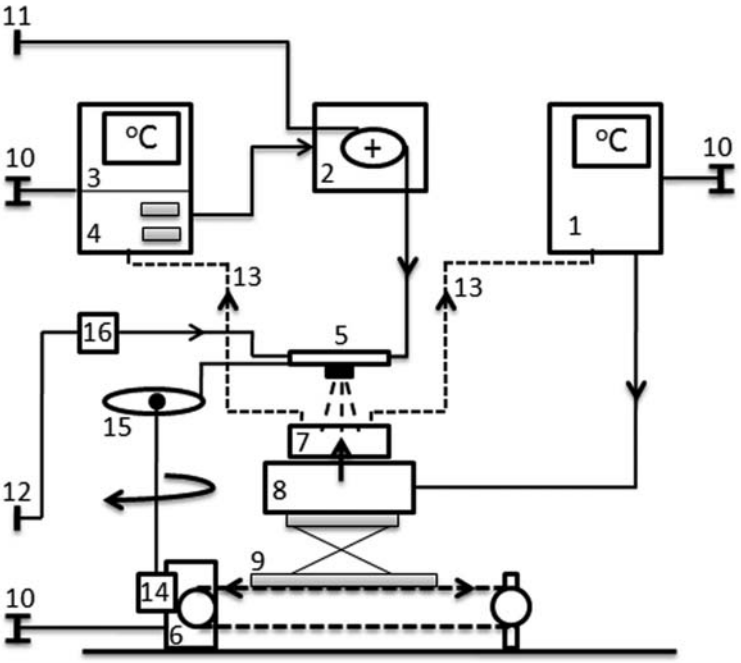

Fig. 3.2 Setup of the spray pyrolysis system (1) temperature controller; (2) peristaltic pump; (3) temperature switch; (4) chronometer (effective spraying and total time); (5) spray nozzle; (6) motor for lateral and circular displacement; (7) heating chamber; (8) heating plate; (9) lateral displacement support; (10) generator; (11) spray solution; (12) carrier gas (N_2); (13) connection to thermocouples; (14) transmission gear; (15) rotating system; (16) flowmeter for the carrier gas (N_2) (after Correa-Lozano et al. 1996)

by heating it at 500°C for 20 min in a muffle furnace with a low, continuous flow of oxygen. The processes were repeated until the SnO_2 coating reached the desired thickness. After the required coating thickness had been achieved, the coating was annealed at 500°C for 60 min. Moreover, spray pyrolysis method was introduced to make the $Ti/SnO_2–Sb_2O_5$ electrode (Correa-Lozano et al. 1996). Figure 3.2 shows the schematic diagram of the spray pyrolysis system. The precursor solution flow and the carrier gas flow were 1.86 and 3 cm^3 min^{-1}, respectively; the nozzle–substrate distance was 17 cm. The carrier gas was nitrogen gas. The reactants were $SnCl_4 \cdot 5H_2O$, $SbCl_3$, HC1 (32%), and ethanol. The $SnCl_4 \cdot 5H_2O$ concentration was fixed at 10% in an ethanol/hydrochloric acid mixture and the $SbCl_3$ concentration was adjusted to obtain the desired Sb percent atomic ratio in the mixture. The $SnO_2–Sb_2O_5$ films were prepared in the temperature region between 400 and 700°C on the substrate. Addition of IrO_2 interlayer between $SnO_2–Sb_2O_5$ and Ti substrate can benefit the service life of the SnO_2-based anodes, due to its high anodic stability and its isomorphous structure with TiO_2 and SnO_2 (Correa-Lozano et al. 1997). Figure 3.3 shows the surface morphology SEM images of $Ti/SnO_2–Sb_2O_5$ and Ti/IrO_2.

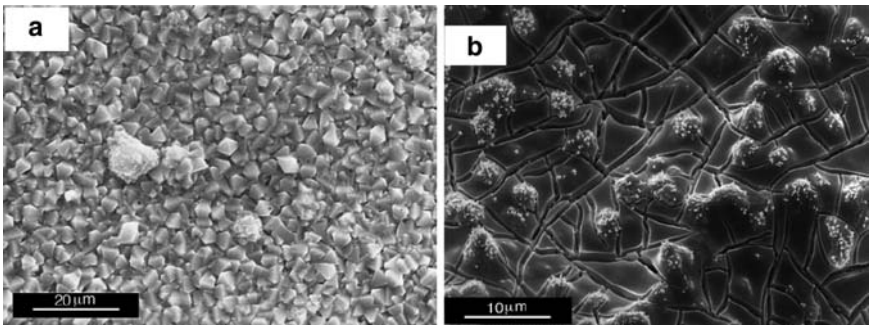

Fig. 3.3 SEM images of **(a)** $Ti/SnO_2{-}Sb_2O_5$ and **(b)** Ti/IrO_2 (after Correa-Lozano et al. 1997)

Coteiro's group studied the influence of the solvent to the ternary oxide, Ru–Ti–Sn, electrode stability (Coteiro et al. 2006). The precursor mixtures were prepared by dissolving $RuCl_3 \cdot nH_2O$, $TiCl_4$, and $SnCl_2 \cdot 2H_2O$ salts into the solvent. Two different solvents, HCl/H_2O (1:1 v/v) or isopropanol, were applied. The results with isopropanol as solvent showed that tin loss can be eliminated and higher electrochemically active area and stability can be achieved, when compared with HCl solution.

3.1.4 Tantalum-Oxide-Based Electrode (Ta_2O_5)

Tantalum oxide shows very high electrochemical stability, and it can be mixed with the catalyst to make the highly stable active electrode (Morimitsu et al. 2000; Ribeiro and De Andrade 2004). Highly oxidizing reagent, ozone, can be produced with PtO_x–Ta_2O_5 as the anode. The maximum ozone concentration was attained when the mole ratio of Pt and Ta was 5:95 (Sata et al. 2004). RuO_2–Ta_2O_5 oxide was prepared through thermal decomposition (Ribeiro and De Andrade 2004). Precursor mixtures were prepared by dissolving the appropriate amounts of $RuCl_3 \cdot xH_2O$ and $TaCl_5$ in isopropilic alcohol. Sandblasted and cleaned Ti-supports were etched in boiling concentrated HCl for 30 min and in boiling 10% oxalic acid for 20 min, sequentially. Then, the precursor mixtures were dropped from a micropipette (~10 mL) on both faces of a pretreated Ti-support base. Afterward, the electrode was dried at low temperature 80 ~ 90°C to evaporate the solvent and then fired at 450 or 500°C for 5 min under 5 dm^3 min^{-1} O_2 flow. This procedure was repeated until the desired nominal oxide loading (~1.4–1.6 mg cm^{-2}) was reached. The layers were finally annealed for 1 h at the same temperature under O_2 flux. Iridium and tantalum oxides electrodes have received much attention as the most dominant catalyst for oxygen evolution, with long working life time (more than 10,000 h under severe operation conditions of 10,000 A m^{-2} current density loading and 60°C temperature) (Rolewicz et al. 1988; Matsunaga et al. 1998). The preparation procedure for IrO_2–Ta_2O_5 consisted of (a) painting a coating solution

on a pretreated Ti substrate, (b) drying it at 120°C, and (c) calcining it at 500°C for 10 min (Morimitsu et al. 2000). The pretreatment of the titanium substrate was carried out by grit blasting and etching in boiling oxalic acid (10 wt%) for 1 h. The coating solution was prepared by dissolving appropriate amounts of $H_2IrCl_6 \cdot 6H_2O$ and $TaCl_5$ into *n*-butanol containing HCl (6 vol%). The above procedures were repeated to obtain the desirable amount of the coating layer.

3.1.5 Rhodium-Oxide-Based Electrode (RhO_x)

RhO_x electrode is one kind of gas evolution electrode, which shows similar activity for oxygen gas evolution with IrO_2, but lower activity than RuO_2 during anodic polarization (Hrussanova et al. 2004). However, it shows higher catalytic performance for hydrogen evolution during cathodic polarization (Morimitsu et al. 2000; Campari et al. 2002). Ti/RhO_x electrodes were prepared by thermal decomposition method (Hrussanova et al. 2004). Precursor solution was prepared with $RhCl_3 \cdot 3H_2O$ dissolved in aqueous HCl solution (10 wt%) to avoid hydrolysis of the precursor before the thermal treatment. The solution was brushed onto a Ti support, the solvent evaporated, and the sample calcined in a furnace in an ambient atmosphere for 7 min at a temperature in the range of 400–600°C. The operation was repeated until the set oxide loading was reached, with final calcination at the same temperature for 3 h.

Besides thermodecomposition, electrochemical deposition has been utilized to make metal-oxide electrode. PbO_2 is one of the favorable catalytic electrodes, in view of its low price, good electrical conductivity, large oxygen overpotential, and chemical inertness. This electrode can be fabricated on conductive substrate with electrochemical deposition method (Zhou et al. 2005; Devilliers et al. 2007; Ghasemi et al. 2007; Kong et al. 2007; Zhou and Gao 2007). The electrocatalysis ability and electrode stability can be modified by doping foreign ions in the film and adjusting the deposition conditions (Velichenko et al. 2002; Mohd and Pletcher 2005; Shi-Yun Al 2005).

3.2 Chemical Vapor Deposition (CVD)

CVD is a synthesis process in which the chemical constituents react in the vapor phase near or on a heated substrate to form a solid deposit (Pierson 1999). The reactions happened in the CVD system can be divided into homogeneous gas phase reactions and heterogeneous substrate surface reactions. Normally, CVD technique is utilized to make thin films. CVD is also defined as a process whereby a thin solid film is synthesized from the gaseous phase by a chemical reaction (Hitchman and Jensen 1993). The CVD apparatus arrangement is dependant on the particular application. The apparatus is made up with three major components: precursors and

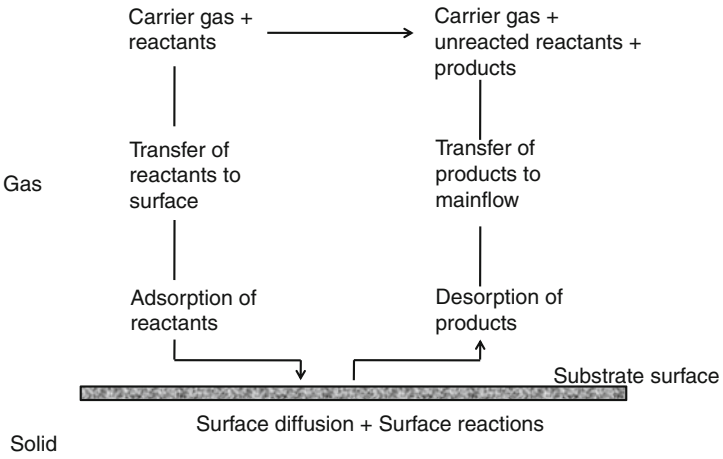

Fig. 3.4 Processes contributing to CVD growth (after Hitchman and Jensen 1993)

their handling, reactors, and the exhaust of by-products. Most chemical reactions in CVD are thermodynamically endothermic, which means energy has to be supplied to the reacting system. Moreover, it means the CVD processes can be initiated and controlled by the introduction of energy. According to the methods of energy input, CVD methods can be categorized into thermal, plasma, photo, and acoustic CVD. Figure 3.4 shows the chemical processes contributing to CVD growth.

Diamond thin-film electrode has become very attractive in the environmental field because of its special chemical and electrochemical properties. As it is known, diamond is the hardest material in the world, which can resist mechanical scratching in its application. Besides, diamond thin-film electrodes possess high anticorrosion property, and it can keep its superb microstructural morphology at high temperatures and current densities in acidic or basic environment. In the aqueous system, it shows weak adsorption of polar molecules, leading to improved resistance to electrode deactivation and fouling. In addition, there are some special electrochemical properties (i) a wide working potential window in aqueous and nonaqueous media, large water splitting potential window during polarization which can reach over 3 V and even to 4 V for high-quality diamond film; (ii) a low and stable background current and low surface double layer capacity, in the range of several $\mu F\,cm^{-2}$, leading to improved signal-to-background ratio (SBR) and signal-to-noise ratio (SNR) during the electroanalysis practice; (iii) good responsiveness for aqueous and nonaqueous redox analytes without any conventional pretreatment; and (iv) long-term response stability even after several months exposing in air. Thanks to these properties, diamond electrodes meet the requirements for a wide range of applications such as water and wastewater treatment and environment monitoring, and electrosynthesis of organic and inorganic compounds (Panizza and Cerisola 2005).

Diamond thin-film electrodes have been studied for decades and by various research groups worldwide. Their superb performance has been proved for the

application in water and wastewater treatment and environmental analysis. *E. coli* can be inactivated with the diamond film electrode as anode in a chloride-free phosphate buffer medium (Jeong et al. 2006). Various persistent and toxic organic pollutants have been mineralized by using diamond film electrode with electrooxidation technique. They show superior electrochemical mineralization performance in treating dyeing or textile wastewater (Hattori et al. 2003; Faouzi et al. 2007), aromatic organic compounds (Canizares et al. 2002; Zhi et al. 2003; Canizares et al. 2005), surfactants (Weiss et al. 2006), organic acid (Martinez-Huitle et al. 2004; Nasr et al. 2005; Louhichi et al. 2006), oil containing wastewater (Taylor et al. 2003), wastewater secondary treatment and filtration effluents (Van Hege et al. 2002; Bejan et al. 2005; Panizza et al. 2006), and complexing agents (Lissens et al. 2003). Compared with different types of DSAs, such as IrO_2, SnO_2, PbO_2, RuO_2, diamond film electrode shows the greatest electrochemical incineration efficiency to degrade organic pollutants (Van Hege et al. 2004; Waterston et al. 2006). Besides the strong oxidizing performance for organic chemicals mineralization and detection, diamond film electrode shows reduction application for metal recovery even from persistent organometallic complexes (Yamaguchi et al. 2006) and shows high sensitivity to detect heavy metal ions in aqueous system in ppb (part per billion) level (Mcgaw et al. 2006), due to the high hydrogen gas evolution potential.

Comninellis's group proposed an indirect electrochemical incineration mechanism with electrosynthesized intermediate of hydroxyl radicals during the oxidation process on diamond film electrode (Foti et al. 1999). Due to the high over potential for oxygen evolution on the diamond electrode (D) in water system, hydroxyl radicals ($^{\cdot}OH$), a kind of strong oxidant, can be formed during water electrolysis on the electrode surface [Reaction (3.1)], and led to the organic pollutants' (OP) oxidation into final products, such as CO_2, H_2O, N_2, NO_3^-, and PO_4^{3-}, etc. [Reaction (3.2)].

$$D + H_2O \rightarrow D(^{\cdot}OH) + H^+ + e^- \quad (3.1)$$

$$D(^{\cdot}OH) + OP \rightarrow D + CO_2 + H_2O + H^+ + N_2 + NO_3^- + PO_4^{3-} + e^- \quad (3.2)$$

$$D(^{\cdot}OH) \rightarrow D + O_2 + H^+ + e^- \quad (3.3)$$

Diamond film electrode has an inert character with weak adsorption properties (Martin et al. 1996; Swain et al. 1998; Pleskov 1999). Weak interactions of D ($^{\cdot}OH$) lead to low anode activity toward oxygen gas evolution [Reaction (3.3)] and high oxidation reactivity to the organic pollutants' incineration [Reaction (3.2)]. Due to the high oxidizing power of the radicals, highly persistent pollutants, which cannot be decomposed with bioremediation method, advanced oxidation process, or even electrooxidation process with other kinds of electrodes, can be successfully degraded with the diamond film electrode.

Furthermore, it has been proved that direct oxidation can happen on the diamond film electrode before the oxygen gas evolution potential (Zhi et al. 2003). Direct oxidation takes place, accompanying with the adsorption of chemical molecules on the diamond electrode surface. An as-grown diamond film with high hydrogen coverage is inert to adsorption of polar molecules (Vinokur, Miller et al. 1996; Yano

et al. 1998), but adsorption may be introduced at high applied potentials, which turns the surface oxygen terminated (Notsu et al. 1999, 2000). Special oxidation peak can be checked during voltammetric tests for various organics. Due to the low potential for direct oxidation, c.a. lower than 2 V (Ag/AgCl sat. KCl), full mineralization cannot be conducted under this condition with reasonable rate, but electroanalytical detection of pollutants and special electrochemical synthesis can be fulfilled under this condition. Diamond film electrode showed well-defined electrochemical analytical use for the detection of ammonia (Ji et al. 2005), pesticides (Codognoto et al. 2006; Pedrosa et al. 2006), phenol and chlorinated phenols (Muna et al. 2004), and adenosine (Xie et al. 2006) in aqueous solutions with concentration as low as nanomolar level and excellent response reproducibility. Electrochemical detection can be influenced by the electrode surface conditions. Take the mineralization of oxalic acid as an example; hydrogen-terminated diamond electrodes exhibited well-defined peaks of oxalic acid oxidation in a wide pH range with good linearity for a concentration range from 50 nM to 10 μM and with a detection limit of 0.5 nM. In contrast, oxygen-terminated diamonds showed no response for oxalic acid oxidation inside the potential window (Ivandini et al. 2006a).

The diamond film has been fabricated on diamond and nondiamond substrates with low-pressure CVD methods. With the CVD methods, the diamond film is normally polycrystalline and microcrystalline. Plasma-assisted chemical vapor deposition (PACVD) and hot-filament chemical vapor deposition (HFCVD) methods are commonly used. These two methods are simple and easy to handle (Angus and Hayman 1988; Yarbrough and Messier 1990; Matsumoto 2000). Hydrogen and hydrocarbon gases are two major precursor gases. Atomic hydrogen, decomposed from hydrogen gas under plasma or high temperature, plays a vital role in the deposition process, including stabilization of the diamond surface, creation of a volatile source of carbon, formation of vacancies on the growth surface, reduction of the surface free energy, formation of carbon radicals, and etching of graphite material (Banholzer 1992; Angus et al. 1993; Sharda et al. 1996). Hydrocarbon gas provides the carbon source for diamond production. Methanol (Sugino et al. 1994), ethanol (Gilbert et al. 1999; Baranauskas et al. 2000), acetone (McNamara and Gleason 1993), and acetylene (Sommer and Smith 1990) have been tried as the carbon source precursors. With the development of CVD technique, methane has become the most common hydrocarbon precursor. The reaction conditions, including gas composition, substrate and gas temperature, reactor chamber pressure, and gas flow rate, have significant effects on diamond crystal quality and film growth rate. Bachmann's group summarized diamond CVD study of over 30 years before 1991 (Bachmann et al. 1991). A C–H–O phase diagram is introduced which provides a common scheme for the diamond CVD methods. Only in a small area in the diagram with low carbon element ratio, diamond can be successfully fabricated. Besides the reaction conditions, the substrate material has a considerable influence on the quality of the deposit, and the gas phase temperature seems to be more important for the diamond deposition rate than other parameters.

Experimental process for diamond deposition is shown in Fig. 3.5. Before the CVD process, seeding pretreatment on the substrates, especially nondiamond

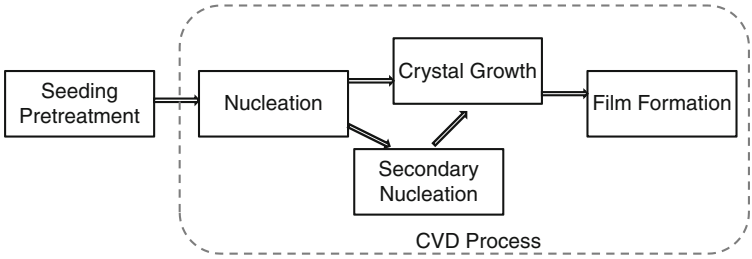

Fig. 3.5 Flow chart of the diamond film growth process

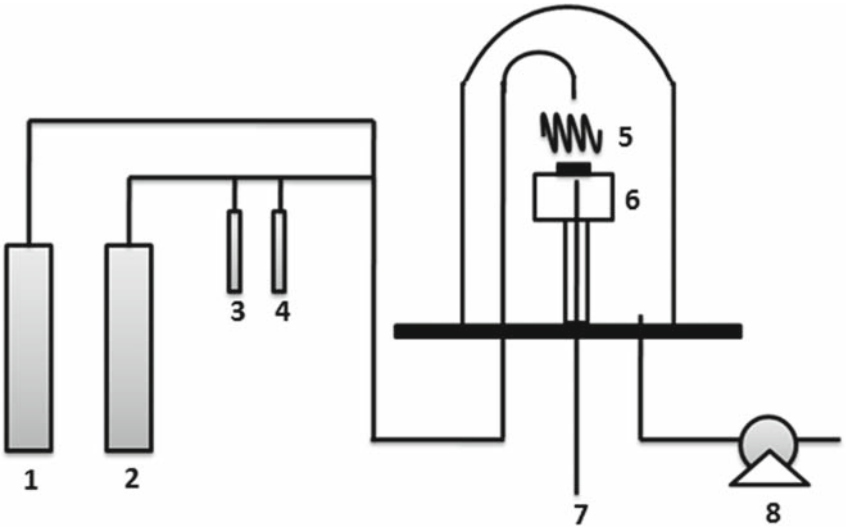

(1) Methane (2) Hydrogen (3) $B(OCH_3)_3$ (4) $CH_2(OCH_3)_2$ (5) Filament (6) Substrate (7) Thermal couple (8) Vacuum Pump

Fig. 3.6 Schematic diagram of hot-filament chemical vapor deposition system (after Guo and Chen 2007a)

materials, is a very important step to enhance the diamond nucleation rate during CVD process. Ultrasonic scratching in the diamond paste, 1 g of synthetic diamond microscale particles dissolved in 10-mL acetone (Guo and Chen 2007a), is one of the most effective and simple pretreatment method. Li and his coworkers (Li et al. 1998) reported that scratching the substrate surface with the diamond paste is effective to improve nucleation process, but Al_2O_3 is not useful for nucleation. During the CVD process, there are two steps, nucleation and crystal growth, before film formation (Fayette et al. 1994).

HFCVD method has been favored by industry (Wilson and Kulisch 1996), because of its special properties, such as relatively low set up cost, easily scaled up to large substrate area, easy operation, and flexibility to three-dimensional geometry (Schafer et al. 2006). Figure 3.6 shows a typical HFCVD system (Guo

and Chen 2007a). In the HFCVD system, high-temperature filament is the power source for series of all the following gas phase and substrate surface heterogeneous reactions. High filament temperature, over 1,900°C, is necessary to make atomic hydrogen efficient, which is very effective for selective deposition of diamond (Venter and Neethling 1994). Due to the high temperature, filament is made from tungsten, tantalum, or rhenium (Sommer and Smith 1990; Okoli et al. 1991). Among the three materials, tungsten is the cheapest one and niobium is the most expensive material. On the other hand, rhenium possesses the longest life, and tungsten shows the shortest life time and the most difficulty for processing. The HFCVD method itself is simple but the quality and property of the diamond layers produced are strongly dependent on the deposition parameters together with the chemical stability of the substrate (Haubner and Lux 1993; Cassidy et al. 1994; Kondoh et al. 1994; Lee et al. 1997). Clear faceted planes were obtained under the following conditions: reactor chamber pressures of 13.3–40 mBar, methane concentration from 0.2 to 2% (volume percentage), gas flow rate less than 800 standard $cm^3\ min^{-1}$ (sccm), distance between the filament and substrate less than 10 mm, and substrate temperature from 500 to 1,100°C (Angus et al. 1988; Kondoh et al. 1994; Singh et al. 1994; Lee et al. 1997; Menon et al. 1998; Gilbert et al. 1999; Hirakuri et al. 2001). Under the typical conditions, the diamond film growth rate is 1–10 $\mu m\ h^{-1}$ (Bachmann et al. 1991). The reaction parameters affect the diamond quality and growth rate, and also the crystal orientation. At higher pressure of 27–40 kPa, (100) facet diamond is the favorable growth surface, whereas (111) is the favorable growth surface at lower pressure (Yu and Flodstrom 1997). The (111) facet is dominant at low methane concentration and (100) is preferred at high methane concentration (Kondoh et al. 1994). The growth rate in the (100) direction exhibits a sharp drop at temperatures where the crystal geometry is changing from octahedral to cubo-octahedral, whereas the growth rate in the (111) direction exhibits a more gradual change with temperature (Menon et al. 1998).

There are some disadvantages for HFCVD method. Filament is relatively easy to break, and its life time is around 100 h. Second, due to the high working temperature, the filament metal element can evaporate into the gas phase and deposit in the diamond film, which is a kind of contamination (Venter and Neethling 1994). Mehta Menon's group reported that tungsten filament yielded the lowest impurity level (few ppm by mass), whereas rhenium yielded the highest (parts per thousand) (Mehta Menon et al. 1999). Metal contamination in the diamond would affect the electronic application of diamond, even in ppm level, but this is not a big problem for the electrochemical application.

In order to prolong working life of filament and broaden the substrate materials choice, some researchers put their effort on studying how to reduce the temperatures. Up to date, halogen-containing chemicals and oxygen-containing chemicals are reported effective to reduce the reaction temperatures. Hong's group reported that chloromethanes (CH_2Cl_2, $CHCl_3$, and CCl_4) were used as carbon sources to grow diamond at low temperature (from 380°C to 700°C) (Hong et al. 1993). In comparison with methane, which is inefficient at growing diamond below 600°C, chloromethane was quite suitable for the growth of diamond films

at low temperature. However, the growth rate at 380°C was only $0.05\,\mu m\,h^{-1}$. Similarly, Corat' group reported that they observed diamond growth under a substrate temperature as low as 390°C with addition of CF_4 in CH_4–H_2 precursor gases in HFCVD system (Corat et al. 1994). Schmidt reported that CHF_3 and C_2H_5Cl made possible a significant decrease in substrate temperature down to 370°C (Schmidt et al. 1997). The effects of chloromethane on diamond nucleation and growth were studied by Wu and Hong (1998) with laser reflective interferometry. They assumed that chloromethane can enhance diamond nucleation at a lower temperature by protecting the residual seeds by diamond-grit scratching from being etched by H atoms. Kim and coworkers reported that when even a small amount of oxygen (about 0.6%) is added, well-faceted diamond films are observed under low substrate temperature of 530°C (Kim et al. 1995). Li and coworkers reported that addition of a small amount of oxygen to the CH_4–H_2 gas permits diamond deposition at filament temperature as low as 1,400°C and substrate temperature down to 450°C. Optimum conditions were found to give reasonable growth rates ($0.5\,\mu m\,h^{-1}$) with high film quality at filament temperatures of 1,750°C and substrate temperatures of 600°C (Li Tolt et al. 1997a). They also reported that H_2O has the similar effect to reduce the reaction temperature in HFCVD system (Li Tolt et al. 1997b). With addition of oxygen gas or oxygen containing chemicals, the diamond film growth rate can be improved (Bruckner and Mantyla 1993; Brunsteiner et al. 1996).

Besides the typical micrometer-size diamond crystal fabricated with HFCVD methods, nanometer-size diamond crystal has been studied in recent years. Ku and Wu (2004) fabricated the nanocrystalline diamond (NCD) films with a thickness of few-hundred nanometers on Si substrates with CCl_4–H_2 precursor gases at a substrate temperature of 610°C. They suggested that both the primary nucleation and the secondary nucleation processes were crucial for the growth of the NCD films. Wang et al. reported that the NCD films were fabricated by decreasing the gas pressure and increasing the concentration of the hydrocarbon of acetone (Wang et al. 2004). The surface of the film is extremely smooth and the grain size is approximately 4–8 nm. There are two keys to fabricate the NCD films using CVD: first one is to increase the nucleation density to 10^9–10^{10} particles per cm^2 during the initial stages and the other is to control the crystal grain growth into nanometer scale. To reduce gas pressure can not only result in the increase in the substrate temperature and dissociation rate of hydrogen gas, but also enhance the free path of radicals group in the reaction chamber. Consequently, the groups with higher velocity and more energy bombard substrate and supply more energy to the surface. The adsorbed radical groups on the surface become more active and promote the ratio of secondary formation of nuclei. Moreover, it is difficult for diamond grain to grow on the occasion of the more and stronger bombardment, which also accelerates the secondary formation of nuclei. NCD films were grown on silicon (100) wafers by Bruhne et al. (2005). Bias voltage was applied to enhance diamond nucleation before diamond film growth, and high methane concentration in hydrogen (3%) with addition of 1% oxygen gas was used, in order to obtain nanocrystalline structure by preventing the cellular growth.

PACVD method is another typical way of making diamond films. Precursor gas molecules can be decomposed into radicals under the effect of plasma. There are three plasma sources commercially available (Davis 1993). Microwave plasma typically uses excitation frequencies of 2.45 GHz. Radio frequency (RF) plasma excitation typically employs frequencies of 13.56 MHz (or less commonly 450 kHz). Direct current plasmas can be run at low electric powers, named as cold plasma, or at high electric powers, which create an arc, named as thermal plasma. Microwave PACVD method is the most common one among the three methods.

Typical deposition parameters for microwave PACVD are as follows: gas composition of 0.1–5% methane in hydrogen, gas flow rate from 50 to 500 sccm, substrate temperature between 400 and 1,000°C, and gas pressure from 5–250 mBar (Davis 1993; Deguchi et al. 1996; Tucker et al. 1996; Ramesham and Rose 1997; Cooper et al. 1998; Ralchenko et al. 1999). Various studies on gas composition modification have been performed. With addition of oxygen, the diamond deposition rate can be enhanced, as well as the diamond quality (Chang et al. 1988; Chen et al. 1989; Chein and Tzeng 1999). By adding oxygen gas up to 2% of hydrogen gas, the diamond deposition rate was found increased linearly (Chen et al. 1989), and the diamond crystal growth rate can reach $20\,\mu m\,h^{-1}$ (Chang et al. 1988). In order to save energy, low-temperature diamond deposition method was studied. The addition of O_2 or CO_2 plays a crucial role in the low-temperature deposition process. Clear faceted diamond film can be fabricated with gas composition of CH_4:CO_2 (29.5:30.5 sccm) at substrate temperature of 420°C, even without adding hydrogen (Stiegler et al. 1996). It was predicted that diamond films may be formed even at temperatures of less than 200°C by using $CH_4 + CO_2$ gas mixtures (Chen et al. 1994). CH_3Cl and CH_2Cl_2 showed the similar effect to oxygen. Chlorine-permuted methane plays an effective role in improving the diamond quality, as well as reducing the deposition substrate temperature to 530°C (Nagano and Shibata 1993). NCD film has been fabricated with the microwave PACVD method. Sharda and coworkers fabricated NCD film on silicon substrate by applying a negative dc bias voltage of 260 V. The reaction condition was as following: a mixture of 5% CH_4 in H_2, chamber pressure of 4 kPa, a microwave power of 1,000 W, and the substrate temperature of 600°C (Sharda et al. 2001). The NCD film can be fabricated in the microwave PACVD system by adjusting the distance between the substrate and the plasma ball in the gas composition of 10% CH_4 in H_2 (Yoshikawa et al. 2001). Gruen's group investigated the transition from microcrystalline to nanocrystalline diamond films grown from $Ar/H_2/CH_4$ microwave plasmas. Microcrystalline grain size and columnar growth have been observed from films produced from $Ar/H_2/CH_4$ microwave discharges with low concentrations of Ar in the reactant gases. By contrast, the films grown from $Ar/H_2/CH_4$ microwave plasmas with a high concentration of Ar in the reactant gases consist of phase pure NCD (Zhou et al. 1998). Liu and his coworkers combined the techniques from Yoshikawa and Gruen. Simultaneous growth of well-faceted microcrystalline diamond and NCD on the same substrate by 1% $CH_4 + 5\%$ $H_2 + 94\%$ Ar microwave plasma was reported (Liu et al. 2004). Soga summarized the NCD fabrication

methods, and categorized them into three groups, e.g., hydrogen-deficient gas phase, biased enhancement of nucleation and growth using CH_4/H_2 gas system, and diamond seeding (Soga et al. 2004). One of the drawbacks when using microwave PACVD is the limitation of substrate area due to the difficulty in enlarging the plasma ball size. Comparatively, RF plasma can be relatively easily generated over much larger areas than microwave plasmas (Davis 1993; Pai et al. 1998).

Diamond is a kind of semiconductor, and pure diamond is nearly nonconductive with high resistivity of $10^{16}\Omega$cm. Good conductivity is needed, when working as an electrode. Doping is an effective way to improve the conductivity of a semiconductor. Doping with boron (Okano et al. 1994; Sugino et al. 1994), as an accepter admixture, allows forming p-type semiconductor and enhancing the conductivity, while high doping levels lead to quasimetallic films. The specific resistance of diamond depends on the content of boron atoms in the film, and it can vary from 10 kΩ cm with the content of boron in diamond of 10^{18} per cm^3 to 10^{-1}–10^{-3} kΩ cm with the content of boron in diamond of 10^{21} per cm^3. There are two ways of introducing boron into the diamond. One is to use volatile boron containing chemicals, e.g., trimethyl borate (Chen et al. 2005; Tian et al. 2006; Guo and Chen 2007a), to supplement into the gas phase via evaporation. The other is to use the solid boron containing chemicals, e.g., B_2O_3 (Okano et al. 1994), placed near the substrate which can be activated into the gas phase under high temperature. Besides boron, nitrogen, sulfur, and phosphorus have been studied as dopants to change diamond into n-type semiconductor (Okano et al. 1994; Koizumi et al. 1998; Haubner et al. 1999).

Substrate material is one crucial factor that should be considered when fabricating diamond film electrodes. Several criteria need to be taken into consideration:

1. Tolerance of high deposition temperature
2. Cost of the material
3. Density and machining property
4. Lattice parameters and thermal expansion coefficients of both the substrate and their related carbides
5. Electrical conductivity of the substrate and the related carbides
6. Chemical stability for the substrate and the related carbides in applied environments

Ti, Ta, Zr, and Nb are preferred, because of their ability of forming stable compact oxides film during anodic polarization. Compared with other metals, titanium has the lowest density, easy machinability, high anticorrosion and quick repassivation electrochemical performance, and relatively low cost (Leyens and Peters 2003). It becomes a preferred choice as the substrate material of diamond film electrode (Drory and Hutchinson 1994; Chen and Lin 1995; Chen et al. 2003; Hian et al. 2003; Gerger et al. 2004; Chen et al. 2005; Guo and Chen 2007a).

A high-quality diamond film electrode needs high purity and quality diamond film fully covering the substrate to limit the exposure of the substrate to the environment. Micro-Raman spectroscopy, X-ray diffraction (XRD), and scanning electron

microscopy (SEM) are three important physical characterization methods. Purity of diamond film can be detected by using micro-Raman spectroscopy. Raman peaks centered at 1,332 cm^{-1} and 1,140 cm^{-1} are related with microcrystalline diamond and NCD sp^3 carbon, respectively, and Raman peaks centered at 1,550 cm^{-1} and 1,580 cm^{-1} are attributed to sp^2 and sp^3 hybridized amorphous carbon and graphite, two kinds of commonly found nondiamond carbon impurities in CVD diamond film (Yarbrough and Messier 1990; Wilson and Kulisch 1996; Nebel and Ristein 2004). It has been reported that the Raman signal is 50 times more sensitive to the nondiamond carbon than to the crystalline diamond (Knight and White 1989). The percentage of diamond carbon in the total carbon content can be quantified with a "Purity Index" (PI) (Guo and Chen 2007a), calculated with the following equation,

$$\mathrm{PI} = \frac{I_\mathrm{D}}{I_\mathrm{D} + \frac{I_\mathrm{C}}{50}},$$

where I_D and I_C are the integrated peak intensity of diamond and nondiamond carbon phase, respectively. XRD can be used to check the crystal orientation, by comparison with the standard diamond database. Peaks at which the 2θ is 43.9, 75.3, and 119.5° are correspondent to the (111), (220), and (400) facet, respectively. Moreover, micro-Raman and XRD can be applied to evaluate the residual stress in the deposited diamond film (Ager and Drory 1993; Chandra et al. 1996; Fu et al. 2003). Residual stress in the diamond film has adverse effect on the stability. Crystallinity of diamond can be checked by measuring the full-width half maximum (FWHM) value of the specific diamond peak in micro-Raman and XRD results. The film morphology and microstructure information can be obtained by using SEM technique. The electrochemical performance can be checked with cyclic voltammetry and impedance spectroscopy techniques. Figures 3.7 and 3.8 show the typical physical and CV characterization results of diamond film electrode.

Besides diamond, carbon nanotubes (CNTs) can be fabricated with the HFCVD method (Dikonimos Makris et al. 2004). Untangled CNTs with smooth walls and high purity were fabricated in a HFCVD reactor on Si substrate. The optimal conditions were substrate temperature 600°C, total pressure 5 mbar, and 10% of CH_4 in H_2. During CNTs fabrication, catalyst is an important factor. Some 3-nm thick nickel film deposited on the substrate was employed as a catalyst, and a 70-nm thick SiO_2 layer was coated between Ni layer and Si substrate in order to prevent dissolvation of Ni into Si. Metal oxide films have been made with CVD methods also. Photocatalytic TiO_2 film was fabricated by using CVD techniques, which will be introduced later in this chapter. Other kinds of metal oxide films, e.g., RuO_2, SnO_2, Ta_2O_5, have been fabricated with CVD methods (Lu et al. 1999; Frohlich et al. 2001; Gopal Ganesan and Eizenberg 2003; Kim et al. 2003b; Papadatos et al. 2004; Huang et al. 2006; Kim 2007). These films are mainly utilized in the electronic and device applications. Their detailed description about the fabrication process will not be given here, because these applications are not related with the environmental application.

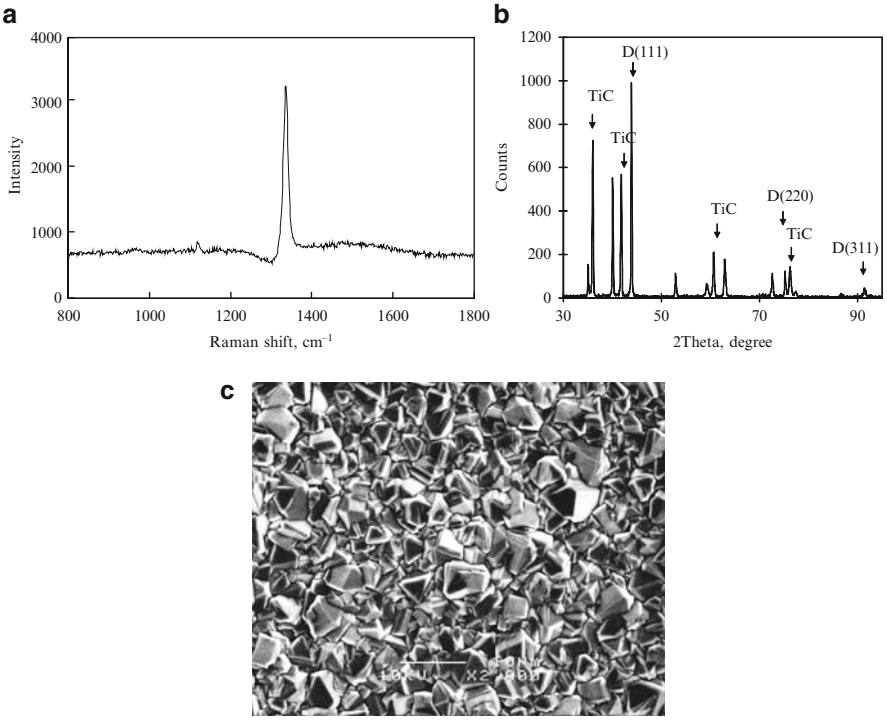

Fig. 3.7 Typical micro-Raman **(a)**, XRD **(b)** and SEM **(c)** characterization results of diamond film deposited on titanium substrate

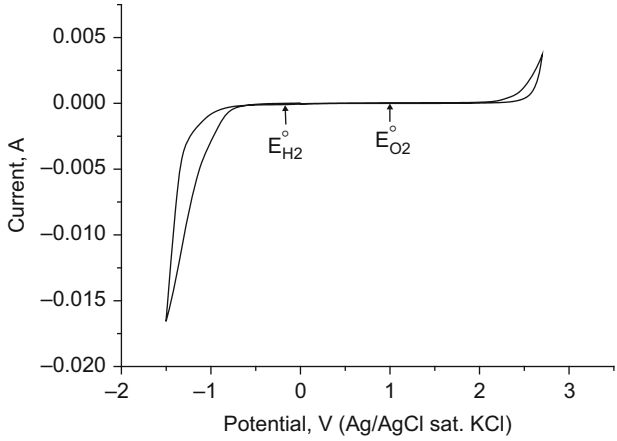

Fig. 3.8 Typical cyclic voltammogram of boron doped diamond film electrode. The result was tested in 0.5 M H_2SO_4 solution at 0.1 V s^{-1} scan rate. The standard hydrogen gas and oxygen gas evolution potentials were marked with $E^{\circ}_{H_2}$ and $E^{\circ}_{O_2}$, respectively (after Guo and Chen 2007b)

3.3 Surface Modifications

All electrodes react with their environment via the surfaces in ways which will determine their electrochemical performance. Properly selected surface modification can effectively enhance the electrode heterogeneous catalysis property, especially selectivity and activity. The bulk materials can be chosen to provide mechanical, chemical, electrical, and structural integrity. In this part, several surface modification methods will be introduced in terms of metal film deposition, metal ion implantation, electrochemical activation, organic surface coating, nanoparticle deposition, glucose oxidase (GOx) enzyme-modified electrode, and DNA-modified electrode.

3.3.1 Metal Film Deposition

Bismuth film coated electrode was found high sensitivity to metal ions (Co^{2+}, Ni^{2+}, Cd^{2+}, Pb^{2+}, Zn^{2+}) in ppb level (Hutton et al. 2006; Kefala and Economou 2006; Svancara et al. 2006), pesticide in $\mu g\,ml^{-1}$ level (Guzsvany et al. 2006), bromate and hydrogen peroxide (Gun et al. 2006; Kefala and Economou 2006). A highly sensitive protocol for measuring trace beryllium (Be) at a mercury-coated electrode was described with a detection limit of $0.25\,\mu g\,l^{-1}$ (Wang et al. 2006b). Detection of selenium (Se^{4+}) at a copper-modified mercury-film electrode was studied. The detection limit was $40\,ng\,l^{-1}$ (0.5 nM) (Zaitsev et al. 2006).

Cathodic electrodeposition is an effective way to coat metal film on electrode substrate. Bismuth film has been cathodically plated on the substrate, such as graphite ex situ (Guzsvany et al. 2006; Svancara et al. 2006), carbon paste (Arribas et al. 2006), glassy carbon electrode (Guzsvany et al. 2006), and Nafion-modified glassy carbon electrode in situ (Kefala et al. 2006). The mercury-coated carbon-fiber electrode was prepared by a 15-min electrodeposition of mercury at −0.8 V from a 0.1 M acetate buffer (pH 4.5) solution containing $20\,mg\,l^{-1}$ mercury (Wang et al. 2006b). Films of copper hydroxide were deposited on the pretreated glassy carbon electrode by voltage cycling between −0.1 and 0.65 V (Casella et al. 2002). Copper was electrodeposited onto the laser-etched carbon fiber with an acidic copper(II) medium through fixing the electrode potential at −1 V for periods up to 30 min (Kilbey et al. 2006).

Mercury was a traditional and highly efficient electrode working as a sensor. Solid amalgam of mercury with different metal is a newly developed way to keep the sensitivity high as well as to reduce environmental toxicity and to improve mechanical stability and simple handling for application. Review on electrodes based on nontoxic solid amalgams (MeSAE) is available elsewhere (Yosypchuk and Novotny 2002). Good sensitivity of atrazine and ametryne herbicides was reported on the copper–mercury amalgam electrode. The detection limit of herbicides obtained in pure water was $3\,\mu g\,l^{-1}$ (De Souza et al. 2006).

3.3.2 Metal Ion Implantation

Iridium-modified diamond film electrodes fabricated by an ion implantation method have been developed for electrochemical detection of As^{3+}. The electrodes exhibited high catalytic activity toward As^{3+} oxidation with the detection limit of 1.5 ppb (20 nM) (Ivandini et al. 2006b). Molecular recognition sites for mercury ions were imprinted in TiO_2 film using stable ground-state complex of 1-amino-8-naphtol-3,6-disodium sulfonate (ANDS) with mercury ions as template. Compared with pure TiO_2 electrode, the imprinted electrode revealed selectivity toward the imprinted ions. Linear calibration plots for mercury ions were obtained with a detection limit of 3.06 nM (Liu et al. 2006). The anodic voltammetric responses for some phenolic compounds can be significantly enhanced at the Sb^{5+} and Fe^{3+} co-doped SnO_2 electrodes. The larger response at the electrode is caused by the enhanced adsorption of the phenolic compounds at Sb sites at the electrode surface via the nonbonded electron pairs of the hydroxyl group in acidic media (He and Mho 2004). The selective detection of glucose in a solution containing interference species such as ascorbic acid and uric acid was performed by using Cu-implanted BDD electrodes (Watanabe et al. 2006).

3.3.3 Electrochemical Activation

Electrode surface activation can be improved simply by electrochemical pretreatment. Determination of nitroaromatic compounds in water and soil spiked samples have been reported at electrochemically activated carbon-fiber microelectrodes. No interference was found from compounds such as hydrazine, phenolic compounds, carbamates, triazines or surfactants. The detection limit obtained can be approximately 0.03 $\mu g\,ml^{-1}$ for all the nitroaromatic compounds (Agui et al. 2005). Chen and coworkers reported an effective field-deployable tool for detecting nitroaromatic compounds with an electrochemically pre-anodized screen-printed carbon electrode (SPE) (Chen et al. 2006).

A semiautomatic screen printer was used to prepare the disposable SPE consisting of carbon as working and counter electrodes and silver pseudoreference electrode, as shown in Fig. 3.9. A stencil with the structure of five continuous electrodes was used in printing the conducting carbon on a flexible polypropylene film. A silver layer was first printed before coating the carbon ink (Acheron) to make an effective conductive nature for the SPE. Then, the unit was cured in a drybox at 100°C for 30 min. After drying, an insulating layer was finally printed over the SPE leaving the working area outside of the insulating cover.

3.3.4 Organic Surface Coating

Surface modification with organic chemicals was introduced. Cations, anions, dissolved oxygen, and organic chemicals in water have been detected with the

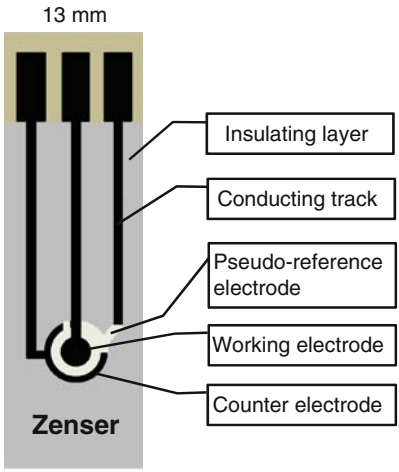

Fig. 3.9 Surface morphology of screen-printed carbon electrode (after Chen et al. 2006)

organic chemical modified electrode (Carrington et al. 2006; Luz et al. 2006; Park et al. 2006; Rahman et al. 2006; Shiddiky et al. 2006; Sun and Zhang 2006; Xiang et al. 2006; Zheng et al. 2006). Organic film can be simply coated by dispersing the organic containing solution on the substrate or soaking the substrate into the solution, and then baked at selected temperature to form the film (Luz et al. 2006; Manisankar et al. 2006; Sun and Zhang 2006). In order to further improve the adhesion between the organic film and the substrate electrode, electrochemical pretreatment is usually applied to modify the surface (Rahman et al. 2006). Li and his coworkers used the electrodeposition method to prepare the poly-1-naphthylamine doped by a ferrocenesulfonic acid (PNAFc) films on a platinum foil by continuous potential cycling between −0.2 and 1.5 V (vs. saturated calomel electrode) for ten cycles (Li et al. 2006b). After polymerization, the PNAFc films were washed thoroughly using a sulfuric acid solution (pH 3.0) to remove unreacted compounds. Figure 3.10 shows the SEM surface morphology images of the PNA- and PNAFc-coated platinum foil electrode.

3.3.5 Nanoparticle Deposition

Due to their small size and high surface area, nanoparticles can be applied to modify electrode surface property. Convenient and sensitive electrochemical sensors to various targets have been set up by using nanoparticle modification. The determination of acetaminophen in a commercial paracetamol oral solution was reported using a multiwall CNTs composite film-modified glassy carbon electrode with a detection limit of 50 nM (Li et al. 2006a). Heavy metal ions, such as arsenite (Dai and Compton 2006; Majid et al. 2006) and lead ion (Cui et al. 2005),

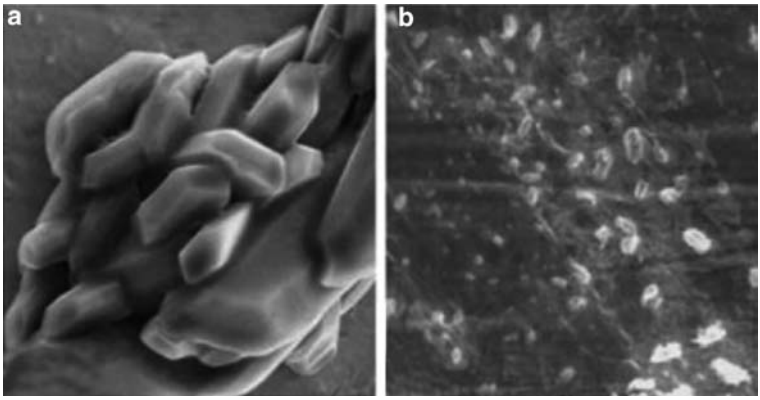

Fig. 3.10 SEM images of **(a)** PNA and **(b)** PNAFc (after Li et al. 2006b)

were detected using gold nanoparticles (Majid et al. 2006), platinum nanoparticle (Dai and Compton 2006), and nanostructured cryptomelane-type potassium manganese oxides (Cui et al. 2005) modified electrode with the detection limit in ppb level. Electrochemical sensor to detect anions in water, such as nitrite (Yang et al. 2005a) and bromated (Li et al. 2006c), was developed based on the gold nanoparticles and CNTs-modified electrodes with a detection limit in micromolar level. Organic chemicals have been successfully detected, including uric acid (UA) and ascorbic acid (AA) (Wei et al. 2006), TNT, and several other nitroaromatics (Hrapovic et al. 2006; Zhang et al. 2006a; Zhang et al. 2006b), with CeO_2 nanoparticles, CNTs, and SiO_2 nanoparticles-modified electrode with the detection limit in micromolar level. The Si-nanoparticle-modified electrode is used as the sensing element for an enzyme-free amperometric electrochemical glucose sensor. The Si-29 particle is significantly more efficient in generating signal current compared to both dissolved and immobilized enzyme (Wang et al. 2006a).

The nanoparticle-modified electrode can be simply developed by dispersing the nanoparticle containing solution on the electrode substrate (Yang et al. 2005a; Svancara et al. 2006; Wang et al. 2006a; Wei et al. 2006; Zhang et al. 2006a). Wang and his coworkers reported a method to fabricate silicon nanoparticle covered wafer shape electrode (Wang et al. 2006a). The 1-nm Si-29 particle was prepared as a water-based colloid. The cleaned heavily doped n-type Si wafer surface was covered with a mask to achieve a working area of about 1×1 mm^2. A drop of 0.1 ml of the Si-29 colloid was spread on the wafer surface, and the sample was incubated for 10 h and then rinsed with deionized water. The particle-covered wafer was prepared as the working electrode. Wei and his coworkers made the CeO_2 nanoparticle-modified electrode by placing the electrochemical pretreated electrode immersed into CeO_2 nanoparticles suspension for 24 h at 4°C, and then rinsed it with water (Wei et al. 2006).

Nanoparticles can be prepared with electrochemical deposition method. Dai and his coworkers made some platinum nanoparticle-modified glassy carbon electrodes

by potential cycling in 0.1 M aqueous KCl containing 1 mM K_2PtCl_6. In each potential cycle, the potential was held at +0.5 V for 0.01 s and at −0.7 V for 10 s. Some 25 cycles were used to prepare the electrodes optimally (Dai et al. 2006).

Surface performance of CNTs can be modified with organic or metal additions (Hrapovic et al. 2006; Li et al. 2006c; Zhang et al. 2006b). Zhang et al. (2006b) made the triphenylene (TP)-modified CNTs. Purified CNTs was dispersed in *N,N*-dimethylformamide (DMF) solution containing TP and ultrasonicated for 5 h. The products were rinsed with DMF to remove the excess TP, dried at 50°C to remove the solvent under vacuum, and finally obtain the functionalized sample of TP-CNTs. The samples of TP-CNTs were dispersed in DMF at a concentration of about 10 mg ml^{-1} and the solution was then dispersed directly onto the substrate surface. After DMF evaporation, a thin TP-CNTs film was formed on the substrate surface. A method to make uniform film consisting of a network of CNTs and metal nanoparticles was introduced by Hrapovic et al. (2006). CNTs were added to metal nanoparticles (Cu, Au, or Pt) containing Nafion (10 vol%), and the resulting suspension was deaerated with argon under sonification for 2 h. The dissolved nanocomposite was dropped on the substrate electrode and then it was dried for 20 min in an oven at 45°C, which resulted in the final product.

3.3.6 GOx Enzyme-Modified Electrode

Selective electrochemical detection of glucose was studied using a glucose oxidase enzyme (GOx)-decorated electrode. Wide linear calibration range has been reported from micromolar to millimolar level. Good detection results have been shown in water sample with common interferents (Ran et al. 1998; Zhao et al. 2006) in blood (Troupe et al. 1998) and in serum (Wu et al. 1996). The electrochemical detection method includes the typical amperometry method (Su et al. 2004; Mashazi et al. 2006; Pauliukaite et al. 2006; Xue et al. 2006) and impedance spectroscopy method (Shervedani et al. 2006). The substrate electrode covered the typical carbon material (Pauliukaite et al. 2006), gold (Mashazi et al. 2006; Shervedani et al. 2006; Xue et al. 2006), as well as diamond film electrode (Wu et al. 1996; Ran et al. 1998; Troupe et al. 1998; Spataru et al. 2004; Su et al. 2004; Zhao et al. 2006). The following sections give more details about the GOx enzyme decoration method.

3.3.6.1 Chemical Deposition

Figure 3.11 shows the chemical deposition process of GOx enzyme assembled 2-mercaptoethanol on gold that was previously modified by cobalt tetracarboxylic acid chloride phthalocyanine self-assembled monolayer gold. Electrochemical biosensor was introduced in the following steps: pretreatment → hydrolysis → functionalized surface → enzyme modification. Shervedani and his coworkers reported a similar

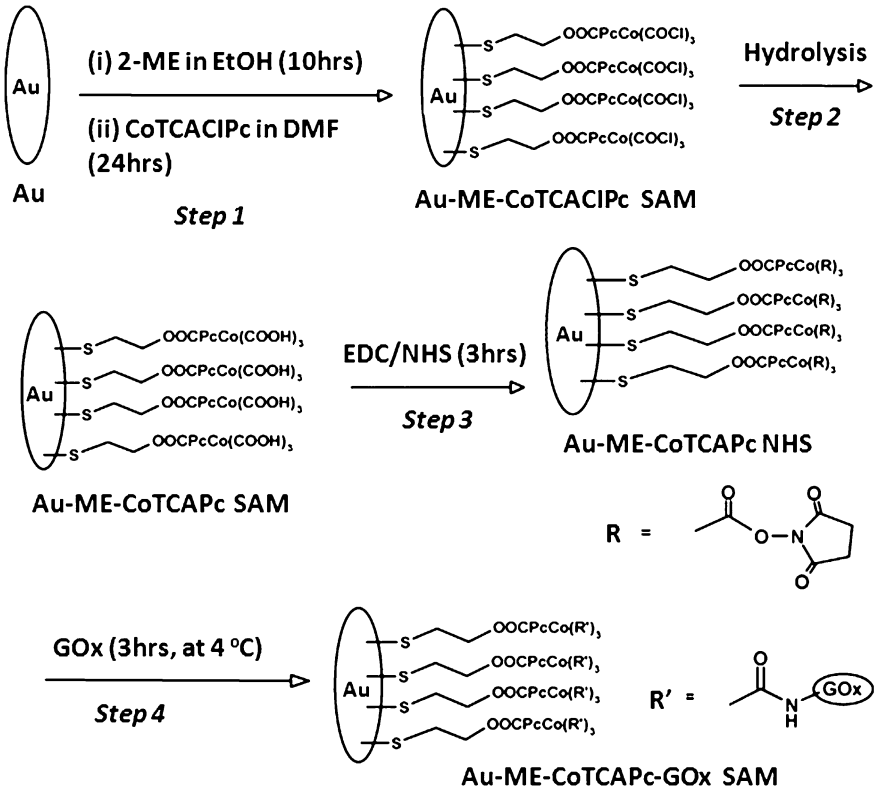

Fig. 3.11 Decoration of GOx enzyme on the Au-ME-CoTCAClPc electrode (after Mashazi et al. 2006)

process to make the GOx enzyme-decorated gold electrode (Shervedani et al. 2006). First, the cleaned gold electrode was modified with 3-mercaptopropionic acid (MPA) to form Au–MPA electrode. Second, the washed and dried Au–MPA electrode was activated in PBS solution containing 1-ethyl-3-(3-dimethylaminopropyl) carbodiimide hydrochloride and *N*-hydroxysuccinimide. Finally, the activated modified electrode was rinsed with the same PBS and immediately placed in PBS containing GOx enzyme for at least 1.5 h to fabricate Au–MPA–GOx SAMs electrode.

Su and his coworkers reported a simple way to make GOx enzyme-decorated diamond film electrode (Su et al. 2004). The enzyme containing solution was prepared in phosphate buffer containing bovine serum album. The mixture was added with glutaraldehyde, afterward. The resulting enzyme solution was rapidly coated onto the cleaned diamond film electrode with NaOH solution at room temperature by a syringe. The electrode was covered and incubated for 1 h at room temperature. After thoroughly washing with water, it was stored in dark at 4°C for use.

3.3.6.2 Sol–Gel Method

With sol–gel method, GOx enzyme was encapsulated onto carbon film electrode coated with the copper hexacyanoferrate (CuHCF) or poly(neutral red) (PNR) mediator (Pauliukaite et al. 2006). There are two steps: (1) surface modification of carbon film electrode with CuHCF using chemical deposition method or with PNR using electrochemical polymerization method and, (2) GOx enzyme deposition. GOx enzyme deposition involves three steps. First, sol–gel solution was prepared by mixing oxysilanes, choosing one from 3-aminopropyltriethoxysilane (APTOS), 3-glycidoxypropyl-trimethoxysilane (GOPMOS), or methyltrimethoxysilane (MTMOS), with water or 0.1 M phosphate buffer solution. Second, the prepared sol–gel solution was carefully mixed with GOx (10%) in 0.1 M phosphate buffer saline (PBS) solution with 50:15 ratio and left for 2 h to equilibrate. Finally, the CuHCF- or PNR-coated carbon film electrodes were immersed in the sol–gel enzyme solutions for 5 min before taking them out for sol–gel formation at 4°C for 3 days.

3.3.6.3 Electrochemical Deposition

Troupe and his coworkers reported a two-step method to electrochemically deposit GOx enzyme on a diamond film electrode (Troupe et al. 1998). In the first step, the GOx and BSA were dissolved in a buffer with pH = 7, greater than their isoelectric points. The BDD electrode was immersed into the solution and biased at 3.5 V for 2 h. Therefore, the negatively charged proteins (GOx and BSA) were drawn to the positively charged electrode. In the second step, the glutaraldehyde (GA) cross-links the protein layer forming a water insoluble barrier.

3.3.7 DNA-Modified Electrode

DNA base sensors for detection of biological agents have the advantages of high sensitivity, selectivity, ability to operate in turbid media, and to be amenable to miniaturization (Shah and Wilkins 2003). The biological agents include bacteria, viruses, and toxins that may be aerosoled deliberately in air, food, or water to spread terrorism and cause disease or death to humans, animals, or plants.

Various electrochemical biosensors have been developed with different special DNA targets. Electrochemical sensors detecting *Salmonella* spp. (Erdem et al. 2006), cancer gene (Feng et al. 2006), and human immunodeficiency virus (HIV) (Niu et al. 2006) have been developed. Different electrode materials have been applied. Genomagnetic assay is developed by using graphite-epoxy composite (GEC) and magneto-GEC (m-GEC) electrodes as electric transducers. The sensitive label-free detection by using GEC or m-GEC electrode as electrochemical transducers was combined with the efficient magnetic separation for improving

selectivity in this assay (Erdem et al. 2006). CeO_2/Chitosan (CHIT) composite matrix was developed for the single-stranded DNA (ssDNA) probe immobilization (Feng et al. 2006). Conducting polymer-based biosensors are likely to cater to the pressing requirements such as biocompatibility, possibility of in vivo sensing, continuous monitoring of drugs or metabolites, multiparametric assays, miniaturization, and high information density (Malhotra et al. 2006).

The use of nanoparticles has extended throughout the field of biosensors in the electrochemical detection of DNA and immunoreactions (Murphy 2006). A wide range of nanoparticles including nanotubes and nanowires, prepared from metals, semiconductor, carbon or polymeric species, have been investigated. The enhanced electrochemistry is due to the ability of the small nanoparticles to reduce the distance between the redox site of a protein and the electrode, since the rate of electron transfer is inversely dependent on the exponential distance between them (Balasubramanian and Burghard 2006). CNT-modified electrodes have been most frequently used for the development of biosensors (Gooding 2005).

Covalent immobilization method will be introduced in detail subsequently to show the making of a DNA-decorated biosensor. Figure 3.12 shows the fabricating process. Five steps are involved before the electrochemical measurement (Riccardi et al. 2006): electrode surface preparation; blocking of the modified electrode surface; HCV-specific oligonucleotide probes immobilization; extraction of the HCV RNA from patient sera; and Avidin–peroxidase labeling. Amperometry was applied with the fabricated biosensor for detection. The enzymatic response was investigated by constant potential amperometry at 0.45 V (vs. Ag/AgCl reference electrode). The current intensity obtained is proportional to amount of HCV amplicons in the samples.

3.4 Ultramicro- or Nanoscale Electrode

Electrodes with dimensions from micrometer to nanometer range are becoming interesting. The advantages arising from these small-sized electrodes include enhanced mass transport, reduced IR drop, and double layer charging effects. These submicrometer-sized electrodes have extended electrochemical methodology into broad new domains of space (single cells, membrane pores), time (steady-state, fast-sweep), chemical medium (nonaqueous solvents, unsupported electrolytes, ice, air), and methodology (kinetics, single molecule studies, AFM, STM, SECM) (Wightman 1981; Montenegro et al. 1991; Heinze 1993; Kawagoe et al. 1993; Barker et al. 1999; Stulik et al. 2000; Yasukawa et al. 2000; Zoski 2002).

Within a regular scanning electrochemical microscopy (SECM) system, the probe microelectrode, called the tip electrode, can be precisely positioned several micrometers away from a substrate under the control of a three-dimensional motorized positioner in the solution containing redox-active species. By scanning the SECM tip within the plane paralleling a substrate surface and simultaneously monitoring tip current (i_T), which is sensitive to the presence of conducting and

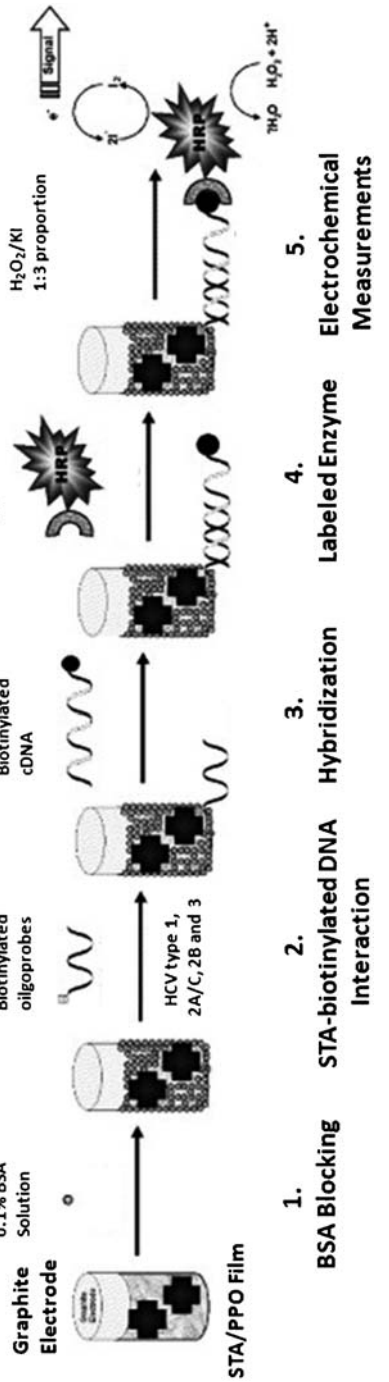

Fig. 3.12 Schematic diagram of the process to fabricated DNA modified electrode (after Riccardi et al. 2006)

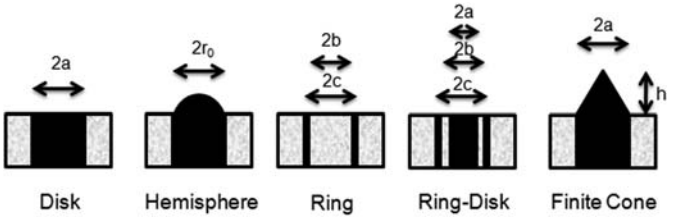

Fig. 3.13 Popular ultra-micro electrode (UME) geometries. *a* radius of disk or finite conical electrode, r_0 radius of hemispherical electrode, *b* inner radius of ring electrode, and *c* outer radius of ring electrode (after Zoski 2002)

electroactive species on the substrate surface, as a function of the tip location, SECM images reflecting the electrochemical properties of the surface could be obtained (Bard et al. 1991; Wipf and Bard 1991a). The dependence of the SECM feedback current on electron-transfer kinetics was used as the basis for imaging variations in electrochemical activity over an electrode surface (Wipf and Bard 1991b; Mirkin and Bard 1992; Mirkin et al. 1992; Pierce et al. 1992; Wang et al. 2006c) and mapping the redox distribution on a substrate surface (Scott et al. 1992; Horrocks et al. 1993; Arca et al. 1995; Lee and Bard 2002; De Souza and Machado 2006; Tel-Vered et al. 2006). Figure 3.13 shows five types of popular ultramicro electrode (UME) geometry shapes. Operationally, a UME has been defined as an electrode having at least one dimension, called the critical dimension, smaller than 25 μm (Zoski 2002). Disk shape electrode is the popular one used in SECM system as a tip. The following will give some examples of the submicroscale electrode fabrication.

Fabrication procedure of gold nanodisk electrodes (NEEs) is schematically shown in Fig. 3.14 (Menon and Martin 1995; Pereira et al. 2006). Step I: A piece of the Au/Au–PC/Au membrane is first affixed to a piece of adhesive aluminum foil tape (Fig. 3.14a). Step II: A rectangular strip of a copper foil, with a conductive adhesive, is then affixed to the upper Au-coated surface of the Au/Au–PC/Au membrane (Fig. 3.14b). This Cu foil tape acts as a current collector and working electrode lead for the NEE. Step III: The upper Au surface layer from the portion of the Au/Au–PC/Au membrane not covered by the Cu foil tape is then removed by simply applying and then removing a strip of Scotch tape. Removal of the Au surface layer exposes the disk-shaped ends of the Au nanowires within the pores of the membrane (Fig. 3.14c). These nanodisks will become the active electrode elements. Step IV: The NEE assembly is heat treated at 150°C for 15 min. This produces a water-tight seal between the Au nanowires and the pore walls. Finally, strips of strapping tape are applied to the lower and upper surfaces of the assembly to insulate the Al and Cu foil tapes (Fig. 3.14d).

Carbon microelectrodes decorated with enzyme were prepared with two different methods (Horrocks et al. 1993). Type A electrode (Fig. 3.15a) was prepared by heat sealing carbon fibers, with diameter of 11 or 8 μm, in 2-mm outer diameter (OD) Pyrex capillaries. The resulting tip geometry was an inlaid microdisk electrode. The carbon microdisk was then coated with the electrically wired enzyme by soaking the

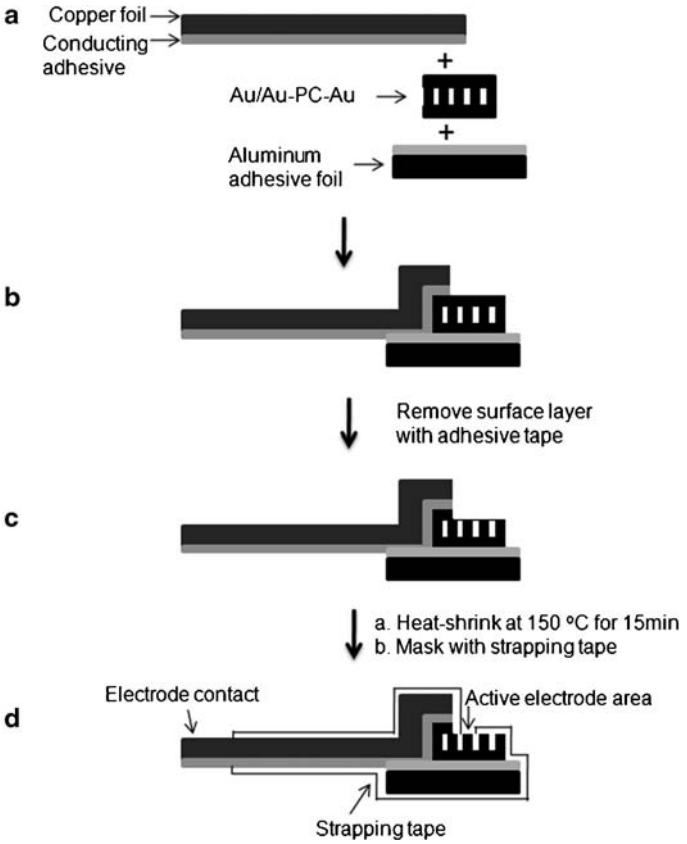

Fig. 3.14 Schematic process for fabrication NEEs (after Menon and Martin 1995)

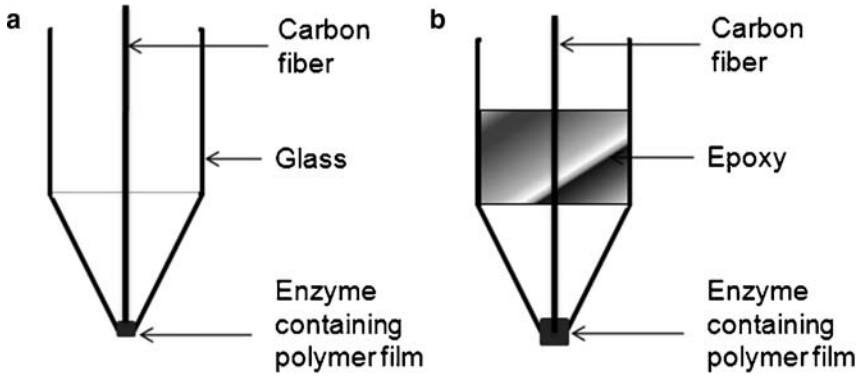

Fig. 3.15 Schematic shape of two different types of carbon microelectrodes decorated with enzyme (after Horrocks et al. 1993)

electrode tip in a drop of the enzyme containing coating solution. The solution was allowed to dry and form a roughly 1 − μm-thick film coating the surface of the tip. The film was cured at ambient temperature in air for a minimum of 2 days. Type B electrode (Fig. 3.15b) was fabricated by the following procedure. A 7-μm diameter carbon fiber was inserted into a 2-mm OD glass tube, and the tube was pulled on a micropipet puller to yield a glass tip of approximately 2-μm OD. The glass tip was then partially filled with a low-viscosity epoxy, leaving a microcylinder as the electrode surface, and was cured at 70°C overnight. The tip was then polished at an angle of 90° with a micropipet beveler to produce smooth carbon surface. Electrical contact to the carbon fiber was made by filling the top of the tube with mercury and inserting a stainless steel wire. The carbon microcylinder tip was coated with the enzyme containing solution.

The procedure for the fabrication of the Pt submicroelectrodes is shown in Fig. 3.16 (Slevin et al. 1999). Namely, Step I: Seal of Pt microwire (Fig. 3.16a). The Pt microwire with 50 μm diameter was mounted in a glass capillary, which was drawn to a fine point using a pipette puller with 3–5 mm microwire protruded from the tip of glass capillary. Step II: Etching Pt microwire (Fig. 3.16b). The protruded Pt wire was electrochemically etched by applying 1.2 V potential between the Pt wire and the counter electrode. The etching procedure was finished when the current decreased to zero. Step III: Microwire insulation (Fig. 3.16c). Insulating paint

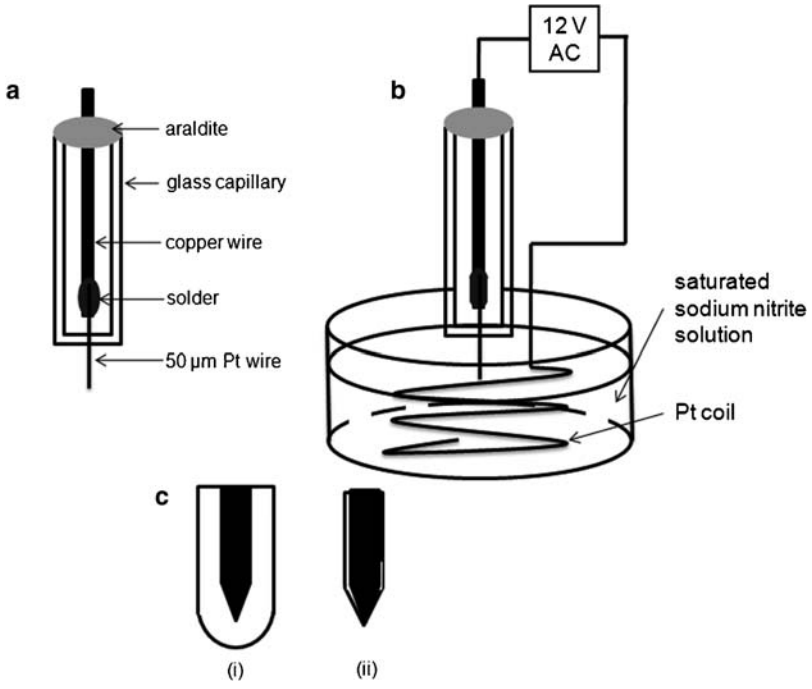

Fig. 3.16 Procedure for fabricating the Pt submicroelectrode (after Slevin et al. 1999)

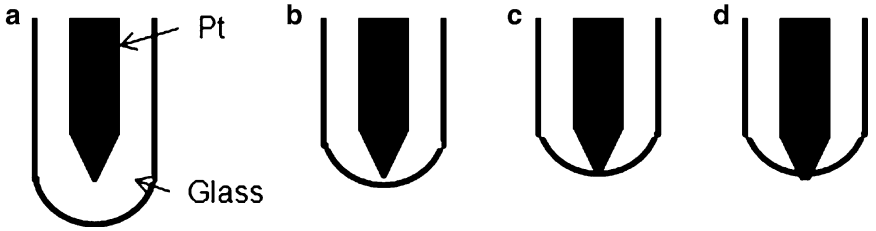

Fig. 3.17 Schematic diagram of the process for removing the seal and getting the exposed micro tip of Pt electrode (after Lee et al. 1991)

film was electrochemically deposited on the wire electrode by anodic or cathodic polarization. The deposited film was hardened by heating at 200°C for 180 s. Film shrinkage during heat curing should leave only the end of the tip exposed, and the exposed area will work as the electrode. Another way to seal and make the exposed tip of the submicroelectrode was shown in Fig. 3.17 (Lee et al. 1991). After sealing of the Pt wire into the Pyrex capillary glass, excess glass near the tip of the Pt wire (Fig. 3.17a) was removed by heating the electrode in the resistive heater coil. Heating was halted just before the Pt tip was exposed (Fig. 3.17b). The end of the electrode was then polished with 0.05-μm alumina paste until the tip of the sharpened Pt wire was exposed (Fig. 3.17c). The diameter of the exposed Pt disk could be controlled from ca. 0.2 to 25 μm by controlling the extent of this final polishing. Further heating for 0.5–1 min caused the glass to pull away from the Pt wire so that the small exposed Pt disk can be protruded from the sealed glass (Fig. 3.17d).

3.5 Concluding Remarks

Electrochemical engineering has gained recognition in recent decades along with the discovery of various capable electrode materials to achieve the desired purpose. In fabricating the electrodes, the heart of an electrochemical process, the thermal decomposition has been widely employed in making metal-oxide film electrodes with advantages of easy processing and low cost. By changing the metal composition, the electrochemical properties of the obtained electrodes can be tailored. CVD methods might be the major method to produce CNTs and various metal-oxide film electrodes, whereas hot-filament and plasma-enhanced CVD methods are the best options for fabrication of diamond film electrodes.

With the help of surface modification, the catalytic activity and selectivity could be manipulated by tailoring the structure of the electrodes. The rapid development of nanotechnology and bioscience has been witnessed by a large number of recent literatures on novel electrodes such as BDD, nanoelectrodes, and biosensors. This trend is likely to remain so for the next decade when the hot research topics for electrochemistry will be in advanced materials, biochemical-related application, and environmental analysis and protection.

References

Ager, J. W. and Drory, M. D. (1993), Quantitative measurement of residual biaxial stress by Raman-spectroscopy in diamond grown on a Ti alloy by chemical-vapor-deposition. Phys. Rev. B, 48(4): 2601–2607.

Agui, L., Vega-Montenegro, D., Yanez-Sedeno, P. and Pingarron, J. M. (2005), Rapid voltammetric determination of nitroaromatic explosives at electrochemically activated carbon-fibre electrodes. Anal. Bioanal. Chem., 382(2): 381–387.

Alves, V. A., Silva, L. A. D., Oliveira, E. D. and Boodts, J. F. C. (1998), Investigation under conditions of accelerated anodic corrosion of the effect of TiO_2 substitution by CeO_2 on the stability of Ir-based ceramic coatings. Mater. Sci. Forum, 289–292: 655–666.

Angelinetta, C., Trasatti, S., Atanasoska, L. D., Minevski, Z. S. and Atanasoski, R. T. (1989), Effect of preparation on the surface and electrocatalytic properties of $RuO_2 + IrO_2$ mixed oxide electrodes. Mater. Chem. Phys., 22(1–2): 231–247.

Angus, J. C. and Hayman, C. C. (1988), Low-pressure, metastable growth of diamond and "diamondlike" phases. Science, 241(4868): 913–921.

Angus, J. C., Argoitia, A., Gat, R., Li, Z., Sunkara, M., Wang, L. and Wang, Y. (1993), Chemical vapour deposition of diamond. Philos. Trans. Phys. Sci. Eng., 342(1664): 195–208.

Arca, M., Mirkin, M. V. and Bard, A. J. (1995), Polymer-films on electrodes. 26. Study of ion-transport and electron-transfer at polypyrrole films by scanning electrochemical microscopy. J. Phys. Chem., 99(14): 5040–5050.

Arribas, A. S., Bermejo, E., Chicharro, M. and Zapardiel, A. (2006), Voltammetric detection of the herbicide metamitron at a bismuth film electrode in nondeaerated solution. Electroanalysis, 18(23): 2331–2336.

Awad, H. S. and Galwa, N. A. (2005), Electrochemical degradation of acid blue and basic brown dyes on Pb/PbO_2 electrode in the presence of different conductive electrolyte and effect of various operating factors. Chemosphere, 61(9): 1327–1335.

Bachmann, P. K., Leers, D. and Lydtin, H. (1991), Towards a general concept of diamond chemical vapour deposition. Diam. Relat. Mater., 1(1): 1–12.

Balasubramanian, K. and Burghard, M. (2006), Biosensors based on carbon nanotubes. Anal. Bioanal. Chem., 385(3): 452–468.

Banholzer, W. (1992), Understanding the mechanism of CVD diamond. Surf. Coat. Technol., 53(1): 1–12.

Baranauskas, V., Ceragioli, H. J., Peterlevitz, A. C., Tosin, M. C. and Durrant, S. F. (2000), Effects of argon dilution of an ethanol/hydrogen gas feed on the growth of diamond by hot-filament chemical vapor deposition. Thin Solid Films, 377–378: 303–308.

Bard, A. J., Fan, F. R. F., Pierce, D. T., Unwin, P. R., Wipf, D. O. and Zhou, F. M. (1991), Chemical imaging of surfaces with the scanning electrochemical microscope. Science, 254(5028): 68–74.

Barker, A. L., Gonsalves, M., MacPherson, J. V., Slevin, C. J. and Unwin, P. R. (1999), Scanning electrochemical microscopy: Beyond the solid/liquid interface. Anal. Chim. Acta, 385(1–3): 223–240.

Beer, H. B., Belgian, Patent 710751 (1968).

Beer, H. B., British, Patent 1147442 (1969).

Beer, H. B., US, Patent 3632498 (1972).

Beer, H. B., US, Patent 3711385 (1973).

Beer, H. B. (1980), The invention and industrial development of metal anodes. J. Electrochem. Soc., 127(8): 303C–307C.

Bejan, D., Sagitova, F. and Bunce, N. J. (2005), Evaluation of electrolysis for oxidative deodorization of hog manure. J. Appl. Electrochem., 35(9): 897–902.

Ben Mansour, L. and Chalbi, S. (2006), Removal of oil from oil/water emulsions using electroflotation process. J. Appl. Electrochem., 36(5): 577–581.

Bergmann, M. E. H. and Koparal, A. S. (2005), Studies on electrochemical disinfectant production using anodes containing RuO_2. J. Appl. Electrochem., 35(12): 1321–1329.

Bergmann, H., Iourtchouk, T., Schops, K. and Bouzek, K. (2002), New UV irradiation and direct electrolysis – promising methods for water disinfection. Chem. Eng. J., 85(2–3): 111–117.

Bruckner, J. and Mantyla, T. (1993), Diamond chemical vapour deposition using tantalum filaments in H_2–CH_4–O_2 gas mixtures. Diam. Relat. Mater., 2(2–4 pt 1): 373–377.

Bruhne, K., Kumar, K. V., Fecht, H. J., Gluche, P. and Floter, A. (2005), Nanocrystalline HFCVD-grown diamond and its industrial applications. Rev. Adv. Mater. Sci., 10(3): 224–228.

Brunsteiner, R., Haubner, R. and Lux, B. (1996), Influence of carbon monoxide – addition to the reaction gas on the hot-filament diamond deposition. Int. J. Refract. Met. Hard Mater., 14(1–3 SPEC. ISS.): 127–135.

Campari, M., Tavares, A. C. and Trasatti, S. (2002), Thermally prepared Ti/RhO_x electrodes – II; H_2 evolution in acidic solution. Chem. Ind. J., 56(6): 231–237.

Canizares, P., Martinez, F., Diaz, M., Garcia-Gomez, J. and Rodrigo, M. A. (2002), Electrochemical oxidation of aqueous phenol wastes using active and nonactive electrodes. J. Electrochem. Soc., 149(8): D118–D124.

Canizares, P., Lobato, J., Paz, R., Rodrigo, M. A. and Saez, C. (2005), Electrochemical oxidation of phenolic wastes with boron-doped diamond anodes. Water Res., 39(12): 2687–2703.

Cardarelli, F., Taxil, P., Savall, A., Comninellis, C., Manoli, G. and Leclerc, O. (1998), Preparation of oxygen evolving electrodes with long service life under extreme conditions. J. Appl. Electrochem., 28(3): 245–250.

Carrington, N. A., Yong, L. and Xue, Z. L. (2006), Electrochemical deposition of sol–gel films for enhanced chromium(VI) determination in aqueous solutions. Anal. Chim. Acta, 572(1): 17–24.

Casella, I. G., Contursi, M. and Desimoni, E. (2002), Amperometric detection of sulfur-containing compounds in alkaline media. Analyst, 127(5): 647–652.

Cassidy, W. D., Evans, E. A., Wang, Y., Angus, J. C., Bachmann, P. K., Hagemann, H.-J., Leers, D. and Wiechert, D. U. (1994), Diamond growth rates and quality: Dependence on gas phase composition. *Materials Research Society Symposium – Proceedings*. Case Western Reserve University, Cleveland, OH.

Chandra, L., Chhowalla, M., Amaratunga, G. A. J. and Clyne, T. W. (1996), Residual stresses and debonding of diamond films on titanium alloy substrates. Diam. Relat. Mater., 5(6–8): 674–681.

Chang, C. P., Flamm, D. L., Ibbotson, D. E. and Mucha, J. A. (1988), Diamond crystal growth by plasma chemical vapor deposition. J. Appl. Phys., 63(5): 1744.

Chatzisymeon, E., Xekoukoulotakis, N. P., Coz, A., Kalogerakis, N. and Mantzavinos, D. (2006), Electrochemical treatment of textile dyes and dyehouse effluents. J. Hazard. Mater., 137(2): 998–1007.

Chein, T. H. and Tzeng, Y. (1999), CVD diamond grown by microwave plasma in mixtures of acetone/oxygen and acetone/carbon dioxide. Diam. Relat. Mater., 8(8–9): 1393–1401.

Chen, X. and Chen, G. (2005a), Investigation of $Ti/IrO_2-b_2O_5-SnO_2$ electrodes for O_2 evolution calcination temperature and precursor composition effects. J. Electrochem. Soc., 152(7).

Chen, X. and Chen, G. (2005b), Stable $Ti/RuO_2 - Sb_2O_5 - SnO_2$ electrodes for O_2 evolution. Electrochim. Acta, 50(20): 4155–4159.

Chen, Q. J. and Lin, Z. D. (1995), Diamond growth on thin Ti wafers via chemical-vapor-deposition. J. Mater. Res., 10(11): 2685–2688.

Chen, C.-F., Huang, Y. C., Hosomi, S. and Yoshida, I. (1989), Effect of oxygen addition on microwave plasma CVD of diamond from CH_4–H_2 mixture. Mater. Res. Bull., 24(1): 87–94.

Chen, C.-F., Chen, S.-H., Ko, H.-W. and Hsu, S. E. (1994), Low temperature growth of diamond films by microwave plasma chemical vapor deposition using $CH_4 + CO_2$ gas mixtures. Diam. Relat. Mater., 3(4–6): 443–447.

Chen, G. H., Chen, X. M. and Yue, P. L. (2000), Electrocoagulation and electroflotation of restaurant wastewater. J. Environ. Eng. -ASCE, 126(9): 858–863.

Chen, X., Chen, G. and Yue, P. L. (2001), Stable Ti/IrO_x–Sb_2O_5–SnO_2 anode for O_2 evolution with low Ir content. J. Phys. Chem. B, 105: 4623–4628.

Chen, G., Chen, X. and Yue, P. L. (2002a), Electrochemical behavior of novel Ti/IrO_x–Sb_2O_5–SnO_2 anodes. 106: 4364–4369.

Chen, X., Chen, G. and Yue, P. L. (2002b), Novel electrode system for electroflotation of wastewater. Environ. Sci. Technol., 36(4): 778–783.

Chen, X., Chen, G., Gao, F. and Yue, P. L. (2003), High-performance Ti/BDD electrodes for pollutant oxidation. Environ. Sci. Technol., 37(21): 5021–5026.

Chen, X., Gao, F. and Chen, G. (2005), Comparison of Ti/BDD and Ti/SnO_2–Sb_2O_5 electrodes for pollutant oxidation. J. Appl. Electrochem., 35(2): 185–191.

Chen, J. C., Shih, J. L., Liu, C. H., Kuo, M. Y. and Zen, J. M. (2006), Disposable electrochemical sensor for determination of nitroaromatic compounds by a single-run approach. Anal. Chem., 78(11): 3752–3757.

Chopra, K. L., Major, S. and Pandya, D. K. (1983), Transparent conductors – a status review. Thin Solid Films, 102(1): 1–46.

Codognoto, L., Tanimoto, S. T., Pedrosa, V. A., Suffredini, H. B., Machado, S. A. S. and Avaca, L. A. (2006), Electroanalytical determination of carbaryl in natural waters on boron doped diamond electrode. Electroanalysis, 18(3): 253–258.

Comninellis, C. (1994), Electrocatalysis in the electrochemical conversion/combustion of organic pollutants for waste water treatment. Electrochim. Acta, 39(11–12): 1857–1862.

Comninellis, C. and Pulgarin, C. (1993), Electrochemical oxidation of phenol for wastewater treatment using SnO2 anodes. J. Appl. Electrochem., 23(2): 108–112.

Comninellis, C. and Vercesi, G. P. (1991a), Characterization of DSA-type oxygen evolving electrodes: Choice of a coating. J. Appl. Electrochem., 21(4): 335–345.

Comninellis, C. and Vercesi, G. P. (1991b), Problems in DSA® coating deposition by thermal decomposition. J. Appl. Electrochem., 21(2): 136–142.

Cooper, J. B., Pang, S., Albin, S., Zheng, J. and Johnson, R. M. (1998), Fabrication of boron-doped CVD diamond microelectrodes. Anal. Chem., 70(3): 464–467.

Corat, E. J., Trava-Airoldi, V. J., Leite, N. F., Pena, A. F. V. and Baranauskas, V. (1994), Low temperature diamond growth with CF_4 addition in a hot filament reactor. *Materials Research Society Symposium – Proceedings*. Spring Meeting, San Fransisco, CA.

Correa-Lozano, B., Comninellis, C. and De Battisri, A. (1996), Physicochemical properties of SnO_2–Sb_2O_5 films prepared by the spray pyrolysis technique. J. Electrochem. Soc., 143(1): 203–209.

Correa-Lozano, B., Comninellis, C. and De Battisti, A. (1997), Service life of Ti/SnO_2–Sb_2O_5 anodes. J. Appl. Electrochem., 27(8): 970–974.

Coteiro, R. D., Teruel, F. S., Ribeiro, J. and De Andrade, A. R. (2006), Effect of solvent on the preparation and characterization of DSA-type anodes containing RuO_2–TiO_2–SnO_2. J. Braz. Chem. Soc., 17(4): 771–779.

Cui, X. L., Liu, G. D., Li, L. Y., Yantasee, W. and Lin, Y. H. (2005), Electrochemical sensor based on carbon paste electrode modified with nanostructured cryptomelane-type manganese oxides for detection of heavy metals. Sensor Lett., 3(1): 16–21.

Da Silva, L. M., Franco, D. V., Forti, J. C., Jardim, W. F. and Boodts, J. F. C. (2006), Characterisation of a laboratory electrochemical ozonation system and its application in advanced oxidation processes. J. Appl. Electrochem., 36(5): 523–530.

Dai, X. and Compton, R. G. (2006), Detection of As(III) via oxidation to As(V) using platinum nanoparticle modified glassy carbon electrodes: Arsenic detection without interference from copper. Analyst, 131(4): 516–521.

Davis, R. F. (1993), *Diamond Films and Coatings: Development, Properties, and Applications*. Noyes Publications, Park Ridge, NJ.

De Souza and Machado, S. A. S. (2006), Study of the electrochemical behavior and sensitive detection of pesticides using microelectrodes allied to square-wave voltammetry. Electroanalysis, 18(9): 862–872.

De Souza, D., De Toledo, R. A., Suffredini, H. B., Mazo, L. H. and Machado, S. A. S. (2006), Characterization and use of copper solid amalgam electrode for electroanalytical determination of triazines-based herbicides. Electroanalysis, 18(6): 605–612.

Deguchi, M., Kitabatake, M. and Hirao, T. (1996), Electrical properties of boron-doped diamond films prepared by microwave plasma chemical vapour deposition. Thin Solid Films, 281–282(1–2): 267–270.

Devilliers, D., Devos, B. and Groult, H. (2007), Dimensionally stable PbO_2 electrodes for lead acid batteries. J. New Mater. Electrochem. Sys., 10(3): 187–193.

Dikonimos Makris, T., Giorgi, R., Lisi, N., Pilloni, L., Salernitano, E., Sarto, F. and Alvisi, M. (2004), Carbon nanotubes growth by HFCVD: Effect of the process parameters and catalyst preparation. Diam. Relat. Mater., 13(2): 305–310.

Drory, M. D. and Hutchinson, J. W. (1994), Diamond coating of titanium alloys. Science, 263(5154): 1753–1755.

Duby, P. (1993), The history of progress in dimensionally stable anodes. J. Miner. Met. Mater. Soc., 45(3): 41–43.

Erdem, A., Pividori, M. I., Lermo, A., Bonanni, A., del Valle, M. and Alegret, S. (2006), Genomagnetic assay based on label-free electrochemical detection using magneto-composite electrodes. Sensor Actuator B Chem., 114(2): 591–598.

Fang, Q., Shang, C. and Chen, G. H. (2006), MS2 inactivation by chloride-assisted electrochemical disinfection. J. Environ. Eng., 132(1): 13–22.

Faouzi, A. M., Nasr, B. and Abdellatif, G. (2007), Electrochemical degradation of anthraquinone dye alizarin reds by anodic oxidation on boron-doped diamond. Dyes Pigments, 73(1): 86–89.

Fayette, L., Mermoux, M. and Marcus, B. (1994), Role of the nucleation step in the growth rate of diamond films. Diam. Relat. Mater., 3(4–6): 480–485.

Feng, K. J., Yang, Y. H., Wang, Z. J., Jiang, J. H., Shen, G. L. and Yu, R. Q. (2006), A nanoporous CeO_2/Chitosan composite film as the immobilization matrix for colorectal cancer DNA sequence-selective electrochemical biosensor. Talanta, 70(3): 561–565.

Ferrer, J. E. and Victori, L. (1994), Oxygen evolution reaction on the iridium electrode in basic medium studied by electrochemical impedance spectroscopy. Electrochim. Acta, 39(4): 581–588.

Fierro, J. L. G. (2006), *Metal Oxides: Chemistry and Applications*. CRC, Boca Raton, FL.

Foti, G., Gandini, D., Comninellis, C., Perret, A. and Haenni, W. (1999), Oxidation of organics by intermediates of water discharge on IrO_2 and synthetic diamond anodes. Electrochem. Solid State Lett., 2(5): 228–230.

Frohlich, K., Machajdik, D., Cambel, V., Luptak, R., Pignard, S., Weiss, F., Baumann, P. and Lindner, J. (2001), Substrate dependent growth of highly conductive RuO_2 films. J. De Phys., 11: Pr11-77-81.

Fu, Y. Q., Du, H. J. and Sun, C. Q. (2003), Interfacial structure, residual stress and adhesion of diamond coatings deposited on titanium. Thin Solid Films, 424(1): 107–114.

Galizzioli, D., Tantardini, F. and Trasatti, S. (1974), Ruthenium dioxide: A new electrode material. I. Behaviour in acid solutions of inert electrolytes. J. Appl. Electrochem., 4(1): 57–67.

Galizzioli, D., Tantardini, F. and Trasatti, S. (1975), Ruthenium dioxide: A new electrode material. II. Non-stoichiometry and energetics of electrode reactions in acid solutions. J. Appl. Electrochem., 5(3): 203–214.

Gao, P., Chen, X. M., Shen, F. and Chen, G. H. (2005), Removal of chromium(VI) from wastewater by combined electrocoagulation – electroflotation without a filter. Purif. Technol., 43(2): 117–123.

Gerger, I., Haubner, R., Kronberger, H. and Fafilek, G. (2004), Investigation of diamond coatings on titanium substrates for electrochemical applications. Diam. Relat. Mater., 13(4–8): 1062–1069.

Ghasemi, S., Mousavi, M. F. and Shamsipur, M. (2007), Electrochemical deposition of lead dioxide in the presence of polyvinylpyrrolidone. A morphological study. Electrochim. Acta, 53(2): 459–467.

Gilbert, D. R., Singh, R. K. and Huang, M. (1999), Chemical vapor deposition of diamond from alcohol precursors at 1.0 torr. Mater. Res. Soc. Symp. Proc., 555: 227–232.

Gooding, J. J. (2005), Nanostructuring electrodes with carbon nanotubes: A review on electrochemistry and applications for sensing. Electrochim. Acta, 50(15): 3049–3060.

Gopal Ganesan, P. and Eizenberg, M. (2003), Chemical vapor deposited RuO_x films: Interfacial adhesion study. Mater. Sci. Eng. B: Solid-State Mater. Adv. Technol., 103(3): 213–218.

Gun, J., Salaun, P. and van den Berg, C. M. G. (2006), Advantages of using a mercury coated, micro-wire, electrode in adsorptive cathodic stripping voltammetry. Anal. Chim. Acta, 571(1): 86–92.

Guo, L. and Chen, G. (2007a), High-quality diamond film deposition on a titanium substrate using the hot-filament chemical vapor deposition method. Diam. Relat. Mater., 16(8): 10.

Guo, L. and Chen, G. (2007b), Long-term stable Ti/BDD electrode fabricated with HFCVD method using two-stage substrate temperature. J. Electrochem. Soc., 154(12).

Guzsvany, V., Kaddar, M., Gaal, F., Bjelica, L. and Toth, K. (2006), Bismuth film electrode for the cathodic electrochemical determination of thiamethoxam. Electroanalysis, 18(13–14): 1363–1371.

Hattori, S., Doi, M., Takahashi, E., Kurosu, T., Nara, M., Nakamatsu, S., Nishiki, Y., Furuta, T. and Iida, M. (2003), Electrolytic decomposition of Amaranth dyestuff using diamond electrodes. J. Appl. Electrochem., 33(1): 85–91.

Haubner, R. and Lux, B. (1993), Diamond growth by hot-filament chemical vapor deposition: State of the art. Diam. Relat. Mater., 2(9): 1277–1294.

Haubner, R., Bohr, S. and Lux, B. (1999), Comparison of P, N and B additions during CVD diamond deposition. Diam. Relat. Mater., 8(2–5): 171–178.

He, D. L. and Mho, S. I. (2004), Electrocatalytic reactions of phenolic compounds at ferric ion co-doped SnO_2 : Sb^{5+} electrodes. J. Electroanal. Chem., 568(1–2): 19–27.

Heinze, J. (1993), Ultramicroelectrodes in electrochemistry. Angew. Chem., 32(9): 1268–1288.

Hian, L. C., Grehan, K. J., Compton, R. G., Foord, J. S. and Marken, F. (2003), Nanodiamond thin films on titanium substrates growth and electrochemical properties. J. Electrochem. Soc., 150(1): E59–E56.

Hirakuri, K. K., Kobayashi, T., Nakamura, E., Mutsukura, N., Friedbacher, G. and Machi, Y. (2001), Influence of the methane concentration on hf-cvd diamond under atmospheric pressure. Vacuum, 63(3): 449–454.

Hitchman, M. L. and Jensen, K. F. (1993), *Chemical Vapor Deposition: Principles and Applications*. Academic, London.

Hong, F. C.-N., Hsieh, J.-C., Wu, J.-J., Liang, G.-T. and Hwang, J.-H. (1993), Low temperature deposition of diamond using chloromethane in a hot-filament chemical vapor deposition reactor. Diam. Relat. Mater., 2(2–4 pt 1): 365–372.

Horrocks, B. R., Schmidtke, D., Heller, A. and Bard, A. J. (1993), Scanning electrochemical microscopy.24. Enzyme ultramicroelectrodes for the measurement of hydrogen-peroxide at surfaces. Anal. Chem., 65(24): 3605–3614.

Hrapovic, S., Majid, E., Liu, Y., Male, K. and Luong, J. H. T. (2006), Metallic nanoparticle-carbon nanotube composites for electrochemical determination of explosive nitroaromatic compounds. Anal. Chem., 78(15): 5504–5512.

Hrussanova, A., Guerrini, E. and Trasatti, S. (2004), Thermally prepared Ti/RhO_x electrodes IV: O_2 evolution in acid solution. J. Electroanal. Chem., 564(1–2): 151–157.

Huang, H., Tan, O. K., Lee, Y. C. and Tse, M. S. (2006), Preparation and characterization of nanocrystalline SnO_2 thin films by PECVD. J. Cryst. Growth, 288(1): 70–74.

Hutton, E. A., Ogorevc, B., Hocevar, S. B. and Smyth, M. R. (2006), Bismuth film microelectrode for direct voltammetric measurement of trace cobalt and nickel in some simulated and real body fluid samples. Anal. Chim. Acta, 557(1–2): 57–63.

Ivandini, T. A., Rao, T. N., Fujishima, A. and Einaga, Y. (2006a), Electrochemical oxidation of oxalic acid at highly boron-doped diamond electrodes. Anal. Chem., 78(10): 3467–3471.

Ivandini, T. A., Sato, R., Makide, Y., Fujishima, A. and Einaga, Y. (2006b), Electrochemical detection of arsenic(III) using iridium-implanted boron-doped diamond electrodes. Anal. Chem., 78(18): 6291–6298.

Iwakura, C., Inai, M., Uemura, T. and Tamura, H. (1981), Anodic evolution of oxygen and chlorine on foreign metal-doped SnO_2 film electrodes. Electrochim. Acta, 26(4): 579–584.

Jasmin Shah, E. W. (2003), Electrochemical biosensors for detection of biological warfare agents. Electroanalysis, 15: 157–167.
Jeong, J., Kim, J. Y. and Yoon, J. (2006), The role of reactive oxygen species in the electrochemical inactivation of microorganisms. Environ. Sci. Technol., 40(19): 6117–6122.
Ji, X. B., Banks, C. E. and Compton, R. G. (2005), The electrochemical oxidation of ammonia at boron-doped diamond electrodes exhibits analytically useful signals in aqueous solutions. Analyst, 130(10): 1345–1347.
Kawagoe, K. T., Zimmerman, J. B. and Wightman, R. M. (1993), Principles of voltammetry and microelectrode surface states. J. Neurosci. Methods, 48(3): 225–240.
Kefala, G. and Economou, A. (2006), Polymer-coated bismuth film electrodes for the determination of trace metals by sequential-injection analysis/anodic stripping voltarnmetry. Anal. Chim. Acta, 576(2): 283–289.
Khelifa, A., Moulay, S. and Naceur, A. W. (2005), Treatment of metal finishing effluents by the electroflotation technique. Desalination, 181(1–3): 27–33.
Kilbey, G., Karousos, N. G., Eglin, D. and Davis, J. (2006), Laser etched carbon fibre composites: Disposable detectors for flow analysis applications. Electrochem. Commun., 8(8): 1315–1320.
Kim, S. D. (2007), Thermal stabilities of metal bottom electrodes for Ta_2O_5 metal-oxide-metal capacitor structure. Curr. Appl. Phys., 7(2): 124–134.
Kim, Y. K., Jung, J. H., Lee, J. Y. and Ahn, H. J. (1995), The effects of oxygen on diamond synthesis by hot-filament chemical vapor deposition. J. Mater. Sci. Mater. Electron., 6(1): 28–33.
Kim, K. W., Lee, E. H., Kim, J. S., Shin, K. H. and Kim, K. H. (2001), Study on the electroactivity and non-stochiometry of a Ru-based mixed oxide electrode. Electrochim. Acta, 46(6): 915–921.
Kim, K. W., Lee, E. H., Kim, J. S., Shin, K. H. and Jung, B. I. (2002), A study on performance improvement of Ir oxide-coated titanium electrode for organic destruction. Electrochim. Acta, 47(15): 2525–2531.
Kim, S., Kim, T. H., Park, C. and Shin, E. B. (2003a), Electrochemical oxidation of polyvinyl alcohol using a RuO_2/Ti anode. Desalination, 155(1): 49–57.
Kim, Y. S., Park, Y. C., Ansari, S. G., Lee, B. S. and Shin, H. S. (2003b), Effect of substrate temperature on the bonded states of indium tin oxide thin films deposited by plasma enhanced chemical vapor deposition. Thin Solid Films, 426(1–2): 124–131.
Kinoshita, K. (1992), *Electrochemical Oxygen Technology*. Wiley, New York.
Knight, D. S. and White, W. B. (1989), Characterization of diamond films by Raman spectroscopy. J. Mater. Res., 4(2): 385–393.
Koizumi, S., Kamo, M., Sato, Y., Mita, S., Sawabe, A., Reznik, A., Uzan-Saguy, C. and Kalish, R. (1998), Growth and characterization of phosphorus doped n-type diamond thin films. Diam. Relat. Mater., 7(2–5): 540–544.
Kondoh, E., Ohta, T., Mitomo, T. and Ohtsuka, K. (1994), Effect of gas-phase composition on the surface morphology of polycrystalline diamond films. Diam. Relat. Mater., 3(3): 270–276.
Kong, J., Shi, S., Kong, L., Zhu, X. and Ni, J. (2007), Preparation and characterization of PbO_2 electrodes doped with different rare earth oxides. Electrochim. Acta, 53(4): 2048–2054.
Kotz, R. and Stucki, S. (1986), Stabilization of RuO_2 by IrO_2 for anodic oxygen evolution in acid media. Electrochim. Acta, 31(10): 1311–1316.
Kotz, R., Stucki, S. and Carcer, B. (1991), Electrochemical waste-water treatment using high overvoltage anodes.1. Physical and electrochemical properties of SnO_2 anodes. J. Appl. Electrochem., 21(1): 14–20.
Ku, C. H. and Wu, J. J. (2004), Effects of CCl_4 concentration on nanocrystalline diamond film deposition in a hot-filament chemical vapor deposition reactor. Carbon, 42(11): 2201–2205.
Lee, Y. and Bard, A. J. (2002), Fabrication and characterization of probes for combined scanning electrochemical/optical microscopy experiments. Anal. Chem., 74(15): 3626–3633.
Lee, C., Miller, C. J. and Bard, A. J. (1991), Scanning electrochemical microscopy – preparation of submicrometer electrodes. Anal. Chem., 63(1): 78–83.

Lee, S. T., Lam, Y. W., Lin, Z., Chen, Y. and Chen, Q. (1997), Pressure effect on diamond nucleation in a hot-filament CVD system. Phys. Rev. B –Condens. Matter Mater. Phys., 55(23): 15937–15941.

Leyens, C. and Peters, M. (2003), *Titanium and Titanium Alloys: Fundamentals* and Applications. Wiley-VCH, Weinheim.

Li, D. M., Hernberg, R. and Mantyla, T. (1998), Diamond nucleation under high CH_4 concentration and high filament temperature. Diam. Relat. Mater., 7(2–5): 188–192.

Li, X. Y., Diao, H. F., Fan, F. X. J., Gu, J. D., Ding, F. and Tong, A. S. F. (2004), Electrochemical wastewater disinfection: Identification of its principal germicidal actions. J. Environ. Eng., 130(10): 1217–1221.

Li, X. Y., Cui, Y. H., Feng, Y. J., Xie, Z. M. and Gu, J. D. (2005), Reaction pathways and mechanisms of the electrochemical degradation of phenol on different electrodes. Water Res., 39(10): 1972–1981.

Li, C. Y., Zhan, G. Q., Yang, Q. D. and Lu, J. J. (2006a), Electrochemical investigation of acetaminophen with a carbon nano-tube composite film electrode. Bull. Korean Chem. Soc., 27(11): 1854–1860.

Li, X., Sun, C. and Zhou, F. (2006b), A novel nitrite sensor based on poly-1-naphthylamine doped by a ferrocenesulfonic-acid-modified electrode. J. Anal. Chem., 61(9): 896–901.

Li, Z. F., Chen, J. H., Pan, D. W., Tao, W. Y., Nie, L. H. and Yao, S. Z. (2006c), A sensitive amperometric bromate sensor based on multi-walled carbon nanotubes/phosphomolybdic acid composite film. Electrochim. Acta, 51(20): 4255–4261.

Liang, W. Y., Qu, J. H., Chen, L. B., Liu, H. J. and Lei, P. J. (2005), Inactivation of microcystis aeruginosa by continuous electrochemical cycling process in tube using Ti/RuO_2 electrodes. Environ. Sci. Technol., 39(12): 4633–4639.

Li Tolt, Z., Heatherly, L., Clausing, R. E. and Feigerle, C. S. (1997a), Hot filament assisted diamond growth at low temperatures with oxygen addition. J. Mater. Res., 12(5): 1344–1350.

Li Tolt, Z., Heatherly, L., Clausing, R. E. and Feigerle, C. S. (1997b), The role of H_2O in enhancing hot filament assisted diamond growth at low temperatures. J. Appl. Phys., 81(3): 1536–1545.

Lipp, L. and Pletcher, D. (1997), The preparation and characterization of tin dioxide coated titanium electrodes. Electrochim. Acta, 42(7): 1091–1099.

Lissens, G., Verhaege, M., Pinoy, L. and Verstraete, W. (2003), Electrochemical decomplexing and oxidation of organic (chelating) additives in effluents from surface treatment and metal finishing. J. Chem. Technol. Biotechnol., 78(10): 1054–1060.

Liu, Y. K., Tzeng, Y., Liu, C., Tso, P. and Lin, I. N. (2004), Growth of microcrystalline and nanocrystalline diamond films by microwave plasmas in a gas mixture of 1% methane/5% hydrogen/94% argon. Diam. Relat. Mater., 13(10): 1859–1864.

Liu, Z. H., Huan, S. Y., Jiang, J. H., Shen, G. L. and Yu, R. Q. (2006), Molecularly imprinted TiO_2 thin film using stable ground-state complex as template as applied to selective electrochemical determination of mercury. Talanta, 68(4): 1120–1125.

Lodowicks, E. and Beck, F. (1994), Basic characteristics of spinel type manganese mixed oxide/titanium composite anodes for electroorganic redox catalysis. Chem. Eng. Technol., 17(5): 338–347.

Louhichi, B., Bensalash, N. and Gadri, A. (2006), Electrochemical oxidation of benzoic acid derivatives on boron doped diamond: Voltammetric study and galvanostatic electrolyses. Chem. Eng. Technol., 29(8): 944–950.

Lu, P., He, S., Li, F. X. and Jia, Q. X. (1999), Epitaxial growth of RuO_2 thin films by metal-organic chemical vapor deposition. Thin Solid Films, 340(1): 140–144.

Luz, R. D. S., Damos, F. S., Tanaka, A. A. and Kubota, L. T. (2006), Dissolved oxygen sensor based on cobalt tetrasulphonated phthalocyanine immobilized in poly-L-lysine film onto glassy carbon electrode. Sensor Actuator B Chem., 114(2): 1019–1027.

Lyons, M. E. G., Lyons, C. H., Michas, A. and Bartlett, P. N. (1993), Heterogeneous redox catalysis at hydrated oxide layers. J. Electroanal. Chem., 351(1–2): 245–258.

Majid, E., Hrapovic, S., Liu, Y. L., Male, K. B. and Luong, J. H. T. (2006), Electrochemical determination of arsenite using a gold nanoparticle modified glassy carbon electrode and flow analysis. Anal. Chem., 78(3): 762–769.

Malhotra, B. D., Chaubey, A. and Singh, S. P. (2006), Prospects of conducting polymers in biosensors. Anal. Chim. Acta, 578(1): 59–74.

Manisankar, P., Selvanathan, G. and Vedhi, C. (2006), Determination of pesticides using heteropolyacid montmorillonite clay-modified electrode with surfactant. Talanta, 68(3): 686–692.

Martin, H. B., Argoitia, A., Landau, U., Anderson, A. B. and Angus, J. C. (1996), Hydrogen and oxygen evolution on boron-doped diamond electrodes. J. Electrochem. Soc., 143(6).

Martinez-Huitle, C. A., Ferro, S. and De Battisti, A. (2004), Electrochemical incineration of oxalic acid – role of electrode material. Electrochim. Acta, 49(22–23): 4027–4034.

Mashazi, P. N., Ozoemena, K. I. and Nyokong, T. (2006), Tetracarboxylic acid cobalt phthalocyanine sam on gold: Potential applications as amperometric sensor for H_2O_2 and fabrication of glucose biosensor. Electrochim. Acta, 52(1): 177–186.

Matsumoto, S. (2000), Development of diamond synthesis techniques at low pressures. Thin Solid Films, 368(2): 231–236.

Matsunaga, M., Morimitsu, M., Meng, H., Kunihiro, T. and Otogawa, R. (1998), *Proceedings of AESF/SFSJ Advanced Surface Technology Forum*. AESF, Orlando, FL.

Mcgaw, E. A. and Swain, G. M. (2006), A comparison of boron-doped diamond thin-film and hg-coated glassy carbon electrodes for anodic stripping voltammetric determination of heavy metal ions in aqueous media. Anal. Chim. Acta, 575(2): 180–189.

McNamara, K. M. and Gleason, K. K. (1993), Comparison of tantalum and rhenium filaments in diamond CVD using selective carbon-13 labeling. J. Electrochem. Soc., 140(2): L22–L24.

Mehta Menon, P., Edwards, A., Feigerle, C. S., Shaw, R. W., Coffey, D. W., Heatherly, L., Clausing, R. E., Robinson, L. and Glasgow, D. C. (1999), Filament metal contamination and Raman spectra of hot filament chemical vapor deposited diamond films. Diam. Relat. Mater., 8(1): 101–109.

Menon, V. P. and Martin, C. R. (1995), Fabrication and evaluation of nanoelectrode ensembles. Anal. Chem., 67(13): 1920–1928.

Menon, P. M., Clausing, R. E., Heatherly, L. and Feigerle, C. S. (1998), The morphology of diamond grown by hot filament chemical vapor deposition. Diam. Relat. Mater., 7(8): 1201–1206.

Mirkin, M. V. and Bard, A. J. (1992), Scanning electrochemical microscopy 18 – thin-layer cell-formation with a mercury pool substrate. J. Electrochem. Soc., 139(12): 3535–3539.

Mirkin, M. V., Fan, F. R. F. and Bard, A. J. (1992), Direct electrochemical measurements inside a 2000-Angstrom thick polymer film by scanning electrochemical microscopy. Science, 257(5068): 364–366.

Mohan, N. and Balasubramanian, N. (2006), In situ electrocatalytic oxidation of acid violet 12 dye effluent. J. Hazard. Mater., 136(2): 239–243.

Mohd, Y. and Pletcher, D. (2005), The influence of deposition conditions and dopant ions on the structure, activity, and stability of lead dioxide anode coatings. J. Electrochem. Soc., 152(6): D97–D102.

Montenegro, M. I., Queirâos, M. A., Daschbach, J. L. and North Atlantic Treaty Organization. Scientific Affairs Division. (1991), *Microelectrodes: Theory and Applications*. Kluwer, Dordrecht.

Morimitsu, M., Otogawa, R. and Matsunaga, M. (2000), Effects of cathodizing on the morphology and composition of IrO_2–Ta_2O_5/Ti anodes. Electrochim. Acta, 46(2–3): 401–406.

Muna, G. W., Tasheva, N. and Swain, G. M. (2004), Electro-oxidation and amperometric detection of chlorinated phenols at boron-doped diamond electrodes: A comparison of microcrystalline and nanocrystalline thin films. Environ. Sci. Technol., 38(13): 3674–3682.

Murphy, L. (2006), Biosensors and bioelectrochemistry. Curr. Opin. Chem. Biol., 10(2): 177–184.

Nagano, T. and Shibata, N. (1993), Diamond synthesis by microwave-plasma chemical vapor deposition using CH_3Cl and CH_2Cl_2 as carbon source. Part 1: Regular papers and short notes and review papers Jpn. J. Appl. Phys., 32(11A): 5067–5071.

Nasr, B., Abdellatif, G., Canizares, P., Saez, C., Lobato, J. and Rodrigo, M. A. (2005), Electrochemical oxidation of hydroquinone, resorcinol, and catechol on boron-doped diamond anodes. Environ. Sci. Technol., 39(18): 7234–7239.

Nebel, C. E. and Ristein, J. (2004), *Thin-Film Diamond II. Elsevier*, Amsterdam.

Niu, S. Y., Zhang, S. S., Wang, L. and Li, X. M. (2006), Hybridization biosensor using di(1,10-phenanthroline) (imidazo[f]1, 10-phenanthroline) cobalt(II) as electrochemical indicator for detection of human immunodeficiency virus DNA. Electroanal. Chem., 597(2): 111–118.

Notsu, H., Yagi, I., Tatsuma, T., Tryk, D. A. and Fujishima, A. (1999), Introduction of oxygen-containing functional groups onto diamond electrode surfaces by oxygen plasma and anodic polarization. Electrochem. Solid State Lett., 2(10): 522–524.

Notsu, H., Yagi, I., Tatsuma, T., Tryk, D. A. and Fujishima, A. (2000), Surface carbonyl groups on oxidized diamond electrodes. J. Electroanal. Chem., 492(1): 31–37.

Okano, K., Kiyota, H., Kurosu, T. and Iida, M. (1994), Doping of diamond. Diam. Relat. Mater., 3(1–2): 35–40.

Okoli, S., Haubner, R. and Lux, B. (1991), Carburization of tungsten and tantalum filaments during low-pressure diamond deposition. Surf. Coat. Technol., 47(1–3): 585–599.

Pai, M. P., Musale, D. V. and Kshirsagar, S. T. (1998), Low-pressure chemical vapour deposition of diamond films in a radio-frequency plasma-assisted hot-filament reactor. Diam. Relat. Mater., 7(10): 1526–1533.

Panizza, M. and Cerisola, G. (2005), Application of diamond electrodes to electrochemical processes. Electrochim. Acta, 51(2): 191–199.

Panizza, M., Zolezzi, M. and Nicolella, C. (2006), Biological and electrochemical oxidation of naphthalenesulfonates. J. Chem. Technol. Biotechnol., 81(2): 225–232.

Papadatos, F., Consiglio, S., Skordas, S., Eisenbraun, E. T., Kaloyeros, A. E., Peck, J., Thompson, D. and Hoover, C. (2004), Chemical vapor deposition of ruthenium and ruthenium oxide thin films for advanced complementary metal-oxide semiconductor gate electrode applications. J. Mater. Res., 19(10): 2947–2955.

Park, S. G., Park, J. E., Cho, E. I., Hwang, J. H. and Ohsaka, T. (2006), Electrochemical detection of ascorbic acid and serotonin at a boron-doped diamond electrode modified with poly(*N*, *N*-dimethylaniline). Res. Chem. Intermed., 32(5–6): 595–601.

Pauliukaite, R., Paquim, A. M. C., Brett, A. M. O. and Brett, C. M. A. (2006), Electrochemical, EIS and AFM characterisation of biosensors: Trioxysilane sol–gel encapsulated glucose oxidase with two different redox mediators. Electrochim. Acta, 52(1): 1–8.

Pedrosa, V. A., Miwa, D., Machado, S. A. S. and Avaca, L. A. (2006), On the utilization of boron dope diamond electrode as a sensor for parathion and as an anode for electrochemical combustion of parathion. Electroanalysis, 18(16): 1590–1597.

Pereira, F. C., Moretto, L. M., De Leo, M., Zanoni, M. V. B. and Ugo, P. (2006), Gold nanoelectrode ensembles for direct trace electroanalysis of iodide. Anal. Chim. Acta, 575(1): 16–24.

Pierce, D. T., Unwin, P. R. and Bard, A. J. (1992), Scanning electrochemical microscopy.17. Studies of enzyme mediator kinetics for membrane-immobilized and surface-immobilized glucose-oxidase. Anal. Chem., 64(17): 1795–1804.

Pierson, H. O. (1999), *Handbook of Chemical Vapor Depostion (CVD): Principles, Technology, and Applications*. Noyes Publications, Norwich, NY.

Pleskov, Y. V. (1999), Synthetic diamond in electrochemistry. Russ Chem Rev, 68(5): 381–392.

Rahman, M. A., Won, M. S., Wei, P. H. and Shim, Y. B. (2006), Electrochemical detection of ClO^{3-}, BrO^{3-}, and IO^{3-} at a phosphomolybdic acid linked 3-aminopropyl-trimethoxysilane modified electrode. Electroanalysis, 18(10): 993–1000.

Rajkumar, D. and Kim, J. G. (2006), Oxidation of various reactive dyes with in situ electrogenerated active chlorine for textile dyeing industry wastewater treatment. J. Hazard. Mater., 136(2): 203–212.

Rajkumar, D., Song, B. J. and Kim, J. G. (2007), Electrochemical degradation of reactive blue 19 in chloride medium for the treatment of textile dyeing wastewater with identification of intermediate compounds. Dyes Pigments, 72(1): 1–7.

Ralchenko, V., Sychov, I., Vlasov, I., Vlasov, A., Konov, V., Khomich, A. and Voronina, S. (1999), Quality of diamond wafers grown by microwave plasma CVD: Effects of gas flow rate. Diam. Relat. Mater., 8(2–5): 189–193.

Ramesham, R. and Rose, M. F. (1997), Electrochemical characterization of doped and undoped CVD diamond deposited by microwave plasma. Diam. Relat. Mater., 6(1): 17–27.

Ran, J. G., Gou, L., Liu, Y., Zheng, C. Q. and Tang, F. Q. (1998), The process of immobilizing enzyme of glucose sensor based on diamond film. Supramol. Sci., 5(5–6): 699–700.

Ribeiro, J. and De Andrade, A. R. (2004), Characterization of RuO_2–Ta_2O_5 coated titanium electrode microstructure, morphology, and electrochemical investigation. J. Electrochem. Soc., 151(10): D106–D112.

Riccardi, C. D. S., Dahmouche, K., Santilli, C. V., da Costa, P. I. and Yamanaka, H. (2006), Immobilization of streptavidin in sol–gel films: Application on the diagnosis of hepatitis C virus. Talanta, 70(3): 637–643.

Rolewicz, J., Comninellis, C., Plattner, E. and Hinden, J. (1988), Characterisation des electrodes de type DSA pour le degagement de O_2 — I. L'electrode Ti/IrO_2–Ta_2O_5. Electrochim. Acta, 33(4): 573–580.

Santana, M. H. P., Faria, L. A. D. and Boodts, J. F. C. (2005), Effect of preparation procedure of IrO_2–Nb_2O_5 anodes on surface and electrocatalytic properties. J. Appl. Electrochem., 5(9): 915–924.

Sata, S., Koizumi, Y., Kaneda, K., Rakuma, T., Okajima, T. and Ohsaka, T. (2004), Electrochemical generation of ozone using DSA-type PtO_x–Ta_2O_5/Ti electrodes. Meeting Abstracts.

Schafer, L., Hofer, M. and Kroger, R. (2006), The versatility of hot-filament activated chemical vapor deposition. Thin Solid Films, 515(3): 1017–1024.

Schmidt, I., Hentschel, F. and Benndorf, C. (1997), Low temperature diamond growth using halogenated hydrocarbons. Solid State Ionics, 101–103(Part 1): 97–101.

Scott, E. R., White, H. S. and Phipps, J. B. (1992), Direct imaging of ionic pathways in stratum-corneum using scanning electrochemical microscopy. Solid State Ionics, 53–6: 176–183.

Shah, J. and Wilkins, E. (2003), Electrochemical biosensors for detection of biological warfare agents, Electroanalysis, 15: 157–167.

Sharda, T., Misra, D. S. and Avasthi, D. K. (1996), Hydrogen in chemical vapour deposited diamond films. Vacuum, 47(11): 1259–1264.

Sharda, T., Soga, T., Jimbo, T. and Umeno, M. (2001), Growth of nanocrystalline diamond films by biased enhanced microwave plasma chemical vapor deposition. Diam. Relat. Mater., 10(9–10): 1592–1596.

Shervedani, R. K., Mehrjardi, A. H. and Zamiri, N. (2006), A novel method for glucose determination based on electrochemical impedance spectroscopy using glucose oxidase self-assembled biosensor. Bioelectrochemistry, 69(2): 201–208.

Shiddiky, M. J. A., Won, M. S. and Shim, Y. B. (2006), Simultaneous analysis of nitrate and nitrite in a microfluidic device with a Cu-complex-modified electrode. Electrophoresis, 27(22): 4545–4554.

Shi-Yun, Al, Jia-Qing, Ll, Luo-Ping, Ll, Hui-Qi, Peng, Ya, Yang and Li-Tong, J. (2005), Electrochemical deposition and properties of nanometer-structure Ce-doped lead dioxide film electrode. Chin. J. Chem. 23: 71–75.

Singh, J., Vellaikal, M. and Dat, R. (1994), Gas flow effects in synthesis of diamond by hot-filament chemical vapor deposition. Thin Solid Films, 238(1): 133–140.

Slevin, C. J., Gray, N. J., Macpherson, J. V., Webb, M. A. and Unwin, P. R. (1999), Fabrication and characterisation of nanometre-sized platinum electrodes for voltammetric analysis and imaging. Electrochem. Commun., 1(7): 282–288.

Soga, T., Sharda, T. and Jimbo, T. (2004), Precursors for CVD growth of nanocrystalline diamond. Phys. Solid State, 46(4): 720–725.

Sommer, M. and Smith, F. W. (1990), Activity of tungsten and rhenium filaments in CH_4/H_2 and C_2H_2/H_2 mixtures. Importance for diamond CVD. J. Mater. Res., 5(11): 2433–2440.

Spasojevic, M., Krstajic, N. and Jaksic, M. (1984), Electrocatalytic optimization of faradaic yields in the chlorate cell process. Surf. Technol., 21(1): 19–26.

Spataru, T., Roman, E. and Spataru, N. (2004), Electrodeposition of cobalt oxide on conductive diamond electrodes for catalytic sensor applications. Rev. Roum. Chim., 49(6): 525–530.

Stiegler, J., Lang, T., Nygard-Ferguson, M., Von Kaenel, Y. and Blank, E. (1996), Low temperature limits of diamond film growth by microwave plasma-assisted CVD. Diam. Relat. Mater., 5(3–5): 226–230.

Stucki, S., Kotz, R., Carcer, B. and Suter, W. (1991), Electrochemical waste water treatment using high overvoltage anodes part II: Anode performance and applications. J. Appl. Electrochem., 21(2): 99–104.

Stulik, K., Amatore, C., Holub, K., Marecek, V. and Kutner, W. (2000), Microelectrodes. Definitions, characterization, and applications (Technical Report). Pure Appl. Chem., 72(8): 1483–1492.

Su, L., Qiu, X. P., Guo, L. H., Zhang, F. H. and Tung, C. H. (2004), Amperometric glucose sensor based on enzyme-modified boron-doped diamond electrode by cross-linking method. Sensor Actuator B, 99(2–3): 499–504.

Sugino, T., Karasutani, K., Mano, F., Kataoka, H., Shirafuji, J. and Kobashi, K. (1994), Characterization of undoped and boron-doped polycrystalline diamond films synthesized by hot-filament chemical vapor deposition using methanol. Diam. Relat. Mater., 3(4–6): 618–622.

Sun, D. and Zhang, H. J. (2006), Electrochemical determination of 2-chlorophenol using an acetylene black film modified glassy carbon electrode. Water Res., 40(16): 3069–3074.

Svancara, I., Baldrianova, L., Tesarova, E., Hocevar, S. B., Elsuccary, S. A. A., Economou, A., Sotiropoulos, S., Ogorevc, B. and Vytras, K. (2006), Recent advances in anodic stripping voltammetry with bismuth-modified carbon paste electrodes. Electroanalysis, 18(2): 177–185.

Swain, G. M., Anderson, A. B. and Angus, J. C. (1998), Applications of diamond thin films in electrochemistry. MRS Bull., 23(9): 56–60.

Taylor, G., Bates, C., Stadelmann, M., Kraft, A. and Matthee, T. (2003), Evaluation of electrooxidation using diamond anodes for the treatment of radioactive contaminated lubricants – preliminary report. New Diam. Front. Carbon Technol., 13(2): 89–96.

Tel-Vered, R., Walsh, D. A., Mehrgardi, M. A. and Bard, A. J. (2006), Carbon nanofiber electrodes and controlled nanogaps for scanning electrochemical microscopy experiments. Anal. Chem., 78(19): 6959–6966.

Tian, Y., Chen, X., Shang, C. and Chen, G. (2006), Active and stable Ti/Si/BDD anodes for electrooxidation. J. Electrochem. Soc., 153(7): 6.

Trasatti, S. (1980), *Electrodes of Conductive Metallic Oxides*. Elsevier, Amsterdam.

Trasatti, S. (1991), Physical electrochemistry of ceramic oxides. Electrochim. Acta, 36(2): 225–241.

Troupe, C. E., Drummond, I. C., Graham, C., Grice, J., John, P., Wilson, J. I. B., Jubber, M. G. and Morrison, N. A. (1998), Diamond-based glucose sensors. Diam. Relat. Mater., 7(2–5): 575–580.

Tucker, D. A., McClure, M. T., Fathi, Z., Sitar, Z., Walden, B., Sutton, W. H., Lewis, W. A. and Wei, J. B. (1996), Microwave plasma assisted CVD of diamond on titanium and Ti-6Al-4v. *Materials Research Society Symposium – Proceedings*.

Van Hege, K., Verhaege, M. and Verstraete, W. (2002), Indirect electrochemical oxidation of reverse osmosis membrane concentrates at boron-doped diamond electrodes. Electrochem. Commun., 4(4): 296–300.

Van Hege, K., Verhaege, M. and Verstraete, W. (2004), Electro-oxidative abatement of low-salinity reverse osmosis membrane concentrates. Water Res., 38(6): 1550–1558.

Velichenko, A. B., Amadelli, R., Baranova, E. A., Girenko, D. V. and Danilov, F. I. (2002), Electrodeposition of co-doped lead dioxide and its physicochemical properties. J. Electroanal. Chem., 527(1–2): 56–64.

Venter, A. and Neethling, J. H. (1994), Effect of filament temperature on the growth of diamond using hot-filament chemical vapor deposition. Diam. Relat. Mater., 3(1–2): 168–172.

Vicent, F., Morallo'n, E., Quijada, C., Va'zquez, J. L., Aldaz, A. and Cases, F. (1998), Characterization and stability of doped SnO_2 anodes. J. Appl. Electrochem., 28(6): 607–612.

Vinokur, N., Miller, B., Avyigal, Y. and Kalish, R. (1996), Electrochemical behavior of boron-doped diamond electrodes. J. Electrochem. Soc., 143(10).

Wang, T., Xin, H. W., Zhang, Z. M., Dai, Y. B. and Shen, H. S. (2004), The fabrication of nanocrystalline diamond films using hot filament CVD. Diam. Relat. Mater., 13(1): 6–13.

Wang, G., Mantey, K., Nayfeh, M. H. and Yau, S. T. (2006a), Enhanced amperometric detection of glucose using Si-29 particles. Appl. Phys. Lett., 89(24).

Wang, J., Thongngamdee, S. and Lu, D. L. (2006b), Adsorptive stripping voltammetric measurements of trace beryllium at the mercury film electrode. Anal. Chim. Acta, 564(2): 248–252.

Wang, K., He, F. Y., Liu, A. L., Xu, J. J., Chen, H. Y. and Xia, X. H. (2006c), Novel coupling mechanism-based imaging approach to scanning electrochemical microscopy for probing the electric field distribution at the microchannel end. Langmuir, 22(16): 7052–7058.

Watanabe, T., Ivandini, T. A., Makide, Y., Fujishima, A. and Einaga, Y. (2006), Selective detection method derived from a controlled diffusion process at metal-modified dia electrodes. Anal. Chem., 78(22): 7857–7860.

Waterston, K., Wang, J. W. J., Bejan, D. and Bunce, N. J. (2006), Electrochemical waste water treatment: Electrooxidation of acetaminophen. J. Appl. Electrochem., 36(2): 227–232.

Wei, Y., Li, M. G., Jiao, S. F., Huang, Q. N., Wang, G. F. and Fang, B. (2006), Fabrication of CeO_2 nanoparticles modified glassy carbon electrode and its application for electrochemical determination of ua and aa simultaneously. Electrochim. Acta, 52(3): 766–772.

Weiss, E., Groenen-Serrano, K. and Savall, A. (2006), Electrochemical degradation of sodium dodecylbenzene sulfonate on boron doped diamond and lead dioxide anodes. J. New Mater. Electrochem. Sys., 9(3): 249–256.

Wightman, R. M. (1981), Microvoltammetric electrodes. Anal. Chem., 53(9): 1125A–1133A.

Wilson, J. I. B. and Kulisch, W. (1996), *Diamond Thin Films*. Akademie Verlag, Berlin.

Wipf, D. O. and Bard, A. J. (1991a), Scanning electrochemical microscopy.7. Effect of heterogeneous electron-transfer rate at the substrate on the tip feedback current. J. Electrochem. Soc., 138(2): 469–474.

Wipf, D. O. and Bard, A. J. (1991b), Scanning electrochemical microscopy.10. High-resolution imaging of active-sites on an electrode surface. J. Electrochem. Soc., 138(5): L4–L6.

Wu, J. J. and Hong, F. C. N. (1998), The effects of chloromethane on diamond nucleation and growth in a hot-filament chemical vapor deposition reactor. J. Mater. Res., 13(9): 2498–2504.

Wu, J. L., Zhu, J. Z., Zhang, G. X., Lin, X. R. and Cheng, N. Y. (1996), Fabrication and application of a diamond-film glucose biosensor based on a H_2O_2 microarray electrode. Anal. Chim. Acta, 327(2): 133–137.

Xiang, L., Cheng, S. and Fang, Z. (2006), A novel nitrite sensor based on poly-1-naphthylamine doped by a ferrocenesulfonic-acid-modified electrode. J. Anal. Chem., 61(9): 896–901.

Xie, S. T., Shafer, G., Wilson, C. G. and Martin, H. B. (2006), In vitro adenosine detection with a diamond-based sensor. Diam. Relat. Mater., 15(2–3): 225–228.

Xue, M. H., Xu, Q., Zhou, M. and Zhu, J. J. (2006), In situ immobilization of glucose oxidase in chitosan-gold nanoparticle hybrid film on prussian blue modified electrode for high-sensitivity glucose detection. Electrochem. Commun., 8(9): 1468–1474.

Yamaguchi, Y., Yamanaka, Y., Miyamoto, M., Fujishima, A. and Honda, K. (2006), Hybrid electrochemical treatment for persistent metal complex at conductive diamond electrodes and clarification of its reaction route. J. Electrochem. Soc., 153(12): J123–J132.

Yang, W. W., Bai, Y., Li, Y. C. and Sun, C. Q. (2005a), Amperometric nitrite sensor based on hemoglobin/colloidal gold nanoparticles immobilized on a glassy carbon electrode by a titania sol–gel film. Anal. Bioanal. Chem., 382(1): 44–50.

Yang, Y. Z., Yang, W. S., Yang, F. L. and Zhang, X. W. (2005b), Electrooxidative degradation of an anthraquinone dye with in-situ electrogenerated active chlorine in a divided flow cell. Chin. J. Chem. Eng., 13(5): 628–633.

Yano, T., Tryk, D. A., Hashimoto, K. and Fujishima, A. (1998), Electrochemical behavior of highly conductive boron-doped diamond electrodes for oxygen reduction in alkaline solution. J. Electrochem. Soc., 145(6): 1870–1876.

Yarbrough, W. A. and Messier, R. (1990), Current issues and problems in the chemical vapor deposition of diamond. Science, 247(4943): 688–696.

Yasukawa, T., Kaya, T. and Matsue, T. (2000), Characterization and imaging of single cells with scanning electrochemical microscopy. Electroanalysis, 12(9): 653–659.

Yoshikawa, H., Morel, C. and Koga, Y. (2001), Synthesis of nanocrystalline diamond films using microwave plasma CVD. Diam. Relat. Mater., 10(9–10): 1588–1591.

Yosypchuk, B. and Novotny, L. (2002), Nontoxic electrodes of solid amalgams. Crit. Rev. Anal. Chem., 32(2): 141–151.

Yu, Z. and Flodstrom, A. (1997), Pressure dependence of growth mode of HFCVD diamond. Diam. Relat. Mater., 6(1): 81–84.

Zaitsev, N. K., Osipova, E. A., Fedulov, D. M., Eremenko, E. A. and Dedov, A. G. (2006), Determination of selenium(IV) by cathodic stripping voltammetry using a copper-modified mercury-film electrode modified with copper. J. Anal. Chem., 61(1): 77–83.

Zhang, H. X., Cao, A. M., Hu, J. S., Wan, L. J. and Lee, S. T. (2006a), Electrochemical sensor for detecting ultratrace nitroaromatic compounds using mesoporous SiO_2-modified electrode. Anal. Chem., 78(6): 1967–1971.

Zhang, H. X., Hu, J. S., Yan, C. J., Jiang, L. and Wan, L. J. (2006b), Functionalized carbon nanotubes as sensitive materials for electrochemical detection of ultra-trace 2,4,6-trinitrotoluene. Phys. Chem. Chem. Phys., 8(30): 3567–3572.

Zhao, W., Xu, J.-J., Qiu, Q.-Q. and Chen, H.-Y. (2006), Nanocrystalline diamond modified gold electrode for glucose biosensing. Biosens. Bioelectron., 22(5): 649–655.

Zheng, H., Dong, H. M., Yan, Z. N., Wen, L. J., Zhang, S. S. and Ye, B. X. (2006), Determination of copper at a glassy carbon electrode modified with langmuir-blodgett film of p-tert-butylthiacalix[4]arene. Electroanalysis, 18(21): 2115–2120.

Zhi, J. F., Wang, H. B., Nakashima, T., Rao, T. N. and Fujishima, A. (2003), Electrochemical incineration of organic pollutants on boron-doped diamond electrode. Evidence for direct electrochemical oxidation pathway. J. Phys. Chem. B, 107(48): 13389–13395.

Zhou, D. and Gao, L. (2007), Effect of electrochemical preparation methods on structure and properties of PbO_2 anodic layer. Electrochim. Acta, 53(4): 2060–2064.

Zhou, D., Gruen, D. M., Qin, L. C., McCauley, T. G. and Krauss, A. R. (1998), Control of diamond film microstructure by ar additions to CH_4/H_2 microwave plasmas. J. Appl. Phys., 84(4): 1981–1989.

Zhou, M., Dai, Q., Lei, L., Ma, C. and Wang, D. (2005), Long life modified lead dioxide anode for organic wastewater treatment: Electrochemical characteristics and degradation mechanism. Environ. Sci. Technol., 39(1): 363–370.

Zoski, C. G. (2002), Ultramicroelectrodes: design, fabrication, and characterization. Electroanalysis, 14(15–16): 1041–1051.

Chapter 4
Modeling of Electrochemical Process for the Treatment of Wastewater Containing Organic Pollutants

Manuel A. Rodrigo, Pablo Cañizares, Justo Lobato, and Cristina Sáez

4.1 Why Is It Important to Use Mathematical Modeling in Electrochemical Wastewater Treatment?

The use of electrochemical technologies for the treatment of organic pollutants contained in industrial wastewaters has received a great deal of attention in recent years. Two of these technologies are especially important: the electrochemically assisted coagulation (or electro-coagulation) that can compete with the conventional chemical coagulation process in the treatment of wastes polluted with colloids or macromolecules or in the treatment of emulsions, and the electrooxidation, that appears as one of the most promising technologies for the treatment of wastewaters containing small-to-medium concentrations $\left(10^0-10^4 \text{ mg COD dm}^{-3}\right)$ of soluble organic compounds.

Both technologies were seem as promising technologies at different periods during the twentieth century, although they did not received significant scientific attention up to the turn of the century. As a consequence, the results obtained in different applications were not satisfactory, and a certain urban legend about the inefficiency of these technologies started to run. Thus, several full-scale electrochemical coagulation plants were commissioned in USA to treat municipal wastewater, and they had to be abandoned due to apparent higher operation cost and some expectations of high initial capital cost, as compared to the case of chemical dosing. Regarding to electrooxidation, the use of this technology rarely overcame the pilot-scale level, as the Faradaic efficiencies were always under the desired values, and the formation of refractory polymers during the treatment was very frequently a very significant process.

At the turn of the twentieth century, some works focused on the study of these technologies have reported very promising results. The proper design of the electrochemical cell to promote electroflocculation and electroflotation processes, the

M.A. Rodrigo (✉)
Department of Chemical Engineering, University of Castilla La Mancha,
Campus Universitario s/n, Ciudad Real, CR 13005, Spain
e-mail: manuel.rodrigo@uclm.es

C. Comninellis and G. Chen (eds.), *Electrochemistry for the Environment*,
DOI 10.1007/978-0-387-68318-8_4,

easiness in the automation, and the use of solar panels to apply the technology in remote sites have become important advantages for the use of electrochemical coagulation plants. In addition, the proper design of the cell to enhance mass transport and the use of new anodic materials like conductive-diamond have allowed achieving high efficiencies in the use of electric energy and, as a consequence, to decrease strongly the operating cost of electrooxidation.

Nevertheless, to make these technologies competitive with the conventional technologies that are in use today (conventional coagulation in case of electrochemical coagulation, or advanced oxidation processes such as Fenton oxidation or ozonation, in case of electrochemical oxidation) more effort has to be done in the next years, and a better understanding of the processes involved must be achieved. In this context, the development of mathematical models that are consistent with the processes occurring in a physical system is a relevant approach, because such models can help to understand what is happening in the treatment process. In turn, a more detailed knowledge of the physical system can be obtained, and tools for a proper design of the processes, or for the analysis of operating problems, are attained. For this reason, several models have been developed in recent years to describe the electrochemical treatment of wastewater containing organic pollutants. These models correspond to different approaches to describe the physical processes occurring within the electrochemical reactors. Previous to the description of these models, some notes about modeling in chemical engineering can help to understand better the approaches proposed by the models.

4.2 Mathematical Modeling in Chemical Engineering

A mathematical model consists, in principle, of a collection of equations that relate some inputs (explicative variables) to some outputs. Its goal is to reproduce the experimental behavior of a physical entity that exists on the real world (in chemical engineering we name these entities as processes).

From the viewpoint of their formulation, mathematical models can be classified into two main categories: phenomenological or empirical. A phenomenological model is that in which the model formulation is based on theoretical principles while an empirical model is that in which model equations are not obtained from these principles, but they are simply a collection of equations that reproduce well the experimental behavior of a system. There is an intermediate type of model, semiempirical model, that use theoretical principles to formulate a process model but not in a strict way, as they also use some assumptions that can be considered as empirical from the formulation perspective.

Actual processes can be very complex, and normally a mathematical model is only going to capture the more significant features of them. So, a model should never be thought of as being the exact equivalent of a physical system. In this context, the description level of a process is much related to the complexity of the model: the more features a model describe, the higher the complexity of the resulting collection

of equations. In this point, it is usual in chemical engineering to try to use models in which process variables do not depend on the position but only on the time. These models are called lumped-parameter models, and in nonsteady-state conditions they take the form of a set of ordinary differential equations, with the time as the only independent parameter. If it is not possible to reproduce a process with such kind of models, and hence the changes with the spatial position are significant, lumped-parameter models are not useful and distributed-parameter models have to be used. In dynamic conditions, these models occur as sets of partial differential equations.

In any chemical or electrochemical process, the application of the conservation principles (specifically to the mass, energy or momentum) provides the outline for building phenomenological mathematical models. These procedures could be made over the entire system, or they could be applied to smaller portions of the system, and later integrated from these small portions to the whole system. In the former case, they give an overall description of the process (with few details but simpler from the mathematical viewpoint) while in the later case they result in a more detailed description (more equations, and consequently more features described).

To complement the equations obtained from the application of the conservation principles, it is required to use some equations based on physical, chemical, or electrochemical laws, that model the primary mechanisms by which changes within the process are assumed to occur (rates of the processes, calculation of properties, etc.). These equations are called constitutive equations and include four main categories of equations: definition of process variables in terms of physical properties, transport rate, chemical and electrochemical kinetics, and thermodynamic equations.

These sets of equations, together with the description level, are the two main distinctive points in the formulation of a phenomenological model. However, the formulation of a model is only one of the stages required to get a model. There are two other important steps that are required previous to the proper use of a model: the parameter estimation and the validation of the model.

After the formulation stage, we have all the equations of the model, but they are not useful yet, because parameters in the equations do not have a particular value. Consequently, the model cannot be used to reproduce the behavior of a physical entity. The parameter estimation procedure consists of obtaining a set of parameters that allows simulation with the model. In many cases, parameters can be found in literature, but in other cases it is required to fit the model to the experimental behavior by using mathematical procedures. The easier and more used types of procedures are those based on the use of optimization algorithms to make minimum the differences between the experimental observations and the model outputs. The more frequently used criterion to optimize the values of the parameters is the least square regression coefficient. In this procedure, a set of values is proposed for all model parameters (one for every parameter) and the model is run. After that, the error criterion is calculated as the sum of the squares of the residues (differences between the values of every experimental and modeled value). Then, an optimization procedure is used to change the values of the model parameters in order to get the minimum value of this criterion.

Once the parameters are calculated, the final stage is the construction of a model, i.e., the validation. This stage consists of checking the results of the model for several different experimental cases. Its goal is to confirm that simulations carried out with the model reproduce the behavior of the processes in a proper way. Some statistical procedures are typically applied in this stage. The best way to validate a model is to compare experimental and modeled data by means of two different tests:

– The regression coefficient
– The analysis of the residues trends

The first test consists of calculating the value of the regression coefficient to compare the actual values of the outputs of the process with the values proposed by the model. To calculate the regression coefficient (4.1) is used, where y_i states for the experimental values of the output, $\hat{y}_i$ are the model values, and y is the average value of the experimental outputs used in the validation

$$r^2 = 1 - \frac{\sum_{i=1}^{N} (y_i - \hat{y}_i)^2}{\sum_{i=1}^{N} (y_i - y)^2}. \tag{4.1}$$

Obviously, the higher the regression coefficient, the better the reproducibility obtained of the system. In this context, it is important to take in mind that the same information that gives the regression coefficient can be obtained visually from the actual output (y_i)–model output ($\hat{y}_i$) graph. If all points lay over the line $y = \hat{y}$, it means that our model describes satisfactorily the process. On the contrary, if points are far away from this line the model has to be reworked.

The second test consists of the analysis of the residues trend vs. the explicative variables and vs. the output. If the graph obtained shows disperse points without a marked trend (white noise), the model does not miss any relevant detail. On the contrary, if a market trend is observed, the model has to be reformulated to include some additional processes or to make a more detailed description.

4.3 Selection of the Description Level in Electrochemical Coagulation and Oxidation Processes

Although electrocoagulation and electrooxidation technologies are very different in nature, both are electrochemical technologies, and both are carried out in electrochemical cells. As a consequence, heterogeneous charge transfer on the surface of electrodes is involved, and from the modeling point of view the system is distributed. This means that the values of the model – outputs (species concentration, temperature, etc.) depend simultaneously on both, the time and the position. This can be clearly observed in Fig. 4.1a, where the intensity of dark in the anodic region represents the local values of COD concentration in a flow-cell with parallel plane

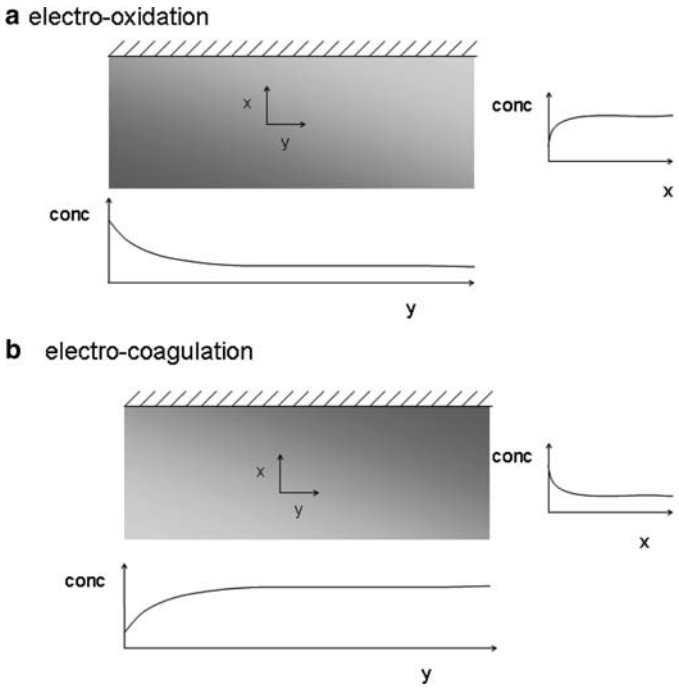

Fig. 4.1 Profiles of concentration in a single flow-cell with parallel plane electrodes (**a**) COD during electrooxidation; (**b**) Aluminum during electrocoagulation

electrodes. If only direct electrochemical processes are assumed to occur, the concentration of COD depends on the distance to the electrode. COD is diminished on the electrode surface and then a profile of concentration between the surface (lower concentration) and the bulk solution (higher concentration) is generated. At the same time, if it is assumed a typical flow channel pattern, the COD decreases in the flow direction. In addition, in nonsteady-state conditions, time will also influence on the value of the variables. Figure 4.1b shows the profiles of aluminum concentration in an electrochemical dissolution process (the darker, the higher the concentration). In this case, the soluble aluminum species are formed on the surface during the process, and consequently their concentration decreases from the electrode surface to the bulk solution. Likewise, as aluminum species are products and not reagents their global concentration increases along the flow direction.

An in-depth description of the electrochemical treatment of organic-polluted wastewater in which the concentration profiles of every compound in the electrochemical cell are calculated is particularly difficult, as it would lead to a very complex mathematical system. This complex situation arises since the concentration of every compound depends on the time and on the distance to the electrode surface, and that the particular concentration of every species for a given case depends on three different mass-transport mechanisms: diffusion, convection, and migration.

In this context, to describe the position dependence of the model species, it is important to take in mind that, in electrochemical wastewater-treatment processes, it can be assumed that in the treated wastewater there is always enough supporting electrolyte to minimize the migration of electroactive species. Hence the primary mass-transport mechanisms are diffusion and convection. Hence, the mass balance of a volume element assuming that reactions are restricted to the electrode surface takes the form of (4.2).

$$\frac{\partial c_i}{\partial t} = D_i \Delta c_i - \vec{u} \cdot \nabla c_i . \tag{4.2}$$

For Newtonian fluids, the relationship between the velocity of a liquid and the forces acting upon it is given by the Navier–Stokes equation. For a noncompressible fluid and considering only convection and viscosity forces (neglecting other forces such as gravity), this equation takes the form of (4.3).

$$\frac{\partial \vec{v}}{\partial t} + \vec{u} \cdot \nabla \vec{u} = -\frac{1}{g} \nabla p + \upsilon \nabla^2 \vec{u}. \tag{4.3}$$

These two equations (4.2) and (4.3) together with (4.4) (continuity equation for incompressible fluids) and with the boundary conditions of the particular reactor define the convective mass transport in electrochemical cells. It is important to take in mind that this exhaustive description is frequently used in electrochemical engineering, especially in cases such as the electroplating processes where the current distribution becomes a key factor in the performance of the process.

$$\nabla \vec{u} = 0. \tag{4.4}$$

However, such a complex system would not be helpful to describe organic-removal wastewater-treatment processes because of its high degree of complexity and, therefore, in an attempt to achieve a useful model, some assumptions could be made in order to simplify the model. Hence the transformation of this distributed-parameter model in a simpler lumped-parameter model is very common in the modeling of wastewater-treatment processes, because it is not very important to obtain detailed information about what happens in every point of the cell but simply to know in a very simple way how the pollution of a influent waste decreases at the outlet of the electrochemical cell. In this context, there are three types of approaches typically used:

– The macroscopic approach, in which it is not taken into account what happens inside the cell in detail, but only an overall view of the system is described. In fact, the system is considered as a black box from the fluid dynamic point of view and then, it is assumed that the cell behaves a mixed tank reactor (the values of the variables only depend on time and not on the position since only one value of every variable describes all positions). This assumption allows simplifying directly all the set of partial differential equations to an easier set of differential equations, one for each model species. For the case of a continuous-operation electrochemical cell, the mass balances take the form shown in (4.5), where $[S_i]$

stands for every model species $\left(\mathrm{g\ m^{-3}}\right)$, q is the volumetric flow rate $\left(\mathrm{m^3\ s^{-1}}\right)$, v is the reactor volume $\left(\mathrm{m^3}\right)$, v_i^j is the stoichiometric coefficient of compound i in process j, r_j is the rate of process j expressed in $\mathrm{g\ s^{-1}}$ (in this text the symbol "r_j" is going to be used to indicate volumetric rates $\mathrm{g\ s^{-1}\ m^3}$), and subindex 0 indicates conditions at the inlet of the reactor.

$$v\frac{\mathrm{d}[S_i]}{\mathrm{d}t} = q_0[S_i]_0 - q[S_i] + \sum_{j=1}^{p} v_i^j r_j. \tag{4.5}$$

This approach is also used to model batch treatments (4.6) with a high value of recycle and in which the produced chemicals are not too active, so they can be considered to live for a sufficiently long time and their concentration results homogeneous in the whole solution. In this case, the initial condition is the concentration of species i at time $t = 0$ ($[S_i]_{t=0}$)

$$v\frac{\mathrm{d}\,[S_i]}{\mathrm{d}t} = \sum_{j=1}^{p} v_i^j r_j. \tag{4.6}$$

– The maximum gradient approach: The dependence of the position is only considered for the maximum gradient direction. Changes in other directions are neglected. This approach is frequently used to describe changes in a plug flow electrochemical cell in which the residence time is important and the more important changes in the species occurs in the flow direction. For the general case of a continuous operation electrochemical cell, the mass balances take the form shown in (4.7), where $\left[S_i^{\mathrm{electr}}\right]$ is the concentration of the species i on the surface of the electrode $\left(\mathrm{g\ m^{-3}}\right)$, k_{m} is the mass-transport coefficient $\left(\mathrm{m\ s^{-1}}\right)$, S is the section of the reactor $\left(\mathrm{m^2}\right)$, and A is the electrodic area $\left(\mathrm{m^2}\right)$.

$$\frac{\partial\,[S_i]}{\partial t} = \frac{q}{S}\frac{\partial\,[S_i]}{\partial x} + k_{\mathrm{m}}A\left([S_i] - \left[S_i^{\mathrm{elect}}\right]\right) + \sum_{j=1}^{p} v_i^j r_j. \tag{4.7}$$

This approach is also used to model batch treatments in which the recycle has a low or medium value In this case, two balances has to be drawn to characterize the discontinuous system: one for the cell (4.8) and the other for the reservoir (4.9)

$$\frac{\partial\,[S_i]}{\partial t} = \frac{q}{S}\frac{\partial\,[S_i]}{\partial x} + \sum_{j=1}^{p} v_i^j r_j, \tag{4.8}$$

$$\frac{\partial\,[S_i]}{\partial t} = \frac{q}{V_{\mathrm{reservoir}}}\left([S_i]_0 - [S_i]\right) + \sum_{j=1}^{p} v_i^j r_j. \tag{4.9}$$

– The mixed maximum gradient/macroscopic approach, in which the profiles in the changes in the variables' values are modeled (only in the direction of maximum change of the process variables) by means of several zones, in which the variables are supposed to depend only on the time and not on the position. The assumption of dividing the electrochemical cell into several zones allows the simplification of the mathematical complexity of the model. Thus, the complex system of partial differential equations (obtained from the mass balance in a nonsimplified system) is reduced to an easier-to-solve system of ordinary differential equations, in which the number of differential equations depends on the number of zones. This approach can be applied when mass transfer is important but it is pretended to obtain a simple model. In this context, a good way to simplify the position dependence of the model is to divide the electrochemical reactor into three zones: two zones close to the electrodes (anode and cathode) and a third zone corresponding to the bulk solution. In these three zones, the concentration of every compound can be considered to be constant with position and is only time dependent. This assumption is valid if the residence time in the electrochemical cell is small, since in this case the profiles of concentration in the flow direction can be assumed to be negligible. For the general case of a continuous operation in electrochemical cell, the mass balances take the form as shown in (4.10)–(4.12), where subindex a, b, and c stands for anodic, bulk, or cathodic conditions, respectively.

$$v_{\mathrm{a}} \frac{\mathrm{d}\left[S_i\right]_{\mathrm{a}}}{\mathrm{d}t} = \left(\sum_{j=1}^{p} v_i^j r_j\right)_{\text{anode}} + k_{\mathrm{m}} A \left(\left[S_i\right]_{\mathrm{b}} - \left[S_i\right]_{\mathrm{a}}\right), \tag{4.10}$$

$$v_{\mathrm{c}} \frac{\mathrm{d}\left[S_i\right]_{\mathrm{c}}}{\mathrm{d}t} = \left(\sum_{j=1}^{p} v_i^j r_j\right)_{\text{cathode}} + k_{\mathrm{m}} A \left(\left[S_i\right]_{\mathrm{b}} - \left[S_i\right]_{\mathrm{c}}\right), \tag{4.11}$$

$$\begin{aligned} v_{\mathrm{b}} \frac{\mathrm{d}\left[S_i\right]_{\mathrm{b}}}{\mathrm{d}t} &= q_0 \left[S_i\right]_{\mathrm{b},0} - q \left[S_i\right]_{\mathrm{b}} + k_{\mathrm{m}} A \left(\left[S_i\right]_{\mathrm{a}} - \left[S_i\right]_{\mathrm{b}}\right) + k_{\mathrm{m}} A \left(\left[S_i\right]_{\mathrm{c}} - \left[S_i\right]_{\mathrm{b}}\right) \\ &\quad + \left(\sum_{j=1}^{p} v_i^j r_j'\right) v_{\mathrm{b}}. \end{aligned} \tag{4.12}$$

This approach is also used to model batch treatments with high recycle rates in which the products generated electrochemically can react rapidly. Consequently, a three region model is required to separate the high reaction rates that occur close to the anodic and cathodic regions from the other slower reactions that occur on the whole volume of the solution (4.13)–(4.15). The initial conditions for these equations are $\left(\left[S_i\right]_{\mathrm{b}}\right)_{(t=0)} = \left(\left[S_i\right]_{\mathrm{b}}\right)_{(t=0)} = \left(\left[S_i\right]_{\mathrm{b}}\right)_{(t=0)} = \left[S_i\right]_{t=0}$

$$v_{\mathrm{a}} \frac{\mathrm{d}\,[S_i]_{\mathrm{a}}}{\mathrm{d}t} = \left(\sum_{j=1}^{p} v_i^j r_j \right)_{\text{anode}} + k_{\mathrm{m}} A \left([S_i]_{\mathrm{b}} - [S_i]_{\mathrm{a}} \right), \tag{4.13}$$

$$v_{\mathrm{c}} \frac{\mathrm{d}\,[S_i]_{\mathrm{c}}}{\mathrm{d}t} = \left(\sum_{j=1}^{p} v_i^j r_j \right)_{\text{cathode}} + k_{\mathrm{m}} A \left([S_i]_{\mathrm{b}} - [S_i]_{\mathrm{c}} \right), \tag{4.14}$$

$$v_{\mathrm{b}} \frac{\mathrm{d}\,[S_i]_{\mathrm{b}}}{\mathrm{d}t} = k_{\mathrm{m}} A \left([S_i]_{\mathrm{a}} - [S_i]_{\mathrm{b}} \right) + k_{\mathrm{m}} A \left([S_i]_{\mathrm{c}} - [S_i]_{\mathrm{b}} \right) + \left(\sum_{j=1}^{p} v_i^j r'_j \right) v_{\mathrm{b}}. \tag{4.15}$$

Besides the description of the position dependence, there is other important description level which has to be defined to formulate a model: the model species. From this perspective, there are two main types of models: those that consider all the significant compounds presented in the reactor as model species (multivariable models) and those that summarize different species into a small number of model species (in the more strict case only one variable and they are called as single-variable models). It is clear that the higher the number of species, the higher the complexity of the simulation. Hence, in the formulation stage it is important to study in detail what it is desired to model and to make a compromise as a function of our modeling goal between the optimum situation for the analysis of the process (many model species) and the optimum situation for the mathematical simulation (few model species).

4.4 Constitutive Equations for Electrochemical Oxidation and Coagulation Processes

In electrochemical coagulation and oxidation processes, to complement the equations obtained from the application of the conservation principles, it is required to use some constitutive equations, that is, equations based on physical, chemical, or electrochemical laws that model the primary mechanisms by which changes within the process are assumed to occur (rates of the processes, calculation of properties, etc.). The more important set of equations can be grouped into three main categories:

- Mass transfer
- Electrochemical kinetics
- Chemical kinetics

In this section these three types will be described.

4.4.1 Mass-Transfer Processes

Mass transfer is a key point in the modeling of the processes that occur in electrochemical cells. In a simple view, to obtain a high efficiency in a direct electrochemi-

cal process, it is required the good performance of the two sequential steps: first the electrochemically active species should arrive to the electrode surface and second, they should be oxidized or reduced. If a drop in the concentration of electroactive species on the electrode surface occurs, the first step becomes the bottleneck of the process and it starts to control the overall rate. Then, it is said that the reaction is mass-transfer controlled. The main cause of this drop in the concentration is the limited rate of transport of the electroactive species from the bulk solution toward the electrode surface. When there are several electroactive species, this will lead to different product conversions (f.i. in electrooxidation processes water oxidation can be promoted vs. the oxidation of organic matter).

Mass-transport processes between two regions are quantified by assuming that the local exchange rate is proportional to the concentration difference between two zones. The mass-transfer rate $\left(\text{in g s}^{-1}\right)$ can be calculated from (4.16), where $\left[S_i^{\text{electr}}\right]$ and $[S_i]$ are the concentrations $\left(\text{g m}^{-3} \text{ or mol m}^{-3}\right)$ of component i in the two zones, respectively; k_{m} $\left(\text{m s}^{-1}\right)$ is the mass-transfer coefficient; and A $\left(\text{m}^2\right)$ is the specific interfacial area between the electrochemical and chemical zones. This expression can also be formulated in terms of the total volume of the reaction system $\left(\text{g s}^{-1}\,\text{m}^{-3}\right)$ by introducing the specific surface of mass-transfer processes (α_{s}) as the ratio between the mass-transfer area and the characteristic volume that concerns this process (4.17). The mass-transfer coefficient (k_{m}) summarizes the transport of species by diffusion, convection, and migration. Hence a lot of parameters influence in its value. However, for typical electrochemical coagulation and oxidation processes, it can be assumed to depend only on the flow rate conditions, because the concentrations of the compounds are low, and hence diffusion and migration are going to be negligible as compared with the conventional mass-transfer mechanisms. Consequently, convention should be the primary transport mechanism in most electrochemical remediation processes.

$$r_i = k_{\text{m}} A \left(\left[S_i^{\text{electr}}\right] - [S_i]\right), \tag{4.16}$$

$$r_i' = k_{\text{m}} \alpha_{\text{s}} \left(\left[S_i^{\text{electr}}\right] - [S_i]\right). \tag{4.17}$$

4.4.2 Electrochemical Processes

To develop any electrochemical process, a voltage should be applied between anodes and cathodes of the cell. This voltage is the addition of several contributions, such as the reversible cell voltage, the overvoltages, and the ohmic drops, that are related to the current in different ways. One of these contributions, the overvoltage, controls the rate of the transfer of electrons to the electrochemically active species through the electrode–electrolyte interface when there is no limitation in the availability of these active species on the interface (no mass-transfer control and no control by a preceding reaction). In this case, the relationship between the current that flows between the anodes and the cathodes of a cell and the overpotential is

given by the well-known Butler–Volmer equation (4.18), where j_0 is the exchange current density, β is the symmetry factor, T is the temperature, F is the Faraday constant, and ν_e is the charge number of the electrode reaction

$$j = j_0 \left(e^{\frac{\beta \nu_e F}{RT} \eta} - e^{-\frac{(1-\beta)\nu_e F}{RT} \eta} \right). \tag{4.18}$$

For large overpotentials (common situation in actual electrochemical oxidation and coagulation processes), one of the terms of the bracket becomes negligible with respect to the other and an important simplification can be done. Thus, for the case of a large positive overpotential, (4.11) can be simplified to (4.19) that is a straight line in a semilog plot known as the equation of Tafel (4.20)

$$j = j_0 e^{\frac{\beta \nu_e F}{RT} \eta}, \tag{4.19}$$

$$\log j = \log j_0 + \frac{\beta \nu_e F}{2.3RT} \eta = \log j_0 + b\eta. \tag{4.20}$$

This equation simplifies the kinetic of a charge-transfer-controlled process to two parameters: the exchange current density j_0 and the Tafel slope b. Both values do not depend not only on the electrochemical reaction but also on the electrode material and on the electrolyte composition.

Once the current is related with the overpotential, the rate of the electrochemical process can be related to the applied current ($I = jA$) by (4.21), where F is the Faraday constant. This expression can be substituted in the mass balance and is used to characterize the generation (reaction) contribution.

$$r = \frac{jA}{\nu_e F}. \tag{4.21}$$

As described in Sect. 4.4.1, this rate can also be expressed in terms of the characteristic volume by using the specific surface of mass transfer (4.22)

$$r' = \frac{j\alpha_s}{\nu_e F}. \tag{4.22}$$

Equation (4.21) gives the total rate of the direct electrochemical processes. If only one process occurs, this equation gives the rate of this process, but if several processes develop at a time, then this equation gives the overall contribution of these partial processes. In principle, (4.23) can be used to determine the rate of every process and the total current will correspond with the addition of the current of all the processes. However, many factor influence on these parameters in actual wastewater-treatment processes, such as conditioning of the electrode surface or the presence of impurities in the electrolyte. This large number of parameters makes not possible to carry out quantitative and reliable calculations on a theoretical basis for electrochemical oxidation or coagulation processes, and it asks for other types of approaches to relate the overall current with the current due to every electrochemical

process. In this context, the simple way to model this, it is to consider that a fraction of the applied current intensity ($\alpha_i^{\text{electrode}}$) corresponds to each process and that the rate of each process can be calculated from (4.23). From (4.21) and (4.23), it is clear that (4.24) must be verified for each electrode.

$$r_i = \frac{I}{F}\alpha_i^{\text{electrode}}, \tag{4.23}$$

$$\sum_i \alpha_i^{\text{electrode}} = 1. \tag{4.24}$$

One of these approaches consists of assuming that the proportion of electrons involved in a particular electrochemical process $\left(\alpha_i^{\text{electrode}}\right)$ can be related with measurable parameters, assuming that the difference between the cell potential and its oxidation/reduction potential (V_i) is the driving force in the distribution of electrons (linear dependence with the overpotentials). Thus, it can be assumed that the fraction of the applied current intensity used in each process depends on the cell potential (ΔV_{work}) and on the oxidation (or reduction) potential (ΔV_i) of each process. The fraction can be calculated using (4.25), where $\Delta V_{\text{work}} = V_{\text{work}} - V_{\text{reference}}$ and $\Delta V_i = V_i - V_{\text{reference}}$. In all cases, ΔV_{work} must be greater than ΔV_i, otherwise process i cannot develop.

$$\alpha_i^{\text{electrode}} = \frac{(\Delta V_{\text{work}} - \Delta V_i)}{\sum_i (\Delta V_{\text{work}} - \Delta V_i)}. \tag{4.25}$$

As long as there are sufficient molecules of all the compounds on the electrode surface, these will be oxidized/reduced depending on the factors $\alpha_i^{\text{electrode}}$. On the contrary, if one of the compounds disappears completely from the electrode surface due to the oxidation/reduction process, the factors must be rearranged to take into account the absence of this compound.

4.4.3 Chemical Processes

The kinetic expressions shown before explain the direct electrochemical processes. However, many of the processes with interest in electrochemical oxidation or coagulation treatments are not direct processes, but simply chemical processes caused by the products generated at the electrode surface (mediated electrochemical processes). In addition, several chemical processes not related to the electrochemical process can occur in the electrochemical cell. Thus, in electrooxidation, the most common case is the mediated oxidation carried out by oxidants electrochemically generated on the electrode surface, such as hydroxyl radicals, hypochlorite, peroxosulphates, or peroxophosphates. In electrochemical coagulation, aluminum species formed during the electrochemical dissolution of the anodes are responsible for the later coagulation reactions.

The kinetics of all these chemical processes must be modeled in the same way as typical chemical processes. Then, it has to be taken in mind that for a given chemical process the kinetic expression must be proposed separately taking into account the experimental performance of this process. However, in the general case, chemical reaction modeling can be performed assuming a second-order kinetic depending on the concentrations of the electrochemically formed species or mediator ($[S_{\text{med}}]$) and the pollutant ($[S_i]$), as shown in (4.26). In this equation k_i is the kinetic constant

$$r_i' = k_i \, [S_{\text{med}}] \, [S_i] \, . \tag{4.26}$$

If the electrochemically generated compounds are very reactive species, the steady-state approximation can be assumed, and a first-order (4.27) or even zero-order (4.28) kinetic can be proposed.

$$r_i' = k_i \, [S_i] \, , \tag{4.27}$$

$$r_i' = k_i \, . \tag{4.28}$$

Independent of the order of the kinetic expression, the effect of temperature in all these processes can be easily introduced in the kinetic constant by means of an Arrhenius type equation (4.29). The effect of temperature is especially important in electrochemical oxidation processes, where the action of oxidants electrochemically generated will be very significant

$$k_i = k_i^0 \mathrm{e}^{-\frac{E}{RT}} . \tag{4.29}$$

In some cases, the reaction rates are very fast and a pseudoequilibrium approach is used to model the system (4.30). This approach consists of assuming that the concentration of species is always close to the equilibrium conditions and hence, they can be calculated using equilibrium constants from the values of other species present in the reaction system. This approach is especially important for the modeling processes in which the reaction rates are fast and when the kinetic rates are ill-defined (because of a large number of species or a lack of experimental data that makes difficult the kinetic analysis)

$$K = \frac{[\text{product}_1] \cdots [\text{product}_n]}{[\text{reagent}_1] \cdots [\text{reagent}_n]} . \tag{4.30}$$

4.5 Electrochemical Oxidation Models

Taking into account the points describe above, in literature there are many models proposed to describe electrochemical-oxidation wastewater-treatment processes (Polcaro and Palmas 1997; Cañizares et al. 1999; Panizza et al. 2001; etc.). They are based on many different description levels and assumptions. In this section, two

of them will be described: one which summarizes the pollution of wastewater in only one model species and that considers a macroscopic approach to formulate the mass balances, and other that considers more detailed profile of concentration to describe the time course of pollutants and intermediates through a mixed maximum gradient/macroscopic approach.

4.5.1 A Single-Variable Model to Describe the Time-Course of the COD During Electrochemical Oxidation Processes

This model was proposed by the group of Comninellis in 2001 (Panizza et al. 2001; Gherardini et al. 2001; Rodrigo et al. 2001). In this model, the pollution in the wastewater is quantified by a single component: the chemical oxygen demand (COD). In addition, it is considered that electrochemical reactions occur very close to the electrodes and the mass-transfer process (quantified by a mass-transfer coefficient k_m) is the controlling stage. This model is particularly suitable to describe galvanostatic treatments with boron-doped diamond (BDD) electrodes which show a high selectivity toward the organic compounds. The formulation of the model starts from the estimation of the limiting current density ($j_{lim}(t)$) from the COD values by (4.31).

$$j_{lim}(t) = 4Fk_m\mathrm{COD}(t). \tag{4.31}$$

In the description of the model, two types of behaviors were considered depending on the value of the limiting current density. The reaction was charge controlled if the applied current density was lower than the limiting current density $\left(j_{appl} < j_{limit}\right)$. In this case, the efficiency is maximum during the wastewater oxidation, and the decrease in COD with time is linear. Conversely, if the applied current density was higher than the limiting current density $\left(j_{appl} > j_{limit}\right)$, the process was mass-transfer controlled. In this case, the efficiency decreases during the oxidation and the decrease in COD with time is exponential. From the mathematical point of view, this behavior can be modeled with (4.32) and (4.33), where the value from which the COD transfer rate limits the overall process rate $\left(\mathrm{COD}_{lim}^{\text{mass transfer}}\right)$ is related to the mass-transfer coefficient through (4.34).

$$\text{If } \mathrm{COD}(t) > \mathrm{COD}_{lim}^{\text{mass transfer}} \text{ then } \mathrm{ICE}(t) = 1, \tag{4.32}$$

$$\text{If } \mathrm{COD}(t) \leq \mathrm{COD}_{lim}^{\text{mass transfer}} \text{ then } \mathrm{ICE}(t) = \frac{\mathrm{COD}(t)}{\mathrm{COD}_{lim}^{\text{mass transfer}}}, \tag{4.33}$$

$$\mathrm{COD}_{lim}^{\text{mass transfer}} = \frac{j_{appl}}{4Fk_m}. \tag{4.34}$$

In these equations, COD (t) is the chemical oxygen demand at time t $\left(\text{mol } O_2\ m^{-3}\right)$, I is the current intensity (A), F is the Faraday constant $\left(96,487\ \text{C mol}^{-1}\right)$, j_{appl} is the applied current density $\left(\text{A m}^{-2}\right)$, k_m the mass-transfer coefficient $\left(\text{m s}^{-1}\right)$, and ICE is the instantaneous current efficiency. For a typical-batch electrochemical

system (with a reactor volume negligible with respect to the reservoir), the following mass balance of the reaction system (4.35) can be obtained. In this case, the initial condition is the concentration of chemical oxygen demand at time $t = 0$ (COD_0)

$$V_R \frac{d\,COD\,(t)}{d_t} = -\frac{I}{4F} ICE\,(t)\,. \tag{4.35}$$

From (4.31), it is clear that the formulation of this model is made for direct electrochemical processes. However, it can be applied (directly without any changes) for systems in which hydroxyl radicals are the main mediators, as these species has a very short lifetime and, consequently, they are only available very close to the anode surface. Hence, processes mediated by these radicals are also mass-transfer controlled. In addition the electrochemical generation of hydroxyl radical is a one-electron charge transfer reaction. Hence the ratio of hydroxyl radicals to electron is 1.

The main advantage of this model is that it does not include any adjustable parameters. Hence, the behavior of the system can be predicted if the experimental conditions (applied current intensity, solution flow rate, and mass-transfer coefficient) are known. The good agreements obtained between model and experimental data validate all the assumptions made in the development of this model. This validation has been carried out with a wide variety of model pollutants including aromatics, nitroaromatics, cloroaromatics, carboxylic acids, alcohols, etc.

However, it is known that in the electrochemical oxidation of wastewaters on BDD other oxidants are generated including peroxosulphates and hydrogen peroxide, depending on the waste composition and on the operation conditions. The effect of these reagents is not considered in the former model, although it should be very important because they are mediated oxidators that extends the oxidation toward more regions in the reactors. To consider this effect, a chemical reaction contribution (4.36) should be added to the previously written model (Cañizares et al. 2005b), where k is a chemical oxidation constant $\left(s^{-1}\right)$.

$$r'_{chem} = k\,COD\,(t)\,. \tag{4.36}$$

This term should only be considered in case that $ICE < 1$, as the maximum decrease in the anodic oxidation of the COD is limited by the value of the current intensity employed. Likewise, this term can account for the generation of COD on the cathode if there are some reversible processes that influence on the system.

4.5.2 *A Multivariable Model to Describe the Time Course of Pollutant, Intermediates, and Final Products During Electrochemical Oxidation Processes*

To know more about the time course of the pollutants and intermediates during an electrochemical oxidation treatment, a more detailed description of the system

should be made (Cañizares et al. 2004a, b). This description should be focused on two items:

– The position and time dependence of every species in the cell
– The model species and the reaction mechanisms that governs their transformation

The first point needs to define the position dependence of species. To describe the changes in the concentration of the electroactive species with the distance to the electrode without increasing excessively the complexity of the mathematical system, the position dependence of the model can be simplified by dividing the electrochemical reactor into three zones (mixed maximum gradient/macroscopic approach): two zones (electrochemical zones) close to the electrodes (anode and cathode) and a third zone corresponding to the bulk solution (chemical zone). In these three zones, the concentration of every compound is considered to be constant with position and is only time dependent. This assumption is valid if the residence time in the electrochemical cell is small, since in this case the profiles of concentration in the flow direction can be assumed to be negligible. Hence, the electrochemical reactor is modeled as the combination of several consecutive stirred-tank reactors. The volume of each zone can be easily calculated if it is assumed that the thickness of the electrochemical zone is equivalent to the Nernst diffusion layer (δ). This assumption is acceptable because direct oxidation and most of the mediated oxidation processes (those with high reaction rates) occur in this zone. The thickness of this zone can be evaluated as a function of the mass-transfer coefficient (k) and the diffusivity (D) using (4.37).

$$\delta = \frac{D}{k} \tag{4.37}$$

The electrode surface area is known and so the volume of each electrochemical zone can be easily calculated by multiplying it by the thickness (δ). The remaining volume of the system corresponds to the volume of the chemical zone. For a typical-batch system, the following mass-balance equations for the anodic (4.38) and cathodic (4.39) electrochemical zones and for the chemical zone (4.40) can be obtained.

$$v_{\mathrm{a}} \frac{\mathrm{d}\,[\mathrm{S}_i]_{\mathrm{a}}}{\mathrm{d}_t} = \sum_{j=1}^{n} \nu_i^j \frac{I}{F} \alpha_j^{\mathrm{anode}} + kA\left([\mathrm{S}_i]_{\mathrm{b}} - [\mathrm{S}_i]_{\mathrm{a}}\right), \tag{4.38}$$

$$v_{\mathrm{c}} \frac{\mathrm{d}\,[\mathrm{S}_i]_{\mathrm{c}}}{\mathrm{d}_t} = \sum_{j=1}^{m} \nu_i^j \frac{I}{F} \alpha_j + kA\left([\mathrm{S}_i]_{\mathrm{b}} - [\mathrm{S}_i]_{\mathrm{c}}\right), \tag{4.39}$$

$$v_{\mathrm{b}} \frac{\mathrm{d}\,[\mathrm{S}_i]_{\mathrm{b}}}{\mathrm{d}_t} = kA\left([\mathrm{S}_i]_{\mathrm{a}} - [\mathrm{S}_i]_{\mathrm{b}}\right) + kA\left([S_i]_{\mathrm{c}} - [S_i]_{\mathrm{b}}\right) + \sum_{j=1}^{p} \nu_i^j r'_j v_{\mathrm{b}}. \tag{4.40}$$

In these equations ν_i^j is the stoichiometric coefficient of compound i in process j and subindexes a, c, and b represent the anodic, cathodic, and chemical (bulk) zone, respectively.

The second item that needs to be fixed is the number of species and the reactions, including the stoichiometric coefficients and also the kinetics of the processes. In this context, in electrochemical oxidation processes it is important to discern between two types of anodes: those that behaves only as electrons sinks (named nonactive) and those that suffer changes during the electrochemical oxidation which influence on the treatment (named active electrodes). In both cases, the main processes related to removal of the pollutant that involves irreversible oxidative routes. Consequently, the reductive processes are less important and it can be presumed that in the cathodic zone only hydrogen evolution occurs. Nevertheless, if some organic compound can be reduced at the cathode, the mass-transfer and the reduction processes must be included in the model scheme.

When a typical nonactive material is employed, the anode only acts as an electron sink. In this particular case, the scheme representing the oxidation processes can be explained as shown in Fig. 4.2. The first process that needs to be considered is the mass transfer of the compounds from the bulk zone to the anodic one. The organic compounds can undergo direct oxidation on the electrode surface. This process can either be one-stage or multistage, and proceeds until the final oxidation product is generated (usually, carbon dioxide). At the same time, the decomposition of water

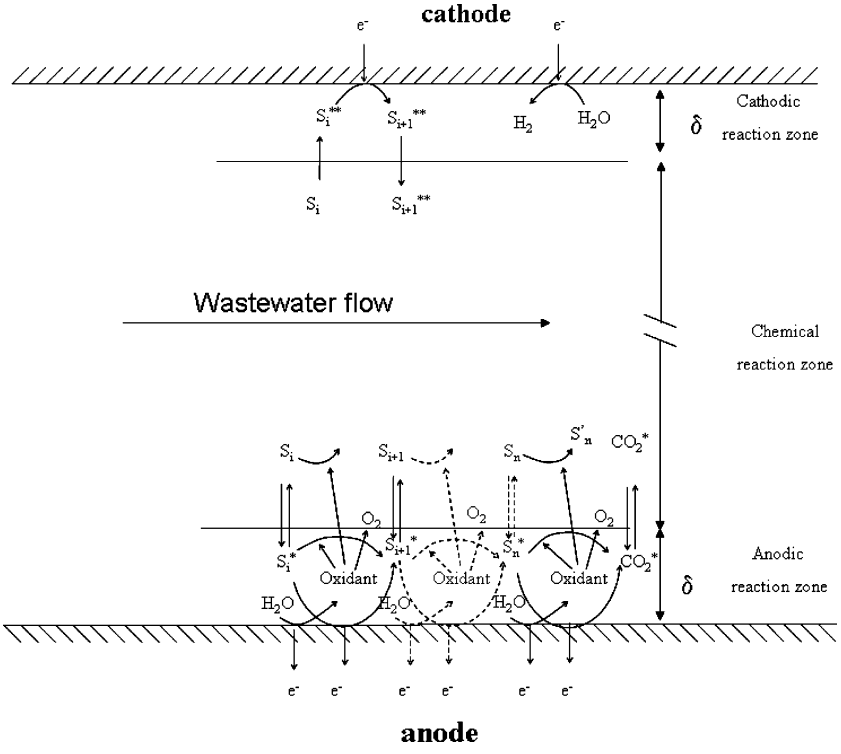

Fig. 4.2 Electrooxidation with nonactive electrodes

molecules can lead to the appearance of hydroxyl radicals. Hydroxyl radicals are not stable and can cause the formation of other oxidants (ozone, hydrogen peroxide, peroxosulphate, chlorine, etc.) that can react chemically with the organic matter through mediated oxidation processes or, alternatively, can promote the formation of oxygen. If these oxidant compounds arrive in the bulk zone, it is necessary to take into account their mass-transfer process and the oxidation of the organics in the bulk zone.

When a typical active material is employed as the anode, a number of additional species generated on the electrode surface must also be considered. They can influence the process performance, causing additional chemical reactions on the electrode surface if the redox couple remains at the surface (i.e., Pt/PtO), or in the bulk solution if the electrogenerated species are dissolved (i.e., Al/Al^{3+}). A scheme outlining the processes that need to be considered in the anodic electrochemical zone is shown in Fig. 4.3. The first process to be taken into account is the formation of oxidized species on the electrode surface. These species can either remain on the surface or move toward the bulk zone. In the latter case, mass transfer to the bulk zone and possible chemical reactions in this zone must be considered.

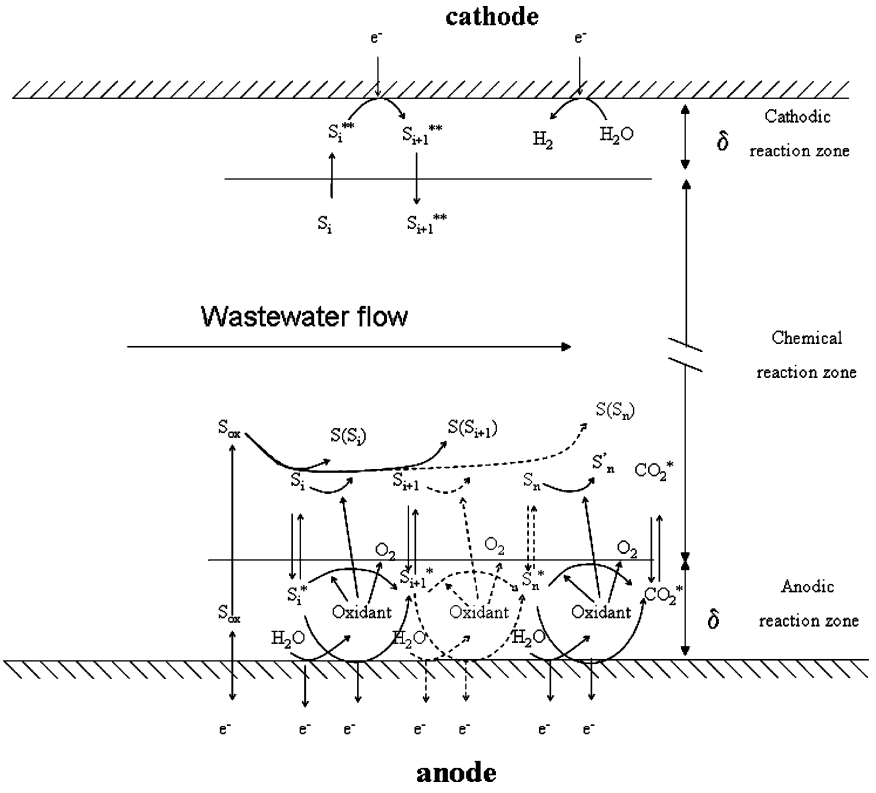

Fig. 4.3 Electrooxidation with active electrodes

At the same time, the mass transfer of the oxidizable compounds from the bulk zone to the anodic zone must also be considered. In this anodic zone, the organic materials can undergo a direct oxidation on the electrode surface – a process similar to that described for nonactive electrodes, in which the anode acts only as an electron sink. At the same time, if the electrogenerated compound remains on the electrode surface, the organic oxidation occurs chemically by electrogenerated oxidants. These processes can either be one-stage or multistage, and they proceed until the final oxidation product is generated (usually carbon dioxide). Simultaneously, the decomposition of water molecules produces oxidants (ozone, hydrogen peroxide, peroxosulphates, chlorine, etc.), that can react with the organic matter through mediated oxidation processes, or can promote the formation of oxygen. If these oxidants arrive in the bulk zone, it is necessary to take into account their mass-transfer processes and the chemical oxidation of the organics in the bulk zone.

To model all the particular processes, kinetics expressions proposed in Sect. 4.4 are used. As an example, Fig. 4.4 shows the application of the model to a particular case (Cañizares et al. 2004a): the oxidation of phenol in a cell with nonactive anodes.

This model has been applied to a wide variety of pollutants including carboxylic acids, phenolic, aminoaromatic, and chloroaromatic compounds. In every case it was able to reproduce the time course of the different species with a great accuracy. This, together with the small number of parameters and with their physical meaning made the model as an important tool to analyze electrochemical oxidation processes.

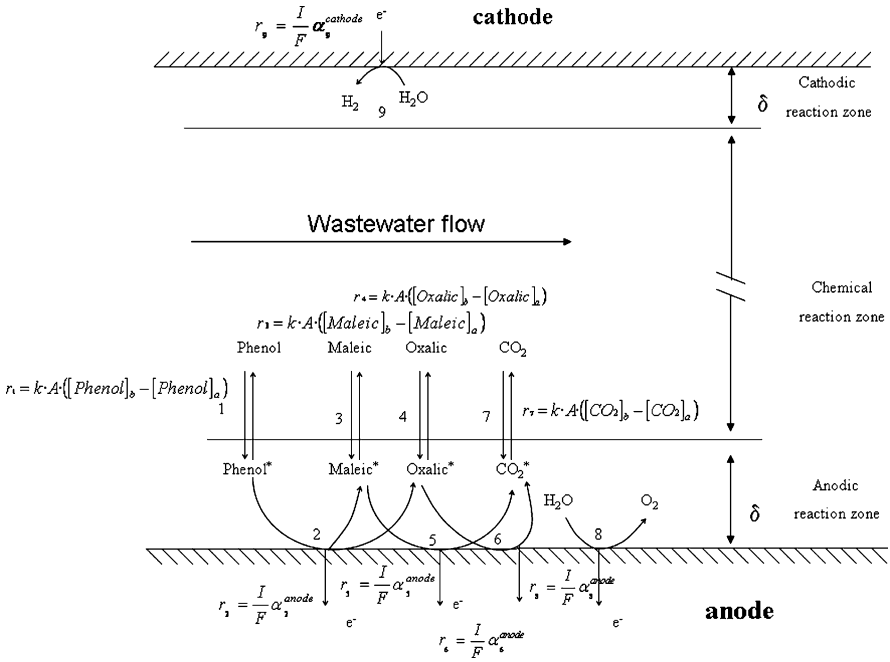

Fig. 4.4 Example of model formulation of phenol oxidation

4.6 Electrochemical Coagulation Models

The electrochemical coagulation is a complex process that can be used to reduce the organic content of many types of industrial wastewaters including those polluted with colloidal particles, macromolecules, or O/W emulsions. This process consists of two sequential processes: the dose of the reagent, which is really the more important electrochemical process, and the subsequent coagulation/flocculation processes. In principle, these later processes are not electrochemical but chemical or physical processes. However, the mobility of the pollutants can be greatly improved due to electrophoretic or the electromigration processes, and consequently electrochemistry should also be considered in the description of these processes.

Modeling of electrochemical coagulation processes has been little investigated (Matteson et al. 1995; Chen et al. 2002; Szpyrkowicz 2005; Cañizares et al. 2005a; Khemis et al. 2006). Most models on electrochemical coagulation are not focused on the description of the dissolution of the electrodes but are focused on the description of the processes that occurs once the coagulant reagents are added to the wastewater. To do this, two different approaches are typically used: one that considers the hydrodynamic conditions as the main factor responsible for the electrochemical coagulation processes and the other that considers the chemical interaction of the reagents and the pollutants as the more significant processes in the description of the electrocoagulation. To illustrate both types of the models, one model example of these two types of approaches is described in this section. Concerning the modeling of the electrochemical dissolution, less work has been done and only very recently a model has been proposed. This model was formulated with the same assumptions as that of the multivariable model of electrochemical oxidation described in Sect. 4.5.2, and it allows describing the aluminum species generated during an electrochemical coagulation process, just from the operation conditions used.

4.6.1 A Single-Variable Model to Describe Electrochemical Coagulation Controlled by Hydrodynamic Conditions

In literature, there are some models in which it is assumed that mass transport is the key point to explain electrochemical coagulation processes. One of the more important contributions is given by Matteson et al. (1995) who model the efficiency of the electrochemical coagulation processes as a function of electrophoretic transport of the colloids toward the anode. However, in this section the attention is going to be focused on the model proposed by Szpyrkowicz in 2005, as it is directly related to the removal of some types of organic compounds (particularly, dyes). This model assumes that coagulation occurs in two successive stages after the dose of the reagent: a destabilization of the pollutants by reaction with coagulating compounds formed in situ during anode dissolution, and a subsequent gas flotation of the particle-agglomerates. Hence the process occurs with two-step mechanisms

$$S_1 \overset{k_1}{\rightarrow} S_2 \overset{k_2}{\rightarrow} S_3$$

The symbol S_1 indicates the initial organic compounds in the solution, S_2 the intermediate form of organic compounds in the solution, and S_3 is the final form of organic compound when they are eliminated from the solution. The first stage behaves as a zero-order reaction (4.41), as it is assumed that neither the pollutant nor the reagent controls the rate of the process. Consequently, for a discontinuous reactor the decrease in the pollutant concentration during this phase is proportional (4.42) to the time lapse (t).

$$\frac{\mathrm{d}S_1}{\mathrm{d}t} = k_1, \tag{4.41}$$

$$\frac{S_{1,t}}{S_{1,0}} = 1 - \frac{k_1}{S_{1,0}} t. \tag{4.42}$$

On the contrary, the performance of the second stage is well described by the first-order kinetics, that is, the higher the concentration of pollutant, the higher the possibility of flocculation (4.43).

$$\frac{\mathrm{d}S_2}{\mathrm{d}t} = k_2 S_1. \tag{4.43}$$

Parameters k_1 and k_2 can be easily related to the hydrodynamic conditions (flow rate, stirring rates) and to the current density by empirical equations. The influence of the current density can also be related to the reagent dose for parameter k_1 and to the bubble generation for parameter k_2 (the flow rate of cathodically generated hydrogen is proportional to the current density). Thus, this semiempirical model considers easily and simultaneously the gas–liquid mass transfer, the collections of solid particles in electroflotation processes, and the effect of the current density.

4.6.2 A Multivariable Model to Describe Electrochemical Coagulation Based on Pseudoequilibrium Approaches

The model that is going to be explained in this section was proposed by the group of Lapicque in 2006 (Khemis et al. 2006) to describe the electrochemical coagulation of organic polluted wastewaters with aluminum, and it is based on the same assumptions that a previously proposed model used to describe the oil–water emulsion breaking process (Carmona et al. 2006).

The model assumes that the coagulation of organics proceeds by complexation of the suspended matter by coagulant reagents, and it postulates a chemical pseudoequilibrium approach to model these processes. According to the model, the concentration of pollutants (which can be expressed as COD) can be divided into three main contributions: pollutants that can coagulate by pH changes without reagent addition (COD_1), pollutants that need the electrochemically generated

reagent to coagulate (COD_2), and pollutants that cannot be removed by these technologies (COD_3). In addition, contribution COD_2 can be divided into two groups: COD available to react COD_{2-1} and COD already reacted (COD_{2-2}).

Likewise, the coagulant electrogenerated (aluminum electrodes are used) is classified into several contributions: aluminum threshold level for coagulation (Al_{min}), free aluminum species (Al_{free}), and aluminum complexed with the pollutants ($Complex_{Al\text{-}COD}$).

The formulation of the model is based on the stoichiometrical equation (4.44) to relate pollutant and coagulant reagent, where coefficient n has to be determined experimentally

$$n\,COD_2 + Al_{free} \leftrightarrow Complex_{Al-COD}. \tag{4.44}$$

According to this reaction the stoichiometry of the process can be modeled according to (4.45). To calculate the concentration of every model species in a batch system, the mass balance of the pollutant species (4.46) that of the reagent species (4.47) and the pseudoequilibrium constant (4.48) should also be considered.

$$COD_{2-2} = 1/n\left[Al_{Complex\ A1\text{-}COD}\right], \tag{4.45}$$

$$COD\,(t) = COD_1 + COD_2 + COD_3, \tag{4.46}$$

$$[Al] = [Al_{min}] + [Al_{free}] + \left[Al_{Complex\ Al\text{-}COD}\right], \tag{4.47}$$

$$K = \frac{[Complex_{Al\text{-}COD}]}{[Al_{free}]\,[COD_2]}. \tag{4.48}$$

These equations are solved for every time step in the simulation. Hence, it is assumed that the system is always on the equilibrium conditions (pseudoequilibrium approach). Model parameters are calculated by mathematical fitting. The good results obtained in the validation, together with the physical meaning of the parameters, are the two main advantages of this model, which can help to understand better the fundamentals of the electrochemical coagulation processes.

4.6.3 A Multivariable Model to Describe Electrochemical Dissolution Processes

In this section it is going to be described a model of electrochemical dissolution of aluminum electrodes previously proposed in literature (Cañizares et al. 2005). According to this model, the more important electrochemical processes that occur in electrochemical coagulation cells are the metal dissolution and the water oxidation and reduction (4.49)–(4.51).

$$Al \rightarrow Al^{3+3} + 3e \tag{4.49}$$

$$2H_2O \rightarrow O_2 + 4H^+ + 4e^- \tag{4.50}$$

$$H_2O + e^- \rightarrow 1/2H_2 + OH^- \tag{4.51}$$

In addition, there are several important chemical processes in electrochemically assisted coagulation. The more important is the chemical dissolution which consists of the oxidation of the metal sheets with the simultaneous reduction of water to form hydrogen. This process is represented by (4.52).

$$2\mathrm{Al} + 6\mathrm{H_2O} \rightarrow 2\mathrm{Al}^{3+} + 3\mathrm{H_2} + 6\mathrm{OH} \tag{4.52}$$

The pH has a strong influence on the chemical dissolution process, and the value of this parameter can increase by several orders of magnitude at alkaline pHs. In this context, it is important to remark that in an electrochemical cell there is a pH profile between anode and cathode. In the anode, the water oxidation process (oxygen evolution) generates a high concentration of protons and thus, a lower pH must be obtained. In the cathode, the water reduction process results in the formation of hydroxyl ions and a higher pH must appear in this zone. Thus, a marked pH profile is expected and the bulk pH is not a good value to determine the rate of chemical dissolution, as it must differ considerably from the actual values on the electrodes surfaces, which is the place where the chemical dissolution is going to take place. To take this into account, the model considers this profile of pH, but in order to simplify the complexity of the mathematical system a mixed maximum gradient/macroscopic approach is used. Consequently the mass balances proposed in this model take the form of the equation proposed in Sect. 4.3 (4.53)–(4.55).

$$\nu_\mathrm{a}\frac{\mathrm{d}\,[\mathrm{S}_i]_\mathrm{a}}{\mathrm{d}t} = kA\left([\mathrm{S}_i]_\mathrm{b} - [\mathrm{S}_i]_\mathrm{a}\right) + r_{\mathrm{electrochem}_{i,\mathrm{a}}} + r'_{\mathrm{chem}_{i,\mathrm{a}}}\nu_\mathrm{a}, \tag{4.53}$$

$$\nu_\mathrm{c}\frac{\mathrm{d}\,[\mathrm{S}_i]_\mathrm{c}}{\mathrm{d}t} = kA\left([\mathrm{S}_i]_\mathrm{b} - [\mathrm{S}_i]_\mathrm{c}\right) + r_{\mathrm{electrochem}_{i,\mathrm{a}}} + r'_{\mathrm{chem}_{i,\mathrm{a}}}\nu_\mathrm{c}, \tag{4.54}$$

$$\nu_\mathrm{b}\frac{\mathrm{d}\,[\mathrm{S}_i]_\mathrm{b}}{\mathrm{d}t} = q\left([\mathrm{S}_i]_0 - [\mathrm{S}_i]_\mathrm{b}\right) + kA\left([S_i]_\mathrm{a} - [S_i]_\mathrm{b}\right) + kA\left([S_i]_\mathrm{c} - [S_i]_\mathrm{b}\right) + r'_{\mathrm{chem}_{i,\mathrm{b}}}\nu_\mathrm{b}. \tag{4.55}$$

In addition to the aluminum chemical dissolution, other important chemical processes that occur in an electrochemical cell are the speciation of the coagulants. Once the aluminum is dissolved (chemically or electrochemically) different species can be formed, depending on the pH of the solution. For the case of aluminum, the reactions involved are shown below (4.56)–(4.60). In this set of equations, it has also been included the carbonate/bicarbonate equilibria (4.61)–(4.62) and ionization of water, due to its high influence on the calculation of the pH value (4.63).

$$\mathrm{Al(OH)_4}^- + \mathrm{H}^+ \rightleftarrows \mathrm{Al\,(OH)_3} \tag{4.56}$$

$$\mathrm{Al\,(OH)_3} + \mathrm{H} \rightleftarrows \mathrm{Al(OH)_2}^+ \tag{4.57}$$

$$\mathrm{Al(OH)_2}^+ + \mathrm{H}^+ \rightleftarrows \mathrm{Al\,(OH)}^{+2} \tag{4.58}$$

$$\mathrm{Al\,(OH)}^{+2} + \mathrm{H}^+ \rightleftarrows \mathrm{Al}^{+3} \tag{4.59}$$

$$\mathrm{Al\,(OH)_3\ (s)} \rightleftarrows \mathrm{Al}^{3+} + 3\mathrm{OH}^- \tag{4.60}$$

$$\mathrm{CO_2} + \mathrm{H_2O} \rightleftarrows \mathrm{H}^+ + \mathrm{HCO_3}^- \tag{4.61}$$

$$HCO_3^- \rightleftarrows CO_3^{2-} + H^+ \tag{4.62}$$

$$H_2O \rightleftarrows OH^- + H^+ \tag{4.63}$$

The concentration of any of these species depends on the total concentration of dissolved aluminum and on the pH, and this makes the system complex from the mathematical point of view and consequently, difficult to solve. To simplify the calculations, mass balances were applied only to a unique aluminum species (the total dissolved aluminum, TDA, instead of the several species considered) and to hydroxyl and protons. For each time step (of the differential equations-solving method), the different aluminum species and the resulting proton and hydroxyl concentration in each zone were recalculated using a pseudoequilibrium approach. To do this, the equilibrium equations (4.64)–(4.71), and the charge (4.72), the aluminum (4.73), and inorganic carbon (IC) balances (4.74) were considered in each zone (anodic, cathodic, and chemical), and a nonlinear iterative procedure (based on an optimization method) was applied to satisfy simultaneously all the equilibrium constants. In these equations (4.64)–(4.74), subindex z stands for the three zones in which the electrochemical reactor is divided (anodic, cathodic, and chemical).

$$\frac{[Al(OH)_4^-]_z \cdot [H^+]_z}{[Al(OH)_3]_z} = 10^{-8.0} \tag{4.64}$$

$$\frac{[Al(OH)_3]_z \cdot [H^+]_z}{[Al(OH)_2^+]_z} = 10^{-5.7} \tag{4.65}$$

$$\frac{[Al(OH)_2^+]_z \cdot [H^+]_z}{[Al(OH)^{2+}]_z} = 10^{-4.3} \tag{4.66}$$

$$\frac{[Al(OH)^{2+}]_z \cdot [H^+]_z}{[Al^{3+}]_z} = 10^{-5.0} \tag{4.67}$$

$$[Al^{3+}]_z \cdot [OH^-]_z^3 = 10^{-32.9} \tag{4.68}$$

$$\frac{[HCO_3^-]_z \cdot [H^+]_z}{[H_2CO_3]_z} = 10^{-6.37} \tag{4.69}$$

$$\frac{[CO_3^{2-}]_z \cdot [H^+]_z}{[HCO_3^-]_z} = 10^{-10.25} \tag{4.70}$$

$$[H^+]_z \cdot [OH^-]_z = 10^{-14.0} \tag{4.71}$$

$$\sum_{\text{anionic species}} n\,[A^{n-}]_z - \sum_{\text{cationic species}} m\,[B^{m+}]_z = 0 \tag{4.72}$$

$$[TDA]_z = [Al^{3+}]_z + [AlOH^{2+}]_z + [Al(OH)_2^+]_z + [Al(OH)_3]_z + [Al(OH)_3]_{sol,z} + [Al(OH)_4^-]_z \tag{4.73}$$

$$[IC]_z = [H_2CO_3]_z + [HCO_3^-]_z + [CO_3^{2-}]_z \tag{4.74}$$

This model is able to reproduce successfully the time course of pH and aluminum in continuous and discontinuous cells and it gives important information about the nature of the processes that occurs inside the electrochemical cells during the dissolution of aluminum.

4.7 Conclusions

Many models are proposed in literature to describe electrochemical coagulation and oxidation processes. They are based on very different simplifications and focused on different aims. Two are the main factors to classify these models: number of species and position dependence of the species. From the perspective of the models species, there are models that consider all the significant compounds presented in the reactor as model species (multivariable models) and others that summarize different species into a small number of model species (in the more strict case, only with one variable and then, they are called single-variable model). In the formulation stage, it is important to study in detail what it is desired to model, and to make a compromise as a function of our modeling goal between the optimum situation for the analysis of the process (many model species) and the optimum situation for the mathematical simulation (few model species). From the viewpoint of the position dependence, an in-depth description of the electrochemical treatment of organic-polluted wastewater in which the concentration profile of every compound in the electrochemical cell is calculated is not useful for the description of organic-wastewater electrochemical-treatment processes. For this reason, different types of approaches (like the macroscopic, the maximum gradient, and the mixed macroscopic/maximum gradient) are used to simplify this position dependence of the variables. Taking into account all these, different models has been proposed in literature and successfully validated with experimental data. They represent different description approaches to the same processes which may be helpful in the design of the processes, in the analysis of operating problems, and also simply to know more about the mechanisms of the processes that occur inside the electrochemical cells.

References

Cañizares, P., Domínguez, J.A., Rodrigo, M.A., Villaseñor, J. and Rodríguez, J. (1999) Effect of the current intensity in the electrochemical oxidation of aqueous phenol wastes at an activated carbon and steel anode. Ind. Eng. Chem. Res. 38(10), 3779–3785.

Cañizares, P., García-Gómez, J., Lobato, J. and Rodrigo, M.A. (2004a) Modeling of wastewater electro-oxidation processes. Part I. General description and application to inactive electrodes. Ind. Eng. Chem. Res. 43, 1915–1922.

Cañizares, P., García-Gómez, J., Lobato, J. and Rodrigo, M.A. (2004b) Modeling of wastewater electro-oxidation processes. Part II. Application to active electrodes. Ind. Eng. Chem. Res. 43, 1923–1931.

Cañizares, P., Carmona, M., Lobato, J., Martínez, F. and Rodrigo, M.A. (2005a). Electrodissolution of aluminium electrodes in electrocoagulation processes. Ind. Eng. Chem. Res. 44, 4178–4185.

Cañizares, P., Lobato, J., Paz, R., Rodrigo, M.A and Sáez, C. (2005b) Electrochemical oxidation of phenolic wastes with boron-doped diamond anodes. Water Res. 39, 2683–2699.

Carmona, M., Khemis, M., Leclerc, J.-P. and Lapicque, F. (2006) A simple model to predict the removal of oils suspensions from water using electrocoagulation technique. Chem. Eng. Sci. 61, 1233–1242

Chen, X., Chen, G. and Yue, P.L. (2002). Investigations on the electrolysis voltage of electrocoagulation. Chem. Eng. Sci. 57, 2449–2455.

Gherardini, L., Michaud, P.A., Panizza, M., Comninellis, Ch. and Vatistas, N. (2001) Electrochemical oxidation of 4-chlorophenol for wastewater treatment – definition of normalized current efficiency (phi). J. Electrochem. Soc. 148, D78–D84.

Khemis, M., Leclerc, J.-P., Tanguy, G., Valentin, G. and Lapicque, F. (2006) Treatment of industrial liquid wastesby electrocoagulation: Experimental investigations and overall interpretation model. Chem. Eng. Sci. 61, 3602–3609.

Matteson, M.J., Dobson, R.L., Glenn, R.W., Kukunoor, N.S., Waits III, W.H. and Clayfield, E.J. (1995) Electrocoagulation and separation of aqueous suspensions of ultrafine particles. Colloids Surf A Physicochem. Eng. Aspects 104, 101–109.

Panizza, M., Michaud, P.A., Cerisola, G. and Comninellis, Ch. (2001) Electrochemical treatment of wastewaters containing organic pollutants on boron-doped diamond electrodes: Prediction of specific energy consumption and required electrode area. Electrochem. Commun. 3, 336.

Polcaro, A.M. and Palmas, S. (1997) Electrochemical oxidation of chlorophenols. Ind. Eng. Chem. Res. 36, 1791–1798.

Rodrigo, M.A., Michaud, P.A., Duo, I., Panizza, M., Cerisola, G. and Comninellis, Ch. (2001) Oxidation of 4-chlorophenol at boron-doped diamond electrode for wastewater treatment. J. Electrochem. Soc. 148, D60–D64.

Szpyrkowicz, L. (2005) Hydrodynamic effects on the performance of electro-coagulation/electroflotation for the removal of dyes from textile wastewater. Ind. Eng. Chem. Res. 44, 7844–7853.

Chapter 5
Green Electroorganic Synthesis Using BDD Electrodes

Ulrich Griesbach, Itamar M. Malkowsky, and Siegfried R. Waldvogel

5.1 Introduction

Electrochemical processes are mostly regarded as "green", due to their pronounced atom efficiency and absence of waste products (Steckhan et al. 2001). In some cases, the reactions on the anode as well as on the cathode can be exploited simultaneously for preparative purposes allowing highly efficient electrochemical processes. These 200% cells fulfil many requirements for a sustainable chemical transformation since no reagent waste is produced. Major advantages for employing electrochemistry are the precise adjustment of redox potentials in a wide range and the influence of current density onto the kinetics of the transformation. However, efficiency and, in particular, selectivity of electrochemical transformations can be triggered by mediators. By mediator the electrode is brought to hidden places which are not accessible by the anodic and cathodic surfaces. Consequently, the active site of enzymes and solid-phase-supported substrates can be part of electrochemical processes (Rao et al. 2006; Nad and Breinbauer 2004; Nad and Breinbauer 2005). The electrocatalytic recycling of reagents is one of the most vivid research areas in this respective field. Consumption and subsequent removal of the supporting electrolyte after electrolysis is often mentioned as a kind of disadvantage in this methodology. However, in most cases very simple supporting electrolytes, e.g. acids, are used or methanol as protic solvent is applied. Some examples demonstrate that ion-exchange resins can substitute the supporting electrolyte avoiding work-up challenges (Jörissen 1996). The electrochemical formation of radicals is an easy-to-control alternative to thermal decomposition of peroxides and photochemistry. Whenever possible, this methodology is applied for production plants. As a result, electrochemical transformations account for approximately 7% of the total industrial electricity consumption (Weissermel and Arpe 1997). Modern strategies like the "paired electrolysis" exploit both electrode reactions for preparative means and increase the efficiency tremendously (Pütter 2001). However, the application of electrochemically generated radicals in organic and

U. Griesbach (✉)
BASF SE, Care Chemicals, Ludwigshafen, Germany
e-mail: ulrich.griesbach@basf.com

C. Comninellis and G. Chen (eds.), *Electrochemistry for the Environment*,
DOI 10.1007/978-0-387-68318-8_5,

biochemical processes is rather limited, because appropriate techniques and, in particular, suitable electrode materials are still missing. Since aqueous media are commonly used in inorganic technical processes, the electrolysis of water is the major side reaction. Electrode materials with a high overpotential for hydrogen and oxygen in cathodic and anodic processes, respectively, can suppress this unwanted drain of electric energy. The investigation and application of boron-doped diamond (BDD) as novel and innovative electrode material in non-destructive chemistry is a new and challenging field. High hopes are placed in this new BDD technology, since tremendous ameliorations in academic and industrial aspects seem to be possible. This is mainly due to the extremely large potential window for BDD in aqueous solutions. In particular, anodic processes allow the formation of OH radicals at potentials well below the onset of oxygen evolution. BDD electrodes thus can be used for new oxidation reactions which otherwise are not possible in water (Iniesta et al. 2001a). In methanol containing solutions, methoxy radicals were also discussed as reactive intermediates (Zollinger et al. 2004a). On the other hand, their use for disinfection, detoxification and wastewater treatment is possible: at intermediate potentials a direct, simple electron transfer occurs, whereas the formation of hydroxyl radicals at highly positive potentials leads to a complete incineration (e.g. of 2-naphthol, 4-chlorophenol and other compounds) via complex oxidation reactions (Rodrigo et al. 2001; Panizza et al. 2001; Ouattara et al. 2003; Zhi et al. 2003; Boye et al. 2002, 2006). Fouling, which is often observed at intermediate potentials, is avoided. Partial oxidation, e.g. of phenol to benzoquinone, is also observed (Iniesta et al. 2001b). Low background currents at BDD electrodes are advantageous for their electroanalytical use (Spataru et al. 2005). Anodic polarization of BDD leads to changes of the properties, such as decrease of the active surface area (Duo et al. 2004). Single crystal orientation and atomic termination have a significant impact onto the electrochemical behaviour (Kondo et al. 2005; Pleskov et al. 2002). Mechanistic investigations often involve the use of the rotating-disc electrode for various redox systems and the study of the influence of the surface state and preconditioning on the rate of electron transfer; comparable studies beyond “simple” electron transfer are scarce (Sopchak et al. 2002). Using the scanning electrochemical microscope, the variation of the electrochemical reactivity was locally resolved (Wilson et al. 2006). Mechanistic studies at high overpotentials were performed by cyclic voltammetry and by measuring concentration changes during bulk electrolysis. The results could be explained by assuming that complete incineration to CO_2 occurs due to the formation of OH spin centres whenever the applied current exceeds the limiting current given by mass transfer. The formation of OH spin centres has been demonstrated using spin traps (Marselli et al. 2003). The influence of the applied potential, diffusion and convection processes is depicted in Fig. 5.1. When a high potential is applied to BDD electrodes the concentration of radical species is dramatically increased and influences the chemical transformations. Since degradation of organic matter is mediated by hydroxyl radicals at highly positive potentials (top), synthetic use of BDD anodes is limited to transformations in protic or only slight aquatic media (centre)

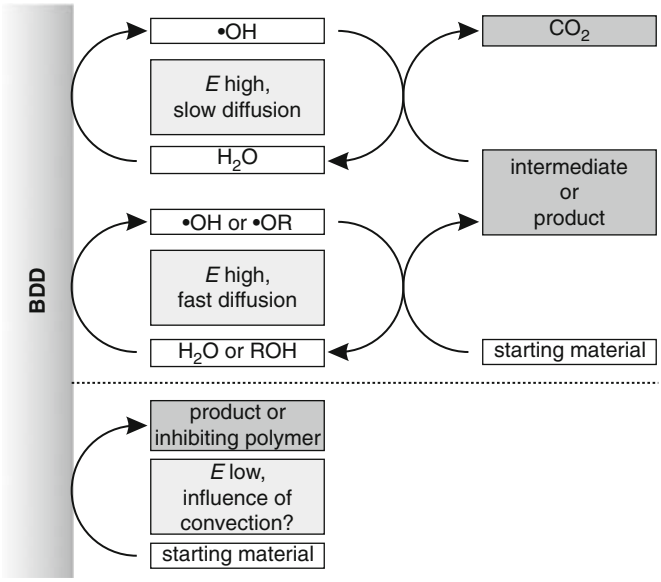

Fig. 5.1 Overview on the influence of applied potential *E* and diffusion or transportation processes at the electrode

as well as to low-potential conversions (bottom). Fast-transportation processes are a significant factor to avoid overoxidation. Therefore, high concentrations of the starting material might be a possibility to exploit BDD electrodes for synthetic purposes.

5.2 Experimental Equipment and Practical Aspects

Electrolysis cells for BDD electrodes are commercially available, e.g. a modular electrochemical cell from CSEM (now Adamant Technologies, Switzerland) (Haenni et al. 2002). Unfortunately, they are designed for wastewater treatment and therefore generally not applicable to organic media. Furthermore, these cell dimensions require relatively large electrodes. In order to work on a smaller scale and to apply various reaction conditions for preparative purposes, a novel cell geometry was developed.

Despite the superior chemical stability of the diamond layer, these electrodes face two challenges. The brittle nature of crystalline silicon limits the mechanical stability of the support, causing eventual loss of the BDD electrode by friction. Furthermore, any contact with the organic electrolyte has to be strictly eliminated, since silicon or niobium support is very prone to corrosion if non-aqueous electrolysis conditions are applied. In contrast to aqueous media, no passivation occurs by oxide

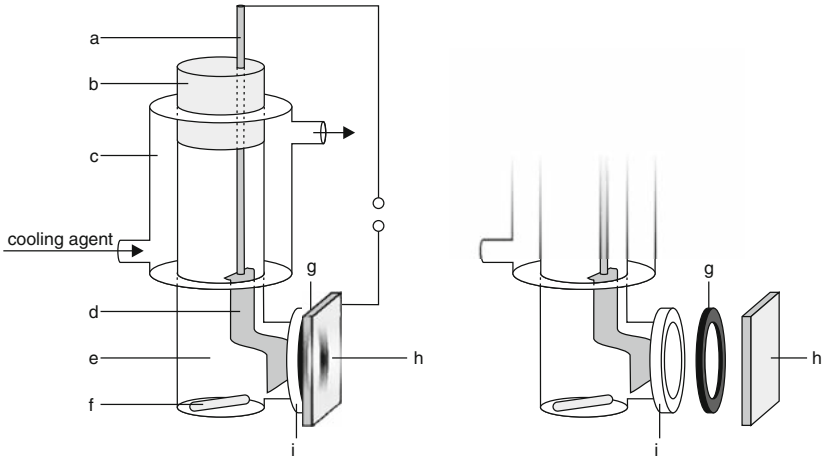

Fig. 5.2 Architecture of the electrolysis cell; *left*: schematically and assembled, *right*: explosion scheme of the flange unit. (**a**) bracket for counter electrode; (**b**) stopper (Teflon^{TM}); (**c**) cooling jacket; (**d**) nickel counter electrode; (**e**) space for electrolyte; (**f**) magnetic stirrer; (**g**) sealing (EPDM); (**h**) BDD electrode; (**i**) flange (glass)

formation. To this aim an arrangement with flange fittings was constructed (Fig. 5.2). In the case of the depicted cell version, electrolyte volumes of 50–70 mL with BDD surface of about 5 cm^2 were applied. The flange arrangement is hold by a standard flange clamp (Malkowsky et al. 2006d).

Employing glass-flange connections allows the use of every planar type of BDD electrode, which is easily contacted by a metal foil on the back. Gratifyingly, fragments of large BDD electrodes can still serve in this experimental setup as electrodes. Particular attention has to be given to the sealing between BDD electrode and the flange of glass. Several materials including Teflon^{TM} and a variety of silicones have been tested. Best results were obtained by a sealing made of EPDM. This rubber is a highly resistant terpolymer and is easily available since it is widely used as foil for garden ponds. Thermal stability was found up to 120°C. Hot organic and aggressive media as well as highly anodic potentials seem not to affect the sealing over a long process time. The depicted cell geometry offers the possibility to heat the electrolyte. Usually, a sand bath or silicon oil heating was applied. The cooling jacket in the upper part keeps the more volatile components in the electrolysis vessel.

5.3 Anodic Transformations

The utmost intriguing feature of polycrystalline BDD material is its very wide potential window in aqueous and protic media of about –1.35 to +2.3 V vs. the normal hydrogen potential. Furthermore, the largest overpotential for the evolution

of oxygen is observed. Therefore, high energetic spin centres like hydroxyl or alkoxy radicals can be created in high concentration in aqueous or alcoholic solutions (Wilson et al. 2006). This opens unique reaction pathways which have previously been considered as inaccessible by electrochemical means. Consequently, there is significant interest to exploit BDD electrodes for preparative purposes, wherein anodic transformations are the most obvious.

5.3.1 Alkoxylation Reactions

BDD electrodes are commonly used for electrochemical (waste) water treatment because of their efficient ability for total organic carbon (TOC) removal. The aim to carry out selective electrochemical processes seems therefore to be self-contradictorily.

The large electrochemical window of BDD electrodes even in non-aqueous solvents like methanol enables transformations which are difficult to access with conventionally used electrode materials.

For some examples, the outcome of direct anodic methoxylations of activated carbons (benzylic, allylic, etc.) at BDD anodes is similar to graphite anodes (Pütter et al. 2003). Further investigation of the reaction mechanism in the case of the methoxylation of *p-tert*-butyltoluene (**1**) – a process of industrial relevance (Bosma et al. 1999) – showed that BDD electrodes favour the occurrence of bibenzylic intermediates **4** which were not observed at graphite electrodes. This difference has been attributed to a mechanism based on the non-catalytic character of BDD electrodes and to the presence of active functionalities on graphite electrodes (Zollinger et al. 2004a).

In the course of the electrochemical conversion, the bibenzylic intermediate **4** is then further converted into the desired products **2** and **3** by cleavage of the central C,C-bond (Fig. 5.3) (Zollinger et al. 2004b). C,C-bond cleavages of stilbene or bibenzyl derivatives are observed at graphite electrodes only at elevated current densities $\left(10\,\mathrm{A\,dm^{-2}}\right)$.

The discovery of a different reaction mechanism of anodic methoxylations on BDD electrodes led to a closer investigation of electrosynthetic possibilities. First of all, BDD electrodes exhibit a 400- mV larger electrochemical window in methanol compared with graphite (Fig. 5.4). This opens access to a series of alkoxylation reactions which are not selective on conventional electrodes.

For example, the anodic methoxylation of formaldehyde dimethylacetal (**5**, FADMA) to trimethyl orthoformate (**6**, TMOF) proceeds well on BDD electrodes in undivided cells (Fig. 5.5) (Fardel et al. 2006). TMOF is obtained in 75% selectivity at 27% FADMA conversion at a charge consumption of $0.4\,\mathrm{F\,mol^{-1}}$ FADMA, according to a current efficiency of 41%. This reaction is not possible using graphite electrodes.

TMOF (**6**) is produced at industrial scale by two major processes. The first proceeds from chloroform and sodium methanolate, but produces three times the

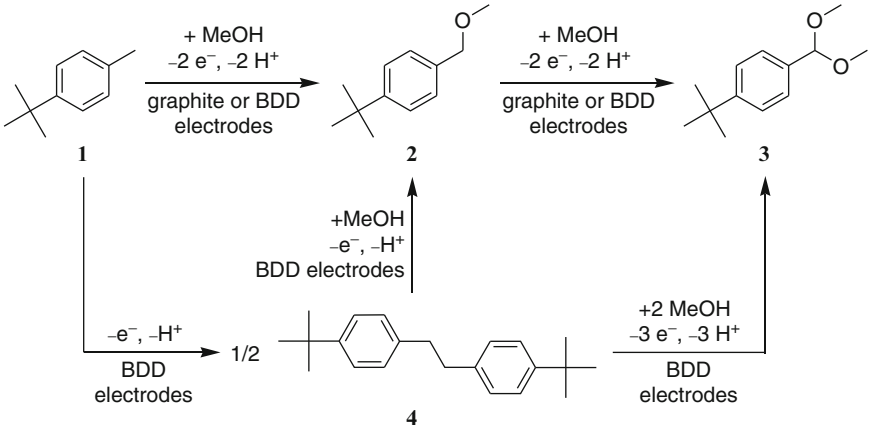

Fig. 5.3 Electrochemical methoxylation of *p-tert*-butyltoluene on different carbon electrodes. The occurrence of the bibenzyl **4** is not observed on graphite electrodes

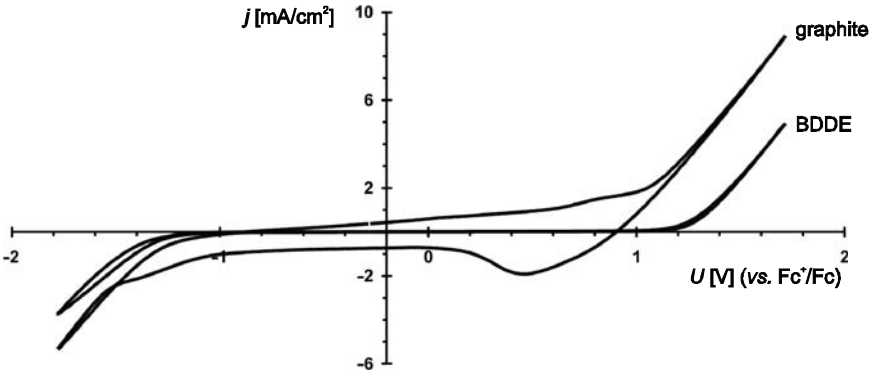

Fig. 5.4 Electrochemical window of MeOH at graphite and BDD electrodes (scan rate $100\,\mathrm{mV\,s^{-1}}$)

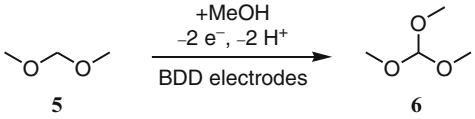

Fig. 5.5 Electrochemical synthesis of trimethylorthoformate (**6**). Reagents and conditions: undivided cell, BDD anode, steel cathode, 24% MeOH, 70% FADMA, $LiN(SO_2CF_3)_2$/NaOMe, 20°C, $9\,\mathrm{A\,dm^{-2}}$

stoichiometry of sodium chloride as waste. The second makes use of methanolysis of cyanhydric acid, which also produces stoichiometric amounts of ammonium chloride and involves high safety costs for the handling of hydrogen cyanide.

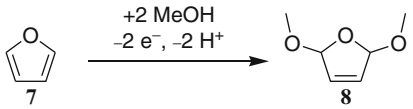

Fig. 5.6 Anodic methoxylation of furan (**7**). Reagents and conditions: (**a**) graphite electrodes: 15% furan in MeOH, 1.2% NaBr, <10°C, 12 A dm^{-2}, yield = 79%, select. 96%, X = 82% at 1.6 F mol^{-1}, current efficiency = 96%; (**b**) BDDE: 8% furan in MeOH, 3% $Bu_4N^+BF_4^-$, 15°C, 10 A dm^2, yield = 75% at 1.5 F mol^{-1}, current efficiency = 99%; yield = 84% at 2.3 F mol^{-1}, current efficiency = 74%

The advantages for the production of TMOF (**6**) on BDD electrodes are on one side the attractive raw materials, which are readily available from syn gas. And on the other side there is no generation of waste salts and safeoperating conditions.

Another example of different electrode mode of action is the methoxylation of furan (**7**) to 2,5-dimethoxy-2,5-dihydrofuran (**8**, DMD), as a masked 1,4-dialdehyde an intermediate for N-heterocycle synthesis and life-science products (Fig. 5.6). On graphite electrodes, this reaction needs a halide salt-like sodium bromide both as supporting electrolyte and mediator (Degner et al. 1978). If the same reaction is carried out on a BDD electrode, a mediator is not needed (Reufer et al. 2004).

5.3.2 Cleavage of C, C-Bonds

A widely applied strategy for the synthesis of various difunctionalized organic molecules, e.g. diols, dialdehydes, etc., relies on the oxidative cleavage of olefinic double bonds. Besides transition metal catalysis for asymmetric synthesis, periodate oxidation and ozonolysis are the standard tools for oxidative bond cleaving reactions. For economic and safety reasons, technically applicable alternatives to osmium-based chemistry and ozonolysis are of great interest.

The synthetic value of double bonds arises from their high reactivity towards simple electrophiles, enophiles and radicals. The latter species can easily be generated by oxidation on BDD electrodes. Thus, advantage can be taken of electrogenerated oxyradicals. Although aliphatic olefins proved to be stable towards electrochemical oxidation on BDD anodes in aqueous media (Bäumer and Schäfer 2005), activated olefins were successfully converted using acidic methanolic electrolytes (Griesbach et al. 2005).

By oxidative C,C-bond cleavage on BDD electrodes phenanthrene (**9**) was transformed into the 1,1′-difunctionalized biaryls **10** and **11**, respectively (Fig. 5.7). Diester **11** was found to be the major product in all the experiments.

Further investigations on the field of oxidative bond cleavage even made single bonds accessible. Thus, biaryls **10** and **11** were similarly obtained by electrooxidation of 9,10-dihydrophenanthrene. Moreover, the cleaving reaction of benzylic carbons was also exploited in the synthesis *p-tert*-butylbenzaldehyde dimethyl acetale (**3**) starting from 1,2-di-(*p-tert*-butylphenyl)ethane (**4**, 1,2-DPTE) (Fig. 5.8) (Zollinger et al. 2004b).

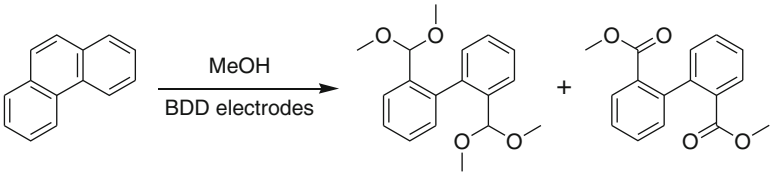

Fig. 5.7 Bond cleavage in phenanthrene to 1,1′-difunctionalized biaryls. Reagents and conditions: BDDE, 2% phenanthrene, 0.5% H_2SO_4 (96%), 3.4 A dm^{-2}, 54°C, 10 F mol^{-1}; yield = 15% (**10**), 39% (**11**)

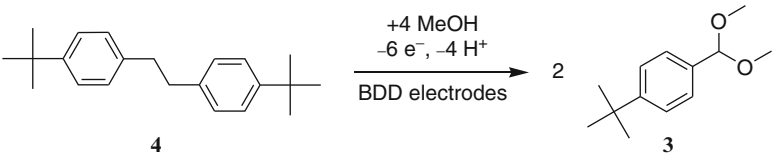

Fig. 5.8 Bond cleavage in 1,2-DPTE in the synthesis of *p-tert*-butylbenzaldehyde dimethyl acetale (**3**). Reagents and conditions: BDDE, 2% 1,2-DPTE, 0.5% H_2SO_4 (96%), MeOH, 3.4 A dm^{-2}, 54°C, 8 F mol^{-1}; yield = 47% (**3**)

Side products from the conversion of 1,2-DPTE (**4**) on BDD electrodes were found to be *p-tert*-butylbenzyl methyl ether (7%) and *p-tert*-butylbenzoic acid methyl ester (6%).

5.3.3 Phenolic Coupling Reactions

The selective oxidative coupling reaction of phenolic moieties to the corresponding biaryl architectures plays a significant role in the synthesis of technically relevant intermediates, e.g. for ligands or natural products (Bringmann et al. 2001). In the past decades, several methodologies were elaborated for the oxidative coupling process of electron-rich arenes. In particular, the selective *ortho*-coupling process of phenols has been addressed by numerous catalytic and stoichiometric approaches, wherein sterically hindered *tert*-butylated phenols as well as naphthols represent preferred substrates (Lessene and Feldman 2002), since simple phenols and derivatives with methyl substituents on the aromatic core tend to side reactions.

Exploiting BDD electrodes in the anodic coupling of phenols was not very promising from the very beginning since several previous studies were devoted to the degradation of phenols, naphthols and chlorinated derivatives thereof (Boye et al. 2002; Panizza et al. 2001; Rodrigo et al. 2001). Treatment by BDD-mediated electrolysis breaks down these persistent aromatic pollutants. In aqueous media a sequence of degradation products is observed: The first intermediates are the corresponding quinones or hydroxylate arenes, followed by maleic acid, fumaric acid and oxalic acid which are then finally mineralized to CO_2 (Boye et al. 2006).

The oxidative *ortho*-coupling reaction of 2,4-dimethylphenol (**12**) became of interest for our laboratories since a demand for this particular compound was recognized (Bartsch et al. 2005). Initial studies including the direct electrolysis in basic media led only in traces to the desired 3,3′,5,5′-tetramethyl-2,2′-biphenol (**13**) and the major components of product mixture consisted of Pummerer's ketone (**14**) and consecutive pentacyclic product **15** (Fig. 5.9) (Malkowsky et al. 2006a). As outlined in Table 5.1 under standard conditions the Pummerer's ketone represents the major product and only traces of the desired compound **13** were found. However, extensive variations of the electrolysis conditions did not ameliorate the situation. In order to circumvent the formation of **14**, a template-directed process was developed (Malkowsky et al. 2006b). This protocol involves several steps: the formation of a tetraphenoxyborate (Malkowsky et al. 2006c), anodic conversion and removal of the boron template. Despite the applicability on larger scale (Rommel et al. 2005), a direct and efficient coupling method was still highly desired.

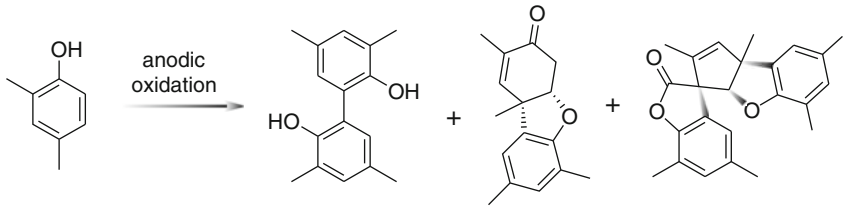

Anode material; conditions	Product ratio **13** : **14** : **15**
Platinum; MeOH	1 : 11 : 6
BDD; solvent free	18 : 1 : 0

Fig. 5.9 Product diversity in the anodic coupling of 2,4-dimethylphenol (**1**)

Table 5.1 Anodic treatment of **12** in organic solvents

Entry	Electrolyte	12 (%)[a]	CE[b] (%)	13 : 14
1	0.1 m Bu_4NBF_4 in MeOH	17	7	10:1
2	0.1 m NaOH in MeOH	15	6	3:2
3	0.1 m H_2SO_4 in MeOH	15	10	4:1
4	0.1 m Bu_4NBF_4 in $CH_3CN/^tBuOH$	16	4	20:1
5	0.1 m Bu_4NBF_4 in CH_2Cl_2/MeOH	11	3	4:3
6	$FeSO_4$, Bu_4NHSO_4, $H_2O/^tBuOMe$	3	n.d.	n.d.

Reaction conditions: 1.5 g **12**, 35-mL electrolyte, BDD anode (layer thickness: 1 μm), $j = 2\ A\ dm^{-2}$, nickel cathode, r.t.
[a] Determined from the crude product by GC using internal standard
[b] Current efficiency

When instead of platinum sheets as electrodes BDD material was employed the **13**:**14** ratio improved tremendously. Surprisingly, this direct electrochemical conversion of **12** gave the desired biphenol **13** in almost exclusive selectivity of 18:1 for **13**:**14**. The typical pentacyclic by-product **15** could not be detected in the crude product. Inspired by the conditions for the electrosynthesis of trimethyl orthoformate (see Sect. 4.3.1 in Chap. 44) we applied to our conversion alcohols as common solvents for organic transformations at BDD electrodes.

For a sufficient conductivity of the electrolyte, protic solvents and supporting electrolytes were necessary. All electrochemical conversions at BDD electrodes favour the desired compound **13**, but it was only obtained in modest yield. Except for **14**, no other low molecular weight by-products could be isolated indicating that oligomeric species were predominantly formed. This deep brown coloured material had resin-type properties but was not further characterized. Noteworthy, the volume of methanol in the cell was reduced by half upon electrolysis. Since simple evaporation could be excluded, the oxidation of methanol to volatile and highly reactive formaldehyde is anticipated. These facts were additionally supported by notable low current efficacies. The surface of the electrode stood intact when performing the transformation in acidic or neutral media, whereas basic electrolyte caused significant corrosion. Several solvent mixtures have been tested in the electrolyte without success. Iron-based mediators led mostly to decomposition and resulted in a very complex mixture, which made it impossible to clearly determine yield and ratio. In order to avoid side reactions that are attributed to the mediating solvent, e.g. methanol, neat phenol **12** was subjected to electrolysis. The conductivity increases with the temperature but is not sufficient for practical purposes. Consequently a supporting electrolyte and a small amount of water were required. Best results were obtained by addition of 11% water and 6% ammonium salt (Fig. 5.10). For a sustainable process development, reduction in the amount of solvent is important and applying a green additive like water will be beneficial. Despite of the large excess of phenol a mediating role of water by preliminary formed hydroxyl radicals cannot be excluded.

Tremendous improvement was achieved when **12** was used neat at higher electrolysis temperature. The yield as well as the selectivity of the transformation could be considerably ameliorated (Table 5.2).

In order to avoid overoxidation or mineralization of the product **13**, the electrolysis was only performed to partial conversion to about 0.4 F mol^{-1} **12**. The workup includes simple and easy to perform steps: First, removal of excess of **12** by a short-path distillation, which recovers non-reacted 2,4-dimethylphenol. Second, partition of the residue with water and *tert*-butylmethyl ether. This particular step provides the supporting electrolyte as aqueous solution. Gratifyingly, upon concentration of

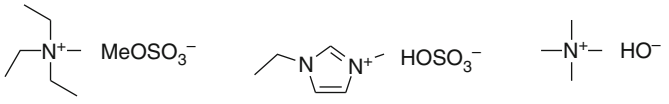

16 **17** **18**

Fig. 5.10 Some supporting electrolytes for the conversion of **12** at BDD electrodes

Table 5.2 Anodic conversion of **12** on BDD electrodes

Entry	Supporting electrolyte	BDD (support, thickness)	**13** (%)[a]	CE[b] (%)	**13 : 14**
1	16	Si, 1 μm	56	29	17:1
2	17	Si, 1 μm	46	42	16:1
3	18	Si, 1 μm	39	30	17:1
4	16	Nb, 10 μm	49	43	18:1
5	16	Si, 10 μm	47	32	19:1

Reaction conditions: 30 g **12**, 4-mL water, 2.2 g ammonium salt, BDD anode, $j = 1\,\mathrm{A\,dm^{-2}}$, nickel cathode, $Q = 0.4\,\mathrm{F\,mol^{-1}}$ **12**, 70°C

[a]From the crude product after distillative removal of excess **12**, determined by GC using internal standard

[b]Current efficiency

the organic layer and slow addition of petrol ether biphenol **13** was obtained as pure crystalline material. This is the most efficient electrochemical access to this particular compound **13**.

Variation of the supporting electrolytes depicted in Fig. 5.10 resulted in the very same selectivity but differed remarkably in the current efficiency (Table 5.2, entries 1, 2 and 3). On the 1 − μm BDD-coated silicon, neutral electrolysis conditions employing **16** gave the best yields in the desired biphenol **13** (entry 1). However, the acidic ionic liquid **17** turned out to be superior concerning the current efficiency of the phenolic oxidation (entry 2). The basic ammonia salt **18** lead to moderate yields and inferior current efficacies (entry 3). Most probably, basic conditions create to electron-rich substrates which might undergo decomposition by overoxidation. When 10 μm diamond-coated supports were used as anodes, the tetraalkyl ammonium methylsulfate **16** gave better results (entry 4). Surprisingly, the nature of the support seems to play an important role for the current efficiency (entries 4 and 5). Since the very same chemoselectivity for the transformation was observed, the loss of efficiency is not based on the oxidative coupling step. These findings indicate that an intermediate spin centre is formed that might undergo background reactions. Further evidence is given by multiple electrolysis runs. The selectivity and the appearance of the BDD electrode looked the very same, whereas the current efficiency dropped from 43% to about 20–25% (e.g. for entry 4). This kind of aging process is also attributed to the nature of BDD material which causes a drain of energy.

For technical purposes a partial conversion with an easy to perform workup is feasible. Therefore, a series of electrolyses were performed to a specific conversion (Fig. 5.11). During electrochemical conversion the amount of **13** increases in a linear fashion up to $0.3\,\mathrm{F\,mol^{-1}}$ **1**. Subsequently, side reactions appear and limit the amount of isolated **13**. For an efficient process and high-quality product, a partial conversion of about 30% is reasonable. Since excess of **12** is easily recovered, virtually no loss of material occurs, creating a good basis for a continuous preparation of **13**.

The anodic transformations for the oxidative coupling were then applied with little success to broader scope of low-melting phenols (Fig. 5.12). Either no conversion

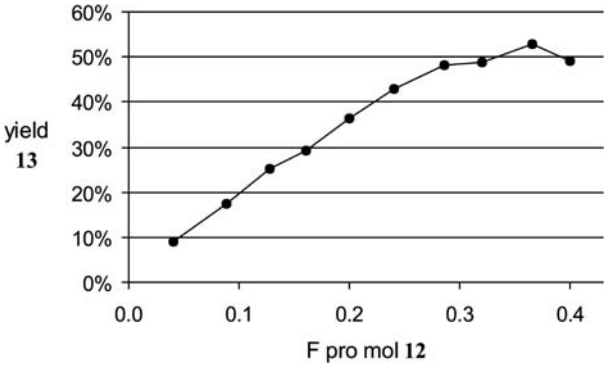

Fig. 5.11 Yield of **13** in dependence on the applied current

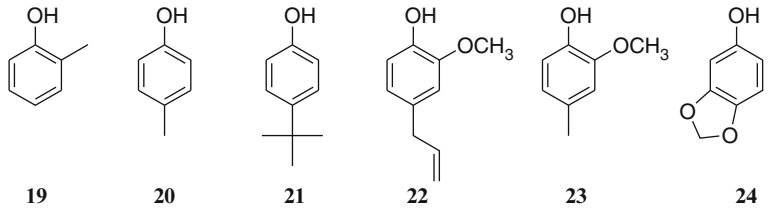

Fig. 5.12 Less successfully tested substrates in the electrolysis at BDD electrodes

was observed or the substrate was completely destructed. When *ortho*-cresol (**19**) was treated by the described protocol, a flow of current was observed without the formation of detectable amounts of product. The same situation was found with *p*-cresol (**20**) and 4-*tert*-butylphenol (**21**). Initially, the lower electron-rich nature of the substrates compared to **12** was anticipated. Electrochemical conversion of guaiacol substituted in position 4 as well as sesamole (**24**) rendered in the formation of tarry products. Obviously, the conditions are still too aggressive for the selective anodic transformation of these phenols at BDD electrodes.

The curious finding is that in the electrochemical conversion of mixtures involving several phenolic substrates the sole product which was detected was **13**. This substrate selectivity is only found at BDD electrodes. The reason for this exclusive substrate selectivity and the particular nature for 2,4-dimethylphenol (**12**) are unclear but currently under investigation.

5.4 Cathodic Transformations

5.4.1 Reduction of Oximes

With regard to cathodic reductions, BDD electrodes have a high overpotential for H_2 evolution by electrolysis of protic electrolytes (Martin et al. 1996). Thus, for

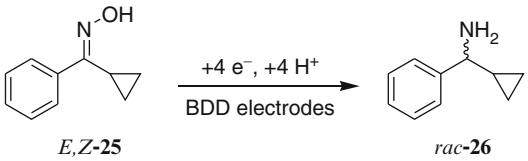

Fig. 5.13 Electrochemical oxime reduction. Reagents and conditions: divided cell, BDD/Nb cathode, 1% $NaOCH_3$ in anhydrous MeOH, 40°C, 3.4 A dm^{-2}, 4 h, yield = 96% (by GC)

electrochemical transformations, BDD cathodes should behave like Pb or Hg cathodes. Consequently, the chemoselective reduction of *E*,*Z*-cyclopropyl phenylketone oxime (*E*,*Z*-**25**) to *rac*-α-cyclopropyl benzylamine (*rac*-**26**) was achieved with 96% yield both on a BDD cathode on a Nb support or Pb cathode using an anhydrous MeOH/NaOMe electrolyte in a divided plate and frame cell (Fig. 5.13) (Griesbach et al. 2005).

Attempted catalytic hydrogenation of oxime *E*,*Z*-**25** ended up with significant amounts of ring-opened compounds hampering distillative purification of the desired compound *rac*-**26**.

The use of electrochemical methods, especially cathodic reduction at BDD electrodes avoiding use of unwanted heavy metals, showed a clear superiority compared to conventional chemical methods in this case. Due to the protective cathodic polarization of the BDD electrodes, no stability and corrosion problems occurred.

5.4.2 Reductive Carboxylation of Aldehydes to α-Hydroxycarboxylic acids

4-Methylmercapto-2-hydroxybutyric acid (**28**) also known as methionin hydroxy analogue (MHA) is an important product used in animal nutrition because of its improved bioavailability compared to the essential amino acid methionin. MHA **28** is produced on a multiple thousand ton scale by reaction of methylmercapto propionaldehyde (**27**, MMP) with cyanhydric acid followed by saponification of the resulting cyanohydrin. An electrochemical approach to MHA is also reported. This procedure makes use of a reductive carboxylation of methylmercapto propionaldehyde (**27**) with a magnesium sacrificial anode (Lehmann et al. 2001, 2002). This reaction proceeds under CO_2 atmosphere in DMF as the solvent and $NBu_4{}^+BF_4{}^-$ as the supporting electrolyte using a magnesium anode and cathode. Application of 5 F mol^{-1} **27** resulted in 75% MHA selectivity at 90% conversion.

If a divided cell is used, this reaction can also be carried out using BDD electrodes, avoiding sacrificial anodes and therefore simplifying workup procedure (Fig. 5.14) (Reufer et al. 2006). The MHA yield of this process is not very high but this is a remarkable example for the versatility of BDD electrodes in preparative electroorganic synthesis.

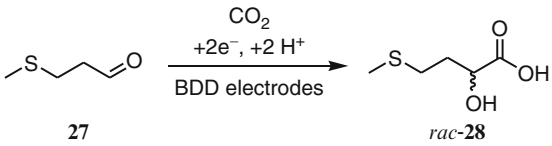

27 *rac*-**28**

Fig. 5.14 Electrochemical carboxylation of aldehydes. Reagents and conditions: divided flow cell, Nafion® membrane, BDD/Si electrodes, $NBu_4^+BF_4^-$ in DMF, 20–25°C, 0.6 A dm^{-2}, 5 h, 27% yield in *rac*-**28** at 88% conversion of **27**

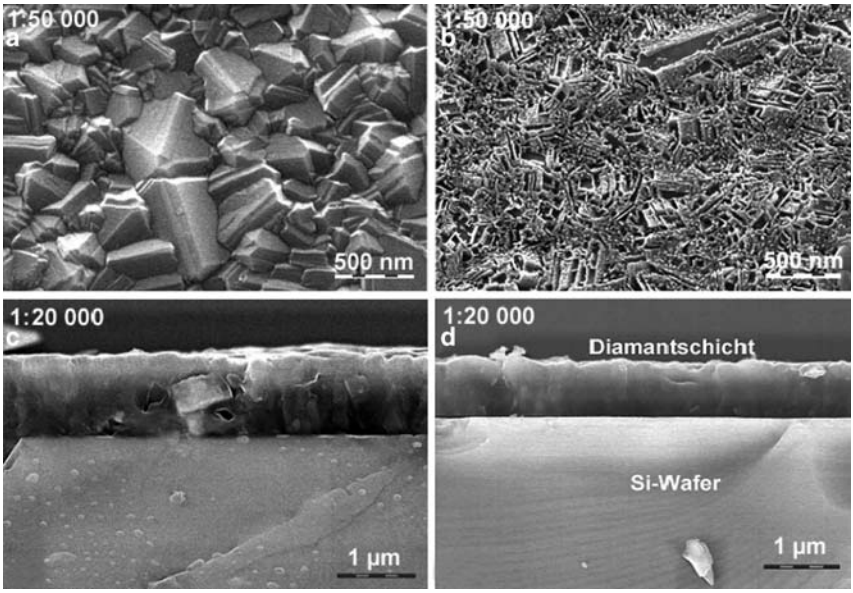

Fig. 5.15 SEM images (*top view and cross section*) of BDD/Si anodes (from *CSEM*, Switzerland) used under different conditions. (**a**) Electrode surface after electrolysis in $MeOH/H_2SO_4$. No degradation of the diamond layer. (**b**) Electrode surface after anodic treatment (∼36 h) in 0.1 M aq. NaOH, containing 3,5-dimethylpyridine. Obvious signs of degradation of the diamond layer, but use in electrosynthesis was still possible. (**c**) Cross section of electrode (**a**), film thickness 1.2 µm as determined by EPMA. (**d**) Cross section of electrode (**b**), film thickness 0.84 µm

5.5 Stability of BDD in Electrolytes

Besides the electrochemical wastewater treatment, preparative organic electrochemical processes are a relatively young field of application for BDD electrodes. As a consequence, there is still much room for improvement of the stability of BDD electrodes under non-aqueous conditions.

The use of sulphuric acid in methanol provides a diamond layer-friendly electrolyte. As shown in Fig. 5.15, aqueous sodium hydroxide changes the morphology of the BDD anode surface (DeClements and Swain 1997) but the electrode can still

be used (Griesbach et al. 2005). A cathodical polarization of niobium-supported BDD electrodes is generally unproblematic whereas care must be taken when using silicon-supported BDD cathodes in basic electrolytes. The silicon support is prone to corrosion in this case because an alkaline and reductive milieu will prevent the formation of a passivating SiO_2 layer.

Furthermore, any contact of the supporting material (Si, Nb, W, Ta and especially Ti) of BDD anodes to a non-aqueous electrolyte has to be strictly eliminated (Malkowsky et al. 2006d), due to the low corrosion resistance of these materials under these conditions. If water is used as electrolyte, the common materials passivate themselves with a metal-oxide layer, preventing further corrosion. The absence of water prevents formation of such a protective layer.

5.6 Future Perspectives

BDD electrodes are innovative and appealing materials of organic electrochemistry, which give access to unusual selective reactions. Under controlled conversion almost no overoxidation or mineralization is observed. In order to exploit the promising potential of this unique electrode material an efficient control of the highly reactive intermediates has to be established. A key role has to be assigned to mediating hydroxyl radicals. Alcohols may serve as mediators, wherein specific alkoxyl moiety will be responsible for triggering the reactivity and transfer of stereo information. Taming the brutal nature of mediating hydroxyl spin centres will also allow the application in electroenzymatic transformations, which are mainly performed in aqueous media. The controlled regeneration of cofactors is still a challenging topic.

For this goal, more fundamental mechanistic studies of redox processes at BDD electrodes will be necessary. With chemically and mechanically more stable BDD/support combinations, preparative organic synthesis and enzymatic applications will conquer the field of research and will bring chemical innovation in a short time to application.

References

Bartsch, M., Baumann, R., Haderlein, G., Flores M.A., Jungkamp, T., Luyken, H., Scheidel, J. and Siegel, W. (2005) Method for the production of adipodinitrile by hydrocyanation of 1,3-butadiene. PCT patent WO20055073167 A1. BASF Aktiengesellschaft, Germany.

Bäumer, U.-St. and Schäfer, H.-J. (2005) Cleavage of alkenes by anodic oxidation. J. Appl. Electrochem. 35, 1283–1292.

Bosma, C, Gouws, S., Loyson, P. and Zeelie, B. (1999) Anodic oxidation of *4-tert*-butyltoluene to *4-tert*-butylbenzaldehyde dimethyl acetal: optimisation and scale-up. S. Afr. J. Chem. 52, 133–144.

Boye, B., Michaud, P.A., Marselli, B., Dieng, M.M., Brillas, E. and Comninellis, Ch. (2002) Anodic oxidation of 4-chlorophenoxyacetic acid on synthetic boron-doped diamond electrodes. New Diam. Front. Carbon Technol. 12, 63–72.

Boye, B., Brillas, E., Michaud, P.A., Comninellis, Ch., Farnia, G. and Sandonà, G. (2006) Electrochemical incineration of chloromethylphenoxy herbicides in acid medium by anodic oxidation with boron-doped diamond electrode. Electrochim. Acta. 51, 2872–2880.

Bringmann, G., Günther, C., Ochse, M., Schupp, M. and Tasler, S. (2001) Biaryls in nature: A multi-facetted class of stereochemically, biosynthetically, and pharmacologically intriguing secondary metabolites. In: Herz, W., Falk, H., Kirby, G.W. and Moore, R.E. (Eds.) Progress in the chemistry of organic natural products, vol. 82, Springer, New York, NY.

DeClements, R. and Swain, G.M. (1997) The formation and electrochemical activity of microporous diamond thin film electrodes in concentrated KOH. J. Electrochem. Soc. 144, 856–866.

Degner, D., Nohe H. and Hannebaum, H. (1978) Verfahren zur elektrolytischen Herstellung von 2,5-Dialkoxy-2,5-dihydrofuranen. German patent DE 2710420 B1. BASF Aktiengesellschaft, Germany.

Duo, I., Levy-Clement, C., Fujishima, A. and Comninellis, Ch. (2004) Electron transfer kinetics on boron-doped diamond Part 1: Influence of anodic treatment. J. Appl. Electrochem. 34, 935–943.

Fardel, R., Griesbach, U., Pütter, H. and Comninellis, Ch. (2006) Electrosynthesis of trimethylorthoformate on BDD electrodes. J. Appl. Electrochem. 36, 249–253.

Griesbach, U., Zollinger, D., Pütter, H. and Comninellis, Ch. (2005) Evaluation of boron doped diamond electrodes for organic electrosynthesis on a preparative scale. J. Appl. Electrochem. 35, 1265–1270.

Haenni, W., Perret, A. and Richen, P. (2002) Large-sized electrode. PCT patent WO 2002061181.

Iniesta, J., Michaud, P.A., Panizza, M. and Commninellis, Ch. (2001a) Electrochemical oxidation of 3-methylpyridine at a boron-doped diamond electrode: applications to electroorganic synthesis and waste water treatment. Electrochem. Commun. 3, 346–351.

Iniesta, J., Michaud, P.A., Panizza, M., Cerisola, G., Aldaz, A. and Commninellis, Ch. (2001b) Electrochemical oxidation of phenol at boron-doped diamond electrode. Electrochim. Acta 46, 3573–3578.

Jörissen, J. (1996) Ion-exchange membranes as solid polymer electrolytes (SPE) in electroorganic synthesis without supporting electrolytes. Electrochim. Acta 41, 553–562.

Kondo, T., Honda, K., Tryk, D.A. and Fujishima, A. (2005) Covalent modification of single-crystal diamond electrode surfaces. J. Electrochem. Soc. 152, E18–E23.

Lehmann, Th., Schneider, R., Reufer, C. and Sanzenbacher, R. (2001) Elektrochemische Carboxylierung zur Synthese von α-Hydroxycarbon-Säuren. Elektronenübertragung in Chemie und Biochemie, Russow, J., Schäfer, H. J. (Eds.), GDCh-Monographie 23, 251–258.

Lehmann, Th., Schneider, R., Weckbecker, Ch., Dunach, E. and Oliviero, S. (2002) Process for the production of 2-hydroxy-4-methylmercaptobutyric acid. International patent WO 02/16671 A1. Degussa AG, Germany.

Lessene, G. and Feldman, K.S. (2002) Oxidative aryl-coupling reactions in synthesis. In: Astruc, D. (Ed.) Modern arene chemistry, Wiley-VCH, Weinheim, 479–538.

Malkowsky, I.M., Rommel, C.E., Wedeking, K., Fröhlich, R., Bergander, K., Nieger, M., Quaiser, C., Griesbach, U., Pütter, H. and Waldvogel, S.R. (2006a) Facile and highly diastereoselective formation of a novel pentacyclic scaffold by direct anodic oxidation of 2,4-dimethylphenol. Eur. J. Org. Chem. 2006, 241–245.

Malkowsky, I.M., Fröhlich, R., Griesbach, U., Pütter, H. and Waldvogel, S.R. (2006b) Facile synthesis and properties of tetraphenoxy borates. Eur. J. Inorg. Chem. 1690–1697.

Malkowsky, I.M., Griesbach, U., Pütter, H. and Waldvogel, S.R. (2006c) Novel template-directed anodic phenol coupling reaction. Chem.-Eur. J. 12, 7482–7488.

Malkowsky, I.M., Griesbach, U., Pütter, H. and Waldvogel, S.R. (2006d) Unexpected highly chemoselective anodic ortho-coupling reaction of 2,4-dimethylphenol on boron-doped diamond electrodes. Eur. J. Org. Chem. 2006, 4569–4572.

Marselli, B., Garcia-Gomez, J., Michaud, P.A., Rodrigo, M.A. and Comninellis, Ch. (2003) Electrogeneration of hydroxyl radicals on boron-doped diamond electrodes. J. Electrochem. Soc. 150, D79–D83.

Martin, H.B., Argoita, A, Landau, U., Anderson, A.B. and Angus, J.C. (1996) Hydrogen and oxygen evolution on boron-doped diamond electrodes. J. Electrochem. Soc. 143, L133–L136.

Nad, S. and Breinbauer, R. (2004) Electroorganic synthesis on the solid phase using polymer beads as supports. Angew. Chem. Int. Ed. 43, 2297–2299.

Nad, S. and Breinbauer, R. (2005) Electroorganic synthesis of 2,5-dialkoxydihydrofurans and pyridazines on solid phase using polymer beads as supports. Synthesis 2005, 3654–3665.

Ouattara, L., Duo, I., Diaco, T., Ivandini, A., Honda, K., Rao, T., Fujishima, A. and Comninellis, Ch. (2003) Electrochemical oxidation of ethylenediaminetetraacetic acid (EDTA) on BDD electrodes: Application to wastewater treatment. New Diam. Front. Carbon Technol. 13, 97–108.

Panizza, M., Michaud, P.A., Cerisola, G. and Comninellis, Ch. (2001) Anodic oxidation of 2-naphthol at boron-doped diamond electrodes. J. Electroanal. Chem. 507, 206–214.

Pleskov, Y.V., Evstefeeva, Y.E., Krotova, M.D., Mishuk, V.Y., Laptev, V.A., Palyanov, Y.N. and Borzdov, Y.M. (2002) Effect of crystal structure on the behavior of diamond electrodes. J. Electrochem. Soc. 149, E260–E264.

Pütter, H. (2001) Industrial electroorganic chemistry. In: Lund, H., Hammerich, O. (Eds) Organic electrochemistry, 4th ed., Marcel Dekker, New York, NY, 1259–1307.

Pütter, H., Weiper-Idelmann, A., Merk, C., Fryda, M., Klages, C.-P., Schäfer, L. and Hampel, A. (2003) Process for the electrochemical conversion of organic compounds on diamond coated electrodes. European patent EP 1 036 861 B1. BASF Aktiengesellschaft, Fraunhofer Gesellschaft, Germany.

Rao, N., Lütz, S., Seelbach, K. and Liese, A. (2006) Basics of bioreaction engineering. In: Liese, A., Seelbach, K. Wandrey, Ch. (Eds.) Industrial biotransfromations, 2nd ed., Wiley-VCH, Weinheim, 115–145.

Reufer, Ch., Lehmann, Th., Sanzenbacher, R. and Weckbecker, Ch. (2004) Verfahren zur anodischen Alkoxylierung von organischen Substraten. German patent DE 10313169 A1. Degussa AG, Germany.

Reufer Ch., Hateley, M., Lehmann, Th., Weckbecker, Ch., Sanzenbacher R. and Bilz, J. (2006) Process for the preparation of α-substituted carboxylic acids from the series comprising α-hydroxycarboxylic acids and N-substituted α-aminocarboxylic acids. European patent EP 1 631 702 B1, Degussa AG, Germany.

Rodrigo, M.A., Michaud, P.A., Duo, I., Panizza, M., Cerisola, G. and Comninellis, Ch. (2001) Oxidation of 4-chlorophenol at boron-doped diamond electrode for wastewater treatment. J. Electrochem. Soc. 148, D60–D64.

Rommel, E., Malkowsky, I.M., Waldvogel, S.R., Pütter, H. and Griesbach, U. (2005) Anodic dimerization of substituted benzenes. PCT patent WO 2005075709 A2, BASF Aktiengesellschaft, Germany.

Sopchak, D., Miller, B., Avyigal, Y. and Kalish, R. (2002) Rotating ring-disk electrode studies of the oxidation of p-methoxyphenol and hydroquinone at boron-doped diamond electrodes. J. Electroanal. Chem. 538, 39–45.

Spataru, N., Spataru, T. and Fujishima, A. (2005) Voltammetric determination of thiourea at conductive diamond electrodes. Electroanalysis 17, 800–805.

Steckhan, E., Arns, Th., Heinemann, W.R., Hilt, G., Hoormann, D., Kröner, L., Lewall, B. and Pütter, H. (2001) Environmental protection and economization of resources by electroorganic and electroenzymatic synthesis. Chemosphere 43, 63–73.

Weissermel, K. and Arpe, H.-J. (1997) Industrial organic chemistry, 3rd ed., VCH, Weinheim.

Wilson, N.R., Clewes, S.L., Newton, M.E., Unwin, P.R. and Macpherson, J.V. (2006) Impact of grain-dependent boron uptake on the electrochemical and electrical properties of polycrystalline boron doped diamond electrodes. J. Phys. Chem. B 110, 5639–5646.

Zhi, J.-F., Wang, H.-B., Nakashima, T., Rao, T.N. and Fujishima, A. (2003) Electrochemical incineration of organic pollutants on boron-doped diamond electrode. Evidence for direct electrochemical oxidation pathway. J. Phys. Chem. B 107, 13389–13395.

Zollinger, D., Griesbach, U., Pütter, H. and Comninellis, Ch. (2004a) Methoxylation of *p-tert*-butyltoluene on boron-doped diamond electrodes. Electrochem. Commun. 6, 600–604.

Zollinger, D., Griesbach, U., Pütter, H. and Comninellis, Ch. (2004b) Electrochemical cleavage of 1,2-diphenylethanes at boron-doped diamond electrodes. Electrochem. Commun. 6, 605–608.

Chapter 6
Domestic and Industrial Water Disinfection Using Boron-Doped Diamond Electrodes

Philippe Rychen, Christophe Provent, Laurent Pupunat, and Nicolas Hermant

6.1 Introduction

With a rapidly growing world population and an increasing pollution, the development of new technologies to treat water becomes a major issue for a sustainable use of water resources. Strategies for ecological water protection generally include development of new or improved industrial processes, which have no or minor effects on the nature.

In this context, electrochemical processes used for recovery or disinfection of water play an important role. Up to some years ago, acceptable efficiencies for electrochemical disinfection applications were achieved with anode materials like noble metals or mixed-metal oxide on titanium anodes, known as DSA® electrodes. In the last years, because of its extreme chemical and physical properties, doped diamond has offered new advances for highly efficient chemical- and chlorine-free disinfection. Despite of its outstanding advantages, diamond had until now a quite "confidential" representation. Main reason for not using diamond as possible electrode material was its unavailability for large area electrodes. In the last years, polycrystalline diamond coatings have made great strides through chemical vapor deposition (CVD) development and are now available on relatively large areas. This availability now leads diamond to be a material of real interest for numerous disinfection applications, either in the wellness and private fields, e.g. for chlorine-free private swimming pools and spas, for rain water disinfection, and for industrial applications such as process and sewage water disinfections. This chapter gives an overview of diamond electrode technology and its use in this particular field.

Ch. Provent (✉)
Adamant Technologies SA, Eplatures-Grise 17, CH-2300 La Chaux-de-Fonds, Switzerland
e-mail: christophe.provent@adamantec.com

C. Comninellis and G. Chen (eds.), *Electrochemistry for the Environment*,
DOI 10.1007/978-0-387-68318-8_6,

6.2 Diamond Electrodes

To allow disinfecting water efficiently by electrochemical means, the material used as electrode should have the following properties:

- A high electrical conductivity (semiconductor up to semimetallic conductivity)
- A long-term chemical, electrochemical, and mechanical stability
- An ability to successively and periodically be used both as anode and as cathode (automatic polarity reversal)
- An excellent nonfouling behavior
- An efficient production mode, with reasonable costs
- The long-term stability of the material is an essential aspect, particularly when a periodical polarity reversal is applied. Using metallic or nonstable materials which could be corroded (mainly under oxygen evolution conditions) induce undesired long-term pollutions in treated waters and moreover generate additional costs linked to frequent replacement of the electrodes.

In the past, a material offering all these properties was not available and as a result industries that are offering disinfection and purification technologies had lost their interest in electrochemical processes. Thanks to boron-doped diamond (BDD) electrodes, such prejudice against these processes should now disappear as a strong sign was given by professionals that awarded disinfection systems using diamond electrodes in the last years (Awards 2004, 2005, 2006, 2007).

BDD electrodes are semiconductor electrodes with microcrystalline structure and relatively rough surfaces on the micrometric scale. Diamond-coated electrodes used for disinfection are chemically, mechanically, and thermally very resistant and show very low corrosion even under high electric charge. Diamond electrodes present no surface redox processes as known from other carbon electrodes (for example glassy carbon).

In the 1990s, research works had evidenced that diamond was an exceptional material. It shows high overpotentials for water electrolysis (hydrogen and oxygen evolution) that offers an electrochemical window which has never been observed with other materials. The wideness of this window depends on the diamond purity and doping level.

6.2.1 Manufacturing

We choose to grow BDD coatings on ceramic substrate, more precisely on silicon. The substrate for BDD electrodes must satisfy some criteria inherent to the preparation condition of BDD coatings itself (Haenni et al. 2004). Main ones are a chemical and mechanical stability at the preparation conditions of diamond coatings (1,000°C in H_2 atmosphere) and an adequate thermal expansion coefficient. Of course silicon satisfies these points and regarding the second one, it is even a material which has one of the closest coefficient as that of BDD ($\sim 3.5 \times 10^{-6} K^{-1}$ compared to

$1.5 \times 10^{-6} K^{-1}$) (Swain 1994; Fryda et al. 1999; Haenni and Fryda 2000). C and Si have similar physicochemical properties, which give the best conditions for long-term stabilities (Haenni et al. 2004).

Specific conductive silicon substrates have to be carefully prepared before use. For the diamond-deposition process, substrates have to be cleaned, seeded with diamond nanocrystalline seeds at high surface density, and then coated with a grown thick diamond film (from less than 1 μm up to several μm) by hot filament chemical vapor deposition (HF-CVD). At Adamant, deposition processes are performed automatically in programmable controlled process units, which allow growing diamond on scale up to 0.5 m^2. The process is performed under low pressure (1 < 0.1 bar) and high temperature (filament temperature ~2,500°C and substrate temperature 800–1,000°C) with a gas mixture composed of CH_4, H_2 (CH_4/H_2 ratio <1%), and a boron source (typically trimethyl boron).

Standard Adamant®-Electrodes, also called BDD/Si for Boron-Doped Diamond on Silicon, are used for water disinfection in the DiaCell®-Technology (Haenni et al. 2001) based systems. They have typical boron doping level of <1,500 ppm, film thickness of <3 μm, and a disk-shape to fit in the DiaCell® modules (Rychen et al. 2003b). A SEM view of a diamond film is shown in Fig. 6.1. Adamant®-Electrodes with other shapes are also produced to fit in other cells and for other applications.

Quality control of BDD electrodes is essential and is performed both by nondestructive and destructive testing methods. Nondestructive methods are either routine methods performed on each electrode (Raman spectroscopy to evaluate sp^3/sp^2

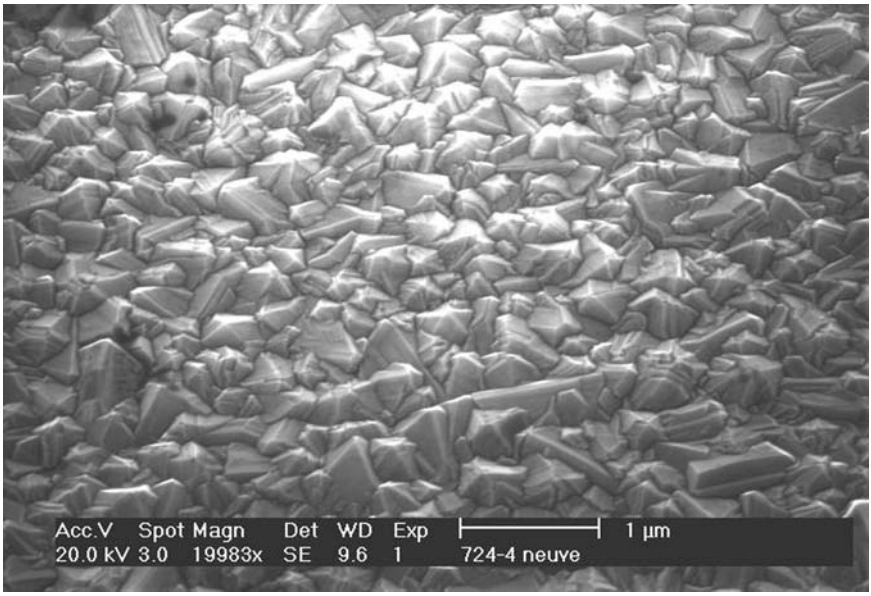

Fig. 6.1 SEM view of a diamond film

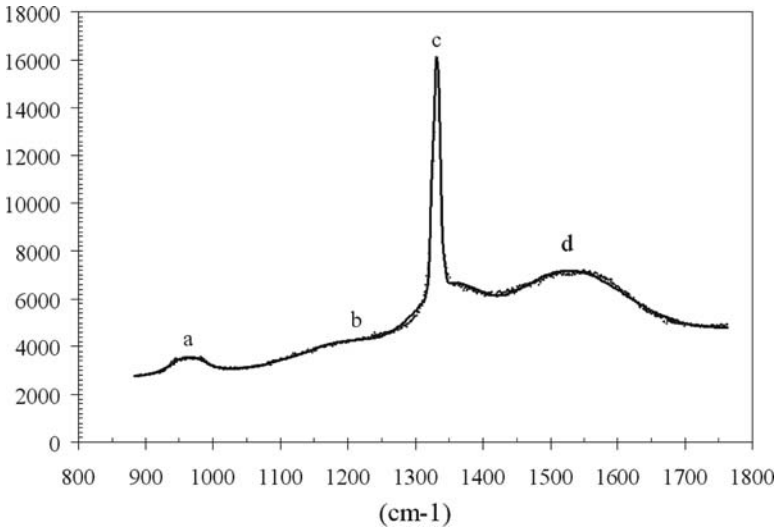

Fig. 6.2 Raman spectrum of boron-doped diamond film on silicon: **(a)** silicon, **(b)** boron atoms, **(c)** diamond (sp3 carbon), and **(d)** other carbon forms (amorphous)

carbon ratio – see Fig. 6.2, weight control, film thickness measurement, and visual control) or nonsystematic testing performed periodically to ensure diamond homogeneity and roughness (scanning electron microscopy – SEM, etc.). Destructive methods are accelerated life-time tests, bending or fracture probe to evaluate film adhesion, scratching, glow discharge optical emission spectroscopy (GDOES) to control boron doping level, etc.

6.2.2 Features and Properties

Great advantages of diamond electrodes are their anodic properties and their wide electrochemical window, the widest known for electrode materials, before water decomposition in aqueous electrolytes takes place (Perret et al. 1999). BDD electrochemical window compared to that of platinum is shown in Fig. 6.3.

In this large potential range, anodic electrochemical production of disinfecting agents can be carried out with high energy efficiency directly from the water molecules and from mineral salts contained in the water with very low by-products (hydrogen or oxygen evolution) (Haenni et al. 1999). This property of diamond electrodes allows performing water disinfection without the addition of chlorine or other chemicals and without mineral salt enrichment or impoverishment of the water. Moreover, it avoids generating toxic chlorinated disinfection by-products (chloramines, THM).

Figure 6.4 shows that the wide potential window of BDD electrode permits anodic potential allowing generation of peroxide-based and radical oxidants, which

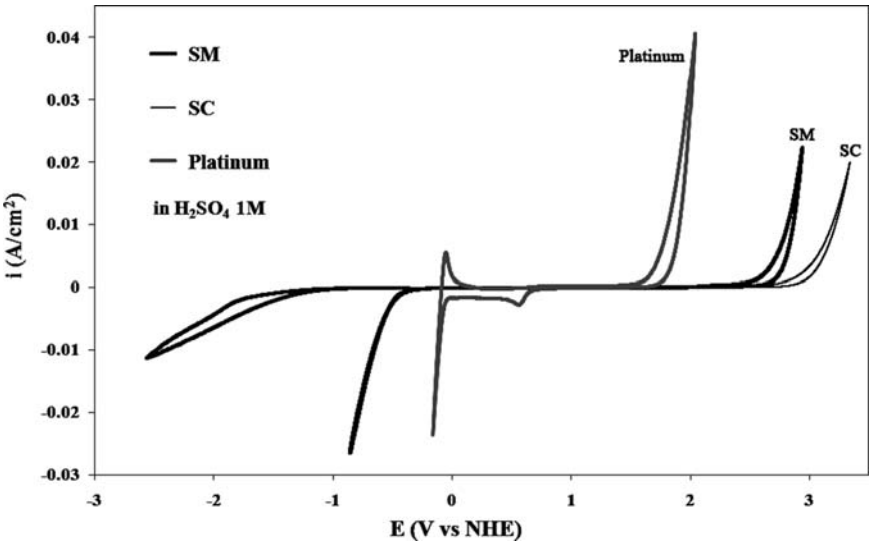

Fig. 6.3 SC (semi-conductor) and SM (semi-metal) BDD electrochemical window compared to that of platinum

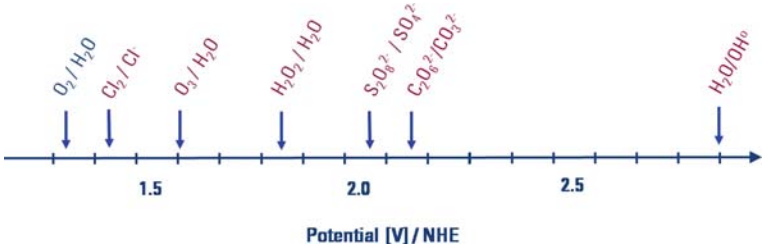

Fig. 6.4 Voltage scale and generated oxidizing species

are far more powerful than more usual oxidants such as hypochlorite. Several academic works (Haenni et al. 1999; Michaud 2002; Sudan Saha et al. 2003) have proven the generation and efficiency of such species either for water disinfection and wastewater treatment.

6.3 Electrolytic Disinfection with Boron-Doped Diamond Electrodes

The first considered disinfection application of BDD/Si electrodes and dedicated cells such as DiaCell® was the treatment of swimming pool water. After the first evaluation, this new technology also proved to be of great interest in numerous other water disinfection applications with the advantage of offering a

chemicalfree disinfection method and avoiding all chlorineinherent drawbacks (Furuta et al. 2005). This point is a major asset both from a practical (no handling and use of harmful aggressive products) and an ecological point of view.

6.3.1 Actives Species, Advantages, and Implementation

During water electrolysis process, DiaCell® and BDD/Si electrodes produce a mixture of powerful persistent oxidants. These active oxygen-based oxidants are generated directly from water and mineral salts naturally dissolved in the water. Such active species are peroxodisulfates, hydrogen peroxide, percarbonates, and ozone and their individual concentrations depend on each of their water composition. After reaction with microorganisms and pollutants, these active species are reduced to their initial mineral salt forms, which can then be oxidized again at the diamond electrodes. The overall process is a cycle that does not induce any long-term enrichment or impoverishment of the water. Academic works (Marselli 2004) also proved that hydroxyl radicals, which are the most powerful oxidizing species after fluorine, are also generated at the electrode. However, this oxidant is so reactive that it is only detected at the electrode surface and offers no persistence at all. Such disinfectant is, however, very useful to perform electrooxidation of refractory organic pollutants and allow destruction of nonbiodegradable compounds.

Disinfection by electrolytic systems operating with diamond electrodes offers several important advantages compared with other existing disinfection methods. Some of these assets are listed below:

1. It does not use chemical products and by the way avoid manipulation and contact risks with these armful species. Moreover, use of chemicals and particularly their reaction by-products often induce reactions such as allergies, irritations, and burnings on human beings. Main by-products generated by chemical disinfection are THM and chloramines which have been proven to be harmful (Villanueva et al. 2004).
2. The mixture of oxidizing species generated with diamond electrodes is far more efficient than a single-disinfectant technique such as chlorine or ozone addition or generation.
3. The persistent effect of the oxidizing species mixture generated with diamond electrodes is an essential asset compared to often-used disinfection techniques such as those using UV-lamps with which treatment is only performed when the water passes in front of the lamps.

For a suitable use in disinfection applications, these diamond electrodes have to be integrated in robust-dedicated modules. The compact, modular, and easy to use DiaCell® concept (several configurations represented in Fig. 6.5) has been developed and is produced specifically for BDD/Si electrodes. Such concept has proven to be very efficient either in the industry or for private use and up to now hundreds of these systems have already been provided and installed on the market worldwide.

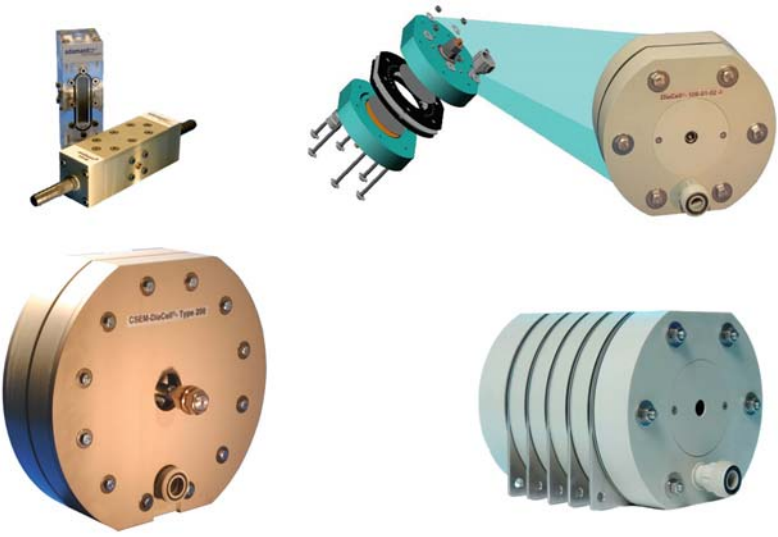

Fig. 6.5 DiaCell®-modules (Mini-Diacell®, DiaCell®-100 (2) and DiaCell®-200)

DiaCell®-100 showed in Fig. 6.5 (right part of the left-hand picture) uses 100-mm circular BDD/Si Adamant®-Electrodes. This module is equipped with two hydraulic fittings (water inlet and outlet) and two electrical connections. It has been designed to operate up to 6 bar of water pressure. Electrical connections (DC and low voltage) are feeding the two monopolar electrodes and one or several (up to 4) bipolar electrodes can also be introduced between these monopolar electrodes to increase the treatment capacity. Depending on configuration, a single module maximum flow can be of $1.2\,m^3\,h^{-1}$ and if needed several ones can be installed in parallel. Modules that integrate separated compartments, membranes, or diaphragms can also be offered.

There are no available simple kits to measure directly the overall disinfectant level when the disinfectant mixture is composed of active oxygen-based disinfectant. Nevertheless such disinfectant can be measured using the DPD method (such method uses *N*,*N*-diethyl-*p*-phenylendiamine and a photometric detection at a wave length of 530 nm). Active oxygen-based disinfectant level is given by a parameter called DPD2 that can be obtained using a differential measurement between DPD3 (overall active oxidants) and DPD1 (free chlorine measurement). For chlorine-based disinfection method, the difference DPD3–DPD1 is used to measure combined chlorine (i.e., chloramines). In the case of disinfection methods based on active oxygen, such parameter gives the concentration of oxidants that are not free chlorine (i.e., active oxygen species). Figure 6.6 shows DPD3 evolutions in water that contain only Na_2SO_4 or $NaHCO_3$, without any chloride. The two lines prove the production of nonchlorinated oxidants which are, respectively, sodium peroxodicarbonate ($Na_2S_2O_8$) and sodium peroxodicarbonate ($NaHC_2O_8$).

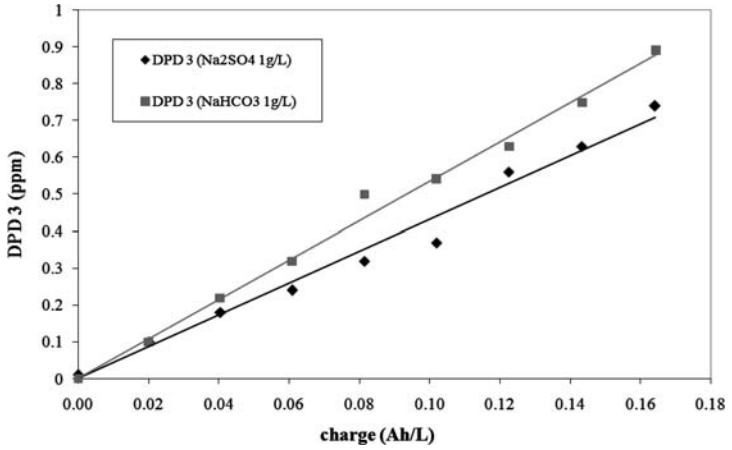

Fig. 6.6 DPD3 production in chloride-free waters as a function of electrical charge

Table 6.1 Efficiency of bacteria inactivation as a function of the treated percentage of the total water volume

Treated part of the total volume (%)	Total germs (CFU/ml) and residual disinfectant concentration (ppm) in samples taken after x min after treatment					
	$X = 5$		$X = 20$		$X = 60$	
	CFU/ml	ppm	CFU/ml	ppm	CFU/ml	ppm
0	60,000	–	60,000	–	60,000	–
5	13,000	0.01	38,000	0.01	16,000	0.01
10	7,000	0.07	4,000	0.02	2,000	0.01
20	1,000	0.14	<1,000	0.07	<1,000	0.02

6.3.2 Data on Several Microorganism Inactivations

Targeted applications are disinfection for swimming pool and spa waters, potable water, industrial cooling towers, hot water circuits, sewage waters, etc. For example, a system composed of two DiaCell®-100 allows daily disinfection of 100 m^3 of water coming out from a sewage treatment plant. Only a part of the volume has to be treated, the remaining being treated afterward; thanks to the persistence of disinfectants, the residual. Data resuming the efficiency of the DiaCell® on such water are presented in Table 6.1. After the treatment, water (<1,000 CFU/ml) can be safely used by the treatment plant team for daily cleaning operations. Such treatment unit offers both economical (lower global installation and operating costs) and ecological advantages compared to the use of potable tap water.

Several studies were carried out on various germs and in different waters. They were performed in comparison with conventional disinfection processes using chlorine dosing or UV lamps. Several microorganisms were studied including *Legionella*

Table 6.2 Microorganism inactivation in artificial seawater using a DiaCell®

Marine microorganism	Concentration in seawater (ml^{-1})	Removal (log^1)	Disinf. needed for inactivation (eq ppm C12)	Contact time for inactivation (min)
Virus H40/E	10^5	3	0.1	<1
Bacteria H40	10^6	7	0.2	<6
Enterococcus faeccalis	10^4	4	0.2	$<6-8$
Vibrio fischerii	10^5	3	0.4	$<1-5$
Pyrocystis fusiformis	10^3	2	2	30–100

Measurements performed with: DiaCell®-101 (1 compartment), I = 0.5 A, flow = 300L/h, t° = 18°C, V = 1L

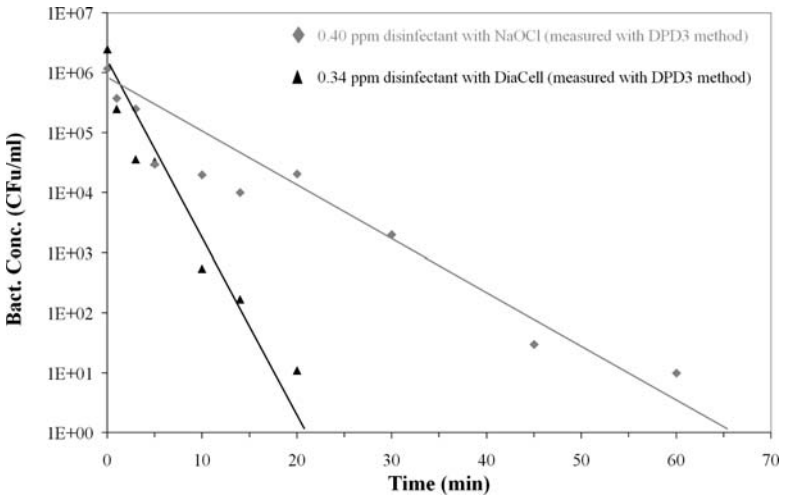

Fig. 6.7 Inactivation efficiency of *Escherichia Coli* in tap water with the DiaCell® compared to conventional disinfection method using sodium hypochlorite dosing (pH = 7.3)

Pneumophila, *H40 bacteria*, *Adenoviridae*, *Escherichia Coli*, *Vibrio Fischerii*, *Pyrocystis Fusiformis prozoan*, etc. (see Table 6.2). All tested microorganisms and even Algae were completely inactivated by disinfectants generated with BDD electrodes at low concentrations (mostly less than 1 ppm). Moreover, this inactivation occurred faster than with conventional methods. The example of *E. coli* inactivation is shown in Fig. 6.7. This graph shows that with approximately the same disinfectant level in the water, either brought by chemical product addition (sodium hypochlorite) or generated with the DiaCell®, the bacteria destruction is approximately three times faster with the electrolysis on diamond electrodes.

Figure 6.8 shows an evaluation performed on a sea microorganism, Marine bacteria H40. Once again, such bacteria are inactivated faster (four time) with Diacell®-generated disinfectants than with the same level of disinfectant introduced with conventional chlorine dosing.

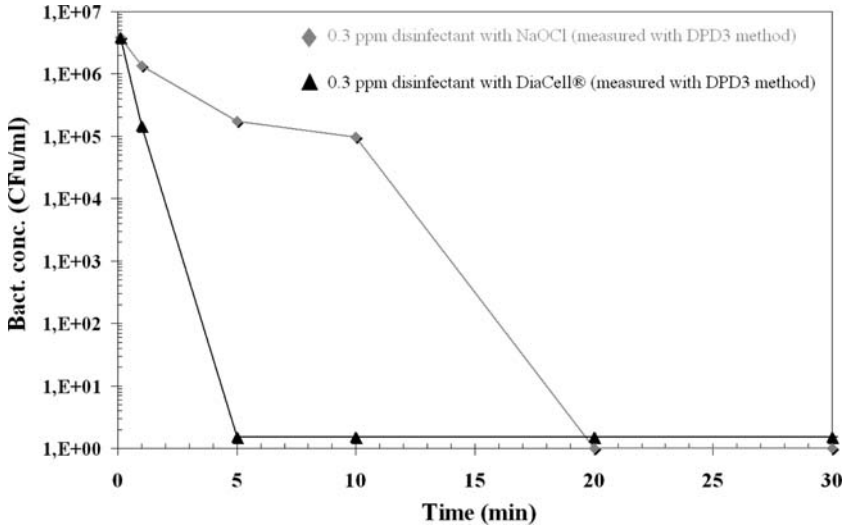

Fig. 6.8 Inactivation efficiency of bacteria H40 in sea water with the DiaCell® compared to conventional disinfection method using sodium hypochlorite dosing. Measurements performed with: DiaCell® − 101 (1 compartment), flow = 300 L h^{-1}, t = 18°C, batch volume = 121

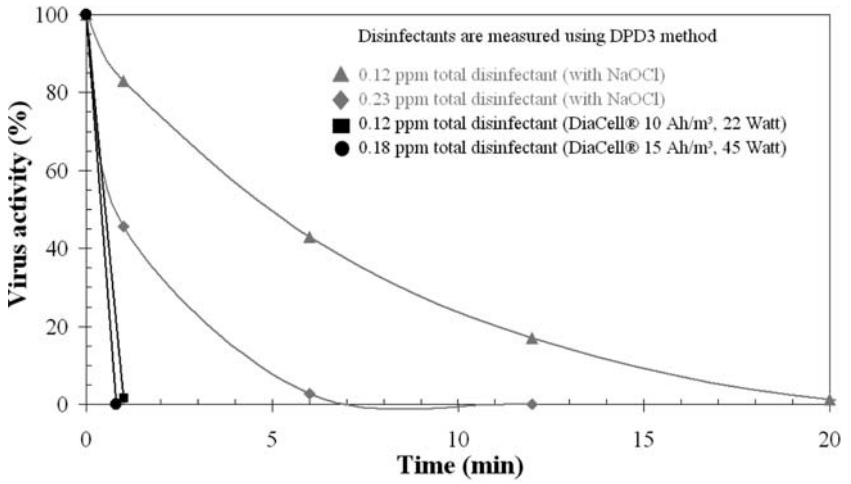

Fig. 6.9 Inactivation efficiency of Adenovirus H40 activity in tap water with the DiaCell® compared to conventional disinfection method using sodium hypochlorite dosing. Measurements performed with: DiaCell®-101 (1 compartment), flow = 300 L h^{-1}, t = 18°C, batch volume = 121

Table 6.2 (Rychen et al. 2003a) summarizes inactivation results obtained on several seawater microorganisms (including bacteria H40) with DiaCell®.

The technology also proved to be very efficient for virus inactivation. Figure 6.9 shows results of Adenovirus H40 inactivation in tap water. Again the diamond

Table 6.3 Biological analysis of a public pool disinfected with a DiaCell®-System (data from the cardiology clinic of Noirmont/Jura/CH)

Date	Mesophile aerobie germs 3 days at 30° C (CFU/mL)	*Escherichia coli* (CFU/mL)	*Pseudomonas aeruginosa* (CFU/mL)	Other pseudomonas (CFU/mL)
Norm	1,000	0	0	–
Prestart measurement	5,940	Not measured	Innumerable high	Innumerable high
19.01.2006	1,300	0	0	0
23.01.2006	0	0	0	0
23 02.2006	560	0	0	0
20.04.2006	696	0	0	22
09.05.2006	0	0	0	0
06.06.2006	1	0	0	0
10.08.2006	268	0	0	0
28.02.2007	420	0	0	0
06.03.2007	684	0	0	0
20.03.2007	664	0	0	0
22.03.2007	0	0	0	0
24.04.2007	120	0	0	0

Analyses were performed in an external lab using conventional standard microbiology techniques

electrodes results are compared to those of chemical product dosing. As shown, treatment with the DiaCell® leads to a strong and rapid inactivation (>99%) of an injection of adenovirus H40 (106 virus/ml) in an electrolyzed raw water $\left(360\,\mu S\,cm^{-1}\right)$ which contains 7 ppm of chloride (chlorine equivalent content of 0.12 ppmCl_2). This inactivation is at least five times faster than with hypochlorite addition.

Field results of public swimming pool disinfection efficiency are shown in Table 6.3. Such table lists parameters that need to be periodically measured, values fixed by law, and the measurement results. Measurements dated 19.01.2006 (2 days after starting the DiaCell®-System) show the germ content of the water since the system was turned on. This table shows the measurement results for several microorganisms such as total Mesophile germs, *E. coli*, and particularly Pseudomonas. Results are particularly interesting regarding *Pseudomonas aeruginosa* bacteria which are somehow chlorine stable. As shown in this table, prestart analysis reveals an innumerable high amount of such bacteria. After few days of treatment, the germ content of the water rapidly decreased and always remained below the norm values for now more than 2 years.

The system is kept automatically controlled at free chlorine levels (DPD1) of less than 0.4 ppm and total disinfectants (DPD3) of less than 1.2 ppm. There is a total absence of any chloramines.

The inactivation of *L. pneumophila* is a great challenge (Furuta et al. 2004; Pupunat and Rychen 2002) as these bacteria, responsible for legionaires' disease, is often detected either in domestic and hospital waters (hot water circuit, air

Table 6.4 Evolution of Legionella population, in water samples treated with DiaCell®, as a function of contact time

Water type	Fresh water 7 ppm chlorides	Fresh water 75 ppm chlorides
Disinfectants concentration (ppm)	0.19	0.71
Contact time after Legionella injection (min)	Legionella inactivation (%)	
1	–	99
5	51	99.9
20	66	99.99
60	90	100

conditioning systems, etc.) or industrial systems (cooling waters, cooling towers, etc.). The DiaCell® technology has been successfully tested against free Legionella infection on several water types. Depending on the water composition, free Legionella was completely inactivated without chemical product additions, with very low current density and short contact times of less than 5 min.

Table 6.4 also shows that the higher the generated oxidant concentration in the treated water is, the faster is the Legionella inactivation. It is interesting to note that bicarbonates in contaminated water were identified as very good support for electrochemical disinfectants production for Legionella inactivation without high chlorine concentration (see Fig. 6.6 for oxidizing species production from sulfates and carbonates).

6.4 Examples of Disinfection Applications: Dedicated Systems and Field/Evaluation Results

As reported in the previous paragraph, one can see that BDD/Si electrodes are very efficient for microorganisms' inactivation. Another great advantage of the active species generated with BDD/Si electrode-based systems is that even if not all of those species are residual, their mixture has a real-persistent effect; thanks to the more stable generated oxidants. This property allows treating only a part of the overall volume (approximately 10%) via a bypass setup and disinfecting the total volume after reinjection in the remaining 90% of the volume. After mixing, the disinfectant brought by the treated 10% of the volume is sufficiently concentrated and have enough long-term effect to ensure a good disinfection of the overall volume.

This partial flow treatment is very important:

- From an economical point of view, as it reduces both investment (smaller system) and operating (smaller energy requirements) costs
- From a safety point of view, as it avoids overoxidizing already generated disinfectants in potentially dangerous species. For example, without such partial flow treatment, a small amount of hypochlorite contained in the water could eventually be oxidized into nondesired chlorate or perchlorate

6.4.1 Swimming Pools (Private and Public)

Up to date, the most developed large-scale application of BDD electrodes in the disinfection field is the automated disinfection of swimming pool water. Dedicated products using the DiaCell® and BDD/Si electrode technologies have been developed both for private and public pools. Such products, Oxineo® and Sysneo®, respectively, for private and public pools (or for industrial process water treatment) are shown in Fig. 6.10.

Compared to other disinfection methods, such systems have the following assets for this application:

- No chlorine smell, no irritated eyes, and no bleaching
- No more dry skin because of chlorine
- No chemicals accumulating in the pool (chlorine stabilizer of chlorine pellets)
- No disinfectants excess as it is maintained at a low level in the pool (0.2–0.5 ppm)
- No need of anti-algae
- Residual action to avoid nonregular or jagged disinfections (advantage compared to not persistent effect of UV disinfection systems)
- Efficient elimination of suntan lotions and oils residues
- Daily pool disinfection without human help to avoid water fouling in case of absence or neglecting
- Compatible and simple adaptation on almost any existing technical pool installation
- No need of strong chemical products addition (exception made for pH correction)
- No need of disinfectant addition (chlorine or else)
- No corrosion, no burned lawn because of the low salt concentration (at least five times weaker than with salt electrolysis systems)
- Self-cleaning system by recurrent polarity reversal (lime stone deposits)
- Very low electrical consumption: between 0.05 and 0.15 $kWh^{-1}\,m^{-3}$ per day depending on the pool's characteristics and bather load.

Fig. 6.10 Oxineo® and a DiaCell®-System (Sysneo®)

Many systems have already been installed in private pools all over the world and several in public pools in Switzerland. Up to now, public pools that are using such systems are essentially medical institutions (hospitals, re-education centers, etc.) and communal pool centers.

6.4.2 Spas

Another very promising application is the rapidly growing market of spa disinfection. These small hot tubs have the particularities of containing from 0.8 up to 2.5 m^3 of hot water (usually around $35 - 40°C$) and to be used by far more people than swimming pools (compared to the small water volume). These two points are responsible for a spectacular bacteria development in the water and often lead to difficulties in treating the water. For such reason, existing disinfection systems usually combine several treatment methods. The most common disinfection method is the use of in situ generated ozone combined with chlorine additions. Such disinfection method has the drawback of leading to very irregular disinfection efficiency as the disinfection is mainly due to the chlorine pellets. Evaluation of Mini-DiaCell® disinfection efficiency in comparison to that of ozone/chlorine method has been performed. The evaluation was performed on a 0.8-m^3 spa that contains a relatively important bacteriological pollution as it was kept at a temperature of 37°C for a period of 4 days without any disinfection (disinfection started at 105 CFU/ml). Operating conditions were Ozonator (6 h/12 h) + weekly chlorine addition; Mini-DiaCell® 101 (4 h/12 h, 60 to 480 Wh per day).

This evaluation showed that with the ozonator + chlorine system the disinfection is mainly due to the chlorine pellet additions as the pollution level decreases after each addition to strongly increase again after few days with only ozone disinfection. The problem with such system is that the spa water is always cycling between an overload of chlorine (after shock chlorination) and a high bacterial pollution when there is no remaining chlorine in the water. With Mini-DiaCell®, the sanitation and stabilization of the water is longer (approximately 7 days), but after this period the bacterial level in the water remains stable at very low level.

6.4.3 Rainwater

Thanks to environmental concerns of industrialized populations and due to the always increasing price of tap water, rainwater collecting tanks become more and more popular to collect "free" water in order to use it for all domestic uses except drinking water (toilets, showers, washing machines, etc.). Installation scheme of such system is shown in Fig. 6.11.

The main problem of such stagnant water is the bacterial development in the tanks and to ensure its future use, this water need to be disinfected. Such disinfection can be done by regular chemical product addition (lot of handling) or UV

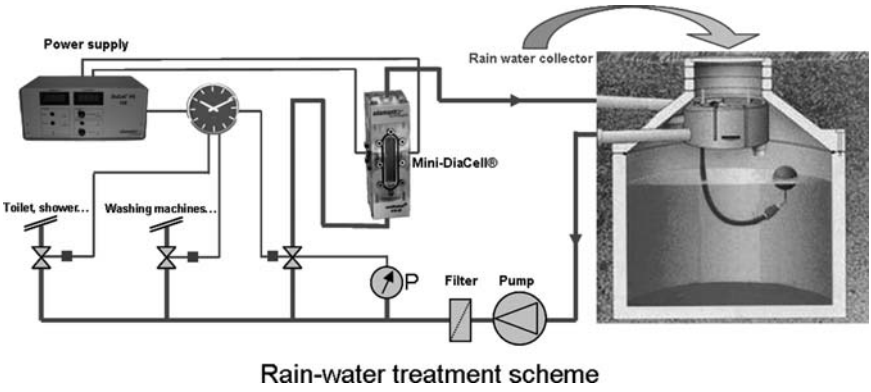

Fig. 6.11 Installation scheme of a Mini-DiaCell® rain water treatment setup

Table 6.5 Evolution of bacteria population in sewage water 5, 20, and 60 min after treatment with DiaCell® as a function of the treated fraction of the total volume ($C0$: initial concentration; $Cx\%$: concentration after treatment of $x\%$ of the total volume)

	Bacterial concentration (CFU/ml)		
Time elapsed after treatment	5 min	20 min	60 min
$C0$	60,000		
$C5\%$	13,000	38,000	16,000
$C10\%$	7,000	4,000	2,000
$C20\%$	1,000	<1,000	<1,000

lamps (high cost and no disinfection of the tank), but for such application a Mini-DiaCell® with BDD/Si electrodes is also a very promising technology. In fact, all the tank water and the tank itself can be maintained disinfected, by applying only a short daily treatment and periodically adding a small amount of mineral salt $\left(\text{approx.}0.4\,\text{g}\,\text{l}^{-1}\right)$ to have a sufficient conductivity. From an economical point of view, the DiaCell® technology is competitive and some units are currently under use successfully for such application.

6.4.4 Sewage Water

The disinfection of sewage water to ensure its use in cleaning operation and daily use is of great interest. For instance in sewage water plants, a large amount of water (having a bacteria concentration of less than 1,000 CFU/ml) is needed for on-site reuse. A typical need is $7.5\,\text{m}^3\,\text{h}^{-1}$ and $100\,\text{m}^3$ per day for a medium size municipal water treatment plant. With a system using BDD/Si electrodes, there is no need to treat the whole water volume to ensure sufficient disinfection. By treating only a part of the volume and reintroducing it in the main flow, it is possible to decrease the bacterial concentration of the overall volume under the allowed limit (see Table 6.5).

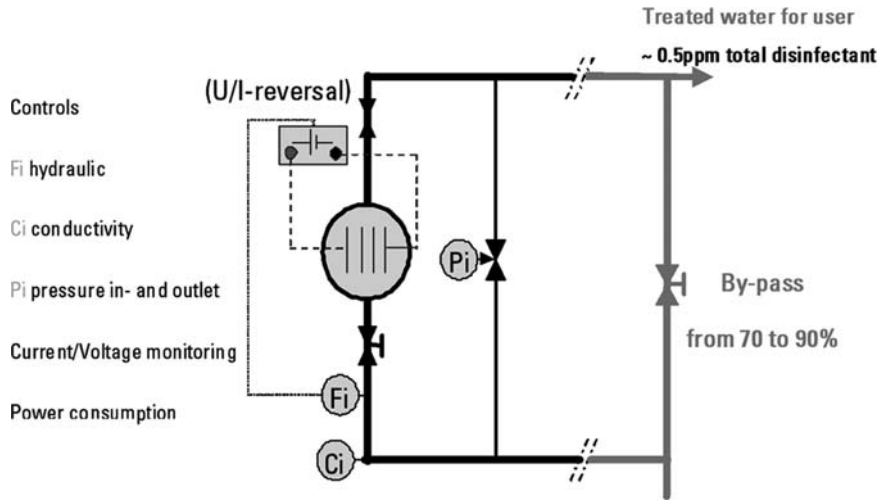

Fig. 6.12 Typical installation scheme for a sewage water treatment plant

Table 6.6 Economical comparison between DiaCell®, UV treatment, and tap water uses for 25,000 m^3 of water dedicated for daily cleaning operations (annual need of a medium size water treatment plant)

Technology	DiaCell®	UV treatment	Tap water
Treatment process	Per batch and/or continuously	During pumping	
Treatment capacity	7.5 $m^3\,h^{-1}$ −14 h (2 DiaCellO 301)	0–33 $m^3\,h^{-1}$ − 24 h (5 UV-Lamp, 0.95 kW)	
Effectiveness	++	−	
Remaining effect (residual)	+	−	
Environmental hazard	−	+	
Size	++	+	
Maintenance	+	−	
Energy (Wh m^{-3})	−150	−230	1.7 USD/m^3
Energy (at 0.17 USD/kWh) (USD/m^3)	0.025	0.039	
Investment (USD)	23,750	26,460	
Consumables (USD/year)	1,830	1,875	
Operating costs (USD/year)	2,500	2,920	42,500

Figure 6.12 shows the typical installation scheme of a DiaCell® BDD/Si-based system for the treatment of sewage water. As mentioned above, the system is installed in a bypass and is secured by a range of hydraulic and physical-sensing devices.

For an annual water need of 25,000 m^3 in such application, Table 6.6 shows an economical comparison between three alternatives: the use of potable tap water and

two disinfection technologies, the well known UV-treatment, and the new DiaCell® technology. As it can be seen, the use of tap water is nonsense as annual operating costs are really high. Regarding the two disinfection technologies, the economical and technical aspects both show that the new DiaCell® technology offers a real progress for such kind of application.

6.4.5 Process Water

Water disinfection is an essential concern in every process in which water is present. Systems such as hot water circuits, cooling and air conditioning systems, industrial cooling towers, etc. all contain water that need to be treated. Hospitals, industries, nuclear power plants, and others are demanding for automated efficient disinfection technologies that only need very little maintenance and no regular human intervention for chemical handling and system cleaning. Another typical industrial application is the algae elimination in testing units that use a continuous flow of water (e.g., in sanitary material manufactures). The feedback from companies that use such units equipped with a DiaCell® system is that this technology is not only efficient to avoid algae development in the water containing parts, but also very effective to destroy already installed algae.

Adamant Technologies offer standard and custom units for such process water disinfection (see Fig. 6.13).

Fig. 6.13 DiaCell®-systems (*left*) and Sysneo® (*right*) water treatment units

6.5 Conclusion

All the works performed up to date in the fields of research, development, manufacturing, and field use of BDD/Si electrodes and systems that include such electrodes have shown that this new material has a huge potential for water disinfection and water treatment in general. Such technology represents a genuine potential to become a new option for realizing a strong and robust disinfection of microorganisms, as it combines a great efficiency and an environmentally friendly process, by avoiding use of chemical product and production of toxic residues in the water.

Major advantages of Adamant®-Electrodes based systems are:

- The long-term sustained action (residual) of oxidizing agents
- The strength of these disinfectants, which are 2−5 times stronger than chlorine or bromine
- The specific design of the systems, as the range of DiaCell® modules and dedicated units is specifically designed for BDD/Si electrodes

As several installations are running since 2−3 years with good feedbacks from users, Adamant has gained a medium-/long-term field experience with BDD electrodes and DiaCell®-based units. These positive references are found in:

- Industrial applications such as cooling tower disinfection, process water disinfection, treatment of waste water from laundry, from chemical industry, etc.
- Public nonindustrial uses,with a main focus on public swimming pools
- Private uses in swimming-pool and spa disinfections, rain-water disinfection, algae elimination in ponds and fountains, etc.

References

Awards: Bronze Award 2004 of EEP – Pollutec Lyon/FR.
Awards: Eco-Conscience Trophy 2005– Lausanne/CH.
Awards: New product trophy 2006 at the World Swimming-pool Show – Lyon/FR.
Awards: Piscina BCN 2007 – Barcelona/SP.
Fryda M., Hermann D., Schäfer L., Klages C.-P., Perret A., Haenni W., Comninellis C. and Gandini D. Properties of diamond electrodes for waste water treatment, New Diam. Front. Carbon Technol. 9 (1999) 229.
Furuta T, Tanaka H., Nishiki Y., Pupunat L., Haenni W. and Rychen P. Legionella inactivation with diamond electrodes, Diam. Relat. Mater. 13 (2004) 2016–2019.
Furuta T., Rychen, Tanaka H., Pupunat L., Haenni W. and Nishiki Y. Application of diamond electrodes for water disinfection, in: A. Fujishima, et al., Editors, Diamond Electrochemistry, BKC, Inc., Tokyo, pp. 525–542 (2005).
Haenni W. and Fryda M. Substrate for diamond electrodes, in: Third Workshop on Diamond Electrodes, Neuchâtel, Switzerland, (2000).
Haenni W., Borel M., Perret A., Correa B., Michaud P.-A. and Comninellis C. Production of oxidants on diamond electrodes, CSEM Scientific Report (1999).
Haenni W., Faure C. and Rychen P. Modular electrochemical cell. Patent WO 02/088430°1, (2001).

Haenni W., Rychen P., Fryda M. and Comninellis C. Industrial applications of diamond electrodes, in: C. E. Nebel and J. Ristein, Editors, Semiconductors and Semimetals, vol. 77 (Thin-film Diamond II), p. 149, (2004).

Marselli B. Electrochemical oxygen transfer reaction on synthetic boron-doped-diamond thin film electrode, PhD thesis no. 3057, EPFL (Ecole Polytechnique Fédérale de Lausanne) (2004).

Michaud P.-A. Comportement anodique du diamant dopé au bore, PhD thesis no. 2595, EPFL (Ecole Polytechnique Fédérale de Lausanne) (2002).

Perret A., Haenni W., Skinner N., Tang X.-M., Gandini D., Comninellis C., Correa B. and Foti G. Electrochemical behaviour of synthetic diamond thin film electrodes, Diam. Relat. Mater. 8 (1999) 820.

Pupunat L. and Rychen P. Inactivation of Legionella with the DiaCell® Water Treatment Technology, CSEM Scientific Report (2002).

Rychen P., Haenni W. and Pupunat L. Water treatment without chemistry, Chimia 57 (2003a) 655.

Rychen P., Pupunat L., Haenni W. and Santoli E. Water treatment applications with BDD Electrodes and the DiaCell® concept, New Diam. Front. Carbon Technol. 13(2) (2003b)109.

Sudan Saha M., Furuta T. and Nishiki Y. Electrochemical synthesis of sodium peroxycarbonate at boron-doped diamond electrodes, Electrochem. Solid-State Lett. 6 (2003) D5.

Swain G.M. The susceptibility to surface corrosion in acidic fluoride media – a comparison of diamond, HOPG and glassy carbon electrodes, J. Electrochem. Soc. (1994) 3382.

Villanueva C.M., Cantor K.P., Cordier S., Jaakkola J.J.K., King W.D., Lynch C.F., Porru S. and Kogevinas M. Disinfection byproducts and bladder cancer, Epidemiology (2004) 357.

Chapter 7
Drinking Water Disinfection by In-line Electrolysis: Product and Inorganic By-Product Formation

M.E. Henry Bergmann

7.1 Introduction

The worldwide supply of safe (disinfected) drinking water is a task of essential importance. Because of the formation of many organic disinfection by-products in conventional chlorination (Krasner et al. 1989; Palacios et al. 2000), new ideas (periodical chlorination, UV treatment, etc.) are being applied in more and more cases. In small-scale disinfection, a growing market for disinfection electrolysers exists. Drinking water is mostly disinfected by flowing through an electrochemical cell using the natural chloride ion content for active chlorine (free available chlorine) formation. Besides this, cells are offered for chlorine-free waters. The increased disinfection ability in electrolysed drinking water is explained by the formation of so-called *mixed oxidants* which are unknown in detail (Kerwick et al. 2005). The method is called in-line electrolysis or named by many other terms and trade marks. The variety of suggested technologies and apparatuses leads to confusion in hygiene officials and other stakeholders. Furthermore, in some variants chloride is added to the drinking water prior to passing through the cell, or water is electrolysed with a chloride concentration differing insignificantly from concentrations permitted for drinking water (250 ppm, all mg L^{-1} concentrations are given here as ppm.)

Literature reports applications for disinfecting medical equipment, oculars (Shimmura et al. 2000), fuel cells, vegetables (Izumi 1999) and green house substrates (internet presentation 2005), pipes and containers in breweries (Gutknecht et al. 1981) or in other fields of food industry (Hernlem and Tsai 2000; Tsai et al. 2002), ship waste waters, etc. Applications outside the drinking water area are mentioned here because many waters are environmentally important and connected with the drinking water chain (Fig. 7.1). Thus, the problem is much more relevant than may at first be expected.

M.E.H. Bergmann (✉)
Departments 6/7, Anhalt University of Applied Sciences, Bernburger Str. 55,
06366 Koethen/Anh., Germany
e-mail: h.bergmann@emw.hs-anhalt.de

C. Comninellis and G. Chen (eds.), *Electrochemistry for the Environment*,
DOI 10.1007/978-0-387-68318-8_7,

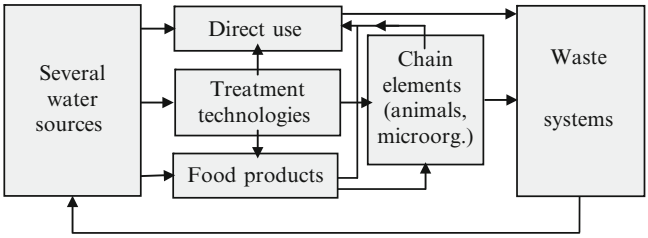

Fig. 7.1 Complex system of interactions for water in its treatment technology paths

Starting from the beginning of research (Reis 1951; Reis and Henninger 1953) many works have been published dealing with selected aspects such as killing efficiency of different microorganisms (Reis 1976; Kirmaier and Schoberl 1980; Reis 1981; Grebenjuk et al. 1990), with the use of different electrode materials such as graphite (Gainer et al. 1975), graphite fibres or composite materials (Stoner et al. 1982; Natishan 1984; Matsunaga et al. 1994), Pt (Kirmaier et al. 1984), Ti (Patermarakis and Fountoukides 1990), IrO_2 (Kraft et al. 1999a) and IrO_2/RuO_2 (Kraft et al. 2003; Bergmann and Koparal 2005d), TiN (Matsunaga et al. 2000), carbon cloth (Matsunaga et al. 1992a) with current modes such as change of polarity, using direct current or applying alternating current of differing frequencies up to some thousand Hz (Rosenberg et al. 1965; Pareilleux and Sicard 1970, Gainer et al. 1975; Gutknecht et al. 1981; Stoner et al. 1982; Porta and Kulhanek 1986) and with others subjects. Newer publications (Fryda et al. 2003; Hupert et al. 2003, Duo 2003) describe the application and modification of so-called boron-doped diamond (BDD) electrodes representing a conductive diamond film on substrates such as niobium and silicon. It was shown that BDD anodes are able to form active chlorine species for disinfection (Ferro et al. 2000; Haenni et al. 2002). But in contrast to the electrocatalytic properties of MIO anodes, BDD anodes produce radicals oxidising other species non-specifically. It is accepted that mainly OH radicals are responsible for oxidation processes (Marselli et al. 2003). The differences in oxidising power of MIO or DSA® and BDD anodes were discussed recently (Foti et al. 1999). A new approach is the clustering of BDD by mixed oxides (Duo et al. 2000) but this application is not known.

There is still a deficit in systematic and complex studies on product and by-product formation during and after the treatment process. On the other hand, confusing terms (*mixed oxidant*, *electroactivated water*, *meta-stabile water*, etc.) are used discussing the higher disinfection power compared to conventional chlorination. In principle, this is a clear indication of unknown or non-specified by-products (Shimizu and Sugawara 1996; Crayton et al. 1997; Hamm 2002; Son et al. 2005; Bergmann et al. 2008). Therefore, the aim of the studies presented here is to demonstrate the potential for DPD formation in complex ways. Electrolysis processes working in the $g\,L^{-1}$ range of chloride concentration are not considered. Also, the reduction of bromide ions and the interaction of products with chlorine species are not a subject of this work.

7.2 Experimental Conditions

7.2.1 Apparatuses

A cell with a rotating anode (rotation rate 300 rpm) 4 mm above a cathode was used in a series of discontinuous experiments at 20°C (Fig. 7.1). Current density was varied between 50 A m^{-2} and 500 A m^{-2} using constant current mode and *Statron* rectifiers. Disk anodes (diameter 35 mm) were made from titanium coated with mixed oxides (50% IrO_2/50% RuO_2 as relative molar concentration) and BDD (producers *Magneto* and *Metakem*/*Condias*). BDD anodes had boron doping between 2,000 and 4,000 ppm. IrO_2 or IrO_2/RuO_2 on Ti (expanded mesh, diameter 40 mm) located 25 mm above the base of the beaker was used as cathode material.

Discontinuous experiments were carried out using a thermostated dark beaker cell with 50–160 mL of electrolyte (artificially prepared water or tap water). The working temperature of 20°C was adjusted with a *Lauda* potentiostat model *RM*6. The anode was rotated using a *MLM MR25/Medingen* unit and contacted through a *Mercotac* contactor (Fig. 7.2). In discontinuous experiments with larger volumes (650–750 mL), a non-divided cell with parallel plate electrodes (20 mm × 50 mm, distance 3 mm) lying in a plane inside the *Plexiglas* half-cells was used. The electrodes were made from titanium and coated with IrO_2/RuO_2 (50%/50%). A centrifugal pump recirculated the electrolyte through glass heat exchangers and a dark beaker (Fig. 7.2). A magnetic stirrer was additionally used inside the beaker. In a few experiments, the cell was divided by a Nafion® separator using space

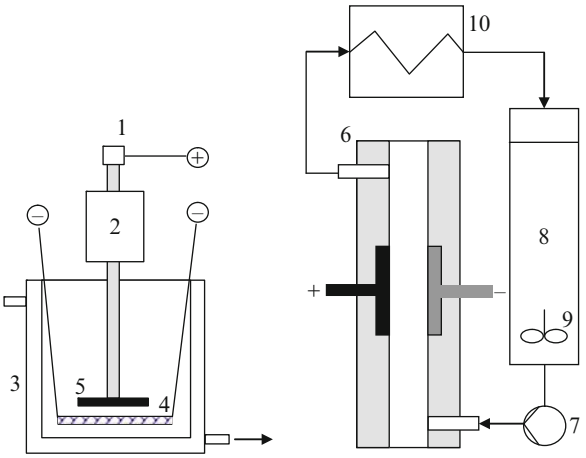

Fig. 7.2 Discontinuous cells used in the experiments – cell with rotating anode (*left*) and flow-through cell with parallel plate electrodes (*right*). (1) Rotating contact, (2) electronically controlled stirrer, (3) thermostated beaker, (4) plate cathode with central hole or expanded mesh cathode, (5) rotating disk or expanded mesh anode, (6) parallel plate cell, (7) centrifugal pump, (8) stirred dark container for sampling, (9) magnetic stirrer, (10) cryostat

frames for a constant flow channel width. Anodic and cathodic cycles were then performed analogous to the non-divided cell. Connecting elements in the flow loop were made from dark *Viton* material highly stable against oxidation. For studies of polarisation curves for modelling, an *EG&G* potentiostat model 283 together with a rotating disc electrode stand (model 616) were used. The anode was a 1-cm^2 Ti disc activated with IrO_2/RuO_2 (*Magneto*) or BDD on niobium. A mercury oxide reference electrode in an outer beaker connected with a salt bridge containing 0.25 M NaOH was used to measure the potential. The cathode was a platinum sheet of size 15 mm × 30 mm. The pH was measured using a *WTW* pH meter *pH 340*, specific conductivity with a conductometer *Cond 340i* from *WTW*. The exact cell current was checked using a multimeter (*MY-64*, *Conrad Electronic*). A UV/Vis spectrophotometer (*Specord 40, Analytik Jena*) was used for special spectroscopic studies in the UV range. Quantitative analysis was carried out using a spectrophotometer (*Nanocolor D100*, *Macherey & Nagel* or *CADAS 40*, *Dr. Lange*).

An *ELCHEMA Model EQCN-700* electrochemical quartz crystal nanobalance was used in combination with an *ELCHEMA Model PS-205B* potentiostat in special experiments. As working crystal, an *ELCHEMA QC-10-AuPB* laboratory quartz crystal with 14 mm of diameter (active area of 0.196 cm^2) was used.

7.2.2 Chemicals

Deionised water for HPLC (specific conductivity less than 0.1 $\mu S\,cm^{-1}$) and very pure chemicals (all as sodium salts) in mg L^{-1} (ppm) range of concentrations were used in the experiments. Chemicals of analytically pure grade with relatively low impurity influence in UV spectra from *Roth* (Na_2CO_3), *Baker* ($NaNO_3$) and *Fisher Scientific and Chempur* (NaCl, Na_2SO_4, NaOH, $CaSO_4$, $Ca(OH)_2$) were taken for preparing artificial electrolytes. Chemicals were partially treated twice (Na_2SO_4) or thrice (Na_2ClO_2) by fractional crystallisation at different temperatures. The deionised water for preparing the artificial drinking water systems was produced in a unit combining reverse osmosis, adsorption and ion exchange (*USF/Seral*).

7.2.3 Analytical Methods

Samples were taken at pre-determined time intervals, immediately diluted if necessary and analysed by spectrophotometry. Samples for IC, if not analysed in the course of or directly after the experiment, were frozen and analysed later.

Perchlorate was analysed using a *Metrosep Dual 4* column (*Metrohm*). H_2O_2 was measured applying *Macherey&Nagel Peroxide 2* test kits based on the peroxidase reaction. Active chlorine was measured by the DPD method (*Dr. Lange LCK 310* or *Macherey&Nagel chlorine/ozone 2* test kits) or by ion chromatography. Because chloride and hypochlorite have overlapping peaks, ion chromatography

analysis was carried out twice with and without hypochlorite elimination. The corresponding values were calculated solving a system of mathematical equations. In selected experiments, active chlorine concentration was calculated from UV spectrum measurements making sure that the sample pH was adjusted to 11.5. Bonded chlorine was measured by the DPD method by adding three drops of KI solution to the sample after determining the active chlorine. Experiments were repeated at least once. Nitrate was analysed in a few experiments applying the spectrophotometrical *Dr. Lange* method LCK 339 reacting nitrate with 2.6-dimethylphenol to 4-nitro-2.6-dimethylphenol. The nitrite analysis was carried out by photospectroscopy using the *Dr. Lange* test LCK 341 (sensitivity 0.002 mg dm^{-3}) and partially by a second method after adding defined volumes of acetic acid, sulphanilic acid and α-naphtol to samples and measuring peaks at 476 nm (sensitivity 0.001 mg dm^{-3}). Mostly, nitrite, nitrate, chloride, hypochlorite, chlorite, chlorate and sulphate were analysed by IC (system *Knauer/Alltech* with *Novasep A-2* anion column and electrochemical detector). Ammonium was measured by a *Knauer* HPLC system (with *Merck L3720* detector).

7.2.4 Bacterial and Yeast Cultures

Eischerichia coli K-12, *Bacillus subtilis DSM* 2277 and *Saccharomyces cerevisiae* Kolin were used as the test-microorganisms. These were supplied by DSM – German Collection of Microorganisms and Cell Cultures. 24–48 h cultures were used for inoculation. For pre-culture, a single colony was inoculated in 100 mL of sterile broth. *E. coli K-12* and *B. subtilis DSM* 2277 were inoculated in Nutrient Broth (*SIFIN*, Germany). *S. cerevisiae* Kolin was inoculated in worth broth (*SIFIN*). *E. coli K*-12 was grown at 37°C for 24 h. *B. subtilis DSM* 2277 and *S. cerevisiae* Kolin were grown at 30°C for 24 h with 180 revolutions per minute (rpm) agitation provided by a rotary stirrer (*Heidolph Unimax 1010*). After 20 h, 30 mL of culture was taken and inoculated in 200 mL of a new sterile broth and incubated for 24 h. After that, all test microorganisms were harvested by centrifuging in a 35-mL conical tube at 10,000 rpm (+5°C) for 5 min and washed with 10 mL sterile drinking water. All stock solutions were prepared by resuspending the final pellet in 10 mL of sterile drinking water. Cell suspensions were diluted with sterile drinking water to the required cell density corresponding to 10^5–10^7 colony forming units per millilitre (CFU mL^{-1}) for use in the experiments. After taking the sample, the reaction was immediately stopped by adding 0.1 mL of 0.1 N sodium thiosulphate solution. The number of viable cells in the samples taken during the experiment was determined by plating and counting colonies. For this purpose, 100 μL of sample was plated on nutrient agar or yeast agar. Two replicate plates were used. *E. coli K*-12 plates were incubated at 37°C for 48 h before counting. *B. subtilis DSM* 2277 and *S. cerevisiae* Kolin were incubated at 30°C for 48 h before counting.

7.2.5 Transmission Electron Microscopy

After taking the sample, the reaction was immediately stopped with 0.1 mL of 0.1 N sodium thiosulphate solution. Copper grids were exposed to 20-μ L samples for 15 min and washed with sterile distilled water. Finally grids were stained in 2% aqueous uranyle acetate for 8 min and dried. The grids were examined with a *Zeiss EM 902* transmission electron microscope (*LEO Elektronenmikroskopie GmbH*).

To determine the cytological status of bacteria after chemical treatment, drops of highly concentrated bacterial suspensions were placed into agar tubes following a defined method (Rovan and Simonsberger 1974). The samples were fixed with 2% glutaraldehyde pH 7.4, buffered with 0.05 M sodium cacodylate and post-fixed in 1% osmium tetroxide pH 7.5. The agar tubes were embedded in EPON 812 (*Serva, Heidelberg*). Prior to embedding in EPON 812, the material was dehydrated in a graded ethanol series and propylene oxide and pre-stained with uranyle acetate. Ultra-thin sections were made on an ultramicrotome *Ultracut (Reichert Jung*). The sections on copper grids were stained with lead citrate and observed using a *Zeiss EM 902* transmission electron microscope at 80 kV.

7.3 Electrochemical In-line Disinfection

7.3.1 Killing of Microorganisms

Disinfection of drinking water is designed to bring the water into a state from which infection is not possible. This means that the majority of microorganisms must be inactivated. Physical and chemical methods are known to achieve this. Electrochemical methods of disinfection must be distinguished depending on the immobilisation state of microorganisms. Matsunaga and co-workers showed that microorganisms adhering to the surface can be inactivated by applying potentials below values of anodic gas formation or chlorine evolution (Matsunaga et al. 1984, 1992b). The work was carried out to study the avoidance of biofilm formation and biofouling. It was found that the cell respiratory activity was destroyed by electrochemical oxidation of CoA in the cell wall. The reaction took approximately 20 min.

Bergmann et al. (2001) demonstrated that this mechanism is improbable for in-line electrolysis. The main reasons for this are the low residence time inside the electrochemical reactor (approximately 1 s) and gas evolution negating the adhering of microorganisms. Even biofilms can be eliminated by short surface polarisation with gas bubble formation (Schultze et al. 2003). Polarisation studies in systems with and without added microorganisms did not show special response. Microorganisms can be considered as charged or bipolar cells but electrophoretic transport (Markitanova and Zenin 1990) would be too slow for significant contribution to electrochemical killing. Thus, theories published in the past on electrochemical inactivation by charge transfer at the electrodes cannot be confirmed. In-line

electrolysis is a process of chemical reactions between microorganisms and species generated electrochemically. Disinfection studies showed that the process may proceed for many minutes. As a result of reactions, organic by-products occur (not discussed here). As shown below, the most probable disinfecting species are active chlorine components, chlorine dioxide, ozone, hydrogen peroxide and several radicals – depending on the operation mode and water matrix.

There is not only one kind of interaction between chemicals and microorganisms. For instance, a cell can die by inhibited mass transfer into the cell, by affecting important cell parts responsible for metabolism or replication and by lyses of cell walls with the resulting outflow of cytoplasm. Hundreds of works exist in literature and also in medical research area. A literature review was published recently (Bergmann et al. 2008). Table 7.1 summarises some effects of selected disinfectants. The main problem in cell damage is obviously that parallel mechanisms exist and that the analysis of species, for example of ROS type, is extremely difficult due to the high reaction rates with kinetic constants in the range of 10^8–10^{10}. Repairing effects seem to exist (Hamelin and Chung 1989). There is no mathematical model taking into account the large variety of possible interactions between microorganisms and chemicals, all the more so in that microorganisms exists in many forms (free or immobilised, biofilms, spores, Gram-positive, Gram-negative, with/without flagella, slime, as spores, etc.).

Kinetic models must consider reaction with the inner (components of cytoplasm) and outer parts of microorganisms (flagella, slime and cell wall). Similar to segregation models in chemical engineering, each microbial cell represents a microreactor where chemicals are able to diffuse through the cell wall and react inside. For example, this is possible for hypochlorous acid and hypochlorite, but, due to the charged cell membrane, HOCl obviously diffuses easier and has better disinfecting ability (Hass 1990).

Figure 7.3 illustrates cell damage patterns obtained by electron microscopy illustrating the discussion. When cytoplasm flows out through a broken wall, the reaction scheme becomes more homogeneous but all scenarios are possible concurrently.

Table 7.1 Effects of killing microorganisms by different disinfectants

Disinfectant	Mechanism	Literature
Chlorine	Inhibition of enzymes necessary for DNA replication	Carlson (1991) and Leyer and Johnson (1997)
Chlorine	Altering of cell walls by amino group oxidation	Sharma and Venkobachar (1979)
ClO_2	Disruption of protein synthesis	Bernarde et al. (1967)
ClO_2	Destruction of glucose oxidase	Junli et al. (1997)
O_3	Destruction of membranes	Christensen and Giese (1954)
O_3	Reaction with glutathione	Scott and Lesher (1963)
O_3	Damage of chromosomal DNA	Ishizaki et al. (1987)
OH radicals	Strand breaking in DNA radicals	Hamelin and Chung (1978)
OH radicals	Reaction with nucleic acids	Von Sonntag (1987)
OH radicals	Deformation of cell surface, wall rupture	Diao et al. (2004)

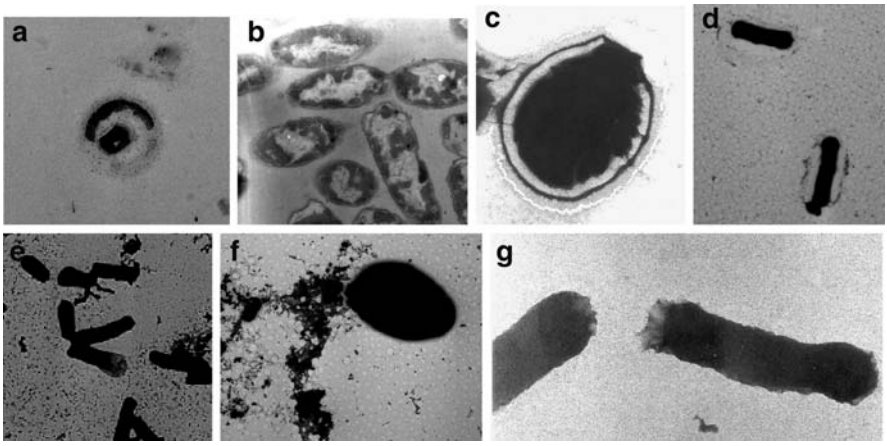

Fig. 7.3 Patterns of damaged cells after reacting with chemicals (initial concentration C_0 of microorganisms (MO) in CFU mL^{-1}). (**a**) *E. coli*, $C_0 = 10^7$, 1 mL MO + 1 mL 0.4 *ppm*ClO_2, $t_{tr} = 5$ min. (**b**) *B. subtilis*, $C_0 = 10^8$, 1 mL MO + 1 mL3%H_2O_2, $t_{tr} = 1$ min. (**c**) *S. cerevisiae*, $C_0 = 10^6$, 1 mL MO + 1 mL electrolysed solution (100 ppm sulphate +100 ppm chloride, 150 mL, 150 mA, rotating IrO_2/RuO_2 anode, 20°C, 10 ppm active chlorine), $t_{tr} = 5$ h. (**d**) *E. coli*, $C_0 = 10^7$, 1 mLHCl + 2.33 mL HCl, $t_{tr} = 1$ min. (**e**) *E. coli*, $C_0 = 10^7$, 1 mL MO + 0.4285 mL1 M$Na_2S_2O_8$, $t_{tr} = 1$ min. (**f**) *S. cerevisiae*, $C_0 = 10^7$, 4 mL MO + 1 mL 0.2 ppm ozone, $t_{tr} = 1$ min. (**g**) *E. coli*, $C_0 = 10^5$, 1 mL MO + 1 mL electrolysed solution (100 ppm sulphate + 100 ppm chloride, 150 mL, 150 mA, rotating IrO_2/RuO_2 anode, 20°C, 6 ppm active chlorine), $t_{tr} = 5$ min

Some of the existing simplified reaction models were published elsewhere (Gyürek and Finch 1998). The influence of active chlorine concentration and kind of microorganism was demonstrated in project work combining electrochemistry and UV irradiation method (Bergmann et al. 2002). Affected cells tend to agglomerate. Figure 7.3a shows a dissolving cell agglomeration after adding chlorine dioxide. Nearly all cells show lyses effects. Figure 7.3b is a transmission picture of cells damaged by H_2O_2. When treatment time is chosen to be longer and peroxide concentration to be higher, cell wall rupture can be found; however, such high concentration values are not typical for in-line electrolysis processes. Yeast cells with relatively thick cell walls seldom disrupt in treatment (c and f) but Fig. 7.3f shows both severe and non-severe damage to cells at the same time because the cell suspension always contains cells of very different lifetime and constitution. Often, cell endings show higher damage (e and g). This can be explained by differing structures of the places for cell division.

7.3.2 The Production of Disinfection Products

The production of disinfecting species must be in agreement with the corresponding rules for drinking water, usually limiting the concentration of species at the point of

addition or at several times from the start of production. A typical time interval is 30 min. Practical application, however, often shows other, not well-controlled situations in the grey zone of in-line applications. Chemicals allowed to be added to drinking water are the active chlorine species, e.g. dissolved chlorine, hypochlorous acid and hypochlorite ions, furthermore, ozone and chlorine dioxide. The situation is complicated by the fact that chloramines are forbidden in many European countries but are allowed to be added in USA. Thus, disinfection products in one region of the world may be disinfection by-products in another region as will be explained in Sect. 7.3.3.4.

Ozone was not measured in the water using MIO anodes but O_3 is a reaction product of electrolysing water poor in chloride ions and using anodes with high oxygen overvoltage. So-called *Membrel* electrolysers with PbO_2 anodes were sold in the past for water-disinfection purposes. BDD anodes are also characterised by ozone generation (Katsuki et al. 1998) and able to work with current efficiency values in the range of some percents. Problems of ozone generation are discussed in Sect. 7.3.3.5. There are new attempts to produce gaseous ozone in water electrolysers using BDD anodes (Thiele and Foerster 2006) but this is not yet a typical case in in-line electrolysis.

Chlorine dioxide is usually not a target of water electrolysis but it may occur when electrolyzing water. This special ClO_2 problem is discussed in Sect. 7.3.3.2.

The mass distribution between the three active chlorine species (see above) is dependant on pH (White 1999). For pH values higher than 4 nearly no dissolved chlorine is present in water whereas for pH values higher then 10 nearly all chlorine exists as hypochlorite. Drinking water is allowed to have pH conditions between 6.5 and 9.5. This consideration is necessary because an electrochemical reactor works with distributed pH parameters. This is due to the fact that the main reaction in electrolysing water containing chloride ions in the ppm range is the splitting of water according to (7.1) and (7.2).

$$\text{Main anodic reaction } H_2O \rightarrow 2H^+ + 0.5O_2 + 2e \tag{7.1}$$

$$\text{Main cathodic reaction } 2H_2O + 2e \rightarrow 2OH^- + H_2 \tag{7.2}$$

This means, at a considered working point, pH is lowest near the anode surface and highest in the vicinity of cathode (Fig. 7.4).

The higher the current density applied, the higher are the differences in anodic and cathodic pH. This behaviour, simplified in Fig. 7.4 by three layers of essentially different pH conditions, is known from electrochemical engineering. The consequences for in-line electrolysis are manifold. For example, the low pH leads to the well-known chlorine formation and dissolution according to (7.3)–(7.6).

$$2Cl^- \rightarrow Cl_2 + 2e \tag{7.3}$$

The mechanism of this reaction on MIO anodes was studied at higher chloride concentrations and was discussed recently (Trasatti 2000).

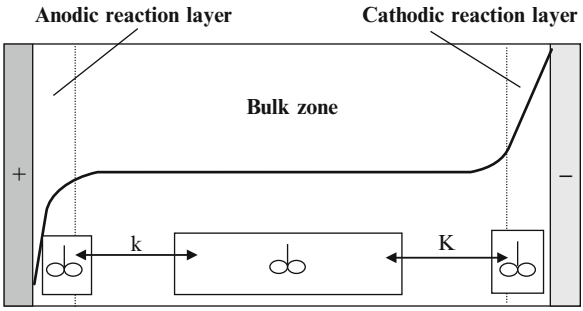

Fig. 7.4 Distribution of pH and formation of different reaction zones in in-line electrochemical cells and possible model structure for different reaction zones coupled by mass transfer

Dissolved chlorine quickly reacts with water near the anode (7.4).

$$Cl_{2,diss.} + H_2O \rightarrow HOCl + H^+ + Cl^- \tag{7.4}$$

Participation of OH^- ions is probable because the kinetic constants for the reaction with hydroxyl ions (7.5) are in the range of 10^{14} (White 1999).

$$Cl_{2,diss.} + OH^- \rightarrow HOCl + Cl^- \tag{7.5}$$

Dissociation of HOCl forms hypochlorite ions (7.6).

$$HOCl \leftrightarrow H^+ + OCl^- \tag{7.6}$$

There are many side reactions significantly depending on pH. So, chlorine dioxide is not stable for lower pH, the reaction rate of chlorite with active chlorine is much higher for lower pH and nitrite reacts faster with active chlorine at very low pH conditions. In addition, reactions in different zones must be taken into consideration if the reaction constants are very high. This is the case for OH radicals and is discussed in Sect. 7.3.3.5.

In-line electrolysis of water differs from technical electrolysis processes in many parameters. The chloride concentration allowed for drinking water is relatively small and not allowed to exceed 250 ppm (in Germany). Other concentration values are also limited that result in low electrical conductivity conditions (maximum 2,500 $\mu S\,cm^{-1}$ in Germany). From the electrochemical point of view, one has to expect strong diffusion control of active chlorine formation. Unfortunately, low diffusion enhancement possibilities exist because the gas evolution [(7.1) and (7.2)] dominates mass transfer. Only the low influence of anode rotation on chlorine formation was measured (Bergmann and Koparal 2005a). In the same work, the migration effect was estimated by analysing the transport equation (7.7) and using mass-transfer equations for the rotating disk electrode. It was shown that migration has a significant influence on the active chlorine formation rate.

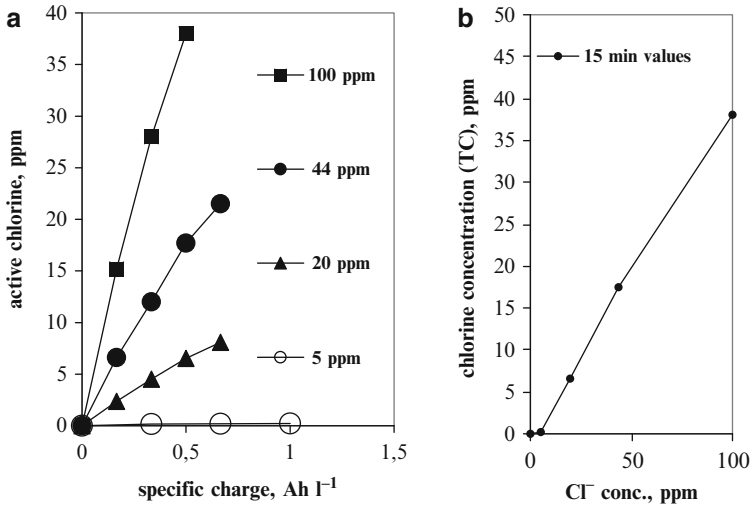

Fig. 7.5 (**a**) Active chlorine concentration vs. specific charge in discontinuous experiments with varying chloride concentration, (**b**) 15 min values of total chlorine concentration, (rotating MIO anode, 300 rpm, Ti cathode, 300 mA, 20–22°C, 0.150 L, 240 ppm sulphate + 10 ppm nitrate + 50 ppm carbonate, as sodium salts, DPD method)

$$N_j = wc_j - D_j \frac{dc_j}{dx} - c_j \frac{\Lambda_j}{zF} \frac{d\Phi}{dx}. \tag{7.7}$$

Indeed, higher chlorine formation at higher cell currents was reported (Kraft et al. 1999a; Bergmann and Koparal 2005d). Consequently, higher chloride concentration may accelerate both diffusion and migration. However, the high voltage drop in the vicinity of electrodes hinders true electrode potential measurement in obtaining polarisation curves (Bergmann and Koparal 2005d). Figure 7.5 shows chlorine formation for varying charge flow and chloride concentrations in discontinuous experiments underlining the discussion. It is surprising that for the lowest chloride concentration chosen the formation efficiency tends to be zero. This is in accordance with many observations that detectable active chlorine concentration can be measured starting from approximately 10 ppm chloride in the water (Hoell 2002). Two explanations are possible:

1. No chlorine is formed during electrolysis.
2. Chlorine is formed but reduced in consecutive side reactions.

Figure 7.6 was obtained by carrying out electrolysis experiments at extremely low chloride concentrations. Both curves show a tendency of chlorine formation and destruction in terms of a spectrophotometrical DPD signal. Even if there are some uncertainties with respect to the DPD method (see Sect. 7.3.3.7) these results support the second theory (2).

IrO_2/RuO_2 anodes show higher chlorine formation compared with IrO_2 anodes (Bergmann 2007a) but anodes containing RuO_2 without IrO_2 often show better

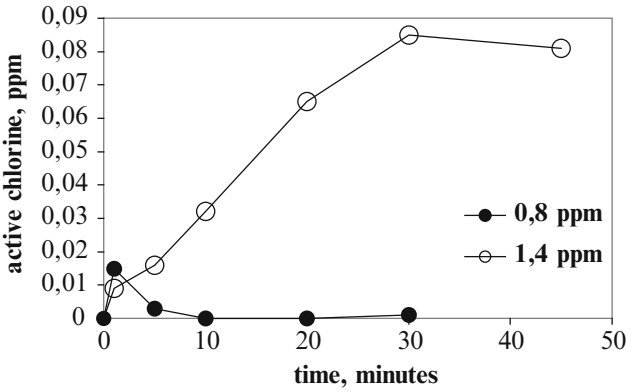

Fig. 7.6 Active chlorine formation in parallel plate cell at very low chloride concentrations as indicated in the legend (IrO_2/RuO_2 electrodes, 150 A m^{-2}, 750 mL, 20°C, 0.8 and 1.4 ppm chloride + 232 ppm sulphate + 5 ppm carbonate as sodium salts)

chlorine formation than IrO_2/RuO_2 anodes. In addition, this formation depends on the electrode supplier, i.e. on the kind of electrode preparation. The situation is known from other publications (Kim et al. 2002). More research is necessary in the field.

Adsorption and co-adsorption of ions on the anode are expected to have a bigger influence on product yield when the ion concentrations are comparable and in the low ppm range. Indeed, reports of a different reaction order with respect to chloride oxidation and the influence of sulphate ions (Trassatti 1981) might be an indicator of adsorption effects. The problem is discussed here in terms of analytical errors (Sect. 7.3.3.7).

Active chlorine can be oxidised on the anode and reduced in cathodic reactions (Krstajic et al. 1987):

$$6ClO^- + 3H_2O \rightarrow 2ClO_3{}^- + 4Cl^- + 6H^+ + 0.5O_2 + 6e \quad (7.8)$$

$$OCl^- + H_2O + 2e \rightarrow Cl^- + 2OH^- \quad (7.9)$$

Own experiments in divided cells using Nafion® membrane separators and hypochlorite solutions in the ppm range of concentration resulted in current efficiency values for active chlorine reduction of a few percent. Shifting the pH to higher values complicated the experiments. A buffer stabilised the pH but the relatively high concentration of buffer ions hindered the electrochemical reaction. Thus, quantification is difficult. Kuhn et al. (1980) showed reduction inhibition when calcareous deposits were precipitated on the cathode, but practical experiments showed the decrease of chlorine production in this case.

Chemical chlorate formation can be neglected by estimating reaction rates with known constants. Electrochemical chlorate formation is discussed in Sect. 7.3.3.1. As considered below, side reactions of active chlorine with disinfection by-products are mainly responsible for lowering the chlorine formation efficiency. It was found

in the experiments using MIO electrodes that maxima of active chlorine formation exist depending upon the current density applied. The maximum is located between 100 A m^{-2} and 200 A m^{-2} and can be explained by different partial polarisation curves for oxygen and chlorine evolution starting from different potentials. The results are consistent with those of other groups (Arikawa et al. 1998) obtained for higher chloride concentrations.

BDD anodes without impurities are not electrocatalytically active because water electrolysis is characterised by the formation of OH radicals (Marselli et al. 2003), ozone (Cho et al. 2005) and hydrogen peroxide (Drogui et al. 2001). One can conclude from radical chemistry that other radicals have to be expected in the anodic reaction layer and, maybe, in the bulk. Foerster and co-workers compared active chlorine formation on Pt and BDD anodes (Foerster et al. 2002). Formation of active chlorine was explained by a mechanism involving the formation of Cl radicals (Ferro et al. 2000):

$$Cl^- \rightarrow Cl + e \tag{7.10}$$

$$2Cl \rightarrow Cl_2 \tag{7.11}$$

An intermediate of the pH-dependent Cl radical formation is $ClOH^-$ (Klaening and Wolff 1985).

For several reasons the mechanism and role of radicals must be discussed. First, the adsorption ability of the chloride ion is very low (Pleskov 2003). Second, not only chlorine but also other oxychlorine products such as chlorate and chlorine dioxide can be found by analysing the treated water and, chloride ions are able to react with other radicals formed by reaction of OH radicals with additional ions. This allows one to conclude that the formation of active chlorine proceeding with the participation of OH radicals [(7.12) and (7.13)] is likely.

$$Cl^- + OH \rightarrow Cl + OH^- \tag{7.12}$$

$$Cl^- + 2OH \rightarrow OCl^- + H_2O \tag{7.13}$$

Higher chloride concentrations and higher current densities form higher amounts of active chlorine but the situation is much more complicated as Fig. 7.7 shows. In addition to the formation of active chlorine and chlorate, both components are decomposed again. One of the resulting products is perchlorate as shown in Sect. 7.3.3.3.

7.3.3 The Production of Inorganic Disinfection By-Products

7.3.3.1 Formation of Chlorate

Chlorate is often found as a by-product in long-term stored hypochlorite liquors for disinfection purposes. The reaction is very slow and proceeds over weeks and

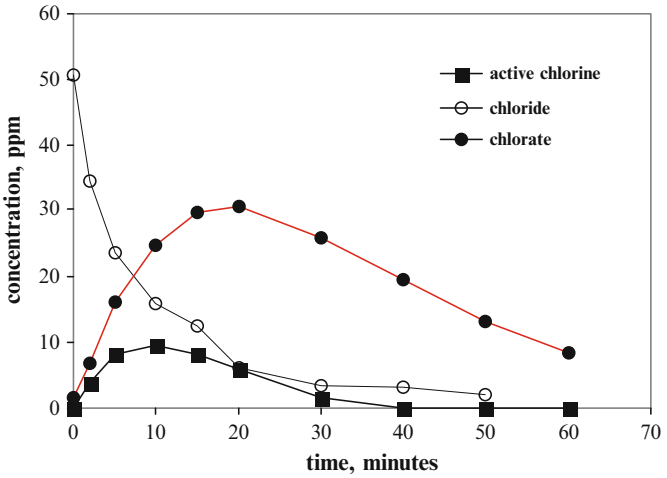

Fig. 7.7 Concentration of chloride, active chlorine and chlorate in discontinuous electrolysis using rotating BDD anode (IrO_2 cathode, 200 A m^{-2}, 100 mL, 300 rpm, 20°C, 50 ppm chloride as NaCl)

months. It was reported in the past (D'Ans and Freund 1957) in confirmation of the so-called Foerster mechanism that for medium pH values (5–9) the reaction is evident in the presence of free hypochlorous acid:

$$OCl^- + 2HOCl \rightarrow ClO_3{}^- + 2H^+ + 2Cl^- \tag{7.14}$$

with the partial reaction steps

$$2OCl^- \rightarrow ClO_2{}^- + Cl^- \tag{7.15}$$

$$OCl^- + ClO_2^- \rightarrow ClO_3^- + Cl^- \tag{7.16}$$

New explanations take into consideration $Cl_2O{\cdot}H_2O$ and $ClO_2{}^-$ species (Adam et al. 1992). Competing reaction (7.17) is much slower.

$$2OCl^- \rightarrow O_2 + 2Cl^- \tag{7.17}$$

In other studies it was found that a maximum of HOCl decomposition exists at pH = 6.89. For the third-order reaction (7.14), catalytic activity of the chloride ion was suggested for hypochlorite decomposition and the stabilising effect of higher pH was quantified in the pH range 9–14 (Adam and Gordon 1999).

However, industrial electrochemical chlorate production is aimed at the chemical path in external reactors because of the higher energy efficiency compared with the summary electrochemical process:

$$6OCl^- + 3H_2O \rightarrow 2ClO_3{}^- + 4Cl^- + 6H^+ + 1.5O_2 + 6e \tag{7.18}$$

or

$$6HOCl + 3H_2O \rightarrow 2ClO_3^- + 4Cl^- + 12H^+ + 1.5O_2 + 6e \quad (7.19)$$

A series of papers tries to explain the electrochemical mechanism in more detail. With respect to RuO_2 anodes, chlorite was suggested as an intermediate in chemical reactions in the acidic anode layer of weakly alkaline solutions of lower chloride content (Czarnetzki and Janssen 1992):

$$2HClO \rightarrow ClO_2^- + 2H^+ + Cl^- \quad (7.20)$$

$$ClO_2^- + HClO \rightarrow ClO_3^- + H^+ + Cl^- \quad (7.21)$$

Electrolysing hypochlorite on Pt in 1 M NaOH chlorite was found to be an intermediate using Raman spectroscopy (Tasaka and Tojo 1985). The authors suggest a stepwise $OCl^- \rightarrow ClO_2^- \rightarrow ClO_3^-$ electrochemical oxidation. The non-selective character of OH radicals lets one conclude that similar stepwise mechanisms are responsible in chloride electrolysis using BDD anodes.

In the concentration range of in-line water disinfection, the occurrence of chlorate is usually denied by cell users and producers. Only a few data exist where the presence of chlorate is mentioned (Cho et al. 2001). Our own studies, however, clearly showed, both with synthetic and real waters and both in laboratory and technical cells, a high chlorate formation potential. For example, the chlorate concentration in technical reactors using BDD or MIO anodes and real drinking water (44 ppm Cl^-) was in the range of some ppm (BDD) and some hundred ppb (MIO) in single-pass operation mode.

Figure 7.8 is a clear demonstration of the different behaviour of the two electrode materials. While chlorate is formed at a nearly constant rate on MIO in the electrochemical reaction, on BDD it is soon consumed (with perchlorate forma-

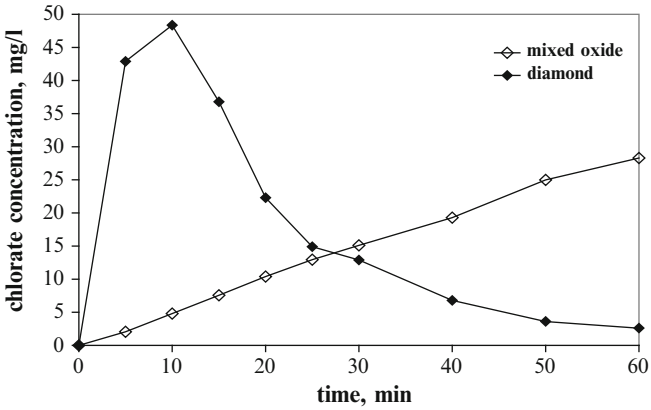

Fig. 7.8 Chlorate formation in discontinuous experiments using rotating IrO_2/RuO_2 and boron-doped diamond anode (IrO_2 cathode, 50 mL, 50 ppm chloride, 200 A m^{-2}, 20°C, 300 rpm, pH = 7 KH_2PO_4/NaOH buffer)

tion). Chlorate was also measured using other anode materials (at varied RuO_2:IrO_2 ratio, Pt). Because chlorate is sometimes limited by regulation in drinking water, its concentration should be controlled when in-line electrolysis is applied.

7.3.3.2 Formation of Chlorine Dioxide

Chlorine dioxide is a powerful disinfectant able to kill free and immobilised microorganisms (Gates 1998). A large bibliography exists in the field. Its main advantage is its lower potential for forming organic DBPs. ClO_2 can be produced in chemical and electrochemical reactions starting from chlorate or chlorite (Kirk-Othmer 1979; Oloman 1996). Thermodynamics suggest reactions starting from chloride and chlorine [(7.22–7.23)] but little is known about the true mechanisms.

$$Cl^- + 2H_2O \rightarrow ClO_2 + 4H^+ + 5e \tag{7.22}$$

$$Cl_2 + 4H_2O \rightarrow 2ClO_2 + 8e \tag{7.23}$$

ClO_2 is extremely easily formed from chlorite even in the ppm concentration range of chlorite (Bergmann 2006a, Pillai et al. 2009):

$$HClO_2 \rightarrow ClO_2 + H^+ + e \tag{7.24}$$

Figure 7.9 shows a superficial effect when chlorite and chloride are present in the electrolysed water. In addition, the pH was chosen to be low by dividing the cell

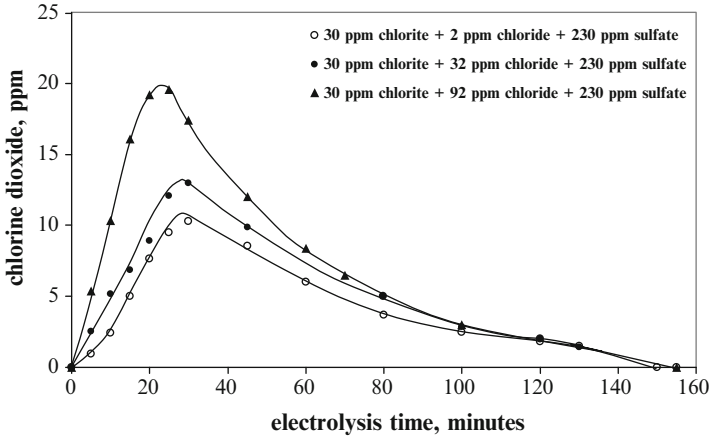

Fig. 7.9 ClO_2 concentration (calculated from 360nm peakheight in UV spectra using a molar coefficient of absorption 1080 M^{-1} cm^{-1}) vs. electrolysis time (divided cell, MIO electrodes, 750 mL, 200 A m^{-2}, 20°C, 230 ppm sulphate + 30 ppm chlorite and varied chloride concentration as indicated)

into two compartments and simulating low pH conditions near the anode in chloride electrolysis. It was found in our own experiments, both in divided and non-divided cells, that more ClO_2 was analysed when the chloride concentration was increased at constant chlorite concentration.

The exponential slope in the beginning could be an indication of both electrochemical and chemical ClO_2 formation.

BDD anodes oxidise chlorite to ClO_2 with reduced efficiency because of easier chlorate and perchlorate formation (see also Fig. 7.13). An optimal current density exists (not shown here).

Thermodynamics allows ClO_2 formation from hypochlorous acid (7.24)

$$HClO + H_2O \rightarrow HClO_2 + 2H^+ + 2e \tag{7.25}$$

but electrolysis of hypochlorous solutions preferably results in chlorate formation.

It was recently found (Bergmann2005a; Bergmann and Koparal 2005c) that under drinking water electrolysis conditions chlorine dioxide is definitely formed. ClO_2 peaks in the UV spectra were temporarily measured especially when experiments were disturbed by gas blocking effects or the interruption of the electrolyte flow (Fig. 7.10).

It is not yet clear if the ClO_2 formation is based on an electrochemical or chemical mechanism or on both. New IC results (not presented here) show that chlorite in low concentration can be present using MIO anodes. (Chlorite formation from ozone and chlorine was also reported recently – Son et al. 2005.) Thus, a peak in electrode polarisation (related to the 10-min value in Fig. 7.10) would allow $HClO_2$ to form (see also mechanism of chlorate formation). During this period the pH is

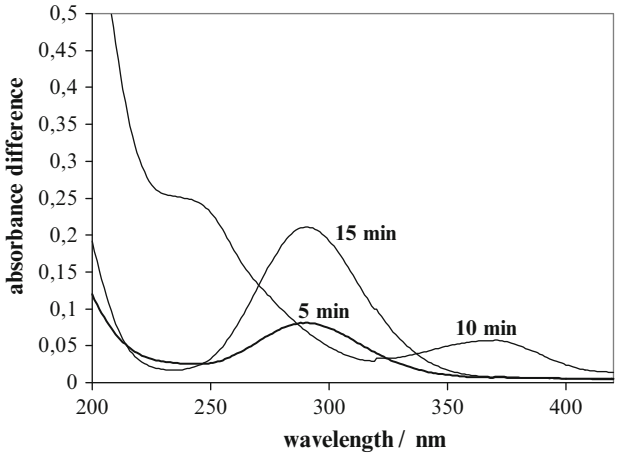

Fig. 7.10 Differential UV spectrogram measured against initial solution in samples from discontinuous water electrolysis (rotating IrO_2/RuO_2 anode, 300 rpm, Ti cathode, 150 mL, 300 mA, pH = 8.67, 20.5°C, 100 ppm sulphate + 100 ppm chloride as Na salts in deionised water)

extremely low and chlorite or chlorous acid can react with hypochlorous acid according to reaction (7.26):

$$2HClO_2 + HClO \rightarrow 2ClO_2 + Cl^- + H_2O + H^+ \quad (7.26)$$

The peak-like increase of absorbance near 230 nm (typical for HOCl) in Fig. 7.10 is probably related to a shift to lower pH values (HOCl formation from OCl^-) and appears to confirm this.

The reaction (7.27)

$$2HClO_2 + Cl_2 \rightarrow 2ClO_2 + 2Cl^- + 2H^+ \quad (7.27)$$

forming the intermediate $[Cl_2O_2]$ is reported as being faster (Emmenegger and Gordon 1967) but higher chlorine concentration would be necessary near the anode. Another option is the fast electrochemical reaction of hypochlorite to chlorate. A reaction path (7.28) is reported for the presence of hydrogen peroxide (formed anodically), but for a much higher concentration range (Burke et al. 1993). It is worth noting this, because hydrogen peroxide is more stable at pH = 4 (Gordon et al. 1998).

$$2NaClO_3 + H_2O_2 + H_2SO_4 \rightarrow 2ClO_2 + O_2 + 2H_2O + Na_2SO_4 \quad (7.28)$$

In fact, active chlorine consumption was observed in disturbed experiments with higher ClO_2 concentration. Chemical formation from active chlorine and chlorite is also favoured due to the reaction behaviour after switching off the electrolysis experiments (Fig 7.11). It can often be seen from the UV spectra that the hypochlorite peak decreases and the ClO_2 peak slightly increases. Increase of ClO_2 concentra-

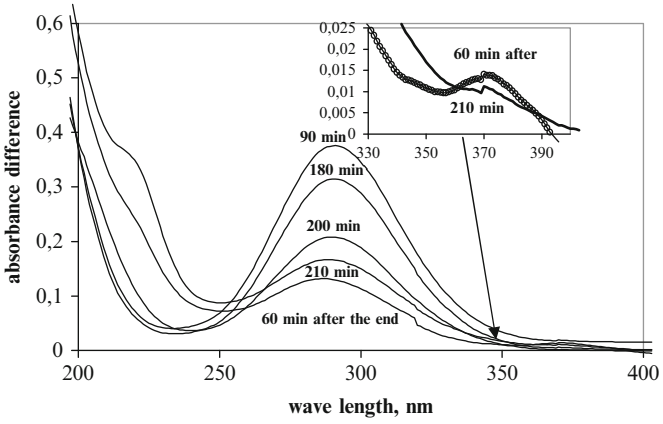

Fig. 7.11 Differential UV spectra measured against initial solution from samples during and after electrolysis switched off at 210 min. (Rotating IrO_2/RuO_2 anode, 300 rpm, IrO_2 cathode, 150 mL, 300 A m^{-2}, 125 ppm chloride + 240 ppm sulphate + 10 ppm nitrate + 2.5 ppm carbonate, pH = 6.8–7.9)

tion can also be measured by applying the Macherey&Nagel test set (Bergmann and Koparal 2005c). ClO_2 is sometimes detectable using the Lisamin Green method for samples during and after electrolysis. Simulating the process by adding hypochlorite and chlorite in higher concentration to the cuvette in excess of chlorite, rapid ClO_2 formation can be easily demonstrated (Fig. 7.11). In contrast to this, it is thought that chlorine dioxide is mainly formed in the pH range 6–10 due to the presence of catalytic metal ions (Gordon and Tachiyashiki 1991). Other researchers (Peintler et al. 1990) report that with excess HOCl and at a higher pH, chlorate formation is the main reaction (7.29).

$$2HOCl + {ClO_2}^- \rightarrow {ClO_3}^- + Cl_2 + H_2O \tag{7.29}$$

In electrolysis using BDD anode chlorite as a ClO_2 precursor may be formed by ozone attacking the hypochlorite ion (von Gunten 2003). The reaction rate is relatively small as well as for chlorite oxidation by ozone. OH radical-based effects are more probable.

So formed, chlorine dioxide may undergo many chemical or electrochemical reactions. With organic matter it again forms chlorite. If ozone is generated, it reacts in the ms-range with chlorine dioxide in competition with the reaction with active chlorine (Gordon et al. 2002):

$$2ClO_2 + O_3 + H_2O \rightarrow 2{ClO_3}^- + O_2 + 2H^+ \tag{7.30}$$

Chlorite is also formed when ClO_2 is reacted with hydrogen peroxide (see also ROS discussion below). Chlorite can be stabilised for many hours at high pH values. In the minute-time scale chlorine dioxide reacts with active chlorine depending on the pH value [(7.31)–(7.32)].

$$2ClO_2 + HOCl + H_2O \longleftrightarrow 2{ClO_3}^- + Cl^- + 3H^+ \tag{7.31}$$

$$2ClO_2 + 2OH^- \longleftrightarrow {ClO_2}^- + {ClO_3}^- + H_2O \tag{7.32}$$

The chlorine/chlorine dioxide system was modelled with real water data. A maximum in chlorite formation was found (Schmidt et al. 1999).

When chlorine dioxide is obtained by anodic chlorite oxidation, with or without the addition of sulphate, it is relatively stable in the minute-to-hour time scale at room temperature in the dark. Complex formation probably stabilises the chlorine dioxide (Gordon and Emmenegger 1966). Unfortunately, observation of this complex under these conditions in water electrolysis is compromised by low optical sensitivity.

It can be summarised that both chlorine dioxide and chlorite can be identified in many experiments at several time intervals. The ClO_2 concentration depends on many influences but experiments with both rotating anode cells and parallel flow-through cells show proportional concentration values compared to the volume factor at constant current load on MIO anodes and using different analysis methods.

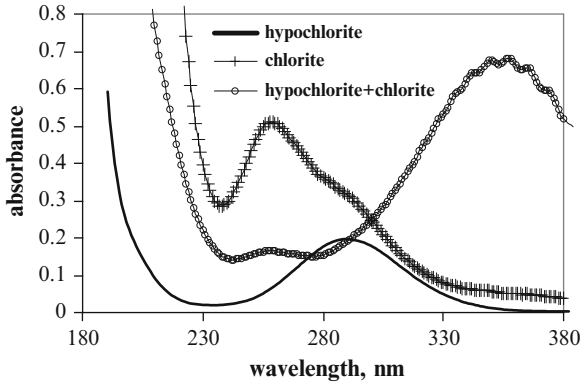

Fig. 7.12 UV spectra showing ClO_2 formation at 360 nm after 1:1 mixing of hypochlorite (ca. 30 ppm) and chlorite (ca. 230 ppm) at room temperature in the dark, reaction time 9 min

This concentration is usually between 0.05 and 0.2 ppm. The large variety of possible ClO_2 consuming reactions makes the analysis difficult. The consumption of chlorine dioxide could contribute to a certain extent to chlorate formation in drinking water (Fig. 7.11).

7.3.3.3 Formation of Perchlorate

The presence of perchlorate is one of the most topical discussions concerning drinking water in USA (Urbansky and Schock 1999; Gu and Coates 2006). Recently, Massachusetts and California set a limiting concentration of 6 ppb and 2 ppb for perchlorate in drinking water. In 2009, the Environmental Protection Agency (EPA) released an interim drinking water health advisory of 15 ppb.

Thermodynamics gives a variety of equations for perchlorate formation as follows [(7.33)–(7.39), with indication of standard potentials vs. SHE].

$$Cl^- + 4H_2O \rightarrow ClO_4^- + 8H^+ + 8e \quad 1.389\,V \tag{7.33}$$

$$Cl_2 + 8H_2O \rightarrow 2ClO_4^- + 16H^+ + 14e \quad 1.389\,V \tag{7.34}$$

$$Cl^- + H_2O \rightarrow HClO + H^+ + 2e \quad 1.494\,V \tag{7.35}$$

$$HClO + H_2O \rightarrow HClO_2 + 2H^+ + 2e \quad 1.645\,V \tag{7.36}$$

$$HClO_2 + H_2O \rightarrow {ClO_3}^- + 3H^+ + 2e \quad 1.214\,V \tag{7.37}$$

$$Cl_2 + 6H_2O \rightarrow 2{ClO_3}^- + 12H^+ + 10e \quad 1.470\,V \tag{7.38}$$

$${ClO_3}^- + H_2O \rightarrow {ClO_4}^- + 2H^+ + 2e \quad 1.189\,V \tag{7.39}$$

Chloric acid may disproportionate:

$$2HClO_3 \leftrightarrow HClO_4 + HClO_2 \tag{7.40}$$

Hydrolysis of ClO_3 and Cl_2O_7 gases also results in perchlorate formation. Chlorine dioxide can be oxidised by ozone with the formation of Cl_2O_6. Hydrolysis results in the formation of perchloric acid [(7.41) and (7.40)].

$$2ClO_2 + O_3 \rightarrow Cl_2O_6 + 0.5O_2 \tag{7.41}$$

$$Cl_2O_6 + H_2O \rightarrow HClO_3 + HClO_4 \tag{7.42}$$

Perchlorate is industrially produced from concentrated chlorate solution using Pt or PbO_2 anodes (Kuhn 1971). The process can be started from chloride or hypochlorite but higher amounts of energy are necessary. Anodes containing RuO_2 are able to produce perchlorate but they are not applied for this purpose. The electrochemical production of perchlorate from concentrated chlorate solution using doped diamond anodes was reported in patent literature (Lehmann 2002). In drinking water, ClO_4^- formation was found in the electrolysis of synthetic and real drinking water using BDD anodes (Bergmann et al. 2007b; Bergmann and Rollin 2007b). Similarly to technical processes, perchlorate can be obtained starting from chloride, hypochlorite, chlorite and chlorate and leads to the suggestion that stepwise oxidation takes place with participating OH radicals [(7.43); Bergmann and Rollin 2007c; Bergmann et al. 2009].

$$Cl^- \xrightarrow{OH} OCl^- \xrightarrow{OH} ClO_2^- \xrightarrow{OH} ClO_2 \xrightarrow{OH} ClO_2^- \xrightarrow{OH} ClO_3^- \xrightarrow{OH} ClO_4^- \tag{7.43}$$

The participation of chlorite and ClO_2 is still speculative because short-lived chlorite is difficult to detect. But chlorite can be a reaction product of active chlorine and ozone (Gordon et al. 2002). When chlorite in the ppm range was electrolysed separately, chlorine dioxide was clearly formed and removed during the discontinuous experiment. In large excess of ozone over chlorite, chlorine dioxide, chlorate and perchlorate are formed by ozone reactions, with ClO_3 as an intermediate (von Gunten 2003). The OH radical-based theory of perchlorate formation from chlorate is supported by the low reaction rates of chlorate with ozone (Langlais et al. 1991) and studies by Siddiqui (Siddiqui 1996).

Surprisingly, perchlorate was found in drinking water simulating cathodic protection systems using iron electrodes (Jackson et al. 2004). The authors concluded perchlorate formation by electrochemical chloride oxidation forming chlorate. This is unlikely for iron anodes. More likely is a mechanism of cathodic peroxide formation from dissolved oxygen. The mechanisms discussed in the literature include different reactive species (Damjanovic 1992), but when hydrogen peroxide is present and bivalent iron from anode dissolution exist, reactions undergo the so-called Electro-Fenton Process with OH radical formation. These oxidise in further steps from chloride to perchlorate. Perchlorate can also be formed as the result of a radical-based chemistry in real and simulated atmospheric processes (Dasgupta et al. 2005).

Figure 7.13 shows the good perchlorate formation potential starting from chlorite and chlorate and forming intermediates (exponential concentration increase). Surprisingly, the addition of sulphate improves the formation starting from chlorite.

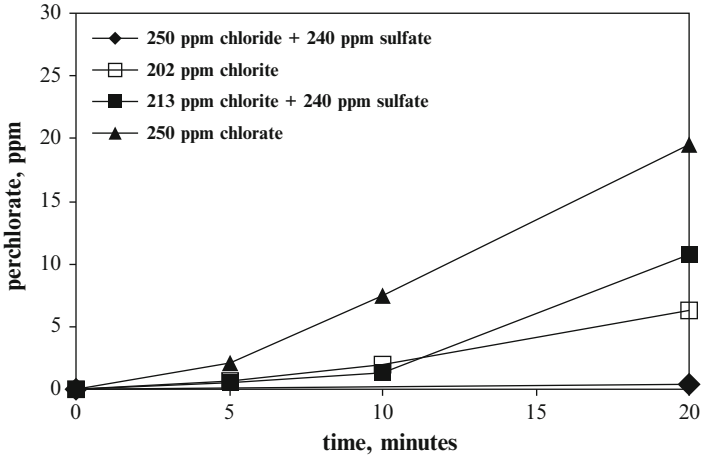

Fig. 7.13 Perchlorate formation in the discontinuous parallel plate cell using BDD electrodes and artificial waters (200 A m^{-2}, 650 mL, 20°C)

Probably, the consumption of OH radicals in competing side reactions is lower. The same tendency was observed in experiments with chloride and chlorate (not shown here).

Using cells with MIO anodes traces of perchlorate were found depending on the chosen conditions. It is not yet clear whether there is an electrocatalytic formation or the formation is supported by radicals. The latter can also be formed on MIO (Kim et al. 2005; Jeong et al. 2009).

It is still worth noting that in an early work (D'Ans et al. 1957) the authors found that perchlorate is a by-product in reacting hypochlorite/hypochlorous acid with chlorate. It is explained by the fast formation of an activated complex $[HCl_2O_4]^-$ that may slowly react to perchlorate, H^+ and Cl^-.

Perchlorate formation in drinking water electrolysis is a serious problem. In experiments using a semitechnical bipolar cell with BDD electrodes and drinking water (40 ppm chloride) even for the lowest current density applied (50 A m^{-2}) perchlorate was measured at 30 ppb using a residence time of approximately 1 s. This behaviour does not recommend BDD cells for drinking water treatment without additional measures.

7.3.3.4 Formation of Nitrogen Containing By-Products

Nitrate ions are allowed in German drinking water up to the limiting concentration of 50 ppm. The limiting concentration for nitrite and ammonium are 0.1 ppm (water works) and 0.5 ppm, respectively. Chloramination is not permitted. Hundreds of publications exist in the field of nitrate electrolysis in acidic, neutral, and alkaline media, mostly for nitrate concentrations in the g L^{-1} range. Depending on the conditions, the formation of nitrite, ammonium, N–O, N–H components and

nitrogen is possible. Brutto kinetic equations usually describe the complicated reaction mechanisms. The problems of drinking water electrolysis are similar to those of water chlorination but differences exist. One example is the formation of nitrite. It is known from electrolysis in weakly alkaline media that at lower cathodic potentials nitrite is formed [(7.44)–(7.47)], whereas at higher potentials ammonium is formed (Bouzek et al. 2003).

$$NO_3^- + H_2O + 2e \rightarrow NO_2^- + 2OH^- \quad (7.44)$$

$$NO_3^- + 6H_2O + 8e \rightarrow NH_3 + 9OH^- \quad (7.45)$$

$$NO_2^- + 5H_2O + 6e \rightarrow NH_3 + 7OH^- \quad (7.46)$$

$$NH_3 + H_2O \leftrightarrow NH_4^+ + OH^- \quad (7.47)$$

Nitrite formation was reported in drinking water electrolysis (Bergmann et al. 2005d). It is surprising because nitrite is thought to be oxidised quickly. However, our own studies of oxidising nitrite ions by oxygen, hydrogen peroxide, ozone and ozone/hydrogen peroxide showed that ozone gives the fastest conversion to nitrate. A significant reaction with hydrogen peroxide is known only for pH values lower than 3.5. From so-called breakpoint chlorination it is known (White 1999) that nitrite is stable if chloramines are present. Figure 7.14 clearly demonstrates nitrite formation in water poor in chloride ions. Formation of ammonium and chloramines according to (7.48) and (7.49) can be seen from Fig. 7.15.

$$HClO + NH_3 \rightarrow NH_2Cl + H_2O \quad (7.48)$$

$$HClO + NH_2Cl \rightarrow NHCl_2 + H_2O \quad (7.49)$$

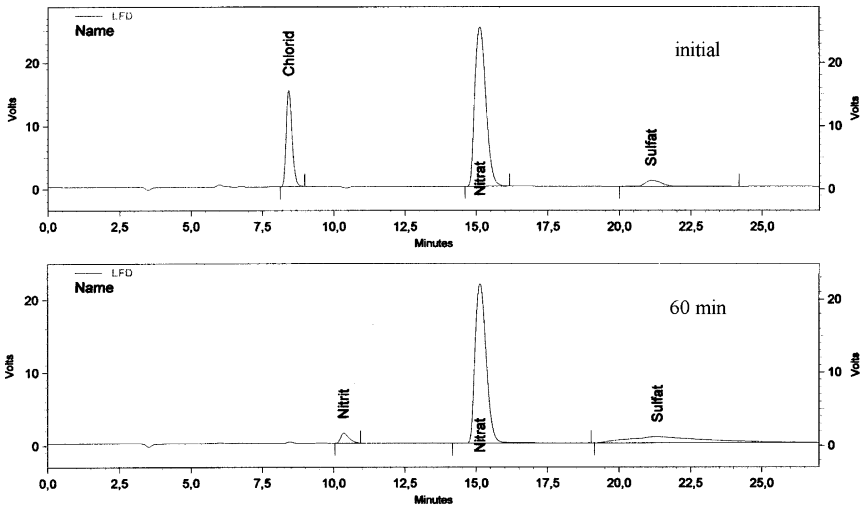

Fig. 7.14 Nitrite detection by IC electrolysing water in a discontinuous cell with rotating BDD anode (300 rpm, IrO_2 cathode, 100 mL, initial concentration 47 ppm nitrate + 9 ppm chloride as sodium salts, 20°C)

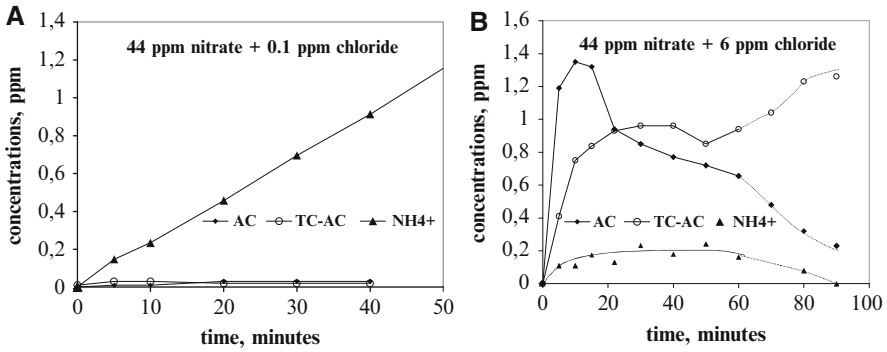

Fig. 7.15 Formation of active chlorine (AC), chloramines (TC-AC) and ammonium (NH^{4+}) in discontinuous electrolysis using MIO electrodes and varying initial chloride concentration (**a**) 0.1 ppm, (**b**) 6 ppm, rotating IrO_2/RuO_2 anode, 300 rpm, IrO_2 cathode, 300 A m^{-2}, 20°C; in experiment (**b**), current was switched off after 60 min

Chloramines were analysed in additional experiments by selective spectrophotometrical procedure (*HACH* method 10171). When the chloride concentration is nearly zero, de facto no chlorine or chloramines (measured as the difference between total and active chlorine) are visible. Ammonium is formed linearly in the cathodic reaction (A). In the second case B, active chlorine is consumed by the ammonium with chloramine formation. After switching off the electrolytic current, this reaction continues until all the chlorine is reacted.

Using BDD anodes and MIO cathodes, enrichment of ammonia was also observed – in contradistinction to other studies using higher ammonium concentration and an IrO_2 anode (Kim et al. 2005). In the combination of BDD anode/BDD cathode, nitrite was oxidised but only relatively slowly. When nitrate was electrolysed, its depletion was lower than 1 ppm for current densities lower than 200 A m^{-2}. An explanation for the relatively low reaction rate between radicals and nitrite is the assumption that ozone or radicals are consumed in faster reactions such as peroxide formation and chlorine oxidation. OH radicals are also able to oxidise chloramines (Huie et al. 2005).

Reactions of chlorine with radicals, hydrogen peroxide or ammonia lower the active chlorine efficiency. Nitrite in the presence of chlorate and perchlorate was found at 0.5 ppb by discontinuously electrolysing real drinking water using a BDD anode and an IrO_2 cathode. Consequently, for water systems such as nitrate/chloride, threshold conditions must exist for measurable active chlorine. This can be seen in Fig. 7.16. Active chlorine can only be detected by analytical means under concrete conditions when the initial chloride concentration is above approximately 10 ppm. The problems discussed here are relevant if the ammonium, chlorine and nitrite concentrations are in similar molaric concentrations. It is not very likely that a technical flow-through reactor produces ammonium, chloramines and nitrite in high quantities.

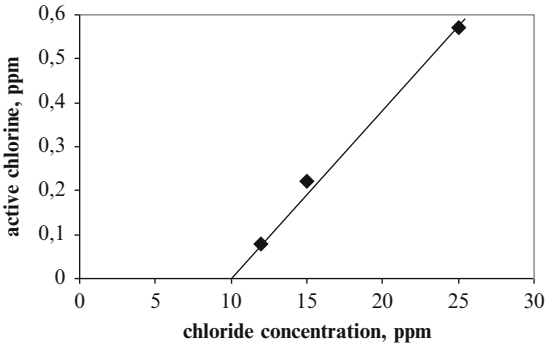

Fig. 7.16 One-minute analysis values of samples electrolysing water poor in chloride ions and varying the chloride concentration (cell with rotating BDD anode, 300 rpm, IrO_2 expended mesh cathode, 200 mA, 37 ppm nitrate + chloride as sodium salts, 160 mL, 20°C)

7.3.3.5 Formation of Reactive Oxygen Species

OH Radical, Hydrogen Peroxide and Ozone

For most types of mixed oxide electrodes, reactive oxygen species (ROS) formation is not predominant. For example, using IrO_2 and RuO_2 cathodes, H_2O_2 was measured with concentrations up to 0.3 ppm, only in chlorine-free waters and in non-divided cells, when dissolved oxygen was present (Bergmann 2005b). A series of other experiments using MIO anodes and adding H_2O_2 prior to the start of experiment showed only slight effects of electrochemical (anodic) H_2O_2 destruction.

As mentioned above water electrolysis on BDD anode leads to OH radical formation:

$$H_2O \rightarrow OH + H^+ + e \tag{7.50}$$

Unfortunately, in a very fast reaction (7.51) these radicals destroy themselves with the formation of peroxide (Hickling 1947) having a much lower oxidation potential.

$$2OH \rightarrow H_2O_2 \tag{7.51}$$

Figure 7.17 depicts the increase of H_2O_2 concentration during discontinuous electrolysis of water containing sodium sulphate. The conclusion can be drawn that the reaction zone in the vicinity of BDD should be reduced as much as possible to transport radicals faster to the bulk, or that an efficient reactor should have high ratios of electrode area to electrolyte volume. In a chlorine-free solution, the DPD test difference TC–AC follows the peroxide concentration pathway because H_2O_2 reacts slowly with I^-.

Another significant reaction on BDD anodes is the generation of ozone from OH (Babak et al. 1994; Michaud et al. 2003). Reduced solubility and high reactivity are responsible for the rare detection of ozone in the liquid phase. If ozone quickly disappears, radical formation from H_2O_2 and ozone in the bulk electrolyte [(7.52) and (7.53)] is negligible.

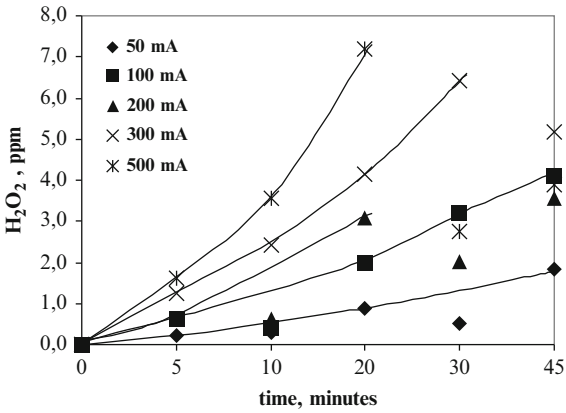

Fig. 7.17 Hydrogen peroxide formation in a discontinuous cell using parallel plate BDD electrodes and varying current density (650 mL, 240 ppm sulphate as sodium salt, 20°C)

$$2O_3 + H_2O \rightarrow 2OH + 3O_2 \tag{7.52}$$

$$H_2O_2 + 2O_3 \rightarrow 2OH + 3O_2 \tag{7.53}$$

The presence of OH radicals, H_2O_2 and O_3 must cause mechanisms known from photolysis, photocatalysis or ozonation (Langlais et al. 1991). New ROS such as O_3^-, O_2^-, O^-, HO_2, HO_3, HO_4 and others are possible; most of them are short lived. Interactions with chloride, carbonate, bicarbonate, sulphate and other ions may form longer lived radicals (Gottschalk et al. 2000; Le Truong et al. 2004). The discussion below makes it clear that there are many indications of OH radicals reacting with other ions.

Chloride ions are consumers of OH radicals whereas active chlorine may consume OH radicals, ozone and hydrogen peroxide. The mechanism of the peroxide reaction with active chlorine depends on the pH as summarised elsewhere (Blum 1989). Summary expressions are:

$$H_2O_2 + Cl_2 \rightarrow 2HCl + O_2 \tag{7.54}$$

$$H_2O_2 + HOCl \rightarrow HCl + H_2O + O_2 \tag{7.55}$$

and

$$HOCl + HO_2^- \leftrightarrow HOOCl + OH^- \tag{7.56}$$

for the case of HO_2^- presence (starting at pH = 7 – Held et al. 1978). The effect can be demonstrated when H_2O_2 is added to the chloride solution for electrolysis (Fig. 7.18).

If present, chlorine dioxide may react with H_2O_2 (Gordon 2001) such as the carbonate radical (Behar et al. 1970):

$$ClO_2 + H_2O_2 + 2OH^- \rightarrow 2ClO_2^- + O_2 + 2H_2O \tag{7.57}$$

$$CO_3^- + H_2O_2 \rightarrow HCO_3^- + HO_2 \tag{7.58}$$

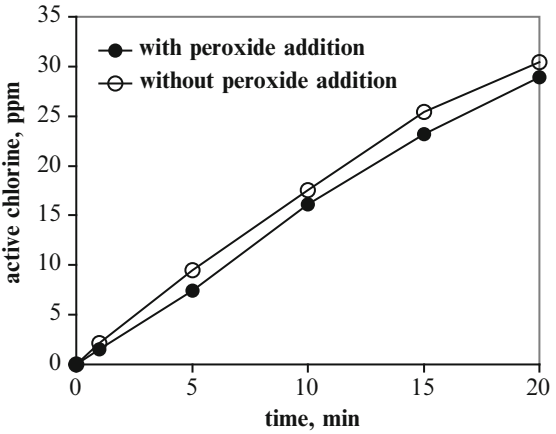

Fig. 7.18 Active chlorine formation in discontinuous cell using rotating MIO anode with and without pre-adding of H_2O_2 (30 rpm, IrO_2 cathode, 205 ppm sulphate + 2 ppm carbonate, sodium salts, pre-addition of 2.5 ppm H_2O_2 in the second experiment)

Percarbonates

As percarbonates components are often named as having the structure $2Na_2CO_3{\cdot}3H_2O_2$ which is in fact carbonate sesquiperhydrate. Percarbonates produced electrochemically differ from this. Peroxodicarbonate ($C_2O_6^{2-}$) was obtained on Pt from 0.14 M to 1.13 M carbonate solution in a first-order reaction (Zhang and Oloman 2005):

$$2CO_3^{2-} \rightarrow C_2O_6^{2-} + 2e \tag{7.59}$$

Hydrolysis gives hydrogen peroxide:

$$C_2O_6^{2-} + 2H_2O \rightarrow H_2O_2 + 2HCO_3^- \tag{7.60}$$

HCO_4^- is an intermediate in this process (Flanagan et al. 1986). Bicarbonate was oxidised using a BDD anode (Saha et al. 2004). Earlier work describes the OH radical reaction with carbonate and bicarbonate as scavengers (Hoigne and Bader 1977) and with rate constants between 10^6 and 10^7 in the form:

$$HCO_3^- + OH \rightarrow H_2O + CO_3^- \tag{7.61}$$

$$CO_3^{2-} + OH \rightarrow OH^- + CO_3^- \tag{7.62}$$

CO_3^- reacts with H_2O_2 to form HCO_3^- and HO_2 with a rate constant of 8×10^5.

By electrolysing carbonate and bicarbonate solutions in the ppm range, (Borutzky et al. 2006) no (using MIO anodes) and negligible (using BDD anode) disinfection activity was measured after adding the electrolysed solution to suspensions of microorganisms. Electrolysis samples analysed by DPD test showed low radical formation ("Wursters Red") so that a small amount of radical formation is likely.

Persulfates

The anodic formation of peroxodisulphate and peroxomonosulphate on Pt is a well-known process [(7.63) and (7.64); Oloman 1996].

$$2SO_4^{2-} - 2e \rightarrow S_2O_8^{2-} \tag{7.63}$$

$$S_2O_8^{2-} + H_2O \rightarrow SO_4^{2-} + SO_5^{2-} + 2H^+ \tag{7.64}$$

$$H_2S_2O_8 + H_2O \rightarrow H_2SO_5 + H_2SO_4 \tag{7.65}$$

Using BDD anodes peroxodisulphate was formed from highly concentrated sulphuric acid (Michaud et al. 2000; Serrano et al. 2002). No data exist on the oxidation of sulphate in drinking water. From our own experiments comparing MIO and BDD anodes in artificial drinking water (Borutzky et al. 2006) it was found that a clear disinfecting effect was reached only in the case when water containing 240 ppm sulphate was electrolysed at 300 A m^{-2} on BDD. Because the water was firstly electrolysed and then added to microorganisms it can be concluded that the disinfection effect is not related to short-lived OH radicals. A probable mechanism is the formation of sulphate radicals:

$$SO_4^{2-} + OH \rightarrow SO_4^{-} + OH^- \tag{7.66}$$

or, more probably,

$$2HSO_4^{-} + 2OH \longrightarrow S_2O_8^{2-} + 2H_2O \tag{7.67}$$

This mechanism is realistic considering the standard potentials of OH, H^+/H_2O – 2.59 V and SO_4^{-}/SO_4^{2-} – 2.43 *P*V (Wardman 1989). There are other indications for the existence of sulphate ion reaction products – a statistically slight decrease of sulphate concentration in discontinuous experiments and the higher formation of perchlorate and ClO_2 in our own experiments starting from chlorite (see also Fig. 7.13). In a recent publication (Polcaro et al. 2007), a superficial disinfection effect was observed when electrolysing chlorine-free water containing sulphate. Other researchers (Le Truong et al. 2004) observed an accelerating effect in sulphate containing waste when ferrous ions were oxidised by H_2O_2 (OH radicals). Thus, sulphate ions in drinking water electrolysis can be considered as reacting scavengers or precursors of mediators supporting the action of OH radicals to a certain extent.

7.3.3.6 The Role of Technology, Operation Mode and Geometric Factors

Many technological aspects have to be taken into consideration and classification is difficult. Some of the most important items in this discussion are:

- Cell operation mode
- The use of separators

– The cell location with respect to the main water stream
– Geometric peculiarities in electrode arrangement

The highest risk of by-product formation is given in discontinuous operation because both products and by-products are recirculated and able to take part in further electrode reaction processes. Accumulation effects at concentrations higher than those permitted are possible.

The use of separators (ion exchange membranes or diaphragms) has a series of advantages. First, the cathodic gas (hydrogen) is not added to the water and reduces the amount of gas in the treated water. Gas diffusion cathodes could remove this cathodic problem, but at higher costs, membrane handling, the catholyte cycle and deposits have prevented their application. Second, the formation of deposits on the cathode is reduced. These deposits are mostly based on the higher pH at the cathode and the favoured formation of carbonates (Kraft et al. 1999b; Gabrielli et al. 1999; Deslouis et al. 1998):

$$HCO_3^- + OH^- \rightarrow CO_3^{2-} + H_2O \tag{7.68}$$

$$Ca^{2+} + CO_3^{2-} \rightarrow CaCO_3 \tag{7.69}$$

The problem can theoretically be reduced when water is transported in a by-pass arrangement through the non-divided or divided cell (Fig. 7.19b, c) and by consecutive flow through anodic and cathodic cell compartments with a decreasing pH in the anolyte (Fig. 7.19d). Cell separation as shown in Fig. 7.19c usually supplies more HOCl than in a non-divided cell. The disinfection power of HOCl is higher than that of hypochlorite ions. But if disinfection continues over many minutes this advantage is reduced adding the catholyte too early to the anolyte.

In affected cells (Fig. 7.20a), deposits can be removed by changing electrode polarity. At low pH calcareous deposits dissolve (7.70)

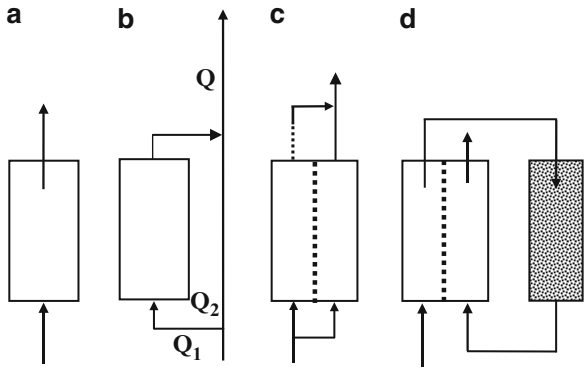

Fig. 7.19 Flow schemes of in-line electrolysis (**a**) single pass of total water stream, (**b**) by-pass arrangement, (**c**) divided cell with by-pass as catholyte, (**d**) divided cell with catalytic bed for product and by-product removal

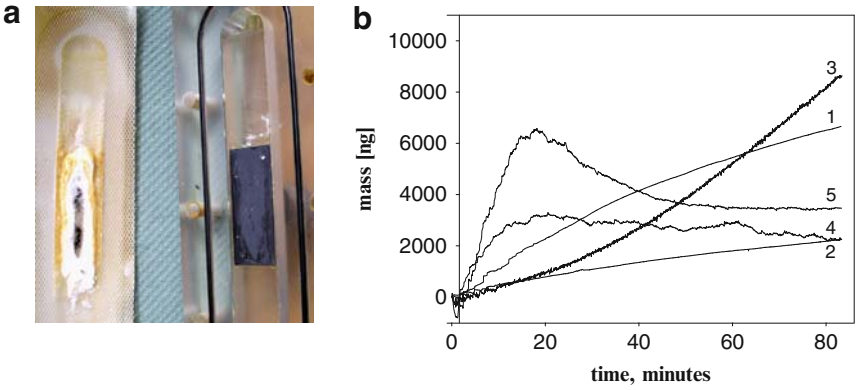

Fig. 7.20 (**a**) Opened half-cells with covered cathode (*left*). (**b**) Mass changes in nanogrammes on the mass balance cathode in waters of different composition [(1) saturated $CaCO_3$, (2) 240 ppm $CaSO_4$+ saturated $CaCO_3$, (3) 240 ppm Na_2SO_4 + $CaCO_3$, (4) saturated $Ca(OH)_2$, (5) saturated $Ca(OH)_2$+ saturated $CaCO_3$]

$$CaCO_3 + 2H^+ \rightarrow Ca^{2+} + CO_2 + H_2O \tag{7.70}$$

Rapid change of polarity damages electrode coating and reduces the lifetime. The period for polarity change depends on water hardness. Other ions such as Mg^{2+} may be involved in deposit formation. In general, different film formation can be considered such as deposits, floating hydroxide films and meta-stable gel-like phases (Barchiche et al. 2003; Kadyk 2005). Figure 7.20b reflects this. If evolving gas breaks off deposit particles from the surface, they can accumulate somewhere in the system. It is difficult to control deposit formation because current distribution focuses on non- or thinner-covered parts, finally covering all the surface (Fig. 7.20a). The efficiency of active species formation decreases in this case. The best method to control the process is the application of quartz microbalance technology (Gabrielli et al. 2002; Kadyk et al. 2006) but for practical purposes, this is too delicate.

Another problem is the by-pass mode (Fig. 7.19b) in discontinuous and continuous electrolysers. If the same amount of produced active chlorine is wanted, the cell in the by-pass regime has to supply a higher concentration, i.e. it has to work at higher current densities, thus increasing the formation of new by-products, because the electrode potential increases. The by-pass mode was simulated (Bergmann and Koparal 2004) assuming a constant current density mass-transfer limited reaction of chloride ions to active chlorine (this assumption is not correct for low chloride concentration between approximately 20 ppm):

$$Cl^- - ne \xrightarrow{\varphi_{\text{diff}}} \text{active chlorine} \tag{7.71}$$

With mass-transfer control, the differential current efficiency can be written:

$$\varphi_{\text{diff}} = k c_{Cl}. \tag{7.72}$$

The mass-balance equation for the ideally stirred reactor is

$$-Q_1\left(c_{\mathrm{Cl}}-c_{\mathrm{Cl}}^0\right)=\frac{Ikc_{\mathrm{Cl}}}{nF} \tag{7.73}$$

that gives (7.74)

$$c_{\mathrm{Cl}}=\frac{c_{\mathrm{Cl}}^0}{1+B} \tag{7.74}$$

with

$$B=\frac{Ik}{nFQ_1} \tag{7.75}$$

Calculating the resulting chloride concentration from (7.74)

$$c=\frac{Q_1c_{\mathrm{cl}}+Q_2c_{\mathrm{cl}}^0}{Q} \tag{7.76}$$

with the recirculation ratio

$$\alpha=\frac{Q_1}{Q} \tag{7.77}$$

one obtains

$$c=\frac{\alpha^2c_{\mathrm{Cl}}^0}{\alpha+B}+(1-\alpha)c_{\mathrm{Cl}}^0 \tag{7.78}$$

that gives results presented in Table 7.2 using an initial concentration of 100 ppm chloride and a set of typical parameters (Bergmann and Koparal 2004). The calculated chloride depletion is proportional to the formed active chlorine.

The maximum depletion of 0.95 is reached when all water is flowing through the cell, comparative calculation of plug flow reactor model would result in a value of 0.912. It is interesting that even for $\alpha = 0.25$ a sufficiently high depletion can be established. For lower recirculation ratios, the active chlorine amounts significantly drop. The calculation shows the possibility of optimisation but knowledge of the parameter k_{Cl} is necessary. Additional limitations are national rules for allowed concentration values in the dosage point making the picture still more complicated.

Variant D in Fig. 7.19 is known from company presentations and describes the production of highly acidic acolytes and the removal of disinfection products and

Table 7.2 Chloride depletion ration related to inlet concentration varying the recirculation rate ($c_{\mathrm{Cl}}^0 = 100$ ppm)

α	0	0.01	0.1	0.25	0.5	0.75	1
Ratio c_{result} to c_{Cl}^0	1	0.9916	0.9655	0.9565	0.9524	0.9508	0.95

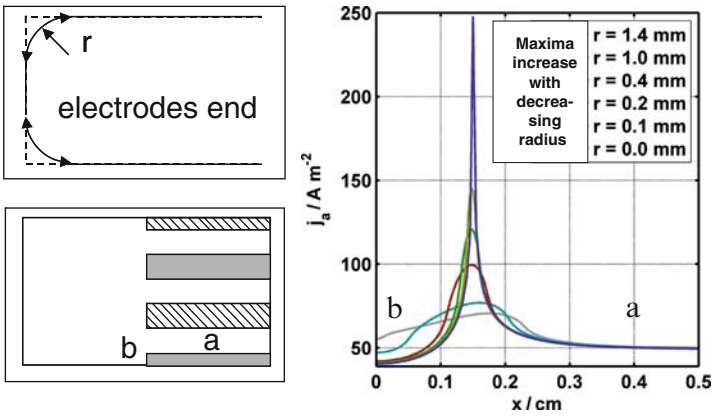

Fig. 7.21 Influence of edge rounding radius on the secondary current density distribution along the surface of plate electrode (parameter x) between location a and b (kinetics obtained from regional tap water study, $c_{Cl^-} = 47$ ppm, average current load $-50\,A\,m^{-2}$; calculated cell voltage for all radius nearly constant value of 6.04 V, electrolyte conductivity $667\,\mu S\,cm^{-1}$).

by-products by adding a catalytic bed into the flow scheme of treated water. No real data are available. Variants with separate catholyte cycles are not shown in Fig. 7.19.

Geometric parameters may influence the current distribution over electrodes. Electrodes in a technical cell are typically arranged in parallel, forming monopolar or bipolar stack constructions. However, slight deviations from parallelism are possible. Furthermore, at least in the flow direction, plate electrodes have open surfaces with a more or less sharp edge profile. And finally, cell producers not only use plate electrodes but also use expanded mesh constructions known for having distributed potential, current density and concentration parameters. Some of these geometric structures were recently modelled using a Femlab simulation system (Kodym et al. 2005, 2006).

The edge-based maxima in Fig. 7.21 demonstrate how these places may function at a clearly higher current density (and by-product formation) compared with the average current density. Thus, edge rounding is a sophisticated method of lowering the risk.

7.3.3.7 Analytical Problems

It was demonstrated that water electrolysis generates mixed oxidant systems. Oxidation–reduction potential (Hsu and Kao 2004) is not the best parameter for system characterisation. In general, the online analysis of generated species is an unsolved problem. Probably, not all electrolysis products are known. This can be seen in analysing the active and total chlorine concentration. The standard method uses DPD but the effect of other chemicals on the DPD method is one reason that active chlorine is sometimes incorrectly measured. Amperometric analysis and

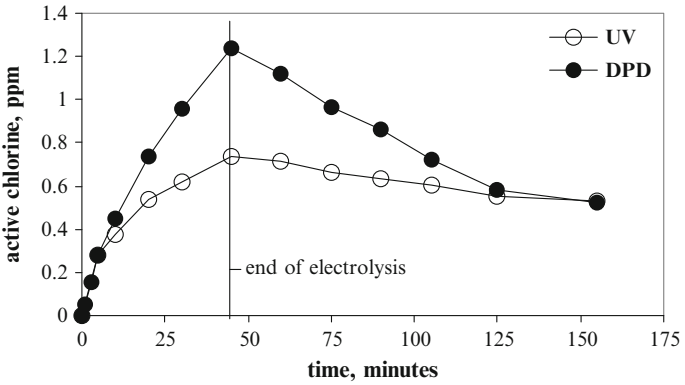

Fig. 7.22 Analysis values of active chlorine in discontinuous experiments using discontinuous parallel plate cell with MIO electrodes. Samples were analysed by DPD and in parallel by UV spectrophotometry after shifting pH to high values by adding 25 µl 2 M NaOH to the 50-mm cuvette (150 mA, 240 ppm sulphate + 25 ppm chloride as sodium salts, 20°C)

iodometric titration are also known for giving incorrect results. The problem was analysed for MIO electrode application in a special publication (Bergmann 2006d). The results can be summarised as follows. DPD methods give increased active chlorine values compared with UV measurement. Amperometric sensors show lower measured values when calcareous deposits cover the electrodes in non-divided cells. The differences between the DPD method and UV spectrum measurements disappear within 1 h after switching off the discontinuous electrolysis (Fig. 7.22).

The ClO_2 values measured by different methods are too small to explain these differences. The differences are higher when the ionic strength is lower. When chloride–sulphate waters are electrolysed, the difference is highest at the lowest sulphate concentration. The difference between the measured total chlorine value and the active chlorine values are additional indicators that components differing from active chlorine species are present.

Obviously, chlorine species are responsible for incorrect measurement if ozone can be excluded. It was speculated that complexes or chlorine oxides such as Cl_2O might be parts of the solution (Beach and Margerum 1990):

$$2HOCl \leftrightarrow Cl_2O \cdot H_2O \tag{7.79}$$

or

$$Cl_2 + HOCl \rightarrow Cl_2O + H^+ + Cl^- \tag{7.80}$$

Many other oxychlorine species are discussed in the literature as possible intermediates in chlorine or chlorite reactions (Cheng and Kelsall 2007). Time-consuming procedures are suggested for the analysis of chlorine–oxygen species typical for chlorine disinfection (Hong and Rapson 1968; Adam and Gordon 1995, White 1999). Ion-selective electrodes are not recommended as our own experience showed.

7.4 Conclusions

In different electrochemical and chemical reactions many inorganic by-products can be formed. A prediction is not possible if the electrolysis conditions are not studied in detail.

The use of doped diamond electrodes is a serious problem because radicals are generated reacting at high reaction rates relatively non-specifically. The risk of forming chlorates, perchlorates and peroxocompounds necessitates discussion by developers and applicants.

There is a suspicion that not all by-products have yet been identified. Incorrect measurement of active chlorine can, in principle, only be explained by the presence of disinfection by-products.

It is strongly recommended, that testing routines are developed and introduced before in-line electrolysers are allowed to be used in practice.

Acknowledgements The author wishes to thank all colleagues and co-workers, which were involved in experiments and discussions. In particular, these thanks are directed to Prof. Johanna Rollin, Dr. Andreas Rittel, Dr. Tatiana Iourtchouk, Dr. Kristin Schoeps, Christine Hummel, Karsten Kresse, Thomas Kadyk, Christian Czichos, Uta M. Borutzky and Renate Zinke (all from Anhalt University Koethen), Prof. Ü. Öütveren, Dr. A. Savas Koparal, Dr. A. Tansu Koparal and Özge Tümöz (Anadolu University Eskisehir), Prof. Karel Bouzek, and Roman Kodym (Institute of Chemical Technology Prague), Dr. F. Ehrig (BAFZ Quedlinburg), to DAAD and Anhalt University for financial support and to German BMBF/AIF Cologne for project organisation – FKZ 1721X04.

List of Symbols, Indices, and Abbreviations

AC	Active chlorine	ppm
B	Constant	
BDD	Boron-doped diamond	
c	Concentration	ppm
Cl, Cl^-	Chloride ion	
diff	Differential	
diss	Dissolved	
D	Coefficient of diffusion	$m^2\ s^{-1}$
DBP	Disinfection by-product	
DPD	N,N-diethyl-p-phenylendiamine	
DSA	Dimensionally stable anodes	
F	Faraday constant	$As\ mol^{-1}$
IC	Ion chromatography	
J	Component j	
k	Constant in (7.69)	$m\ s^{-1}$
K, k	Mass-transfer coefficients	$L\ mol^{-1}$

MIO	Mixed oxide	
MO	Microorganism suspension	
n	Number of electrons	$\mathrm{mol\,s^{-1}\,m^{-2}}$
N	Molaric flux	
ROS	Reactive oxygen species	
rpm	Revolutions per minute	
SHE	Standard hydrogen electrode	
TC	Total chlorine	ppm
t_{tr}	Treatment time	min, h
Q	Volumetric flow rate	$\mathrm{m^3\,s^{-1}}$
V	Volume	$\mathrm{m^3}$
w	Velocity	$\mathrm{m\,s^{-1}}$
x	Coordinate	m
z	Charge number	
α	Recirculation ratio	
Λ	Equivalent ionic conductivity	$\mathrm{m^2\,A\,V^{-1}\,mol^{-1}}$
Φ	Electrical potential	V
Φ	Current efficiency	
0	Initial or inlet value	

References

Adam, L.C. and Gordon, G. (1995) Direct and sequential potentiometric determination of hypochlorite, chlorite, and chlorate ions when hypochlorite ion is present in large excess. Anal. Chem. 67, 535–540.

Adam, L.C., Fabian, I., Suzuki, K. and Gordon, G. (1992) Hypochlorous acid decomposition in the pH 5–8 region. Inorg. Chem. 31, 3534–3541.

Adams, L. and Gordon, G. (1999) Hypochlorite ion decomposition: Effects of temperature, ionic strength, and chloride ion. Inorganic. Chem. 38, 1299–1304.

Arikawa, T., Murakami, Y. and Takasu, Y. (1998) Simultaneous determination of chlorine and oxygen evolving at RuO_2/Ti and RuO_2–TiO_2/Ti anodes by different electrochemical mass spectroscopy. J. Appl. Electrochem. 28, 511–516.

Babak, A.A., Amadelli, R., De Battisti, A. and Fateev, V.N. (1994) Influence of anions on oxygen/ozone evolution on PbO_2/spe and PbO_2/Ti electrodes in neutral pH media. Electrochim. Acta 39, 1597–1602.

Barchiche, Ch., Deslouis, C., Festy, D., Gil, O., Refait, Ph., Touzain, S. and Tribollet, B. (2003) Characterization of calcareous deposits in artificial seawater by impedance techniques. 3-Deposit of $CaCO_3$ in the presence of Mg(II). Electrochim. Acta 48, 1645–1654.

Beach, M.W. and Margerum, D.W. (1990) Kinetics of oxidation of tetracyanonickelate(II) by chlorine monoxide, chlorine, and hypochlorous acid and kinetics of chlorine monoxide formation. Inorg. Chem. 29, 1225–1232.

Behar, D., Czapski, G. and Duchovny, I. (1970) Carbonate radical in flash photolysis and pulse radiolysis of aqueous carbonate solutions. J. Phys. Chem. 74, 2206–2210.

Bergmann, M.E.H. (2005a) About the chlorine dioxide formation during electrochemical drinking water disinfection (in German). GWF Wasser Abwasser 146, 126–133.

Bergmann, H., Iourtchouk, T., Schoeps, K. and Ehrig, F. (2001) What is the so-called anodic oxidation and what can it do? (in German). GWF Wasser Abwasser 142, 856–869.

Bergmann, H., Iourtchouk, T., Schoeps, K. and Bouzek, K. (2002) New UV irradiation and direct electrolysis-promising methods for water disinfection. J. Chem. Eng. 85, 111–117.

Bergmann, H. and Koparal, A.S. (2004) The flow-through technology of disinfecting drinking and technical waters (in German) part 2. Galvanotechnik 95, 3037–3043.

Bergmann, M.E.H. (2005a) On the chlorine dioxide formation during electrochemical drinking water disinfection (in German). GWF Wasser Abwasser 146, 126–133.

Bergmann, M.E.H. (2005b) The formation of H2O2 in drinking water electrolysis. 56th Annual Meeting of the International Society of Electrochemistry – Busan, Korea, September 26–30, *Book of Abstracts*, p. 892.

Bergmann, H. and Koparal, A.S. (2005c) Problems of chlorine dioxide formation during electrochemical disinfection. Electrochim. Acta 50, 5218–5228.

Bergmann, M.E.H. and Koparal A.S. (2005d) Studies on electrochemical disinfectant production using anodes containing RuO2. J. Appl. Electrochem. 35, 1321–1329 and Erratum (2006) 36, 845–846.

Bergmann,M.E.H. and Koparal, A.S. (2006a) Chlorine dioxide formation from chloride and chlorite solutions of very low concentrations. Industrial Water, Frankfurt, 6–8 February 2006, *Book of Abstracts*, pp. 181–185.

Bergmann, M.E.H., Rollin, J., Koparal, A.S. and Kresse, K. (2006b) What is the ominous chlorine consumption in the disinfectant production from drinking water electrolysis? *Proceedings 57th Annual Meeting of the International Society of Electrochemistry, 27 Aug. to 1 Sept., Edinburgh/UK*, p. S5.O-4.

Bergmann, H. and Rollin, J. (2006c) Product and by-product formation using doped diamond anodes in disinfection electrolysis of drinking water. 1. European Conference on Environmental Application of Advanced Oxidation Processes (EAAOP), Chania/Greece, *Conference Materials Full text version* P198, pp. 1–6 and *Book of Abstracts*, p. 218.

Bergmann, M.E.H. (2006d) On DPD method application for drinking water disinfection analysis (in German). GWF Wasser Abwasser 147, 780–786.

Bergmann, M.E.H. (2007a) On the electrochemical flow-through electrolysis for the production of waters with disinfecting ability (in German). In: Suchentrunk, R. (ed.) *Jahrbuch fuer Oberflaechentechnik*, Leuze, Saulgau, pp. 315–330.

Bergmann, H., Rollin, J., Czichos, C. and Roemer, D. (2007b) Perchlorate analysis in drinking water electrolysis-a new application for Ion Chromatography (in German). Labo, 26–28.

Bergmann, M.E.H., Koparal, A.T., Koparal, A.S., Schoeps, K., Iourtchouk, T. and Ehrig, F. (2008) The influence of products and by-products obtained by drinking water electrolysis on microorganisms. Microchem. Journ. 89, 98–107.

Bergmann, M.E.H., Rollin, J. and Iourtchouk, T. (2009) The occurrence of perchlorate during drinking water electrolysis using BDD electrodes. Electrochim. Acta 54, 2102–2107.

Bernarde, M.A., Snow, W.B. and Olivieri, P. (1967) Kinetics and mechanism of bacterial disinfection by chlorine dioxide. Appl. Microbiol. 15, 257–265.

Blum, E. (1989) Studies on chemical disinfection reactions using hydrogen peroxide and chlorine in drinking water treatment, PhD Thesis, KfK 4619, Kernforschungszentrum Karlsruhe.

Borutzky, U., Bergmann, H. and Junghannss, U. (2006) Disinfection ability of drinking water treated by electrolysis using doped diamond electrodes, Proceedings 1. European Conference on Environmental Application of Advanced Oxidation Processes (EAAOP), Chania/Crete (Greece), *Book of Abstracts*, p. 229 and *CD full text version* P207, pp. 1–6.

Bouzek, K., Bergmann, H. and Paidar (2003) Nitrate removal from drinking and process water (in German). In ALPHA Informationsgesellschaft GmbH (ed.) *Handbuch Umweltwissenschaften*, *Ausgabe 2003/2004*, Lampertheim, pp. 81–89.

Burke, M., Tenney, J., Indu, B., Hoq, M.F., Carr, S. and Ernst, W.R. (1993) Kinetics of hydrogen peroxide-chlorate reaction in the formation of chlorine dioxide. Ind. Eng. Chem. Res. 32, 1449–1456.

Carlson, S. (1991) Fundamentals of water disinfection, J. Water SRT-Aqua 40, 346–356.

Cheng, C.Y. and Kelsall, G.H. (2007) Models of hypochlorite production in electrochemical reactors with plate and porous electrode. J. Appl. Electrochem. 37, 1203–1217.
Cho, J., Choi, H., Kim, I.S. and Amy, G. (2001) Chemical aspects and by-products of electrolyser. Water Sci. Technol. Water Supply 1, 159–167.
Cho, E.-I., Kim, G.-S., Park, J.-E. and Park, S.-G. (2005) Ozone generation with boron-doped diamond electrodes and its application. In: Fushima, A. and co-ed. *Diamond Electrochemistry*, Elsevier, Amsterdam, pp. 502–524.
Christensen, E. and Giese, A.C. (1954) Changes in absorption spectra of nucleic acids and derivatives following exposure to ozone and ultraviolet radiation. Arch. Biochem. Biophys. 51, 208–216.
Crayton, C., Camper, A. and Warwood, B. (1997) Evaluation of mixed oxidants for the disinfection and removal of biofilms from distribution systems, *Proceedings of the American Water Eorks Association Water Quality Technology Conference*, 3A6/1–3A6/17.
Damjanovic, A. (1992) Progress in the studies of oxygen reduction during the last thirty years. In: Murphy, O.J., Srinivasan, S. and Conway, B.E. (eds.) *Electrochemistry in Transition*, Plenum, New York, NY, pp.107–146.
D'Ans, J. and Freund, H.E. (1957) Kinetic studies 1. About the formation of chlorate from hypochlorite (in German). Zeitschrift fuer Elektrochemie 61, 10–18.
Dasgupta, P.K., Martinelango, P.K., Jackson, W.A., Anderson, T.A., Tian, K., Tock, R.W. and Rajagopalan, S. (2005) The origin of naturally occurring perchlorate: The role of atmospheric processes. Environ. Sci. Technol. 39, 1569–1575.
Deslouis, C., Festy, D., Gil, O., Ruis, G., Touzain, S. and Tribollet, E. (1998) Characterization of calcereous deposits in artificial sea water by impedance techniques-I. Deposit of CaCO3 without Mg(OH)2. Electrochim. Acta 43, 1891–1901.
Diao, H.F., Li, X.Y., Gu, J.D., Shi, H.C. and Xie, Z.M. (2004) Electron microscopic investigation of the bactericidal action of electrochemical disinfection in comparison with chlorine, ozonation and Fenton reaction. Process Biochem. 39, 1421–1426.
Drogui, P., Elmaleh, S., Rumeau, M., Bernard, C. and Rambaud, A. (2001) Hydrogen peroxide production by water electrolysis: Application to disinfection. J. Appl. Electrochem. 31, 877–882.
Duo, I. (2003) Control of electron transfer kinetics at boron-doped diamond electrodes by surface modification, PhD Thesis, Ecole Polytechnique Federale Lausanne.
Duo, I., Michaud, P.A., Haenni, W., Perret, A. and Comninellis, Ch. (2000) Activation of boron-doped diamond with IrO2 clusters. Electrochem. Solid-State Lett. 3, 325–326.
Emmenegger, F. and Gordon, G. (1967) The rapid interaction between sodium chlorite and dissolved chlorine. Inorg. Chem. 6, 633–635.
Ferro, S., De Battisti, A., Duo, I., Comninellis, Ch., Haenni, W. and Perret, A. (2000) Chlorine evolution at highly boron-doped diamond electrodes. J. Electrochem. Soc. 147, 2614–2619.
Flanagan, J., Jones, D.P., Griffith, W.P., Skapski, A.C. and West, A.P. (1986) On the existence of peroxocarbonates in aqueous solution. J. Chem. Soc. Chem. Commun. 1, 20–21.
Foerster, H.J., Thiele, W., Fassler, D. and Guenter, K. (2002) Comparative investigation on hypochlorite formation on platinum and diamond electrodes. New Diam. Front. Carbon Technol. 12, 99–105.
Foti, G., Gandini, D., Comninellis, Ch., Perret, A. and Haenni, W. (1999) Production of oxidants on diamond electrodes. Electrochem. Solid-State Lett. 2, 228.
Fryda, M., Matthee, T., Mulcahy, S., Hampel, A., Schaefer, L. and Troester, I. (2003) Fabrication and application of Diachem® electrodes. Diam. Relat. Mater. 12, 1950–1965.
Gabrielli, C., Maurin, G., Perrot, H., Poindessous, G. and Rosset, R. (2002) Investigation of electrochemical calcareous scaling potentiostatic current- and mass–time transients. J. Electroanal. Chem. 538/539, 133–143.
Gainer, J.L., Kirwan, D.L. and Stoner, G.E. (1975) Enzymatic and electrochemical disinfection of pathogens in air and water. *Technical Report*, Nat Sci. Found. Res. Appl. Nat. Needs NSFR/RA (U.S.), pp. 48–54.
Gates, D.J. (1998) *The Chlorine Dioxide Handbook*, American Water Works Association, Denver.
Gordon, G. (2001) Is all chlorine dioxide created equal? J. AWWA 93, 163–174.

Gordon, G. and Emmenegger, F. (1966) Complex ion formation between ClO2 and ClO2–. Inorg. Nucl. Chem. Lett. 2, 395–398.
Gordon, G. and Tachiyashiki, S. (1991) Kinetics and mechanism of formation of chlorate ion from the hypochlorous acid/chlorite ion reaction at pH 6–10. Environ. Sci. Technol. 25, 468–474.
Gordon, G., Gauw, R., Emmer, G. and Bubnis, B. (1998) The kinetics and mechanism of ClO3- formation following the electrolysis of salt brine: What role do ClO2 and/or O3 play? ACH-Models Chem. 135, 799–809.
Gordon, G., Bolden, R. and Emmert, G. (2002) Measuring oxidant species in electrolysed salt brine solutions. J. AWWA 94, 111–120.
Gottschalk, C., Libra, J.A. and Saupe, A. (2000) Ozonation of water and waste water, Wiley-VCH, Weinheim.
Grebenjuk, V.D., Korchak, G.I., Sobolevskaja, T.T., Konovalova, I.D., Aksilenko, H.D. and Atamanov, M.Yu. (1990) Electrochemical detoxification (in Russian). Khim. Technol. Vody 12, 78–80.
Gu, B., Coates, J. D. (Eds.), *Perchlorate, Environmental Occurrence, Interactions and Treatment*. Springer, Berlin 2006.
Gutknecht, J., Hartmann, F., Kirmaier, N., Reis, A. and Schoeberl, M. (1981) Anodic Oxidation as a water disinfecting process in food plants and breweries (in German). GIT Fachz. Lab. 25, 472–481.
Gyürek, B.L. and Finch, G.R. (1998) Modeling water treatment chemical disinfection kinetics. J. Environ. Eng. 124, 783–793.
Haas, C.N. (1990) Disinfection. In: Pontius FA (ed.), *Water Quality and Treatment, A Handbook of Community Water Supplies*, 4th ed., Chapter 14, Technical editor, American Water Works Association, New York, NY.
Haenni, W., Gobet, J., Perret, A., Pupunat, L., Rychen, P., Comninellis, C. and Corea, B. (2002) Loop-controlled production of chlorine for disinfection of pool water using boron-doped diamond electrodes. New Diam. Front. Carbon Technol. 12, 83–88.
Hamelin, C. and Chung, Y.S. (1978) Role of the pol, rec, and dna gene products in the repair of lesions produced Escherichia coli DNA by ozone. Stud. Biophys. 68, 229–235.
Hamelin, C. and Chung, Y.S. (1989) Repair of ozone-induced DNA lesions in *Escherichia coli* B cells. Water Res. 214, 253–255.
Hamm, B. (2002) Disinfection by-product reduction using on-site generated mixed oxidants in groundwater treatment. Water Cond. Purif. 44, 24–27.
Held, A.M., Halko, D.J. and Hurst, J.K. (1978) Mechanisms of chlorine oxidation of hydrogen peroxide. J. Am. Chem. Soc. 100, 5732–5740.
Hernlem, B.J. and Tsai, L.-S. (2000) Chlorine generation and disinfection by electroflotation. J. Food Sci. 65, 834–837.
Hickling, A. (1947) Some anomalies in the concept of electrode potential as the determining factor in the occurrence of anodic reactions. Disc. Faraday Soc. 1, 227–229.
Hoell, K.(ed.) (2002) *Wasser*, Walter de Gruyter, Berlin, p. 610.
Hoigne, J. and Bader, H. (1977) Influence of Carbonate on the oxidation ability of ozone and OH radicals (in Germ). Vom Wasser 48, 283–304.
Hong, C.C. and Rapson, W.H. (1968) Analysis of chlorine dioxide, chlorous acid, chlorite, chlorate, and chloride in composite mixtures. Can. J. Chem. 46, 2061–2064.
Hsu, S.-Y. and Kao, H.-Y. (2004) Effects of storage conditions on chemical and physical properties of electrolysed oxidizing water. J. Food Eng. 65, 465–471.
Huie, R.E., Poskrebyshev, G.A. and Neta, P. (2005) Reactions of monochloramine with *OH and e-aqu and subsequent reactions of *NH2 and *NHCl with O2. *Proceedings Annual Meeting of the ACS*, Division of Environmental Chemistry, Washington, pp. 472–474.
Hupert, M., Muck, A., Wang, J., Stotter, J., Cvackova, Z., Haymond, S., Show, Y. and Swain, G.M. (2003) Conductive diamond thin-films in electrochemistry. Diam. Relat. Mater. 12, 1940–1949.
Internet presentation (2005) *Advanced systems for substrate sterilization*. http://www.substrate-tech.com/producers.html (access 21. Feb. 2005).

Ishizaki, K., Sawadaishi, K., Miura, K. and Shinriki, N. (1987) Effect of ozone on plasmid DNA of *Eschericha coli in situ*. Water Res. 21, 823–827.

Izumi, H. (1999) Electrolysed water as a disinfectant for fresh-cut vegetables. J. Food Sci. 64, 536–539.

Jackson, A., Arunagiri, S., Tock, R., Anderson, T. and Rainwater, K. (2004) Technical note: Electrochemical generation of perchlorate in municipal drinking water systems. J. AWWA 96, 103–108.

Jeong, J., Kim, C. and Yoon, J. (2009) The effect of electrode material on the generation of oxidants and microbial inactivation in the electrochemical disinfection processes. Wat. Res. 43, 895–901.

Junli, H., Li., Nanqi, R. and Fang, M.A. (1997) Disinfection effect of chlorine dioxide on bacteria in water. Water. Res. 31, 607–613.

Kadyk, T. (2005) Diploma thesis: Comparative analysis of measuring techniques to investigate the scaling of the cathode indirect water disinfection electrolysis, Department 6, Anhalt University, Koethen/Germany.

Kadyk, T., Bergmann, M.E.H. and Bouzek, K. (2006) Comparative analysis of measuring techniques to investigate the scaling of the cathode in direct water disinfection electrolysis, *Proceedings 57th Annual Meeting of the International Society of Electrochemistry, 27 Aug. to 1 Sept., Edinburgh, UK*.

Katsuki, N., Takahashi, E., Toyoda, M., Kurosu, T., Iida, M., Wakita, S., Nishiki, Y. and Shimamumune (1998) Water electrolysis using diamond thin-film electrodes. J. Electrochem. Soc. 145, 2358–3262.

Kerwick, M.I., Reddy, S.M., Chamberlain, A.H.L. and Holt, D.M. (2005) Electrochemical disinfection, an environmentaly acceptable method of drinking water disinfection? Electrochim. Acta 50, 5270–5277.

Kim, K.-W., Lee, E.-E., Kim, J.-S., Shin, K.-H. and Jung, B.-I. (2002) Material and organic destruction characteristics of high temperature-sintered RuO2 and IrO2 electrodes. J. Electrochem. Soc. 149, D187–D192.

Kim, K.-W., Kim, Y.-J., Kim, I.-T., Park, G.-I. and Lee, E.-H. (2005) The electrolytic decomposition mechanism of ammonia to nitrogen at an IrO2 anode. Electrochim. Acta 50, 4356–4364.

Kirk-Othmer (1979) *Encyclopedia of Chemical Technology*, 3.ed., vol. 5, Wiley, New York, NY.

Kirmaier, N. and Schoberl, M. (1980) The anodic oxidation a new practical method for water disinfection (in German). GIT Fachz. Lab. 24, 443–455.

Kirmaier, N., Hose, G.H. and Reis, A. (1984) Theory, process engineering and practical results of anodic oxidation, Neue Deliwa-Zeitschrift 35, 260–266.

Klaening, U.K. and Wolff, T. (1985) Laser flash photolysis of HOCl, ClO-, HBrO and BrO- in aqueous solution. Reaction of Cl- and Br- ions. Ber. Bunsenges. Phys. Chem. 89, 243–245.

Kodym, R., Bergmann M.E.H. and Bouzek, K. (2005) First results of modelling geometry factors in electrolysis cells for direct drinking water disinfection. *Proceedings 56th Annual Meeting of the International Society of Electrochemistry, September 26–30, Busan/Korea*, p. 896.

Kodym, R., Bergmann, H. and Bouzek, K. (2006) Results of modelling electrodes and reactors for the direct electrochemical drinking water electrolysis. *Proceedings 57th Annual Meeting of the International Society of Electrochemistry, 27 Aug. to 1 Sept., Edinburgh/UK*, p. S5-P16.

Kraft, A., Stadelmann, M., Blaschke, M., Kreysig, D., Sandt, B. and Schroeder, F. (1999a) Electrochemical water disinfection, part I: Hypochlorite production from very dilute chloride solutions. J. Appl. Electrochem. 29, 861–868.

Kraft, A., Blaschke, M., Kreysig, D., Sandt, B., Schroeder, F. and Rennau, J. (1999b) Electrochemical water disinfection. Part II: Hypochlorite production from potable water, chlorine consumption and the problem of calcareous deposits. J. Appl. Electrochem. 29, 895–902.

Kraft, A., Wuensche, M., Stadelmann, M. and Blaschke, M. (2003) Electrochemical water disinfection. Recent Res. Dev. Electrochem. (India) 6, 27–55.

Krasner, S.W., McGuire, M.J., Jacangelo, J.G. and Patania, N.L. (1989) The occurrence of disinfection by-products in U.S. drinking water. J. AWWA 81, 41–53.

Krstajic, N., Nakic, V. and Spasojevic, M. (1987) Hypochlorite production. I. A model of the cathodic reactions. J. Appl. Electrochem. 17, 77–81.

Kuhn, A.T. (1971) *Industrial Electrochemical Processes*, Elsevier, Amsterdam.

Kuhn, A.T., Hamzah, H. and Collins, G.C.S. (1980) The inhibition of the cathodic reduction of hypochlorite by films deposited at the cathode surface. J. Chem. Technol. Biotechnol. 30, 423–428.

Langlais, B., Reckhow, D.A. and Brink, D.R. (1991) *Ozone in Water Treatment-Application and Engineering*, Lewis Publishers, Boca Raton, FL.

Lehmann, T. (2002) DE-OS 102 58 652 A1 (German Patent Application).

Le Truong, G., De Laat, J. and Legube, B. (2004) Effect of chloride and sulfate on the rate of oxidation of ferrous ion by H2O2. Water Res. 38, 2384–2394.

Leyer, G.J. and Johnson, E.A. (1997) Acid adaptation sensitizes Salmonella typhimurium to hypochlorous acid. Appl. Environ. Microbiol. 63, 461–467.

Markitanova, L.I. and Zenin, G.S. (1990) Mechanism of inactivation of coliform bacteria during electrochemical treatment of water (in Russ.). Khim. Technol. Vody (Leningrad) 12, 658–661.

Marselli, B., Garcia-Gomez, J., Michaud, P.-A., Rodrigo, M.A. and Comninellis, Ch. (2003) Electrogeneration of hydroxyl radicals on boron doped diamond electrodes. J. Electrochem. Soc. 150, D79–D83.

Matsunaga, T., Namba, Y. and Nakajima, T. (1984) Electrochemical sterilization of microbial cells. Bioelectrochem. Bioenerg. 13, 393–400.

Matsunaga, T., Nakasono, S., Takamura, T., Burgess, J.G., Nakamura, N. and Sode, K. (1992a) Disinfection of drinking water by using a novel electrochemical reactor employing carbon-cloth electrodes. Appl. Environ. Microbiol. 58, 686–689.

Matsunaga, T., Nakasono, S. and Masuda, S. (1992b) Electrochemical sterilization of bacteria adsorbed on granular activated carbon. FEMS Microbiol. Lett. 93, 255–260.

Matsunaga, T., Nakasono, S., Kitajima, Y. and Horiguchi, K. (1994) Electrochemical disinfection of bacteria in drinking water using activated carbon fibers. Biotechnol. Bioeng. 43, 429–433.

Matsunaga, T., Okochi, M., Takahashi, M., Nakayama, T., Wake, H. and Nakamura, N. (2000) TiN electrode reactor for disinfection of drinking water Water Res. 34, 3117–3122.

Michaud, P.-A., Mahe, E., Haenni, W., Perret, A. and Comninellis, Ch. (2000) Preparation of peroxodisulfuric acid using boron-doped diamond thin film electrodes. Electrochem. Solid-State Lett. 3, 77–79.

Michaud, P.-A., Panniza, M., Quattara, L., Diaco, T., Foti, G. and Comninellis, Ch. (2003) Electrochemical oxidation of water on boron-doped diamond thin film electrodes. J. Appl. Electrochem. 33, 151–154.

Natishan, P.M. (1984) The use of composite electrodes for the electrochemical disinfection of recirculating fluids. PhD thesis, Faculty of the School of Engineering and Applied Science, University of Virginia.

Oloman, C. (1996) *Electrochemical Processing for the Pulp and Paper Industry*, The Electrochemical Consultancy, Underhill.

Palacios, M., Pampillon, J.F. and Rodriguez, M.E. (2000) Organohalogenated compounds levels in chlorinated drinking water and current compliance with quality standards throughout the European Union. Water Res. 34, 1002–1016.

Pareilleux, A. and Sicard, N. (1970) Lethal effects of electric current on *Echerichia coli*. Appl. Environ. Microbiol. 19, 421–424.

Patermarakis, G. and Fountoukides, E. (1990) Disinfection of water by electrochemical treatment, Water Res. 24, 1491–1496.

Peintler, G., Nagypal, I. and Epstein, I.R. (1990) Kinetics and mechanism of the reaction between chlorite ion and hypochlorous acid. J. Phys. Chem. 94, 2954–2958.

Pillai, K.C., Kwon, T.O., Park, B.B. and Moon, I.S. (2009) Studies on process parameters for chlorine dioxide production using IrO2 anode in an un-divided electrochemical cell. J. Haz. Mat. 164, 812–819.

Pleskov, Y.V. (2003) The electrochemistry of diamond. In: Alkire, R.C. and Kolb, D.M. (eds.) *Advances in Electrochemical Science and Engineering*, vol. 8, Wiley-VCH, Weilheim, pp. 209–269.

Polcaro, A.M., Vacca, A., Maskia, M., Palmas, S., Pompej, R. and Laconi, S. (2007) Characterization of a stirred tank electrochemical cell for water disinfection processes. Electrochim. Acta 52, 2595–2602.

Porta, A. and Kulhanek, A. (1986) Process for the electrochemical decontamination of water polluted by pathogenic germs with peroxide formed in situ. US Patent No. 4.619.745.

Reis, A. (1951) The anodic oxidation as an inactivator of pathogenic substances and processes (in German). Klin. Wschr. 29, 484–485.

Reis, A. (1976) Sterilization and decomposition of noxious organic substances by anodic oxidation (in German) GIT Fachz. Lab. 20, 197–204.

Reis, A. (Editor) (1981) *Anodische Oxidation in der Wasser- und Lufthygiene*, GIT Verlag, Darmstadt.

Reis, A. and Henninger, T. (1953) Destruction of malignant growth energy by anodic oxidation (in German). Klin. Wschr. 31, 39–40.

Rosenberg, B., van Camp, L. and Krigas, T. (1965) Inhibition of cell division in Escherichia coli by electrolysis products from a platinum electrode. Nature 209, 698–699.

Rovan E. and Simonsberger P. (1974) The mini-agar-tube method for electronmicroscopic preparation of cell suspensions and small tissue samples (in German). Mikroskopie 30, 129–134.

Saha, M.S., Furutu, T. and Nishiki Y. (2004) Conversion of carbon dioxide to peroxycarbonate at boron-doped diamond electrode. Electrochem. Commun. 6, 201–204.

Schmidt, W., Boehme, U., Sacher, F. and Brauch, H.-J. (1999) Formation of chlorate by disinfection of drinking water (in German). Vom Wasser 93, 109–126.

Schultze, J.W., Khan, W., Woolfaardt, G.M., Rohns, H.-P., Irmscher, R. and Schoening, J. (2003) High resolution gravimetric, optical and electrochemical investigations of microbial biofilm formation in aqueous systems. Electrochim. Acta 48, 3363–3372.

Scott, D.B.M. and Lesher, E.C. (1963) Effect of ozone on survival and permeability of Escherichia coli. J. Bacteriol. 85, 567–576.

Serrano, K., Michaud, P.A., Comninellis, Ch. and Savall, A. (2002) Electrochemical preparation of peroxodisulfuric acid using boron doped diamond thin film electrodes. Electrochim. Acta 48, 431–436.

Sharma, A.K. and Venkobachar, C. (1979) Effect of prechlorination on coagulation of algae. J. Environ. Health 21, 16–22.

Shimizu, Y. and Sugawara, H. (1996) Virucidal and bactericidal effects of electrolyzed oxidizing water and hypochlorous acid. Jpn. J. Oral Biol. 38, 564–571.

Shimmura, S., Matsumoto, K., Yaguchi, H., Okuda, T., Miyajima, S., Negi, A., Shimazaki, J. and Tsubota, K. (2000) Acidic electrolyse water in the disinfection of the ocular surface. Exp. Eye Res. 70, 1–6.

Siddiqui, M.S. (1996) Chlorine-ozone interactions: Formation of chlorate. Wat. Res. 30, 2160–2170.

Son, H., Cho, M., Kim, J., Oh, B., Chung, H. and Yoon, J. (2005) Enhanced disinfection efficiency of mechanically mixed oxidants with free chlorine. Water Res. 39, 721–727.

Stoner, G.E., Cahen, G.L., Sachyani, M. and Gileadi, E. (1982) The mechanism of low frequency AC electrochemical disinfection. Bioelectrochem. Bioenerg. 9, 229–243.

Tasaka, A. and Tojo T. (1985) Anodic oxidation mechanism of hypochlorite ion on platinum electrode in alkaline solution. J. Electrochem. Soc. 132, 1855–1859.

Thiele, W. and Foerster, H.-J. (2006) Progress in electrochemical ozone generation and disinfection of ultra-pure water using new electrochemical cell with polymer membrane separators (in German). *Proceedings of the Annual GDCh Meeting, Bayreuth 2006*.

Trasatti, S. (ed.) (1981) *Studies in Physical and Theoretical Chemistry 11-Electrodes of Conductive Metallic Oxides, Part B*, Elsevier, Amsterdam.

Trasatti, S. (2000) Electrocatalysis: Understanding the success of DSA. Electrochim. Acta 45, 2377–2385.

Tsai, L.S., Hernlem, B. and Huxsoll, C.C. (2002) Disinfection and solids removal of poultry chiller water by electroflotation. J. Food Sci. 67, 2160–2164.
Urbansky, E.T. and Schock, M.R. (1999) Issues in managing the risks associated with perchlorate in drinking water. J. Environ. Manage. 56, 79–95.
Von Gunten, U. (2003) Ozonation of drinking water: Part II. Disinfection and by-product formation in presence of bromide, iodide or chlorine. Water Res. 37, 1469–1487.
Von Sonntag, C. (1987) *The Chemical Basis of Radiation Biology*, Taylor and Francis, London.
Wardman, P. (1989) Reduction potentials of one-electron couples involving free radicals in aqueous solution. J. Phys. Chem. Ref. Data 18, 1637–1755.
White, G.C. (1999) *Handbook of Chlorination and Alternative Disinfectants*, 4.ed., Wiley, New York, NY.
Zhang, J. and Oloman, C.W. (2005) Electro-oxidation of carbonate in aqueous solution on a platinum rotating disk electrode. J. Appl. Electrochem. 35, 945–953.

Chapter 8
Case Studies in the Electrochemical Treatment of Wastewater Containing Organic Pollutants Using BDD

Anna Maria Polcaro, M. Mascia, S. Palmas, and A. Vacca

8.1 Introduction

Electrochemistry offers new and interesting approaches to industrial wastewater treatment: in particular, electrochemical combustion is a very attractive process for solutions in which, although the pollutant concentration is low, its presence makes the waste toxic (Rajeshwar and Ibanez 1997).

Despite certain advantages, such as the versatility of the process and the simplicity of the reactors in terms of construction and management (which makes them particularly suitable for automation), the electrochemical treatment still represents a niche process: practical application of this technique to wastewater treatment has been limited by the difficulty in finding anode materials with such specific characteristics that the process is economically competitive.

Among the several materials which have been proposed as anode, synthetic boron-doped diamond (BDD) has received great attention in the last decades as a new electrode material, opening up a new branch known as the *electrochemistry of diamond electrodes* (Alfaro et al. 2006). Its peculiar characteristics such as hardness, stability up to high anodic potentials and the wide potential range over which discharge of water does not occur make BDD an excellent material for different electrochemical applications. So, until 1999 most of the studies on BDD focused only on its structural properties and after this date attention was also paid on its possible practical applications for diagnostic and analytical purposes. The peculiarities of BDD also suggested its use as anode to oxidise organics in clear water or wastewater, the first patent being appeared since 1995 (Carey et al. 1995). Then, BDD anodes have been widely proposed to oxidative treatment of both synthetic and real wastewaters containing either inorganic and/or organic compounds. A very wide number of scientific papers and patents have been published, so that citation of all the papers which have appeared in the literature is very difficult. Figure 8.1 wants to be a representative picture of the main classes of compounds whose oxidation at BDD has been proposed since 1999.

A.M. Polcaro (✉)
Dip. Ingegneria Chimica e mat., University of Cagliari, Italy
e-mail: polcaro@dicm.unica.it

C. Comninellis and G. Chen (eds.), *Electrochemistry for the Environment*,
DOI 10.1007/978-0-387-68318-8_8,

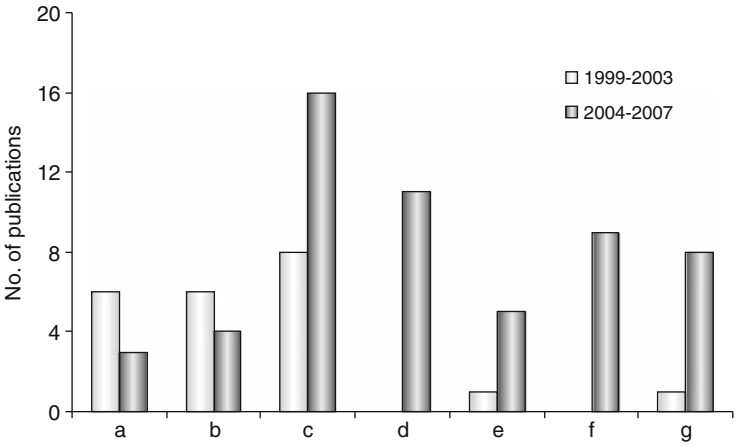

Fig. 8.1 Number of publications on electrochemical treatment of the major classes of organics at BDD: (**a**) phenol, (**b**) aliphatics, (**c**) substituted phenols and other aromatics, (**d**) Drugs and pesticides, (**e**) Surfactants, (**f**) Dyes, (**g**) Real wastewaters

Initially, the interest was on the oxidation of model substances or, in any case, of substances whose oxidation was already studied by other technologies, the results of which could be used for comparison. Phenol and oxalic acid were often considered to model the behaviour of the aromatic and aliphatic fractions of the waste, respectively. Single component artificial solutions were firstly considered. Then, attention was focused also to different substances, such as substituted phenols, or more complex molecules such as those of dyes. Moreover, an increasing number of papers dealt with the treatment of real wastes but in any case, at the moment, the study is performed on a laboratory scale or, in a few cases, on a pilot scale. Some studies reported the treatment of multi-component solutions which better simulate the real composition of the waste, at least concerning some peculiar characteristics of it. This is the case, e.g., of works on oxidation of dyes in which chlorides were added to the model solutions.

Attention was always paid on the analysis of the different processes involved during degradation of the organics. Granted that BDD performed well in all the examined cases, leading in most of the studies to complete mineralization of the pollutant, some doubts still remain on the comprehension of the reaction mechanism, which represents a crucial point when the best operative conditions have to be individuated in order to optimise the process in terms of yield and costs. As sketched in Fig. 8.2, several series/parallel steps may be involved in the oxidative process at BDD: direct electron exchange may occur at the electrode surface (b) and, at the same time, the decomposition of water molecules can lead to the appearance of hydroxyl radicals (c) which are able to oxidize the organic compounds. This process can occur in either one stage or multiple stages, and it proceeds until the final oxidation product is generated (usually carbon dioxide). As the hydroxyl radicals are concerned, they are not stable and they can cause the formation of other oxidants

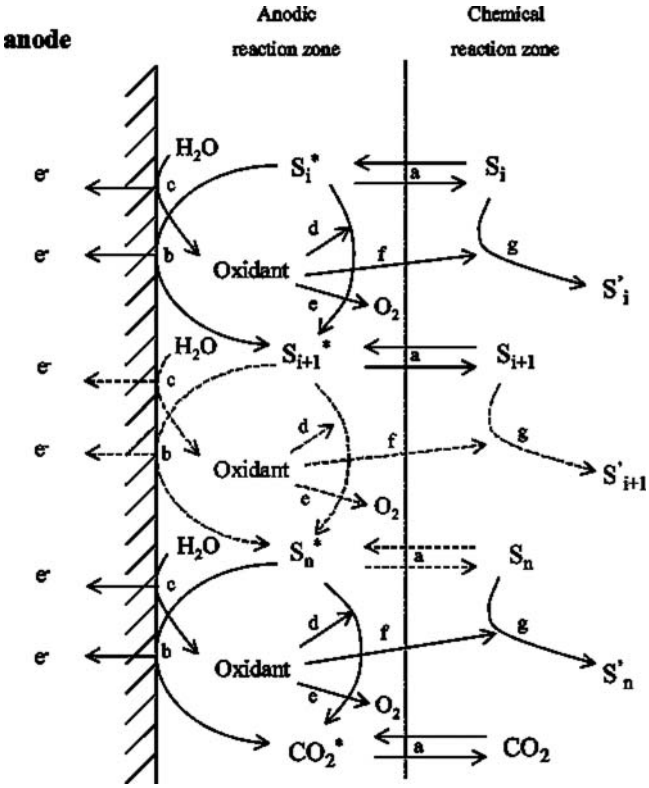

Fig. 8.2 Electrochemical processes considered in the anodic zone (Cañizares et al. 2004b).

(ozone, hydrogen peroxide, peroxodisulphate, chlorine, etc.) that can in turn, react chemically with the organic matter through mediated oxidation processes (d) or, alternatively, they can promote the formation of oxygen (e). If these oxidant compounds reach the bulk zone, it is necessary to take into account their mass-transfer process (f) and the oxidation of the organics in the bulk zone (g) (Cañizares et al. 2004b).

Depending on different factors, such as nature of the organic substrate, nature and composition of the supporting electrolyte and imposed operative conditions, the whole process may be only controlled by one or more steps which can lead to different performances of BDD anodes.

A review of the main classes of compounds which have been studied at this electrode material is reported as follows. In particular, the papers on oxidation of model substances are firstly examined and then specific paragraphs are devoted to the other classes of organics such as phenolic compounds, pesticides and drugs, dyes and surfactants which represent typical wastes that make particular problems of degradation with traditional wastewater treatment technologies.

8.2 Oxidation of Model Substances

As pointed above, great attention was initially paid on oxidation of *phenol* which was assumed as model substance to represent the aromatic fraction of the pollutants in the waste. On the basis of the initial studies (Perret et al. 1999), the similar trend of the removal rates of phenol, TOC and COD were interpreted by a direct oxidation of phenol up to CO_2:

$$C_6H_5OH + 11H_2O \rightarrow 6CO_2 + 28H^+ + 28e^- \tag{8.1}$$

This was also confirmed by HPLC analysis which showed that only very small amounts of intermediates were originated (hydroquinone, benzoquinone, maleic and oxalic acids).

Further studies (Iniesta et al. 2001) on the oxidative degradation of phenol allowed to highlight the importance of the reactant concentration and the current density on the process. The experimental results showed that in the region of water stability ($E < 2.3$V vs. SHE) direct electron transfer on the electrode surface can occur. However, this reaction resulted in the electrode fouling because a polymeric film may be formed on BDD surface. In the region of water decomposition ($E > 2.3$V vs. SHE) hydroxyl radicals were generated at the electrode surface, avoiding its fouling. During electrolysis performed in a batch reactor under galvanostatic conditions, if the phenol concentration was high and the current density was low, only aromatic compounds were formed, for low phenol conversion and aliphatic compounds were also produced when the reactant conversion increased. Under these conditions, the phenol concentration decreased linearly with the electrolysis time and a nearly unity value was calculated for the instantaneous current efficiency (ICE), defined as (Comninellis and Pulgarin 1991):

$$\mathrm{ICE} = \mathrm{FV}\frac{[(\mathrm{COD})_t - (\mathrm{COD})_{t+\Delta t}]}{8I\ \Delta t}, \tag{8.2}$$

where $(\mathrm{COD})_t$ and $(\mathrm{COD})_{t+\Delta t}$ are the chemical oxygen demands at times t and $t + \Delta t$ $\left(\mathrm{g\,dm^{-3}}\right)$, respectively; I is the current (A); F is the Faraday constant $\left(96{,}487\,\mathrm{C\,mol^{-1}}\right)$; V is the volume of electrolyte $\left(\mathrm{dm^3}\right)$ and 8 is the equivalent mass of oxygen $\left(\mathrm{g\,eq^{-1}}\right)$.

Under conditions of high current density and low phenol concentration, the complete combustion to CO_2 was obtained. In this case, due to the high local concentration of OH radicals, the anodic oxidation was a fast reaction under diffusion control, so that the instantaneous current efficiency decreased during the electrolysis as phenol was oxidised.

Actually, a wide range of experimental conditions exists in which the disappearance of the reactant occurs under diffusion control but its mineralization is not complete.

An overall analysis (Polcaro et al. 2003) suggested that the behaviour of the process only depended on the ratio γ between the imposed current density (i)

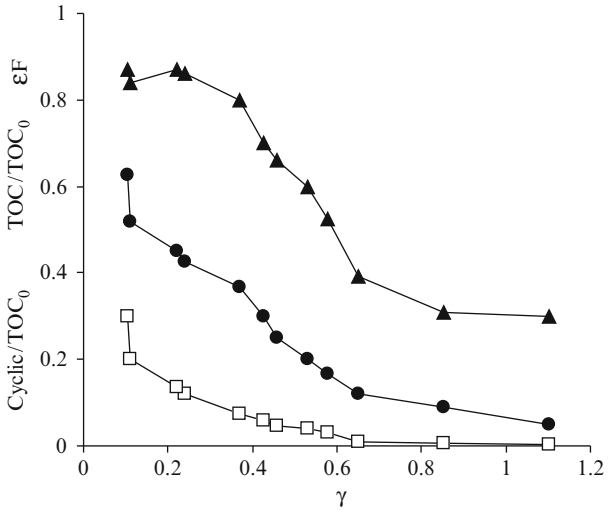

Fig. 8.3 Trend of TOC (*circles*), dissolved carbon attributable to cyclic intermediates (*squares*), both normalised with respect to TOC_0, and faradic yield (*triangles*) as a function of γ

and the initial value of limiting current density for the mineralization of phenol ($28Fk_mC_{F0}$). The values of distribution of intermediates, percentage of mineralization and Faradic yield only depended on γ, whatever the experimental conditions which generated the particular γ value (Fig. 8.3).

The kinetics of the process was considered as oxidative reactions in series with each other, but in parallel with respect to the OH, so that the concentration of OH radicals in the reaction zone was determined by the fastest reaction step. As a consequence, if the value of the imposed current was sufficiently high to complete the first oxidative step of phenol to hydroquinone ($i = 2Fk_mC_{0F}$ which corresponded to $\gamma \geq 0.07$) which involves two electrons, the disappearance of phenol was mass-transfer controlled but the total mineralization was not achieved. In these conditions, the concentration of OH was too low to provoke an appreciable reaction rate of the less oxidisable intermediates. Thus, the products of the first oxidative step accumulated in the laminar film, from which they diffused to the bulk solution where they were identified.

When higher values of γ were adopted for the electrolyses, the flux of OH was higher than that required for the first oxidative step and a greater amount of OH was available for the further steps. In these conditions, the presence of highly oxidized intermediates was experimentally revealed, and when the original reactant disappeared from the solution, high mineralization was achieved. On the other hand, the high concentration of OH radicals enhanced the production of O_2, so decreasing the Faradic yield of the process.

As the degradation of more oxidized compounds is considered, due to their intrinsic lower reactivity toward further oxidation, a reaction mechanism different from that evidenced for phenol has to be expected. Of particular concern is the work

of Zhi and co-workers (Zhi et al. 2003) in which bulk electrolyses of phenol and sodium formate were performed in order to investigate on the different contributions to the whole oxidation mechanism of direct oxidation of the reactant or indirect reaction mediated by hydroxyl radicals. The results of this work showed that both the processes could be involved, being the extent of the two possible mechanisms different for phenol or little anions such as formate. Direct oxidation contribute was found to be more significant for formate than for phenol, indicating the probability of higher sorption of formate on the oxygen-terminated diamond surface. In both cases, the extent of direct reaction was found to decrease with increasing potentials due to the competing reaction of hydroxyl radical formation.

The importance of the superficial state of diamond was also pointed out in a recent work by Ivandini et al. (2006) in which oxidation of oxalic acid was considered.

Among the more oxidized compounds, *oxalic acid* has received significant attention (Martinez-Huitle et al. 2004, 2005; Ivandini et al. 2005) because often it constitutes the final product in the oxidative process of organics. It is generally selected as a model compound to represent the aliphatic fraction of organic substrate in the waste.

In the cited work (Ivandini et al. 2006), the authors outlined that the oxygen-terminated BDD performed worst than the hydrogen-terminated one because the carboxyl functional groups of the oxalic acid molecule may be repulsed by the negative O-terminated electrode surface.

Also in the case of oxalic acid, the reaction mechanism may involve hydroxyl radicals which, depending on the electrode activity and on the applied current, may not be favourable for the reaction of interest.

From a global analysis of the results, it is evident that electrosorption is a necessary pre-requisite for a fast electro-oxidation of these substances to take place (Sargisyan and Vasil'ev 1982; Bock et al. 2002). The nature of the electrode material always resulted of such a great importance that the reactivity of oxalic acid has been considered by the authors as one more example of "volcano plot", in which, at least up to certain current values, maximum performance was obtained at Pd, Pt and Au electrodes, while Os and glassy carbon represented the two minimum extremes. Among the investigated materials, the best performance of high applied current was obtained at PbO_2 anodes in which a strong adsorption of oxalic acid was achieved: in such conditions oxidation was fast and was only limited by the mass transfer. In fact, thanks to the lack of higher oxidation states, the performance of PbO_2 electrodes remained good also at high current density, condition at which the performance of many electrode materials results to be affected by the possible oxidation state changes of the metal cations. In case of Pt electrodes, for example, three-dimensional oxide phase is formed, with improved catalytic activity towards the parasite oxygen evolution reaction, so causing a drop in efficiency of oxalic acid oxidation (Horànyi 1974).

When adsorption of oxalic acid was hindered, either by adsorbed hydroxyl radicals [as at Os electrodes (Sargisyan et al. 1982)] or by a low adsorption capacity (as at glassy carbon or BDD electrodes), the rate of anodic oxidation reached minimum values. However, the same authors underlined that compared with glassy carbon, a

better performance of BDD was obtained attributable to its low adsorption capability also with respect to OH radicals which were produced at its surface, allowing the reaction to proceed in the "reaction cage" nearby the electrode (Gandini et al. 2000).

8.3 Oxidation of Phenolic Compounds

Phenols and substituted phenols such as chlorinated phenols and related aromatic compounds are known to be usual components of industrial wastes. Some of the larger and more common sources of wastewater containing phenolic compounds are pulp and paper mills, petrochemical refineries, plastics and glue manufacturers, coke plants, food industries and leachate from municipal waste dumps (Rao et al. 2002). Many phenolic compounds are thought to be highly toxic and carcinogenic so they are considered to be priority pollutants.

Because of their high environmental impact, the removal process of phenolic compounds from wastewaters was widely investigated by means of different technologies and a very large number of papers can be found in the old and recent literature: we just mention here some of them as an example (Posada et al. 2006; Meng et al. 2006; Suarez-Ojeda et al. 2005; Beltran et al. 2005; Yermakova et al. 2006). The electrochemical oxidation of phenolic compounds was also widely studied at different anodic materials (Comninellis and Pulgarin 1993; Saracco et al. 2000, 2001; Cañizares et al. 2002, 2004a, b, 2005b; Iniesta et al. 2001; Louhichi et al. 2006; Fino et al. 2005).

The behaviour that is generally observed at BDD anodes for these compounds was analogous to that of phenol. As an example we can consider a paper by Nasr et al. (2005) which examined the oxidative degradation of *p*-hydroxybenzoic acid, cathecol and hydroquinone performed in a batch reactor either in $HClO_4$ 1 M or KH_2PO_4/K_2HPO_4 0.3 M as supporting electrolyte: the process was found to follow a first-order kinetics as indicated by the good linearity of the trend of $\ln(C/C_0)$ vs. time. The value of the kinetic constant deduced from the slope of this straight line well agrees with the mass-transfer coefficient of the reactant under the hydrodynamic conditions adopted in the experiments.

Also electrochemical oxidation of 4-chlorophenol performed in H_2SO_4 medium, in the potential region of electrolyte decomposition resulted in a complete incineration of reactant by electrogenerated OH radicals (Rodrigo et al. 2001).

As general trend, it can be observed that for most of the studied phenolic compounds the anodic oxidation at BDD was very fast and, if the applied current density was sufficiently high, the kinetics of the process was under mass-transfer control and it was not appreciably dependent on the nature of the substituting groups in the aromatic ring, as it was reported at more usual electrode materials, like platinum (Torres et al. 2003).

The results demonstrated that, in the oxidation of substituted phenols, the first stage of the reaction generally consisted in the detachment of the functional group from the aromatic ring, followed by the formation of non-substituted phenols and

quinones. Only in a subsequent step, the opening of the aromatic ring occurred: due to its low reactivity, oxalic acid often represented the intermediate product prior to the complete mineralization (Polcaro et al. 2002).

No strong differences were observed when multicomponent mixtures of phenols (phenol, benzyl alcohol, 1-phenyl-ethanol and *m*-cresol) were treated (Morao et al. 2004): the experimental results were interpreted well by assuming that all the components in the mixture were degraded in the same time and that the combustion of the compounds to CO_2 occurred at the anode surface by means of hydroxyl radicals electrogenerated. The instantaneous current efficiency was unity, until the reaction became diffusion controlled.

The effect of the possible homogeneous oxidation mediated by long-life oxidants in the bulk solution was also investigated. The importance of this homogeneous contribute was found to be dependent on the nature and concentration of both the organic substrate and the ionic species contained in the electrolyte solution.

In this context, the oxidation of chlorophenol at BDD, even when performed in H_2SO_4 1 M with production of high concentration of peroxidisulphates, was found to occur at the interface, with a process only controlled by the mass transfer of the reactant towards the anode (Rodrigo et al. 2001).

Similar results were also found during oxidation of nitrophenols (Cañizares et al. 2004d; Cañizares et al. 2004c) which were degraded by the scheme in Fig. 8.4.

According to this model, the first stage in the treatment of nitrophenols aqueous wastes was the release of the nitro group from the aromatic ring. As a consequence, phenols or quinones were formed. These organic compounds were oxidized first to carboxylic acids (maleic and oxalic) and later to carbon dioxide. Also the cathodic reaction steps were considered in the global process when the electrochemical cell was undivided: at the cathode, the reduction of the nitro to the amine group and the transformation of nitrate into ammonia were observed. In alkaline media, aminophenols were polymerised and transformed into a dark brown solid.

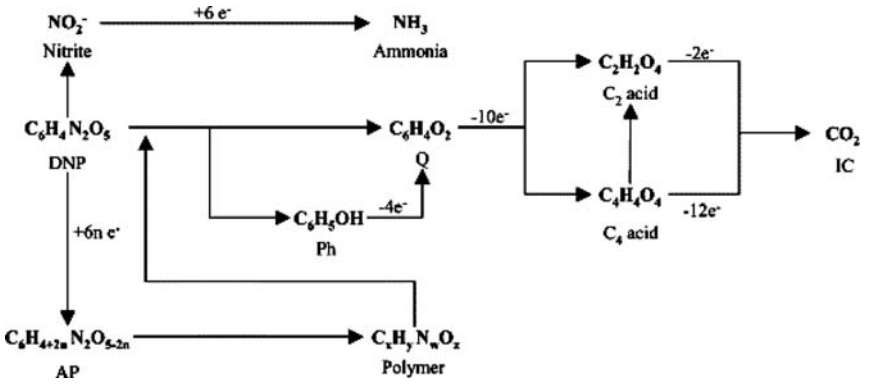

Fig. 8.4 Sketch of the simple mechanistic model proposed to explain the main processes occurring in the electrochemical treatment of 2,4-dinitrophenol wastes using BDD anodes (Cañizares et al. 2004d).

However, although the oxidation process was ascribed to either direct reaction on the electrode surface, or mediated by peroxodisulphate and other inorganic reagents electrogenerated at the anode surface, the linear decrease of the Faradic yield down to zero in the investigated range of concentration was interpreted as an indication of a process under diffusive control. This leads to the conclusion that the oxidative degradation of the compounds essentially occurred at the electrode interface.

More recent work (Cañizares et al. 2005b) demonstrated that in particular conditions, when the supporting electrolyte contained high concentration of sulphate, mass transfer was no more influent: Most of the electrochemical oxidation of aromatics could be considered as a chemical reaction in the bulk solution (rather than a direct electrochemical step), in which the mediation of the electrogenerated species became the dominant contribution to the whole oxidative process. Oxidation of phenol, hydroquinone, 1,2,4-trihydroxybenzene, as well as chloro- and nitro-substituted phenols in sulphate solutions at different pH was considered. In the applied conditions, the efficiencies of the process strongly depended on the concentration of organic pollutants and their nature while the influence of the current density was less important. Although at the end of the treatment all the investigated pollutants were removed from the solution, different reaction products were indicated depending on the original reactant. Carbon dioxide was the major product in the treatment of non-substituted hydroxybenzenes, whereas chlorinated aromatics also dealt with the formation of volatile organic compounds and nitrogenated-phenolic compounds with the formation of polymeric material.

The complexity of the processes involved in the electrochemical oxidation at BDD anodes was also evidenced during the degradation of an olive oil mill wastewater, which represents an actual industrial waste characterised by a high fraction of phenolic and polyphenolic compounds (Cañizares et al. 2006c). The waste was the effluent of a wastewater treatment plant consisting of a Fenton reactor followed by a settler and a sand filter, in which the waste generated in an olive oil mill was treated. The residual COD of the waste was nearly 700 mg dm^{-3} which cannot be further oxidized by the Fenton process, but the exact composition of the waste was not given. Also in this case the results demonstrated a good performance of BDD to oxidize organics with a process which occurred not only at the interface, by means of OH radicals, but also throughout other mechanisms such as direct exchange of electrons between electrode and substrate as well as homogeneous chemical reaction by oxidant electrogenerated and diffused to the bulk solution. It was shown that the presence of Na_2SO_4, from which $S_2O_8{}^{2-}$ may be produced, increased the average efficiency of COD removal, whereas the addition of chlorides decreased the efficiency. This behaviour is very surprising because the addition of Cl^- in the electrolytic process generally causes the formation of ClO^- which in turn increases the degradation efficiency. In order to justify this behaviour at BDD anodes, the authors suggested that, due to the high anodic potential typical of these electrodes, the oxidation of Cl^- leads to $ClO_3{}^-$ and $ClO_4{}^-$ that do not show oxidizing capacity (Bergmann et al. 2002).

8.4 Oxidation of Dyes

The environmental problem of dye industry wastes is highlighted by estimates that up to 50,000 tons of dye are discharged annually from dyehouses worldwide (Brown 1987). These wastes constitute a significant source of environmental pollution due to their visibility and recalcitrance, because dyes are highly coloured and designed to resist chemical, biochemical and photochemical treatments. Among dyes the aromatic azo-dyes, which contain the $-N = N-$ chromophore, comprise about two-thirds of the total (Fernandes et al. 2004).

Different technologies have been proposed to treat this kind of waste (Kusvuran et al. 2004, 2005; Aris and Sharratt 2004; Mollah et al. 2004; Yu et al. 2005; Park et al. 1999). Oxidative biological degradation of azo-dyes was often inefficient or incomplete. Chemically advanced oxidation processes (AOP) gave better results leading to the partial oxidation of the pollutants with generation of products which were more amenable to subsequent biooxidation, while reductive treatment of azo-dyes produced aromatic amines, many of which are known mutagens or carcinogens (Josephy 1996).

Also the electrochemical treatment of dyes has been proposed and some interesting results were obtained by Hastie and co-workers (Hastie et al. 2006) who examined both reductive and oxidative electrolyses of Orange II (sodium 4-(2-hydroxy-l-naphthylazo) benzenesulfonate) synthetic solutions. Among the different materials (BDD, SnO_2 and IrO_2) which were tested as anode, BDD exhibited the best performance: The order of efficacy (BDD > SnO_2 > IrO_2) was consistent with the efficiency of producing hydroxyl radicals at these three anode materials. At BDD it was supposed that most molecules that suffer electrochemical attack became completely mineralized, as assessed by the loss of TOC which roughly mirrored the loss of substrate concentration. Mineralization occurred because hydroxyl radical attack on the substrate initiated a cascade of radical chain oxidation steps, whose efficiency was enhanced by participation of the O_2 that was also formed at the anode. The effect of the structure of the cell (divided or undivided) was also pointed out in this work (Hastie et al. 2006). When undivided cell was used, cathodic reduction produced anilines which appeared to be persistent towards anodic oxidation at acid pH. A different reaction mechanism was supposed in the presence of Cl^- ions, which were added to the synthetic solution to represent better the actual composition of dye waste which often contains this anion. Under these conditions the degradation of the waste seemed to occur mainly in the bulk solution mediated by ClO^- produced from the anodic oxidation of chlorides.

The oxidation of azo dyes (methyl orange, eriochrome black T and Congo red) was studied by other authors (Cañizares et al. 2006a) in an undivided flow cell, in a solution containing 500 mg L^{-1} of Na_2SO_4. The complete mineralization was achieved for all the dyes. However, the reaction mechanism appeared to be complex and in some way different from that obtained in the treatment of many phenolic compounds (Cañizares et al. 2002, 2004a, 2004b, 2004d, 2005a, 2005b; Iniesta et al. 2001; Panizza and Cerisola 2004). In those cases, the experimental data were

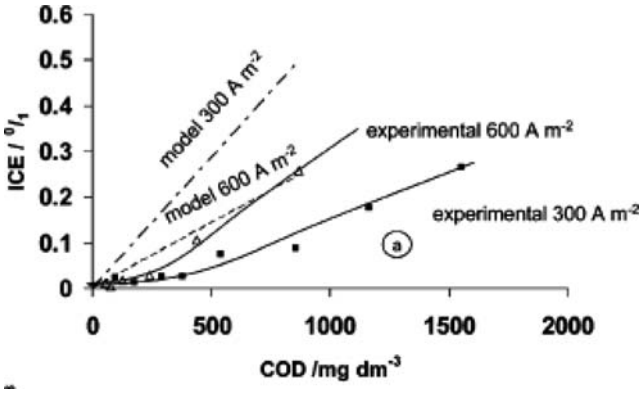

Fig. 8.5 Influence of the current density in the efficiency of the process (Na_2SO_4, 500 mg dm^{-3}, natural pH; $T = 25°C$). Changes in the instantaneous current efficiency (ICE) with the residual COD during electrolyses: (*triangles*) 600 and (*squares*a) 300 A m^{-2} of current density (Cañizares et al. 2006a)

fitted well by the model which assumed direct electrochemical reaction in the anode surface with efficiencies only limited by mass transport. In contrast, in the cited work (Cañizares et al. 2006a), especially when low concentrations of COD were considered, the differences between the experimental data and the model proposed in the literature were very significant. In fact, as shown in Fig. 8.5, although the direct electrooxidation model predicts that, for a given COD, the efficiency decreases linearly with the current density, the experimental efficiency data obtained in this work showed an important increase with the current. This suggested that in this case the oxidation of organics did not occur by direct electrooxidation at the anode surface: The mediation by $S_2O_{8-}{}^2$ originated at the anode was supposed to be the most effective oxidant in diluted solution. At higher concentrations also a direct reaction by OH radicals was considered in order to interpret the trend of the experimental data.

The effectiveness of the anodic treatment at BDD was also tested with an insoluble dye-like dispersed indigo (Bechtold et al. 2006), a typical dye used for cotton work clothes and blue jeans. Also in this case the treatment was effective leading to the complete decolourisation of the solution. The current yield was found to decrease with the applied current indicating a direct oxidation at the electrode interphase under diffusive control. The addition of NaCl up to 144 mg L^{-1} did not enhance the rate of the decolourisation, as well as persulphate, eventually formed from sulphate present in the supporting electrolyte, resulted ineffective.

The effectiveness of OH radicals in the oxidative decolourisation of various dyes has been also assessed by Flox et al. (2006b), who obtained the complete mineralization of the dye by electro-Fenton and photoelectro-Fenton processes using an undivided cell with a Pt or BDD anode.

8.5 Oxidation of Pesticides and Drugs

Herbicides were used in long-time applications in agriculture and for most of them the long-term effects on the soil and water were not known. The accumulation of herbicides or of their metabolites determined a relatively high contamination level of ground and surface waters. The pollution of pharmaceutical drugs can be due to emission from production sites, direct disposal of overplus drugs in households, excretion after drug administration to humans and animals and treatments throughout the water in fish farms.

Since these pollutants resist to biodegradation, powerful oxidation methods have to be searched to remove them from waters, thus avoiding their potential adverse health effects on humans and animals (Brillas et al. 2004, 2005; Flox et al. 2006a; Sires et al. 2006b, 2007; Skoumal et al. 2006).

Among the several kinds of herbicides, phenoxyderivatives like chlorophenoxycarboxylic acids were considered as model substances to assess the powerful of these oxidative techniques towards herbicides. Good results were obtained with advanced oxidation processes in which OH radicals were produced by chemical, photochemical and photocatalytic systems (Pignatello 1992; Sun and Pignatello 1993; Trillas et al. 1995; Modestov and Lev 1998; Brillas et al. 2003; Chu and Ching 2003; Gora et al. 2006; Toepfer et al. 2006). Also the oxidative degradation of herbicides at BDD was widely studied (Polcaro et al. 2004; Boye et al. 2006; Brillas et al. 2004 and reference therein).

In particular, the degradation of chloromethylphenoxy herbicides was studied in different supporting electrolytes, at different current densities and solution pH (Boye et al. 2006; Flox et al. 2006a). The reaction mechanism was pointed out and the reaction intermediates were individuated. In all the cases, the results demonstrated that complete mineralization of the pollutants was achieved. When electrolyses were carried out in $HClO_4$ which is not susceptible of further oxidation, the process was interpreted by a series of steps (Fig. 8.6) in which OH radicals were the oxidising agents: the oxidative demolition occurred only at potential greater than 2.6 V vs. SHE, when water is decomposed to give OH. At lower potential, the formation of polymers occurred which started from the electrochemical oxidation of the reactant to give cationic radicals and then phenoxy radicals. The complete mineralization was achieved at current density $i > 8\,\text{mA}\,\text{cm}^{-2}$: as the applied current increased, an increase of the rate of reactant disappearance was registered as well as

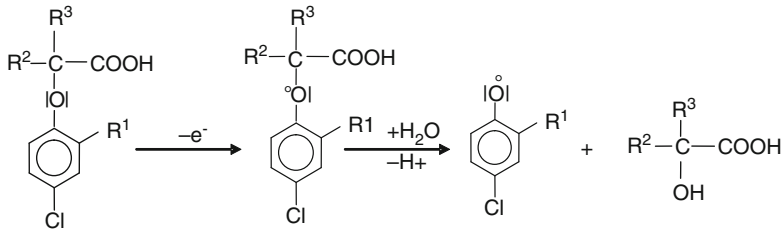

Fig. 8.6 Oxidative removal of phenoxy herbicide (Boye et al. 2006)

a considerable increase of the amount of charge required for its complete mineralization. When the imposed current reached 30 mA cm^{-2}, the oxidation occurred by OH radicals at a high reaction rate and the process was completely controlled by the mass transfer of the reactant to the anode surface.

Acidic aqueous solutions of clofibric acid (2-(4-chlorophenoxy)-2-methylpropionic acid), the bioactive metabolite of various lipid-regulating drugs, were degraded by anodic oxidation at Pt and BDD anodes (Sires et al. 2006a) in sulphate medium. In this case, the oxidising species originated by sulphates were not active in oxidising clofibric acid, thus leading to the conclusion that only OH radicals were able to produce effective demolition of this recalcitrant compound. Very interesting comparison was presented in the same work, between the results obtained at the two anode materials. Conversely to what generally found for most of the organic compounds, clofibric acid resulted to be more rapidly destroyed on Pt than on BDD anodes. A strong adsorption of both clofibric acid and OH radicals at the Pt surface was assumed to be responsible for this behaviour. Chlorophenol and hydroxybutyric acid were individuated as intermediates of the first reaction stage, whereas aliphatic acids were subsequently formed. However, when the final transformation to CO_2 is considered, the results indicated that BDD was more effective than Pt: carboxylic acids remained stable at Pt, while they were completely mineralised at BDD.

Atrazine and its derivates represent another class of herbicides whose complete mineralization even by AOPs makes some problems due to the scarce degradability of cyanuric acid, the main intermediate which originated during the oxidation of triazines. In particular experimental conditions, oxidation of triazine compounds such as atrazine and 2-chloro-4,6-diammino-1,3,5-triazine was successfully obtained at BDD (Polcaro et al. 2005) at which mineralization of cyanuric acid was effectively achieved. When electrolyses were performed in sulphate medium, the decrease of the reactant concentration was faster than that in $HClO_4$ medium, indicating that the mediation by persulphate ions was effective in the removal of the reactant. However, since $S_2O_8{}^{2-}$ ions were not able to degrade the more resistant molecule of cyanuric acid, so the global process did not result enhanced. This fact indicated that the degradation of cyanuric acid was only achieved at the electrode/solution interface by means of free OH radicals, the production of which was affected by the concomitant oxidation of the electrolyte. This was considered to be the reason for the observed reaction trend and to justify why the demolition of cyanuric acid and the consequent removal of solution TOC were not favoured by the presence of sulphuric acid in solution.

8.6 Oxidation of Surfactants

Surfactants such as alkyl sulphates (AS), alkyl ethoxysulphates (AES) and linear alkylbenzene sulfonates (LAS) are the major cleaning ingredients found in household and personal care products. The annual North American consumption volumes of AS and AES for 2003 were estimated to be 260 and 1,083 million pounds, respectively (Modler et al. 2004).

Although biological systems are effective in the removal of LAS, some difficulties have been found in the treatment of wastewater with high LAS concentrations, mainly connected to the formation of foams, self-regulation capacity of the pH in wastewater and long retention time of treatment to accomplish complete pollutant removal (Cavalli et al. 1993). Thus, alternative treatments, such as photodegradation (Hermann et al. 1997) or oxidation with ozone (Rice 1997), were proposed to treat wastewater with a high LAS concentration.

In this context also, the electrochemical oxidation was proposed as effective process of wastewater treatment. Among surfactants, sodium dodecyl benzenesulfonate is generally assumed to represent anionic surfactants, whereas hexadecyltrimethylammonium chloride is assumed as representing the cationic class.

Oxidation of sulphuric solutions of anionic surfactants was considered by Panizza and co-workers (Panizza et al. 2005) which compared the performance of ternary Ti–Ru–Sn oxide and BDD electrodes during oxidative treatment of synthetic and real wastewater containing sodium dodecyl benzenesulfonate. The authors demonstrated that the anionic surfactant was mineralised at active Ti–Ru–Sn electrodes only when a certain amount of chlorides were added to the solution. The process mainly occurred in homogeneous reaction by means of the oxidant species originated by chlorides, since it was not influenced by the stirring velocity of the solution.

A complete removal of the surfactant was obtained at BDD in which, in absence of chlorides, mineralization was achieved by a direct involving of OH radicals originated at the electrode surface, with a process which resulted controlled by the mass transfer. The results from oxidation at BDD performed with a real car wash wastewater confirmed those obtained from model solutions. Conversely, at ternary oxide electrodes the efficiency was lower than that measured for model solutions; as suggested by the authors, the presence of heavy metals, which caused the decomposition of electrogenerated active chlorine, could be the reason of this behaviour.

The degradation of anionic surfactants was also considered by other authors and compared with that of cationic surfactants (Lissens et al. 2003). Although mineralization to CO_2 was obtained in both cases, the electrochemical oxidation of the cationic surfactant was found to proceed at higher rate and higher Faradic yield than that of anionic surfactant (Fig. 8.7).

Also in this case the process seemed to occur mainly in the bulk: no effect was observed as the flow conditions were varied (from 0.05 to 0.25 $dm^3\ min^{-1}$), indicating that the process was not under diffusion control. However, most of the mediated oxidation seemed to occur by oxidation products of chlorides rather than sulphates: the authors assessed that the addition of Na_2SO_4 up to $1\ g\ L^{-1}$ had only a minor effect on TOC removal of both surfactants.

The relevant effect of chlorides was instead highlighted by the higher rate of TOC removal for the cationic rather than for the anionic surfactant. In this respect, it was assumed that the extra input of chlorides, which was present in the solution during cationic surfactant oxidation, caused two effects: the first was the formation of chlorine substances evolving from chlorides which may react instantaneously with the cationic surfactant, causing an initially higher oxidation and surfactant deactivation

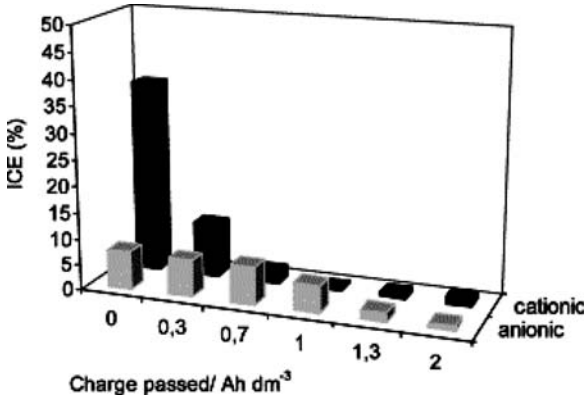

Fig. 8.7 ICE values during the electrolysis at a BDD electrode of anionic and cationic surfactant solution. Electrolyte: 0.0615 mM sodium dodecylbenzenesulfonate solution; 0.07 mM hexadecyltrimethyl ammonium chloride solution, $i = 4\,\mathrm{mA\,cm^{-2}}$ (Lissens et al. 2003)

rate compared to the anionic surfactant. Second, the lower water solubility of the formed chlorinated compounds and the lower molecular weight of the cationic surfactant enhanced the adsorption on hydrophobic carbon surfaces (e.g., on a BDD electrode). Both effects might explain the higher initial oxidation rate and surfactant deactivation rate of the alkyl ammonium chloride (cationic) compared with the alkyl sulfonate (anionic).

8.7 Economic Considerations

The economic viability is a key factor to allow a practical application of a given process. Also in the case of electrochemical oxidation at BDD, an economic assessment of the process, mainly in terms of minimisation of the energy demand, is required to extend the laboratory scale results to industrial applications. Traditional processes such as biological treatment, clarification, wet air oxidation, membrane bioreactor technologies, are more economic and, when warranted, they are more appropriated. However, due to the increasingly stringent regulations that apply to wastewaters and drinking waters, the use of less economic AOPs is sometime required in order to reduce COD of particular pollutant wastes. Other than costs, suppose that a selected AOP is effective in the oxidation of a particular pollutant, the production of by-products is the first aspect to be investigated in order to establish the suitability of the process. In this regards, the possibility to obtain the almost complete mineralization of the pollutant is a favourable characteristic which makes the electrochemical treatment at BDD as an attractive process for the wastewater treatment.

As the economic aspects are concerned, the overall costs, represented by the sum of capital costs, operating costs and maintenance have to be considered. For an electrochemical process, the operating costs are mainly determined by the energy consumption (CE).

For the removal of COD in aqueous solutions, CE (Wh) can be calculated using the following formula:

$$\mathrm{CE} = \frac{F \times \Delta\mathrm{COD} \times V \times U}{3{,}600 \times 8\eta}, \tag{8.3}$$

where ΔCOD is the removed COD ($\mathrm{gO_2\,m^{-3}}$), V the volume of solution $\left(\mathrm{m^3}\right)$, U the cell voltage (V), η the average current efficiency for COD removal and F is the Faraday constant ($\mathrm{C\,eq^{-1}}$).

The cell voltage U is the sum of the voltage which is thermodynamically and kinetically necessary for performing the electrochemical reaction U_{ec} (about 3 V at BDD anode) and the voltage drop ΔU due to the resistance of the electrolyte. For parallel plate electrodes this voltage drop is given by:

$$\Delta U = \frac{i \times d}{\Lambda}, \tag{8.4}$$

where d is the electrode distance (cm), Λ the conductivity ($\mathrm{mS\,cm^{-1}}$) and i is the current density ($\mathrm{mA\,cm^{-2}}$).

In general, current efficiency [η in (8.3)] has to be determined by laboratory experiments. However, for such compounds as phenol which are susceptible of a fast reaction with OH radicals, the model proposed by Iniesta et al. (2001) may be used. Following this model, when the galvanostatic electrolysis is performed in a batch reactor and the process is only limited by the mass transfer of the reactant to the electrode surface, η is equal to 1 when the applied current density is lower than the initial limiting current density for mineralization of the reactant:

$$i_{\mathrm{L}}^{0} = 4Fk_{\mathrm{m}}\mathrm{COD}_0, \tag{8.5}$$

where k_{m} is the average mass-transport coefficient in the electrochemical reactor and 4 is the number of exchanged electrons per mole of O_2. When the reactant conversion is higher than X_{cr} (defined as the conversion for which the initial limiting current is equal to the applied current density), a Faradic yield can be evaluated by:

$$\bar{\eta} = \frac{X}{1 - \alpha\left[1 + \ln\left(\frac{1-X}{\alpha}\right)\right]} \quad \text{where } \alpha = \frac{i}{i_{\mathrm{lim}}^{0}}. \tag{8.6}$$

The energy consumption remains constant with conversion (X) until the critical conversion X_{cr} value is reached and then it increases, due to mass-transport limitations. The energy consumption increases also with α value due to an increase of the rate of secondary reactions.

According to this model the complete mineralization of phenol at BDD from a solution containing $0.5\,g\,L^{-1}$ of reactant requires $18\,kWh\,kg\,COD^{-1}$ when α is equal to 0.37 and the cell voltage is 3.6 V. Similar value of energetic consumption was also calculated by Kraft et al. (2003).

The capital costs depend on the anode area; although information on industrial scale cost of diamond anodes are not currently available, this parameter is of great relevance. In order to evaluate the electrode area which is needed for the elimination of a given loading P ($mol\,COD\,s^{-1}$), the following equation can be used:

$$A = 4F\frac{XP}{\bar{\eta}i}. \tag{8.7}$$

The whole cost of the process depends on such different parameters as reactant concentration, electrolyte composition or cell design and a reliable comparison with other technologies is often impeded by the lack of data on industrial or at least on pilot scale.

However, if the attention is focused on the removal of phenol from aqueous solutions, a possible comparison may be done in terms of energy demand and effectiveness. Al Momani et al. (2004) compared the performances of ozonisation, photolysis and UV/H_2O_2, photocatalysis and Fenton for the treatment of phenol solutions. Fenton-based process showed the highest removal rate, whereas the treatment with ozone was the less-expensive process; among the UV-based processes, the UV/H_2O_2 showed the higher removal rate.

Kusic et al. (2006) showed that, although all the traditional AOP can oxidise the phenol, mineralization was low since the best performances were obtained in a combined $UV/O_3/H_2O_2$ process, in which the removal of TOC was equal to 58%: the combined $UV/O_3/H_2O_2$ process should be preferred to the less-expensive O_3 process.

As pointed out above, the complete mineralization of $0.5\,g\,L^{-1}$ phenol at BBD anode requires $18\,kWh\,kg\,COD^{-1}$; assuming a price of the electrical energy of $0.07\,Euro\,kWh^{-1}$, the operative cost of this treatment results $1.26\,Euro\,kg\,COD^{-1}$ which is less than that evaluated for ozonisation, the less-expensive traditional AOP (Kraft et al. 2003).

When the waste contains more complex molecules such as compounds refractory to oxidation with OH radicals, as well as in the presence of inorganic ions which can be precursor of long-life oxidants, the Faradic yield cannot be calculated by (8.3) and different alternatives have been proposed. Faouzi and co-worker (Faouzi et al. 2006) proposed a comparison between electrochemical oxidation at BDD anodes and Fenton and Ozone treatments for the removal of dyes: a specific parameter OCC (oxygen-equivalent chemical-oxidation capacity) was proposed which is defined as the kg of O_2 equivalent to the quantity of oxidant used in each AOP to treat $1\,m^3$ of wastewater. As highlighted by the authors, the parameter OCC may only give information on the chemical efficiency of the oxidants, but it does not give any information related to the real cost of the treatment, as the oxidants can

have very different prices. Results showed that all the three technologies were able to successfully decolourise the wastes during the first oxidation times, which means that the breakage of the azo moiety is one of the first steps in the oxidation mechanisms. However, the efficiency and the mineralization percentage were found to be strongly dependent on the oxidation technique and on the concentration of pollutant: for low concentration of azo-dyes, the oxidants were used with the highest efficiency in the Fenton process and with the lowest efficiency in the electrochemical oxidation. Nevertheless, electrochemical oxidation attained the highest mineralization percentage and the Fenton the worst. Conversely, during the first stages of the treatment of highly loaded wastes, the three technologies studied attained the same efficiency in the use of oxidants. This suggested that the lower efficiency observed for the electrochemical oxidation in the treatment of diluted wastes may be due to mass-transport limitations. The accumulation of refractory carbon during the final stages of the Fenton process is an important drawback for the use of this technology, and it disappoints its use for the treatment of highly loaded wastes.

In many cases, the most appropriated use of AOP may be as a stage of a combined biological/chemical process. AOP can be used as pre-treatment step to enhance biodegradability of the waste or as a complementary treatment to remove residual bio-refractory component if the biological treatment is not adequate to ensure the water-quality standards.

As the electrochemical oxidation at BDD anodes is concerned, its use as first treatment step was tested to enhance the biodegradability of wastewaters with high organic load; although the Faradic yield was high, the high charge required for the complete mineralization advises against the use of the only electrochemical treatment.

A recent paper of Cañizares and co-workers (Cañizares et al. 2006b) reported the results of the electrolyses at BDD of different substituted phenols showing a significant decrease of the toxicity during the treatment. However, it was not possible to establish a dependence between decrease of toxicity and residual COD, because different reactants were oxidised to intermediates characterised by different toxicity.

Another study (Polcaro et al. 2002) showed that when different substances were present in the waste, the selectivity of anodic treatment at BDD towards the different compounds may be low, and a significant enhancement of biodegradation was achieved only for high COD removal, requiring a high amount of current.

The electrochemical oxidation at BDD as final treatment in a combined two-step biological/electrochemical process was investigated by Panizza et al. (2006) for the removal of naphthalene sulfonates contained in infiltration water of an industrial site. Mono and disulfonate naphthalenes were easily removed in the biological step, whereas bio-refractory compounds with complex molecules were oxidised by electrolysis at BDD anodes. With this combination the energy demand was significantly lowered with respect to that required in a single electrochemical step.

8.8 Conclusions

Analysis of the results obtained during electrochemical treatment at BDD anodes shows that organic compounds refractory to other oxidation techniques are successfully oxidised. This indicates that in the near future this technology can become one of the most interesting and advanced oxidation processes. However, the results reported in literature on this topic demonstrate that different behaviours can be expected, depending on the composition of the wastewater, in particular on the chemistry of organics and supporting electrolyte. As pointed out above, while for some compounds, such as phenol, the degradation only occurs at the interface through the mediation of OH radicals, and under mass-transfer control, other compounds such as azo-dyes show a different behaviour. For these species, even in diluted solution, mass transfer is not the limiting step of the process, and the inorganic oxidants generated by oxidation of water or salts contained in the water are mainly responsible for the oxidation. However, the unspecific oxidation of all substances by the hydroxyl radicals leads to possible side reactions: unwanted substances such as chlorates, perchlorates, chlorites and other oxidation products can be formed. This has to be considered when designing electrochemical water-treatment devices with diamond anodes. In particular, when addition of salts to the waste is required to increase the conductivity of the electrolyte and decrease the cell potential, an appropriate choice of the electrolyte is very important.

Further investigation is needed in order to clarify better the role of the long-life oxidants produced in the bulk solution and to establish their fate during oxidative treatment. Moreover, the specific composition of the waste has to be considered in order to evaluate if, rather than as main process, the electrochemical treatment with diamond anodes can be more efficiently used in combined processes in which this technology may be used as a pre-treatment or a finishing stage.

References

Alfaro, M.A.Q., Ferro, S., Martinez-Huitle, C.A. and Vong, Y.M.(2006) Boron doped diamond electrode for the wastewater treatment. J. Braz. Chem. Soc. 17, 227–236

Al Momani, F., Sans, C. and Esplugas, S. (2004) A comparative study of the advanced oxidation of 2,4-dichlorophenol. J. Hazard. Mater. 107, 123–129

Aris, A. and Sharratt, P.N. (2004) Fenton oxidation of Reactive Black 5: Effect of mixing intensity and reagent addition strategy. Environ. Technol. 25, 601–612

Bechtold, T., Turcanu, A. and Schrott, W. (2006) Electrochemical decolourisation of dispersed indigo on boron-doped diamond anodes. Diam. Relat. Mater. 15, 1513–1519

Beltran, F.J., Rivas, F.J. and Gimeno, O. (2005) Comparison between photocatalytic ozonation and other oxidation processes for the removal of phenols from water. J. Chem. Technol. Biotechnol. 80, 973–984

Bergmann, H., Iourtchouk, T., Schops, K. and Bouzek, K. (2002) New UV irradiation and direct electrolysis – Promising methods for water disinfection. Chem. Eng. J. 85, 111–117

Bock, C., Smith, A. and MacDougall, B. (2002) Anodic oxidation of oxalic acid using WOx based anodes. Electrochim. Acta 48, 57–67

Boye, B., Brillas, E., Marselli, B., Michaud, P.A., Comninellis, Ch., Farnia, G. and Sandona, G. (2006) Electrochemical incineration of chloromethylphenoxy herbicides in acid medium by anodic oxidation with boron-doped diamond electrode. Electrochim. Acta 51, 2872–2880

Brillas, E., Calpe, J.C. and Cabot, P.L. (2003) Degradation of the herbicide 2,4-dichlorophenoxyacetic acid by ozonation catalyzed with Fe2+ and UVA light. Appl. Catal. B: Environ. 46, 381–391.

Brillas, E., Boye, B., Sires, I., Garrido, J. A., Rodriguez, R.M., Arias, C., Cabot, P. and Comninellis, Ch. (2004) Electrochemical destruction of chlorophenoxy herbicides by anodic oxidation and electro-Fenton using a boron-doped diamond electrode. Electrochim. Acta 49, 4487–4496

Brillas, E., Sires, I., Arias, C., Cabot, P.L., Centellas, F., Rodriguez, R.M. and Garrido, J.A. (2005) Mineralization of paracetamol in aqueous medium by anodic oxidation with a boron-doped diamond electrode. Chemosphere 58, 399–406

Brown, D. (1987) Effects of colorants in the aquatic environment. Chemosphere, 12, 397–404

Cañizares, P., Díaz, M., Domínguez, J.A., García-Gómez, J. and Rodrigo, M.A. (2002) Electrochemical oxidation of aqueous phenol wastes on synthetic diamond thin-film electrodes. Ind. Eng. Chem. Res. 41, 4187–4194

Cañizares, P., García-Gómez, J., Saez, C. and Rodrigo, M.A. (2004a) Electrochemical oxidation of several chlorophenols on diamond electrodes. Part II. Influence of waste characteristic and operating conditions. J. Appl. Electrochem. 34, 87–94

Cañizares, P., Garcia-Gomez, J., Lobato, J. and Rodrigo, M.A. (2004b) Modeling of wastewater electro-oxidation processes. Part I. General description and application to inactive electrodes. Ind. Eng. Chem. Res. 43, 1915–1922

Cañizares, P., Saez, C., Lobato, J. and Rodrigo, M.A. (2004c) Electrochemical treatment of 4-nitrophenol-containing aqueous wastes using boron-doped diamond anodes. Ind. Eng. Chem. Res. 43, 1944–1951

Cañizares, P., Saez, C., Lobato, J. and Rodrigo, M.A. (2004d) Electrochemical treatment of 2,4-dinitrophenol aqueous wastes using boron-doped diamond anodes. Electrochim. Acta 49, 4641–4650

Cañizares, P., Díaz, M., Domínguez, J.A., Lobato, J. and Rodrigo, M.A. (2005a) Electrochemical treatment of diluted cyanide aqueous wastes. J. Chem. Technol. Biotechnol. 80, 565–573

Cañizares, P., Lobato, J., Paz, R., Rodrigo, M.A. and Saez, C. (2005b) Electrochemical oxidation of phenolic wastes with boron-doped diamond anodes. Water Res. 39, 2687–2703

Cañizares, P., Gadri, A., Lobato, J., Nasr, B., Paz, R., Rodrigo, M.A. and Saez, C. (2006a) Electrochemical oxidation of azoic dyes with conductive-diamond anodes. Ind. Eng. Chem. Res. 45, 3468–3473

Cañizares, P., Saez, C., Lobato, J. and Rodrigo, M.A. (2006b) Detoxification of synthetic industrial wastewaters using electrochemical oxidation with boron-doped diamond anodes. J. Chem. Technol. Biotechnol. 81, 352–358

Cañizares, P., Martinez, L., Paz, R., Saez, C., Lobato, J. and Rodrigo, M.A. (2006c) Treatment of Fenton-refractory olive oil mill wastes by electrochemical oxidation with boron-doped diamond anodes. J. Chem. Technol. Biotechnol. 81, 1331–1337

Carey, J.J., Christ, C.S. and Lowery, S.N., US Patent 5 399 247, 1995.

Cavalli, L., Gellera, A. and Landone, A. (1993) LAS removal and biodegradation in a wastewater treatment plant. Environ. Toxicol. Chem. 12, 1777–1788

Chu, W. and Ching, M. H. (2003) Modeling the ozonation of 2,4-dichlorophoxyacetic acid through a kinetic approach. Water. Res. 37, 39–46

Comninellis, Ch. and Pulgarin, C. (1991) Anodic oxidation of phenol for waste water treatment. J. Appl. Electrochem. 21,

Comninellis, Ch. and Pulgarin, C. (1993) Electrochemical oxidation of phenol for wastewater treatment using SnO_2 anodes. J. Appl. Electrochem. 23, 108–112

Faouzi, M., Cañizares, P., Gadri, A., Lobato, J., Nasr, B., Paz, R., Rodrigo, M.A. and Saez, C. (2006) Advanced oxidation processes for the treatment of wastes polluted with azoic dyes. Electrochim. Acta 52, 325–331

Fernandes, A., Morão, A., Magrinho, M., Lopes, A. and Gonçalves, I. (2004) Electrochemical degradation of C. I. Acid Orange 7. Dyes Pigm. 61, 287–296

Fino, D., Jara, C., Saracco, G., Specchia, V. and Spinelli, P. (2005) Deactivation and regeneration of Pt anodes for the electro-oxidation of phenol. J. Appl. Electrochem. 35, 405–411

Flox, C., Cabot, P.L., Centellas, F., Garrido, J.A., Rodriguez, R.M., Arias, C. and Brillas, E. (2006a) Electrochemical combustion of herbicide mecoprop in aqueous medium using a flow reactor with a boron-doped diamond anode. Chemosphere 64, 892–902

Flox, C., Ammar, S., Arias, C., Brillas, E., Vargas-Zavala, A.V. and Abdelhedi, R., (2006b) Electro-Fenton and photoelectro-Fenton degradation of indigo carmine in acidic aqueous medium. Appl. Catal. B: Environ. 67, 93–104

Gandini, D., Mahe, E., Michaud, P.A., Haenni, W., Perret, A. and Comninellis, Ch. (2000) Oxidation of carboxylic acids at boron-doped diamond electrodes for wastewater treatment. J. Appl. Electrochem. 30, 1345–1350

Gora, A., Toepfer, B., Puddu, V. and Li Puma, G. (2006) Photocatalytic oxidation of herbicides in single-component and multicomponent systems: Reaction kinetics analysis. Appl. Catal. B: Environ. 65, 1–10

Hastie, J., Bejan, D., Teutli-Leon, M. and Bunce, N.J. (2006) Electrochemical methods for degradation of Orange II (sodium 4- (2-hydroxy-l-naphthylazo) benzenesulfonate). Ind. Eng. Chem. Res. 45, 4898–4904

Hermann, R., Gerke, J. and Ziechmann, W. (1997) Photodegradation of the surfactants Na-dodecylbenzenesulfonate and dodecylpyridinium-chloride as affected by humic substances. Water Air Soil Pollut. 98, 43–55

Horányi, G.(1974) On the adsorption of organic compounds on platinized platinum electrodes. J. Electroanal. Chem. 51, 163–178

Iniesta, J., Michaud, P.A., Panizza, M., Cerisola, G., Aldaz, A. and Comninellis, Ch. (2001) Electrochemical oxidation of phenol at boron-doped diamond electrode. Electrochim. Acta 46, 3573–3578

Ivandini, T.A., Naono, Y., Nakajima, A. and Einaga, Y. (2005) Gold-nanoparticle-dispersed boron-doped diamond electrodes for electrochemical oxidation of oxalic acid. Chem. Lett. 34, 1086–1087

Ivandini, T.A., Rao, T.N., Fujishima, A. and Einaga, Y. (2006) Electrochemical oxidation of oxalic acid at highly boron-doped diamond electrodes. Anal. Chem. 78, 3467–3471

Josephy, P. D. (1996) *Molecular Toxicology*, Oxford University Press, New York, NY

Kraft, A., Stadelmann, M. and Blaschke, M. (2003) Anodic oxidation with doped diamond electrodes: A new advanced oxidation process. J. Hazard. Mater. 103, 247–261

Kusic, H., Koprivanac, N. and Bozic, A.L. (2006) Minimization of organic pollutant content in aqueous solution by means of AOPs: UV- and ozone-based technologies. Chem. Eng. J. 123, 127–137

Kusvuran, E., Gulnaz, O., Irmak, S., Atanur, O. M., Ibrahim Y. H. and Erbatur, O. (2004) Comparison of several advanced oxidation processes for the decolorization of Reactive Red 120 azo dye in aqueous solution. J. Hazard. Mater. 109, 85–93

Kusvuran, E., Irmak, S., Ibrahim Y.H., Samil, A. and Erbatur, O. (2005) Comparison of the treatment methods for decolorization and mineralization of Reactive Black 5 azo dye. J. Hazard. Mater. 119, 109–116.

Lissens, G., Pieters, J., Verhaege, M., Pinoy, L. and Verstraete, W. (2003) Electrochemical degradation of surfactants by intermediates of water discharge at carbon-based electrodes. Electrochim. Acta 48, 1655–1663

Louhichi, B., Bensalash, N. and Gadri, A. (2006) Electrochemical oxidation of benzoic acid derivatives on boron doped diamond: Voltammetric study and galvanostatic electrolyses, Chem. Eng. Technol. 29, 944–950

Martinez-Huitle, C.A., Ferro, S. and De Battisti, A. (2004) Electrochemical incineration of oxalic acid: Role of electrode material. Electrochim. Acta, 49, 4027–4034

Martinez-Huitle C.A., Ferro, S. and De Battisti, A. (2005) Electrochemical incineration of oxalic acid: Reactivity and engineering parameters. J. Appl. Electrochem. 35, 1087–1093

Meng, X.G., Zhu, J., Yan, J., Xie, J.Q., Kou, X.M., Kuang, X.F., Yu, L.F. and Zeng, X.C. (2006) Studies on the oxidation of phenols catalyzed by a copper(II)-Schiff base complex in aqueous solution under mild conditions. J. Chem. Technol. Biotechnol. 81, 2–7

Modestov, A.D. and Lev, O. (1998) Photocatalytic oxidation of 2,4-dichlorophenoxyacetic acid with titania photocatalyst. Comparison of supported and suspended TiO_2. J. Photochem. Photobiol. A: Chem. 112, 261–270

Modler, R.F., Gubler, R. and Inoguchi Y. (2004) *Detergent Alcohols, Chemical Economics Handbook Marketing Research Report*, SRI International, Menlo Park, CA

Mollah, M.Y., Pathak, S.R., Patil, P.K., Vayuvegula, M., Agrawal, T.S., Gomes, J.A.G., Kesmez, M. and Cocke, D.L. (2004) Treatment of Orange II azo-dye by electrocoagulation (EC) technique in a continuous flow cell using sacrificial iron electrodes. J. Hazard. Mater. 109, 165–171

Morao, A., Lopes, A., Pessoa de Amorim, M.T. and Goncalves, I.C. (2004) Degradation of mixtures of phenols using boron doped diamond electrodes for wastewater treatment. Electrochim. Acta 49, 1587–1595

Nasr, B., Abdellatif, G., Cañizares, P., Saez, C., Lobato, J. and Rodrigo, M.A. (2005) Electrochemical oxidation of hydroquinone, resorcinol, and catechol on boron-doped diamond anodes. Environ. Sci. Technol. 39, 7234–7239

Panizza, M. and Cerisola, G. (2004) Influence of anode material on the electrochemical oxidation of 2-naphthol. Part 2. Bulk electrolysis experiments. Electrochim. Acta 49, 3221–3226

Panizza, M., Delucchi M., and Cerisola, G. (2005) Electrochemical degradation of anionic surfactants, J. Appl. Electrochem. 35, 357–361

Panizza, M., Zolezzi, M. and Nicolella, C. (2006) Biological and electrochemical oxidation of naphthalenesulfonates. J. Chem. Technol. Biotechnol. 81, 225–232

Park, T.J., Lee, K.H., Jung, E.J. and Kim, C.W. (1999) Removal of refractory organics and color in pigment wastewater with Fenton oxidation. Water Sci. Technol. 39, 189–192

Perret A., Haenni, W., Skinner, N., Tang, X.M., Gandini, D., Comninellis, Ch., Correa B. and Foti G. (1999) Electrochemical behaviour of synthetic diamond thin film electrodes. Diam. Relat. Mater. 8, 820–823

Pignatello, J.J. (1992) Dark and photoassisted iron (3+)-catalyzed degradation of chlorophenoxy herbicides by hydrogen peroxide. Environ. Sci. Technol. 26, 944–951

Polcaro, A.M., Mascia, M, Palmas, S. and Vacca, A. (2002) Electrochemical oxidation of phenolic and other organic compounds at boron doped diamond electrodes for wastewater treatment: Effect of mass transfer. Ann. Chim. 93, 967–976

Polcaro, A.M., Vacca, A., Palmas, S. and Mascia, M. (2003) Electrochemical treatment of wastewater containing phenolic compounds: Oxidation at boron-doped diamond electrodes. J. Appl. Electrochem. 33, 885–892

Polcaro, A.M., Mascia, M., Palmas, S. and Vacca, A. (2004) Electrochemical degradation of diuron and dichloroaniline at BDD electrode. Electrochim. Acta, 49, 649–656

Polcaro, A.M., Vacca, A., Mascia, M. and Palmas, S. (2005) Oxidation at boron doped diamond electrodes: An effective method to mineralise triazines. Electrochim. Acta 50, 1841–1847

Posada, D., Betancourt, P., Liendo, F. and Brito, J.L. (2006) Catalytic wet air oxidation of aqueous solutions of substituted phenols. Catal. Lett. 106, 81–88

Rajeshwar, K. and Ibanez, J. (1997) *Fundamentals and Applications in Pollution Abatement*, Academic, New York, NY

Rao, T.N., Terashima, C., Sarada, B.V., Tryk, D.A. and Fujishima, A. (2002) Electrochemical oxidation of chlorophenols at a boron-doped diamond electrode and their determination by high-performance liquid chromatography with amperometric detection. Anal. Chem. 74, 895–902

Rice, R.G. (1997) Applications of ozone for industrial wastewater treatment. A review. Ozone Sci. Eng. 18, 477–515

Rodrigo, M.A., Michaud, P.A., Duo, I., Panizza, M., Cerisola, G. and Comninellis, Ch. (2001) Oxidation of 4-chlorophenol at boron-doped diamond electrode for wastewater treatment. J. Electrochem. Soc. 148, D60–D64

Saracco, G., Solarino, L., Aigotti, R., Specchia, V. and Maja, M. (2000) Electrochemical oxidation of organic pollutants at low electrolyte concentrations. Electrochim. Acta, 46, 373–380

Saracco, G., Solarino, L., Specchia, V. and Maja, M. (2001) Electrolytic abatement of biorefratory organics by combining bulk and electrode oxidation processes. Chem. Eng. Sci. 56, 1571–1578

Sargisyan, S.A. and Vasil'ev, Yu. B. (1982) Kinetics and mechanism of the electrooxidation of oxalic acid at a platinum electrode. Sov. Electrochem. 18, 848–853

Sires, I., Cabot, P.L., Centellas, F., Garrido, J.A., Rodriguez, R.M., Arias, C. and Brillas, E. (2006a) Electrochemical degradation of clofibric acid in water by anodi.c oxidation. Comparative study with platinum and boron-doped diamond electrodes. Electrochim. Acta 52, 75–85

Sires, I., Garrido, J.A., Rodriguez, R.M., Cabot, P.L., Centellas, F., Arias, C. and Brillas, E., (2006b) Electrochemical degradation of paracetamol from water by catalytic action of Fe2+, Cu2+, and UVA light on electrogenerated hydrogen peroxide. J. Electrochem. Soc.153, D1–D9

Sires, I., Arias, C., Cabot, P.L., Centellas, F., Garrido, J. A., Rodriguez, R.M. and Brillas, E., (2007) Degradation of clofibric acid in acidic aqueous medium by electro-Fenton and photoelectro-Fenton. Chemosphere 66, 1660–1669

Skoumal, M., Cabot, P.L., Centellas, F., Arias, C., Rodriguez, R.M., Garrido, J.A. and Brillas, E., (2006) Mineralization of paracetamol by ozonation catalyzed with Fe2+, Cu2+ and UVA light. Appl. Catal. B: Environ. 66, 228–240

Suarez-Ojeda, M.E., Stuber, F., Fortuny, A., Fabregat, A., Carrera, J. and Font, J. (2005) Catalytic wet air oxidation of substituted phenols using activated carbon as catalyst. Appl. Catal. B: Environ. 58, 105–114

Sun, Y. and Pignatello, J.J. (1993) Photochemical reactions involved in the total mineralization of 2,4-D by iron(3+)/hydrogen peroxide/UV. Environ. Sci. Technol. 27, 304–310

Toepfer, B., Gora, A. and Li Puma, G. (2006) Photocatalytic oxidation of multicomponent solutions of herbicides: Reaction kinetics analysis with explicit photon absorption effects. Appl. Catal. B: Environ. 68, 171–180

Torres, R.A., Torres, W., Peringer, P. and Pulgarin, C. (2003) Electrochemical degradation of p-substituted phenols of industrial interest on Pt electrodes. Attempt of a structure-reactivity relationship assessment. Chemosphere 50, 97–104

Trillas, M., Peral, J. and Domènech, X. (1995) Redox photodegradation of 2,4-dichlorophenoxyacetic acid over TiO2. Appl. Catal. B: Environ. 5, 377–387

Yermakova, A., Mikenin, P.E. and Anikeev, V.I. (2006) Phenol oxidation in supercritical water in a well-stirred continuous reactor. Theor. Found. Chem. Eng. 40, 168–174

Yu, F.Y., Li, C.W. and Kang, S.F. (2005) Color, dye and doc removal, and acid generation during Fenton oxidation of dyes. Environ. Technol. 26, 537–544

Zhi, J.F., Wang, H.B., Rao, T.N., Fujishima, A. and Nakashima, T. (2003) Electrochemical incineration of organic pollutants on boron-doped diamond electrode. Evidence for direct electrochemical oxidation pathway. J. Phys. Chem. B 107, 13389–13395

Chapter 9
The Persulfate Process for the Mediated Oxidation of Organic Pollutants

N. Vatistas and Ch. Comninellis

9.1 Introduction

In the field of wastewater treatment, the oxidation reaction of organic pollutants by dissolved oxygen is not impeded by thermodynamics but by the high activation energy of the reaction. In fact, thanks to the catalytic action of enzymes; biological treatment allows a sufficiently high oxidation rate to be obtained for many pollutants, but not for those that are bio-refractory and need to be oxidized using highly active oxidants.

A highly active oxidant such as the hydroxyl radical ($OH^{\cdot}$), oxidizes both wastewater organic and inorganic compounds with high oxidation rates (Buxton et al. 1988), thus this radical is rapidly consumed and its action occurs only in the region where it is produced. Consequently, if the production region contains a high concentration of organic pollutants or a large enough flow of these species reaches this region then the produced radical is efficiently used and is not lost in the oxidation of other species.

The Boron-Doped Diamond (BDD) anode produces highly active hydroxyl radicals on its surface (Iniesta et al. 2001a) thus the treatment of wastewater with this type of anodes requires an adequate flow of organic pollutants toward the anodic region, to achieve a very efficient process. When during the treatment the concentration and flow of organic pollutants is significantly reduced, only a portion of the hydroxyl radicals that are produced oxidize the inorganic species of wastewater and the efficiency of the treatment drops.

Less-active oxidants such as persulfate $\left(S_2O_8{}^{2-}\right)$, percarbonate $\left(C_2O_6{}^{2-}\right)$, and hydrogen peroxide (H_2O_2) are all efficiently produced with BDD anodes (Michaud et al. 2000, 2003; Serrano et al. 2002; Saha et al. 2003, 2004; Katsuki et al. 1998; Kraft et al. 2006). These oxidants are relatively stable at ambient conditions and are defined as *precursors* due to their characteristic of generating highly active inorganic radicals when a catalyst or a form of energy is used

N. Vatistas (✉)
Chemical Engineering Department, University of Pisa Via Diotisalvi, 2, 56126 Pisa, Italy
e-mail: vatistas@ing.unipi.it

C. Comninellis and G. Chen (eds.), *Electrochemistry for the Environment*,
DOI 10.1007/978-0-387-68318-8_9,

(Dogliotti and Hayon 1967; Hayou et al. 1972; Walling 1975; Thompson 1981). The stability of these precursors and the controlled oxidative action they show permit their production in the anodic region and the successive activation after their mixing with the organic pollutants. In other words, these precursors produced with the BDD anodes introduce new possibilities of mediated oxidation during electrochemical treatment.

The mediated oxidation method is not new and it is considered during treatments with the conventional anodes. As an example in the electro-Fenton process the production of precursor (H_2O_2) and catalyst (Fe^{2+}) on the two electrodes of the cell is promoted. In this case, the subsequent diffusion and mixing of the produced species generates hydroxyl radicals in the bulk of the solution that efficiently eliminate the organic pollutants from the wastewater (Do and Chen 1994; Brillas et al. 1996; Alvarez-Gallegos and Pletcher 1999; Panizza and Cerisola 2001; Zhang et al. 2006). A similar mediated oxidation during electrochemical treatment is proposed for wastewater containing chloride ions at neutral or basic conditions. In this case, thanks to the basic condition of wastewater; the produced chlorine generates the more soluble hypochlorite (ClO^-), which efficiently oxidizes the organic pollutants. Results of experimental tests have shown the significant contribution of mediated oxidation during the electrochemical wastewater treatment (Czarnetzki and Janssen 1992; Comninellis and Nerini 1995; Szpyrkowicz et al. 2005).

Experimental tests have shown that persulfate is produced during electrochemical treatment of effluent containing organic pollutants and sulfate ions with BDD anodes, and the effect of this precursor on the organic pollutant oxidation has to be considered in order to explain the experimental results (Michaud et al. 2000; Canizares et al. 2004). Moreover, a theoretical model has been proposed that includes the contribution of the mediated oxidation, and the parameters of this model is estimated by the fitting of the experimental results (Canizares et al. 2003). It is evident that in this case the contribution of mediated oxidation depends on the following operating conditions (1) temperature of wastewater, (2) applied current density, (3) quantity of sulfate ions, and (4) introduction time of sulfate ions in the wastewater. These conditions have not been systematically considered, thus the real possibilities of mediated oxidation with this precursor have not been clearly described.

This chapter therefore proposes a systematic study of mediated oxidation using persulfate as precursor. The initial part of this chapter will consider the conditions of hydroxyl radical production on the BDD anode and mass-transfer limitation, and these conditions will be related to the range of the operating parameters of the electrochemical treatment. The range that assures the maximum efficiency of the treatment will be estimated, together with the possibility of its extension using mediated oxidation.

The second part of this chapter will deal with the performance of mediated oxidation with persulfate and the BDD anode using the single-cell treatment method. Experimental tests at different temperatures and concentrations of organic pollutants, with and without the mediated oxidation, will be done to detect the effect of operating parameters on the overall efficiency of the electrochemical treatment.

Finally, the last part of the chapter contains the proposal of a mediated oxidation method in two new steps that will improve both mechanisms of mediated oxidation, i.e., production and activation of precursor and an increase in the positive contribution of mediated oxidation.

9.2 Kinetic and Mass-Transfer Barriers and Mediated Oxidation

Electrochemical treatment tests of organic pollutants with the BDD anode have shown that the high selectivity is due to its high over-potential with respect to the oxygen evolution reaction. The primary effect of this fact is that a high anodic potential is reached by applying a relatively low current density, which allows the efficient generation of the highly active hydroxyl radicals in the anodic region.

The hydroxyl radicals produced oxidized organic compounds, and even the inorganic ions that reach the anodic region, and also maintain the BDD surface clean. In fact, experimental results show that if the anodic potential is not high enough to produce hydroxyl radicals, a polymeric film covers the surface of BDD anode, and this film blocks the progress of the electrochemical treatment (Iniesta et al. 2001b). In other words, the BDD anode shows two qualitatively different operating regimes that can be easily controlled during the treatment by the value of the applied current density or by the anodic potential.

In this context, the minimal anodic potential that maintains the BDD surface clean can be defined as *the minimal hydroxyl production potential* $\left(E_{k,\min}\right)$, and similarly the required current density to reach this potential can be defined as *the minimal hydroxyl production current density* $\left(i_{k,\min}\right)$. Definition of the above parameters allows us to state that the anodic surface is maintained clean if the applied current density $\left(i_{\text{appl}}\right)$ satisfies the following condition (9.1) during the treatment.

$$i_{k,\,\min} \leq i_{\text{appl}}. \tag{9.1}$$

An optimal use of the applied current density requires one further condition: the flow of organic pollutants toward the anodic surface must be sufficient to consume the produced hydroxyl radicals on the same surface. The maximum flow of organic pollutants toward the anode can be expressed as limiting current density (i_{lim}), and this further condition assumes the form (9.2).

$$i_{\text{appl}} \leq i_{\text{lim}}. \tag{9.2}$$

The combination of the above two conditions (9.1) and (9.2), gives the following range of applied current density (9.3):

$$i_{k,\,\min} \leq i_{\text{appl}} \leq i_{\text{lim}}. \tag{9.3}$$

If the applied current satisfies this condition (9.3), the BDD anode remains clean and the current efficiency assumes its maximum value ($\eta = 1.0$).

The previously reported condition requires a relationship between the limiting current density and COD, which is measured during the treatment. An exact determination of this relationship is a complicate task but if it is assumed that all the organic compounds that reach the anodic surface are instantaneously transformed into inorganic ones, (9.4) relates the value of the limiting current density to the COD (Gherardini et al. 2001):

$$i_{\text{lim}} = 4Fk_{\text{m}}\text{COD}, \tag{9.4}$$

where F is the Faraday constant and k_{m} is the mass transfer coefficient.

As (9.4) shows, the limiting current density decreases during treatment due to the decreasing organic pollutants' concentration. When the limiting current density reaches the minimal hydroxyl production current density $\left(i_{\text{lim}} = i_{k,\text{min}}\right)$, the previous range of applied current density given by the condition (9.3) is reduced to its minimum value (9.5):

$$i_{\text{appl, min}} = i_{k,\text{min}}. \tag{9.5}$$

Combining (9.4) and (9.5) produces (9.6), which estimates the minimal COD value that assures maximum current efficiency:

$$\text{COD}_{k,\text{min}} = i_{k,\text{min}}/4Fk_{\text{m}}. \tag{9.6}$$

In fact, if the COD value of the wastewater falls below $\text{COD}_{k,\text{min}}$, during the electrochemical treatment, there is an insufficient flow of organic pollutants reaching the anode to consume the generated hydroxyl radical. Consequently, the excess of generated hydroxyl radicals in this region are consumed in the oxidation of other species.

Figure 9.1 indicates the whole region of operating conditions that concern the electrochemical treatment. This whole region is separated into four regions by the line of limiting current i_{lim} and the line of minimal hydroxyl production current density $i_{k,\text{min}}$. The BDD anode is maintained clean in the regions I and II, while an organic film is formed on the surface which obstructs the oxidation process (anode fouling) in the regions III and IV. Only the conditions in the region II permit the anode to remain clean and the treatment to occur with the maximum value of current efficiency. The same figure also shows the characteristic COD values of wastewater $\left(\text{COD}_{\text{in}},\ \text{COD}_{k,\text{min}},\ \text{and}\ \text{COD}_{\text{f}}\right)$.

During a typical batch electrolysis, the minimal COD value can be estimated $\left(\text{COD}_{k,\text{min}} = 4.25\,\text{mmol dm}^{-3}\ \text{or}\ 136\,\text{ppm}\right)$ by assuming a typical value of minimal hydroxyl production current density $\left(i_{k,\text{min}} = 5.0\,\text{mA cm}^{-2}\right)$, and a characteristics value of mass-transfer coefficient $\left(k_{\text{m}} = 3 \times 10^{-5}\,\text{m s}^{-1}\right)$. The obtained minimal COD value is higher than the final treatment value that is usually required (COD_{f}). Consequently, it can be stated that the electrochemical treatment loses a part of electric charge supplied in secondary reactions in this final step $\left(\text{COD}_{\text{f}} < \text{COD} < \text{COD}_{k,\text{min}}\right)$.

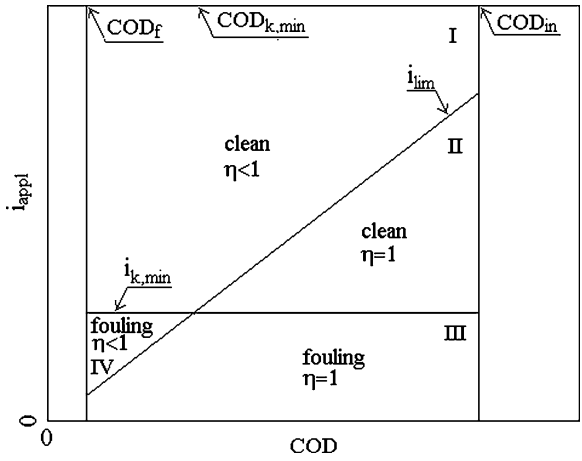

Fig. 9.1 The operating regions of the electrochemical wastewater treatment with BDD anodes

9.3 The Mediated Oxidation with Persulfate

To increase the efficiency of the electrochemical wastewater treatment process with conventional anodic materials, the mediated oxidation method has been proposed. This method avoids the production of oxygen, thanks to the generation of precursors that are successively transformed to active oxidants. When the BDD anodes are used, a positive contribution of the generated active oxidants can also be foreseen, but only in the previously defined region IV of the treatment. The production of strong oxidants in this region avoids the mass-transfer limitation and treatment efficiency is recovered.

It is important to note that mediated oxidation using the conventional anodic materials is applied in order to improve the low oxidative action of these materials. Consequently, with these materials mediated oxidation is required during the whole electrochemical treatment, while with the BDD anodes this oxidation is only needed in the region IV of the treatment when the mass-transfer regime limits the treatment efficiency.

9.3.1 Production of Persulfate

The success of mediated oxidation is related to the efficient production and activation of precursors. Experimental tests exploring the production of precursors with the BDD anode point out that the persulfate precursor is produced with a high-current efficiency ($\eta > 0.95$) when the electrolyte contains a high concentration of sulfate ions $\left(\mathrm{C} > 2.0\,\mathrm{mol\,dm^{-3}}\right)$ and the process temperature is low ($T < 10°\mathrm{C}$) (Michaud et al. 2000; Serrano et al. 2002). The effect of concentration of sulfate

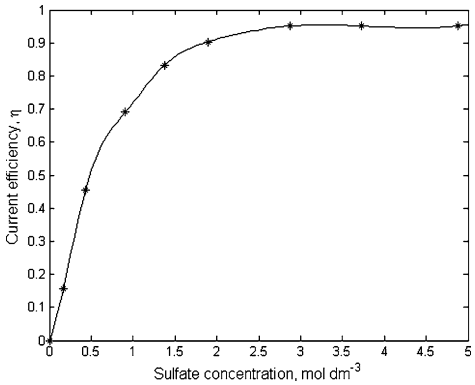

Fig. 9.2 Current efficiency vs. concentration of sulfate on BDD electrode. Current density 23 mA cm^{-2}, temperature 9°C (from Serrano et al. 2002)

on the current efficiency with BDD anodes is reported in Fig. 9.2. It is important to note that the value of this efficiency is higher than the convectional platinized titanium, tantalum, or nobium anodes used in industrial electrosynthesis (about 70–75%) (Ibl and Vogt 1981).

This large value of current efficiency is higher than that for the production of alternative precursors such as percarbonate and hydrogen peroxide (Saha et al. 2003, 2004; Katsuki et al. 1998; Michaud et al. 2003; Kraft et al. 2006).

9.3.2 Activation of Persulfate

The activation of persulfate occurs via the generation of the highly active sulfate radical ($SO_4^{-\cdot}$), and this step requires a transition metal catalyst (Ag^+, Fe^{2+},Mn^{2+}, etc.) or a form of energy (heat, UV light, etc.). Heat activation has been studied in detail from some time to explain the degradation of persulfate in aqueous solutions (Kolthoff and Müller 1951; Berlin 1986; Tanner and Osmar 1987):

$$S_2O_8^{2-} \rightarrow 2SO_4^{-\cdot} \tag{9.7}$$

The thermally activated persulfate can oxidize the organic compounds and initial studies in this field have examined the fundamental aspects of this oxidation (Kolthoff and Müller 1951; Allen 1951; House 1962; Gallopo and Edwards 1971; Goulden and Anthony 1978; Berlin 1986). The application of this oxidation has recently been considered in the treatment of groundwater and soils contaminated by bio-refractory organic pollutants. Experimental results obtained in the typical temperature range of this field (20–50°C) indicate the important effect of temperature in eliminating the initial organic pollutants. In particular, the mean half-life of the organic pollutants at the lower temperatures is rather long ($t_{1/2} = 10\,h$). (Liang et al. 2003; Huang et al. 2005).

In the field of wastewater treatments, thermally activated persulfate has also been proposed and tested in a process called *direct chemical oxidation* (DCO) (Anipsitakis and Dionisiou 2002). In addition, the available literature contains promising experimental results at high-temperature range (110–390°C). These results demonstrate that use of this oxidant permits high oxidation rates to be achieved, i.e., the elimination of 4-chloro-3-methylphenol is completed with a very short reaction time $\left(3 < t_{1/2} < 59\,\mathrm{s}\right)$ (Kronholm et al. 2001).

9.4 Alternative Methods of Mediated Oxidation

Mediated oxidation with conventional anodic materials has already been applied using a cell in which direct and mediated oxidation occurs. It is important to note that the objective when using conventional anodic materials was to improve the low oxidative action of these anodes, not to improve the mass-transfer limitation found with BDD anodes. Consequently, it is not taken for granted that the single-step method is the most suitable one.

In the single-step method, both production of persulfate and oxidation of organic pollutants occur at the same temperature. Operating at a high temperature, the mediated oxidation rate is high but little persulfate is produced, while at a low temperatures more persulfate is produced but the mediated oxidation rate is low. In this single-step case, the temperature is the most important treatment parameter.

A two-step mediated oxidation method can be proposed that separates the persulfate production step from its activation and organic pollutants' oxidation. In this way, the optimum conditions of temperature and concentration can be adopted in order to reach the maximum efficiency of mediated oxidation.

9.4.1 Single-Step Mediated Oxidation Method

As previously reported with single-step mediated oxidation, temperature has a complex effect. This complexity can be partially reduced by comparing the characteristic times of mediated and direct oxidation that occurs, respectively, in the bulk of the wastewater and on the anodic surface. In this field, a pseudo-first-order rate is normally assumed for mediated oxidation and consequently the characteristic time of the mediated oxidation (τ_{med}) is related with the half-life of the pollutants $t_{1/2}$ by (9.8).

$$\tau_{\mathrm{med}} = t_{1/2}/\ln 2. \tag{9.8}$$

The characteristic time of direct electrochemical oxidation (τ_{dir}) is easily estimated during the mass-transfer regime and is derived by (9.9).

$$\tau_{\mathrm{dir}} = V/(k_{\mathrm{m}}S), \tag{9.9}$$

where k_m is the mass-transfer coefficient, S the anodic surface, and V is the volume of wastewater to be treated.

Temperature variation has a strong effect on the characteristic time of the mediated oxidation but not on that of the direct oxidation. Consequently the positive or negative contribution of the mediated oxidation has an effect when the characteristic time of the mediated oxidation is less than that of the direct oxidation ($\tau_{med} < \tau_{dir}$).

To evaluate this process, salicylic acid has been used as a model of organic pollutant. In all the experimental tests, a constant current density was applied $(15.8\,\text{mA cm}^{-2})$. The organic pollutant was used at two different levels of concentrations $(3.6 \text{ and } 7.2\,\text{mmol dm}^{-3})$, in order to include the mediated oxidation during the final or entire treatment time. Sulfuric or perchloric acids were used at the same concentration $(1\,\text{mol dm}^{-3})$ to assure the same pH value in the wastewater. The use of perchloric acid impeded mediated oxidation while maintaining the same conductivity and acid condition in the wastewater as in the case of wastewater containing sulfuric acid.

A two-compartment cell was adopted to avoid the reduction of produced persulfate in the cathode and an ion-selective membrane, Nafion® N117/H^+, separated the two compartments of the cell. A circular BDD anode was used and a cathode with the same surface $(S = 63\,\text{cm}^2)$ was used. Two thermostatted tanks maintained the temperature of both solutions constant, while the recirculation of the solutions in the cell by two pumps assured a constant mass-transfer coefficient in the anodic and cathodic region during the test $(k_m = 2.0 \times 10^{-5}\,\text{m s}^{-1})$. The characteristic time of the direct oxidation was calculated in this series of tests ($\tau_{dir} = 1.10\,\text{h}$), with the previous relationship (9.9).

Figure 9.3 reports the values of dimensionless organic pollutants' concentration (COD/COD_{in}) vs. treatment time. These results are for two experimental tests with

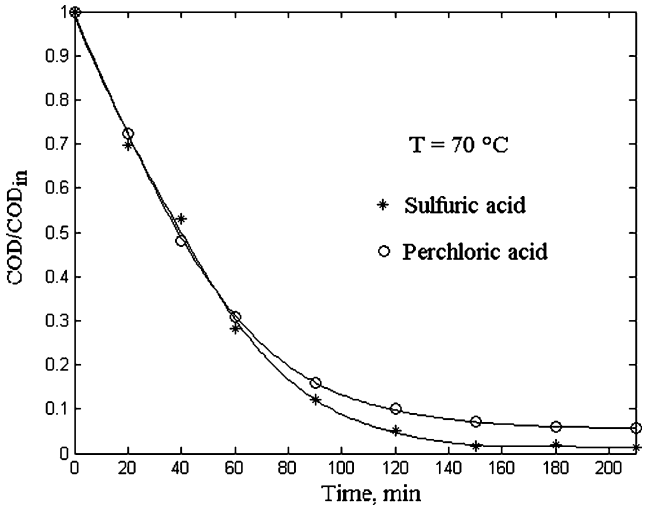

Fig. 9.3 COD/COD_{in} vs. treatment time, with a low initial salicylic acid and sulfuric or perchloric acid. Salicylic acid concentration 3.6 mmol dm^{-3}, sulfuric acid or perchloric acid concentration 1 mol dm^{-3}, temperature 70°C, applied current density 15.8 mA cm^{-2}

the same value of temperature (70° C) and applied current density $\left(15.8\,\text{mA cm}^{-2}\right)$. The wastewater in the two tests contained, respectively, sulfuric acid and perchloric acid. Both tests were performed using the same low initial concentration of salicylic acid $\left(3.6\,\text{mmol dm}^{-3}\right)$, in order to operate at the conditions of mass-transfer regime during treatment.

Comparison of the results obtained indicates that the test performed using sulfuric acid reaches lower values of dimensionless concentration of organic pollutants ($\text{COD}/\text{COD}_{\text{in}}$), with respect to the test with the perchloric acid. This result points out that mediated oxidation with the persulfate has a positive contribution on the elimination of organic pollutants. The same tests were also done at ambient temperature and the results obtained (not reported here) were compared. In this case, the contribution of mediated oxidation was not observed, due to the higher characteristic time of the mediated oxidation at ambient temperature ($\tau_{\text{med}} = 14\,\text{h}$), with respect to the characteristic time of the direct electrochemical treatment time ($\tau_{\text{dir}} = 1.10\,\text{h}$).

Figure 9.4 reports the results of the subsequent two tests at 70°C that featured a higher concentration of salicylic acid with respect to the previous ones $\left(7.2\,\text{mmol dm}^{-3}\right)$. In these two tests, the electrochemical treatment is not subject to mass-transfer limitation from the outset, i.e., the cell initially operates in chemical regime and only operates in the mass-transfer regime in the final stage. These tests were used to examine the contribution of the mediated oxidation throughout the entire treatment, i.e., when the wastewater contains sulfate. Comparison of the obtained results shows that mediated oxidation initially has a small negative contribution, while at the end of the treatment this contribution becomes positive. In order to explain this result, it is assumed that the persulfate production step occurs

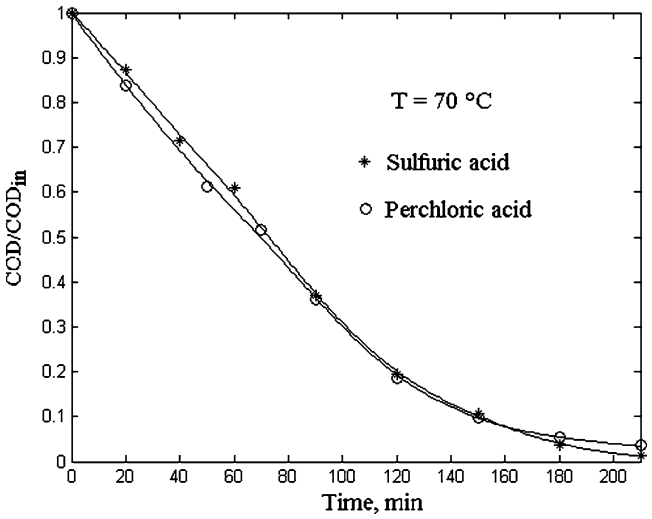

Fig. 9.4 $\text{COD}/\text{COD}_{\text{in}}$ vs. treatment time, with a high initial salicylic acid and sulfuric or perchloric acid. Salicylic acid concentration 7.2 mmol dm^{-3}, sulfuric acid concentration or perchloric acid concentration 1 mol dm^{-3}, temperature 70°C, and applied current density 15.8 mA cm^{-2}

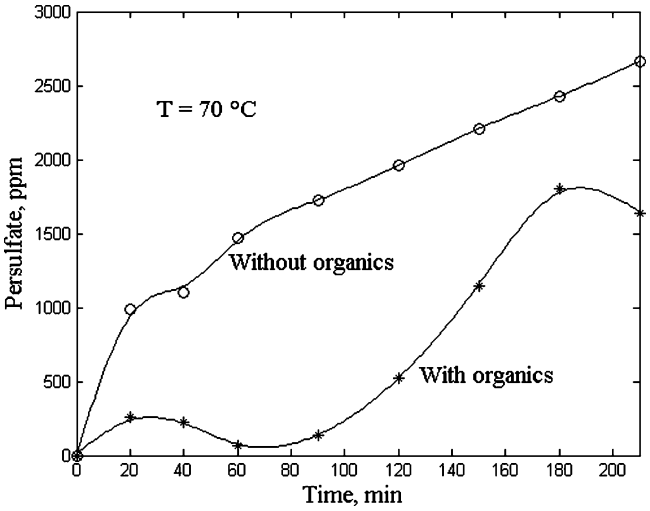

Fig. 9.5 Persulfate concentration vs. treatment time of two solution containing initially sulfuric acid solutions with and without salicylic acid. Initial sulfuric acid concentration 1 mol dm^{-3}, initial salicylic acid concentration 3.6 mmol dm^{-3}, temperature 70°C, and applied current density 15.8 mA cm^{-2}

throughout the treatment, even during the initial phase with a low current efficiency and in this case the positive contribution of mediated oxidation in the final mass-transfer regime is partially eliminated by its negative contribution in the preceding chemical regime.

In order to confirm the previous assumption, Fig. 9.5 shows the persulfate produced during two different tests. One is related with the sulfuric acid reported in Fig. 9.4, while the other is a specific test performed at the same operating conditions but without salicylic acid. The first aspect to note is the rapid production of persulfate at the initial time, when the salicylic acid concentration is high. This result indicates that despite the high flow of organic pollutants toward the anode, a portion of the furnished current is used to oxidize the sulfate ions, and thus not all the furnished current is used for salicylic acid oxidation. Moreover, the reported persulfate concentration in the solution without organic pollutants indicates that persulfate is produced under the same operating conditions with a low current efficiency ($0.1 < \eta < 0.4$). These results confirm the previous assumptions on the negative and positive contribution of mediated oxidation during the treatment.

9.4.2 Two-Step Mediated Oxidation Method

An improvement in mediated oxidation can be expected by increasing the efficiency of persulfate production and the oxidation rate of organic pollutants. These objectives can be reached with a new two-step mediated oxidation method that separates

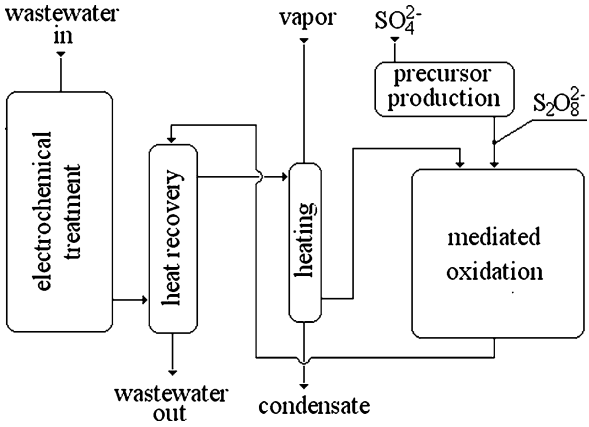

Fig. 9.6 Scheme of wastewater treatment with an initial electrochemical treatment with BDD anodes and a successive two-step mediated oxidation, with the precursor produced locally with the use of the same kind of anodes

the production from the activation and oxidation mechanisms. In the first step, a small electrochemical cell electrolyzes a low-temperature electrolyte of high sulfate ions concentration. The efficiently produced persulfate is introduced to the pre-heated wastewater, where the persulfate is then activated and the organic pollutants are efficiently oxidized.

Figure 9.6 reports a scheme of this two-step mediated oxidation process. The wastewater is subjected to an initial electrochemical treatment with BDD anodes. With this treatment, the organic pollutants' concentration reaches $COD_{k,\min}$ with maximum current efficiency. In the subsequent treatment, pollutants' elimination occurs through mediated oxidation by the introduced persulfate, which is activated by the previously heated wastewater. The same figure also shows that a part of required heat is recovered by the treated wastewater.

The success of proposed two-step process depends on the efficient production of persulfate and on the rate and yield of mediated oxidation. Both efficient production and yield value are related to the consumed electric energy, while the oxidation rate is related to the required volume of the reaction vessel.

As previously reported the persulfate is produced easily, safely, and in small quantities with the use of cells with BDD anodes.

9.4.2.1 Yield of Organic Pollutants' Oxidation

Yield during the oxidation of organic pollutants has not been considered in literature, and for this reason first a relationship for the estimation of yield is reported here and following this, a series of oxidation tests has been performed to estimate both yield and oxidation rate.

The yield of organic pollutant oxidation by persulfate y is defined as the ratio of stoichiometric persulfate variation for the oxidation of organic pollutant ΔC_s, with respect to the persulfate that is effectively consumed ΔC:

$$y = \Delta C_s / \Delta C. \tag{9.10}$$

The value of yield can be related to a specific instant of oxidation process (point yield) or with the complete process (integral yield) (Carbery 1976).

The quantity of persulfate consumed can be obtained by measuring its concentration in solution, while the stoichiometric quantity must be related to the elimination of organic pollutants. Usually during treatment, the whole organic compound concentration is measured by COD in order to know the oxidation progress. The yield estimation (9.10) requires a relationship between the variation of COD and the variation of C_s and this relationship is given by (9.11).

$$\Delta C_s = 2\Delta \mathrm{COD}. \tag{9.11}$$

The above equation is obtained by the stoichiometry of persulfate degradation.

$$S_2O_8{}^{2-} + H_2O \rightarrow 2SO_4{}^{2-} + 2H^+ + (1/2)O_2 \tag{9.12}$$

The substitution of (9.10) into (9.11) allows the yield to be related to measured quantities during the treatment:

$$y = 2\Delta \mathrm{COD} / \Delta C_s. \tag{9.13}$$

The above relationship can be used for the estimation of the yield during the oxidation of organic pollutants by the persulfate.

9.4.2.2 Chemical Oxidation of Salicylic Acid

Figure 9.7 reports the measured COD values during the oxidation vs. treatment time at tested temperatures (70, 80, and 90°C). Comparison of the results shows the strong effect of temperature on the time required to complete the treatment due to the activation of persulfate. Moreover, the low final value of COD reached shows that the excess of persulfate used is sufficient for the complete elimination of salicylic acid.

Figure 9.8 reports the logarithmic ratio of persulfate $\ln(C/C_{in})$ during oxidation tests. These results indicate that the rate of persulfate elimination is not of the first order respect to its concentration. If it is assumed that the elimination of persulfate is principally due to the oxidation of organic pollutants, then the oxidation of these organics is not first order with respect to the persulfate concentration.

Despite the nonlinear oxidation rate obtained, the kinetic constants have been estimated by assuming a pseudo-first-order oxidation rate. The estimated mean values

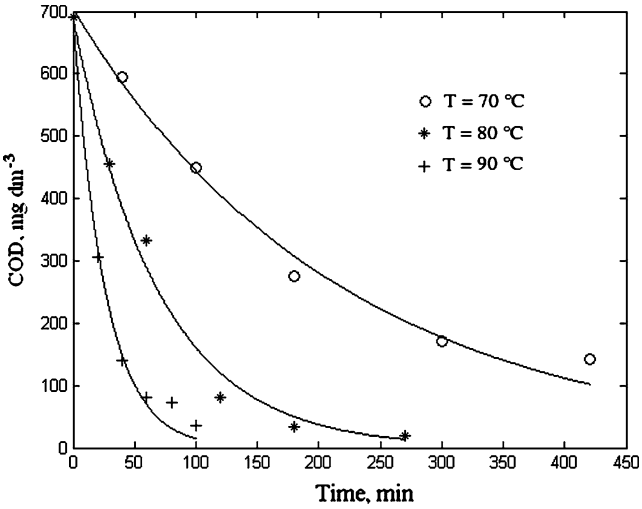

Fig. 9.7 COD vs. oxidation time, at 70, 80, and 90°C; pH 13.0; persulfate concentration 56 mmol dm^{-3}; and salicylic acid concentration 3 mmol dm^{-3}

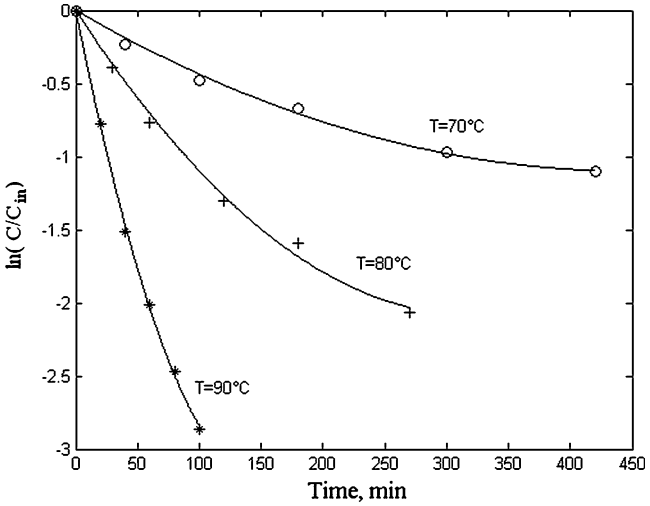

Fig. 9.8 $\ln(C/C_{in})$ vs. oxidation time, at 70, 80, and 90°C; pH 13.0; persulfate concentration 56 mmol dm^{-3}; and salicylic acid concentration 3 mmol dm^{-3}

of kinetic parameter (k) at the various test temperatures are used to fit the Arrhenius law, and activation energy and pre-exponential factors of the pollutants' oxidation have been estimated $\left(E_a = 123\,\text{kJ mol}^{-1},\ A_0 = 1.73 \times 10^{16}\,\text{min}^{-1}\right)$.

Figure 9.9 shows the change of persulfate concentration, one deriving directly from its measurement and the other indirectly by the Chemical Oxygen Demand

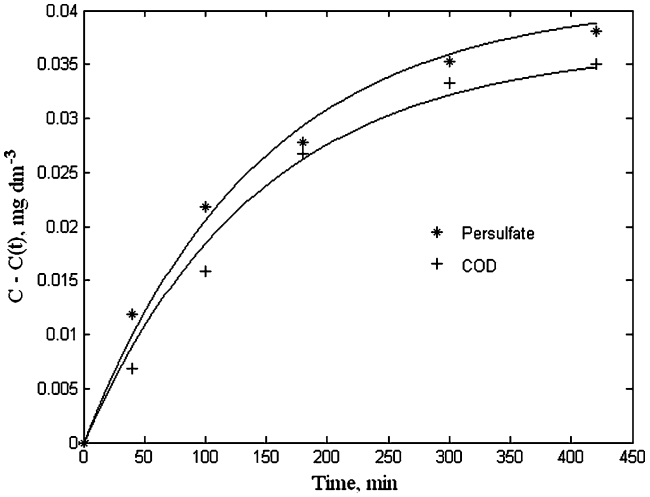

Fig. 9.9 Persulfate reduction obtained by direct measurement (*asterisk*), and indirectly by the measured values of COD (*plus*) vs. oxidation time, at 70, 80, and 90°C; pH 13.0; persulfate concentration 56 mmol dm^{-3}; and salicylic acid concentration 3 mmol dm^{-3}

measurements. In the same figure they are also reported the two fitting curves. The higher curve is related to the direct measurement and concern the whole consumption of persulfate, while the lower one is related to the consumption of persulfate that concerns the oxidation of organic compounds and is calculated using measured COD values. These results are from the oxidation test at 70°C, also the other tests at different temperatures shown a similar behavior.

The yield values are calculated using (9.13) and the estimated value was found to be high ($y \cong 0.90$). This result indicates that persulfate is principally used to oxidize organic pollutants and only a minimal part of this oxidant is used for other oxidation reactions.

9.5 Conclusions

This chapter examines the possibility of using mediated oxidation during the electrochemical treatment of wastewater with BDD anodes, and a comparison is made of the difference in the mediated oxidation contribution using a BDD anode respect to the conventional anodic materials. The contribution of this oxidation in the conventional anodic materials is the improvement of the low oxidative action of these anodes throughout the entire treatment, while in the case of BDD anode, a positive contribution is only found during the mass-transfer regime that occurs at the end of the electrochemical treatment.

By considering the specific characteristic of BBD anode, i.e., the production of hydroxyl radicals, a separation is obtained between the region of the maximum

current efficiency and the region of lower efficiency related to the mass-transfer regime. The characteristics of the mediated oxidation for the BDD anode are initially examined so mediated oxidation can be applied efficiently.

The existing single-step mediated oxidation method is considered, together with a new version, consisting of two separate steps that improve all the mechanisms of this oxidation. Experimental tests have performed using the single- and two-step mediated oxidation methods and the results of these tests are reported. Comparison of these results finds that the contribution of mediated oxidation is low for the single-step method; while this contribution is higher when the two-step mediated oxidation method is applied.

References

Allen, T. (1951). The oxidation of oxalate ion by peroxydisulfate. J. Am. Chem. Soc. 73, 3589–3593.

Alvarez-Gallegos and D. Pletcher (1999). The removal of low level organics via hydrogen peroxide formed in a reticulated vitreous carbon cathode cell. Part 2: The removal of phenols and related compounds from aqueous effluents. Electrochim. Acta 44, 2483–2492.

Anipsitakis, K. and D. Dionisiou (2002). Transition metal/UV-based advance oxidation technologies for water decontamination. Appl. Catal. B: Environ. 54, 155–163.

Berlin, A. (1986). Kinetics of radical-chain decomposition of persulfate in aqueous solutions of organic compounds. Kinetic Catal. 27, 34–39.

Brillas, E., E. Mur, and J. Casado (1996). Iron(II) catalysis of the mineralization of aniline using a carbon-PTFE O_2-FED cathode. J. Electrochem. Soc. 143, L49–L53.

Buxton, G., C. Greenstock, W. Helman, and A. Ross (1988). Critical review of rate constants for reactions of hydrated electrons, hydrogen atoms and hydroxyl radicals in aqueous solution. J. Phys. Chem. Ref. Data 17, 513–886.

Canizares, P., J. Lobato, and M. Rodrigo (2003). Electrochemical oxidation of aqueous caboxylic acid wastes using diamond thin-film electrodes. Ind. Eng. Chem. Res. 42, 956–962.

Canizares, P., J. Garcja-Gomez, C. Saez, and M. Rodrigo (2004). Electrochemical oxidation of several chlorophenols on diamond electrodes. Part II. Influence of waste characteristic and operating conditions. J. Appl. Electrochem. 34, 87–94.

Carbery, J. (1976). *Chemical and Catalytic Reaction Engineering*. McGraw-Hill, New York, NY.

Comninellis, C. and A. Nerini (1995). Anodic oxidation of phenol in the presence of NaCl for wastewater treatment. J. Appl. Electrochem. 24, 23–28.

Czarnetzki, L. and L. Janssen (1992). Formation of hypochlorite, chlorate and oxygen during NaCl electrolysis from alkaline solutions at an RuO_2/TiO_2 anode. J. Appl. Electrochem. 22, 315–324.

Do, J. and P. Chen (1994). In-situ oxidative degradation of formaldehyde with hydrogen peroxide electrogenerated on the modified graphites. J. Appl. Electrochem. 24, 936–942.

Dogliotti, L. and E. Hayon (1967). Flash photolysis of persulfate in aqueous solutions. Study of sulfate and ozonite anions. J. Phys. Chem. 71, 2511–2516.

Gallopo, A. and J. Edwards (1971). Kinetics and mechanism of the spontaneous and metal modified oxidation of ethanol by peroxydisulfate ion. J. Org. Chem. 36, 4089–4096.

Gherardini, L., P. Michaud, M. Panizza, C. Comninellis, and N. Vatistas (2001). Electrochemical oxidation of 4-chlorophenol for wastewater treatment: Definition of normalized current efficiency. J. Electrochem. Soc. 148, D78–D82.

Goulden, P. and D. Anthony (1978). Kinetics of uncatalyzed peroxydisulfate oxidation of organic materials in fresh water. Anal. Chem. 50, 953–958.

Hayou, E., A. Treinin, and J. Wilf (1972). Electronic spectra, photochemistry and autoxidation mechanism of sulfite–bisulfite–pyrosulfite systems. J. Am. Chem. Soc. 94, 47–57.

House, D. (1962). Kinetics and mechanism of oxidation by peroxydisulfate. Chem. Rev. 62, 185–203.

Huang, K., Z. Zhao, G. Hoag, A. Dahmani, and B. Block (2005). Degradation of volatile organic compounds with thermally activated persulfate oxidation. Chemosphere 61, 551–560.

Ibl, N. and H. Vogt (1981). In: J.O.'M. Bockris, B.E. Conway, E. Yeager, R.E. White (Eds), *Comprehensive Treatise of Electrochemistry*, vol. 2, pp. 224. Plenum, New York, NY.

Iniesta, J., P. Michaud, M. Panizza, G. Cerisola, A. Aldaz, and C. Comninellis (2001a). Electrochemical oxidation of phenol at boron-doped diamond electrode. Electrochim. Acta 46, 3573–3578.

Iniesta, J., P. Michaud, M. Panizza, G. Cerisola, A. Aldaz, and C. Comninellis (2001b). Electrochemical oxidation of phenol at boron-doped diamond electrode. Electrochim. Acta 46, 3573–3578.

Katsuki, N., E. Takashashi, M. Toyoda, T. Kuosu, M. Iida, S. Wakika, Y. Nishiki, and T. Shimamune (1998). Water electrolysis using diamond thin-film electrodes. J. Electrochem. Soc. 145, 2358–2362.

Kolthoff, I. and J. Müller (1951). The chemistry of persulfate: I. The kinetics and mechanism of the persulfate ion in aqueous medium. J. Am. Chem. Soc. 73, 3055–3059.

Kraft, A., M. Stadelmann, M. Wünsche, and M. Blaschke (2006). Electrochemical ozone production using diamond anodes and a solid polymer electrolyte. Electrochem. Commun. 8, 883–886.

Kronholm, J., H. Metsala, K. Hartonen, and M. Riekkola (2001). Oxidation of 4-chloro-3-methylphenolin pressurized hot water/supercritical with potassium persulfate as oxidant. Environ. Sci. Technol. 35, 3247–3251.

Liang, C., C. Bruell, M. Marley, and K. Sperry (2003). Thermally activated persulfate oxidation of trichloroethylene (tce) and 1,1,1-trichloroethane in acqueous systams and soil slurries. Soil Sediment Contam. 12, 207–228.

Michaud, P., E. Mahe, W. Haenni, A. Perret, and C. Comninellis (2000). Preparation of peroxodisulfuric acid using boron-doped diamond thin film electrodes. Electrochem. Solid State 3, 77–79.

Michaud, P., M. Panizza, L. Quattara, T. Diaco, G. Foti, and C. Comninellis (2003). Electrochemical oxidation of water on synthetic boron-doped diamond thin film anodes. J. Appl. Electrochem. 33, 151–154.

Panizza, M. and G. Cerisola (2001). Removal of organic pollutants from industrial wastewater by electrogenerated Fenton's reagent. Water Res. 36, 3987–3992.

Saha, M., T. Furuta, and Y. Nishita (2003). Electrochemical synthesis of sodium peroxycarbonate at boron-doped diamond electrodes. Electrochem. Solid State 6, D5–D7.

Saha, M., T. Furuta, and Y. Nishita (2004). Conversion of carbon dioxide to peroxycarbonate at boron-doped diamond electrode. Electroch. Commun. 6, 201–204.

Serrano, K., P. Michaud, C. Comninellis, and A. Savall (2002). Electrochemical preparation of peroxodisulfuric acid using boron doped diamond thin film electrodes. Electrochim. Acta 48, 431–436.

Szpyrkowicz, L., M. Radaelli, and S. Daniele (2005). Electrocatalysis of chlorine evolution on different materials and its influence on the performance of an electrochemical reactor for indirect oxidation of pollutants. Catal. Today 100, 425–429.

Tanner, D. and S. Osmar (1987). Oxidative decarbonation on the mechanism of potassium persulfate promoted decarbonation reaction. J. Org. Chem. 52, 4689–4693.

Thompson, R. (1981). Catalytic decomposition of peroxymonosulfate in aqueous perchloric acid by dual catalysts. Inorg. Chem. 20, 1005–1010.

Walling, C. (1975). Fenton's reagent revisited. Accounts Chem. Res., 8, 125–131.

Zhang, H., D. Zhang, and J. Zhou (2006). Removal of COD from landfill leachate by electro-Fenton method. J. Hazard. Mater. 135, 106–111.

Chapter 10
Electrocoagulation in Water Treatment

Huijuan Liu, Xu Zhao, and Jiuhui Qu

10.1 Theoretical Aspect

10.1.1 Principle of Electrocoagulation

EC is a complicated process involving many chemical and physical phenomena that use consumable electrodes (Fe/Al) to supply ions into the water stream. It has been discovered over the last hundred years both in batch and continuous applications. During the late nineteenth century, EC has been applied in several large-scale water treatment plants in London (Matteson et al. 1995), while electrolytic sludge treatment plants were operated as early as 1911 in various parts of USA (Vik et al. 1984). Fe/Al is dissolved from the anode generating corresponding metal ions, which immediately hydrolyze to polymeric iron or aluminum hydroxide. These polymeric hydroxides are excellent coagulating agents. The consumable (sacrificial) metal anodes are used to continuously produce polymeric hydroxides in the vicinity of the anode. Coagulation occurs when these metal cations combine with the negative particles carried toward the anode by electrophoretic motion. Contaminants present in the wastewater stream are treated either by chemical reactions and precipitation or by physical and chemical attachment to colloidal materials being generated by the electrode erosion. They are then removed by electroflotation, sedimentation, and filtration. In conventional coagulation process, coagulating chemicals are added. By contrast, these coagulating agents are generated in situ in EC process. The basic process can be summarized in Fig. 10.1.

In the EC process, the destabilization mechanism of the contaminants, particulate suspension, and breaking of emulsions may be summarized as follows. (1) Compression of the diffuse double layer around the charged species by the interactions of ions generated by oxidation of the sacrificial anode. (2) Charge neutralization of the

J. Qu (✉)
State Key Laboratory of Environmental Aquatic Chemistry,
Research Center for Eco-Environmental Sciences, Chinese Academy of Sciences,
Beijing, People's Republic of China
e-mail: jhqu@rcees.ac.cn

C. Comninellis and G. Chen (eds.), *Electrochemistry for the Environment*,
DOI 10.1007/978-0-387-68318-8_10,

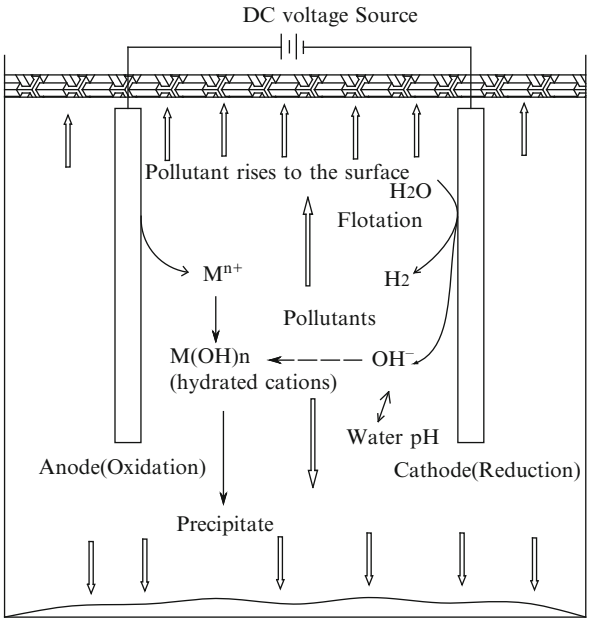

Fig. 10.1 Schematic diagram of a two-electrode electrocoagulation cell

ionic species present in wastewater by counter ions produced by the electrochemical dissolution of the sacrificial anode. These counter ions reduce the electrostatic interparticle repulsion to the extent that the van der Waals attraction predominates, thus causing coagulation. A zero net charge results in the process. (3) Floc formation: the floc formed as a result of coagulation creates a sludge blanket that entraps and bridges colloidal particles that are still remaining in the aqueous medium.

Water is also electrolyzed in a parallel reaction, producing small bubbles of oxygen at the anode and hydrogen at the cathode. These bubbles attract the flocculated particles and float the flocculated pollutants to the surface through natural buoyancy. In addition, the following physiochemical reactions may also take place in the EC cell (Paul 1996) (1) cathodic reduction of impurities present in wastewater; (2) discharge and coagulation of colloidal particles; (3) electrophoretic migration of the ions in solution; (4) electroflotation of the coagulated particles by O_2 and H_2 bubbles produced at the electrodes; (5) reduction of metal ions at the cathode; and (6) other electrochemical and chemical processes.

10.1.2 Reactions at the Electrodes and Electrodes Assignment

A simple electrocoagulation reactor is made up of one anode and one cathode. When a potential is applied from an external power source, the anode material undergoes

oxidation, while the cathode will be subjected to reduction or reductive deposition of elemental metals. The electrochemical reactions with metal M as anode may be summarized as follows:
At the anode:

$$M_{(s)} \rightarrow M_{(aq)}{}^{n+} + n\,e^{-} \tag{10.1}$$

$$2H_2O_{(1)} \rightarrow 4H^{+}{}_{(aq)} + O_{2(g)} + 4e^{-} \tag{10.2}$$

At the cathode:

$$M_{(aq)}{}^{n+} + n\,e^{-} \rightarrow M_{(s)} \tag{10.3}$$

$$2H_2O_{(l)} + 2e^{-} \rightarrow 2H_{2(g)} + 2OH^{-} \tag{10.4}$$

If iron or aluminum electrodes are used, the generated $Fe_{(ag)}{}^{3+}$ or $Al_{(aq)}{}^{3+}$ ions will immediately undergo further spontaneous reactions to produce corresponding hydroxides and/or polyhydroxides. These compounds have strong affinity for dispersed particles as well as counter ions to cause coagulation. The gases evolved at the electrodes may impinge on and cause flotation of the coagulated materials (Jiang et al. 2002).

To improve the performances of an EC, it may be necessary to interchange the polarity of the electrode intermittently. Usually, a two-electrode EC cell is not suitable for wastewater treatment because of a workable rate of metal dissolution. The use of electrodes with large surface area is required and performance improvement has been achieved by using EC cells either with monopolar electrodes or with bipolar electrodes. The schematic diagram of monopolar and bipopar electrodes in series connections is shown in Fig. 10.2 (Golder et al. 2007). The parallel arrangement essentially consists of pairs of conductive metal plates placed between two parallel electrodes and a DC power source. In a monopolar arrangement, each pair of "sacrificial electrodes" is internally connected with each other, and has no interconnection with the outer electrodes. This arrangement of monopolar electrodes with cells in series is electrically similar to a single cell with many electrodes and interconnections. The experimental setup also requires a resistance box to regulate the flow of current and a multimeter to read the current values. The conductive metal plates or

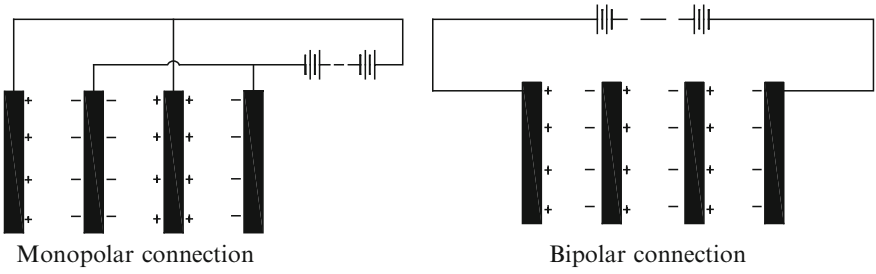

Fig. 10.2 Schematic diagram of a monopolar and bipolar electrodes in series connections

rods used in EC fabrication are commonly known as “sacrificial electrodes.” The sacrificial electrode and the cathode may be made up of the same or of different materials.

In a bipolar arrangement, the sacrificial electrodes are placed between the two parallel electrodes without any electrical connection. The two monopolar electrodes are connected to the electric power source with no interconnections between the sacrificial electrodes. This cell arrangement provides a simple setup, which facilitates easy maintenance. When an electric current is passed through the two electrodes, the neutral sides of the conductive plate will be transformed to charged sides, which have opposite charge compared with the parallel side beside it. The sacrificial electrodes are known as bipolar electrodes. It has been reported that EC cell with monopolar electrodes in series connection was more effective where aluminum electrodes were used as sacrificial and iron was used as anode and cathode. And, electrocoagulation with Fe/Al (anode/cathode) was more effective for the treatment process than Fe/Fe electrode pair (Modirshahla et al. 2007).

10.1.3 Electrode Passivation and Activation

Electrode passivation, specifically of aluminum electrodes, has been widely observed and recognized as detrimental to reactor performance. This formation of an inhibiting layer, usually an oxide on the electrode surface, will prevent metal dissolution and electron transfer, thereby limiting coagulant addition to the solution. Over time, the thickness of this layer increases, reducing the efficacy of the electrocoagulation process. The use of new materials, different electrode types and arrangements (Pretorius et al. 1991), and more sophisticated reactor operational strategies (such as periodic polarity reversal of the electrodes) have certainly let to significant reductions of impact passivation. In addition, addition of anions will also slow down the electrode passivation. The positive effect was as follows: $Cl^- > Br^- > I^- > F^- > ClO_4^- > OH^-$ and SO_4^{2-}. Specially, addition of a certain amount of Cl^- into the aqueous solution will inhibit the electrode passivation process largely. It is also necessary to rinse regularly the surface of the electrode plates. Generally, iron is used in wastewater treatment and aluminum is used in water treatment because there are a definite amount of metal ions required to remove a given amount of pollutants and iron is relatively cheaper. The aluminum plates are also finding application in wastewater treatment either alone or in combination with iron plates due to the high coagulation efficiency of Al^{3+}. When there are a significant amount of Ca^{2+} or Mg^{2+} ions in water, the cathode material is recommended to be stainless steel.

Apart from a technical focus on quantifying interactions between the foundation technologies and an economic focus on the relative cost of electrocoagulation, future research also needs to examine reliable means of reducing electrode passivation.

10.1.4 Comparison Between Electrocoagulation and Chemical Coagulation

Chemical coagulation and electrocoagulation have the same phenomenon in which the charged particles in colloidal suspension are neutralized by mutual collision with metallic hydroxide ions and are agglomerated, followed by sedimentation or flotation. The difference between electrocoagulation and chemical coagulation is mainly in the way of which aluminum or iron ions are delivered (Zhu et al. 2005; Avsar et al. 2007). Electrocoagulation is a process consisting of creating metallic hydroxide flocks within the water by electrodissolution of the soluble anodes, usually made of iron or aluminum. In chemical coagulation, hydrolyzing metal salts, based on aluminum or iron, e.g., aluminum and ferric sulfates and chlorides, are very widely used as coagulants in water treatment. There are some advantages for EC compared to chemical coagulation, which are as follows:

1. In the chemical coagulation process, the hydrolysis of the metal salts will lead to a pH decrease and it is always needed to modulate the effluent pH. The chemical coagulation is highly sensitive to pH change and effective coagulation is achieved at pH 6–7. While in the electrocoagulation, the pH neutralization effect made it effective in a much wide pH range (4–9).
2. Flocs formed by EC are similar to chemical floc. But, EC floc tends to be much larger, contains less bound water, is acid resistant, and is more stable. In the chemical coagulation process, it is always followed by sedimentation and filtration. While in the electrocoagulation process, it can be followed by sedimentation or flotation. The gas bubbles produced during electrolysis can carry the pollutant to the top of the solution where it can be more easily concentrated, collected, and removed.
3. Sludge formed by EC tends to be readily settable and easy to de-water, because it is composed of mainly metallic oxides/hydroxides. Above all, it is a low-sludge producing technique.
4. Use of chemicals is avoided in EC process. Thus, it need not neutralize excess chemicals, and secondary pollution caused by chemical substances that are added can be avoided.
5. The EC process has the advantage of treating the water with low temperature and low turbidity. In this case, the chemical coagulation has difficulty in achieving a satisfying result.
6. EC requires simple equipment and is easy to be operated.

The disadvantages of EC are as follows. (1) The “sacrificial electrodes” are dissolved into wastewater as a result of oxidation, and need to be regularly replaced. (2) The passivation of the electrodes over time has limited its implementation. (3) The use of electricity may be expensive in many places. (4) High conductivity of the wastewater suspension is required (Yildiz et al. 2007).

10.2 Typical Designs of the EC Reactors

Electrocoagulation reactors have been built in a number of configurations. Each system has its own set of advantages and disadvantages. It is important to design the EC cell so that maximum efficiency can be achieved.

Among the electrocoagulation reactors, the first major distinction is whether a reactor was configured as a batch or a continuous system. It is clear that the majority of applications fall into the latter category, having a continuous feed of wastewater and operating under (pseudo) steady-state conditions. A key advantage for such reactor systems is that their coagulant requirements are essentially fixed, a major advantage in terms of both design and operation. Batch reactor applications typically operate with a fixed wastewater volume per treatment cycle, which suffer from the perceived disadvantage that those conditions within the reactor change with time.

The second major distinction between alternative reactor designs is the role of flotation. Reactors that do not exploit the separation of aggregated pollutant via electrochemically generated bubbles are regarded as "coagulation only" processes, while reactors that integrate flotation into their design and operation are classed as "coagulation and flotation" processes. Integrated units have two main pollutant removal paths – flotation and settling (Holt et al. 2002). Separation by settling is the more common option, with the fact that electrolytic gases are also being produced simultaneously with the dosing process often viewed as an unnecessary operational complication (Vik et al. 1984). The difference between pollutant removal by settling or flotation will seem to be the current density. A low current produces a low bubble density, leading to a low upward momentum-flux condition that encourages sedimentation over flotation. When the current is increased, the bubble density increases, which results in a greater upward momentum flux. Thus, the contaminants may be removed by flotation.

10.2.1 Liquid Flow Assignment

Generally, the liquid flow is in parallel connection (Fig. 10.3), which is easy to be fabricated. However, liquid flow is low in parallel connection and it is not beneficial for Al ion diffusion and Al coagulant formation as well as adsorption (Mameri et al. 1998). Additionally, if the Al ion cannot be transferred, the electrode will be passivated. Thus, overpotential will be increased and the electrical energy will be consumed. By contrast, the liquid flow rate in series connection will be increased (Fig. 10.3). Certainly, the flow rate cannot be increased too high in order to not to destroy the coagulant. The results of the treatment of a textile wastewater by EC process using various liquid flow assignments were reported. Two electrode materials, aluminum and iron, were connected in three modes namely, monopolar-parallel (MP-P), monopolar-serial (MP-S), and bipolar-serial (BP-S). For MP-P, anodes and cathodes are in parallel connection; the current is divided between all the electrodes in relation to the resistance of the individual cells. Hence, a lower potential

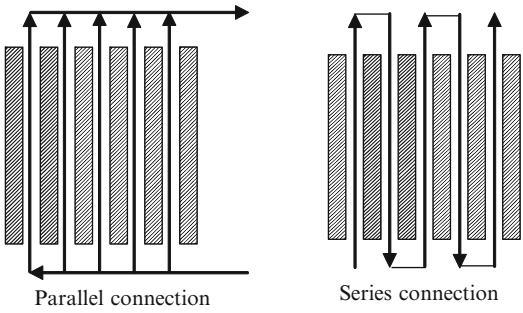

Fig. 10.3 Schematic diagram of liquid flow in parallel or series connection

difference is required in parallel connection, when compared with serial connections. For MP-S, each pair of sacrificial electrodes is internally connected with each other, because the cell voltages sum up a higher potential difference required for a given current. For BP-S, there is no electrical connection between inner electrodes, only the outer electrodes are connected to the power supply. Outer electrodes are monopolar and inner ones are bipolar. This connection mode has simple setup and has less maintenance cost during operation. COD and turbidity removals are selected as performance criteria. For a high COD removal, acidic medium is preferable for both electrode materials. And, process economy is as important as removal efficiencies during the process evaluation test. Various direct and indirect cost items including electrical, sacrificial electrodes, labor, sludge handling, maintenance, and depreciation costs have been considered in the calculation of the total cost. The results show that monopolar parallel mode is the most cost effective for both electrode types (Kobya et al. 2007).

10.3 Factors Affecting Electrocoagulation

10.3.1 Effect of Current Density or Charge Loading

Operating current density is very important in electrocoagulation because it is the only operational parameter that can be controlled directly. In this system, electrode spacing is fixed and current is a continuous supply. Current density directly determines both coagulant dosage and bubble generation rates and strongly influences both solution mixing and mass transfer at the electrodes.

In an EC experiment, the electrode or electrode assembly is usually connected to an external DC source. The amount of metal dissolved or deposited is dependent on the quantity of electricity passed through the electrolytic solution. A simple relationship between current density ($\mathrm{A\,cm^{-2}}$) and the amount of substances (M) dissolved (g of $\mathrm{M\,cm^{-2}}$) can be derived from Faraday's law:

$$w = \frac{itM}{Nf}, \tag{10.5}$$

where w is the quantity of electrode material dissolved (g of M cm^{-2}), i the current density (A cm^{-2}), t the time in s; M the relative molar mass of the electrode concerned, n the number of electrons in oxidation/reduction reaction, and f is the Faraday's constant, 96,500 C mol^{-1}.

It is expected that there should be an agreement between the calculated amount of substances dissolved as a result of passing a definite quantity of electricity and the experimental amount determined. Usually a good agreement is obtained (Vik et al. 1984). One uncertainty is in the measurement of potential of the EC cell. The measured potential is the sum of three components:

$$\eta_{AP} = \eta_k + \eta_{Mt} + \eta_{IR}, \tag{10.6}$$

where η_{AP} is the applied overpotential (V), η_k the kinetic overpotential (V), η_{Mt} the concentration overpotential (V), and η_{IR} is the overpotential caused by solution resistance or IR drop (V).

The IR drop is related to the distance (d in cm) between the electrodes, surface area (A in m^2) of the cathode, specific conductivity of the solution (κ in mS m^{-1}), and the current (I in A). The IR drop can be easily minimized by decreasing the distance between the electrodes and increasing the area of crossing section of the electrodes and the specific conductivity of the solution. The IR drop can be easily minimized by decreasing the distance between the electrodes and increasing the area of cross section of the electrodes and the specific conductivity of the solution. Concentration overpotential (η_{Mt}, V), also known as mass transfer or diffusion overpotential, is caused by the change in analytic concentration occurring in the proximity of the electrode surface due to electrode reaction. This overpotential is caused by the differences in electroactive species concentration between the bulk solution and the electrode surface. This condition occurs when the electrochemical reaction is sufficiently rapid to lower surface concentration of electroactive species below that of the bulk solution. The overpotential is small when reaction rate constant is much smaller than the mass-transfer coefficient. The mass-transport overpotential (η_{Mt}, V) can be reduced by increasing the masses of the metal ions transported from the anode surface to the bulk of the solution and can be achieved by enhancing the solution turbulence. It can also be overcome by passing electrolyte solution from anode to cathode at a higher velocity by using some mechanical means. With the increase in the current, both kinetic and concentration overpotential increase.

The current density is the key operational parameter, affecting not only the system's response time but also strongly influencing the dominant pollutant separation mode. The highest allowable current density may not be the most efficient mode of running the reactor. It is well known that the optimal current density will invariably involve a trade-off between operational costs and efficient use of the introduced coagulant. At the meantime, the current density depends on solution pH, temperature, flow rate, etc.

As summarized by Chen (2004), the supply of current to the electrocoagulation system determines the amount of Al^{3+} or Fe^{2+} ions released from the respective

electrodes. For aluminum, the electrochemical equivalent mass is 335.6 mg $(Ah)^{-1}$. For iron, the value is 1,041 mg $(Ah)^{-1}$. In order for the electrocoagulation system to operate for a long period of time without maintenance, its current density is suggested to be 20–25 A m^{-2} unless there are measures taken for a periodical cleaning of the surface of electrodes. The current density selection should be made with other operating parameters such as pH, temperature, as well as flow rate to ensure a high current efficiency. The current efficiency for aluminum electrode can be 120–140% while that for iron is around 100%. The overall 100% current efficiency for aluminum is attributed to the pitting corrosion effect especially when there are chlorine ions present. The current efficiency depends on the current density as well as the types of the anions. Significantly enhanced current efficiency, up to 160%, was obtained when low-frequency sound was applied to iron electrodes (Kovatchva and Parlapanski 1999). The quality of the treated water depends on the amount of ions produced (mg) or charge loading, the product of current and time (Ah). Table 10.1 gives the values of the required Al^{3+} for treating some typical pollutants in water treatment (Kul'skii et al. 1978). The operating current density or charge loading can be determined experimentally if there are not any reported values available. There is a critical charge loading required. Once the charge loading reaches the critical value, the effluent quality does not show significant improvement for further current increase (Chen et al. 2000).

10.3.2 Effect of Conductivity

When the electrolytic conductivity is low, the current efficiency will decrease. And, high-applied bias potential is needed which will lead to the passivation of electrode and increase treatment cost. Generally, NaCl was added in order to increase the electrolytic conductivity. Active chloride will also produce in the Cl^- electrolysis, which will contribute to the water disinfection (Wong et al. 2002). And, the addition of Cl^- will also decrease the negative effect of $CO_3{}^{2-}$ and $SO_4{}^{2-}$. The presence of $CO_3{}^{2-}$ and $SO_4{}^{2-}$ will lead to the deposition of Ca^{2+} and Mg^{2+} and formation of oxide layer, which will decrease the current efficiency rapidly. It is

Table 10.1 The aluminum demand and power consumption for removing pollutants from water

		Preliminary purification		Purification	
Pollutant	Unit quantity	Al^{3+} (mg)	E $(Wh\,m^{-3})$	Al^{3+} (mg)	E $(Wh\,m^{-3})$
Turbidity	1 mg	0.04–0.06	5–10	0.15–0.2	20–40
Color	1 unit	0.04–0.1	10–40	0.1–0.2	40–80
Silicates	1 mg/SiO_2	0.2–0.3	20–60	1–2	100–200
Irons	1 mg Fe	0.3–0.4	30–80	1–1.5	100–200
Oxygen	1 mg O_2	0.5–1	40–200	2–5	80–800
Algae	1,000	0.006–0.025	5–10	0.02–0.03	10–20
Bacteria	1,000	0.01–0.04	5–20	0.15–0.2	40–80

therefore recommended that among the anions present, there should be 20% Cl^- to ensure a normal operation of electrocoagulation in water treatment. However, NO_3^- widely present in the water solution nearly has no effect on the EC process.

10.3.3 Effect of Temperature

The water temperature will also influence the electrocoagulation process. Al anode dissolution was investigated in the water temperature range from 2 to 90°C. The Al current efficiency increase rapidly when the water temperature increase from 2 to 30°C. The temperature increase will speed up the destructive reaction of oxide membrane and increase the current efficiency. However, when the temperature was over 60°C, the current efficiency began to decrease. In this case, the volume of colloid $Al(OH)_3$ will decrease and pores produced on the Al anode will be closed. The above factors will be responsible for the decreased current efficiency.

10.3.4 Effect of pH

The pH of solution plays an important role in electrochemical and chemical coagulation process (Chen et al. 2000). Under certain conditions, various complex and polymer compounds can be formed via hydrolysis and polymerization reaction of electrochemically dissolved Al^{3+}. The formation of Al^{3+} single-core coordination compounds can be described as follows:

$$Al^{3+} + H_2O \rightarrow Al(OH)^{2+} + H^+ \tag{10.7}$$

$$Al(OH)^{2+} + H_2O \rightarrow Al(OH)_2{}^+ + H^+ \tag{10.8}$$

$$Al(OH)_2{}^+ + H_2O \rightarrow Al(OH)_3 + H^+ \tag{10.9}$$

$$Al(OH)_3 + H_2O \rightarrow Al(OH)_4{}^- + H^+ \tag{10.10}$$

With the extension of hydrolysis of Al^{3+}, multicore coordination compounds and $Al(OH)_3$ precipitate can be formed.

$$Al^{3+} \rightarrow Al(OH)_n{}^{3-n} \rightarrow Al_2(OH)_2{}^{4+} \rightarrow Al_{13}\,\text{complex} \rightarrow Al(OH)_3 \tag{10.11}$$

In the pH range of 4–9, $Al(OH)^{2+}$, $Al(OH)_2{}^+$, $Al_2(OH)_2{}^{4+}$, $Al(OH)_3$, and $Al_{13}(OH)_{32}{}^{7+}$ are formed. The surface of these compounds has large amounts of positive charge, which can lead to adsorption electrochemistry neutralization and net catching reaction. At pH $>$ 10, $Al(OH)_4{}^-$ is dominant, and the coagulation effect rapidly decreases. At low pH, Al^{3+} is dominant, which has no coagulation effect.

In the chemical coagulation process, pH is needed to be adjusted because the pH of solution will decrease with the addition of coagulants. In the electrochemical coagulation, the evolution of H_2 at the cathode will increase the OH^- concentration. Thus, pH in the aqueous solution will increase when the pH of original water is in the range of 4–9. However, when the pH of the original water is higher than 9, the pH of the treated water will decrease. Compared with the chemical coagulation, electrocoagulation can neutralize the pH of the treated water to some extent via following reactions.

$$Al + 3H^+ \rightarrow Al^{3+} \tag{10.12}$$

$$Al^{3+} + 3H_2O \rightarrow Al(OH)_3 + 3H^+ \tag{10.13}$$

$$Al(OH)_3 + OH^- \rightarrow Al(OH)_4{}^- \tag{10.14}$$

Under acid conditions, CO_2 can be purged with the evolution of H_2 and O_2. Particularly, Al dissolution occurs by (10.4)–(10.24). And, the formed $Al(OH)_3$ also dissolve, reaction (10.12) occurs to the left easily. These reactions are responsible for the increase of solution's pH. At high pH, reaction (10.13) occurs to the right easily, Ca^{2+} and Mg^{2+} can precipitate with $Al(OH)_3$. At higher pH, reaction (10.14) proceeds. These processes are responsible for the decrease of aqueous pH.

10.4 Application of Electrocoagulation in Water Treatment

EC is a process consisting of creating metallic hydroxides flocs within the wastewater by electrodissolution of soluble anodes, usually made of iron or aluminum. It was found that anodized aluminum was more effective than the aluminum ion introduced in the form of aluminum sulfate solution. In water and wastewaters treatment, electrocoagulation has been widely used to treat potable water, urban wastewater, oil wastes, textile wastewater, suspended particles, chemical and mechanical polishing waste, fluoride containing water, and heavy metal containing solutions (Hu et al. 2005; Adhoum et al. 2004; Yildiz et al. 2007; Kumar et al. 2004; Gomes et al. 2007; Parga et al. 2005; Golder et al. 2007; Hansen et al. 2007; Mollah et al. 2004; Wu et al. 2008). The removal of surfactants can also be achieved efficiently by using electrochemical coagulation not depending on the type of surfactant. Removal efficiency of nearly 100% has been achieved for the solution of $300\,mg\,L^{-1}$ in a short time of 4 min (Onder et al. 2007). The treatability of waters containing high concentration of NOMs using iron cast electrodes has been explored based on removal efficiency by electrocoagulation method. Effects of initial humic substance concentration, applied potential, and supporting electrolyte type on the electrocoagulation have been investigated. It can be concluded that electrocoagulation is an effective method for the treatment of waters containing MOMs (Yildiz et al. 2007). Here, we take the removal of arsenic, dyes, and heavy metal from water as examples to explain the EC process and its mechanism in water treatment.

10.4.1 Arsenic Removal from Water by EC

Arsenic in drinking water is a worldwide concern due to its toxicity and carcinogenicity. In order to minimize these health risks, the World Health Organization (WHO) has set a guideline limit of $10\,\mu g\,L^{-1}$ in drinking water. In natural water, arsenic is primarily present in inorganic forms and exists in two predominant species, arsenate (As(V)) and arsenite (As(III)). As(V) is the major arsenic species in well-oxygenated water, whereas As(III) is the dominant arsenic in groundwater.

EC is a simple, efficient, and promising method to remove arsenic form water. Arsenic removal efficiencies with different electrode materials follow the sequence: iron > titanium > aluminum. The process was able to remove more than 99% of arsenic from an As-contaminated water and met the drinking water standard of $10\,\mu g\,L^{-1}$ with iron electrode. Compared with the iron electrodes, aluminum electrodes obtained lower removal efficiency. The plausible reason for less arsenic removal by aluminum in comparison to iron could be that the adsorption capacity of hydrous aluminum oxide for As(III) is much lower in comparison to hydrous ferric oxides. Comparative evaluation of As(III) and As(V) removal by chemical coagulation (with ferric chloride) and electrocoagulation has been done. The comparison revealed that EC has better removal efficiency for As(III), whereas As(V) removal by both processes was nearly same (Kumar et al. 2004).

Gomes et al. (2007) reported that As(III) ions are partly converted to As(V) during EC process. Crystalline iron oxides (magnetite, iron oxide), iron oxyhydroxide (lepidocrocite), aluminum hydroxide (bayerite), and aluminum oxyhydroxide (diaspore), as well as some interaction between the two phases were generated during the EC process. They also indicated the presence of amorphous or ultrafine particular phase in the floc. The substitution of Fe^{3+} ions by Al^{3+} ions in the solid surface has been observed also, which indicated a removal mechanism of arsenic in these metal hydroxides and oxyhydroxides by providing larger surface area for arsenic adsorption via retarding the crystalline formation of iron oxides. Electrocoagulation of As (V) in wastewaters is a promising remediation tool. Experiments with three different process designs showed the possibility of removing arsenic as adsorbed to or co-precipitate with iron(III)hydroxide. Applying electrocoagulation with a modified flow and an air lift reactor, in both cases practically all arsenic was eliminated from a $100\,mg\,As(V)\,L^{-1}$ solution with current densities of around $1.2\,A\,dm^{-2}$ (Parga et al. 2005).

10.4.2 Other Heavy Metal Removal from Water by EC

Most of the metals such as copper, nickel, chromium, silver, and zinc are harmful when they are discharged without treatment. The most widely used method for the treatment of metal polluted wastewater is precipitation with NaOH and coagulation with $FeSO_4$ or $Al_2(SO_4)_3$ with subsequent time-consuming sedimentation. Other methods include adsorption, ion exchange, and reverse osmosis. Each method has

its disadvantages. EC is a promising method to remove heavy metal from water and has the advantages of simple equipment, easy operation, high removal efficiency, high removal rate, and no need pH adjustment.

Take the treatment of electroplating wastewater containing Cu^{2+}, Zn^{2+}, and Cr(VI) as an example. When using aluminum as electrode, Cu^{2+}, Zn^{2+}, and Cr(VI) could be effectively removed by the EC process when the pH was kept between 4 and 8. The removal rates of copper and zinc were found to be five times quicker than chromium because of a difference in the removal mechanisms. Coprecipitation of $Cu(OH)_2$ and $Zn(OH)_2$ may play a dominant role in the removal mechanism of the corresponding metallic ions. For Cr(VI), it was firstly reduced to Cr(III) at the cathode surface and then removed by coprecipitated process to $Cr(OH)_3$. When the pH was higher than 8, a dramatic decrease of the removal efficiency of chromium is observed, while removal yields of Cu^{2+} and Zn^{2+} remained very high. At alkaline pH between 8 and 10, $Cr_2O_7{}^{2-}$ ions are converted to soluble chromate ($CrO_4{}^{2-}$) anions, which can explain the low removal rate.

When using Fe as electrode, Fe^{2+} was formed by direct electrochemical reduction at the anode surface. Simultaneously, higher oxidized metal compounds like Cr(VI) may be reduced to Cr(III) by Fe^{2+} in acidic solution, as (10.15)–(10.17).

$$Fe \rightarrow Fe^{2+} + 2e \tag{10.15}$$

$$Cr_2O_7{}^{2-} + 6Fe^{2+} + 14H^{+} \rightarrow 2Cr^{3+} + 6Fe^{3+} + 7H_2O \tag{10.16}$$

$$CrO_4{}^{2-} + 3Fe^{2+} + 8H^{+} \rightarrow Cr^{3+} + 3Fe^{3+} + 4H_2O \tag{10.17}$$

On the cathode, in addition to the formation of H_2, Cr(VI) can be directly reduced to Cr(III) on the cathodes, which can be expressed as (10.18)–(10.20).

$$2H^{+} + 2e \rightarrow H_2 \tag{10.18}$$

$$Cr_2O_7{}^{2-} + 6e + 14H^{+} \rightarrow 2Cr^{3+} + 7H_2O \tag{10.19}$$

$$CrO_4{}^{2-} + 3e + 8H^{+} \rightarrow Cr^{3+} + 4H_2O \tag{10.20}$$

Additionally, H_2 formed at the cathode increase the pH of the wastewater thereby inducing precipitation of Cr^{3+} and Fe^{3+} as corresponding hydroxides $Cr(OH)_3$ and $Fe(OH)_3$ (Golder et al. 2007).

10.4.3 Dye Removal from Water by EC

Dye is a ubiquitous class of synthetic organic pigments. The traditional treatment methods for dye effluents include physical–chemical method and biological process. The biological methods are cheap and simple to apply, but cannot be applied to most textile wastewaters because most commercial dyes are toxic to the organisms used in the process and result in sludge bulking. The EC technique is considered to be an effective tool for treatment of textile wastewaters with high removal efficiency.

A number of authors have reported the treatments of textile dye wastewater by EC technique (Mollah et al. 2004; Wu et al. 2008). There are two mechanisms for the dye decolorization (1) precipitation and (2) adsorption. At low pH, the precipitation is dominant. At pH > 6.5, the adsorption is the main process.

Precipitation:

$$\text{Dyes} + \text{Monomeric Al} \rightarrow [\text{Dyes Monomeric Al}]\,(\text{s})\ \text{pH} = 4.0 - 5.0 \quad (10.21)$$

$$\text{Dyes} + \text{Polymeric Al} \rightarrow [\text{Dyes Polymeric Al}](\text{s})\ \text{pH} = 5.0 - 6.0 \quad (10.22)$$

Adsorption:

$$\text{Dyes} + \text{Al(OH)}_{3(\text{s})} \rightarrow\rightarrow [\text{particle}] \quad (10.23)$$

$$[\text{Dyes Polymeric Al}]_{(\text{s})} + \text{Al(OH)}_{3(\text{s})} \rightarrow\rightarrow\rightarrow [\text{particles}] \quad (10.24)$$

Freshly formed amorphous $Al(OH)_3(s)$ "sweep flocs" have large surface areas which is beneficial for a rapid adsorption of soluble organic compounds and trapping of colloidal particles. Finally, these flocs are removed easily from aqueous medium by sedimentation or flotation.

Iron and aluminum are used as sacrificial electrode materials in the treatment of textile wastewater by EC. In acidic medium, COD and turbidity removal efficiencies of aluminum are higher than those of iron, while in neutral and weakly alkaline medium iron is more efficient. High conductivity is in favor of high process performances and low operating cost. For the same turbidity and COD removal efficiencies, iron requires a lower current density than aluminum. Operating time and current density exhibit similar effects on the process performances and the operating cost. The energy consumption is lower with iron, while the electrode consumption is lower generally with aluminum. If anode potential is sufficiently high, secondary reactions may occur, including direct oxidation of organic compounds and of Cl^- ← ions present in wastewater.

The dye removal efficiency decreased with increase in the initial concentration. In a bipolar EC reactor with iron electrodes, using NaCl as electrolyte, the removal efficiency of orange II decreased from 90.4 to 55% with the increase in the initial dye concentration from 10 to 50 mg L^{-1} at constant voltage of 40 V and a current strength of 159.5 A m^{-2}. The high treatment efficiency is considered to be due to chemical coagulation involving maghemite (γ-Fe_2O_3) and/or magnetite (Fe_3O_4) produced in the system as well as electrooxidation. The results of XRD analyses of the residue confirmed the presence of magnetite (Fe_3O_4) and maghemite (γ-Fe_2O_3) in EC process (Canizares et al. 2006). Misawa et al. (199) reported that either goethite (α-FeOOH) or magnetite (Fe_3O_4) is produced depending upon the pH of the environment. At acidic condition, γ-Fe_2O_3 was formed; in slightly basic and strongly basic condition Fe_3O_4 and α-FeOOH were formed, respectively by the (10.25)–(10.26).

$$6\text{Fe(OH)}_{2(\text{s})} + \text{O}_{2(\text{aq})} \rightarrow 2\text{Fe}_3\text{O}_{4(\text{s})} + 6\text{H}_2\text{O} \quad (10.25)$$

$$4\text{Fe(OH)}_{2(\text{s})} + \text{O}_{2(\text{aq})} \rightarrow 4\alpha\text{–FeOOH}_{(\text{s})} + 2\text{H}_2\text{O} \quad (10.26)$$

As for the acid red 14 removal by EC, 95% color removal and 85% COD removal were obtained when the pH ranged from 6 to 9, time of electrolysis was approximately 4 min and current density was approximately 80 A m^{-2}. The results also showed that an EC cell with monopolar electrodes had higher color removal efficiency than an EC cell with bipolar electrodes. Furthermore, within an EC cell, the series connection of the monopolar electrodes was more effective for the treatment process than the parallel connection in color removal (Daneshvar et al. 2004).

EC has the advantage of consumed less material and produced less sludge, and the pH of the medium was more stabilized than that of chemical coagulation for similar COD and turbidity removal levels. Cost calculations for dye removal by EC show that, in the case of iron electrode, operating cost is approximately 0.1 US$ per kg COD removed, and for aluminum, it is 0.3 US$ per kg COD removed. Electrode consumption cost accounts nearly 50% of the total cost for iron, and 80% of the total cost for aluminum (Bayramoglu et al. 2004). This paper presents the comparative results with respect to electrode configurations on the economic performance of treatment of textile wastewater by EC process. Aluminum and iron electrode materials were used as sacrificial electrode in parallel and series connection modes. Various direct and indirect cost items including electrical, sacrificial electrodes, labor, sludge handling, maintenance, and depreciation costs were considered in the calculation of the total cost per m^3 of wastewater taken from a textile plant with a capacity of 1,000 m^3 per day. The results showed that MP-P was the most cost effective for Fe and Al electrodes.

10.5 A New Bipolar EC–EF Process for Wastewater Treatment

The separation of the flocculated sludge formed by EC process can be accomplished by precipitation or flotation (Yavuz 2007; Szpyrkowicz 2007). However, preliminary experiment showed that the hydrogen gas produced at the aluminum cathode in an electrocoagulation cell was not so fine that could float only about 60% of the total solids. In our research group, a combinative bipolar EC–EF process was developed to treat laundry wastewater (Ge et al. 2004).

Figure 10.4 showed the flowchart of the experimental EC–EF system in our research work. In the bipolar EC–EF unit, three aluminum plates placed between two titanium electrodes having opposite charges will undergo anodic reactions on the positive side while on the negative side cathodic reactions take place. The objectives of using this bipolar EC–EF reactor were to neutralize pollutant charge, generate ultrafine bubbles, and separate the coagulated flocs from water.

The main anodic reactions are as follows:
Ti anode:

$$2H_2O \rightarrow O_2 + 4H^+ + 4e \tag{10.27}$$

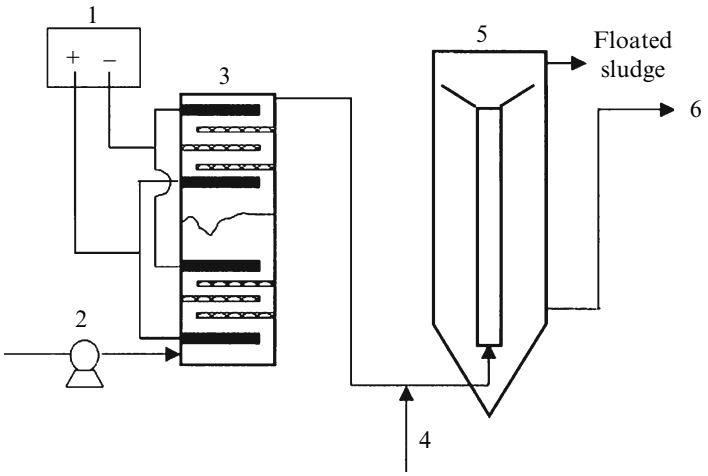

Fig. 10.4 Flowchart of the experimental system: (1) DC power supply, (2) pump, (3) electrochemical cell (*solid bar*: Ti electrode and *space bar*: Al electrode), (4) polymer electrolyte injection, (5) separator, and (6) effluent

Al positive side:

$$\mathrm{Al} \rightarrow \mathrm{Al}^{3+} + 3\mathrm{e} \tag{10.28}$$

The hydrolysis and polymerization of Al^{3+} under appropriate pH conditions subsequently give rise to the formation of such species as $\mathrm{Al(OH)}^{2+}$, $\mathrm{Al_2(OH)_2}^{4+}$, $\mathrm{Al(OH)_3}$, and charged hydroxo cationic complexes, which can effectively remove pollutants. In this study, titanium metal is chosen as anode material mainly for its cheapness and high stability. Some materials with high oxygen evolution have also been reported. When there are some Cl^- in the solution, some reactions will occur on the anode by (10.29)–(10.31).

$$2\mathrm{Cl}^- \rightarrow \mathrm{Cl_2} + 2\mathrm{e} \tag{10.29}$$

$$\mathrm{Cl_2} + \mathrm{H_2O} \rightarrow \mathrm{HClO} + \mathrm{H}^+ + \mathrm{Cl}^- \tag{10.30}$$

$$\mathrm{HClO} \rightarrow \mathrm{H}^+ + \mathrm{ClO}^- \tag{10.31}$$

It is generally believed that there are three possible mechanisms involved in the process: electrocoagulation, electroflotation, and electrooxidation. However, it can be suggested that, during the bipolar EC–EF process, bipolar aluminum electrodes are mainly responsible for electrocoagulation.

The process successfully removed turbidity, COD, phosphate, and MBAS simultaneously in the pH range of 5–9. The COD removal was greater than 70%. And the removal efficiencies of MBAS, turbidity, and P-phosphate could be reached above 90%. Based on the laboratory test of laundry wastewater, $1.5\,\mathrm{m^3\,h^{-1}}$ pilot scale EC–EF equipment was manufactured and mounted on a mobile truck. The

Table 10.2 Pilot scale field test results

	Harbin, Heilongjiang		Wuxi, Jiangsu		Shunyi, Beijing	
	Influent	Effluent	Influent	Effluent	Influent	Effluent
Conductivity (μS)	1,904–786	956–675	830–712	719–655	1,159–897	735–589
pH	9.56–7.83	8.15–7.24	10.68–9.77	8.73–7.92	9.35–8.45	8.09–7.77
Turbidity (NTU)	583–471	12.3–8.26	78.0–32.2	11.2–10.5	810–225	4.25–1.41
COD $(\mathrm{mg\,L^{-1}})$	1,090–785	45.6–32.4	65.9–31.8	11.2–5.3	890–628	71.2–59.3
MBAS $(\mathrm{mg\,L^{-1}})$	72.3–64.5	11.2–9.6	14.6–8.3	2.9–1.7	72.5–57.6	8.9–5.8

equipment mainly consisted of an EC–EF tank and a separator. The field test results are shown in Table 10.2. As for the laundry wastewater of Shunyi (Beijing), when polyaluminum chloride (10% Al_2O_3) was used, the dosage was $1,200\,\mathrm{mg\,L^{-1}}$, equal to $63.5\,\mathrm{mg\,L^{-1}}$ Al^{3+}, to achieve the same residual turbidity. The settled sludge amounted to nearly 40% of the total volume. For the electrochemical process (32 V/30 A, $1.5\,\mathrm{m^3\,h^{-1}}$), the Al^{3+} consumption was $6.72\,\mathrm{mg\,L^{-1}}$. Table 10.1 also indicated that the pH of the treated wastewater was neutralized and the electrical conductivity was reduced. It can be seen that the bipolar EC–EF process was different from other coagulation/flotation processes.

References

Adhoum, N., Monser, L., Bellakhal, N., Belgaied, J. (2004). Treatment of electroplating wastewater containing Cu^{2+}, Zn^{2+}, and Cr(VI) by electrocoagulation. J. Hazard. Mater. **112**, 207–213.

Avsar, Y., Kurt, U., Gonullu, T. (2007). Comparison of classical chemical and electrochemical processes for treating rose processing wastewater. J. Hazard. Mater. **148**, 340–345.

Bayramoglu, M., Kobya, M., Can, O., Sozbir, M. (2004). Operating cost analysis of electrocoagulation of textile dye wastewater. Sep. Purif. Technol. **37**, 117–125.

Canizares, P., Martinez, P., Jimenez, C., Lobato, J., Rodrigo, M.A. (2006). Coagulation and electrocoagulation of wastes polluted with dyes. Environ. Sci. Technol. **40**, 6418–6424.

Chen, G.H (2004). Electrochemical technologies in wastewater treatment. Sep. Purif. Technol. **38**, 11–41.

Chen, X., Chen, G.H., Yue, P.L. (2000). Separation of pollutants from restaurant wastewater by electrocoagulation. Sep. Purif. Technol. **19**, 65–76.

Daneshvar, N., Sorkhabi, H.A., Kasiri, M. (2004). Decolorization of dye solution containing Acid Red 14 by electrocoagulation with a comparative investigation of different electrode connections. J. Hazard. Mater. **112**, 55–62.

Ge, J.T., Qu, J.H., Lei, P.J., Liu, H.J. (2004). New bipolar electrocagulation–electroflotation process for the treatment of laundry wastewater. Sep. Purif. Technol. **36**, 33–39.

Golder, A.K., Samanta, A.N., Ray, S. (2007). Removal of Cr^{3+} by electrocoagulation with multiple electrodes: biopolar and monopolar configurations. J. Hazard. Mater. **141**, 653–661.

Gomes, J.A.G., Daida, P., Kesmez, M., Weir, M., Moreno, H., Parga, J.R., Irwin, G., McWhinney, H., Grady, T., Peterson, E., Cocke, D.L. (2007). Arsenic removal by electrocoagulation using combined Al–Fe electrode system and characterization of products, J Hazard Mater. **139**, 220–231.

Hansen, H.K., Nunez, P., Raboy, D., Schippacasse, I., Grandon, R. (2007). Electrocoagulation in wastewater containing arsenic: comparing different process designs. Electrochim. Acta **52**, 3464–3470.

Holt, P.K., Barton, G.W., Wark, W., Mitchell, C.A. (2002). A quantitative comparison between chemical dosing and electrocoagulation. Colloids Surf. A. **211**, 233–248.

Hu, C.Y., Lo, S.L., Kuan, W.H., Lee, Y.D. (2005). Removal of fluoride from semiconductor wastewater by electrocoagulation–flotation. Water Res. **39**, 895–901.

Jiang, J.Q., Graham, N., Andre, C., Kelsall, G.H., Brandon, N. (2002). Laboratory study of electrocoagulation–flotation for water treatment. Water Res. **36**, 4064–4078.

Kobya, M., Bayramoglu, M., Eyvaz, M. (2007). Techno-economical evaluation of electrocoagulation for the textile wastewater using different electrode connections. J. Hazard. Mater. **148**, 311–318.

Kovatchva, V.K. and Parlapanski, M.D. (1999). Sono-electrocoagulation of iron hydroxides. Colloids Surf. A **149**, 603–608.

Kul'skii, L.A., Strokach, P.P., Slipchenko, VA., Saigak, E.I. (1978). *Water Purification by Electrocoagulation*, Budivel'nik, Kiev,.

Kumar, P.R. Chaudhari, S., Khilar, K.C., Mahajan, S.P. (2004). Removal of arsenic from water by electrocoagulation Chemosphere **55**, 1245–1252.

Mameri, N., Yeddou, A.R., Lounici, H., Belhocine, D., Grib, H., B. Bariou. (1998). Defluoridation of septentrional Sahara water of North Africa by electrocoagulation process using bipolar aluminium electrodes. Water. Res. **32**, 1604.

Matteson, M.J., Dobson, R.L., Glenn, R.W.J., Kukunoor, N.S., Waits, W.H.I., Clayfield, E.J. (1995). Electrocoagulation and separation of aqueous suspensions of ultrafine particles. Colloids Surf. A **104**, 101–109.

Misawa, T., Kyuno, T., Suëtaka, W., Shimodaira, S. (1971). The mechanism of atmospheric rusting and the effect of Cu and P on the rust formation of low alloy steels. Corros. Sci. **11**, 35–48.

Modirshahla, N., Behnajady, M.S., Kooshaiian, S. (2007). Investigation of the effect of different electrode connections on the removal efficiency of tartrazine from aqueous solutions by electrocoagulation. Dyes Pigm. **74**, 249–257.

Mollah, M., Pathak, S., Patil, P., Vayuvegula, M. (2004). Treatment of orange II azo-dye by electrocoagulation (EC) technique in a continuous flow cell using sacrificial iron electrodes. J. Hazard. Mater. **109**, 165–171.

Onder, E., Koparal, A.S., Ogutveren, U.B. (2007). An alternative method for the removal of surfactants from water: electrochemical coagulation. Sep. Purif. Technol. **52**, 527–532.

Parga, J.R., Cocke, D.L., Valenzuela, J.L., et al. (2005). Arsenic removal via electrocoagulation from heavy metal contaminated groundwater in La Comarca Lagunera México J Hazard Mater. **124**, 247–254.

Paul, A.B. *Proceedings of the 22nd WEDC Conference on Water Quality and Supply, New Delhi, India*, 1996, p. 286.

Pretorius, W.A., Johannes, W.G., Lempert, G.G. (1991). Eelectrolytic iron flocculant production with a bipolar electrode in series arrangement. Water SA **17**, 133–138.

Szpyrkowicz, L. (2007). Hydrodynamic effects on the performance of electro-coagulation/electroflotation for the removal of dyes from textile wastewater. Ind. Eng. Chem. Res. **44**, 7844–7853.

Vik, E.A., Carlson, D.A., Eikun, A.S., Gjessing, E.T., (1984). Electrocoagulation of potable water. Water Res. **18**, 1355–1360.

Wong, H.M., Shang, C., Cheung, Y.K., Chen, G. (2002). Chloride assisted electrochemical disinfection, in: *Proceedings of the Eighth Mainland-Taiwan Environmental Protection Conference*, Tsin Chu, Taiwan.

Wu, C.H., Chang, C.L., Kuo, C.Y. (2008). Decolorization of procion red MX-5B in electrocoagulation (EC), UV/TiO_2 and ozone-related systems. Dyes Pigm. **76**, 187–194.

Yavuz, Y. (2007). EC and EF processes for the treatment of alcohol distillery wastewater. Sep. Purif. Technol. **53**, 135–140.

Yildiz, Y.S., Koparal, A.S., Irdemez, S., Keskinler, B. (2007). Electrocoagulation of synthetically prepared waters containing high concentration of NOM using iron cast electrodes. J. Hazard. Mater. **B139**, 373–380.

Zhu, B.T., Cliford, D.A., Chellam, S. (2005). Comparison of electrocoagulation and chemical coagulation pretreatment for enhanced virus removal using microfiltration membranes. Water Res. **39**, 3098–3108.

Chapter 11
Electroflotation

Xueming Chen and Guohua Chen

11.1 Theoretical

11.1.1 Electrochemical Reactions and Gas Generating Rate

In EF, the oxygen and hydrogen bubbles are generated at an anode and a cathode, respectively, as below

$$2H_2O = O_2 + 4H^+ + 4e \text{ at the anode} \tag{11.1}$$

$$2H^+ + 2e = H_2 \text{ at the cathode} \tag{11.2}$$

The total reaction is

$$2H_2O = 2H_2 + O_2 \tag{11.3}$$

Equation (11.3) demonstrates that the amount of hydrogen gas generated is twice that of oxygen gas. The gas generating rate can be calculated according to the Faraday's law:

$$Q_H = \frac{IV_0}{n_H F}, \tag{11.4}$$

$$Q_O = \frac{IV_0}{n_O \dot{F}}, \tag{11.5}$$

where Q_H is the hydrogen gas generating rate ($L\,s^{-1}$) at the normal state; Q_O the oxygen gas generating rate ($L\,s^{-1}$) at the normal state; V_0 the molar volume of gases at the normal state ($22.4\,L\,mol^{-1}$); F the Faraday's constant ($96,500\,C\,mol^{-1}$

X. Chen (✉)
Environmental Engineering Department, Zhejiang University, 38 Zheda Road, Hangzhou, Zhejiang Province, People's Republic of China
e-mail: chenxm@zju.edu.cn

C. Comninellis and G. Chen (eds.), *Electrochemistry for the Environment*,
DOI 10.1007/978-0-387-68318-8_11,

electrons); n_H the electrons transfer number of H_2 (2 mol electrons per mole of H_2); and n_O is the electrons transfer number of O_2 (4 mol electrons per mole of O_2).

The total gases generating rate is

$$Q_g = Q_H + Q_O = \frac{IV_0}{F}\left(\frac{1}{n_H} + \frac{1}{n_O}\right) = 1.74 \times 10^{-4} I, \tag{11.6}$$

where Q_g is the total gases generating rate ($L\,s^{-1}$) at the normal state.

11.1.2 Electrolysis Voltage and Specific Energy Consumption

The electrolysis voltage between two electrodes is the summation of the equilibrium potential difference, anode overpotential, cathode overpotential, and ohmic potential drop of the aqueous solution as shown below (Scott 1995; Chen et al. 2002c):

$$U = E_{eq} + \eta_a + |\eta_c| + \frac{d}{\kappa} i, \tag{11.7}$$

where U is the electrolysis voltage (V); E_{eq} the equilibrium potential difference for water split (V); η_a the anode overpotential (V); η_c the cathode overpotential (V); d the interelectrode distance (m); κ the solution conductivity ($S\,m^{-1}$); and i is the current density ($A\,m^{-2}$).

Usually, overpotentials include activation overpotentials and concentration overpotentials. They are related to many factors including the electrochemical properties of electrodes, the current density used, and the pH value of the solution. Therefore, direct calculation of the electrolysis voltage using (11.7) is still difficult, and experimental measurement is necessary. However, it is useful to point out that the electrolysis voltage required in an EF process is mainly from the ohmic potential drop of the aqueous phase, especially when the conductivity is low and the current density is high. Since the ohmic potential drop is proportional to the interelectrode distance, reducing this distance is of great importance for reducing the electrolysis energy consumption. In addition, when the conductivity is low, direct application of EF consumes large amount of electricity. For this case, addition of table salt (NaCl) is helpful (Ibrahim et al. 2001).

The specific energy consumption of EF during electrolysis can be calculated according to (11.8):

$$W = \frac{IU}{1{,}000 Q_w} = \frac{qU}{1{,}000}, \tag{11.8}$$

where W is the specific energy consumption ($kWh\,m^{-3}$); I the electrolysis current (A); Q_w the water flow rate ($m^3\,h^{-1}$); and $q = I/Q_w$ is the charge loading ($Ah\,m^{-3}$).

11.2 Features of EF

11.2.1 Bubbles' Size

Flotation is a complicated process. Its separation efficiency depends not only on the properties of suspended substances the volume ratio of the gas bubbles to the suspended substances, and the retention time of the flotation tank, but also on the bubbles' size. Usually, the smaller the bubbles are, the higher the flotation efficiency is. This is simply because smaller bubbles can provide larger specific surface area for particles attachment. Therefore, generation of finely dispersed bubbles is highly desired for any flotation processes.

EF can produce much smaller bubbles than DAF and many other flotation methods. This is one of the most attractive features of the EF process. Usually, the sizes of bubbles generated electrolytically obey a log–normal distribution (Fukui and Yuu 1985). Table 11.1 gives the typical bubble sizes reported in literatures (Glembotskii et al. 1975; Ketkar et al. 1991; Burns et al. 1997; Chen 2002). The mean diameters of the hydrogen and oxygen bubbles generated in EF range from 17 to 50 μm. In contrast, the typical mean diameters of the bubbles released in DAF are 48–58 μm using a pressurized water release unit (Burns et al. 1997), and about 60 μm using a needle valve (De Rijk et al. 1994); the dispersed air flotation produced bubbles with diameters of 75–655 μm (Ahmed and Jameson 1985). The

Table 11.1 Typical bubble sizes generated electrolytically

Mean diameter (μm)		Electrode	Experimental conditions	Reference
H_2	17	Pt	pH 7, current density 250 A m^{-2}	Glembotskii et al. (1975)
	17	Fe		
	25	C		
O_2	30	Pt		
H_2	22–34	Stainless steel plate	pH 9, current density 125–375 A m^{-2}	Ketkar et al. (1991)
	28–39	200 mesh		
	32–45	100 mesh		
	37–49	60 mesh		
O_2	42–48	Pt plate		
	38–50	200 mesh		
H_2	19–38	Graphite	Na_2SO_4 solution, current density 6.3–34 A m^{-2} for H_2 and 5.8–152 A m^{-2} for O_2	Burns et al. (1997)
O_2	17–38	Graphite		
$H_2 + O_2$	23–35	Ti/IrO_x–Sb_2O_5–SnO_2 (anode) Ti (cathode)	Na_2SO_4 solution, current density 133–400 A m^{-2}	Chen (2002)

much smaller bubbles generated electrolytically means that EF has higher efficiency for separating of suspended substances than the conventional flotation processes.

It should be noted that the size of bubbles generated electrolytically depends on pH. The hydrogen bubbles are smallest at neutral pH, while the size of oxygen bubbles increases with pH (Glembotskii et al. 1975). Llerena et al. (1996) found that the recovery of sphalerite was optimal at pH between 3 and 4 using buffer solution. They also documented that within this pH range, the hydrogen bubbles were the smallest, about $16 \pm 2\,\mu m$. Deviation of pH away from 3 to 4 resulted in an increase in the size of the hydrogen bubbles. At pH of 6, the mean hydrogen bubbles' diameter was $27\,\mu m$; at pH of 2, the hydrogen bubbles were about $23\,\mu m$ when the current density was all fixed at $500\,A\,m^{-2}$ using a 304 SS wire.

The size of the bubbles is also associated with the electrode material and current density. The stainless steel plate gives the finest bubbles (Ketkar et al. 1991). An increase in current density results in a decrease in bubbles' size. Nevertheless, Burns et al. (1997) reported that such a decrease of bubbles' size with increase in current density was true only at the low end of current densities. Chen (2002) found that the smallest bubbles were obtained at a current density of $267\,A\,m^{-2}$.

Moreover, it needs to point out that the electrode surface state can affect the size of bubbles significantly. Pretreatment of the electrode surface by sandblast and or/etching with boiled hydrochloric acid is beneficial for the reduction of bubbles' size.

11.2.2 Operation

The operation of EF is very simple. This is another important feature for EF. By varying current, it becomes possible to create any gas bubble concentration in the flotation medium to fit the variation of the water flow rate and the suspended substances' concentration from time to time. If necessary, a gas medium with very great surface area can be formed easily during EF, thereby increasing the probabilities of bubble–particle collision and adhesion and the formation of tenacious particle–bubble complexes (Mallikarjunan and Venkatachalam 1984).

11.2.3 Simultaneous Separation and Disinfection

When chloride ions are present, it is also possible to achieve simultaneous separation and disinfection for water and wastewater treatment by electrolytic generation of chlorine:

$$2Cl^- = Cl_2 + 2e \text{ at an anode} \quad (11.9)$$

$$Cl_2 + H_2O = HOCl + HCl \quad (11.10)$$

$$HOCl = H^+ + OCl^- \quad (11.11)$$

The combined phenomena make EF an attractive technology for the treatment and reuse of food-process water streams or even as a direct fluid food-processing operation where separation and disinfection are required (Hernlem and Tsai 2000; Tsai et al. 2002).

11.3 Electrodes System

11.3.1 Cathodes

Metals and alloys are usually selected as cathodes for hydrogen evolution in EF. For most cases, stainless steel is a good choice because it is cheap and readily available. Nickel is known to have low overpotential for hydrogen evolution. Therefore, usage of a nickel cathode can save energy consumption. Titanium is expensive, but it is very stable. Therefore, this metal can be selected as a cathode material in treatment of corrosive wastewaters.

11.3.2 Anodes

Compared with cathodes, available anodes are much less because severe electrochemical corrosion may occur when common metals and alloys are used as anodes. Actually, the lack of stable and cheap anodes was one of the key factors that limited the wide application of EF in industry. Fortunately, this problem has been well solved due to the quick development of cost-effective anodes in recent years.

Graphite, PbO_2, and Pt are among the most common nonconsumable anode materials. Graphite and PbO_2 anodes are cheap and easily available, and thus have been widely investigated for oxygen evolution in EF (Burns et al. 1997; Ho and Chan 1986; Hosny 1996). However, the durability of graphite is poor. Its service life (SL) is only 6–24 months in part due to the oxidation of C to CO_2 and to physical wear arising from gas evolution (Novak et al. 1982). In fact, the once widely employed graphite anodes have been replaced by the dimensionally stable anodes (DSA) in chlorine-alkali industry. The stability of PbO_2 is also poor. Ho and Chan (1986) investigated the corrosion of PbO_2 anodes and found that the concentrations of Pb^{2+} ions present in solutions ranged from 0.06 to 0.68 mg L^{-1} after 24 h of electrolysis. Therefore, graphite and PbO_2 are not good oxygen evolution anodes for EF. A few researchers reported the use of Pt or Pt-plated meshes as anodes for EF (Ketkar et al. 1991; Poon 1997). They are much more stable than graphite and

PbO_2. However, their known high costs make large-scale industrial applications impracticable.

The DSA invented by Beer in the late 1960s are the most important anodes that are used nowadays in electrochemical engineering. Usually, DSA use conductive precious metal oxides (RuO_2, IrO_2, etc.) as electrocatalysts and nonconductive metal oxides (TiO_2, Ta_2O_5, ZrO_2, Nb_2O_5, etc.) as dispersing or stabilizing agents, which are coated on valve metal substrates (Ti, Ta, Zr, W, Nb, Bi) with a thermal decomposition method (Beer 1972; Novak et al. 1982).

It is well known that TiO_2–RuO_2 types of DSA® discovered by Beer possess high quality for chlorine evolution in the chlor-alkali industry. However, their service lives are short for oxygen evolution (Hine et al. 1979). In the last two decades, IrO_x-based DSA have received much attention. IrO_x presents a service life about 20 times longer than that of the equivalent RuO_2 (Alves et al. 1998). In general, Ta_2O_5, TiO_2, and ZrO_2 are used as stabilizing or dispersing agents to save cost and/or to improve the coating property (Rolewicz et al. 1988; Comninellis and Vercesi 1991; Vercesi et al. 1991; Cardarelli et al. 1998). Occasionally, a third component such as CeO_2 is also added (Alves et al. 1998; Alves et al. 1994). It should be noted that although incorporation of Ta_2O_5, TiO_2, and ZrO_2 can save IrO_x loading, the requirement of molar percentage of the precious Ir component is still very high. The optimal IrO_x contents are 80 mol% for IrO_x–ZrO_2, 70 mol% for IrO_x–Ta_2O_5, and 40 mol% for IrO_x–TiO_2, below which electrode service lives decrease sharply (Comninellis and Vercesi 1991). Among the various electrocatalysts mentioned above, IrO_x–Ta_2O_5 has the highest electrochemical stability. The IrO_x–Ta_2O_5-coated titanium electrodes (Ti/IrO_x–Ta_2O_5) have been successfully used as anodes of EF (Mraz and Krysa 1994; Chen et al. 2000). Nevertheless, due to consumption of large amounts of the IrO_x, Ti/IrO_x–Ta_2O_5 electrodes are very expensive, limiting their wide application.

The recently developed Ti/IrO_x–Sb_2O_5–SnO_2 anodes have extremely high electrochemical stability and good electrocatalytic activity for oxygen evolution (Chen et al. 2001; Chen et al. 2002a, b; Chen and Chen 2005). A Ti/IrO_x–Sb_2O_5–SnO_2 electrode containing only 2.5 mol% of IrO_x nominally in the oxide coating could be used for 437 h in the accelerated life test performed in 3 M H_2SO_4 solution at a current density of $10,000\ A\ m^{-2}$ (Chen et al. 2002b). In contrast, the service life of Ti/IrO_x is 355 h under the same condition (Chen et al. 2001). This means that the Ti/IrO_x–Sb_2O_5–SnO_2 electrode not only saves 97.5% of the precious Ir content, but also exceeds the conventional Ti/IrO_x in electrochemical stability. The significant saving of IrO_x is attributed to good conductivity of Sb_2O_5–SnO_2, formation of a solid solution, bonding improvement as well as compact structure of the IrO_x–Sb_2O_5–SnO_2 film.

The electrode service life is strongly dependent on the current density used. A simple model relating the service life to the current density (i) has been obtained (Chen et al. 2001):

$$\mathrm{SL} \propto \frac{1}{i^n}, \tag{11.12}$$

where n ranges from 1.4 to 2.0.

According to (11.12), the service life of $Ti/IrO_x–Sb_2O_5–SnO_2$ for EF application (SL_{EF}) at a current density (i_{EF}) can be estimated:

$$SL_{EF} = SL_a \left(\frac{i_a}{i_{EF}} \right)^n , \tag{11.13}$$

where SL_a and i_a are the service life and the current density under the accelerated lifetest conditions.

Using (11.13), the service life of the $Ti/IrO_x–Sb_2O_5–SnO_2$ anode containing 2.5 mol% of IrO_x nominally in the oxide coating is calculated to be about 8 years at a current density of 500 A m^{-2} in acid solution. Considering the lower current density used and nearly neutral operating environments, such an anode is believed stable enough for use in EF.

11.3.3 Electrodes Arrangement

The electrodes can be arranged in different patterns. Usually a plate electrode is installed at the bottom, while a screen electrode is fixed at 10–50 mm above the plate electrode as shown in Fig. 11.1 (Alexandrova et al. 1994; Llerena et al. 1996; Il'in and Sedashova 1999; Mostefa and Tir 2004; Khelifa et al. 2005). In such an arrangement, only the upper screen electrode faces the water flow, while the bottom electrode does not interact with the flow directly. Therefore, the bubbles generated at the bottom electrode cannot be dispersed immediately into the water being treated. This not only decreases the availability of the effective small bubbles, but also increases the possibility of breaking the flocs formed previously, affecting the flotation efficiency. In addition, if the conductivity is low, energy consumption will be unacceptably high due to the large interelectrode spacing required for preventing the short circuit between the upper flexible screen electrode and the bottom plate electrode. This renders EF economically unfavorable in competing with the conventional DAF. Moreover, the maintenance of the electrodes system is a problem because the screen electrode is easy to be twined by undesirable deposits such as fabric, and difficult to clean once twined.

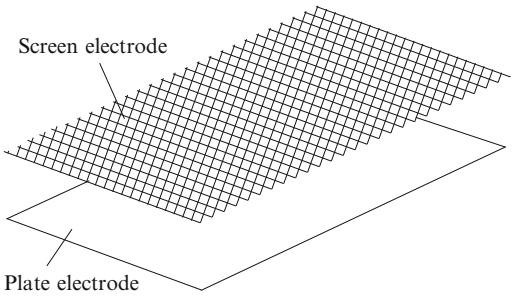

Fig. 11.1 Conventional electrodes arrangement

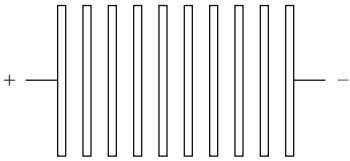

Fig. 11.2 Vertical electrodes arrangement

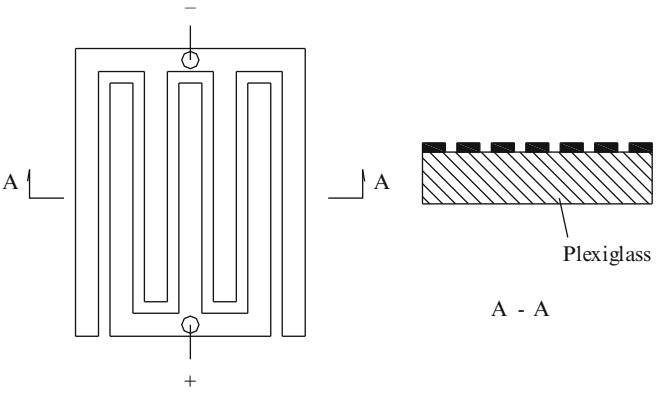

Fig. 11.3 Open electrodes arrangement

The electrodes can also be arranged vertically as shown in Fig. 11.2 (Hernlem and Tsai 2000; Tsai et al. 2002; Choi et al. 2005). For such an arrangement, both the anodes and the cathodes are designed as plate shape, and therefore they can be fixed easily. However, the bubbles generated trend to rise along the surfaces of the electrodes, which is often observed in the electrocoagulation process (Chen et al. 2000) resulting in a quick bubbles coalesce and thereby affecting the flotation efficiency.

Moreover, the electrodes can be arranged openly with the fork-like anode and cathode placed on the same plane as shown in Fig. 11.3 (Chen et al. 2002b; Shen et al. 2003). Effective flotation is obtained because of quick dispersion of the small bubbles generated into the water flow. Quick bubble dispersion is essentially as important as the generation of tiny bubbles. When the anode and the cathode are leveled, such an open configuration allows both the cathode and the anode to contact the water flow directly. Therefore, the bubbles generated at both electrodes can be dispersed into water rapidly and attach onto the flocs effectively, ensuring high flotation efficiency. Another open electrodes arrangement is shown in Fig. 11.4 (Gao et al. 2005). It has the advantage of the uniform property of the surface of an electrode. The open configuration has been proven quite effective in the flotation of oil and suspended solids (Chen et al. 2002b). Significant electrolysis energy saving has also been obtained due to the small interelectrode gap used in the open arrangement system. As mentioned before, the electrolysis voltage required in an EF process is mainly from the ohmic potential drop of the solution resistance, especially when

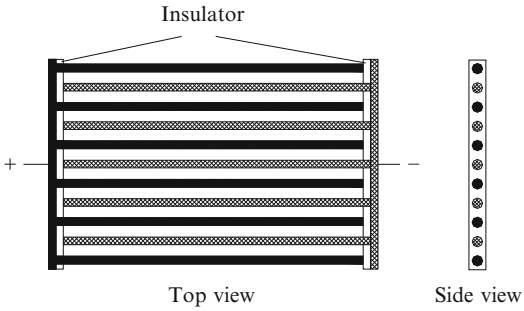

Fig. 11.4 Alternative open electrodes arrangement

the conductivity is low and the current density is high. Accordingly, the electrolysis energy consumption can be reduced as the interelectrode distance decreases. For the conventional electrode system (Fig. 11.1), due to the easy short circuit between the upper flexible screen electrode and the bottom electrode, use of a very small spacing is technically difficult. But for the electrodes system shown in Figs. 11.3 and 11.4, the interelectrode gap can be as small as 2 mm.

11.4 Typical Designs

11.4.1 Single-Stage EF

The EF unit can be designed as various configurations. For most cases, a single-stage EF with a horizontal flow is a good choice due to its simplicity. A prototype single-stage EF system is shown in Fig. 11.5 (Poon 1997). The unit was built using a platinum-clad columbium screen as an anode, and a stainless steel screen as a cathode. The anode had an area of 1.35 m^2, and was positioned at the bottom. The water depth above the cathode was about 98 cm. The flow rate and the effective volume were 1.1 $m^3\ h^{-1}$ and 1.4 m^3, respectively. The system has been successfully used for groundwater decontamination.

An alternative to the design above is the single-stage EF with a vertical flow as shown in Fig. 11.6. Such as system may have higher separation efficiency due to the uniform distribution of the flow.

When the treatment scale is large, a single-stage EF with a contacting chamber and a separating chamber as shown in Fig. 11.7 can be considered. In such an EF system, the electrodes area can be reduced significantly. However, its separation efficiency may decrease because the fragments dropping from the scum layer during skimming cannot be floated to the top again.

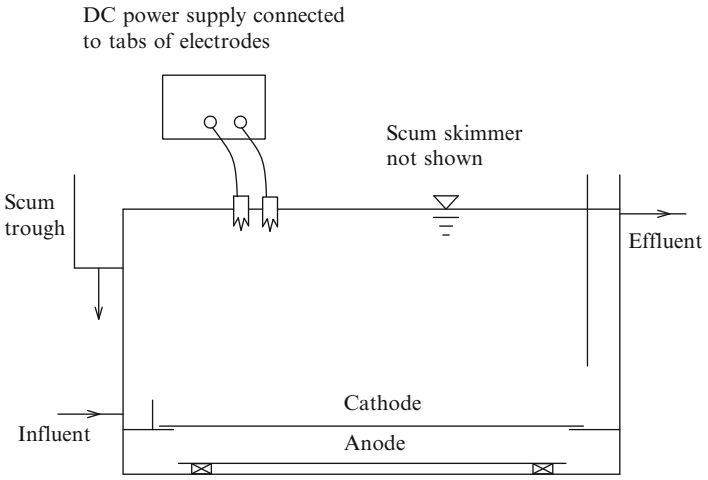

Fig. 11.5 Single-stage EF with a horizontal flow

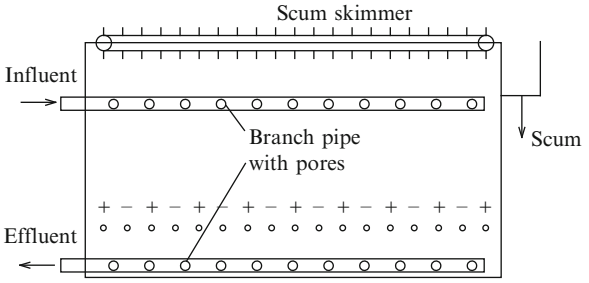

Fig. 11.6 Single-stage EF with a vertical flow

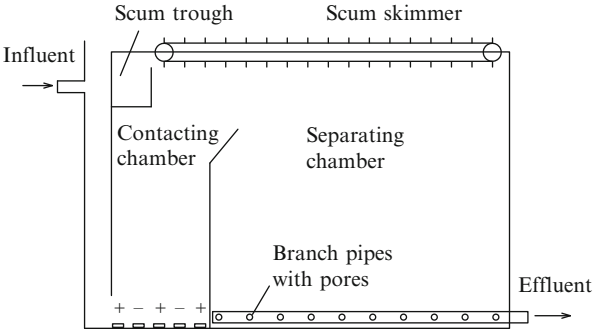

Fig. 11.7 Single-stage EF with a contacting chamber and a separating chamber

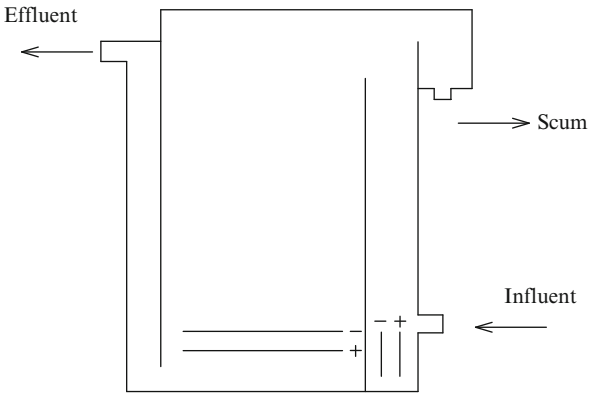

Fig. 11.8 Two-stage EF

11.4.2 Two-Stage EF

In order to improve separation efficiency, two-stage EF systems can be used. A typical two-stage EF system is shown in Fig. 11.8 (Il'in and Sedashova 1999). In the first stage, there is vigorous mixing because of the rapid production of gas bubbles due to the high current, which accelerates the formation of the flotation complexes and the displacement of them to the surface, with the foam layer receiving 80–90% of the impurities to be extracted. The secondary stage has a current loading selected to provide for bubbles to float up under conditions close to laminar, which provides for extracting suspended impurities of size less than 10 μm. There is an additional purification effect due to the filtration of the solution through the dense layer of bubbles. The liquid moves downward and the purified effluent is drawn off under the electrode unit.

11.4.3 Combination of EF with EC

In order to separate finely dispersed particles effectively, EF can be combined with chemical flocculation or EC (Chen 2004). Figure 11.9 shows the combination of EF and EC for oily wastewater treatment (Chen et al. 2002b). In such a process, EC mainly plays the role of destabilizing and aggregating the fine particles, while EF is responsible for floating the flocs formed in the effluent of the EC. Fork-like $Ti/IrO_2–Sb_2O_5–SnO_2$ and titanium are used as the anode and the cathode, respectively, for EF; and aluminum plates are used as the anodes and cathodes for EC. Oil separation is very effective. Even at a charge loading as low as 0.5 Faraday per m^3, the oil is reduced from 710 mg L^{-1} to around 10 mg L^{-1} with a removal efficiency over 98%. As the charge loading increases to 1.5 Faraday per m^3, the oil content in the effluent is only 4 mg L^{-1}. SS separation is also effective. The concentration of

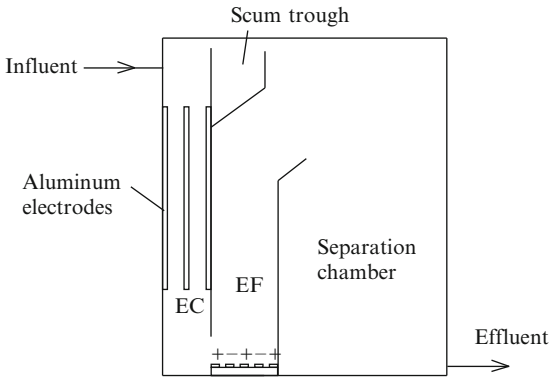

Fig. 11.9 Combined EC–EF

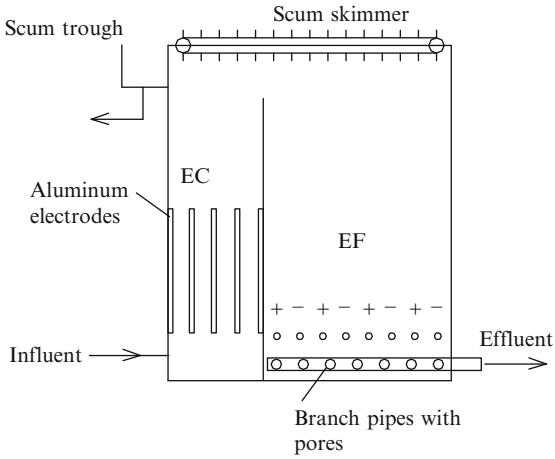

Fig. 11.10 Alternative combined EC–EF

SS can be reduced from 330 to 74 mg L^{-1} at a charge loading of 0.5 Faraday per m^3 and to only 17 mg L^{-1} at a charge loading of 3.0 Faradays per m^3. The combined EF and EC has two significant advantages over the other processes: shorter retention time and drier sludge produced. Ten minutes are enough to achieve effective pollutant removal. This is a very attractive advantage for densely populated areas where the compactness of the treatment facility is particularly concerned.

For large-scale application, a combined EC–EF system as shown in Fig. 11.10 can be considered. The system is simple in configuration. More importantly, scum collection becomes easy due to the direct connection of EC and EF at the top However, it should be noted that the co-current EC is usually not as effective as the counter-current EC. Therefore, a slight increase in charge loading is probably required.

11.5 Water and Wastewaters Treated by EF

In water and wastewaters treatment, flotation has been widely used for separating oil and low-density suspended solids. EF, as an electrochemical version of flotation, usually has higher separation efficiency than the conventional DAF due to its much smaller hydrogen and oxygen bubbles generated electrolytically. This technique has been proven effective in treating oily wastewater or oil–water emulsion (Balmer and Foulds 1986; Hosny 1996; Il'in and Sedashova 1999; Ibrahim et al. 2001; Khelifa et al. 2005; Mansour and Chalbi 2006), mining wastewater (Alexandrova et al. 1994), groundwater (Poon 1997), food processing wastewater (Kubritskaya et al. 2000; Hernlem et al. 2000; Tsai et al. 2002), restaurant wastewater (Chen et al. 2000), industrial sewage (Il'in et al. 2002), heavy metals containing effluent (Srinivasan and Subbaiyan 1989; Mostefa and Tir 2004; Casqueira et al. 2006), and many other water and wastewaters (Llerena et al. 1996; Il'in and Kolesnikov 2001; Park et al. 2002).

References

Ahmed, N. and Jameson, G.J. (1985) The effect of bubble size on the rate of flotation of fine particles. Int. J. Miner. Process 14, 195–215.

Alexandrova, L., Nedialkova, T. and Nishkov, I. (1994) Electroflotation of metal ions in waste water. Int. J. Miner. Process. 41, 285–294.

Alves, V.A., Silva, L. A. D. Boodts, J.F.C. and Trasatti, S. (1994) Kinetics and mechanism of oxygen evolution on IrO_2-based electrodes containing Ti and Ce acidic solutions. Electrochim Acta 39, 1585–1589.

Alves, V.A., Silva, L.A.D., Oliveira, E.D. and Boodts, J.F.C. (1998) Investigation under conditions of accelerated anodic corrosion of the effect of TiO_2 substitution by CeO_2 on the stability of Ir-based ceramic coatings. Mater. Sci. Forum 289–292, 655–666.

Balmer, L.M. and Foulds, A.W. (1986) Separation oil from oil-in-water emulsions by electroflocculation/electroflotation. Filtr. Separ 23(11/12), 366–369.

Beer, H.B. (1972) Electrode and coating therefore. USA Patent 3,632,498.

Burns, S.E., Yiacoumi, S. and Tsouris, C. (1997) Microbubble generation for environmental and industrial separations. Separ. Purif. Technol. 11, 221–232.

Cardarelli, F., Taxil, P., Savall, A., Comninellis, Ch., Manoli, G. and Leclerc, O. (1998) Preparation of oxygen evolving electrodes with long service life under extreme conditions. J. Appl. Electrochem. 28, 245–250.

Casqueira, R.G., Torem, M.L. and Kohler, H.M. (2006) The removal of zinc from liquid streams by electroflotation. Miner. Eng. 19, 1388–1392.

Chen, X.M. (2002) High-performance electrodes for wastewater treatment. PhD thesis presented to the Hong Kong University of Science and Technology.

Chen, G. (2004) Electrochemical technologies in wastewater treatment Separ. Purif. Technol. 38, 11–41.

Chen, X.M. and Chen, G. (2005) Investigation of $Ti/IrO_2–Sb_2O_5–SnO_2$ electrodes for O_2 evolution. J. Electrochem. Soc. 152(7), J59–J64.

Chen, G., Chen, X.M. and Yue, P.L. (2000) Electrocoagulation and electroflotation of restaurant wastewater. J. Environ. Eng.-ASCE 126, 858–863.

Chen, X.M., Chen, G. and Yue, P. L. (2001) Stable $Ti/IrO_x - Sb_2O_5 - SnO_2$ anode for O_2 evolution with low Ir content. J. Phys. Chem. B 105, 4623–4628.

Chen, G., Chen, X.M. and Yue, P.L. (2002a) Electrochemical behaviour of Novel Ti/IrO_x–Sb_2O_5–SnO_2 anodes. J. Phys. Chem. B 106, 4364–4369.
Chen, X.M., Chen, G. and Yue, P.L. (2002b) Investigation on the electroysis voltage of electrocoagulation. Chem. Eng. Sci. 57, 2449–2455.
Chen, X.M., Chen, G. and Yue, P.L. (2002c) Novel electrode system for electroflotation of wastewaters, Environ. Sci. Technol. 36(4), 778–783.
Choi, Y.G., Kim, H.S., Park, Y.H., Jeong, S.H., Son, D.H., Oh, Y.K. and Yeom, I.T. (2005) Improvement of the thickening and dewatering characteristics of activated sludge by electroflotation (EF) Water. Sci. Technol. 52(10–11), 219–226.
Comninellis, Ch. and Vercesi, G.P. (1991) Characterization of DSA-type oxygen evolving electrodes: choice of a coating. J. Appl. Electrochem. 21, 335–345.
De Rijk, S.E., van der Graaf, J.H.J.M. and den Blanken, J.G. (1994) Bubble size in flotation thickening. Water Res. 28, 465–473.
Elmore, F.E. (1905) A process for separating certain constituents of subdivided ores and like substances, and apparatus therefore. British Patent 13,578.
Fukui, Y. and Yuu, S. (1985) Removal of colloidal particles in electroflotation. AIChE J. 31(2), 201–208.
Gao, P., Chen, X.M, Shen, F. and Chen, G. (2005) Removal of chromium (VI) from wastewater by combined electrocoagulation-electroflotation without a filter. Separ. Purif. Technol. 43, 117–123.
Glembotskii, V. A., Mamakov, A.A., Ramanov, A. M. and Nenno, V.E. (1975) *11th International Mineral Processing Congress, Caglairi*, pp. 562–581.
Hernlem, B.J. and Tsai, L.S. (2000) Chlorine generation and disinfection by electroflotation. J. Food Sci. 65, 834–837.
Hine, F., Yasuda, M., Noda, T., Yoshida, T. and Okuda, J. (1979) Electrochemical behavior of the oxide-coated metal anodes. J. Electrochem. Soc. 126, 1439–1445.
Ho, C.C. and Chan, C.Y. (1986) The application of lead dioxide-coated titanium anode in the electroflotation of palm oil mill effluent. Water Res. 20, 1523–1527.
Hosny, A.Y. (1996) Separating oil from oil–water emulsions by electroflotation technique. Separ. Technol. 6, 9–17.
Ibrahim, M.Y., Mostafa, S.R., Fahmy, M.F.M. and Hafez, A.I. (2001) Utilization of electroflotation in remediation of oily waste water. Separ. Sci. Technol. 36, 3749–3762.
Il'in, V.I. and Kolesnikov, V.A. (2001) Electroflotation purification of radioactive waste waters. Atom. Energy 91, 551–554.
Il'in, V. I. and Sedashova, O.N. (1999) An electroflotation method and plant for removing oil products from effluents. Chem. Petrol. Eng. 35, 480–481.
Il'in, V.I., Kolesnikov, V.A. and Parshina, Y. I. (2002) Purification of highly concentrated industrial sewage from the porcelain and faience industry by the electric flotation method. Glass Ceram. 59(7–8), 242–244.
Ketkar, D.R., Mallikarjunan, R. and Venkatachalam, S. (1991) Electroflotation of quartz fines. Int. J. Miner. Process. 31, 127–138.
Khelifa, A., Moulay, S. and Naceur, A.W. (2005) Treatment of metal finishing effluents by the electroflotation technique. Desalination 181, 27–33.
Kubritskaya, T.D., Drako, I.V., Sorokina, V.N. and Drondina, R.V. (2000) Use of electrochemical methods to purify the waste water from the production of concentrates in the food industry. Surf. Eng. Appl. Electrochem. 6, 62–68.
Llerena, C., Ho, J. C. K. and Piron, D.L. (1996) Effect of pH on electroflotation of sphalerite. Chem. Eng. Commun. 155, 217–228.
Mallikarjunan, R. and Venkatachalam, S. (1984) Electroflotation-a review. In: *Proceeding of the International Symposium on Electrochemistry in Mineral and Metal Processing*, 165th Meeting of Electrochemistry Society, Cincinnati, OH, USA, pp. 233–256.
Mansour, L. B. and Chalbi, S. (2006) Removal of oil from oil/water emulsions using electroflotation process. J. Appl. Electrochem. 36, 577–581.

Mostefa, N.M. and Tir, M. (2004) Coupling flocculation with electroflotation for waste oil/water emulsion treatment: Optimization of the operating conditions. Desalination 161, 115–121.

Mraz, R. and Krysa, J. (1994) Long service life IrO_2/Ta_2O_5 electrodes for electroflotation. J. Appl. Electrochem. 24, 1262–1266.

Novak, D.M., Tilak, B.V. and Conway, B.E. (1982) Fundamental and applied aspects of anodic chlorine production In: J.O. Bockris, B.E. Conway and R.E. White (Eds), *Modern Aspects of Electrochemistry* vol. 14 Plenum New York, NY, pp. 195–318.

Park, J., Jung, Y., Han, M. and Lee, S. (2002) Simultaneous removal of cadmium and turbidity in contaminated soil-washing water by DAF and electroflotation. Water Sci. Technol. 46 (11–12), 225–230.

Poon, C.P.C. (1997) Electroflotation for groundwater decontamination. J. Hazard. Mater. 55, 159–170.

Rolewicz, J., Comninellis, Ch., Plattner, E. and Hinden, J. (1988) Characterisation des electrodes de type DSA pour le degagement de O_2 — I. l'electrode $Ti/IrO_2–Ta_2O_5$. Electrochim. Acta 33, 573–580.

Scott, K. (1995) *Electrochemical Processes for Clean Technology*. Royal Society of Chemistry Cambridge.

Shen, F., Chen, X.M., Gao, P. and Chen, G. (2003) Electrochemical removal of fluoride ions from industrial waste water. Chem. Eng. Sci. 58, 987–993.

Srinivasan, V. and Subbaiyan, M. (1989) Electroflotation studies on Cu, Ni, Zn, and Cd with ammonium dodecyl dithiocarbamate. Separ. Sci. Technol. 24, 145–150.

Tsai, L.S., Hernlem, B. and Huxsoll, C.C. (2002) Disinfection and solids removal of poultry chiller water by electroflotation. J. Food Sci. 67, 2160–2164.

Vercesi, G.P., Rolewicz, F. and Comninellis, Ch. (1991) Characterization of DSA-type oxygen evolving electrodes: choice of base metal Thermochim. Acta 176, 31–47.

Chapter 12
Electroreduction of Halogenated Organic Compounds

Sandra Rondinini and Alberto Vertova

12.1 Introduction

Since the early works of Winkel and Proske (1936) on the electroreduction of 1,3-dichloroacetone and other halogenated carbonyl compounds and of von Stackelberg and Stracke (1949) on the polarographic behaviour of several aliphatic and aromatic halocompounds, the electroreduction of organic halides has been a key topic in organic electrochemistry studies (Peters 2001; Lund 2002), which coupled the voltammetric investigations (Kolthoff and Lingane 1941; Meites 1965; Zuman 1967; Feldberg 1969; Andrieux and Savéant 1986; Bard and Faulkner 1999; Hammerich 2001) to the synthetic potentialities of controlled potential electrolyses (Chaussard et al. 1989; Fontana 1993; Koshechko et al 1994; Rondinini et al. 1998; Inokuchi and Kusumoto 2001; Simonet and Peters 2004; Gennaro et al. 2004; Simonet 2005; Scialdone et al. 2005; Isse et al. 2005a). More recently, the possibility of efficiently removing the halogen group from the substrate has been considered for environmental applications (Juttner et al. 2000; Rondinini et al. 2001a; Hori et al. 2003; Rondinini and Vertova 2004; Fiori et al. 2005; Ju et al. 2006; Laine and Cheng 2007), as valid alternative to the more popular and exhaustive electrooxidative process of total degradation, described in a recent review paper (Chen 2004) and in several contributions on the mineralization of chlorophenoxy herbicides (Brillas et al. 2004; Boye et al. 2006), mono- and poly-halogenated phenolic wastes (Gherardini et al. 2001; Rodrigo et al. 2001; Oturan et al. 2001; Canizares et al. 2005) and other chlorinated aromatic compounds (Polcaro et al. 2004).

Organic halides are utilized in a wide range of industrial processes as solvents and as building blocks for intermediates, value added chemicals and large production materials (e.g. polymers and resins). They have (or have had) a wide usage in a large variety of applications that range from herbicides/fungicides/pesticides in agriculture and woods disinfestations, to thermal and mechanical fluids. They might form as secondary pollutants in primary waste treatments (e.g. in thermal

S. Rondinini (✉)
Dipartimento di Chimica Fisica ed Elettrochimica, Università degli Studi di Milano, Milan, Italy
e-mail: sandra.rondinini@unimi.it

C. Comninellis and G. Chen (eds.), *Electrochemistry for the Environment*,
DOI 10.1007/978-0-387-68318-8_12,

decomposition plants (Ryu et al. 2006; Briois et al. 2007; Öberg et al. 2007), in oxidative degradations (Comninellis and Nerini 1995; Naumczyk et al. 1996; Kimbrough and Suffet 2002; De Lima Leite et al. 2003; Cherepy and Wildenschild 2003), in naturally occurring processes, under the effect of ultraviolet radiation (Fram et al. 2002; Liu et al. 2002) and in productive processes (Juttner et al. 2000; Deutscher and Cathro 2001; Bailey 2001).

Most of the persistent organic pollutant (POP), listed in the Stockholm Convention and its successive amendments (EC 850/2004; EC COM (2004) 537; EC COM (2006) 242; EC COM (2006) 252) (see Table 12.1), are halogenated organic compounds, which conjugate toxicity with high chemical stability, lipophilicity, accumulation-in-the-food-chain capability and long-range diffusivity. In this context, soil and ground-water remediation become key issues of the environmental protection and restoration.

According to their source, the wastes containing halocompounds range from concentrated organic solutions/emulsions to very dilute aqueous phases, to airborne streams, thus representing serious challenges in developing suitable treatment methodologies.

Over the years, the electrochemical methods have proven to be highly effective in the detoxification of wastes, since unlike conventional physico-chemical techniques (e.g. thermal degradation or chemical oxidation) they provide mild reaction conditions, avoid the secondary pollution effects chained to the excess reagents and are easily adapted even to small-size treatment needs.

Although the oxidative electrochemical processes are more widely used and studied, since they generally lead to the total degradation (mineralization) of the compounds, the electroreductive treatments are progressively attracting the interests of scientists and operators because they might potentially lead to the partial recovering/recycling of chemicals or to the production of value-added substances (Baizer and Wagenknecht 1973; Cabot et al. 2004; Titov et al. 2006).

In the following, the state-of-the-art of the electroreductive dehalogenation processes for environmental applications is critically reviewed in terms of substrates, electrode materials, reaction media, process and cell design and performances.

12.2 The Reaction Pathways

The mechanism of the electrochemical cleavage of the C–X (X = F, Cl, Br and I) bond has been extensively studied (see for example, Miller and Riekena 1969; Pause et al. 2000; Costentin et al. 2003; Wang et al. 2004; Sanecki and Skitał 2007) and theoretical models (Battistuzzi et al. 1993; Kuznetsov et al. 2004; Zhang et al. 2005; Golinske and Voss 2005), mostly based on the Marcus theory (Marcus 1964) for the homogeneous and heterogeneous (electrochemical) electron transfer (ET), have been formulated (Savéant 1987, 2000; Maran et al. 2001; Costentin et al. 2006a, b) and tested with the aim to predict the experimental outcomes.

Table 12.1 List of persistent halogenated organic pollutants (including CASnumber)

Aldrin – $C_{12}H_8Cl_6$

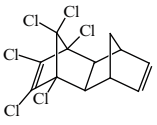

309-00-2

Chlordane – $C_{10}H_6Cl_8$

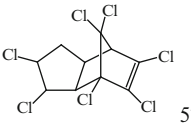

57-74-9

Dieldrin – $C_{12}H_8Cl_6O$

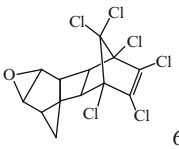

60-57-1

Endrin – $C_{12}H_8Cl_6O$

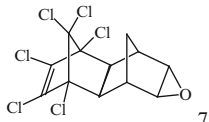

72-20-8

Heptachlor – $C_{10}H_5Cl_7$

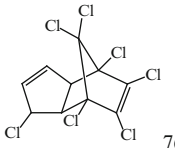

76-44-8

Hexachlorobenzene – C_6Cl_6

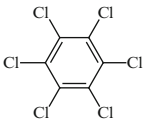

118-74-1

Mirex – $C_{10}Cl_{12}$

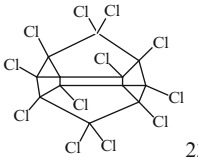

2385-85-5

Toxaphene[a]

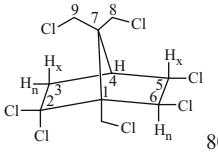

800 1-35-2

Polychlorinated Biphenyls (PCB)

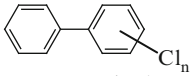

1336-36-3 and others

Hexabromobiphenyl

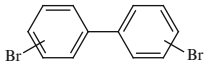

355-01-8

Chlordecone – $C_{10}Cl_{10}O$

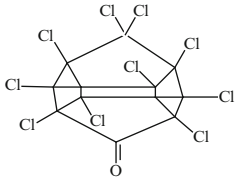

143-50-0

DDT (1,1,1-trichloro-2,2-bis (4-chlorophenyl) ethane) – $C_{14}H_9Cl_5$

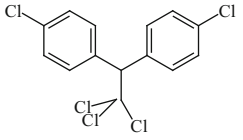

50-29-3

(continued)

Table 12.1 (continued)

Hexachlorocyclohexane[b] (HCH) $C_6H_6Cl_6$, including lindane

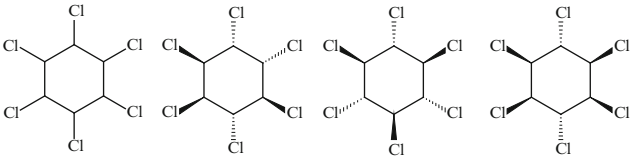

608-73-1 (α) 319-84-6 (β) 319-85-7 (γ) 658-89-9

Hexachlorobutadiene C_4Cl_6

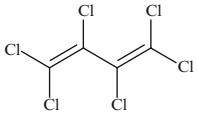

87-68-3

octabromodiphenyl ether $C_6H_2Br_8O$

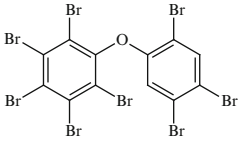

32536-52-0

Pentachlorobenzene – C_6HCl_5

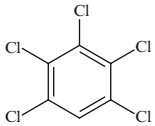

608-93-5

Polychlorinated naphthalenes

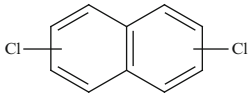

Polychiorinated dibenzo-p-dioxins (PCDD) and dibenzofurans (PCDF)

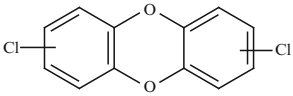

PCDD

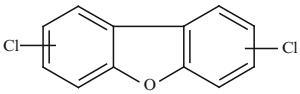

PCDF

[a] A mixture of over 670 substances

[b] Hexachlorocyclohexane (HCH) is the name of a technical mixture of various isomers. Only α-, β- and γ-HCH is of toxicological relevance

According to the theory (Costentin et al. 2006a), the dissociative ET process can be summarized in the following scheme:

$$RX + e^- \rightleftarrows RX^{\cdot -} \tag{12.1}$$

$$RX^{\cdot -} \rightarrow R^{\cdot} + X^- \tag{12.2}$$

$$RX + e^- \rightarrow R^{\cdot} + X^- \tag{12.3}$$

$$R^{\cdot} + e^- \rightarrow R^- \tag{12.4}$$

Here, reactions (12.1) and (12.2) represent the stepwise pathway, in which an intermediate radical anion is formed before the breaking of the C–X bond, while reaction (12.3) represents the simultaneous ET+C–X cleavage of the concerted pathway.

In dependence on the substrate and on the working conditions (solvent, supporting electrolyte, electrode material and potential), a second ET reaction (12.4) leads to the organic anion. Both anion and/or radical can react with solvent, hydrogen/proton donors and/or other RX molecules (or their organic moieties) to give propagation reaction products like dimers and hydrodehalogenated species, as in reactions (12.5b)–(12.5c).

$$R^{\cdot}(R^{-}) + HA \rightarrow RH + A^{\cdot}(A^{-}) \tag{12.5a}$$

$$R^{-} + RX \rightarrow R - R + X^{-} \tag{12.5b}$$

$$R^{\cdot} + R^{\cdot} \rightarrow R - R \tag{12.5c}$$

In many instances HX elimination can lead to double/triple bond formation (Costentin et al. 2003; Simonet 2004; Liu et al. 2000), while in the presence of suitable reagents [e.g. activated olefins (Brown and Harrison 1969; Baizer and Chruma 1972; Leonel et al. 1998; Peters 2001, Lund 2002; Barhdadi et al. 2003) or carbon dioxide (Baizer et al. 1973; Perichon et al. 1986; Chaussard et al. 1989; Koshechko et al 1994; Koshechko and Kiprianova 1999; Isse and Gennaro 2002a, b, 2003; Isse et al. 2002, 2005a, b; Gennaro et al. 2004)] addition products can be obtained.

Note that the ET reactions may also occur in homogeneous conditions, which represent a further route to degradation, via reducing mediator species continuously regenerated at the electrode (Scheme 1) (Rusling et al. 1990; Zhou et al. 1996; Nedelec et al. 1997; Isse and Gennaro 2004; Robert and Savéant 2005; Costentin et al. 2006a; Magdesieva et al. 2006; Vaze and Rusling 2006).

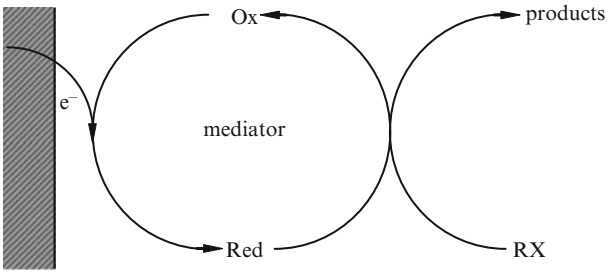

Scheme 1

In addition the mediator can be immobilized on the electrode surface, a feature that can be exploited also for analytical purposes (Betterton et al. 1995; Burris et al. 1996; Liu et al. 2006).

Finally, the indirect dehalogenation, via electrolytic production of atomic hydrogen, represents a possible alternative, especially when operating in protonated solvents, under background current conditions, on cathodes activated with noble metal particles (e.g. Pd, Ru, Rh, Ir, Au) (Cheng et al. 1997; Tsyganok et al. 1998; Tsyganok and Otsuka 1999; Iwakura et al. 2004).

The variety of possible products and by-products, which represents one of the most stimulating aspects in synthetic organic electrochemistry, constitutes a challenge when dealing with environmental applications, for which the total conversion of the substrates and the absence of secondary pollutants are crucial issues in the development and implementation of waste detoxification. In this context, while it is evident that no effective generalization can be done in the treatment of different substrates, which require specific studies for the adoption of successful degradation conditions, some general features can be recognized as underpinning elements, which have to be considered in the research and development of the treatment process.

12.3 The Combined Role of Electrode Material and Reaction Medium

The choice of the cathode material is extremely critical for the process, as it governs the reaction pathway, the selectivity and the specific energy consumption.

At the same time, the poor water solubility of most of the halogenated compounds implies the use of non-aqueous or mixed solvents which, in turn, require the choice of appropriate supporting electrolytes for ensuring the electrical conductivity of the reaction medium. While this last aspect can also be addressed by accurate cell design and appropriate process conditions, it has to be noted that tetraalkylammonium salts, currently used in the majority of voltammetric studies and preparative electrolyses, have their role on the reaction paths and products distribution (Tsyganok et al. 1999; Rondinini et al. 1999, 2000; Peters 2001; Ardizzone et al. 2002). In addition, in the absence of water and of any other source of protons, strong hydrogen scavengers like alkyl carbanions can deprotonate the tetraalkylammonium cations, which, in turn, degrade to the corresponding trialkylamine and olefin (Peters 2001).

Despite the advantages that the total non-aqueous environment offers the electroreductive studies on halocompounds, most of the degradation processes have to be applied to part of or total aqueous streams.

In these cases, as well as in protic solvents and/or in the presence of hydrogen/proton donors, the direct RX reaction at the electrode is frequently in concurrence with the hydrogen evolution reaction (HER), the more probable the less reactive the organic halide. Consequently, taking into account that the RX reactivity decreases in the series $I < Br < Cl < F$, dechlorination and to some extent debromination are low-current-yield processes, unless specific materials are used, which either activate the C–X reduction or strongly deactivate HER. In the former case, silver is the most promising (Rondinini et al. 1998, 1999, 2000, 2001a, b; Guerrini et al. 1998; Delli et al. 1998; Sonoyama and Sakata 1998; Schizodimou et al. 1999) and increasingly studied electrode material (Köster et al. 2001; Fedurco et al. 2001; Fiori et al. 2002, 2005; Ardizzone et al. 2002, 2003a; Isse et al. 2002a, 2005a, 2006a–d; Sonoyama et al. 2002; Gennaro et al. 2004;

Rondinini et al. 2004; Falciola et al. 2006; Titov et al. 2006; Doherty et al. 2007), sided by Pd, Ni, Pt, Fe and stainless steel, while mercury, lead (Sonoyama et al. 1998, 2002) and tin are the most popular material of the latter group.

In the case of silver, its well-known strong specific interactions with halide anions (Valette et al. 1978; Foresti et al. 1998; Mussini et al. 2003; Migani and Illas 2006) are assumed to be at the base of its remarkable electrocatalytic activity towards the target reactions, which allows the development of low specific energy consumption processes, thanks to the concomitant reduction of cell voltage, increase of current efficiency and substrate conversion. Although the mechanistic aspects of the electroreductive pathways of halocompounds on silver are still debated (Isse et al. 2006a, c), the effectiveness of the use of Ag cathodes in the dehalogenation of organic halides has already been proved for a variety of substrates and, in the particular case of aqueous media, for halophenols and volatile organic chlorides. Figure 12.1 reports the cyclic voltammetry reduction peak potentials observed on Ag, in comparison with the corresponding values observed on glassy carbon (GC), for several categories of organohalides (data listed in Table 12.2). Data refer mainly to non-aqueous solvents, acetonitrile (ACN), dimethylformamide (DMF) and room temperature ionic liquids (RTIL), because of both solubility limitations and the need to extend the potential window on the negative side as much as possible, as required by the use of GC for most of the comparative studies.

As can be noted, all the iodides studied so far (circles) are almost equivalently reactive on silver, while exhibit on GC a secondary modulation effect chained to the organic moiety structure. On Ag, to appreciate the influence of bulky molecular structures (as in the case of haloadamantanes), or poorly activated C–X bonds (as in the case of long linear alkyl chain halides), it is necessary to consider the less reactive bromide (squares) and chloride (full triangles) derivatives. The difference between the reduction potentials on Ag and on GC ranges from 0.3 to 1.4 V, thus implying a substantial saving in the specific energy consumption. The remarkable

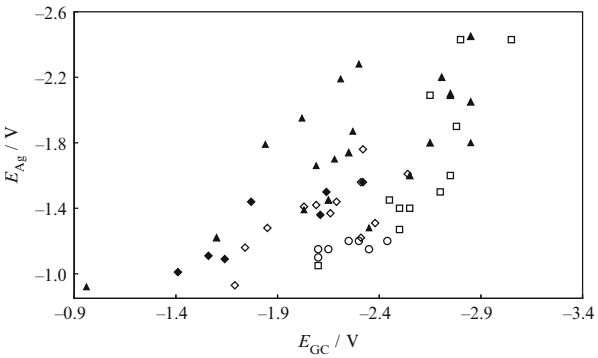

Fig. 12.1 Reduction peak potential values measured on silver, E_{Ag} (V), against the parallel values measured on glassy carbon, E_{GC} (V). Symbols denote: *circles* iodo, *squares* bromo, *triangles* chloroderivatives and diamonds – freons, respectively; *full diamonds* freons in DMF, *empty diamonds* freons in RTIL

Table 12.2 Reduction peak potential values measured on silver, E_{Ag} (V), and the parallel values measured on glassy carbon, E_{GC} (V)

	Substance		E_{Ag} (V)	E_{GC} (V)
1	Dichloromethane		−2.18	−2.66[a]
2	Trichloromethane	1st Peak	−1.41	−2.10[a]
		2nd Peak	−1.99	−2.70[a]
3	Tetrachloromethane	1st Peak	−1.27	−1.55[a]
		2nd Peak	−1.74	−2.20[a]
		3rd Peak	−2.10	−2.70[a]
4	1,1,2 Trichloroethane		−1.60	−2.50[a]
5	1,1,2,2-Tetrachloroethane	1st Peak	−1.30	−2.30[a]
		2nd Peak	−1.82	−2.80[a]
6	F113 ($CF_2ClCFCl_2$)		−1.36	−2.06
7	F114B2 (CF_2BrCF_2Br)		−1.09	−1.59
8	F113B2 ($CF_2BrCFClBr$)		−1.01	−1.36
9	F114B2[b]		−1.44	−1.72
10	F114B2[c]		−1.16	−1.69
11	F114B2[d]		−1.28	−1.80
12	F114B2[e]		−1.42	−2.04
13	F113B2[b]		−1.11	−1.51
14	F113B2[c]		−0.93	−1.64
15	F113B2[d]		−1.44	−2.14
16	F113B2[e]		−1.41	−1.98
17	F13B1[b] (CF_3Br)		−1.56	−2.27
18	F13B1[c]		−1.56	−2.26
19	F13B1[d]		−1.61	−2.49
20	F13B1[e]		−1.31	−2.33
21	F113[b]		−1.50	−2.09
22	F113[c]		−1.37	−2.11
23	F113[d]		−1.76	−2.27
24	F113[e]		−1.22	−2.26
25	1-I-buthane		−1.15	−2.30
26	2-I-buthane		−1.15	−2.10
27	1-I,2-CH_3-propane		−1.20	−2.39
28	2-I,2-CH_3-propane		−1.10	−2.05
29	1-I-hexane		−1.20	−2.20
30	1-Br-hexane		−2.09	−2.60
31	1-Br,6-OH-hexane		−1.50	−2.65
32	1-Br,8-OH-octane		−1.60	−2.70
33	1-I-adamantane		−1.15	−2.05
34	1-Br-adamantane		−2.43	−2.75
35	2-Br-adamantane		−2.43	−3.00
36	Acetobromoglucose		−1.27	−2.45
37	Acetochloroglucose		−2.05	−2.80
38	2,4,6-Tribromophenol		−1.05	−2.05
39	2-Bromophenol		−1.40	−2.45
40	3-Bromophenol		−1.45	−2.40

(continued)

Table 12.2 (continued)

41	4-Bromophenol	−1.40	−2.50
42	4-Chlorophenol	−1.80	−2.60
43	1-Metoxy,4-I-benzene	−1.20	−2.25
44	1-Metoxy,4-Br-benzene	−1.90	−2.73
45	1-Metoxy,4-Cl-benzene	−2.45	−2.80
46	9-Cl-anthracene	−1.79	−1.79
47	1-Cl-naphthalene	−2.19	−2.16
48	4-Cl-benzonitrile	−1.95	−1.97
49	3-Cl-pyridine	−2.28	−2.25
50	Benzylchloride	−1.70	−2.13
51	3-CF3-benzylchloride	−1.66	−2.04
52	4-NO2-benzylchloride	−0.92	−0.91
53	1-Chloroacetonitrile	−1.39	−1.98
54	(1-Chloroethyl)benzene	−1.87	−2.22

Unless otherwise specified, all potentials are measured vs. the saturated calomel electrode (SCE)
(1–5) Fiori et al. (2005), 0.1 M $TEABF_4$ in ACN; (6–8) Titov et al. (2006), LiBF4 in DMF vs. Ag/AgCl; (9–24) Doherty et al. (2007) vs. Pt pseudo-reference electrode; (25–31) and (33–35) Rondinini et al. (2001b), 0.1 M $TEAClO_4$ in ACN; (32) Rondinini et al. (2004), 0.1 M $TEAClO_4$ in ACN; (36 and 37) Rondinini et al. (2000), 0.1 M $TEAClO_4$ in ACN; (38–45) Rondinini et al. (2001a, b), 0.1 M $TEAClO_4$ in ACN; (46–54) Isse et al. (2006a), 0.1 M TEABF4 in ACN
[a] Costentin et al. (2003)
[b] 0.1 M TBAF in DMF
[c] 1-butyl-3-methylimidazolium bistriflimide ($BmimNTF_2$)
[d] 1-butyl-1-methylpyrrolidinium bistriflimide ($BmpyrNTF_2$)
[e] 1-butyl-3-methylimidazolium hexafluorophosphate ($BmimPF_6$)

silver behaviour is attributed to a three-actor process involving the metal surface, the organic moiety and the bridging halide, which results in the confinement of the substrate in a reaction cage, a condition depictable also in terms of an attenuated radical intermediate, R. . .X. . .Ag (Rondinini et al. 2001b; Ardizzone et al. 2003b).

Note that for a few compounds, 9-chloro-anthracene, 1-chloro-naphtalene, 4-Cl-benzonitrile, 3-Cl-pyridine and 4-Cl-nitrobenzene, which are reported to undergo outer-sphere dissociative ET (Isse et al. 2006a), the difference between Ag and GC is negligible.

Palladium, palladium alloys and palladized supports are also widely used (Li and Farrell 2000; Liu et al. 2001; Chen et al. 2003; Cheng et al. 2003a, b, 2004a; Miyoshi et al. 2004c; Simonet 2005; Simonet et al. 2006) and are known to lead preferentially to totally saturated products, in connexion with their catalytic activity toward hydrogen evolution and hydrogenation reactions. In addition, the palladium capability of absorbing hydrogen can contribute to promote indirect hydrodehalogenation (Cheng et al. 1997). Interestingly, the reaction pathway might substantially differentiate not only from Ag, as previously outlined, but also from Pt. Platinum, in turn, has also been widely employed (Horanyi and Torkos 1982; Kotsinaris et al. 1998; Schizodimou et al. 1999; Liu et al. 2001; Hori et al. 2003; Chen et al. 2003; Simonet et al. 2004; Miyoshi et al. 2004a; Ju et al. 2006; Titov et al. 2006), especially in

non-aqueous environment, in which the existence of Pt cluster anions is documented (Simonet 2006). Less precious and expensive metals, like Ni, Cu, Fe and stainless steel are also frequently used (Sonoyama et al. 1998, 2002; Schizodimou et al. 1999; Fedurco et al. 2001; Hori et al. 2003; Cheng et al. 2003a; Cabot et al. 2004).

In the case of iron, and of other less noble metals, the reductive hydrodehalogenation of the substrates via metal dissolution has received much attention, especially for on-site remediation processes (e.g. reactive barriers). Although the dehalogenation is based on a corrosion process, rather than on an electrolytic process, the flourishing literature of the past few years prompted us to provide a selection of the bibliographic references (Boronina et al. 1995; Warren et al. 1995; Roberts et al. 1996; Farrell et al. 2000; Alonso et al. 2002; Kluyev et al. 2002; Dombek et al. 2004; Lowry and Johnson 2004; Mishra and Farrell 2005; Moglie et al. 2006; Laine et al. 2007).

In the case of high hydrogen overvoltage materials, mercury and metal amalgams have for a long time been the preferred electrode materials (Peters 2001; Baizer et al. 1972) for both voltammetric studies [originally, polarography at dropping mercury electrode (DME)] and preparative electrolyses, also thanks to its specific interactions with inorganic and organic halides, which has a synergistic effect in providing separations larger than 100 mV between the reduction potential of many substrates and the inset of the background current. Despite the huge impact that mercury has had on the research and development of the electroreductive processes of halogenated organic compounds, since the Minamata case (Uchini et al. 2005), its use is progressively abandoned under the impulse of the strong environmental motivations. Similarly, Pb and Cd, and their amalgams, suffer the same drawbacks. Moreover, their use as cathodes, as well as the use of tin and mercury, in non-aqueous media, leads to the high-yield formation of organometallic compounds (R_nMe, Me = Hg, Pb, Cd, Sn and R = alkyl, benzyl, aryl), a feature widely used in synthetic organic chemistry.

Intermediate behaviour between the high and low hydrogen overvoltage metals is exhibited by carbon-based electrodes, including specific carbon phases like glassy carbon, graphite, etc. In fact, carbon materials are known for their almost total inertness toward the C–X cleavage reactions and parallelly do not exhibit specific activation for HER. They are low cost and robust (under reductive conditions) materials, particularly adapt to industrial applications, since they are easily produced in different forms (sponge, felt, fibre, cloth, etc.) and provide high real-to-geometrical surface ratios. Carbon supports are also extensively used for noble-metal-modified electrodes, thus providing a tool for reducing the loading of the precious components.

12.4 Cell Design and Operations

The engineering of the electrochemical cell is a key step for the successful implementation of the target process. While this is true for any electrochemical process, and extended treatment of cell design and operations and of the relevant

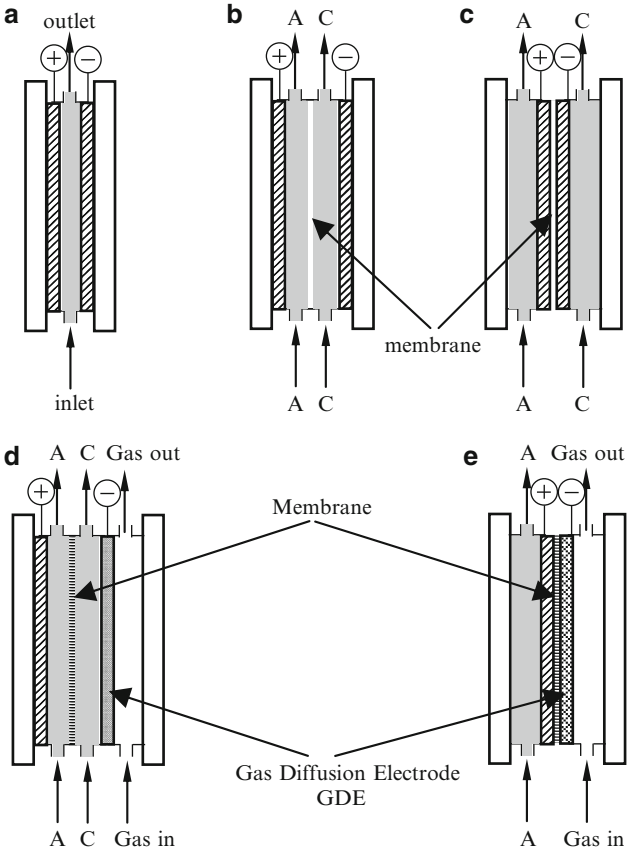

Fig. 12.2 Plate-and-frame electrolyser schemes: (**a**) undivided cell; (**b**) membrane-divided cell; (**c**) solid polymer electrolyte (SPE) reactor; (**d**) membrane-divided cell with GDE; (**e**) SPE–GDE reactor. Liquid compartments are denoted in *grey*

figures of merits is available in the appropriate literature (Wendt and Kreysa 1999; Pletcher 1982), a brief summary of the underlying features of the different cell schemes is provided.

The most popular is the plate-and-frame scheme in Fig. 12.2, which has the advantage of being easily adapted to the process needs, in terms of both the choice of the total electrode area, by simply adding/removing elementary units, and of the use of membranes or separators for obtaining two-compartment units. In fact, although undivided cells are always to be preferred in order to reduce investment and operating costs, the separation between catholyte and anolyte can be adopted to (1) avoid the mutual interference from the products of the electrode reactions, (2) prevent the loss of value-added products by anodic degradation, (3) allow the use of different solvents in the two compartments (e.g. water in the anodic and non-aqueous solvent in the cathodic one), (4) maintain effective separation between

gaseous products, and, more generally, when the process is under development, for an easy recovery/separation/analysis of the reaction mixture. In addition, the substitution of a liquid electrolyte (catholyte and/or anolyte) with a cation or an anion exchange membrane allows the adoption of a solid polymer electrolyte (SPE) reactor for the treatment of volatile compounds and non-conducting wastes (Cheng et al. 2004b, c; Ju et al. 2006). Note that all schemes in Fig. 12.2 revert from the plug-flow-reactor (PFR) to the stirred-tank-reactor (STR) behaviour in the limiting case of total recycling, thus including the undivided and divided (H-cell) laboratory electrolytic cells.

Despite their intrinsic simplicity, the plate-and-frame reactors require accurate selection of the materials, especially when the electrolytic processes are performed in non-aqueous solvents and/or deal with substrates which are currently used as solvents, as in the case of volatile organic chlorides. Special attention should be paid to the selection of the gaskets, for long-term operational stability. Moreover, in the case of the SPE scheme, porous electrodes should be adopted, to allow for optimal contact between electrode, electrolyte and reactants/products. In this case, mass-transfer limitations into the porous structure should be carefully considered.

For undivided cells, a valid alternative is provided by the stirred tank reactor (STR), which is characterized by a high flexibility in the use of different electrode structures and shapes. The adoption of a sacrificial anode (Gennaro et al. 2004) and/or specific fluidodynamic conditions (He et al. 2004a) avoids most of the drawbacks connected with parasitic electrode reactions.

The mechanical stirring usually provides good mass-transfer conditions. The additional use of ultrasound (Compton et al. 1996; De Lima Leite et al. 2002; Ragaini et al. 2001) and microwave devices (Tsai et al. 2002) is reported to have beneficial effects.

A tri-dimensional electrode reactor geometry was studied by He et al. (2004a, b) to overcome the problem of low conductivity media (≥ 1 S m^{-1}). The reduction of model carbon tetrachloride was performed on a porous copper foam with good conversion rates and almost total dehalogenation of the substrate.

12.5 Electroreductive Treatments of Halogenated Organic Pollutants

In the electroreductive treatments of halogenated organic pollutants the goal is either the complete dehalogenation (mostly hydrodehalogenation) of the substrates to ease their further treatment (e.g. improve their biodegradability), or their transformation into value-added compounds (e.g. selective removal of halogens, carboxylation/carbonylation).

According to their chief molecular features, they can be grouped into the following categories.

12.5.1 Organic Volatile Halides

A large family, whose most representative compounds are chlorinated solvents like CH_2Cl_2 (pharmaceuticals, chemical processing, aerosols, etc.), $CHCl_3$, CCl_4, $Cl_2C{=}CCl_2$ (dry and metal cleaning), and $Cl_2C{=}CHCl$ (metal cleaning and specialty adhesives). They are not included in the POP list because of their relatively short atmospheric life time, e.g. 6–8 days trichloroethylene and 5–6 months tetrachloroethylene and dichloromethane.

Baizer et al. (1972) extensively studied the electroreduction of carbon tetrachloride in the presence of electrophiles for synthetic purposes. Since then the formation of the dichloro-dianion (CCl_2^{2-}) or -carbene (Takita et al. 1990) was considered for the synthesis of cyclopropane derivatives. Recently, carbene formation was observed in the direct reduction of CCl_4 and DDT (1,1-bis(*p*-chlorophenyl)-2,2,2-trichloroethane) on hemin-modified TiO_2 supports (Stromberg et al. 2006).

In the presence of water, CCl_4 was electrolytically reduced on different cathode materials (Ag, Al, Au, Cu, Fe, Ni, Pd and Zn) (Liu et al. 1999). Primary products included $CHCl_3$, CH_2Cl_2 and CH_4; traces of CH_3Cl, C_2H_4, C_2H_6 and C_3H_8 were also detected. Subsequent studies were performed by the same school adopting different reactors and cathode materials. On copper foam cylindrical cathodes, total hydrodehalogenation and good conversion rates were obtained (He et al. 2004a, b). Using a SPE reactor equipped with Pd- and Pt-based gas diffusion electrodes (GDE), the reduction of gas-phase CCl_4 to CH_4 was obtained together with lower chlorinated products, tri- and di-chloromethane (Liu et al. 2001). Concomitantly the degradation of tri- (TCE) and per-chloroethene (PCE) was also tested. For TCE, the reactivity decreased in the series of cathode materials: Pd > Ni > Co > Ag > Cu > Zn, and the predominant products were ethane, ethene, 1-buthene and *trans*- and *cis*-2-buthene. Chlorine containing products (TCE, *cis*- and *trans*-dichloroethene) accounted for less than 3% of the PCE transformed at Pd/C. More recently, an optimized MEA-GDE (MEA = membrane-electrode-assembly) system based on a 20% Pt catalyst was applied to treat gas-phase trichloroethylene (Ju et al. 2006), for which the indirectly reduction by electrolytic hydrogen is suggested.

Specific interactions with Ni (Wang et al. 2004) are reported to be at the base of the almost total conversion of CCl_4 to methane, thus suggesting that the preferred reaction path is not the sequential dechlorination, usually observed on other cathodes [e.g. Fe and glassy carbon (Liu et al. 2000; Costentin et al. 2003; Li et al. 2000)]. This is an important feature for the treatments based on permeable reactive barriers, because the intermediate species are also toxic and are much more slow reactants than carbon tetrachloride. A high yield in methane was also observed on vitamin B12 – modified silver electrode (Betterton et al. 1995).

In addition, the degradation of C1 and C2 polyhalogenated substrates has been reported in non-aqueous (Kotsinaris et al. 1998), aqueous (Horanyi et al. 1982; Liu et al. 2000; Li et al. 2000; Chen et al. 2003) and mixed (Hori et al. 2003; Rondinini et al. 2004; Fiori et al. 2005) solvents, under different operating conditions. The reduction of CH_2Cl_2 on Ni and Cu in ACN resulted in the formation not only of methane and chloromethane, but also of ethylene, propene and buthene

(Kotsinaris et al. 1998), while on Ag and Pt cathodes methane was the main product. Rondinini et al. (2004) observed the preferential formation of methane from polychloromethane on silver in ACN, DMF and aquo-organic solvents. Trichloroethene and trichloromethane were hydrodehalogenated in aqueous solution at different pHs by Chen et al. (2003) on platinized and palladized ceramic (ebonex) supports. Main reaction products were ethane, ethene and HCl for the former substrate, and methane and HCl for the latter. In a preceding study (Chen et al. 1999) in oxidative conditions, they observed the parallel degradation to carbon-containing products (mainly CO_2) and, in neutral or alkaline pH, Cl^-/ClO_3^- as the only chloro-containing products.

12.5.2 Chlorofluorocarbons

Because of their environmental impact, chlorofluorocarbons (CFC) represent a separate category of volatile organic halides.

Although the production of CFCs was stopped since 1996 as a result of international agreements, there are still large amounts in stock. The estimated amount of banked CFCs are 2.25 Mton, about 45% being trichlorofluoromethane (CFC 11) and about 45% dichlorodifluoromethane (CFC 12) (Cabot et al. 2004), which have to be treated. However, degradation processes imply a double loss, in terms of both energy requirements and destruction of valuable fluoro-containing compounds, for which conversion into useful products appears to be more attractive. In this context, the electrolytic reduction processes, with their selective removal of chloro atoms, seem to provide a suitable and promising technique. Earlier works report the reduction of 1,1,2-trichloro-1,2,2-trifluoroethane (CFC 113) and 1,2-dichloro-1,1,2,2-tetrafluoroethane (CFC 114) to chlorotrifluoroethylene (CTFE) and tetrafluoroethylene on different electrodes and various reacting media (Savall et al. 1990a, b; Montecatini Edison S.p.a., Italian Pat. 852,487 (1969); Wawzonek and Willging 1977). Trifluoroethene (TFE) was obtained on Pb cathodes in $MeOH/H_2O$ in the presence of $PdCl_2$ from CFC 113 (Cabot et al. 1997).

More recently CCl_2F_2 (CFC-12) was converted at Ag, Cu, Au, Pt, Ni and Pb electrodes in acetonitrile and propylene carbonate, to CF_2CF_2 (the monomer for PTFE production), CH_2F_2 (a candidate for refrigeration applications), CH_3F and small amounts of $CHClF_2$ and CH_4 (Schizodimou et al. 1999; Georgolios et al. 2001). Persinger and co-authors (Persinger et al. 2004) investigated that the reduction of CFC 113 by cobalt(I)salen (salen = 2, 2′-ethylenebis(nitrilomethylidene)diphenol, *N*,*N*′-ethylenebis(salicylimine)) electrogenerated at a carbon cathode in dimethylformamide (DMF) containing tetra-*n*-butylammonium tetrafluoroborate ($TBABF_4$) as a supporting electrolyte in dependence on the electrode potential, chlorotrifluoroethene, trifluoroethene and 1,1,1,2-tetrafluoroethane were obtained. CFC 113 was treated by Cabot et al. (2004) in a Cu cathode–hydrogen diffusion anode cell, in $MeOH/H_2O$ mixture in the presence of NH_4Cl or tetrabutylammonium perchlorate (or both) as supporting electrolyte and of 50 ppm $PdCl_2$ as reduction promoter. CFC 11 was treated similarly, but in the absence of the palladium salt. The two

substrates were dechlorinated stepwise to difluoroethene and methane, respectively. The latter was obtained with >90% current efficiency from CFC 11 in the presence of tetraalkylammonium salt. The same salt, however, resulted to interfere, in the case of CFC 113, with the electrodeposition of Pd, thus depressing the electrolyser performance.

Titov and co-authors (Titov et al. 2006) studied the electrodehalogenation of C-2 freons ($CF_2ClCFCl_2$, $CF_2BrCFClBr$ and CF_2BrCF_2Br) on different cathodes, namely Ag, Pt and glassy carbon. In comparison with the other materials, silver has a promoting effect on the formation of the target products, chlorotrifluoro- and tetrafluoroethenes. Ag, Pt and glassy carbon were used as working electrode also in the reduction of freons in RTIL (Doherty et al. 2007). Although current intensities and reduction potentials resulted significantly affected by ohmic losses, the electrocatalytic properties of Ag are reported to be retained also in RTIL media.

Up to 12 kinds of metals were used by Sonoyama and co-authors (Sonoyama et al. 1998) in their studies on the degradation of CFC 12 at GDE. At Zn-, Ag-, Cu-, and In-supported GDEs CFC-12 dechlorinated and defluorinated to methane as a principal product. Pb-supported GDE induced only dechlorination of CFC-12 and produced difluoromethane (HFC-32) in high selectivity (92.6%). When massive Pb, Cu and Ag cathodes were used under high-pressure conditions, the conversion to tetrafluroethene was obtained in high yields (up to 70%) only on Pb (Sonoyama et al. 2002).

12.5.3 Polyhaloacetic Acids

Polyhaloacetic acids and their partially hydrodehalogenated products represent a second important family of herbicide-/pesticide-derived substrates. In their review on the environmental applications of industrial electrochemistry, Juttner and co-authors (Juttner et al. 2000) documented the electroreductive dechlorination of dichloroacetic acid (a by-product of monochloroacetic acid), a way to recover the valuable compound and avoid wastes. The electrochemical reduction of polychloro- and polybromo-derivatives was performed by Korshin and Jensen (2001) on Cu and Au cathodes. Complete dehalogenation was obtained for all substrates, but for monochloroacetic acid. To overcome the intrinsic poor reactivity of the monochloro-derivative the photoelectrochemical properties of a p-doped SiC electrode were investigated (Schnabel et al. 2001); however, the dehalogenation stopped at monochloroacetic acid.

12.5.4 Polyhalophenols

An important family of herbicides and pesticides, their precursors and/or by-products, is represented by polyhalophenols and polyhalophenoxy-acids and

-esthers. Partial detoxifications of industrial and agricultural wastes as well as site remediation by electrochemical reductive treatments have been widely studied.

Tsyganok and co-authors (Tsyganok et al. 1996) studied the dechlorination of the commercial pesticide 2,4-D (2,4-dichlorophenoxyacetic acid) using different carbon materials. Phenoxyacetic acid was obtained with 80% selectivity and 10–14% current efficiency, at 75% substrate conversion. Cheng and co-authors (Cheng et al. 2003a–c, 2004a–e) investigated in detail the electrochemical hydrodehalogenation of dichloro- and dibromo-phenols in aqueous and oil phases in a SPE reactor. Data on electrolyser design and performances are provided in a series of well-concerted papers. Comparison between two-compartment H-cell and SPE reactor for the treatment of aqueous halophenols was performed on the basis of in situ FTIR studies (Chetty et al. 2004). In the investigated conditions, current efficiencies up to 90% were obtained with the H-cell, and 50% with the SPE reactor. The dechlorination of chlorophenols on Zn and Ni electrodes in propylene carbonate was investigated by Lin et al. (Lin and Tseng 2000). On zinc, the dechlorination of a variety of chlorophenols (pentachlorophenol, 2,3,4,6-tetrachlorophenol, 2,4,5-trichlorophenol, 2,4-dichlorophenol and 2-chlorophenol) was achieved, in dependence of the electrode potential. 2,3,4,6-tetrachlorophenol was dechlorinated step-by-step until complete dechlorination was obtained. Rondinini et al. studied the electrodehalogenation of several bromo- and chlorophenols in non-aqueous and mixed solvents on silver cathodes by cyclic voltammetry and preparative electrolyses (Rondinini et al. 2001a; Fiori et al. 2002). In all media, the complete hydrodehalogenation of 2,4,6-tribromophenol can be achieved with good current efficiencies. Stepwise debromination could be observed: 2,4,6-tribromophenol was firstly reduced to 2,4- and 2,6-dibromophenols, which converted into 2-, and 4-brophenols and finally to phenol.

12.5.5 Polychlorohydrocarbons

1,2,3-Trichlorobenzene (1,2,3-TCB), a model sample of POPs, was dechlorinated under inert gas atmosphere, using different type of sintered cathode materials (Miyoshi et al. 2004a). Sintered RuO_2(major)/Pt/PdO, Pt(major)/IrO_2/RuO_2, RuO_2, PdO, Pt, PdO/Pt, Pd/Pt and plain Pd plate gave dechlorination yields of 91, 81, 59, 96, 53, 97, 82 and 70%, respectively.

The same group highlighted the beneficial effect of adopting a membrane-divided cell with aqueous NaOH anolyte and non-aqueous (ACN) catholyte. The degradation of 1,2,3-TCB was performed on glassy carbon (cyclic voltammetry experiments) and Pd (preparative electrolyses) cathodes (Miyoshi et al. 2004b, c).

Chlorobenzene, 1,2,3,5-tetrachlorobenzene and lindane (γ-hexachlorocyclohexane) were dechlorinated in different solvents on plain and metal-modified carbon cloth cathodes. In dimethylsufoxide and ACN, chlorobenzene was dechlorinated even on plain carbon materials, while Pd-coated and Zn-coated cathodes were necessary to perform degradation in methanol and water, respectively (Kulikov et al. 1996).

The use of metal–complex mediators was applied by Nunnecke and co-authors (Nunnecke and Voss 1999) to the dechlorination of chlorinated benzenes and dibenzofurans. The main products were chlorobenzene and unsubstituted dibenzofurans, respectively.

Mediated dechlorination of β-methylallyl chloride (extensively used in the polymer industry), via in situ electrochemically generated $[\mathrm{Co\,(I)\,(2,2'\text{-bipyridine})_3}]^+$, was achieved by Muthuraman and co-authors (Muthuraman and Pillai 2006) in aqueous solutions, in the presence of cationic surfactants.

12.5.6 Other Compounds

Atrazine (2-chloro-4-ethylamino-6-isopropylamino-s-triazine), a photosynthetic inhibitor that is used in large quantities for weed control in corn and sorghum, has been treated electrochemically in aqueous solution on reticulated vitreous carbon cathode in the presence of noble-metal catalysts (Stock and Bunce 2002). Electrocatalytic hydrogenolysis to 2-ethylamino-4-isopropylamino-s-triazine occurs in quantitative yield, and is most efficient with Pd-based catalysts. Current efficiency increases with increasing atrazine and catalyst concentration, and decreasing current density. The Authors observed a time lag between the start of the electrolysis and the appearance of the dechlorinated products, which was attributed to the absorption of hydrogen by the palladium lattice. As alternative to the electrochemical treatment, the degradation of chlorinated triazines by zero-valent-iron was already mentioned (Dombek et al. 2004).

Partial dechlorination of Mirex, a persistent polychlorinated olygocyclic insecticide, in MeOH on Pb cathodes is reported by Gassmann and co-authors (Gassman et al. 1995).

12.5.7 Sensors

The electroreductions on mediator-modified electrodes can be also used for analytical purposes. Although this aspect is beyond the scope of this section, a sample of the most recent results are presented.

Wright and co-authors (Wright et al. 1999) studied the properties of a polyethyleneoxide myoglobine-modified electrode in the reductive dehalogenation of hexachloroethane in ethanolic solutions, and the observed catalytic response resulted linearly dependent on the bulk concentration of the substrate.

Immobilized haemoglobin (Hb) was applied by Liu and co-authors (Liu et al. 2006) to the dehalogenation of haloethanes (hexachloroethane, pentachloroethane, tetrachloroethane, etc.). The observed fast electron-transfer reactions observed in aqueous-organic solvents are promising for the detection of the

substrates. The co-immobilization of Hb and sodium montmorillonite (a cationic conducting clay) on a pyrolitic graphite electrode was used for the detection of trichloroacetic acid (Fan et al. 2000). Hb was found to maintain its native structure and stability in the film.

Detection of trichloroacetic acid via dechlorination to its di- and monochloroderivatives was also studied on a pyrolitic graphite electrode modified by Hb immobilized in poly-3-hydrobutyrate membrane (Ma et al. 2005).

The effective electrochemical detection of several organic halides (trichloroacetic acid, ethylene dibromide, tetrachloroethylene, trichloroethylene, dichloroacetic acid, 2,4,6-trichlorophenol, 2,4-dichlorophenoxy acetic acid, methoxychloride, etc.) in aqueous and organic solutions via Co and Fe macrocyclic complex-based films was studied by Alatorre and co-authors (Alatorre et al. 2000).

12.6 Conclusions

In the next decades, energetic and environmental issues are expected to drive key actions for the sustainable development of human activities. In these fields, electrochemistry can provide mature technologies which range from energy conversion and storage to environmental protection and remediation. The electrolytic processes offer effective, low-impact methods not only for the detoxification of wastes but also for the recovery of reagents and recycling of materials. In addition, conspicuous energy savings can be achieved by improving process efficiency, reducing raw material consumption and avoiding secondary pollutant production.

In this context, the electroreduction of halogenated organic compounds offers an effective route not only to the detoxification of wastes but also to their valorization as in the case of CFCs and, generally, of volatile organic halides.

The wide category of halocompounds represents a serious challenge for natural waters, soils and atmosphere. Because of their toxicity combined with high chemical stability, lipophilicity, accumulation-in-the-food-chain capability and long-range diffusivity, several chlorinated and brominated organic substances are included in the list of POPs.

The main reaction paths for the electroreductive cleavage of the carbon–halogen bond lead to total or partial dehalogenated products with the formation of C–H and/or single, double and triple C–C bonds according to the prevailing coupling or elimination reactions.

In all cases a strong influence of the operating conditions (medium, supporting electrolyte, cell design and hydrodynamics) and of the electrode material is observed. Among the large variety of metals and metal alloys investigated so far, silver- and carbon-based electrodes hold prominent positions, the former for its outstanding electrocatalytic activity towards C–X electroreductions, the latter for the cumulative effect of robustness, inexpensiveness and workability.

A selection of electrolysis cells with their working conditions is reported to discuss the aspects related with the scaling-up of the simple one- or two-compartment

laboratory cells, and review the adoption of special cell (e.g. SPE) or electrode (e.g. tri-dimensional) geometries, sacrificial anodes and enhanced mass-transfer equipments (e.g. ultrasound).

The description of the electroreductive treatments of organic halides is subdivided into the following sections: organic volatile halides, CFCs, polyhaloacetic acids, polyhalophenols, polychlorohydrocarbons and other compounds. These sections are meant to complete the discussion and information, provided in the preceding parts, by focussing on each specific category of compounds and their related working examples.

Finally, some recent analytical applications of electroreduction processes as sensors are presented.

Acknowledgments The financial support of the MUR-Università degli Studi di Milano (FIRST) is gratefully acknowledged.

References

Alatorre Ordaz, A., Manriquez Rocha, J., Acevedo Aguilar, F.J., Gutierrez Granados, S. and Bedioui, F. (2000) Electrocatalysis of the reduction of organic halide derivatives at modified electrodes coated by cobalt and iron macrocyclic complex-based films: Application to the electrochemical determination of pollutants. Analusis 28, 238–244.

Alonso, F., Beletskaya, I.P. and Yus, M. (2002) Metal-mediated reductive hydrodehalogenation of organic halides. Chem. Rev. 102, 4009–4091.

Andrieux, C.P. and Savéant, J.-M. (1986) Electrochemical reactions. In: Bernasconi, C.F. (Eds.) *Investigations of Rates and Mechanisms of Reaction, Techniques of Chemistry*, vol. 6, Ch 2.1, Wiley, New York, NY, p. 305.

Ardizzone, S., Cappelletti, G., Mussini, P.R., Rondinini, S. and Doubova, L.M. (2002) Adsorption competition effects in the electrocatalytic reduction of organic halides on silver. J. Electroanal. Chem. 532, 285–293.

Ardizzone, S., Cappelletti, G., Mussini, P.R., Rondinini, S. and Doubova, L.M. (2003a) Electrodeposited polycrystalline silver electrodes: Surface control for electrocatalytical studies. Russ. J. Electrochem. (translation of Elektrokhimija) 39, 170–176.

Ardizzone, S., Cappelletti, G., Doubova, L.M., Mussini, P.R., Passeri, S. and Rondinini, S. (2003b) The role of surface morphology on the electrocatalytic reduction of organic halides on mono- and polycrystalline silver. Electrochim. Acta. 48, 3789–3796.

Bailey, R.E. (2001) Global hexachlorobenzene emissions. Chemosphere 43, 2167–182.

Baizer, M.M. and Chruma, J.L. (1972) Electrolytic reductive coupling. XXI. Reduction of organic halides in the presence of electrophiles. J. Org. Chem. 37, 1951–60.

Baizer, M.M. and Wagenknecht, J.H. (1973) Electrolytic preparation of esters from organo halides. (Monsanto Co., USA) US Patent 3764492 19731009; Application: US 72–216721 19720110.

Bard, A.J. and Faulkner, L.R. (1999) *Electrochemical Methods*, Wiley, New York, NY.

Barhdadi, R., Courtinard, C., Nedelec, J.-Y. and Troupel, M. (2003) Room-temperature ionic liquids as new solvents for organic electrosynthesis. The first examples of direct or nickel-catalyzed electroreductive coupling involving organic halides. Chem. Commun. (Cambridge) 12, 1434–1435.

Battistuzzi, G., Borsari, M. and Fontanesi, C. (1993) Theoretical study of the electroreduction of halogenated aromatic compounds. Part 2. Bromine and chlorine derivatives in different organic solvents. J. Chem. Soc. Faraday Trans. 89, 3931–3939.

Betterton, E.A., Arnold, R.G., Kuhler, R.J. and Santo, G.A. (1995) Reductive dehalogenation of bromoform in aqueous solution. Environ. Health Perspect. 103(Suppl. 5), 89–91.

Boronina, T., Klabunde, K.J. and Sergeev, G. (1995) Destruction of organohalides in water using metal particles: Carbon tetrachloride/water reaction with magnesium, tin, and zinc. Environ. Sci. Technol. 29, 1511–1517.

Boye, B., Brillas, E., Marselli, B., Michaud, P.-A., Comninellis, C., Farnia, G. and Sandonà, G. (2006) Electrochemical incineration of chloromethylphenoxy herbicides in acid medium by anodic oxidation with boron-doped diamond electrode. Electrochim. Acta, 51, 2872–2880.

Brillas, E., Boye, B., Sires, I., Garrido, J.A., Rodriguez, R.M., Arias, C., Cabot, P.-L. and Comninellis, Ch. (2004) Electrochemical destruction of chlorophenoxy herbicides by anodic oxidation and electro-Fenton using a boron-doped diamond electrode. Electrochim. Acta, 49, 4487–4496.

Briois, C., Ryan, S., Tabor, D., Touati, A. and Gullett, B.K. (2007) Formation of polychlorinated dibenzo-*p*-dioxins and dibenzofurans from a mixture of chlorophenols over fly ash: Influence of water vapor. Environ. Sci. Technol. 41, 850–856.

Brown, O.R. and Harrison, J.A. (1969) Reactions of cathodically generated radicals and anions. J. Electroanal. Chem. Int. Electrochem. 21, 387–407.

Burris, D.R., Delcomyn, Smith and Roberts, L.A. (1996) Reductive dechlorination of tetrachloroethylene and trichloroethylene catalyzed by vitamin B-12 in homogeneous and heterogeneous systems. Environ. Sci. Technol. 30, 3047–3052.

Cabot, P.L., Centelles, M., Segarra, L. and Casado, J. (1997) Palladium-assisted electrodehalogenation of 1,1,2-trichloro-1,2,2-trifluoroethane on lead cathodes combined with hydrogen diffusion anodes. J. Electrochem. Soc. 144, 3749–3757.

Cabot, P.L., Segarra, L. and Casado, J. (2004) Electrodegradation of chlorofluorocarbons in a laboratory-scale flow cell with a hydrogen diffusion anode. J. Electrochem. Soc. 151, B98–B104.

Canizares, P., Lobato, J., Paz, R., Rodrigo, M.A. and Saez, C. (2005) Electrochemical oxidation of phenolic wastes with boron-doped diamond anodes. Water Res. 39, 2687–2703.

Chaussard, J., Troupel, M., Robin, Y., Jacob, C. and Jubasz, J.P. (1989) Scale-up of electrocarboxylation reactions with a consumable anode. J. Appl. Electrochem. 19, 345–348.

Chen, G. (2004) Electrochemical technologies in wastewater treatment. Sep. Purif. Technol, 38, 11–41.

Chen, G., Betterton, E.A. and Arnold, R.G. (1999) Electrolytic oxidation of trichloroethylene using a ceramic anode. J. Appl. Electrochem. 29, 961–970.

Chen, G., Betterton, E.A., Arnold, R.G. and Ela, W.P. (2003) Electrolytic reduction of trichloroethylene and chloroform at a Pt- or Pd-coated ceramic cathode. J. Appl. Electrochem. 33, 161–169.

Cheng, I.F., Fernando, Q. and Korte, N. (1997) Electrochemical dechlorination of 4-chlorophenol to phenol. Environ. Sci. Technol. 31, 1074–1078.

Cheng, H., Scott, K. and Christensen, P.A. (2003a) Electrochemical hydrodehalogenation of chlorinated phenols in aqueous solutions. J. Electrochem. Soc. 150, D17–D24.

Cheng, H., Scott, K. and Christensen, P.A. (2003b) Electrochemical hydrodehalogenation of chlorinated phenols in aqueous solutions. J. Electrochem. Soc. 150, D25–D29.

Cheng, H., Scott, K. and Christensen, P.A. (2003c) Hydrodehalogenation of 2,4-dibromophenol by electrochemical reduction. J. Appl. Electrochem. 33, 893–899.

Cheng, H., Scott, K. and Christensen, P.A. (2004a) Feasibility study of electrochemical hydrodehalogenation of 2,4-dibromophenol in a paraffin oil. Electrochim. Acta 49, 729–735.

Cheng, H., Scott, K. and Christensen, P.A. (2004b) Design and operation of a solid polymer electrolyte reactor for electrochemical hydrodehalogenation. Chem. Eng. J. (Amsterdam) 102, 161–170.

Cheng, H., Scott, K. and Christensen, P.A. (2004c) Engineering aspects of electrochemical hydrodehalogenation of 2,4-dichlorophenol in a solid polymer electrolyte reactor. Appl. Catal. A: General 261, 1–6.

Cheng, H., Scott, K. and Christensen, P.A. (2004d) Electrochemical hydrodehalogenation of 2,4-dichlorophenol in paraffin oil and comparison with aqueous systems. J. Electroanal. Chem. 566, 131–138.

Cheng, H., Scott, K. and Christensen, P.A. (2004e) Electrochemical hydrodehalogenation of 2,4-dibromophenol in paraffin oil using a solid polymer electrolyte reactor. Environ. Sci. Technol. 38, 638–642.

Cherepy, N.J. and Wildenschild, D. (2003) Electrolyte management for effective long-term electro-osmotic transport in low-permeability soils. Environ. Sci. Technol. 37, 3024–3030.

Chetty, R., Christensen, P.A., Golding, B.T. and Scott, K. (2004) Fundamental and applied studies on the electrochemical hydrodehalogenation of halogenated phenols at a palladised titanium electrode. Appl. Catal. A: General 271, 185–194.

Comninellis, Ch. and Nerini, A. (1995) Anodic oxidation of phenol in the presence of NaCl for wastewater treatment. J. Appl. Electrochem. 25, 23–28.

Compton, R.G., Marken, F. and Rebbitt, T.O. (1996) Sonovoltammetric measurement of the rates of electrode processes with fast coupled homogeneous kinetics: Making macroelectrodes behave like microelectrodes. Chem. Commun. (Cambridge) 1017–1018.

Costentin, C., Robert, M. and Savéant, J.-M. (2003) Successive removal of chloride ions from organic polychloride pollutants. Mechanisms of reductive electrochemical elimination in aliphatic gem-polychlorides, α, β-polychloroalkenes, and α, β-polychloroalkanes in mildly protic medium. J. Am. Chem. Soc. 125, 10729–10739.

Costentin, C., Robert, M. and Savéant, J.-M. (2006a) Electron transfer and bond breaking: Recent advances. Chem. Phys. 324, 40–56.

Costentin, C., Robert, M. and Savéant, J.-M. (2006b) Electrochemical concerted proton and electron transfers. Potential-dependent rate constant, reorganization factors, proton tunneling and isotope effects. J. Electroanal. Chem. 588, 197–206.

Delcomyn, C.A., Smith, M.H. and Roberts, L.A. (1996) Reductive dechlorination of tetrachloroethylene and trichloroethylene catalyzed by vitamin B-12 in homogeneous and heterogeneous systems. Environ. Sci. Technol. 30, 3047–3052.

De Lima Leite, R.H., Cognet, P., Wilhelm, A.-M. and Delmas, H. (2002) Anodic oxidation of 2,4-dihydroxybenzoic acid for wastewater treatment: Study of ultrasound activation. Chem. Eng. Sci. 57, 767–778.

De Lima Leite, R.H., Cognet, P., Wilhelm, A.-M. and Delmas, H. (2003) Anodic oxidation of 2,4-dihydroxybenzoic acid for wastewater treatment. J. Appl. Electrochem. 33, 693–701.

Delli, E., Kyriacou, G. and Lambrou, C. (1998) Electrochemical reduction of CCl_2F_2 on Nafion solid polymer electrolyte composite electrodes. Chem. Commun. (Cambridge). 16, 1693–1694.

Deutscher, R.L. and Cathro, K.J (2001) Organochlorine formation in magnesium electrowinning cells. Chemosphere 43, 147–155.

Doherty, A.P., Koshechko, V., Titov, V. and Mishura, A. (2007) Freon electrochemistry in room-temperature ionic liquids. J. Electroanal. Chem. 602, 91–95.

Dombek, T., Davis, D., Stine, J. and Klarup, D. (2004) Degradation of terbutylazine (2-chloro-4-ethylamino-6-terbutylamino-1,3,5- triazine), deisopropyl atrazine (2-amino-4-chloro-6-ethylamino-1,3,5-triazine), and chlorinated dimethoxy triazine (2-chloro-4,6-dimethoxy-1,3, 5-triazine) by zero valent iron and electrochemical reduction. Environ. Pollut. 129, 267–275.

EC 850/2004 Persistent Organic Pollutants. O. J. Eur. Union, 30.04.2004, L158/1–43.

EC Decision, Proposal COM (2004) 537, 04.08.2004. Amendments to Annexes I–III of the 1998 Protocol to the 1979 Convention on Long Range Transboundary Air Pollution on Persistent Organic Pollutants and to Annexes A–C of the Stockholm Convention on Persistent Organic Pollutants.

EC Regulation, Proposal COM (2006) 242, 31.05.2006, Amending Annex IV to Regulation (EC) No 850/2004 of the European Parliament and of the Council on Persistent Organic Pollutants and Amending Directive 79/117/EEC.

EC Regulation, Proposal COM (2006) 252, 31.05.2006, Amending Annex V to Regulation (EC) No 850/2004 of the European Parliament and of the Council on Persistent Organic Pollutants and Amending Directive 79/117/EEC.

Falciola, L., Gennaro, A., Isse, A.A., Mussini, P.R. and Rossi M. (2006) The solvent effect in the electrocatalytic reduction of organic bromides on silver. J. Electroanal. Chem. 593, 47–56.

Fan, C., Zhuang, Y., Li, G., Zhu, J., Zhu, D. (2000) Direct electrochemistry and enhanced catalytic activity for hemoglobin in a sodium montmorillonite film. Electroanalysis 12, 1156–1158.

Farrell, J., Kason, M., Melitas, N. and Li, T. (2000) Investigation of the long-term performance of zerovalent iron for reductive dechlorination of trichloroethylene. Environ. Sci. Technol. 34, 514–521.

Fedurco, M., Sartoretti, C.J. and Augustynski, J. (2001) Reductive cleavage of the carbon-halogen bond in simple methyl and methylene halides. Reactions of the methyl radical and carbene at the polarized electrode/aqueous solution interface. Langmuir 17, 2380–2387.

Feldberg, S.W. (1969) Digital simulation. In: Bard, A.J. (Ed.) *Electroanalytical Chemistry*, vol. 3, CRC, Boca Raton, FL.

Fiori, G., Mussini, P.R., Rondinini, S. and Vertova, A. (2002) Selective dehalogenation of bromophenols on ag electrocatalyst. Ann. Chim. (Milan) 92, 963–972.

Fiori, G., Rondinini, S., Sello, G., Vertova, A., Cirja, M. and Conti, L. (2005) Electroreduction of volatile organic halides on activated silver cathodes. J. Appl. Electrochem. 35, 363–368.

Fontana, A. (1993) Electrochemical methods in organic chemistry. II: Industrial applications Chim. Nouv. 11, 1232–1236.

Foresti, M.L., Innocenti, M., Forni, F. and Guidelli, R. (1998) Electrosorption valency and partial charge transfer in halide and sulfide adsorption on Ag(111). Langmuir 14, 7008–7016.

Fram, M.S., Berghouse, J.K., Bergamaschi, B.A., Fujii, R., Goodwin, K.D. and Clark, J.F. (2002) Water-quality monitoring and studies of the formation and fate of trihalomethanes during the third injection, storage, and recovery test at Lancaster, Antelope Valley, California, March 1998 through April 1999. *US Geological Survey, Open-File Report 02–102, Sacramento, CA, USA*.

Gassman, J., Voss, J. and Adiwidjaja, G. (1995) Electroreduction of organic compounds. 25. Electrochemical dehalogenation of chlorinated insecticides. Zeit. Natur. B: Chem. Sci. 50, 953–958.

Gennaro, A., Sanchez-Sanchez, C.M., Isse, A.A. and Montiel V. (2004) Electrocatalytic synthesis of 6-aminonicotinic acid at silver cathodes under mild conditions. Electrochem. Commun. 6, 627–631.

Georgolios, N., Kyriacou, G. and Ritzoulis, G. (2001) Electrochemical reduction of dichlorodifluoromethane on silver and lead electrodes. J. Appl. Electrochem. 31, 207–212.

Gherardini, L., Michaud, P.A., Panizza, M., Comninellis, Ch. and Vatistas N. (2001) Electrochemical oxidation of 4-chlorophenol for wastewater treatment: Definition of normalized current efficiency. J. Electrochem. Soc. 148, D78–D82.

Golinske, D. and Voss, J. (2005) Electroreduction of organic compounds, 35. Quantum chemical calculations of reaction pathways for the cathodic dehalogenation of chloro-dibenzo-furans and oligo-chlorobenzenes. Zeit. Natur. B: Chem. Sci. 60, 780–786.

Guerrini, M., Mussini, P.R., Rondinini, S., Torri, G. and Vismara, E. (1998) Electrochemical reduction of halogenosugars on silver: A new approach to C-disaccharides. Chem. Commun. 15, 1575–1575.

Hammerich, O. (2001) Methods for studies of electrochemical reactions. In: Lund, H. and Hammerich, O. (Eds) *Organic Electrochemistry*, 4th ed., Marcel Dekker, New York, NY, pp. 95–182.

He, J., Saez, A.E., Ela, W.P., Betterton, E.A. and Arnold, R.G. (2004a) Destruction of aqueous-phase carbon tetrachloride in an electrochemical reactor with a porous cathode. Ind. Eng. Chem. Res. 43, 913–923.

He, J., Ela, W.P., Betterton, E.A., Arnold, R.G. and Saez, A.E. (2004b) Reductive dehalogenation of aqueous-phase chlorinated hydrocarbons in an electrochemical reactor. Ind. Eng. Chem. Res. 43, 7965–7974.

Horanyi, G. and Torkos, K. (1982) Electrocatalytic reduction of some halogenated derivatives of methane and acetic acid at a platinized platinum electrode in acid medium. J. Electroanal. Chem. Int. Electrochem. 140, 329–346.

Hori, Y., Murata, K. and Oku, T. (2003) Electrochemical dechlorination of chlorinated hydrocarbons – electrochemical reduction of chloroform in acetonitrile/water mixtures at high current density. Chem. Lett. 32, 230–231.

Inokuchi, T. and Kusumoto, M. (2001) Selective dehalogenation of 6,6-dibromopenicillanates by indirect electroreduction with diphenyl diselenide as a recyclable mediator. J. Electroanal. Chem. 507, 34–36.

Isse, A.A. and Gennaro, A. (2002a) Electrocatalytic carboxylation of benzyl chlorides at silver cathodes in acetonitrile. Chem. Commun. (Cambridge) 2798–2799.

Isse, A.A. and Gennaro, A. (2002b) Electrochemical synthesis of cyanoacetic acid from chloroacetonitrile and carbon dioxide. J. Electrochem. Soc. 149, D113–D117.

Isse, A.A. and Gennaro, A. (2003) Electrochemical reduction of benzyl bromide in the presence of carbon dioxide. Indian J. Chem. Sec. A Inorg. Phys. Theor. Anal. Chem. 42, 751–757.

Isse, A.A. and Gennaro, A. (2004) Homogeneous reduction of haloacetonitriles by electrogenerated aromatic radical anions: Determination of the reduction potential of $^{\cdot}CH_2CN$. J. Phys. Chem. A 108, 4180–4186.

Isse, A.A., Galia, A., Belfiore, C., Silvestri, G. and Gennaro, A. (2002) Electrochemical reduction and carboxylation of halobenzophenones. J. Electroanal. Chem. 526, 41–52.

Isse, A.A., Ferlin, M.G. and Gennaro, A. (2005a) Electrocatalytic reduction of arylethyl chlorides at silver cathodes in the presence of carbon dioxide: Synthesis of 2-arylpropanoic acids. J. Electroanal. Chem. 581, 38–45.

Isse, A.A., Scialdone, O., Galia A. and Gennaro A. (2005b) The influence of aluminium cations on electrocarboxylation processes in undivided cells with Al sacrificial anodes. J. Electroanal. Chem. 585, 220–229.

Isse, A.A., Falciola, L., Mussini, P.R. and Gennaro, A. (2006a) Relevance of electron transfer mechanism in electrocatalysis: The reduction of organic halides at silver electrodes. Chem. Commun. 344–346.

Isse, A.A., Gottardello, S., Maccato, C. and Gennaro A. (2006b) Silver nanoparticles deposited on glassy carbon. Electrocatalytic activity for reduction of benzyl chloride. Electrochem. Commun. 8, 1707–1712.

Isse, A.A., De Giusti, A. and Gennaro, A. (2006c) One- versus two-electron reaction pathways in the electrocatalytic reduction of benzyl bromide at silver cathodes. Tetrahedron Lett. 47, 7735–7739.

Isse, A.A., De Giusti, A., Gennaro, A., Falciola, L. and Mussini, P.R. (2006d) Electrochemical reduction of benzyl halides at a silver electrode. Electrochim. Acta 51, 4956–4964.

Iwakura, C., Tsuchiyama, Y., Higashiyama, K., Higuchi, E. and Inoue, H. (2004) Successive hydrogenation and dechlorination systems using palladized ion exchange membranes. J. Electrochem. Soc. 151, D1–D5.

Ju, X., Hecht, M., Galhotra, R.A., Ela, W.P., Betterton, E.A., Arnold, R.G. and Saez, A.E. (2006) Destruction of gas-phase trichloroethylene in a modified fuel cell. Environ. Sci. Technol. 40, 612–617.

Juttner, K., Galla, U. and Schmieder, H. (2000) Electrochemical approaches to environmental problems in the process industry. Electrochim. Acta 45, 2575–2594.

Kimbrough, D.E. and Suffet, I.H. (2002) Electrochemical removal of bromide and reduction of THM formation potential in drinking water. Water Res. 36, 4902–4906.

Kluyev, N., Cheleptchikov, A., Brodsky, E., Soyfer, V. and Zhilnikov, V. (2002) Reductive dechlorination of polychlorinated dibenzo-p-dioxins by zerovalent iron in subcritical water. Chemosphere 46, 1191–1193.

Kolthoff, I.M. and Lingane, J.J. (1941) *Polarography, Interscience*, New York, NY.

Korshin, G.V. and Jensen, M.D. (2001) Electrochemical reduction of haloacetic acids and exploration of their removal by electrochemical treatment. Electrochim. Acta 47, 747–751.

Koshechko, V.G. and Kiprianova, L.A. (1999) Electrochemically activated insertion of fluoroalkyl groups into organic and inorganic substrates. Theor. Exp. Chem. (Translation of Teoreticheskaya i Eksperimental'naya Khimiya) 35, 18–36.

Koshechko, V.G., Titov, V.E. and Sednev, D.V. (1994) New route for producing acrylic acid copolymers, based on electrochemical carboxylation of poly(vinyl halide)s and polybutadiene. Polymer 35, 1787–1788.

Köster, F., Dinjus, E. and Dunach, E. (2001) Electrochemical selective incorporation of CO_2 into terminal alkynes and diynes. Eur. J. Org. Chem. 13, 2507.

Kotsinaris, A., Kyriacou, G. and Lambrou, Ch. (1998) Electrochemical reduction of dichloromethane to higher hydrocarbons. J. Appl. Electrochem. 28, 613–616.

Kulikov, S.M., Plekhanov, V.P., Tsyganok, A.I., Schlimm, C. and Heitz, E. (1996) Electrochemical reductive dechlorination of chloroorganic compounds on carbon cloth and metal-modified carbon cloth cathodes. Electrochim. Acta 41, 527–31.

Kuznetsov, A.M., German, E.D., Masliy, A.N. and Korshin, G.V. (2004) A density functional study of dissociative electron transfer reactions with participation of halogenated methanes. J. Electroanal. Chem. 573, 315–325.

Laine D.F. and Cheng I.F. (2007) The destruction of organic pollutants under mild reaction conditions: A review. Microchem. J. 85, 183–193.

Leonel, E., Paugam, J.P., Condon-Gueugnot, S. and Nedelec, J.-Y. (1998) Cyclopropane formation by electroreductive coupling of activated olefins and gem-polyhalo compounds. Tetrahedron 54, 3207–3218.

Li, T. and Farrell, J. (2000) Reductive dechlorination of trichloroethene and carbon tetrachloride using iron and palladized-iron cathodes. Environ. Sci. Technol. 34, 173–179.

Lin, C.H. and Tseng, S.K. (2000) Electrochemically reductive dechlorination of chlorophenol using nickel and zinc electrodes. Water Sci. Technol. 42, 167–172.

Liu, Z., Arnold, R.G., Betterton, E.A. and Festa, K.D. (1999) Electrolytic reduction of CCl_4. Effects of cathode material and potential on kinetics, selectivity, and product stoichiometry. Environ. Eng. Sci. 16, 1–13.

Liu, Z., Betterton, E.A. and Arnold, R.G. (2000) Electrolytic reduction of low molecular weight chlorinated aliphatic compounds: Structural and thermodynamic effects on process kinetics. Environ. Sci. Technol. 34, 804–811.

Liu, Z., Arnold, R.G., Betterton, E.A. and Smotkin, E. (2001) Reductive dehalogenation of gas-phase chlorinated solvents using a modified fuel cell. Environ. Sci. Technol 35, 4320–4326.

Liu, P.Y., Zheng, M.H. and Xu, X.B. (2002) Phototransformation of polychlorinated dibenzo-p-dioxins from photolysis of pentachlorophenol on soils surface. Chemosphere 46, 1191–1193.

Liu, H.-H., Wan, Y.-Q. and Zou, G.-L. (2006) Direct electrochemistry and electrochemical catalysis of immobilized haemoglobin in an ethanol-water mixture. Anal. Bioanal. Chem. 385, 1470–1476.

Lowry, GV and Johnson, KM. (2004) Congener-specific dechlorination of dissolved PCBs by microscale and nanoscale zerovalent iron in a water/methanol solution. Environ. Sci. Technol. 38, 5208–5216.

Lund, H. (2002) A century of organic electrochemistry. J. Electrochem. Soc. 149, S21–S33.

Ma, X., Liu, X., Xiao, H., Li, G. (2005) Direct electrochemistry and electrocatalysis of haemoglobin in poly-3-hydroxybutyrate membrane. Biosens. Bioelectron. 20, 1836–1842.

Magdesieva, T.V., Graczyk, M., Vallat, A., Nikitin, O.M., Demyanov, P.I., Butin, K.P. and Vorotyntsev, M.A. (2006) Electrochemically reduced titanocene dichloride as a catalyst of reductive dehalogenation of organic halides. Electrochim. Acta 52, 1265–1280.

Maran, F., Wayner, D.D.M. and Workentin, M.S. (2001) Kinetics and mechanism of the dissociative reduction of C–X and X–X bonds (X = O, S). Adv. Phys. Org. Chem. 36, 85–166.

Marcus, R.A. (1964) Chemical and electrochemical electron-transfer theory. Annu. Rev. Phys. Chem. 15, 155–196.

Meites, L. (1965) *Polarographic Techniques*, 2nd ed., Wiley-Interscience, New York, NY.

Migani, A. and Illas, F. (2006) A systematic study of the structure and bonding of halogens on low-index transition metal surfaces. J. Phys. Chem. 110, 11894–11906.

Miller, L.L. and Riekena, E. (1969) The electrochemical reduction of vynil bromides. J. Org. Chem. 34, 3359–3362.

Mishra, D. and Farrell, J. (2005) Understanding nitrate reactions with zerovalent iron using tafel analysis and electrochemical impedance spectroscopy. Environ. Sci. Technol. 39, 645–650.

Miyoshi, K., Kamegaya, Y. and Matsumura, M. (2004a) Electrochemical reduction of organohalogen compound by noble metal sintered electrode. Chemosphere 56, 187–193.

Miyoshi, K., Kamegaya, Y. and Matsumura, M. (2004b) Destruction of 1, 2, 3-trichlorobenzene in sediment extract by Na ion supply system. Electrochemistry 72, 830–832.

Miyoshi, K., Alfafara, C.G., Matsumura, M. (2004c) Dechlorination of organohalogen compounds by an electrocatalytic cation supply system. J. Electroanal. Chem. 568, 293–300.

Moglie, Y., Alonso, F., Vitale, C., Yus, M. and Radivoy, G. (2006) Active-iron-promoted hydrodehalogenation of organic halides. Appl. Catal. A: General 313, 94–100.

Montecatini Edison S.p.a., (1969) Italian Patent, 852,487.

Mussini, P.R., Ardizzone, S., Cappelletti, G., Longhi, M., Rondinini, S. and Doubova, L.M. (2003) Surface screening effects by specifically adsorbed halide anions in the electrocatalytic reduction of a model organic halide at mono- and polycrystalline silver in acetonitrile. J. Electroanal. Chem. 552, 213–221.

Muthuraman, G. and Pillai, K.C. (2006) Dechlorination of β-methylallyl chloride by electrogenerated $\left[\text{Co(I) (bipyridine)}_3\right]^+$: An electrochemical study in the presence of cationic surfactants. J. Colloid Interface Sci. 297, 687–695.

Naumczyk, J., Szpyrkowicz, L., De Faveri, M.D. and Zilio-Grandi F. (1996) Electrochemical treatment of tannery wastewater containing high strength pollutants. Process Saf. Environ. Protect. 74, 59–68.

Nedelec, J.-Y., Perichon, J. and Troupel, M. (1997) Organic electroreductive coupling reactions using transition metal complexes as catalysts. Top. Curr. Chem. 185, 141–173.

Nunnecke, D. and Voss, J. (1999) Electroreduction of organic compounds. Part 32. Indirect electrodehalogenation of chloro arenes in methanol mediated by nickel complexes. Acta Chem. Scand. 53, 824–829.

Öberg, T., Öhrström, T. and Bergström, J. (2007) Metal catalyzed formation of chlorinated aromatic compounds: A study of the correlation pattern in incinerator fly ash. Chemosphere 67, S185–S190.

Oturan, M.A., Oturan, N., Lahitte, C. and Trevin, S. (2001) Production of hydroxyl radicals by electrochemically assisted Fenton's reagent: Application to the mineralization of an organic micropollutant, pentachlorophenol. J. Electroanal. Chem. 507, 96–102.

Pause, L., Robert, M. and Savéant, J.-M. (2000) Reductive cleavage of carbon tetrachloride in a polar solvent. An example of a dissociative electron transfer with significant attractive interaction between the caged product fragments. J. Am. Chem. Soc. 122, 9829–9835.

Perichon, J., Sock, O. and Troupel, M. (1986) Electrosynthesis of carboxylic acids. Ger. Offen. DE 3522304 A1 19860102 Patent Application: DE 85–3522304 19850621. Priority: FR 84–9787 19840621, p. 32.

Persinger, J.D., Hayes, J.L., Klein, L.J., Peters, D.G., Karty, J.A. and Reilly, J.P. (2004) Catalytic reduction of 1,1,2-trichloro-1,2,2-trifluoroethane (CFC-113) by cobalt(I) salen electrogenerated at vitreous carbon cathodes. J. Electroanal. Chem. 568, 157–165.

Peters, D.G. (2001) Halogenated organic compounds. In: H. Lund and O. Hammerich (Eds.) *Organic Electrochemistry*, 4th ed., Marcel Dekker, New York, NY, pp. 341–377.

Pletcher, D. (1982) *Industrial Electrochemistry*, Chapman and Hall, London.

Polcaro, A.M., Mascia, M., Palmas, S. and Vacca, A. (2004) Electrochemical degradation of diuron and dichloroaniline at BDD electrode. Electrochim. Acta 49, 649–656.

Ragaini, V., Selli, E., Bianchi L.C. and Pirola C. (2001) Sono-photocatalytic degradation of 2-chlorophenol in water: Kinetic and energetic comparison with other techniques. Ultrason. Sonochem. 8, 251–258.

Robert, M. and Savéant, J.-M. (2005) Electroenzymatic reactions. Investigation of a reductive dehalogenase by means of electrogenerated redox cosubstrates. J. Am. Chem. Soc. 127, 13583–13588.

Roberts, A.L., Totten, L.A., Arnold, W.A., Burris, D.R. and Campbell, T.J. (1996) Reductive elimination of chlorinated ethylenes by zerovalent metals. Environ. Sci. Technol. 30, 2654–2659.

Rodrigo, M.A., Michaud, P.A., Duo, I., Panizza, M., Cerisola, G. and Comninellis, Ch. (2001) Oxidation of 4-chlorophenol at boron-doped diamond electrode for wastewater treatment. J. Electrochem. Soc. 148, D60–D64.

Rondinini, S. and Vertova, A. (2004) Electrocatalysis on silver and silver alloys for dichloromethane and trichloromethane dehalogenation. Electrochim. Acta 49, 4035–4046.

Rondinini, S., Mussini, P.R., Sello, G., Vismara, E. (1998) Glycosyl halides as building blocks for the electrosynthesis of glycosides. J. Electrochem. Soc. 145, 1108–1112.

Rondinini, S., Mussini, P.R., Cantù, G. and Sello, G. (1999) Cathode and medium effects on the electroreductive glucosidation of phenols. Phys. Chem. Chem. Phys. 1, 2989–2995.

Rondinini, S., Mussini, P.R., Crippa, F. and Sello, G. (2000) Electrocatalytic potentialities of silver as a cathode for organic halide reductions. Electrochem. Commun. 2, 491–496.

Rondinini, S., Mussini, P.R., Specchia, M. and Vertova, A. (2001a) The electrocatalytic performance of silver in the reductive dehalogenation of bromophenols. J. Electrochem Soc. 148, D102–D107.

Rondinini, S., Mussini, P.R., Muttini, P. and Sello, G. (2001b) Silver as a powerful electrocatalyst for organic halide reduction: The critical role of molecular structure. Electrochim. Acta, 46, 3245–3258.

Rusling, J.F., Miaw, C.L. and Couture, E.C. (1990) Electrocatalytic dehalogenation of α-haloacetic acids by vitamin B12. Inorg. Chem. 29, 2025–2027.

Ryu, J.-Y., Choi, K.-C. and Mulholland, J.A. (2006) Polychlorinated dibenzo-p-dioxin (PCDD) and dibenzofurna (PCDF) isomer patterns from municipal waste combustion: Formation mechanism fingerprints. Chemosphere. 65, 1526–1536.

Sanecki, P.T. and Skitał, P.M. (2007) The electroreduction of alkyl iodides and polyiodides. The kinetic model of EC(C)E and ECE-EC(C)E mechanisms with included transfer coefficient variability. Electrochim. Acta 52, 4675–4684.

Savall, A., Abdelhedi, R., Dalbéra, S. and Bouguerra, M.L. (1990a) Reduction electrochimique du trichloro-1,1,2-trifluoroethane: Effet catalytique de l'ion ammonium. Electrochim. Acta, 35, 1727–1737.

Savall, A., Abdelhedi, R., Dalbéra, S. and Bouguerra, M.L. (1990b) Réduction électrochimique du trichloro-1,1,2 trifluoroéthane: étude de la corrosion chimique de cathodes de zinc. J. Appl. Electrochem. 20, 1045–1052.

Savéant, J.-M. (1987) A simple model for the kinetics of dissociative electron transfer in polar solvents. Application to the homogeneous and heterogeneous reduction of alkyl halides. J. Am. Chem. Soc. 109, 6788–6795.

Savéant, J.-M. (2000) Electron transfer, bond breaking and bond formation. Adv. Phys. Org. Chem. 35, 117–192.

Schizodimou, A., Kyriacou, G. and Lambrou, C. (1999) Electrochemical reduction of dichlorodifluoromethane in acetonitrile medium to useful fluorinated compounds. J. Electroanal. Chem. 471, 26–31.

Schnabel, C., Worner, M., Gonzalez, B., Del Olmo, I. and Braun, A.M., (2001) Photoelectrochemical characterization of p- and n-doped single crystalline silicon carbide and photoinduced reductive dehalogenation of organic pollutants at p-doped silicon carbide. Electrochim. Acta 47, 719–727.

Scialdone, O., Galia, A., La Rocca, C. and Filardo, G. (2005) Influence of the nature of the substrate and of operative parameters in the electrocarboxylation of halogenated acetophenones and benzophenones. Electrochim. Acta 50, 3231–3242.

Simonet, J. (2005) The one electron reduction of primary alkyl iodides at palladiated surfaces. A convenient and general source of alkyl radicals. J. Electroanal. Chem. 583, 34–45.

Simonet, J. (2006) The platinized platinum interface in super-dry solvents: Cathodic reversible reactivity and morphology modifications in the presence of tetramethylammonium salts. J. Electroanal. Chem. 593, 3–14.

Simonet, J. and Peters, D.G. (2004) Electrochemical conversion of primary alkyl halides to alkenes at platinum cathodes. J. Electrochem. Soc. 151, D7–D12.

Simonet, J., Poizot, P. and Laffont, L. (2006) A copper–palladium alloy usable as cathode material mode of formation and first examples of catalytic cleavages of carbon-halide bonds. J. Electroanal. Chem. 591, 19–26.

Sonoyama, N. and Sakata, T. (1998) Electrochemical decomposition of CFC-12 using gas diffusion electrodes. Environ. Sci. Technol. 32, 375–378.

Sonoyama, N., Ezaki, K., Fujii, H. and Sakata, T. (2002) Electrochemical conversion of CFC-12 to tetrafluoroethylene: Electrochemical formation of difluorocarbene. Electrochim. Acta, 47, 3847–3851.

Stock, N.L. and Bunce, N.J. (2002) Electrocatalytic dechlorination of atrazine. Can. J. Chem. 80, 200–206.

Stromberg, J.R., Wnuk, J.D., Pinlac, R.A.F. and Meyer, G.J. (2006) Multielectron transfer at heme-functionalized nanocrystalline TiO_2: Reductive dechlorination of DDT and CCl_4 forms stable carbene compounds. Nanoletters 6, 1284–1286.

Takita, Y., Yamada, H., Hashira, M. and Ishihara, T. (1990) Conversion of 1,1,2-Trichloro-1,2,2-trifluoroethane (CFC 113) over TiO_2-supported metal and metal oxide catalysts. Chem. Lett. 715–718.

Titov, V.E., Mishura, A.M. and Koshechko, V.G. (2006) The effect of the cathode material on the electrochemical activation and dehalogenation of C-2 freons. Theor. Exp. Chem. 42, 224–228.

Tsai, Y-C., Coles, B.A., Compton, R.G. and Marken, F. (2002) Microwave activation of electrochemical processes: Enhanced electrodehalogenation in organic solvent media. J. Am. Chem. Soc. 124, 9784–9788.

Tsyganok, A.I. and Otsuka, K. (1999) Selective dechlorination of chlorinated phenoxy herbicides in aqueous medium by electrocatalytic reduction over palladium-loaded carbon felt. Appl. Catal. B. Environ. 22, 15–26.

Tsyganok, A., Otsuka, K., Yamanaka, I., Plekhanov, V. and Kulikov, S. (1996) Selective electrochemical dehalogenation of 2,4-dichlorophenoxy acetic acid in MeCN at room temperature. Chem Lett. 25, 261–262.

Tsyganok, A.I., Yamanaka, I. and Otsuka, K. (1998) Pd-loaded carbon felt as the cathode for selective dechlorination of 2,4-dichlorophenoxyacetic acid in aqueous solution. J. Electrochem. Soc. 145, 3844–3850.

Tsyganok, A.I., Yamanaka, I. and Otsuka, K. (1999) Dechlorination of chloroaromatics by electrocatalytic reduction over palladium-loaded carbon felt at room temperature. Chemosphere 39, 1819–1831.

Uchini, M., Hirano, T., Satoh, H., Nakagawa, M. and Wakamiya, J. (2005) The severity of Minamata disease declined in 25 years: Temporal profile of the neurological findings analyzed by multiple logistic regression model. Tohoku J. Exp. Med. 205, 53–63.

Valette, G., Hamelin, A. and Parsons, R. (1978) Specific adsorption on silver single crystals in aqueous solutions. Z. Phys. Chem. Neue Fol. 113, 71–89.

Vaze, A. and Rusling, J.F. (2006) Microemulsion-controlled reaction sites in biocatalytic films for electrochemical reduction of vicinal dibromides. Langmuir 22, 10788–10795.

von Stackelberg, M. and Stracke, W. (1949) Das Polarographische Verhalten ungesättiger und halogenierte Kohlenwasserstoffe. Z. Elektrochem. Angew. Phys. Chem. 53, 118–125.

Wang, J., Blowers, P. and Farrell, J. (2004) Understanding reduction of carbon tetrachloride at nickel surfaces. Environ. Sci. Technol. 38, 1576–1581.

Warren, K.D., Arnold, R.G., Bishop, T.L., Lindholm, L.C. and Betterton, E.A. (1995) Kinetics and mechanism of reductive dehalogenation of carbon tetrachloride using zero-valence metals. J Hazard. Mater. 41, 217–227.

Wawzonek, S. and Willging, S. (1977) Continuous electrochemical preparation of chlorotrifluoroethylene. J. Electrochem. Soc. 124, 860–861.

Wendt, H. and Kreysa, G. (1999) *Electrochemical Engineering. Science and Technology in Chemical and Other Industries*, Springer-Verlag, Berlin.

Winkel, A. and Proske, G. (1936) Über die elektrolytische Reduktion organischer Verbindungen an den Quecksilber-tropfelektrode. Ber. Dtsch. Chem. Ges. B 69, Mitteil I, 693–706; Mitteil II, 1917–1929.

Wright, M., Honeychurch, M.J., Hill, H. and Allen O. (1999) Bioelectrochemical dehalogenations via direct electrochemistry of poly(ethylene oxide)-modified myoglobin. Electrochem. Commun. 1, 609–613.

Zhang, N., Blowers, P. and Farrell, J. (2005) Ab initio study of carbon-chlorine bond cleavage in carbon tetrachloride. Environ. Sci. Technol. 39, 612–617.

Zhou, D.-L., Carrero, H. and Rusling, J.F. (1996) Radical vs anionic pathway in mediated electrochemical reduction of benzyl bromide in a bicontinuous microemulsion. Langmuir 12, 3067–3074.

Zuman, P. (1967) *Substituent Effects in Organic Polarography*, Plenum, New York, NY.

Chapter 13
Principles and Applications of Solid Polymer Electrolyte Reactors for Electrochemical Hydrodehalogenation of Organic Pollutants

Hua Cheng and Keith Scott

13.1 Introduction

Halogenated organic compounds consist of a large group of potentially toxic pollutants, including aliphatics, olefins, aromatics, etc. They are widely distributed at many existing and former industrial sites and contaminated the environment. Disposal of such compounds to landfill is now virtually precluded by environmental legislation. Incineration is an energy-intensive process due to the high operation temperatures and, in addition, produces harmful substances (e.g. dioxins) and causes adverse public reaction. Other alternatives, such as bio-remediation and chemical dehalogenation (Hitchman et al. 1995), have been investigated. However, the products of bio-remediation are often toxic and, in some cases, may be more toxic than the parent compounds (Criddle and McCarty 1991). There are great challenges to achieve micro-organism survival in a halogenated-compound environment, as well as a necessity for long-term operation, e.g., months for the bio-remediation of PCBs (Grittini et al. 1995; Hitchman et al. 1995). Chemical hydrodehalogenation (HDH) using, for example, $LiAlH_4$ and $NaBH_4$, is too expensive for practical applications (Appleton 1996; Hitchman et al. 1995; Schmal et al. 1986). Alternatively, zero-valent metals (e.g. iron, zinc and tin) have been employed to treat halogenated hydrocarbons in wastewaters and groundwaters (Connors and Rusling 1983; Fennelly and Roberts 1998; Hitchman et al. 1995; Matheson and Tratnyek 1994; Tratnyek 1996). For instance, a mixture of 22% granular iron and 78% sand was installed as a permeable "wall" across the path of a contaminant plume at Canadian Forces Base, Borden, Ontario. Approximately 90% of the trichloroethene and 86% of the tetrachloroethene were removed by reductive dechlorination within the wall, with no measurable decrease in performance over the 5-year duration of the test (O'Hannesin and Gillham 1998). Unfortunately, this method has slow reaction kinetics and very low effectiveness, particularly for

H. Cheng (✉)
School of Chemical Engineering and Advanced Materials, Newcastle University, Newcastle upon Tyne, UK
e-mail: hua.cheng@ncl.ac.uk

C. Comninellis and G. Chen (eds.), *Electrochemistry for the Environment*,
DOI 10.1007/978-0-387-68318-8_13,

halogenated aromatic compounds (Hitchman et al. 1995; Tratnyek 1996). Catalytic HDH is another option, but it has to be operated at high temperature (above 400°C in most cases) and high pressure (e.g. 10 MPa) to provide high reaction rates, but often cause rapid catalyst deactivation and introduce safety concerns due to unacceptable use of hydrogen in large-scale treatment facilities (Aramendia et al. 1999; Connors and Rusling 1983; Hitchman et al. 1995; Schmal et al. 1986; Yak et al. 1999).

Recently, electrochemical HDH has emerged as an attractive technique to destroy halogenated organic wastes (Bonfatti et al. 1999; Cheng et al. 1997, 2001, 2003a–d, 2004a–e; Chetty et al. 2003, 2004; Dabo et al. 2000; Kulikov et al. 1996; Schmal et al. 1986; Zhang and Rusling 1995). In an electrochemical HDH process, toxic materials are removed from gases and liquids using the electron as a main reagent rather than redox chemicals. In principle, electrochemical technology is environmentally compatible because the electron is a "clear reagent"; it is also selective, efficient, cheap, controllable and flexible. Hence electrochemical reductive HDH is considered a promising solution to the ecological problem posed by halogenated organic compounds (Marrocino et al. 1987). A striking feature of electrochemical reductive HDH is the capability to remove halogen components selectively from halogenated organics, which eliminates the main toxic source of this type of compound. In addition, the electrochemical HDH can be operated at ambient temperature and pressure, without the use of additional chemicals, and HDH products are also easier to remediate.

13.2 Background

The majority of HDH research has concentrated on mechanisms of the electrochemical process (Bonfatti et al. 1999; Cheng et al. 1997, 2001, 2003a–d, 2004a–e; Chetty et al. 2003, 2004; Dabo et al. 2000; Kulikov et al. 1996; Schmal et al. 1986; Marrocino et al. 1987), which are complex and, even for a simple mono-halogenated aliphatic compound RX, apart from other possible chemical reactions, the mechanism can be either a one-electron radical mechanism:

$$RX + e^- \rightarrow (RX^{\cdot})^- \rightarrow R^{\cdot} + X^- + H_2O \rightarrow RH + HX + OH^- \quad (13.1a)$$

$$2R^{\cdot} \rightarrow RR \quad (13.1b)$$

or a two-electron hydrogenation mechanism:

$$RX + 2H^+ + 2e^- \rightarrow RH + HX \quad (13.2)$$

Fourier transform infrared measurements have shown that electrochemical HDH of halogenated phenols produced the phenolate anion, followed by a sequence of electron additions and halide expulsions leading, via the intermediate radical, to phenol (Chetty et al. 2003, 2004).

The HDH products usually depended on electrolysis conditions, e.g. the electrochemical HDH of polyhalogenated aliphatic compounds produced various products at different potentials:

$$\mathrm{RCl_4} + \mathrm{H^+} + 2\mathrm{e^-} \xrightarrow{-0.78\,\mathrm{V\ vs.\ RHE}} \mathrm{RHCl_3} + \mathrm{H} + 2\mathrm{e} \xrightarrow{-1.67\mathrm{V\,vs.RHE}} \mathrm{RH_2Cl_2} + \mathrm{H^+} + 2\mathrm{e^-} \xrightarrow{-2.30\,\mathrm{V\ vs.\ RHE}} \mathrm{RH_3Cl} \tag{13.3}$$

The nature of the cathode has been found to have major effect on the efficiency of electrochemical HDH of halogenated compounds. For instance, the HDH of 12 mM chlorobenzene at carbon cloth or lead cathodes gave conversions up to 95% with a current efficiency of 20%, lower conversion and efficiency (<5%) were observed using platinum, titanium or nickel cathodes (Zanaveskin et al. 1996). A 100% electrochemical HDH of 153 ppm 4-chlorophenol to phenol was achieved using a palladium-coated carbon cloth cathode (Balko et al. 1993). Unfortunately, several environmentally unacceptable materials, such as Hg and Pb, have also been used as cathodes (Bonfatti et al. 1999; Kulikov et al. 1996).

In general, the majority of work was carried out in standard electrochemical cells, which required added electrolyte and non-aqueous solvents (Aramendia et al. 1999; Zanaveskin et al. 1996). A flow-through cell with a carbon-fibre cathode was used to dehalogenate pentachlorophenol (PCP); however, the current efficiency was very low (ca. 1%) and the energy consumption was high, about 400 kWh $(\mathrm{kgPCP})^{-1}$ (Schmal et al. 1986). This performance renders the approach unattractive with respect to treatment of large volumes of organic wastes and inappropriate for the remediation of aqueous streams. It is clear that an environmentally benign cheap and efficient hydrodehalogenation technology is required to attract industrial use. Therefore, an HDH reactor using the SPE technology was designed and operated (Cheng et al. 1997, 2001, 2003a–d, 2004a–e; Chetty et al. 2003, 2004) and it is described in the following sections.

13.3 The Solid Polymer Electrolyte Hydrodehalogenation Reactor

13.3.1 Principle of Solid Polymer Electrolyte Reactors

The central part of the electrochemical HDH reactor is the use of solid polymer electrolyte (SPE). A typical membrane material belongs to the fully fluorinated polyethene-based family: polytetrafluoroethylene (PTFE) (known by the trade name Teflon), shown in Fig. 13.1.

Fig. 13.1 Structure of polytetrafluoroethylene

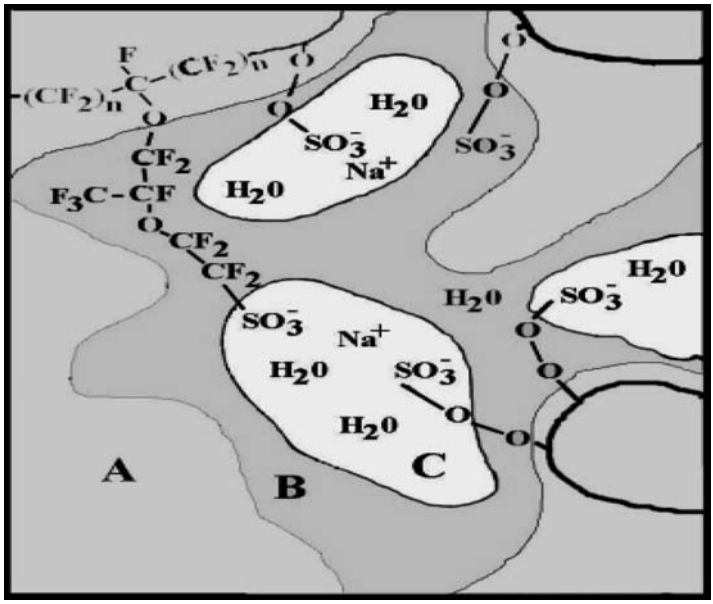

Fig. 13.2 Structure of perfluorosulphonic acid co-polymer (Nafion®). The Yeager Three Phase Model, based on a three-phase clustered system with interconnecting channels within the polymer. (**a**) Fluorocarbon backbone, (**b**) interfacial region of relatively large fractional void volume containing some pendant side chains, some water and sulphate groups, (**c**) clustered regions

PTFE is a very chemically resistant material which is very hydrophobic (repels water) but does not have inherent ion exchange capabilities. Thus to convert this material into an ion-exchange material further processing is required. This requires the introduction of a side-chain which is then sulphonated. The classic side chain, used by DuPont, consists of a vinyl ether to which sulphonic acid is chemically bonded (Fig. 13.2).

Introduction of the side chain with the bonded ionic group makes the material partially hydrophilic, due to the attached sulphonate group, as well as ion conducting. The classic (benchmark) material developed by DuPont goes under the name of Nafion®.

The perfluorosulfonic acid family of membranes includes a range of alternative products from different manufacturers, using for example different side chains, but generally the inherent characteristics are similar as follows:

- They exhibit exceptionally high chemical stability – stable against strong bases, strong oxidising and reducing acids, Cl_2, H_2 and O_2 at temperatures up to 125°C.

- They are mechanically strong and can be formed into thin films down to 30–40 μm.
- They have high acidity with high conductivity (and ion-exchange capacity) when wet.
- They are highly stable in operation. In selected fuel cell tests (and water electrolysis systems), lifetimes of over 50,000 h have been demonstrated.

The principle reason why the ionomer membranes function well as ion conducting materials is that the sulphonate groups form into clusters, which is very hydrophilic and attract water. These clusters effectively form channels through which H^+ ion can move quite freely under a potential gradient. A model of a Nafion type of membrane is shown in Fig. 13.2, consisting of hydrophilic (PTFE) regions surrounding the regions of high water content formed by the sulphonic acid.

The fundamental principle of SPE reactors is the coupling of the transport of electrical charges, i.e. an electrical current with a transport of ions (cations or anions), through a SPE membrane due to an externally applied (e.g. electrolysis) or internally generated (e.g. fuel cells) electrical potential gradient. For example, in a chlorine/alkaline SPE reactor (Fig. 13.3), the anode and cathode were separated by a cation–SPE membrane (e.g. Nafion® 117) forming two compartments, containing the anolyte (e.g. 25 wt% NaCl solution) and the catholyte (e.g. dilute sodium hydroxide), respectively.

When an electrical potential is applied between the electrodes, chlorine ions in the anode chamber migrate towards the anode where they are oxidised and form chlorine gas. The sodium ions from the salt solution migrate through the membrane towards the cathode where it is reduced to sodium metal, which immediately reacts with water to form sodium hydroxide and hydrogen gas. The overall reaction is:

$$2NaCl + 2H_2O = Cl_2 + H_2 + 2NaOH \tag{13.4}$$

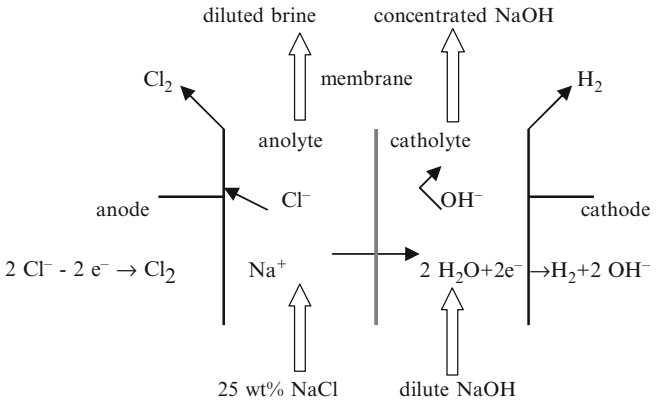

Fig. 13.3 The principle of a chlorine/alkaline solid polymer electrolyte reactor

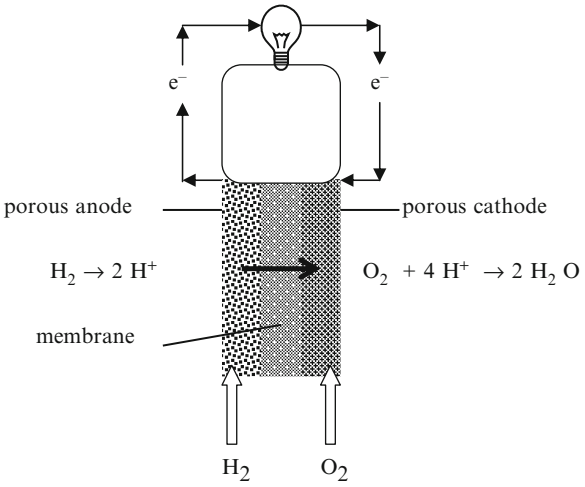

Fig. 13.4 The principle of an H_2–O_2 fuel cell

In a fuel cell, chemical energy is converted into electrical energy. For instance, in an H_2–O_2 fuel cell (Fig. 13.4), porous electrodes and catalyst layers are separated by a SPE membrane (e.g. Nafion® 117).

Hydrogen passes through the anode and reacts in the catalyst layer forming protons and releasing electrons at the anode to an electric circuit. The protons migrate through the membrane and react in the catalyst layer with oxygen and electrons to form water. The overall reaction is the oxidation of hydrogen by oxygen to form water:

$$H_2 + \frac{1}{2}O_2 = H_2O \tag{13.5}$$

In this case, the reaction has a negative Gibb's free energy and electrical energy is generated.

In principle, oxidation could occur simultaneously during a HDH (reduction) reaction. For example any de-halogenated compounds could be oxidised to CO_2 in the anode compartment. Thus in the case of pentachlorophenol the phenol produced by the HDH could be oxidised at a suitable anode (e.g. boron-doped diamond) to CO_2:

$$Cl_5C_6OH\,(PCP) + 10e^- + 5H^+ \rightarrow C_6H_5OH + 5Cl^- \tag{13.6}$$

$$C_6H_5OH + 11H_2O \rightarrow 6CO_2 + 28e^- + 28H^+ \tag{13.7}$$

13.3.2 SPE HDH Reactor Equipment

The flow sheet of the SPE HDH test system is shown in Fig. 13.5.

The reactor can be operated in a batch recycle mode. One of the advantages of SPE HDH technology is that separation and recycling of a supporting electrolyte are unnecessary, which can greatly reduce process cost.

13.3.3 Principle of the SPE HDH Reactor

Figure 13.6 shows the principle of the SPE HDH reactor using a Nafion® 117 membrane to separate anolyte and catholyte chambers.

A porous anode and cathode are attached to each surface of the membrane, forming a membrane-electrode assembly, similar to that employed in SPE fuel cells. Electrochemical reactions (electron transfer+hydrogenation) occur at the interfaces between the ion exchange membrane and electrochemically active layers of electrodes. Electrochemical reductive HDH occurred at the interfaces between the ion exchange membrane and the cathode catalyst layer when an electrical current is applied between the electrodes:

$$RX_n + n\,H^+ + 2n\,e^- \rightarrow RH_n + n\,X^- \tag{13.8}$$

where X is halogen atom and R is an organic skeleton.

Electrogenerated protons $\left(H^+ \text{ ions}\right)$, from the anode reaction, migrate through the membrane towards the cathode under the influence of the applied electric field. These protons are typically produced by the oxidation of water which also forms

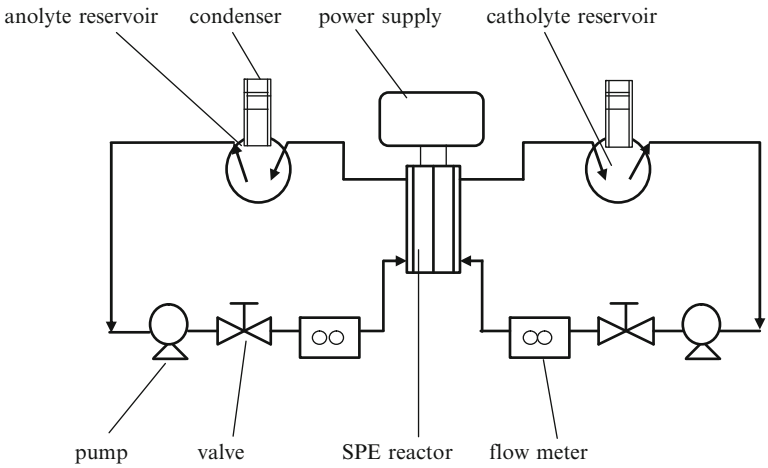

Fig. 13.5 Flow sheet for the SPE HDH rig used at Newcastle

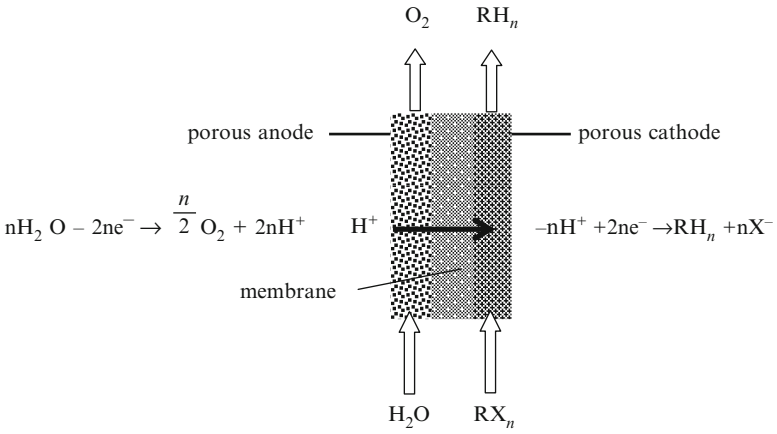

Fig. 13.6 Principle of the SPE HDH reactor

oxygen and are involved in the hydrogenation reaction or are reduced to atomic and molecular hydrogen at the cathode. There are other products, from the HDH process, such as hydrogen, evolved at cathode which would be a cause of current inefficiency.

The SPE HDH reactor is flexible in terms of structural materials and functions, e.g. electrode materials could be mesh- or carbon-supported gas diffusion ones; the SPE could be a cation or anion exchange membrane (e.g. Nafion® 117 or FuMATech FT-FKE-S) and the reactor can treat either aqueous or non-aqueous (e.g. a paraffin oil) wastes with or without supporting electrolytes.

13.3.4 Parameters Used for Performance Evaluation

The percentage of halogenated organics removal (PR, %), space–time yield (STY, $\mathrm{kg\,m^{-3}\,h^{-1}}$), current efficiency (CE, %) and energy consumption (ECN, $\mathrm{kWh\,kg^{-1}}$) are used to evaluate the HDH process performance. They are defined as:

$$\mathrm{PR} = \frac{C_0 - C_t}{C_0}, \tag{13.9}$$

$$\mathrm{STY} = \frac{36 \times a \times j \times \mathrm{CE} \times M_{\mathrm{FW}}}{n \times F}, \tag{13.10}$$

$$\mathrm{ECN} = \frac{n \times F \times E_{\mathrm{Cell}}}{\mathrm{CE} \times M_{\mathrm{FW}}} \tag{13.11}$$

where C_0 and C_t are concentrations of halogenated organics at start and at electrolysis time t, respectively; a is a specific area $\left(\mathrm{m^{-1}}\right)$, defined as a ratio of the electrode area to the actual volume in the reactor; j is the current density $\left(\mathrm{A\,m^{-2}}\right)$; n is the number of electrons in the concerned reaction; F is the Faraday constant

$(96{,}500\,\mathrm{C\,mol^{-1}})$; M_{FW} is the molar mass $(\mathrm{kg\,mol^{-1}})$; E_{Cell} is the cell voltage; and CE is the current efficiency, which was calculated as that part of current (or charge) passed to convert RX_n to RH_n and intermediates.

The total energy consumption includes the energy used for the HDH process, heaters and pumps.

13.3.5 Voltammetry

Figure 13.7 shows typical linear sweep voltammograms (LSV) obtained using a Ti mesh-supported Pd cathode in 0.05 M sodium sulphate solutions with or without pentachlorophenol (PCP) and 2,4-dichlorophenol (DCP).

The addition of PCP and DCP to the catholyte caused an increase in cathodic current densities, compared to that observed in the blank solution. The increase in current was due to the HDH reaction and to hydrogen evolution:

$$Cl_5C_6OH\,(PCP) + 10e^- + 5H^+ \rightarrow C_6H_5OH + 5Cl^- \tag{13.6}$$

$$Cl_2C_6H_3OH\,(DCP) + 4e^- + 2H^+ \rightarrow C_6H_5OH + 2Cl^- \tag{13.12}$$

$$2H^+ + 2e^- \rightarrow H_2 \tag{13.13}$$

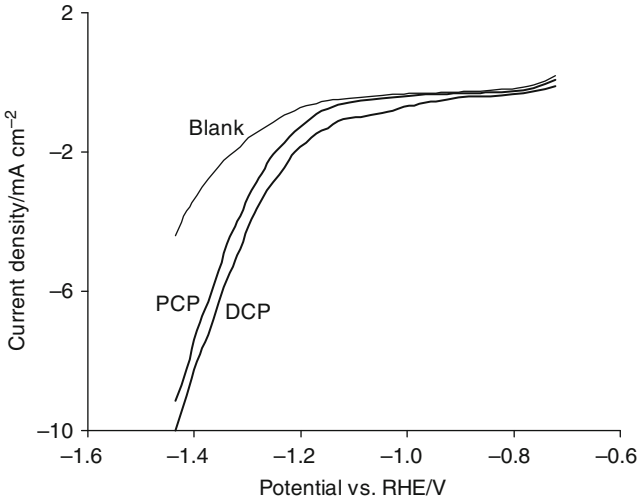

Fig. 13.7 Linear sweep voltammograms for electrochemical HDH of pentachlorophenol (PCP) and 2,4-dichlorophenol (DCP) on a Ti mesh-supported Pd cathode ($2\,\mathrm{mg\,Pd\,cm^{-2}}$, $4\,\mathrm{cm^2}$). Cell: H-cell divided by a Nafion® 117 membrane. Anode: Pt mesh $(10\,\mathrm{cm^2})$. Catholyte: 0.05 M Na_2SO_4 (pH 3) solution without (*blank*) or with saturated PCP and DCP. Anolyte: 0.05 M Na_2SO_4 (pH 3) solution. Scan rate: $5\,\mathrm{mV\,s^{-1}}$. Temperature: $21.5 \pm 0.5°C$

In particular, the rapid increase in current density at potentials more negative than −1.2 V vs. RHE was accompanied by rapid evolution of hydrogen bubbles at the cathode. These data show that using voltammetric measurements can provide information on the HDH of halogenated organics, but cannot investigate the HDH reaction and the hydrogen evolution separately. More data to guide reactor design and process development can only be obtained from quantitative electrolysis.

13.3.6 Percentage of Halogenated Organics Removal and Space–Time Yield

Figure 13.8 shows the effect of cathode catalysts on the HDH of an aqueous saturated PCP solution in the SPE HDH reactor.

The palladised cathode gave the greatest percentage of PCP removal due to its superior capability to produce and store hydrogen. The poor performance at the iron cathode was mainly a result of its instability under the HDH condition. Both instability and poisoning of catalyst by intermediates were responsible for the poorer performance of the Ni cathode.

The electrochemical HDH is much more effective than a chemical HDH, as compared in Fig. 13.8. In "chemical HDH" the same reactor with a Ti mesh-supported Pd catalyst was used. The PR for the HDH of PCP using a poor Ni cathode was even higher than that achieved in the chemical HDH, e.g. 20% against 15% at 120 min (Cheng et al. 2003a).

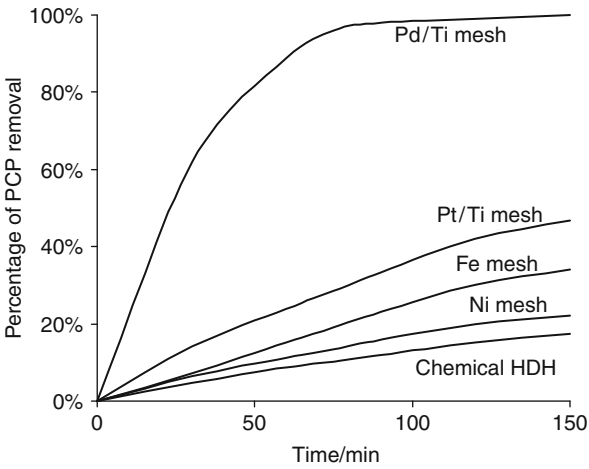

Fig. 13.8 Change in the percentage of pentachlorophenol (PCP) removal for the electrochemical HDH of saturated aqueous solution using a Nafion® 117 membrane reactor. Active area: 20 cm^2. Cathode: Pd or Pt/Ti mesh (2 mg Pd or Pt cm^{-2}), Fe or Ni mesh. Anode: Pt/Ti mesh (2 mg Pt cm^{-2}). Anolyte: Water. Flow rate: 100 ml min^{-1}. Applied current density: 10 mA cm^{-2}. Temperature: 17 ± 0.5°C

In addition to operate with aqueous waste streams, a striking feature of the HDH reactor is its capability to carry out HDH in non-aqueous and very poorly conducting aqueous media. Figure 13.9 shows variations in percentage of DCP removal and

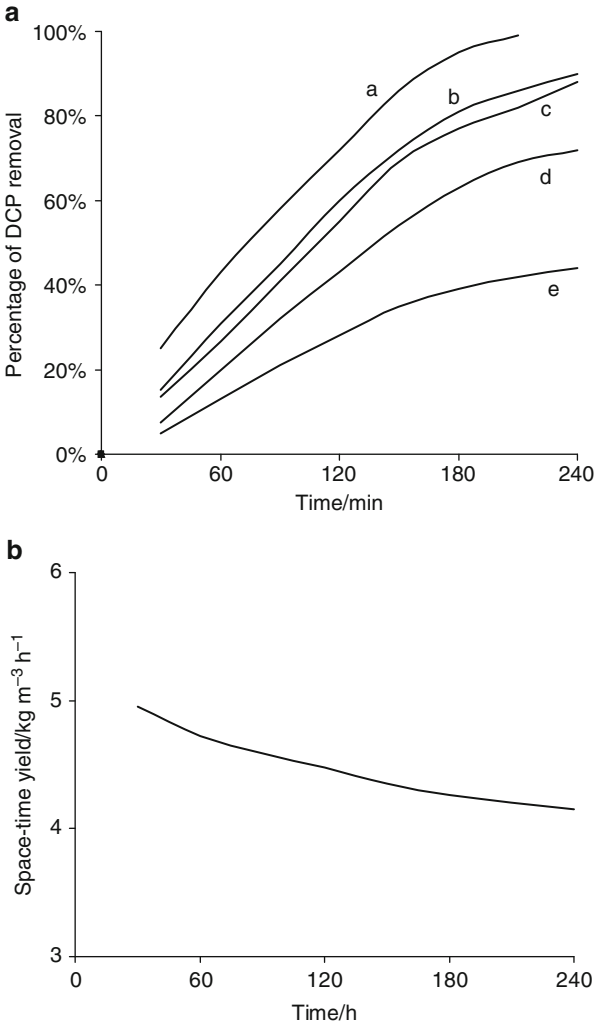

Fig. 13.9 (**a**) Variations in percentage of 2,4-dichlorophenol (DCP) removal for the electrochemical HDH of DCP in paraffin oil media. Anolyte: 0.5 M H_2SO_4 aqueous solution $(100\,cm^3)$. Cathode: Pd/Ti mini-mesh $(2\,mg\,Pd\,cm^{-2})$. Volume: $100\,cm^3$. Curves a: 19.1°C, 5 mM and $10\,mA\,cm^{-2}$; b: 40°C, 20 mM and $10\,mA\,cm^{-2}$; c: 19.1°C, 20 mM and $10\,mA\,cm^{-2}$; d: 19.1°C, 20 mM and $20\,mA\,cm^{-2}$; e: 19.1°C, 20 mM and $5\,mA\,cm^{-2}$. Other conditions are as in Fig. 13.6. (**b**) Variations in space–time yield for the electrochemical HDH of DCP in paraffin oil media. Anolyte: 0.5 M H_2SO_4 aqueous solution $(100\,cm^3)$. Cathode: Pd/Ti mini-mesh $(2\,mg\,Pd\,cm^{-2})$. Data were collected at 19.1°C and $10\,mA\,cm^{-2}$ in a catholyte of 20 mM DCP in paraffin oil $(100\,cm^3)$. Other conditions are as in Fig. 13.6

STY for the electrochemical HDH of DCP in paraffin oil. In this case, a sulphuric acid aqueous solution was used as the anolyte, which decreased the cell resistance that arose from the application to the non-aqueous catholyte, making the process possible. As shown in Fig. 13.9a (curves c, d and e), moderate current densities, i.e. around 10 mA cm^{-2}, were necessary to achieve better performance; high current densities, such as 20 mA cm^{-2}, caused severe side reactions, e.g. hydrogen evolution at the cathode (13.13) and oxygen evolution at the anode:

$$2H_2O \rightarrow O_2 + 4H^+ + 4e^- \tag{13.14}$$

Figure 13.9a also shows that high temperature (e.g. 40°C, curve b) promoted faster reaction kinetics and enhanced the HDH capacity. Not surprisingly, the percentage of DCP removal was higher at lower DCP concentration (5 mM vs. 20 mM, curve a vs. curve c).

Figure 13.9b shows the change in STY for the electrochemical HDH of 20 mM DCP in paraffin oil, which varied between 4.2 and 5 kg m^{-3} h^{-1}.

Figure 13.10 shows a change in STY during the electrochemical HDH of 200 mM 2,4-dibromophenol (DBP) in paraffin oil:

$$Br_2C_6H_3OH\,(DBP) + 4e^- + 2H^+ \rightarrow C_6H_5OH + 2Br^- \tag{13.15}$$

Change in ratio of the waste volume (cm^3) to the cathode geometric surface area (cm^2) was achieved using varying waste volumes between 50 and 1,000 cm^3 in

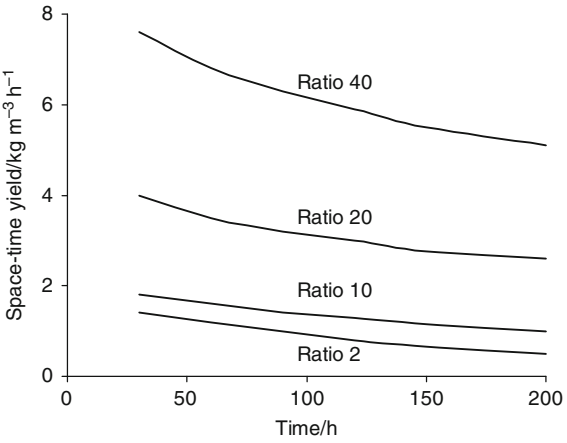

Fig. 13.10 Change in space–time yield during the electrochemical HDH of 200 mM DBP in paraffin oil media using a Nafion® 117 membrane reactor. Ratios of the waste volume (cm^3) to the cathode geometric surface area (cm^2) are indicated in figure. Cathode: Three-layer Ti mesh-supported Pd (25 cm^2, 2 mg Pd cm^{-2}). Anode: Three-layer Ti mesh-supported Pt (25 cm^2, 2 mg Pt cm^{-2}). Controlled current density: 10 mA cm^{-2}. Catholyte: 200 mM DBP in paraffin oil $(50–1{,}000\,cm^3)$. Anolyte: 0.5 M H_2SO_4 aqueous solution $(50–1{,}000\,cm^3)$. Flow rate: 100 ml min^{-1}. Temperature: 18.5 ± 0.5°C

a reactor with a fixed electrode surface area. The STY ranged between 0.5 and 7.6 (kgDBP) $m^{-3}\,h^{-1}$, depending on electrolysis conditions. The data suggest that increasing the ratio of the waste volume to the cathode surface area can greatly enhance the HDH rates.

13.3.7 Selectivity

Another characteristic of the HDH reactor is its high selectivity to desired products. For instance, DCP was selectively converted to phenol with only a small amount (less than 1%) of intermediates, such as 2-chrolophenol (CP) formed (Fig. 13.11):

$$Cl_2C_6H_6OH\,(DCP) + 2e^- + H^+ \rightarrow ClC_6H_4OH\,(CP) + Cl^- \qquad (13.16)$$

This behaviour is of particular importance for a practical waste treatment process where intermediates may be more toxic than the original halogenated compounds.

13.3.8 Current Efficiency and Energy Consumption

Efficient use of electrical energy was achieved in the HDH reactor. Figure 13.12 shows current efficiency and energy consumption for the electrochemical HDH of DCP in paraffin oil. Here the unit for energy consumption is defined as kWh $(kg\,DCP)^{-1}$.

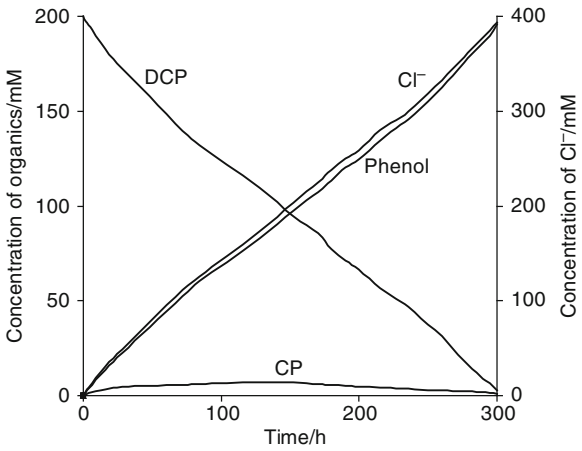

Fig. 13.11 Variations in concentrations during the electrochemical HDH of DCP in paraffin oil media. Catholyte: 200 mM DCP in paraffin oil $\left(1{,}000\,cm^3\right)$. Other conditions are as in Fig. 13.7

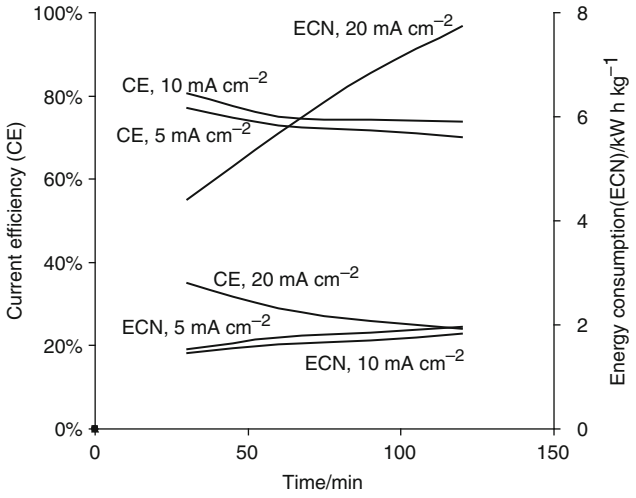

Fig. 13.12 Variations in current efficiency and energy consumption for the electrochemical HDH of 20 mM DCP in paraffin oil at different current densities. Other conditions are as in Fig. 13.7

Both current efficiency and energy consumption were related to the current densities. Current efficiencies were above 75% at a current density of 10 mA cm^{-2} but below 35% at 20 mA cm^{-2} due to side reactions, such as the hydrogen evolution. A moderate current density, e.g. 10 mA cm^{-2}, gave lower energy consumption, e.g. 1.5–1.8 vs. 4.4–7.8 kWh kg^{-1} at 10 and 20 mA cm^{-2}, respectively. Higher and lower current densities could not balance the rates of hydrogen production and consumption and, hence, caused lower performance.

13.3.9 Stability of the HDH Reactor

To be used in a realistic process, the HDH reactor should provide long-term operation. Figure 13.13 shows data for 250 h continuous operation for the HDH of 150 mM DBP in paraffin oil $(1{,}000\,cm^3)$ using a Nafion® 117 membrane with Ti mesh-supported Pd cathode and Pt anode, at a current density of 10 mA cm^{-2}. An anolyte of 0.5 M H_2SO_4 aqueous solution $(1{,}000\,cm^3)$ was used.

The cell voltage changed between 2.7 and 2.9 V. After an operation, the same reactor treated other waste systems successfully, also on a long-term basis. The data demonstrated that the Pd cathodes can be subjected for a relatively long HDH operation.

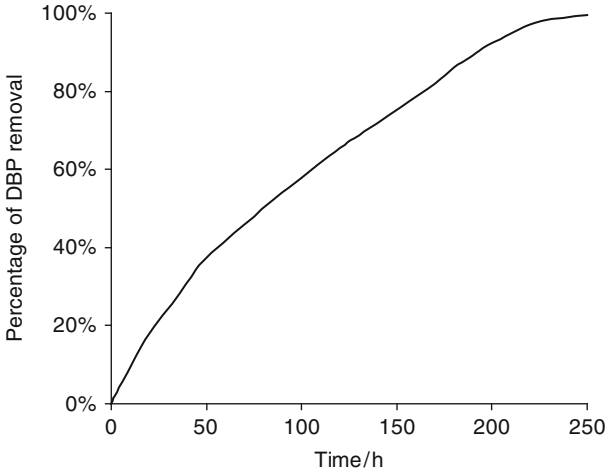

Fig. 13.13 Long-term evaluation data for the electrochemical HDH of 150 mM 2, 4-dibromophenol (DBP) in paraffin oil. Catholyte: 150 mM DBP in paraffin oil $(1,000\,\mathrm{cm}^3)$. Anolyte: 0.5 M H_2SO_4 aqueous solution $(1,000\,\mathrm{cm}^3)$. Other conditions are as in Fig. 13.8

13.4 Conclusion

Electrochemical HDH in a SPE reactor is a promising method to treat aqueous and non-aqueous halogenated organic waste. High percentage of halogenated organics (above 95%) can be achieved with high selectivity (up to 98%), high current efficiency (up to 98.5%), high STYs (up to $8.0\,\mathrm{kg\,m^{-3}\,h^{-1}}$) and low energy consumption $(2.2\,\mathrm{kWh\,kg^{-1}})$. The cathode material had a decisive influence on HDH with respect to both reaction rate and efficiency. Palladised cathodes were much more effective than other cathodes. Moderate current densities (around $10\,\mathrm{mA\,cm^{-2}}$) promoted high rates of HDH and high efficiency. The long-term HDH, up to 250 h, demonstrated that reasonable rate and the acceptable efficiency can be achieved for continuous operation. A performance improvement can be achieved by material and process optimisation, such as optimising catalysts and reactor structure, and by maintaining high reactant concentrations via a concentrating line.

Overall the advantages of the HDH process include:

- Clean reduction using only electrons
- Minimal by-products produced
- Can operate with aqueous and non-aqueous waste streams
- Can operate with streams of varying pH and which are electrically non-conducting
- Reactor has stable operation
- Low energy consumption
- Capable to treat a large range of halogenated organics
- Potential for simultaneous reduction and oxidation.

Acknowledgment The authors thank the United Kingdom Engineering and Physical Sciences Research Council (EPSRC) for funding. The work was performed in research facilities provided through an EPSRC/HEFCE Joint Infrastructure Fund award (No. JIF4NESCEQ).

References

Appleton, E. L. (1996) A nickel-iron wall against contaminated groundwater. Environ. Sci. Technol. 30, 536A–539A.

Aramendia, M. A., Borau, V., Garcia, I. M., Jimenez, C., Marinas, J. M. and Urbano, F. J. (1999) Influence of the reaction conditions and catalytic properties on the liquid-phase hydrobromination of bromobenzene over palladium supported catalysts: activity and deactivation. Appl. Catal. B: Environ. 20, 101–110.

Balko, E. N., Przybylski, E. and Trentini, F. V. (1993) Exhaustive liquid-phase catalytic hydrodehalogenation of chlorobenzenes. Appl. Catal. B: Environ. 2, 1–8.

Bonfatti, F., Ferro, S., Lavezzo, F., Malacarne, M., Lodi, G. and Battisti, A. De (1999) Electrochemical incineration of glucose as a model organic substrate. I. Role of the electrode material. J. Electrochem. Soc. 146, 2175–2179.

Chen, G., Wang, Z. and Xia, D. (2004) Electrochemically reductive dechlorination of micro amounts of 2,4,6-trichlorophenol in aqueous medium on molybdenum oxide containing supported palladium. Electrochim. Acta 50, 933–937.

Cheng, I. F., Fernando, Q. and Korte, N. (1997) Electrochemical dechlorination of 4-chlorophenol to phenol. Environ. Sci. Technol. 31, 1074–1078.

Cheng, H., Scott, K. and Christensen, P. A. (2001) Electrochemical HDH of chlorinated organics. In: E. W. Brooman, C. M. Doyle, C. Cominellis and J. Winnick (Eds.), *Energy and Electrochemical Processes for a Cleaner Environment*, PV 2001–23, Proceedings of the International Symposium held during the 2001 Joint International Meeting of the ECS and ISE in San Francisco, CA, Fall 2001, pp. 45–58.

Cheng, H., Scott, K. and Christensen, P. A. (2003a) Electrochemical hydrodechlorination of chlorinated phenols in aqueous solutions – Part I. Material aspects. J. Electrochem. Soc. 150, D17–D24.

Cheng, H., Scott, K. and Christensen, P. A. (2003b) Electrochemical hydrodechlorination of chlorinated phenols in aqueous solutions – Part II. Effect of operating parameters. J. Electrochem. Soc. 150, D25–D29.

Cheng, H., Scott, K. and Christensen, P. A. (2003c) Hydrodehylogenation of 2, 4-dibromophenol by electrochemical reduction. J. Appl. Electrochem. 33, 893–899.

Cheng, H., Scott, K. and Christensen, P. A. (2003d) Electrolysis cell and method, The UK patent application number: 0210017.0 (Application ref. RJW/NP5966247), 2003.

Cheng, H., Scott, K. and Christensen, P. A. (2004a) Electrochemical hydrodehalogenation of 2, 4-dichlorophenol in paraffin oil and comparison with aqueous systems. J. Electroanal. Chem. 566, 131–138.

Cheng, H., Scott, K. and Christensen, P. A. (2004b) Feasibility study of electrochemical hydrodehalogenation of 2, 4-dibromophenol in a paraffin oil. Electrochim. Acta 49, 729–735.

Cheng, H., Scott, K. and Christensen, P. A. (2004c) Engineering aspects of electrochemical hydrodehalogenation of 2, 4-chlorophenol in a solid polymer electrolyte reactor. Appl. Catal. A: General 261, 1–6.

Cheng, H., Scott, K. and Christensen, P. A. (2004d) Influence of reactor design on electrochemical hydrodehalogenation of 2, 4-dibromophenol in a paraffin oil – cathode effect. Environ. Sci. Technol. 38, 638–642.

Cheng, H., Scott, K. and Christensen, P. A. (2004e) Design and operation of a solid polymer electrolyte reactor for electrochemical hydrodehalogenation. Chem. Eng. J. 102, 161–170.

Chetty, R., Christensen, P. A. and Golding, B. T. (2003) In situ FTIR studies on the electrochemical reduction of halogenated phenols. Chem. Commun. (8), 984–985.
Chetty, R., Christensen, P. A., Golding, B. T. and Scott, K. (2004) Fundamental and applied studies on the electrochemical hydrodehalogenation of halogenated phenols at a palladised titanium electrode. Appl. Catal. A: General 271, 185–194.
Connors, T. F. and Rusling, J. F. (1983) Removal of chloride from 4-chlorobiphenyl and 4, 4′-dichlorobiphenyl by electrocatalytic reduction. J. Electrochem. Soc. 130, 1120–1121.
Criddle, C. S. and McCarty, P. L. (1991) Electrolytic model system for reductive dehalogenation in aqueous environments. Environ. Sci. Technol. 25, 973–978.
Dabo, P., Cyr, A., Laplante, F., Jean, F., Menard, H. and Lessard, J. (2000) Electrocatalytic dehydrochlorination of pentachlorophenol to phenol or cyclohexanol. Environ. Sci. Technol. 34, 1265–1268.
Fennelly, J. P. and Roberts, A. L. (1998) Reaction of 1,1,1-trichloroethane with zero-valent metals and bimetallic reductants. Environ. Sci. Technol. 32, 1980–1988.
Grittini, C., Macomson, M., Fernando, Q. and Korte, N. (1995) Rapid dechlorination of polychlorinated biphenyls on the surface of a Pd/Fe bimetallic system. Environ. Sci. Technol. 29, 2898–2900.
Hitchman, M. L., Spackman, R. A., Ross, N. C. and Agra, C. (1995) Disposal methods for chlorinated aromatic waste. Chem. Soc. Rev. 423–430.
Kulikov, S. M., Plekhanov, V. P., Tsyganov, A. I., Schlimm, C. and Heitz, E. (1996) Electrochemical reductive dechlorination of chlororganic compounds on carbon cloth and metal-modified carbon cloth cathodes. Electrochim. Acta 41, 527–531.
Marrocino, J. M., Coeuret, F. and Langglois, S. (1987) A first investigation of flow-through porous electrodes made of metallic felts or foams. Electrochim. Acta 32, 1303–1309.
Matheson, L. J. and Tratnyek, P. G. (1994) Reductive dehalogenation of chlorinated methanes by iron metal. Environ. Sci. Technol. 28, 2045–2053.
O'Hannesin, S. F. and Gillham, R. W. (1998) Long-term performance of an in situ "iron wall" for remediation of VOCs, Ground Water 36, 164–170.
Schmal, D., van Erkel, J. and van Duin, P. J. (1986) Electrochemical reduction of halogenated compounds in process waster water. Ichem. Symp. Ser. 98, 259–269.
Tratnyek, P. G. (1996) Putting corrosion to use: remediating contaminated ground water with zero-valent metals. Chem. Ind. 499–503.
Yak, H. K., Wenclawiak, B. W., Cheng, I. F., Doyle, J. G. and Wai, C. M. (1999) Reductive dechlorination of polychlorinated biphenyls by zerovalent iron in subcritical Water. Environ. Sci. Technol. 33, 1307–1310.
Zanaveskin, L. N., Averganov, V. A. and Treger, Y. A. (1996) Prospects for the development of methods for the processing of organohalogen waste. Characteristic features of the catalytic hydrogenolysis of halogen-containing compounds. Russ. Chem. Rev. 65, 617–624.
Zhang, S. and Rusling, J. F. (1995) Dechlorination of polychlorinated biphenyls on soils and clay by electrolysis in a bicontinuous microemulsion. Environ. Sci. Technol. 29, 1195–1199.

Chapter 14
Preparation, Analysis and Behaviors of Ti-Based SnO_2 Electrode and the Function of Rare-Earth Doping in Aqueous Wastes Treatment

Yujie Feng, Junfeng Liu, and Haiyang Ding

14.1 Introduction: Background and Significance

Aromatic compounds are common pollutants in the waste effluent from many industrial sectors, such as petroleum refineries, synthetic chemical plants, plastics, pulp and paper, textiles, detergent, pesticide and herbicide, and pharmaceutical factories. Wastewater containing aromatic chemicals is refractory, and is often toxic to biological treatment processes. Electrochemical degradation is an attempt, which is attractive for environmental compatibilities, such as simplicity, robustness in structure, and easy operation (Walsh and Mills 1993; Esplugas et al. 1994; Masten and Davies 1994; Brillas et al. 2000; Santiago et al. 2002; Ricardo et al. 2003; Rajkumar and Palanivelu 2004), and especially electrolysis can be used as a pretreatment technology to detoxify ahead of biotreatment, rather than mineralizing them completely with high cost. EC process has the potential to be developed as a cost-effective technology for the treatment of toxic pollutants in low-volume applications.

Although organic wastes in general can be oxidized at numerous electrode materials (Beck and Schulz 1987; Comninellis 1994; James et al. 1999; Vukovic et al. 1999; Rodgers et al. 1999; Habazaki et al. 2002; Ya and Hans 2002), the electrochemical effects depend on the kinds and structure of anode materials (Stucki et al. 1991a; Feng and Li 2003). The current efficiency was usually found poor with the electrode graphite or Ni (James et al. 1999). Some organics can be degraded quickly at Pt anode, but it is reported that phenols can cause the inactivation of Pt anode by the deposition of oligomers (Comninellis and Pulgarin 1991). A great success development has been obtained since the discovery of dimensionally stable anodes (DSA) in 1966 (Beer 1976). DSA, also called dimensionally stable electrode

Y. Feng (✉)
State Key Laboratory of Urban Water Resource and Environment, Harbin Institute of Technology, No 73, Huanghe Road, Harbin 150090, Heilongjiang, People's Republic of China
e-mail: yujief@hit.edu.cn

C. Comninellis and G. Chen (eds.), *Electrochemistry for the Environment*,
DOI 10.1007/978-0-387-68318-8_14,

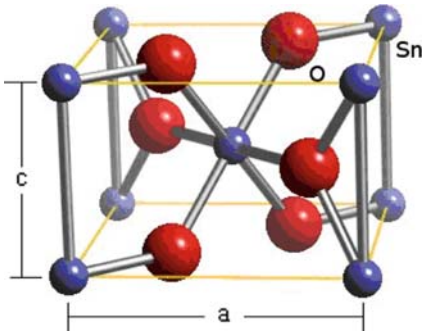

Fig. 14.1 Crystal structure of SnO_2

(DSE), precious metal-coated titanium anodes (PMTA), oxide-coated titanium anode (OCTA), or activated titanium anode (ATA) are composed of a thin layer (a few micrometers) of metal oxides (RuO_2, IrO_2, SnO_2, PbO_2, etc.) on a base metal, such as Ti, Zr, Ta, etc. (Chopra et al. 1983). Researchers' results showed that electrodes either composed of SnO_2 or with a component of SnO_2 in the catalayers can possess better degradable ability for organic degradation (Comninellis and Vercesi 1991; Stucki et al. 1991b; Comninellis and Pulgarin 1993; Houk et al. 1998; Vicent et al. 1998; Steve et al. 1999; Polcaro et al. 1999).

The structure of unit cell of SnO_2 is listed in Fig. 14.1. Sn atom is in the center of octahedron, with six oxygen atoms around. The crystal parameters of SnO_2 lies $a = b = 0.4737$ nm and $c = 0.3185$ nm. The radii of O^{2-} and Sn^{4+} are 0.14 nm and 0.071 nm, respectively (Jarzebski and Marton 1976).

Pure SnO_2 crystal is a kind of n-type semiconductor, which has wide E_g value (3.5–4.3 eV) (Kötz et al. 1991; Supothina and Guire 2000) and cannot be used as conductor. The conductivity of SnO_2 can be enhanced by adding some doping atoms. For most cases, Sb as doping atoms is applied into crystal SnO_2 and new energy bands can be induced.

In terms of heterocatalytic characteristics, it is worthy to note that the catalytic characteristics could be changed with the structure variation of the catalyst. For rare earth, there are many f-electron orbits of rare earth atoms and, when element of rare earth was doped into the DSA-coating materials, additional energy bands can be induced in the structure of coating metal oxides. This might help to develop convenient channels for electrons transition and help to enhance the electrocatalytic characteristics of the anodes also.

It is clearly important to know the different electrocatalytic behaviors of some potential DSA anodes and it is also important to obtain the influences of some incorporated elements on the properties of the resulting oxides coatings of DSA anodes. This present chapter focuses on our research related to electrochemical degradation of model substrates – phenol by the SnO_2 anode and rare-earth doping SnO_2 electrode, including fabrication electrodes, analysis method, and the evaluation of the characteristics of the electrodes.

14.2 Electrode Fabrication Methods

To achieve a catalytic layer on base materials is the "core" process for DSA-electrode fabrication. To ensure the layer stability, it is important to try to make the layer better adhesion with the base surface. We have tried several methods in the electrode preparation, including pretreatment, pyrolysis technologies, and electrodeposition. Till now, our research revealed that the electrode service life and the behaviors have been influenced by the electrode preparation methods and technological factors.

14.2.1 Pretreatment of the Ti-Base Metal

Usually there are some fatty grease or titanium oxides on the surface of fresh titanium surface, which might influence the layer solidification. The following steps should be useful for the treatment of Ti-base metal plate (Feng et al. 2003; Li et al. 2005).

- Polish thoroughly with a 80–320-grit sandpaper, till the surface became even and a little coarse.
- Degreased in 40% NaOH at 80°C for 2 h, to remove the fatty grease. And then etched in 15% oxalic acid at 98°C for 2 h to remove the oxides thoroughly in the Ti-base surface, followed by a thorough washing with deionized (DI) water. The treated Ti plates became gray, losing their metallic sheen.

14.2.2 Dip-Pyrolysis Method

"Dip" is a process that drives the Ti plates into the dipping solution, which contained elements in DSA electrodes. There are some important methods, such as puttering, spray pyrolysis, dipping, chemical vapor deposition (CVD), physical vapor deposition, etc., that can be employed in catalytic layer fabrication. We developed a kind of "dip-pyrolysis" method, including a serious repeats of "dipping – drying" and finally pyrolysis in high temperature.

In this process, the temperature and the Sb doping content are the main factors for the catalytic ability of the electrodes.

- *Calcined temperature*. Based on the degrading reaction of the component in dipping solution, temperatures of 400°C, 500°C, 600°C, 700°C, and 800°C were tested at the same pyrolysis time. From the results for phenol degradation (Fig. 14.2), a similar degradation results obtained at the pyrolysis temperature 500°C and 600°C.

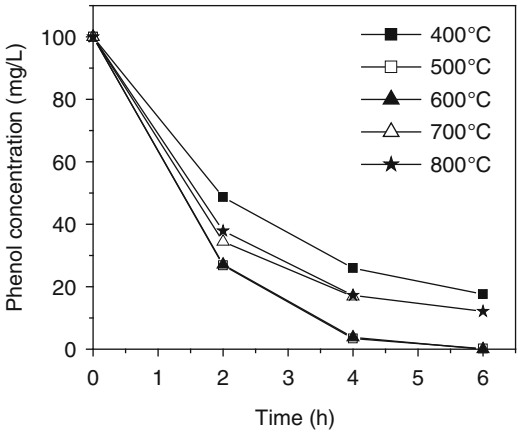

Fig. 14.2 Effect of preparation temperature on phenol degradation, phenol: 100 mg L^{-1}; electrolyte: 0.25 M Na_2SO_4; anode: SnO_2; cathode: stainless steel; current density: 10 mA cm^{-2}

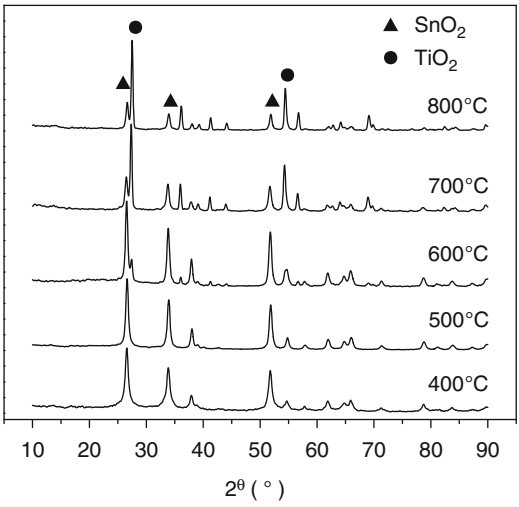

Fig. 14.3 XRD patterns of Ti/SnO_2–Sb anodes prepared at different temperature

The XRD of SnO_2 electrode at different calcined temperature (Fig. 14.3) showed that the square rutile SnO_2 can be detected at 400°C and 500°C pyrolysis temperature. When calcined temperature increased, a rutile TiO_2 can also be found in the layer which might induce poor electrocatalysis of the electrodes.

- *Content of Sb in the crystals of* SnO_2. Proper doping of Sb can increase the conductivity and also the electrocatalytic ability of the SnO_2 electrodes. Usually the behavior of the electrode do not vary much more when Sb content lies in 3–6%. But higher or smaller doping can decrease the service life of the electrode.

14.2.3 Electrodeposition

It is helpful for the electrochemical degradation ability by getting a uniform layer on base metals. Electrodeposition is convenient and is an effective way to realize this. Sb and Sn metals can be prepared either by co-electrodeposition together or by a sequencing electrodeposition. We developed a sequencing electrodeposition method which is more useful for more uniform and more effective layers.

Procedures for the preparation of Ti/SnO_2–Sb electrodes by electrodeposition method can be followed by the following steps: The Ti substrates were first cathodic electrodeposited in the sulfuric acid solution including Sn^{2+} and followed in the citric acid solution including Sb^{3+} with the same current density of 10 mA cm^{-2} at 35°C (the voltage is controlled as 3.2 V). The Sn^{2+} and Sb^{3+} irons were deposited on the Ti electrode with formation of Sn and Sb separately due to electrochemical redox process. Deposition time can be used to adjust the mole ratio of Sn/Sb. Such procedures should be repeated 3–5 times depending on the request for the electrode. Finally, the electrodes should be calcined at higher temperature for 3 h to obtain the Ti/SnO_2–Sb electrode.

The degradation curves of several kinds of electrodes in 100 mL (100 mg L^{-1}) phenol solution are shown in Fig. 14.4. Compared with other electrodes, higher catalytic activity was observed for the electrodes obtained by electrodeposition with a pyrolysis temperature of 550°C.

14.2.4 Technologies for Nanometer Coating Fabrication

Fabrication of SnO_2 nanometer coating is more difficult than that of normal coating due to the control of crystal size. There are several technologies for the fabrication of SnO_2 nanometer coating, such as sol–gel, electrodeposition, chemical vapor

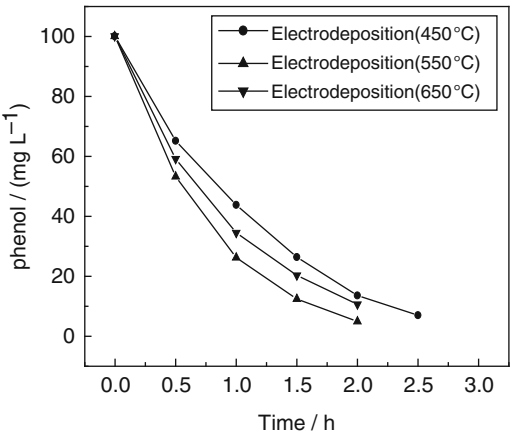

Fig. 14.4 Degradation of phenol of SnO_2 electrode prepared with electrodeposition method (with different calcined temperature)

deposition, and sputtering (Correa-lozano et al. 1996; Liu et al. 2004). But sol–gel method is a relatively simple, effective, and convenient way to realize nanocoating.

We developed a sol–gel method to fabricate the SnO_2 nanometer coating on Ti-base metal by the following steps (Liu et al. 2006). (1) *Sol solution*. The aqueous solution of $SnCl_4$ and $SbCl_3$ is added drop wise to aqueous ammonia solution and a kind of precipitation was formed. (2) *Coating solution*. The precipitation is isolated by centrifuging and washed with distilled water several times and after that dissolved in aqueous oxalic acid solution at 50–70°C. This is used as the coating solution. (3) *Dipping and pyrolysis*. Put Ti-base metal (after pretreatment) into the coating solution, then dry and heat it under air flow at a high annealing temperature for 3 h. This process should be repeated two times, and SnO_2 electrodes with nanometer coating are obtained. The pyrolysis temperature has great influences on the performance of the electrode formed (Fig. 14.5) and the temperature of 600°C was found a niche temperature for nanocoating fabrication. For the electrocatalytic ability, nanocoating is also behaved better that of the normal size of SnO_2 electrode (Fig. 14.5).

The XRD patterns of electrodes fabricated at different temperatures (Fig. 14.6) showed that rutile SnO_2 was detected at every temperature. Diffraction lines of electrode prepared at 500°C are broadened, indicating the nanosized crystallites in the surface coating of the electrode. When the annealing temperature increases from 500 to 700°C, the intensity of the peaks increases sharply and it means that the crystal of electrode surface grows more integrated. Better electrocatalytic ability can be achieved.

14.2.5 Technologies of Increasing the Life Service of the Electrodes

Although SnO_2 electrode possesses better electrocatalytic ability for organic degradation, a most important problem for the SnO_2 electrode is its shorter service life

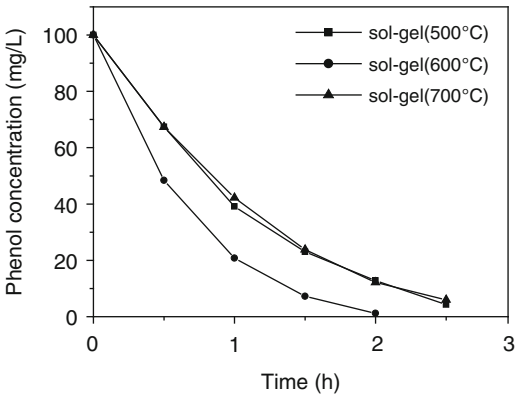

Fig. 14.5 Effect of preparation temperature on phenol degradation, phenol: 100 mg L^{-1}; electrolyte: 0.25 M Na_2SO_4; anode: SnO_2 with nanometer coating; cathode: stainless steel

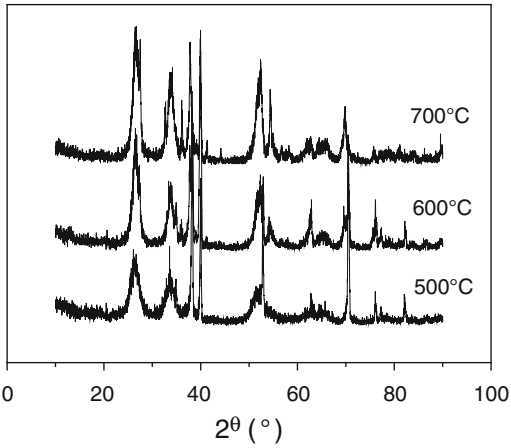

Fig. 14.6 XRD patterns of electrodes with nanometer coating prepared at different temperature

in application (Lozano et al. 1997). The factors which induced the service-life descending are very complicated and have not researched thoroughly, although we have already accumulated much more knowledge of SnO_2. Technologies of increasing the service life of SnO_2 electrode are optimizing the process of thermal oxidation, adding interlayer et al. The most effective technology is adding interlayer between Ti base and SnO_2 coating. The interlayer is regarded as a "bridge" or "glue" which can connect the base metal and the catalyst layer together.

The service life is defined as the time the electrode can be used without eletrocatalytic ability descending. The value can be got by an intensive experiment at larger electric current with the formula below

$$t = (I_1/I)^{2*} t_1,$$

where, I_1 stands for current density in larger current experiment test; I stands for normal current density; t_1 stands for service life with larger current experiment test, and t stands for service life at normal current density.

Usually it is effective to install an interlayer between Ti-base metal and the layer of SnO_2. The interlayer possesses different behavior that depends on the structure and the installation technologies. In our lab, several kinds of interlayers are designed (You et al. 2004; Cui et al. 2005; Feng and Liu 2006; Feng et al. 2006) and some achievements have been achieved (Table 14.1).

- *Electrocatalytic behavior*. The time for 100 mL (100 mg L^{-1}) phenol degradation in 0.25 M Na_2SO_4 electrolyte, $I = 0.10\,mA\,cm^{-2}$
- *Service life*. The using time calculated in larger current experiment test.
  The radius of Ru atom is in the middle of that of Sn atom and Ti atom. The three elements can form stabilized solid solution during thermal oxidation and it can resist the formation of nonconductive TiO_2. That is the reason why SnO_2 electrode with interlayer processes longer service life. RuO_2 coating has low oxygen evolution potential, which will result in low electrocatalytic

Table 14.1 Behaviors of electrodes with inter-layers

Element contained in interlayer	Electrocatalytic behavior	Service life
Co	4 h	170 days
Mn	4 h	180 days
Ru	6 h	350 days
Ru, Sn	3 h	310 days

characteristics. While doping Sn element in RuO_2 coating can obviously enhance the oxygen evolution potential of SnO_2 electrode. Therefore, SnO_2 electrodes with interlayer containing Ru and Sn elements own higher electrocatalytic characteristics and longer service life.

14.3 Analysis Method

14.3.1 Analysis of the Degradation Solution

For analysis, the degradation effects and research on the degradation pathway of organics, phenols, and some intermediates should be quantity analyzed.

The pathway of phenol degradation has been researched by some researchers (see Sect. 14.4.3). So, it is important to install an effective analysis method to investigate the intermediate variation during electrodegradation. Gas chromatograph (GC), high performance liquid chromatograph (HPLC), and also IC, UV, etc. are main measures to get these information. And it should be noted that the analysis conditions are different for different organics.

- Analysis for Phenol, Hydroquinone, Benzoquinone, and Catechol: Phenol, hydroquinone, benzoquinone and catechol can be detected with the ®C18 column (ID = 3.91 mm, length = 50 mm) and a UV detector at working wavelength of 190–400 nm. Methanol/water (1/1, V/V) can be selected as the mobile phase at a flow rate of 0.5 mL min^{-1}. $A0.2\mu m$ membrane filter is necessary before injection.
- Analysis for Intermediate Organic Acids: For the organic acids analysis, the column can be selected as Waters Symmetry® dC18 column (ID = 3.91 mm, length = 50 mm) and the wavelength for UV detector used was around 190–300 nm. The mobile phase switched to 20 mM NaH_2PO_4 at a flow rate of 0.5 mL min^{-1}. Based on the above conditions, phenol and the intermediates can be separated and analyzed (Figs. 14.7 and 14.8).

The peak at retention time of 2.609 min stands for hydroquinone, the peak (t_R = 3.200 min) is identified as benzoquinone (Fig. 14.7).

There are lots of intermediates in Fig. 14.8. Although not all the peaks can be identified in Fig. 14.8, at least some importance can be founded such

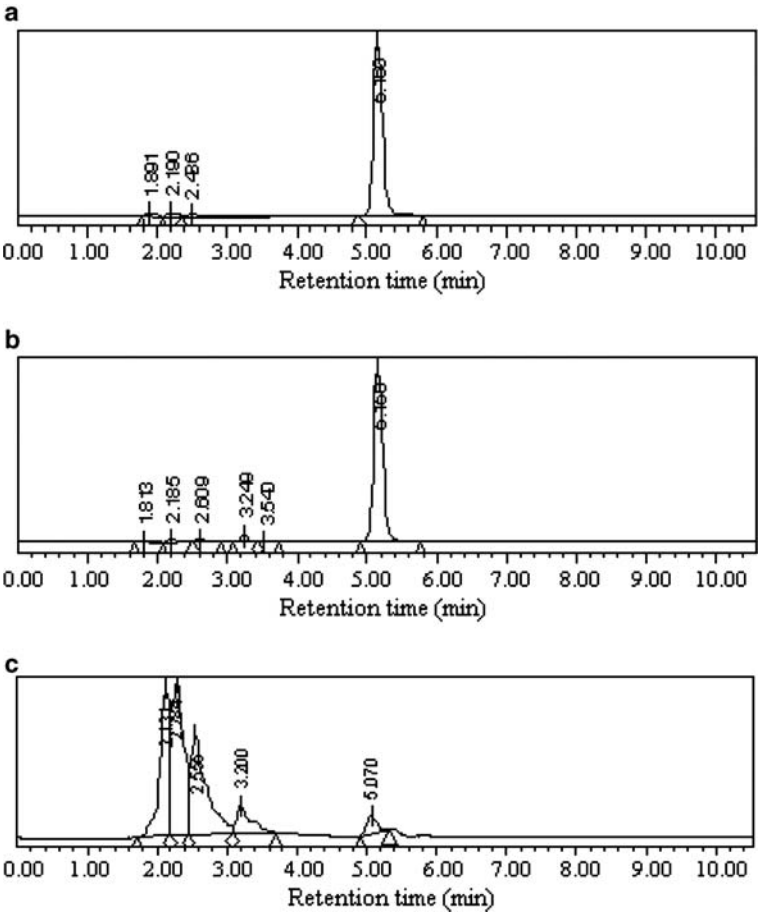

Fig. 14.7 HPLC chromatogram electrochemical degradation of phenol at **(a)** 0 min; **(b)** 15 min; and **(c)** 120 min; phenol: 100 mg L^{-1}

as formic acid ($R = 3.396$ min), α-oxoglutaric acid ($t_R = 4.457$ min), maleic acid ($t_R = 6.508$ min), fumaric acid ($t_R = 7.817$ min), and 2,4-muconic acid ($t_R = 12.167$ min). The quantification (Feng et al. 2007) of some of these intermediates was conducted with HPLC (Fig. 14.9). It is clear to see that the condition above mentioned is suitable for some intermediates' separation and quantity analysis.

UV Analysis Applied: For the whole organic amounts, we can also employ UV to know the information of organic degradation statues. Usually the scan from 200 to 400 nm and the total organic amounts can be estimated by the strength of the absorbing value. Also, some typical organic has its unique absorbing peak at some wavelength, so we can estimate the amounts of the organics. For example phenol, benzoquinone, maleic acid, etc. has their unique absorb position in UV curves (Fig. 14.10).

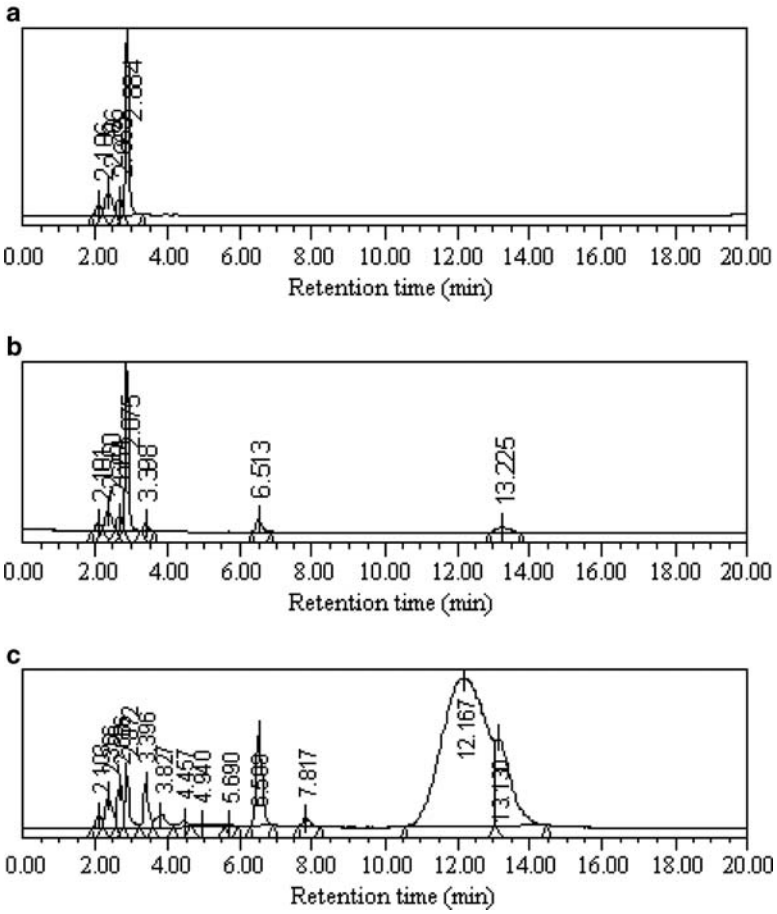

Fig. 14.8 HPLC chromatogram electrochemical degradation of phenol at **(a)** 0 min; **(b)** 15 min; and **(c)** 120 min; phenol: 100 mg L^{-1} (for organic acids analysis)

We selected several different electrodes as catalytic anodes and phenol as model substrate (Feng et al. 2003). The degradation solution was scanned at 200–400 nm. We can see that the behavior of the electrode is different (Fig. 14.11).

It can be concluded that opening of aromatic ring of phenol was taken place from the disappeared peak of 269.32 nm of phenol in the electrolysis process. Electrolysis then stops at different stage with various carboxylic acids. Much more organic compounds remained in the electrolyte when Ti/RuO_2 (a) and Ti/Sb–Sn–RuO_2 (b) were selected as anodes, and this means that oxidation ability for organic compounds on these two anodes is poor. Almost no organic substrates remained in electrolyte when $\beta - PbO_2$ (d) was selected as anodes, and lower absorbency was detected at 290 nm. These results showed that high efficiency both for phenol oxidation to benzoquinone, and benzoquinone oxidation, which is related with aromatic rings opening, can be got on lead dioxides anodes. Although relative lower organic acid

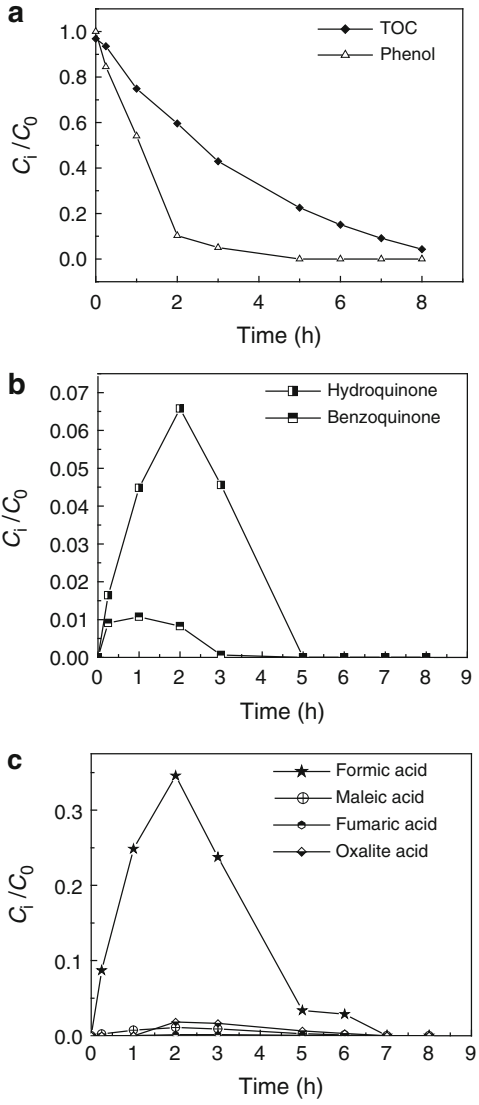

Fig. 14.9 The quantity analysis of intermediates during phenol degradation. **(a)** TOC and phenol variety; **(b)** hydroquinone and benzoquinone; and **(c)** some organic acids

remained in the electrolyte when Pt was selected as anodes, but it is obvious that Pt anodes have high efficiency for phenol oxidation and lower for benzoquinone oxidation (much more benzoquinone accumulated in the initial electrolysis period). Comparing with electrode of Ti/RuO_2 and $Ti/Sb–Sn–RuO_2$, less organic acid remained in the electrolyte when same charge passed with the electrode of Gd-doped $Ti/SnO_2–Sb_2O_3/RuO_2$ (c). The introduction of Gd makes the electrolysis to take place easier on the direction of oxidation than the direction of reduction as reported by many. The results we obtained from UV scan are corresponding with the degradation results, which showed that UV is an efficient method for analyzing the solution.

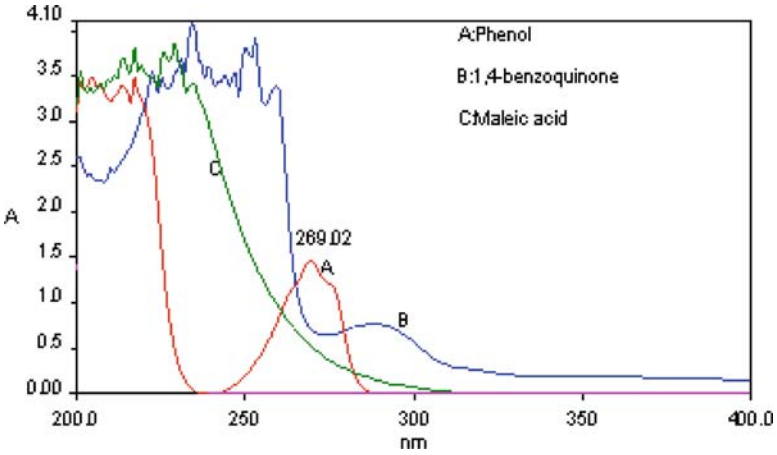

Fig. 14.10 Standard UV scan curves of phenol and some possible intermediates

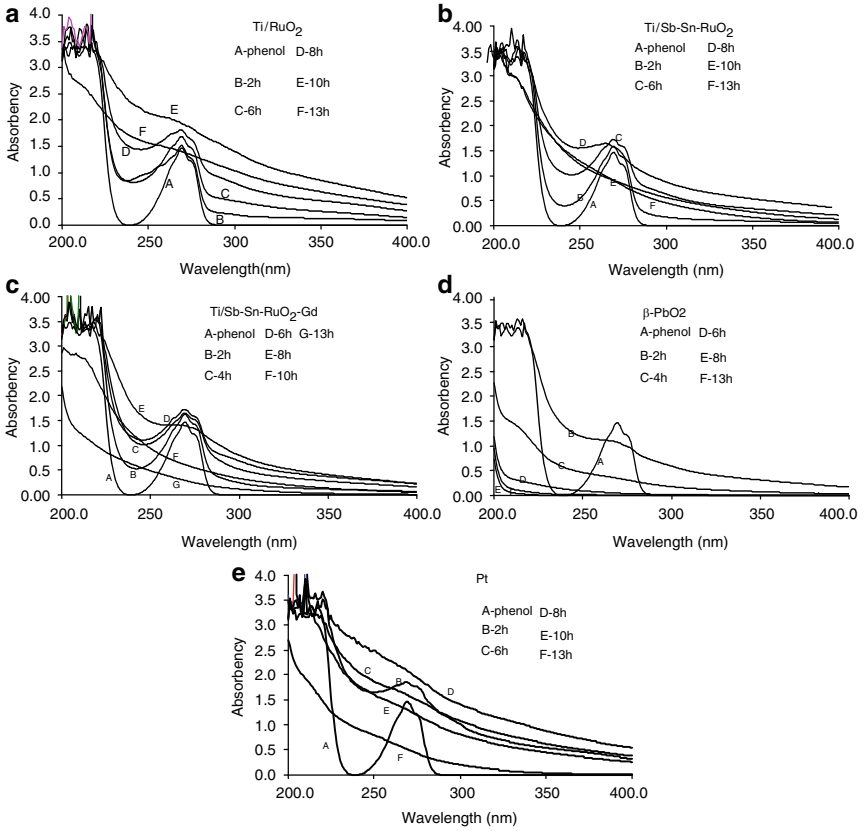

Fig. 14.11 UV scan results at 200–400 nm of the electrolyte at different electrolysis time, with electrode of **(a)** Ti/RuO_2, **(b)** $Ti/Sb–Sn–RuO_2$, **(c)** $Ti/Sb–Sn–RuO_2–Gd$, **(d)** PbO_2, and **(e)** Pt

14.3.2 Structure of the Electrodes

The molecular structure of the electrode has great influences on the behavior of the catalytic electrode, so it is important to get the exact structure information. There are many structural analysis methods being used for semiconductor materials. Here we listed some in the following sections.

14.3.2.1 Crystal Structure of Electrodes

X-ray diffraction (XRD) is a good measure to understand the structure of materials. We can get much information by XRD.

Usually we can read the electrode structure from the diffraction peaks recorded according to the JCPDS. We selected an example listed in Fig. 14.12 (Liu et al. 2006). The serial peaks appeared at 35.0°, 38.3°, 40.0°, 70.6°, and 76.1° were agreed with the Ti metal (JCPDS No.05–0682) and the peaks appeared at 26.6°, 33.7°, and 51.8° stand for SnO_2 ((JCPDS No.21–1250). Therefore, the electrode surface was mainly SnO_2 crystal processed in a tetragonal rutile-type structure. If the diffraction peaks were broadened like that of the electrode prepared at 500°C, it means the nanocrystallites in surface coating. If the intensity of peaks increases sharply, it indicates that the crystal of electrode surface grows more integrated.

The particle sizes of SnO_2 crystal in the samples can be calculated by well-known Scherrer formula from diffraction lines 110 (appeared at 26.6°). The particle sizes of electrodes prepared at 500°C, 600°C, and 700°C for 3 h were 8.5, 10.2, and 11.9 nm, respectively. This data tells us that the electrodes process nanometer structure and SnO_2 crystal of electrode surface does not reunite seriously.

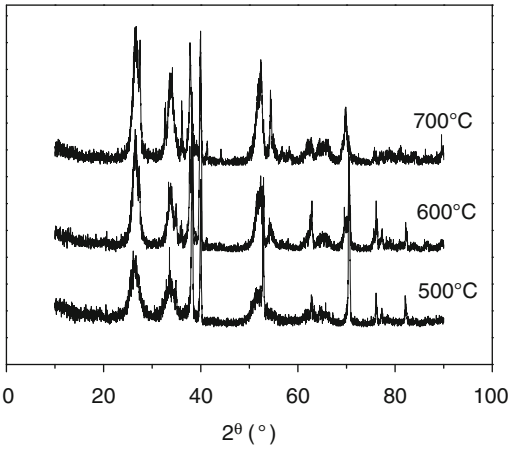

Fig. 14.12 X-ray diffraction pattern of electrodes prepared at an annealing temperature of 700°C, 600°C and 500°C for 3 h

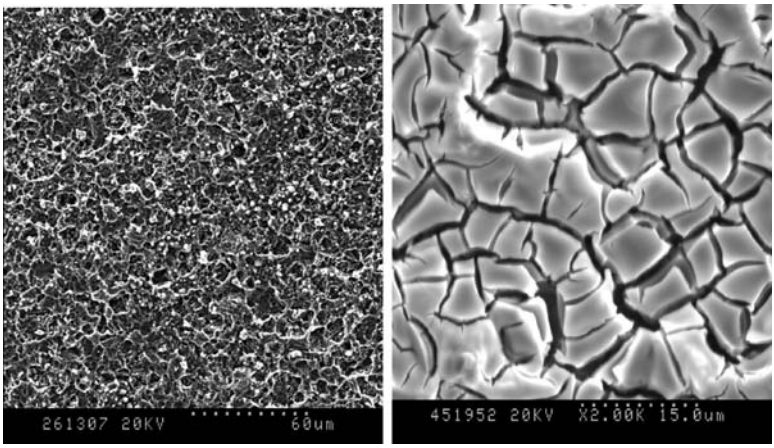

Fig. 14.13 Microstructure of SnO_2 electrodes with nanometer coating and SnO_2 electrodes with normal coating

14.3.2.2 Micrograph of the Electrodes

SEM or TEM is a useful tool to investigate the micrograph of the electrodes' surfaces. The image of the electrode can give us some information about the coating quality and implied some service-life information. For those nanometers, they also can imply some information about the crystal sizes.

Here is an example of SEM picture (Liu et al. 2006) listed in Fig. 14.13. The surface of SnO_2 electrodes with nanometer coating is covered by SnO_2 crystal symmetrically, and has no crack appeared at the surface of SnO_2 electrodes with normal coating. The cracks in the surface may cause oxidation of Ti-base metal during electrocatalytic reaction and descending of the service life. This means that SnO_2 electrodes with nanometer coating have better coating quality and longer service life. We also can use the scale marked in the bottom of SEM picture to estimate the crystal size.

14.3.2.3 Chemical Environmental Analysis with XPS

X-ray photoelectron spectroscopy (XPS), also called electron spectroscopy for chemical analysis (ESCA), is a useful measure to know chemical environment of elements in material surface. The strength of XPS is its ability to identify different chemical states. This function is useful in physics, chemistry and material science, such as oxidation/corrosion products, adsorbed species or thin-film growth processes. Analysis of insulators is possible, and XPS is also capable of semiquantitative analysis.

Table 14.2 The deconvoluted components of Sn3d5/2 in electrode with nanometer coating

Binding energy (eV)	Content (%)
486.000	2.58
486.654	97.42

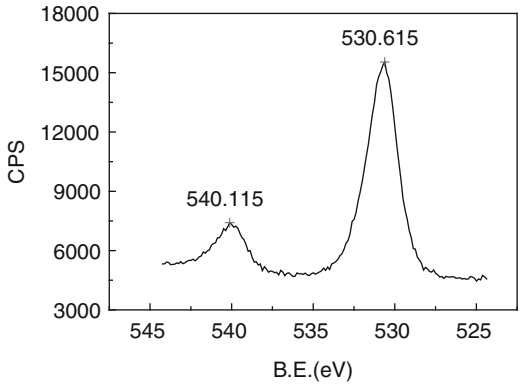

Fig. 14.14 XPS pattern of Sb3d in electrode with nanometer coating

For XPS, spectral information is collected from a depth of 2–20 atomic layers, depending on the materials studied. Different chemical states resulting from compound formation are reflected in the photoelectron peak positions and shapes. We can use it to identify the chemical states of elements in the electrode surface, and also the content of special chemical state.

Here is an example of application of XPS (Liu et al. 2006). The binding energy of $Sn3d_{5/2}$ in SnO_2 nanometer coating is 486.615 eV, and it corresponds to the standard binding energy 486.654 eV of $Sn3d_{5/2}$ in SnO_2 crystal. And the results of the deconvoluted components of $Sn3d_{5/2}$ as shown in Table 14.2 also indicate that Sn element in SnO_2 nanometer coating exists in the form of Sn (IV).

The binding energies of $Sb3d_{5/2}$ and O1s in SnO_2 nanometer coating are 530.615 eV and 530.865 eV (Figs. 14.14 and 14.15); the XPS peaks of $Sb3d_{5/2}$ and O1s were superposed. The chemical environment of Sb element can only be determined by the binding energy of $Sb3d_{3/2}$ ($E_B = 540.115$ eV). It corresponds to the standard binding energy of $Sb3d_{3/2}$ in Sb_2O_5 crystal, and Sb element in SnO_2 nanometer coating exists in the form of Sb (V).

Information of Unpaired Electrons

Electron paramagnetic resonance (EPR) is a spectroscopic technique detecting chemical species that have unpaired electrons. A great number of materials contain such paramagnetic entities, which may occur either as electrons in unfilled conduction bands, electrons trapped in radiation damaged sites, or as free radicals, various transition ions, biradicals, triplet states, impurities in semiconductors, as well as other types. Solids, liquids and gases are all accessible to EPR.

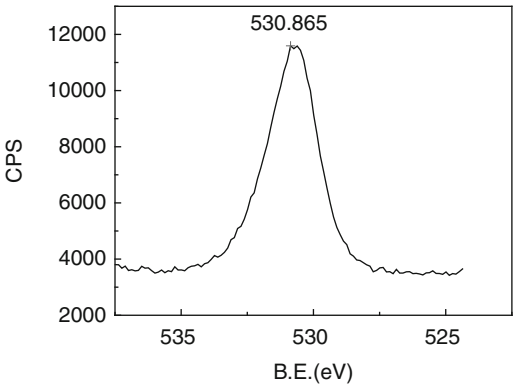

Fig. 14.15 XPS pattern of O1s in electrode with nanometer coating

Researchers are capable of obtaining detailed information about many topics of scientific interest. For example, chemical kinetics, electron exchange, electrochemical processes, crystalline structure, fundamental quantum theory, catalysis, and polymerization reactions have all been studied with great success.

We can know the information of radicals generated during EC reactions and oxygen vacancies in SnO_2 crystal lattice. We also can infer electrocatalytic characteristics from the concentration of oxygen vacancies.

Here is an example of the application of EPR (Cui et al. 2005a). Considering the fact that there are no unpaired electrons in the structure of either Sn^{4+} or Sb^{5+}, oxygen vacancy should be the only producer for EPR signals of all the samples. The g values of electrodes with Sb doping amount 6% and 12% are 14.6 and 6.2 (Fig. 14.16). Higher g value enable electrode to have more oxygen vacancy and better electrocatalytic ability. It is easy to understand that the concentration of oxygen vacancies in SnO_2 crystal lattice decreased with increasing of Sb atoms, as the higher valence of Sb^{5+} needs more oxygen atoms to make charge balance when Sn^{4+} atoms in crystal lattice are replaced.

14.3.3 Electrochemical Analysis

14.3.3.1 Cyclic Voltammograms Analysis

Cyclic voltammograms (CV) is a kind of electrochemical analysis method and is a linear-sweep voltammetry with the scan continued in the reverse direction at the end of the first scan; this cycle can be repeated a number of times. Usually it is used in the field of electrochemistry. The function of CV in electrocatalytic analysis of electrodes might be in these parts (a) kinetics; (b) mechanism of electrode reactions; and (c) corrosion studies.

Here we give an example listed in Figs. 14.17 and 14.18 to give a whole image of how to use CV to analysis electrode ability. From Fig. 14.17 (Pt, Ti/RuO_2,

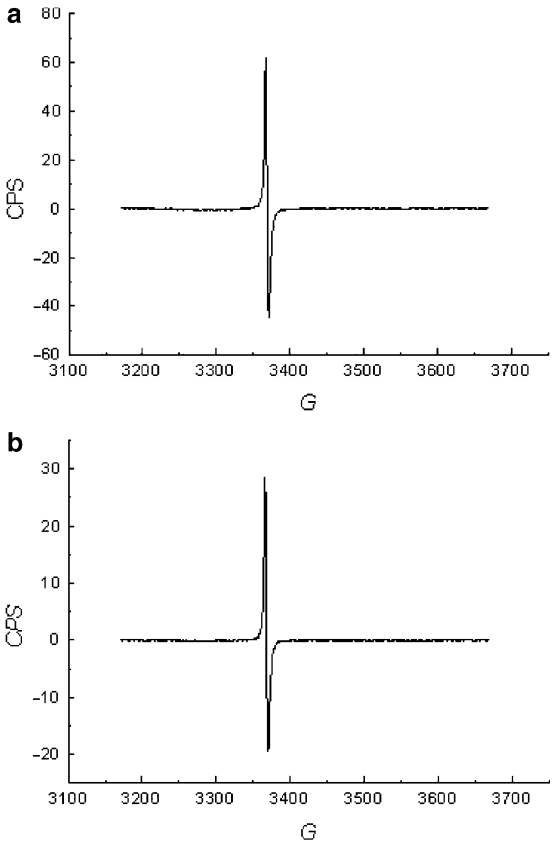

Fig. 14.16 EPR spectrum of electrodes with Sb doping amount 6% **(a)** and 12% **(b)**

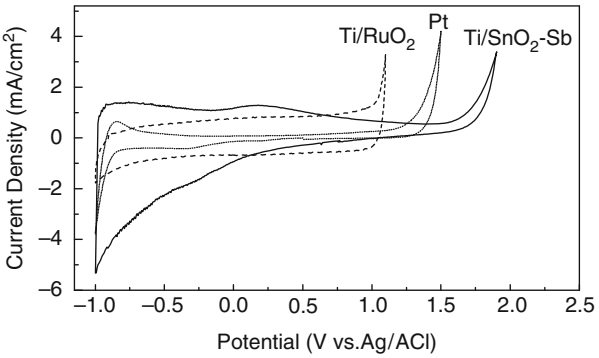

Fig. 14.17 Comparison of cyclic voltammograms of several electrodes in 0.25 mol L^{-1} Na_2SO_4 solution

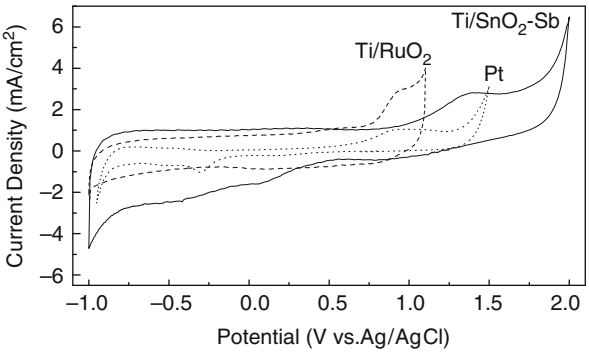

Fig. 14.18 Comparison of cyclic voltammograms of several electrodes in 0.25 mol L^{-1} Na_2SO_4 solution (phenol concentration = 500 mg L^{-1})

and Ti/SnO_2–Sb electrodes in 0.25 mol $L^{-1}$$Na_2SO_4$ solution absent of phenol), a great difference among oxygen evolution reaction of Pt, Ti/RuO_2, and Ti/SnO_2–Sb electrodes can be found, and their oxygen evolution potentials is in the sequence of Ti/RuO_2 < Pt < Ti/SnO_2–Sb. Figure 14.18 exhibits cyclic voltammograms of Pt, Ti/RuO_2, and Ti/SnO_2–Sb electrodes in 0.25 mol $L^{-1}$$Na_2SO_4$ solution with 500 mg L^{-1} phenol. Compared with Figs. 14.17 and 14.18, in 0.25 mol $L^{-1}$$Na_2SO_4$ solution with 500 mg L^{-1} phenol system, oxygen peaks of Pt, Ti/RuO_2, and Ti/SnO_2–Sb electrodes existed at 0.93 V, 0.95 V, and 1.40 V (vs. Ag/AgCl), respectively. The oxygen peaks can be considered as the phenol oxide/redox reaction peaks occurring at the surface of Pt, Ti/RuO_2, and Ti/SnO_2–Sb electrodes. From Fig. 14.18, electrocatalytic oxidation of phenol occurring on the surface of Pt, Ti/RuO_2, and Ti/SnO_2–Sb electrodes is irreversible. The oxidation potentials of phenol on the Pt, Ti/RuO_2, and Ti/SnO_2–Sb electrodes are different due to the different oxidation paths for phenol, which is resulting from the varied structures of Pt, Ti/RuO_2, and Ti/SnO_2–Sb electrodes (Ding et al. 2007). In addition, the current values of phenol oxidation peaks for Pt, Ti/RuO_2, and Ti/SnO_2–Sb electrodes are varied, whose sequence is Pt < Ti/SnO_2–Sb < Ti/RuO_2. The current value of oxidation peak is lower than that of Ti/RuO_2 and Ti/SnO_2–Sb electrodes, indicating that Pt electrode has poorer ability on direct electrocatalytic oxidation of phenol than Ti/RuO_2 and Ti/SnO_2–Sb electrodes, and Ti/RuO_2 electrodes have the strongest ability on direct electrocatalytic oxidation of phenol. However, the past study of our work showed that the capacity of degradation of phenol by these electrodes was in the sequence of Ti/RuO_2 < Pt < Ti/SnO_2–Sb (Li et al. 2005), which was not corresponding with their capacity by direct electrocatalytic oxidation of phenol. This indicated that there was an indirect electrocatalytic oxidation process occurring during the degradation of phenol. Indirect electrocatalytic oxidation process can produce high active group (such as $^{\cdot}OH$) with strong oxidation capacity, which can degrade and oxide the organics and enhance the electrocatalytic oxidation capacity of the electrodes.

14.3.3.2 Tafel Curve

Tafel curve is overpotential of the electrode and the current density passing through the electrode $\eta = a + b \log i$, is an efficient measure to be applied in electrochemistry. The Tafel slope can be used to address the catalytic activity of the catalytic material and also provide information about the mechanism of the reaction. Here we also give an example to address this (Fig. 14.19).

Tafel curves of Pt, Ti/RuO_2, and Ti/SnO_2–Sb were tested using polarization in 0.1 mol $L^{-1}H_2SO_4$ solution, as shown in Fig. 14.19. The logarithm of current density is in line with the potentials of the electrodes, which is corresponding to Tafel equation (14.1)

$$\eta = a + b \log I, \tag{14.1}$$

where b can be obtained from (14.1)

$$b = \frac{\partial \eta}{\partial \log I}. \tag{14.2}$$

From Fig. 14.19, the evolution potentials of the electrodes are in the sequence of $Ti/RuO_2 < Pt < Ti/SnO_2$–Sb, which is in accordance with the oxygen evolution sequence of $Ti/RuO_2 < Pt < Ti/SnO_2$–Sb obtained from Figs. 14.1 and 14.2. The oxygen evolution potentials of the electrodes are different due to their varied material compositions, and different conditions for preparing the electrodes resulted in varied structures, properties, and oxygen evolution potentials of the electrodes. The oxygen evolution potentials of Ti/RuO_2, Pt, and Ti/SnO_2–Sb electrodes with the current density of 0.1 mA cm^{-2} are in the sequence of 1.19, 1.51, and 1.81 V (vs. Ag/AgCl), respectively. According to (14.2), the slopes of Tafel curves for Ti/RuO_2, Pt, and Ti/SnO_2–Sb electrodes are 50, 150, and 450 mV, respectively. The slope values of Tafel curves for different electrodes reflect the dominating steps of oxygen evolution reaction. When anodic potential enhances, active site (M) on the electrode has electrochemical reaction with H_2O with product of M–OH (Johnson et al. 2000).

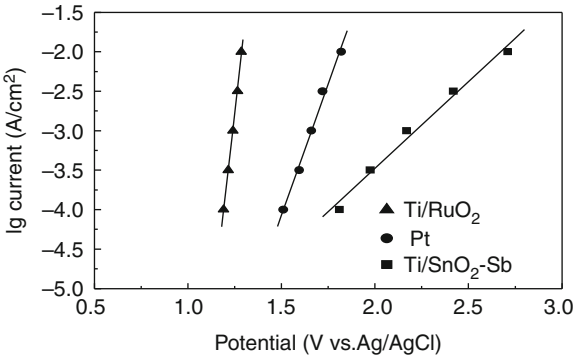

Fig. 14.19 The Tafel curves of Pt, Ti/RuO_2, and Ti/SnO_2–Sb electrodes

Ti/SnO_2–Sb electrode has higher oxygen evolution potential and oxygen evolution becomes difficult, which facilitates the reaction from M–OH to ·OH. The difference of the oxygen evolution potentials of Ti/RuO_2, Pt, and Ti/SnO_2–Sb electrodes becomes evident electrodes with high current density. For example, the oxygen evolution of Ti/SnO_2–Sb electrode is 1.4 V higher than that of Ti/RuO_2 electrode with the current density of 10 mA cm^{-2}, which indicates that Ti/SnO_2–Sb electrode restrains oxygen evolution more seriously than that of Ti/RuO_2 electrode, and Ti/SnO_2–Sb electrode needs higher oxygen evolution potential to have the same oxygen evolution reaction rate for Ti/RuO_2 electrode. Therefore, Ti/SnO_2–Sb electrode can produce more ·OH with higher current density, which accords with the prophase result (Zhao et al. 2000).

14.3.3.3 Electrochemical Impedance Spectroscopy Tests

Electrochemical impedance spectroscopy (EIS) is a powerful tool for examining the processes occurring at the electrode surfaces. EIS is a kind of electrochemical analysis method which can be used in the characterization of batteries, fuel cells, and corrosion phenomena.

Comparisons of electrochemical impedance spectroscopy of freshly prepared electrodes and after accelerated life test can give us some information of the deactivation mechanism.

Figure 14.20 listed the EIS results of SnO_2 electrode in 0.5 mol L^{-1} H_2SO_4 solution and 1.0 mol L^{-1} NaOH solution. The potentials are 2.0 and 1.0 V (vs. Ag/AgCl), respectively, and the frequency range is 100 kHz–100 mHz. It is evident that the impedance arcs are enhanced greatly after the service-life tests, indicating increased resistance. The equivalent circuit which best fits the experimental EIS data is a R_s ($C_f R_f$) ($C_d R_{ct}$) combination, as shown in Fig. 14.21. R_s, C_f, R_f, C_d, and R_{ct} correspond to solution resistance, membrane capacitance, membrane resistance, double layer capacitance, and charge-transfer resistance, respectively. The simulated results are listed in Table 14.3. Seen from Table 14.3, the membrane resistance and the charge-transfer resistance is enhanced greatly after accelerated life tests both in 0.5 mol L^{-1} H_2SO_4 solution and 1.0 mol L^{-1} NaOH solution. The membrane resistances of the freshly prepared electrode are 4.29 and 2.95 Ω, and they are 1,231 and 90.55 Ω after the accelerated life tests in 0.5 mol L^{-1} H_2SO_4 solution and 1.0 mol L^{-1} NaOH solution, respectively. However, the membrane capacitance of the electrode was reduced to 10% of the original value or so, which explained that the electrode activity sites decreased greatly. The double capacitance varied more significantly between the freshly prepared electrode and after accelerated life tests, with 1.0% of the original value or more. It is implied that the electrode surface was occupied by the electrochemical inertia matter, and the charge-transfer resistance increased, resulting in hard charge transfer. It is probable that the TiO_2 membrane with poor conductivity is formed on the electrode surface.

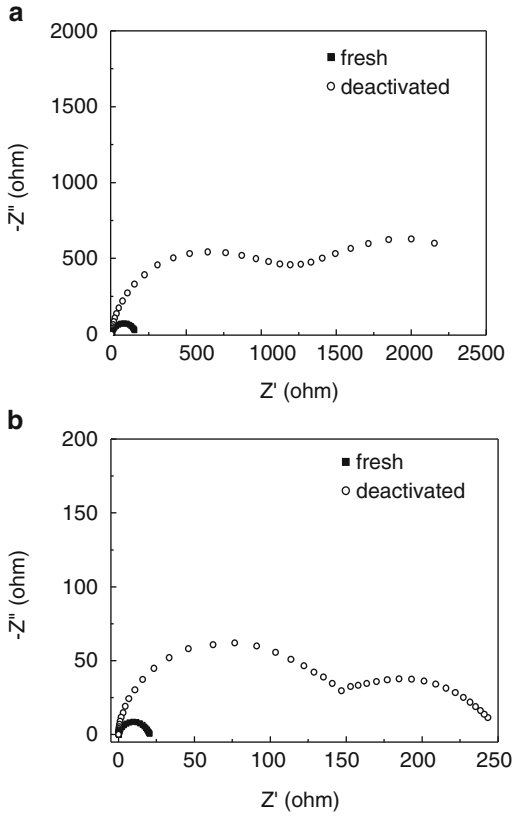

Fig. 14.20 Comparison of electrochemical impedance spectra of freshly prepared electrodes and after accelerated life test in 0.5 mol L^{-1} H_2SO_4 solution **(a)** and in 1.0 mol L^{-1} NaOH solution **(b)**

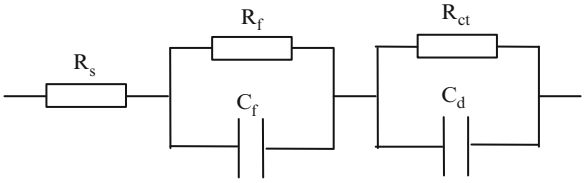

Fig. 14.21 Equivalent circuit used in the simulation of the experimental results

Table 14.3 Simulated results of EIS

Solution	Electrode	C_f (mF)	R_f (Ω)	C_d (mF)	R_{ct} (Ω)
H_2SO_4	Fresh	5.92	4.59	1.59	342
	Deactivated	0.618	1,231	1.8×10^{-2}	1,157
NaOH	Fresh	8.03	2.95	4.13	16.3
	Deactivated	0.911	90.6	9.38×10^{-3}	140.3

14.3.4 Summary

Available analysis methods are important for evaluation of the electrocatalytic abilities of electrodes. It is complicated to have a whole estimation system. New evaluation, new technologies, and methods are always needed and also very important for developing new electrode materials.

14.4 Characteristics of Rare-earth Doped Ti-Base SnO_2 Electrode

14.4.1 Sb Doping SnO_2 Electrode

For organic compounds degradation, Ti-base SnO_2 electrodes showed better behaviors than any other DSA electrodes, especially for the nanostructure.

Figure 14.22 listed a result both for nano- and normal size SnO_2 electrodes. The degradation possesses first-order regulation and the kinetic parameter is 0.03479, which is much higher than reported (Beck and Schulz 1987; Panizza et al. 2000; Cui et al. 2005).

For nanocoating and normal size SnO_2, they both have crystal structure with tetragonal rutile-type structure, but crystals of SnO_2 with nanosize are smaller and have higher concentration of oxygen vacancies. Smaller crystal size means larger surface area, and enables more reaction to take place together. Higher concentration of oxygen vacancies means that oxidation of organic compounds is the main reaction instead of oxygen evolution reaction. SnO_2 nanometer coating has no cracks, while SnO_2 normal coating has many cracks. More cracks in electrode surface can cause descending of the service life. Therefore, different structures bring them different abilities.

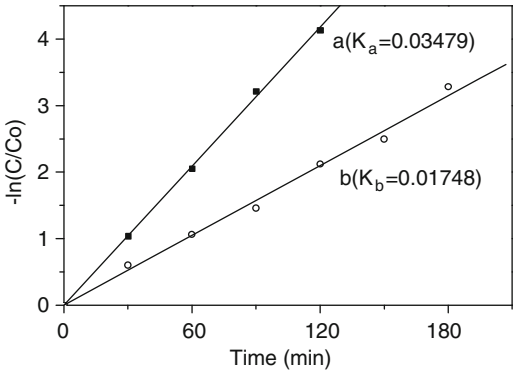

Fig. 14.22 Phenol degradation dynamics of electrode with nanometer coating **(a)** and electrode with normal coating **(b)**

14.4.2 *Effects of Rare-Earth Doping on Structure and Performance of Ti/Sb–SnO_2 Electrode*

Four kinds of rare-earth (Dy, Eu, Nd and Gd) doping SnO_2 electrodes were prepared by following the conditions described before (Cui et al. 2004; Wang and Feng 2005; Feng et al. 2005; Wang et al. 2005).

Till now, we do not wholly understand for the mechanism and rare-earth function on the electrode ability. But our research showed that the oxygen evolution potential varied in different rare-earth doping and this might be confirmed by the main factors which have relation with the catalytic ability as shown in Fig. 14.23. Figure 14.24 displayed Tafel curves of earth-doped Ti/SnO_2–Sb electrodes measured at 2.0–2.5 V(vs. Ag/AgCl).The electrode has higher oxygen evolution potential, and it facilitates to produce more OH. The electrode with higher oxygen evolution potential would have stronger activity of catalytic oxidation of the organics. Therefore, the electrocatalytic activity of earth-doped Ti/SnO_2–Sb electrodes was in the following sequence: Ti/SnO_2–Sb–Nd electrode > Ti/SnO_2–Sb–Dy electrode > Ti/SnO_2–Sb–Gd electrode > Ti/SnO_2–Sb–Eu electrode.

There are many other factors which can influence Cerium, Europium, Gadolinium, and Dysprosium on electrocatalytic ability of Ti/Sb–SnO_2 anodes, such as heat-treatment temperature, REs content, etc. Usually different micrographs of the electrodes can also induce variation of the ability of the electrodes. With an energy dispersive spectrometer (EDS), we also found that REs and Sb atoms were both enriched toward anode's surface layer when REs were introduced (Table 14.4). X-ray diffraction (XRD) implied some characteristics of the coating crystal structure. The unit cell of SnO_2 on REs-doped Ti/Sb–SnO_2 anodes expanded slightly compared with Ti/Sb–SnO_2 anode. Introducing Eu, Gd, and Dy restrained the upgrowth of SnO_2 grains while Ce slightly promoted its upgrowth. Based on the experimental and the theoretical analysis, it is argued that the electrocatalytic activity of SnO_2 anodes might be influenced by lattice oxygen, active sites, crystal grain size, metal ion redox couples, and oxygen evolution potential.

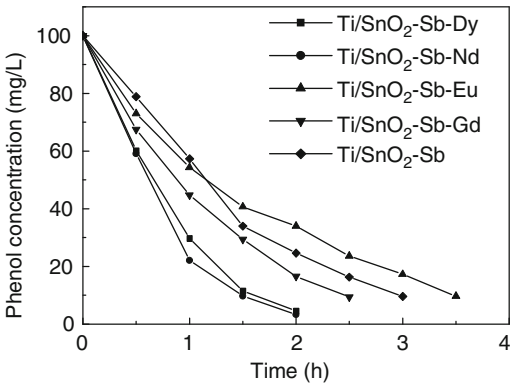

Fig. 14.23 Phenol degradation on different electrode with rare earth doping

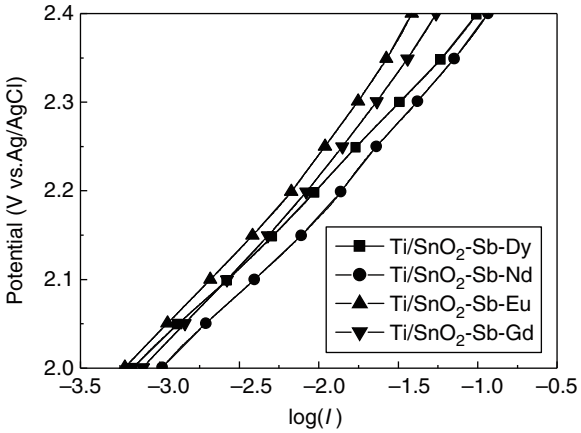

Fig. 14.24 Tafel curves of Dy, Nd, Eu, and Gd doped Ti/Tafel curves of Dy, Nd, Eu, and Gd doped Ti/SnO2–Sb electrodes in 0.5 M H_2SO_4 solution

Table 14.4 EDS data of REs and Sb-doped Ti/Sb–SnO_2 electrodes

Electrode samples	Sn	Sb/mol%		Gd/mol%	
		Theory data	Practice data	Theory data	Practice data
Ce/2%	100	6.4	18.22	2.0	9.24
Gd/2%	100		6.53	2.0	8.04
Eu/2%	100		13.7	2.0	10.6
Dy/2%	100		13.69	2.0	5.52

14.4.3 Reaction Pathway of Electrochemical Degradation of Phenol on Ti/SnO_2–Sb Electrodes

Till now, many degradation pathways have been proposed by some researchers. Basically, the phenol degradation was regarded as basic three process (1) from phenol to benzoquinone, catechol and hytroquinone, (2) organic acids formed based on aromatic rings being opened and (3) the organic acids transformed to CO_2 and H_2O (Howard 1984; Comninellis and Pulgarin 1993; Boudence 1996; Duprez 1996; Steve 1999; Santos 2005)

$$\text{Phenol} \rightarrow \text{aromatic intermediates} \rightarrow \text{fatty acids} \rightarrow H_2O + CO_2$$

A possible pathway was proposed in our previous study (6), which was proposed deepens on different electrode structure (Fig. 14.25).

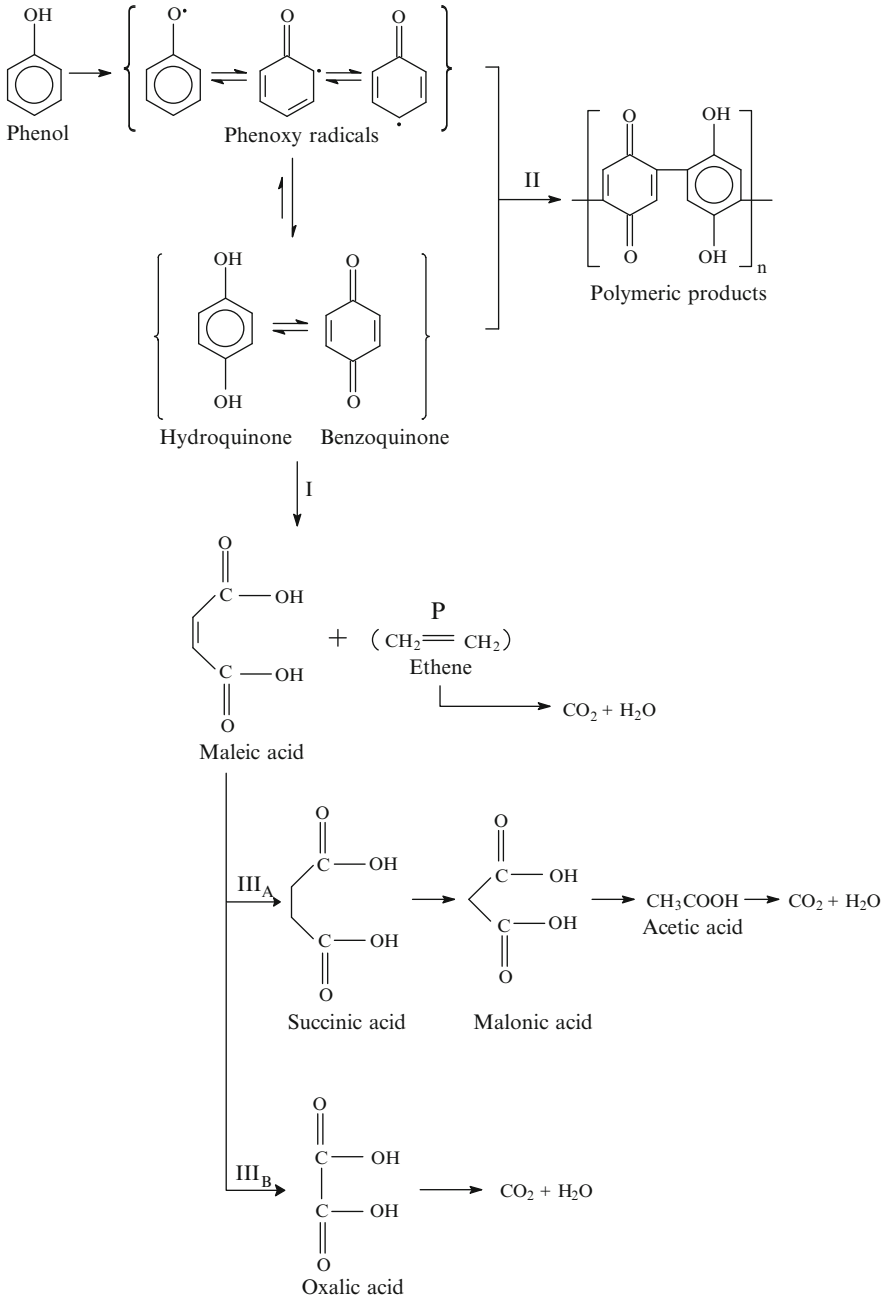

Fig. 14.25 Phenol degradation pathway

14.4.4 Summary

The section presented some information about the SnO_2 electrode and rare-earth doped SnO_2 electrode on the electrochemical phenol degradation process, and should be helpful for the application of electrocatalysis in the field of environment as well as for the preparation of electrocatalytic anodes.

SnO_2 electrode with nanostructure have better behaviors on phenol degradation than the electrode with nanosize. Rare-earth doping can change the electrode behavior and appropriate doping can enhance the ability for the electrode to electrocatalytic degradation of phenols. The electrode structures have great influences on the behavior of organic degradation and on the degradation pathway.

Acknowledgment The author thanks his students, Junfeng Liu, Haiyang Ding, Yuhong Cui, Baiyan Cui, Zhengqian Liu, etc., who finished most of the data in this part, and also thanks Junfeng Liu and Haiyang Ding for their efforts in editing the words and drawing the figures. The author also thanks Dr. X. Y. Li in the University of Hong Kong for his support on some analysis for phenol degradation and some creative suggestion on the students' research. The project is supported by the National Science Fund of China (50278022 and 50638020), the Chinese 973 Key Project (2004CB41850), and also the Provincial Science Fund for Excellent Youth in Heilongjiang Province. The author also thanks the financial support of the research.

References

Beck, F. and Schulz, H. (1987) Cr–Ti–Sb oxide composite anodes, electro-organic oxidation. J. Appl. Electrochem. 17, 914–924.

Beer, H.B. (1976) Electrodes and coating thereof. US Patent 3632498.

Boudence, J.L. (1996) Electrochemical oxidation of aqueous phenol at a carbon black slurry electrode. J. Appl. Catal. A, General 143, 185–202.

Brillas, E., Calpe, J.C. and Casado, J. (2000) Mineralization of 2, 4-D by advanced electrochemical oxidation processes. Water Res. 34, 2253–2262.

Chopra, K. L., Major, S. and Pandya, D.K. (1983) Transparent conductors – A status review. Thin Solid Film 102, 1–15.

Comninellis, C. (1994) Electrocatalysis in the electrochemical conversion/combussion of organic pollutants for waste water treatment. Electrochem. Acta 39(11/12), 1857–1862.

Comninellis, C. and Pulgarin, C. (1991) Anodic oxidation of phenol for waste water treatment. J. Appl. Electrochem. 21, 703–708.

Comninellis, C. and Pulgarin, C. (1993) Electrochemical oxidation of phenol for wastewater treatment using SnO_2 anodes. J. Appl. Electrochem. 23, 108–112.

Comninellis, C. and Vercesi, G.P. (1991) Characterization of DSA-type oxygen evolving electrodes, choice of coating. J. Appl. Electrochem. 21(4), 335–340.

Correa-lozano, B., Comninellis, C. and Battisti, A.D. (1996) Preparation of SnO_2–Sb_2O_5 films by the spray pyrolysis technique. J. Appl. Electrochem. 26, 83–89.

Cui, Y.H. and Feng, Y.J. (2005) EPR study on Sb doped Ti-base SnO_2 electrodes. J. Mater. Sci. 40(17), 4695–4697.

Cui, Y.H., Liu, Z.Q., Liu, Z.G. and Feng, Y.J. (2004) Preparation and investigation of Ti-based SnO_2 electrode doped with Ce element. J. Funct. Mater. 35, 2035–2039 (in Chinese).

Cui, Y.H., Feng, Y.J. and Liu, J.F. (2005a) Performance of Ti-base SnO_2 electrode with an interlayer containing Mn element. Chin. J. Mater. Res. 19(1), 47–53 (in Chinese).

Cui, Y.H., Feng, Y.J. and Liu, J.F. (2005b) Preparation and characterization on Sb doped Ti-base SnO_2 electro-catalytic electrodes. J. Funct. Mater. 36(2), 234–237 (in Chinese).
Ding, H.Y., Feng, Y.J. and Liu, J.F. (2007) Comparison of electrocatalytic performance of different anodes with cyclic voltammetry and Tafel curves. Chin. J. Catal. 28(7), 646–650 (in Chinese).
Duprez, D. (1996) Catalytic oxidation of organic compounds in aqueous media. Catal. Today 29, 317–322.
Esplugas, S., Yue, P.L. and Perverz, M.I. (1994) Degradation of 4-chlorophenol by photolytic oxidation. Water Res. 28, 1323–1328.
Feng, Y. J. and Li, X.Y. (2003) Electro-catalytic oxidation of phenol on several metal-oxide electrodes in aqueous solution. Water Res. 37(10), 2399–2407.
Feng, Y.J. and Liu, J.F. (2006) Preparation of a kind of DSA electrode with nanometer coating. 200610010182.6.
Feng, Y.J., Cui, Y.H. and Wang, J.J. (2005) Preparation and characterization of Dy doped Ti-base SnO_2/Sb electro-catalytic electrodes. Chin. J. Inorganic Chem. 21(6), 836–841 (in Chinese).
Feng, Y.J., Cui, Y.H. and Liu, J.F. (2006) Preparation method of rare-earths doped SnO_2 electrode based on Ti. 200610010184.5.
Feng, Y.J., Cui, B.Y., Li, X.Y., Cui, Y.H. and Liu, J.F. (2007) Degradation pathway of electrochemical oxidation of phenol on Ti base SnO2 anode. 207th ACS Meeting, August, Boston, USA.
Habazaki, H., Hayashi, Y. and Konno, H. (2002) Characterization of electrodeposited WO_3 films and its application to electrochemical wastewater treatment. Electrochim. Acta 47, 4181–4188.
Houk, L.L., Johnson, S.K., Feng, J., Houk, R.S. and Johnson, D.C. (1998) Electrochemical incineration of benzoquinone in aqueous media using a quaternary metal oxide electrode in the absence of a soluble supporting electrolyte. J. Appl. Electrochem. 28, 1167–1177.
Howard, R.D. (1984) Mechanism of the oxidation of aqueous phenol with dissolved oxygen. Ind. Eng. Chem. Fundam. 23, 387–392.
James, D.R., Wojciech, J. and Nigel, J.B. (1999) Electrochemical oxidation of chlorinated phenols. Environ. Sci. Technol. 33, 1453–1457.
Jarzebski, Z.M. and Marton, J.P. (1976) Physical properties of SnO_2 materials. Preparation and defect structure. J. Electrochem. Soc. 123(7), 199C–205C.
Johnson, D.C., Feng, J. and Houk L.L. (2000) Direct electrochemical degradation of organic wastes in aqueous media. Electrochim. Acta 46(2–3), 323–330.
Kötz, R., Stucki, S. and Carcer, B. (1991) Electrochemical waste water treatment using high overvoltage anodes. Part I, Physical and electrochemical properties of SnO_2 anodes. J. Appl. Electrochem. 21, 14–20.
Li, X.Y., Cui, Y.H., Feng, Y.J., Xie, Z.M. and Gu, J.D. (2005) Reaction pathways and mechanisms of the electrochemical degradation of phenol on different electrodes. Water Res. 39(10), 1972–1981.
Liu, P.Y., Chen, J.F. and Sun, W.D. (2004) Characterizations of SnO_2 and SnO_2, Sb thin films prepared by PECVD. Vacuum 76, 7–11.
Liu, J.F., Feng, Y.J., Sun, L.X. and Qian, Z.G. (2006) Investigation on preparation and electrocatalytic characteristics of Ti-base SnO_2 electrode with nano-coating. Mater. Sci. Technol. 14(2), 200–203 (in Chinese).
Lozano, B.C., Comnonellis, C. and Battisti, A.D. (1997) Service life of Ti/SnO_2–Sb_2O_5 anodes. J. Appl. Electrochem. 27, 970–974.
Masten, S.J. and Davies, S.H. (1994) The use of ozonation to degrade organic contaminants in wastewaters. Environ. Sci. Technol. 28, 180A–185A.
Panizza, M., Bocca, C. and Cerisola, G. (2000) Electrochemical treatment of wastewater containing polyaromatic organic pollutants. Water Res. 34(9), 2601–2605.
Polcaro, A.M., Palmas, S. and Renoldi, F. (1999) On the performance of Ti/SnO_2 and Ti/PbO_2 anodes in electrochemical degradation of 2-chlorophenol for wastewater treatment. J. Appl. Electrochem. 29(2), 147–151.
Rajkumar, D. and Palanivelu, K. (2004) Electrochemical treatment of industrial wastewater. J. Hazard. Mater. B113, 123–129.

Ricardo, A.T., Victor, S. and Walter, T. (2003) Electrochemical treatment of industrial wastewater containing 5-amino-6-methyl-2-benzimidazolone. Toward an electrochemical–biological coupling. Water Res. 37, 3118–3124.

Rodgers, J.D., Jedral, W. and Bunce, N.J. (1999) Electrochemical oxidation of chlorinated phenols. Environ. Sci. Technol. 33(9), 1453–1457.

Santiago, E., Jaime, G. and Sandra, C. (2002) Comparison of different advanced oxidation processes for phenol degradation. Water Res. 36, 1034–1042.

Santos, A. (2005) Kinetic model of wet oxidation of phenol at basic pH using a copper catalyst. Chem. Eng. Sci. 60, 4866–4878.

Steve, K.J. (1999) Electrochemical incineration of 4-chlorophenol of products and intermediates by mass spectrometry. J. Environ. Sci. Technol. 33, 2638–2644.

Steve, K.J., Linda, L.H., Feng, J., Houk, R.S. and Johnson, D.C. (1999) Electro-chemical incineration of 4-chlorophenol and the identification of products and intermediates by mass spectrometry. Environ. Sci. Technol. 33, 2638–2644.

Stucki, S., Kötz, R., Carcer, B. and Suter, W. J. (1991a) Electrochemical waste-water treatment using high overvoltage anodes. 2. Anode performance and applications. Appl. Electrochem. 21, 99–104.

Stucki, S., kötz, R., Carcer, B., et al. (1991b) Electrochemical waste water treatment using high overvoltage anodes. Part II, Anode performance and applications. J. Appl. Electrochem. 21(2), 99–104.

Supothina, S. and Guire, M.R.D. (2000) Characterization of SnO_2 thin films grown from aqueous solutions. Thin Solid Films 371, 1–9.

Vicent, E., Morallon, E., Quijada, C. and Vazquez, J.L. (1998) Characterization and stability of doped SnO_2 anodes. J. Appl. Electrochem. 28, 607–612.

Vukovic, M., Marijan, D. and Cukman, D. (1999) Electrocatalytic activity and anodic stability of electrodeposited ruthenium–rhodium coatings on titanium. J. Mater. Sci. 34, 869–874.

Walsh, F. and Mills, G. (1993) Electrochemical techniques for a cleaner environment. Chem. Ind. 8, 576–580.

Wang, J. and Feng, Y.J. (2005) Effect of preparation method on electrocatalysis of rare earth Gd doping SnO_2/Sb electrode. J. Jilin University (Science Edition). 43(4), 546–550 (in Chinese).

Wang, J., Feng, Y.J. and Liu, Z.Q. (2005) Study of the influences of Gd doping on the characteristics of SnO_2 catalytic electrodes. J. Funct. Mater. 36(6), 877–880 (in Chinese).

Ya, X. and Hans, T.K. (2002) An experimental investigation of chemical oxygen demand removal from the wastewater containing oxalic acid using three-phase three-dimensional electrode reactor. Adv. Environ. Res. 7, 139–145.

You, H., Cui, Y.H., Feng, Y.J., Liu, J.F. and Cai, W.M. (2004) Preparation and investigation of Ti-based SnO_2 electrode with an inter layer containing Co element. Mater. Sci. Technol. 12(3), 230–233 (in Chinese).

Zhao, G., Zhou, B. and Zhu, Z. (2000) Research on process analysis and intermediate of electrolytic degradation process of phenol water solution. J. Tongji University 28(5), 597–599.

Chapter 15
Wet Electrolytic Oxidation of Organics and Application for Sludge Treatment

Roberto M. Serikawa

15.1 Introduction

Sewage treatment systems are the major source of organic sludge emissions and the amount produced in Japan reached 428 million m^3 in 2003. This issue has become a global concern, as the huge amount of sludge emitted increases every year because of the diffusion of sewage nets in the infrastructure of urban areas. Roughly 34% of this organic sludge is dewatered or digested and returned in green areas as a soil conditioner or fertilizer. Sewage sludge can provide a large part of the nitrogen and phosphorus requirements of many crops. However, a large variety and quantity of pharmaceutical and personal-care products enter the sewage via daily domestic use. Although they are dilute, most of these compounds have limited biological degradability in the sewage treatment system and become concentrated in the sludge by sorption (Ternes et al. 2004). Accumulation of these potentially harmful compounds together with toxic heavy metals, endocrine disruptors, and pathogenic and parasitic organisms that can be found in the sludge means that reusing it agriculturally poses a potential risk to both human health and the environment. The environmental and human health consequences of reusing the sludge in the agricultural sector are still unclear, but some countries have already forbidden returning the sludge to the agricultural land.

Roughly 36% of all organic sludge is placed in landfills after its volume has been reduced. Current landfill sites are expected to be exhausted in less than 10 years, and environmental concerns, as well as lack of acceptance by local communities, mean that securing new sites is becoming increasingly difficult. New methods to reduce the amount of sludge at its source are being developed, including using ozone (Saktaywin et al. 2005, 2006), ultrasonic waves (Cao et al. 2006; Rai et al. 2004), and solubilization techniques. These techniques make the suspended organic solids

R.M. Serikawa (✉)
Ebara Research Co., Ltd, Honfujisawa, Japan
e-mail: serikawa.roberto@er.ebara.co.jp

C. Comninellis and G. Chen (eds.), *Electrochemistry for the Environment*,
DOI 10.1007/978-0-387-68318-8_15,

soluble rather than reducing the chemical oxygen demand (COD) of sludge. Solubilized liquors are recycled in aeration tanks and the COD is removed with a biological treatment. The organics are mineralized into CO_2 by the metabolism of microorganisms. In this sludge reduction method, it is necessary to restrict the solubilization dose to balance it with the capacity of the biological tank and avoid any deterioration in the quality of the effluent water. Reports indicate that ozone solubilization, when properly applied in biological treatments and depending on the type of sewage, can reduce excess sludge by up to 100% (Sakai et al. 1997). Methane fermentation is another practical technique that allows the recovery of energy in the form of biogas from organic sludge and reduces the COD. Because of its low biodegradability, organic sludge is mixed with other biodegradable waste before undergoing methane fermentation. Also, making the sludge soluble beforehand is reported to improve the biodegradability of methane fermentation (Hogan et al. 2004). Typical COD reduction in anaerobic digestion is around 65–85%, but the methane fermentation itself produces sludge by-products. The final organic sludge after methane fermentation can be dewatered using a screw press or other mechanical method after the sludge is coagulated and sedimented by adding chemical flocculants. Incineration is the ultimate treatment for all organic sludge. Dewatered organic sludge still has a water content of roughly 90%, most of which is water inside or strongly attached to the cells of micro-organisms. Because of the high water content of sludge it has to be incinerated or burnt at $800 - 1,000°C$ together with other solid waste with a high calorific value or by adding some fuel. Some modern incinerators operate at even higher temperatures and the inorganic components or ash is melted, locking the heavy metals inside the slag. Roughly 20–30% of sewage sludge is burned in cement kilns and reused as a construction material.

While sludge incineration is widely practiced on a full-scale basis, wet oxidation (Lendormi et al. 2001) is again becoming the focus of attention as an alternative to incineration, and new facilities for wet oxidation are being constructed in Europe. The beginning of wet oxidation for treating sludge goes back to the early 1950s and 1960s, when the concept and basic process was developed by F. J. Zimmermann in USA. The organic sludge is oxidized at a high temperature and under high-pressure conditions using air as an oxidizer. Operational temperatures are lower than those of incineration and thermal energy for water evaporation is not required. This allows an auto-thermal operation in which the organic pollutants serve as the fuel. Several variations of wet oxidation have been developed up till now, and some process uses oxygen gas, liquid oxygen or hydrogen peroxide in place of air. The working temperature varies from 120°C to temperatures near the critical point of water (374°C), depending on the type of wet oxidation. The working pressures are usually higher than the saturated vapor pressure to ensure the presence of a liquid phase and the fluidity of the reactants inside the reactors. Super critical water oxidation can also be considered as an extension to the process of wet oxidation, differing in the respect that the operating temperatures and pressures are higher than the critical point of water (374°C, 22 MPa). The use of a heterogeneous catalyst in wet oxidation allows

a lower working temperature to be used and ensures the degradation of compounds that are refractory in conventional wet oxidation processes. However, catalyzed wet oxidation systems can encounter some difficulties when treating wastewater that contains scaling components. Calcium and magnesium can easily cause poisoning of the catalyst when present in concentrations higher than 60 ppm. Noncatalyzed wet oxidation, where the reaction performance mainly depends on the reaction temperature, seems to be a solution for treating organic sludge. A 97% reduction in the volume of sludge and a roughly 85% removal rate of COD can be easily achieved with wet oxidation treatment at 350°C (Shananblesh and Shimizu 2000). Although some soluble COD remains in the treated water, these soluble organics are identified as mainly volatile fatty acids (VFA), which are a good substrate for biological treatment.

Wet electrolytic oxidation (WEO) is basically a wet oxidation system, differing in that the oxidation reactions are assisted by electrochemical reactions. The basic concept was born from a simple idea to perform wet oxidation without using high pressure compressors to inject oxidizers into the reactor. The idea was to produce nascent oxygen in situ in the reactor by water electrolysis. This idea seemed to be attractive since high-pressure compressors are usually expensive and the cost of compressing the oxidizer (air) accounts for a large portion of the running costs of a wet oxidation facility.

The potential required for oxygen evolution in water electrolysis becomes lower as temperature increases (Flarshein et al. 1986). At $200 - 300$°C, around twice as many ionic products of liquid water are produced compared with the ionic products under ambient conditions, and a large number of dissociated H^+ and OH^- can enhance the electrochemical reactions. The diffusion coefficient of some organics in aqueous media, experimentally obtained by microelectrode measurement and predicted by the Stokes–Einstein relation, are reported to be 20 times higher at 304°C compared with at 25°C (Liu et al. 1997). The water solubility of some organics, such as benzene, increases by a factor of 10 at 200°C and they become completely miscible at 297°C (Bard et al. 1988). The improved kinetics and greatly increased mass transfer rates imply operations at higher current density and throughputs (MacDonalds et al. 1986).

All this information in the research literature encourages the use of a wet-oxidation process with in situ oxygen produced by water electrolysis. However, a crucial problem related to safety must be solved. The hydrogen that is generated in twice the amount of the oxygen generated has to be separated from the oxygen inside the wet oxidation reactor. The lower explosion limit of hydrogen is just 4 vol% under atmospheric conditions and the difficulty is how to avoid forming a potentially explosive gaseous mixture inside a wet oxidation reactor. For electrolysis at lower temperatures and pressures, divided cells that use separation membranes can easily solve this problem. However, there is no feasible polymer electrolyte or solid-oxide electrolyte material that can be used as a separation membrane in the harsh and high-temperature conditions found in the wet oxidation reactors.

15.2 Peculiar Electrolysis of Aqueous Solution at Higher Temperatures

Although the formation of an explosive gas composed of hydrogen, oxygen or chlorine is expected when conducting electrolysis of aqueous solutions in closed and undivided pressure cells, the electrochemical reaction with subcritical water results in a completely different reaction (Serikawa et al. 2000).

Figure 15.1 illustrates the electrolysis products as a function of temperature when charging 2A-DC in 150 mL of 2 wt% NaCl aqueous solution for 1 h inside a 300-mL electrolytic autoclave. The gaseous products were measured using gas chromatography and free residual chlorine was measured using a DPD method, collecting samples directly from the autoclave. The experimental details can be found elsewhere (Serikawa et al. 2000). At temperatures lower than 100°C, there is a clear evolution of hydrogen, oxygen and chlorine which is detected as free residual chlorine, because of the progress of the well-known following electrolysis.

$$2H_2O + 2e^- \rightarrow H_2 + 2OH^- \quad (15.1)$$

$$2H_2O \rightarrow O_2 + 2H^+ + 2e^- \quad (15.2)$$

$$Cl^- + H_2O \rightarrow HOCl + H^+ + 2e^- \quad (15.3)$$

The evolution of hydrogen, oxygen and chlorine is strongly suppressed as the temperature increases. Chlorine evolution is not detected at temperatures higher than 150°C. Oxygen evolution is not detected at temperatures higher than 250°C. Traces of hydrogen are detected even at higher temperatures but the amount is extremely small compared with the amount supposed to be produced by Faraday's law. Electrolysis of water under subcritical conditions can take place without producing oxygen and hydrogen. These findings allow the conclusion that electrolyzing water as an oxidizer supply can be performed safely inside the wet oxidation reactors without the need to use separation membranes.

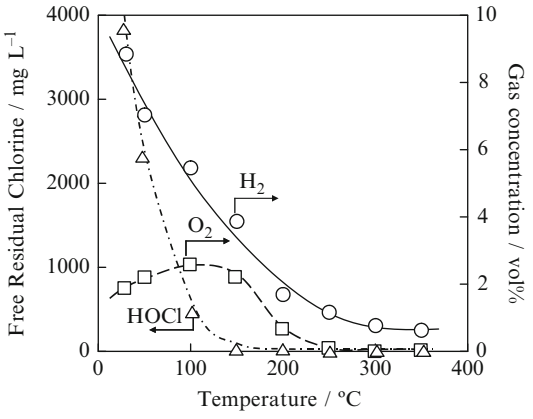

Fig. 15.1 Temperature influence on the electrolysis product of aqueous NaCl solution

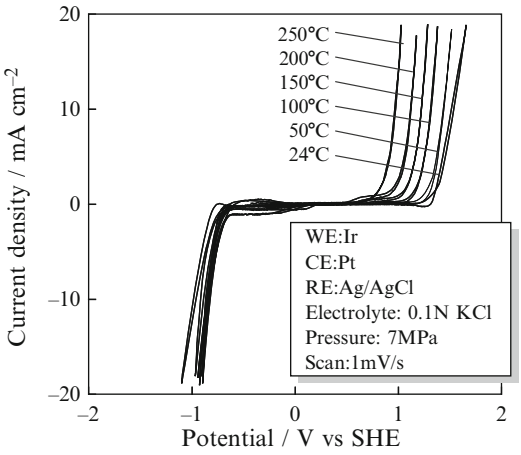

Fig. 15.2 Temperature influence on the thermodynamic windows of aqueous NaCl solution

However, if oxygen evolution cannot be detected during subcritical water electrolysis, another question arises about the efficiency of producing nascent oxygen in situ in a wet oxidation reactor. The evolution of oxygen, chlorine and hydrogen is highly suppressed during the subcritical water electrolysis of an aqueous NaCl solution, but electrolytic reactions are taking place. Indeed, the cyclic voltammetry investigation of a chloride solution in Fig. 15.2 clearly shows peaks corresponding to anodic and cathodic peak currents, even at 250°C.

At higher temperatures the thermodynamic window becomes narrow because of the overpotentials decrease for oxygen evolution, but anodic and cathodic reactions are clearly taking place. The suppression mechanism of usual electrolysis products under subcritical water conditions is not completely understood. A possible explanation is that the oxidizer species formed at the anode is preferentially reduced at the cathode, thereby suppressing the evolution of hydrogen at the cathode. Bard and his coworkers have done pioneering work on electrochemical measurements at near-critical and supercritical fluids in a series of nine publications (Bard et al. 1988). Although the experimental conditions are not the same and the work focuses on electrochemical measurements, they did not find any evidence of such suppression of oxygen or hydrogen evolution in subcritical water conditions. The reactions that suppress hydrogen or oxygen evolution can occur at places besides the electrode interface and are not purely electrochemical. Although any direct chemical reaction between hydrogen and oxygen inside the reactor is unlikely, hydrogen is known to be a difficult compound to oxidize under subcritical water conditions. Thus, the catalytic effects of high-temperature chloride solutions, electrode materials or autoclave materials are also possible explanations for these reactions. The most probable explanation for the chlorine disappearance is thermal degradation.

15.3 Wet Electrolytic Oxidation of Organics

Although the oxidizer species cannot be detected during electrolysis under subcritical water conditions, efficient oxidation can take place when some organics are present. Figure 15.3 shows a case of degradation of 2-aminoethanol (MEA) when applying 12A-DC in 150 mL of solution containing 2 wt% NaCl as a supporting electrolyte at 25°C and 7 MPa. Different concentrations of MEA are degraded with the same ratio, while the applied current is kept constant. The H_2:CO_2:N_2 volumetric ratio in the gaseous product is 13:4:1, showing that the overall WEO reaction can be written as follows.

$$2C_2H_4OHNH_2 + 6H_2O \rightarrow 13H_2 + 4CO_2 + N_2 \tag{15.4}$$

Several organics including acetic acid were confirmed to be efficiently mineralized by WEO (Serikawa et al. 2000) accompanied by hydrogen evolution. Although the absence of organics suppresses the evolution of hydrogen, WEO reaction produces hydrogen in the presence of organics. Please note that hydrogen is generated but oxygen is not produced and the reaction product is still a nonexplosive gas mixture. Other recent work (Sasaki et al. 2007; Goto et al. 2004) has also confirmed hydrogen evolution during the hydrothermal electrolysis of biomass-related compounds. Hydrogen is produced because of the cathodic reduction of water, but further addition of an oxidizer can suppress this water reduction and enhance the mineralization reaction.

Figure 15.4 illustrates the reaction products of WEO of acetic acid with and without added oxygen gas. Here, 2A-DC was applied to 150 mL of 4,000 mg L^{-1} acetic acid solution having 2 wt% NaCl at 250°C and 7 MPa. In the experiment without any added oxygen gas, an inert gas (argon) was pressurized in the head space of the electrolytic autoclave (150 mL). For the experiment with oxygen, a gas mixture

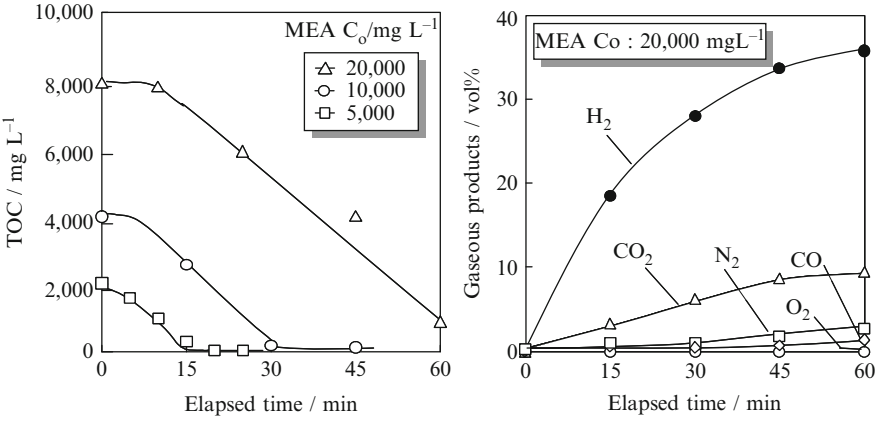

Fig. 15.3 Degradation and products of MEA after WEO treatment

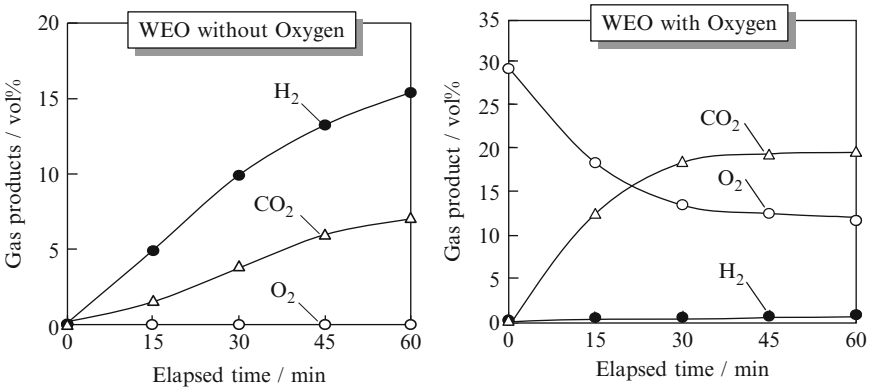

Fig. 15.4 Gaseous product from WEO of acetic acid with and without added oxygen

containing 30 vol% oxygen with argon balance was pressurized in the autoclave. The addition of oxygen for WEO of organics clearly suppresses the generation of hydrogen. For WEO of acetic acid, two reactions can be written, depending on whether or not oxygen is added.

$$CH_3COOH + 2H_2O \rightarrow 4H_2 + 2CO_2 \text{ (without oxygen)} \quad (15.5)$$

$$CH_3COOH + 2O_2 \rightarrow 2CO_2 + 2H_2O \text{ (with oxygen)} \quad (15.6)$$

$$2H_2O + 2e^- \rightarrow H_2 + 2OH^- \text{ (without oxygen)} \quad (15.7)$$

$$2H_2O + O_2 + 2e^- \rightarrow H_2O_2 + 2OH^- \text{ (with oxygen)} \quad (15.8)$$

The electrical charge required for reaction (15.5) is 8 F and for reaction (15.6) is 4 F. Accordingly, the addition of an external oxidizer can decrease the electrical power consumption by a factor of 2.

The cathodic reaction during the WEO of organics also changes depending on whether or not oxygen is present [(15.7) and (15.8)]. When oxygen gas is added, the cathodic reaction reduces dissolved oxygen gas rather than water in accordance with the redox potential. The reaction in WEO is thermodynamically limited rather than kinetically limited.

Cathodic reduction of oxygen explains the suppression of hydrogen when oxygen is added in WEO of organics. The oxygen is transformed to a more active form of oxygen [represented as H_2O_2 in (15.8)] at the cathode, and that can further oxidize the organics.

Figure 15.5 shows the influence of electrical charge in WEO of acetic acid with added oxygen.

Even with added oxygen, degradation of acetic acid clearly depends on the electrical charge and the controlling mechanism is electrochemical rather than chemical oxidation. Acetic acid is a component that is known to oxidize minimally under wet oxidation conditions (see 0 A line).

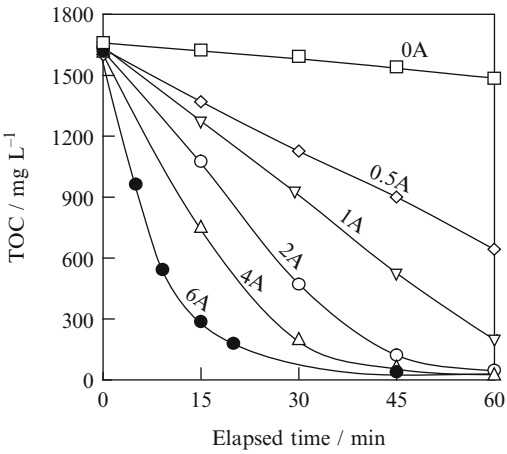

Fig. 15.5 Influence of electrical charge during WEO of acetic acid with added oxygen at 250°C

Another relevant aspect that can be considered in performing electrochemical oxidation at higher temperatures is related to the use of chloride ions as a supporting electrolyte. Chloride ions were found to catalyze the electrolytic oxidation of organics at room temperature because of the participation of electrogenerated hypochlorous acid (Comninellis and Nerini 1995). However, this electrolytic oxidation under room conditions was reported to be followed by the formation of harmful organochlorinated (AOX) by-products. The formation of AOX compounds can also be suppressed by increasing the reaction temperatures. Figure 15.6 illustrates the AOX, TOC and gases after WEO treatment of phenol as a function of temperature. Figure 15.6a shows the AOX concentration in the aqueous phase and gas phase. The AOX in the aqueous phase was 800 ppm after a 13.3 Ah L^{-1} charged electrooxidation at 30°C and this decreased as the reaction temperature increased. The AOX in the aqueous solution is attributed to the chlorophenols confirmed by GC-MS analysis. The AOX in the gas phase is because of the formation of volatile chlorinated compounds such as trichloromethane, which results from the degradation of chlorophenols. The AOX in the gas phase shows a peak in concentration at 150°C. Aqueous phase and gas phase AOX are strongly suppressed in all electrolysis conducted at temperatures higher than 200°C. This kind of behavior of AOX byproducts with increases in electrolysis temperature is not particular to phenol and can be extended for other organics. Separate experiments using EDTA and 2-aminoethanol in place of phenols have shown analogous results with an elevated concentration of AOX compounds at low temperature electrolysis and undetectable amounts for electrolysis conducted at temperatures higher than 200°C. Two explanations can be given for the absence of AOX byproducts under WEO conditions.

The first is that the oxidation mechanism of organics in WEO occurs directly at the electrode surface, without evolving intermediate reactions that form chlorinated compounds, and that can be supported by the fact that free residual chlorine is not detected in the effluent samples for all electrolysis conducted at temperatures higher

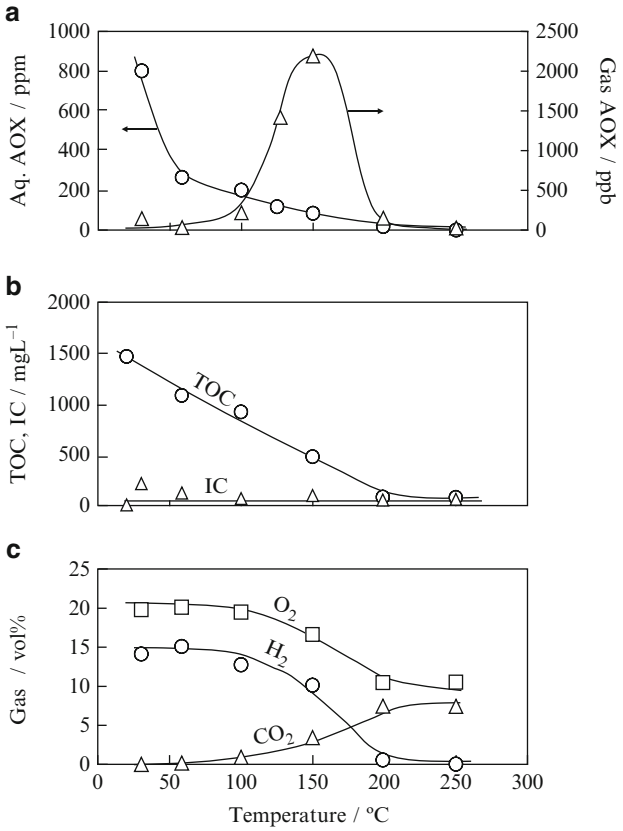

Fig. 15.6 Influence of temperature on phenol electrooxidation. Condition: 150 mL of 19 mM phenol with 2 wt% NaCl, 2 Ah and 3 MPa air initially charged

than 200°C. The second explanation is that there is an intermediate chlorination mechanism followed by a subsequent dechlorination of AOX compounds. Highly stable chlorinated aromatics, such as PCBs, were reported to be dechlorinated under alkaline hydrothermal conditions (Yamazaki et al. 1980). Similar hydrothermal dechlorination can occur, for example, at the cathode vicinity where the pH is alkaline in WEO. Nevertheless, organochlorinated by-products are strongly suppressed when the temperatures are higher than 200°C evidencing the "clean" aspect of WEO reactions. Figure 15.6b illustrates the TOC concentration as a function of electrolysis temperature when aqueous phenol is electrolyzed. A negligible TOC decrease was observed for electrolysis at 30°C. The degradation rate of phenol reported by Comninellis' group (Comninellis et al. 1955) is higher because of the high pH (12.2) used in their experiments. An alkaline solution increases the solubility of phenols in the aqueous phase, thereby improving the electrooxidation. In the case discussed here, the pH was not adjusted and was weakly acidic (5.8). The

electrolysis temperature greatly influenced the TOC removal rate. For electrolysis at 250°C, the TOC removal rate was 95% at charging 13.3 Ah L^{-1}. Free-residual chlorine in the effluent was 8 mg L^{-1} at 30°C electrolysis and was undetected at temperatures higher than 150°C. Separate experiments using the same electrolytic autoclave without adding phenol resulted in the production of 3800 mg L^{-1} of free residual chlorine at 30°C electrolysis and an undetectable amount at temperatures higher than 150°C. This indicates that the formed hypochlorous acid at low temperature electrolysis is almost completely consumed by phenol chlorination or by autodegradation without promoting oxidation of organics. The gaseous product analysis shown in Fig 15.6c also supports this theory. A negligible amount of CO_2 was measured at 30°C electrolysis. A pronounced increase in CO_2 concentration was observed with the increase in the reaction temperature and this reached 8 vol% at 200°C. The decrease of O_2 and H_2 concentration with the increase in temperature indicates that electrolytic oxidation under hydrothermal conditions takes place, thereby consuming the oxygen gas and suppressing the evolution of hydrogen at the cathode. Please note that the initial concentration of oxygen gas is 21 vol% because of the initially charged air in the autoclave. The oxygen in Fig. 15.6c comes from the initially charged air and not from the anodic oxygen evolution of WEO

15.4 Behavior of Organic Sludge Under Hydrothermal Conditions

Before starting to explain the treatment of organic sludge by WEO, this section describes the basic behavior of organic sludge under hydrothermal conditions. An example of the water quality of typical organic sludge is given in Table 15.1. This sludge was produced in a commercial methane fermentation facility treating sewage sludge, night soil and garbage.

Table 15.1 Typical water quality of organic sludge (methane fermentation sludge)

Analysis item	Unit	
MLSS	mg L^{-1}	34,000
MLVSS	mg L^{-1}	23,000
T-COD_{Cr}	mg L^{-1}	45,000
S-COD_{Cr}	mg L^{-1}	5,900
T-BOD	mg L^{-1}	2,600
S-BOD	mg L^{-1}	450
T-Sugar	mg L^{-1}	5,700
S-Sugar	mg L^{-1}	760
EC	mS cm^{-1}	8.2
pH	–	7.7
Color	degree	2,400
VFA	mg L^{-1}	25

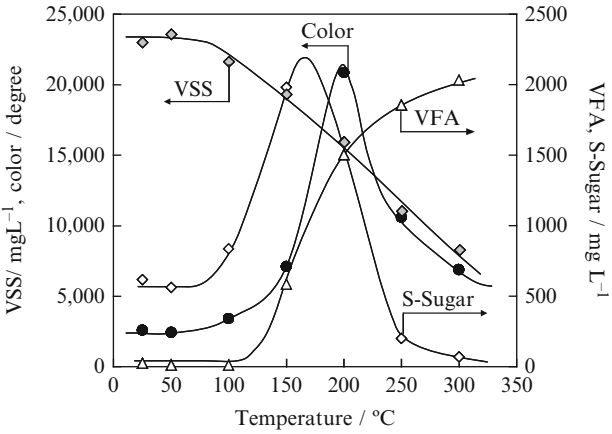

Fig. 15.7 Influence of temperature on hydrothermal reaction of organic sludge

Figure 15.7 shows the results of hydrothermal treatment when 150 mL of the sludge listed in Table 15.1 was charged into the autoclave and kept at various temperatures for 30 min. No electrical current or oxygen was used in these experiments and the results illustrated in Fig. 15.7 are caused purely by thermal effects. The organics in the form of suspended solids (VSS) start to decrease at temperatures higher than 100°C because of thermal solubilization. The first compound that appears as the result of solubilization is soluble sugar (S-Sugar), because of the hydrolysis of the organic compounds in the sludge. The origin of the soluble sugar is attributed to the polymeric sugars that make up the cell wall of methanogenic microorganisms. The soluble sugar achieves a maximum yield at 180°C. Although not illustrated in this figure, amino acids are also produced at similar temperatures because of the hydrolysis of proteins. A further increase in the temperature causes the degradation of S-Sugars and appearance of color compounds that achieve a maximum concentration at 200°C. These color compounds often appear when treating organic waste under subcritical water conditions and they are extremely problematic. These color compounds dye the treated water a dark black color and usually cannot be removed by biological processes. The production of color compounds in subcritical water is attributed to the progress of a melanoidin reaction between amino acids and soluble sugars. A further increase in the reaction temperature to higher than 250°C causes a decrease in colors and an increase in the production of VFA. The VFA are composed of acetic acid, lactic acid, formic acid, and propionic acid. Among the VFA, acetic acid is a very stable compound under subcritical water conditions. The VFA are produced because of the partial oxidation of organic compounds in the sludge.

For a combined process with a biological system, it is interesting to convert the sludge to VFA as much as possible. The VFA provide a good substrate for the biological process and can be readily treated in anaerobic or aerobic processes.

15.5 Wet Electrolytic Oxidation of Organic Sludge

As described in Sect. 15.4, when submitting the organic sludge to a hydrothermal treatment there is a production of problematic color compounds at 200°C. In the WEO, the color is erased by the electrochemical reaction. Figure 15.8 shows the color behavior of WEO-treated water as a function of electrical charge and reaction temperature. The color that appears at 200°C clearly decreases with an increase in electrical charge. Although the color disappears, the VFA amount in WEO treatment can be increased as a function of applied electrical charge (Fig. 15.9).

Another relevant aspect of sludge treatment by WEO that should be considered is related to the dewatering properties of organic sludge. A large part of the water in organic sludge is located inside or strongly attached to the cells of microorganisms. The gel-like compound that surrounds cells of microorganisms retains a large amount of water and increases the viscosity of the sludge. Usually, it is difficult to dewater organic sludge by filtration because of this viscosity and a precipitation procedure is needed that uses a huge amount of chemical coagulants. However, WEO can degrade these viscous compounds, drastically decreasing the viscosity of the sludge. Furthermore, the cell walls of the microorganisms rupture because of thermal effects thereby releasing the water inside. Some of the thermally degraded cell walls are transformed to small particles of char-like products in WEO. These char particles naturally precipitate and can be easily removed from the treated water by filtration. The filtrate after WEO treatment is transparent and almost colorless. Figure 15.10 shows the morphological changes of organic sludge before and after WEO treatment.

The filtrate still contains dissolved COD compounds that can be removed by biological processes. Complete COD removal of sludge by WEO is possible but no longer recommended. The initial T-COD concentration of this sludge was $45\,g\,L^{-1}$ (see Table 15.1). According to the Faraday's law, an electrical charge of $151\,kAh\,m^{-3}$ of sludge will be required for complete COD removal. Considering

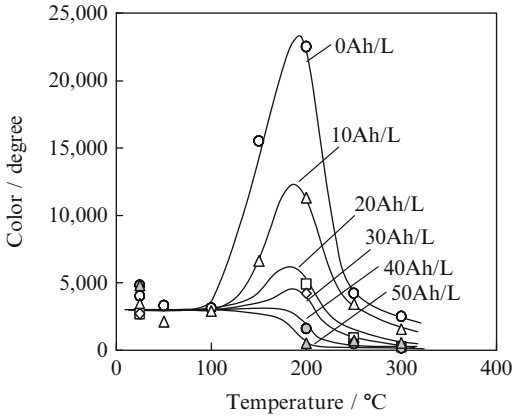

Fig. 15.8 Color erasing by electrochemical effects in WEO of organic sludge

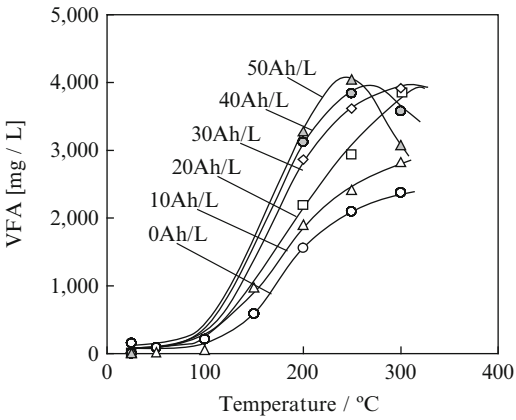

Fig. 15.9 Increase in VFA yield by electrochemical effects in WEO of organic sludge

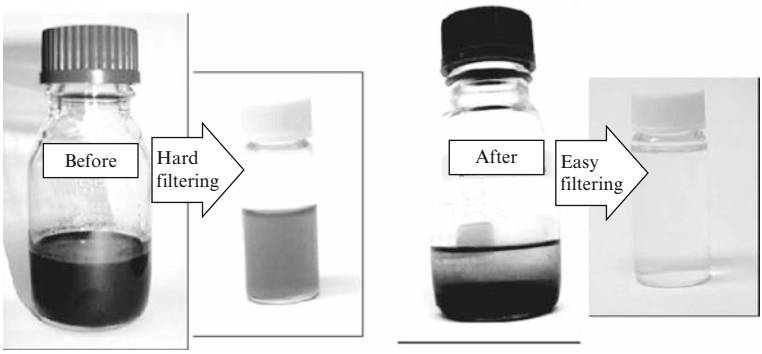

Fig. 15.10 Organic sludge before and after WEO treatment

that the voltage between the electrodes in the WEO is around 5 V, an electrical power of 755 kWh m^{-3} of sludge will be required for total COD removal.

This level of electrical power consumption is usually prohibitive for commercial treatment of organic sludge, suggesting the need to couple WEO with a biological process. The WEO product should have an improved biodegradability if it is to be treated by a biological process.

One reference for this biodegradability is the BOD/COD ratio. The BOD/COD ratio of the original sludge was 6%, but after the WEO treatment this value could be increased to higher than 50%. The BOD/COD ratio increased with the increase in temperature and electrical charge, and that was attributed to the formation of VFA.

The BOD/COD ratio is an indicator of biodegradability for an aerobic process but the WEO was also found to increase the biodegradability for anaerobic treatment. The filtrate from WEO treatment of organic sludge at 250°C was submitted to a methane fermentation test. Figure 15.11 shows the methane yield for the filtrate of WEO, in which different electrical charges were applied. A clear increase in the methane yield was observed with the increase in the electrical charge of WEO. The

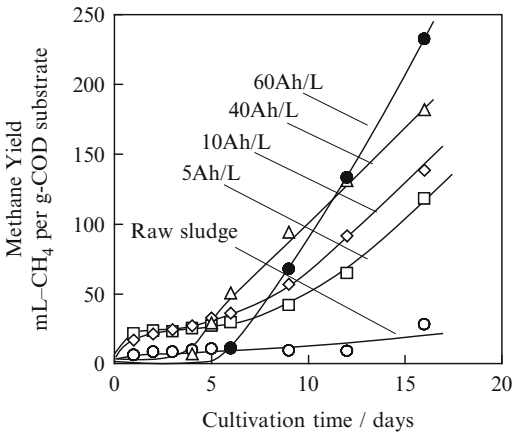

Fig. 15.11 Methane fermentation of organic sludge after WEO treatment

methane yield from raw sludge was very low because the residue had already been treated by methane fermentation. The aqueous product from the WEO treatment has good biodegradability in aerobic and anaerobic biological processes.

15.6 Materials for WEO

The proper choice of anode material, cathode material and reactor material are of particular importance in conducting WEO treatments. The reaction takes place high temperature at oxidizing conditions in the presence of organics and salts, which make the reaction environment extremely corrosive.

Table 15.2 lists the results of a test on anode material under accelerated-corrosion conditions using high current densities under WEO conditions at 250°C. The materials that were classified as having a low stability showed a high level of corrosion, dissolution or delamination with failure in less than 50 h under accelerated test conditions. The materials classified as having medium stability cleared the 50-h test but showed localized corrosion or partial delamination of coating layers. The material classified as having a high stability showed no visible changes in the electrode surface after the 50-h test.

Platinum and gold anodes are unstable and dissolution of these materials is accelerated by an increase in temperature (test samples n.1, n.2) when the electrolyte solution contains chloride ions. Platinum sample n.1 showed visual surface dissolution and weight loss during the 50-h test, and the gold-coated tantalum lost all the gold layers in less than 5 h. Iridium electrodes (test samples n.3, n.4) showed no visible changes after the 50-h test. An iridium anode seems to work better when it is made from pure metallic iridium. Iridium oxide electrodes prepared by thermal decomposition (test sample n.5) on tantalum substrate are less stable, possibly because of the porous morphology of the coating oxide layer. Although this sample cleared

Table 15.2 Anode material stability test for WEO

n	Sample	Test sample specification	I $(\mathrm{mA\,cm^{-2}})$	Stability
1	Pt	99.9% purity Pt disk	3,200	Medium
2	Au/Ta	Au (3 μm) coated on Ta disk by electroplating	3,200	Low
3	Ir	99.9% purity Ir disk	3,200	High
4	Ir/Ta	Ir (3 μm) coated on Ta disk by electroplating	3,200	High
5	Ir/Ta	Ir (3 μm) coated on Ta by thermal decomposition	3,200	Medium
6	Ir/Ti	Ir (3 μm) coated on Ti by thermal decomposition	3,200	Low
7	T15Pd	JIS grade12 Pd–Ti alloy	3,200	Low
8	BDD	CVD-coated borondoped diamond	150	Low

Electrolyte: $5,000\,\mathrm{mg\,L^{-1}}$ acetic acid with $2,000\,\mathrm{mg\,L^{-1}}$ chloride ion aq. solution, $T = 250°\mathrm{C}$ and $P = 7\,\mathrm{MPa}$

the 50h test, some delamination of the coating layer was observed. The stability of iridium oxide coated on titanium (test piece n.6) showed a low stability compared with using tantalum as a substrate. The delaminated area was larger in this sample and the remaining coated area showed losses of iridium when measured by X-ray fluorescence. The stability of the coated electrodes by thermal decomposition also depends on the substrate material. Titanium is not suitable as an anode substrate. Test sample n.7 for example, which is a titanium alloy containing palladium that is considered to be more stable than pure titanium, completely dissolved after 3 h under accelerated test conditions. Also, boron-doped diamond (BDD) was tested here at usual current densities of $150\,\mathrm{mA\,cm^{-2}}$. Diamond electrodes made of CVD are a promising electrode material for low-temperature electrolysis but at a working temperature of 250°C a complete delamination occurred in a few minutes.

Lead oxide and tin oxide are often found in research literature as anode materials, but there is little indication that these materials are stable at higher temperatures. These electrodes were not tested here because of the possibility that the heavy metals would leach into the electrolyte solution.

Conventional techniques for detecting the anode failure by increasing the potential could not be used under WEO conditions. With low-temperature electrolysis, when the coating layers of the electrode delaminate, the exposed passivation layer of titanium and tantalum substrate causes an increase in the voltage between the electrodes. However, under WEO conditions, even with a complete delamination of the coating layers, the voltage does not increase. No protective passivation layer seems to form at WEO by anodic polarization. Metallic titanium, when exposed to WEO conditions, was found to be directly converted to white titanium oxide powder inside the electrolytic autoclave (test sample n.7). Tantalum was found to be more robust than titanium and no dissolution was found even with complete delamination of the Au layer (test sample n.2). In addition, no voltage increase was observed for tantalum during this test.

Table 15.3 Cathode material stability test for WEO

n	Test sample	Test piece specification	i $(\mathrm{mA\,cm^{-2}})$	Stability
9	SS400	JIS G3101 steel	3,200	Low
10	SUS 316	JIS Cr16-Ni12-Mo2 iron alloy	3,200	Low
11	Nickel 276	JIS Mo16-Cr15- Fe4-W3 nickel alloy	3,200	Medium
12	Nickel 22	JIS Cr21-Mo13-Fe4-W3 nickel alloy	3,200	Medium
13	Nickel 625	JIS NCF625 nickel alloy	3,200	Medium
14	TP 340	JIS-grade 2 titanium	3,200	High
15	TP 550	JIS-grade 4 titanium	3,200	High
16	T64	JIS-grade 60 Al6-V4 titanium alloy	3,200	Medium

Electrolyte: $5,000\,\mathrm{mg\,L^{-1}}$ acetic acid with $2,000\,\mathrm{mg\,L^{-1}}$ chloride ion aq. solution, $T = 250°\mathrm{C}$ and $P = 7\,\mathrm{MPa}$

Table 15.3 list the results of the cathode material test under accelerated corrosion conditions using high-current densities in WEO at 250°C. Steel (sample n.9) and stainless steel (sample n.10) showed a high corrosion rate over their whole surface and are not suitable as a cathode material for WEO. Cathodic protection against corrosion does not work for these materials under WEO conditions. Alloys with high nickel content (samples n.11, n.12, and n.13) passed the 50-h test under accelerated conditions, though they showed some localized corrosion on the surface. Although these nickel alloys have a high tensile strength at higher temperatures, they were found to be unsuitable for direct exposure with the electrolyte solution in WEO reaction. Samples n.14 and n.15, which are titanium with different purity grades, cleared the 50-h test, showing no visible corrosion. Titanium alloy T64 (sample n.16) passed the 50-h test, but had some localized corrosion on its surface. The titanium alloy had less surface corrosion than the nickel alloys but it too cannot be used for direct exposition under the WEO reaction environment.

From the test results listed in Tables 15.2 and 15.3, and from the experience gained in building and running continuous WEO apparatus for some years, the author will make some brief comments on a suitable material for WEO.

For anodes, the best material found up to now is metallic iridium. Although the actual price of iridium is only 20% that of platinum on a weight-for-weight basis, the cost of manufacturing the whole anode from iridium is still prohibitive. Some possible options for manufacturing large electrodes include either iridium foil attached to a tantalum substrate or electroplated iridium. Titanium alloy T64, and nickel alloys 276, 22, and 625 are usually good materials for a high-temperature and high-pressure reactor, but cannot be used in place of direct contact with the electrolyte solution in a WEO reactor. When used as a construction material for a WEO reactor, they have to be properly lined with titanium. Titanium was found to be a suitable material for the cathode in WEO. However, because of its low tensile strength at higher temperatures, titanium cannot be used as a material for pressure vessels and must be limited to use as a lining material. Stainless steel 316 or even

common steel can be used as a reactor material, if properly lined with titanium. To reinforce a high-pressure reactor against corrosion, a cathodic current is preferably applied to titanium-lined walls or the titanium lining can be directly used as the cathode.

15.7 Conclusions

Wet electrolytic oxidation is an electrochemically assisted wet oxidation process in which the reaction can be controlled by varying the electrical charge, thereby offering new parameter other than reaction temperature for handling the degree of reaction. The electrolytic reaction under WEO conditions is thermodynamically limited rather than kinetically limited, allowing water to be electrolyzed without generating any hydrogen or oxygen. The organochlorinated compounds that are formed in usual electrooxidation are strongly suppressed with WEO oxidation, evidencing a clean chloride evolved reaction. When applied to organic sludge treatment, colors are decreased and VFA yields are increased, and consequently the biodegradability of the treated water is improved, allowing further biological processing. The reaction environment of WEO is extremely corrosive and suitable material must be selected. Iridium as an anode and a titanium reactor liner as a cathode were found to be suitable material for the WEO process.

Acknowledgment The author acknowledges the New Energy and Industrial Technology Development Organization (NEDO) of Japan for their financial support related to the treatment of organic sludge by WEO.

References

Bard, A. J., Flarshein, W. M. and Johnston, K. P. (1988) High-pressure electrochemical oxidation of benzene at a lead dioxide electrode in aqueous bisulfate solution at 25°C to 250°C. J. Electrochem. Soc. 135, 1939–1944.

Cabrera, C. R. and Bard A. J. (1989) Electrochemistry in near-critical and supercritical fluids. Part 8. Methyl viologen, decamethylferrocene, $Os(bpy)_3^{2+}$ and ferrocene in acetonitrile and the effect of pressure on diffusion coefficients under supercritical conditions. J. Electroanal. Chem. 273, 147–160.

Cabrera, C. R. Garcia, E. and Bard, A. J. (1989) Electrochemistry in near-critical and supercritical fluids. Part 7. SO_2. J. Electroanal. Chem. 260, 457–460.

Cao, X. Q., Chen, J., Cao, Y. L., Zhu, J. Y. and Hao, X. D. (2006) Experimental study on sludge reduction by ultrasound. Water Sci Technol 54, 87–93.

Comninellis, C. and Nerini, A. (1995) Anodic oxidation of phenol in the presence of NaCl for wastewater treatment. J. Appl. Electrochem. 25, 23–28.

Crooks R. M. and Bard A. J. (1987) Electrochemistry in near-critical and supercritical fluids. 4. Nitrogen heterocycles, nitrobenzene and solvated electrons in ammonia at temperature to 150°C J. Phys. Chem. 91, 1274–1284.

Crooks, R. M. and Bard, A. J. (1988a) Electrochemistry in near-critical and supercritical fluids. Part VI. The electrochemistry of ferrocene and phenazine in acetonitrile between 25 and 300°C. J. Electroanal. Chem. 243, 117–131.

Crooks, R. M. and Bard, A. J. (1988b) Electrochemistry in near-critical and supercritical fluids. Part V. The dimerization of quinoline and acridine radical anions in ammonia from 70°C to 150°C. J. Electroanal. Chem. 240, 253–279.

Crooks, R. M., Fan, F. F. and Bard, A. J. (1984) Electrochemistry in near-critical and supercritical fluids. 1. Ammonia J. Am. Chem. Soc. 106, 6851–6852.

Flarshein, W. M. and Johnston, K. (1988) High-pressure electrochemical oxidation of benzene at a lead dioxide electrode in aqueous bisulfate solution at 25°C to 250°C. J. Electrochem. Soc.: Electrochem Sci Technol 135, 1939–1944.

Flarshein, W. M., Tsou, Y., Trachtenberg, L., Johnston, K. P. and Bard, A. J. (1986) Electrochemistry in near-critical and supercritical fluids. 3. Studies of Br^-, I^-, and hydroquinone in aqueous solution. J. Phys. Chem. 90, 3857–3862.

Goto, M., Sasaki, M., Yamamoto, K., Kuroda, T. (2004) Hydrothermal electrolysis of bio-related compounds, *Proceedings of Third International Meeting on High Pressure Chemical Engineering*.

Hogan, F., Mormede, S., Clark, P. and Crane, M. (2004) Ultrasonic sludge treatment for enhanced anaerobic digestion. Water Sci. Technol. 50, 25–32.

Lendormi, T., Prevot, C., Doppenberg, F., Foussard, J. N. and Debellefontaine, H. (2001) Subcritical wet oxidation of municipal sewage sludge: comparison of batch and continuous experiments. Water Sci. Technol. 44, 161–169.

Liu, C., Snyder, S. R. and Bard, A. J. (1997) Electrochemistry in near-critical and supercritical fluids. 9. Improved apparatus for water systems (23°C–385°C). The oxidation of hydroquinone and iodide. J. Phys. Chem. 101, 1180–1185.

MacDonalds, A. C., Fan, F. F. and Bard, A. J. (1986) Electrochemistry in near-critical and supercritical fluids. 2. Water. Experimental techniques and copper (II) system. J. Phys. Chem. 90, 196–202.

Rai, C. L., Struenkmann, G., Mueller, J. and Rao, P. G. (2004) Influence of ultrasonic disintegration on sludge growth reduction and its estimation by respirometry. Environ. Sci. Technol 38, 5779–5785.

Sakai, Y., Fuakase, T., Yasui, H. and Shibata, M. (1997) An activated sludge process without excess sludge production. Water Sci. Technol. 36, 163–170.

Saktaywin, W., Tsuno, H., Nagare, H., Soyama, T. and Weerapakkaroon (2005) Advanced sewage treatment process with excess sludge reduction and phosphorus recovery. Water Res 39, 902–910.

Saktaywin, W., Tsuno, H., Nagare and Soyama, T. (2006) Operation of a new sewage treatment process with technologies of excess sludge reduction and phosphorus recovery. Water Sci. Technol. 53, 217–227.

Sasaki, M., Yamamoto, K. and Goto M. (2007) Reaction mechanism and pathway for hydrothermal electrolysis of organic compounds J Mater Cycles Waste Manage 9(1), 40–46.

Serikawa, R. M., Isaka, M., Su, Q., Usui, T., Nishimura, T., Sato, H. and Hamada, X. (2000) Wet electrolytic oxidation of organic pollutants in wastewater treatment. J. Appl. Electrochem. 30, 875–883.

Shananblesh, A. and Shimizu, Y. (2000) Treatment of sewage sludge using hydrothermal oxidation-technology application challenges. Water Sci. Technol. 41, 85–92.

Ternes, T. A., Joss, A. and Siegrist H. (2004) Scrutinizing pharmaceuticals and personal care products in wastewater treatment. Environ. Sci. Technol. 38, 393A–399A.

Yamazaki, N., Yasui, T. and Matsuoka, K. (1980) Hydrothermal decomposition of polychlorinated biphenils. Environ. Sci. Technol. 14, 550–552.

Chapter 16
Environmental Photo(electro)catalysis: Fundamental Principles and Applied Catalysts

Huanjun Zhang, Guohua Chen, and Detlef W. Bahnemann

16.1 Introduction

Since the demonstration by Honda and Fujishima of the photoelectrolysis of water using a TiO_2 electrode under an anodic bias potential (Fujishima and Honda 1972), intensive research efforts have been devoted to the study of photocatalytic performances of semiconductor materials (Hoffmann et al. 1995). Before touching the details of any photocatalytic process using semiconductors, it is crucial to clarify a few fundamental definitions which are most relevant in this context. The electronic energy structure within a semiconductor consists of three distinguished regimes, i.e., the conduction band, the valence band, and the forbidden zone. The forbidden zone represents a region in which energy states do not exist for an ideal, undoped semiconductor. Energy states only exist above and below this region. Taking the energy level of the electron in the vacuum as reference and as the uppermost level, the upper band is called the conduction band, and the lower one is called the valence band. In terms of energy, the difference between the upper edge of the valence band and the lower edge of the conduction band is called bandgap $\left(E_g\right)$ of the semiconductor. If the two levels can be described with the same wavevector, the semiconductor is considered to have a direct bandgap; otherwise it has an indirect bandgap. The bandgap is one of the most critical parameters defining the optical properties of semiconductors.

A semiconductor immersed into a solvent (in most cases water) and illuminated with photons exceeding its bandgap energy will be called a photocatalyst provided that at its surface it is able to catalyze reactions with $\Delta G < 0$ (e.g., the oxidation of organic compounds by molecular oxygen). In case endothermic reactions such as the splitting of water into O_2 and H_2 are found to occur at the semiconductor surface upon ultra-bandgap illumination the system will be called photosynthetic and will be able to store part of light energy in the form of chemical energy. Most studies of photocatalytic reactions are nowadays focused on particulate systems

D.W. Bahnemann (✉)
Institut für Technische Chemie, Leibniz Universität Hannover, Hannover, Germany
e-mail: bahnemann@iftc.uni-hannover.de

C. Comninellis and G. Chen (eds.), *Electrochemistry for the Environment*,
DOI 10.1007/978-0-387-68318-8_16,

(Ollis et al. 1991; Gerischer and Heller 1992; Gerischer 1995), employing either transparent colloidal suspensions of semiconductor nano particles or light scattering suspensions of larger semiconductor particles, due to the apparent reality that particles possess much higher surface area (therefore enabling hopefully higher yields of utilizing the incoming light energy called photonic efficiency) than their bulk counterparts. The photocatalyst particles can actually be regarded as individual microelectrodes, always kept under open circuit potential, inside which charge carriers (electrons and holes) can be generated upon bandgap irradiation, i.e., the incident photons have higher energies than the bandgap of the semiconductor. The thus formed charge carriers then travel to the particle surface to participate in possible chemical reactions with surface-adsorbed species. This is a highly simplified description of photocatalytic reactions which as will be shown below turn out to be rather more complicated, however, if one takes a closer scrutiny.

16.2 Description of Photocatalytic Systems

16.2.1 The Semiconductor–Electrolyte Interface in the Absence of Redox Systems

Most researchers have studied photocatalytic reactions in an aqueous environment. It is therefore essential to understand the semiconductor–electrolyte interface, preferably from an energetic point of view. To illustrate this, the semiconductor–electrolyte interface in the absence of redox species is depicted in Fig. 16.1 (Memming 2001). Compared with metal electrodes, the charge-carrier density

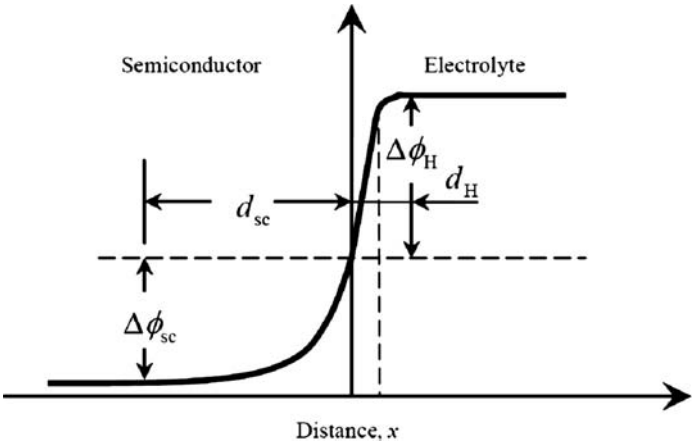

Fig. 16.1 Potential distribution at the semiconductor–electrolyte interface [Copyright Wiley-VCH Verlag GmbH & Co. KGaA. Reproduced with permission from Memming (2001)]

in semiconductor electrodes is much lower, even if they are doped. Therefore, when the semiconductor is brought into contact with an electrolyte, the so-called Helmholtz double layer having a potential drop of $\Delta\phi_H$ over a distance d_H is formed on the solution side. On the solid side, the counter charge (i.e., the charge to neutralize that on the solution side due to bonding or specific adsorption of, for example, hydroxyl ions) is distributed over a certain range below the surface. Correspondingly, a potential drop $\Delta\phi_{sc}$ is formed across this so-called space charge region, the dimension of which is denoted as d_{sc}, as indicated in Fig. 16.1. Here the diffuse layer in the solution has been neglected assuming that a high ion concentration is applied. The potential and charge distribution within the space charge region in the solid is described by the Poisson equation as follows

$$\frac{d^2\Delta\phi_{sc}}{dx^2} = -\frac{1}{\varepsilon\varepsilon_0}\rho(x) \tag{16.1}$$

in which ε is the dielectric constant of the material and ε_0 is the permittivity of free space. The charge density $\rho(x)$ is given by

$$\rho(x) = e\left[N_d - N_a - n(x) + p(x)\right] \tag{16.2}$$

in which x is the distance from the surface and N_d and N_a are the fixed ionized donor and acceptor densities, respectively, introduced by the doping of the semiconductor. The electron and hole densities, $n(x)$ and $p(x)$, vary with the distance x according to the following equations

$$n(x) = N_c \exp\left(-\frac{E_c(x) - E_F}{kT}\right), \tag{16.3}$$

$$p(x) = N_v \exp\left(-\frac{E_v(x) - E_F}{kT}\right), \tag{16.4}$$

where N_c is the density of states at the lower edge of the conduction band and N_v is the density of states at the upper edge of the valence band. $E_c(x)$ is the energy of the lower edge of the conduction band which varies with the distance x and $E_v(x)$ the energy of the upper edge of the valence band. E_F is the Fermi level energy of the semiconductor, which is defined in solid-state physics as the highest occupied energy level within the crystal at 0 K. For an intrinsic semiconductor, the position of its Fermi level can be calculated from

$$E_F = \frac{E_c + E_v}{2} + \frac{kT}{2}\ln\left(\frac{N_v}{N_c}\right) = \frac{E_c + E_v}{2} + \frac{kT}{2}\ln\left(\frac{m_h^*}{m_e^*}\right) \tag{16.5}$$

in which m_e^* and m_h^* are the effective masses of electrons and holes, respectively.

Within the space charge region, since the Fermi level is expected to be constant, the position of the energy bands $E_c(x)$ and $E_v(x)$ vary with distance. If the

charge-carrier densities in the bulk of the semiconductor are n_0 for electrons and p_0 for holes, then

$$n(x) = N_0 \exp\left(-\frac{E_c(x) - E_c^b}{kT}\right) = N_0 \exp\left(-\frac{e\Delta\phi_{sc}(x)}{kT}\right), \tag{16.6}$$

$$p(x) = p_0 \exp\left(-\frac{E_v(x) - E_v^b}{kT}\right) = p_0 \exp\left(\frac{e\Delta\phi_{sc}(x)}{kT}\right), \tag{16.7}$$

in which E_c^b and E_v^b are the energy levels of the conduction and valence bands in the bulk. These two equations imply a Boltzmann distribution of charge carriers in the space charge region. In the bulk of the semiconductor, i.e., at sufficient distance from the surface, charge neutrality must be obeyed. Then

$$N_d - N_a = n_0 - p_0. \tag{16.8}$$

Inserting (16.2), (16.6), (16.7), and (16.8) into (16.1) one obtains the so-called Poisson-Boltzmann equation:

$$\frac{d^2\Delta\phi_{sc}}{dx^2} = \frac{e}{\varepsilon\varepsilon_0}\left[n_0 - p_0 - n_0 \exp\left(-\frac{e\Delta\phi_{sc}}{kT}\right) + p_0 \exp\left(\frac{e\Delta\phi_{sc}}{kT}\right)\right]. \tag{16.9}$$

Without going into much mathematical detail, the capacity of the space charge region is derived by solving the Poisson–Boltzmann equation as

$$C_{sc} = \frac{\varepsilon\varepsilon_0}{L_D}\cosh\left(\frac{e\Delta\phi_{sc}}{kT}\right) \tag{16.10}$$

in which the so-called Debye length is defined by

$$L_D = \left(\frac{\varepsilon\varepsilon_0 kT}{2n_i e^2}\right)^{1/2}, \tag{16.11}$$

where n_i is the intrinsic carrier density given by the equilibrium equation $n_0 p_0 = n_i^2$. From (16.10) one recognizes that the space charge capacity C_{sc} depends strongly on the potential drop $\Delta\phi_{sc}$ across the space charge region.

16.2.2 The Semiconductor–Electrolyte Interface in the Presence of Redox Systems

In the presence of a redox system dissolved in the electrolyte, as long as there exists an energy difference between the Fermi level of the semiconductor and the redox couple, to reach the equilibrium conditions charge-carrier transfer occurs across the semiconductor–liquid interface via the energy bands, i.e., the conduction or valence band of the semiconductor. At the equilibrium point, the Fermi level of the redox

system, $E_{\mathrm{F,\ redox}}$, is equivalent to the electrochemical potential of the electrons in the redox system, as shown in the following equation:

$$E_{\mathrm{F,\ redox}} = \bar{\mu}_{\mathrm{e,\ redox}} = \mu^{0}_{\mathrm{e,\ redox}} + kT \ln\left(\frac{C_{\mathrm{ox}}}{C_{\mathrm{red}}}\right) \tag{16.12}$$

in which C_{ox} and C_{red} are the concentrations of the Ox and Red species being in equilibrium according to the following reaction:

$$\mathrm{Ox} + \mathrm{e}^{-} \rightleftharpoons \mathrm{Red} \tag{16.13}$$

Conventionally, the corresponding redox potential is given on a scale using the normal hydrogen electrode (NHE) or the saturated calomel electrode (SCE) as reference electrode.

The Gerischer model (Gerischer 1959, 1961), which has the advantage that energy levels of localized electron states in an electrolyte solution can be introduced, is usually employed to illustrate the charge-carrier transfer between the semiconductor and the redox system at the interface. In a very simplified version of the Gerischer model as illustrated in Fig. 16.2, the redox system is characterized by a set of occupied states centered around the energy value of E^{0}_{red} and a set of empty states centered around E^{0}_{ox}. Correspondingly, the densities of the electronic states, i.e., D_{red} for the occupied and D_{ox} for the empty states, are proportional to the concentration of the reduced (C_{red}) and oxidized (C_{ox}) species in the redox system, respectively, as given by

$$D_{\mathrm{red}}(E) = C_{\mathrm{red}} W_{\mathrm{red}}(E), \tag{16.14}$$

$$D_{\mathrm{ox}}(E) = C_{\mathrm{ox}} W_{\mathrm{ox}}(E), \tag{16.15}$$

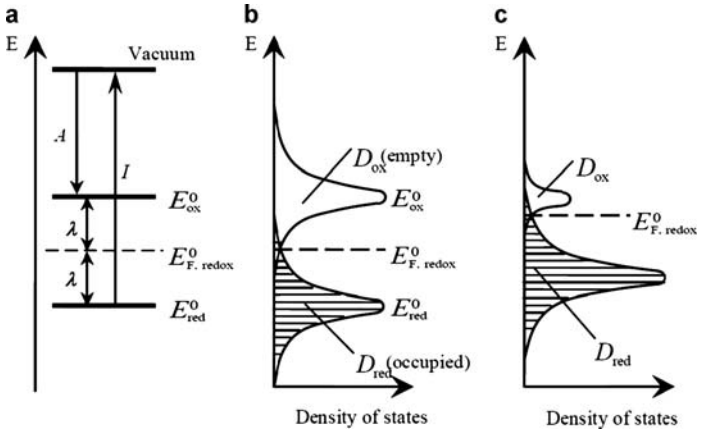

Fig. 16.2 Electron energies of a redox system vs. density of states: (**a**) E^{0}_{red} for occupied states, E^{0}_{ox} for empty states, A as electron affinity and I as ionization energy of the redox system; (**b**) the corresponding distribution functions at $C_{\mathrm{ox}} = C_{\mathrm{red}}$; (**c**) the distribution functions at $C_{\mathrm{ox}} \ll C_{\mathrm{red}}$ [Copyright Wiley-VCH Verlag GmbH & Co. KGaA. Reproduced with permission from Memming (2001)]

in which $W_{red}(E)$ describes the distribution of the occupied electronic levels and $W_{ox}(E)$ the distribution of the empty levels. These two distribution functions are dependent on the reorganization energy λ (Fig. 16.2a) which is accompanied by the rearrangement of the solvation shell and the solvent dipoles after the fast electron transfer between the reduced and the oxidized species in the solution, and have the following forms:

$$W_{red}(E) = (4kT\lambda)^{-1/2} \exp\left[-\frac{\left(E - E^0_{F,\,redox} - \lambda\right)^2}{4kT\lambda}\right], \tag{16.16}$$

$$W_{ox}(E) = (4kT\lambda)^{-1/2} \exp\left[-\frac{\left(E - E^0_{F,\,redox} + \lambda\right)^2}{4kT\lambda}\right]. \tag{16.17}$$

As shown in Fig. 16.2b, at equal concentrations, the distributions of the reduced and oxidized species are equivalent at the standard electrochemical potential of the redox couple, $E^0_{F,\,redox}$. By varying the concentrations of the redox species a shift of the Fermi level (where D_{red} and D_{ox} are equal) of the redox system is induced according to the Nernst equation (Fig. 16.2c).

At the semiconductor–electrolyte interface, the electron transfer rate depends on the density of energy states on both sides of the interface. For example, the electron transfer from the redox system to the conduction band of the semiconductor generates an anodic current

$$j_c^+ = ek_0 C_{red} \int_{E_F}^{\infty} (1 - f(E))\, \rho(E) \exp\left[-\frac{\left(E - E^0_{F,\,redox} - \lambda\right)^2}{4kT\lambda}\right] dE. \tag{16.18}$$

The subscript "c" and superscript "+" of j indicate that the current is generated via the "conduction" band and is an "anodic" current. k_0 is the electron-transfer rate constant. $\rho(E)$ is the distribution of energy states in the semiconductor. $f(E)$ is the Fermi energy distribution function as given in

$$f(E) = \frac{1}{1 + \exp\left(\dfrac{E - E_F}{kT}\right)}. \tag{16.19}$$

In most cases, the overlap between energy states on both sides of the interface is limited to a small energy range, the electron transfer is therefore assumed to be within 1 kT at the edge of the conduction band. The integral in (16.18) can be approximated using $dE = 1\,kT$ and $E = E_c^s$. Then one obtains

$$j_c^+ = ek_0 \left(1 - f\left(E_c\right)\right) \rho\left(E_c\right) \left\{ C_{red} \exp\left[-\frac{\left(E_c^s - E^0_{F,\,redox} - \lambda\right)^2}{4kT\lambda}\right]\right\} \tag{16.20}$$

in which the product of C_{red} and the exponential function corresponds to the density of occupied states of the redox system at the energy of the lower edge of the conduction band on the surface where $E = E_c^s$. The density of states in the semiconductor at the lower edge of the conduction band is

$$\rho(E_c) = N_c = \frac{2\left(2\pi m_e^* kT\right)^{3/2}}{h^3}, \tag{16.21}$$

where N_c is the density of energy states within few kT above the conduction band edge. Usually, most of the energy states in the conduction band are empty, i.e., $1 - f \approx 1$, therefore

$$(1 - f(E_c))\,\rho(E_c) \approx N_c. \tag{16.22}$$

Then (16.20) can be written as

$$j_c^+ = ek_0 N_c C_{red} \exp\left[-\frac{\left(E_c^s - E_{F,\,redox}^0 - \lambda\right)^2}{4kT\lambda}\right]. \tag{16.23}$$

It is clear from (16.23) that the anodic current is independent of the electrode potential, since the equation contains only constant parameters for a given system.

The cathodic current due to electron transfer from the conduction band of the semiconductor to the empty states of the redox system is given by

$$j_c^- = ek_0 f(E_c)\,\rho(E_c)\,C_{ox} \exp\left[-\frac{\left(E_c^s - E_{F,\,redox}^0 + \lambda\right)^2}{4kT\lambda}\right] \tag{16.24}$$

in which the product $f(E_c)\rho(E_c)$ at $E = E_c^s$ is the density of occupied states at the bottom of the conduction band on the surface. It is equivalent to the density of free electrons on the surface n_s, which is dependent on the potential drop across the space charge region as given by

$$n_s = n_0 \exp\left(-\frac{e\Delta\phi_{sc}}{kT}\right). \tag{16.25}$$

The net current due to the electron transfer via the conduction band is then the sum of j_c^- and j_c^+, which continues to be nonzero until the electrochemical potentials of the electrons are equal on both sides of the interface. This leads to a further modification of the space charge region in the semiconductor, on top of the simple semiconductor–electrolyte case in the absence of redox systems. Accordingly, if one visualizes the electron energy states in the space charge region, the energy bands are usually drawn as energy vs. distance plots. The so-called "band bending" simply refers to the bending or curvature in such plots, as shown in Fig. 16.3. Other than via the energy bands, charge transfer can also occur via the surface states at the interface, which will, however, not be further discussed in this section.

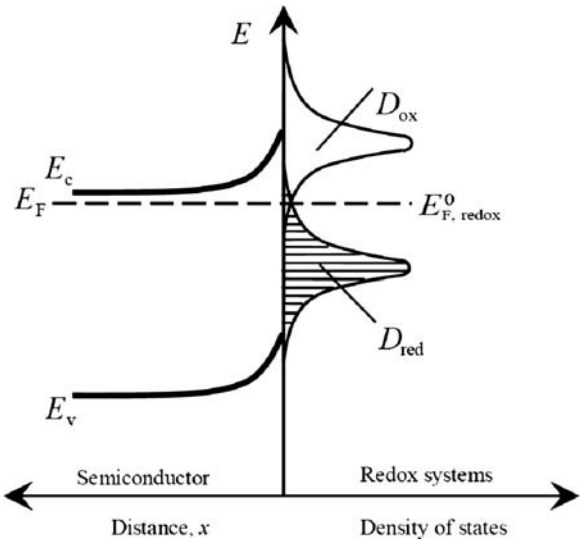

Fig. 16.3 Electron energies of a semiconductor electrode in contact with a redox system [Copyright Wiley-VCH Verlag GmbH & Co. KGaA. Reproduced with permission from Memming (2001)]

16.2.3 The Semiconductor–Liquid Interface Under Illumination

If the semiconductor is illuminated by photons more energetic than its bandgap energy, the equilibrium achieved at the interface in the dark is now disturbed by the excitation of electrons from the valence band to the conduction band. Besides this band–band transition, in a real, i.e., nonideal system also other electronic transitions can be induced upon light excitation, including the excitation of an electron from a donor state or an impurity level into the conduction band, and the formation of an exciton. The latter represents a bound state between an electron and a hole due to their Coulomb attraction. Its energy is close to the conduction band, and thermal excitation can hence feasibly split the exciton into an independent electron and hole. In this section, however, only the band–band transition is considered during the analysis of charge transfer processes occuring at the semiconductor–liquid interface under illumination.

The absorption of a photon results in the formation of an electron–hole pair. This process is of special interest if minority carriers, i.e., the holes in an n-type and the electrons in a p-type semiconductor, are involved in the charge transfer. Thereby, the density of the minority carriers can be increased upon light excitation, by orders of magnitude, as compared with that in the dark. For a n-type semiconductor, the minority carriers (holes) generated in the space charge region are subsequently driven to the interface by the "built-in" electric field. Those generated outside this region can only reach the space charge region by diffusion, and then continue the relayed

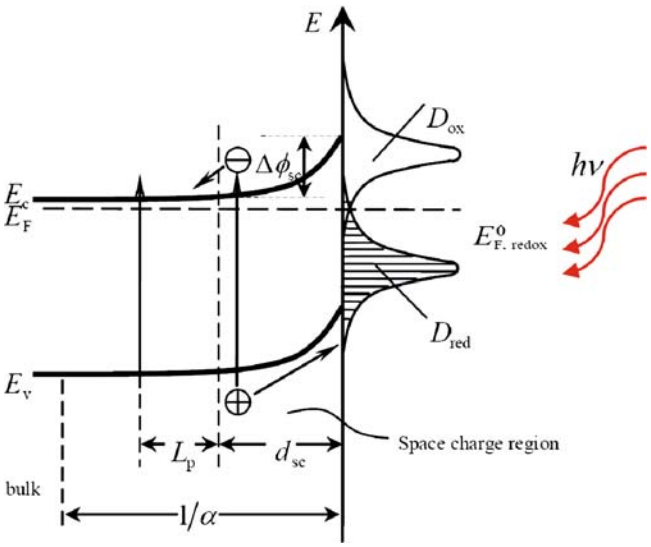

Fig. 16.4 Charge transfer at the n-type semiconductor–solution interface under illumination [Copyright Wiley-VCH Verlag GmbH & Co. KGaA. Reproduced with permission from Memming (2001)]

transfer driven by the electric field. The general minority carrier transfer process across the semiconductor–solution interface occuring under illumination of a n-type semiconductor is illustrated in Fig. 16.4.

Overall, only the holes photogenerated within the range of $L_p + d_{sc}$ will reach the surface, i.e., the interface between the semiconductor and the electrolyte, if negligible recombination within the space charge region is assumed. The distance L_p, defined as the hole diffusion length, across which the minority carriers travel without recombination is usually limited due to the electron–hole recombination outside the space charge region. To obtain the photocurrent density, one needs to solve the diffusion equation for holes in the bulk using Reichman's method, as given by

$$D\frac{\mathrm{d}^2 p}{\mathrm{d}x^2} - \frac{p - p_0}{\tau} + I\alpha \exp(-\alpha x) = 0 \tag{16.26}$$

in which D is the diffusion coefficient; p the hole density; p the equilibrium hole density; τ the lifetime of holes; I the monochromatic photon flux across the semiconductor which is dependent on the distance from the interface; α the absorption coefficient of the semiconductor, a wavelength-dependent parameter defined as

$$\alpha = \frac{1}{d} \ln \frac{I_0}{I}, \tag{16.27}$$

where d is the thickness of the semiconductor; I_0 the incident photon flux on the surface at $x = 0$; and I is the transmitted photon flux. Subject to the wide range

of bandgap energies of different semiconductors, their absorption coefficients vary typically between 10^3 and 10^6 cm^{-1}, depending on the wavelength of the incident photons. The inverse of α is called the depth of penetration (of light), the distance at which the radiant power decreases to 1/e of its incident value if the Naperian absorption coefficient is adopted. Accordingly, the depth of penetration of different semiconductors also varies over a wide range, typically from tens of nanometers to microns.

The three terms on the left-hand side of (16.26) account, respectively, for the diffusion, recombination, and generation of holes under illumination. Without advancing into mathematical details, one obtains the hole current density at the interface between the bulk and the space charge region, i.e., the diffusion current density j_{diff}, as given by

$$j_{\mathrm{diff}} = -j_0\left(\frac{p_{\mathrm{d}}}{p_0} - 1\right) + \frac{eI_0\alpha L_{\mathrm{p}}}{1+\alpha L_{\mathrm{p}}}\exp\left(-\alpha d_{\mathrm{sc}}\right) \tag{16.28}$$

in which p_0 is the hole density in the bulk ($x = \infty$); p_{d} is the hole density at $x = d_{\mathrm{sc}}$ that is related to the hole density p_{s} on the semiconductor surface under illumination via

$$p_{\mathrm{s}} = p_{\mathrm{d}}\exp\left(\frac{\mathrm{e}\Delta\phi_{\mathrm{sc}}}{kT}\right). \tag{16.29}$$

j_0 is a saturation current density which represents the generation/recombination rate of holes in the bulk of the semiconductor as given by

$$j_0 = \frac{\mathrm{e}Dn_{\mathrm{i}}^2}{N_{\mathrm{D}}L_{\mathrm{p}}}, \tag{16.30}$$

where n_i is the intrinsic electron density equivalent to $(n_0 p_0)^{1/2}$; N_{D} is the density of donor states; and the hole diffusion length L_{p} is herein defined as $(D\tau)^{1/2}$. A typical value of L_{p} for GaAs has been given as 1μm (Memming 2001). Meanwhile, the thickness of the space charge region, d_{sc} can be estimated by

$$d_{\mathrm{sc}} = \frac{1}{e}\left(\frac{2\Delta E_{\mathrm{F}}\varepsilon\varepsilon_0}{N_{\mathrm{D}}}\right)^{1/2}. \tag{16.31}$$

To quantitatively sense the dimension of d_{sc} using the dielectric constant $\varepsilon = 11.68$ and typical density of donor states $N_{\mathrm{D}} = 10^{17}\mathrm{cm}^{-3}$ of Si and assuming $\Delta E_{\mathrm{F}} = 0.5\,\mathrm{eV}$, one obtains that d_{sc} is in the order of 0.1 μm. Within the space charge region where it is assumed that no recombination occurs, excitation of holes leads to the current

$$j_{\mathrm{sc}} = eI_0\left[1 - \exp\left(-\alpha d_{\mathrm{sc}}\right)\right]. \tag{16.32}$$

If recombinations at the semiconductor–solution interface are also neglected, the total hole current at the semiconductor surface is then given by the sum of j_{diff} and j_{sc}. Together with (16.28), this summation leads to

$$\begin{aligned} j_{\mathrm{v}} &= j_{\mathrm{diff}} + j_{\mathrm{sc}} = -j_0 \left(\frac{p_{\mathrm{d}}}{p_0} - 1 \right) + \frac{e I_0 \alpha L_{\mathrm{p}}}{1 + \alpha L_{\mathrm{p}}} \exp\left(-\alpha d_{\mathrm{sc}}\right) \\ &\quad + e I_0 \left[1 - \exp\left(-\alpha d_{\mathrm{sc}}\right)\right] \\ &= -j_0 \left[\frac{p_{\mathrm{s}}}{p_0} \exp\left(-\frac{e\Delta\phi_{\mathrm{sc}}}{kT} \right) - 1 \right] + \frac{e I_0 \alpha L_{\mathrm{p}}}{1 + \alpha L_{\mathrm{p}}} \exp\left(-\alpha d_{\mathrm{sc}}\right) \\ &\quad + e I_0 \left[1 - \exp\left(-\alpha d_{\mathrm{sc}}\right)\right]. \end{aligned} \tag{16.33}$$

Again, the subscript "v" in (16.33) indicates that the charge transfer occurs via the valence band. This current density must also be equal to the hole current derived from the surface hole densities. In a way similar to that used for deriving (16.23) and (16.24), the anodic and cathodic current via the valence band can be obtained as

$$j_{\mathrm{v}}^{+} = \mathrm{e} k_0 p_{\mathrm{s}} C_{\mathrm{red}} \exp\left[-\frac{\left(E_{\mathrm{v}}^{\mathrm{s}} - E_{\mathrm{F,\,redox}}^{0} - \lambda\right)^2}{4kT\lambda} \right], \tag{16.34}$$

$$j_{\mathrm{v}}^{-} = \mathrm{e} k_0 N_{\mathrm{v}} C_{\mathrm{ox}} \exp\left[-\frac{\left(E_{\mathrm{v}}^{\mathrm{s}} - E_{\mathrm{F,\,redox}}^{0} + \lambda\right)^2}{4kT\lambda} \right], \tag{16.35}$$

in which p_{s} is the hole density at the surface of the semiconductor; N_{v} is the density of states at the upper edge of the valence band; and $E_{\mathrm{v}}^{\mathrm{s}}$ is the energy of the upper edge of the valence band at the surface of the semiconductor. At equilibrium in the dark, the anodic and cathodic currents are equal in magnitude, which can be regarded as a saturation current density j_{v}^{0} determined by the rate of hole transfer at the interface via the valence band as follows:

$$\begin{aligned} j_{\mathrm{v}}^{0} &= j_{\mathrm{v}}^{+}\big|_{\mathrm{equilibrium}} = \mathrm{e} k_0 p_{\mathrm{s}}^{0} C_{\mathrm{red}} \exp\left[-\frac{\left(E_{\mathrm{v}}^{\mathrm{s}} - E_{\mathrm{F,\,redox}}^{0} - \lambda\right)^2}{4kT\lambda} \right] \\ &= j_{\mathrm{v}}^{-}\big|_{\mathrm{equilibrium}} = \mathrm{e} k_0 N_{\mathrm{v}} C_{\mathrm{ox}} \exp\left[-\frac{\left(E_{\mathrm{v}}^{\mathrm{s}} - E_{\mathrm{F,\,redox}}^{0} + \lambda\right)^2}{4kT\lambda} \right]. \end{aligned} \tag{16.36}$$

Equation (16.36) is subject to the condition $p_{\mathrm{s}} = p_{\mathrm{s}}^{0}$. The density of states at the upper edge of the valence band N_{v} barely changes since the valence band is almost always full, i.e., N_{v} is almost constant whether or not an equilibrium is achieved.

In a nonequilibrium situation upon illumination, the net current density due to the hole transfer from the semiconductor surface to the solution can be obtained as

$$j_{\mathrm{v}} = j_{\mathrm{v}}^{+} - j_{\mathrm{v}}^{-} = j_{\mathrm{v}}^{+}\big|_{\mathrm{equilibrium}} \frac{p_{\mathrm{s}}}{p_{\mathrm{s}}^{0}} - j_{\mathrm{v}}^{-}\big|_{\mathrm{equilibrium}} = j_{\mathrm{v}}^{0} \left(\frac{p_{\mathrm{s}}}{p_{\mathrm{s}}^{0}} - 1 \right) \tag{16.37}$$

p_{s}^{0} is related to the bulk hole density p_0 by the Boltzmann distribution function

$$p_s^0 = p_0 \exp\left(\frac{e\Delta\phi_{sc}^0}{kT}\right), \tag{16.38}$$

in which $\Delta\phi_{sc}^0$ is the potential drop across the space charge region under the equilibrium condition in the dark. From (16.37) and (16.38), one obtains

$$\frac{p_s}{p_0} = \left(\frac{j_v}{j_v^0}+1\right)\exp\left(\frac{e\Delta\phi_{sc}^0}{kT}\right). \tag{16.39}$$

Inserting (16.39) into (16.33) leads to

$$j_v = \frac{j_0 + eI_0\left[1 - \frac{\exp(-\alpha d_{sc})}{1+\alpha L_p}\right] - j_0\exp\left(-\frac{e\eta}{kT}\right)}{1 + \frac{j_0}{j_v^0}\exp\left(-\frac{e\eta}{kT}\right)}, \tag{16.40}$$

in which $\eta = \Delta\phi_{sc} - \Delta\phi_{sc}^0$ is the overpotential created upon illumination; the new term j_g called the generation current is defined as

$$j_g = j_0 + eI_0\left[1 - \frac{\exp(-\alpha d_{sc})}{1+\alpha L_p}\right] = j_0 + j_{ph}, \tag{16.41}$$

where j_{ph} is the so-called photocurrent density.

Equation (16.40), though rather complex in form, is of remarkable importance because it describes the overall charge transfer process via the valence band at a n-type semiconductor electrode for both anodic and cathodic polarizations. As mentioned earlier, j_0 represents the generation/recombination rate of holes in the bulk of the semiconductor and j_0 represents the rate of hole transfer at the interface. The ratio j_0/j_v^0 indicates whether the generation/recombination or the surface kinetics of the hole transfer is rate determining. If $j_0/j_v^0 \gg 1$, i.e., the rate is controlled by surface kinetics due to slow hole injection, then

$$j_v = j_v^0\left[\exp\left(\frac{e\eta}{kT}\right) - 1\right] + j_{ph}\frac{j_v^0}{j_0}\exp\left(-\frac{e\eta}{kT}\right), \tag{16.42}$$

which leads to a constant current $-j_v^0$ under high negative polarization in the dark. If $j_0/j_v^0 \ll 1$, i.e., the current is controlled by the generation/recombination rate, then

$$j_v = j_0\left[1 - \exp\left(-\frac{e\eta}{kT}\right)\right] + j_{ph}. \tag{16.43}$$

It is straightforward that under high positive polarization, the current levels off to a constant being the sum of j_0 and j_{ph}. Since the charge carriers to be transferred across the interface are minority carriers, j_0 is usually of very small magnitude and depends on material properties such as diffusion coefficient and the diffusion length of minority carriers, as expressed in (16.30). For instance, using typical values of the parameters in (16.30) for Si electrodes, the dark current density j_0 is found to be in

the order of 10^{-12} A cm^{-2}, which is a hardly detectable value. Such small currents can be considerably enhanced by light excitation. The limiting value is obtained once all excited minority carriers reach the surface where they are consumed in the reaction process. However, this is still a simplified analysis of charge transfer at the illuminated semiconductor–electrolyte interface because, for example, the cathodic dark current is hitherto assumed to be only due to the injection of holes into the valence band of the n-type semiconductor. More complexities will arise if other effects such as surface states are introduced, which will not be further discussed here.

16.2.4 Photocatalytic Reactions at Semiconductor Particles

16.2.4.1 Charge Transfer at Semiconductor Particles

In photocatalytic reactions, the essential advantage of using semiconductor particles is their large surface area. Besides, the photogenerated charge carriers can easily reach the surface before they recombine, so that a high quantum yield (which will be defined later) can also be expected. However, two reactions, an oxidation and a reduction must proceed simultaneously at the same particle surface (otherwise the particle will be charged up, eventually leading to the termination of the overall reaction), as presented in Fig. 16.5. The slower process then determines the overall reaction rate. In this regard, the particle behaves practically as a microelectrode kept always under open circuit potential with the anodic and cathodic current being equal in magnitude.

Using larger-sized semiconductor particles, the partial currents in the dark are of rather limited magnitude under open-circuit conditions, because the majority carrier (e.g., electrons for a n-type semiconductor) density at the surface is small due to the depletion layer beneath the electrode surface, as indicated in Fig. 16.5a. In contrast, no space charge region is formed in much smaller particles of size $d \ll d_{sc}$ (Fig. 16.5b). Upon light excitation, some minority carriers (e.g., holes for n-type materials) in larger particles are transferred to the electron donor in the solution, which results in a negative charging of the particle that alleviates the positive space charge. Accordingly, this event causes a flattening of energy bands (see the dashed line in Fig. 16.5a), equivalent to a negative shift of the rest potential of a bulk electrode under illumination.

Using much smaller semiconductor particles ($d \ll d_{sc}$), the photogenerated electrons and holes can be easily transferred to the surface and react with the electron and hole acceptors, provided that the energetic requirements are fulfilled. The average transit time τ_{tr} within a particle of diameter d can be obtained by solving Fick's diffusion law as

$$\tau_{tr} = \frac{d^2}{4\pi^2 D}. \tag{16.44}$$

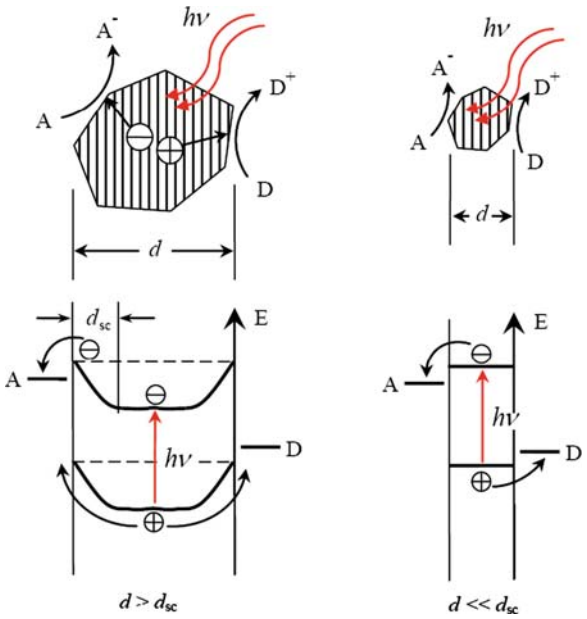

Fig. 16.5 Charge-carrier transfer at large (*left*) and small (*right*) semiconductor particles in the presence of an electron donor D and an acceptor A [Copyright Wiley-VCH Verlag GmbH & Co. KGaA. Reproduced with permission from Memming (2001)]

Taking typical values of $D = 0.1\,\mathrm{cm^2 s^{-1}}$ and $d = 20\,\mathrm{nm}$, the average transit time is about 1 ps, which is much shorter than the recombination time so that most charge carriers can reach the surface before recombination.

16.2.4.2 Quantum Size Effect

As mentioned previously, nanosized semiconductor particles have been very popular as photocatalysts due to their large surface area. Yet the most striking feature of the semiconductor nanoparticles is the remarkable change in their optical absorption spectra due to size reduction, compared with the bulk materials (Linsebigler et al. 1995; Alivisatos 1996a, b). For example, the bandgap of CdS can be tuned between 2.5 and 4.5 eV as the size is varied from a macroscopic crystal down to the molecular regime. This interesting phenomenon has been addressed with success using the effective mass model. As mentioned earlier, in bulk semiconductors, light excitation results in the formation of electron–hole pairs, which experience a Coulomb interaction and can form excitons with usually small binding energy (<0.03 eV) and large radius. The exciton radius can be calculated based on the Bohr

radius of an electron in a H atom modified by introducing the dielectric constant of the semiconductor and its reduced effective mass m^* with the latter being given by

$$m^* = \left(\frac{1}{m_e^*} + \frac{1}{m_h^*}\right)^{-1}. \tag{16.45}$$

Using a "particle in a box" model with an infinite potential drop at the wall as the boundary condition, and taking into account that the exciton consists of an electron–hole pair, the Schrödinger equation can be solved yielding the energy of the lowest excited state (Brus 1983, 1984; Rossetti et al. 1984), i.e., the lower edge of the conduction band, as

$$E(R) = E_g + \frac{h^2}{8m_0 m^* R^2} - \frac{1.8e^2}{\varepsilon R}, \tag{16.46}$$

in which m_0 is the electron mass in vacuum. According to (16.46), when a semiconductor has a reduced effective mass significantly smaller than the free electron mass, a large variation of its bandgap can be expected. Examples of such semiconductors are given: CdS ($m_e^* = 0.21\,m_0$, $m_h^* = 0.80\,m_0$), CdSe ($m_e^* = 0.13\,m_0$, $m_h^* = 0.45\,m_0$), GaAs ($m_e^* = 0.067\,m_0$, $m_h^* = 0.082\,m_0$) and ZnO ($m_e^* = 0.24\,m_0$, $m_h^* = 0.45\,m_0$) (Bahnemann et al. 1987a; Wong and Searson 1999). There are, however, semiconductors with larger effective mass due to which quantization does only occur once particle sizes reach the molecular regime, e.g., in small clusters. One example is TiO_2 which has been the most intensively studied photocatalyst materials in the past decades. Experimentally, TiO_2 particles synthesized with an average size between 5 and 20 nm were confirmed to exhibit the bandgap properties of the bulk solid. However, when the TiO_2 particle size is controlled below 3 nm (i.e., corresponding to clusters consisting of a few hundred TiO_2 molecules), a quantum size effect could also be identified indicating a bandgap increase of ~0.25 eV (Kormann et al. 1988). To precisely explore the quantum size effect, it should be emphasized that the bandgap shifts can only be measured with sufficient precision employing colloidal suspensions possessing a sufficiently narrow size distribution. Besides dispersed particles, techniques have also been available for fabrication of semiconductor films consisting of nanocrystalline particles (Wong and Searson 1999). Such films may exhibit similar quantum-size effects as individual particles, depending on the effective mass of the semiconductor as just described.

Accompanying the bandgap widening due to reduced particle size, electrons at the lower edge of the conduction band and holes at the upper edge of the valence band then possess higher negative and positive potentials, respectively. In consequence, electrons and holes can be expected to have a higher reduction and oxidation power, respectively, in such quantized particles.

Besides bandgap widening, variation of semiconductor particle size has also possible interesting consequences on the charge-carrier transfer in photocatalytic reactions. For instance, differences in the pathways of the photocatalytic reaction of acetic acid between a system using a TiO_2 bulk electrode short-circuited to a Pt electrode and that using Pt-loaded TiO_2 particles provide a very suitable illustration

of such size-dependent consequences (Kraeutler and Bard 1978). Using spatially separated electrodes, acetic acid is oxidized by photogenerated holes at the illuminated TiO_2 electrode to form $CH_3^{\cdot}$ radicals which then combine with each other to yield ethane, while H_2 evolution is the result at the Pt electrode. Distinctively, at the Pt-loaded TiO_2 particles, a photogenerated electron (most likely trapped at Pt sites) and a hole are able to reduce a proton and oxidize acetic acid to yield surface-adsorbed hydrogen H_{ad} and a $CH_3^{\cdot}$ radical, respectively. Then at adjacent TiO_2 and Pt sites, methane can be formed due to the reaction between a neighboring H_{ad} and a $CH_3^{\cdot}$. Another interesting consequence of the size effect concerns the density of photons absorbed by semiconductor particles. Considering two colloidal suspensions containing semiconductors of different particle sizes and assuming that all photons are absorbed in both, the time interval between the absorption of two photons in the smaller-particle suspension can be exceedingly larger than that in the bigger-particle suspension. This difference can be very influential on those reaction pathways which require multiple-electron transfer.

16.2.4.3 Photonic Efficiency and Quantum Yield in Photocatalytic Systems

Studies on heterogeneous photocatalysis have been undertaken extensively worldwide, employing significantly diverse experimental conditions including illumination, photocatalyst preparation, and reactor design. To allow the comparison of experimental data between different research laboratories, a unified, unambiguous definition of the efficiencies of photocatalytic processes is compulsory.

The term photonic efficiency (η) is defined as the ratio of the rate of a photocatalytic reaction (usually the initial rate) to the rate of incident photons entering the system at a given wavelength interval. This parameter attracts the most attention for photocatalysis applications in that it does provide a basis for an engineering efficiency. On the other hand, the quantum yield, ϕ is defined as the ratio of the quantity of reactant molecules consumed or product molecules formed to the quantity of absorbed photons at a given wavelength. In practice, this ratio is often alternatively measured by the reaction rate and the absorption rate of the photon flow, i.e., the volumetric rate corresponding to a given reactant (or product) divided by the rate of photons absorbed in the system, as given by

$$\phi = r/I_{\mathrm{a}}, \tag{16.47}$$

in which r is the photocatalytic reaction rate and I_{a} is the absorbed photon flux. The latter can be obtained from

$$I_{\mathrm{a}} = I_0 \times F, \tag{16.48}$$

in which I_0 is the incident photon flux and F is the integrated absorption fraction in the system over the useful wavelength range calculated as follows:

$$F = \frac{\int_{\lambda_1}^{\lambda_2} I_\lambda T_\lambda^{\mathrm{F}} f_\lambda \mathrm{d}\lambda}{\int_{\lambda_1}^{\lambda_2} I_\lambda T_\lambda^{\mathrm{F}} \mathrm{d}\lambda}, \tag{16.49}$$

where I_λ is the relative incident photon flux in the wavelength interval dλ; I_λ^F is the transmittance of the filter used in the experiment; and f_λ is the fraction of photons absorbed at wavelength λ as given by

$$f_\lambda = 1 - T_\lambda = 1 - 10^{-A_\lambda} \tag{16.50}$$

in which T_λ and A_λ are the transmittance and absorbance, respectively, of the photocatalytic system at wavelength λ. I_0 and F can be determined by actinometry and spectrophotometry, respectively.

16.3 Materials for Photocatalysis

Thin-film photoelectrodes are needed in photoelectrocatalytic systems to apply a bias potential, either for the photoelectrode characterization or to facilitate the photocatalytic reactions. However, to be able to present a more comprehensive view on the performance of different materials, our subsequent discussions will focus on particulate semiconductor photocatalysts since the latter have been much more extensively investigated. Their electronic band structure (i.e., both the bandgap energy and the positions of CB and VB) is the key factor to determine whether or not a semiconductor material is suitable for a specific photocatalytic reaction, as will be demonstrated by reviewing a number of selected metal oxides and coupled/composite materials based on various semiconductors.

16.3.1 Single Semiconductors

16.3.1.1 TiO_2

The virtues of TiO_2, high photostability (i.e., the resistance to photocorrosion), low cost, and nontoxicity, have allowed it to be widely used in photocatalytic applications, including the degradation of organic pollutions in aqueous and gaseous phases, removal of heavy metals from contaminated waters, hydrogen gas generation from photocatalytic water splitting, etc. Studies of TiO_2 photocatalysis have been increasingly thriving since the first pioneering articles appeared in the 1970s (Fujishima and Honda 1972; Frank and Bard 1975, 1977a, b). Anatase and rutile TiO_2 are commonly used as photocatalysts, with anatase showing a higher photocatalytic activity in most cases (Linsebigler et al. 1995). The difference in their photocatalytic activity arises from their different lattice structures and electronic band structures.

It has been generally accepted that upon bandgap illumination of TiO_2 particles the physical events simply proceed as follows: First, electrons are raised into CB and holes left in VB of TiO_2; then a portion of the electrons and holes successfully reach the particle surface where subsequent chemical reactions can take place.

Experimental techniques, such as pulsed laser photolysis and transient absorption spectroscopy (Bahnemann et al. 1984a; Bahnemann et al. 1984b, 1997), are useful to probe the behavior of photogenerated charge carriers in the degradation of organic pollutants by aqueous colloidal suspensions of TiO_2. Upon pulsed laser excitation, electrons and holes are generated inside a TiO_2 particle. Their subsequent behavior can then be probed by the transient absorption spectroscopy technique. To do this, it is necessary to identify the absorption bands of electrons and holes. However, a precise assignment of the electron and hole absorption is rather difficult because their absorption spectra are very broad and the bands overlap each other in the visible wavelength range (Bahnemann et al. 1997). Optically transparent colloidal TiO_2 systems are best chosen to investigate the transient absorption of photogenerated charge carriers. Considerable progress in synthetic methods to produce extremely small TiO_2 clusters (Bahnemann 1993) makes it possible for such investigations to be carried out under well-defined experimental conditions (Colombo and Bowman 1995; Serpone et al. 1995).

Detailed spectroscopic investigations on aqueous colloidal TiO_2 suspensions upon bandgap irradiation in the absence of any hole scavengers showed that, while photogenerated electrons are trapped instantaneously, i.e., on the timescale of nanoseconds, holes can be trapped in electronically shallow or deep states. Deeply trapped holes are rather long lived and inactive, while shallowly trapped holes, which are in a thermally activated equilibrium with free holes, exhibit a very high oxidation potential as probed by using dichloroacetate (DCA^-) and thiocyanate (SCN^-) as substrates (Bahnemann et al. 1997). In another recent work by Yoshihara et al. (2004), the free and trapped electrons and trapped holes were identified employing transient absorption spectra. Their reactivity was evaluated by transient absorption spectroscopy in the presence of hole- and electron-scavengers indicating that the trapped electrons and holes are localized at the surface of the TiO_2 particles and the free electrons are distributed in the bulk, as depicted in Fig. 16.6.

The primary cause for the photocatalytic activity of TiO_2 is believed to be the formation of $^{\cdot}OH$ radicals by rapid conversion of photogenerated holes upon contact with the adsorbed H_2O molecules on TiO_2 according to the following reaction pathways (Gao et al. 2002; Wang et al. 2003a, 2006a):

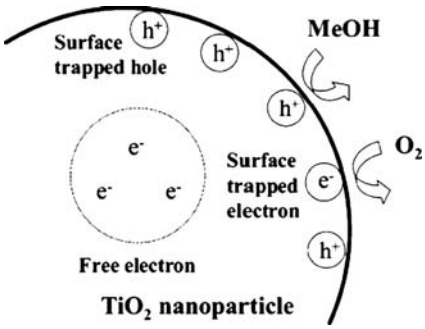

Fig. 16.6 Spatial distribution of photogenerated charge carriers in TiO_2 [Reprinted with permission from Yoshihara et al. (2004). Copyright (2004) American Chemical Society]

$$TiO_2 + hv\left(\geq E_g\right) \rightarrow h^+_{VB} + e^-_{CB}, \tag{16.51}$$

$$h^+_{VB} + e^-_{CB} \rightarrow TiO_2 + \text{heat}, \tag{16.52}$$

$$h^+_{VB} + \equiv Ti^{IV}OH/H_2O \rightarrow \equiv Ti^{IV}OH^{\cdot+}/OH^{\cdot+} + H^+. \tag{16.53}$$

These highly active $^{\cdot}OH$ radicals are capable of mineralizing most organic pollutant molecules. Oxygen molecules dissolved in H_2O, which usually serve as scavengers of photogenerated electrons, also lead to the formation of $^{\cdot}OH$ radicals. Other oxidizing routes have also been proposed, including direct oxidation by the photogenerated holes (Bahnemann et al. 1997; Yoshihara et al. 2004), generation of oxidizing species from reactions involving intermediates formed in the solution (Richard and Boule 1995), etc.

Besides colloidal TiO_2, various nanosized TiO_2 particulate aqueous suspensions have also been used in photocatalytic degradation of organic molecules such as methanol (Wang et al. 2002b, 2004a), dichloroacetate, oxalic acid, phenols, dyes, and other pollutants including herbicides, pesticides, and their derivatives, etc. Commercially available TiO_2 products such as Degussa P25 and Sachtleben Hombikat UV100 have also been studied for different reactions (Wang et al. 2001a, 2002a; Siemon et al. 2002), with the former being regarded as a model photocatalyst widely used as a reference to be compared with other photocatalytic materials.

The photocatalytic activity of TiO_2 toward a specific reaction depends on both, its physicochemical properties such as primary particle size, degree of aggregation, surface area, crystalline structures, etc. and external conditions such as irradiation intensity, pH of the aqueous system, the presence/absence of electron/hole scavengers, and the bias potential if applied for TiO_2 film photoelectrodes. These factors are often interactively affecting the overall photocatalytic activity (Hoffmann et al. 1995).

Particle size, degree of aggregation, and surface area determine the adsorption ability of TiO_2 photocatalysts for substrate molecules, which has proven to be a prerequisite for many photocatalytic reactions to proceed efficiently. Most currently used and commercially available photocatalyst powders, for example, consist of nanocrystalline primary particles that are aggregated to form secondary structures with dimensions in the micrometer range. Aggregation of particles would inevitably reduce their total surface area exposed to the outer environment, leading to a lowered photocatalytic activity as observed in many reaction systems. Only in a certain special agglomerated fashion, i.e., adjacent crystallites are aligned in a given crystallographic orientation to enable a strong electronic coupling between the primary particles, can the photocatalytic activity be maintained at a high level due to the so-called "antenna effect" (Wang et al. 2003a, 2006a). Compared to randomly agglomerated TiO_2 particles, a chain of well-aligned particles will act as the antenna system to transfer the photon energy from the spot of light absorption to the reaction site since the electron-transfer resistance at the grain boundaries is considerably reduced in these nanowires formed upon the aggregation of individual nanoparticles. Based on similar arguments, due to the attraction of both high surface area (hence high adsorption capacity) and crystallite alignment, mesoporous TiO_2

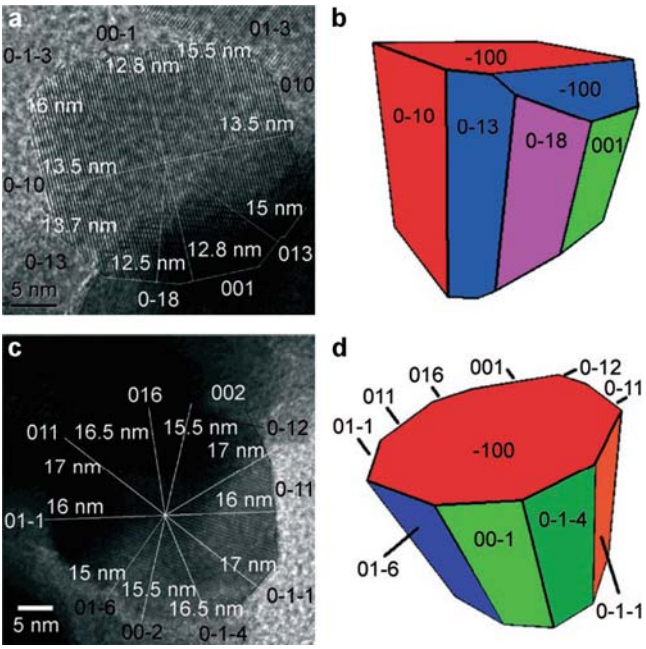

Fig. 16.7 HRTEM micrographs and reconstructed shapes of anatase TiO_2 nanoparticles: (**a, b**) truncated cube; (**c, d**) prism [Copyright Wiley-VCH Verlag GmbH & Co. KGaA. Reproduced with permission from Feldhoff et al. (2007)]

films with ordered structures have also been actively developed recently as efficient photocatalysts (Antonelli and Ying 1995; Bach et al. 1998; Yu et al. 2002a, b; Crepaldi et al. 2003; Tang et al. 2004; Choi et al. 2006; Pan and Lee 2006; Sakatani et al. 2006). The employed illumination mode can also affect the adsorption property of TiO_2 particles via a deaggregation scheme (Wang et al. 2004a, 2006a), in which high intensity, e.g., pulsed laser irradiation, induces the deaggregation of particles through non-adiabatic heat transfer following the electron-hole recombination. This exposes more surface area for the adsorption of the target molecules that was originally blocked due to particle–particle aggregation. This deaggregation scheme is considerably valid since most TiO_2 nanoparticles do not exhibit a spherical shape, as revealed by a high-resolution transmission electron microscopy (HRTEM) study shown in Fig. 16.7, but possess flat facets upon contact of which the adsorption sites can be notably reduced in number (Feldhoff et al. 2007).

Consequently, the knowledge of the adsorption behavior of different molecules onto the TiO_2 surface provides more profound insight into the mechanisms of the corresponding photocatalytic reactions (Blesa et al. 2000; Weisz et al. 2001, 2007; Mendive et al. 2008). In this regard, Attenuated Total Reflection-Fourier Transform Infrared Spectroscopy (ATR-FTIR) serves as a powerful tool to probe the interactions between the TiO_2 surface and organic molecules, e.g. carboxylic acids (Araujo et al. 2005; Mendive et al. 2005, 2006). For example, three forms of oxalate

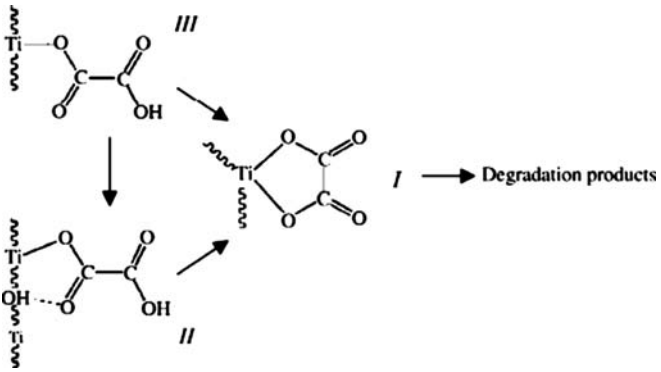

Fig. 16.8 Schematic evolution of the surface composition of oxalates chemisorbed on TiO_2 surface during UV illumination [Reprinted from Mendive et al. (2005), Copyright (2005), with permission from Elsevier]

structures are formed upon chemisorption of oxalic acid on the TiO_2 surface in a low-pH aqueous system, as illustrated in Fig. 16.8, with complex (I) being the most stable and complex (III) being the least stable one. Sequential ATR-FTIR spectra of these adsorbed oxalates under UV illumination suggested that the photocatalytic oxidation of oxalate proceeds through the most stable surface complex, i.e., complex (I) in Fig. 16.8. Complexes (II) and (III) undergo structural rearrangements to replenish the surface availability of complex (I) during its oxidation.

The pH of the aqueous environment of the TiO_2 particles appears to be one of the most influential external conditions determining their photocatalytic activity. Apparently, the adsorption behavior of TiO_2 surfaces toward ionic species can be directly modified by changing the pH of the solution: at lower pH, the TiO_2 surface is protonated to be positively charged which favors the adsorption of anionic species from the solution; at higher pH, the surface is negatively charged thus repelling anionic species from approaching the surface. On the other hand, the pH also bears an influence on the levels of energy bands in TiO_2. At ambient temperature (298 K), the flatband potential, E_{fb}, of a single-crystal TiO_2 photoelectrode varies with pH according to

$$E_{fb} = E_{fb(pH=0)} - 0.059\,pH, \tag{16.54}$$

where $E_{fb(pH=0)}$ is the flatband potential of the photoelectrode at 25°C at pH 0. In other words, the flatband potential shifts cathodically by 59 mV upon changing the pH by one unit. The value of $E_{fb(pH=0)}$ for rutile TiO_2 photoelectrodes has been determined to be 0.06, –0.038, or −0.05 V (vs. NHE) by different researchers. Particulate TiO_2 also exhibits such a Nernstian pH dependence at 25°C as reported by Duonghong et al. (1982) using colloidal TiO_2 composed mainly of amorphous and anatase TiO_2:

$$E_{fb}\,(TiO_2\ \text{particle}) = -(0.12 \pm 0.02) - 0.059pH\,(\text{vs. NHE})\,. \tag{16.55}$$

The difference between the $E_{fb(pH=0)}$ values of particulate and film photoelectrode TiO_2 can, for example, be explained by the different crystal structures of particles

and electrodes. Anatase particles possess a larger bandgap than rutile particles and electrodes. As the valence band position appears to be rather insensitive to the TiO_2 lattice structure, this difference is thus reflected in a more negative value of $E_{fb(pH=0)}$ of anatase particles than of rutile electrodes. Since the flatband potential is usually very close to the Fermi level of electrons and the conduction band edge in n-type TiO_2, the pH dependence of E_{fb} also determines the position of the conduction band edge, and hence the rate of interfacial electron transfer. Consequently, reduction reactions initiated by conduction band electrons will be more favored (i.e., occur at a higher rate or yield) at high pH values while oxidation processes are favored at low pH values. Depending upon the desired reactions, the proper choice of pH will therefore be crucial for the overall process efficiency. Since this so-called Nerstian behavior is by no means limited to TiO_2 but is a general phenomenon of almost any semiconductor/water interface, the above considerations can readily be generalized for all of the subsequently described systems.

16.3.1.2 ZnO

ZnO has a similar bandgap to TiO_2 as shown in Fig. 16.9 and is expected to exhibit similar photocatalytic capacity to that of TiO_2, provided that this property is largely dependent on the energy level of CB and VB. Therefore, it has been comparatively studied with TiO_2 concerning its photocatalytic performance (Amalric et al. 1994; Richard 1994; Yeber et al. 2000; Khodja et al. 2001; Sakthivel et al. 2003; Daneshvar et al. 2004; Jing et al. 2004b; Seven et al. 2004). The main drawback of particulate ZnO in an aqueous environment is, however, its chemical instability:

$$\mathrm{ZnO} + 2\mathrm{H}^+_{aq} \rightleftharpoons Zn^{2+}_{aq} + \mathrm{H_2O} \tag{16.56}$$

$$\mathrm{ZnO} + \mathrm{H_2O} \rightleftharpoons \mathrm{Zn\,(OH)_2} \tag{16.57}$$

Hence, the pH range in which ZnO is found to exist in the stable form is very limited (Bahnemann et al. 1987a).

ZnO has shown photocatalytic activities toward the reduction or oxidation of several compounds (Richard et al. 1992; Sakthivel et al. 1999, 2001; Khodja et al. 2001; Jing et al. 2002, 2004b; Akyol et al. 2004; Chakrabarti and Dutta 2004; Daneshvar et al. 2004; Yatmaz et al. 2004) including organic dyes and pulp and paper bleaching effluents, etc. Similar oxidation pathways to those of TiO_2 were confirmed in ZnO photocatalysis, including the formation of $^{\cdot}OH$ radicals as well as the direct oxidation by photogenerated holes, etc. But the implementation of ZnO photocatalytic systems has not been as flourishing as TiO_2 systems, mainly due to its unsatisfying photostability. Under prolonged optical irradiation, ZnO suffered from photodecomposition, which is mainly attributed to the oxidation of ZnO from solid phase into aqueous phase by holes according to the following reaction (Fujishima et al. 1981):

$$\mathrm{ZnO} + 2h^+_{VB} \rightarrow \mathrm{Zn^{2+}} + \frac{1}{2}\mathrm{O_2} \tag{16.58}$$

Although its photocatalytic application is not as successful as TiO_2, ZnO has been attracting more and more attention in other fields, including sensors (Wan et al. 2004; Ozgur et al. 2005; Pearton et al. 2005), optoelectronics (Wang et al. 2004b), and field emission units (Studenikin et al. 1998; Li et al. 2000; Kong et al. 2001).

16.3.1.3 SnO_2

SnO_2 is also an n-type semiconductor with bandgap energy of ~3.8 eV, which corresponds to an optical absorption edge below 330 nm. However, the CB position of SnO_2 is such that it is incapable of reducing oxygen molecules (Fig. 16.9). Therefore, in the past, semiconductors of such kind have not been considered as suitable photocatalysts that can be used individually. On the other hand, such materials may have an advantage regarding their band structures and can possibly provide another

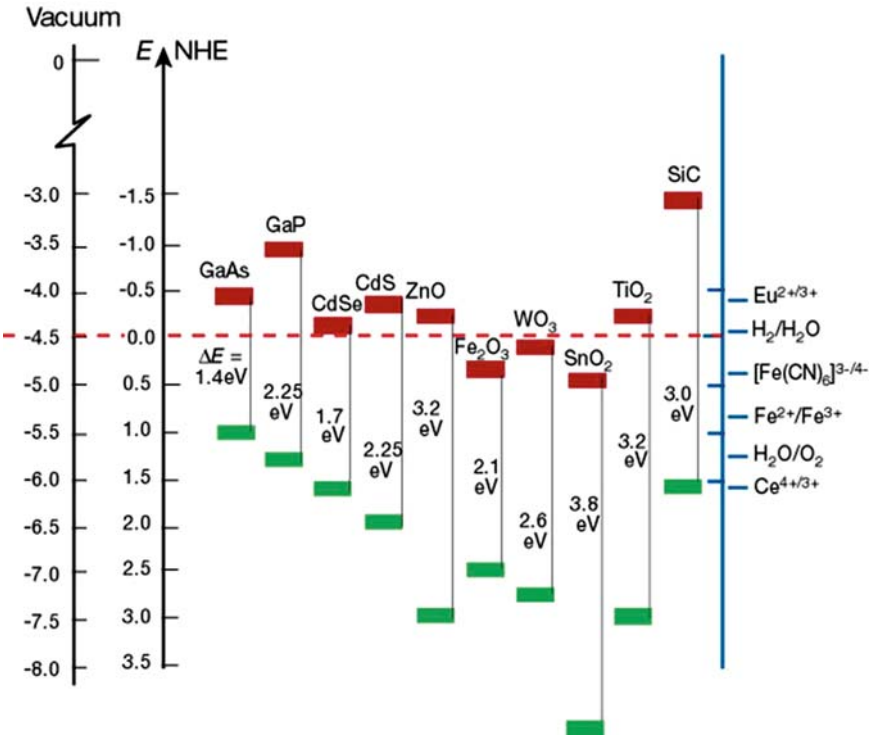

Fig. 16.9 CB and VB energy levels of several semiconductors. (The semiconductors are in contact with aqueous electrolyte at pH 1. The energy scale is indicated in electron volts using either the normal hydrogen electrode (NHE) or vacuum level as reference. On the *right* the standard potentials of several redox couples are presented against the standard hydrogen electrode potential.) [Reprinted by permission from Macmillan Publishers Ltd: [Nature] (Grätzel 2001), copyright (2001)]

way to serve in photocatalytic systems, i.e., when coupled with other semiconductors with suitable matching of band levels (Vinodgopal and Kamat 1995). This has been demonstrated in a number of publications (Vinodgopal and Kamat 1995; Vinodgopal et al. 1996; Wang et al. 2002a; Cun et al. 2004; Zhang et al. 2004) details of which will be given in Sect. 16.3.2. A much narrower bandgap of 2.53 eV was also reported for SnO_2, corresponding to an absorption edge of 490 nm (Wang et al. 2002a). Quite recently, an interesting type of SnO_2 photocatalyst, nanosized V-shaped bipods, was reported by Wang and coworkers (Wang et al. 2006b), and the materials showed a broad photoresponse in the visible region deep up to ~550 nm. This was believed to be due to the presence of oxygen vacancies, together with abundant surface states.

16.3.1.4 WO_3, Fe_2O_3 and CdS

WO_3, Fe_2O_3, and CdS are jointly discussed in the same section simply because of their similar and relatively narrow bandgaps, 2.6, 2.1, and 2.25 eV, respectively, which make them capable of being excited by visible light. Figure 16.9 shows that the upper edge of the VB of WO_3 is close to that of TiO_2, which is exceeding the H_2O/O_2 oxidation potential. Thus, the photogenerated holes in WO_3 upon bandgap excitation are capable of oxidizing a wide range of compounds. The advantage of WO_3 as a photocatalyst is that the bandgap is only ~2.6 eV, which is ~0.6 eV narrower than TiO_2. Therefore, more visible light can be harnessed by WO_3 from the sunlight spectrum (Santato et al. 2001). Another virtue of WO_3 is its remarkable photostability in acidic aqueous solutions making it a powerful photocatalyst, e.g., for the treatment of wastewater contaminated by organic acids (Monllor-Satoca et al. 2006). For example, formic acid and Rhodamine B have been reported to be effectively degraded on WO_3 photoelectrodes.

Another important application of WO_3 is photocatalytic water splitting to produce hydrogen gas using visible solar light, due to its narrow bandgap. Earlier studies of the photoelectrochemical behavior of both polycrystalline and monocrystalline WO_3 provided instructive knowledge for the development of photocatalytic water-splitting systems (Hodes et al. 1976; Hardee and Bard 1977). The difficulty in the overall water splitting (both reduction and oxidation of H_2O molecules are to be achieved) by WO_3 is that the lower edge of the CB lies below the redox potential of H_2O/H_2, as illustrated in Fig. 16.9. This means that the reduction of water molecules to generate hydrogen gas is thermodynamically unfavorable (Gissler and Memming 1977). Applying a bias potential to the system can overcome the energy barrier for the photogenerated electrons to be ejected into the adsorbed water molecules (Santato et al. 2001). Coupling with other semiconductor materials (Abe et al. 2005) and doping by metal ions (Hwang et al. 2002; Hameed et al. 2004) are other alternatives to make use of the oxidation power of WO_3 for water splitting. WO_3 also found interesting applications in electrochromic (Papaefthimiou et al. 2001; Badilescu and Ashrit 2003; Baeck et al. 2003) and photochromic (Shigesato 1991; Bechinger et al. 1996; Su et al. 1997; Xu et al. 2000;

Kim et al. 2006b) devices such as large area displays and "smart windows" because WO_3 films can be switched between different optical states under different electrochemical or optical conditions. The electrochromic effect is caused by the electrochemical reaction between the WO_3 electrode and protons in the electrolyte solution, under the influence of a bias potential to provide charge carriers (electrons in this case). The electrons can then create color centers by reducing the W^{6+} species to W^{5+} species. The photochromism effect of WO_3 is due to the formation of an identical absorption band upon light irradiation (Bechinger et al. 1993). This process is completely reversible by exposing the reduced sample to oxygen gas.

The band structure of α-Fe_2O_3 is quite similar to that of WO_3, with the VB edge exceeding the standard redox potential of H_2O/O_2 and the CB edge being lower than the standard redox potential of H_2/H_2O. Upon optical irradiation, the recombination of the photogenerated charge carriers is reported to be very rapid (within 1 ns) if no electron or hole scavengers were present in the electrolyte (Faust et al. 1989). In the presence of appropriate scavengers, however, the holes can function as powerful oxidants, and the electrons as moderately powerful reductants. For example, S^{4+} species, such as aqueous SO_2, HSO_3^- and SO_3^{2-} etc., have been shown to be readily oxidized on the surface of α-Fe_2O_3 (Frank and Bard 1977; Leland and Bard 1987). Using Fe^{3+} as the electron scavengers, α-Fe_2O_3 is capable of oxidizing H_2O to evolve oxygen gas (Ohmori et al. 2000). A bias potential can also help to achieve a total H_2O splitting under visible irradiation (Khan and Akikusa 1999). A number of organic compounds (e.g. salicylic acid (Pal and Sharon 1998), phenols (Pulgarin and Kiwi 1995), azo dyes, and 2-naphthol (Kawahara et al. 2006)) can also be photocatalytically degraded on α-Fe_2O_3 photocatalysts, either by adding sacrificial scavengers or through the application of a bias potential, although the efficiency remains to be improved.

In the area of photoelectrochemistry, CdS has been the most heavily studied II–VI group semiconductor. It has a higher VB edge as compared with the above-mentioned metal oxides, as shown in Fig. 16.9. This is because the VBs of metal oxides are mainly formed by O2p states, while that of CdS is formed by S2p states. The electronegativity of S is smaller than that of O, resulting in the different VB positions. Quantum size effects, represented by the markedly different properties of materials when their sizes decrease, were often emphasized in the study of CdS semiconductors. For example, the onset of light absorption by CdS varies significantly as the particles decrease in size. Moreover, this quantum size effect can be maintained during the assembly of CdS films from quantum-sized CdS particles (Hirai et al. 2002; Granot et al. 2004; Baron et al. 2005). For example, assembly of p-aminothiophenol-capped CdS nanoparticles onto a p-aminothiophenol-functionalized Au electrode was achieved by electropolymerization, resulting in a flexible charge-carrier behavior upon optical irradiation under the bias potential (Granot et al. 2004). Chemoselective photocatalytic reduction of aromatic azides to aromatic amines was recently reported on CdS quantum dots in the presence of sacrificial electron donors (Warrier et al. 2004). As commonly seen in other low CB edge semiconductors, CdS also suffers from photocorrosion by photogenerated holes (Meissner and Memming 1988). Moreover, as reported by

Meissner et al. (Meissner et al. 1986), there might even be fundamental problems concerning the principle ability of CdS to form molecular hydrogen from water in a photoelectrochemical cell based upon the position of its conduction band edge. This problem has been recently addressed by a new method for the preparation of CdS electrodes, meanwhile obtaining high photocatalytic activity toward hydrogen production (Jing and Guo 2006).

16.3.2 Coupled Semiconductors

Coupling between different semiconductors in photocatalytic systems was designed to alleviate the charge-carrier recombination in individual photoelectrodes. A good matching of their CB and VB levels can realize a vectorial transfer of photogenerated charge carriers from one to the other as illustrated in Fig. 16.10, where the relative positions of the energy bands of the two particles are shown in terms of energetic rather than spatial level. After coupling in the shown manner, the energy gap between corresponding band levels drives the charge carriers from one particle to its neighbor to form a spatial separation between electrons and holes. But coupling of semiconductors does not always enhance the charge separation, because the design of a coupled photoelectrode relies on the band structures of its components, which are determined by many other factors (e.g. surface area, defect density, crystallinity, and quantum size effects). More detailed aspects of such coupling effects will be discussed below for a few examples.

Other than the mutually photosensitive components, coupling between one photosensitive and another nonsensitive (e.g., very wide bandgap) semiconductor may also have positive effects on the photocatalytic performance of the sensitive one. For example, Kisch and Weiss (Weiss et al. 2001; Kisch and Weiss 2002) studied the SiO_2-supported CdS photoelectrode in an organic addition reaction, and found that the enhanced photocatalytic activity was related to the changes in bandgap and flatband potential of CdS, which originates from an electronic semiconductor–support interaction mediated by [Si]–O–Cd–S bonds.

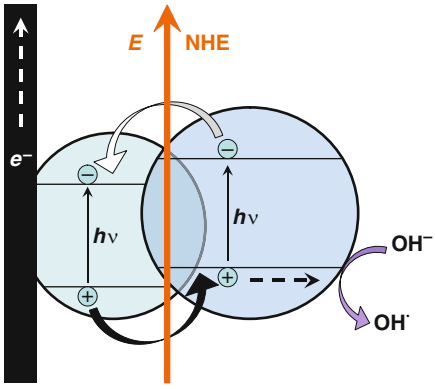

Fig. 16.10 Coupling two different semiconductor particles and charge-carrier separation

16.3.2.1 TiO_2/WO_3

The coupling scheme depicted in Fig. 16.10 has been achieved for WO_3/TiO_2 photoelectrodes. As shown in an earlier study (Do et al. 1994) concerning the effect of adding WO_3 to TiO_2 on the photocatalytic activity of TiO_2, the observed enhanced photocatalytic degradation of 1,4-dichlorobenzene was explained by the increased electron transfer from TiO_2 to WO_3 via the formation of an intermediate W(V) species, together with the increased surface acidity in the coupled photoelectrode. Protonated surface hydroxyl groups, and hence the surface acidity, can promote the electron transfer from the CB of TiO_2 to adsorbed oxygen molecules (Papp et al. 1994). In a study by Kwon et al. (2000), the role of the increased surface acidity due to WO_3 addition was confirmed by treating the photocatalytic reactions on WO_3/TiO_2 electrodes using the Langmuir–Hinshelwood equation (Hidaka et al. 1992) as follows:

$$r = \frac{kKC}{1 + KC}, \tag{16.59}$$

where r is the rate of photocatalytic reaction; k is the reaction rate constant only related to the illumination source, the catalyst activity, and the reaction media, but not to the structure of the reactants; K represents the equilibrium adsorption constant and is a function of the reactant molecular structure; and C denotes the concentration of the reactant. The magnitude of k is indicative of the decomposition rate of the adsorbed organic molecules, which is closely related with the charge-carrier separation and trapped charge density on the surface. Meanwhile, K represents the adsorption efficiency of the organic compounds, which is intimately related to the Lewis surface acidity of the particles. Therefore, the contribution to the enhanced photocatalytic activity by WO_3 incorporation can be divided into two aspects (1) improved charge-carrier separation and (2) increased surface adsorption affinity. The authors suggested that under certain circumstances the second might be the predominant effect. As proposed by Miyaochi et al. (2002) who studied the effect of layered WO_3/TiO_2 structures, both the surface hydrophilicity of the top TiO_2 layer and the photocatalytic oxidation efficiency for the test molecule methylene blue were increased, which was also explained by a charge-carrier transfer between the TiO_2 and WO_3 layers.

The TiO_2/WO_3 coupling does not always enhance the photocatalytic activity of TiO_2. For example, too much loading of WO_3 shows adverse effects because some W sites can act as charge recombination centers according to the following scheme (Keller et al. 2003):

$$W^{6+} + e^-_{(TiO_2)CB} \rightarrow W^{5+} \tag{16.60}$$

$$W^{5+} + h^+_{(TiO_2)VB} \rightarrow W^{6+} \tag{16.61}$$

Another negative example was reported to be due to the difference in WO_3 crystallinity. Higashimoto et al. (2006) studied two systems of TiO_2 coupled with either amorphous or crystalline WO_3. Their bandgap calculations on the two systems

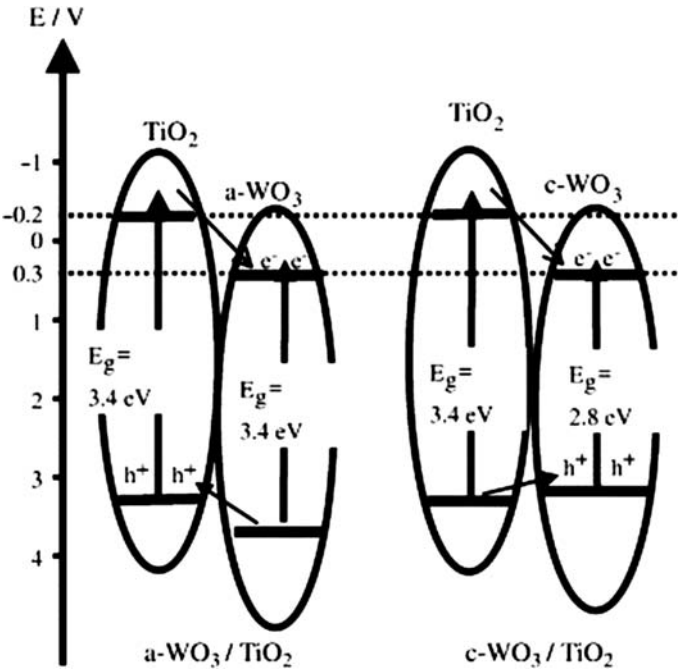

Fig. 16.11 Energetic diagram of amorphous- and crystalline-WO_3/TiO_2 [Reprinted from Higashimoto et al. (2006), Copyright (2006), with permission from Elsevier]

revealed different CB and VB positions of amorphous and crystalline WO_3, and so are the different CB positions between TiO_2 and WO_3 in the two systems, as depicted in Fig. 16.11.

The band structures in the crystalline-WO_3/TiO_2 couple do not favor the separation but rather the recombination of charge carriers. Although the CB electron transfer is favored in amorphous-WO_3/TiO_2, the bandgaps and band edge levels in WO_3 and TiO_2 may vary from sample to sample due to different preparation methods (Miyauchi et al. 2000; Higashimoto et al. 2006). Therefore, the fabrication of coupled semiconductors with controlled band structure properties is still a challenging task.

16.3.2.2 TiO_2/SnO_2

As mentioned in Sect. 16.3.1.3, SnO_2 has a very large bandgap (~3.8 eV) and has been traditionally viewed as a bad candidate for photocatalytic applications. However, coupling SnO_2 with other semiconductors can greatly enhance its photocatalytic activities for organic pollutants degradation (Bedja and Kamat 1995; Vinodgopal and Kamat 1995; Vinodgopal et al. 1996; Kamat 1997; Levy et al. 1997; Hattori et al. 2000; Kanai et al. 2004), especially when an external bias potential is applied (Vinodgopal and Kamat 1995).

Vinodgopal and Kamat (1995) reported a very rapid decolorization of acid orange 7 using a coupled SnO_2/TiO_2 photoelectrode under a bias potential. They ascribed the enhanced degradation rate as an improved charge separation due to a good matching in energy levels (E_{CB} for $SnO_2 = 0$ V vs. NHE at pH 7, while for TiO_2 $E_{CB} = -0.5$ V vs. NHE at pH 7). The anodic bias potential was also reported to be responsible for the enhancement in photocatalytic activity by driving away the electrons into the conduction band of SnO_2, thus promoting the oxidation of dye molecules on the TiO_2 surface where photogenerated holes are more abundant. The photoelectrocatalytic degradation of naphthol blue black by a similar system (Vinodgopal et al. 1996) again was significantly improved compared with pure TiO_2, due to the enhanced charge separation between TiO_2 and SnO_2 nanoparticles. As the content of SnO_2 was increased, the influence of oxygen on both the short-circuit photocurrent and the open-circuit photovoltage became less and less significant, indicating the rapid injections of electrons from TiO_2 into SnO_2 before recombination with the holes or being scavenged by the oxygen molecules. A scheme depicting this coupled photoelectrode is shown in Fig. 16.12. The network of three-dimensionally interconnected nanoparticles of both kinds generates sufficient contact points between these two kinds of particles and thus a large SnO_2/TiO_2 interface.

Another coupling approach is to deposit one type of semiconductor film over another, thus a clear-cut two-dimensional interface layer will be achieved. Employing this approach, the charge-carrier transfer between TiO_2 and SnO_2 was also confirmed as the dominant factor for the improved photocatalytic activity. Hattori et al. (2000, 2001) prepared the double-layer SnO_2/TiO_2 coupled films (as shown in Fig. 16.13) and studied their photocatalytic activity toward both the oxidation of formic acid and 1,3,5,7-tetramethylcyclotetrasiloxane and the reduction of Ag^+ and bis(2-dipyridyl)disulfide. By comparing the amount of CO_2 evolved, the photooxidation of formic acid on the SnO_2/TiO_2 couple was confirmed to occur more efficiently than on pure TiO_2 films. The degradation of 1,3,5,7-tetramethylcyclotetrasiloxane was also more efficient on the coupled SnO_2/TiO_2 films. On the other hand, photocatalytic reduction processes on the SnO_2/TiO_2 couple were found to be less efficient than on pure TiO_2 films. These results are unanimously in consistence with the vectorial charge-carrier transfer as proposed earlier (Vinodgopal and Kamat 1995; Vinodgopal et al. 1996). Note that the

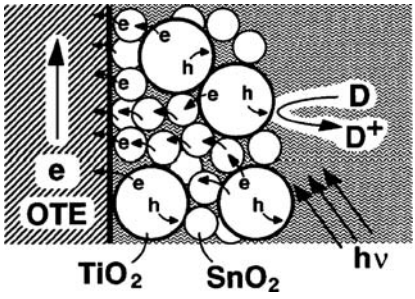

Fig. 16.12 Idealized photoinduced charge separation in a SnO_2/TiO_2 semiconductor film [Reprinted with permission from Vinodgopal et al. (1996). Copyright (1996) American Chemical Society]

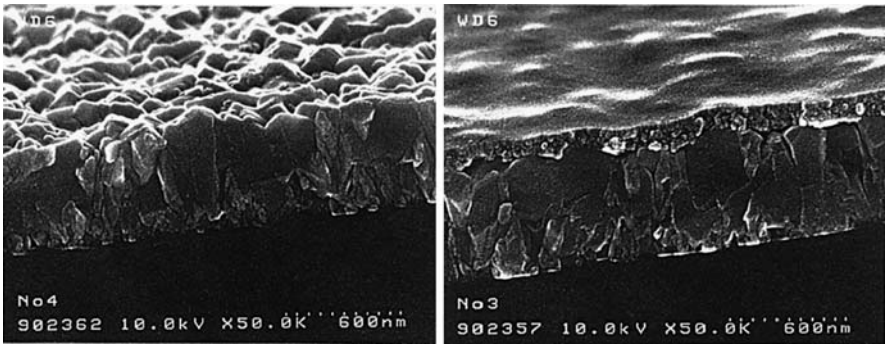

Fig. 16.13 SnO_2 and TiO_2/SnO_2 deposited on glass substrate (Hattori et al. 2000) (Reproduced by permission of The Electrochemical Society)

electrode substrates in these studies are nonconducting, therefore electrons transferred from TiO_2 into SnO_2 can only exit these layers via the edges of the SnO_2 layer in contact with the electrolyte (Hattori et al. 2000).

Shang et al. (2004) also confirmed the positive effect of the coupled semiconductors by the higher photocatalytic degradation of formaldehyde on SnO_2/TiO_2 bilayers which were compared with pure TiO_2. They further studied the effect of the thickness of the TiO_2 layer on the photocatalytic activity of the couple. As the TiO_2 thickness increased, the activity was found to decline, until a similar value as that of the pure TiO_2 film was attained. As the TiO_2 layer became thicker, more and more electrons generated far away from the SnO_2/TiO_2 interface recombine with the holes before they can reach the region of the interface in which a gradient can "pull" them toward the SnO_2 CB. The outermost TiO_2 region functioned very much the same way as a pure TiO_2 film did. If TiO_2 was firstly deposited on the glass substrate, followed by depositing a SnO_2 layer over the TiO_2 film, the photocatalytic activity of this couple was much lower than that of the glass/SnO_2/TiO_2 configuration. This again supports the coupling effect in that the electrons in the SnO_2 conduction band now cannot be transferred into TiO_2 due to the energy barrier. More complex patterns can also be formed in combining SnO_2 and TiO_2 layers into a film photoelectrode (Cao et al. 2001; Kawahara et al. 2001). As shown in Fig. 16.14, a first layer of SnO_2 followed by two layers of TiO_2 stripes orthogonal to each other resulted in much higher activity, as compared with nonpatterned structures.

16.3.2.3 TiO_2/CdS

Similar coupling schemes as those described in Sect. 16.3.2.1 can be used for CdS/TiO_2 photoelectrodes. The relative energetic positions of CBs and VBs between CdS and TiO_2 are shown in Fig. 16.15. Both the CB and VB of CdS particles are higher than their counterparts in the TiO_2 particles (Srinivasan et al. 2006). The smaller bandgap of CdS ($\sim$2.5 eV) enables it to absorb visible light to generate

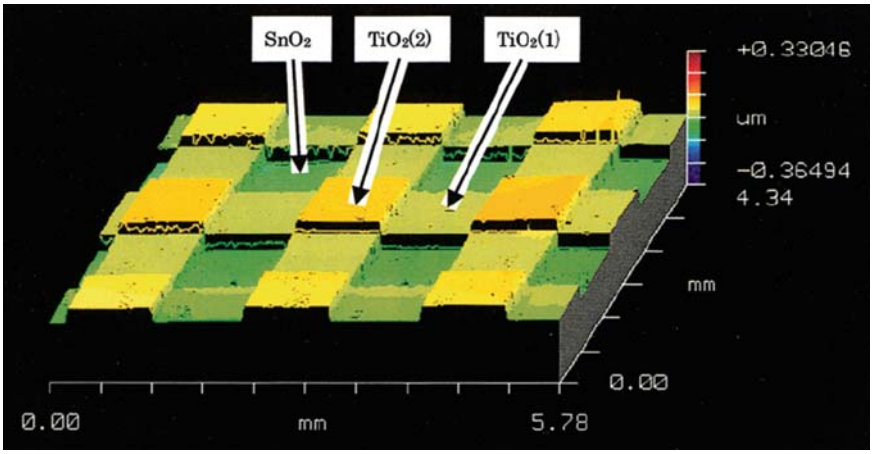

Fig. 16.14 3D imaging of a cross-patterned SnO_2/TiO_2 coupled film. (The SnO_2 layer was at the *bottom*, with two orthogonal TiO_2 stripes on top.) [Reprinted with permission from Kawahara et al. (2001). Copyright (2001) American Chemical Society]

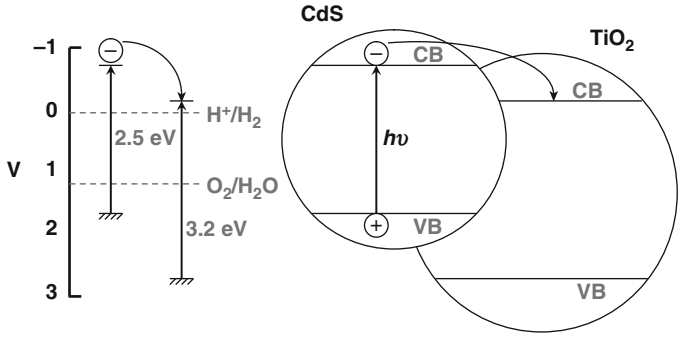

Fig. 16.15 Band positions in the coupled TiO_2/CdS system (Srinivasan et al. 2006)

electrons and holes. Subsequently the electrons will flow from the CB of CdS to the CB of the adjacent TiO_2, leaving the holes behind in the VB of CdS. The enhanced charge separation under visible-light illumination has made the couple widely used in the photo(electro)catalytic reactions, e.g., for the degradation of organic pollutants (Kumar and Jain 2001; Yin et al. 2001; Bessekhouad et al. 2004, 2006; Tristao et al. 2006), in the production of hydrogen gas (So et al. 2004; Jang et al. 2006), and in visible-light-driven solar cells (Robel et al. 2006), etc.

Studies on the coupling effect between CdS and TiO_2 can be traced back to the early 1980s, when the hydrogen generation via photocatalytic H_2S splitting by CdS was found to be enhanced upon the addition of TiO_2 particles (Serpone et al. 1984). Spanhel et al. (1987) also found a tenfold increase in the quantum yield for the photoreduction of methylviologen by using coupled CdS/TiO_2 particulates.

Evans et al. (1994) suggested that the CB electron transfer from CdS to TiO_2 could be completed on a timescale of picoseconds, resulting in a significantly slower recombination for the charge carriers formed upon light absorption in CdS.

Earlier research on TiO_2/CdS couples was mostly limited to colloidal systems, and CdS was usually the dominant component. Subsequent research started to reverse this trend by using CdS as a "sensitizer." The small amount of CdS dispersed in TiO_2 matrix can absorb visible light, making the coupled photocatalyst sensitive to visible light. Yu et al. (2003) prepared a CdS-sensitized TiO_2 nanocrystalline photocatalyst and obtained much higher activity toward the degradation of methylene blue under visible-light illumination ($\lambda > 400$ nm) than with pure TiO_2 or pure CdS, respectively, due to the rectified electron transfer from CdS to TiO_2, as shown by the formation of Ti^{3+} observed in electron paramagnetic resonance (EPR) spectra (Wu et al. 2006). Wang et al. (2006c) prepared a coupled TiO_2/CdS hydrogel with a CdS loading of only about 0.9%. The hydrogel consisted of uniform crystalline CdS particles (~2 nm in size) well dispersed in TiO_2. At this size, the quantum size effect from CdS could be expected, i.e., the bandgap of CdS was widened to increase the energy difference between the CBs of CdS and TiO_2. Meanwhile, the coupled semiconductor was still sensitive to visible light for the degradation of methylene blue under visible light (excitation wavelength longer than 420 nm). The degradation mainly took place on the TiO_2 surface since most of the CdS surface was covered by the TiO_2 matrix.

Another benefit of a such-structured couple is that the surrounding TiO_2 matrix can protect the CdS quantum dots against photocorrosion, which has been a major problem for CdS photocatalysts to be used in aqueous environments (Bessekhouad et al. 2006). The effects of quantized TiO_2 particles were also studied in TiO_2/CdS couples. Sant and Kamat (2002) prepared extremely small TiO_2 particles coupled with CdS. The quantum size effects from both TiO_2 and CdS were confirmed by the blue shift of the absorption edges as the size of the particles decreased. When the TiO_2 size came down to 0.5 nm, the bandgap of TiO_2 was widened by 0.85 eV. This in turn shifted the energy of the conduction band edge of TiO_2 by over 0.5 eV toward negative values. Such a shift in CB of TiO_2 now created an energy barrier for the electron transfer from CdS to TiO_2, because the CB edge of TiO_2 had become more negative than that of CdS. This was confirmed by the CdS emission spectra, i.e., the quenching of CdS emission (the electron transfer from CdS to TiO_2) could no longer be observed as the TiO_2 particle size dropped to 0.5 nm with CdS size remaining unchanged, as illustrated in Fig. 16.16.

It is straightforward that an adequate physical and electric contact (e.g., an ohmic contact) between different semiconductors in the coupled semiconductor assembly is necessary for an effective transfer and hence a significant separation of the charge carriers. Thus, many efforts have been dedicated in this regard. Jang et al. (2006) prepared a coupled CdS/TiO_2 photocatalyst by coupling CdS nanoparticles with TiO_2 nanosheets to maximize the contact between the two phases. The such-coupled photocatalyst showed higher activity for hydrogen production and methylene blue degradation under visible-light illumination ($\lambda > 420$ nm) than a physical mixture of CdS nanoparticles and TiO_2 nanorods. Coaxial arrays of TiO_2/CdS sheath/core

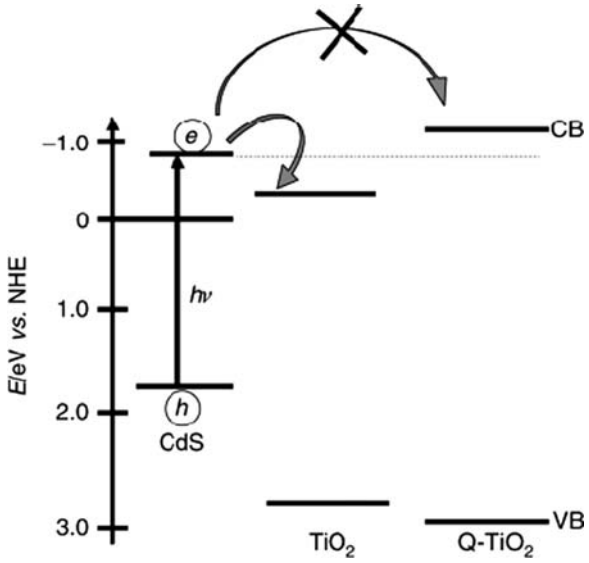

Fig. 16.16 Energy level diagram of quantized TiO_2/CdS coupled semiconductors [Sant and Kamat (2002) – Reproduced by permission of the PCCP Owner Societies]

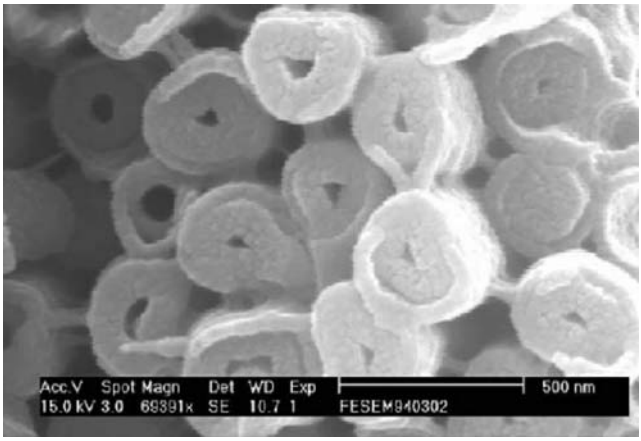

Fig. 16.17 SEM image of TiO_2/CdS nanocables prepared by templated liquid-phase deposition [Reprinted from Hsu et al. (2005), Copyright (2005), with permission from Elsevier]

couples were also prepared to increase the contact interface (Hsu et al. 2005), as shown in Fig. 16.17. The outer layer of the TiO_2 sheath was firstly grown guided by an anodic aluminum oxide template; then the CdS core was grown within the TiO_2 sheath. This coupling mode has been found to be highly favorable for the vectorial electron transfer between the coaxial CdS and TiO_2.

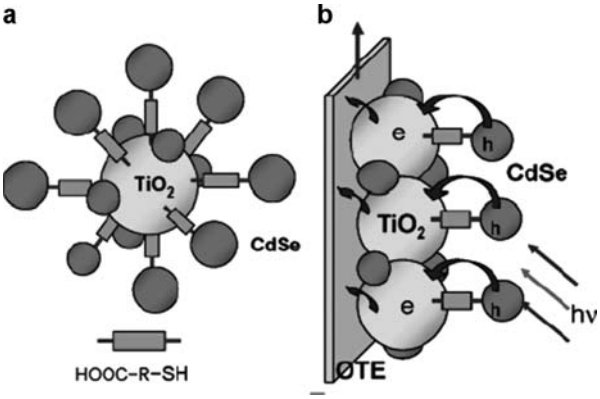

Fig. 16.18 TiO_2/CdSe couple linked by organic molecules: (**a**) particle–particle; (**b**) particle–film [Reprinted with permission from Robel et al. (2006). Copyright (2006) American Chemical Society]

While the above-mentioned methods tried to couple TiO_2 with CdS via a direct contact between hard particles, a "soft" coupling scheme was also proposed. Robel et al. (2006) used bifunctional organic molecules as the surface modifier to link up CdSe quantum dots (QDs) with TiO_2 nanoparticles, as shown in Fig. 16.18. The optical absorption properties of the QDs remain unchanged but the emission yield decreases by ~80% when linked to TiO_2. This indirectly proved the hypothesis that TiO_2 nanoparticles are interacting with the excited CdSe QDs via a vectorial electron transfer scheme. It should be emphasized that the photoactivity strongly depends on the physicochemical properties of the coupled semiconductors, such as the surface area, porosity, adsorption capacity, distribution of the active sites, etc. Upon coupling, besides the vectorial charge transfer, the original properties of the components might also be modified. This complicates the comparison of photoactivity before and after coupling. In many cases, only the total photocatalytic activity, which is a collective performance based on many factors, was studied.

16.3.3 Noble Metal/Semiconductor Composites

Combining noble metals with semiconductor photocatalysts on a nanometer scale was proposed to enhance the photocatalytic activity due to their different Fermi levels, characterized by the work function of the metals and the band structure of the semiconductors. Upon contact, a Schottky barrier (Gao et al. 1991; Schierbaum et al. 1991; Linsebigler et al. 1995) can be formed between semiconductor and metal particle, leading to a rectified charge-carrier transfer similar to that in the coupled semiconductors. As shown in Fig. 16.19, irradiation by photons with higher energy than the semiconductor bandgap generates electrons in the CB of the semiconductor, and raises its Fermi level to more negative values (Subramanian et al. 2004).

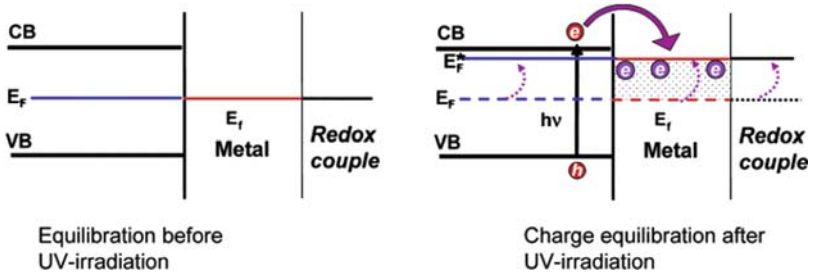

Fig. 16.19 Electron transfer and Fermi level shift at the metal/semiconductor interface [Reprinted with permission from Subramanian et al. (2004). Copyright (2004) American Chemical Society]

Then, the energetic difference at the semiconductor/metal interface drives the electrons from the CB of the semiconductor into the metal nanoparticles. The Fermi level of the metal is thereby also negatively shifted so that a secondary electron transfer can occur between the metal and electron acceptors in the redox couples from the surrounding electrolyte. A large number of reports on nanosized Ag, Au, and Pt combined with photocatalysts such as TiO_2 have indeed shown increased photoactivity which was hence explained by this effect (Sano et al. 2000; Yu and Zhao 2000).

16.3.3.1 Ag/TiO_2

Photoinduced Charge Transfer in Ag/TiO_2

Combination of Ag and TiO_2 can be achieved in different manners. For instance, Ag nanoparticles can be deposited on the TiO_2 surface by photoassisted reduction of Ag^+ ions in aqueous solution under UV illumination (Friedmann et al. 2007). Ag/TiO_2 core/shell structures can also be obtained, for example, by firstly reducing Ag^+ ions to form an Ag core and hydrolyzing titanium-(triethanolaminato)isopropoxide to form a TiO_2 shell around the Ag particle (Hirakawa and Kamat 2004, 2005). In the absence of electron scavengers, such materials have shown the ability to store the photogenerated electrons transferred from TiO_2 to the Ag cores upon UV excitation, as shown in Fig. 16.20. The electron transfer continued until a Fermi level equilibrium was established between Ag and TiO_2. The shift of the surface plasmon resonance band was used to measure the number of electrons stored in the Ag core, with an estimation of 66 electrons per Ag/TiO_2 core/shell structure. This electron storage ability shows the importance of such structures in photon energy conversion by storing electrons during excitation and delivering them back in the dark. But their photocatalytic activity was limited, as indicated by C_{60}/C_{60}^- probe under UV irradiation (Hirakawa and Kamat 2005). Similar electron transfer and Fermi level equilibration were also observed in noble metal/ZnO nanocomposites (Wood et al. 2001).

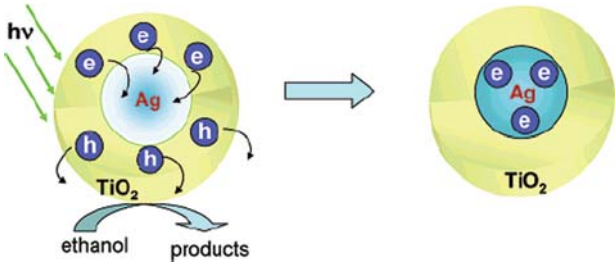

Fig. 16.20 Electron accumulation in Ag/TiO_2 core–shell particles [Reprinted with permission from Hirakawa and Kamat (2004). Copyright (2004) American Chemical Society]

Photocatalytic Performance of Ag/TiO_2

High photoactivity of Ag/TiO_2 nanocomposites has been reported, for example, in the decoloration of methyl orange solutions (Yu et al. 2005b). This was attributed to the multiheterojunctions formed by Ag/TiO_2 (anatase), Ag/TiO_2 (rutile), anatase/rutile, etc. Although anatase TiO_2 has been known to be more active than rutile, their coexistence has a positive effect on the photocatalytic activity, as exemplified by the highly active Degussa P25 with a two-phase formula (Sun et al. 2003). Ag nanoparticles were also intercalated between TiO_2 nanosheets, and a larger photocurrent can be obtained as compared with pure TiO_2 films (He et al. 2004). This was explained by the enhanced photoelectron conduction between TiO_2 layers due to metallic Ag. Under visible-light irradiation (wavelengths longer than 470 nm), photooxidation of Rhodamine B by Ag/TiO_2 can be achieved due to the following mechanisms (Sung-Suh et al. 2004) (1) The dye molecules are photosensitive and can be excited to generate electrons which are then transferred to the CB of TiO_2; (2) TiO_2 under visible-light illumination only acts as the electron acceptor from the excited dye due to its large bandgap; (3) the Ag nanoparticles attract the electrons from the CB of TiO_2 due to the Schottky-barrier effect; and (4) Ag nanoparticles can also act as efficient dye-adsorption sites, where oxidant species can be formed from electron scavenging by adsorbed oxygen molecules. Under bias potential, Ag/TiO_2 thin-film photoelectrodes on ITO glass can efficiently degrade formic acid. Both, Ag loading and the bias potential are responsible for the increased activity. Ag not only traps the photoelectrons from TiO_2 but also assists the bias electric field to drive them into the external circuit.

Photocatalytic reduction has also been studied employing Ag/TiO_2 nanocomposite powders with very small Ag clusters (diameter $\sim$1.5 nm) and low Ag loading ($\sim$0.24 wt%) prepared by a photoassisted deposition method (Tada et al. 1999, 2000, 2004). The composite shows very high efficiency toward the photocatalytic reduction of nitrobenzene and bis(2-dipyridyl)disulfide. The Ag^0 nanoclusters attracting the photoelectrons from the CB of TiO_2 worked as selective adsorption/reduction sites for nitrobenzene and bis(2-dipyridyl)disulfide, while the TiO_2 surface with trapped photogenerated holes served as oxidation sites. The high efficiency for such reactions was explained by the combined effects of selective

adsorption and rectified charge separation. Photoactivity enhancement was also observed for the photoreduction of selenate ions by Ag/TiO_2 (Tan et al. 2003). Without Ag, the selenate was firstly reduced by photoelectrons to Se^0. Then upon the exhaustion of selenate in the solution, the as-formed Se^0 was further reduced to H_2Se. In the presence of Ag, the selenate was directly reduced to H_2Se. The photoelectrons were thought to be transferred from TiO_2 to Se^0 via Ag. The accumulation of electrons in Se^0 before the exhaustion of Se(VI) led to the reduction of Se^0 to Se^{2-}. It is necessary to take into account the reaction kinetics to elucidate the mechanism of this photoreduction process, besides thermodynamics considerations (i.e., the Fermi level differences between TiO_2, Ag, Se^{4+}/Se^0, Se^0/Se^{2-} etc.).

Coexistence of Metallic and Ionic Ag

It is the contact between metallic particles and semiconductors that forms the Schottky barrier between them, but noble metals do not always exist in the pure metallic form in these composites. A certain part of the metals can be oxidized to form ions. Xin et al. (2005) reported three types of silver species, including Ag_2O, AgO, and Ag^0, in the Ag/TiO_2 composites prepared by a sol–gel method. At lower Ag loadings (<0.3 mol%), silver mainly exists as Ag_2O and AgO; while at higher loadings (up to 5 mol%), all three types exist with Ag^0 being the dominant one. Ag_2O may introduce impurity band levels within the material. The oxygen-related surface states are multiple due to various valence states of Ag species. Two O1s peaks from Ag–O and Ag^0-adsorbed O were confirmed besides the lattice O, surface bridging O, and the surface hydroxyl O in TiO_2. The improved photocatalytic degradation of Rhodamine B by the Ag/TiO_2 indicates that both ionic and metallic silver can effectively capture the photogenerated electrons and enhance the photoactivity of TiO_2. Kumar and Mathur (2004) studied the photooxidation of aniline using Ag/Ag^+-loaded TiO_2, and also found an improvement in the photoactivity due to similar reasons.

Photostability of Ag^0

Noble metal nanoparticles are expected to undergo morphology transformation after long time exposure to light (Ah et al. 2000; Stathatos and Lianos 2000; Einaga et al. 2003; Sun et al. 2003; Kawahara et al. 2005). For example, Ag particles 40–60 nm in size in water can be fragmented into smaller particles when exposed to highly energetic laser pulses (Kamat et al. 1998). Photoinduced structural changes were also observed in Ag nanoparticles deposited on glass (Murakoshi et al. 2002). Moreover, optical irradiation was used for synthesis purposes to convert Ag nanoparticles into triangular nanoprisms with special optical properties (Jin et al. 2001). The size- and morphology dependency of the catalytic activity of nanomaterials has been well emphasized in the literature (Jana et al. 1999; Pradhan et al. 2001; Roucoux et al. 2002; Narayanan and El-Sayed 2003; Cozzoli

et al. 2004a). Moreover, the electron or hole scavengers in solution can also affect the oxidation or reduction of the metals (Subramanian et al. 2003). For example, in a Ag/TiO_2-nanorod composite, the Ag particles diminished upon UV irradiation with oxygen as electron scavenger in the solution (Cozzoli et al. 2004b). Recognition of such problems is of great importance in designing high-efficiency nanocomposite photocatalysts (Zhang and Yu 2005).

Photochromism of Ag/TiO_2

Photochromic materials, which change their colors reversibly in response to light, can be used in smart windows, displays, and memory devices (Yao et al. 1992). While conventional photochromic materials respond monochromatically, multicolor photochromism often requires combinations of different materials or filters. If this can be achieved on a single material, photochromic devices would find broader applications such as rewritable color copy paper, electronic paper, and multi-wavelength optical memory (Irie 2000). Tatsuma and coworkers (Ohko et al. 2003; Naoi et al. 2004, 2005) recently explored an interesting property of Ag/TiO_2 film, as shown in Fig. 16.21. The film color was initially brownish-gray. Upon visible-light irradiation, it was changed to be identical to the incident light and could be changed back to brownish-gray under UV light. This multicolor response arose from the broad absorption of the Ag/TiO_2 film ranging from 350 to 700 nm, due to the diversity in size and morphology of Ag particles, and the high refractive index of the TiO_2 matrix.

16.3.3.2 Au/TiO_2

Despite its bulk inertness, Au nanoparticles with diameters smaller than 5 nm on TiO_2 supports have shown high catalytic activity in chemical reactions

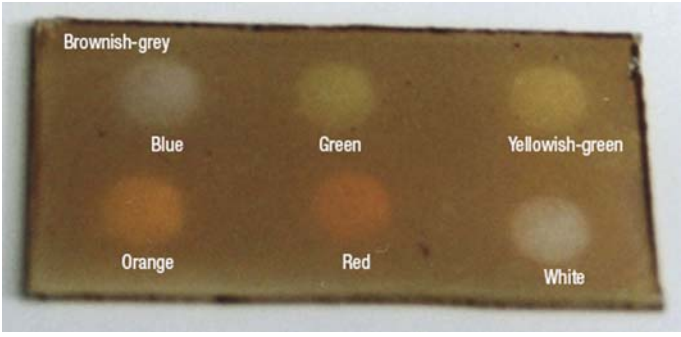

Fig. 16.21 Multicolored Ag/TiO_2 film [Reprinted by permission from Macmillan Publishers Ltd: [Nature Materials] (Ohko et al. 2003), copyright (2003)]

such as low-temperature CO oxidation (Bollinger and Vannice 1996; Grunwaldt et al. 1999; Lee et al. 2004), water–gas-shift reaction, and epoxidation of propylene (Hayashi et al. 1998). Au nanoparticles are also able to enhance photocatalytic reactions if incorporated into photocatalysts like TiO_2 (Bamwenda et al. 1995). For example, Au/TiO_2 photoelectrodes under visible-light irradiation generate photocurrents due to Au surface-plasmon resonance. Photoelectrocatalytic production of hydrogen gas using Au/TiO_2 film electrodes was also attempted (Zhao et al. 1996). Different preparation methods such as impregnation, photodeposition, deposition–precipitation, and sol–gel have been employed to achieve Au/TiO_2 composites. Their photoactivity indeed showed a dependency on the preparation methods. Mechanisms concerning the role of Au nanoparticles were investigated by the aid of electrochemical, photochemical, and spectroelectrochemical probing techniques (Nakato et al. 1988; Zhao et al. 1996). For example, due to the stability of C_{60}^- in N_2 and the ease to follow its optical absorption at 1,075 nm, C_{60}/C_{60}^- redox couples were used as a convenient probe to determine the Fermi level of the Au/TiO_2 composite system. According to the report by Subramanian et al. (Jakob et al. 2003; Subramanian et al. 2004), the Fermi level shift in Au/TiO_2 composites showed a size dependency (20 mV for 8 nm, 40 mV for 5 nm, and 60 mV for 3 nm Au particles). The influence of Au particle size on the photoelectrochemical behavior of the respective Au/TiO_2 system was probed by isolating the individual charge transfer steps as shown in Fig. 16.22. Upon UV irradiation in the presence of ethanol, photoelectrons were trapped at Ti^{4+} sites in the TiO_2 nanoparticle suspension. After addition of Au nanoparticles with controlled size, the trapped electrons were then transferred to Au, indicated by the decreased blue coloration. Once C_{60} was introduced, the electrons trapped at the Au nanoparticles were further transferred to reduce C_{60} to form C_{60}^- as confirmed by the quantifiable increase in the 1,075 nm absorption intensity. This probing technique is very helpful for understanding photoreduction processes on these nanocomposite materials.

Photocatalytic Oxidation by Au/TiO_2

Au/TiO_2 nanocomposites have shown high activity for photocatalytic degradation of various organic compounds. Li et al. (Li and Li 2001) studied photooxidation of methylene blue by Au-loaded TiO_2 in aqueous solutions. The high Schottky barrier

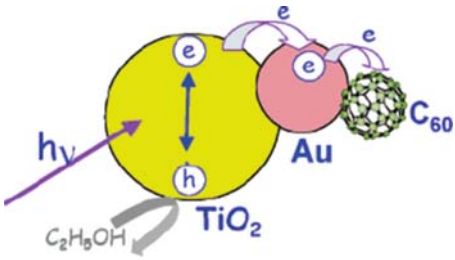

Fig. 16.22 Photoelectron transfer in a Au/TiO_2 nanocomposite probed by C_{60}/C_{60}^- couple [Reprinted with permission from Subramanian et al. (2004). Copyright (2004) American Chemical Society]

existing between TiO_2 and Au nanoparticles facilitated the photoelectron transfer out of the CB of TiO_2 and enhanced the electron/hole separation. Meanwhile, the existence of ionic Au^+ and Au^{3+} species served as traps for charge carriers, which also contributed to the charge separation. Au loadings should be controlled properly to achieve the optimum performance. This is because Au ionic impurity levels can also act as charge recombination centers which become relevant, in particular, at very high Au loadings. A similar tendency was found in Au/TiO_2 thin-film composites with Au deposited over the TiO_2 layer via electron beam evaporation (Arabatzis et al. 2003). Employing these structures, the highest photoactivity for methyl orange degradation was obtained at a surface Au concentration of about 0.8 $\mu g\ cm^{-2}$. The Au particle size also affected the performance. As the Au concentration increased, its particle size also increased to benefit the photoelectron transfer because the distance between trapped electrons and remaining holes became larger. Very high Au loadings, however, resulted in a high coverage of the TiO_2 surface area, leaving a smaller surface exposed for light absorption and methyl orange adsorption. Compared with bare TiO_2, enhancement in phenol photodegradation was also reported on Au/TiO_2 thin-film electrodes (Sonawane and Dongare 2006).

Plasmon-Induced Electron Transfer in Au/TiO_2

Based on their experimental results concerning ethanol and methanol photooxidation by Au/TiO_2 composites under visible-light illumination, Tatsuma et al. (Tian and Tatsuma 2005) proposed a plasmon-induced charge separation scheme. They observed a surprising phenomenon, in which the photoelectrons were excited from Au nanoparticles and transferred to the CB of TiO_2 (Wood et al. 2001; Subramanian et al. 2004). Meanwhile, the oxidized Au species accepted electrons from the donor molecules present in the solution to recover the charge balance. The process is illustrated in Fig. 16.23.

The photocatalytic activity of Au/TiO_2 nanocomposites mainly depends on the effectiveness of electron transfer between Au and TiO_2 resulting in an improved electron–hole separation. The charge transfer behavior is dictated by the specific electronic structures of both Au and TiO_2. The so-called Schottky-barrier effect only provides the conceptual explanations on how the charge transfer proceeds. Other factors such as particle sizes, lattice defects, oxygen vacancies, surface states in both components (Okazaki et al. 2004), and the chemical environment surrounding the heterojunctions also influence the characteristics of the heterojunctions within the composite materials.

16.3.3.3 Pt/TiO_2

Platinization of semiconductor photocatalysts like TiO_2 has become a routine practice to enhance the photoactivity (Lee and Choi 2004). Pt nanoparticles showed very fast electron trapping from semiconductor CB upon light excitation (Wood

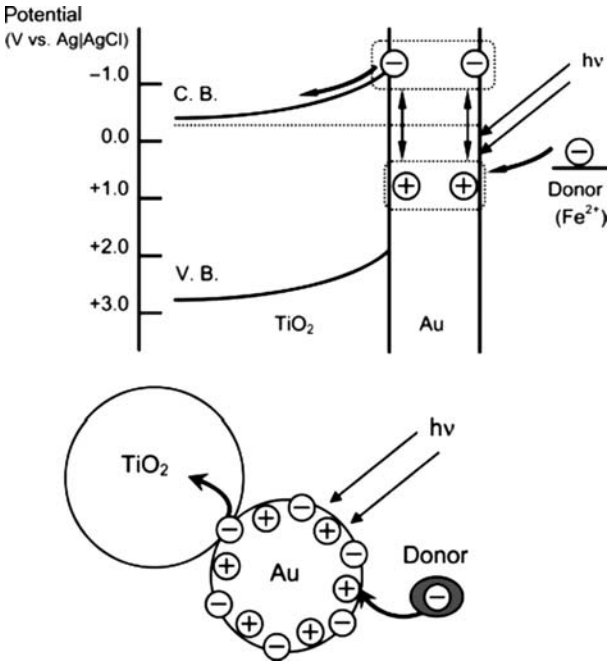

Fig. 16.23 Charge separation upon visible-light irradiation on Au/TiO_2 [Reprinted with permission from Tian and Tatsuma (2005). Copyright (2005) American Chemical Society]

et al. 2001). Other factors such as selective adsorption of reactants at the Pt surface may also contribute to the observed activity enhancement. There were also cases where Pt-loading showed no positive effects on the photocatalytic performance (Linsebigler et al. 1996; Keller et al. 2003; Sun et al. 2003). This indicates that the charge-carrier transfer in a Pt/semiconductor composite is as complicated as for the Ag and Au counterparts.

Platinized TiO_2 has long been used as the photocatalyst for a variety of reactions (Henglein et al. 1981; Bahnemann et al. 1984b, 1987b; Wang et al. 2004a). The role of Pt nanocontacts as electron traps was confirmed by transient absorption spectra analysis of Pt/TiO_2 powders (Furube et al. 2001). As shown in Fig. 16.24, in addition to the normal decay of the transient absorption of the trapped CB electrons in TiO_2 at 600 nm due to the electron/hole recombination following 390-nm excitation, a new decay component lasting a few picoseconds was observed and interpreted as the photoelectron migration from TiO_2 to Pt. For pure TiO_2 samples, no such decay occurred within 25ps. This clearly proved that the charge-carrier separation can be enhanced by Pt trapping of the electrons from the CB of TiO_2. In consistence with this mechanism, a recent study (Nakajima et al. 2004a, b) revealed that the photoluminescence of Pt/TiO_2 under UV irradiation was blue-shifted upon increasing the Pt content. The excited electrons accumulated in the Pt particles possess higher energy, so that the electron/hole recombination emitted shorter-wavelength luminescence, as compared with that of pure TiO_2.

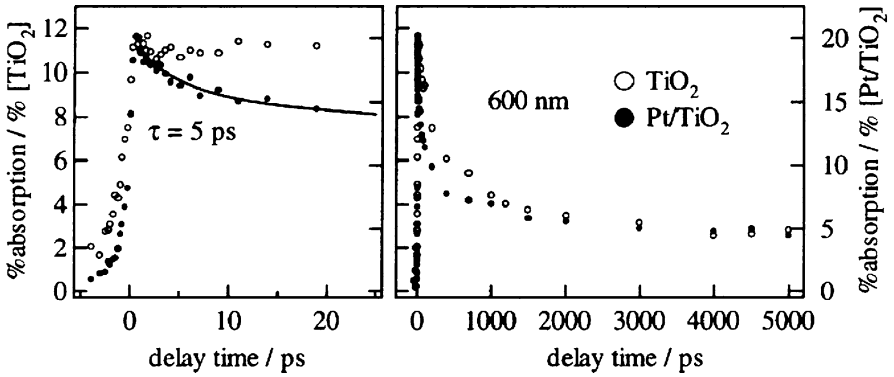

Fig. 16.24 Transient absorption spectra of irradiated TiO_2 and Pt/TiO_2 [Reprinted from Furube et al. (2001), Copyright (2001), with permission from Elsevier]

Bahnemann et al. (1984a, b) studied the surface trapping of photoelectrons and holes in a platinized TiO_2 sol and assigned the trapping mode to different scavengers by laser flash photolysis technique combined with transient absorption spectroscopy. Anpo et al. (1991) compared the effect of Pt loading on the photoactivity for the hydrogenation of $CH_3C{=}CH$ and C_3H_6 by TiO_2 and ZnO, and found that Pt increased the photoactivity for both catalysts. Electron trapping by adsorbed protons on Pt may be responsible for this enhancement. A comparative study on photocatalytic H_2 generation between Pt/TiO_2 and Au/TiO_2 powders suggested that Pt can be a better trapping site for photoelectrons than Au (Bamwenda et al. 1995). Another comparison was made between Ag/TiO_2, $Pt/Ag/TiO_2$, and Pt/TiO_2 catalysts for the photocatalytic dehydrogenation of 1-propanol (Sclafani and Herrmann 1998). In $Pt/Ag/TiO_2$, the photoelectrons can be effectively transferred from TiO_2 via Ag to Pt clusters where chemically dissociated hydrogen was adsorbed to generate H_2. Favorable adsorption of reactants on Pt clusters was also confirmed in the photooxidation of CO (Einaga et al. 2003). Uchida et al. (1998) proposed a novel configuration of Pt/TiO_2 electrodes for the photodegradation of 1,2,4-trichlorobezene (TCB). As shown in Fig. 16.25, TiO_2 and PTFE particles were firstly deposited together on an ITO substrate via an electrophoretic method. Then Pt nanoparticles were photodeposited into the TiO_2/PTFE matrix. PTFE showed affinity toward both O_2 and TCB, which led to efficient TCB adsorption and photoelectron consumption for O_2 reduction. Pt particles promoted the electron transfer within the matrix and their reaction with O_2 molecules.

Zhao et al. (2002) studied the photodestruction of sulforhodamine-B in Pt/TiO_2 suspension under visible light illumination. The electrons excited from dye molecules were accepted by Pt islands. The accumulated electrons then react with O_2 to form $O_2^{-\cdot}$ and subsequently $^{\cdot}OH$, which ultimately caused the self-destruction of the dye molecules. Photocatalytic destruction of oxalic acid (Iliev et al. 2006) and H_2 generation (Sreethawong et al. 2006) from aqueous methanol solution were also promoted by platinizing TiO_2. Under anoxic conditions, products from

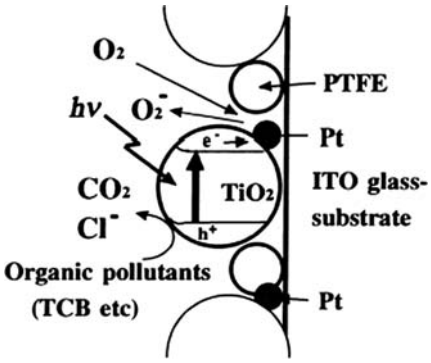

Fig. 16.25 Pt-loaded TiO_2-PTFE film photoelectrode deposited on ITO glass substrate [Reprinted from Uchida et al. (1998), Copyright (1998), with permission from Elsevier]

photocatalytic reactions using Pt/TiO_2 may be different from those using pure TiO_2. For example, although the reaction rate of alkylamine degradation was increased by the presence of Pt, some undesirable toxic byproducts were also generated (Lee and Choi 2004). Quan et al. (2004) reported a synergetic effect on the photoelectrocatalytic degradation of 2,4-dichlorophenoxyacetic acid using $Pt/TiO_2/Ti$ electrodes. The degradation efficiency was higher than the sum of individual photocatalytic and electrochemical efficiencies. Suppression of charge-carrier recombination benefits from the trapping of photoelectrons by Pt while the charge-carrier separation is improved by the external bias potential.

16.3.4 Doped Semiconductors

Wide bandgap semiconductor materials have long been serving as active photocatalysts. But their main drawback is just this wide bandgap, as this only allows very limited utilization of solar energy. Accordingly, the red shift of their absorption edge into the visible-light region has been widely attempted. Sensitization by dye molecules has shown encouraging results in dye-sensitized solar cells (O'Regan and Grätzel 1991; Bach et al. 1998; Grätzel 2001; Kay and Grätzel 2002; Wang et al. 2003b). However, in most photocatalytic systems, the dyes are usually not stable once the photocatalyst is exposed to bandgap illumination. Another way to shift the absorption toward the visible region is to dope the semiconductors with ionic species. Although not all the results were successful, quite a few studies provided very encouraging results for the development of visible-light-active photocatalysts. While the light absorption edge could be red-shifted by this type of doping, the photoactivity after doping may not necessarily be improved. The measured absorption spectra of a photocatalyst is the overlapped results from several absorption bands of different origins such as intrinsic bulk absorption, surface state absorption, absorptions from defects, etc. As a result, the absorption by intrabandgap states may not form sufficiently strong oxidants for certain reactions. The absorption spectra for a photocatalyst should not be expected to match entirely with the action spectra

of its photocatalytic performance. Although numerous theoretical and experimental results concerning doped photocatalysts have already been published, a clear mechanistic understanding concerning the role of dopants and the photocatalytic behavior is far from being established.

16.3.4.1 Nonmetal-Ion Doped Photocatalysts

Earlier studies (Saha and Tompkins 1992; Lee et al. 1995) on anionic doping used N-containing TiO_2 obtained from thermal oxidation of TiN or chemical vapor deposition with titanium(IV) isopropoxide and nitrous oxide. Other choices of dopants included C, F, S, P, etc., which have been subject to investigations on optical absorption, photocatalytic activity, and/or band structure calculations. Nitrogen has been the most intensively studied nonmetal-ion dopant for TiO_2, as can be seen from the yearly increasing number of publications on N-doped TiO_2. Even for this single dopant, various mechanisms have been proposed to explain its effect on the light absorption and photoactivity of such-doped TiO_2, i.e., the bandgap narrowing by overlapping between N2p and O2p orbitals (Asahi et al. 2001; Morikawa et al. 2001), the creation of oxygen vacancies (Ihara et al. 2003; Serpone 2006), the generation of intrabandgap surface states, or combined effects between them (Sakthivel and Kisch 2003). A schematic diagram shown in Fig. 16.26 displays these possible mechanisms (Serpone 2006).

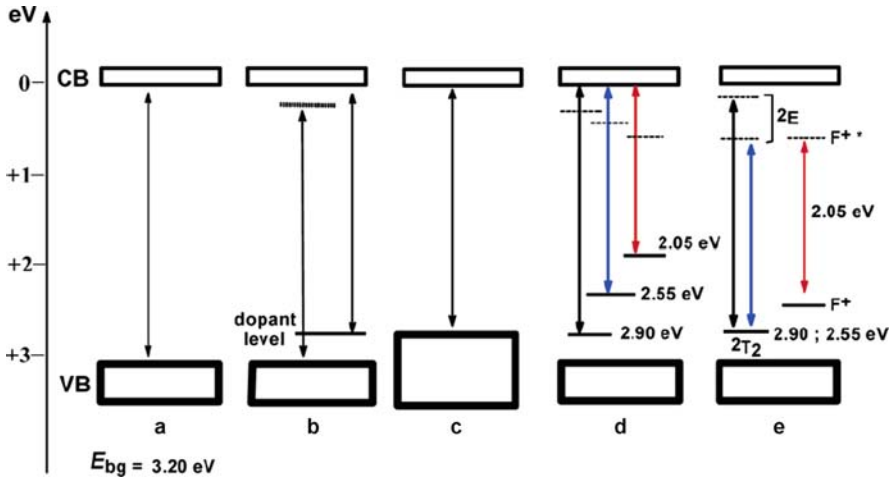

Fig. 16.26 Various schemes of band structure change of: (**a**) Pure anatase TiO_2; (**b**) Doped-TiO_2 with localized dopant levels near the CB and VB edges; (**c**) Bandgap narrowing due to VB broadening; (**d**) Localized dopant levels and electronic transitions to the CB; (**e**) Electronic transitions of dopant levels near the VB edge to corresponding excited states for Ti^{3+} and F^{+} centers [Reprinted with permission from Serpone (2006). Copyright (2006) American Chemical Society]

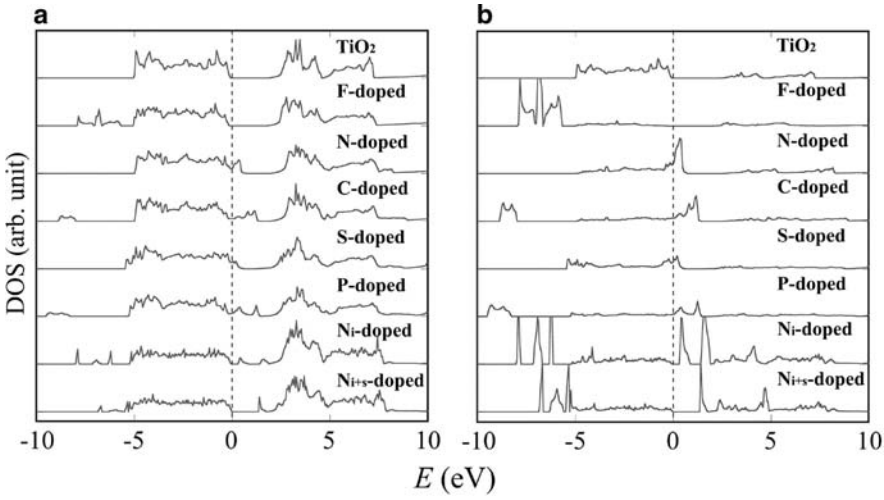

Fig. 16.27 Total DOSs of doped anatase TiO_2 (**a**) and the projected DOSs into the doped anion sites (**b**). The results for N-doping at the interstitial site (N_i-doped) and that at both substitutional and interstitial sites (N_{i+s}-doped) are also shown [from Asahi et al. (2001); Reprinted with permission from AAAS]

Bandgap Narrowing

Asahi and coworkers (Asahi et al. 2001) published the results from both theoretical density-of-states (DOS) calculations of the band structures and photocatalytic experiments of nonmetal-ion doped TiO_2 in 2001. They claimed that among C, N, F, P, and S, the most effective substitutional dopant was N for the bandgap narrowing of TiO_2. As shown in Fig. 16.27, the calculated p states from N dopants mix with O2p states from TiO_2 to narrow the bandgap and effectively transfer the photoexcited charge carriers to the reactive sites at the TiO_2 surface within their lifetime. Although doping by S shows a similar bandgap narrowing, the ionic radius of S is too big to enable it to be substitutionally incorporated into the TiO_2 lattice. (This may not be a serious problem if S-doped TiO_2 is prepared by thermal oxidation of TiS_2 instead of using S to attack the O in the TiO_2 lattice (Takeshita et al. 2006).) The states introduced by C and P are located energetically too deep with in the bandgap of TiO_2 to promptly transfer the charge carriers to the surface reactive sites.

For the interstitial N doping and substitutional-and-interstitial N doping, calculations indicate the existence of molecular dopants with bonding states quite similar to those of NO and N_2 molecules. Such dopants give rise to bonding states below the O2p valence bands and antibonding states deep in the bandgap (Fig. 16.27b, N_i-doped and N_{i+s}-doped), which hardly interact with the band states of TiO_2 and therefore are not effective to transfer the photogenerated charges carriers. This argument was confirmed by testing the visible-light-driven photocatalytic degradation of aqueous methylene blue and gaseous acetaldehyde and by XPS analysis of the atomic-N peak area (corresponding to a binding energy of 396 eV (Saha and

Tompkins 1992)), because the N-doped TiO_2 sample with the highest fraction of atomic N state (calculated as the area of the 396 eV peak relative to the total area of the 396, 400 with 402 eV peaks, with the latter two peaks corresponding to the molecularly chemisorbed states (Saha and Tompkins 1992)) shows the highest photocatalytic degradation rate. Contrary opinions exist about whether substitutional or interstitial N-doping is more effective. Diwald et al. (2004) doped TiO_2(110) single crystals with N by an NH_3 treatment at 870 K and found that it is the interstitial nitrogen that was responsible for the red shift of the optical absorption down to a lower energy.

The work by Asahi et al. initiated a new wave of research aiming to find visible-light-active photocatalysts based on doped TiO_2, which seemed to be able to benefit from the guidance of theoretical calculations, although their reliability could not be easily estimated. Umebayashi et al. (2002) found that the mixing of S3p states with the VB of anatase TiO_2 resulted in a bandgap narrowing of S-doped TiO_2 which is consistent with Asahi et al.'s results. Based on first principles calculations, Yamamoto et al. (2004) also obtained a bandgap narrowing of rutile TiO_2 induced by S doping. Based on plane-wave-based pseudopotential density functional theory calculations, Tian and Liu (2006) presented a similar bandgap narrowing by mixing O2p with S3p states in a S-doped anatase TiO_2. Recently, Wang and Lewis (2006) re-calculated the band structures of C, N, and S-doped TiO_2, showing that their dopant of choice was C for the development of visible-light-active TiO_2-based photocatalysts, in contrast to the suggestion by Asahi et al. that the energy states induced by C do not effectively overlap and mix with O2p states. However, despite all these obvious differences these groups of authors do share a common recognition concerning the bandgap narrowing by mixing the O2p orbitals with the introduced energy states near the VB edge of TiO_2. Experimentally, Umebayashi et al. (2003b) investigated the optical properties of S-doped anatase TiO_2 prepared by annealing TiS_2. The diffuse reflectance spectra showed that the absorption edge was shifted toward the lower energy region due to the bandgap narrowing by mixing S3p states with the TiO_2 VB. By studying the visible-light-active C-doped TiO_2 made from thermal oxidation of TiC powders, Irie et al. (2003) suggested that the bandgap narrowing could be seen even at a low carbon loading ($\sim$0.32%). It is obvious from these results that considerable hesitation concerning the reliability of theoretical calculations, aiming for the prediction of the electronic band structures of doped semiconductors, is most certainly indicated because the predictions of these studies just do not agree with each other. Moreover, a large number of experiments seem to prove that it is not by bandgap narrowing but by newly formed localized energy states that the visible-light absorption of doped TiO_2 is enhanced.

Formation of Intrabandgap Energy States

States Close to the Conduction Band Edge

Color centers constitute one type of intrabandgap energy states in semiconductor materials. Color centers are, for example, formed in a metal oxide upon the loss

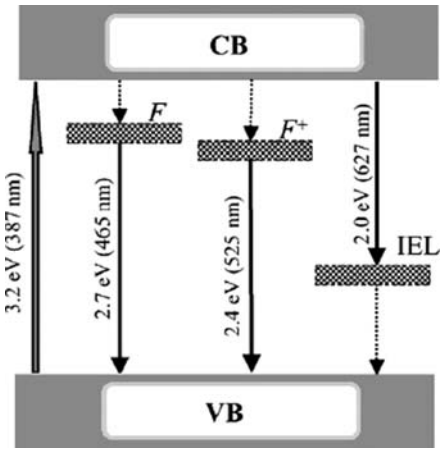

Fig. 16.28 Possible energy states between the CB and VB of fluorine-doped TiO_2 [Reprinted from Li et al. (2005), Copyright (2005), with permission from Elsevier]

of an oxygen atom; the electron pair that remains trapped at the remaining cavity gives rise to the formation of a so-called F center; a positively charged F^+ center is equivalent to a single electron residing at the oxygen vacancy; the electron-pair deficient oxygen vacancy is referred to as a doubly charged F^{++} center; the electrons left in the cavity can also react with adjacent Ti^{4+} ions to yield Ti^{3+} centers (Lu et al. 2001b; Li et al. 2005a).

In most fluoride (F^-)-doped TiO_2 photocatalysts, the main reason for the improved light absorption was assigned to the color centers formed upon F^- incorporation. For example, Li et al. (2005b) studied F^--doped TiO_2 from spray pyrolysis of H_2TiF_6 and found a high photocatalytic activity toward the decomposition of gaseous acetaldehyde under both UV and visible-light irradiation. XPS analysis revealed two types of color centers in the sample, i.e., the oxygen vacancies with either two trapped electrons (F centers) or one trapped electron (F^+ centers). As indicated in the excitation/emission pathways shown in Fig. 16.28, both types of color centers form trapped states below the CB edge of TiO_2 (0.53 eV for F centers and 0.84 eV for F^+ centers, respectively) as deduced from the photoluminescence spectra. Ho and coworkers (Ho et al. 2006) prepared hierarchical-structured F^--doped TiO_2 nanospheres exhibiting visible-light photoactivity which was also explained by the extrinsic absorption resulting from the color centers formed upon F^--doping. Ihara et al. (2003) prepared a N-doped TiO_2 photocatalyst by calcination of the hydrolysis products of Ti $(SO_4)_2$ with ammonia. The resulting powder showed visible-light absorption between 400 and 550 nm that was interpreted as being due to the creation of oxygen vacancies preferably at the grain boundaries of TiO_2. These oxygen vacancies will in turn reduce both, cation charge and coordination number, leading to localized states between the CB and the VB of TiO_2 (without pinning their positions) and thus allowing excitation pathways to be initiated with subbandgap energy (Bilmes et al. 2000). Lin et al. (2005) quantified the position of the donor states introduced by oxygen vacancies by theoretical calculations, as being localized at 0.15–0.30 eV below the CB edge. Martyanov et al. (2004) prepared

oxygen-deficient TiO_2 by annealing TiO and Ti_2O_3 powders under O_2 atmosphere. In this way, the interference from N-doping on oxygen vacancies could be excluded since no N was involved in the preparation of TiO_2.

Oxygen vacancies were also attributed as being responsible for the visible-light-activity of C- and S-doped TiO_2. Li et al. (2005c) prepared C-doped titania by carbonization of anatase TiO_2, and the product showed optical absorption bands up to 700 nm and much higher photooxidation activity for gas-phase benzene than pure TiO_2 under artificial solar irradiation. These observations were explained by the presence of oxygen vacancies and the formation of Ti^{3+} levels between the CB and VB. Yu and coworkers (Yu et al. 2005a) observed considerable antibacterial photoactivity of S-doped TiO_2 for killing bacteria under visible-light illumination that was explained by the formation of intrabandgap S^{6+} states close to the CB edge of TiO_2. Ohno et al. (2003, 2004) proposed that sulfur incorporated into the TiO_2 lattice mainly substitutes Ti^{4+} with S^{4+} based on XPS analysis. (The S^{6+} peaks found in their XPS spectra were claimed to be sulfuric acid adsorbed on the TiO_2 surface.) First-principles calculations carried out by Ohno et al. indicate the formation of S^{4+} states near the CB edge of TiO_2 that account for the visible-light absorption and photoactivity for 2-propanol decomposition. Note that S dopants do not always substitute Ti with the specific doping mode depending largely on the methods of preparation (Ohno et al. 2004; Takeshita et al. 2006). Theoretical calculations also showed that oxygen vacancies in TiO_2 lattices are also able to accommodate S atoms (Rodriguez et al. 2001). Visible-light-active P-doped TiO_2 was also prepared and it was reported that phosphorus atoms exist in their pentavalent form and act as impurity levels to trap photogenerated electrons (Shi et al. 2006). Based on the common features reported for most doped TiO_2 photocatalysts, i.e., the formation of oxygen vacancies and color centers that are inevitably due to a partial reduction of TiO_2 at a certain point during the preparations of the materials, Serpone (Kuznetsov and Serpone 2006; Serpone 2006) argued that the red-shift of the absorption edge is indeed caused by such color centers (Fig. 16.26e).

States Close to the Valence Band Edge

Theoretical calculations by Lin et al. (2005) suggested that N-doping did not narrow the bandgap of TiO_2 by mixing O2p with N2p orbitals, even at much higher N concentrations than those used by Asahi et al. (2001). Instead, their calculations predicted that the N2p states are localized near the top of the VB of TiO_2. Only at very high dopant levels ($\sim$20%) would the N2p states mix with the O2p orbitals, leading to a bandgap narrowing. However, in practice, too much N loading results in the formation of TiN, which is not transparent in the visible region. Moreover, it is questionable whether or not a semiconductor can maintain its chemical and electronic structural integrity after incorporating a large amount of foreign dopants (Serpone 2006). The highest experimentally achieved N loading in TiO_2 was reported to be 8% (Ma et al. 2005), which is far below the amount required for a bandgap narrowing as calculated by Lin et al. While the dopant loading is pertinent to the properties of the doped materials, their distribution within the materials, which

is closely related to the preparation methods, should never be ignored. As shown by Takeshita and coworkers (Takeshita et al. 2006), even with similar sulfur loadings in TiO_2, different distribution of S resulted in significant differences in their photoactivity under visible-light illumination. Di Valentin et al. (2005) conducted density functional theory (DFT) calculations revealing that besides the substitutional N2*p* states, states formed by interstitial N are located higher than substitutional N2*p* states above the VB edge and are expected to also contribute to the red-shift of the absorption edge. However, these interstitial N dopants might behave as strong hole trapping sites thus reducing the direct oxidizing power of doped TiO_2 (Mrowetz et al. 2004).

Theoretical calculation results predicting localized states above the VB edge have been confirmed by some photocatalytic experiments using N-doped TiO_2 photoelectrodes. Nakamura et al. (2004) determined the mid-bandgap surface state positions by studying the photooxidation of various hole scavengers (e.g., SCN^-, Br^-, I^- etc.) with unique oxidation potentials, under both UV and visible-light irradiation. The estimated energy levels of the surface states are shown in Fig. 16.29. Hence, the possibility of a bandgap narrowing resulting from an overlapping between O2*p* and N2*p* orbitals was excluded by the observed oxidizing power variation of the photogenerated holes under different irradiation conditions.

Miyauchi et al. (2004) supported this conclusion by testing the photoactivity of N-doped TiO_2 under visible-light illumination. They compared the photocatalytic decomposition of 1-propanol under UV and visible-light illumination, and found that the reaction rate under UV irradiation is much higher than that under visible-light illumination. If the visible-light activity of N-doped TiO_2 were due to the mixing of N2*p* with O2*p* levels, then the photoactivity should not differ much under these different irradiation conditions. However, the quantum yield (defined

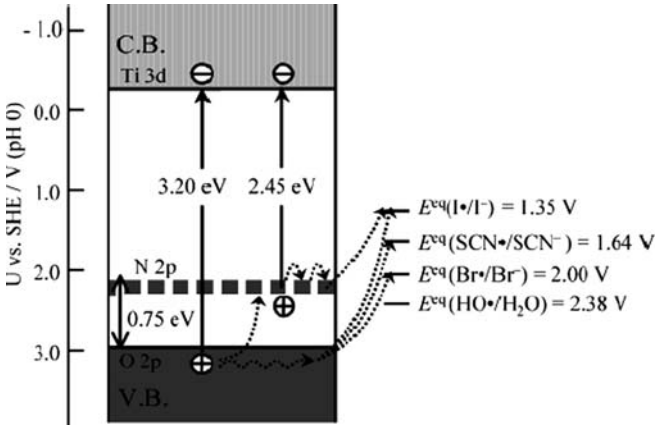

Fig. 16.29 Band structure of N-doped TiO_2 with the oxidation potentials of a few redox couples [Reprinted with permission from Nakamura et al. (2004). Copyright (2004) American Chemical Society]

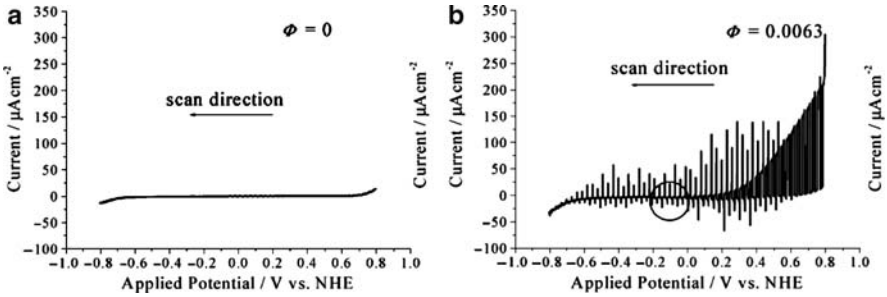

Fig. 16.30 $i - V$ characteristics of pure TiO_2 (**a**) and N-doped TiO_2 (**b**) irradiated by white light [Reprinted with permission from Lindgren et al. (2003). Copyright (2003) American Chemical Society]

as the number of oxidized 1-propanol molecules per absorbed photon) of N-doped TiO_2 is lower than that of pure TiO_2 under UV irradiation. This suggested a negative effect of N-doping, i.e., the energy states formed by doping acted as the recombination centers for electrons and holes and should thus be located in the mid-bandgap region between VB and CB.

The possible role of dopant species as recombination centers was also confirmed by other researchers. Lindgren et al. (2003) studied the photoelectrochemical i–V characteristics of a N-doped TiO_2 film electrode under modulated irradiation. As shown in Fig. 16.30, white light hardly caused any photoresponse for the undoped TiO_2 film electrode (Fig. 16.30a), whereas there was an obvious photoresponse with the N-doped TiO_2 (Fig. 16.30b). Pronounced photocurrent transients could be seen in a wide bias-potential range around the photocurrent onset, indicated by the circle in Fig. 16.30b. The transients together with the nearly linear increase of the photocurrent under positive bias-potential are typical indicators for a high electron/hole recombination rate under stable irradiation.

Sakthivel and Kisch (2003) prepared nitrogen-doped (0.08–0.13 wt%) titania by hydrolysis of $TiCl_4$ with nitrogen-containing bases, followed by a 400°C calcination in air. Diffuse reflectance spectra showed that the thus prepared catalyst could absorb visible light (wavelength between 400 and 520 nm). The bandgap energy of the doped TiO_2 was estimated to be 3.12 eV by plotting the modified Kubelka–Munk function as a function of the photon energies. This bandgap is slightly smaller than that of pure anatase TiO_2 and was ascribed to a bandgap narrowing due to a modest anodic shift of the CB edge. Since the light absorption edge was 520 nm (2.39 eV, which is much smaller than 3.12 eV), the authors proposed that some localized energy states above the VB edge must exist. The positions of these states were determined by measuring the wavelength dependence of the photooxidation of different charge-carrier scavengers. The final band structure suggested by these authors is shown in Fig. 16.31.

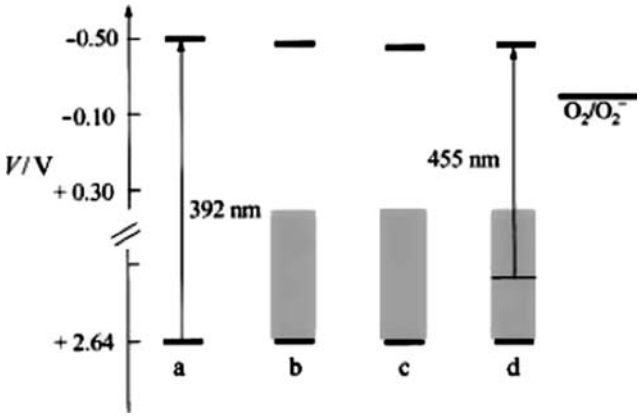

Fig. 16.31 Electrochemical potentials (vs. NHE) for band edges, surface states (*shaded areas*) and oxygen reduction at pH 7 for TiO_2 and N-doped TiO_2 [Copyright Wiley-VCH Verlag GmbH & Co. KGaA. Reproduced with permission from Sakthivel and Kisch (2003)]

16.3.4.2 Metal-Ion-Doped Photocatalysts

In metal-ion-doped semiconductors, there are also two different positions that the dopant ions can occupy in the semiconductor lattice, i.e., substitutional and interstitial. If the ionic radius of the dopant is similar to that of the matrix cation, the dopant will conveniently take the substitutional mode; if the dopant radius is much smaller than the matrix cation, interstitial doping is also possible (Serpone et al. 1994). Some studies even suggest that the interstitial doping is possible for dopant ions larger than the matrix cation (Shah et al. 2002). Note that the dopant ions should be within an appropriate concentration to exclude a phase separation between the dopant and the matrix (Wang et al. 2001b; Miyake and Kozuka 2005). Compared with the valence states of the matrix cations, cationic dopants can be divided into two categories: those with valence states higher than those of the matrix cations and those with valence states which are lower than those of the matrix cations. In the TiO_2 matrix, these two types of dopants behave in distinctly different ways, i.e., the higher-valence dopants act as electron donors and are therefore called n-type dopants, while the lower-valence dopants act as electron acceptors and are called p-type dopants.

Transition metal dopants influence wide bandgap semiconductor photocatalysts with at least two effects (Karakitsou and Verykios 1993; Serpone et al. 1994): changing the bulk electronic structure of the matrix semiconductor [resulting in, e.g., changes in the position of the Fermi level, the formation of new energy levels by the interaction of the dopant with the matrix lattice, changes of the electron conductivity within the matrix semiconductor (Bally et al. 1998; Sharma and Bhatnagar 1999)] and/or modification of the surface properties. The latter can be linked with the variations of the thickness of the space charge layer, changes in the concentration of surface states, and the initiation of photocorrosion processes (Wilke and Breuer 1999;

Carp et al. 2004). Earlier studies focused on metal-ion-doped photocatalysts can be traced back to the 1980s (Grätzel and Howe 1990). Electron paramagnetic resonance (EPR) was applied by these authors to study the doped TiO_2 to discriminate the various doping modes in both anatase and rutile TiO_2. Since then, doping of photocatalysts with metal ions has been investigated extensively with the consequence that nearly all metals in the periodic table of elements have been tried as dopants (Kikkawa et al. 1991; Karakitsou and Verykios 1993; Serpone et al. 1994; Litter and Navio 1996; Ranjit Viswanathan 1997; Navio et al. 1998, 1999; Wilke and Breuer 1999; Iwasaki et al. 2000; Wang et al. 1999, 2000a, b, 2004a, c; Yu and Zhao 2000; Gesenhues 2001; Klosek and Raftery 2001; Di Paola et al. 2002; Xu et al. 2002; Yu et al. 2002b, 2006; Yuan et al. 2002; Zheng et al. 2003; Arana et al. 2004; Cao et al. 2004; Jing et al. 2004a, 2005; Yang et al. 2004; Kim et al. 2005, 2006a; Sahoo et al. 2005; Bettinelli et al. 2006; Colmenares et al. 2006; Colon et al. 2006; Ha et al. 2006; Lee et al. 2006; Mohamed and Al-Esaimi 2006; Ohno et al. 2006; Tsuge et al. 2006). For this section, only some mechanistic principles and a few examples based on doped-TiO_2 have been selected to illustrate the influence of metal-ion dopants on photocatalysts.

Formation of New Energy Levels

Upon metal-ion doping, new energy states can be formed either within or beyond the bandgap of semiconductors. The diagram in Fig. 16.32 qualitatively provides a scenario illustrating where the dopant levels could be within the energy diagram of a metal-ion-doped TiO_2 (Serpone et al. 1994).

For Cr and Fe ions, their most frequently employed valence states are Cr^{3+} and Fe^{3+}, respectively. If these cations are incorporated into the TiO_2 lattice by substituting Ti^{4+} cations, the electroneutrality as a whole requires the simultaneous

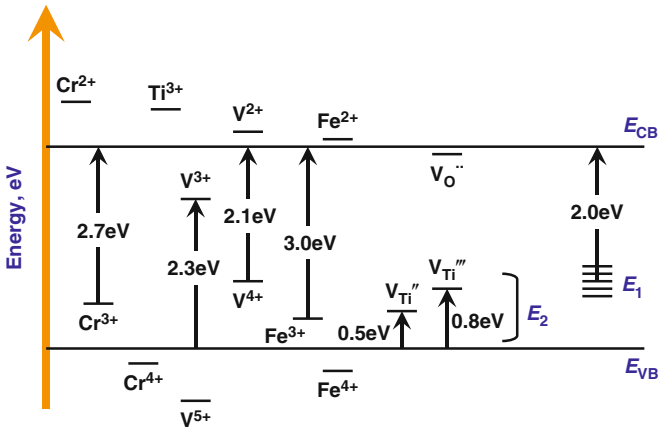

Fig. 16.32 Energy states in TiO_2 after being doped by Fe, Cr and V ions [Reprinted with permission from Serpone et al. (1994). Copyright (1994) American Chemical Society]

formation of oxygen vacancies, the amount of which should be equal to half of the substitutional trivalent cation dopants incorporated at Ti^{4+} sites, as shown in (16.62):

$$M_2O_3 \rightarrow 2|M^{III}|'_{Ti} + V_0^{\cdot\cdot} + 3O_0 \tag{16.62}$$

where M refers to the corresponding metals (Fe or Cr); $V_0^{\cdot\cdot}$ represents the oxygen vacancy, the energy level of which lies slightly below the CB edge as shown in Fig. 16.32; O_0 denotes the oxygen atom at its normal lattice site. Consequently, only a fraction of the dopant centers will have a full-coordination sphere of lattice oxygen atoms, while the other dopant centers are in the position of having an oxygen vacancy at the nearest neighbor site. Similarly, for pentavalent dopants such as V^{5+}, the following equation holds:

$$2M_2O_5 \rightarrow 4|M|^{5\cdot}_{Ti} + 5V^{4'}_{Ti} + 10O_0 \tag{16.63}$$

where $V^{4'}_{Ti}$ represents cation vacancies which are good hole acceptors (as shown in Fig. 16.32, after excitation holes in the VB can be trapped at these sites to form V_{Ti}''' and V_{Ti}'' states above the VB edge); $|M|^{5\cdot}_{Ti}$ denotes the defect sites which are good electron acceptors (upon acceptance of one or two photoelectrons, V^{4+} and V^{3+} states can be formed within the bandgap).

Increase of Visible-Light Absorption

Due to the formation of intrabandgap energy levels, the light absorption edge can be red-shifted by electronic transitions from the VB to these levels and/or from these levels to the CB. For Cr^{3+}-doped TiO_2, both the Cr^{3+} states and the visible-light activity were confirmed by many research groups (Karvinen 2003; Umebayashi et al. 2003; Osterwalder et al. 2005). Zhu et al. (2006) prepared Cr^{3+}-doped TiO_2 by a sol–gel/hydrothermal procedure, and observed visible-light absorption at a doping level between 0.15 and 0.30%. An absorption shoulder at around 450 nm was ascribed to the excitation of Cr^{3+} resulting in generation of CB electrons. Lu and coworkers (Lu et al. 2001a) prepared Cr^{3+}-doped TiO_2 by a diffusion-doping-sensitization technique. Their products showed an absorption edge at around 750 nm. Ghicov et al. (2007) recently reported enhanced visible-light absorption up to 520 nm by TiO_2 nanotubes doped with Cr^{3+} by ion implantation. Although a certain amount of defects was created during ion implantation that could potentially act as recombination centers, such adverse effect could be minimized by reannealing the doped TiO_2 samples. Umebayashi et al. (2003) also reported that Cr-dopant levels appeared close to the VB edge of TiO_2 following the material preparation by an ion implantation method.

For Fe^{3+}-doped TiO_2, the red shift of the absorption edge was ascribed to the excitation of $3d$-Fe^{3+} electrons to the CB of TiO_2 (Litter and Navio 1996), or the charge transfer between dopant ions (Fe^{2+} and Fe^{4+}) via the CB. Wang and coworkers (Wang et al. 2000a, 2003a, 2006a, d) described a sol–gel method to

prepare Fe(III)-doped TiO_2 nanopowders with high uniformity of Fe(III) distribution throughout the TiO_2 matrix, which was considered to be responsible for the high quantum efficiency of the materials in the photocatalytic oxidation of methanol to form formaldehyde. Yamashita and coworkers (Yamashita et al. 2003) prepared iron-doped TiO_2 by ion implantation exhibiting visible-light absorption up to 600 nm. Jeong et al. (2005) observed a red shift in the absorption edge of Fe-doped TiO_2 films deposited on glass substrates. Zhou et al. (2006) prepared mesoporous Fe-doped TiO_2 powders and found that the absorption was red-shifted as the dopant concentration increased from 0.05 to 0.25 at.%. Zhang and coworkers (Zhang et al. 2006) prepared Fe-doped TiO_2 supported on activated carbon which also showed a red shift in its light absorption edge. Very recently, Wang et al. (2006d) demonstrated that Fe^{3+}-doped TiO_2 nanopowders prepared by plasma oxidative pyrolysis could degrade methyl orange under visible-light irradiation. Nahar et al. (2006) prepared Fe-doped TiO_2 by calcination of Fe_xTiS_2 (x was varied from 0.002 to 0.01). The material was able to photocatalytically degrade phenol under visible-light illumination (405–436 nm). Teoh et al. (2007) prepared Fe-doped TiO_2 by flame spray pyrolysis which showed considerable activity toward the degradation of oxalic acid under visible-light illumination above 400 nm. Other metal (e.g. Mn (Dvoranova et al. 2002); V, Co (Gracia et al. 2004); Ni (Jing et al. 2005; Kim et al. 2006a); Mg (Hwang et al. 2002); and Pt (Zang et al. 1998; Macyk et al. 2003; Kim et al. 2005)) ion-doped photocatalysts were also found to exhibit visible-light activities. Although quite a large number of examples exist in the literature of materials exhibiting enhanced light-absorption properties, it should be pointed out that the absorption of light is a necessary yet not sufficient condition to promote the photocatalytic activity (Gracia et al. 2004).

Changing the Lifetime of Charge Carriers and Photoactivity

Metal-ion dopants can greatly alter the lifetime of photogenerated charge carriers, and thus the photocatalytic activities. At appropriate concentrations, the dopants can selectively trap one charge carrier thus allowing the other one to reach the particle surface to be able to take part in the desired redox reactions. For example, Grätzel and Howe (1990) demonstrated by electron paramagnetic resonance measurements that doping of colloidal TiO_2 particles with Fe^{3+} and V^{4+} resulted in a drastic augmentation in the lifetime of the photogenerated electron/hole pairs upon bandgap irradiation, which would recombine within a few nanoseconds without these dopants. Quite a few photocatalytic activity measurements for metal-ion-doped TiO_2 also confirmed the enhancement of charge-carrier lifetime and the corresponding photocatalytic activity (Sakthivel et al. 2004; Yu et al. 2006).

On the other hand, the dopant ions can also act as recombination centers for photoelectrons and holes thus decreasing the photocatalytic performance (Dvoranova et al. 2002). The frequently reported decrease in photoactivity of metal-ion-doped TiO_2 with increasing dopant concentration above a certain doping level is a good illustration of this phenomenon. In fact, visible-light photoactivity could hardly be

observed for a Fe^{3+}-doped TiO_2 at a Fe loading of 10 wt%, although the visible-light absorption was very considerable. Radecka et al. (2004) studied the photoelectrochemical behavior of Cr^{3+}-doped TiO_2 electrodes and found that the addition of Cr^{3+} led to an increase in the recombination of photogenerated charge carriers, and therefore the energy conversion efficiency for the doped electrodes was lower than that of an undoped TiO_2 electrode. Wilke and Breuer (1999) examined the relationship between dopant concentration, charge-carrier lifetime, and photocatalytic performance of Cr^{3+}- and Mo^{5+}-doped TiO_2. Their study revealed that for both Cr^{3+}- and Mo^{5+}-doped TiO_2, the lifetime of the charge carriers was drastically decreased from about 90 μs for pure TiO_2 down to about 25 μs at a dopant concentration of 1 at.%. Meanwhile, the photocatalytic activity decreased to a low level with dopant concentrations below 1 at.% for both systems. This was ascribed to the substitutional doping by the cations which act as recombination centers. Wang and coworkers (Wang et al. 2006d) studied the photodegradation of methyl orange by both pure and Fe^{3+}-doped TiO_2 nanopowders under UV irradiation, and found that the photoactivity of the former is higher than that of the latter, which was explained by the more serious recombination loss of charge carriers in Fe^{3+}-doped TiO_2.

All the examples given above are seemingly suggesting that a direct relationship exists between the charge-carrier lifetime and the photoactivity for metal-ion-doped photocatalysts. The longer the lifetime, the higher the photoactivity. However, such a statement should not be generalized because the relationship between the charge-carrier lifetime and the photoactivity is not straightforward and unambiguous. As pointed out by Bahnemann and coworkers (Bahnemann et al. 1997), photogenerated holes could be trapped either deeply or shallowly. Those deeply trapped holes which were rather long lived exhibited almost no activity, i.e., they were not able to oxidize dichloroacetate (DCA^-). Shallowly trapped holes, on the other hand, were able to oxidize DCA^- almost instantaneously $\left(t_{1/2} < 5\ \mu s\right)$. Moreover, there are also other effects caused by metal-ion doping on the photoactivity of catalysts, such as change of the surface hydrophilicity (Yu et al. 2005c; Arpac et al. 2007), change of the adsorption ability toward reactant molecules, shifting of Fermi levels (Karakitsou and Verykios 1993), change of the thickness of the space charge region near the surface, and induction of crystalline phase transitions within the catalysts (Gracia et al. 2004). Sometimes these factors may exhibit opposite effects when being present simultaneously (Ranjit and Viswanathan 1997; Yu et al. 2005c).

Although in this review the different ways to increase the efficiency of photocatalysts, e.g., coupled semiconductors, deposition of noble metals, and doping, have been discussed separately, these techniques can also be combined to achieve synergetic effects in improving the photocatalytic performance. In a recent report, Tada et al. (2006) showed that an Au/TiO_2 photocatalyst was capable to effectively photoreduce elemental S to S^{2-} in an aqueous environment (Kiyonaga et al. 2006). Based on this finding, the authors prepared an $Au/CdS/TiO_2$ nanocomposite photocatalyst by the selective deposition of CdS on Au deposited on the surface of TiO_2 nanoparticles. Convincing evidence was presented that a vectorial electron transfer takes place from TiO_2 via-Au-to CdS under irradiation, as a result of the simultaneous excitation of CdS and TiO_2. Under these reaction conditions the CdS surface

was found to predominantly function as the reductive site leaving the exposed TiO_2 surface as the oxidizing site, as probed by the photodeposition of Pt metal selectively on the CdS surface. This observation is in clear contrast to the simple electrochemical picture in which according to the energetic positions of CB and VB in TiO_2 and CdS (cf. Fig. 16.9), the former should be the place for the reduction processes and the latter for the oxidation reactions.

16.4 Concluding Remarks

The photocatalytic oxidation of mainly organic pollutants in water and air as one of the advanced oxidation processes has been proven to be an effective technique for environmental remediation. To develop efficient photocatalytic systems, high-quality semiconductor-based materials have been actively studied in recent years. Among a wide spectrum of semiconductors, TiO_2 has attracted significant attention over the past decades due to its excellent performance as photocatalysts under UV-light irradiation. The maturity in synthesis methods for various nanostructures based on TiO_2 allows further enhancement of its photocatalytic performance. Considerable efforts have also been devoted to developing visible-light-sensitive materials to extend the usable solar energy spectrum into the longer-wavelength region. Although the photocatalysts reviewed here only cover a small portion of the whole range of applicable materials, both theoretical and experimental evidence has been accumulated to support that such materials can serve as the basis upon which highly efficient photocatalysts for solar energy utilization can be developed.

References

Abe, R., T. Takata, H. Sugihara and K. Domen (2005). Photocatalytic overall water splitting under visible light by TaON and WO_3 with an IO_3^-/I^- shuttle redox mediator. Chemical Communications 2005(30), 3829–3831.

Ah, C.S., H.S. Han, K. Kim and D.J. Jang (2000). Photofragmentation dynamics of *n*-dodecanethiol-derivatized silver nanoparticles in cyclohexane. Journal of Physical Chemistry B, 104(34), 8153–8159.

Akyol, A., H.C. Yatmaz and M. Bayramoglu (2004). Photocatalytic decolorization of remazol red RR in aqueous ZnO suspensions. Applied Catalysis B-Environmental, 54(1), 19–24.

Alivisatos, A.P. (1996a). Perspectives on the physical chemistry of semiconductor nanocrystals. Journal of Physical Chemistry, 100(31), 13226–13239.

Alivisatos, A.P. (1996b). Semiconductor clusters, nanocrystals, and quantum dots. Science, 271(5251), 933–937.

Amalric, L., C. Guillard and P. Pichat (1994). Use of catalase and superoxide-dismutase to assess the roles of hydrogen-peroxide and superoxide in the TiO_2 or ZnO photocatalytic destruction of 1,2-dimethoxybenzene in water. Research on Chemical Intermediates, 20(6), 579–594.

Anpo, M., K. Chiba, M. Tomonari, S. Coluccia, M. Che and M.A. Fox (1991). Photocatalysis on native and platinum-loaded TiO_2 and ZnO catalysts-origin of different reactivities on wet and dry metal-oxides. Bulletin of the Chemical Society of Japan, 64(2), 543–551.

Antonelli, D.M. and J.Y. Ying (1995). Synthesis of hexagonally packed mesoporous TiO_2 by a modified sol–gel method. Angewandte Chemie-International Edition in English, 34(18), 2014–2017.

Arabatzis, I.M., T. Stergiopoulos, D. Andreeva, S. Kitova, S.G. Neophytides and P. Falaras (2003). Characterization and photocatalytic activity of Au/TiO_2 thin films for azo-dye degradation. Journal of Catalysis, 220(1), 127–135.

Arana, J., J.M. Dona-Rodriguez, O. Gonzalez-Diaz, E.T. Rendon, J.A.H. Melian, G. Colon, J.A. Navio and J.P. Pena (2004). Gas-phase ethanol photocatalytic degradation study with TiO_2 doped with Fe, Pd and Cu. Journal of Molecular Catalysis A-Chemical, 215(1–2), 153–160.

Araujo, P.Z., C.B. Mendive, L.A.G. Rodenas, P.J. Morando, A.E. Regazzoni, M.A. Blesa and D. Bahnemann (2005). FT-IR-ATR as a tool to probe photocatalytic interfaces. Colloids and Surfaces A-Physicochemical and Engineering Aspects, 265(1–3), 73–80.

Arpac, E., F. Sayilkan, M. Asilturk, P. Tatar, N. Kiraz and H. Sayilkan (2007). Photocatalytic performance of Sn-doped and undoped TiO_2 nanostructured thin films under UV and Vis-lights. Journal of Hazardous Materials, 140(1–2), 69–74.

Asahi, R., T. Morikawa, T. Ohwaki, K. Aoki and Y. Taga (2001). Visible-light photocatalysis in nitrogen-doped titanium oxides. Science, 293(5528), 269–271.

Bach, U., D. Lupo, P. Comte, J.E. Moser, F. Weissortel, J. Salbeck, H. Spreitzer and M. Grätzel (1998). Solid-state dye-sensitized mesoporous TiO_2 solar cells with high photon-to-electron conversion efficiencies. Nature, 395(6702), 583–585.

Badilescu, S. and P.V. Ashrit (2003). Study of sol–gel prepared nanostructured WO_3 thin films and composites for electrochromic applications. Solid State Ionics, 158(1–2), 187–197.

Baeck, S.H., K.S. Choi, T.F. Jaramillo, G.D. Stucky and E.W. McFarland (2003). Enhancement of photocatalytic and electrochromic properties of electrochemically fabricated mesoporous WO_3 thin films. Advanced Materials, 15(15), 1269–1273.

Bahnemann, D.W. (1993). Ultrasmall metal oxide particles: Preparation, photophysical characterization, and photocatalytic properties. Israel Journal of Chemistry, 33, 115–136.

Bahnemann, D., A. Henglein, J. Lilie and L. Spanhel (1984a). Flash photolysis observation of the absorption spectra of trapped positive holes and electrons in colloidal TiO_2. Journal of Physical Chemistry, 88(4), 709–711.

Bahnemann, D., A. Henglein and L. Spanhel (1984b). Detection of the intermediates of colloidal TiO_2-catalysed photoreactions. Faraday Discussions of the Chemical Society, 78, 151–163.

Bahnemann, D.W., C. Kormann and M.R. Hoffmann (1987a). Preparation and characterization of quantum size zinc oxide: A detailed spectroscopic study. Journal of Physical Chemistry, 91(14), 3789–3798.

Bahnemann, D.W., J. Mönig and R. Chapman (1987b). Efficient photocatalysis of the irreversible one-electron and two-electron reduction of halothane on platinized colloidal titanium dioxide in aqueous suspension. Journal of Physical Chemistry, 91(14), 3872–3788.

Bahnemann, D.W., M. Hilgendorff and R. Memming (1997). Charge carrier dynamics at TiO_2 particles: Reactivity of free and trapped holes. Journal of Physical Chemistry B, 101(21), 4265–4275.

Bally, A.R., E.N. Korobeinikova, P.E. Schmid, F. Levy and F. Bussy (1998). Structural and electrical properties of Fe-doped TiO_2 thin films. Journal of Physics D-Applied Physics, 31(10), 1149–1154.

Bamwenda, G.R., S. Tsubota, T. Nakamura and M. Haruta (1995). Photoassisted hydrogen-production from a water–ethanol solution – a comparison of activities of $Au–TiO_2$ and $Pt–TiO_2$. Journal of Photochemistry and Photobiology A-Chemistry, 89(2), 177–189.

Baron, R., C.H. Huang, D.M. Bassani, A. Onopriyenko, M. Zayats and I. Willner (2005). Hydrogen-bonded CdS nanoparticle assemblies on electrodes for photoelectrochemical applications. Angewandte Chemie-International Edition, 44(26), 4010–4015.

Bechinger, C., G. Oefinger, S. Herminghaus and P. Leiderer (1993). On the fundamental role of oxygen for the photochromic effect of WO_3. Journal of Applied Physics, 74(7), 4527–4533.

Bechinger, C., E. Wirth and P. Leiderer (1996). Photochromic coloration of WO_3 with visible light. Applied Physics Letters, 68(20), 2834–2836.

Bedja, I. and P.V. Kamat (1995). Capped semiconductor colloids – synthesis and photoelectrochemical behavior of TiO_2-capped SnO_2 nanocrystallites. Journal of Physical Chemistry, 99(22), 9182–9188.

Bessekhouad, Y., D. Robert and J. Weber (2004). Bi_2S_3/TiO_2 and CdS/TiO_2 heterojunctions as an available configuration for photocatalytic degradation of organic pollutant. Journal of Photochemistry and Photobiology A-Chemistry, 163(3), 569–580.

Bessekhouad, Y., N. Chaoui, M. Trzpit, N. Ghazzal, D. Robert and J.V. Weber (2006). UV/Vis versus visible degradation of acid orange II in a coupled CdS/TiO_2 semiconductors suspension. Journal of Photochemistry and Photobiology A-Chemistry, 183(1–2), 218–224.

Bettinelli, M., A. Speghini, D. Falcomer, M. Daldosso, V. Dallacasa and L. Romano (2006). Photocatalytic, spectroscopic and transport properties of lanthanide-doped TiO_2 nanocrystals. Journal of Physics-Condensed Matter, 18(33), S2149–S2160.

Bilmes, S.A., P. Mandelbaum, F. Alvarez and N.M. Victoria (2000). Surface and electronic structure of titanium dioxide photocatalysts. Journal of Physical Chemistry B, 104, 9851–9858.

Blesa, M.A., A.D. Weisz, P.J. Morando, J.A. Salfity, G.E. Magaz and A.E. Regazzoni (2000). The interaction of metal oxide surfaces with complexing agents dissolved in water. Coordination Chemistry Reviews, 196, 31–63.

Bollinger, M.A. and M.A. Vannice (1996). A kinetic and drifts study of low-temperature carbon monoxide oxidation over Au–TiO_2 catalysts. Applied Catalysis B-Environmental, 8(4), 417–443.

Brus, L.E. (1983). A simple-model for the ionization-potential, electron-affinity, and aqueous redox potentials of small semiconductor crystallites. Journal of Chemical Physics, 79(11), 5566–5571.

Brus, L.E. (1984). Electron–electron and electron–hole interactions in small semiconductor crystallites – the size dependence of the lowest excited electronic state. Journal of Chemical Physics, 80(9), 4403–4409.

Cao, L.X., H.B. Wan, L.H. Huo and S.Q. Xi (2001). A novel method for preparing ordered SnO_2/TiO_2 alternate nanoparticulate films. Journal of Colloid and Interface Science, 244(1), 97–101.

Cao, Y.A., W.S. Yang, W.F. Zhang, G.Z. Liu and P.L. Yue (2004). Improved photocatalytic activity of Sn^{4+} doped TiO_2 nanoparticulate films prepared by plasma-enhanced chemical vapor deposition. New Journal of Chemistry, 28(2), 218–222.

Carp, O., C.L. Huisman and A. Reller (2004). Photoinduced reactivity of titanium dioxide. Progress in Solid State Chemistry, 32(1–2), 33–177.

Chakrabarti, S. and B.K. Dutta (2004). Photocatalytic degradation of model textile dyes in wastewater using ZnO as semiconductor catalyst. Journal of Hazardous Materials, 112(3), 269–278.

Choi, H., E. Stathatos and D.D. Dionysiou (2006). Sol–gel preparation of mesoporous photocatalytic TiO_2 films and TiO_2/Al_2O_3 composite membranes for environmental applications. Applied Catalysis B-Environmental, 63(1–2), 60–67.

Colmenares, J.C., M.A. Aramendia, A. Marinas, J.M. Marinas and F.J. Urbano (2006). Synthesis, characterization and photocatalytic activity of different metal-doped titania systems. Applied Catalysis A-General, 306, 120–127.

Colombo Jr, D.P. and R.M. Bowman (1995). Femtosecond diffuse reflectance spectroscopy of TiO_2 powders. Journal of Physical Chemistry, 99(30), 11752–11756.

Colon, G., M. Maicu, M.C. Hidalgo and J.A. Navio (2006). Cu-doped TiO_2 systems with improved photocatalytic activity. Applied Catalysis B-Environmental, 67(1–2), 41–51.

Cozzoli, P.D., R. Comparelli, E. Fanizza, M.L. Curri, A. Agostiano and D. Laub (2004a). Photocatalytic synthesis of silver nanoparticles stabilized by TiO_2 nanorods: A semiconductor/metal nanocomposite in homogeneous nonpolar solution. Journal of the American Chemical Society, 126(12), 3868–3879.

Cozzoli, P.D., E. Fanizza, R. Comparelli, M.L. Curri, A. Agostiano and D. Laub (2004b). Role of metal nanoparticles in TiO_2/Ag nanocomposite-based microheterogeneous photocatalysis. Journal of Physical Chemistry B, 108(28), 9623–9630.

Crepaldi, E.L., G. Soler-Illia, D. Grosso, F. Cagnol, F. Ribot and C. Sanchez (2003). Controlled formation of highly organized mesoporous titania thin films: From mesostructured hybrids to mesoporous nanoanatase TiO_2. Journal of the American Chemical Society, 125(32), 9770–9786.

Cun, W., X.M. Wang, B.Q. Xu, J.C. Zhao, B.X. Mai, P. Peng, G.Y. Sheng and H.M. Fu (2004). Enhanced photocatalytic performance of nanosized coupled ZnO/SnO_2 photocatalysts for methyl orange degradation. Journal of Photochemistry and Photobiology A-Chemistry, 168(1–2), 47–52.

Daneshvar, N., D. Salari and A.R. Khataee (2004). Photocatalytic degradation of azo dye acid red 14 in water on ZnO as an alternative catalyst to TiO_2. Journal of Photochemistry and Photobiology A-Chemistry, 162(2–3), 317–322.

Di Paola, A., E. Garcia-Lopez, S. Ikeda, G. Marci, B. Ohtani and L. Palmisano (2002). Photocatalytic degradation of organic compounds in aqueous systems by transition metal doped polycrystalline TiO_2. Catalysis Today, 75(1–4), 87–93.

Di Valentin, C., G. Pacchioni, A. Selloni, S. Livraghi and E. Giamello (2005). Characterization of paramagnetic species in n-doped TiO_2 powders by EPR spectroscopy and DFT calculations. Journal of Physical Chemistry B, 109(23), 11414–11419.

Diwald, O., T.L. Thompson, T. Zubkov, E.G. Goralski, S.D. Walck and J.T.J. Yates (2004). Photochemical activity of nitrogen-doped rutile TiO_2(110) in visible light. Journal of Physical Chemistry B, 108, 6004–6008.

Do, Y.R., W. Lee, K. Dwight and A. Wold (1994). The effect of WO_3 on the photocatalytic activity of TiO_2. Journal of Solid State Chemistry, 108(1), 198–201.

Duonghong, D., J. Ramsden and M. Grätzel (1982). Dynamics of interfacial electron-transfer processes in colloidal semiconductor systems. Journal of the American Chemical Society, 104(11), 2977–2985.

Dvoranova, D., V. Brezova, M. Mazur and M.A. Malati (2002). Investigations of metal-doped titanium dioxide photocatalysts. Applied Catalysis B-Environmental, 37(2), 91–105.

Einaga, H., M. Harada, S. Futamura and T. Ibusuki (2003). Generation of active sites for CO photooxidation on TiO_2 by platinum deposition. Journal of Physical Chemistry B, 107(35), 9290–9297.

Evans, J.E., K.W. Springer and J.Z. Zhang (1994). Femtosecond studies of interparticle electron-transfer in a coupled CdS–TiO_2 colloidal system. Journal of Chemical Physics, 101(7), 6222–6225.

Faust, B.C., M.R. Hoffmann and D.W. Bahnemann (1989). Photocatalytic oxidation of surfur dioxide in aqueous suspension of α-Fe_2O_3. Journal of Physical Chemistry, 93, 6371–6381.

Feldhoff, A., C. Mendive, T. Bredow and D. Bahnemann (2007). Direct measurement of size, three-dimensional shape, and specific surface area of anatase nanocrystals. Chemphyschem, 8(6), 805–809.

Frank, S.N. and A.J. Bard (1975). Semiconductor electrodes. II. Electrochemistry at n-type titanium dioxide electrodes in acetonitrile solutions. Journal of the American Chemical Society, 97(26), 7427–7433.

Frank, S.N. and A.J. Bard (1977a). Heterogeneous photocatalytic oxidation of cyanide and sulfite in aqueous solutions at semiconductor powders. Journal of Physical Chemistry, 81, 1484–1488.

Frank, S.N. and A.J. Bard (1977b). Heterogeneous photocatalytic oxidation of cyanide ion in aqueous solutions at titanium dioxide powder. Journal of the American Chemical Society, 99(1), 303–304.

Friedmann, D., H. Hansing and D. Bahnemann (2007). Primary processes during the photodeposition of Ag clusters on TiO_2 nanoparticles. Zeitschrift fur Physikalische Chemie, 221(3), 329–348.

Fujishima, A. and K. Honda (1972). Electrochemical photolysis of water at a semiconductor electrode. Nature, 238(5358), 37–38.

Fujishima, A., T. Kato, E. Maekawa and K. Honda (1981). Mechanism of the current doubling effect. I. The ZnO photoanode in aqueous solution of sodium formate. Bulletin of the Chemical Society of Japan, 54, 1671–1674.

Furube, A., T. Asahi, H. Masuhara, H. Yamashita and M. Anpo (2001). Direct observation of a picosecond charge separation process in photoexcited platinum-loaded TiO_2 particles by femtosecond diffuse reflectance spectroscopy. Chemical Physics Letters, 336(5–6), 424–430.

Gao, Y.M., W. Lee, R. Trehan, R. Kershaw, K. Dwight and A. Wold (1991). Improvement of photocatalytic activity of titanium(IV) oxide by dispersion of Au on TiO_2. Materials Research Bulletin, 26(12), 1247–1254.

Gao, R.M., J. Stark, D.W. Bahnemann and J. Rabani (2002). Quantum yields of hydroxyl radicals in illuminated TiO_2 nanocrystallite layers. Journal of Photochemistry and Photobiology A-Chemistry, 148(1–3), 387–391.

Gerischer, H. (1959). Metal and semiconductor electrode processes. Journal of the Electrochemical Society, 106(8), C200.

Gerischer, H. (1961). Electrode processes. Annual Review of Physical Chemistry, 12, 227–254.

Gerischer, H. (1995). Photocatalysis in aqueous-solution with small TiO_2 particles and the dependence of the quantum yield on particle-size and light-intensity. Electrochimica Acta, 40(10), 1277–1281.

Gerischer, H. and A. Heller (1992). Photocatalytic oxidation of organic-molecules at TiO_2 particles by sunlight in aerated water. Journal of the Electrochemical Society, 139(1), 113–118.

Gesenhues, U. (2001). Al-doped TiO_2 pigments: Influence of doping on the photocatalytic degradation of alkyd resins. Journal of Photochemistry and Photobiology A-Chemistry, 139(2–3), 243–251.

Ghicov, A., B. Schmidt, J. Kunze and P. Schmuki (2007). Photoresponse in the visible range from Cr doped TiO_2 nanotubes. Chemical Physics Letters, 433(4–6), 323–326.

Gissler, W. and R. Memming (1977). Photoelectrochemical processes at semiconducting WO_3 layers. Journal of the Electrochemical Society, 124, 1710–1714.

Gracia, F., J.P. Holgado, A. Caballero and A.R. Gonzalez-Elipe (2004). Structural, optical, and photoelectrochemical properties of m^{n+}-TiO_2 model thin film photocatalysts. Journal of Physical Chemistry B, 108(45), 17466–17476.

Granot, E., F. Patolsky and I. Willner (2004). Electrochemical assembly of a CdS semiconductor nanoparticle monolayer on surfaces: Structural properties and photoelectrochemical applications. Journal of Physical Chemistry B, 108(19), 5875–5881.

Grätzel, M. (2001). Photoelectrochemical cells. Nature, 414(6861), 338–344.

Grätzel, M. and R.F. Howe (1990). Electron paramagnetic resonance studies of doped TiO_2 colloids. Journal of Physical Chemistry, 94(6), 2566–2572.

Grunwaldt, J.D., M. Maciejewski, O.S. Becker, P. Fabrizioli and A. Baiker (1999). Comparative study of Au/TiO_2 and Au/ZrO_2 catalysts for low-temperature co oxidation. Journal of Catalysis, 186(2), 458–469.

Ha, M.G., E.D. Jeong, M.S. Won, H.G. Kim, H.K. Pak, J.H. Jung, B.H. Shon, S.W. Bae and J.S. Lee (2006). Electronic band structure and photocatalytic activity of m-doped TiO_2 (m = Co and Fe). Journal of the Korean Physical Society, 49, S675–S679

Hameed, A., M.A. Gondal and Z.H. Yamani (2004). Effect of transition metal doping on photocatalytic activity of WO_3 for water splitting under laser illumination: Role of 3d-orbitals. Catalysis Communications, 5(11), 715–719.

Hardee, K.L. and A.J. Bard (1977). Semiconductor electrodes X. Photoelectrochemical behavior of several polycrystalline metal oxide electrodes in aqueous solutions. Journal of the Electrochemical Society, 124, 215–224.

Hattori, A., Y. Tokihisa, H. Tada and S. Ito (2000). Acceleration of oxidations and retardation of reductions in photocatalysis of a TiO_2/SnO_2 bilayer-type catalyst. Journal of the Electrochemical Society, 147(6), 2279–2283.

Hattori, A., Y. Tokihisa, H. Tada, N. Tohge, S. Ito, K. Hongo, R. Shiratsuchi and G. Nogami (2001). Patterning effect of a sol–gel TiO_2 overlayer on the photocatalytic activity of a TiO_2/SnO_2 bilayer-type photocatalyst. Journal of Sol–Gel Science and Technology, 22(1–2), 53–61.

Hayashi, T., K. Tanaka and M. Haruta (1998). Selective vapor-phase epoxidation of propylene over Au/TiO_2 catalysts in the presence of oxygen and hydrogen. Journal of Catalysis, 178(2), 566–575.

He, J.X., P.J. Yang, H. Sato, Y. Umemura and A. Yamagishi (2004). Effects of Ag-photodeposition on photocurrent of an ITO electrode modified by a hybrid film of TiO_2 nanosheets. Journal of Electroanalytical Chemistry, 566(1), 227–233.

Henglein, A., B. Lindig and J. Westerhausen (1981). Photochemical electron storage on colloidal metals and hydrogen formation by free radicals. Journal of Physical Chemistry, 85(12), 1627–1628.

Hidaka, H., J. Zhao, E. Pelizzetti and N. Serpone (1992). Photodegradation of surfactants. 8. Comparison of photocatalytic processes between anionic sodium dodecylbenzenesulfonate and cationic benzyldodecyldimethylammonium chloride on the TiO_2 surface. Journal of Physical Chemistry, 96(5), 2226–2230.

Higashimoto, S., M. Sakiyama and M. Azuma (2006). Photoelectrochemical properties of hybrid WO_3/TiO_2 electrode. Effect of structures of WO_3 on charge separation behavior. Thin Solid Films, 503(1–2), 201–206.

Hirai, T., Y. Bando and I. Komasawa (2002). Immobilization of CdS nanoparticles formed in reverse micelles onto alumina particles and their photocatalytic properties. Journal of Physical Chemistry B, 106(35), 8967–8970.

Hirakawa, T. and P.V. Kamat (2004). Photoinduced electron storage and surface plasmon modulation in $Ag@TiO_2$ clusters. Langmuir, 20(14), 5645–5647.

Hirakawa, T. and P.V. Kamat (2005). Charge separation and catalytic activity of $Ag@TiO_2$ core-shell composite clusters under UV-irradiation. Journal of the American Chemical Society, 127(11), 3928–3934.

Ho, W., J.C. Yu and S. Lee (2006). Synthesis of hierarchical nanoporous f-doped TiO_2 spheres with visible light photocatalytic activity. Chemical Communications 2006(10), 1115–1117.

Hodes, G., D. Cahen and J. Manasson (1976). Tungsten trioxide as a photoanode for a photoelectrochemical cell (pec). Nature, 260, 312–313.

Hoffmann, M.R., S.T. Martin, W.Y. Choi and D.W. Bahnemann (1995). Environmental applications of semiconductor photocatalysis. Chemical Reviews, 95(1), 69–96.

Hsu, M.C., I.C. Leu, Y.M. Sun and M.H. Hon (2005). Fabrication of $CdS@TiO_2$ coaxial composite nanocables arrays by liquid-phase deposition. Journal of Crystal Growth, 285(4), 642–648.

Hwang, D.W., J. Kim, T.J. Park and J.S. Lee (2002). Mg-doped WO_3 as a novel photocatalyst for visible light-induced water splitting. Catalysis Letters, 80(1–2), 53–57.

Ihara, T., M. Miyoshi, Y. Iriyama, O. Matsumoto and S. Sugihara (2003). Visible-light-active titanium oxide photocatalyst realized by an oxygen-deficient structure and by nitrogen doping. Applied Catalysis B-Environmental, 42(4), 403–409.

Iliev, V., D. Tomova, L. Bilyarska, A. Eliyas and L. Petrov (2006). Photocatalytic properties of TiO_2 modified with platinum and silver nanoparticles in the degradation of oxalic acid in aqueous solution. Applied Catalysis B-Environmental, 63(3–4), 266–271.

Irie, M. (2000). Diarylethenes for memories and switches. Chemical Reviews, 100(5), 1685–1716.

Irie, H., Y. Watanabe and K. Hashimoto (2003). Carbon-doped anatase TiO_2 powders as a visible-light sensitive photocatalyst. Chemistry Letters, 32(8), 772–773.

Iwasaki, M., M. Hara H. Kawada, H. Tada and S. Ito (2000). Cobalt ion-doped TiO_2 photocatalyst response to visible light. Journal of Colloid and Interface Science, 224(1), 202–204.

Jakob, M., H. Levanon and P.V. Kamat (2003). Charge distribution between UV-irradiated TiO_2 and gold nanoparticles: Determination of shift in the fermi level. Nano Letters, 3(3), 353–358.

Jana, N.R., T.K. Sau and T. Pal (1999). Growing small silver particle as redox catalyst. Journal of Physical Chemistry B, 103(1), 115–121.

Jang, J.S., S.H. Choi, H. Park, W. Choi and J.S. Lee (2006). A composite photocatalyst of CdS nanoparticles deposited on TiO_2 nanosheets. Journal of Nanoscience and Nanotechnology, 6(11), 3642–3646.

Jeong, L.H., J.H. Ahn, B.H. Kim, Y.S. Jeon, K.O. Jeon and K.S. Hwang (2005). Effect of Fe-doping on the crystallinity and the optical properties of TiO_2 thin films. Journal of the Korean Physical Society, 46(2), 559–561.

Jin, R.C., Y.W. Cao, C.A. Mirkin, K.L. Kelly, G.C. Schatz and J.G. Zheng (2001). Photoinduced conversion of silver nanospheres to nanoprisms. Science, 294(5548), 1901–1903.

Jing, D.W. and L.J. Guo (2006). A novel method for the preparation of a highly stable and active CdS photocatalyst with a special surface nanostructure. Journal of Physical Chemistry B, 110(23), 11139–11145.

Jing, L.Q., Z.L. Xu, Y.G. Du, X.J. Sun, L. Wang, X.Q. Zhou, H.Y. Shan and W.M. Cai (2002). Investigation on photocatalytic oxidation degradation of n-C_7H_{16} over zno ultrafine particles. Chemical Journal of Chinese Universities-Chinese, 23(5), 871–875.

Jing, L.Q., X.J. Sun, B.F. Xin, B.Q. Wang, W.M. Cai and H.G. Fu (2004a). The preparation and characterization of La doped TiO_2 nanoparticles and their photocatalytic activity. Journal of Solid State Chemistry, 177(10), 3375–3382.

Jing, L.Q., B.F. Xin F.L. Yuan, B.Q. Wang, K.Y. Shi, W.M. Cai and H.G. Fu (2004b). Deactivation and regeneration of ZnO and TiO_2 nanoparticles in the gas phase photocatalytic oxidation of n-C_7H_{16} or SO_2. Applied Catalysis A-General, 275(1–2), 49–54.

Jing, D.W., Y.J. Zhang and L.J. Guo (2005). Study on the synthesis of Ni doped mesoporous TiO_2 and its photocatalytic activity for hydrogen evolution in aqueous methanol solution. Chemical Physics Letters, 415(1–3), 74–78.

Kamat, P.V. (1997). Native and surface modified semiconductor nanoclusters. Molecular Level Artificial Photosynthetic Materials, 44, 273–343.

Kamat, P.V., M. Flumiani and G.V. Hartland (1998). Picosecond dynamics of silver nanoclusters. Photoejection of electrons and fragmentation. Journal of Physical Chemistry B, 102(17), 3123–3128.

Kanai, N., T. Nuida, K. Ueta, K. Hashimoto, T. Watanabe and H. Ohsaki (2004). Photocatalytic efficiency of TiO_2/SnO_2 thin film stacks prepared by DC magnetron sputtering. Vacuum, 74(3–4), 723–727.

Karakitsou, K.E. and X.E. Verykios (1993). Effects of altervalent cation doping of TiO_2 on its performance as a photocatalyst for water cleavage. Journal of Physical Chemistry, 97(6), 1184–1189.

Karvinen, S.M. (2003). The effects of trace element doping on the optical properties and photocatalytic activity of nanostructured titanium dioxide. Industrial and Engineering Chemistry Research, 42(5), 1035–1043.

Kawahara, T., Y. Konishi, H. Tada, N. Tohge and S. Ito (2001). Patterned TiO_2/SnO_2 bilayer type photocatalyst. 2. Efficient dehydrogenation of methanol. Langmuir, 17(23), 7442–7445.

Kawahara, K., K. Suzuki, Y. Ohka and T. Tatsuma (2005). Electron transport in silver-semiconductor nanocomposite films exhibiting multicolor photochromism. Physical Chemistry Chemical Physics, 7(22), 3851–3855.

Kawahara, T., K. Yamada and H. Tada (2006). Visible light photocatalytic decomposition of 2-naphthol by anodic-biased α-Fe_2O_3 film. Journal of Colloid and Interface Science, 294(2), 504–507

Kay, A. and M. Grätzel (2002). Dye-sensitized core-shell nanocrystals: Improved efficiency of mesoporous tin oxide electrodes coated with a thin layer of an insulating oxide. Chemistry of Materials, 14(7), 2930–2935.

Keller, V., P. Bernhardt and F. Garin (2003). Photocatalytic oxidation of butyl acetate in vapor phase on TiO_2, Pt/TiO_2 and WO_3/TiO_2 catalysts. Journal of Catalysis, 215(1), 129–138.

Khan, S.U.M. and J. Akikusa (1999). Photoelectrochemical splitting of water at nanocrystalline n-Fe_2O_3 thin-film electrodes. Journal of Physical Chemistry B, 103(34), 7184–7189.

Khodja, A.A., T. Sehili, J.F. Pilichowski and P. Boule (2001). Photocatalytic degradation of 2-phenylphenol on TiO_2 and ZnO in aqueous suspensions. Journal of Photochemistry and Photobiology A-Chemistry, 141(2–3), 231–239.

Kikkawa, H., B. O'Regan and M.A. Anderson (1991). The photoelectrochemical properties of Nb-doped TiO_2 semiconducting ceramic membrane. Journal of Electroanalytical Chemistry, 309(1–2), 91–101.

Kim, S., S.J. Hwang and W.Y. Choi (2005). Visible light active platinum-ion-doped TiO_2 photocatalyst. Journal of Physical Chemistry B, 109(51), 24260–24267.

Kim, D.H., K.S. Lee, Y.S. Kim, Y.C. Chung and S.J. Kim (2006a). Photocatalytic activity of Ni 8 wt%-doped TiO_2 photocatalyst synthesized by mechanical alloying under visible light. Journal of the American Ceramic Society, 89(2), 515–518.

Kim, K., C. Seo and H. Cheong (2006b). Photochromic mechanism in a-WO_3 thin films based on Raman spectroscopic studies. Journal of the Korean Physical Society, 48(6), 1657–1660.

Kisch, H. and H. Weiss (2002). Tuning photoelectrochemical and photocatalytic properties through electronic semiconductor–support interaction. Advanced Functional Materials, 12(8), 483–488.

Kiyonaga, T., T. Mitsui, M. Torikoshi, M. Takekawa, T. Soejima and H. Tada (2006). Ultrafast photosynthetic reduction of elemental sulfur by Au nanoparticle-loaded TiO_2. Journal of Physical Chemistry B, 110(22), 10771–10778.

Klosek, S. and D. Raftery (2001). Visible light driven v-doped TiO_2 photocatalyst and its photooxidation of ethanol. Journal of Physical Chemistry B, 105(14), 2815–2819.

Kong, Y.C., D.P. Yu, B. Zhang, W. Fang and S.Q. Feng (2001). Ultraviolet-emitting ZnO nanowires synthesized by a physical vapor deposition approach. Applied Physics Letters, 78(4), 407–409.

Kormann, C., D.W. Bahnemann and M.R. Hoffmann (1988). Preparation and characterization of quantum-size titanium dioxide. Journal of Physical Chemistry, 92(18), 5196–5201.

Kraeutler, B. and A.J. Bard (1978). Heterogeneous photocatalytic preparation of supported catalysts. Photodeposition of platinum on TiO_2 powder and other substrates [12]. Journal of the American Chemical Society, 100(13), 4317–4318.

Kumar, A. and A.K. Jain (2001). Photophysics and photochemistry of colloidal CdS-TiO_2 coupled semiconductors – photocatalytic oxidation of indole. Journal of Molecular Catalysis A-Chemical, 165(1–2), 265–273.

Kumar, A. and N. Mathur (2004). Photocatalytic oxidation of aniline using Ag^+-loaded TiO_2 suspensions. Applied Catalysis A-General, 275(1–2), 189–197.

Kuznetsov, V.N. and N. Serpone (2006). Visible light absorption by various titanium dioxide specimens. Journal of Physical Chemistry B, 110, 25203–25209.

Kwon, Y.T., K.Y. Song, W.I. Lee, G.J. Choi and Y.R. Do (2000). Photocatalytic behavior of WO_3-loaded TiO_2 in an oxidation reaction. Journal of Catalysis, 191(1), 192–199.

Lee, J.S. and W.Y. Choi (2004). Effect of platinum deposits on TiO_2 on the anoxic photocatalytic degradation pathways of alkylamines in water: Dealkylation and n-alkylation. Environmental Science and Technology, 38(14), 4026–4033.

Lee, D.H., Y.S. Cho, W.I. Yi, T.S. Kim, J.K. Lee and H.J. Jung (1995). Metalorganic chemical-vapor-deposition of TiO_2-n anatase thin-film on Si substrate. Applied Physics Letters, 66(7), 815–816.

Lee, S.S., C.Y. Fan, T.P. Wu and S.L. Anderson (2004). Co oxidation on Au-n/TiO_2 catalysts produced by size-selected cluster deposition. Journal of the American Chemical Society, 126(18), 5682–5683.

Lee, K., N.H. Leea, S.H. Shin, H.G. Lee and S.J. Kim (2006). Hydrothermal synthesis and photocatalytic characterizations of transition metals doped nano TiO_2 sols. Materials Science and Engineering B-Solid State Materials for Advanced Technology, 129(1–3), 109–115.

Leland, J.K. and A.J. Bard (1987). Photochemistry of colloidal semiconducting iron oxide polymorphs. Journal of Physical Chemistry, 91, 5076–5083.

Levy, B., W. Liu and S.E. Gilbert (1997). Directed photocurrents in nanostructured TiO_2/SnO_2 heterojunction diodes. Journal of Physical Chemistry B, 101(10), 1810–1816.

Li, X.Z. and F.B. Li (2001). Study of Au/Au^{3+} − TiO_2 photocatalysts toward visible photooxidation for water and wastewater treatment. Environmental Science and Technology, 35(11), 2381–2387.

Li, Y., G.W. Meng, L.D. Zhang and F. Phillipp (2000). Ordered semiconductor ZnO nanowire arrays and their photoluminescence properties. Applied Physics Letters, 76(15), 2011–2013.

Li, D., H. Haneda, S. Hishita and N. Ohashi (2005a). Visible-light-driven N-F-codoped TiO_2 photocatalysts. 2. Optical characterization, photocatalysis, and potential application to air purification. Chemistry of Materials, 17(10), 2596–2602.

Li, D., H. Haneda, S. Hishita, N. Ohashi and N.K. Labhsetwar (2005b). Fluorine-doped TiO_2 powders prepared by spray pyrolysis and their improved photocatalytic activity for decomposition of gas-phase acetaldehyde. Journal of Fluorine Chemistry, 126(1), 69–77.

Li, Y.Z., D.S. Hwang, N.H. Lee and S.J. Kim (2005c). Synthesis and characterization of carbon-doped titania as an artificial solar light sensitive photocatalyst. Chemical Physics Letters, 404(1–3), 25–29.

Lin, Z.S., A. Orlov, R.M. Lambert and M.C. Payne (2005). New insights into the origin of visible light photocatalytic activity of nitrogen-doped and oxygen-deficient anatase TiO_2. Journal of Physical Chemistry B, 109(44), 20948–20952.

Lindgren, T., J.M. Mwabora, E. Avendano, J. Jonsson, A. Hoel, C.G. Granqvist and S.E. Lindquist (2003). Photoelectrochemical and optical properties of nitrogen doped titanium dioxide films prepared by reactive DC magnetron sputtering. Journal of Physical Chemistry B, 107(24), 5709–5716.

Linsebigler, A.L., G.Q. Lu and J.T. Yates (1995). Photocatalysis on TiO_2 surfaces – principles, mechanisms, and selected results. Chemical Reviews, 95(3), 735–758.

Linsebigler, A., C. Rusu and J.T. Yates (1996). Absence of platinum enhancement of a photoreaction on TiO_2–Co photooxidation on $Pt/TiO_2(110)$. Journal of the American Chemical Society, 118(22), 5284–5289.

Litter, M.I. and J.A. Navio (1996). Photocatalytic properties of iron-doped titania semiconductors. Journal of Photochemistry and Photobiology A-Chemistry, 98(3), 171–181.

Lu, T.C., Y.Z. Liu, L.B. Lin, X.T. Zu, J.M. Zhu and L.P. Wu (2001a). Influence of transition-metal Cr doping on optical properties of rutile single crystal. Journal of Inorganic Materials, 16(2), 373–376.

Lu, T.C., S.Y. Wu, L.B. Lin and W.C. Zheng (2001b). Defects in the reduced rutile single crystal. Physica B-Condensed Matter, 304(1–4), 147–151.

Ma, T.L., M. Akiyama, E. Abe and I. Imai (2005). High-efficiency dye-sensitized solar cell based on a nitrogen-doped nanostructured titania electrode. Nano Letters, 5(12), 2543–2547.

Macyk, W., G. Burgeth and H. Kisch (2003). Photoelectrochemical properties of platinum(IV) chloride surface modified TiO_2. Photochemical and Photobiological Sciences, 2(3) 322–328.

Martyanov, I.N., S. Uma, S. Rodrigues and K.J. Klabunde (2004). Structural defects cause TiO_2-based photocatalysts to be active in visible light. Chemical Communications 2004(21), 2476–2477.

Meissner, D. and R. Memming (1988). Photoelectrochemistry of cadmium sulfide. 1. Reanalysis of photocorrosion and flat-band potential. Journal of Physical Chemistry, 92, 3476–3483.

Meissner, D., R. Memming, B. Kastening and D. Bahnemann (1986). Fundamental problems of water splitting at cadmium-sulfide. Chemical Physics Letters, 127(5), 419–423.

Memming, R. (2001). Semiconductor electrochemistry. Weinheim, Wiley-VCH

Mendive, C.B., D.W. Bahnemann and M.A. Blesa (2005). Microscopic characterization of the photocatalytic oxidation of oxalic acid adsorbed onto TiO_2 by FTIR-ATR. Catalysis Today, 101(3–4), 237–244.

Mendive, C.B., T. Bredow, M.A. Blesa and D.W. Bahnemann (2006). ATR-FTIR measurements and quantum chemical calculations concerning the adsorption and photoreaction of oxalic acid on TiO_2. Physical Chemistry Chemical Physics, 8(27), 3232–3247.

Mendive, C.B., T. Bredow, A. Feldhoff, M. Blesa and D. Bahnemann (2008). Adsorption of oxalate on rutile particles in aqueous solutions: A spectroscopic, electron-microscopic and theoretical study. Physical Chemistry Chemical Physics, 10(14), 1960–1974.

Miyake, H. and H. Kozuka (2005). Photoelectrochemical properties of $Fe_2O_3 - Nb_2O_5$ films prepared by sol–gel method. Journal of Physical Chemistry B, 109(38), 17951–17956.

Miyauchi, M., A. Nakajima, K. Hashimoto and T. Watanabe (2000). A highly hydrophilic thin film under 1 muW/cm^2 UV illumination. Advanced Materials, 12(24), 1923–1927.

Miyauchi, M., A.K. Nakajima, T. Watanabe and K. Hashimoto (2002). Photoinduced hydrophilic conversion of TiO_2/WO_3 layered thin films. Chemistry of Materials, 14(11), 4714–4720.

Miyauchi, M., A. Ikezawa, H. Tobimatsu, H. Irie and K. Hashimoto (2004). Zeta potential and photocatalytic activity of nitrogen doped TiO_2 thin films. Physical Chemistry Chemical Physics, 6(4), 865–870.

Mohamed, M.M. and M.M. Al-Esaimi (2006). Characterization, adsorption and photocatalytic activity of vanadium-doped TiO_2 and sulfated TiO_2 (rutile) catalysts: Degradation of methylene blue dye. Journal of Molecular Catalysis A-Chemical, 255(1–2), 53–61.

Monllor-Satoca, D., L. Borja, A. Rodes, R. Gomez and P. Salvador (2006). Photoelectrochemical behavior of nanostructured WO_3 thin-film electrodes: The oxidation of formic acid. ChemPhysChem, 7(12), 2540–2551.

Morikawa, T., R. Asahi, T. Ohwaki, K. Aoki and Y. Taga (2001). Band-gap narrowing of titanium dioxide by nitrogen doping. Japanese Journal of Applied Physics Part 2-Letters, 40(6A), L561–L563

Mrowetz, M., W. Balcerski, A.J. Colussi and M.R. Hoffmann (2004). Oxidative power of nitrogen-doped TiO_2 photocatalysts under visible illumination. Journal of Physical Chemistry B, 108(45), 17269–17273.

Murakoshi, K., H. Tanaka, Y. Sawai and Y. Nakato (2002). Photoinduced structural changes of silver nanoparticles on glass substrate in solution under an electric field. Journal of Physical Chemistry B, 106(12), 3041–3045.

Nahar, S., K. Hasegawa and S. Kagaya (2006). Photocatalytic degradation of phenol by visible light-responsive iron-doped TiO_2 and spontaneous sedimentation of the TiO_2 particles. Chemosphere, 65(11), 1976–1982.

Nakajima, H., T. Mori and M. Watanabe (2004a). Influence of platinum loading on photoluminescence of TiO_2 powder. Journal of Applied Physics, 96(1), 925–927.

Nakamura, R., T. Tanaka and Y. Nakato (2004b). Mechanism for visible light responses in anodic photocurrents at n-doped TiO_2 film electrodes. Journal of Physical Chemistry B, 108(30), 10617–10620.

Nakato, Y., K. Ueda, H. Yano and H. Tsubomura (1988). Effect of microscopic discontinuity of metal overlayers on the photovoltages in metal-coated semiconductor–liquid junction photoelectrochemical cells for efficient solar energy conversion. Journal of Physical Chemistry, 92, 2316–2324.

Naoi, K., Y. Ohko and T. Tatsuma (2004). TiO_2 films loaded with silver nanoparticles: Control of multicolor photochromic behavior. Journal of the American Chemical Society, 126(11), 3664–3668.

Naoi, K., Y. Ohko and T. Tatsuma (2005). Switchable rewritability of $Ag - TiO_2$ nanocomposite films with multicolor photochromism. Chemical Communications 2005(10), 1288–1290.

Narayanan, R. and M.A. El-Sayed (2003). Effect of catalysis on the stability of metallic nanoparticles: Suzuki reaction catalyzed by PVP-palladium nanoparticles. Journal of the American Chemical Society, 125(27), 8340–8347.

Navio, J.A., G. Colon, M. Trillas, J. Peral, X. Domenech, J.J. Testa, J. Padron, D. Rodriguez and M.I. Litter (1998). Heterogeneous photocatalytic reactions of nitrite oxidation and Cr(VI) reduction on iron-doped titania prepared by the wet impregnation method. Applied Catalysis B-Environmental, 16(2), 187–196.

Navio, J.A., J.J. Testa, P. Djedjeian, J.R. Padron, D. Rodriguez and M.I. Litter (1999). Iron-doped titania powders prepared by a sol–gel method. Part II: Photocatalytic properties. Applied Catalysis A-General, 178(2), 191–203.

Ohko, Y., T. Tatsuma, T. Fujii, K. Naoi, C. Niwa, Y. Kubota and A. Fujishima (2003). Multicolour photochromism of TiO_2 films loaded with silver nanoparticles. Nature Materials, 2(1), 29–31.

Ohmori, T., H. Takahashi, H. Mametsuka and E. Suzuki (2000). Photocatalytic oxygen evolution on α-Fe_2O_3 films using Fe^{3+} ion as a sacrificial oxidizing agent. Physical Chemistry Chemical Physics, 2(15), 3519–3522.

Ohno, T., T. Mitsui and M. Matsumura (2003). Photocatalytic activity of S-doped TiO_2 photocatalyst under visible light. Chemistry Letters, 32(4), 364–365.

Ohno, T., M. Akiyoshi, T. Umebayashi, K. Asai, T. Mitsui and M. Matsumura (2004a). Preparation of S-doped TiO_2 photocatalysts and their photocatalytic activities under visible light. Applied Catalysis A-General, 265(1), 115–121.

Ohno, T., T. Tsubota, M. Toyofuku and R. Inaba (2004b). Photocatalytic activity of a TiO_2 photocatalyst doped with C^{4+} and S^{4+} ions having a rutile phase under visible light. Catalysis Letters, 98(4), 255–258.

Ohno, T., Z. Miyamoto, K. Nishijima, H. Kanemitsu and X.Y. Feng (2006). Sensitization of photocatalytic activity of S- or N-doped TiO_2 particles by adsorbing Fe^{3+} cations. Applied Catalysis A-General, 302(1), 62–68.

Okazaki, K., Y. Morikawa, S. Tanaka, K. Tanaka and M. Kohyama (2004). Electronic structures of Au on TiO_2(110) by first-principles calculations. Physical Review B, 69(23), 8

Ollis, D.F., E. Pelizzetti and N. Serpone (1991). Photocatalyzed destruction of water contaminants. Environmental Science and Technology, 25(9), 1522–1529.

O'Regan, B. and M. Grätzel (1991). A low-cost, high-efficiency solar-cell based on dye-sensitized colloidal TiO_2 films. Nature, 353(6346), 737–740.

Osterwalder, J., T. Droubay, T. Kaspar, J. Williams, C.M. Wang and S.A. Chambers (2005). Growth of Cr-doped TiO_2 films in the rutile and anatase structures by oxygen plasma assisted molecular beam epitaxy. Thin Solid Films, 484(1–2), 289–298.

Ozgur, U., Y.I. Alivov, C. Liu, A. Teke, M.A. Reshchikov, S. Dogan, V. Avrutin, S.J. Cho and H. Morkoc (2005). A comprehensive review of ZnO materials and devices. Journal of Applied Physics, 98(4), 103

Pal, B. and M. Sharon (1998). Photocatalytic degradation of salicylic acid by colloidal Fe_2O_3 particles. Journal of Chemical Technology and Biotechnology, 73(3), 269–273.

Pan, J.H. and W.I. Lee (2006). Preparation of highly ordered cubic mesoporous WO_3/TiO_2 films and their photocatalytic properties. Chemistry of Materials, 18(3), 847–853.

Papaefthimiou, S., G. Leftheriotis and P. Yianoulis (2001). Advanced electrochromic devices based on WO_3 thin films. Electrochimica Acta, 46(13–14), 2145–2150.

Papp, J., S. Soled, K. Dwight and A. Wold (1994). Surface-acidity and photocatalytic activity of TiO_2, WO_3/TiO_2, and MoO_3/TiO_2 photocatalysts. Chemistry of Materials, 6(4), 496–500.

Pearton, S.J., D.P. Norton, K. Ip, Y.W. Heo and T. Steiner (2005). Recent progress in processing and properties of ZnO. Progress in Materials Science, 50(3), 293–340.

Pradhan, N., A. Pal and T. Pal (2001). Catalytic reduction of aromatic nitro compounds by coinage metal nanoparticles. Langmuir, 17(5), 1800–1802.

Pulgarin, C. and J. Kiwi (1995). Iron oxide-mediated degradation, photodegradation, and biodegradation of aminophenols. Langmuir, 11(2), 519–526.

Quan, X., S. Chen, J. Su, J.W. Chen and G.H. Chen (2004). Synergetic degradation of 2,4-D by integrated photo- and electrochemical catalysis on a Pt doped TiO_2/Ti electrode. Separation and Purification Technology, 34(1–3), 73–79.

Radecka, M., M. Wierzbicka, S. Komornicki and M. Rekas (2004). Influence of Cr on photoelectrochemical properties of TiO_2 thin films. Physica B-Condensed Matter, 348(1–4), 160–168.

Ranjit, K.T. and B. Viswanathan (1997). Synthesis, characterization and photocatalytic properties of iron-doped TiO_2 catalysts. Journal of Photochemistry and Photobiology A-Chemistry, 108(1), 79–84.

Richard, C. (1994). Photocatalytic reduction of benzoquinone in aqueous ZnO or TiO_2 suspensions. New Journal of Chemistry, 18(4), 443–445.

Richard, C. and P. Boule (1995). Reactive species involved in photocatalytic transformations on zinc-oxide. Solar Energy Materials and Solar Cells, 38(1–4), 431–440.

Richard, C., A.M. Martre and P. Boule (1992). Photocatalytic transformation of 2,5-furandimethanol in aqueous ZnO suspensions. Journal of Photochemistry and Photobiology A-Chemistry, 66(2), 225–234.

Robel, I., V. Subramanian, M. Kuno and P.V. Kamat (2006). Quantum dot solar cells. Harvesting light energy with CdSe nanocrystals molecularly linked to mesoscopic TiO_2 films. Journal of the American Chemical Society, 128(7), 2385–2393.

Rodriguez, J.A., J. Hrbek, J. Dvorak, T. Jirsak and A. Maiti (2001). Interaction of sulfur with TiO_2 (110): Photoemission and density-functional studies. Chemical Physics Letters, 336(5–6), 377–384.

Rossetti, R., J.L. Ellison, J.M. Gibson and L.E. Brus (1984). Size effects in the excited electronic states of small colloidal CdS crystallites. Journal of Chemical Physics, 80(9), 4464–4469.

Roucoux, A., J. Schulz and H. Patin (2002). Reduced transition metal colloids: A novel family of reusable catalysts? Chemical Reviews, 102(10), 3757–3778.

Saha, N.C. and H.G. Tompkins (1992). Titanium nitride oxidation chemistry – an X-ray photoelectron-spectroscopy study. Journal of Applied Physics, 72(7), 3072–3079.

Sahoo, C., A.K. Gupta and A. Pal (2005). Photocatalytic degradation of crystal violet (Ci basic violet 3) on silver ion doped TiO_2. Dyes and Pigments, 66(3), 189–196.

Sakatani, Y., D. Grosso, L. Nicole, C. Boissiere, G. Soler-Illia and C. Sanchez (2006). Optimised photocatalytic activity of grid-like mesoporous TiO_2 films: Effect of crystallinity, pore size distribution, and pore accessibility. Journal of Materials Chemistry, 16(1), 77–82.

Sakthivel, S. and H. Kisch (2003). Photocatalytic and photoelectrochemical properties of nitrogen-doped titanium dioxide. Chemphyschem, 4(5), 487–490.

Sakthivel, S., B. Neppolian, M. Palanichamy, B. Arabindoo and V. Murugesan (1999). Photocatalytic degradation of leather dye, acid green 16 using ZnO in the slurry and thin film forms. Indian Journal of Chemical Technology, 6(3), 161–165.

Sakthivel, S., B. Neppolian, M. Palanichamy, B. Arabindoo and V. Murugesan (2001). Photocatalytic degradation of leather dye over ZnO catalyst supported on alumina and glass surfaces. Water Science and Technology, 44(5), 211–218.

Sakthivel, S., B. Neppolian, M.V. Shankar, B. Arabindoo, M. Palanichamy and V. Murugesan (2003). Solar photocatalytic degradation of azo dye: Comparison of photocatalytic efficiency of ZnO and TiO_2. Solar Energy Materials and Solar Cells, 77(1), 65–82.

Sakthivel, S., M.V. Shankar, M. Palanichamy, B. Arabindoo, D.W. Bahnemann and V. Murugesan (2004). Enhancement of photocatalytic activity by metal deposition: Characterisation and photonic efficiency of Pt, Au and Pd deposited on TiO_2 catalyst. Water Research, 38(13), 3001–3008.

Sano, T., N. Negishi, D. Mas and K. Takeuchi (2000). Photocatalytic decomposition of N_2O on highly dispersed Ag^+ ions on TiO_2 prepared by photodeposition. Journal of Catalysis, 194(1), 71–79.

Sant, P.A. and P.V. Kamat (2002). Interparticle electron transfer between size-quantized CdS and TiO_2 semiconductor nanoclusters. Physical Chemistry Chemical Physics, 4(2), 198–203.

Santato, C., M. Odziemkowski, M. Ulmann and J. Augustynski (2001). Crystallographically oriented mesoporous WO_3 films: Synthesis, characterization, and applications. Journal of the American Chemical Society, 123(43), 10639–10649.

Schierbaum, K.D., U.K. Kirner, J.F. Geiger and W. Gopel (1991). Schottky-barrier and conductivity gas sensors based upon Pd/SnO_2 and Pt/TiO_2. Sensors and Actuators B-Chemical, 4(1–2), 87–94.

Sclafani, A. and J.M. Herrmann (1998). Influence of metallic silver and of platinum–silver bimetallic deposits on the photocatalytic activity of titania (anatase and rutile) in organic and aqueous media. Journal of Photochemistry and Photobiology A-Chemistry, 113(2), 181–188.

Serpone, N. (2006). Is the band gap of pristine TiO_2 narrowed by anion- and cation-doping of titanium dioxide in second-generation photocatalysts? Journal of Physical Chemistry B, 110(48), 24287–24293.

Serpone, N, E. Borgarello and M. Grätzel (1984). Visible-light induced generation of hydrogen from H_2S in mixed semiconductor dispersions – Improved efficiency through inter-particle electron-transfer. Journal of The Chemical Society – Chemical Communications, 6, 342–344.

Serpone, N., D. Lawless, J. Disdier and J.M. Herrmann (1994). Spectroscopic, photoconductivity, and photocatalytic studies of TiO_2 colloids – naked and with the lattice doped with Cr^{3+}, Fe^{3+}, and V^{5+} cations. Langmuir, 10(3), 643–652.

Serpone, N., D. Lawless, R. Khairutdinov and E. Pelizzetti (1995). Subnanosecond relaxation dynamics in TiO_2 colloidal sols (particle sizes $Rp = 1.0 - 13.4$ nm). Relevance to heterogeneous photocatalysis. Journal of Physical Chemistry, 99(45), 16655–16661.

Seven, O., B. Dindar, S. Aydemir, D. Metin, M.A. Ozinel and S. Icli (2004). Solar photocatalytic disinfection of a group of bacteria and fungi aqueous suspensions with TiO_2, ZnO and Sahara desert dust. Journal of Photochemistry and Photobiology A-Chemistry, 165(1–3), 103–107.

Shah, S.I., W. Li, C.P. Huang, O. Jung and C. Ni (2002). Study of Nd^{3+}, Pd^{2+}, Pt^{4+}, and Fe^{3+} dopant effect on photoreactivity of TiO_2 nanoparticles. Proceedings of the National Academy of Sciences of the United States of America, 99, 6482–6486.

Shang, J., W.Q. Yao, Y.F. Zhu and N.Z. Wu (2004). Structure and photocatalytic performances of glass/SnO_2/TiO_2 interface composite film. Applied Catalysis A-General, 257(1), 25–32.

Sharma, R.K. and M.C. Bhatnagar (1999). Improvement of the oxygen gas sensitivity in doped TiO_2 thick films. Sensors and Actuators B-Chemical, 56(3), 215–219.

Shi, Q., D. Yang, Z.Y. Jiang and J. Li (2006). Visible-light photocatalytic regeneration of NADH using p-doped TiO_2 nanoparticles. Journal of Molecular Catalysis B-Enzymatic, 43(1–4), 44–48.

Shigesato, Y. (1991). Photochromic properties of amorphous WO_3 films. Japanese Journal of Applied Physics Part 1-Regular Papers Short Notes and Review Papers, 30(7), 1457–1462.

Siemon, U., D. Bahnemann, J.J. Testa, D. Rodriguez, M.I. Litter and N. Bruno (2002). Heterogeneous photocatalytic reactions comparing TiO_2 and Pt/TiO_2. Journal of Photochemistry and Photobiology A-Chemistry, 148(1–3), 247–255.

So, W.W. K.J. Kim and S.J. Moon (2004). Photo-production of hydrogen over the CdS–TiO_2 nanocomposite particulate films treated with $TiCl_4$. International Journal of Hydrogen Energy, 29(3), 229–234.

Sonawane, R.S. and M.K. Dongare (2006). Sol–gel synthesis of Au/TiO_2 thin films for photocatalytic degradation of phenol in sunlight. Journal of Molecular Catalysis A-Chemical, 243(1), 68–76.

Spanhel, L., H. Weller and A. Henglein (1987). Photochemistry of semiconductor colloids. 22. Electron ejection from illuminated cadmium sulfide into attached titanium and zinc oxide particles. Journal of the American Chemical Society, 109, 6632–6635.

Sreethawong, T., Y. Suzuki and S. Yoshikawa (2006). Platinum-loaded mesoporous titania by single-step sol–gel process with surfactant template: Photocatalytic activity for hydrogen evolution. Comptes Rendus Chimie, 9(2), 307–314.

Srinivasan, S., J. Wade and E.K. Stefanakos (2006). Visible light photocatalysis via CdS/TiO_2 nanocompositematerials. Journal of Nanomaterials, 2006, 87326(1–7).

Stathatos, E. and P. Lianos (2000). Photocatalytically deposited silver nanoparticles on mesoporous TiO_2 films. Langmuir, 16(5), 2398–2400.

Studenikin, S.A., N. Golego and M. Cocivera (1998). Fabrication of green and orange photoluminescent, undoped ZnO films using spray pyrolysis. Journal of Applied Physics, 84(4), 2287–2294.

Su, L.Y., J.H. Fang and Z.H. Lu (1997). Photochromic and photoelectrochemical behavior of thin semiconductor WO_3 films. Materials Chemistry and Physics, 51(1), 85–87.

Subramanian V., E.E. Wolf and P.V. Kamat (2003). Influence of metal/metal ion concentration on the photocatalytic activity of TiO_2–Au composite nanoparticles. Langmuir, 19(2), 469–474.

Subramanian, V., E.E. Wolf and P.V. Kamat (2004). Catalysis with TiO_2/gold nanocomposites. Effect of metal particle size on the fermi level equilibration. Journal of the American Chemical Society, 126(15), 4943–4950.

Sun, B., A.V. Vorontsov and P.G. Smirniotis (2003). Role of platinum deposited on TiO_2 in phenol photocatalytic oxidation. Langmuir, 19(8), 3151–3156.

Sung-Suh, H.M., J.R. Choi, H.J. Hah, S.M. Koo and Y.C. Bae (2004). Comparison of Ag deposition effects on the photocatalytic activity of nanoparticulate TiO_2 under visible and UV light irradiation. Journal of Photochemistry and Photobiology A-Chemistry, 163(1–2), 37–44.

Tada, H., K. Teranishi and S. Ito (1999). Additive effect of sacrificial electron donors on Ag/TiO_2 photocatalytic reduction of bis(2-dipyridyl)disulfide to 2-mercaptopyridine in aqueous media. Langmuir, 15(20), 7084–7087.

Tada, H., K. Teranishi, Y. Inubushi and S. Ito (2000). Ag nanocluster loading effect an TiO_2 photocatalytic reduction of bis(2-dipyridyl)disulfide to 2-mercaptopyridine by H_2O. Langmuir, 16(7), 3304–3309.

Tada, H., T. Ishida, A. Takao and S. Ito (2004). Drastic enhancement of TiO_2-photocatalyzed reduction of nitrobenzene by loading Ag clusters. Langmuir, 20(19), 7898–7900.

Tada, H., T. Mitsui, T. Kiyonaga, T. Akita and K. Tanaka (2006). All-solid-state z-scheme in $CdS–Au–TiO_2$ three-component nanojunction system. Nature Materials, 5(10), 782–786.

Takeshita, K., A. Yamashita, T. Ishibashi, H. Onishi, K. Nishijima and T. Ohno (2006). Transient IR absorption study of charge carriers photogenerated in sulfur-doped TiO_2. Journal of Photochemistry and Photobiology A-Chemistry, 177(2–3), 269–275.

Tan, T.T.Y., C.K. Yip, D. Beydoun and R. Amal (2003). Effects of nano-Ag particles loading on TiO_2 photocatalytic reduction of selenate ions. Chemical Engineering Journal, 95(1–3), 179–186.

Tang, J., Y.Y. Wu, E.W. McFarland and G.D. Stucky (2004). Synthesis and photocatalytic properties of highly crystalline and ordered mesoporous TiO_2 thin films. Chemical Communications 2004(14), 1670–1671.

Teoh, W.Y., R. Amal, L. Madler and S.E. Pratsinis (2007). Flame sprayed visible light-active $Fe–TiO_2$ for photomineralisation of oxalic acid. Catalysis Today, 120(2), 203–213.

Tian, F.H. and C.B. Liu (2006). DFT description on electronic structure and optical absorption properties of anionic s-doped anatase TiO_2. Journal of Physical Chemistry B, 110(36), 17866–17871.

Tian, Y. and T. Tatsuma (2005). Mechanisms and applications of plasmon-induced charge separation at TiO_2 films loaded with gold nanoparticles. Journal of the American Chemical Society, 127(20), 7632–7637.

Tristao, J.C., F. Magalhaes, P. Corio and M.T.C. Sansiviero (2006). Electronic characterization and photocatalytic properties of CdS/TiO_2 semiconductor composite. Journal of Photochemistry and Photobiology A-Chemistry, 181(2–3), 152–157.

Tsuge, Y., K. Inokuchi, K. Onozuka, O. Shingo, S. Sugi, M. Yoshikawa and S. Shiratori (2006). Fabrication of porous TiO_2 films using a spongy replica prepared by layer-by-layer self-assembly method: Application to dye-sensitized solar cells. Thin Solid Films, 499(1–2), 396–401.

Uchida, H., S. Katoh and M. Watanabe (1998). Photocatalytic degradation of trichlorobenzene using immobilized TiO_2 films containing poly(tetrafluoroethylene) and platinum metal catalyst. Electrochimica Acta, 43(14–15), 2111–2116.

Umebayashi, T., T. Yamaki, H. Itoh and K. Asai (2002). Band gap narrowing of titanium dioxide by sulfur doping. Applied Physics Letters, 81, 454–456.

Umebayashi, T., T. Yamaki, T. Sumita, S. Yamamoto, S. Tanaka and K. Asai (2003a). UV-ray photoelectron and ab initio band calculation studies on electronic structures of Cr- or Nb-ion implanted titanium dioxide. Nuclear Instruments and Methods in Physics Research Section B-Beam Interactions with Materials and Atoms, 206, 264–267.

Umebayashi, T., T. Yamaki, S. Tanaka and K. Asai (2003b). Visible light-induced degradation of methylene blue on S-doped TiO_2. Chemistry Letters, 32(4), 330–331.

Vinodgopal, K. and P.V. Kamat (1995). Enhanced rates of photocatalytic degradation of an azo-dye using SnO_2/TiO_2 coupled semiconductor thin-films. Environmental Science and Technology, 29(3), 841–845.

Vinodgopal, K., I. Bedja and P.V. Kamat (1996). Nanostructured semiconductor films for photocatalysis. Photoelectrochemical behavior of SnO_2/TiO_2 composite systems and its role in photocatalytic degradation of a textile azo dye. Chemistry of Materials, 8(8), 2180–2187.

Wan, Q., Q.H. Li, Y.J. Chen, T.H. Wang, X.L. He, J.P. Li and C.L. Lin (2004). Fabrication and ethanol sensing characteristics of ZnO nanowire gas sensors. Applied Physics Letters, 84(18), 3654–3656.

Wang, H. and J.P. Lewis (2006). Second-generation photocatalytic materials: Anion-doped TiO_2. Journal of Physics-Condensed Matter, 18(2), 421–434.

Wang, Y.Q., H.M. Cheng, Y.Z. Hao, J.M. Ma, W.H. Li and S.M. Cai (1999). Photoelectrochemical properties of metal-ion-doped TiO_2 nanocrystalline electrodes. Thin Solid Films, 349(1–2), 120–125.

Wang, C.Y., D.W. Bahnemann and J.K. Dohrmann (2000a). A novel preparation of iron-doped TiO_2 nanoparticles with enhanced photocatalytic activity. Chemical Communications 2000(16), 1539–1540.

Wang, Y.Q., H.M. Cheng, L. Zhang, Y.Z. Hao, J.M. Ma, B. Xu and W.H. Li (2000b). The preparation, characterization, photoelectrochemical and photocatalytic properties of lanthanide metal-ion-doped TiO_2 nanoparticles. Journal of Molecular Catalysis A-Chemical, 151(1–2), 205–216.

Wang, C., D.W. Bahnemann and J.K. Dohrmann (2001a). Determination of photonic efficiency and quantum yield of formaldehyde formation in the presence of various TiO_2 photocatalysts. Water Science and Technology, 44(5), 279–286.

Wang, J.A., R. Limas-Ballesteros, T. Lopez, A. Moreno, R. Gomez, O. Novaro and X. Bokhimi (2001b). Quantitative determination of titanium lattice defects and solid-state reaction mechanism in iron-doped TiO_2 photocatalysts. Journal of Physical Chemistry B, 105(40), 9692–9698.

Wang, C., J.C. Zhao, X.M. Wang, B.X. Mai, G.Y. Sheng, P. Peng and J.M. Fu (2002a). Preparation, characterization and photocatalytic activity of nano-sized ZnO/SnO_2 coupled photocatalysts. Applied Catalysis B-Environmental, 39(3), 269–279.

Wang, C.Y., J. Rabani, D.W. Bahnemann and J.K. Dohrmann (2002b). Photonic efficiency and quantum yield of formaldehyde formation from methanol in the presence of various TiO_2 photocatalysts. Journal of Photochemistry and Photobiology A-Chemistry, 148(1–3), 169–176.

Wang, C.Y., C. Böttcher, D.W. Bahnemann and J.K. Dohrmann (2003a). A comparative study of nanometer sized Fe(III)-doped TiO_2 photocatalysts: Synthesis, characterization and activity. Journal of Materials Chemistry, 13(9), 2322–2329.

Wang, P., S.M. Zakeeruddin, J.E. Moser, M.K. Nazeeruddin, T. Sekiguchi and M. Grätzel (2003b). A stable quasi-solid-state dye-sensitized solar cell with an amphiphilic ruthenium sensitizer and polymer gel electrolyte. Nature Materials, 2(6), 402–407.

Wang, C.Y., R. Pagel, D.W. Bahnemann and J.K. Dohrmann (2004a). Quantum yield of formaldehyde formation in the presence of colloidal TiO_2-based photocatalysts: Effect of intermittent illumination, platinization, and deoxygenation. Journal of Physical Chemistry B, 108(37), 14082–14092.

Wang, X.D., C.J. Summers and Z.L. Wang (2004b). Large-scale hexagonal-patterned growth of aligned ZnO nanorods for nano-optoelectronics and nanosensor arrays. Nano Letters, 4(3), 423–426.

Wang, Y.M., S.W. Liu, M.K. Lu S.F. Wang, F. Gu, X.Z. Gai, X.P. Cui and J. Pan (2004c). Preparation and photocatalytic properties of Zr^{4+}-doped TiO_2 nanocrystals. Journal of Molecular Catalysis A-Chemical, 215(1–2), 137–142.

Wang, C.Y., R. Pagel, J.K. Dohrmann and D.W. Bahnemann (2006a). Antenna mechanism and deaggregation concept: Novel mechanistic principles for photocatalysis. Comptes Rendus Chimie, 9(5–6), 761–773.

Wang, G., W. Lu, J.H. Li, J. Choi, Y.S. Jeong, S.Y. Choi, J.B. Park, M.K. Ryu and K. Lee (2006b). V-shaped tin oxide nanostructures featuring a broad photocurrent signal: An effective visible-light-driven photocatalyst. Small, 2(12), 1436–1439.

Wang, J.Y., Z.H. Liu, Q. Zheng, Z.K. He and R.X. Cai (2006c). Preparation of photosensitized nanocrystalline TiO_2 hydrosol by nanosized cds at low temperature. Nanotechnology, 17(18), 4561–4566.

Wang, X.H., J.G. Li, H. Kamiyama, Y. Moriyoshi and T. Ishigaki (2006d). Wavelength-sensitive photocatalytic degradation of methyl orange in aqueous suspension over iron(III)-doped TiO_2 nanopowders under UV and visible light irradiation. Journal of Physical Chemistry B, 110(13), 6804–6809.

Warrier, M., M.K.F. Lo, H. Monbouquette and M.A. Garcia-Garibay (2004). Photocatalytic reduction of aromatic azides to amines using CdS and CdSe nanoparticles. Photochemical and Photobiological Sciences, 3(9), 859–863.

Weiss, H., A. Fernandez and H. Kisch (2001). Electronic semiconductor–support interaction – a novel effect in semiconductor photocatalysis. Angewandte Chemie-International Edition, 40(20), 3825–3827.

Weisz, A.D., A.E. Regazzoni and M.A. Blesa (2001). ATR-FTIR study of the stability trends of carboxylate complexes formed on the surface of titanium dioxide particles immersed in water. Solid State Ionics, 143(1), 125–130.

Weisz, A.D., A.E. Regazzoni and M.A. Blesa (2007). Stability of surface complexes formed at the TiO_2/water interface. Croatica Chemica Acta, 80(3–4), 325–332.

Wilke, K. and H.D. Breuer (1999). The influence of transition metal doping on the physical and photocatalytic properties of titania. Journal of Photochemistry and Photobiology A-Chemistry, 121(1), 49–53.

Wong, E.M. and P.C. Searson (1999). ZnO quantum particle thin films fabricated by electrophoretic deposition. Applied Physics Letters, 74(20), 2939–2941.

Wood, A., M. Giersig and P. Mulvaney (2001). Fermi level equilibration in quantum dot-metal nanojunctions. Journal of Physical Chemistry B, 105(37), 8810–8815.

Wu, L., J.C. Yu and X. Fu (2006). Characterization and photocatalytic mechanism of nanosized CdS coupled TiO_2 nanocrystals under visible light irradiation. Journal of Molecular Catalysis AChemical, 244(1–2), 25–32.

Xin, B.F., L.Q. Jing, Z.Y. Ren, B.Q. Wang and H.G. Fu (2005). Effects of simultaneously doped and deposited Ag on the photocatalytic activity and surface states of TiO_2. Journal of Physical Chemistry B, 109(7), 2805–2809.

Xu, N., M. Sun, Y.W. Cao, J.N. Yao and E.G. Wang (2000). Influence of pH on structure and photochromic behavior of nanocrystalline WO_3 films. Applied Surface Science, 157(1–2), 81–84.

Xu A.W., Y. Gao and H.Q. Liu (2002). The preparation, characterization, and their photocatalytic activities of rare-earth-doped TiO_2 nanoparticles. Journal of Catalysis, 207(2), 151–157.

Yamamoto, T., F. Yamashita, I. Tanaka, E. Matsubara and A. Muramatsu (2004). Electronic states of sulfur doped TiO_2 by first principles calculations. Materials Transactions, 45, 1987–1990.

Yamashita, H., M. Harada, J. Misaka, M. Takeuchi, B. Neppolian and M. Anpo (2003). Photocatalytic degradation of organic compounds diluted in water using visible light-responsive metal ion-implanted TiO_2 catalysts: Fe ion-implanted TiO_2. Catalysis Today, 84(3–4), 191–196.

Yang, Y., X.J. Li, J.T. Chen and L.Y. Wang (2004). Effect of doping mode on the photocatalytic activities of Mo/TiO_2. Journal of Photochemistry and Photobiology A-Chemistry, 163(3), 517–522.

Yao, J.N., K. Hashimoto and A. Fujishima (1992). Photochromism induced in an electrolytically pretreated MoO_3 thin-film by visible-light. Nature, 355(6361), 624–626.

Yatmaz, H.C., A. Akyol and M. Bayramoglu (2004). Kinetics of the photocatalytic decolorization of an azo reactive dye in aqueous ZnO suspensions. Industrial and Engineering Chemistry Research, 43(19), 6035–6039.

Yeber, M.C., J. Rodriguez, J. Freer, N. Duran and H.D. Mansilla (2000). Photocatalytic degradation of cellulose bleaching effluent by supported TiO_2 and ZnO. Chemosphere, 41(8), 1193–1197.

Yin, H.B., Y. Wada, T. Kitamura, T. Sakata, H. Mori and S. Yanagida (2001). Enhanced photocatalytic dechlorination of 1,2,3,4-tetrachlorobenzene using nanosized CdS/TiO_2 hybrid photocatalyst under visible light irradiation. Chemistry Letters (4), 334–335.

Yoshihara, T., R. Katoh, A. Furube, Y. Tamaki, M. Murai, K. Hara, S. Murata, H. Arakawa and M. Tachiya (2004). Identification of reactive species in photoexcited nanocrystalline TiO_2 films by wide-wavelength-range (400–2,500 nm) transient absorption spectroscopy. Journal of Physical Chemistry B, 108(12), 3817–3823.

Yu, J.G. and X.J. Zhao (2000). Ag-doped TiO_2 composite thin films prepared by sol–gel and its photocatalytic activity. Rare Metal Materials and Engineering, 29(6), 390–393.

Yu, J.C., J.G. Yu and J.C. Zhao (2002a). Enhanced photocatalytic activity of mesoporous and ordinary TiO_2 thin films by sulfuric acid treatment. Applied Catalysis B-Environmental, 36(1), 31–43.

Yu, J.G., J.C. Yu, B. Cheng and X.J. Zhao (2002b). Photocatalytic activity and characterization of the sol–gel derived Pb-doped TiO_2 thin films. Journal of Sol–Gel Science and Technology, 24(1), 39–48.

Yu, J.G., J.C. Yu, W.K. Ho and Z.T. Jiang (2002c). Effects of calcination temperature on the photocatalytic activity and photo-induced super-hydrophilicity of mesoporous TiO_2 thin films. New Journal of Chemistry, 26(5), 607–613.

Yu, J.C., L. Wu, J. Lin, P. Li and Q. Li (2003). Microemulsion-mediated solvothermal synthesis of nanosized CdS-sensitized TiO_2 crystalline photocatalyst. Chemical Communications, 9(13), 1552–1553.

Yu, J.C., W.K. Ho, J.G. Yu, H. Yip, P.K. Wong and J.C. Zhao (2005a). Efficient visible-light-induced photocatalytic disinfection on sulfur-doped nanocrystalline titania. Environmental Science and Technology, 39(4), 1175–1179.

Yu, J.G., J.F. Xiong, B. Cheng and S.W. Liu (2005b). Fabrication and characterization of Ag-TiO_2 multiphase nanocomposite thin films with enhanced photocatalytic activity. Applied Catalysis B-Environmental, 60(3–4), 211–221.

Yu, J.G., M.H. Zhou, H.G. Yu, Q.J. Zhang and Y. Yu (2005c). Enhanced photoinduced super-hydrophilicity of the sol–gel-derived TiO_2 thin films by Fe-doping. Materials Chemistry and Physics, 95(2–3), 193–196.

Yu, J.G., H.G. Yu, C.H. Ao, S.C. Lee, J.C. Yu and W.K. Ho (2006). Preparation, characterization and photocatalytic activity of in situ Fe-doped TiO_2 thin films. Thin Solid Films, 496(2), 273–280.

Yuan Z.H., J.H. Jia and L.D. Zhang (2002). Influence of Co-doping of Zn(II) plus Fe(III) on the photocatalytic activity of TiO_2 for phenol degradation. Materials Chemistry and Physics, 73(2–3), 323–326.

Zang, L., C. Lange, I. Abraham, S. Storck, W.F. Maier and H. Kisch (1998). Amorphous microporous titania modified with platinum(IV) chloride – a new type of hybrid photocatalyst for visible light detoxification. Journal of Physical Chemistry B, 102(52), 10765–10771.

Zhang, L.Z. and J.C. Yu (2005). A simple approach to reactivate silver-coated titanium dioxide photocatalyst. Catalysis Communications, 6(10), 684–687.

Zhang, M.L., T.C. An, X.H. Hu, C. Wang, G.Y. Sheng and J.M. Fu (2004). Preparation and photocatalytic properties of a nanometer ZnO–SnO_2 coupled oxide. Applied Catalysis A-General, 260(2), 215–222.

Zhang, X.W., M.H. Zhou and L.C. Lei (2006). Co-deposition of photocatalytic Fe doped TiO_2 coatings by MOCVD. Catalysis Communications, 7(7), 427–431.

Zhao, G., H. Kozuka and T. Yoko (1996). Sol–gel preparation and photoelectrochemical properties of TiO_2 films containing Au and Ag metal particles. Thin Solid Films, 277(1–2), 147–154.

Zhao, W., C.C. Chen, X.Z. Li, J.C. Zhao, H. Hidaka and N. Serpone (2002). Photodegradation of sulforhodamine-b dye in platinized titania dispersions under visible light irradiation: Influence of platinum as a functional co-catalyst. Journal of Physical Chemistry B, 106(19), 5022–5028.

Zheng, H.L., M.F. Tang, Y.K. Gong, X.J. Deng and B.H. Wu (2003). Study on preparation of lanthanum-doped TiO_2 nanometer thin film materials and its photocatalytic activity. Spectroscopy and Spectral Analysis, 23(2), 246–248.

Zhou, M.H., J.G. Yu and B. Cheng (2006). Effects of Fe-doping on the photocatalytic activity of mesoporous TiO_2 powders prepared by an ultrasonic method. Journal of Hazardous Materials, 137(3), 1838–1847.

Zhu, J.F., Z.G. Deng, F. Chen, J.L. Zhang, H.J. Chen, M. Anpo, J.Z. Huang and L.Z. Zhang (2006). Hydrothermal doping method for preparation of Cr^{3+} −TiO_2 photocatalysts with concentration gradient distribution of Cr^{3+}. Applied Catalysis B-Environmental, 62(3–4), 329–335.

Chapter 17
Solar Disinfection of Water by TiO_2 Photoassisted Processes: Physicochemical, Biological, and Engineering Aspects

Angela Guiovana Rincón and Cesar Pulgarin

17.1 Introduction

The most common used techniques for water disinfection are chlorination, heating, and ozonation. The negative effect of chlorination is the appearance of trihalomethanes (THMs) as by-products of its reaction with organic matter (Cooper et al. 1993). It also gives drinking water an unpleasant taste (Mercalf 2005). When used for irrigation, chlorine is often phytotoxic. Other methods, e.g., ozonation, are either moderately expensive or involve high consumption of energy that is usually not sustainably produced. In this respect, the use of solar energy as an alternative to chlorination has recently been explored because this technology could be economically viable for communities in regions with a high of sunlight radiation. The bactericidal effect of sunlight has been known for many years (Whitelam and Codd 1985).

Sunlight is able to inactivate microorganisms due to the synergistic effect of the UV and IR parts of sunlight. The main type of UV-B-induced DNA lesions consists in the formation of dimeric pyrimidine photoproducts cause inhibition of DNA replication and also bacterial mutations (Britt 1996).

The practical use of solar disinfection in drinking water was first studied by Acra et al., who filled polyethylene bags with water before exposing them to full sunlight. Recently, a review of solar disinfection used as a water treatment method has been published (Reed 2004).

The disinfecting effect of solar light can be enhanced by addition of a catalyst and the generated system belongs to the group of advanced oxidation processes (AOPs). AOPs could be an attractive alternative for the treatment of contaminated ground, surface, and wastewaters containing hardly biodegradable anthropogenic substances as well as for the purification and disinfection of drinking water (Hoffmann et al. 1995). Although AOPs use different reacting systems, all are characterized by the same chemical feature: production of $^{\cdot}OH$ radical (Hoigne 1997). Photoinduced AOP can be roughly divided into heterogeneous and homogeneous processes.

A.G. Rincón (✉)
California Institute of Technology, Division of Engineering and Applied Science, Pasadena, CA 91125, USA
e-mail: agrincon@caltech.edu

C. Comninellis and G. Chen (eds.), *Electrochemistry for the Environment*,
DOI 10.1007/978-0-387-68318-8_17,

In the case of heterogeneous photocatalytic oxidation via TiO_2, when the TiO_2 semiconductor is suspended in water and irradiated with near UV ($\lambda < 385\,nm$), the absorption of one UV photon generates electron/hole pairs (eCB^-/hvB^+) separated in the conduction band (CB) and the valence band (VB) of the semiconductor, respectively. $^{\cdot}OH$ radicals are generated by the reaction of holes and electrons, respectively with donors and acceptors of electrons [(17.1)–(17.7)]. The $^{\cdot}OH$ radical is highly toxic toward microorganisms and very reactive in the oxidation of organic substances. Therefore, the solar photocatalytic treatment could not only become a disinfecting method but also an efficient way to degrade organic matter. Reduction of the amount of organic matter present in drinking water sources makes chlorinated drinking water harmless for human consumption.

$$TiO_2 + hv \rightarrow TiO_2(e^- + h^+) \tag{17.1}$$

$$TiO_2(h^+) + RX_{ad} \rightarrow TiO_2 + RX_{ad}^{\cdot +} \tag{17.2}$$

$$TiO_2(h^+) + H_2O_{ad} \rightarrow TiO_2 + {}^{\cdot}OH_{ad} + H^+ \tag{17.3}$$

$$TiO_2(h^+) + {}^- OH_{ad} \rightarrow TiO_2 + {}^{\cdot}OH_{ad} \tag{17.4}$$

$$TiO_2(e^-) + O_2 \rightarrow TiO_2 + O_2^{\cdot -} \tag{17.5}$$

$$O_2^{\cdot -} + H^+ \rightarrow HO_2^{\cdot} \tag{17.6}$$

$$O_2^{\cdot -} + HO_2^{\cdot} \rightarrow {}^{\cdot}OH + O_2 + H_2O_2 \tag{17.7}$$

The earliest example of the semiconductor photocatalysis application as a method of disinfection was published by Matsunaga et al. (1985). This work reveals that TiO_2 particles were effective in the inactivation of bacteria, such as *Lactobacillus acidophilus*, *Saccharomyces cerevisiae*, and *Escherichia coli*. To date more than 200 studies are related with this subject and at least three reviews were dedicated to photocatalytic disinfection (Blake et al. 1999; Srinivasan and Somasundaram 2003; Carp et al. 2004). Some general conclusions on TiO_2 disinfection are reported below and the literature will be discussed more specifically throughout the chapter.

Most of the TiO_2 disinfection studies focus on bacteria and cancer cells (Blake et al. 1999), but a few studies also on other microorganisms, such as yeast (Serpone et al. 2006), fungi (Sichel et al. 2007a), and viruses (Sjogren and Sierka 1994) (Belháová et al. 1999). The most currently investigated topic is the photoinactivation kinetics for different bacterial groups under different experimental conditions.

Disinfecting rates or inactivation times are usually not comparable from study to study, due to widely varying operational parameters and reactor configurations. Reactor configurations range from small volume Pyrex beakers and Petri dishes (typically 1–10 cm^3 using illumination from the top by tubular lamp) (Bekbolet 1997; Huang et al. 2000; Sunada et al. 2003) to the design and construction of large volume reactors (0.01–0.1 m^3) (Ireland et al. 1993; Rincón and Pulgarin 2004a; Fernandez et al. 2005).

The different microorganisms sensitivities toward TiO_2 photocatalysis follows the order: virus > bacterial cell gram positive > gram negative > bacterial spores

(Matsunaga et al. 1985; Saito et al. 1992; Sjogren and Sierka 1994; Pham et al. 1995; Bekbolet 1997; Butterfield et al. 1997; Lee et al. 1997; Rincón and Pulgarin 2004b), and it suggests that several microorganisms respond differently to the complexity and thickness of the cell envelope, which comprises the cell and cytoplasmic membrane.

Kinetic investigation of the *E. coli* cells photokilling was shown to involve two steps, an initial lower rate killing step, followed by a higher one (Maness et al. 1999; Rincón and Pulgarin 2003).

Only few studies explored the mechanisms leading to cell death (or inactivation) (Matsunaga et al. 1985; Saito et al. 1992; Ireland et al. 1993; Kikuchi et al. 1997; Sunada et al. 1998; Maness et al. 1999; Huang et al., 2000; Salih 2002; Sunada et al. 2003; Gogniat et al. 2006). These mechanisms have not yet very fully understood and some explanations are contradictory. The first killing mechanism implies an oxidation of the intracellular coenzyme a (CoA), which inhibits the cell respiration and subsequently causes cell death as a result of a direct contact between TiO_2 and the target cell (Matsunaga et al. 1985). The second killing mode suggests that bacterial death is caused by a significant disorder in the cell permeability and by the decomposition of the cell walls (Saito et al. 1992). It is suggested that the cell wall damages might take place prior to cytoplasmic membrane damages (Sunada et al. 1998; Huang et al. 2000). Photocatalytic treatment progressively increases the cell permeability and subsequently allows free efflux of intracellular constituents, which eventually lead to cell death. Up to now, the development of large scale photocatalytic reactors for practical applications of water disinfection has not been investigated enough and further research is necessary in this field.

17.2 Experimental Part

17.2.1 Photoreactors and Light Sources

17.2.1.1 Pyrex Glass Bottle Illuminated by Solar Lamp

A Pyrex glass bottle of 50-mL capacity was used as batch reactor. In these flasks 40 mL of water was the total volume. Solar irradiation was simulated by a Hanau Suntest (AM1) lamp. Total radiation measurements were carried out with an YSI corporation power meter. Experiments were performed at room temperature (25°C) reaching up to 32°C during irradiation.

17.2.1.2 Coaxial Photocatalytic Reactor

A complete description of the pilot system called CAPHORE (Coaxial Photocatalytic Reactor) was presented previously (Rincón and Pulgarin 2005). The illuminated part of the setup is connected with a nonilluminated bioreactor (Biolafitte).

The illuminated part of the system is composed of two glass tubes which contain neon lamps. Two Philips 36-W black actinic lights are employed for irradiation in such a way that their center passes through the reactor axis. The sterile bioreactor was inoculated with bacterial culture in demineralized water; both parts of the system were sterilized before and after each experiment. The bacterial suspension and the suspended TiO_2 circulate in a 4-L closed circuit. A small pump (Little Giant Pump Comp.) ensures circulation of water through the system; the pipe is a PVC-Nylon Solaflex. Temperature and pH measurements, addition of gas (O_2 or N_2) as well as the sampling are done in the bioreactor.

17.2.1.3 Compound Parabolic Reactor CPC

A complete description was presented previously (Rincón and Pulgarin 2004a). Solar ultraviolet radiation is determined by means of a global UV radiometer (KIPP&ZONEN, model CUV3). Solar-UV power varies during experiments, especially when clouds are passing by. Data combination from several days and their comparison with other photocatalytic experiments is done by the application of the following equation.

$$Q_{\mathrm{UV},n} = Q_{\mathrm{UV},n-1} + \Delta t_n \overline{\mathrm{UV}}_{\mathrm{G},n} \frac{A_{\mathrm{CPC}}}{V_{\mathrm{TOT}}},$$

where $\Delta t_n = t_n - t_{n-1}$, t_n is the experimental time for each sample, $\mathrm{UV}_{\mathrm{G},n}$ is the average $\mathrm{UV_G}$ (global UV radiation) during t_n, $A_{\mathrm{CPC}} = 3.08\,\mathrm{m}^2$, $V_{\mathrm{TOT}} = 35\,\mathrm{L}$, and $Q_{\mathrm{UV},n}$ is the accumulated energy incident on the photoreactor for each sample during the experiment per unit of volume ($\mathrm{kJ\,L^{-1}}$). The total solar radiation was measured by means of a radiometer KIPP&ZONEN, model CUV4.

17.2.2 Materials

The photocatalyst was TiO_2 Degussa P-25 (mainly anatase, specific surface area $50\,\mathrm{m^2\,g^{-1}}$). TiO_2 in suspension was used in all photocatalytic experiments. Sodium hydrogen phosphate, sodium bicarbonate, sodium nitrate, sodium sulfate, sodium chloride, potassium sulfate, potassium bicarbonate, potassium hydrogen phosphate, potassium sulfate, potassium nitrate, potassium chloride, and iron chloride were used without further purification and were supplied by Fluka (Buchs, Switzerland).

17.2.3 Bacterial Strain and Growth Media

A complete description was presented previously (Rincón and Pulgarin 2004a, b, 2007a, b). The bacterial strain used was *Escherichia coli* K12 (ATCC 23716) and

was supplied by DSM, German Collection of Microorganisms and Cell Cultures. *E. coli* K12 was inoculated into Luria Bertani (LB) medium and grown overnight at 37°C by constant agitation under aerobic conditions. LB solution was then sterilized by autoclaving for 20 min at 121°C. Aliquots of the overnight culture were inoculated into sterilized LB medium and incubated aerobically at 37°C. At an exponential growth phase, bacterial cells were collected by centrifugation and the bacterial pellet was washed with a tryptone solution. Finally, the bacterial pellet was resuspended in tryptone solution and diluted in different water types to the required cell density corresponding to $10^3 - 10^6$ colony forming units per milliliter ($CFU\,mL^{-1}$). Thereafter, bacterial suspension was exposed to the sunlight irradiation. Samples were taken during illumination period and after 24 h in the subsequent dark period. Samples were plated on agar Plate-Count-Agar (PCA, Merck, Germany) plates. Colonies were counted after 24-h incubation at 37°C.

17.3 Physicochemical Aspects

17.3.1 TiO_2 Concentration

The optimal TiO_2 concentration reported in the literature for photodisinfection studies is ranged from 0.1 to $3\,g\,L^{-1}$ (Blake et al. 1999; Maness et al. 1999; Saito et al. 1992). For each experimental system, an optimum, depending on the reactor geometry can be determined.

In this work, the influence of TiO_2 concentration on *E. coli* inactivation was investigated in the range of $0.0025{-}2\,g\,L^{-1}$ at two different light intensities. In general, the time required for total inactivation increases as TiO_2 concentration decreases. Figure 17.1a (10^7 CFU) shows that the initial inactivation rate (r_0)

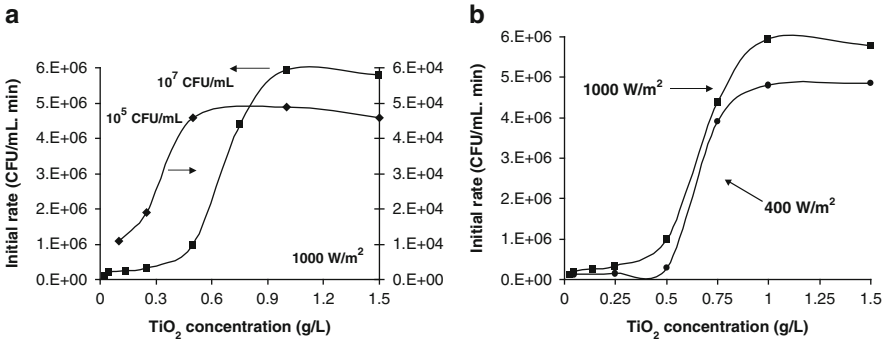

Fig. 17.1 Initial rate of bacterial inactivation as a function of TiO_2 concentration. (**a**) For an initial bacterial concentration of 10^7 (*filled square*) and 10^5 CFU mL^{-1} (*filled diamond*) at 1,000 W m^{-2}. (**b**) For an initial bacterial concentration of 10^7 at 1,000 W m^{-2} (*filled square*) and 400 W m^{-2} (*filled circle*). Solar simulator

determined after 5 min of illumination, increases with the amount of catalyst to a plateau at 1 g L^{-1} corresponding probably to the complete absorption of the incident light by TiO_2. Thus, at TiO_2 concentrations higher than 1 g L^{-1}, the weak light penetration into the bulk of the solution makes the photoactivity of the catalyst less effective and the concomitant action of light on bacteria (direct photolysis) is also diminished. At high TiO_2 concentrations, terminal reactions [(17.8) and (17.9)], could also contribute to the diminution of the bacterial inactivation. In (17.9), $^{\cdot}OH$ will readily dimerize to form H_2O_2 which will produce $HO_2^{\cdot}$. This hydroperoxyl radical is less reactive and does not seem to contribute to the oxidative process (Legrini et al. 1993).

$$^{\cdot}OH + {}^{\cdot}OH \rightarrow H_2O_2 \tag{17.8}$$

$$H_2O_2 + {}^{\cdot}OH \rightarrow H_2O + HO_2^{\cdot} \tag{17.9}$$

The shape of the relation between initial deactivation rate and TiO_2 concentration in the whole range between 0.0025 and 1.5 g L^{-1} of TiO_2 varies in function of initial bacterial concentration and light intensity as shown in Fig. 17.1a, b. The maximal initial inactivation rate appears at TiO_2 concentration around 0.5 g L^{-1} for 10^5 CFU mL^{-1} of initial concentration of bacteria, while values around 1.0 g L^{-1} for 10^7 CFU mL^{-1} were found (Fig. 17.1a). *E. coli* inactivation rate increasing with light intensity was observed (Fig. 17.1b). This implies that saturation of TiO_2 acting as a photosensitizer has not been reached when moving to 1,000 W m^{-2}. Higher light intensity increases the amount of h_{vb}^{+}, $^{\cdot}OH$ radicals, and other oxidative radicals generated at the TiO_2 surface active in the bacterial destruction (Ollis et al. 1991). In addition, for values above 1.0 g L^{-1} of TiO_2 (in Fig. 17.1), the initial rates of bacterial inactivation were negatively affected by the progressive increase of TiO_2. A similar result was observed when *E. coli* inactivation was studied in wastewater taken at the outlet of a biological wastewater treatment plant (Vidy, Lausanne, Switzerland in November of 2000), using the same initial concentration of 10^7 CFU mL^{-1} and at a light intensity of 1,000 W m^{-2} as in Milli-Q water. The optimal concentrations of TiO_2 were around 0.5 and 1.0 g L^{-1} for wastewater and Milli-Q water, respectively. These results suggest that the optimal TiO_2 concentration also depends on the chemical matrix of water (see Sect. 17.3.2).

17.3.2 Presence of Natural Anions

In photocatalytic disinfection in the presence of anions, there are at least three interactions or equilibria (a) anion–bacteria, (b) anion–TiO_2, and (c) TiO_2–bacteria. These interactions are affected by the light (Rincón and Pulgarin 2004c). Photocatalysis damages the cell walls and membranes to a high extent, so that the sudden change of chemical species in their environment achieves the membrane disorganization or even the cell lyses.

A negative effect on the TiO_2 photocatalytic disinfection was found by the addition of HCO_3^-, $H_2PO_4^-$, Cl^-, SO_4^{-2}, and NO_3^- ($0.2\,mmol\,L^{-1}$) to *E. coli* suspension in the presence of TiO_2. HCO_3^- and $HPO_4^{-2}/H_2PO_4^-$ decrease the inactivation rates in a larger extend than NO_3^-, Cl^-, and SO_4^{-2}.

This inhibition could be due to:

1. Anions (A^-) reduce the oxidation rate by scavenging the oxidizing radical species ($^{\bullet}Ox$), such as $^{\cdot}OH$ and $HO_2^{\bullet}$ radicals [(17.10)–(17.12)]. For example, HCO_3^-/CO_3^{-2} reacts with the $^{\cdot}OH$ radical, producing the less reactive anion radical $CO_3^{\cdot -}$ [(17.11) and (17.12)] (Chen et al. 1997). This radical shows a wide range of reactivity with organic molecules but it is mainly a selective electrophilic reagent, and its reactions are slower than those of $^{\cdot}OH$. However, by comparing the sequence of the $^{\cdot}OH$ quenching by different anions to the photocatalytic disinfection rate, no correlation was found. This is illustrated by the fact that SO_4^{-2} has the highest reaction constant with $^{\cdot}OH$ radicals, but does not inhibit the photocatalytic disinfection to the largest extent. Thus, the inhibition of the photocatalytic disinfection is not exclusively due to the scavenging of $^{\cdot}OH$ by anions.

$$^{\cdot}Ox + A^- \rightarrow A^{\cdot} + Ox^- \tag{17.10}$$

$$^{\cdot}OH + HCO_3^- \rightarrow CO_3^{\cdot -} + H_2O \tag{17.11}$$

$$^{\cdot}OH + CO_3^{-2} \rightarrow CO_3^{\cdot -} + OH^- \tag{17.12}$$

2. There is adsorption of anions and organic substances in the active surfaces of TiO_2. This effect has been specially studied for phosphates which are adsorbed in TiO_2 surface and block light penetration. It has been reported (Poulina and Mikhailova 1995) that HPO_4^{-2} has a higher inhibiting capacity of TiO_2 than HCO_3^- during the photocatalytic degradation of organic compounds. These authors postulated that adsorption of phosphate takes place as a ligand attached to a surface Ti^{4+} ion by an exchange reaction between the surface hydroxyl groups of TiO_2 and $H_2PO_4^-$. This bonding is stronger than that of Cl^-. Such mechanism can also be postulated for the adsorption of SO_4^{-2} in the TiO_2 surface, while NO_3^- and HCO_3^- appear to be an intermediate case. Furthermore, $H_2PO_4^-$ reacts with $^{\cdot}OH$ to form $H_2PO_4^{\cdot}$ which is not as reactive as $^{\cdot}OH$.
3. Anions compete for the photogenerated holes. For example, HCO_3^- probably acts as scavengers of h^+ formed on the TiO_2 surface (17.13) reducing the inactivation rate (Abdullah et al. 1990). HCO_3^- partially inhibits the photocatalytic reactions by generation of a negatively charged layer on the TiO_2 surface; therefore the TiO_2 surface charge becomes less positive, leading to the decrease in the adsorption of bacteria.

$$h^+ + HCO_3^- \rightarrow HCO_3^{-\cdot} \tag{17.13}$$

The adsorption of ions on TiO_2 is influenced by the competitive anion uptake by bacteria. In the system in the presence of light, anions TiO_2, and without bacteria,

SO_4^{-2} was less adsorbed in TiO_2 than NO_3^- and Cl^-. Nevertheless, SO_4^{-2} inhibits *E. coli* inactivation to a higher extent than Cl^- and NO_3^-. This suggests that other mechanisms about anion adsorption on TiO_2 are involved in the inhibition of the photocatalytic disinfection by certain anions.

Using optical microscopy and flow cytometry, it was shown (Gogniat et al. 2006) that adsorption of *E. coli* cells depends on the composition of the solution. Authors confirmed by flow cytometry that the membrane integrity was very rapidly and drastically affected by photocatalytic treatment, and this fact was directly correlated with loss of culturability. Whereas, all cells were adsorbed before illumination in (NaCl/KCl solution), only 5% of cells adhered to TiO_2 particles in phosphate buffer solution (PBS). On starting illumination, bacterial adsorption on TiO_2 in PBS increased with increasing illumination time (Gogniat et al. 2006). Moreover, there is a correlation between the loss of culturability and the enhancement of the bacterial adsorption in TiO_2. Accordingly, aggregation of bacteria and TiO_2, as well as the adsorption between bacteria and TiO_2 aggregates change as a function of ionic strength of solution and is probably affected in a different way by the presence or absence of light. Thus cell adsorption to TiO_2 and consequently the *E. coli* inactivation rate is modified (generally increased) during the illumination.

The inhibition sequence of *E. coli* photocatalytic inactivation as a function of the type of anion has followed a similar shape of that reported by other authors (Chen et al. 1997) for the photocatalytic degradation of organic substances, namely higher inhibition of $H_2PO_4^-/HPO_4^{-2}$, HCO_3^- and SO_4^{-2}. However, by modifying the pH, the inhibiting effect of inorganic salts could be modified (Hu et al. 2003; Epling and Lin 2002). Thus in a solution containing inorganic substances and bacteria, pH which modifies the chemical properties of inorganic ions can meaningfully affect the photocatalytic disinfection process. But the ions toxicity which depends on its concentration can also represent a supplementary stress for the bacteria affecting both their metabolism and the osmotic strength of solutions. The turbidity and optic absorption very often generated in the presence of anions, influences also the light penetration and consequently diminishes its effect on both bacteria and TiO_2.

On the other hand, the photoelectrocatalytic disinfection of *E. coli* suspensions by TiO_2 in a sparged photoelectrochemical reactor has been reported (Christensen et al. 2003). They found that phosphate addition poisons both the electrode and particulate-slurry systems in a partially reversible way. While, bicarbonate detrimental effect was irreversible after washing the electrodes with cold water. It was also demonstrated (Koizumi and Taya 2002) that the photocatalytic inactivation of phage MS2 with TiO_2 was inhibited when NO_3^-, SO_4^{-2}, and $HPO_4^{-2}/H_2PO_4^-$, K^+, or Ca^{+2} were present in the reaction mixture. The inhibitory effects were explained from the direct proportionality between the inactivation rate constants and the quantities of the phage adsorbed in the TiO_2 surface.

When water contains a mixture on the same natural anions, a retard effect on photocatalytic disinfection was observed. As expected, the time required for complete bacterial inactivation change as a function of the concentration of anion in the mixture (Rincón and Pulgarin 2007b). However, *E. coli* inactivation rate is accelerated in some experiments carried out using natural waters, filtered and spiked with

E. coli, when compared to that of bacteria suspended in MQW. This type of water probably contains, in addition of natural anions, chemical photosensitizers (organic or inorganic) which increase the detrimental action of light on bacteria.

Organic substances are also present in natural waters. The composition and the concentration of organics such as humic compounds are different in surface waters, groundwater, and wastewater. Consequently, absorptivity of light by these studied waters may then be affected by the nature of these UV absorbing chromophores as well as by the intermediates generated during the photocatalytic reaction. Organic compounds present in these waters can either positively affect the photocatalytic disinfection by the enhancement of ROS production (Whitelam and Codd 1985) or negatively by competing with bacteria for the photogenerated oxidative species (Rincón et al. 2001). Thus, photocatalytic disinfection experiments carried out using ultra-pure waters do not perfectly simulate the actual situation in natural waters.

The response of bacteria to the photocatalytic inactivation results from a combination of antagonistic and synergistic effects of different water components. Then, the response of bacteria generated by an individual substance could be very different from that observed if the same substance is accompanied by other chemicals. Photolytic treatment was also affected by chemical composition of water. The significant difference observed between both treatments indicates the specific action mode of each system (Rincón and Pulgarin 2007b). However, the extent of this observed difference depends on the type of water. Thus, for practical applications each type of water has to be considered as a specific case.

In addition, bacteria recovery is dependent on the chemical composition of water.

17.3.3 Presence of Iron

No difference was observed in the photocatalytic bacterial inactivation with $0.5\,g\,L^{-1}$ of TiO_2 in the absence or presence of $0.3\,mg\,L^{-1}\,Fe^{+3}$ (Fig. 17.2). In these conditions, the TiO_2 screens the light absorbance of Fe^{+3} and protects bacteria against the inactivation action of the UV–Vis/Fe^{+3} system (Rincón and Pulgarin 2006). This is confirmed with lower TiO_2 concentrations, the beneficial effect of Fe^{+3} addition on the photocatalytic *E. coli* inactivation was observed. The beneficial effect of Fe^{+3} ions on water disinfection for TiO_2 concentrations lower than $0.5\,g\,L^{-1}$ is attributed to electron trapping at the semiconductor surface. Fe^{+3} behaves as an electron scavenger, thus preventing the recombination of electron–hole pairs (17.14). This reaction is thermodynamically favorable with regard to the oxide-reductive potential of Fe(III)/Fe(II) (E versus NHE $= +0.77$ V) and that of the conduction band of TiO_2 (-0.1 to 0.2 V).

The trapping of photoelectrons (17.14) leaves photogenerated holes available for reaction with hydroxyl ions to form hydroxyl radicals. Decreased activity above the optimum metal ions concentration is possibly due to the oxidation of Fe^{2+} by hydroxyl radicals or holes. The competition of holes between Fe^{+2} and OH− means that less $OH^{\cdot}$ radicals would be generated for the bacteria inactivation. The reactivity

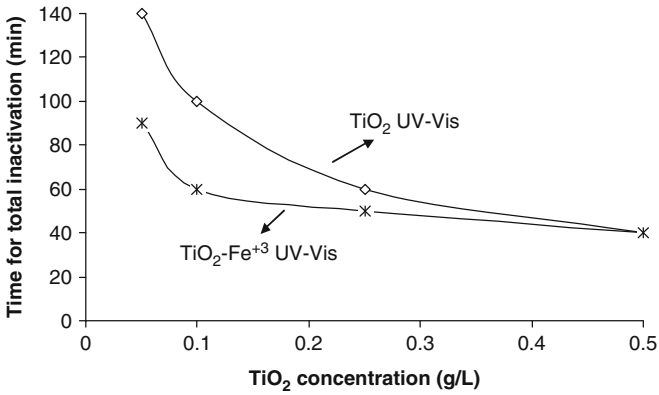

Fig. 17.2 Time for total inactivation versus TiO_2 concentration for the systems UV–Vis/TiO_2/Fe^{+3} and UV–Vis/TiO_2. TiO_2 at 0.05, 0.1, 0.25, and 0.5 g L^{-1}; Fe^{+3} at 0.3 mg L^{-1}. 1,000 W m^{-2} of light intensity in solar simulator. *E. coli* was suspended in deionized water

of the iron aquocomplexes with e- photogenerated at the conduction band of TiO_2 could be positive or negative as a function of the iron species present in the medium (Mest'ankova et al. 2004).

$$Fe^{3+} + e^- \rightarrow Fe^{2+} \tag{17.14}$$

The presence of Fe^{+3}/Fe^{+2} in TiO_2 suspension strongly influences the reaction of hydrogen peroxide generation and surface peroxidic groups (Brezova et al. 1995). In the combined system $Fe/TiO_2/h\nu$, the re-oxidation reactions of Fe(II) to Fe(III) on the TiO_2 surface is due to oxidants species such as $HO^{\cdot}$, $O_2^{\cdot -}$, $HO_2^{\cdot}$, and H_2O_2. The reaction of Fe^{+2} with H_2O_2 photogenerated by the system TiO_2/UV–Vis (17.15) represents a supplementary source of $HO^{\cdot}$ radicals resulting in the increase of the bacterial inactivation rate in the irradiated systems. With the addition of TiO_2 in the solution of Fe(III), the Fenton reaction increases the re-oxidation rate of Fe(II) and consequently favors the photocatalytic cycle Fe(III) ↔ Fe(II), which seems to be the limiting process in the degradation of pollutants by iron complexes (Mest'ankova et al. 2004).

H_2O_2 produced during the TiO_2-mediated photocatalysis may diffuse across the cell membrane and produce intracellular $^{\cdot}OH$ radicals according to the known Fenton mechanism (17.15).

$$M^{(n-1)+} + H_2O_2 + H^+ \rightarrow M^{n+} + {}^{\cdot}OH + H_2O \tag{17.15}$$

As mentioned above, Fig. 17.2 showed that no additional effect of Fe^{+3} was observed at 0.5 g L^{-1} of TiO_2 concentration. Moreover, for 1 g L^{-1} of TiO_2 concentration total disinfection (<1 CFU mL^{-1}) in the absence or presence of Fe^{+3} is within the same time span (not shown here). These results may be due to the following reasons. (1) In the range of TiO_2 concentration between 0.5 and 1 g L^{-1} the efficiency of the photocatalytic disinfection is higher than low TiO_2 concentrations

(Sect. 17.3.1). Consequently, low quantity of Fe^{+3} added is not enough to trap electrons and increases $^{\cdot}OH$ production. (2) The size of TiO_2 and TiO_2–bacteria aggregates changes upon the increase of TiO_2 concentration and the presence of Fe^{+3}. The charge interaction between *E. coli* (negatively charged) and TiO_2 (slightly positively charged) is affected. This affects the TiO_2–bacteria adsorption, which is necessary for the bactericidal effect of TiO_2 photocatalysis. But the main parameter affecting the TiO_2 aggregation state is the pH. Then, the pH (6.5–5) changes during TiO_2 photocatalysis affect both the size of TiO_2 aggregates and the species of iron aqua complexes presented in the solution. (3) Bacteria are also very sensitive to the chemical changes produced during the solar irradiation (Rincón and Pulgarin 2004c).

Some years ago, the near-UV photocatalytic disinfection of Phage MS2 in aqueous TiO_2 suspension was reported (Sjogren and Sierka 1994). A level of inactivation of phage MS2 of 90% increased to 99.9% after 2 μM ferrous sulfate was added. Hydroxyl radical oxidation, with Fenton reaction enhancement, is suspected to be primarily responsible for the viral degradation. In other study, MS2 bacteriophage and *B. fragilis* phage were exposed to TiO_2 photocatalytic inactivation with addition of $FeSO_4$ (4 μM) and an increase in the inactivation efficiency was also observed (Armon et al. 1998).

17.3.4 pH Influence

Photocatalytic *E. coli* inactivation (TiO_2 P25) in Milli-Q water was not affected by modifications of initial pH between 4.0 and 9.0 (Rincón and Pulgarin 2004c). However, modification of the pH during the illumination by successive acid addition (without TiO_2) resulted in a greater diminution of bacteria compared with the no acidified system. That suggests that photocatalytic disinfection results from the accumulative and possible synergistic effect of three factors: pH modification, direct action of light, and attack of photogenerated oxidative species.

E. coli presented in a TiO_2 suspension were inactivated after 2 h of irradiation by a sunlight lamp with a concomitant decrease of pH from 7.0 to 4.0; or 8.5 to 5.9; or 6.0 to 5.2 respectively. As the reaction time progresses, and the suspension pH moves to more acidic pH values, the TiO_2 surface becomes positively charged, thus favoring the TiO_2 electrostatic attraction with *E. coli*. Chemisorbed water on the TiO_2 surface allows the valence band hole transfer induced by light irradiation through the reaction (17.16) (Bahnemann et al. 1994; Dhananjeyan et al. 2001).

$$h_{vb}^{+} + H_2O \rightarrow H^{+} + {}^{\cdot}OH \tag{17.16}$$

On strictly electrostatic basis, the *E. coli* abatement should be much less favored at pH 8.5 than at pH values of 4.5 and 6.0, since *E. coli* is negatively charged between pH 3 and pH 9, and TiO_2 Degussa P-25 surface becomes more positively charged up to pH 7.0, because the isoelectric point (IEP) is 6.5. However, this was

not the case; the kinetic of the inactivation was the same for the different initial pH. Thus, electrostatic attraction between the *E. coli* and TiO_2 Degussa P-25 is not a determining factor in the kinetics of *E. coli* photoinactivation.

Contrary to that, *E. coli* survival kinetic for a positively charged Millenium 5S-300A, with an IEP of 7 follows what is expected from repulsion or the attraction between the TiO_2 and *E. coli*. The same behavior was observed for Tayca TKS201 (IEP of 7) and Tayca TKS 203 with IEP <3. Surface and crystallographic parameters are similar for Tayka TKS 201 and Tayka TKS 203 with exception of the IEP (Gumy et al. 2006a). Then, negatively charged TiO_2 was not efficient in activating *E. coli* because of the electrostatic repulsions with the negative outer membrane.

In addition, a change in the initial pH of solution containing chemical substances and bacteria would change not only the equilibrium (i.e., amphoteric) of certain anions but also the ionic strength, and modify the dynamic interactions between TiO_2 and bacteria and consequently the response of bacteria to the light irradiation.

17.3.5 Physicochemical Characteristics of Suspended TiO_2

Thirteen different TiO_2 samples suitable for water disinfection were systematically characterized, according to their physicochemical properties (Gumy et al. 2006a). Except for two mixed catalysis anatase-rutile from Degussa, P25, and P25 TN90, all photocatalysis were pure anatase crystalline. The particle sizes of the TiO_2 samples varied from about 5 to 700 nm, and was inversely correlated with the BET specific surface area (ranged from 9 to 335 $m^2\ g^{-1}$). Surface properties of the colloidal suspensions measured by electroacoustic methods were evaluated at different pH values. The aggregate size appeared to be dependent on the pH value of the solution. The IEP of the TiO_2 samples ranged from very acidic (IEP, 3) to neutral values.

Interestingly, BET specific surface area, particle, and aggregate size seemed not to be correlated with *E. coli* inactivation. However, surface charges appeared to be crucial for the TiO_2 and bacteria interaction. Indeed, negatively charged TiO_2, i.e., TiO_2 with acidic IEP, were not efficient in *E. coli* inactivation probably due to the electrostatic repulsions with the negatively charged outer membrane of the *E. coli* (Gumy et al. 2006). This phenomenon was observed while investigating the photocatalysis experiment at different pH values (Sect. 17.3.4). These results suggest that the preparation method, superficial charge, the size of the aggregates, and the crystallographic structure of TiO_2, together, play an important role during the interfacial transference of charge between TiO_2 and *E. coli*. The optimization and interrelation of these parameters could allow an increase in bacterial inactivation.

17.3.6 Supported TiO_2

Several microorganisms have been reported to be inactivated by fixed TiO_2, and those include *E. coli* (Ireland et al. 1993; Jacoby et al. 1998; Kikuchi et al. 1997;

Kuhn et al. 2003; Matsunaga et al. 1988; Salih 2002; Sunada et al. 1998, 2003), *Vibrio alginolyticus* (Nakayama et al. 1998), *Pseudomonas aeruginosa* (Amezaga-Madrid et al. 2002; Lonnenn et al. 2005), *Lactobacillus acidophilus*, *Saccharomyces cerevisiae* (Matsunaga et al. 1985), *Bacillus subtilis*, *Micrococcus luteus* (Wolfrum et al. 2002), *Lactobacillus casei*, and Phage PL-1 (Kashige et al. 2001). However, most of these studies describe small batch systems (few mL) where the TiO_2 catalyst is fixed as a thin film on glass support. More specifically, they tend to focus on assessing the biocidal effect of the TiO_2 once fixed, and to determine the exact mechanisms leading to the bacteria outer membranes' alteration rather than developing a potential applicability for large-scale water treatment. Nonetheless, continuously recirculated flow reactors have also been studied (Ireland et al. 1993; Wolfrum et al. 2002), and showed a relative efficiency but were rarely compared to suspended TiO_2 or direct sunlight effect. Indeed, when suspended vs. fixed TiO_2 were compared for the purpose of bacterial inactivation, the later always appeared to be less efficient (Rincón and Pulgarin 2003; Salih 2002).

Fixed TiO_2 efficiency, however, could be improved while applying a potential in electrophotochemical assays and reached even better results than suspended TiO_2 (Butterfield et al. 1997; Christensen et al. 2003, 2005; Dunlop et al. 2002). For practical disinfection applications of fixed TiO_2, two types of reactors have been investigated. The first one, a batch system without water recirculation, based on the SODIS technology (Duffy et al. 2004; Lonnenn et al. 2005), consisted of PET bottles with the catalyst being coated on the bottle wall or on intern solid supports. The second were large-scale continuously recirculated reactors with intern pieces supporting the catalyst (Fernandez et al. 2005).

17.3.6.1 TiO_2 Fixed in Nafion Membranes

Immobilization of catalyst: TiO_2-P25 fixed on Nafion membranes inactivate *E. coli* with efficiencies close to that observed for bacterial suspensions containing the same concentration of suspended TiO_2 (25 mg in 40 mL) (Rincón and Pulgarin 2003). The low TiO_2 concentration used in both fixed and suspended form explains the little beneficial effect of the photocatalytic process on deactivation compared with direct photolysis. Fixation of TiO_2 concentration higher than 25 mg L^{-1} would result in a diminution of light penetration, limiting also the efficiency of the process. Hence a compromise between these two parameters has to be found. In terms of applicability of this system, other supports cheaper than Nafion should be explored.

17.3.6.2 TiO_2 Fixed on Glass

TiO_2 immobilized (Gel deposition technique) on Pyrex glass was tested for *E. coli* inactivation. Figure 17.3 shows that the required total time to inactivate bacteria, using immobilized TiO_2 on glass was higher than that observed with suspended TiO_2 at the same concentrations (40, 20, and 10 mg of TiO_2 P-25 in 40 mL of

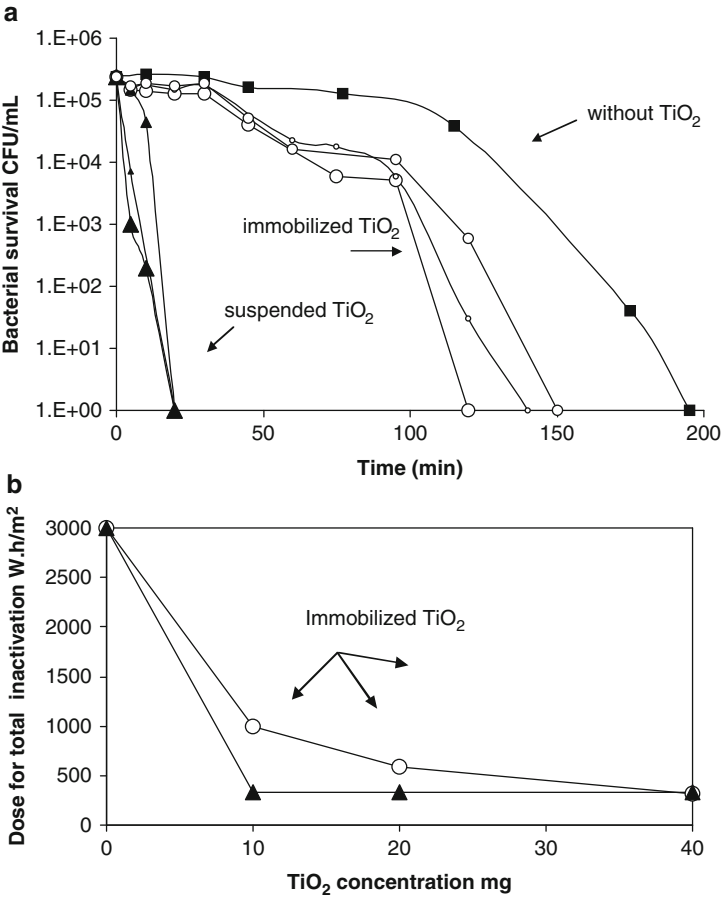

Fig. 17.3 (**a**) Bacterial inactivation by light, in the presence of TiO_2 P-25 fixed in glass, for an initial concentration of 10^5 CFU mL^{-1} and 10 (*open circle*), 20 (*open circle*), and 40 mg (*open circle*) of TiO_2. System without TiO_2 addition (*filled square*), 10 (*filled triangle*), 20 (*filled triangle*), and 40 mg (*filled triangle*) of TiO_2 suspended TiO_2. (**b**) Dose required for reach total *E. coli* inactivation of suspended (*filled triangle*) and fixed TiO_2 (*open circle*). Simulated sunlight

water). The order in the deactivation efficiency using immobilized TiO_2 was, 10 mg >20 mg >40 mg, which is in accordance with the decrease of the wall thinness formed by TiO_2 deposit and consequently the portion of light reaching the bulk of the bacterial suspension. The dose (Intensity × illumination time) necessary for total inactivation as a function of catalyst concentration is shown in Fig. 17.3b. The dose for total inactivation of *E. coli* using TiO_2 in suspension was independent on catalyst concentration in the tested range, suggesting that in this type of reactor, even at 10 mg L^{-1} of suspended TiO_2, the $^{\cdot}OH$ generation is not a limiting factor. For fixed TiO_2, the dose necessary for the total inactivation decreases by increasing the fixed TiO_2 concentration. All concentrations of suspended TiO_2 revealed the

same behavior than 40 mg of immobilized TiO_2 meaning that the optimal fixed TiO_2 concentration, in this type of photoreactor, was found between 20 and 40 mg (against less than 10 mg if suspended TiO_2) in contact with 40 mL of stirred water.

Some factors influencing the photocatalytic activity of immobilized TiO_2 are (1) diminution of specific surface of catalyst accessible to light and bacteria; (2) the TiO_2 support could enhance the recombination of photogenerated electron/hole pairs; (3) the pathway followed by the light to reach TiO_2 layers which are in contact with bacterial suspension increases in this case with the concentration of fixed TiO_2, because the light source is outside the reacting system; (4) limitation of oxygen diffusion in the deeper layers of TiO_2; (5) immobilized catalyst is less exposed than the suspended one to chiral and friction forces which would avoid its deactivation; (6) the mean distance between bacteria and immobilized TiO_2 increases and causes a diminution of the probability of attack by $^{\cdot}OH$ as compared with suspended TiO_2; (7) due to catalyst fixation there is no penetration of the little TiO_2 beads (30–50 nm) into bacteria ($\sim 1\mu m$) to cause intracellular damage; (8) the reactor geometry determines the light distribution and its availability for fixed TiO_2 excitation.

17.3.6.3 TiO_2 Coated on Fibrous Web

TiO_2 photoactivity on bacteria inactivation was performed with the catalyst supports (web support NW10 and KN47) and two types of catalyst P25 and PC500 from Ahlstrom. The experiments were carried out using fixed and suspended TiO_2 and blank light. The fibrous web was coated first with SiO_2 binder, then with 12 g m^{-3} of P25 TiO_2 and only with SiO_2 binder without TiO_2.

It was found that neither the type of web supports nor the nature of the TiO_2 seemed to influence the bacteria inactivation kinetics (Gumy 2006). No enhancement was observed with fixed catalysis compared with light only (Fig. 17.4), for the

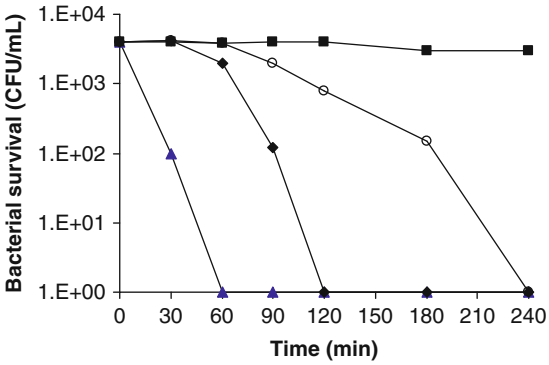

Fig. 17.4 *E. coli* survival with TiO_2 P25 fixed on NW10 (*filled diamond*), without TiO_2 (*open circle*) as a function of time. Suspended TiO_2 (*filled triangle*). Dark control with fixed TiO_2 0.2 g L^{-1} (*filled square*). Caphore system

tested concentrations during the first hour of treatment. Indeed, the photocatalytic effect of fixed TiO_2 starts after 1 h of illumination. A total bacterial inactivation was reached after 2 h while it was reached after 1 h using suspend TiO_2. In the dark, during 3 h, inactivation or bacterial adsorption on fibrous web did not occur (trace "filled square").

The less-efficient activities of TiO_2 coated on NW10 web can be partially attributed to the presence of the silica-binder used for TiO_2 fixation. Indeed, at pH = 7, the surface of TiO_2 is neutral, but the surface of SiO_2 is negatively charged, once coated with TiO_2 (IEP of SiO_2 = 2). Therefore, the negatively charged surface decreases the adsorption of negatively charged bacteria by electrostatic repulsion, thus decreasing the photocatalytic activity (Gumy et al. 2006b). A similar behavior had already been observed during degradation experiments of anionic organic compounds with the same supported TiO_2 (Guillard et al. 2003a, b; Pizarro et al. 2005). Moreover, previous studies also showed that positively charged TiO_2 supports strongly favored bacteria inactivation (Butterfield et al. 1997; Christensen et al. 2003). Hence, as there is no adsorption of bacteria on the fixed TiO_2 and that reactions occur certainly mainly at, or close to, the surface of TiO_2 (and not in the solution), the average distance between bacteria and catalyst appears here to be an important limiting factor for the photocatalytic inactivation of bacteria. The average distance between bacteria and immobilized TiO_2 increases, compared to suspended TiO_2, and the probability of an attack by oxidative species $^{\cdot}OH$ radical decreases as compared with suspended TiO_2.

17.3.7 Oxygen Concentration

As mentioned above, dissolved oxygen molecules accept electrons from the conduction band of TiO_2 and are transformed into superoxide anion radicals, which react with H_2O and generate other oxidative species such as $^{\cdot}OH$ or H_2O_2 [(17.1)–(17.6)].

The effectiveness of the CAPHORE was tested using water contaminated with a mixed *E. coli* and *Bacillus* sp. population. *E. coli* was found to be more sensitive to photocatalytic treatment than *Bacillus* sp. Bacterial inactivation was dependent on the oxygen concentration and the chemical composition of water. It was observed that the presence of oxygen clearly enhanced the inactivation process of the mixed culture. A sharp drop in dissolved oxygen was observed during photocatalytic disinfection in the presence of a mixture of organic and inorganic matter. In this situation, photogenerated ROS simultaneously attack the bacteria and the organic compounds, leading to heavy consumption of O_2, which is involved in the photocatalytic production of ROS. The effect of oxygen on bacterial photocatalytic inactivation is crucial in water containing a large amount of organic matter. For practical reasons, good oxygenation of this kind of water seems to be essential to prevent the inhibition of bacterial inactivation.

Other authors have discussed the role of DO in water on bacterial inactivation by photocatalysis. Wei et al. reported that bactericidal activity increased with the concentration of DO; they used suspended TiO_2 and solar irradiation. The composition

of the gas flowing in the solutions exerted a dramatic effect on the bacterial activity of irradiated TiO_2 when switched from 100% O_2 to 100% N_2 (Wei et al. 1994). Reed and coworkers reported that even in the absence of TiO_2, solar disinfection depends on the DO concentration (Reed 2004; Reed et al. 2000).

17.4 Biological Aspects

17.4.1 Initial Bacterial Concentration

The initial bacteria population is an important parameter, during the evaluation of the photocatalytic water disinfection efficiency. Examples of photocatalytic inactivation starting at four different initial *E. coli* concentrations confirmed the fact that longer time is required for bacterial inactivation when the initial concentration of bacteria is higher (not shown here). This behavior corresponds to a first-order kinetic (Huang et al. 1998; Rincón and Pulgarin 2004a, b; Wei et al. 1994). However, the total deactivation rate calculated for the whole photocatalytic treatment duration and expressed in CFU min^{-1} mL^{-1} is 10^4 times higher for an initial concentration of 10^7 CFU mL^{-1} than for an initial one of 10^2 CFU mL^{-1}.

17.4.2 Physiological State of Bacteria

Experiments in which bacteria were illuminated at two different growth states, stationary and exponential phase and two different generations were performed (Fig. 17.5). Bacteria collected from the culture at their stationary phase were less readily inactivated in the presence and absence of TiO_2 than those taken at exponential growth phase. This difference is highlighted when TiO_2 is not added.

To our knowledge, no systematic study of the impact of TiO_2 photocatalytic inactivation of different types of bacteria at different physiological states has been performed. However, the influences of the growth state of bacteria on UV disinfection have been documented (Kadavy et al. 2000; Morton and Haynes 1969; Lewis and Burt Maxcy 1984). There are a number of studies reporting stationary phase bacteria that are more resistant to irradiation than exponential phase cells. The stationary-phase response to environmental changes involves the synthesis of a set of proteins which confer on *E. coli* cells a marked resistance to several stress conditions, including heat shock, oxidation (UV light), hyperosmolarity, acidity, and nutrient scarcity (Child et al. 2002; Murno et al. 1995). We can assume that similar events occur under photocatalytic treatment and the resistance of microorganisms to these conditions is not only dependent on the type of bacteria but also on their growth state. Nevertheless, in the present study (Fig. 17.6), bacterial recovery after total photocatalytic inactivation was not observed after 24 h in the dark with a culture taken either in exponential or in stationary phase.

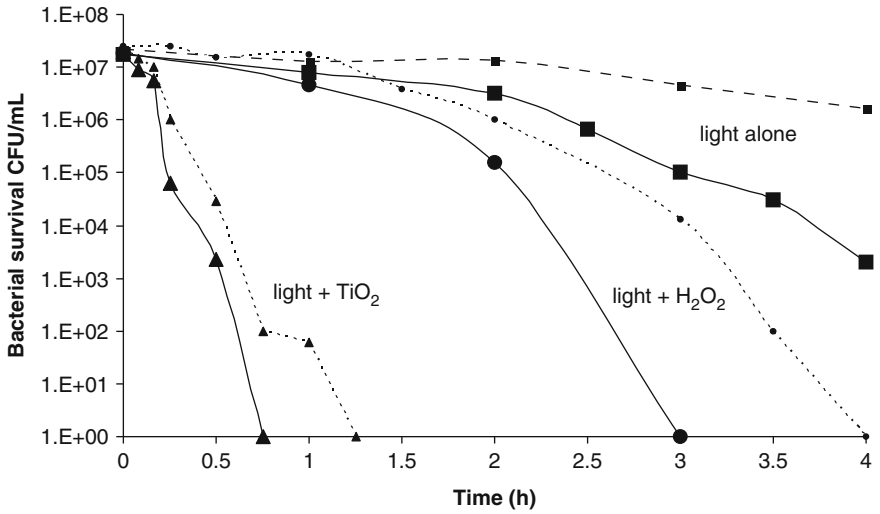

Fig. 17.5 Influence of the generation of *E.coli* K_{12} on light inactivation of bacteria for the systems with (*filled triangle*) and without (*filled square*) TiO_2 addition. System with H_2O_2 addition (*filled circle*). Third generation (*dashed line*), seven generation (*continuous line*). TiO_2 ($1\,g\,L^{-1}$), H_2O_2 ($10\,mg\,L^{-1}$). Sun Simulated lamp

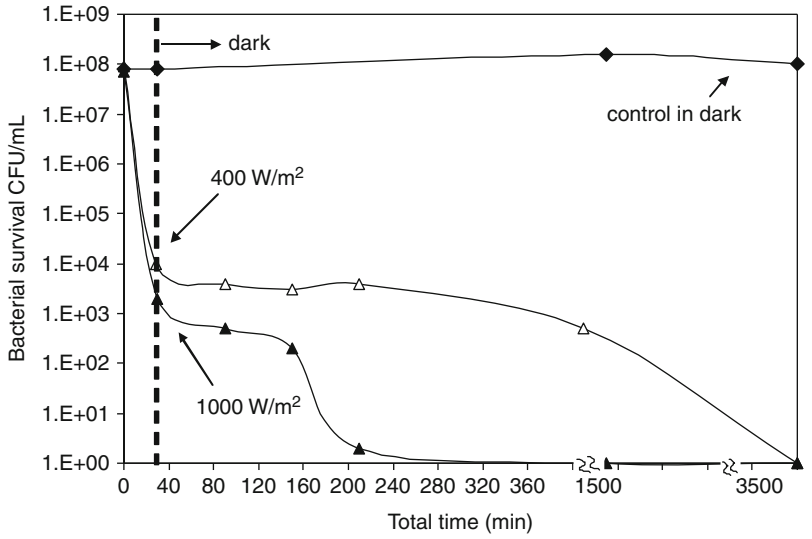

Fig. 17.6 Continuous irradiation of *E. coli* during 30 min in solar simulator, at 400 and $1{,}000\,W\,m^{-2}$. Durability of disinfection in the dark (24 and 60 h). $V_{TOT} = 40\,mL$, $TiO_2 = 0.5\,g\,L^{-1}$, deionized water. *Black dotted line* signifies commencement of dark incubation

The influence of the generation of *E. coli* is illustrated in Fig. 17.5. Bacteria harvested at the third generation of culture were less sensitive to irradiation than those taken from the seventh one. This effect of bacteria generation was observed in three

illuminated systems (1) light alone, (2) light plus H_2O_2, and (3) light plus TiO_2. According to our study, these mutations make bacteria more sensitive to photocatalytic attack (Rincón and Pulgarin 2004b).

17.5 Technological Aspects

In this section, the behavior of an *E. coli* suspension during the subsequent dark period is discussed in order to estimate the potential of using the solar (photocatalytic) treatment process in real water disinfection situations. Photocatalytic disinfection at field scale is illustrated using water from the Leman Lake (LLW). Other aspects when using a pilot reactor such as dose, circulation rate and catalyst concentrations are discussed.

17.5.1 Durability of Disinfection and Postirradiation Events

The main advantage of using chlorine for drinking water disinfection is that the presence of a residual amount of oxidant assures bacterial inhibition during water transport and storage. During the photolytic and photocatalytic processes, generated oxidant species have a far shorter half-life time than chlorine. Thus, when phototreatment is applied, it is important not only to determine the time required to reach complete disinfection of water but also to verify the durability of the photodisinfection. For these reasons, at the end of the illumination of *E. coli* within photolytic and photocatalytic conditions, the bacterial suspensions were examined under permanent agitation during a subsequent dark period of 60 h.

Some experiments were carried out using a solar lamp in controlled conditions of the laboratory. After reaching a complete photocatalytic bacterial inactivation of the *E. coli* suspended in the water, no bacterial regrowth was observed after 8, 24 48, and 60 h of dark incubation at 37°C. By contrast, in the absence of TiO_2, bacterial regrowth was observed. In another experiment, water was irradiated for 30 min a time when some bacteria are still cultivable; thereafter, the bacterial suspensions were examined under permanent agitation during a subsequent dark period of 60 h (Fig. 17.6). As expected, photocatalytic inactivation was accelerated by the increase in light intensity. After irradiation at 400 W m^{-2} (trace "open triangle"), culturable bacteria gradually reached 1 CFU mL^{-1} after 60 h in the dark. When the process was conducted at 1,000 W m^{-2} (trace "filled triangle"), the inactivation of bacteria was continuous also in the dark as it was observed in the former experiments carried out at 400 W m^{-2}. But at 1,000 W m^{-2} the post irradiation events were drastically accelerated. For instance, *E. coli* treated at 1,000 W m^{-2} for 10 min (dose: 167 Wh m^{-2}) reached a value of <1 CFU mL^{-1} after around 3 h in the dark. In contrast to that, if a light intensity of 400 W m^{-2} was applied for 30 min (dose: 200 Wh m^{-2}), the total disinfection was attained only after 60 h. This fact suggests that, in our experimental

conditions, the "residual disinfecting effect" of the photocatalytic process observed during the subsequent dark period is dependent on the light intensity, but not on the dose. To assure no bacterial regrowth before water consumption, the effective disinfection time (EDT) required for total killing of bacteria has to be determined during the evaluation of the solar disinfection process. In the illuminated system without catalyst, the EDT was not reached (no shown here). Thus, if all bacteria were not killed, the recovery of the damaged bacteria and/or the cellular reproduction of the not affected cells could occur in the dark.

17.5.2 Water Disinfection by Sunlight Using a CPC Photoreactor

A CPC photoreactor (Sect. 17.2.2) represents an approximation to the real-field application of solar technology for water decontamination. Thirty-five liters of natural water was used to suspend *E. coli* in the absence or presence of TiO_2. In the absence of TiO_2 (Fig. 17.7a), active *E. coli* concentration decreases as the accumulated energy increases to 15.5 kJ L^{-1} with an asymptotic tendency between 12 and 15.5 kJ L^{-1}. Bacterial concentrations below the detection limit (1 CFU mL^{-1}) are not reached during illumination probably because: (1) some bacteria recover their culturability; (2) the decrease of UV intensity and modification of the visible spectral composition during the experimentation time; and (3) replication of the remaining culturable cells (Rincón and Pulgarin 2007a, b).

Figure 17.7b shows that active *E. coli* concentration decreases as the accumulated energy increases to 37.5 kJ L^{-1}. Total bacterial inactivation (<1 CFU mL^{-1}) was reached after 5.5 h of phototreatment. As mentioned above, the decrease on bacterial culturability is due to the direct action of UV light and the indirect action of organic and inorganic photosensitizers present in LLW.

Note that the initial concentration of bacteria in Fig. 17.7a is 1,000 times higher than that of Fig. 17.7b. A low bacterial load requires less time to reach a bacterial concentration below the detection limit (1 CFU mL^{-1}). However, the efficiency of the photolytic and photocatalytic disinfection rates are higher for a high concentration of bacteria (like 10^6–10^7 CFU mL^{-1}) than for small concentration (10^2 CFU mL^{-1}) as explained in the Sect. 17.4.1 (Rincón and Pulgarin 2004b).

17.5.3 Water Disinfection by Sunlight and TiO_2 Using a CPC Photoreactor

0.02 g L^{-1} of TiO_2 was enough to enhance the solar disinfection of 35 L of *E. coli* contaminated water in CPC solar photoreactor. Figure 17.8 shows that active *E. coli* concentration decreases as the accumulated energy increases and arrives to nondetectable level (<1 CFU mL^{-1}) when 13 kJ L^{-1} are applied.

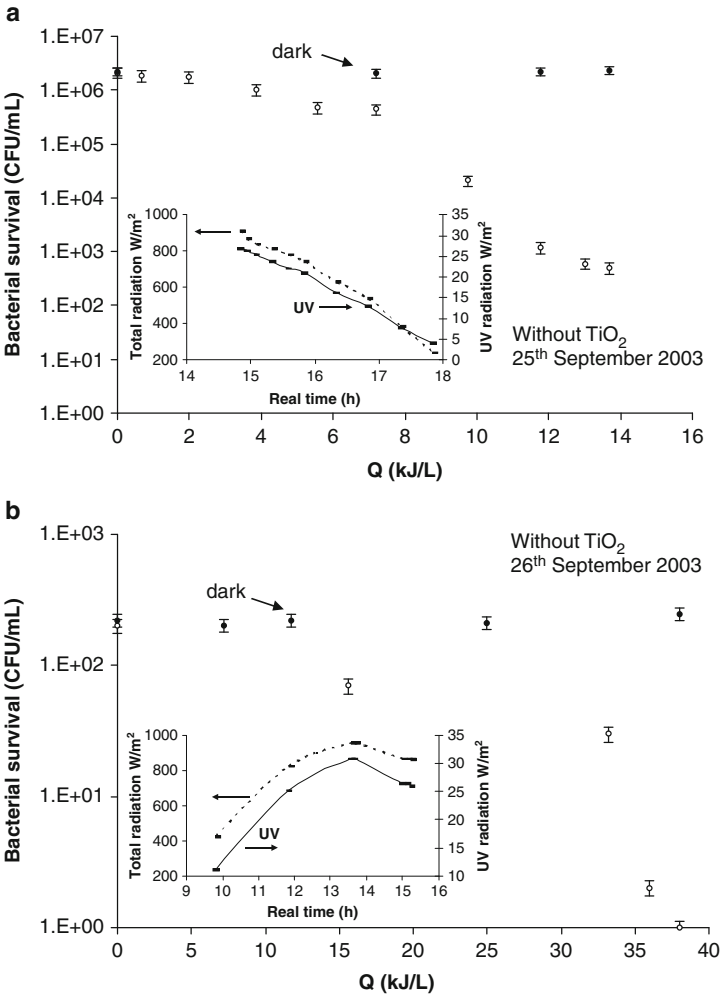

Fig. 17.7 Inactivation of *E. coli* by sunlight in a CPC photoreactor. The insert contains the UV (*continuous line*) and total (*dashed line*) solar irradiation measured during the period of the experiment. 25th (**a**) and 26th (**b**) September 2003, in Lausanne, Switzerland. Dark control for samples that corresponds to 0, 1, 2, and 3 h of the illumination exposure. Conditions: $V_{TOT} = 35$ L, recirculation rate $= 20.5\,\mathrm{L\,min^{-1}}$, illumination time $= 3$ h (**a**) and 5 h (**b**), natural pH. Type of water: LLW. The *bars* show the SD of four samples

17.5.4 Postirradiation Events at Field-Scale Experiments

To study the durability of solar disinfection at field scale, the final samples of Figs. 17.7a, b and 17.8 were incubated in the dark. During the solar treatment in the absence of catalyst, presented in Fig. 17.7a, total bacterial inactivation was not reached and bacterial recovery was observed during the subsequent dark period

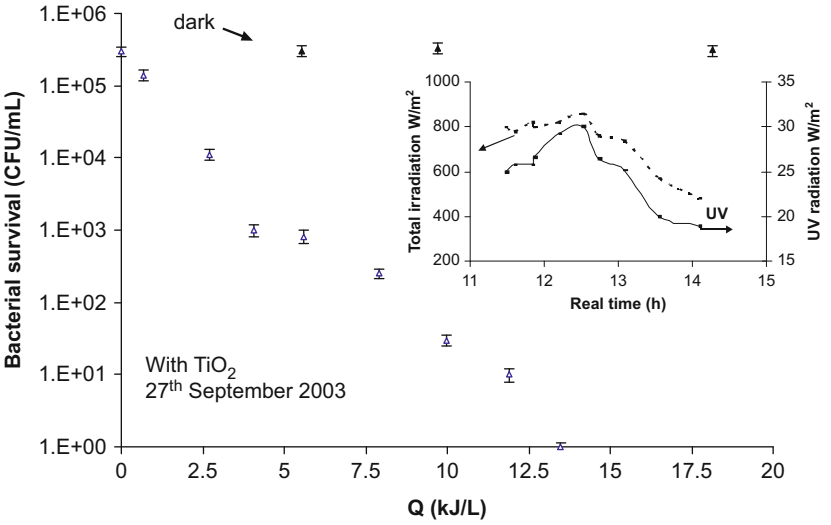

Fig. 17.8 Inactivation of *E. coli* by sunlight in the presence of TiO_2 in CPC photoreactor. The insert contains the UV (*continuous line*) and total (*dashed line*) solar irradiation measured during the period of the experiment. 27th September 2003 in Lausanne, Switzerland. Dark control for samples that corresponds to 0, 1, 2, and 3 h of the illumination exposure. Conditions: TiO_2 = 0.02 g L^{-1}, V_{TOT} = 35 L, recirculation rate = 20.5 L min^{-1}, illumination time = 3 h. Water from Leman lake. The *bars* show the SD of four samples taken at the same moment. Initial concentration 10^5 CFU mL^{-1}

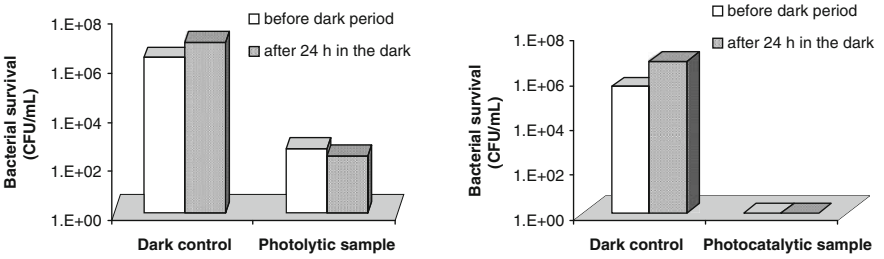

Fig. 17.9 Durability of solar disinfection without catalyst experiment of Fig. 17.7a, September 25th (**a**). Durability of solar disinfection with catalyst experiment of September 27th, 2003 (**b**). Initial and final samples were incubated for 24 h in the dark

(Fig. 17.9a). Even in the experiment shown in Fig. 17.7b, total inactivation was reached during illumination, bacterial recovery was still observed after 24 h in the dark (not shown here). Therefore, in the studied conditions, a bacteriostatic but not bactericidal effect of photolytic treatment occurred. Conditions are favorable for *E. coli* replication since even the nonilluminated sample undergoes growth (Fig. 17.9a); although, the low concentration of dissolved organic carbon in Leman lake water limits the bacterial growth. Thus, in the experiment shown in

Fig. 17.7a, b EDT_{24} was not reached after 5.5 and 3 h of illumination, respectively. Consequently, in these conditions a longer time of illumination would be necessary to reach the EDT_{24}.

In the presence of TiO_2, total photocatalytic inactivation (Fig. 17.8) and no bacterial regrowth was observed after stopping the treatment, as shown in Fig. 17.9b, suggesting that this treatment induces strong and lethal bacteria damages. Similar behavior after photocatalytic disinfection via TiO_2 has been reported in our previous papers (Rincón and Pulgarin 2004b, c). In this latter work, it has also been demonstrated that residence time of water in the illuminated part of the system, light intensity, and the period of the day selected for the treatment (morning, afternoon) strongly influence the EDT (Rincón and Pulgarin 2004a).

Other photocatalytic disinfection experiments (not shown here) were carried out and in all cases EDT_{24} was reached before 3 h of phototreatment (Rincón and Pulgarin 2004). In preceding works, a "residual disinfection effect" was observed at laboratory and field scale after solar photocatalytic treatment (Rincón and Pulgarin 2004a, b, 2005, 2007b, c).

17.5.5 Dose in Water Disinfection

As with chemical disinfection, the performance of UV irradiation systems (especially with 254-nm lamps) is determined by the disinfectant UV dose. In the case of solar disinfection of water, dose can then be calculated from the average solar UV intensity and the residence time in the irradiated part of the reactor: dose $= I \times t_r$, where dose is the solar UV dose (Wh m^{-2}), I is the average intensity (W m^{-2}), and t is the residence time (h). Note that only the UV part of the solar spectra is taken into account.

In order to compare the effect of solar illumination applied at different seasons of the year (2003) and at different moments of the day, we calculated for each period the solar UV dose necessary to reach approximately 99.9900% of *E. coli* inactivation. As expected, the dose necessary to inactivate a similar quantity of bacteria is higher in the absence (37.28–43.74 W m^{-2}) than in the presence of TiO_2 (17.204–23.720 W m^{-2}).

In general, similar doses do not result in the same bacterial inactivation. For example, in one experiment (August 19, 2003) a dose of 19.52 Wh m^{-2} achieved less bacterial inactivation (active *E. coli* $\gg$ 1 CFU mL^{-1}) than in the experiment 5 with a dose of only 17.04 Wh m^{-2} (August 19, 2003). These results were explained (Rincón and Pulgarin 2004) because of (1) the solar spectra characteristics change with the day period and seasons; the relative UV and visible wavelengths intensities, characteristics of each season, and day period significantly affect the solar photoinactivation, photoreactivation as well as the bacterial behavior in the subsequent dark period, (2) the nonlinear dependence on light intensity, (3) the temperature in different seasons and consequently the oxygen level in water could also influence the process.

The nonproportionality between UV disinfection and dose received was confirmed in experiments carried out with reactor (CPC) illuminated surface. Then, a better performance would be expected from larger exposed area from the basic tenets of disinfection kinetics as described by Chick's Law, since the bacteria receive more illumination time (and hence more UV dose) in the 3-m^2 configuration compared to the 1 m^2 (McLoughlin 2004). However, using the same photoreactor, once the minimum solar dose has been received, the disinfection efficacy is not particularly enhanced by any further increase of dose (Sichel et al. 2007b) which is consistent with our findings in experiments carried out at laboratory scale (Rincón and Pulgarin 2004a, b).

It has been reported, in the presence (Rincón and Pulgarin 2003) or absence of TiO_2 (Sommer et al. 1998), a greater effectiveness of applying a high UV intensity for short time than applying a lower intensity for a long period of time was observed. Then, *E. coli* survival was affected differently under similar doses also at laboratory scale. This effect may be due to the action of repair enzymes in the cell which are more negatively influenced by UV intensities (Sommer et al. 1998).

For the precedent discussion, the solar UV dose is not a good parameter to accurately predict and standardize the impact of solar photocatalytic process on bacteria. According to our results and for practical applications; we propose to determine the EDT_x for each specific condition. Thereafter, the obtained EDT_x value can be raised of a certain percentage in order to introduce a range of security for users (Rincón and Pulgarin 2004a). This EDT_x is dependent not only on the classical parameters such as chemical characteristics of water (Rincón and Pulgarin 2007a, b, c), type and concentration of bacteria, reactor geometry, etc., but also on the UV and visible composition of sunlight spectra in different geographic locations, seasons, and period of day.

17.5.6 Flow Rate and TiO_2 Concentration

The aim of this section is to quantify the influence of some operating parameters such as flow rate, catalyst concentration, initial bacterial concentration, and reactor volume. These parameters affect reactor efficiency evaluation and therefore subsequent optimization of the disinfection system.

The photocatalytic process depends on the flow rate because of (1) the stress produced by mechanical agitation inside the reactor and (2) the possibility of bacteria being adsorbed or reaching the catalyst. Experiments in the presence or absence of TiO_2 were made using 13.5 and 20 L min^{-1} (Rincón and Pulgarin 2004a, 2007a, b, c). Even though the lowest flow rate produces the highest residence time, on the illuminated part of the reactor, of bacteria under solar radiation, the efficiency of bacteria inactivation is still the lowest. This could be attributed to the capacity of bacteria to adapt to stressful conditions such as incoming solar photons inside the reactor, which could easily be developed if residence time was long enough. Later

results are in accordance with that reported recently by Fernandez et al. (2005), they found that 22.5 L min^{-1} yields higher efficiency than 13 L min^{-1}, which is higher than 5.0 L min^{-1}. However, opposite tendencies occur during solar photocatalytic disinfection when TiO_2 was fixed; in this case a flow rate between 10 and 2 L min^{-1} was used and photocatalytic disinfection effectiveness tend to increase with decreasing flow rates (Sichel et al. 2007b, c). Low flow rates result in a high retention time in the illuminated part of the reactor and then a better interaction between bacterial cells and photocatalysis which is the principal factor when immobilized TiO_2 is used (Sect. 17.3.6).

In addition, the control in the dark should be taken into account in order to know about the effect of mechanical agitation toward bacteria. Some results had shown the impact that mechanical stress in the CPC reactors has the viability of *E. coli* cells (Gumy 2006) which is inversely proportional to the anion (Cl^-) concentration of the solution (Sichel et al. 2007c). Decrease of mechanical stress, as expected, when the concentration of anions increases in solution because the osmotic shock on bacteria is reduced compared with that observed in distilled water (Rincón and Pulgarin 2004, 2007).

Concerning catalyst concentration when using CPC photoreactors, the experiments had shown a nonhigh influence of this parameter between 0.02 and 0.1 g L^{-1}, as we found in experiment carried out at laboratory scale (Sect. 2.1). However, a slight enhance on the efficiencies were found using 0.1 g L^{-1} of TiO_2 (Rincón and Pulgarin 2004a, 2007a, c). Another group of authors reported that the disinfection rate is independent of catalyst concentration in the range of 0.025 and 0.05 g L^{-1} using a CPC photoreactor and slurry TiO_2 (Fernandez et al. 2005) while in the range of 0.003 and 0.009 g L^{-1}, no difference was observed and even in some experiments disinfection in the absence of TiO_2 was more effective than the photocatalytic system (McLoughlin et al. 2004).

In general, the time as well as the energy (kJ L^{-1}) required to reach total disinfection of water in the presence and absence of TiO_2 was strongly dependent on the initial concentration of bacteria ranging between 10^2 and 10^6 CFU mL^{-1} (Rincón and Pulgarin 2007a, b, c) as observed in laboratory experiments (Sect. 17.4.1).

The total volume affects the residence time in the nonilluminated part of the reactor, if the surface of illumination does not vary. It was reported that higher volume of phototreated water (90 L) results in a decrease in the solar disinfection when compared with the lower volume (56 L, 70 L) (Rincón and Pulgarin 2004a). Thus, retention time on the nonilluminated part of the reactor increases of volume increase, favoring dark repair and then decreases the disinfection.

However, we had observed that the influence of the above parameters in experiments carried out in pilot scale is masked by the final point chosen for comparison of the results, because as described in Sect. 17.6 the spectral characteristics of the days are not the same and then the point when the wall is over passed in terms of time, energy, and intensity is different for each experiment (Rincón and Pulgarin 2007a, b, c).

17.6 Outgoing Work in Photocatalytic Disinfection

Small doses of sunlight have a postirradiation effect in laboratory and field-scale photoreactors. The solar photocatalytic disinfection is correlated to the accumulated energy (Q, kJ L^{-1}): experimental time always plays an important role; some groups are at the moment working in this aspect.

For a specific situation: to determine the minimum amount of irradiated catalyst to inactivate bacteria and the efficient disinfection time (EDT_x) as well as the optimization of the ratio of dark/illuminated areas became a key factor in the application of photocatalytic disinfection.

When the TiO_2 in slurry is used, no regrowth was found after a specific dark period. However, it is not clear whether solar photocatalysis with supported TiO_2 avoid the *E. coli* regrowth once the "zero" is achieved. The interaction between the catalyst and the bacteria is the determinant factor; in addition, the interaction is depending on the chemical matrix of water and geometrical characteristics of the photoreactors. This subject should be studied in more detail.

Concerning the technological point, the development of solar collectors to higher UV flux concentrations, the combination of photocatalytic and thermal effect in the same collector, and the study of series manufacturing techniques incorporating new materials are investigated by some groups.

To study the action of the photocatalytic system at the genetical level of bacteria should contribute to the understanding of the bacterial disinfection mechanism.

References

Abdullah, M., Low, G.K.C. and Mattheus, R.W. (1990) Effects of common inorganic anions on rates of photoctalytic degradation of organic carbon over illuminated titanium dioxide. J. Phys. Chem. 94, 6820–6825.

Amezaga-Madrid, P., Nevarez-Moorillon, G.V., Orrantia-Borunda, E. and Miki-Yoshida, M. (2002) Photoinduced bactericidal activity against *Pseudomonas aeruginosa* by TiO2 based thin films. FEMS Microbiol. Lett. 211, 183–188.

Armon, R., Laot, N., Narkis, N. and Neeman, I. (1998) Photocatalytic inactivation of different bacteria and bacteriophages in drinking water at different TiO_2 concentration with or without exposure to O_2. J. Adv. Oxid. Technol. 3, 145–150.

Bahnemann, D., Cunningham, J., Fox, M.A., Pelizzetti, E., Pichat, P. and Serpone, N. (1994) *Photocatalytic treatment of waters*. Lewis Publishers, Boca Raton, FL.

Bekbolet, M. (1997) Photocatalytic bactericidal activity of TiO2 in aqueous suspensions of *Escherichia coli*. Water Sci. Technol. 35, 95–100.

Belháová, L., Krýsa, J., Geryk, J. and Jirkovský, J. (1999) Inactivation of microorganisms in a flow-through photoreactor with an immobilized TiO2 layer. J. Chem. Technol. Biotechnol. 74, 149–154.

Blake, D.M., Maness, P.C., Huang, Z., Wolfrum, E.J., Huang, J. and Jacoby, W.A. (1999) Application of the photocatalytic chemistry of titanium dioxide to disinfection and the killing of cancer cells. Separ. Purif. Methods 28, 1–50.

Brezova, V., Blazkova, A., Borosova, E., Ceppan, M. and Fiala, R. (1995) The influence of dissolved metal ions on the photocatalytic degradation of phenol in aqueous TiO_2 suspensions. J. Mol. Catal. A: Chem. 98, 109–116.

Britt, A.B. (1996) DNA damage and repair in plants. Annu. Rev. Plant. Physiol. Plant. Mol. Biol. 47, 75–100.

Butterfield, I.M., Christensen, P.A., Curtis, T.P. and Gunlazuardi, J. (1997) Water disinfection using an immobilised titanium dioxide film in a photochemical reactor with electric field enhancement. Water Res. 31, 675–677.

Chen, H.Y., Zahraa, O. and Bouchy, M. (1997) Inhibition of the adsorption and photocatalytic degradation of an organic contaminant in an aqueous suspension of TiO_2 by inorganic ions. J. Photochem. Photobiol. A: Chem. 108, 37–44.

Child, M., Strike, P., Pickup, R. and Edwards, C. (2002) *Salmonella typhimurium* displays cyclical patterns of sensitivity to UV-C killing during prolonged incubation in the stationary phase of growth. FEMS Microbiol. Lett. 213, 81–85.

Christensen, P.A., Curtis, T.P., Egerton, T.A., Kosa, S.A.M. and Tinlin, J.R. (2003) Photoelectrocatalytic and photocatalytic disinfection of E. coli suspensions by titanium dioxide. Appl. Catal. B: Environ. 41, 371–386.

Christensen, P.A., Egerton, T.A., Kosa, S.A.M., Tinlin, J.R. and Scott, K. (2005) The photoelectrocatalytic oxidation of aqueous nitrophenol using a novel reactor. J. Appl. Electrochem. 35, 683–692.

Cooper, W.J., Cadavid, E., Nickelsen, M.G., Lin, K.J., Kurucz, C.N. and Waite, T.D. (1993) Removing THMS from drinking-water using high-energy electron-beam irradiation. J. Am. Water Work Assoc. 85, 106–112.

Crap O., Huisman, C.L. and Reller, A. (2004) Photoinduced reactivity of titanium dioxide. Prog. Solid State Chem. 32, 33–177.

Dhananjeyan, M.R., Mielczarski, E., Thampi, R.K., Buffat, P., Bensimon, M., Kulik, J., Mielczarski, J. and Kiwi, J. (2001) Photodynamics and surface characterization of TiO2 and Fe2O3 photocatalysts immobilized on modified polyethylene films. J. Phys. Chem. B 105, 12046–12055.

Duffy, E.F., Al Touati, F., Kehoe, S.C., McLoughlin, O.A., Gill, L.W., Gernjak, W., Oller, I., Maldonado, M.I., Malato, S. and Cassidy, J. (2004) A novel TiO_2-assisted solar photocatalytic batch-process disinfection reactor for the treatment of biological and chemical contaminants in domestic drinking water in developing countries. Solar Energy 77, 649–655.

Dunlop, P.S.M., Byrne, J.A., Manga, N. and Eggins, B.R. (2002) The photocatalytic removal of bacterial pollutants from drinking water. J. Photochem. Photobiol. A: Chem. 148, 355–363.

Epling, G.A. and Lin, C. (2002) Investigation of retardation effects on the titanium dioxide photodegradation system. Chemosphere 46, 937–944.

Fernandez, P., Blanco, J., Sichel, C. and Malato, S. (2005) Water disinfection by solar photocatalysis using compound parabolic collectors. Catal. Today 101, 345–352.

Gogniat, G., Thyssen, M., Denis, M., Pulgarin, C. and Dukan, S. (2006) The bactericidal effect of TiO_2 photocatalysis involves adsorption onto catalyst and the loss of membrane integrity. FEMS Microbiol. Lett. 258, 18–24.

Guillard, C., Disdier, J., Monnet, C., Dussaud, J., Malato, S., Blanco, J., Maldonado, M.I. and Herrmann, J.-M. (2003a) Solar efficiency of a new deposited titania photocatalyst: Chlorophenol, pesticide and dye removal applications. Appl. Catal. B: Environ. 46, 319–332.

Guillard, C., Lachheb, H., Houas, A., Ksibi, M., Elaloui, E. and Herrmann, J.-M. (2003b) Influence of chemical structure of dyes, of pH and of inorganic salts on their photocatalytic degradation by TiO2 comparison of the efficiency of powder and supported TiO2. J. Photochem. Photobiol. A: Chem. 158, 27–36.

Gumy, D. (2006) Factors influencing photocatalytic drinking water detoxification and disinfection by suspended and fixed TiO2, PhD Thesis, EPFL 3586, p. 170.

Gumy, D., Morais, C., Bowen, P., Pulgarin, C., Giraldo, S., Hajdu, R. and Kiwi, J. (2006a) Catalytic activity of commercial of TiO_2 powders for the abatement of the bacteria (*E. coli*) under solar simulated light: Influence of the isoelectric point. Appl. Catal. B: Environ. 63, 76–84.

Gumy, D., Rincon, A.G., Hajdu, R. and Pulgarin, C. (2006b) Solar photocatalysis for detoxification and disinfection of water: Different types of suspended and fixed TiO2 catalysts study. Solar Energy 80, 1376–1381.

Hoffmann, M., Martin, S., Choi, W. and Bahnemann, D. (1995) Environmental applications of semiconductor photocatalysis. Chem. Rev. 95, 69–96.

Hoigne, J. (1997) Inter-calibration of OH radical sources and water quality parameters. Water Sci. Technol. 35, 1–8.

Hu, C., Yu, J.C., Hao, Z. and Wong, P.K. (2003) Effects of acidity and inorganic ions on the photocatalytic degradation of different azo dyes. Appl. Catal. B: Environ. 46, 35–47.

Huang, N., Xiao, Z., Huang, D. and Yuan, C. (1998) Photochemical disinfection of Escherichia coli with a TiO2 colloid solution and a self-assembled TiO2 thin film. Supramol. Sci. 5, 559–564.

Huang, Z., Maness, P.C., Blake, D.M., Wolfrum, E.J., Smolinski, S.L. and Jacoby, W.A. (2000) Bactericidal mode of titanium dioxide photocatalysis. J. Photochem. Photobiol. A: Chem. 130, 163–170.

Ireland, J.C., Klostermann, P., Rice, E.W. and Clark, R.M. (1993) Inactivation of *Escherichia coli* by titanium-dioxide photocatalytic oxidation. Appl. Environ. Microbiol. 59, 1668–1670.

Jacoby, W.A., Maness, P.C., Wolfrum, E.J., Blake, D.M. and Fennell, J.A. (1998) Mineralization of bacterial-cell mass on a photocatalytic surface in air. Environ. Sci. Technol. 32, 2650–2653.

Kadavy, D.R., Shaffer, J.J., Lott, S.E., Wolf, T.A., Bolton, C.E., Gallimore, W.H., Martin, E.L., Nickerson, K.W. and Kokjohn, T.A. (2000) Influence of infected cell growth state on bacteriophage reactivation levels. Appl. Environ. Microbiol. 66, 5206–5212.

Kashige, N., Kakita, Y., Nakashima, Y., Miake, F. and Watanabe, K. (2001) mechanism of the photocatalytic inactivation of lactobacillus case I Phage PL-1 by titania thin film. Curr. Microbiol. 42, 184–189.

Kikuchi, Y., Sunada, K., Iyoda, T., Hashimoto, K. and Fujishima, A. (1997) Photocatalytic bactericidal effect of TiO2 thin-films – Dynamic view of the active oxygen species responsible for the effect. J. Photochem. Photobiol. A: Chem. 106, 51–56.

Koizumi, Y. and Taya, M. (2002) Photocatalytic inactivation rate of phage MS2 in titanium dioxide suspensions containing various ionic species. Biotechnol. Lett. 24, 459–462.

Kuhn, K.P., Chaberny, I.F., Massholder, K., Stickler, M., Benz, V.W., Sonntag, H.-G. and Erdinger, L. (2003) Disinfection of surfaces by photocatalytic oxidation with titanium dioxide and UVA light. Chemosphere 53, 71–77.

Lee, S., Nishida, K., Otaki, M. and Ohgaki, S. (1997) Photocatalytic inactivation of phage Q-beta by immobilized titanium-dioxide mediated photocatalyst. Water Sci. Technol. 35, 101–106.

Legrini, O., Oliveros, E. and Braun, M.A. (1993) Photochemical processes for water treatment. Chem. Rev. 93, 671–698.

Lewis, C.K. and Burt Maxcy, R. (1984) Effect of physiological age on radiation resistance of some bacteria that are highly radiation resistant. Appl. Environ. Microbiol. 47, 915–918.

Lonnenn, J., Kilvington, S., Kehoe, S.C., Touati, F.A. and McGuigan, K.G. (2005) Solar and photocatalytic disinfection of protozoan, fungal and bacterial microbes in drinking water. Water Res. 39, 877–883.

Maness, P.-C., Smolinski, S., Blake, D.M., Huang, Z., Wolfrum, E.J. and Jacoby, W.A. (1999) Bactericidal activity of photocatalytic TiO2 reaction: Toward an understanding of its killing mechanism. Appl. Environ. Microbiol. 65, 4094–4098.

Matsunaga, T., Tomoda, R., Nakajima, T. and Wake, H. (1985) Photoelectrochemical sterilization of microbial cells by semiconductor powders. FEMS Microbiol. Lett. 29, 211–214.

Matsunaga, T., Tomoda, T., Nakajima, T., Nakamura, N. and Komine, T. (1988) Continuous-sterilization system that uses photosemiconductor powders. Appl. Environ. Microbiol. 54, 1330–1333.

McLoughlin, O.A., Fernández, P., Gernjak, W., Malato, S. and Gilla, L.W. (2004) Photocatalytic disinfection of water using low cost compound parabolic collectors. Solar Energy 77, 625–633.

Mercalf, E. (2005) *Waste water engineering treatment and reuse*. McGraw Hill, New York, NY.

Mest'ankova, H., Mailhot, G., Pilichowski, J.-F., Krysa, J., Jirkovsky, J.x.r. and Bolte, M. (2004) Mineralisation of monuron photoinduced by Fe(III) in aqueous solution. Chemosphere 57, 1307–1315.

Morton, A.R. and Haynes, R.H. (1969) Changes in the ultraviolet sensitivity of *Escherichia coli* during growth in bath cultures. J. Bacteriol. 97, 1379–1385.

Murno, P.M., Flatatau, G.N., Clement, L.R. and Gauthier, M.L. (1995) Influence of the RpoS (KatF) sigma factor on maintenance of viability and culturability of *Escherichia coli* and *Salmonella typhimurium* in seawater. Appl. Environ. Microbiol. 61, 1853–1858.

Nakayama, T., Wake, H., Ozawa, K., Kodama, H., Nakamura, N. and Matsunaga, T. (1998) Use of a titanium nitride for electrochemical inactivation of marine bacteria. Environ. Sci. Technol. 32, 798–801.

Ollis, D., Pelizzetti, E. and Serpone, N. (1991) Photocatalysed destruction of water contaminants. Environ. Sci. Technol. 25, 1522–1529.

Pham, H.N., McDowell, T. and Wilkins, E. (1995) Photocatalytically mediated disinfection of water using TiO_2 as a catalyst and spore-forming *Bacillus-Pumilus* as a model. J. Environ. Sci. Health A Environ. 30, 627–636.

Pizarro, P., Guillard, C., Perolb, N. and Herrmann, J.M. (2005) Photocatalytic degradation of Imazapyr in water: Comparison of activities of different supported and unsupported TiO2-based catalysts. Catal. Today 101, 211–218.

Poulina, A. and Mikhailova, S.S. (1995) Influence of impurities on adsorption interaction between surfactants and titanium dioxide. Colloid J. 57, 116–117.

Reed, R.H. (2004) The inactivation of microbes by sunlight: Solar disinfection as a water treatment process. Adv. Appl. Microbiol. 54, 333–365.

Reed, R.H., Mani, S.K. and Meyer, V. (2000) Solar photo-oxidative disinfection of drinking water: Preliminary field observations. Lett. Appl. Microbiol. 30, 432–436.

Rincón, A.G. and Pulgarin, C. (2003) Photocatalytical inactivation of *E. coli*: Effect of (continuous-intermittent) light intensity and of (suspended-fixed) TiO_2 concentration. Appl. Catal. B: Environ. 44, 263–284.

Rincón, A.G. and Pulgarin, C. (2004a) Field solar *E.coli* inactivation in the absence and presence of TiO_2: Is UV solar dose an appropriate parameter for standarization of water solar disinfection?. Solar Energy 77, 635–648.

Rincón, A.G. and Pulgarin, C. (2004b) Bactericidal action of illuminated TiO_2 on pure *Escherichia coli* and natural bacterial consortia: Post irradiation events in the dark and assessment of the effective disinfection time. Appl. Catal. B: Environ. 49, 99–112.

Rincón, A.G. and Pulgarin, C. (2004c) Effect of pH, inorganic ions, organic matter and H_2O_2 on *E. coli* K_{12} photocatalytic inactivation by TiO_2: Implications in solar water disinfection. Appl. Catal. B. Environ. 51, 283–302.

Rincón, A.G. and Pulgarin, C. (2005) Use of coaxial photocatalytic reactor (CAPHORE) in the TiO_2 photo-assisted treatment of mixed *E. coli* and *Bacillus* sp. and bacterial community present in wastewater. Catal. Today 101, 331–344.

Rincón, A.G. and Pulgarin, C. (2006) Comparative evaluation of Fe^{+3} and TiO_2 photoassisted processes in solar photocatalytic disinfection of water. Appl. Catal. B: Environ. 63, 222–231.

Rincón, A.G. and Pulgarin, C. (2007a) Fe3+ and TiO2 solar-light-assisted inactivation of *E. coli* at field scale. Implications in solar disinfection at low temperature of large quantities of water. Catal. Today 122, 128–136

Rincón, A.G. and Pulgarin, C. (2007b) Solar photolytic and photocatalytic disinfection of water at laboratory and field scale. Effect of the chemical composition of water and study of the postirradiation events. Solar Energy Eng. 129, 100–110.

Rincón, A.G., and Pulgarin C. (2007c) Absence of *E. coli* regrowth after Fe^{3+} and TiO_2 solar photoassisted disinfection of water in CPC solar photoreactor. Catal. Today. 124, 204–214.

Rincón, A.G., Pulgarin, C., Adler, N. and Peringer, P. (2001) Interaction between *E. coli* inactivation and DBP-precursors – dihydroxybenzene isomers – in the photocatalytic process of drinking-water disinfection with TiO_2. J. Photochem. Photobiol. A: Chem. 139, 233–241.

Saito, T., Iwase, T., Horie, J. and Morioka, T. (1992) Mode of photocatalytic bactericidal action of powdered semiconductor TiO2 on mutans Streptococci. J. Photochem. Photobiol. B: Biol. 14, 369–379.

Salih, F.M. (2002) Enhancement of solar inactivation of *Escherichia coli* by titanium dioxide photocatalytic oxidation. J. Appl. Microbiol. 92, 920–926.
Serpone, N., Salinaro, A., Horikoshi, S. and Hidaka, H. (2006) Beneficial effects of photoinactive titanium dioxide specimens on plasmid DNA, human cells and yeast cells exposed to UVA/UV B simulated sunlight. J. Photochem. Photobiol. A: Chem. 179, 200–212.
Sichel, C., de Cara M., Tello, J., Blanco, J. and Fernandez-Ibanez, P. (2007a). Solar photocatalytic disinfection of agricultural pathogenic fungi: Fusarium species. Appl. Catal. B: Environ. 74, 152–160.
Sichel, C., Tello, J., de Cara, M. and Fernandez-Ibanez P. (2007b) Effect of UV solar intensity and dose on the photocatalytic disinfection of bacteria and fungi. Catal. Today. 129, 152–60.
Sichel, C., Blanco, J., Malato, S. and Fernández-Ibáñez, P. (2007c) Effects of experimental conditions on *E. coli* survival during solar photocatalytic water disinfection. J. Photochem. Photobiol. A: Chem. 189, 239–246.
Sjogren, J.C. and Sierka, R.A. (1994) Inactivation of phage Ms-2 by iron-aided titanium-dioxide photocatalysis. Appl. Environ. Microbiol. 60, 344–347.
Sommer, R., Haider, T., Cabaj, A., Pribil, W. and Lhotsky, M. (1998) Time dose reciprocity in UV disinfection of water. Water Sci. Technol. 38, 145–150.
Srinivasan C., and Somasundaram, N. (2003) Bactericidal and detoxification effects of irradiated semiconductor catalyst TiO_2. Curr. Sci. 85, 1431–1438.
Sunada, K., Kikuchi, Y., Hashimoto, K. and Fujishima, A. (1998) Bactericidal and detoxification effects of TiO2 thin-film photocatalysts. Environ. Sci. Technol. 32, 726–728.
Sunada, K., Watanabe, T. and Hashimoto, K. (2003) Studies on photokilling of bacteria on TiO2 thin film. J. Photochem. Photobiol. A: Chem. 156, 227–233.
Wei, C., Lin, W.Y., Zainal, Z., Williams, N.E., Zhu, K., Kruzic, A.P., Smith, R.L. and Rajeshwar, K. (1994) Bactericidal activity of TiO_2 photocatalyst in aqueous-media – Toward a solar-assisted water disinfection system. Environ. Sci. Technol. 28, 934–938.
Whitelam, G.C. and Codd, G.A. (1985) Damaging effects of light on microorganisms. In: Herbert, R.A. and Codd, G.A. (Eds.) *Microbes in extreme environments*. Academic, London, pp. 129–169.
Wolfrum, E.J., Huang, J., Blake, D.M., Maness, P.-C., Huang, Z., Fiest, J. and Jacoby, W.A. (2002) Photocatalytic oxidation of bacteria, bacterial and fungal spores, and model biofilm components to carbon dioxide on titanium dioxide-coated surfaces. Environ. Sci. Technol. 36, 3412–3419.

Chapter 18
Fabrication of Photoelectrode Materials

Huanjun Zhang, Xinyong Li, and Guohua Chen

18.1 Sol–Gel Methods

Sol–gel synthesis has been widely used for making transition-metal oxide solids with fine-scaled microstructures (Anderson and Bard 1995; Antonelli and Ying 1995; Lakshmi, Patrissi and Martin 1997b). In this method, normally the corresponding metal alkoxides or other salts are used as precursors, which are dissolved in acidic aqueous or organic-solvent-based solutions (Shang, Yao, Zhu and Wu 2004) at controlled temperatures, and the resulted colloidal solution can be kept stable for months. Pore and particle sizes no greater than a few nanometers can be easily achieved in the freshly derived gels. These gels have a hydrous solid skeleton that contains a large amount of hydroxyl groups. Annealing is usually indispensable for dehydroxylation to achieve sufficient crystallinity to give the desired combination of mechanical, catalytic, and optoelectronic properties for their applications (Wu, Wang and Rusakova 1999). In fact, many methods discussed in the following context more or less involve (either based on or combined with) the sol–gel method (Kim and Anderson 1994; Sunada, Kikuchi, Hashimoto and Fujishima 1998), therefore discussions on this method are placed here prior to all the other methods.

The sol–gel method has been used for over two decades to produce TiO_2 films from aqueous-based TiO_2 (Anderson, Gieselmann and Xu 1988). A typical recipe of this method includes preparing a Ti-precursor solution by mixing it with HNO_3 in H_2O, refluxing the mixture at elevated temperature (normally 80°C), transferring the TiO_2 sol onto a conducting glass substrate, and finally annealing the coated film at high temperatures.

Nonaqueous-based TiO_2 sols have also been used. For example, Anderson and Bard (1995) prepared a TiO_2/SiO_2 composite film photoelectrode using an alcohol-solvent-based sol–gel method, in which the gels were obtained from the

G. Chen (✉)
Department of Chemical and Biomolecular Engineering, Hong Kong University of Science and Technology, Kowloon, Hong Kong
e-mail: kechengh@ust.hk

C. Comninellis and G. Chen (eds.), *Electrochemistry for the Environment*,
DOI 10.1007/978-0-387-68318-8_18,

acid-catalyzed hydrolysis of tetraisopropyl orthotitanate (TIOT) and tetraethoxysilane (TEOS). The TIOT/TEOS mixture was added dropwise to a solution of 2-propanol containing a small amount of concentrated HCl at 0°C while being stirred in an ice bath. A molar quantity of water four times the total moles of Ti and Si species was added dropwise under vigorous stirring to form the gel.

Using similar these recipes, other researchers (Kim and Anderson 1994; Sunada et al. 1998; Shang et al. 2004) prepared TiO_2 or TiO_2-based photoelectrodes to study their photoelectrocatalytic properties. For example, taking the advantage of the different hydrolysis rates of titanium ethoxide (TEOT) and TEOS precursors, Jung and Park (2000) prepared silica-embedded TiO_2 composites. Butterfield et al. (1997) used a chemical composition of $Ti(O\text{-}i\text{-}C_3H_7)_4$:$H_2O$:$C_2H_5OH$:HCl = 1:1:8:0.008 in molar ratio, while Yu et al. (2000) used a chemical composition of $Ti(OC_4H_9)_4$:C_2H_5OH:H_2O:$NH(C_2H_4OH)_2$ =1:26.5:1:1 to prepare the TiO_2 sol. Shang et al. (2004) prepared TiO_2/SnO_2 composite photoelectrodes using TiO_2 and SnO_2 sols. (The SnO_2 sol was obtained by dissolving $SnCl_2$ hydrates in ethanol at desired concentrations.) Ohyama et al. (1997) prepared highly oriented ZnO films using $Zn(CH_3COO)_2$ hydrate and monoethanolamine dissolved in 2-methoxyethanol to form a homogeneous ZnO sol. Dip coating and thermal annealing were in these three reports to form the TiO_2 or ZnO films over supporting substrates. Santato and coworkers (2001) developed a novel sol–gel method to prepare nanostructured WO_3 film electrodes using tungstic acid as the precursor. The tungstic acid was collected in ethanol, followed by the addition of an organic stabilizer such as poly(ethylene glycol) (PEG 300) to form a viscous, pale yellowish colloidal solution with much higher stability than that obtained without adding organic stabilizers. The WO_3 films were obtained by spreading the colloidal solution onto conducting glass substrates, followed by drying and annealing in oxygen flow at 400–550°C. Ichinose and coworkers (1997) proposed a "surface sol–gel" method to prepare metal-oxide films over other substrates. This method is actually a layer-by-layer sol–gel process, which usually consists of four steps: chemisorption of metal alkoxide precursors; rinsing; hydrolysis of the metal alkoxides; and drying the monolayer. By repeating these steps, multilayer metal-oxide films could be assembled with a precise thickness control down to the molecular level. Some other novel sol–gel based (and/or related) fabrication methods will be discussed in the following sections.

18.2 Film Assembly Using Particles

18.2.1 Simple Sintering of Particles

Early studies on the photoelectrochemical behaviors of semiconductors used film-structured photoelectrodes prepared via simple sintering of their particles. For example, TiO_2 film photoelectrodes were fabricated by applying TiO_2 particulate

suspension over optically transparent electrodes (e.g., conducting glass), as reported by Hidaka et al. (1995, 1996), followed by drying and sintering at elevated temperatures. The suspension could be either water- (Hidaka et al. 1995) or alcohol-based. Applying the TiO_2 particulate suspensions could be achieved by dip-coating or spin-coating methods (Song, Park, Kwon, Lee, Chung and Lee 2001), as commonly used for producing film structures over supporting materials (McMurray, Byrne, Dunlop and McAdams 2005). The TiO_2 particles were connected to each other and the as-formed TiO_2 films could strongly adhere to the glass substrates (Vinodgopal and Kamat 1995). The suspension applying/sintering process was repeated for a few cycles to control the film thickness (or it can be achieved by varying the concentration of the particulate suspensions) (Choi, Hong, Chang and Cho 2000). Composite semiconductor films composed of different particles (e.g., SnO_2 and TiO_2) can also be made by this method (Nasr, Kamat and Hotchandani 1998). Normally the particles sintered into the films would keep their original sizes and morphologies if the sintering temperature was not too high (otherwise neckings could be formed between particles), and the control over other geometrical properties (e.g., surface roughness and inner porosity of the films) was limited using this method.

18.2.2 Layer-by-Layer Self-Assembly

The layer-by-layer self-assembly (LBLSA) method has been used to prepare uniform monolayer and multilayer thin-film structures incorporating organic components, biopolymers, virus particles and other molecules (Decher, Hong and Schmitt 1992; Decher 1997). The driving force behind this process is the ionic interaction between opposite charges of different components in adjacent layers. This technique has the advantage of allowing subtle molecular-level control over the film composition and thickness. The products are independent of the substrate size and topology. The assembly process is easy to operate and does not require high-temperature sintering.

The LBLSA method can also be used to produce multilayered thin-film structures containing inorganic components such as semiconductor nanoparticles. Normally polyelectrolytes are employed to provide electrostatic attractions with the inorganic materials in the next layer and to reduce the defect formation within the multilayer structures. For the films used as photoelectrodes, the organic polyelectrolyte components in the films should be burned out to form a robust structure. The control of pH in the component solutions is critical, because it strongly influences the dissociation of the polyelectrolyte molecules and the surface charge density of the inorganic particles. Hao and coworkers (2005) produced TiO_2 photoelectrodes on quartz substrates by this technique. A poly(sodium-4-styrenesulfonate) (PSS) solution and a positively charged TiO_2-sol solution were used to submerge the substrate, followed by extensive rinsing between adjacent immerging. The thickness of the multilayered TiO_2/PSS films was controlled by choosing the appropriate number of cycles. After thermal treatment nanoporous TiO_2 granular films were obtained

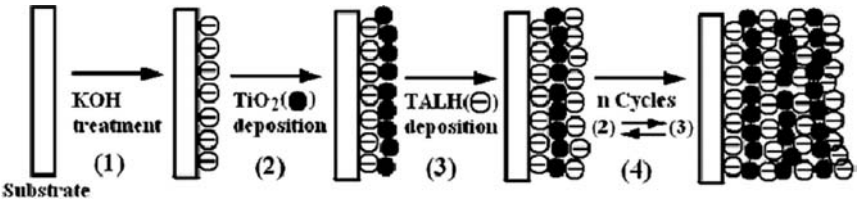

Fig. 18.1 LBLSA process for fabrication of TiO_2/TALH multilayered films [reprinted from Kim et al. (2006), copyright (2006), with permission from Elsevier]

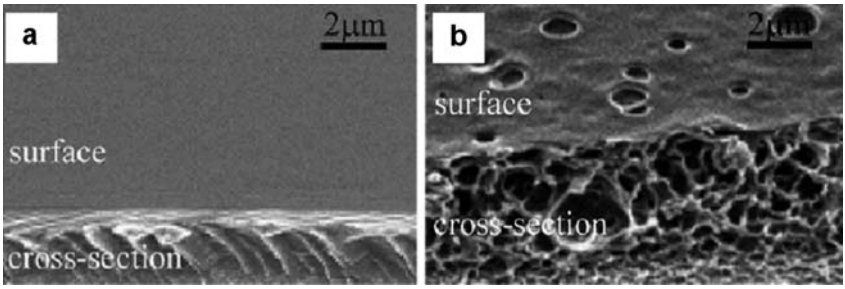

Fig. 18.2 TiO_2 films from LBLSA: (**a**) immersed and (**b**) not immersed in silver acetate solution [reprinted from Tsuge et al. (2006), copyright (2006), with permission from Elsevier]

with photocatalytic activity in the degradation of Rhodamine B. Kim et al. (2006) reported TiO_2 multilayered thin-film photoelectrodes using similar polyelectrolyte components but different TiO_2 precursor that contains both 7-nm-sized TiO_2 sol solution and titanium(IV) bis(ammonium lactato) dihydroxide (TALH) with negative charges after dissociation in water. The molecular structure of the assembled film is shown in Fig. 18.1. Without thermal treatment, the final product showed activity in photocatalytic degradation of methyl orange under UV light.

Highly porous TiO_2 films could also be obtained upon exposure to a silver acetate solution after cycles of LBLSA, as reported by Tsuge et al. (2006), and the spongy structure brought significant enhancement on the energy conversion efficiency of this film photoelectrode. The morphology of both normal and highly spongy films is shown in Fig. 18.2.

18.2.3 Electrophoretic Deposition

Electrophoretic deposition (EPD) is a colloidal process in which the charged colloidal particles are driven by a dc electric field to deposit on a substrate, forming a condensed film. This process is a combination of electrophoresis and deposition (Sarkar and Nicholson 1996). It has a long history and the first application was in 1927 for ThO_2 and tungsten deposition on a platinum cathode. Recently, photocatalyst semiconductor nanoparticles/microparticles have also been assembled by this

technique to form film-structured electrodes on top of indium tin oxide (ITO) glass substrates. Matsuda and coworkers (2006) prepared TiO_2/SiO_2 composite films consisting of spherical microparticles which showed high activity in photocatalytic reactions probed by the I^-/I_2 redox couple under UV irradiation. In their method, the TiO_2/SiO_2 core-shell-structured microparticles were dispersed in acetone containing I_2 and poly(vinylidene fluoride). The resultant suspension was subjected to a dc electric field between an ITO glass cathode and a stainless steel spiral counter electrode. Uchikoshi et al. (2004) combined EPD with a magnetic field to prepare TiO_2 films with control over the crystalline orientation of the particles. By varying the angle between the electric and the magnetic fields, the dominant crystal orientation at the surface was controlled, and it could be retained after phase transition from anatase to rutile.

18.3 Aqueous Phase Deposition

18.3.1 Electrodeposition

Electrodeposition of dissolved precursors (especially in aqueous solutions) is a low cost and scalable method which is well suited to the mass production of thin films of metal-oxide semiconductors such as TiO_2, Cu_2O, WO_3, and ZnO. Control of temperature, pH and the deposition potential are important because the corresponding electrochemical reactions within the deposition bath mainly depend on these parameters.

Kavan et al. (1993) proposed an anodic electrodeposition method to prepare TiO_2 films over various substrates by oxidative hydrolysis of $TiCl_3$ in aqueous acidic solutions. The TiO_2 films, possessing the anatase structure after annealing at 450°C, showed high photoelectrochemical activity as the photoanode in an I^-/I_2 regenerative cell. One layer of such-electrodeposited TiO_2 film over conventional TiO_2 particulate layers also enhanced the short-circuit photocurrent and open-circuit photovoltage in dye-sensitized solar cells (Nazeeruddin, Kay, Rodicio, Humphrybaker, Muller, Liska, Vlachopoulos and Grätzel 1993).

Cathodic electrodeposition can be used to produce TiO_2 thin films over ITO glass substrate, as reported by Natarajan and Nogami (1996). They prepared the deposition bath by dissolving Ti powders with H_2O_2 and ammonia solution first (a gel was obtained after heating to remove excess H_2O_2 and NH_3) and then dissolving the TiO^{2+}-gel in H_2SO_4 or HNO_3 solution. An et al. (2005) added cationic surfactants (such as cetyltrimethylammonium bromide, CTAB) can serve as the deposition-promoting agent to cathodically deposit TiO_2 films in $TiCl_3$ or $TiCl_4$ aqueous solutions containing KNO_3. The main reactions in the deposition baths were proposed as follows (An et al. 2005):

$$\begin{aligned}&\text{(a) } NO_3^- + H_2O + 2e^- \rightarrow NO_2^- + 2OH^-\\&\text{(b) } TiO^{2+} + 2OH^- \rightarrow TiO(OH)_2 \quad \text{(for } TiCl_4 \text{ precursor)}\\&\text{(c) } TiOH^{2+} + 2OH^- \rightarrow Ti(OH)_3 \quad \text{(for } TiCl_3 \text{ precursor)}\end{aligned} \tag{18.1}$$

The beneficial effect of CTAB was to increase the deposition (film growth) rate due to the less electrostatic repulsion between NO_3^- ions and the cathode after adsorbing CTA^+ cations (anionic or nonionic surfactants did not show this effect).

Deposition of Cu_2O films over TiO_2 underlayer on OTC glass substrates was reported using the cathodic electrodeposition in an aqueous solution of cupric acetate and sodium acetate (Tang, Chen, Jia, Zhang and Li 2005). The temperature of the deposition bath showed a strong influence on both the morphology and the deposition rate, and highly porous Cu_2O films could be obtained by keeping the deposition bath temperature at 60°C. The morphology of the film was shown in Fig. 18.3.

WO_3 films can also be made using electrodeposition by dissolving tungsten powder in aqueous hydrogen peroxide solution containing 2-propanol (Luo and Hepel 2001). After being annealed at 400°C, the WO_3 films showed higher photocatalytic activity for the degradation of a textile diazo dye, naphthol blue black, as compared with the TiO_2 nanoparticulate film electrode.

Based on cathodic electrodeposition of TiO_2 and WO_3 films, de Tacconi and coworkers (2003) provided a method to cathodically electrodeposit TiO_2/WO_3 composite films via the control of a pulsed deposition potential. By mixing the deposition baths for both TiO_2 and WO_3, the authors applied a pulsed potential

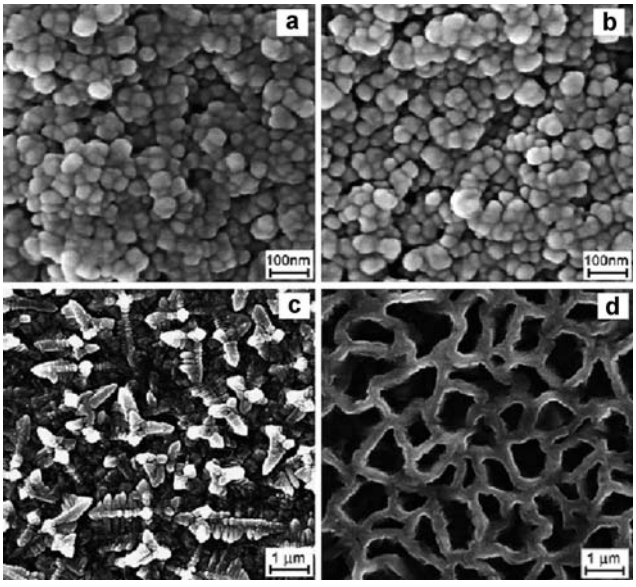

Fig. 18.3 Cu_2O films obtained by electrodeposition at various temperatures: (**a**) 0°C, (**b**) 30°C, (**c**) 45°C and (**d**) 60°C [reprinted from Tang et al. (2005), copyright (2005), with permission from Elsevier]

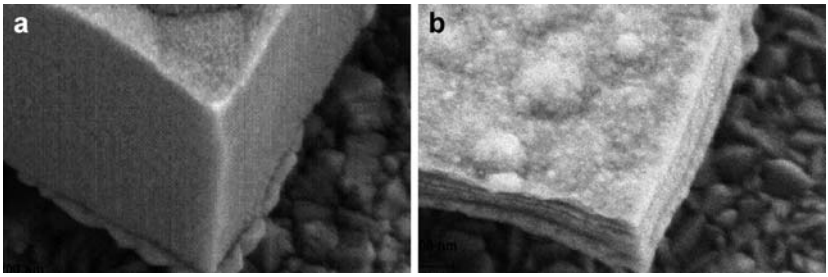

Fig. 18.4 Contrast between TiO_2/WO_3 composite films electrodeposited by (**a**) pulsed-potential deposition in a single deposition bath and (**b**) sequential deposition in different baths [reprinted from Somasundaram et al. (2006), copyright (2006), with permission from Elsevier]

sequence during which −0.45 and −0.95 V were used to trigger the deposition of WO_3 and WO_3–TiO_2, respectively. The duration of the two potentials was controlled to achieve an appropriate ratio between TiO_2 and WO_3 in the film. But the incident photon-to-current efficiency (IPCE) measurements suggested that this pulsed-potential method in a single-deposition bath provided less satisfactory coupling effects between TiO_2 and WO_3 than sequential electrodeposition of TiO_2 and WO_3 in separate deposition baths. SEM results, as shown in Fig. 18.4, revealed that layered TiO_2/WO_3 films could be obtained using the latter method, which might be responsible for the more efficient separation of photogenerated electrons and holes.

Electrodeposition has also been frequently used to fabricate ZnO films. Peulon and Lincot (1996) obtained ZnO thin films on tin oxide/glass substrate by a cathodic electrodeposition process using an aqueous zinc salt solution containing dissolved oxygen, according to the following diffusion and reaction steps:

$$\begin{aligned}
&\text{(a)}\ O_{2,\text{bulk}} \rightarrow O_{2,\text{surface}} \\
&\text{(b)}\ {Zn^{2+}}_{\text{bulk}} \rightarrow {Zn^{2+}}_{\text{surface}} \\
&\text{(c)}\ O_{2,\text{surface}} + 2H_2O + 4e^- \rightarrow 4{OH^-}_{\text{surface}} \\
&\text{(d)}\ {Zn^{2+}}_{\text{surface}} + 2{OH^-}_{\text{surface}} \rightarrow ZnO + H_2O \\
&\text{(e)}\ {OH^-}_{\text{surface}} \rightarrow {OH^-}_{\text{bulk}}
\end{aligned} \tag{18.2}$$

where (a), (b), and (e) are the diffusion steps accounting for the transfer of materials between the bulk solution and the electrode surface; (c) is the electrochemical step for oxygen reduction; and (d) represents the formation of ZnO on the substrate. It was proposed that the growth of such films is a heterogeneous process under quasithermodynamic equilibrium conditions at the electrode/electrolyte interface. The deposition temperature, deposition bath composition, and the nature of the substrate influenced the final properties of the films. The SEM images shown in Fig. 18.5 display the effect of the deposition conditions on the structure of the ZnO films. Efforts have also been made to modify the film structure and properties by introducing structure-directing agents (such as surfactants) in

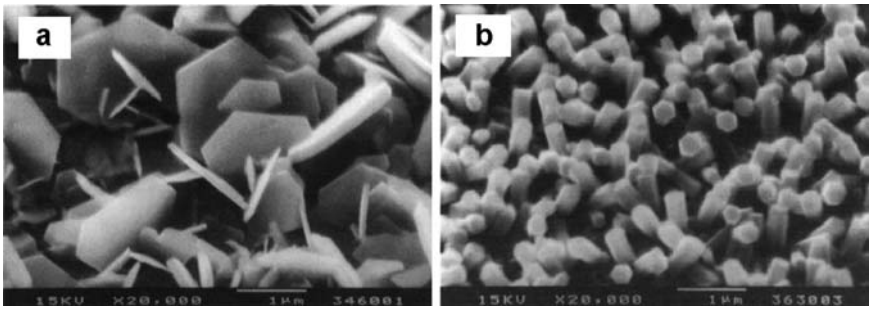

Fig. 18.5 ZnO films deposited with: (**a**) high zinc concentration on Au substrate; (**b**) low zinc concentration on tin oxide/glass substrate (Peulon and Lincot 1998) [reproduced by permission of The Electrochemical Society]

the electrodeposition bath (Oekermann, Yoshida, Schlettwein, Sugiura and Minoura 2001; Choi, Lichtenegger, Stucky and McFarland 2002).

Simultaneous electrodeposition of ZnO and dye molecules from aqueous solution was reported as well to achieve a deeper penetration of the dye molecules into the inorganic film, as compared with those obtained by adsorption of dye molecules by the pre-assembled particles (mostly limited to the top layers). Yoshida and coworkers (2000) conducted such deposition process in an aqueous solution of $Zn(NO_3)_2$ and eosin Y at 70°C and obtained ZnO/eosin Y dye-sensitized semiconductor films without high temperature annealing. The eosin Y molecules condensed at a sufficiently high concentration at both inside and on the surface of the film, which improved light absorption and IPCE.

18.3.2 Hydrothermal Methods

Hydrothermal methods have been widely used to fabricate well-ordered, highly crystalline materials (Sayari, Liu, Kruk and Jaroniec 1997; Feng and Xu 2001; Wang and Li 2002; Liu and Zeng 2003). Yoshida, Zhang and coworkers (2002) prepared nanocrystalline TiO_2 films by low-temperature hydrothermal treatment of a paste containing nanocrystalline TiO_2 powder and titanium salts (such as $TiCl_4$, $TiOSO_4$, and Ti(IV) alkoxide). The titanium salts were crystallized to form a chemical "glue" between the TiO_2 particles, resulting in crack-free, robust porous thick films up to 18 μm at temperatures as low as 100°C. With such thickness, the light-harvesting capacity could be maintained high which is not surprising, and the IPCE of the films was also promising because of the improved electron transport in the film since the connection of anatase TiO_2 particles was improved by the additional thin TiO_2 layer. Subsequent high-temperature annealing further elongated the electron lifetime upon the removal of the residual organic species, which might otherwise act as the surface states and recombination centers. Hosono et al. (2004) reported a hydrothermal

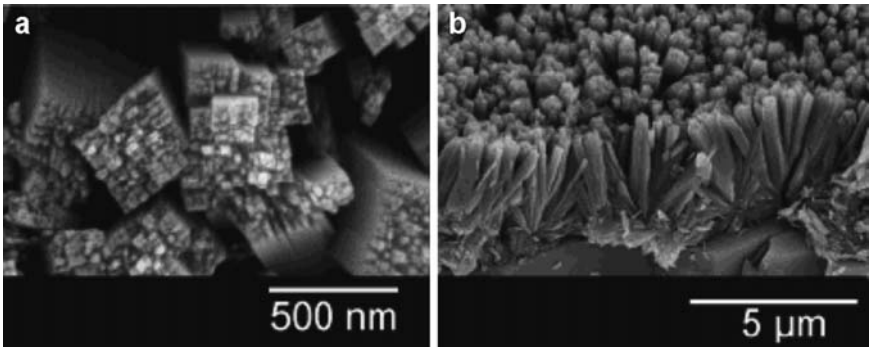

Fig. 18.6 Rutile TiO_2 films deposited by hydrothermal method: (**a**) top view; (**b**) cross-section view [reprinted with permission from Hosono et al. (2004), copyright 2004 American Chemical Society]

method to fabricated highly crystalline (nearly single-crystalline) rutile TiO_2 films over glass substrates. Hydrothermal treatment was conducted on an aqueous $TiCl_3$ solution containing high-concentration NaCl in Teflon-lined autoclaves at 200°C. The substrate was covered completely and continuously by the TiO_2 film consisting of rectangular parallel submicron pipes 150–250 nm in width and 3–4 μm in length, as shown in Fig. 18.6.

Guo et al. (2005a, b) reported the hydrothermal growth of large area, densely packed and well-oriented single-crystalline ZnO nanorod arrays on ITO substrates. To obtain high-quality ZnO nanorods, they firstly modified the ITO substrate surface by a few cycles of spin coating of an aqueous zinc nitrate/methenamine solution followed by annealing at 200°C. Then hydrothermal growth was carried out at 95°C by immersing the modified substrate in a diluted solution containing the same precursors. The resultant ZnO films consisted of well-aligned ZnO nanorod with diameters typically smaller than 150 nm and their thickness were around 4 μm, as shown in Fig. 18.7. The films exhibited high photoconversion efficiency as dye-sensitized photoelectrodes [the IPCE was comparable to much thicker ZnO nanoparticulate films tested under identical conditions (Rensmo, Keis, Lindstrom, Sodergren, Solbrand, Hagfeldt, Lindquist, Wang and Muhammed 1997)].

18.3.3 Electrochemical Anodization

TiO_2 nanotubes has been attracting attention in photoelectrochemical applications because they are believed to be capable of transferring electrons more efficiently than conventional nanoporous TiO_2 films (Adachi, Murata, Okada and Yoshikawa 2003). TiO_2 nanotubes can be synthesized by a variety of methods, such as sol–gel (Zhang, Bando and Wada 2001), sonochemical (Zhu, Li, Koltypin, Hacohen and Gedanken 2001) and surfactant-templated methods

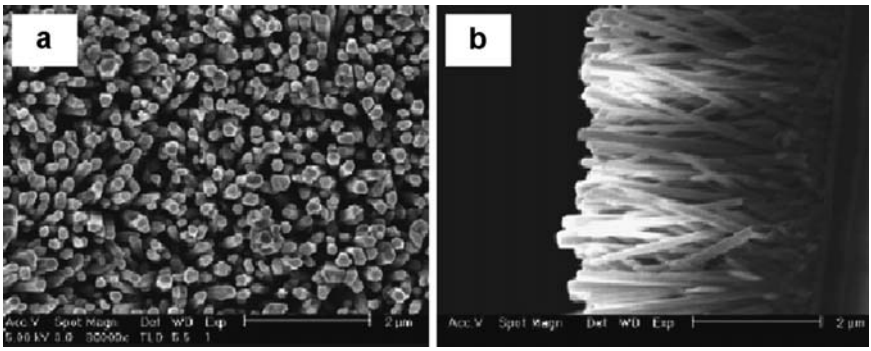

Fig. 18.7 ZnO nanorod arrays deposited on ITO substrates by hydrothermal method: (**a**) top view; (**b**) cross-section view [reprinted from Guo et al. (2005a), copyright (2005), with permission from Elsevier]

(Adachi et al. 2003). Recently, Shankar and coworkers (2007) has successfully developed a templateless method to directly from highly ordered TiO_2 nanotube arrays suitable for photoelectrodes.

Briefly, this method consists of the following steps: (1) a thin layer (∼500 nm) of Ti was RF sputtered onto FTO glass substrate; (2) the resulted film was anodized at a constant potential in an electrolyte solution of 0.5% HF and + acetic acid mixed at desired ratio; (3) after annealing at elevated temperatures, they obtained crystalline TiO_2 nanotube-array films of 360 nm thick, and with pore diameters of ∼46 nm and wall thickness of ∼17 nm (Mor, Shankar, Paulose, Varghese and Grimes 2006). By varying the electrolytes (fluoride ion-containing baths supplemented by dimethyl sulfoxide, formamide, ethylene glycol, and *N*-methylformamide, etc.) and the anodization voltage, TiO_2 nanotubes with lengths up to 220 μm (Shankar et al. 2007), pore diameters ranging from 20 to 150 nm, and length-to-width aspect ratio of ∼835 could be achieved, together with a remarkable photoconversion efficiency of 16.25% for H_2O photoelectrolysis (Paulose, Shankar, Yoriya, Prakasam, Varghese, Mor, Latempa, Fitzgerald and Grimes 2006). Figure 18.8 gives the SEM images of the resulted TiO_2 nanotube arrays. Using similar procedures, nanoporous Fe_2O_3 films were also fabricated with controlled pore size and length (Prakasam, Varghese, Paulose, Mor and Grimes 2006).

Other groups have also reported the fabrication of TiO_2 nanotube-based film electrodes by electrochemical anodization. For example, Quan et al. (2005) synthesized TiO_2 nanotube array films by anodizing Ti sheets in a 0.2 wt% HF aqueous solution under a potential of 20 V at room temperature. Their electrodes showed high and stable photoelectrocatalytic efficiency for the degradation of pentachlorophenol under UV irradiation. TiO_2 nanotube arrays can also be further coupled with other photosensitive materials such as polyoxometalate (POM) to form a composite photoelectrode by a hydrothermal method, as reported by Xie (2006), and the composite photoelectrode showed a high efficiency for photoelectrocatalytic degradation of bisphenol A due to the promotion of interfacial charge transfer caused

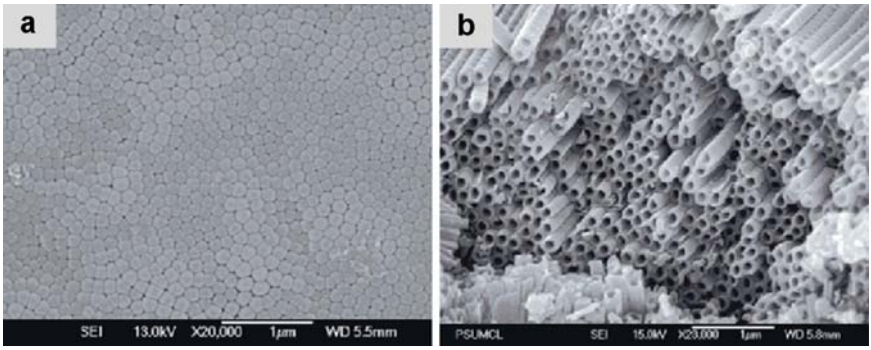

Fig. 18.8 Bottom surface (**a**) and top surface (**b**) of a TiO_2 nanotube-array grown at 60 V in an ethylene glycol electrolyte containing 0.25 wt% NH_4F [reprinted with permission from Paulose et al. (2006), copyright 2006 American Chemical Society]

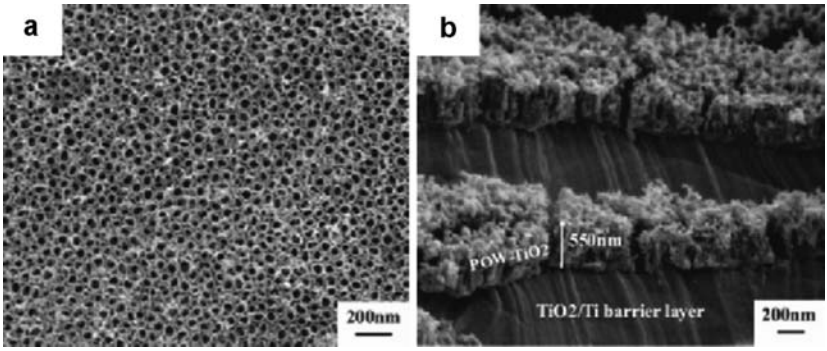

Fig. 18.9 SEM images of TiO_2 nanotube arrays (**a**) and coupled POM/TiO_2 film (**b**) [Xie (2006); copyright Wiley-VCH Verlag GmbH & Co. KGaA; reproduced with permission]

by the coupling modification. The SEM images of the TiO_2 nanotubes and the coupled POM/TiO_2 film are shown in Fig. 18.9. Feng et al. (2007) studied the formation of TiO_2 nanotube arrays under a wide range of pH conditions and found that not only acidic conditions but also neutral and basic conditions were suitable for the fabrication of TiO_2 nanotube arrays. By applying a more viscous electrolyte solution containing, for example, glycerol to inhibit the local current, concentration and pH fluctuations during the anodization process, very smooth-walled TiO_2 nanotube arrays have been obtained (Macak, Tsuchiya, Taveira, Aldabergerova and Schmuki 2005).

18.3.4 Template Methods

Template methods have been applied to synthesize semiconductor photocatalysts with well-ordered structures including nanowires (Miao, Xu, Ouyang, Guo, Zhao and Tang 2002), nanorods (Limmer, Seraji, Wu, Chou, Nguyen and Cao 2002),

nanotubes (Lakshmi, Dorhout and Martin 1997a; Lakshmi et al. 1997b) and nanoporous films. Generally, well-ordered materials that are feasibly dissolved via chemical methods can be used as "hard" templates. Polymeric materials, on the other hand, can serve as "soft" templates for the fabrication of ordered mesoporous films (Soler-Illia, Crepaldi, Grosso and Sanchez 2003).

18.3.4.1 "Hard" Template Methods

The most commonly used hard templates are anodic aluminum oxide (AAO) and track-etched polycarbonate membranes, both of which are porous structured and commercially available. The pore size and thickness of the membranes can be well controlled, which then determine the dimension of the products templated by them. The pores in the AAO films prepared electrochemically from aluminum metals form a regular hexagonal array, with diameters of 200 nm commercially available. Smaller pore diameters down to 5 nm have also been reported (Martin 1995). Without external influences, capillary force is the main driving force for the Ti-precursor species to enter the pores of the templates. When the pore size is very small, electrochemical techniques have been employed to enhance the mass transfer into the nanopores (Limmer et al. 2002).

Charles Martin's group has been working on the fabrication of nanoporous alumina membrane templates (Che, Lakshmi, Fisher and Martin 1998; Lee, Mitchell, Trofin, Nevanen, Soderlund and Martin 2002) and subsequent synthesis of nanostructured metal-oxide materials, including TiO_2, ZnO, WO_3, MnO_2, V_2O_5, and Co_3O_4, within the nanopores of the alumina membranes (Martin 1995; Lakshmi et al. (1997a, b)). They combined the sol–gel synthesis with the template method to fabricate for example, nanotubules and nanofibrils of TiO_2 using titanium isopropoxide as the precursor. First, a TiO_2 sol was formed within the mixture of titanium isopropoxide, ethanol, water, and HCl; the alumina template membrane was then dipped into the sol for desired amount of time, removed and dried in air, followed by thermal treatment to crystallize the TiO_2 products; finally after removing the alumina template in aqueous base solution, TiO_2 tubules or fibrils could be obtained. In this process, initially the TiO_2 sol was adsorbed on to the pore walls by forming Ti–O–Al bonds with Al–OH sites on the pore wall. After a longer time of contact, the pores could be further filled to form nanofibrils. Operation at higher temperatures also facilitated the formation of TiO_2 nanofibrils within shorter time. The TiO_2 nanofibers showed high activity for the decomposition of salicylic acid.

Direct sol filling was suggested to have potential limitations in that the sols commonly have a very low solid content ($\sim$5 vol%) which might not be high enough to form condense packing of solids in the pores. Increasing the concentration of the sol would result in a highly viscous sol that is very difficult to be transferred into the pores driven by the capillary force alone. Therefore, shrinkage, cracking, and defects can be formed by the large volume change upon drying when the solvent content is removed. To overcome this limitation, electrophoretic motion was introduced by an applied electric field to increase the mass transfer of the TiO_2 sol particles, which

were positively charged by appropriately controlling the pH of their environment, into the nanopores of the template membrane. Limmer and coworkers (2001, 2002) demonstrated that this method could effectively increase the density of the sol inside the polycarbonate membrane, and a less significant shrinkage was observed after the samples were fired at 700–800°C to crystallize the nanorods. Note that the polycarbonate membrane could be burned off at around 400°C, i.e., below the temperature at which the metal oxide could be fully crystallized. Some of the insufficiently crystallized nanorods with low mechanical strength could be broken or distorted during the firing process. Recently, this method has also been applied to the production of transparent conducting ITO membranes, which have an apparent resistivity of 5Ω cm (Limmer, Cruz, and Gao 2004).

The electrophoretic sol–gel template method could overcome the pore size limitation to certain extent (down to a few tens of nanometers), but it is still limited by the size of the sol particles which were preformed prior to being subjected to the electric field. To address this problem, Miao et al. (2002) reported an electrochemical sol–gel template method in which the sol particles were generated within the pores of the AAO template membrane, as shown in Fig. 18.10.

The hydroxyl ions were first generated from the cathodic reduction of the nitrate ions in a stock solution containing TiO^{2+} ions (Natarajan and Nogami 1996). These hydroxyl ions increased the local pH in the pores of the AAO template, leading to

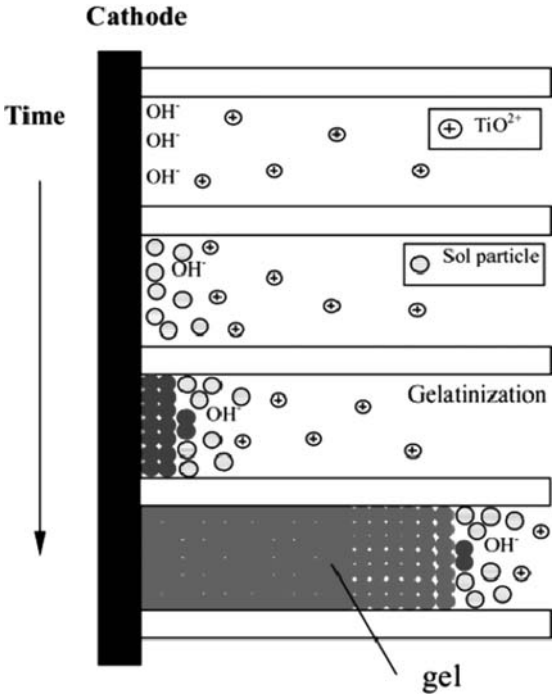

Fig. 18.10 Illustration of the electrochemical sol–gel template process. [reprinted with permission from Miao et al. (2002), copyright 2002 American Chemical Society]

the formation of titanium oxyhydroxide sol particles which was further converted into a network of gel by bond formation between the sol particles within the pores of the template. Finally, the thermal treatment and the removal of the AAO template resulted in the TiO_2 single-crystalline nanowire arrays. This method successfully pushed the template-pore-size limit down to around 10 nm and a much higher surface area of the products could be achieved. Another advantage is that a higher packing density of the sol particles could be obtained because of the high pH gradient constructed at the bottom of the pores, hence less shrinkage and cracking happened during the thermal treatment especially for the smaller-diameter pores since the pH gradient is higher in this case than that for larger-diameter pores.

18.3.4.2 "Soft" Template Methods

Soft polymeric materials, for example, the so-called block copolymers, have been successfully used as templates for the synthesis of well-ordered, mesoporous nanostructured materials (Yang, Deng, Zhao, Feng, Pine, Chmelka, Whitesides and Stucky 1998; Zhao, Feng, Huo, Melosh, Fredrickson, Chmelka and Stucky 1998a; Zhao, Huo, Feng, Chmelka and Stucky 1998 b). This method is also named "evaporation-induced self-assembly" (Grosso, Babonneau, Sanchez, Soler-Illia, Crepaldi, Albouy, Amenitsch, Balkenende and Brunet-Bruneau 2003; Choi, Mamak, Coombs, Chopra and Ozin 2004; Choi, Mamak, Speakman, Chopra and Ozin 2005), which can produce a variety of mesostructured shapes including powders, films, monoliths and aerosols. A recent review has covered more details of the copolymer-templated synthesis methods (Soler-Illia et al. 2003). For the fabrication of TiO_2 mesoporous films, commercially available block copolymers (such as Pluronic P123 and F127) are dissolved and mixed with an acidified alcoholic solution containing the TiO_2 precursors, for example, titanium(IV) ethoxide or propoxide. Aging of the solution is usually required before the film casting. Control over the temperature and the relative humidity of the film-aging environment is very important for the formation of ordered mesostructures. Slow temperature-increasing calcinations lead to the removal of the organic components and crystallization of the inorganic walls of the mesoporous structures. The TiO_2 films exhibited much higher photocatalytic activities than conventionally assembled films (Wark, Tschirch, Bartels, Bahnemann and Rathousky 2005). Such films can be further modified, for instance, by introducing noble metal nanoclusters into the mesopores (Yu, Wang, Wu, Ho, Zhang and Zhou 2004; Wang, Yu, Yip, Wu, Wong and Lai 2005) to enhance the photocatalytic activities. Stucky's group reported film-structured Ag/TiO_2 photoelectrodes using surfactant-directed titania as the support (Andersson, Birkedal, Franklin, Ostomel, Boettcher, Palmqvist and Stucky 2005). Hexagonal mesoporous titania film was first made by dip coating quartz slides from the titanium precursor mixed with Pluronic P123 as the structure-directing agent. As low burning temperature as 250°C was used to keep the long-range order of the mesoporous film. The remaining surfactant which was not completely burned off at this temperature was said to reduce the silver ions and form metallic silver nanoparticles.

18.3.5 Methods for Synthesis of Composite Photoelectrodes

The above-mentioned aqueous-phase methods have shown their ability to produce structure-controlled (on the nanometer scale) photoelectrodes. In this section, several other methods operated in aqueous phase will be briefly discussed with a focus on the synthesis of composite photocatalysts such as bimetal oxides and metal/semiconductor nanocomposite materials.

18.3.5.1 Wet Impregnation Method

Wet impregnation method in some publications it was also called the incipient wetness impregnation method (Song et al. 2001; Bowker, Millard, Greaves, James and Soares 2004) is a widely applied technique to synthesize composite photocatalysts (Papp, Soled, Dwight and Wold 1994; Pal, Sharon and Nogami 1999; Reddy, Chowdhury and Smirniotis 2001; Shchukin and Caruso 2003; Bandyopadhyay, Birkner, van den Berg, Klementiev, Schmidt, Grunert and Gies 2005), metal ion-doped semiconductors (Di Paola, Marci, Palmisano, Schiavello, Uosaki, Ikeda and Ohtani 2002; Tayade, Kulkarni, and Jasra 2006), and metal/semiconductor nanocomposites (Haruta, Uphade, Tsubota and Miyamoto 1998; Bowker et al. 2004; Jing, Li, Wang, Xin, Fu, Wang and Cai 2005; Li, Liu, Nag and Croziers 2005b; Bavykin, Lapkin, Plucinski, Torrente-Murciano, Friedrich and Walsh 2006). The general route consists of the following steps: (1) the supporting material (e.g., metal-oxide particles or films) is first impregnated with aqueous solutions of the target precursors (such as metal ions); (2) after standing for desired amount of time, water is evaporated by heating the impregnated sample; (3) the dried solid is further burned at desired temperatures to form, the final products. For example, WO_3/TiO_2 and MoO_3/TiO_2 composite nanopowders were prepared by impregnating TiO_2 nanoparticles with aqueous ammonia solution of H_2WO_4 and aqueous solution of ammonium paramolybdate, followed by drying and burning at different temperatures (Papp et al. 1994). Dispersion of MoO_3 on various binary and ternary metal oxide supports (TiO_2/ZrO_2, TiO_2/Al_2O_3, TiO_2/SiO_2, $TiO_2/SiO_2/ZrO_2$, etc.) has also been reported (Reddy et al. 2001). The resulted metal-oxide composite powders can be fixed onto conducting support to serve as electrodes for photoelectrocatalytic applications.

Direct synthesis of film-structured TiO_2/ITO, TiO_2/ZrO_2/ITO, TiO_2/In_2O_3/ITO and TiO_2/SnO_2/ITO photoelectrodes have also been achieved by impregnating organic templates with aqueous TiO_2 sols, as reported by Shchukin and Caruso (2003). Cellulose acetate and polyamide membrane filters were used as the organic templates, which were first attached to the conducting surface of the ITO glass substrate. Then the templates were immersed in the target aqueous metal oxide sols (or their mixtures at desired molar ratios) and stored at room temperature in the dark for 24 h. Water was evaporated by heating at 60°C, followed by calcination at 500°C to burn out the organic templates and result in highly porous films supported

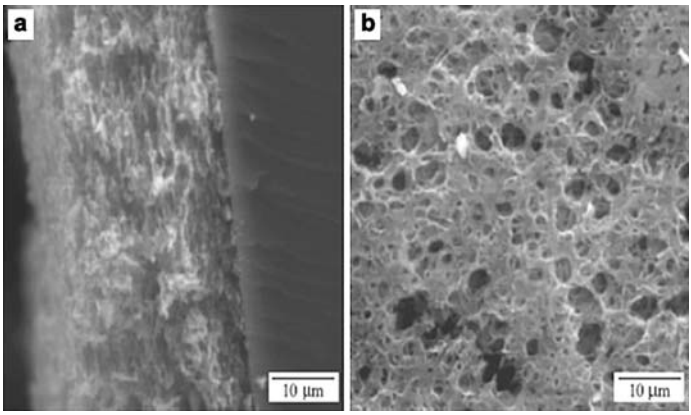

Fig. 18.11 TiO_2 film supported on ITO surface: (**a**) view from the edge and (**b**) view from the top surface of the titania film [Shchukin and Caruso (2003) Copyright Wiley-VCH Verlag GmbH & Co. KGaA, reproduced with permission]

on ITO substrate. The morphology of the TiO_2/ITO film is shown in Fig. 18.11. Its photoelectrochemical activity was twice that of a spin-coated titania film electrode. TiO_2/ZrO_2/ITO, TiO_2/In_2O_3/ITO and TiO_2/SnO_2/ITO films showed different photocatalytic activities, depending on the molar ratio between TiO_2 and the other metal oxide component and the nature of it.

Metal ion-doped TiO_2 photocatalysts can be synthesized by the wet impregnation method. The difference between such materials and the mixed metal oxides is that the impregnated metal ions in the former take the substitutional or interstitial sites of the TiO_2 lattice (which depends on their relative ionic radius to Ti^{4+} cations and does not significantly alter the XRD pattern and the crystallinity of TiO_2), while in the latter the impregnated metal species can form its own localized oxide phase segregated from TiO_2 and can be detected from XRD measurements. TiO_2 photocatalysts doped by metal ions of Co, Cr, Cu, Fe, Mo, V, W, and Ni have all been prepared by this method (Di Paola et al. 2002; Tayade et al. 2006).

Noble metal nanoparticles deposited on TiO_2 support have also been achieved using the wet impregnation method. An aqueous stock solution of noble metal precursors (such as chloroauric acid in the case of gold (Bowker et al. 2004)) was first prepared to impregnate the TiO_2 substrates at desired loadings. Different from the metal ion-doped TiO_2, the noble metal ionic species in this case normally undergo a reduction process during the aging or heating process to form metallic nanocrystals. Li and coworkers (2005b) also reported an in situ reduction of Ni^{2+} ions on TiO_2 support to form metallic Ni/TiO_2 heterojunctions at atomic resolution as observed using environmental transmission electron microscopy.

18.3.5.2 Photodeposition

Photodeposition has been frequently used in synthesizing metal/semiconductor composite materials such as Ag/TiO_2, Pt/TiO_2 and Au/TiO_2 (Tada, Teranishi, Inubushi and Ito 2000; Tada, Mitsui, Kiyonaga, Akita and Tanaka 2006; Vorontsov, Stoyanova, Kozlov, Simagina and Savinov 2000; Soejima, Tada, Kawahara and Ito 2002; Chan and Barteau 2005). It takes the advantage of the semiconductor photocatalysts under irradiation to reduce the metal precursors in an aqueous or organic solution, and metal nanoparticles are deposited on the surface of the photocatalyst particles. Normally the metal precursors (for example, $AgNO_3$ for Ag, $HAuCl_4$ for Au or H_2PtCl_6 for Pt) are first dissolved to make a solution, in which the photocatalyst particles are loaded and dispersed. Then the system is subjected to bandgap irradiation to deposit the noble metal nanoparticles on the photocatalyst surface. Chan and Barteau (2005) used this method on a small scale (on a TEM copper grid loaded with TiO_2 particles) and observed the formation of Au/TiO_2 nanocomposites as exemplified in the TEM images in Fig. 18.12. Tada et al. (2006) proved that the Au/TiO_2 photocatalyst was capable of fast photoreduction of elemental S to S^{2-} in an aqueous environment (Kiyonaga, Mitsui, Torikoshi, Takekawa, Soejima and Tada 2006). Based on this finding, they synthesized a $Au/CdS/TiO_2$ nanocomposite photocatalyst with selective deposition of CdS at the Au spots on the surface of TiO_2 nanoparticles, as illustrated in Fig. 18.13. Subsequent photodeposition of Pt on this material could also be achieved to give more complex structures.

Cozzoli and coworkers (2004) synthesized Ag/TiO_2 nanocomposites by photodeposition of Ag from a $CHCl_3$ solution of surfactant-stabilized TiO_2 nanorods containing $AgNO_3$ as the Ag precursor. Careful control of the irradiation condition was able to give the Ag/TiO_2 nanocomposites with various Ag particle-size and its contact modes with the TiO_2 nanorods. Film-structured photoelectrodes

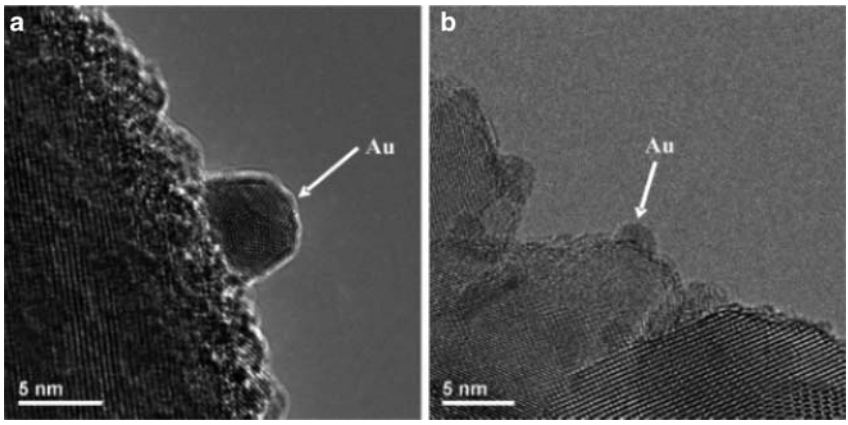

Fig. 18.12 Au/TiO_2 nanocomposites obtained by photodeposition on different TiO_2 nanoparticles ((**a**) commercial and (**b**) prepared by MOCVD) in $HAuCl_4$ solution [reprinted with permission from Chan and Barteau (2005), Copyright 2005 American Chemical Society]

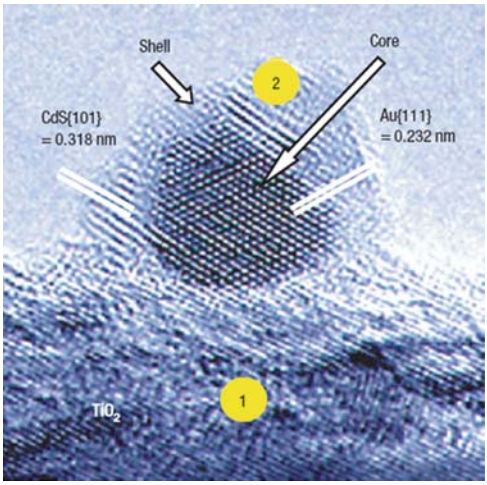

Fig. 18.13 Geometrical structure of $Au/CdS/TiO_2$ composite nanoparticle formed on TiO_2 [adapted by permission from Macmillan Publishers Ltd: Nature Materials (Tada et al. 2006), copyright (2006)]

loaded with noble metal nanoparticles were also fabricated using the photodeposition method. He and coworkers (2003) fabricated $Ag/TiO_2/ITO$ photoelectrodes by photodeposition of Ag onto TiO_2 films supported on ITO glass. Combined with a layer-by-layer assembly technique, He and coworkers (2004) prepared another type of Ag-loaded TiO_2/ITO photoelectrode. In this method, TiO_2 nanosheets were first hybridized with an Ru(II) complex, and then the hybridized species was deposited on an ITO substrate, followed by dipping it into an aqueous $AgNO_3$ solution. The film was subjected to UV irradiation to form the Ag nanoparticle-loaded photoelectrode. Jin and Shiraishi (2004) conducted photodeposition of Pd, Cu and Pt nanoparticles on a transparent TiO_2 film supported by a glass tube, and the product showed increased activity in the photocatalyticoxidation of several organic compounds in water.

18.3.5.3 Deposition–Precipitation

The deposition–precipitation method as proposed by Haruta et al. (1993) provides another way to synthesize composite materials with noble metal nanoparticles over metal-oxide supports. The synthesis of gold and platinum nanoparticles supported on various metal oxide substrates (such as TiO_2, ZnO, CeO_2, Co_3O_4 and Fe_2O_3) (Bamwenda, Tsubota, Nakamura and Haruta 1995; Boccuzzi, Chiorino, Tsubota and Haruta 1996; Centeno, Carrizosa and Odriozola 2003; Moon, Lee, Park and Hong 2004; Zanella, Delannoy and Louis 2005; Li, Comotti and Schuth 2006) has been continually reported in the past one and a half decades.

In a typical deposition–precipitation method (for example, to synthesize gold nanoparticles supported by TiO_2), an aqueous solution of $HAuCl_4$ is heated and the pH is adjusted to a desired value; then an appropriate amount of TiO_2 nanopowders is added to the solution. After aging the slurry for an effective adsorption of the metal precursor onto the surface of TiO_2, the mixture is washed and the solid content is separated out. The solids are dried and calcined in air at moderate temperatures to result in metallic gold nanoparticles on TiO_2 surface. The mechanism of the formation of metallic gold and the oxidation states of the gold species after being deposited on TiO_2 surface are still to be elucidated (Zanella 2005; Dimitratos, Villa, Bianchi, Prati and Makkee 2006; Venkov, Fajerwerg, Delannoy, Klimev, Hadjiivanov and Louis 2006). It seems that the "precipitation" part is missing from the "deposition–precipitation" term. Actually the precipitation part has been originally designed to obtain metal hydroxide supports from aqueous solution of metal salts prior to the deposition of metal nanoparticles. Obviously it is not a suitable way to prepare TiO_2 by aqueous precipitation. For other metal oxides (e.g., Fe_2O_3 (Khoudiakov, Gupta and Deevi 2005)), the precipitation procedure has indeed been included using suitable salts under an alkaline environment. Nowadays due to the easy availability of nanosized metal-oxide materials, direct application of such metal oxides as the supporting materials in the deposition–precipitation method is common practice (Zanella, Giorgio, Henry and Louis 2002; Zanella and Louis 2005; van Bokhoven, Louis, Miller, Tromp, Safonova, and Glatzel 2006; Weiher, Beesley, Tsapatsaris, Delannoy, Louis, van Bokhoven and Schroeder 2007). It is suggested that the supporting materials should have a surface area of at least $50\,m^2\,g^{-1}$ (Bond and Thompson 1999). Besides working as photocatalysts (You, Chen, Zhang and Anpo 2005), such materials are also under intensive investigation in gold-catalyzed chemical reactions including low-temperature CO oxidation.

18.4 Gas-Phase Deposition

Generally, gas phase deposition for the fabrication of photoelectrodes possess the advantage of direct formation of highly crystalline films that do not need post-thermal treatments as often required in the aqueous phase deposition methods discussed in Sect. 18.3. But the equipments for conducting gas phase deposition are more expensive because conditions like high vacuum are frequently required during the operation processes. In this section, recent developments in the fabrication of photoelectrodes using chemical vapor deposition (CVD), spray pyrolysis, magnetron sputtering, and ion implantation will be discussed.

18.4.1 CVD Methods

CVD has been a powerful technique in synthesizing film-structured materials (such as metal-oxide semiconductors, diamond-related materials and carbon nanotubes)

with a variety of morphologies and properties. In a typical CVD process, the substrate is exposed to one or more volatile precursors, which react and/or decompose on the surface of the substrate to produce the desired deposit. Frequently, volatile byproducts are also formed, which are removed from the reaction region by carrier gas through the reaction chamber. In the fabrication of film-structured semiconductor photoelectrodes, some new techniques has been incorporated into traditional CVD, and new methods such as metal-organic chemical vapor deposition (MOCVD) (Babelon, Dequiedt, Mostefa-Sba, Bourgeois, Sibillot and Sacilotti 1998; Gauthier, Bourgeois, Sibillot, Maglione and Sacilotti 1999; Lee, Park and Ko 2000; Lee, Huang and Wu 2005; Won, Wang, Jang and Choi 2001; Lo Nigro, Toro, Malandrino and Fragala 2003; Zhang, Zhou and Lei 2006), light-induced CVD (Halary, Benvenuti, Wagner and Hoffmann 2000; Murakami, Kijitori, Kawashima and Miyasaka 2004; Halary-Wagner, Bret and Hoffmann 2005), aerosol-assisted CVD (Backman, Auvinen and Jokiniemi 2005; Conde-Gallardo, Guerrero, Fragoso and Castillo 2006; Palgrave and Parkin 2006), plasma-enhanced CVD (Okuyama, Honma and Ohno 1999; Karches, Morstein, von Rohr, Pozzo, Giombi and Baltanas 2002) and ion-beam-induced CVD (Espinos, Fernandez, Caballero, Jimenez, Sanchez-Lopez, Contreras, Leinen and GonzalezElipe 1997) have been successfully developed. A few examples will be given here to illustrate their application to fabricate TiO_2-based photoelectrodes.

The most widely used precursors for the CVD-synthesis of TiO_2 thin films are $TiCl_4$ and titanium isopropoxide. The chemical nature of the precursors has been shown to have a direct influence on the properties of the deposited TiO_2 films, as reported by Evans and coworkers (2006). The existence of oxygen in titanium isopropoxide molecules makes it possible for an intramolecular reaction to take place.

A typical atmospheric-pressure CVD process was exemplified by the work of Hyett et al. (2006). The authors fabricated TiO_2 thin films over float glass substrates using $TiCl_4$ and ethyl-acetate as precursors. After being vaporized in heated bubblers, the precursors were introduced to the deposition region, and the substrate temperature was adjusted to control the crystal orientation and phase of the deposited TiO_2 films. Low pressure conditions can also be used to make TiO_2 films using the CVD method. The reduced pressure in the deposition chamber could reduce the unwanted gas-phase reactions and improve the film uniformity across the substrates. MOCVD uses metal-organic precursors or a mixture of them to fabricate both pure and doped materials. For example, Nd^{3+}, Pd^{2+}, Pt^{4+} or Fe^{3+} ion-doped TiO_2 was synthesized using titanium isopropoxide and acetylacetonates of the corresponding metals as the precursors (Shah, Li, Huang, Jung and Ni 2002). Plasma-enhanced CVD allows significant reduction in the substrate temperature, as compared with conventional CVD processes. This makes it possible to deposit materials with poor thermal tolerance. A high deposition rate of 900 nm min^{-1} could be obtained. Besides, the control of the plasma-induced reactions also allows one to optimize the film composition and its microstructure (Yang and Wolden 2006). Aerosol-assisted CVD generates aerosol droplets (for example, by an ultrasonic humidifier) containing the precursor solution which was transferred by the carrier gas to the reaction region. This method has been used when the precursors

are nonvolatile or thermally unstable under the conditions typical in a conventional atmospheric-pressure CVD process. Moreover, by designing precursors specifically for the aerosol-assisted CVD, the restrictions of volatility and thermal stability can be loosened and new precursors and films can be investigated. For example, gold nanoparticles in toluene solution containing titanium isopropoxide or tungsten phenoxide could be used as the precursors to deposit Au/TiO_2 or Au/WO_3 composite films by the aerosol-assisted CVD (Palgrave and Parkin 2006). Light-induced CVD enables manipulating light beams with high spatial resolution on the substrate surface, thus achieving localized deposition of film-structures. Both lamps and laser beams have been utilized to heat the substrates at temperatures much lower than that for conventional thermal CVD processes (Halary-Wagner et al. 2004).

18.4.2 Spray Pyrolysis

Spray pyrolysis has been an attractive synthesis route for nanostructured films because large-scale thin films can be produced feasibly on various types of substrates (such as glass and stainless steel) (Kim and Yoon 1991; Zhang, Zhu and Brodie 1992; Cui, Shen, Gao, Dwight and Wold 1993; Okuya, Prokudina, Mushika and Kaneko 1999; Teleki, Pratsinis, Kalyanasundaram and Gouma 2006). For the fabrication of TiO_2-based films, the precursors frequently used here are similar to those used in CVD methods, including titanium isopropoxide and $TiCl_4$. In this method, the substrate is preheated to desired temperatures; then the pyrolysis procedure is initiated using compressed gas (e.g., air or oxygen) to spray the precursor solution and form a mist over the substrate. The temperature of the substrate should be maintained high enough to burn off the organic content in the precursor solution and leave behind a compact TiO_2 thin film. The temperature can be lowered upon the landing of the cool mist, therefore, an intermittent operation can be practiced for the recovery of the substrate temperature. Repeated cycles of spray-pyrolysis can produce films with desired thickness. The final crystal structure of the product usually depends on the specific precursor solutions employed. An example of such-made TiO_2 film is shown in Fig. 18.14. The film was deposited over a glass substrate using an isopropanol solution of titanium isopropoxide/$TiCl_4$ as the precursor, and the substrate temperature was 430°C (Okuya et al. 1999).

Compact TiO_2 layer incorporated in dye-sensitized solar cells has been deposited using this method (Peng, Jungmann, Jager, Haarer, Schmidt and Thelakkat 2004). Aqueous solution of peroxo-titanium complex was also used as the precursor solution to produce TiO_2 films using spray-pyrolysis (Natarajan, Fukunaga and Nogami 1998). Other metal-oxide semiconductor films such as WO_3 (Ortega, Martinez, Acosta and Magana 2006) and ZnO (Studenikin, Golego and Cocivera 1998; Paraguay, Estrada, Acosta, Andrade and Miki-Yoshida 1999) have also been fabricated by this method. Because the precursor solutions can be easily prepared by simply mixing various species at desired molar ratios (especially for water soluble salts), a variety of doped semiconductor films (Badawy 1997; Bougrine, El Hichou,

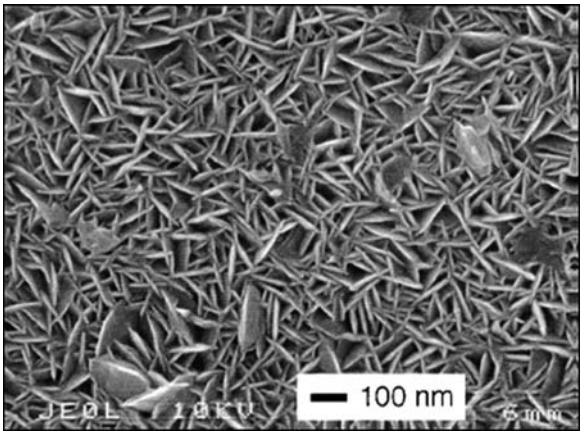

Fig. 18.14 TiO_2 film deposited by spray-pyrolysis method using $TiCl_4$/titanium isopropoxide as the precursor [reprinted from Okuya et al. (1999), copyright 1999, with permission from Elsevier]

Addou, Ebothe, Kachouane and Troyon 2003; Manivannan, Seehra, Majumder and Katiyar 2003; Li, Haneda, Hishita, Ohashi and Labhsetwar 2005a; Ilican, Caglar, Caglar and Yakuphanoglu 2006; Teoh, Amal, Madler and Pratsinis 2007) have been produced by spray pyrolysis. For instance Badawy (1997) prepared indium-incorporated TiO_2 thin films with an ethanol solution of a $TiCl_4/InCl_3$ mixture and the spray-pyrolysis process was operated at 450°C. Bougrine et al. (2003) synthesized Sn-doped ZnO films using an aqueous mixture of $ZnCl_2$ and $SnCl_2$ with the temperature of the glass substrate maintained at 450°C. Manivannan et al. (2003) obtained cobalt-doped TiO_2 films using an ethanol solution of titanium acetylacetonate and cobalt nitrate, which was sprayed by N_2 gas over glass substrates kept at 400°C followed by annealing at 500°C in air to remove the organic contaminants. Li and coworkers (2005a) used H_2TiF_6 as the single-component precursor to prepare fluorine-doped TiO_2 photocatalysts. Ilican et al. (2006) prepared In-doped ZnO nanofiber thin films over glass substrates at 350°C, using zinc acetate hydrate and indium chloride dissolved in the H_2O/methanol mixture as the precursor solution. Because the precursor species can be premixed to achieve a homogeneous distribution in their solution, this method is useful for the synthesis of homogeneously doped materials.

18.4.3 Magnetron Sputtering

Magnetron sputtering, one type of physical vapor deposition (PVD) method, is a powerful and flexible method that can be used to coat virtually any surface with a wide range of materials. It removes atomized materials from a solid by high-energy bombardment of its surface layers with ions or neutral particles. Prior to the

sputtering process, a high vacuum should be achieved, followed by the introduction of a closely controlled flow of an inert gas to raise the pressure to the minimum needed to operate the magnetrons. After a proper type of power is supplied to a magnetron sputtering system, positive ions driven by the electric field collides with the atoms at the surface of the target solid, accompanied by an energy transfer which, if larger than about three times the surface binding energy, will make the surface atoms sputtered. The type of power supply depends on the target materials, i.e., for pure metals a DC power supply can be used (Zheng, Wang, Xiang and Wang 2001), while for semiconductors and insulators a pulsed DC or a radio-frequency power supply is required. Deposition can be carried out in either nonreactive (inert gas only such as Ar) or reactive (inert and reactive gas such as N_2 or O_2 mixed with Ar) discharges with single- or multielemental targets. During the magnetron sputtering process, a magnetic field is used to trap secondary electrons close to the targets, which follow helical paths around the magnetic field lines undergoing more ionizing collisions with neutral gaseous near the target. This enhances the ionization of the plasma near the target and leads to a higher sputtering rate. Meanwhile it is capable of sustaining the plasma at a lower pressure. Following a condensation of the sputtered species, films can be obtained on the substrate placed close to the target material.

Magnetron sputtering has been applied to fabricate a wide range of film-structured photocatalyst electrodes, including pure semiconductors (Weinberger and Garber 1995; Dumitriu, Bally, Ballif, Hones, Schmid, Sanjines, Levy and Parvulescu 2000; Takeda, Suzuki, Odaka and Hosono 2001; Ohno, Sato, Kon, Song, Yoshikawa, Suzuki, Frach and Shigesato 2003), ion-doped semiconductors (Lindgren, Mwabora, Avendano, Jonsson, Hoel, Granqvist and Lindquist 2003; Visinescu, Sanjines, Levy, Marcu and Parvulescu 2005; Kitano, Funatsu, Matsuoka, Ueshima and Anpo 2006) and metal-oxide composites (Takahashi, Nakabayashi, Yamada and Tanabe 2003; Kanai, Nuida, Ueta, Hashimoto, Watanabe and Ohsaki 2004; Liu, Zhao, Zhang, Zhao, He and Feng 2005). In the following context a few examples will be given to emphasize some key parameters (such as the sputtering pressure the substrate temperature, and the chemical nature of the reactive sputtering gas) that influence the structure and properties of the films obtained.

High-quality photocatalytically active TiO_2 films have been deposited by the magnetron sputtering method. For example, Weinberger and Garber (1995) prepared highly crystalline (without post-annealing), porous microcolumnar-packed anatase TiO_2 films (as shown in Fig. 18.15) by reactive DC magnetron sputtering using titanium metal target and O_2/Ar sputtering. The films showed high activity for photodecomposition of gaseous pollutants such as C_2H_2 and C_2Cl_3H in air.

Zheng, Wang, Xiang and Wang and coworkers (2001) deposited TiO_2 thin films on glass substrates in a DC magnetron sputtering system using a mixture of Ar and O_2 under 5.0 Pa pressure in the deposition chamber, and the substrate temperature was kept at 200°C during the sputtering process. Yamagishi et al. (2003) prepared polycrystalline anatase TiO_2 thin films on glass substrates (as shown in Fig. 18.16) using an radio frequency (RF) magnetron sputtering method under varied sputtering pressures. The authors revealed a dependency of their photocatalytic activity on the sputtering pressure, i.e., the activity decreased with the decrease in the total

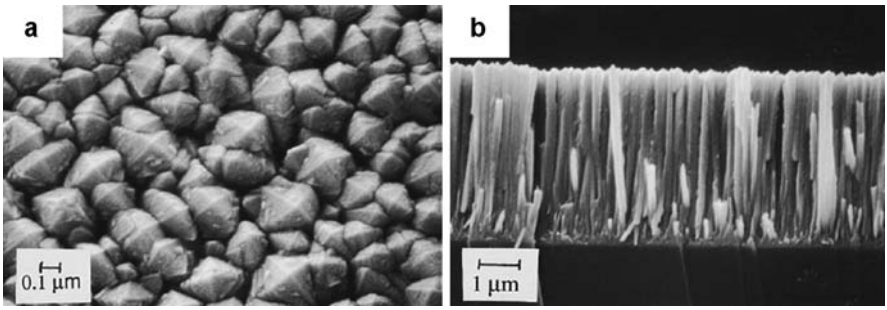

Fig. 18.15 TiO_2 films deposited by reactive DC magnetron sputtering: (**a**) Top view and (**b**) cross-sectional view [reprinted with permission from Weinberger and Garber (1995), Copyright 1995, American Institute of Physics]

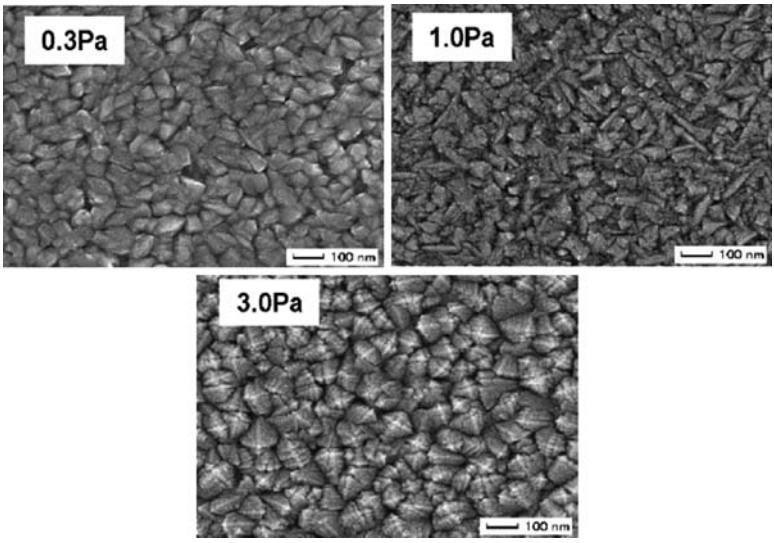

Fig. 18.16 TiO_2 thin films deposited by RF magnetron sputtering under various pressure [reprinted from Yamagishi et al. (2003), copyright 2003, with permission from Elsevier]

sputtering pressure in the range of 0.3–3 Pa because of the defect level generated by the bombardment of the high-energy particles on the growing film surface. Similar trends were confirmed by Zerman and Takabayashi (2003), who also found that the photocatalytic activity of magnetron sputtering-deposited TiO_2 films increased with the increasing film thickness if the films were prepared at higher sputtering pressures.

Zhang and coworkers (2004) studied the influence of the Ar gas flow rate on the properties of the deposited TiO_2 films and found that the photocatalytic degradation of methyl orange was enhanced when the Ar flow rate increased, which was ascribed to the dependency of both the crystallite size of TiO_2 and the optical properties (transmittance and reflectance) of the films on the Ar flow rate. The

operation mode of the magnetron also has an influence on the crystallinity and the photocatalytic performance of the sputtered TiO_2 photoelectrodes, as reported by Glöβ and coworkers (2005). Kikuchi et al. (2006) fabricated visible-light-sensitive TiO_2 films over optically transparent electrode (OTE) substrates by RF magnetron sputtering of a high-purity sintered TiO_2 target in an Ar/O_2 mixture. The working pressure inside the sputtering chamber was kept at 1.0 and 2.0 Pa, the temperature was controlled at 400 and 600°C, and the substrate holder was rotated for uniform deposition of TiO_2. The light absorption of such-deposited TiO_2 films could be extended into visible region at wavelengths up to 600 nm (Matsuoka, Kitano, Takeuchi, Anpo and Thomas 2005) that was caused by the decrease in the O/Ti ratio from the surface ($O/Ti = 2.00$) to the bottom ($O/Ti = 1.93$), i.e., the creation of oxygen vacancies. The films were capable of photocatalytic splitting of water under visible-light irradiation, though the IPCE was still limited due to the recombination of photogenerated electrons and holes.

Nitrogen-doped TiO_2 films have been successfully fabricated by magnetron sputtering methods by adding N_2 as a reactive gas into the sputtering chamber. Lindgren, Mwabora, Avendano, Jonsson, Hoel, Granqvist and Lindquist and coworkers (2003) deposited nitrogen-doped TiO_2 films by DC magnetron sputtering using a mixture of Ar, N_2, and O_2. Their characterization results showed that the crystal structure of the films varied from rutile to anatase depending on the nitrogen content, i.e., the portion of anatase phase increased with increasing the nitrogen content, which was controlled by increasing the N_2 pressure in the sputtering chamber. All the N-doped TiO_2 films showed visible-light absorption in the wavelength range from 400 to 535 nm. Similarly, Anpo Katino and coworkers (2005, 2006) introduced nitrogen into the sputtering gas (Ar) in the magnetron sputtering system and obtained N-doped TiO_2 film photoelectrodes showing photocatalytic activity for water splitting under anodic bias and visible-light irradiation with wavelengths up to 550 nm. The extent of substitution of nitrogen into the lattice oxygen positions of TiO_2 can also be controlled by changing the N_2/Ar ratio. The surface morphology and roughness of the deposited N-doped TiO_2 films were influenced by the concentration of N_2. But the nitrogen-doping level does not always go up with increasing the N_2 flow rate. Tu et al. (2006) fabricated p-type nitrogen-doped ZnO films by RF magnetron sputtering with Ar gas mixed with various concentrations of N_2. Their XPS data showed a decrease of N/Zn atomic ratio as the N_2 flow rate was increased. P-type nitrogen-doped Cu_2O films were also deposited by reactive RF magnetron sputtering using Cu metal as the target and $Ar/O_2/N_2$ as the sputtering gas (Ishizuka, Kato, Maruyama and Akimoto 2001).

Metal ion-doped or binary-oxide semiconductor films can be obtained by magnetron (co-)sputtering using appropriate combination of various metals (and/or their oxides) as the target material. The deposition conditions should be closely controlled to achieve a homogeneous distribution of the metal ion dopants because the two target materials may have different sputtering rates. By mixing different amounts of alumina powders as the Al doping source with ZnO powders, Kim and coworkers (1997) prepared Al-doped ZnO films on glass or Si substrates. A bandgap widening was observed, depending on both the Al doping level and the microstructure of the films. Using titanium and iron mixed metal target, Zhang

et al. (2003) prepared Fe-doped TiO_2 films by the pulsed DC magnetron cosputtering method. In this case, the Fe_2O_3 phase occurred in the high iron concentration samples. Liu et al. (2005) fabricated TiO_2/CeO_2 composite films using TiO_2/CeO_2 composite disks as the target operated at temperatures lower than 150°C, and the films showed enhanced photoactivity due to the existence of CeO_2 which favored the photogenerated electron transfer as compared with pure TiO_2 films. Layered composite metal-oxide films, such as TiO_2/WO_3 (Takahashi et al. 2003) and TiO_2/SnO_2 (Kanai et al. 2004), were also deposited by sequential reactive magnetron sputtering with different metals (or metal oxides) as the targets. Pulsed laser deposition (PLD) (Beck, Sasaki and Koshizaki 1999; Hidaka, Ajisaka, Horikoshi, Oyama, Zhao and Serpone 2001; Inoue, Yuasa and Okoshi 2002; Suda, Kawasaki, Ueda and Ohshima 2004, 2005; Xu, Mi and Wang 2006) and thermal or electron beam evaporation (Oh, Kim, Hahn, and Kim 2003; Modes, Scheffel, Metzner, Zywitzki and Reinhold 2005; Yang, Yang, Shiu, Chang and Wong 2006; Hsu, Yang, Chen and Wong 2007) have also been applied for the deposition of photoelectrodes, the details of which will however not be covered here.

18.4.4 Ion-Implantation

Ion-implanted nanocomposite photocatalysts has been recently developed by Anpo and coworkers (1998; 2000) for the synthesis of visible-light-sensitive photocatalysts. The key component of this system is the ion implanter, a typical setup of which is shown in Fig. 18.17. It consists of a metal ion source, a mass analyzer, and a high-voltage ion accelerator. The metal ions from the source are accelerated in

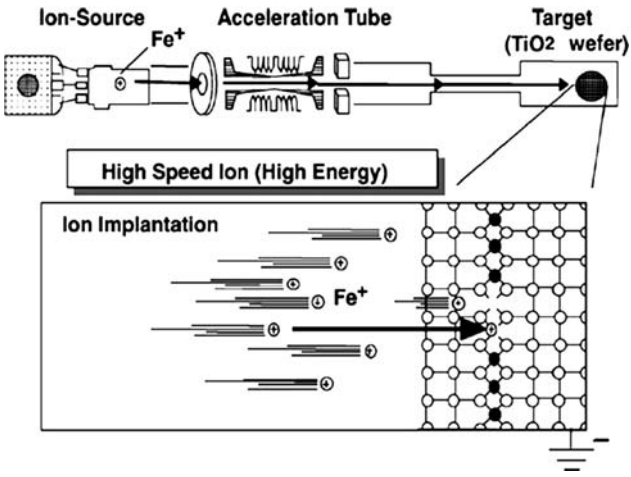

Fig. 18.17 Diagram of a metal ion-implantation system [reprinted from Yamashita et al. (2003), copyright 2003, with permission from Elsevier]

the electronic field and injected to the sample target (a semiconductor wafer such as TiO_2) as the ion beam. These metal ions interact with the sample surface in different manners, depending on their kinetic energy. The metal ions accelerated under high energy conditions (~150 keV) can be implanted into the bulk of the samples. For the synthesis of ion-doped materials, post-thermal treatments were conducted so that a phase separation and a precipitation of guest ion species should not be formed within the host materials but a relatively uniform distribution of the implanted ions should be maintained. In addition, phase-separated metal nanoparticles embedded inside the semiconductor matrix can also be prepared by ion-implantation followed by an annealing process (Sun, Zhu, Fromknecht, Linker and Wang 2004; Wang, Zhang, Shutthanandan, Thevuthasan and Duscher 2004).

Anpo et al. (1999, 2001) studied the TiO_2 photocatalysts modified by ion implantation with various transition metal ions such as Cr, V, Co, Fe and Ni followed by annealing in oxygen atmosphere at around 450°C, and found that the light absorption bands of the doped TiO_2 were in all cases largely shifted towards the visible region. A comparison on the absorption spectra between the ion-implanted and the chemically doped TiO_2 showed that ion-implantation modified the electronic properties of TiO_2 in a way different from that of chemical-doping, and the spectra were shown in Fig. 18.18. In the former case (Fig. 18.18a), the absorption band was obviously red-shifted to wavelengths longer than 500 nm, depending on the amount and kind of ions implanted into TiO_2, while in the latter case (Fig. 18.18b), only a new absorption shoulder (rather than a whole new absorption band) could be observed at around 420 nm, which was ascribed to the impurity levels within the bandgap.

The ion-implanted TiO_2 also excelled the chemically doped counterpart in photocatalytic performance because the former showed photocatalytic activities for a few selected reactions under visible-light irradiation, while the same reaction did not proceed with the latter sample. For example, V-doped TiO_2 produced by ion implantation was capable of photodegrading 2-propanol diluted in H_2O under O_2 atmosphere, leading to the formation of acetone and finally CO_2 under visible-light

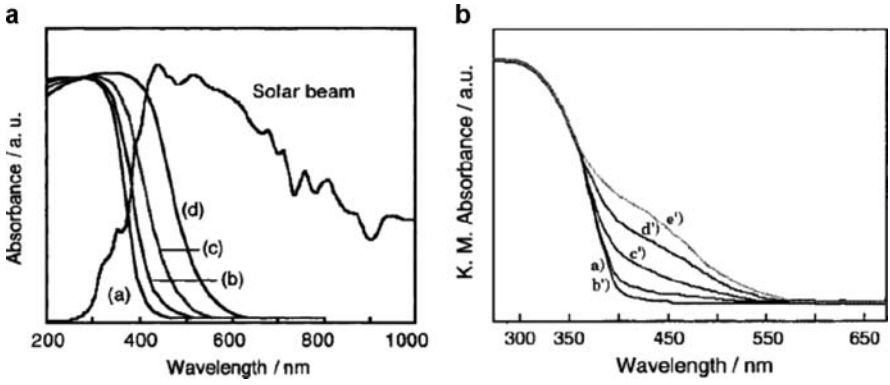

Fig. 18.18 Optical absorption spectra of Cr-doped TiO_2 prepared by (**a**) ion-implantation method and (**b**) chemically doping method (After Anpo et al. 2001)

irradiation (Yamashita, Harada, Misaka, Takeuchi, Ikeue and Anpo 2002). The same photocatalyst could also catalyze the photohydrogenation reaction of methylacetylene with H_2O to form CH_4 when irradiated by light of wavelengths longer than 450 nm. Moreover, by comparing the photocatalytic activities under UV irradiations, the authors also suggested that the implanted species at appropriate doping levels did not act as recombination centers for the photogenerated electrons and holes while the chemically doped species did. For the ion-implanted catalysts, it was proposed that optimal conditions should exist in the depth and number of metal ions implanted to achieve the best photocatalytic performance.

In another way of ion implantation, titanium dioxide catalysts were successfully anchored onto porous silica glass substrates with various Ti contents using $TiCl_4$ as the Ti ion source (Yamashita, Honda, Harada, Ichihashi, Anpo, Hirao, Itoh and Iwamoto 1998). Acceleration at an energy level of 30–100 keV implanted Ti ions into the surface layers of the silica glass, replacing the host atoms there. The amount of the implanted Ti ions could be controlled by varying the duration time of the implantation process. Post-thermal treatment in O_2 gas at 450°C was conducted before being used as photocatalysts. The Ti ions were implanted as tetrahedral titanium oxide moieties which was believed to be responsible for the high photocatalytic activity of liquid-phase mineralization of 2-propanol.

Various doped or composite photocatalysts with visible-light activity have been produced by ion implantation. Zheng and coworkers (2002a) implanted Sn^{4+} ions via a Ti-substituting mode into TiO_2 thin films deposited by RF magnetron sputtering method, and the photocatalytic activity in the degradation of Rhodamine B was improved due to the implanted Sn species. The authors also observed a negative effect by Fe-ion implantation on the photoactivity of Fe-doped TiO_2 as compared with undoped TiO_2. Ferric ions as the recombination centers were proposed to be one of the possible causes (Zheng et al. 2002b). In a report by Tesfamichael et al. (2005), nitrogen gas was ionized to create the ion beam to implant TiO_2 films coated on conducting glass substrates. A maximum N concentration of 6.08 at.% was obtained using the highest ion dose and ion-implanting energy. The authors correlated the transmittance of the implanted films with the N concentration, showing that increasing N concentration led to a decrease in the transmittance of the films possibly because of the increased number of defects in the films, and this can be minimized by annealing at temperatures above 400°C. Ghicov and coworkers (2006) implanted N ions onto the anatase TiO_2 nanotube films produced by electrochemical Ti oxidation, and found that the N-ion implantation caused a serious structural alteration of the films, as shown in Fig. 18.19. By studying their photoelectrochemical responses under UV and visible irradiations, the authors suggested a dual effect of the N-ion implantation, that is, the defect states introduced by ion implantation acted as traps for photogenerated electron–hole pairs, thus decreasing the photocurrent in the UV range; but on the other hand, an efficient N-doping led to a significant increase in photoresponse in the visible range. Hou et al. (2006) confirmed that annealing is indispensable for V-doped TiO_2 films prepared by ion implantation to exhibit photocatalytic activity under visible-light irradiation, because the unannealed samples did not show such activities. The authors also explained the decreased quantum

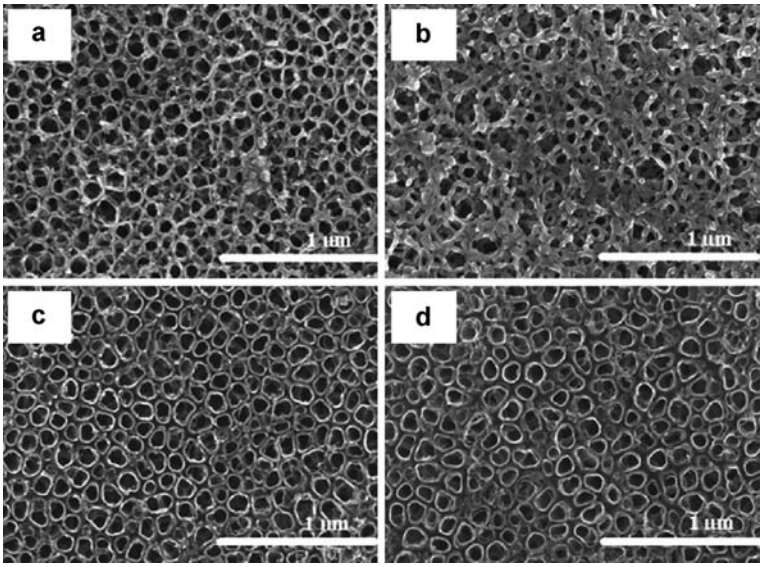

Fig. 18.19 Top views of SEM images of nanotube layers: Amorphous structures of N-ion implanted TiO_2 nanotubes at 1×10^{15} ions per cm^2 (**a**) and 1×10^{16} ions per cm^2 (**b**); annealed anatase TiO_2 nanotube films before ion implantation at 1×10^{15} ions per cm^2 (**c**) and 1×10^{16} ions per cm^2 (**d**) [reprinted from Ghicov et al. (2006), copyright 2006, with permission from Elsevier]

efficiency when the amount of the implanted V ions exceeded its optimum value (determined to be 1×10^{16} ions per cm^2) by the possibility that the overdosed V ions which could not find more substituting positions would then reside at the interstitial space as the recombination centers for photogenerated charge carriers. Zhou and coworkers (2006) studied the photocatalytic activities of V^+-doped TiO_2 for the complete oxidation of formic acid under visible light ($\lambda > 450$ nm). Photocatalytic degradation of gaseous formaldehyde by Cr ion-implanted TiO_2 films was also studied under visible-light irradiation in a parallel-plate reactor (Lam, Leung, Leung, Vrijinoed, Yam and Ng 2007).

The above-mentioned examples demonstrate the synthesis of ion-doped photocatalysts by implantation methods with or without post-annealing. In particular for transition metal ion-implanted samples, no separated phases of metal oxides were found from the implanted ion sources. In some implantation processes using noble metal-containing species, noble metal nanoparticles have been commonly observed after the implanted samples were subjected to annealing. Tsuji et al. (2005, 2006) prepared the Ag ion-implanted rutile and anatase TiO_2 after annealing at above 400°C and observed Ag metal nanoparticles in the surface region of the TiO_2 films, which were responsible for the improved photocatalytic activity for the decolorization of methylene blue. Wang et al. (2004) conducted high-energy Au ion-implantation process and obtained Au nanoclusters inside TiO_2 films after high-temperature annealing. After closely examining the implanted samples by HRTEM

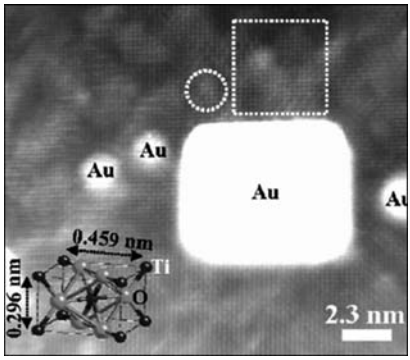

Fig. 18.20 Representative STEM-HAADF image of the Au ion-implanted TiO_2 operated at 300 K and subsequently annealed at 1,275 K, revealing large Au clusters, which are labeled by Au. The *dashed line circled* region is Au atoms conglomerated region [reprinted with permission from Wang et al. (2004), copyright 2004, American Institute of Physics]

and high angle annular dark-field (HAADF) imaging as shown in Fig. 18.20, the authors suggested that Au atoms were in substitutional Ti atomic columns in the TiO_2 lattice prior to the nucleation of Au, and the size and spatial distribution of the Au nanoclusters showed dependence on the implantation temperature. Without post-annealing treatments, gold nanoparticles embedded in the near-top layers of TiO_2 and $SrTiO_3$ films were also observed by Sun et al. (2004). The formation of noble metal nanoparticles in these processes might be caused by the special chemical nature of noble metal ionic species (e.g., the high oxidizing power at elevated temperatures). It was also proposed that the formation of a supersaturated solid solution of the implanted species should be necessary to produce embedded nanoparticles (Meldrum, Haglund, Boatner and White 2001).

18.5 Concluding Remarks

Photocatalysis has provided promising means of addressing the energy and environmental-protection issues, and its success relies on the availability of high-performance photoelectrocatalytic materials. Recent developments of new approaches for the fabrication of photoelectrode materials and their related applications are presented in this chapter. Major efforts have been devoted to achieving higher photocatalytic activities by enhanced light absorption and improved separation between the photogenerated charge carriers. Doped semiconductors, coupled semiconductors with different bandgaps and composite materials with heterojunctions between, for example, semiconductors and noble metals have been successfully fabricated by the selectively reviewed methods. Other beneficial structural features such as high surface area and porosity within the photoelectrode materials could also be realized by some of these methods.

References

Adachi, M., Murata, Y., Okada, I. and Yoshikawa, S. (2003). Formation of titania nanotubes and applications for dye-sensitized solar cells. J. Electrochem. Soc. 150(8), G488–G493.

An, H. J., Jang, S. R., Vittal, R., Lee, J. and Kim, K. J. (2005). Cationic surfactant promoted reductive electrodeposition of nanocrystalline anatase TiO_2 for application to dye-sensitized solar cells. Electrochimica Acta 50(13), 2713–2718.

Anderson, C. and Bard, A. J. (1995). Improved photocatalyst of TiO_2/SiO_2 prepared by a sol–gel synthesis. J. Phys. Chem. 99(24), 9882–9885.

Anderson, M. A., Gieselmann, M. J. and Xu, Q. Y. (1988). Titania and alumina ceramic membranes. J. Membr. Sci. 39(3), 243–258.

Andersson, M., Birkedal, H., Franklin, N. R., Ostomel, T., Boettcher, S., Palmqvist, A. E. C. and Stucky, G. D. (2005). Ag/AgCl-loaded ordered mesoporous anatase for photocatalysis. Chem. Mater. 17(6), 1409–1415.

Anpo, M. (2000). Use of visible light. Second-generation titanium oxide photocatalysts prepared by the application of an advanced metal ion-implantation method. Pure Appl. Chem. 72(9), 1787–1792.

Anpo, M., Ichihashi, Y., Takeuchi, M. and Yamashita, H. (1998). Design of unique titanium oxide photocatalysts by an advanced metal ion-implantation method and photocatalytic reactions under visible light irradiation. Res. Chem. Intermed. 24(2), 143–149.

Anpo, M., Ichihashi, Y., Takeuchi, M. and Yamashita, H. (1999). Design and development of unique titanium oxide photocatalysts capable of operating under visible light irradiation by an advanced metal ion-implantation method. Sci. Technol. Catal. 1998. 121, 305–310.

Anpo, M., Kishiguchi, S., Ichihashi, Y., Takeuchi, M., Yamashita, H., Ikeue, K., Morin, B., Davidson, A. and Che, M. (2001). The design and development of second-generation titanium oxide photocatalysts able to operate under visible light irradiation by applying a metal ion-implantation method. Res. Chem. Intermed. 27(4–5), 459–467.

Antonelli, D. M. and Ying, J. Y. (1995). Synthesis of hexagonally packed mesoporous TiO_2 by a modified sol–gel method. Angew. Chem. Int. Ed. Engl. 34(18), 2014–2017.

Babelon, P., Dequiedt, A. S., Mostefa-Sba, H., Bourgeois, S., Sibillot, P. and Sacilotti, M. (1998). SEM and XPS studies of titanium dioxide thin films grown by MOCVD. Thin Solid Films 322(1–2), 63–67.

Backman, U., Auvinen, A. and Jokiniemi, J. K. (2005). Deposition of nanostructured titania films by particle-assisted MOCVD. Surf. Coat. Technol. 192(1), 81–87.

Badawy, W. A. (1997). Preparation, electrochemical, photoelectrochemical and solid-state characteristics of indium-incorporated TiO_2 thin films for solar cell fabrication. J. Mater. Sci. 32(18), 4979–4984.

Bamwenda, G. R., Tsubota, S., Nakamura, T. and Haruta, M. (1995). Photoassisted hydrogen-production from a water–ethanol solution – A comparison of activities of Au–TiO_2 and Pt–TiO_2. J. Photochem. Photobiol. A-Chem. 89(2), 177–189.

Bandyopadhyay, M., Birkner, A., van den Berg, M. W. E., Klementiev, K. V., Schmidt, W., Grunert, W. and Gies, H. (2005). Synthesis and characterization of mesoporous MCM-48 containing TiO_2 nanoparticles. Chem. Mater. 17(15), 3820–3829.

Bavykin, D. V., Lapkin, A. A., Plucinski, P. K., Torrente-Murciano, L., Friedrich, J. M. and Walsh, F. C. (2006). Deposition of Pt, Pd, Ru and Au on the surfaces of titanate nanotubes. Top. Catal. 39(3–4), 151–160.

Beck, K. M., Sasaki, T. and Koshizaki, N. (1999). Characterization of nanocomposite materials prepared via laser ablation of Pt/TiO_2 bi-combinant targets. Chem. Phys. Lett. 301(3–4), 336–342.

Boccuzzi, F., Chiorino, A., Tsubota, S. and Haruta, M. (1996). FTIR study of carbon monoxide oxidation and scrambling at room temperature over gold supported on ZnO and TiO_2. J. Phys. Chem. 100(9), 3625–3631.

Bond, G. C. and Thompson, D. T. (1999). Catalysis by gold. Catal. Rev. Sci. Eng. 41(3–4), 319–388.

Bougrine, A., El Hichou, A., Addou, M., Ebothe, J., Kachouane, A. and Troyon, M. (2003). Structural, optical and cathodoluminescence characteristics of undoped and tin-doped ZnO thin films prepared by spray pyrolysis. Mater. Chem. Phys. 80(2), 438–445.

Bowker, M., Millard, L., Greaves, J., James, D. and Soares, J. (2004). Photocatalysis by Au nanoparticles: Reforming of methanol. Gold Bull. 37(3–4), 170–173.

Butterfield, I. M., Christensen, P. A., Hamnett, A., Shaw, K. E., Walker, G. M., Walker, S. A. and Howarth, C. R. (1997). Applied studies on immobilized titanium dioxide films as catalysts for the photoelectrochemical detoxification of water. J. Appl. Electrochem. 27(4), 385–395.

Centeno, M. A., Carrizosa, I. and Odriozola, J. A. (2003). Deposition-precipitation method to obtain supported gold catalysts: dependence of the acid–base properties of the support exemplified in the system $TiO_2-TiO_xN_y-TiN$. Appl. Catal. A-Gen. 246(2), 365–372.

Chan, S. C. and Barteau, M. A. (2005). Preparation of highly uniform Ag/TiO_2 and Au/TiO_2 supported nanoparticle catalysts by photodeposition. Langmuir 21(12), 5588–5595.

Che, G. L., Lakshmi, B. B., Fisher, E. R. and Martin, C. R. (1998). Carbon nanotubule membranes for electrochemical energy storage and production. Nature 393(6683), 346–349.

Choi, W., Hong, S. J., Chang, Y. S. and Cho, Y. (2000). Photocatalytic degradation of polychlorinated dibenzo-*p*-dioxins on TiO_2 film under UV or solar light irradiation. Environ. Sci. Technol. 34(22), 4810–4815.

Choi, K. S., Lichtenegger, H. C., Stucky, G. D. and McFarland, E. W. (2002). Electrochemical synthesis of nanostructured ZnO films utilizing self-assembly of surfactant molecules at solid–liquid interfaces. J. Am. Chem. Soc. 124(42), 12402–12403.

Choi, S. Y., Mamak, M., Coombs, N., Chopra, N. and Ozin, G. A. (2004). Thermally stable two-dimensional hexagonal mesoporous nanocrystalline anatase, meso-nc-TiO_2: Bulk and crack-free thin film morphologies. Adv. Funct. Mater. 14(4), 335–344.

Choi, S. Y., Mamak, M., Speakman, S., Chopra, N. and Ozin, G. A. (2005). Evolution of nanocrystallinity in periodic mesoporous anatase thin films. Small 1(2), 226–232.

Conde-Gallardo, A., Guerrero, M., Fragoso, R. and Castillo, N. (2006). Gas-phase diffusion and surface reaction as limiting mechanisms in the aerosol-assisted chemical vapor deposition of TiO_2 films from titanium diisopropoxide. J. Mater. Res. 21(12), 3205–3209.

Cozzoli, P. D., Comparelli, R., Fanizza, E., Curri, M. L., Agostiano, A. and Laub, D. (2004). Photocatalytic synthesis of silver nanoparticles stabilized by TiO_2 nanorods: A semiconductor/metal nanocomposite in homogeneous nonpolar solution. J. Am. Chem. Soc. 126(12), 3868–3879.

Cui, H., Shen, H. S., Gao, Y. M., Dwight, K. and Wold, A. (1993). Photocatalytic properties of titanium (IV) oxide thin-films prepared by spin coating and spray pyrolysis. Mater. Res. Bull. 28(3), 195–201.

de Tacconi, N. R., Chenthamarakshan, C. R., Rajeshwar, K., Pauporte, T. and Lincot, D. (2003). Pulsed electrodeposition of WO_3–TiO_2 composite films. Electrochem. Commun. 5(3), 220–224.

Decher, G. (1997). Fuzzy nanoassemblies: Toward layered polymeric multicomposites. Science 277(5330), 1232–1237.

Decher, G., Hong, J. D. and Schmitt, J. (1992). Buildup of ultrathin multilayer films by a self-assembly process. 3. Consecutively alternating adsorption of anionic and cationic polyelectrolytes on charged surfaces. Thin Solid Films 210(1–2), 831–835.

Dimitratos, N., Villa, A., Bianchi, C. L., Prati, L. and Makkee, M. (2006). Gold on titania: Effect of preparation method in the liquid phase oxidation. Appl. Catal. A-Gen. 311, 185–192.

Di Paola, A., Marci, G., Palmisano, L., Schiavello, M., Uosaki, K., Ikeda, S. and Ohtani, B. (2002). Preparation of polycrystalline TiO_2 photocatalysts impregnated with various transition metal ions: Characterization and photocatalytic activity for the degradation of 4-nitrophenol. J. Phys. Chem. B 106(3), 637–645.

Dumitriu, D., Bally, A. R., Ballif, C., Hones, P., Schmid, P. E., Sanjines, R., Levy, F. and Parvulescu, V. I. (2000). Photocatalytic degradation of phenol by TiO_2 thin films prepared by sputtering. Appl. Catal. B-Environ. 25(2–3), 83–92.

Espinos, J. P., Fernandez, A., Caballero, A., Jimenez, V. M., Sanchez-Lopez, J. C., Contreras, L., Leinen, D. and GonzalezElipe, A. R. (1997). Ion-beam-induced CVD: An alternative method of thin film preparation. Chem. Vapor Deposit. 3(4), 219–226.

Evans, P., Pemble, M. E. and Sheel, D. W. (2006). Precursor-directed control of crystalline type in atmospheric pressure CVD growth of TiO_2 on stainless steel. Chem. Mater. 18(24), 5750–5755.

Feng, S. H. and Xu, R. R. (2001). New materials in hydrothermal synthesis. Accounts Chem. Res. 34(3), 239–247.

Feng, X. J., Macak, J. M. and Schmuki, P. (2007). Robust self-organization of oxide nanotubes over a wide pH range. Chem. Mater. 19(7), 1534–1536.

Gauthier, V., Bourgeois, S., Sibillot, P., Maglione, M. and Sacilotti, M. (1999). Growth and characterization of AP-MOCVD iron doped titanium dioxide thin films. Thin Solid Films 340(1–2), 175–182.

Ghicov, A., Macak, J. M., Tsuchiya, H., Kunze, J., Haeublein, V., Kleber, S. and Schmuki, P. (2006). TiO_2 nanotube layers: Dose effects during nitrogen doping by ion implantation. Chem. Phys. Lett. 419(4–6), 426–429.

Göß, D., Frach, P., Zywitzki, O., Modes, T., Klinkenberg, S. and Gottfried, C. (2005). Photocatalytic titanium dioxide thin films prepared by reactive pulse magnetron sputtering at low temperature. Surf. Coat. Technol. 200(1–4), 967–971.

Grosso, D., Babonneau, F., Sanchez, C., Soler-Illia, G., Crepaldi, E. L., Albouy, P. A., Amenitsch, H., Balkenende, A. R. and Brunet-Bruneau, A. (2003). A first insight in the mechanisms involved in the self-assembly of 2D-hexagonal templated SiO_2 and TiO_2 mesostructured films during dip-coating. J. Sol–Gel Sci. Technol. 26(1–3), 561–565.

Guo, M., Diao, P. and Cai, S. M. (2005a). Hydrothermal growth of perpendicularly oriented ZnO nanorod array film and its photoelectrochemical properties. Appl. Surf. Sci. 249(1–4), 71–75.

Guo, M., Diao, P., Wang, X. D. and Cai, S. M. (2005b). The effect of hydrothermal growth temperature on preparation and photoelectrochemical performance of ZnO nanorod array films. J. Solid State Chem. 178(10), 3210–3215.

Halary, E., Benvenuti, G., Wagner, F. and Hoffmann, P. (2000). Light induced chemical vapour deposition of titanium oxide thin films at room temperature. Appl. Surf. Sci. 154, 146–151.

Halary-Wagner, E., Wagner, F. and Hoffmann, P. (2004). Titanium dioxide thin-film deposition on polymer substrate by light induced chemical vapor deposition. J. Electrochem. Soc. 151(9), C571–C576.

Halary-Wagner, E., Bret, T. and Hoffmann, P. (2005). Light-induced CVD of titanium dioxide thin films I: Kinetics of deposition. Chem. Vapor Deposit. 11(1), 21–28.

Hao, W. C., Pan, F. and Wang, T. M. (2005). Photocatalytic activity TiO_2 granular films prepared by layer-by-layer self-assembly method. J. Mater. Sci. 40(5), 1251–1253.

Haruta, M., Tsubota, S., Kobayashi, T., Kageyama, H., Genet, M. J. and Delmon, B. (1993). Low-temperature oxidation of Co over gold supported on TiO_2, α-Fe_2O_3, and Co_3O_4. J. Catal. 144(1), 175–192.

Haruta, M., Uphade, B. S., Tsubota, S. and Miyamoto, A. (1998). Selective oxidation of propylene over gold deposited on titanium-based oxides. Res. Chem. Intermed. 24(3), 329–336.

He, C., Xiong, Y., Chen, J., Zha, C. H. and Zhu, X. H. (2003). Photoelectrochemical performance of Ag–TiO_2/ITO film and photoelectrocatalytic activity towards the oxidation of organic pollutants. J. Photochem. Photobiol. A-Chem. 157(1), 71–79.

He, J. X., Yang, P. J., Sato, H., Umemura, Y. and Yamagishi, A. (2004). Effects of Ag-photodeposition on photocurrent of an ITO electrode modified by a hybrid film of TiO_2 nanosheets. J. Electroanal. Chem. 566(1), 227–233.

Hidaka, H., Asai, Y., Zhao, J. C., Nohara, K., Pelizzetti, E. and Serpone, N. (1995). Photoelectrochemical decomposition of surfactants on a TiO_2/TCO particulate film electrode assembly. J. Phys. Chem. 99(20), 8244–8248.

Hidaka, H., Nagaoka, H., Nohara, K., Shimura, T., Horikoshi, S., Zhao, J. and Serpone, N. (1996). A mechanistic study of the photoelectrochemical oxidation of organic compounds on a TiO_2/TCO particulate film electrode assembly. J. Photochem. Photobiol. A-Chem. 98(1–2), 73–78.

Hidaka, H., Ajisaka, K., Horikoshi, S., Oyama, T., Takeuchi, K., Zhao, J. and Serpone, N. (2001). Comparative assessment of the efficiency of TiO_2/OTE thin film electrodes fabricated by three deposition methods – Photoelectrochemical degradation of the DBS anionic surfactant. J. Photochem. Photobiol. A-Chem. 138(2), 185–192.

Hosono, E., Fujihara, S., Kakiuchi, K. and Imai, H. (2004). Growth of submicrometer-scale rectangular parallelepiped rutile TiO_2 films in aqueous $TiCl_3$ solutions under hydrothermal conditions. J. Am. Chem. Soc. 126(25), 7790–7791.

Hou, X. G., Hao, F. H., Fan, B., Gu, X. N., Wu, X. Y. and Liu, A. D. (2006). Modification of TiO_2 photocatalytic films by V^+ ion implantation. Nucl. Instrum. Methods Phys. Res. Sect. B-Beam Interact. Mater. Atoms 243(1), 99–102.

Hsu, S. W., Yang, T. S., Chen, T. K. and Wong, M. S. (2007). Ion-assisted electron-beam evaporation of carbon-doped titanium oxide films as visible-light photocatalyst. Thin Solid Films 515(7–8), 3521–3526.

Hyett, G., Green, M. and Parkin, I. P. (2006). X-ray diffraction area mapping of preferred orientation and phase change in TiO_2 thin films deposited by chemical vapor deposition. J. Am. Chem. Soc. 128(37), 12147–12155.

Ichinose, I., Senzu, H. and Kunitake, T. (1997). A surface sol–gel process of TiO_2 and other metal oxide films with molecular precision. Chem. Mater. 9(6), 1296–1298.

Ilican, S., Caglar, Y., Caglar, M. and Yakuphanoglu, F. (2006). Electrical conductivity, optical and structural properties of indium-doped ZnO nanofiber thin film deposited by spray pyrolysis method. Phys. E 35(1), 131–138.

Inoue, N., Yuasa, H. and Okoshi, M. (2002). TiO_2 thin films prepared by PLD for photocatalytic applications. Appl. Surf. Sci. 197, 393–397.

Ishizuka, S. O., Kato, S., Maruyama, T. and Akimoto, K. (2001). Nitrogen doping into Cu_2O thin films deposited by reactive radio-frequency magnetron sputtering. Jpn. J. Appl. Phys. Part 1-Regular Papers Short Notes & Review Papers 40(4B), 2765–2768.

Jin, S. and Shiraishi, F. (2004). Photocatalytic activities enhanced for decompositions of organic compounds over metal-photodepositing titanium dioxide. Chem. Eng. J. 97(2–3), 203–211.

Jing, L. Q., Li, X. Q., Li, S. D., Wang, B. Q., Xin, B. F., Fu, H. G., Wang, D. J. and Cai, W. M. (2005). XPS and SPS studies on nanometer Au/TiO_2 photocatalyst. Chin. J. Catal. 26(3), 189–193.

Jung, K. Y. and Park, S. B. (2000). Enhanced photoactivity of silica-embedded titania particles prepared by sol–gel process for the decomposition of trichloroethylene. Appl. Catal. B-Environ. 25(4), 249–256.

Kanai, N., Nuida, T., Ueta, K., Hashimoto, K., Watanabe, T. and Ohsaki, H. (2004). Photocatalytic efficiency of TiO_2/SnO_2 thin film stacks prepared by DC magnetron sputtering. Vacuum 74(3–4), 723–727.

Karches, M., Morstein, M., von Rohr, P., Pozzo, R. L., Giombi, J. L. and Baltanas, M. A. (2002). Plasma-CVD-coated glass beads as photocatalyst for water decontamination. Catal. Today 72(3–4), 267–279.

Kavan, L., O'Regan, B., Kay, A. and Grätzel, M. (1993). Preparation of TiO_2 (anatase) films on electrodes by anodic oxidative hydrolysis of $TiCl_3$. J. Electroanal. Chem. 346(1–2), 291–307.

Khoudiakov, M., Gupta, M. C. and Deevi, S. (2005). Au/Fe_2O_3 nanocatalysts for CO oxidation: A comparative study of deposition – precipitation and coprecipitation techniques. Appl. Catal. A-Gen. 291(1–2), 151–161.

Kikuchi, H., Kitano, M., Takeuchi, M., Matsuoka, M., Anpo, M. and Kamat, P. V. (2006). Extending the photoresponse of TiO_2 to the visible light region: Photoelectrochemical behavior of TiO_2 thin films prepared by the radio frequency magnetron sputtering deposition method. J. Phys. Chem. B 110(11), 5537–5541.

Kim, D. H. and Anderson, M. A. (1994). Photoelectrocatalytic degradation of formic-acid using a porous TiO_2 thin-film electrode. Environ. Sci. Technol. 28(3), 479–483.

Kim, T. H. and Yoon, K. H. (1991). Photoeffects in SnO_2 film electrodes deposited by spray pyrolysis. J. Appl. Phys. 70(5), 2739–2744.

Kim, K. H., Park, K. C. and Ma, D. Y. (1997). Structural, electrical and optical properties of aluminum doped zinc oxide films prepared by radio frequency magnetron sputtering. J. Appl. Phys. 81(12), 7764–7772.

Kim, J. H., Fujita, S. and Shiratori, S. (2006). Fabrication and characterization of TiO_2 thin film prepared by a layer-by-layer self-assembly method. Thin Solid Films 499(1–2), 83–89.

Kitano, M., Takeuchi, M., Matsuoka, M., Thomas, J. M. and Anpo, M. (2005). Preparation of visible light-responsive TiO_2 thin film photocatalysts by an RF magnetron sputtering deposition method and their photocatalytic reactivity. Chem. Lett. 34(4), 616–617.

Kitano, M., Funatsu, K., Matsuoka, M., Ueshima, M. and Anpo, M. (2006). Preparation of nitrogen-substituted TiO_2 thin film photocatalysts by the radio frequency magnetron sputtering deposition method and their photocatalytic reactivity under visible light irradiation. J. Phys. Chem. B 110(50), 25266–25272.

Kiyonaga, T., Mitsui, T., Torikoshi, M., Takekawa, M., Soejima, T. and Tada, H. (2006). Ultrafast photosynthetic reduction of elemental sulfur by Au nanoparticle-loaded TiO_2. J. Phys. Chem. B 110(22), 10771–10778.

Lakshmi, B. B., Dorhout, P. K. and Martin, C. R. (1997a). Sol–gel template synthesis of semiconductor nanostructures. Chem. Mater. 9(3), 857–862.

Lakshmi, B. B., Patrissi, C. J. and Martin, C. R. (1997b). Sol–gel template synthesis of semiconductor oxide micro- and nanostructures. Chem. Mater. 9(11), 2544–2550.

Lam, R. C. W., Leung, M. K. H., Leung, D. Y. C., Vrijinoed, L. L. P., Yam, W. C. and Ng, S. P. (2007). Visible-light-assisted photocatalytic degradation of gaseous formaldehyde by parallel-plate reactor coated with Cr ion-implanted TiO_2 thin film. Solar Energy Mater. Solar Cells 91(1), 54–61.

Lee, H. Y., Park, Y. H. and Ko, K. H. (2000). Correlation between surface morphology and hydrophilic/hydrophobic conversion of MOCVD-TiO_2 films. Langmuir 16(18), 7289–7293.

Lee, S. B., Mitchell, D. T., Trofin, L., Nevanen, T. K., Soderlund, H. and Martin, C. R. (2002). Antibody-based bio-nanotube membranes for enantiomeric drug separations. Science 296(5576), 2198–2200.

Lee, M. K., Huang, J. J. and Wu, T. S. (2005). Electrical characteristics improvement of oxygen-annealed MOCVD-TiO_2 films. Semicond. Sci. Technol. 20(6), 519–523.

Li, D., Haneda, H., Hishita, S., Ohashi, N. and Labhsetwar, N. K. (2005a). Fluorine-doped TiO_2 powders prepared by spray pyrolysis and their improved photocatalytic activity for decomposition of gas-phase acetaldehyde. J. Fluorine Chem. 126(1), 69–77.

Li, P., Liu, J. Y., Nag, N. and Croziers, P. A. (2005b). Atomic-scale study of in situ metal nanoparticle synthesis in a Ni/TiO_2 system. J. Phys. Chem. B 109(29), 13883–13890.

Li, W. C., Comotti, M. and Schuth, F. (2006). Highly reproducible syntheses of active Au/TiO_2 catalysts for CO oxidation by deposition-precipitation or impregnation. J. Catal. 237(1), 190–196.

Limmer, S. J., Seraji, S., Forbess, M. J., Wu, Y., Chou, T. P., Nguyen, C. and Cao, G. Z. (2001). Electrophoretic growth of lead zirconate titanate nanorods. Adv. Mater. 13(16), 1269–1272.

Limmer, S. J., Seraji, S., Wu, Y., Chou, T. P., Nguyen, C. and Cao, G. Z. (2002). Template-based growth of various oxide nanorods by sol–gel electrophoresis. Adv. Funct. Mater. 12(1), 59–64.

Limmer, S. J., Cruz, S. V. and Cao, G. Z. (2004). Films and nanorods of transparent conducting oxide ITO by a citric acid sol route. Appl. Phys. A-Mater. Sci. Process. 79(3), 421–424.

Lindgren, T., Mwabora, J. M., Avendano, E., Jonsson, J., Hoel, A., Granqvist, C. G. and Lindquist, S. E. (2003). Photoelectrochemical and optical properties of nitrogen doped titanium dioxide films prepared by reactive DC magnetron sputtering. J. Phys. Chem. B 107(24), 5709–5716.

Liu, B. and Zeng, H. C. (2003). Hydrothermal synthesis of ZnO nanorods in the diameter regime of 50 nm. J. Am. Chem. Soc. 125(15), 4430–4431.

Liu, B. S., Zhao, X. J., Zhang, N. Z., Zhao, Q. N., He, X. and Feng, J. Y. (2005). Photocatalytic mechanism of TiO_2–CeO_2 films prepared by magnetron sputtering under UV and visible light. Surf. Sci. 595(1–3), 203–211.

Lo Nigro, R., Toro, R., Malandrino, G. and Fragala, I. L. (2003). Heteroepitaxial growth of nanostructured cerium dioxide thin films by MOCVD on a (001) TiO_2 substrate. Chem. Mater. 15(7), 1434–1440.

Luo, J. and Hepel, M. (2001). Photoelectrochemical degradation of naphthol blue black diazo dye on WO_3 film electrode. Electrochim. Acta 46(19), 2913–2922.

Macak, J. M., Tsuchiya, H., Taveira, L., Aldabergerova, S. and Schmuki, P. (2005). Smooth anodic TiO_2 nanotubes. Angew. Chem. Int. Ed. 44(45), 7463–7465.

Manivannan, A., Seehra, M. S., Majumder, S. B. and Katiyar, R. S. (2003). Magnetism of Co-doped titania thin films prepared by spray pyrolysis. Appl. Phys. Lett. 83(1), 111–113.

Martin, C. R. (1995). Template synthesis of electronically conductive polymer nanostructures. Accounts Chem. Res. 28(2), 61–68.

Matsuda, A., Higashi, Y., Tadanaga, K. and Tatsumisago, M. (2006). Hot-water treatment of sol–gel derived SiO_2–TiO_2 microparticles and application to electrophoretic deposition for thick films. J. Mater. Sci. 41(24), 8101–8108.

Matsuoka, M., Kitano, M., Takeuchi, M., Anpo, M. and Thomas, J. M. (2005). Photocatalytic water splitting on visible light-responsive TiO_2 thin films prepared by a RF magnetron sputtering deposition method. Top. Catal. 35(3–4), 305–310.

McMurray, T. A., Byrne, J. A., Dunlop, P. S. M. and McAdams, E. T. (2005). Photocatalytic and electrochemically assisted photocatalytic oxidation of formic acid on TiO_2 films under UVA and UVB irradiation. J. Appl. Electrochem. 35(7–8), 723–731.

Meldrum, A., Haglund, R. F., Boatner, L. A. and White, C. W. (2001). Nanocomposite materials formed by ion implantation. Adv. Mater. 13(19), 1431–1444.

Miao, Z., Xu, D. S., Ouyang, J. H., Guo, G. L., Zhao, X. S. and Tang, Y. Q. (2002). Electrochemically induced sol–gel preparation of single-crystalline TiO_2 nanowires. Nano Lett. 2(7), 717–720.

Modes, T., Scheffel, B., Metzner, C., Zywitzki, O. and Reinhold, E. (2005). Structure and properties of titanium oxide layers deposited by reactive plasma activated electron beam evaporation. Surf. Coat. Technol. 200(1–4), 306–309.

Moon, S. W., Lee, G. D., Park, S. S. and Hong, S. S. (2004). Catalytic combustion of chlorobenzene over V_2O_5/TiO_2 catalysts prepared by the precipitation-deposition method. React. Kinet. Catal. Lett. 82(2), 303–310.

Mor, G. K., Shankar, K., Paulose, M., Varghese, O. K. and Grimes, C. A. (2006). Use of highly-ordered TiO_2 nanotube arrays in dye-sensitized solar cells. Nano Lett. 6(2), 215–218.

Murakami, T. N., Kijitori, Y., Kawashima, N. and Miyasaka, T. (2004). Low temperature preparation of mesoporous TiO_2 films for efficient dye-sensitized photoelectrode by chemical vapor deposition combined with UV light irradiation. J. Photochem. Photobiol. A-Chem. 164(1–3), 187–191.

Nasr, C., Kamat, P. V. and Hotchandani, S. (1998). Photoelectrochemistry of composite semiconductor thin films. Photosensitization of the SnO_2/TiO_2 coupled system with a ruthenium polypyridyl complex. J. Phys. Chem. B 102(49), 10047–10056.

Natarajan, C. and Nogami, G. (1996). Cathodic electrodeposition of nanocrystalline titanium dioxide thin films. J. Electrochem. Soc. 143(5), 1547–1550.

Natarajan, C., Fukunaga, N. and Nogami, G. (1998). Titanium dioxide thin film deposited by spray pyrolysis of aqueous solution. Thin Solid Films 322(1–2), 6–8.

Nazeeruddin, M. K., Kay, A., Rodicio, I., Humphrybaker, R., Muller, E., Liska, P., Vlachopoulos, N. and Grätzel, M. (1993). Conversion of light to electricity by *cis*-X_2bis(2,2′-bipyridyl-4,4′-dicarboxylate)ruthenium(II) charge-transfer sensitizers ($X = Cl^-$, Br^-, I^-, CN^-, and SCN^-) on nanocrystalline TiO_2 electrodes. J. Am. Chem. Soc. 115(14), 6382–6390.

Oekermann, T., Yoshida, T., Schlettwein, D., Sugiura, T. and Minoura, H. (2001). Photoelectrochemical properties of ZnO/tetrasulfophthalocyanine hybrid thin films prepared by electrochemical self-assembly. Phys. Chem. Chem. Phys. 3(16), 3387–3392.

Oh, S. H., Kim, D. J., Hahn, S. H. and Kim, E. J. (2003). Comparison of optical and photocatalytic properties of TiO_2 thin films prepared by electron-beam evaporation and sol–gel dip-coating. Mater. Lett. 57(26–27), 4151–4155.

Ohno, S., Sato, D., Kon, M., Song, P. K., Yoshikawa, M., Suzuki, K., Frach, P. and Shigesato, Y. (2003). Plasma emission control of reactive sputtering process in mid-frequency mode with dual cathodes to deposit photocatalytic TiO_2 films. Thin Solid Films 445(2), 207–212.

Ohyama, M., Kozuka, H. and Yoko, T. (1997). Sol–gel preparation of ZnO films with extremely preferred orientation along (002) plane from zinc acetate solution. Thin Solid Films 306(1), 78–85.

Okuya, M., Prokudina, N. A., Mushika, K. and Kaneko, S. (1999). TiO_2 thin films synthesized by the spray pyrolysis deposition (SPD) technique. J. Eur. Ceram. Soc. 19(6–7), 903–906.

Okuyama, H., Honma, K. and Ohno, S. (1999). Photocatalytic activity of ultrafine TiO_2 particles synthesized by an RF plasma CVD. J. Jpn. Inst. Met. 63(1), 74–81.

Ortega, J. M., Martinez, A. I., Acosta, D. R. and Magana, C. R. (2006). Structural and electrochemical studies of WO_3 films deposited by pulsed spray pyrolysis. Solar Energy Mater. Solar Cells 90(15), 2471–2479.

Pal, B., Sharon, M. and Nogami, G. (1999). Preparation and characterization of TiO_2/Fe_2O_3 binary mixed oxides and its photocatalytic properties. Mater. Chem. Phys. 59(3), 254–261.

Palgrave, R. G. and Parkin, I. P. (2006). Aerosol assisted chemical vapor deposition using nanoparticle precursors: A route to nanocomposite thin films. J. Am. Chem. Soc. 128(5), 1587–1597.

Papp, J., Soled, S., Dwight, K. and Wold, A. (1994). Surface-acidity and photocatalytic activity of TiO_2, WO_3/TiO_2, and MoO_3/TiO_2 photocatalysts. Chem. Mater. 6(4), 496–500.

Paraguay, F., Estrada, W., Acosta, D. R., Andrade, E. and Miki-Yoshida, M. (1999). Growth, structure and optical characterization of high quality ZnO thin films obtained by spray pyrolysis. Thin Solid Films 350(1–2), 192–202.

Paulose, M., Shankar, K., Yoriya, S., Prakasam, H. E., Varghese, O. K., Mor, G. K., Latempa, T. A., Fitzgerald, A. and Grimes, C. A. (2006). Anodic growth of highly ordered TiO_2 nanotube arrays to 134 μ m in length. J. Phys. Chem. B 110(33), 16179–16184.

Peng, B., Jungmann, G., Jager, C., Haarer, D., Schmidt, H. W. and Thelakkat, M. (2004). Systematic investigation of the role of compact TiO_2 layer in solid state dye-sensitized TiO_2 solar cells. Coord. Chem. Rev. 248(13–14), 1479–1489.

Peulon, S. and Lincot, D. (1996). Cathodic electrodeposition from aqueous solution of dense or open-structured zinc oxide films. Adv. Mater. 8(2), 166–170.

Peulon, S. and Lincot, D. (1998). Mechanistic study of cathodic electrodeposition of zinc oxide and zinc hydroxychloride films from oxygenated aqueous zinc chloride solutions. J. Electrochem. Soc. 145(3), 864–874.

Prakasam, H. E., Varghese, O. K., Paulose, M., Mor, G. K. and Grimes, C. A. (2006). Synthesis and photoelectrochemical properties of nanoporous iron (III) oxide by potentiostatic anodization. Nanotechnology 17(17), 4285–4291.

Quan, X., Yang, S. G., Ruan, X. L. and Zhao, H. M. (2005). Preparation of titania nanotubes and their environmental applications as electrode. Environ. Sci. Technol. 39(10), 3770–3775.

Reddy, B. M., Chowdhury, B. and Smirniotis, P. G. (2001). An XPS study of the dispersion of MoO_3 on TiO_2–ZrO_2, TiO_2–SiO_2, TiO_2–Al_2O_3, SiO_2–ZrO_2, and SiO_2–TiO_2–ZrO_2 mixed oxides. Appl. Catal. A-Gen. 211(1), 19–30.

Rensmo, H., Keis, K., Lindstrom, H., Sodergren, S., Solbrand, A., Hagfeldt, A., Lindquist, S. E., Wang, L. N. and Muhammed, M. (1997). High light-to-energy conversion efficiencies for solar cells based on nanostructured ZnO electrodes. J. Phys. Chem. B 101(14), 2598–2601.

Santato, C., Odziemkowski, M., Ulmann, M. and Augustynski, J. (2001). Crystallographically oriented mesoporous WO_3 films: Synthesis, characterization, and applications. J. Am. Chem. Soc. 123(43), 10639–10649.

Sarkar, P. and Nicholson, P. S. (1996). Electrophoretic deposition (EPD): Mechanisms, kinetics, and application to ceramics. J. Am. Ceram. Soc. 79(8), 1987–2002.

Sayari, A., Liu, P., Kruk, M. and Jaroniec, M. (1997). Characterization of large-pore MCM-41 molecular sieves obtained via hydrothermal restructuring. Chem. Mater. 9(11), 2499–2506.

Shah, S. I., Li, W., Huang, C. P., Jung, O. and Ni, C. (2002). Study of Nd^{3+}, Pd^{2+}, Pt^{4+}, and Fe^{3+} dopant effect on photoreactivity of TiO_2 nanoparticles. Proc. Natl Acad. Sci. USA 99, 6482–6486.

Shang, J., Yao, W. Q., Zhu, Y. F. and Wu, N. Z. (2004). Structure and photocatalytic performances of glass/SnO_2/TiO_2 interface composite film. Appl. Catal. A-Gen. 257(1), 25–32.

Shankar, K., Mor, G. K., Prakasam, H. E., Yoriya, S., Paulose, M., Varghese, O. K. and Grimes, C. A. (2007). Highly-ordered TiO_2 nanotube arrays up to 220 μm in length: Use in water photoelectrolysis and dye-sensitized solar cells. Nanotechnology 18(6), 11.

Shchukin, D. G. and Caruso, R. A. (2003). Inorganic macroporous films from preformed nanoparticles and membrane templates: Synthesis and investigation of photocatalytic and photoelectrochemical properties. Adv. Funct. Mater. 13(10), 789–794.

Soejima, T., Tada, H., Kawahara, T. and Ito, S. (2002). Formation of Au nanoclusters on TiO_2 surfaces by a two-step method consisting of Au(III)-complex chemisorption and its photoreduction. Langmuir 18(11), 4191–4194.

Soler-Illia, G., Crepaldi, E. L., Grosso, D. and Sanchez, C. (2003). Block copolymer-templated mesoporous oxides. Curr. Opin. Colloid Interface Sci. 8(1), 109–126.

Somasundaram, S., Chenthamarakshan, C. R., de Tacconi, N. R., Basit, N. A. and Rajeshwar, K. (2006). Composite WO_3–TiO_2 films: Pulsed electrodeposition from a mixed bath versus sequential deposition from twin baths. Electrochem. Commun. 8(4), 539–543.

Song, K. Y., Park, M. K., Kwon, Y. T., Lee, H. W., Chung, W. J. and Lee, W. I. (2001). Preparation of transparent particulate MoO_3/TiO_2 and WO_3/TiO_2 films and their photocatalytic properties. Chem. Mater. 13(7), 2349–2355.

Studenikin, S. A., Golego, N. and Cocivera, M. (1998). Fabrication of green and orange photoluminescent, undoped ZnO films using spray pyrolysis. J. Appl. Phys. 84(4), 2287–2294.

Suda, Y., Kawasaki, H., Ueda, T. and Ohshima, T. (2004). Preparation of high quality nitrogen doped TiO_2 thin film as a photocatalyst using a pulsed laser deposition method. Thin Solid Films 453–54, 162–166.

Suda, Y., Kawasaki, H., Ueda, T. and Ohshima, T. (2005). Preparation of nitrogen-doped titanium oxide thin film using a PLD method as parameters of target material and nitrogen concentration ratio in nitrogen/oxygen gas mixture. Thin Solid Films 475(1–2), 337–341.

Sun, K., Zhu, S., Fromknecht, R., Linker, G. and Wang, L. M. (2004). Formation of single-layered Au nanoparticles in Au ion implanted TiO_2 and $SrTiO_3$. Mater. Lett. 58(5), 547–550.

Sunada, K., Kikuchi, Y., Hashimoto, K. and Fujishima, A. (1998). Bactericidal and detoxification effects of TiO_2 thin film photocatalysts. Environ. Sci. Technol. 32(5), 726–728.

Tada, H., Teranishi, K., Inubushi, Y. and Ito, S. (2000). Ag nanocluster loading effect on TiO_2 photocatalytic reduction of bis(2-dipyridyl)disulfide to 2-mercaptopyridine by H_2O. Langmuir 16(7), 3304–3309.

Tada, H., Mitsui, T., Kiyonaga, T., Akita, T. and Tanaka, K. (2006). All-solid-state Z-scheme in CdS–Au–TiO_2 three-component nanojunction system. Nat. Mater. 5(10), 782–786.

Takahashi, T., Nakabayashi, H., Yamada, N. and Tanabe, J. (2003). Photocatalytic properties of TiO_2/WO_3 bilayers deposited by reactive sputtering. J. Vac. Sci. Technol. A 21(4), 1409–1413.

Takeda, S., Suzuki, S., Odaka, H. and Hosono, H. (2001). Photocatalytic TiO_2 thin film deposited onto glass by DC magnetron sputtering. Thin Solid Films 392(2), 338–344.

Tang, Y. W., Chen, Z. G., Jia, Z. J., Zhang, L. S. and Li, J. L. (2005). Electrodeposition and characterization of nanocrystalline cuprous oxide thin films on TiO_2 films. Mater. Lett. 59(4), 434–438.

Tayade, R. J., Kulkarni, R. G. and Jasra, R. V. (2006). Transition metal ion impregnated mesoporous TiO_2 for photocatalytic degradation of organic contaminants in water. Ind. Eng. Chem. Res. 45(15), 5231–5238.

Teleki, A., Pratsinis, S. E., Kalyanasundaram, K. and Gouma, P. I. (2006). Sensing of organic vapors by flame-made TiO_2 nanoparticles. Sens. Actuator B-Chem. 119(2), 683–690.

Teoh, W. Y., Amal, R., Madler, L. and Pratsinis, S. E. (2007). Flame sprayed visible light-active Fe–TiO_2 for photomineralisation of oxalic acid. Catal. Today 120(2), 203–213.

Tesfamichael, T., Will, G. and Bell, J. (2005). Nitrogen ion implanted nanostructured titania films used in dye-sensitised solar cells and photocatalyst. Appl. Surf. Sci. 245(1–4), 172–178.

Tsuge, Y., Inokuchi, K., Onozuka, K., Shingo, O., Sugi, S., Yoshikawa, M. and Shiratori, S. (2006). Fabrication of porous TiO_2 films using a spongy replica prepared by layer-by-layer self-assembly method: Application to dye-sensitized solar cells. Thin Solid Films 499(1–2), 396–401.

Tsuji, H., Sakai, N., Sugahara, H., Gotoh, Y. and Ishikawa, J. (2005). Silver negative-ion implantation to sol–gel TiO_2 film for improving photocatalytic property under fluorescent light. Nucl. Instrum. Methods Phys. Res. Sect. B-Beam Interact. Mater. Atoms 237(1–2), 433–437.

Tsuji, H., Sakai, N., Gotoh, Y. and Ishikawa, J. (2006). Photocatalytic properties of sol–gel titania film under fluorescent-light irradiation improved by silver negative-ion implantation. Nucl. Instrum. Methods Phys. Res. Sect. B-Beam Interact. Mater. Atoms 242(1–2), 129–132.

Tu, M. L., Su, Y. K. and Ma, C. Y. (2006). Nitrogen-doped p-type ZnO films prepared from nitrogen gas radio-frequency magnetron sputtering. J. Appl. Phys. 100(5), 4.

Uchikoshi, T., Suzuki, T. S., Tang, F., Okuyama, H. and Sakka, Y. (2004). Crystalline-oriented TiO_2 fabricated by the electrophoretic deposition in a strong magnetic field. Ceram. Int. 30(7), 1975–1978.

van Bokhoven, J. A., Louis, C., Miller, J. T., Tromp, M., Safonova, O. V. and Glatzel, P. (2006). Activation of oxygen on gold/alumina catalysts: In situ high-energy-resolution fluorescence and time-resolved X-ray spectroscopy. Angew. Chem. Int. Ed. 45(28), 4651–4654.

Venkov, T., Fajerwerg, K., Delannoy, L., Klimev, H., Hadjiivanov, K. and Louis, C. (2006). Effect of the activation temperature on the state of gold supported on titania: An FT-IR spectroscopic study. Appl. Catal. A-Gen. 301(1), 106–114.

Vinodgopal, K. and Kamat, P. V. (1995). Electrochemically assisted photocatalysis using nanocrystalline semiconductor thin-films. Solar Energy Mater. Solar Cells 38(1–4), 401–410.

Visinescu, C. M., Sanjines, R., Levy, F., Marcu, V. and Parvulescu, V. I. (2005). Tantalum doped titania photocatalysts: Preparation by dc reactive sputtering and catalytic behavior. J. Photochem. Photobiol. A-Chem. 174(2), 106–112.

Vorontsov, A. V., Stoyanova, I. V., Kozlov, D. V., Simagina, V. I. and Savinov, E. N. (2000). Kinetics of the photocatalytic oxidation of gaseous acetone over platinized titanium dioxide. J. Catal. 189(2), 360–369.

Wang, X. and Li, Y. D. (2002). Selected-control hydrothermal synthesis of α- and β-MnO_2 single crystal nanowires. J. Am. Chem. Soc. 124(12), 2880–2881.

Wang, C. M., Zhang, Y., Shutthanandan, V., Thevuthasan, S. and Duscher, G. (2004). Microstructure of precipitated au nanoclusters in TiO_2. J. Appl. Phys. 95(12), 8185–8193.

Wang, X. C., Yu, J. C., Yip, H. Y., Wu, L., Wong, P. K. and Lai, S. Y. (2005). A mesoporous Pt/TiO_2 nanoarchitecture with catalytic and photocatalytic functions. Chem. Eur. J. 11(10), 2997–3004.

Wark, M., Tschirch, J., Bartels, O., Bahnemann, D. and Rathousky, J. (2005). Photocatalytic activity of hydrophobized mesoporous thin films of TiO_2. Microporous Mesoporous Mater. 84(1–3), 247–253.

Weiher, N., Beesley, A. M., Tsapatsaris, N., Delannoy, L., Louis, C., van Bokhoven, J. A. and Schroeder, S. L. M. (2007). Activation of oxygen by metallic gold in Au/TiO_2 catalysts. J. Am. Chem. Soc. 129(8), 2240–2241.

Weinberger, B. R. and Garber, R. B. (1995). Titanium-dioxide photocatalysts produced by reactive magnetron sputtering. Appl. Phys. Lett. 66(18), 2409–2411.

Won, D. J., Wang, C. H., Jang, H. K. and Choi, D. J. (2001). Effects of thermally induced anatase-to-rutile phase transition in MOCVD-grown TiO_2 films on structural and optical properties. Appl. Phys. A-Mater. Sci. Process. 73(5), 595–600.

Wu, N. L., Wang, S. Y. and Rusakova, I. A. (1999). Inhibition of crystallite growth in the sol–gel synthesis of nanocrystalline metal oxides. Science 285(5432), 1375–1377.

Xie, Y. B. (2006). Photoelectrochemical reactivity of a hybrid electrode composed of polyoxophosphotungstate encapsulated in titania nanotubes. Adv. Funct. Mater. 16(14), 1823–1831.

Xu, P., Mi, L. and Wang, P. N. (2006). Improved optical response for N-doped anatase TiO_2 films prepared by pulsed laser deposition in $N_2/NH_3/O_2$ mixture. J. Cryst. Growth 289(2), 433–439.

Yamagishi, M., Kuriki, S., Song, P. K. and Shigesato, Y. (2003). Thin film TiO_2 photocatalyst deposited by reactive magnetron sputtering. Thin Solid Films 442(1–2), 227–231.

Yamashita, H., Honda, M., Harada, M., Ichihashi, Y., Anpo, M., Hirao, T., Itoh, N. and Iwamoto, N. (1998). Preparation of titanium oxide photocatalysts anchored on porous silica glass by a metal

ion-implantation method and their photocatalytic reactivities for the degradation of 2-propanol diluted in water. J. Phys. Chem. B 102(52), 10707–10711.
Yamashita, H., Harada, M., Misaka, J., Takeuchi, M., Ikeue, K. and Anpo, M. (2002). Degradation of propanol diluted in water under visible light irradiation using metal ion-implanted titanium dioxide photocatalysts. J. Photochem. Photobiol. A-Chem. 148(1–3), 257–261.
Yamashita, H., Harada, M., Misaka, J., Takeuchi, M., Neppolian, B. and Anpo, M. (2003). Photocatalytic degradation of organic compounds diluted in water using visible light-responsive metal ion-implanted TiO_2 catalysts: Fe ion-implanted TiO_2. Catal. Today 84(3–4), 191–196.
Yang, W. L. and Wolden, C. A. (2006). Plasma-enhanced chemical vapor deposition of TiO_2 thin films for dielectric applications. Thin Solid Films 515(4), 1708–1713.
Yang, P. D., Deng, T., Zhao, D. Y., Feng, P. Y., Pine, D., Chmelka, B. F., Whitesides, G. M. and Stucky, G. D. (1998). Hierarchically ordered oxides. Science 282(5397), 2244–2246.
Yang, T. S., Yang, M. C., Shiu, C. B., Chang, W. K. and Wong, M. S. (2006). Effect of N_2 ion flux on the photocatalysis of nitrogen-doped titanium oxide films by electron-beam evaporation. Appl. Surf. Sci. 252(10), 3729–3736.
Yoshida, T., Terada, K., Schlettwein, D., Oekermann, T., Sugiura, T. and Minoura, H. (2000). Electrochemical self-assembly of nanoporous ZnO/eosin Y thin films and their sensitized photoelectrochemical performance. Adv. Mater. 12(16), 1214–1217.
You, X. F., Chen, F., Zhang, J. L. and Anpo, M. (2005). A novel deposition precipitation method for preparation of Ag-loaded titanium dioxide. Catal. Lett. 102(3–4), 247–250.
Yu, J. G., Zhao, X. J. and Zhao, Q. N. (2000). Effect of surface structure on photocatalytic activity of TiO_2 thin films prepared by sol–gel method. Thin Solid Films 379(1–2), 7–14.
Yu, J. C., Wang, X. C., Wu, L., Ho, W. K., Zhang, L. Z. and Zhou, G. T. (2004). Sono- and photochemical routes for the formation of highly dispersed gold nanoclusters in mesoporous titania films. Adv. Funct. Mater. 14(12), 1178–1183.
Zanella, R. and Louis, C. (2005). Influence of the conditions of thermal treatments and of storage on the size of the gold particles in Au/TiO_2 samples. Catal. Today 107–08, 768–777.
Zanella, R., Giorgio, S., Henry, C. R. and Louis, C. (2002). Alternative methods for the preparation of gold nanoparticles supported on TiO_2. J. Phys. Chem. B 106(31), 7634–7642.
Zanella, R., Delannoy, L. and Louis, C. (2005). Mechanism of deposition of gold precursors onto TiO_2 during the preparation by cation adsorption and deposition–precipitation with NaOH and urea. Appl. Catal. A-Gen. 291(1–2), 62–72.
Zhang, S., Zhu, Y. F. and Brodie, D. E. (1992). Photoconducting TiO_2 prepared by spray pyrolysis using $TiCl_4$. Thin Solid Films 213(2), 265–270.
Zhang, M., Bando, Y. and Wada, K. (2001). Sol–gel template preparation of TiO_2 nanotubes and nanorods. J. Mater. Sci. Lett. 20(2), 167–170.
Zhang, D. S., Yoshida, T. and Minoura, H. (2002). Low temperature synthesis of porous nanocrystalline TiO_2 thick film for dye-sensitized solar cells by hydrothermal crystallization. Chem. Lett. (9), 874–875.
Zhang, W. J., Li, Y., Zhu, S. L. and Wang, F. H. (2003). Fe-doped photocatalytic TiO_2 film prepared by pulsed dc reactive magnetron sputtering. J. Vac. Sci. Technol. A 21(6), 1877–1882.
Zhang, W. J., Li, Y., Zhu, S. L. and Wang, F. H. (2004). Influence of argon flow rate on TiO_2 photocatalyst film deposited by dc reactive magnetron sputtering. Surf. Coat. Technol. 182(2–3), 192–198.
Zhang, X. W., Zhou, M. H. and Lei, L. C. (2006). Co-deposition of photocatalytic Fe doped TiO_2 coatings by MOCVD. Catal. Commun. 7(7), 427–431.
Zhao, D. Y., Feng, J. L., Huo, Q. S., Melosh, N., Fredrickson, G. H., Chmelka, B. F. and Stucky, G. D. (1998a). Triblock copolymer syntheses of mesoporous silica with periodic 50 to 300 angstrom pores. Science 279(5350), 548–552.
Zhao, D. Y., Huo, Q. S., Feng, J. L., Chmelka, B. F. and Stucky, G. D. (1998b). Nonionic triblock and star diblock copolymer and oligomeric surfactant syntheses of highly ordered, hydrothermally stable, mesoporous silica structures. J. Am. Chem. Soc. 120(24), 6024–6036.
Zheng, S. K., Wang, T. M., Xiang, G. and Wang, C. (2001). Photocatalytic activity of nanostructured TiO_2 thin films prepared by dc magnetron sputtering method. Vacuum 62(4), 361–366.

Zheng, S. K., Wang, T. M., Hao, W. C. and Shen, R. (2002a). Improvement of photocatalytic activity of TiO_2 thin film by Sn ion implantation. Vacuum 65(2), 155–159.

Zheng, S. K., Wang, T. M., Wang, C. and Xiang, G. (2002b). Photocatalytic activity study of TiO_2 thin films with and without Fe ion implantation. Nucl. Instrum. Methods Phys. Res. Sect. B-Beam Interact. Mater. Atoms 187(4), 479–484.

Zhou, J. K., Takeuchi, M., Zhao, X. S., Ray, A. K. and Anpo, M. (2006). Photocatalytic decomposition of formic acid under visible light irradiation over V-ion-implanted TiO_2 thin film photocatalysts prepared on quartz substrate by ionized cluster beam (ICB) deposition method. Catal. Lett. 106(1–2), 67–70.

Zhu, Y. C., Li, H. L., Koltypin, Y., Hacohen, Y. R. and Gedanken, A. (2001). Sonochemical synthesis of titania whiskers and nanotubes. Chem. Commun. 24, 2616–2617.

Chapter 19
Use of Both Anode and Cathode Reactions in Wastewater Treatment

Enric Brillas, Ignasi Sirés, and Pere Lluís Cabot

19.1 Introduction

In the last decade, indirect electro-oxidation methods based on the cathodic electrogeneration of hydrogen peroxide are being developed for the treatment of acidic wastewaters containing toxic and refractory (nonbiodegradable) organic pollutants. They are environmentally friendly techniques considered as electrochemical advanced oxidation processes (Brillas et al. 2000), since their main oxidant is the in situ electrogenerated hydroxyl radical ($^{\bullet}$OH). The most usual method is electro-Fenton that can be easily applied using divided and undivided electrolytic cells. In the first case, $^{\bullet}$OH is produced by the catalytic Fenton's reaction of Fe^{2+} with electrogenerated H_2O_2, whereas in the second one this radical is also formed from water oxidation at the anode surface. The electro-Fenton process in undivided cells then profits from the oxidative ability of both anode and cathode reactions, being more efficient to destroy organics than anodic oxidation with electrogenerated H_2O_2. Its oxidation power depends on the kind of anode, cathode, and metallic ion catalyst (Fe^{2+}, Fe^{3+}, Cu^{2+}, etc.) used. Novel indirect electro-oxidation methods like photoelectro-Fenton and peroxi-coagulation have been recently proposed to enhance the efficiency of electro-Fenton in undivided cell taking into account the catalytic action of UVA light and the alternative use of a sacrificial iron anode, respectively. Fundamentals, laboratory experiments, and environmental applications of these emerging techniques are discussed in this chapter.

E. Brillas (✉)
Laboratori d'Electroquímica dels Materials i del Medi Ambient, Departament de Química Física, Facultat de Química, Universitat de Barcelona, Martí i Franquès 1–11, 08028 Barcelona, Spain
e-mail: brillas@ub.edu

C. Comninellis and G. Chen (eds.), *Electrochemistry for the Environment*,
DOI 10.1007/978-0-387-68318-8_19,

19.2 Fundamentals of Indirect Electro-oxidation Methods Based on H_2O_2 Electrogeneration

Hydrogen peroxide is a "green" chemical that leaves O_2 and water as by-products. It is used to bleach pulp and paper and textiles, clean electronic circuits, and delignify agricultural wastes, as well as a disinfectant in medical and industrial applications and as an oxidant in synthesis and wastewater treatment (Plant and Jeff 1994; Pletcher 1999; Drogui et al. 2001a, b). However, the direct treatment with applied H_2O_2 shows some limitations by its low oxidation power, since it can only attack reduced sulfur compounds, cyanides, chlorine (it is reduced to chloride ion), and certain organics such as aldehydes, formic acid, and some nitro-organic and sulfo-organic compounds. More effective wastewater treatments have been proposed by activating H_2O_2 with an iron catalyst (Fenton's reagent), ozone, or UVC light at $\lambda_{max} = 254\,nm$. These chemical and photochemical methods are advanced oxidation processes where organic pollutants can be destroyed efficiently by the in situ generated strong oxidant $^{\bullet}OH$. In this section, we will see that this oxidant radical can also be produced by means of alternative indirect electro-oxidation methods based on the generation of H_2O_2 from the cathodic reduction of O_2.

19.2.1 Cathodic Electrogeneration of Hydrogen Peroxide

It is known since 1882 that hydrogen peroxide can be formed in aqueous NaOH by the cathodic reduction of dissolved O_2 at high surface area carbon electrodes (Traube 1882). From this pioneering work, a large number of papers and patents have been published dealing with the electrogeneration of alkaline H_2O_2 solutions from pure O_2 and air using carbon-based cathodes for different purposes. More recently, the electrogeneration of H_2O_2 in acid medium has been applied to wastewater remediation. In this scenario, the reduction of dissolved O_2 on reticulated vitreous carbon (RVC), graphite, and carbon-felt cathodes and directly injected O_2 or air to gas diffusion have been mainly reported. Several papers have also checked the reduction of O_2 at a mercury cathode for wastewater treatment (Tzedakis et al. 1989; Ventura et al. 2002), but the use of this toxic material is discarded for environmental applications.

The overall two-electron reduction of O_2 gas to H_2O_2 in acid medium proceeds as follows (Foller and Bombard 1995):

$$O_{2(g)} + 2H^+ + 2e^- \rightarrow H_2O_2 \tag{19.1}$$

Hydrogen peroxide production and stability depend on several factors like the cell configuration, the cathode used, and the experimental conditions applied. Electrochemical reduction on the cathode surface by reaction (19.2) and in much lesser

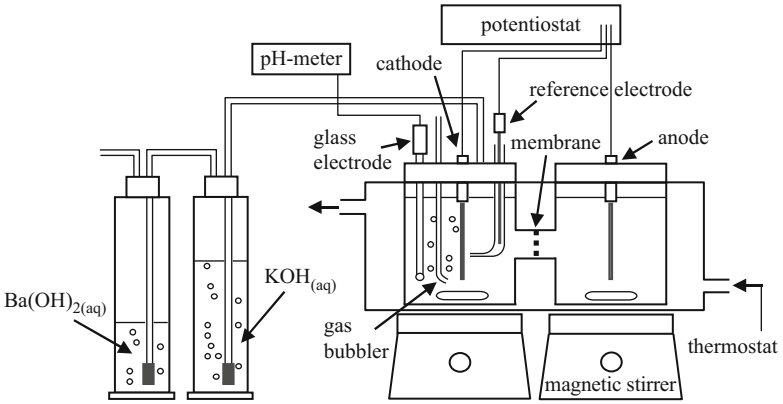

Fig. 19.1 Sketch of an H-type two-compartment cell and equipment utilized for cathodic electrogeneration of H_2O_2 and degradation of organics. O_2 is bubbled near the cathode and released CO_2 was collected and quantified [adapted from Sudoh et al. (1986)]

extent disproportion in the bulk solution by reaction (19.3) are general parasite reactions which result in the loss of product or a lowering of observed current efficiency (Alvarez Gallegos et al. 2005):

$$H_2O_2 + 2e^- \rightarrow 2OH^- \tag{19.2}$$

$$2H_2O_2 \rightarrow O_{2(g)} + 2H_2O \tag{19.3}$$

For an H-type two-compartment cell with a graphite cathode (see scheme in Fig. 19.1), Sudoh et al. (1986) reported a maximum current efficiency of 85% for H_2O_2 production in 0.5 M Na_2SO_4 as the catholyte by applying a cathodic potential (E_{cat}) of −0.6 V vs. Ag/AgCl/saturated KCl at pH 3 under O_2 sparging. They also found a gradual increase in H_2O_2 concentration with prolonging electrolysis time in the pH range 1–3. Do and Chen (1993) described similar results using the same electrolytic system and showed a drop in current efficiency for E_{cat} more negative than −0.39 V vs. Ag/AgCl/3 M KCl due to the side reaction (19.2) along with H_2 evolution from direct proton reduction and H_2O_2 decomposition via reaction (19.3) when temperature rises from 25°C. A sparging O_2 rate higher than 5 $cm^3\ s^{-1}$ was needed to keep the catholyte saturated with this gas (solubility ≈1 mM) while it is transfered from the bulk to the cathode to be reduced to H_2O_2 by reaction (19.1). Da Pozzo et al. (2005a) confirmed this behavior for a graphite cathode in several divided three-electrode cells, determining current efficiencies as high as 85% for H_2O_2 production in 0.04 M Na_2SO_4 + 0.05 M $NaHSO_4$ as the catholyte at the optimum $E_{cat} = -0.6$ V vs. SCE, practically independent of time.

Alvarez-Gallegos and Pletcher (1998) used the flow divided three-electrode cell fed with O_2 and flow circuit depicted in Fig. 19.2 to generate H_2O_2 at a three-dimensional RVC cathode. Maximum current efficiencies of 56–68% were obtained for 10 mM HCl and 10 mM H_2SO_4 (pH ≈ 2) as catholytes at E_{cat} values

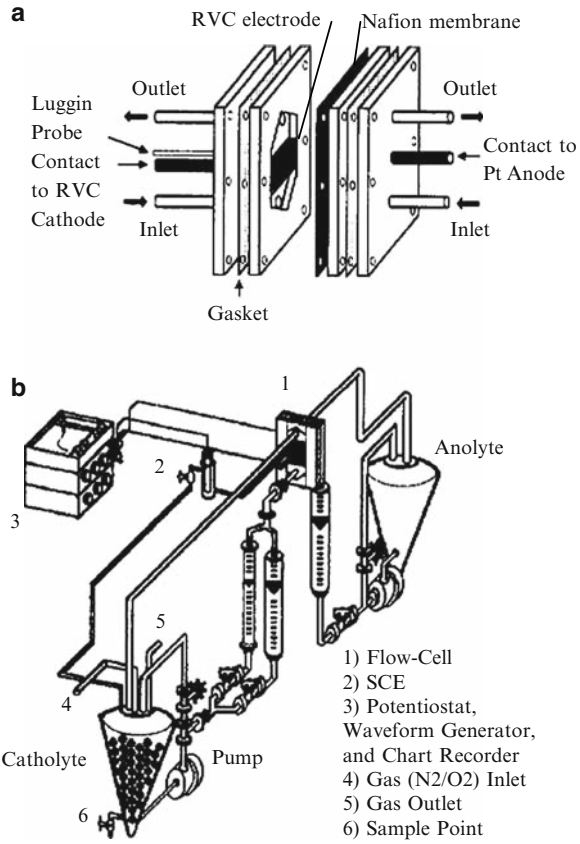

Fig. 19.2 Sketches of (**a**) a flow divided three-electrode cell with an RVC cathode and (**b**) the flow circuit used for H_2O_2 electrogeneration (Alvarez-Gallegos et al. 1998)

between −0.4 and −0.7 V vs. SCE, which slightly increased by adding NaCl and Na_2SO_4 as background electrolyte, respectively. Harrington and Pletcher (1999) further explored the ability of a carbon-polytetrafluoroethylene (PTFE) O_2-diffusion cathode to form H_2O_2 in a 0.05 M Na_2SO_4 solution of pH 2 using a small divided three-electrode cell, but they found that H_2O_2 concentration reaches a steady value of 5 mM at $E_{cat} = -0.5$ V vs. SCE due to its fast decomposition. These results disagree with those reported by Da Pozzo et al. (2005a), who found a constant H_2O_2 production with current efficiency >90% when an E_{cat} value of −0.9 V vs. SCE is applied to a carbon-PTFE O_2-fed cathode immersed in a 0.04 M Na_2SO_4 + 0.05 M $NaHSO_4$ as the catholyte of a three-electrode cell. Current efficiencies >95% for H_2O_2 electrogeneration have also been obtained for a similar O_2-diffusion cathode in a divided Pt/O_2 electrolytic cell containing a KCl solution of pH 3.0–3.5 as the catholyte under galvanostatic electrolysis at 80 mA (Boye et al. 2006).

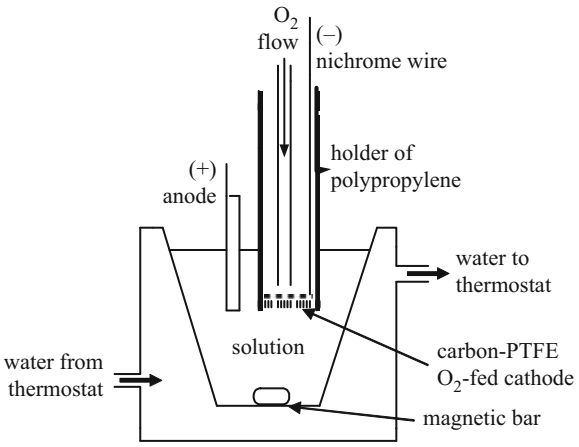

Fig. 19.3 Scheme of an open and undivided Pt/O_2 cell of 100 cm^3 capacity with an O_2-diffusion cathode used for the degradation of organic pollutants by indirect electro-oxidation methods with Pt, BDD, and Fe anodes (Brillas et al. 1995)

A very different behavior is found when undivided electrolytic cells are used for H_2O_2 production. Figure 19.3 presents a scheme of an open and undivided Pt/O_2 cell containing a 10-cm^2 Pt sheet anode, a 3-cm^2 carbon-PTFE O_2-fed cathode, and 100 cm^3 of a 0.05 M Na_2SO_4 solution of pH 3.0 vigorously stirred with a magnetic bar (Brillas et al. 1996). For this system, H_2O_2 is gradually accumulated during the initial 3 h of electrolysis up to reach a steady value, as can be seen in Fig. 19.4 at 450 mA (curve *a*), 300 mA (curve *b*), and 100 mA (curve *e*) (Brillas et al. 2000). The steady H_2O_2 content increases with increasing current and it is attained just when its electrogeneration rate becomes equal to its oxidation rate to O_2 via hydroperoxyl radical $\left(HO_2^{\bullet}\right)$ at the Pt anode surface by the following reactions (Brillas et al. 1995):

$$H_2O_2 \rightarrow HO_2^{\bullet} + H^+ + e^- \tag{19.4}$$

$$HO_2^{\bullet} \rightarrow O_{2(g)} + H^+ + e^- \tag{19.5}$$

Similar trends for H_2O_2 accumulation have also been described by Badellino et al. (2006) in an undivided Pt/RVC cell under potentiostatic control (see a scheme of this kind of cell in Fig. 19.5) and by Wang et al. (2005) in an undivided RuO_2/carbon-felt cell under galvanostatic control. These results confirm the anodic decomposition of H_2O_2 with formation of intermediate $HO_2^{\bullet}$ from reaction (19.4), a much weaker oxidant than $^{\bullet}OH$.

Recently, Xie and Li (2006a) suggested the conversion of electrogenerated H_2O_2 into $^{\bullet}OH$ on a TiO_2–Ti semiconductor anode illuminated with UVA light at $\lambda_{max} =$ 360 nm using the undivided cell sketched in Fig. 19.6 containing 13 cm^3 of 0.01 M Na_2SO_4 and an RVC cathode controlled by an SCE as the reference electrode. They found a much lower H_2O_2 accumulation in the TiO_2–Ti/RVC cell than in a Pt/RVC

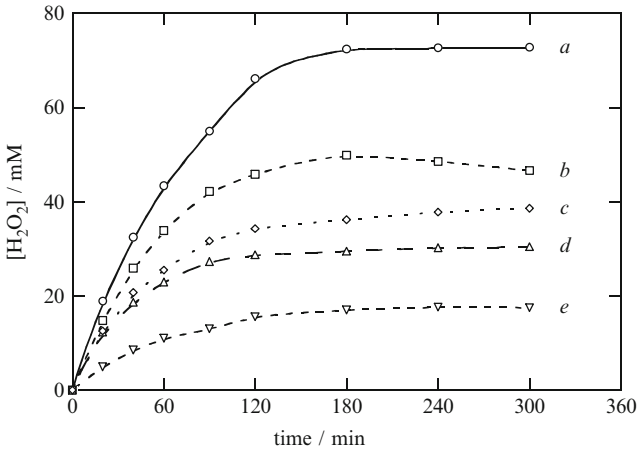

Fig. 19.4 Concentration of accumulated H_2O_2 vs. time during the electrolysis of 100 cm^3 of a 0.05 M Na_2SO_4 + H_2SO_4 solution of pH 3.0 at 25°C in the Pt/O_2 cell of Fig. 19.3. (**a, b, e**) Without Fe^{2+} (anodic oxidation with electrogenerated H_2O_2), (**c**) with 1 mM Fe^{2+} (electro-Fenton conditions), (**d**) in the presence of 1 mM Fe^{2+} and under 6-W UVA irradiation (photoelectro-Fenton conditions). Applied current: (**a**) 450, (**b, c, d**) 300,(**e**) 100 mA (Brillas et al. 2000)

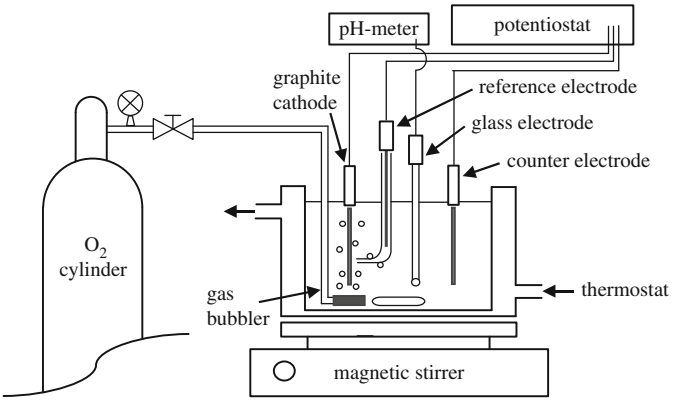

Fig. 19.5 Scheme of an undivided electrolytic cell fed with oxygen to electrogenerate H_2O_2 for the treatment of wastewaters [adapted from Panizza et al. (2001)]

one under comparable electrolytic conditions, along with an enhancement of the oxidation power of the photoelectrochemical system to destroy pollutants. This behavior is explained by the expected promotion of one electron from the valence band to the conduction band $\left(e_{CB}^-\right)$ of TiO_2 by UVA light with production of a hole $\left(h^+\right)$ from reaction (19.6), followed by the direct reduction of accumulated H_2O_2 with e_{CB}^- to yield $^\bullet OH$ by reaction (19.7):

$$TiO_2 + h\nu \rightarrow h^+ + e_{CB}^- \tag{19.6}$$

$$e_{CB}^- + H_2O_2 \rightarrow {}^\bullet OH + OH^- \tag{19.7}$$

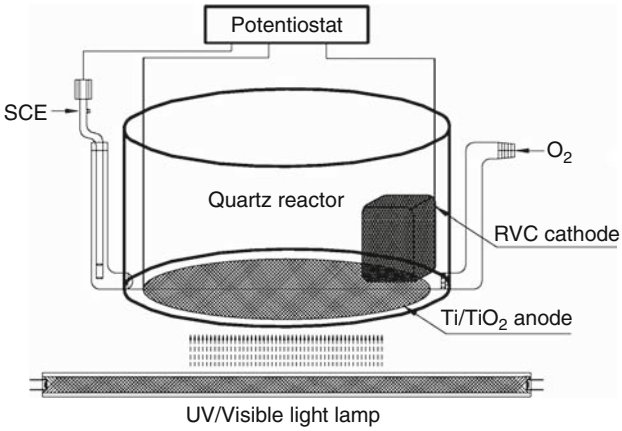

Fig. 19.6 Schematic diagram of the photoreactor equipment with a cylindrical quartz cell containing a three-electrode assembly fed with oxygen (Xie et al. 2006a)

$^{\bullet}OH$ can also be formed by oxidation of water with h^+ (Xie and Li 2006) as follows:

$$H_2O + h^+ \rightarrow {}^{\bullet}OH + H^+ \tag{19.8}$$

19.2.2 Anodic Oxidation with Electrogenerated H_2O_2

Anodic oxidation is one of the most common electrochemical technologies for the treatment of wastewaters with low contents of organics pollutants. In acid medium, this method involves the destruction of contaminants with adsorbed $^{\bullet}OH$ generated at the surface of a high O_2-overpotential anode as intermediate during water oxidation to O_2 (Comninellis and De Battisti 1996; Panizza and Cerisola 2005):

$$H_2O \rightarrow {}^{\bullet}OH + H^+ + e^- \tag{19.9}$$

$^{\bullet}OH$ is the second most strong oxidizing agent known after fluorine due to its high standard potential ($E°$ ($^{\bullet}OH/H_2O$) = 2.80 V vs. SHE). This radical is then able to react nonselectively with organics giving dehydrogenated or hydroxylated derivatives up to total mineralization, i.e., overall conversion into CO_2, water, and inorganic ions (sulfate, nitrate, chloride, etc. depending on the heteroatoms of the organic pollutant).

The use of a classical anode such as Pt in anodic oxidation usually leads to a partial mineralization of wastewaters containing aromatics due to the formation of final short-chain carboxylic acids, as oxalic acid, that hardly react with $^{\bullet}OH$. Overall mineralization is feasible with a boron-doped diamond (BDD) anode that possesses a much greater O_2 overpotential compared to Pt, thus producing a higher amount of

reactive $^{\bullet}OH$ with ability to destroy such aliphatic acids. Evidence on the formation of this radical from reaction (19.9) with concomitant evolution of O_2 in active (like Pt) and nonactive (like BDD) anodes in acid medium has been reported (Marselli et al. 2003). In addition, in sulfate medium other weaker oxidants such as peroxodisulfate ion and ozone can be competitively formed with $^{\bullet}OH$ at the BDD anode from the following reactions (Panizza et al. 2005):

$$2HSO_4^- \rightarrow {S_2O_8}^{2-} + 2H^+ + 2e^- \quad (19.10)$$

$$3H_2O \rightarrow O_{3(g)} + 6H^+ + 6e^- \quad (19.11)$$

Several indirect electro-oxidation methods based on H_2O_2 electrogeneration have then been proposed by combining a high O_2-overpotential anode and a cathode that produces hydrogen peroxide in an undivided electrolytic cell to decontaminate wastewaters under the action of oxidizing species formed from both anode and cathode reactions. The simplest technique without catalysts is the so-called anodic oxidation with electrogenerated H_2O_2. An example is the Pt/O_2 cell of Fig. 19.3 containing 100 cm^3 of 0.05 M Na_2SO_4 of pH 3.0. This system accumulates H_2O_2 during electrolysis at 450, 300, and 100 mA, as shown in curves *a*, *b*, and *e* of Fig. 19.4, respectively. However, this method is not more useful in practice than direct anodic oxidation (without H_2O_2) for wastewater treatment, since pollutants undergo similar destruction rate in both cases because their main oxidant is $^{\bullet}OH$ formed at the anode surface from reaction (19.9), with much smaller participation of other weaker oxidants like H_2O_2, $HO_2^{\bullet}$, ${S_2O_8}^{2-}$, and O_3 formed from reactions (19.1), (19.4), (19.10), and (19.11), respectively. Examples on the degradation of some organics by anodic oxidation with electrogenerated H_2O_2 using undivided cells with a Pt or BDD anode, to show the much higher oxidation power that possesses the electro-Fenton process with Fe^{2+} as catalyst under comparable electrolytic conditions, will be given below.

19.2.3 Electro-Fenton Method

The electro-Fenton method, called electrogenerated Fenton's reagent (EFR) by Sudoh et al. (1986), consists in the degradation of an acidic wastewater in an electrolytic cell where H_2O_2 is continuously supplied to it by reaction (19.1) in the presence of a small quantity of Fe^{2+} or Fe^{3+} as catalyst. Under these conditions, Fe^{2+} and electrogenerated H_2O_2 react to produce $^{\bullet}OH$ and Fe^{3+} by the following well-known Fenton's reaction (Sudoh et al. 1986; Sun and Pignatello 1993; De Laat and Gallard 1999):

$$Fe^{2+} + H_2O_2 \rightarrow Fe^{3+} + {}^{\bullet}OH + OH^- \quad (19.12)$$

An advantage of this method is the catalytic behavior of the Fe^{3+}/Fe^{2+} system. Thus, Fe^{2+} can be regenerated mainly from the reduction of Fe^{3+} at the cathode

by reaction (19.13) and in smaller extent from the reduction of Fe^{3+} with H_2O_2 by reaction (19.14), with $HO_2^{\bullet}$ by reaction (19.15) and/or with organic radical intermediates $R^{\bullet}$ by reaction (19.16):

$$Fe^{3+} + e^- \rightarrow Fe^{2+} \tag{19.13}$$

$$Fe^{3+} + H_2O_2 \rightarrow Fe^{2+} + H^+ + HO_2^{\bullet} \tag{19.14}$$

$$Fe^{3+} + HO_2^{\bullet} \rightarrow Fe^{2+} + H^+ + O_{2(g)} \tag{19.15}$$

$$Fe^{3+} + R^{\bullet} \rightarrow Fe^{2+} + R^+ \tag{19.16}$$

Reactions (19.13)–(19.16) propagate Fenton's reaction (19.12) with the continuous production of $^{\bullet}OH$ giving rise to the fast destruction of organic pollutants in the bulk solution. However, a part of this radical is lost by the oxidation of Fe^{2+} from reaction (19.17) and by decomposition of H_2O_2 from reaction (19.18):

$$Fe^{2+} + {}^{\bullet}OH \rightarrow Fe^{3+} + OH^- \tag{19.17}$$

$$H_2O_2 + {}^{\bullet}OH \rightarrow HO_2^{\bullet} + H_2O \tag{19.18}$$

The rate of Fenton's reaction (19.12) can also decay by oxidation of Fe^{2+} in the bulk with $HO_2^{\bullet}$ by reaction (19.19) and at the anode by reaction (19.20) when an undivided cell is used:

$$Fe^{2+} + HO_2^{\bullet} \rightarrow Fe^{3+} + HO_2^- \tag{19.19}$$

$$Fe^{2+} \rightarrow Fe^{3+} + e^- \tag{19.20}$$

Several authors (Alvarez-Gallegos et al. 1998; Brillas et al. 1996, 2000, 2004a; Badellino et al. 2006) confirmed the fall of H_2O_2 concentration in solution under electro-Fenton conditions in comparison to that accumulated in the absence of Fe^{2+} due to reactions (19.12), (19.14), and (19.18). This trend can be deduced from comparison of curves *b* and *c* of Fig. 19.4 obtained when 100 cm^3 of 0.05 M Na_2SO_4 of pH 3.0 without and with 1 mM Fe^{2+}, respectively, are electrolyzed in an undivided Pt/O_2 cell at 300 mA. It has also been reported the concomitant decay of Fe^{2+} content during the electro-Fenton process (Alvarez-Gallegos et al. 1998; Brillas et al. 1996). The regeneration of Fe^{2+} from Fe^{3+} reduction by reaction (19.13) on a graphite cathode has been exhaustively studied by Qiang et al. (2003), who demonstrated that the optimum potential for this reduction is $E_{cat} = -0.1$ V vs. SCE and that the regeneration rate for Fe^{2+} is accelerated by increasing cathode area surface and solution temperature.

In an undivided electrolytic cell, the electro-Fenton process leads to the destruction of organics contained in wastewaters by simultaneous oxidation with $^{\bullet}OH$ formed at the anode surface from reaction (19.9) and in the medium from Fenton's reaction (19.12). Parallel slower reaction of pollutants with weaker oxidants such as H_2O_2, $HO_2^{\bullet}$, $S_2O_8^{2-}$, and O_3 formed from reactions (19.1), (19.4), (19.10), and (19.11), respectively, is also possible. In addition, final carboxylic acids can form complexes with iron ions that are difficult to be oxidized by $^{\bullet}OH$. We will see the notable influence of the anode material (Pt or BDD) on the degradation of these compounds in further sections.

Some papers (Brillas et al., 2004a; Sirés et al. 2006) have explored the effect of Cu^{2+} as co-catalyst in the electro-Fenton treatment of organics. The Cu^{2+}/Cu^{+} system is also catalytic (Sharma and Millero 1988; Gallard et al. 1999) involving the reduction of Cu^{2+} to Cu^{+} with $HO_2^{\bullet}$ by reaction (19.21) and/or with organic radicals $R^{\bullet}$ by reaction (19.22)

$$Cu^{2+} + HO_2^{\bullet} \rightarrow Cu^{+} + H^{+} + O_{2(g)} \tag{19.21}$$

$$Cu^{2+} + R^{\bullet} \rightarrow Cu^{+} + R^{+} \tag{19.22}$$

followed by regeneration of Cu^{2+} by oxidation of Cu^{+} with H_2O_2 from the following Fenton-like reaction:

$$Cu^{+} + H_2O_2 \rightarrow Cu^{2+} + {}^{\bullet}OH + OH^{-} \tag{19.23}$$

An enhancement of the oxidation power of the electro-Fenton process with both Fe^{2+} and Cu^{2+} as catalysts should then be expected due to the additional generation of $^{\bullet}OH$ from reaction (19.23), but a more significant effect on the oxidation of final aliphatic acids has been found by the easier oxidation of their complexes with Cu^{2+} than with Fe^{3+}, as described below.

19.2.4 Photoelectro-Fenton Method

The photoelectro-Fenton method involves the simultaneous irradiation of the wastewater with UVA light while it is degraded by electro-Fenton in an undivided cell. UVA irradiation favors the regeneration of Fe^{2+} from additional photoreduction of $Fe(OH)^{2+}$, which is the predominant Fe^{3+} species in acid medium (Sun et al. 1993):

$$Fe(OH)^{2+} + h\nu \rightarrow Fe^{2+} + {}^{\bullet}OH \tag{19.24}$$

The acceleration of H_2O_2 destruction mainly from Fenton's reaction (19.12) due to the above Fe^{2+} regeneration under UVA illumination can be corroborated by comparing curves *c* (without UVA light) and *d* (with UVA light) of Fig. 19.4 determined during the electrolysis of 100 cm^3 of a solution containing 0.05 M Na_2SO_4 and 1 mM Fe^{2+} of pH 3.0 in an undivided Pt/O_2 cell at 300 mA.

In the photoelectro-Fenton process the mineralization of organic pollutants can be enhanced by the production of more $^{\bullet}OH$ from reaction (19.24) and the additional acceleration of Fenton's reaction (19.12). However, we will see that the main action of UVA irradiation is the photodecomposition of complexes between Fe^{3+} and some final aliphatic acids, as for example oxalic acid (Zuo and Hoigné 1992).

19.2.5 Peroxi-coagulation Method

The peroxi-coagulation method uses a sacrificial iron anode to treat a wastewater in an undivided cell containing a cathode that electrogenerates H_2O_2 from reaction (19.1). In this process, soluble Fe^{2+} is continuously supplied to the solution from the oxidation of a Fe anode as follows (Brillas et al. 1997, 1998b):

$$Fe \longrightarrow Fe^{2+} + 2e^- \tag{19.25}$$

Fe^{2+} thus formed is quickly oxidized by electrogenerated H_2O_2 from Fenton's reaction (19.12) yielding a Fe^{3+} saturated solution, whereas the excess of this ion precipitates as hydrated Fe(III) oxide ($Fe(OH)_3$). Organics can then be removed from the wastewater by the combined action of their degradation with $^{\bullet}OH$ generated by Fenton's reaction (19.12) and their coagulation with the high amount of $Fe(OH)_3$ precipitate formed. No hydrogen peroxide is accumulated in the bulk. Peroxi-coagulation differs from classical electrocoagulation with a Fe anode and an inert cathode, where soluble organics are not oxidized by the absence of electrogenerated H_2O_2, although they can be separated from the medium by precipitation of their complexes with injected iron ions. A related procedure is the so-called anodic Fenton treatment (Pratap and Lemley 1998; Wang and Lemley 2001, 2002, 2003; Wang et al. 2004) in which H_2O_2 is directly added to the treated solution contained in the anodic compartment of a divided cell with a Fe anode. This method will not be explained here because it does not use cathode reactions for wastewater treatment.

19.3 Electro-Fenton Degradation of Organics Using a Divided Cell

This section is devoted to discuss the main results obtained for the treatment of organics in wastewaters by electro-Fenton using a divided cell usually with a cationic membrane (e.g., of Nafion) to separate the anolyte and catholyte. Although the anode reactions do not affect the degradation of pollutants under these conditions, it is interesting to know the characteristics of their homogeneous oxidation with $^{\bullet}OH$ when this radical is uniquely formed in the medium from Fenton's reaction (19.12).

The electro-Fenton method (or EFR) was initially used for synthetic purposes considering the hydroxylation of aromatics in the cathodic compartment of a divided cell. Thus, the production of phenol from benzene (Tomat and Vecchi 1971; Tzedakis et al. 1989), (methyl)benzaldehydes and (methyl)benzyl alcohols from toluene or polymethylbenzenes (Tomat and Rigo 1976,1979, 1984, 1985) by adding Fe^{3+} to generate Fe^{2+} via reaction (19.13), as well as benzaldehyde and cresol isomers from toluene or acetophenone and ethylphenol isomers from ethylbenzene (Matsue et al. 1981) with direct addition of Fe^{2+}, have been described. Further studies have reported the polyhydroxylation of salicylic acid (Oturan et al. 1992)

and benzoic acid (Oturan and Pinson 1995) at pH 3 by $^{\bullet}OH$ generated on a mercury cathode at $E_{cat} = -0.5$V vs. SCE with addition of Fe^{3+}. Mono-, di-, and trihydroxylated derivatives of chlorophenoxy herbicides and other aromatic pesticides using a Hg cathode (Oturan et al. 1999a) or a carbon-felt cathode (Aaron and Oturan 2001) and the metabolites of riluzole using a carbon cathode (Oturan et al. 1999b) under similar experimental conditions have also been identified.

As far as we know, Sudoh et al. (1986) were the first to use the electro-Fenton process for wastewater treatment. They degraded 170 cm^3 of O_2-saturated phenol solutions with Fe^{2+} as catalyst in the cathodic compartment of the H-type Pt/graphite cell of Fig. 19.1 at $E_{cat} = -0.6$ V vs. Ag/AgCl/saturated KCl. Under these conditions, phenol is mineralized to CO_2 via hydroquinone, catechol, *p*-benzoquinone, muconic acid, and maleic acid as intermediates. The current efficiency was >60% for 260–2,600 mg O_2 dm^{-3} of initial chemical oxygen demand (COD) at pH 3 and the optimum Fe^{2+} content was 2 mM for 2.5 mM phenol. Recently, a similar H-type cell with a stainless steel anode and an RVC cathode has been utilized to successfully decolorize the industrial wastewaters containing azo dyes (Alvarez Gallegos et al. 2005). The energy needed for the treatment was supplied by a solar panel and iron ions released from anode oxidation passed the membrane to produce the oxidant $^{\bullet}OH$ by Fenton's reaction (19.12) with electrogenerated H_2O_2 in the cathodic compartment containing the O_2-saturated wastewater.

Ponce de Leon and Pletcher (1995) reported the degradation of 2.5 dm^3 of formaldehyde solutions saturated with O_2 under batch recycling in a flow divided cell with an RVC cathode (similar to that of Fig. 19.2) at $E_{cat} = -0.6$ V vs. SCE. Total organic carbon (TOC) analysis of electrolyzed solutions confirmed their complete mineralization to CO_2 under electro-Fenton conditions. The greatest current efficiency was 24% for the removal of 75% of 12 mg dm^{-3} formaldehyde with 0.5 mM $FeCl_2$ at pH 3 after 2,000 s of treatment. Addition of 10 mM NaCl or 10 mM HCl to this solution caused a slower degradation. Following the study on H_2O_2 electrogeneration in the flow reactor and circuit of Fig. 19.2 above explained, Alverez-Gallegos and Pletcher (1999) used this system to treat 1 dm^3 of O_2-saturated 0.05 M $Na_2SO_4 + H_2SO_4$ solutions of pH 2 containing different organics and 1mM Fe^{2+} at $E_{cat} = -0.7$ V vs. SCE. The COD of solutions with phenol, cresol, catechol, *p*-benzoquinone, aniline, oxalic acid, and the azo dye amaranth was reduced from 50 to 500 mg O_2 dm^{-3} to below 10 mg O_2 dm^{-3} with a current efficiency >50%. Harrington et al. (1999) also examined the oxidation ability of electro-Fenton to mineralize 80 cm^3 of aqueous 0.05 M Na_2SO_4 solutions with 0.5–3 mM phenol, aniline, acetic acid, formaldehyde, or three azo dyes and 1 mM Fe^{2+} in the pH range 1–3 using a small divided cell with a 2.3-cm^2 carbon-PTFE O_2-fed cathode at E_{cat} from −0.4 to − 1.4 V vs. SCE. The best current efficiencies (60–70%) were found at pH 2 for 90% COD removal, without significant influence of the applied potential. Energy costs <14 kWh m^{-3} were estimated for these optimum conditions assuming a cell that operates with a voltage of 5 V.

Oturan's group has extensively studied the mineralization process and the oxidation intermediates of aromatic pollutants degraded in the cathodic compartment of a divided three-electrode cell with a carbon-felt working cathode surrounding

Table 19.1 Absolute second-order rate constant for the reaction of several organic pollutants with $^{\cdot}OH$ formed during the electro-Fenton process with Fe^{3+} as catalyst in divided and undivided Pt/carbon felt cells at room temperature (Oturan et al. 2000; Oturan et al. 2000, 2001; Gözmen et al. 2003; Edelahi et al. 2004; Hanna et al. 2005)

Pollutant	Cell	Experimental conditions	$k_2 \times 10^{-10}(M^{-1}s^{-1})$
2,4-D	Divided	H_2SO_4, pH 2, −0.5 V vs. SCE	3.5
2,4-Dichlorophenol			3.3
2,4-Dichlororesorcinol			3.2
4,6-Dichlororesorcinol			3.9
p-Nitrophenol		HCl, pH 2, −0.5 V vs. SCE	1.2
p-Nitrocatechol			1.0
Hydroquinone			1.6
1,2,4-Trihydroxybenzene			0.86
Pentachlorophenol		H_2SO_4, pH 3, −0.55 V vs. SCE	0.36
Bisphenol A		HCl, pH 2, −0.5 V vs. SCE	1.0
Diuron	Undivided	H_2SO_4, pH 3, 100 mA	0.48
Hydroxypropyl-β-cyclodextrin		H_2SO_4, pH 3, 30 mA	0.88

the anodic compartment containing a Pt counter electrode. Electro-Fenton treatments were performed with 110−200 cm^3 of O_2-saturated aqueous solutions with 0.5−2 mM Fe^{3+} of pH 2–3 at E_{cat} close to −0.5 V vs. SCE. Table 19.1 summarizes the second-order rate constant (k_2) determined for the fast reaction of several aromatics with $^{\bullet}OH$ produced in this system, along with the experimental conditions applied. Oturan (2000) found that the electro-Fenton process with 1 mM Fe^{3+} allows the total removal of 2 mM 2,4-D (2,4-dichlorophenoxyacetic acid) after passing 700 C. Figure 19.7 shows the rapid TOC decay of a solution with 1 mM of this herbicide up to about 90% mineralization at 2,000 C. HPCL analysis of treated solutions revealed the formation of hydroxylated products like 2,4-dichlorophenol, 2,4-dichlororesorcinol, and 4,6-dichlororesorcinol, along with totally or partially dechlorinated derivatives such as chlorohydroquinone, chloro-*p*-benzoquinone, and 1,2,4-trihydroxybenzene. Similarly, Oturan et al. (2000) reported the total destruction of 4 mM *p*-nitrophenol with 0.5 mM Fe^{3+} after consumption of 1,000 C and 95% COD removal for 1 mM of this compound after applying 800 C. *p*-Nitrocatechol, 4-nitropyrogallol, benzoquinone, hydroquinone, and 1,2,4-trihydroxybenzene were detected as aromatic intermediates, along with maleic, fumaric, and oxalic acids as major generated carboxylic acids. Oturan et al. (2001) described the slower TOC abatement of a saturated pentachlorophenol (0.03 mM) solution up to 82% mineralization after consumption of 1,500 C, with total release of all chlorine as Cl^- ion. Tetrachloro-*o*-benzoquinone and tetrachloro-*p*-benzoquinone were identified as by-products. In a further work Bisphenol A was comparatively degraded using 1 mM Fe^{3+} or 1 mM Cu^{2+} as catalyst (Gözmen et al. 2003). The same k_2-value of $1.0 \times 10^{10}\ M^{-1}s^{-1}$ (see Table 19.1) was found in both cases, but the treatment with Fe^{3+} was more efficient

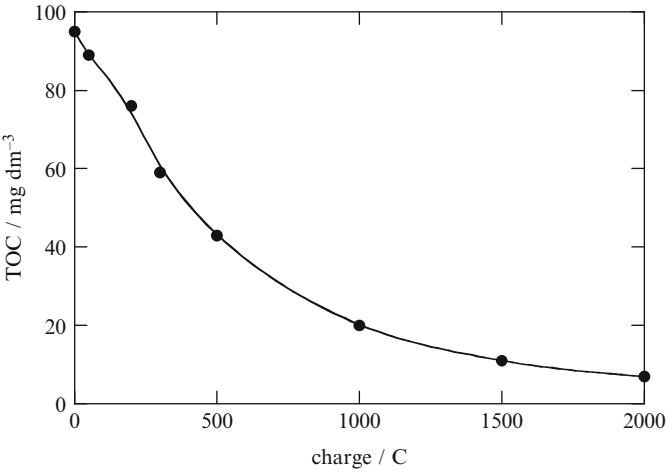

Fig. 19.7 TOC decay with total charge passed during the mineralization of 125 cm^3 of an O_2-saturated 220 mg dm^{-3} 2,4-D (2,4-dichlorophenoxyacetic acid) solution with 1 mM Fe^{3+} in H_2SO_4 of pH 2 at room temperature in the cathodic compartment of a divided Pt/carbon felt cell at $E_{cat} = -0.5$V vs. SCE giving a current of 60 mA [adapted from Oturan (2000)]

in terms of total mineralization vs. charge utilized. In this case, 82% mineralization was attained after applying 10,000 C to 200 cm^3 of a 0.7 mM Bisphenol A solution. The direct reaction of this compound with $^{\bullet}OH$ produces *ortho*- and *meta*-monohydroxylated derivatives, which are oxidized to a dihydroxylated product. Subsequent degradation of these products leads to aromatic intermediates like phenol, hydroquinone, catechol, resorcinol, *p*-benzoquinone, etc., and carboxylic acids like butendioic, 4-oxobutenoic, acetic, and formic. The electro-Fenton treatment of organophosphorus herbicides (Guivarch et al. 2003a) and azo dyes (Guivarch et al. 2003b) has also been reported. Figure 19.8 illustrates the quick COD removal obtained for 0.32 mM malathion, 0.50 mM TEPP (tetraethyl-pyrophosphate), and 0.09 mM parathion ethyl solutions with 2 mM Fe^{3+} in 10^{-2} M H_2SO_4, which are mineralized >80% at 6,000 C. A similar fast COD decay was also found for aqueous solutions of the azo-dyes Azobenzene, *p*-Methyl Red, and Methyl Orange, producing hydroquinone, *p*-benzoquinone, pyrocatechol, 4-nitrocatechol, 2,3,5-trihydroxynitrobenzene, and *p*-nitrophenol as main by-products.

Irmak et al. (2005) also utilized an analogous divided Pt/carbon-felt cell to destroy 300 cm^3 of an O_2-saturated 0.6 mM 4-chloro-2-methylphenol solution with Fe^{2+} as catalyst in H_2SO_4 of pH 2.7 by electro-Fenton and photoelectro-Fenton at $E_{cat} = -0.55$ V vs. SCE. The solution was irradiated with UVC light of $\lambda_{max} = 254$ nm in photoelectro-Fenton. After applying 141 C to a solution with 1.8 mM Fe^{2+} for 300 min, the photoelectro-Fenton process led to overall mineralization with total release of Cl^-. This process was much faster than the comparable electro-Fenton one, as expected from the additional photolysis of complexes of Fe^{3+} with pollutants and the production of more $^{\bullet}OH$ from reaction (19.24).

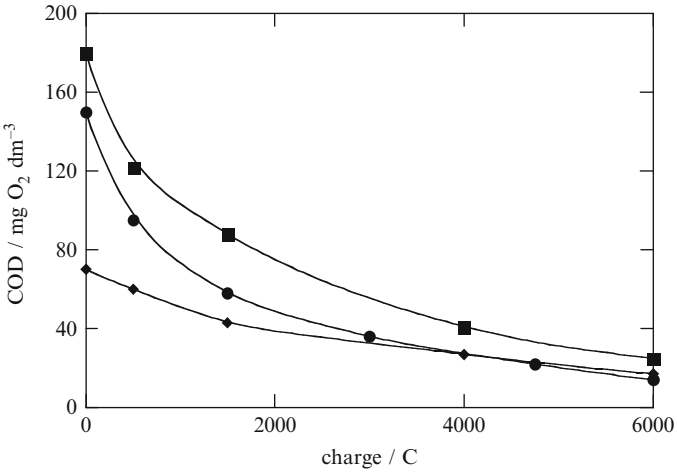

Fig. 19.8 Chemical oxygen demand evolution of O_2-saturated (*filled square*) 0.32 mM malathion, (*filled circle*) 0.50 mM TEPP (tetraethyl-pyrophosphate), and (*filled diamond*) 0.09 mM parathion ethyl solutions with 2 mM Fe^{3+} in 10^{-2} M H_2SO_4 at room temperature in the cathodic compartment of a divided Pt/carbon felt cell at $E_{cat} = -0.55$ V vs. SCE [adapted from Guivarch et al. (2003a)]

Fockedey and Van Lierde (2002) proposed an interesting approach to degrade wastewaters in a divided cell by $^{\bullet}$OH formed from both, water oxidation by reaction (19.9) at a SbO_2-doped SnO_2-coated Ti foam anode and Fenton's reaction (19.12) with H_2O_2 electrogenerated at an RVC cathode sparged with O_2. Two pumps were used to independently flow the effluent containing up to 3 g dm^{-3} phenol and 0.25 M Na_2SO_4 through the anodic and cathodic compartments of an Electrocell AB. The best operative conditions were found at pH 3 with 50 mg dm^{-3} of catalyst Fe^{2+} and 20 mg dm^{-3} of dissolved O_2, yielding an energy consumption of 2.68 Ah g^{-1} COD and a current efficiency of about 125% (the maximum efficiency expected for both coupled anode and cathode oxidations is 200%).

19.4 Treatment of Wastewaters Using an Undivided Cell Under Potentiostatic Control

Organic pollutants can be destroyed more efficiently with $^{\bullet}$OH produced from both anode and cathode reactions if they are degraded in an undivided electrolytic cell with cathodic electrogeneration of H_2O_2 under potentiostatic or galvanostatic control. The use of an undivided cell is energetically advantageous in comparison to a divided one because the energetic penalty of the ohmic drop of the membrane separating the anolyte and catholyte is avoided. In this section, relevant work on the treatment of wastewaters in undivided three-electrode cells is described.

Panizza and Cerisola (2001) used the cell of Fig. 19.5 with a 1-cm^2 Pt wire anode and a 15-cm^2 graphite-felt cathode to treat 200 cm^3 of an industrial wastewater mainly containing naphthalene- and antraquinone-sulphonic acids with 1,350 mg O_2 dm^{-3} of COD at pH 4 and 35°C. From current/potential curves, the H_2O_2 electrogeneration was found optimal at $E_{cat} = -1$ V vs. SCE under O_2 sparging. Maximum COD removal of 87% and color fading of 89% were obtained by electro-Fenton with 3 mM Fe^{2+} after 15 h of electrolysis. A similar Pt/graphite cell has also been utilized by Song-hu and Xiao-hua (2005) for the degradation of 200 cm^3 of solutions of various chlorophenols with 3.8 mg dm^{-3} Fe^{2+} or 3.2 mg dm^{-3} Fe^{3+} in 0.14 M Na_2SO_4 + H_2SO_4 of pH 2.5 at a cell voltage of 5 V ($E_{cat} = -0.55$ V vs. SCE) and room temperature. Concentrations between 16 and 35 mg dm^{-3} of chlorophenols were completely removed in 120–240 min following a pseudo-first-order reaction with $^{\bullet}OH$. The corresponding rate constant (k_1) decreased in the sequence: 2,4-dichlorophenol ($k_1 = 6.6 \times 10^{-2}$ min^{-1}) > 2, 4,6-trichlorophenol ($k_1 = 3.4 \times 10^{-2}$ min^{-1}) > pentachlorophenol ($k_1 = 1.9 \times 10^{-2}$ min^{-1}) > 4– chlorophenol ($k_1 = 1.3 \times 10^{-2}$ min^{-1}). Dechlorination with loss of Cl^- was detected during the decay of all compounds.

Meinero and Zerbinati (2006) degraded comparatively 200 cm^3 of 100 mg dm^{-3} 4-chloroaniline solutions in 0.1–0.05 M Na_2SO_4 + H_2SO_4 of pH 3.0 by anodic oxidation in a Pt/Ti cell at a constant voltage of 7 V and by anodic oxidation with electrogenerated H_2O_2 and electro-Fenton in a Pt/carbon cloth cell at $E_{cat} = -1$ V vs. Ag/AgCl under air sparging. The best degradation efficiency was found for the electro-Fenton process with 1 mM Fe^{2+}. Further application of this method to a wastewater containing chloroanilines, obtained by washing a polluted soil, showed 75% COD removal with an energy consumption of 0.3 kWh g^{-1} COD corresponding to 41.8 kWh m^{-3}. Badellino et al. (2006) also degraded 130 cm^3 of 100 mg dm^{-3} of 2,4-D in 0.3 M K_2SO_4 + H_2SO_4 solutions of pH 3.5 at 10°C in a Pt/RVC cell with 25 mg dm^{-3} O_2 at $E_{cat} = -1.6$ V vs. SCE by means of different methods such as anodic oxidation with electrogenerated H_2O_2, electro-Fenton with 1 mM Fe^{2+}, and photoelectro-Fenton with 1 mM Fe^{2+} under a 8-W UVC irradiation. Although UVC light photolyzes 2,4-D, the role of illumination was very poor in the degradation process since similar 67–69% mineralization was attained after 90% 2,4-D removal by electro-Fenton and photoelectro-Fenton, a value higher than 58% obtained for anodic oxidation. The electro-Fenton process is preferable by its lower energy consumption of 0.05 kWh g^{-1} TOC in comparison to 0.98 kWh g^{-1} TOC for photoelectro-Fenton. Intermediates like 2,4-dichlorophenol, 2,4-dichlororesorcinol, 4,6-dichlororesorcinol, and 2-chlorophenol were identified in all processes.

Recently, novel electro-Fenton procedures based on the oxidation with $^{\bullet}OH$ simultaneously generated by photoelectrocatalysis via reaction (19.7) using a TiO_2–Ti photoanode irradiated with UVA light and Fenton's reaction (19.12) have been proposed. Thus, Xie et al. (2006b) used the TiO_2–Ti/RVC cell of Fig. 19.6 to degrade 80 cm^3 of solutions with 0.1 mM azo dye Orange G and 17.2 mg dm^{-3} Fe^{2+} adjusted to pH 3.0 with HCl. The RVC working electrode was controlled at −0.71 V as cathode bias potential to electrogenerate H_2O_2.

This electro-Fenton photoelectrocatalytic process was much more effective than photoelectro-Fenton in a similar Pt/RVC cell with UVA irradiation, yielding 97% dye removal and 74% TOC reduction at 300 min, due to the additional production of $^{\bullet}OH$ at the TiO_2–Ti anode from reaction (19.7). Peralta-Hernández et al. (2006) have designed a flow annular photoelectrochemical reactor consisting of an outer cylindrical carbon-cloth cathode of 5.3-cm diameter, an inner cylindrical TiO_2–Ti photoanode of 1.0 cm diameter and a central 75 mW cm^{-2} UVA lamp for photoanode illumination. This electro-Fenton photoelectrocatalytic system operated in batch recycle mode and gave higher decolorization and mineralization of O_2-saturated solutions with 2 mg dm^{-3} of the dye Direct Yellow 52 and 0.5 mM Fe^{2+} in 0.05 M Na_2SO_4 + H_2SO_4 of pH 2 than electro-Fenton in the absence of UVA light by applying $E_{cat} = -0.7$ V vs. $Hg/HgSO_4$ and a liquid flow of 100 cm^3 min^{-1}.

19.5 Degradation of Organic Pollutants Using an Undivided Cell Under Galvanostatic Control

A higher number of papers have been published dealing with the degradation of organic pollutants at constant current in undivided cells by different indirect electro-oxidation methods based on H_2O_2 electrogeneration, where the effect of experimental parameters such as pH, temperature, applied current, and pollutant and catalyst concentrations on the mineralization processes have been clearly established. Most work has been performed by Oturan's group using a Pt/carbon-felt cell and also by our group using Pt/O_2, BDD/O_2, and Fe/O_2 cells, which are separately presented in subsections below. It is also interesting to remark the paper published by Hsiao and Nobe (1993), who studied the hydroxylation of 4 mM chlorobenzene and 1 mM phenol with 5 mM Fe^{2+} in 0.1 M Na_2SO_4 + H_2SO_4 at pH 3.8 under batch recycle mode in the undivided flow reactor shown in Fig. 19.9. The oxygen evolved at the anode and Fe^{3+} were reduced downstream to H_2O_2 and Fe^{2+}, respectively, at the RVC cathode, so that no O_2 was sparged. Unfortunately, the process rate in this system was not high enough for practical purposes, probably limited by its low H_2O_2 production. Phenol and 4-chlorophenol were obtained from chlorobenzene, while phenol yielded catechol, resorcinol, and hydroquinone. Wang et al. (2005) described the electro-Fenton treatment of 500 cm^3 of O_2-saturated solutions with 200 mg dm^{-3} of the azo dye Acid Red 14 and different Fe^{2+} contents in 0.05 M Na_2SO_4 + H_2SO_4 of pH 3.0 using a Ru/carbon-felt cell at constant current. After 6 h of electrolysis at 360 mA after addition of 1 mM Fe^{2+}, 70% TOC removal and complete decolorization were found. TOC removal gradually increased with increasing current from 120 to 500 mA and Fe^{2+} concentration up to 1 mM, but the mineralization rate dropped at greater Fe^{2+} contents. This behavior is typical of the electro-Fenton process, as further reported for a Pt/O_2 cell. On the other hand, Yuan et al. (2006) explored the degradation of 200 cm^3 of solutions of several nitrophenols in 25 g dm^{-3} Na_2SO_4 + H_2SO_4 of pH 3.0 by electro-Fenton with 0.5 mM Fe^{2+} and by anodic oxidation using a Pt/graphite cell at 50 mA. The electro-Fenton

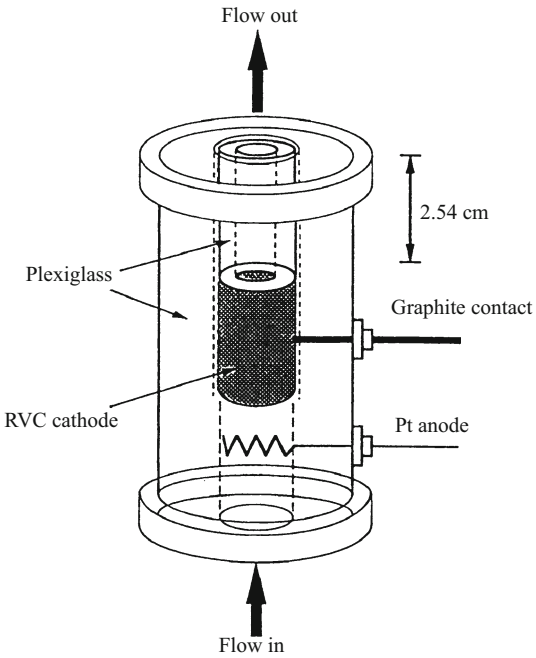

Fig. 19.9 Sketch of the flow undivided electrochemical reactor working in batch recycle mode designed for the hydroxylation of chlorobenzene and phenol (Hsiao et al. 1993)

process gave a faster decay of all compounds following the sequence: 4-nitrophenol > 2-nitrophenol > 2,4-dinitrophenol >3-nitrophenol > phenol. Since no significant amounts of released NO_3^- and NO_2^- ions were detected after 4-nitrophenol mineralization, they proposed the initial cathode reduction to 4-aminophenol, followed by the oxidation of this intermediate to hydroquinone and *p*-benzoquinone with $^\bullet$OH produced from Fenton's reaction (19.12), as reaction pathway.

19.5.1 Pt/Carbon-Felt Cell

Recently, Oturan's group has extended its research on the electro-Fenton treatment of pollutants to an undivided Pt/carbon-felt cell under current control using the same configuration and experimental conditions as stated above for the divided Pt/carbon-felt cell. This procedure was first used by this group to treat 125 cm^3 of an O_2-saturated 40 mg dm^{-3} diuron solution with 0.5 mM Fe^{3+} in H_2SO_4 of pH 3 at 100 mA (Edelahi et al. 2004). A fast reaction between the herbicide and $^\bullet$OH, with a k_2-value of 4.8×10^9 M^{-1} s^{-1} (see Table 19.1), was found leading to its disappearance in 10 min, whereas the solution TOC was reduced by 93% after applying 1,000 C. Hanna et al. (2005) further degraded soil extracts solutions

containing high pentachlorophenol loads. These extractions were made by adding hydroxypropyl-β-cyclodextrin (HPCD) to soil effluents that allowed an increase up to 3.5 times of the concentration of pentachlorophenol during the water flush of the soil. Although the reaction of $^{\bullet}OH$ with HPCD is more rapid than with pentachlorophenol (see the corresponding k_2-values in Table 19.1), it was found that a HPCD content of 5 mM in an O_2-saturated solution with 0.5 mM Fe^{3+} at pH 3 accelerated the decay rate of 0.1 mM pentachlorophenol, probably due to the formation of a ternary complex of pentachlorophenol–HPCD–iron that is directly oxidized by this radical. Total disappearance of pentachlorophenol and 90% COD abatement were achieved after 11 h of electrolysis of 125 cm^3 of a soil extract solution with 0.15 mM pentachlorophenol, 5 mM HPCD, and 0.5 mM Fe^{3+} of pH 3 at 50 mA. Accumulation of short-chain carboxylic acids such as monochloroacetic, dichloromaleic, acetic, formic, and oxalic was detected during the mineralization process. The electro-Fenton treatment of a real olive oil mill wastewater has been reported by Bellakhal et al. (2006). Complete COD removal of 100 cm^3 of an O_2-saturated 1:50 (v/v) diluted sample with 1.84 g O_2 dm^{-3} of initial COD and 0.5 mM Fe^{3+} of pH 3.0 was achieved after 9 h of electrolysis at 200 mA (charge consumed of 7,000 C). The sample became colorless after the application of 4,000 C, when all polyaromatics are completely destroyed. These results evidence the suitability of this method for the remediation of industrial wastewaters from agricultural activities.

19.5.2 Pt/O_2 Cell

Our group has comparatively studied the mineralization of organics by anodic oxidation with electrogenerated H_2O_2, electro-Fenton, and photoelectro-Fenton using the open, thermostated, cylindrical, and undivided Pt/O_2 cell of Fig. 19.3 containing 100 cm^3 of contaminated solution vigorously stirred with a magnetic bar. The anode was a 10 − cm^2 Pt sheet and the cathode was a 3-cm^2 carbon-PTFE electrode placed at the extreme of a polypropylene holder and mounted onto a Ni screen that served as current distributor, in contact with a nichrome wire as electrical connection. This electrode is directly fed with pure O_2 at a flow rate of 12-20 cm^3 min^{-1}, which diffuses to the interface of its carbon surface with the liquid where it is reduced to H_2O_2 by reaction (19.1). No O_2 bubbling in the bulk is then needed during electrolysis. For direct anodic oxidation without H_2O_2 accumulation (Brillas et al. 2002), a 3-cm^2 graphite bar was employed as alternative cathode. Aromatic pollutants of industrial wastewaters such as aniline (Brillas et al. 1996, 1998a) and 4-chlorophenol (Brillas et al. 1998b), as well as common herbicides present in the aquatic environment such as 2,4-D (Brillas et al. 2000), 4-CPA or 4-chlorophenoxyacetic acid (Boye et al. 2002), 2,4,5-T or 2,4,5,trichlorophenoxyacetic acid (Boye et al. 2003c), MCPA or 4-chloro-2-methylphenoxyacetic acid (Brillas et al. 2003d), and dicamba or 3,6-dichloro-2-methoxybenzoic acid (Brillas et al. 2003a), were degraded in this cell. The contaminated solutions contained 0.05 M Na_2SO_4 as background electrolyte

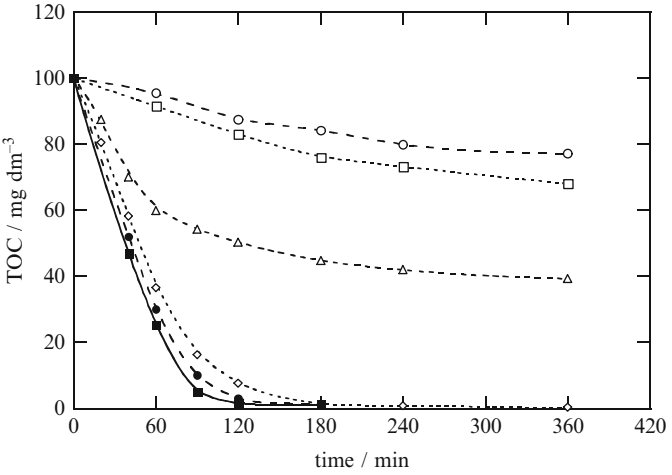

Fig. 19.10 TOC removal with electrolysis time for the degradation of 100 cm^3 of 266 mg dm^{-3} 2,4,5-T (2,4,5-trichlorophenoxyacetic acid) solutions in 0.05 M Na_2SO_4 + H_2SO_4 of pH 3.0 at 35°C. (*Open circle*) Anodic oxidation in a Pt/graphite cell at 100 mA. (*Open square*) Anodic oxidation with electrogenerated H_2O_2 in a Pt/O_2 cell at 100 mA. (*Open triangle*) Electro-Fenton with 1 mM Fe^{2+} in a Pt/O_2 cell at 100 mA. Photoelectro-Fenton with 1 mM Fe^{2+} and UVA irradiation in a Pt/O_2 cell at: (*open diamond*) 100, (*filled circle*) 300, and (*filled square*) 450 mA (Boye et al. 2003c)

and H_2SO_4 to adjust its pH in the range 2.0–6.0. Electrolyses were performed at constant current between 100 and 450 mA, usually maintaining the temperature at 25 or 35°C. Electro-Fenton and photoelectro-Fenton treatments were carried out by adding 0.2–2 mM $FeSO_4$ to the starting solutions. In photoelectro-Fenton the solution was irradiated with UVA light supplied by a 6-W fluorescent black light blue tube placed at 7 cm above its surface.

An example of the comparative degradation behavior found for the above methods can be seen in Fig. 19.10, where the TOC abatement with time for 266 mg dm^{-3} of 2,4,5-T at pH 3.0, 100 mA, and 35°C is presented. The oxidation power of treatments increases in the sequence: anodic oxidation $\leq$ anodic oxidation with electrogenerated H_2O_2 < electro-Fenton < photoelectro-Fenton. The low degradation rate in direct anodic oxidation can be ascribed to the small concentration of reactive $^{\bullet}$OH formed on the Pt anode surface from reaction (19.9), which is the main oxidizing agent of organics. The slightly faster TOC removal in anodic oxidation with electrogenerated H_2O_2 agrees with the expected additional poor destruction of pollutants with the weak oxidant H_2O_2. In contrast, electro-Fenton with 1 mM Fe^{2+} yields a much faster degradation during its first stages due to the existence of quick homogeneous reactions of organics with the great amount of $^{\bullet}$OH produced from Fenton's reaction (19.12), although at long electrolysis time the solution accumulates by-products that are not attacked by this radical. The photodecomposition of such by-products and/or the enhancement of the generation

rate of $^{\bullet}OH$ by reaction (19.24) can explain the highest mineralization rate of photoelectro-Fenton giving rise to complete mineralization.

The same relative oxidation power was found for the above methods in the degradation of all aromatics, as deduced from the percentages of TOC removal after 3 h of electrolysis of solutions with 100 mg dm^{-3} TOC of 4-CPA, MCPA, 2,4-D, and 2,4,5-T at pH 3.0 and 100 mA given in Table 19.2. All initial chlorine of these compounds was released as Cl^-, which remained stable in solution. The apparent current efficiency (ACE) for these trials was then calculated from the following equation:

$$\text{ACE} = [\Delta(\text{TOC})_{\text{exper}}/\Delta(\text{TOC})_{\text{theor}}] \times 100 \tag{19.26}$$

where $\Delta(\text{TOC})_{\text{exper}}$ is the experimental TOC decay in solution and $\Delta(\text{TOC})_{\text{theor}}$ is the theoretically calculated TOC removal assuming that the applied electrical charge (=current × time) is only consumed in the mineralization process. The $\Delta(\text{TOC})_{\text{theor}}$ values for chlorophenoxy herbicides were obtained considering that they are transformed into carbon dioxide and chloride ion according to reaction (19.27) for 4-CPA, reaction (19.28) for MCPA, reaction (19.29) for 2,4-D, and reaction (19.30) for 2,4,5-T:

$$C_8H_7ClO_3 + 13H_2O \rightarrow 8CO_2 + Cl^- + 33H^+ + 32e^- \tag{19.27}$$

$$C_9H_9ClO_3 + 15H_2O \rightarrow 9CO_2 + Cl^- + 39H^+ + 38e^- \tag{19.28}$$

$$C_8H_6Cl_2O_3 + 13H_2O \rightarrow 8CO_2 + 2Cl^- + 32H^+ + 30e^- \tag{19.29}$$

$$C_8H_5Cl_3O_3 + 13H_2O \rightarrow 8CO_2 + 3Cl^- + 31H^+ + 28e^- \tag{19.30}$$

Table 19.2 shows that the ACE values thus determined at 3 h of electrolysis are 3.1–6.0% for anodic oxidation with Pt and electrogenerated H_2O_2, 14–20% for electro-Fenton with Pt, and 25–29% for photoelectro-Fenton with Pt, related to a mineralization of 12–19%, 53–66%, and 90–96%, respectively. In all methods, the efficiency dropped with prolonging electrolysis time due to the gradual presence in solution of fewer amounts of pollutants that are more hardly oxidizable with $^{\bullet}OH$.

For electro-Fenton and photoelectro-Fenton, an increase in current always caused quicker mineralization rate, as can be seen in Fig. 19.10 for the photoelectro-Fenton process of 2,4,5-T. This is due to the production of greater amount of $^{\bullet}OH$ at the anode surface from reaction (19.9) and/or in the medium from Fenton's reaction (19.12) since more H_2O_2 is accumulated (see Fig. 19.4). However, the ACE value gradually decreased at higher current because of the greater relative increase in rate of nonoxidizing reactions of $^{\bullet}OH$ like its anodic oxidation to O_2 as follows:

$$2^{\bullet}OH \rightarrow O_{2(g)} + 2H^+ + 2e^- \tag{19.31}$$

and its destruction with Fe^{2+} and H_2O_2 by reactions (19.17) and (19.18), respectively. In contrast, a higher efficiency was obtained with raising initial pollutant content, evidencing the acceleration of the destruction of organics with $^{\bullet}OH$ and the concomitant decay in rate of its nonoxidizing reactions. All pollutants were more

Table 19.2 Percentage of TOC removal and apparent current efficiency (ACE) determined after 3 h of treatment of 100 cm^3 of solutions of chlorophenoxyacetic acid herbicides with a concentration equivalent to 100 mg dm^{-3} TOC in 0.05 M Na_2SO_4 + H_2SO_4 of pH 3.0 by different indirect electro-oxidation methods under comparable conditions at 100 mA

Herbicide	Method[a]	T (°C)	% TOC removal	ACE	k_1 (min^{-1})
4-CPA	AO-Pt	35	19	5.6	4.9×10^{-3}
	AO-BDD		54	16	5.4×10^{-3}
	EF-Pt		66	20	0.12
	EF-BDD		75	22	0.27
	PEF-Pt		96	29	0.16
	PC		86	26	0.14
MCPA	AO-Pt	35	19	6.0	5.9×10^{-3}
	AO-BDD		58	18	7.0×10^{-3}
	EF-Pt		65	20	0.12
	EF-BDD		76	24	0.14
	PEF-Pt		91	29	0.14
	PC		85	27	0.17
2,4-D	AO-Pt	25	13	3.6	7.9×10^{-3}
	AO-BDD	35	57	16	7.1×10^{-3}
	EF-Pt	25	57	16	0.18
	EF-BDD	35	78	22	0.31
	PEF-Pt	25	90	25	0.23
	PC		76	21	0.19
2,4,5-T	AO-Pt	35	12	3.1	1.2×10^{-2}
	AO-BDD		59	15	6.6×10^{-3}
	EF-Pt		53	14	0.11
	EF-BDD		80	21	0.24
	PEF-Pt		99	26	0.12
	PC		84	22	0.16

The last column collects the rate constant corresponding to their pseudo-first-order decay with $^{\bullet}OH$ (Boye et al. 2002,2003a–c; Brillas et al. 2003b–d, 2004b)

[a]*AO-Pt* Anodic oxidation with electrogenerated H_2O_2 in a Pt/O_2 cell, *AO-BDD* anodic oxidation with electrogenerated H_2O_2 in a BDD/O_2 cell, *EF-Pt* electro-Fenton with 1 mM Fe^{2+} in a Pt/O_2 cell, *EF-BDD* electro-Fenton with 1 mM Fe^{2+} in a BDD/O_2 cell, *PEF-Pt* photoelectro-Fenton with 1 mM Fe^{2+} and UVA light in a Pt/O_2 cell, and *PC* peroxi-coagulation in a Fe/O_2 cell

efficiently degraded at pH 3.0, near the optimum pH of 2.8 for Fenton's reaction (19.12), since it produces the major quantity of oxidant $^{\bullet}OH$ in electro-Fenton and photoelectro-Fenton with a Pt anode. At pH 3.0 similar degradation rates were found up to 1 mM Fe^{2+}, whereas higher Fe^{2+} contents caused a decrease in TOC removal due to the faster consumption of generated $^{\bullet}OH$ with this ion by reaction (19.17).

The decay kinetics for initial pollutants was followed by reversed-phase HPLC chromatography. As illustrated in Fig. 19.11 for 2,4,5-T, the pollutant concentration underwent a slow, but similar, drop in anodic oxidation and anodic oxidation with electrogenerated H_2O_2 as expected if $^{\bullet}OH$ formed from reaction (19.9) on Pt is the main oxidant. A much faster destruction rate was always found for electro-Fenton and photoelectro-Fenton because of the production of greater amount of $^{\bullet}OH$ from Fenton's reaction (19.12).

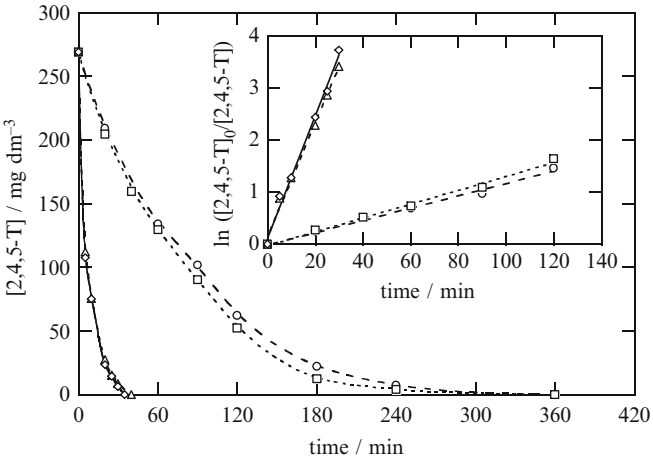

Fig. 19.11 2,4,5-T concentration decay during the same treatments of Fig. 19.10 at 100 mA. The *inset panel* shows its kinetic analysis assuming a pseudo-first-order reaction for 2,4,5-T

Kinetic analysis of all concentration decays fit well with the equation related to a pseudo-first-order reaction (see the inset panel of Fig. 19.11). The last column of Table 19.2 lists the k_1-values thus determined for the comparative treatments of chlorophenoxy herbicides. Similar k_1 values can be observed for all electro-Fenton and photoelectro-Fenton treatments with Pt. This discards direct photolysis of herbicides by UVA light and significant participation of reaction (19.24) to generate $^{\bullet}$OH.

GC-MS and HPLC analyses of electrolyzed solutions allowed the detection of aromatic intermediates such as "*p*-benzoquinone and nitrobenzene" for aniline, "4-chlorocatechol" for 4-chlorophenol, "4-chlorophenol, 4-chlorocatechol, hydroquinone, and *p*-benzoquinone" for 4-CPA, "4-chloro-*o*-cresol, mehylhydroquinone, and methyl-*p*-benzoquinone" for MCPA, "2,4-dichlorophenol, 4,6-dichlororesorcinol, chlorohydroquinone, and chloro-*p*-benzoquinone" for 2,4-D, and "2,4,5-trichloro-phenol, 2,5-dichlorohydroquinone, 4,6-dichlororesorcinol, and 2,5-dihydroxy-*p*-benzoquinone" for 2,4,5-T. In general, these by-products persisted in solution while the initial pollutant was degraded.

A high number of short-chain carboxylic acids coming from the cleavage of the benzenic ring of aromatics and the release of aliphatic lateral chains were identified by ion-exclusion HPLC chromatography analysis of electrolyzed solutions. All these acids were also quickly removed, except the final oxalic acid that persisted for long time. The evolution of this acid during the treatments of 2,4,5-T is depicted in Fig. 19.12. Oxalic acid is slowly accumulated in both anodic oxidation treatments because of the slow degradation of precedent by-products. However, it is accumulated to reach a steady concentration in electro-Fenton and rapidly decomposes in photoelectro-Fenton. These trends can be explained by the formation of a high proportion of Fe^{3+}-oxalate complexes since high amounts of Fe^{3+}

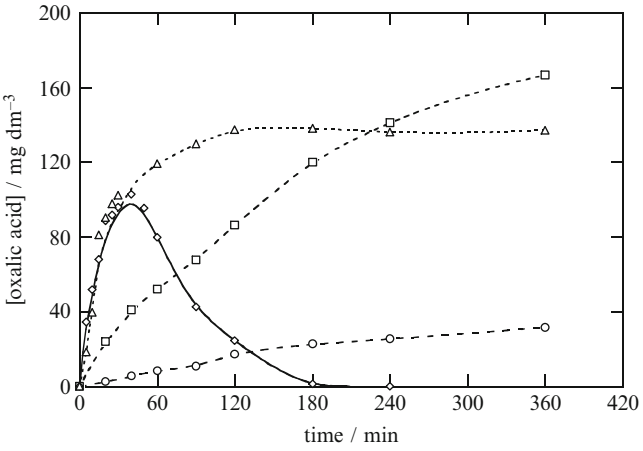

Fig. 19.12 Evolution of oxalic acid concentration with electrolysis time during the same treatments of 2,4,5-T as given in Fig. 19.10 at 100 mA

are produced from Fenton's reaction (19.12). The low oxidation ability of $^{\bullet}$OH to destroy the Fe^{3+}–oxalate complexes formed justifies the slow TOC abatement at the end of electro-Fenton (see Fig. 19.10), while the fast photodecarboxylation of such complexes by UVA light accounts for the total mineralization achieved in photoelectro-Fenton. This satisfactorily explains the higher oxidation power of photoelectro-Fenton.

From the results obtained for 2,4,5-T degradation, the reaction sequence of Fig. 19.13 has been proposed by the different treatments tested in a Pt/O_2 cell. The process is initiated by the formation of 2,4,5-trichlorophenol and glycolic acid from the breakage of the C(1)–O bond of the herbicide. The subsequent nonselective attack of $^{\bullet}$OH on C(4)- and C(5)-positions of 2,4,5-trichlorophenol gives 2,5-dichlorohydroquinone and 4,6-dichlororesorcinol, respectively, which are oxidized to 2,5-dihydroxy-*p*-benzoquinone. These dechlorination reactions yield the complete loss of all chlorine atoms as chloride ions. Further degradation of 2,5-dihydroxy-*p*-benzoquinone leads to a mixture of malic, maleic, and fumaric acids, which are oxidized to oxalic acid. This acid can also be produced from dehydrogenation of glycolic acid, followed by hydroxylation of the resulting glyoxylic acid. Glycolic and glyoxylic acids undergo a parallel oxidation to formic acid, which is directly converted into CO_2. Oxalic acid is slowly transformed into CO_2 by the two anodic oxidation methods, whereas in the indirect electro-oxidation treatments with iron ions, it mainly forms Fe^{3+}–oxalate complexes. These species are very stable in electro-Fenton and rapidly photodecompose under the action of UVA light, with loss of Fe^{2+}, in photoelectro-Fenton.

The degradation of a solution with 100 mg dm^{-3} TOC of the herbicide amitrole (3-amino-1,2,4-triazole) of pH 3.0 in the Pt/O_2 cell of Fig. 19.3 has been further studied by Da Pozzo et al. (2005b). Complete decontamination was achieved by electro-Fenton with 1 mM Fe^{2+}, although with a low accumulation of released

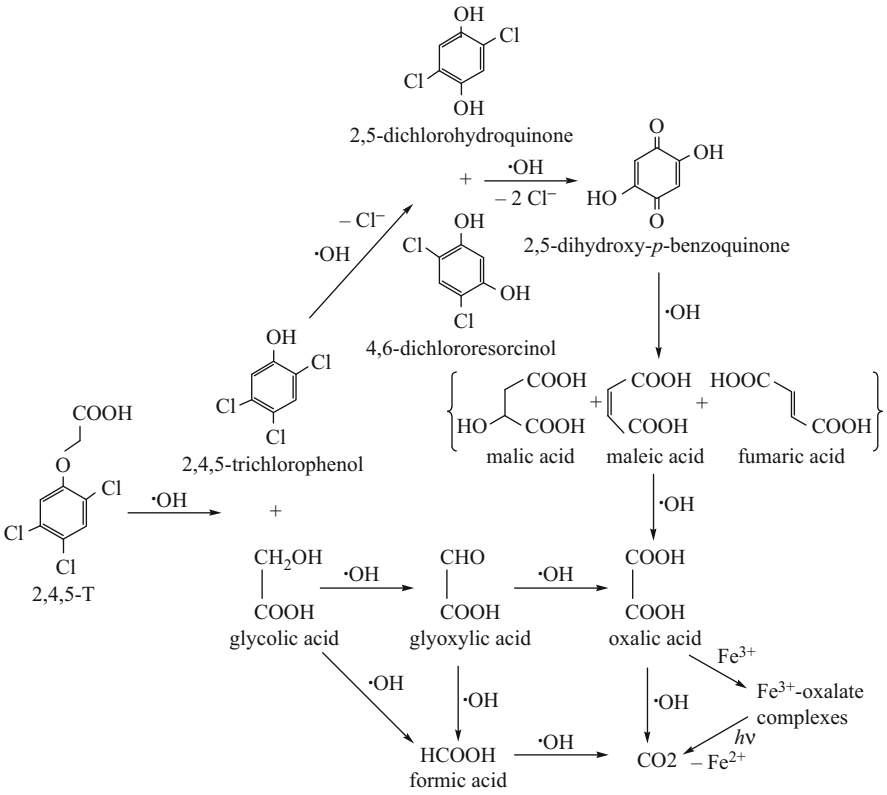

Fig. 19.13 Proposed reaction sequence for 2,4,5-T degradation in acid aqueous medium by electro-Fenton and photoelectro-Fenton using a Pt/O_2 cell [adapted from Boye et al. (2003c)]

NO_3^- and NH_4^+ ions as expected if volatile *N*-products are lost during the mineralization process. A similar behavior was found for the treatments of the same amitrole solution by anodic oxidation using Pt/stainless steel and BDD/stainless steel cells, but electro-Fenton yielded the quickest degradation due to the higher production of $^\bullet$OH from Fenton's reaction (19.12).

The effect of Cu^{2+} as co-catalyst on the electro-Fenton and photoelectro-Fenton processes of nitrobenzene (Brillas et al. 2004a) and paracetamol (Sirés et al. 2004, 2006) has been explored in the same Pt/O_2 cell. Solutions with 100 mg dm^{-3} nitrobenzene of pH 3.0 and up to 1 g dm^{-3} paracetamol in the pH range 2.0–6.0 in 0.05 M $Na_2SO_4 + H_2SO_4$ were electrolyzed between 100 and 450 mA at 25°C and 35°C, respectively. The oxidation power in the presence of catalysts increased in the sequence: 1mM $Cu^{2+} \leq$ 1mM Cu^{2+} + UVA light < 1 mM $Fe^{2+} \ll$ 1 mM Fe^{2+} + 1 mM $Cu^{2+} \approx$ 1 mM Fe^{2+} + UVA light < 1 mM Fe^{2+} + 1 mM Cu^{2+} + UVA light. Anodic oxidation with electrogenerated H_2O_2 led to very poor degradation, which was slightly enhanced in the presence of 1 mM Cu^{2+} without and with UVA light due to the low production of $^\bullet$OH by reaction (19.9) at the Pt anode and

reaction (19.23) under the action of the Cu^{2+}/Cu^{+} system. In the electro-Fenton process with 1 mM Fe^{2+}, less than 70% mineralization was obtained because of the formation of stable complexes of Fe^{3+} with by-products. These complexes are photodecomposed by UVA light in photoelectro-Fenton giving almost total mineralization. Complete decontamination is feasible using 1 mM Fe^{2+} and 1 mM Cu^{2+} since $^{\bullet}OH$ can destroy the complexes between Cu^{2+} and intermediates. The positive synergistic effect of all the catalysts allows the quickest mineralization using 1 mM Fe^{2+} and 1 mM Cu^{2+} under UVA irradiation. In this procedure, the fastest paracetamol degradation was found at pH 3.0 and its efficiency increased with raising pollutant concentration and decreasing current.

NO_3^- and NH_4^+ ions were released during nitrobenzene and paracetamol treatments, respectively. *o*-Nitrophenol, *m*-nitrophenol, *p*-nitrophenol, 4-nitrocatechol, and maleic, fumaric, and oxalic acids were detected as by-products of nitrobenzene, whereas hydroquinone, *p*-benzoquinone, ketomalonic, and maleic, fumaric, oxalic, and oxamic acids were identified as intermediates of paracetamol. It was found that Cu^{2+} and/or UVA light did not affect the decay rates of nitrobenzene and paracetamol, as well as the evolution of their intermediates, except that of complexes of Fe^{3+} and Cu^{2+} with the final oxalic and/or oxamic acids. Figure 19.14 shows that the use of Cu^{2+} alone yields a small accumulation of Cu^{2+}–oxalate and Cu^{2+}–oxamate complexes due to the slow degradation of pollutants. When only Fe^{2+} is added, Fe^{3+}–oxalate and Fe^{3+}–oxamate complexes cannot be mineralized by $^{\bullet}OH$, thus limiting the oxidation ability of the electro-Fenton process. The efficient photodecomposition of Fe^{3+}–oxalate complexes, along with a slower photolysis of Fe^{3+}–oxamate ones, explains the faster mineralization of photoelectro-Fenton. By combining Fe^{2+} and Cu^{2+}, Fe^{3+}–oxalate, Fe^{3+}–oxamate, Cu^{2+}–oxalate, and Cu^{2+}–oxamate complexes are produced, but uniquely Cu^{2+} complexes are destroyed. The quickest and total mineralization of paracetamol with $Fe^{2+} + Cu^{2+} +$ UVA light is due to the oxidation of Cu^{2+}–oxalate and Cu^{2+}–oxamate complexes with $^{\bullet}OH$ in parallel to the photodegradation of their Fe^{3+} complexes by UVA light.

The above catalytic effects of Fe^{2+}, Cu^{2+}, and UVA light on the conversion of oxamic and oxalic acids into CO_2 are reflected in the proposed sequence for paracetamol degradation of Fig. 19.15. The pathway involves the formation of oxamic acid from the oxidation of acetamide, previously released when paracetamol gives hydroquinone, whereas oxalic acid proceeds from the oxidation of ketomalonic, maleic, and fumaric acids, coming from the degradation of hydroquinone via *p*-benzoquinone.

19.5.3 BDD/O_2 Cell

Our group has also investigated the influence of a BDD anode, with much higher oxidation power than Pt, on the anodic oxidation with electrogenerated H_2O_2 and electro-Fenton treatments of chlorophenoxy herbicides (Brillas et al. 2004b). Solutions with 100 mg dm^{-3} TOC of 4-CPA, MCPA, 2,4-D, and 2,4,5-T of pH 3.0 were

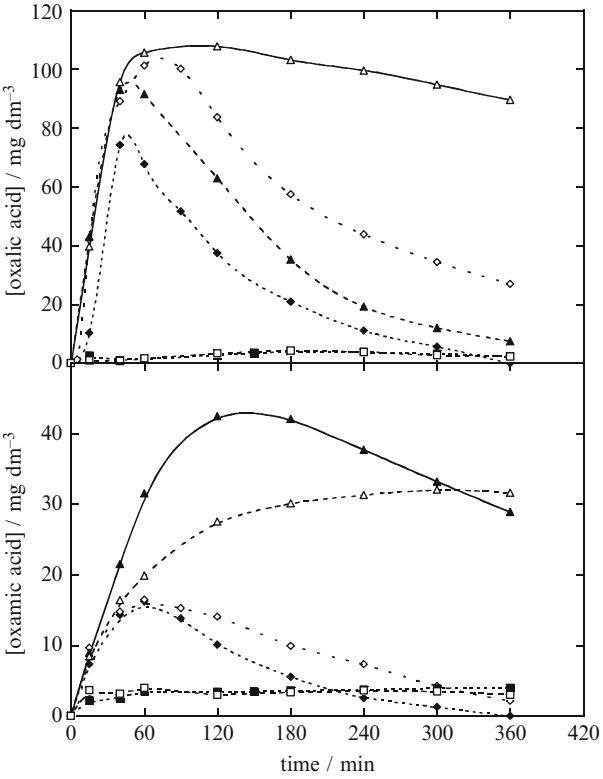

Fig. 19.14 Time course of the concentration of oxalic and oxamic acids during the degradation of 157 mg dm^{-3} paracetamol solutions in 0.05 M $Na_2SO_4 + H_2SO_4$ of pH 3.0 at 300 mA and at 35°C using a Pt/O_2 cell with the following catalysts: (*open square*) 1 mM Cu^{2+}, (*filled square*) 1 mM Cu^{2+} + UVA light, (*open triangle*) 1 mM Fe^{2+}, (*filled triangle*) 1 mM Fe^{2+} + UVA light, (*open diamond*) 1 mM Fe^{2+} + 1mM Cu^{2+}, and (*filled diamond*) 1 mM Fe^{2+} + 1mM Cu^{2+} + UVA light [adapted from Sirés et al. (2006)]

electrolyzed at 100 mA and 35°C in an undivided BDD/O_2 cell with the configuration of Fig. 19.3. A 3-cm^2 BDD thin layer deposited on a conductive Si sheet was used as the anode. As can be seen in Fig. 19.16, the TOC of all herbicide solutions is removed at similar rate in each procedure, attaining total mineralization after 6–8 h (specific charge of 6 − 8 Ah dm^{-3}) of electro-Fenton and 9–10 h (specific charge of 9 − 10 Ah dm^{-3}) of anodic oxidation. Although the degradation rate at the first stages (up to approximately 2 h) of electro-Fenton is very fast, a slightly shorter time than anodic oxidation is needed for achieving overall mineralization. Both methods with BDD are then much more efficient than the homologous ones with Pt (see Table 19.2), which do not allow total decontamination under comparable conditions (see Fig. 19.10). The greater oxidation ability of these methods using a BDD/O_2 cell in comparison to a Pt/O_2 one cannot be related to a faster reaction of aromatic pollutants with the higher amount of reactive $^{\bullet}OH$ that is expected to

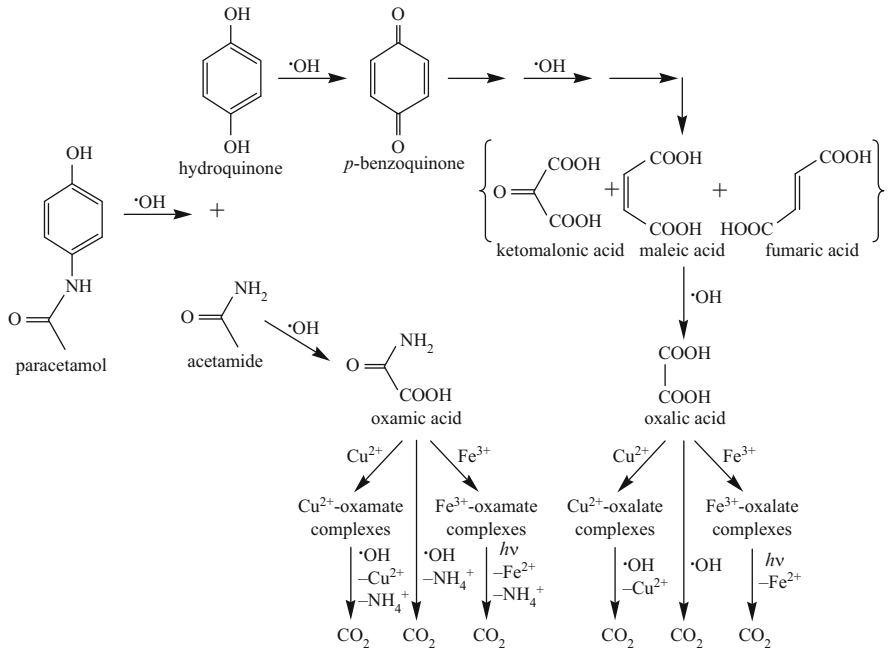

Fig. 19.15 Proposed reaction sequence for paracetamol degradation in acid medium by the catalytic action of Fe^{2+}, Cu^{2+}, and/or UVA light using a Pt/O_2 cell [adapted from Sirés et al. (2006)]

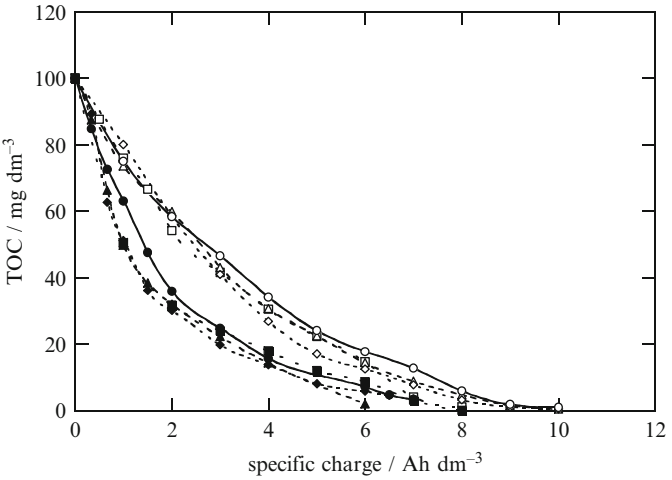

Fig. 19.16 TOC removal vs. consumed specific charge for the treatment of 100 cm^3 of: (*open circle, filled circle*) 194 mg dm^{-3} 4-CPA (4-chlorophenoxyacetic acid), (*open square, filled square*) 200 mg dm^{-3} MCPA (4-chloro-2-methylphenoxyacetic acid), (*open triangle, filled triangle*) 230 mg dm^{-3} 2,4-D, (*open diamond, filled diamond*) 266 mg dm^{-3} 2,4,5-T solutions in 0.05 M $Na_2SO_4 + H_2SO_4$ of pH 3.0 at 100 mA and at 35°C using a BDD/O_2 cell. (*open circle, open square, open triangle, open diamond*) Anodic oxidation with electrogenerated H_2O_2, (*filled circle, filled square, filled triangle, filled diamond*) electro-Fenton with 1 mM Fe^{2+} (Brillas et al. 2004b)

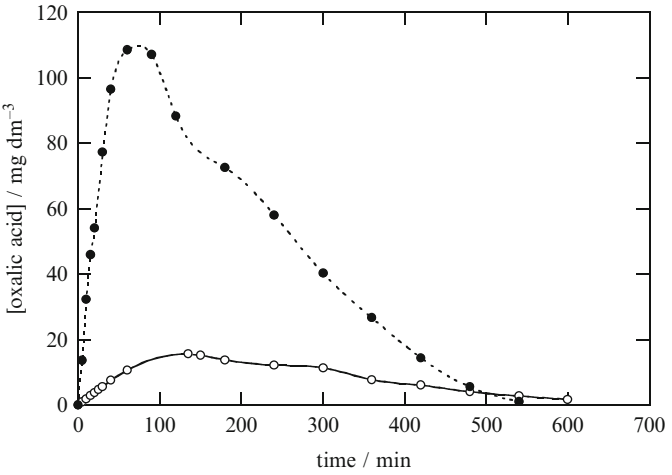

Fig. 19.17 Evolution of oxalic acid concentration during the treatment of 194 mg dm^{-3} 4-CPA solutions in a BDD/O_2 cell under the same conditions as reported in Fig. 19.16. (*Open circle*) Anodic oxidation with electrogenerated H_2O_2 and (*filled circle*) electro-Fenton with 1 mM Fe^{2+}

be formed on BDD from reaction (19.9), since initial herbicides always followed a pseudo-first-order decay with a quite similar k_1 value for each method in both cells, as can be seen in Table 19.2. These results confirm their quicker reaction with $^{\bullet}$OH in the medium than on Pt or BDD surface. Their primary phenol intermediates such as 4-chlorophenol for 4-CPA, 4-chloro-*o*-cresol for MCPA, 2,4-dichlorophenol for 2,4-D, and 2,4,5-trichlorophenol for 2,4,5-T also rapidly react with the same oxidant, since they were uniquely detected while starting herbicides were destroyed. Analyses of generated carboxylic acids revealed the large persistence of the final oxalic acid or its Fe^{3+} complexes during these treatments in the BDD/O_2 cell. This behavior is illustrated in Fig. 19.17 for 4-CPA degradation. The persistence of large amount of Fe^{3+}–oxalate complexes in electro-Fenton with BDD cannot be ascribed to their oxidation by $^{\bullet}$OH in the bulk since they are stable in electro-Fenton with Pt (see Fig. 19.12) and hence, they are mineralized by reaction with $^{\bullet}$OH at the BDD surface. The slow destruction of such complexes on BDD explains the long time needed for the total decontamination of herbicides by electro-Fenton. This occurs at similar times to those needed for anodic oxidation with BDD in which oxalic acid is accumulated at low concentrations (see Fig. 19.17) because it is practically removed at the same rate as it is produced. Cl^- ion released in all the treatments was slowly oxidized to Cl_2 gas on BDD (Ferro et al. 2000):

$$2Cl^- \rightarrow Cl_{2(g)} + 2e^- \tag{19.32}$$

The great oxidation power of electro-Fenton with BDD has also been confirmed in the comparative treatment of acidic aqueous solutions containing up to 0.9 g dm^{-3} of the dye Indigo Carmine by electro-Fenton and photoelectro-Fenton using BDD/O_2 and Pt/O_2 cells (Flox et al. 2006). The application of both methods

with 1 mM Fe^{2+} in the Pt/O_2 cell led to partial mineralization of the dye. In contrast, complete decontamination with loss of NH_4^+ was found using electro-Fenton with BDD and 1 mM Fe^{2+} and when 1 mM Fe^{2+} and 0.25 mM Cu^{2+} were combined as catalysts in photoelectro-Fenton with Pt. The first procedure gave similar degradation rate in the pH range 2.0–4.0, whereas the second one was more potent up to 0.44 g dm^{-3} of Indigo Carmine at pH 3.0. A higher mineralization rate was found with increasing current density and initial dye content. The Indigo Carmine decay always followed a pseudo-zero-order reaction. The aromatic derivatives isatin 5-sulfonic acid, indigo, and isatin were transformed into final oxalic and oxamic acids. Kinetic results corroborated the destruction of the dye and its aromatic by-products mainly by $^{\bullet}OH$ formed in the bulk from Fenton's reaction (19.12). The electro-Fenton process with BDD allowed the total mineralization of Fe^{3+}–oxalate and Fe^{3+}–oxamate complexes under the action of $^{\bullet}OH$ on the anode surface. In the presence of Fe^{2+} and Cu^{2+}, the photoelectro-Fenton process with Pt involved the photolysis of Fe^{3+}–oxalate complexes by UVA light, while competitive Cu^{2+}–oxalate and Cu^{2+}–oxamate complexes were mineralized by $^{\bullet}OH$ in the medium. This study again confirms the positive catalytic action of combining Fe^{2+}, Cu^{2+}, and UVA light for the treatment of wastewaters with aromatic pollutants.

19.5.4 Fe/O_2 Cell

The peroxi-coagulation treatment of 100 cm^3 of acidic solutions of different aromatics has been reported by us using an undivided Fe/O_2 cell with the configuration of Fig. 19.3. This method has been successfully applied to remove aniline (Brillas et al. 1997), 4-chlorophenol (Brillas et al. 1998b), 4-CPA (Brillas et al. 2003c), MCPA (Boye et al. 2003a), 2,4,5-T (Boye et al. 2003b), and 2,4-D and dicamba (Brillas et al. 2003b) under comparable experimental conditions to those used in a Pt/O_2 cell. Since the sacrificial Fe anode is quantitatively oxidized to Fe^{2+} by reaction (19.25) (Brillas et al. 1997, 1998b) and large amounts of $Fe(OH)_3$ precipitate, the pH of the solution increases continuously and needs to be periodically regulated during electrolysis by adding H_2SO_4 to the medium. For each pollutant, the same by-products and released inorganic ions were detected using electro-Fenton, photoelectro-Fenton, and peroxi-coagulation because $^{\bullet}OH$ is the main oxidant. In peroxi-coagulation, this radical is produced by Fenton's reaction between both electrogenerated H_2O_2 and Fe^{2+}.

As an example of the degradative behavior of this process, Fig. 19.18 presents the comparative TOC–time plots determined for 100 mg dm^{-3} TOC of chlorophenoxyacetic and chlorobenzoic herbicides of pH 3.0 at 100 mA under pH regulation. The soluble TOC is quickly reduced during the first 2 h, but at longer time a much slower degradation occurs by the presence of hardly oxidizable products. At 3 h of this treatment, a 76–86% of TOC decay with 21–27% of current efficiency was found for the chlorophenoxyacetic herbicides, values higher than those obtained for electro-Fenton but lower than those determined for

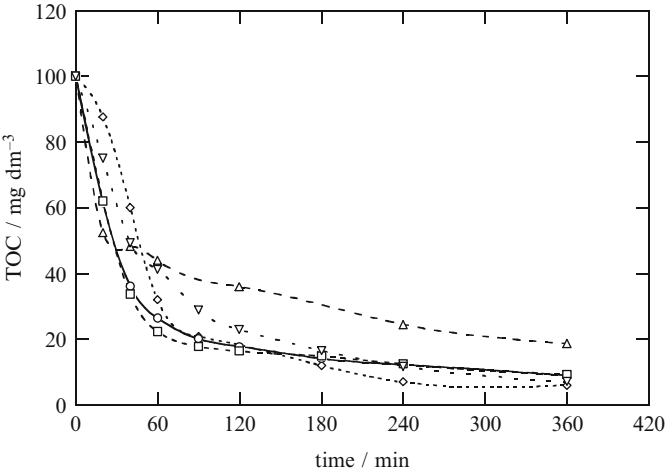

Fig. 19.18 TOC abatement for the peroxi-coagulation degradation in a Fe/O_2 cell of 100 cm^3 of: (*open circle*) 200 mg dm^{-3} 4-CPA, (*open square*) 194 mg dm^{-3} MCPA, (*open up triangle*) 230 mg dm^{-3} 2,4-D, (*open diamond*) 230 mg dm^{-3} dicamba (3,6-dichloro-2-methoxybenzoic acid), (*open down triangle*) 269 mg dm^{-3} 2,4,5-T solutions in 0.05 M $Na_2SO_4 + H_2SO_4$ of pH 3.0 at 100 mA and at 35°C under pH regulation (Brillas et al. 2003b)

photoelectro-Fenton (see Table 19.2). The decay of these compounds in peroxi-coagulation followed a pseudo-first-order reaction with quite similar k_1 values to those obtained for electro-Fenton and photoelectro-Fenton under comparable conditions (see Table 19.2). This agrees with their oxidation mainly by the $^{\bullet}$OH radicals produced from Fenton's reaction (19.12). The fast TOC removal at the first stages of their peroxi-coagulation process (see Fig. 19.18) can then be ascribed to the rapid oxidation of all organics with $^{\bullet}$OH, along with the coagulation of some intermediates with the $Fe(OH)_3$ precipitate formed. The existence of coagulation during the peroxi-coagulation process was confirmed by determining the percentage of TOC removal and percentages of coagulated and mineralized TOC after electrolysis. Table 19.3 summarizes the values obtained for these parameters after 6 h of treatment of the above herbicides. These data show that the coagulation and mineralization paths compete at 100 mA, but the increase in current causes the acceleration of TOC abatement with predominance of coagulation over mineralization. The quicker generation of $^{\bullet}$OH when current raises then enhances the oxidation of herbicides yielding a larger proportion of by-products that are retained by the greater quantity of $Fe(OH)_3$ precipitate produced, thus avoiding their further mineralization. Low contents of the oxalic acid as the ultimate product were detected in the final electrolyzed solutions, indicating that their Fe^{3+} complexes are very slowly removed by coagulation with the $Fe(OH)_3$ precipitate. Comparative treatments under UVA illumination (photoperoxi-coagulation process) only allowed a slight enhancement of TOC decay because UVA irradiation is largely absorbed by the $Fe(OH)_3$ precipitate (Boye et al. 2003a; Brillas et al. 2003c).

Table 19.3 Percentage of TOC removal and percentages of coagulated and mineralized TOC obtained after 6 h of photo peroxi-coagulation treatment of 100 cm^3 of chlorophenoxyacetic and chlorobenzoic acids solutions with an herbicide concentration equivalent to 100 mg dm^{-3} TOC in 0.05 M Na_2SO_4 + H_2SO_4 of pH 3.0 at 35°C in a Fe/O_2 cell at different currents and under pH regulation (Boye et al. 2003a, b; Brillas et al. 2003b, c)

Herbicide	Current (mA)	% TOC removal	% Coagulated TOC	% Mineralized TOC
4-CPA	100	91	48	43
MCPA	100	92	49	43
2,4-D	100	81	38	43
	300	92	45	47
	450	92	50	42
dicamba	100	94	48	46
2,4,5-T	300	94	94	0
	450	94	94	0
	100	93	54	39

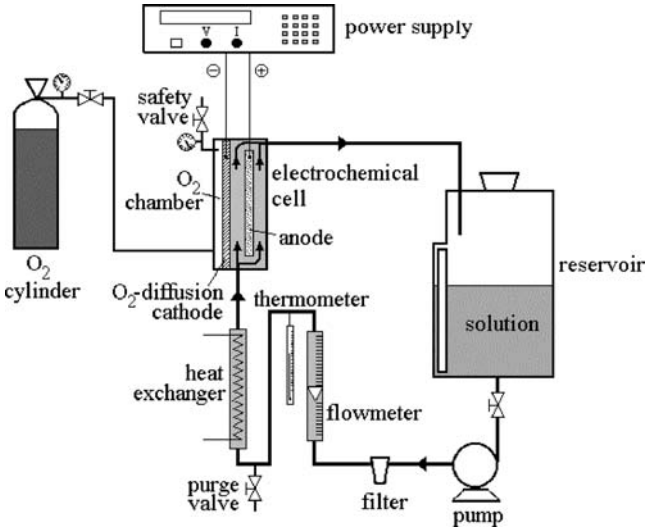

Fig. 19.19 Sketch of the flow plant with an undivided filter-press two-electrode electrochemical reactor fed with oxygen used for the degradation of 30 dm^3 of aniline solutions by electro-Fenton and peroxi-coagulation (Brillas et al. 2002)

Brillas and Casado (2002) have reported the degradation of 30 dm^3 of 1 g dm^{-3} aniline solutions in 0.05 M Na_2SO_4 + H_2SO_4 of pH 3.0 at 40°C using the lab-scale plant of Fig. 19.19 containing an Electrocell AB with 100-cm^2 electrodes in batch recycle mode. The electro-Fenton process with 1 mM Fe^{2+} in a Pt/O_2 cell gave a violet insoluble polymer and soluble TOC was rapidly reduced by 61% in 2 h at 20 A, but it slowly decreased at longer times. Peroxi-coagulation in a Fe/O_2 cell was much more effective with >95% TOC removal in 4 h at the same current. Apparent efficiencies as high as 700% and 900% were calculated from (19.26) after

30 min of electro-Fenton and peroxi-coagulation, respectively, as expected if a large proportion of by-products are separated from the medium as insoluble polymers or by coagulation with $Fe(OH)_3$. The energy cost for total decontamination after 4 h of peroxi-coagulation at 20 A was ca. 60 kWh m^{-3}, whereas about 70 kWh m^{-3} were consumed to attain 65% degradation by electro-Fenton under the same conditions. Comparative anodic oxidation with electrogenerated H_2O_2 in the Pt/O_2 cell only led to 18% mineralization in 6 h with a high energy cost of 502 kWh m^{-3}, indicating that it is not useful in practice.

Boye et al. (2005) treated 200 cm^3 of synthetic solutions containing up to 2 g dm^{-3} of gallotannic acid in 2.0 g dm^{-3} KCl of pH 3 at 80 mA and 400 cm^3 of a real wastewater from vegetal tanning processes with COD $>$ 100,000 mg O_2 dm^{-3} at 1.5 A by electrocoagulation and peroxi-coagulation using Fe/Pt and Fe/O_2 cells, respectively, at room temperature. Complete removal of gallotannic acid via precipitation of its Fe^{3+} complexes was found for both treatments, although the soluble COD was more efficiently removed by the peroxi-coagulation process due to the quicker generation of Fe^{3+} from Fenton's reaction (19.12). In contrast, the real wastewater solely reached 40% COD removal with formation of a black precipitate by electrocoagulation after the consumption of 54,000 C dm^{-3}, whereas peroxi-coagulation yielded almost total destruction of both tannin and nontannin (mainly proteins) pollutants under the same conditions. These results confirm the viability of the peroxi-coagulation method to decontaminate concentrated effluents at the end of industrial tanning.

A recent paper of Boye et al. (2006) reports the degradation of 200 cm^3 of solutions containing up to 6 mM gallic acid in 2.0 g dm^{-3} KCl of pH 3 at 80 mA and room temperature. The electro-Fenton method with 1 mM Fe^{2+} in a Pt/O_2 cell gave 70% TOC removal as maximum at 4 h, whereas the comparable photoelectro-Fenton process under 6-W UVA irradiation led to 90% TOC abatement. This behavior is explained by the expected mineralization of pollutants with $^{\bullet}OH$ to produce stable Fe^{3+}–oxalate complexes that can only be photodecarboxylated by UVA light. In contrast, the electrocoagulation method using a Fe/Pt yielded 95% decontamination in 2 h because complexes between gallic acid and Fe^{3+} quickly precipitate. This precipitation process, along with parallel mineralization of initial pollutant and its by-products with $^{\bullet}OH$ and coagulation with $Fe(OH)_3$, explains that overall decontamination is reached in less than 2 h by peroxi-coagulation in a Fe/O_2 cell. Peroxi-coagulation can then be much more effective than electro-Fenton and photoelectro-Fenton for wastewater remediation when insoluble complexes of Fe^{3+} with pollutants are formed.

19.6 Conclusions

It has been shown that indirect electro-oxidation methods based on H_2O_2 electrogeneration such as electro-Fenton, photoelectro-Fenton, and peroxi-coagulation are promising techniques for an effective and efficient decontamination of acidic wastewaters containing persistent organic pollutants. They are environmentally

friendly electrochemical methods that use oxidant species like $^{\bullet}OH$ produced from anode and cathode reactions in an undivided electrolytic cell. These techniques are economic, with moderate energetic spent even in the treatment of effluents with low salt content, and can be easily scaled-up for industrial wastewater remediation. Iron ions and other metallic ions used as catalysts can be recovered by precipitation of their hydroxides at neutral pH and reused in further runs. Aromatic pollutants are more efficiently mineralized by electro-Fenton than by anodic oxidation with electrogenerated H_2O_2 under comparable conditions. The efficiency of the electro-Fenton process depends on both, the anode and the cathode utilized, but it is limited by the formation of Fe^{3+} complexes with final carboxylic acids such as oxalic and oxamic. The use of a BDD anode always gives overall mineralization at long electrolysis times. The degradation rate of electro-Fenton is enhanced when iron ions and Cu^{2+} are combined as catalysts. The photoelectro-Fenton process is also more efficient and yields total decontamination since UVA light rapidly photodecomposes the Fe^{3+} complexes with the final carboxylic acids. The operational time and cost of photoelectro-Fenton are expected to be significantly reduced if inexpensive sunlight is applied as alternative UVA source. Peroxi-coagulation with a Fe anode is also very effective, although separation of pollutants in the precipitate formed usually predominates over their mineralization.

References

Aaron, J. –J. and Oturan, M. A. (2001) New photochemical and electrochemical methods for the degradation of pesticides in aqueous media. Environmental applications. Turk. J. Chem. 25, 509–520.

Alvarez-Gallegos, A. and Pletcher, D. (1998) The removal of low level organics via hydrogen peroxide formed in a reticulated vitreous cathode cell. Part 1. The electrosynthesis of hydrogen peroxide in aqueous acidic solutions. Electrochim. Acta 44, 853–861.

Alverez-Gallegos, A. and Pletcher, D. (1999) The removal of low level organics via hydrogen peroxide formed in a reticulated vitreous carbon cathode cell. Part 2: The removal of phenols and related compounds from aqueous effluents. Electrochim. Acta 44, 2483–2492.

Alvarez Gallegos, A., Vergara García, Y. and Zamudio, A. (2005) Solar hydrogen peroxide. Solar Energy Mater. Solar Cells 88, 157–167.

Badellino, C., Rodrigues, C. A. and Bertazzoli, R. (2006) Oxidation of pesticides by in situ electrogenerated hydrogen peroxide: Study for the degradation of 2,4-dichlorophenoxyacetic acid. J. Hazard. Mater. B137, 856–864.

Bellakhal, N., Oturan, M. A., Oturan, N. and Dachraoui, M. (2006) Olive oil mill wastewater treatment by the electro-Fenton Process. Environ. Chem. 3, 345–349.

Boye, B., Dieng, M. M. and Brillas, E. (2002) Degradation of herbicide 4-chlorophenoxyacetic acid by advanced electrochemical oxidation methods. Environ. Sci. Technol. 36, 3030–3035.

Boye, B., Brillas, E. and Dieng, M. M. (2003a) Electrochemical degradation of the herbicide 4-chloro-2-methylphenoxyacetic acid in aqueous medium by peroxi-coagulation and photoperoxi-coagulation. J. Electroanal. Chem. 540, 25–34.

Boye, B., Dieng, M. M. and Brillas, E. (2003b) Electrochemical degradation of 2,4,5-trichlorophenoxyacetic acid in aqueous medium by peroxi-coagulation. Effect of pH and UV light. Electrochim. Acta 48, 781–790.

Boye, B., Dieng, M. M. and Brillas, E. (2003c) Anodic oxidation, electro-Fenton and photoelectro-Fenton treatments of 2,4,5-trichlorophenoxyacetic acid. J. Electroanal. Chem. 557, 135–146.
Boye, B., Farnia, G., Sandonà, G., Buso, A. and Giomo, M. (2005) Removal of vegetal tannins from wastewater by electroprecipitation combined with electrogenerated Fenton oxidation. J. Appl. Electrochem. 35, 369–374.
Boye, B., Brillas, E., Buso, A., Farnia, G., Flox, C., Giomo, M. and Sandonà, G. (2006) Electrochemical removal of gallic acid from aqueous solutions. Electrochim. Acta 52, 256–262.
Brillas, E. and Casado, J. (2002) Aniline degradation by Electro-Fenton and peroxi-coagulation processes using a flow reactor for wastewater treatment. Chemosphere 47, 241–248.
Brillas, E., Bastida, R. M., Llosa, E. and Casado, J. (1995) Electrochemical destruction of aniline and 4-chloroaniline for wastewater treatment using a carbon-PTFE O_2-fed cathode. J. Electrochem. Soc. 142, 1733–1741.
Brillas, E., Mur, E. and Casado, J. (1996) Iron(II) catalysis of the mineralization of aniline using a carbon-PTFE O_2-fed cathode. J. Electrochem. Soc. 143, L49–L53.
Brillas, E., Sauleda, R. and Casado, J. (1997) Peroxi-coagulation of aniline in acidic medium using an oxygen diffusion cathode. J. Electrochem. Soc. 144, 2374–2379.
Brillas, E., Mur, E., Sauleda, R., Sánchez, L., Peral, J., Domènech, X. and Casado, J. (1998a) Aniline mineralization by AOP's: Anodic oxidation, photocatalysis, electro-Fenton and photoelectro-Fenton processes. Appl. Catal. B: Environ. 16, 31–42.
Brillas, E., Sauleda, R. and Casado, J. (1998b) Degradation of 4-chlorophenol by anodic oxidation, electro-Fenton, photoelectro-Fenton, and peroxi-coagulation processes. J. Electrochem. Soc. 145, 759–765.
Brillas, E., Calpe, J. C. and Casado, J. (2000) Mineralization of 2,4-D by advanced electrochemical oxidation processes. Water Res. 34, 2253–2262.
Brillas, E., Baños, M. A. and Garrido, J. A. (2003a) Mineralization of herbicide 3, 6-dichloro-2-methoxybenzoic acid in aqueous medium by anodic oxidation, electro-Fenton and photoelectro-Fenton. Electrochim. Acta 48, 1697–1705.
Brillas, E., Boye, B., Baños, M. A., Calpe, J. C. and Garrido, J. A. (2003b) Electrochemical degradation of chlorophenoxy and chlorobenzoic herbicides in acidic aqueous medium by the peroxi-coagulation method. Chemosphere 51, 227–235.
Brillas, E., Boye, B. and Dieng, M. M. (2003c) Peroxi-coagulation and photoperoxi-coagulation treatments of the herbicide 4-chlorophenoxyacetic acid in aqueous medium using an oxygen-diffusion cathode. J. Electrochem. Soc. 150, E148–E154.
Brillas, E., Boye, B. and Dieng, M. M. (2003d) General and UV-assisted cathodic Fenton treatments for the mineralization of herbicide MCPA. J. Electrochem. Soc. 150, E583–E589.
Brillas, E., Baños, M. A., Camps, S., Arias, C., Cabot, P. L., Garrido, J. A. and Rodríguez, R. M. (2004a) Catalytic effect of Fe^{2+}, Cu^{2+} and UVA light on the electrochemical degradation of nitrobenzene using an oxygen-diffusion cathode. New J. Chem. 28, 314–322.
Brillas, E., Boye, B., Sirés, I., Garrido, J. A., Rodríguez, R. M., Arias, C., Cabot, P. L. and Comninellis, Ch. (2004b) Electrochemical destruction of chlorophenoxy herbicides by anodic oxidation and electro-Fenton using a boron-doped diamond electrode. Electrochim. Acta 49, 4487–4496.
Comninellis, Ch and De Battisti, A. (1996) Electrocatalysis in anodic oxidation of organics with simultaneous oxygen evolution. J. Chim. Phys. 93, 673–679.
Da Pozzo, A., Di Palma, L., Merli, C. and Petrucci, E. (2005a) An experimental comparison of a graphite electrode and a gas diffusion electrode for the cathodic production of hydrogen peroxide. J. Appl. Electrochem. 35, 413–419.
Da Pozzo, A., Merli, C., Sirés, I., Garrido, J. A., Rodríguez, R. M. and Brillas, E. (2005b) Removal of the herbicide amitrole from water by anodic oxidation and electro-Fenton. Environ. Chem. Lett. 3, 7–11.
De Laat, J. and H. Gallard, H. (1999) Catalytic decomposition of hydrogen peroxide by Fe(III) in homogeneous aqueous solution: Mechanism and kinetic modeling. Environ. Sci. Technol. 33, 2726–2732.

Do, J. -S. and Chen, C. -P. (1993) In situ oxidative degradation of formaldehyde with electrogenerated hydrogen peroxide. J. Electrochem. Soc. 140, 1632–1637.

Drogui, P., Elmaleh, S., Rumeau, M., Bernard, C. and Rambaud, A. (2001a) Hydrogen peroxide production by water electrolysis: Application to disinfection. J. Appl. Electrochem. 31, 877–882.

Drogui, P., Elmaleh, S., Rumeau, M., Bernard, C. and Rambaud, A. (2001b) Oxidising and disinfecting by hydrogen peroxide produced in a two-electrode cell. Water Res. 35, 3235–3241.

Edelahi, M. C., Oturan, N., Oturan, M. A., Padellec, Y., Bermond, A. and El Kacemi, K. (2004) Degradation of diuron by the electro-Fenton process. Environ. Chem. Lett. 1, 233–236.

Ferro, S., De Battisti, A., Duo, I., Comninellis, Ch., Haenni, W. and Perret, A. (2000) Chlorine evolution at highly boron-doped diamond electrodes. J. Electrochem. Soc. 147, 2614–2619.

Flox, C., Ammar, S., Arias, C., Brillas, E., Vargas-Zavala, A. V. and Abdelhedi, R. (2006) Electro-Fenton and photoelectro-Fenton degradation of indigo Carmine in acidic aqueous medium. Appl. Catal. B: Environ. 67, 93–104.

Fockedey, E. and Van Lierde, A. (2002) Coupling of anodic and cathodic reactions for phenol electro-oxidation using three-dimensional electrodes. Water Res. 36, 4169–4175.

Foller, P. C. and Bombard, R. T. (1995) Processes for the production of mixtures of caustic soda and hydrogen peroxide via the reduction of oxygen. J. Appl. Electrochem. 25, 613–627.

Gallard, H., De Laat, J. and Legube, B. (1999) Comparative study of the rate of decomposition of H_2O_2 and of atrazine by Fe(III)/H_2O_2, Cu(II)/H_2O_2, Fe(III)/Cu(II)/H_2O_2. Rev. Sci. Eau 12, 715–728.

Gözmen, B., Oturan, M. A., Oturan, N. and Erbatur, O. (2003) Indirect electrochemical treatment of bisphenol A in water via electrochemically generated Fenton's reagent. Environ. Sci. Technol. 37, 3716–3723.

Guivarch, E., Oturan, N. and Oturan, M. A. (2003a) Removal of organophosphorus pesticides from water by electrogenerated Fenton's reagent. Environ. Chem. Lett. 1, 165–168.

Guivarch, E., Trevin, S., Lahitte, C. and Oturan, M. A. (2003b) Degradation of azo dyes in water by electro-Fenton process. Environ. Chem. Lett. 1, 38–44.

Hanna, K., Chiron, S. and Oturan, M. A. (2005) Coupling enhanced water solubilization with cyclodextrin to indirect electrochemical treatment for pentachlorophenol contaminated soil remediation. Water Res. 39, 2763–2773.

Harrington, T. and Pletcher, D. (1999) The removal of low levels of organics from aqueous solutions using Fe(II) and hydrogen peroxide formed in situ at gas diffusion electrodes. J. Electrochem. Soc. 146, 2983–2989.

Hsiao, Y. L. and Nobe, K. (1993) Hydroxylation of chlorobenzene and phenol in a packed bed flow reactor with electrogenerated Fenton's reagent. J. Appl. Electrochem. 39, 943–946.

Irmak, S., Yavuz, H. I. and Erbatur, O (2005) Degradation of 4-chloro-2-methylphenol in aqueous solution by electro-Fenton and photoelectro-Fenton processes. Appl. Catal. B: Environ. 63, 243–248.

Marselli, B., Garcia-Gomez, J., Michaud, P. -A., Rodrigo, M. A. and Comninellis, Ch. (2003) Electrogeneration of hydroxyl radicals on boron-doped diamond electrodes. J. Electrochem. Soc. 150, D79–D83.

Matsue, T., Fujihira, M. and Osa, T. (1981) Oxidation of alkylbenzenes by electrogenerated hydroxyl radical. J. Electrochem. Soc. 128, 2565–2569.

Meinero, S. and Zerbinati, O. (2006) Oxidative and energetic efficiency of different electrochemical oxidation processes for chloroanilines abatement in aqueous medium. Chemosphere 64, 386–392.

Oturan, M. A. (2000) An ecologically effective water treatment technique using electrochemically generated hydroxyl radicals for in situ destruction of organic pollutants: Application to herbicide 2,4-D. J. Appl. Electrochem. 30, 475–482.

Oturan, M. A. and Pinson, J. (1995) Hydroxylation by electrochemically generated OH radicals. Mono- and polyhydroxylation of benzoic acid: Products and isomer distribution. J. Phys. Chem. 99, 13948–13954.

Oturan, M. A., Pinson, J., Deprez, D. and Terlain, B. (1992) Polyhydroxylation of salicylic acid by electrochemically generated hydroxyl radicals. New J. Chem. 16, 705–710.
Oturan, M. A., Aaron, J. J., Oturan, N. and Pinson, J. (1999a) Degradation of chlorophenoxyacid herbicides in aqueous media, using a novel electrochemical method. Pestic. Sci. 55, 558–562.
Oturan, M. A., Pinson, J., Oturan, N. and Deprez, D. (1999b) Hydroxylation of aromatic drugs by the electro-Fenton method. Formation and identification of the metabolites of riluzole. New J. Chem. 23, 793–794.
Oturan, M. A., Peiroten, J., Chartrin, P. and Acher, A. J. (2000) Complete destruction of *p*-nitrophenol in aqueous medium by electro-Fenton method. Environ. Sci. Technol. 34, 3474–3479.
Oturan, M. A., Oturan, N., Lahitte, C. and Trevin, S. (2001) Production of hydroxyl radicals by electrochemically assisted Fenton's reagent. Application to the mineralization of an organic micropollutant, pentachlorophenol. J. Electroanal. Chem. 507, 96–102.
Panizza, M. and Cerisola, G. (2001) Removal of organic pollutants from industrial wastewater by electrogenerated Fenton's reagent. Water Res. 35, 3987–3992.
Panizza, M. and Cerisola, G. (2005) Application of diamond electrodes to electrochemical processes. Electrochim. Acta 51, 191–199.
Peralta-Hernández, J. M., Meas-Vong, Y., Rodríguez, F. J., Chapman, T. W., Maldonado, M. I. and Godínez, L. A. (2006) In situ electrochemical and photo-electrochemical generation of the Fenton reagent: A potentially important new water treatment technology. Water Res. 40, 1754–1762.
Plant, L. and Jeff, M. (1994) Hydrogen peroxide: A potent force to destroy organics in wastewater. Chem. Eng. 101, 16–20.
Pletcher, D. (1999) Indirect oxidations using electrogenerated hydrogen peroxide. Acta Chem. Scand. 53, 745–750.
Ponce De Leon, C. and Pletcher, D. (1995) Removal of formaldehyde from aqueous solutions via oxygen reduction using a reticulated vitreous carbon cathode cell. J. Appl. Electrochem. 25, 307–314.
Pratap, K. and Lemley, A. T. (1998) Fenton electrochemical treatment of aqueous atrazine and metolachlor. J. Agric. Food Chem. 46, 3285–3291.
Qiang, Z., Chang, J. H. and Huang, C. P. (2003) Electrochemical regeneration of Fe^{2+} in Fenton oxidation processes. Water Res. 37, 1308–1319.
Sharma, V. K. and Millero, F. J. (1988) Oxidation of copper(I) in seawater. Environ. Sci. Technol. 22, 768–771.
Sirés, I., Arias, C., Cabot, P. L., Centellas, F., Rodríguez, R. M., Garrido, J. A. and Brillas, E. (2004) Paracetamol mineralization by advanced electrochemical oxidation processes for wastewater treatment. Environ. Chem. 1, 26–28.
Sirés, I., Garrido, J. A., Rodríguez, R. M., Cabot, P. L.,Centellas, F., Arias, C. and Brillas, E. (2006) Electrochemical degradation of paracetamol from water by catalytic action of Fe^{2+}, Cu^{2+}, and UVA light on electrogenerated hydrogen peroxide. J. Electrochem. Soc. 153, D1–D9.
Song-hu, Y. and Xiao-hua, L. (2005) Comparison treatment of various chlorophenols by electro-Fenton method: Relationship between chlorine content and degradation. J. Hazard. Mater. B118, 85–92.
Sudoh, M., Kodera, T., Sakai, K., Zhang, J. Q. and Koide, K. (1986) Oxidative degradation of aqueous phenol effluent with electrogenerated Fenton's reagent. J. Chem. Eng. Jpn 19, 513–518.
Sun, Y. and Pignatello, J. J. (1993) Photochemical reactions involved in the total mineralization of 2,4-D by $Fe^{3+}/H_2O_2/UV$. Environ. Sci. Technol. 27, 304–310.
Tomat, R. and Rigo, A. (1976) Electrochemical production of hydroxyl radicals and their reaction with toluene. J. Appl. Electrochem. 6, 257–261.
Tomat, R. and Rigo, A. (1979) Oxidation of polymethylated benzenes promoted by hydroxyl radicals. J. Appl. Electrochem. 9, 301–305.
Tomat, R. and Rigo, A. (1984) Electrochemical oxidation of toluene promoted by hydroxyl radicals. J. Appl. Electrochem. 14, 1–8.

Tomat, R. and Rigo, A. (1985) Electrochemical oxidation of aliphatic hydrocarbons promoted by inorganic radicals. I. Hydroxyl radicals. J. Appl. Electrochem. 15, 167–173.
Tomat, R. and Vecchi, E. (1971) Electrocatalytic production of hydroxyl radicals and their oxidative addition to benzene. J. Appl. Electrochem. 1, 185–188.
Traube, M. (1882) Ueber die Aktivirung des Sauerstoffs. Ber. Dtsch. Chem.Ges. 15, 2434–2443.
Tzedakis, T., Savall, A. and Clifton, M. J. (1989) The electrochemical regeneration of Fenton's reagent in the hydroxylation of aromatic substrates: Batch and continuous processes. J. Appl. Electrochem. 19, 911–921.
Ventura, A., Jacquet, G., Bermond, A. and Camel, V. (2002) Electrochemical generation of the Fenton's reagent: Application to atrazine degradation. Water Res. 36, 3517–3522.
Wang, Q. and Lemley, A. T. (2001) Kinetic model and optimization of 2,4-D degradation by anodic Fenton treatment. Environ. Sci. Technol. 35, 4509–4514.
Wang, Q. and Lemley, A. T. (2002) Oxidation of diazinon by anodic Fenton treatment. Water Res. 36, 3237–3244.
Wang, Q. and Lemley, A. T. (2003) Oxidative degradation and detoxification of aqueous carbofuran by membrane anodic Fenton treatment. J. Hazard. Mater. B98, 241–255.
Wang, Q., Scherer, E. M. and Lemley, A. T. (2004) Metribuzin degradation by membrane anodic Fenton treatment and its interaction with ferric ion. Environ. Sci. Technol. 38, 1221–1227.
Wang, A., Qu, J., Ru, J., Liu, H. and Ge, J. (2005) Mineralization of an azo dye Acid Red 14 by electro-Fenton's reagent using an activated carbon fiber cathode. Dyes Pigments 65, 227–233.
Xie, Y. -B. and Li, X. -Z. (2006a) Degradation of Bisphenol A in aqueous solution by H_2O_2-assisted photoelectrocatalytic oxidation. J. Hazard. Mater. B138, 526–533.
Xie, Y. -B. and Li, X. -Z. (2006b) Interactive oxidation of photoelectrocatalysis and electro-Fenton for azo dye degradation using TiO_2-Ti mesh and reticulated vitreous carbon electrodes. Mater. Chem. Phys. 95, 39–50.
Yuan, S., Tian, M., Cui, Y., Lin, L. and Lu, X. (2006) Treatment of nitrophenols by cathode reduction and electro-Fenton methods. J. Hazard. Mater. B137, 573–580.
Zuo, Y. and Hoigné, J. (1992) Formation of hydrogen peroxide and depletion of oxalic acid in atmospheric water by photolysis of iron(III)-oxalato complexes. Environ. Sci. Technol. 26, 1014–1022.

Index

D

E

Q

R

S